

International Baltic Earth Secretariat Publication No. 3, June 2014

3rd International Lund Regional-Scale Climate Modelling Workshop

21st Century Challenges in Regional Climate Modelling

Lund, Sweden, 16-19 June 2014

Workshop Proceedings

Editors:
Lars Bärring
Marcus Reckermann
Burkhardt Rockel
Markku Rummukainen

LUND UNIVERSITY

Baltic Earth
Earth System Science for the Baltic Sea Region

Impressum

International Baltic Earth Secretariat Publications
ISSN 2198-4247

International Baltic Earth Secretariat
Helmholtz-Zentrum Geesthacht GmbH
Max-Planck-Str. 1
D-21502 Geesthacht, Germany

www.baltic-earth.eu
balticearth@hzg.de

Front page photo: Spring in Lund (Mikael Risedal)

Workshop Organizers and Sponsors





























Associated Organisations







Scientific Workshop Committee

- Babatunde Abiodun (South Africa)
- Raymond Arritt (U.S.A.)
- Lars Bärring (Sweden)
- Michel Déqué (France)
- Jason Evans (Australia)
- Jens Hesselbjerg Christensen (Denmark)
- Elizabeth Kendon (U.K.)
- Rupa Kumar Kolli (Switzerland)
- René Laprise (Canada)
- Ruby Leung (U.S.A)
- Markku Rummukainen (Sweden)
- Burkhardt Rockel (Germany)
- Silvina Solman (Argentina)
- Izuru Takayabu (Japan)
- Shuyu Wang (China)

Organizing Committee

- Markku Rummukainen (Sweden)
- Lars Bärring (Sweden)
- Marcus Reckermann (Germany)
- Burkhardt Rockel (Germany)
- Jens Hesselbjerg Christensen (Denmark)

Preface

This *Third International Lund Regional-scale Climate Modelling Workshop* is a follow-up to the regional scale climate modelling workshops held in Lund, Sweden, in 2004 and in 2009. The science has since then progressed over yet additional half decade, and it is timely to again take stock of where we are, what the current challenges are, and how we can further advance the science on regional-scale climate modelling to meet future expectations and demands. The overall aim of the workshop is to review the overall and specific developments in the field over the last five years, to discuss pertinent issues, and to consider emerging new avenues and challenges. In addition to the scientific sessions, the workshop provides opportunities for working meetings for networks, projects and training. The workshop addresses four themes:

Regional Climate and Earth System Models; Coupled modelling at regional scales is advancing, with Regional Climate Models (RCM) evolving to coupled models of atmosphere-ocean-sea ice, climate-vegetation, climate-biogeochemistry and aerosols. How can they advance research on climate feedback at regional scales?

Very-high-resolution RCMs; The resolution of RCMs continues to increase. More models are now being applied at resolutions of 5-10 km, and some down to 1-2 km. This requires adaptation and new developments in dynamics and physical parameterizations, including non-hydrostatic models. Statistical downscaling approaches also progress.

Challenges to RCM evaluation and application; RCMs with new components and higher resolution imply new model evaluation issues, such as the need for very-high-resolution evaluation data. Relevant developments in advanced statistics, hybrid downscaling approaches, nudging techniques, performance-based metrics and comprehensive added value aspects are fundamental issues to be explored under this topic.

RCM Ensembles; Coordinated experimentation with RCMs is advancing. This brings about many pertinent issues. What is the best design for a regional climate model ensemble? What determines the choice of GCMs and RCMs? Is weighting of ensemble members feasible? Can we account for model independence? Does the ensemble variance provide a good estimate of uncertainty in the regional climate projections?

The workshop collects more than 200 experts and we are very happy to see that this involves colleagues from all over the world, including many young scientists. The number of presentations, as documented in this volume, is 206.

The workshop is jointly organized and funded by Lund University, the Swedish Meteorological and Hydrological Institute (SMHI), the Danish Meteorological Institute (DMI), Helmholtz-Zentrum Geesthacht (HZG) and the International Baltic Earth Secretariat. The scientific committee was responsible for preparing the workshop content and the scientific programme, while practical and logistic arrangements were managed by the organizing committee.

We are grateful for a generous endorsement and financial support by the following organizations: the World Meteorological Organization (WMO); the World Climate Research Programme (WCRP); the Swedish Research Council Formas; the Centre for Regional Change in the Earth System (CRES), the Mistra-SWECIA research programme on climate, impacts and adaptation, the Strategic Research Areas MERGE and eSSENCE, and the Programme for Risk Information on Climate Change (SOUSEI).

Last but not least, we would like to thank Hanna Holm, Annika Malmgren Widerberg and Silke Köppen for the smooth preparation and running of the workshop.

May 2014

Lars Bärring, Marcus Reckermann, Burkhardt Rockel and Markku Rummukainen

Editors

Contents

Topic 1 Regional Climate and Earth System Models

Role of atmosphere-ocean coupling in the simulation of a polar low: a case study with the COAWST modeling system
Muralidhar Adakudlu, Sobolowski, S. 1

Medicanes in an ocean–atmosphere coupled regional climate model
Naveed Akhtar, Brauch, J., Dobler, A., Béranger, K., Ahrens, B. 3

Use of RCMs, cryosphere, and biosphere models to assess hydrological changes in mountain regions: results from the EU/FP7 "ACQWA" Project
Martin Beniston 5

Forcing a hydrological discharge model with RCM and GCM outputs in the Euphrates-Tigris Basin: Evaluation of the model performance and projected river discharges
Deniz Bozkurt, Sen, O. L., Hagemann, S. 6

Coupling of COSMO/CLM and NEMO in two regions
Jennifer Brauch, Früh, B., Pham, T.V., Akhtar, N., Ahrens, B. 8

Modeling Arctic Climate with a Regional Arctic System Model (RASM)
John Cassano, DuVivier, A., Hughes, M., Roberts, A., Brunke, M., Craig, A., Fisel, B., Gutowski, W., Maslowski, W., Nijssen, B., Osinski, R., Zeng, X. 10

Regional climate and streamflow projections in North America under IPCC CMIP5 scenarios
Hsin-I Chang, Castro, C., Troch, P., Mukherjee, R. 12

Regional Climate and Earth System Models – Added Value Revisited
Jens Hesselbjerg Christensen 14

Surface Heat Budget over the North Sea in Climate Change Simulations
Christian Dieterich, Wang, S., Schimanke, S., Gröger, M., Klein, B., Hordoir, R., Samuelsson, P., Liu, Y., Höglund, A., Meier, H.E.M. 15

A new regional climate system model setup for the EuroCORDEX domain
Alberto Elizalde, Mathis, M., Mikolajewicz, U. 17

Towards a LMD regional Earth simulator with WRF
Lluis Fita, Arsouze, T., Stéfanon, M. Berthou, S., Bastin, S., Polcher, J., Mailler, S., Drobinski, P., Hourdin, F., Fairhead, L. 19

The study and modeling of rainfall spatial and temporal changes in East Azarbaijan, Iran
Hojjatollah Fouladi Osgouei, Zarghami, M. 20

Added value of interactive air-sea coupling assessed from hindcast simulations for the North and Baltic seas
Matthias Gröger, Dieterich, C., Schimanke, S., Meier, H.E.M. 22

Assessing environmental changes and risks using a regional coupled ocean – atmosphere – sediment model
Alexandra Gronholz, Paul, A., Schulz, M. 24

Impacts of different coupling methods on regional atmosphere - ocean simulations
Ha Ho Hagemann, Rockel, B., Kapitza, H., Behrens, J. 26

The impact of two land-surface schemes on the characteristics of summer precipitation over East Asia from the RegCM4 simulations
Suchul Kang, Im, E.-S., Ahn, J.-B. 28

Arctic climate variability and change in the regional models RCA and RCAO
Torben Koenigk, Berg, P., Döscher, R. 30

Improvement of simulated monsoon precipitation over South-Asia with a regionally coupled model ROM
Pankaj Kumar, Sein, D., Cabos, W., Jacob, D. 32

Coupled regional climate and hydrology modelling at the catchment scale
Morten Andreas Dahl Larsen, Drews, M., Refsgaard, J.C., Jensen, K.H., Butts, M.B., Christensen, J.H., Christensen, O.B. 34

Sea Salt Generation Function in the Baltic Sea region as the important component to regional atmospheric model
Piotr Markuszewski, Petelski, T., Piskozub, J., Jakacki, J. 36

Challenges in regional climate system modeling for the Baltic Sea and North Sea regions
H.E. Markus Meier and members of the Baltic Earth Working Group on Regional Climate System Modelling 38

Sea state projections for the North Sea: Impact of climate change on very high waves?
Jens Möller, Groll, N., Heinrich, H. 40

Contribution of anthropogenic aerosols to the Euro-Mediterranean climate trends since 1980 using a regional coupled modelling approach
Pierre Nabat, Somot, S., Mallet, M., Sanchez-Lorenzo, A., Wild, M. 41

The potential impacts of forestation in mitigating climate change over Southern Africa
Myra Naik, Abiodun, B.J. 43

Simulation of snowbands on the Baltic Sea with coupled model COSMO-CLM/NEMO
Trang Van Pham, Brauch, J., Früh, B., Ahrens, B. 45

Analysis of nucleation events in the European boundary layer using the regional aerosol-climate model REMO-HAM
Joni-Pekka Pietikäinen, Mikkonen, S., Hamed, A., Hienola, A.I., Birmili, W., Kulmala, M., Laaksonen, A. 47

On the importance of inclusion of air-sea interactions in the simulation of austral summer precipitation over southern Africa using a regional model
Venkata Ratnam Jayanthi, Morioka, Y., Behera, S.K., Yamagata, T. 49

Air-Sea Interactions in a Coupled Atmosphere-Ocean Model for the Baltic Sea
Thomas Raub, Lehmann, A., Jacob, D. 51

Impacts of aerosols in the CORDEX-Europe domain using the regional aerosol-climate model REMO-HAM
Armelle Reca C. Remedio, Teichmann, C., Pietikäinen, J.-P., Sudarchikova, N., Jacob, D., Brasseur, G. 52

Simulated canopy vegetation effects on snow conditions for a forest site using the Multi-Energy Balance option in SURFEX
Patrick Samuelsson, Boone, A., Gollvik, S. 54

The sensitivity of major Baltic inflows simulated with the RCM NEMO-Nordic
Semjon Schimanke, Dieterich, C., Gröger, M., Meier, H.E.M. 56

Regionally coupled modelling of the Tropical Atlantic
Dmitry Sein, Cabos, W., Jacob, D. 57

Future climate change RCP4.5 and RCP8.5 scenarios downscaling for the Northern Europe with the focus on the North and Baltic Seas
Dmitry Sein, Cabos, W., Jacob, D. 59

Recent development in regional earth system modelling
Jun She, Tian, T., Madsen, K.C., Poulsen, J.W., Berg, P., Jonasson, L. 61

Land-cover dynamics and feedbacks in RCMs: State-of-the-art, outlook, and lessons learned
Benjamin Smith 63

Med-CORDEX: a first coordinated inter-comparison of fully-coupled regional climate system models (RCSM) for the Mediterranean
Samuel Somot, Ruti, P., Med-CORDEX Group 65

Soil moisture interaction with surface climate for different vegetation types in the La Plata Basin
Anna Sörensson, Berbery, H. 67

Coupled atmosphere – wave simulations of high-impact weather systems in the North-Atlantic and Baltic Region
David Sproson, Sahlée, E., Wu, L., Rutgersson, A. 69

Testing coupling techniques for a regional climate model : What are the advantages?
Marc Stéfanon, Polcher, J. 70

Ocean feedback mechanism in a coupled atmosphere-ocean model system for the North Sea
Jian Su, Moseley, C., Elizalde, A., Sein, D., Mayer, B., Pohlmann, T. 71

An impact of historical land-cover conversion on regional climate change during winter in Hokkaido Island, Japan
Shiori Sugimoto, Sato, T., Sasaki, T. 72

Simulation of the surface mass balance of the ice caps in Arctic Canada and Patagonia with the Regional Atmospheric Climate Model RACMO2
Willem Jan Van de Berg, Lenaerts, J., Van Meijgaard, E., Van den Broeke, M. 74

Development and evaluation of a new regional coupled atmosphere-ocean model in the North Sea and the Baltic Sea
Shiyu Wang, Dieterich, C., Döscher, R., Höglund, A., Hordoir, R., Meier, H.E.M., Samuelsson, P., Schimanke, S. 76

Potential mechanism of vegetation-induced reduction in tropical rainfall in Africa: Analysis based on regional Earth system model simulations
Minchao Wu, Smith, B., Schurgers, G., Siltberg, J., Rummukainen, M., Samuelsson, P. Jansson, C. 78

Comparison of air-sea momentum parameterizations in atmosphere-wave coupled system: Storm cases study
Lichuan Wu, Rutgersson, A., Sproson, D., Sahlée, E. 79

Severity of climate change dictates the direction of biophysical feedbacks of vegetation change to Arctic climate - results from the coupled regional climate-vegetation model CMIP5 simulations
Wenxin Zhang, Jansson, C., Miller, P. A., Smith, B., Samuelsson, P. 81

Dynamical downscaling with RIEMS over East Asia
Deming Zhao, Fu, C., Yan, X. 82

Topic 2 Very-high-resolution RCMs

Using High Resolution climate Modelling to Study the Effect of Climate Change on Lylan Valley Ground Water Characteristic in Kirkuk City in Iraq
Sameer S. Al-Juboori, Omer, F.M. 83

Amplified climate change signal due to urban expansion at local scales from a regional climate model
Daniel Argüeso, Evans, J.P., Fita, L., Pitman, A.J., Di Luca, A. 84

Cloud-resolving regional climate modeling approach in decade-long simulations
Nikolina Ban, Schmidli, J., Schär, C. 86

Downscaling of precipitation for the Himalayas using WRF model
Bhuwan Chandra Bhatt 88

Ensuring a robust regional model experimental design for future projection of extreme weather during the North American monsoon in the Southwest U.S.
Christopher L. Castro, Chang, H.-I., Luong, T., Jares, M., Lahmers, T., Carrillo, C. 89

Precipitation intensity and return level change projections by a convective-permitting regional climate model
Steven C. Chan, Kendon, E.J., Fowler, H.J., Roberts, N.M., Blenkinsop, S. 91

Feasibility Study of Very High Resolution Regional Climate Modelling Through Grid Telescoping Applied to the Canadian Regional Climate Model (CRCM5)
Mélissa Cholette, Laprise, R. 92

Land surface feedbacks on spring precipitation in the Netherlands
Emma Daniels, Lenderink, G., Hutjes, R.W.A., Ronda, R. Holtslag, A.A.M. 94

High-resolution sensitivity studies over Crete with the non-hydrostatic regional climate model REMO-NH
Bastian Eggert, Marien, L., Jacob, D. 96

Pursuing high resolution downscaling for hydrological applications in the Victorian Climate Initiative (VicCI)
Marie Ekström 98

Climate change signal of convective precipitation through convection permitting climate model simulations
Giorgia Fosser, Khodayar, S., Berg, P. 100

Impact of using the surface scheme SURFEX within ALARO-0 for the ERA-Interim high-resolution dynamical downscaling over Belgium
Oliver Giot, De Troch, R., Hamdi, R., Deckmyn, A., Termonia, P. 101

Implementation and initial results from convection-resolving Pan-European TerrSysMP and WRF simulations
Klaus Goergen, Keune, J., Gasper, F., Shrestha, P., Sulis, M., Knist, S., Ohlwein, C., Kollet, S., Simmer, C., Vereecken, H. 103

Simulating historical wind storms in Switzerland with WRF: identification of the optimal setup and its performance in high-resolution simulations
Juan Jose Gomez-Navarro, Messmer, M., Raible, C. 105

Precipitation in complex orography simulated by the regional climate model RCA3
Ivan Guettler, Stepanov, I., Nikulin, G., Jones, C., Branković, Č. 107

Impact of the horizontal resolution on extremes investigated with convection-resolving COSMO-CLM simulations
Oliver Gutjahr , Heinemann, G., Schefczyk, L. 109

Air quality and climate interaction within urban environment
Tomas Halenka, Huszar, P., Belda, M., Zemankova, K. 111

Assessment of three dynamical urban climate downscaling methods: Application for Brussels and Paris
Rafiq Hamdi 113

Implementation of the tidal forces into the models of the selected Svalbard fjords
Jaromir Jakacki, Przyborska, A., Kosecki, S. 114

Application of High-resolution RCM to Climate Change Projection and Urban Climatology Research
Nobuyuki Kayaba, Harada, M., Yamada, T., Murai, H., Hagiya, S., Oikawa, Y. 116

Very high resolution regional climate modeling – Benefits and future prospects
Elizabeth J. Kendon 118

Climate change projections for the North Sea from three coupled high-resolution models
Birgit Klein, Bülow, K., Dieterich, C., Heinrich, H. Hüttl-Kabus, S., Mayer, B., Meier, H.E.M., Mikolajewicz, U., Narayan, N., Pohlmann, T., Rosenhagen, G., Sein, D., Su, J. 120

Urban Climate Projection in Tokyo for the 2050's August: Impact of Urban Planning Scenarios and RCMs
Hiroyuki Kusaka, Suzuki-Parker, A., Aoyagi, T., Adachi, S.A., Yamagata, Y. 122

Response of hourly precipitation extremes to temperature and moisture perturbations: Results from a mesoscale model
Geert Lenderink, Attema, J., Loriaux, J., Van Meijgaard, E. 124

A Review of Very High Resolution Climate Modeling
L. Ruby Leung 126

Simulating extreme precipitation in the island of Crete with non-hydrostatic high-resolution RCMs
Petter Lind, Lindstedt, D., Jones, C., Kjellström, E. 127

A new regional climate model operating at the meso-gamma scale performance over Europe
David Lindstedt, Lind, P., Jones, C., Kjellström, E. 128

Convection permitting regional climate simulations of precipitation over a southwestern region of Japan
Akihiko Murata, Sasaki, H., Hanafusa, M., Nosaka, M. 129

Evaluation of the coupling between NWP and LES-based CFD models for simulating urban boundary layer flows
Hiromasa Nakayama, Takemi, T., Nagai, H. 131

The GAME project: challenges in modeling circulation of Svalbard fjords
Jacek Piskozub, Jakacki, J., Kosecki, S., Przyborska, A. 133

Simulation of salty bottom water penetration in a Deep
Nadezda Podrezova, Tsarev, V. 134

Projection of Future Climate Change around Japan in a Non-hydrostatic Regional Climate Model
Hidetaka Sasaki, Murata, A., Oh'izumi, M., Kurihara, K. 136

Usage of high-resolution dynamical downscaling around East and South-East Asia
Izuru Takayabu 139

Convection permitting climate simulations (CPCS) – Lessons learned at the Wegener Center
Heimo Truhetz, H., Prein, A., Gobiet, A. 141

Reproducibility of Regional difference of Altitudinal Dependence of Snow Depth using 1.5km High Resolution Experiments
Fumichika Uno, Kawase, H., Ishizaki, N.N., Yoshikane, T., Hara, M., Kimura, F., Iyobe, T., Kawashima, K. 143

Investigations of urban climate characteristics with SURFEX/TEB model: Preliminary results for Budapest city
Gabriella Zsebeházi, Krüzselyi, I., Szépszó, G. 145

Topic 3 Challenges for RCM evaluation and application

Objective type comparison and classification of precipitations variability over Ethiopia based on CORDEX simulations and GPCP datasets
Nigus Hiluf Abay 147

How well do regional climate models simulate extreme rainfall events in South Africa?
Babatunde J. Abiodun, Abba Omar, S. 148

Climate projection over the East Asia based on RCP scenarios using WRF
Joong-Bae Ahn, Hong, J.-Y. 150

CRCM5: performance errors, boundary forcing errors and climate projections over India
Adelina Alexandru, Sushama, L. 152

Impacts of using spectral nudging on COSMO-CLM simulations of single Vb-events
Ivonne Anders, Paumann, M., Chimani, B., Hofstätter, M. 154

The Indian Summer Monsoon Projections: Climate variability or Climate Change?
Shakeel Asharaf, Ahrens, B. 156

Submesoscale hydrodynamic response of the Black Sea coastal zone to the surface forcing provided by the regional climate model
Andrii Bagaiev, Ivanov, V.A., Demyshev, S.G. 158

Capitalizing on high resolution projections in application on regional climate change adaptation planning in Japan
Yingjiu Bai, Kaneko, I., Kobayashi, H., Sasaki, H., Hanafusa, M., Kurihara, K., Takayabu, I., Murata, A. 160

A new high-resolution European region reanalysis dataset for RCM evaluation and calibration – First tests and comparison to other datasets
Lars Bärring, Landelius, T., Wilcke, R.A., Dahlgren, P., Nikulin, G., Villaume, S., Undén, P., Kållberg, P. 162

On the integrated climate assessment using climate classification
Michal Belda, Halenka, T., Kalvova, J., Holtanova, E. 164

Statistical downscaling for assessing GCMs, RCMs and vice versa
Rasmus Benestad, Mezghani, A., Landgren, O., Haugen, J.-E., Haakenstad, H. 166

Creating a model consistent reference data set for bias correction applications
Peter Berg, Bosshard, T., Yang, W. 167

Evaluation of regional climate model simulations over Central Europe using the new high-resolution HYRAS precipitation climatology
Susanne Brienen, Früh, B., Walter, A., Tsusilova, K., Becker, P. 169

Climate Change Projections over CORDEX East Asia Domain using Multi-RCMs
Dong-Hyun Cha, Kim, G.-Y., Jun, C.-S., Lee, D.-K., Oh, S.-G., Suh, M.-S. 171

Climate information for decision making – The challenge of responding to user needs
Diane Chaumont, Isabelle Charron, David Huard 173

Potential Added Value of COSMO-CLM in Simulating Extreme Precipitation over East Africa
Bedassa R. Cheneka, Früh, B., Brienen, S., Fröhlich, K., Asharaf, S. 175

Limited-Area Energy Budget for the Canadian RCM
Marilys Clément, Laprise, R., Nikiéma, O. 177

Role of domain size and grid resolution on the accuracy of regional climate simulations with the COSMO-CLM model over the Mediterranean region
Dario Conte, Lionello, P. 179

Challenges of tracking extratropical cyclones in regional climate models
Hélène Côté, Grise, K.M., Son, S.-W., De Elia, R., Frigon, A. 181

Sensitivity of the NHRCM simulation of the southwest monsoon rainfall over the Philippines to model resolution
Faye T. Cruz, Sasaki, H., Narisma, G.T. 183

Probabilistic climate scenarios for risk assessment in Japan
Koji Dairaku, Ueno, G., Takayabu, I. 185

Dynamical downscaling and socio-economic land use scenarios for regional scale adaptation to climate change in Tokyo metropolitan area
Koji Dairaku, Yamagata, Y., Hirano, J., Seya, H., Tsunematsu, N., Nakamichi, K. 187

Assessment of add-value of ensemble dynamical downscaling in Japan
Koji Dairaku, Iizuka, S., Tsunematsu, N., Hirano, J., Sasaki, W., Pielke Sr., R.A. 189

Some sources of bias in the Eurocordex historical runs
Michel Déqué, Alias, A., Dubois, C., Somot, S. 191

A framework to study the potential benefits of using high-resolution regional climate model simulations
Alejandro Di Luca, De Elia, R., Laprise, R. 192

Identifying cyclones in high-resolution RCM simulations and reanalysis
Alejandro Di Luca, Evans, J.P., Argüeso, D. 194

Evaluation of fifth-generation Canadian Regional Climate Model (CRCM5) simulations using Stage IV precipitation analyzes over the eastern United States
Mamadou Insa Diop, Laprise, R., Torlaschi, E. 196

Exploiting regional climate modeling in the Arctic
Ralf Döscher, Königk, T., Berg, P., Johansson, M. 198

Evaluation of a surface temperature simulation over Tunisia using the WRF model
Bilel Fathalli, Pohl, B., Castel, T., Safi, M.J. 200

Typhoons in regional climate model simulations
Frauke Feser, Barcikowska, M. 202

Exploring new evaluation methods for RCM exercises. Using Australian soundings for the NARCliM experiment
Lluis Fita, Liles, S., Evans, J.P., Argüeso, D. 203

Representation of Heavy Precipitation Events over the western Mediterranean region in regional climate models
Giorgia Fosser , Nuissier, O., Dubois, C., Somot, S. 204

Challenges for RCM evaluation and application when moving to high resolutions
Hayley J Fowler, Kendon, E. J., Blenkinsop, S., Chan, S. C., Roberts, N., Ferro, C.A.T. 205

From high-resolution simulations to the client
Anne Frigon, Biner, S., De Elia, R. 207

Evaluation of CORDEX-REMO simulations applying a new high-resolution gridded dataset for the Carpathian region
Borbála Gálos, Szalai, S., Rechid, D., Teichmann, C., Kriegsmann, A., Jacob, D. 208

Climate model results for wind speed and direction over the North Sea
Anette Ganske, Rosenhagen, G., Heinrich, H. 210

Is it possible to separate model calibration and evaluation? A multi-physics study with modern radiation and soil datasets
Markel Garcia-Diez, Fernandez, J., Vautard, R. 211

Development, validation and application of a single-column atmosphere model in the framework of the Canadian RCM with an application to deep Lake Geneva
Stephane Goyette, Marjorie Perroud..... 213

Estimation of future temperature and sea ice extremes of the Baltic Sea
Jari Haapala, An, B.W., Juva, K. 215

Future Climate Changes over East Asia by the RCP scenarios downscaled using the Regional Spectral Model
Suryun Ham, Yoshimura, K. 216

The KLIWAS Project: Adapting Shipping and Waterways to Climate Change – The North Sea Case
Hartmut Heinrich, Tinz, B., Rosenhagen, G., Klein, B., Klein, H., Ganske, A., Bülow, K., Schade, N., Möller, J., Hüttl-Kabus, S., Löwe, P., Gates, L. 218

Web Processing Services for Climate Data – with Examples for Impact Modelers
Nils Hempelmann, Ehbrecht, C., Falk, W., Parham, P. 220

The Change of Cherry First-flowering Date over South Korea Projected from Downscaled IPCC AR5 Simulation
Jina Hur, Ahn, J.-B., Shim, K.-M. 221

Model based analysis of decade scale variability of Baltic Sea hydrography
Katriina Juva, An, B.W., Haapala, J. 223

Stochastic modelling of future daily weather in consistency with RCM projections and the observed spatio-temporal structure
Denise Keller, Fischer, A.M., Frei, C., Liniger, M.A., Appenzeller, C., Knutti, R. 225

Differences in future European climate change between an RCM ensemble and the underlying GCMs
Erik Kjellström, Nikulin, G., Samuelsson, P., Kupiainen, M., Hansson, U., Jones, C. 227

Evaluating temperature distributions in a high-resolution RCM at 6 km horizontal resolution over Europe
Erik Kjellström, Lind, P., Lindstedt, D., Landelius, T. 229

The representation of recent Siberian snow cover in the regional climate model COSMO-CLM
Katharina Klehmet, Geyer, B., Rockel, B. 231

Validation of Cordex data over Cote d'Ivoire
Kouakou Kouadio, Konare, E., Kouakou, K.G., Diedhiou, A. 233

Accurate Boundary Conditions for Regional Climate Modeling
Marco Kupiainen 234

Spatially explicit climate model evaluation with complex networks
Stefan Lange, Feldhoff, J.H., Donges, J.F., Volkholz, J., Kurths, J. 235

Evaluation of River Discharge Simulated by Regional Climate Modeling over the Korean Region and Sensitivity on Resolution of River Routing Scheme
Ji-Woo Lee, Hong, S.-Y., Ester Kim, J.-E., Yoshimura, K., Ham, S., Joh, M. 236

Quantifying uncertainty in observed rainfall datasets across Africa: A probabilistic history
Chris Lennard, Dosio, A., Nikulin, G. 238

Atmospheric circulation and precipitation in regional climate models during major heat waves in Central Europe
Ondřej Lhotka, Kyselý, J. 240

Studies of scale interaction in a two-way nesting climate model
Laurent Li, Li, S., Le Treut, H. 242

Large Scale Meteorological Patterns Associated with Temperature Extremes in the North American Regional Climate Change Assessment Program Hindcast Experiment
Paul C. Loikith, Waliser, D.E., Kim, J., Lee, H., Neelin, J.D., McGinnis, S., Lintner, B., Mattmann, C., Mearns, L.O. 243

Markovian behaviour of dry spells over the Iberian Peninsula using ESCENA regional climate models
Noelia López-Franca, Sánchez, E., Domínguez, M., Losada, T., Romera, R. 245

Comparison of North-American CORDEX simulations with the Canadian Regional Climate Model (CRCM5) at 0.44°, 0.22° and 0.11°: Does the simulated climate get better with higher resolution?
Philippe Lucas-Picher, Laprise, R., Winger, K. 247

A regional climate model hindcast downscaling study of screen level temperature and precipitation for Estonia and the Baltic Sea region
Aarne Männik, Luhamaa, A., Zirk, M., Rõõm, R. 249

Identifying added value in two high-resolution climate simulations over Scandinavia
Stephanie Mayer, Fox Maule, C., Sobolowski, S., Christensen, O.B., Sørup, H.J.D., Pinya, M.A.S., Arnbjerg-Nielsen, K., Barstad, I. 251

The link between El Niño Southern Oscillation (ENSO) and the Southern African rainfall in a Regional Climate Model
Arlindo Meque, Abiodun, B.J. 253

Using WRF to analyse the role of Vb-events in extreme precipitations over Central Europe
Martina Messmer, Gomez-Navarro, J.J., Raible, C. 255

Simulation of high-altitude frontal zones in the tropopause and their role in the formation of the synoptic situation and climatic variability in the Northern Hemisphere and Europe region
Yaroslav Mitskevich, Partasenok, I. 257

Simulation of the African hydroclimate using the HadGEM3-RA regional climate model: Resolution versus parametrisation dependence
Wilfran Moufouma-Okia, Jones, R. 259

Evaluation of projected changes in extreme precipitation with increasing spatial resolution
Trevor Q. Murdock, Sobie, S.R., Cannon, A.J. 260

Climate-type based analysis of RegCM4 model performance over the Philippines
Gemma T. Narisma, Discar, A. 262

Performance evaluation of Regional Climate Model (RegCM4) in simulating the climate over Indian region
Sridhara Nayak, Manabottam, M., Suman, M. 264

An analysis of Precipitation-Temperature relationship: Responses from Multiple RCM simulations over Japan
Sridhara Nayak, Dairaku, K. 266

Contradicting projected changes in precipitation over West Africa from the CMIP5 and CORDEX simulations
Grigory Nikulin, Kjellström, E., Jones, C., Samuelsson, P., Kupiainen, M., Hansson, U., CORDEX Africa Team 267

Mistral and its Siblings in RCMs
Anika Obermann, Somot, S., Ahrens, B. 268

How well does HIRHAM5 model simulate present day climate over East Africa?
Sarah Emerald Osima, Hewitson, B., Stendel, M. 270

Projected Changes in Air Temperature and Precipitation Climatology in Central Asia CORDEX Region 8 by Using RegCM4.3.5
Tugba Ozturk, Türkes, M., Kurnaz, M. L. 272

Regional climate model evaluation of atmospheric conditions leading to severe weather and large precipitable water events
Dominique Paquin, De Elia, R., Frigon, A. 273

Sensitivity of ERA-Interim driven RegCM4 precipitation to horizontal resolution
Mirta Patarčić, Cindrić, K., Branković, Č. 275

Character analysis of observation data for model evaluation and land use changes
Swantje Preuschmann, Jacob, D. 277

Examining the impact of domain size on tropical cyclone simulations and projections over Vietnam in a regional climate model downscaling of a 5 member GCM ensemble
Grace Redmond, Hein, D., Hodges, H. 279

On the variability in a regional climate model using dynamical downscaling with frequent reinitializations
Thomas Remke, Jacob, D. 280

Evaluation of Dynamical Downscaling Resolution Effect on Wind Energy Forecast Value for a Wind Farm in Central Sweden
Martin Haubjerg Rosgaard, Hahmann, A.N., Nielsen, T.S., Giebel, G., Sørensen, P.E., Madsen, H. 282

A Markov chain method to determine the dynamic properties of compound extremes and their near future climate change signal
Katrin Sedlmeier, Mieruch, S., Schädler, G. 284

Evaluating teleconnection responses of the CORDEX models: A case study over Eastern Africa
Hussen Seid, Lennard, C., Hewitson, B. 285

Simulation Strategies for Optimal Detection of Regional Climate Model Response to Parameter Modifications
Leo Separovich, De Elia, R., Laprise, R. 287

Systematic temperature and precipitation biases in the CLARIS-LPB ensemble simulations over South America and possible implications for climate change projections
Silvina Solman 289

Diagnostic Budget Study of the Internal Variability of Ensemble Simulations of HIRHAM5 for the Arctic
Anja Sommerfeld, Nikiema, O., Rinke, A., Dethloff, K., Laprise, R. 291

Uncertainties in the regional climate models simulations of South-Asian summer monsoon and climate change
Faisal Saeed Syed, Iqbal, W., Syed, A.A.B. 293

Assessment of methods for downscaling European wind storms.
Simon Tucker, Buonomo, E., Jones R. 294

A realistic land cover change trajectory, including re-vegetation, reveals substantial climate impact of deforestation in the Congo basin
Nicole P.M. van Lipzig, Akkermans, T., Thiery, W., Moonen, P., Verbist, B., Muys, B. 295

Can an RCM improve on large scales within its domain – How much to this end does the resolution help?
Katarina Veljovic, Mesinger, F. 296

Strategies and measures for determining the skill of dynamical downscaling
Hans von Storch..... 297

Impacts of boundary layer parameterization schemes and air-sea coupling on WRF simulation of East Asian summer monsoon
Ziqian Wang, Duan, A., Wu, G. 299

Future of precipitation in Poland – projections for XXI century
Joanna Wibig, Jędruszkiewicz, J., Piotrowski, P..... 301

Impact of BOB tropical storms on Tibetan Plateau precipitation and soil moisture
Zhixiang Xiao, Duan, A. 302

Dry spells: RCMs performance to simulate present climate and projections for future climate in South America
Pablo Zaninelli, Carril, A.F., Menéndez, C.G., Sánchez, E. 304

Comparisons of simulated climate changes of Eastern China using WRF with Noah and Noah-MP land surface scheme
Xuezhen Zhang, Hu, Y. 306

WRF sensitivity to physics parameterizations over the MENA-CORDEX domain
George Zittis, Hadjinicplaou, P., Lelieveld, J. 308

Parameter tuning and calibration of RegCM3 with MIT-Emanuel cumulus parameterization scheme over CORDEX East Asian domain
Liwei Zou, Qian, Y., Zhou, T., Yang, B..... 310

Topic 4 RCM Ensembles

Regime-dependent validation of simulated surface wind speed in coastal areas of the North Sea
Ivonne Anders, Rockel, B. 313

Use of a multiple GCM and mixed physics ensemble of regional climate simulations to evaluate trends in extreme precipitation
Raymond W. Arritt, Groisman, P.Y., Daniel, A.R. 315

Seasonal forecasting: Opportunities and challenges for use of regional climate models
Raymond Arritt W., Castro, C.L. 317

Seasonal Ensemble Simulations in East Africa
Shakeel Asharaf, Cheneka, R.B., Brienen, S., Fröhlich, B., Nikulin, G., Früh, B., and the EUPORIAS East Africa Team 319

Availability of CORDEX output through the ESGF network
Ole Bøssing Christensen 320

Europe in a 6 Degrees Warmer Climate
Ole Bøssing Christensen, Yang, S., Boberg, F., Fox Maule, C., Olesen, M., Drews, M., Sørup, H.J.D., Christensen, J.H. 321

Quantifying uncertainty in regional climate model projections over Western Canadian watersheds
Charles L. Curry, Weaver A.J., Caya, D., Giguère, M., Wiebe, W. 323

Global Warming Impacts on Great Lakes Basin Precipitation Extremes
Marc d'Orgeville, Peltier, W.R., Erler, A.R. 324

On Reliability of Regional Decadal Ensemble Prediction for Europe
Fatemeh Davary Adalatpanah, Früh, B., Lenz, C.-J., Becker, P. 325

Future snowfall in western and central Europe projected with a high-resolution regional climate model ensemble
Hylke De Vries, Lenderink, G., Van Meijgaard, E. 327

Weather Extremes in Regional Climate Ensembles
James Done, Pai Mazumder, D. 329

Including model performance and independence in ensemble design
Jason Evans, Argüeso, D., Di Luca, A., Olson, R., Fita, L. 331

Selection of a best subset of GCM-RCMs from an ensemble for impact studies
Cathrine Fox Maule, Christensen, O.B., Thejll, P. 332

Simulation of medicanes over the Mediterranean Sea: multi-model analysis of the impact of high resolution and ocean-atmosphere coupling
Miguel Ángel Gaertner, Domínguez, M., Romera, R., Gil, V., Sánchez, E., Gallardo, C., EURO-CORDEX and Med-CORDEX teams 334

Assessing the sensitivity in the ensemble building from RCMs for hydrological applications
Sandra Galiano Garcia, Giménez, O., Giraldo Osorio, J.D. 336

COSMO-CLM and RCA4 Multimodel ensemble Projections for the West African Monsoon
Emiola O. Gbobaniyi, Anders, I. 338

Use of RCM ensembles to produce regional climate projections: Key issues and the CORDEX perspective
Filippo Giorgi 339

Exploring a three-stage dynamical downscaling with empirical correction of sea-surface temperature using CRCM5 over the CORDEX-Africa domain
Leticia Hernández-Díaz, Laprise, R., Nikiéma, O., Winger, K. 340

Evaluation of the Performance of Regional Climate Models from CORDEX-East Asia
Bo Huang, Polanski, S., Cubasch, U. 342

The Euro-CORDEX initiative: A new generation of regional climate scenarios for Europe
Daniela Jacob, Gobiert, A., Teichmann, C., Truhetz, H. 343

Seasonal-to-decadal prediction and opportunities for downscaling
Noel Keenlyside 345

The elevation dependency of 21st century European climate change in a multi-RCM ensemble
Sven Kotlarski, Lüthi, D., Schär, C. 346

The European summer climate in a surrogate experiment
Nico Kröner, Kotlarski, S., Fischer, E., Lüthi, D., Schär, C. 348

Investigating structural dependencies between AOGCM models and their impact on regional-scale climate-change projections
Martin Leduc, Laprise, R., De Elia, R. 350

Bayesian model averaging to combine surface temperatures simulated in the North America Regional Climate Change Assessment Program
Huikyo Lee, Braverman, A., Mattmann, C., Waliser, D., Loikith, P., Kim, J. 352

Regional Arctic Climate System Model (RASM): An overview and selected results on sea ice sensitivity to variable parameter space
Wieslaw Maslowski, Osinski, R., Roberts, A., Kinney, J.-C., Cassano, J. 354

Regional climate modeling of Arctic temperature extremes and their variability
Heidrun Matthes, Rinke, A., Königk, T., Scinocca, J., Dethloff, K. 356

Strategic sub-selection of CMIP5 GCMs for dynamical downscaling
Carol McSweeney, Jones, R. 357

How to establish the value of multiple GCM-RCM simulation programs
Linda O. Mearns, Dominguez F., Garfin, G., Gutowski W., Hammerling D., Lettenmaier D., Leung R., Michaels S., Pryor S., Sain, S. 359

Selecting climate simulations for impact studies based on multivariate patterns of climate change
Thomas Mendlik, Gobiet, A. 361

Energy cycle associated with Inter-member Variability in a large ensemble of simulations of the Canadian RCM (CRCM5)
Oumarou Nikiéma, Laprise, R. 362

Precipitation in the EURO-CORDEX 0.11 ° and 0.44 simulations: High resolution, High benefits?
Andreas Prein, Gobiet, A., Truhetz, H., Keuler, K., Görgen, K., Teichmann, C., Fox Maule, C., Van Meijgaard, E., Déqué, M., Nikulin. G., Vautard, R., Kjellström, E., Colette, A. 364

The design and interpretation of RCM ensembles: Lessons from GCM simulations in the Coupled Model Intercomparison Project
Jouni Räisänen and Jussi. S. Ylhäisi 366

South America regional temperature and precipitation projections for the end of XXIst century from CLARIS-LPB ensemble of RCMs
Enrique Sánchez, Samuelsson, P., Da Rocha, R., Li, L., Marengo, J., Remedio, A., Berbery, H. 368

Using a Circulation Type Classification to Investigate the Internal Variability in Regional Climate Model Simulations over Europe
Kevin Sieck, Jacob, D. 370

Improvement of Climate Projections and Reduction of their Uncertainties Using a Sequential Learning Algorithm
Ehud Strobach, Bel G 372

An overview of the SOUSEI multi GCM/RCM dynamical downscaling ensemble
Asuka Suzuki-Parker, Takayabu, I., Mizuta, R., Kusaka, H., Dairaku, S., Adachi, S.A., Ishizaki, N.N.. 374

Sampling downscaling method and ist application to Hokkaido summer climate
Tamaki Y., Inatsu M., Nakano, N., Kuno, R. 376

Estimation of the probability distribution of monthly mean temperature by a regression model
Genta Ueno, Iba, Y., Dairaku, K., Takayabu, I. 378

Regional modeling approaches to study the recent shift in East African long rains
Nicolas Vigaud, Robertson, A., Lyon, B. 380

A stochastic regional scale climate change projection experiment using incremental dynamical downscaling and analysis system
Yasutaka Wakazuki, Hara, M., Kimura, F. 382

Reducing model ensemble size for climate change impact application – A case study
Renate A.I. Wilcke, Bärring, L., Mendlik, T. 384

Climate change scenarios over complex topography: assessing the added value of dynamical downscaling
Elias Zubler, Fröb, F., Fischer, A.M., Liniger, M.A., Appenzeller, C. 386

Baltic Earth

Baltic Earth - Earth System Science for the Baltic Sea Region
An open research network to achieve an improved Earth system understanding of the Baltic Sea region
H. E. Markus Meier, Anna Rutgersson, Marcus Reckermann and the Baltic Earth Interim Science Steering Group 389

Author Index

Abay, N.H. 147
Abba Omar, S. 148
Abiodun, B.J. 43, 148, 253
Adachi, S.A. 122, 374
Adakudlu, M. 1
Ahn, J.-B. 28, 150, 221
Ahrens, B. 3, 8, 45, 156, 268
Akhtar, N. 3, 8
Akkermans, T. 295
Alexandru, A. 152
Alias, A. 191
Al-Juboori, S.S. 83
An, B.W. 215
Anders, I. 154, 313, 338
Aoyagi, T. 122
Appenzeller, C. 225, 386
Argüeso, D. 84, 194, 203, 331
Arnbjerg-Nielsen, K. 251
Arritt, R.W. 315, 317
Arsouze, T. 19
Asharaf, S. 156, 175, 319
Attema, J. 124
Bagaiev, A. 158
Bai, Y. 160
Baltic Earth Working Group on RCSM 38
Ban, N. 86
Barcikowska, M. 202
Bärring, L. 162, 384
Barstad, I. 251
Bastin, S. 19
Becker, P. 169, 325
Behera, S.K. 49
Behrens, J. 26
Bel, G. 372
Belda, M. 111, 164
Benestad, R. 166
Beniston, M. 5
Béranger, K. 3
Berbery, H. 67, 368
Berg, Per 61
Berg, Peter 30, 100, 167, 198
Berthou, S. 19
Bhatt, B.C. 88
Biner, S. 207
Birmili, W. 47
Blenkinsop, S. 91, 205
Boberg, F. 14, 321
Boone, A. 54
Bosshard, T. 167
Bozkurt, D. 6
Branković, Č. 107, 275
Brasseur, G. 52
Brauch, J. 3, 8, 45
Braverman, A. 352
Brienen, S. 169, 175, 319
Brunke, M. 10
Bülow, K. 120, 218
Buonomo, E. 294
Butts, M.B. 34
Cabos, W. 32, 57, 59
Cannon, A.J. 260
Carril, A.F. 304
Carrillo, C. 89
Cassano, J. 10, 354
Castel, T. 200
Castro, C.L. 12, 89, 317
Caya, D. 323
Cha, D.-H. 171
Chan, S.C. 91, 205
Chang, H.-I. 12, 89
Charron, I. 173
Chaumont, D. 173
Cheneka, R.B. 175, 319
Chimani, B. 154
Cholette, M. 92
Christensen, J.H. 14, 34, 321
Christensen, O.B. 34, 251, 320, 321, 332
Cindrić, K. 275
Clément, M. 177
Colette, A. 364
Conte, D. 179
CORDEX Africa Team 267
Côté, H. 181
Craig, A. 10
Cruz, F.T. 183
Cubasch, U. 342
Curry, C.L. 323
D'Orgeville, M. 324
Da Rocha, R. 368
Dahlgren, P. 162
Dairaku, K. 185, 187, 189, 266, 378
Dairaku, S. 374
Daniel, A.R. 315
Daniels, E. 94
Davary Adalatpanah, F. 325
De Elia, R. 350

De Troch, R. 101
De Vries, H. 327
Deckmyn, A. 101
Demyshev, S.G. 158
Déqué, M. 191, 364
Dethloff, K. 291, 356
Di Luca, A. 84, 192, 194, 331
Diedhiou, A. 233
Dieterich, C. 15, 22, 56, 76, 120
Diop, M.I. 196
Discar, A. 262
Dobler, A. 3
Dominguez, M. 359
Done, J. 329
Donges, J.F. 235
Döscher, R. 30, 76, 198
Dosio, A. 238
Drews, M. 34, 321
Drobinski, P. 19
Duan, A. 299, 302
Dubois, C. 191, 204
DuVivier, A. 10
Eggert, B. 96
Ehbrecht, C. 220
Ekström, M. 98
Elizalde, A. 17, 71
Erler, A.R. 324
Ester Kim, J.E. 236
EUPORIAS East Africa Team 319
EURO-CORDEX Team 334
Evans, J.P. 84, 194, 203, 331
Fairhead, L. 19
Falk, W. 220
Fathalli, B. 200
Feldhoff, H.H. 235
Fernandez, J. 211
Ferro, C.A.T. 205
Feser, F. 202
Fischer, A.M. 225, 386
Fischer, E. 348
Fisel, B. 10
Fita, L. 19, 84, 203, 331
Fosser, G. 100, 204
Fouladi Osgouei, H. 20
Fowler, H.J. 91
Fox Maule, C. 251, 321, 332, 364
Frei, C. 225
Frigon, A. 181, 207, 273
Fröb, F. 286
Fröhlich, B. 319
Fröhlich, K. 175
Früh, B. 8, 45, 169, 175, 319, 325
Fu, C. 82
Gaertner, M.A. 334
Gallardo, C. 334
Gálos, B. 208
Ganske, A. 210, 218
Garcia Galiano, S. 336
Garcia-Diez, M. 211
Garfin, G. 359
Gasper, F. 103
Gates, L. 218
Gbobaniyi, E.O. 338
Geyer, B. 231
Giebel, G. 282
Giguère, M. 323
Gil, V. 334
Giménez, O. 336
Giorgi, F. 339
Giot, G. 101
Giraldo Osorio, J.D. 336
Gobiet, A. 141, 361, 364
Gollvik, S. 54
Gomez-Navarro, J.J. 105, 255
Goergen, K. 103
Goyette, S. 213
Grise, K.M. 181
Gröger, M. 15, 22, 56
Groisman, P.Y. 315
Groll, N. 40
Gronholz, A. 24
Guettler, I. 107
Gutjahr, O. 109
Gutowski, W. 10, 359
Haakenstad, H. 166
Haapala, J. 215, 223
Hadjinicplaou, P. 308
Hagemann, H.H. 26
Hagemann, S. 6
Hagiya, S. 116
Hahmann, A.N. 282
Halenka, T. 111, 164
Ham, S. 216, 236
Hamdi, R. 101, 113
Hamed, A. 47
Hammerling, D. 359
Hanafusa, M. 129, 160
Hansson, U. 227, 267
Hara, M. 143, 382
Harada, M. 116

Haugen, J.-E. 166
Hein, D. 279
Heinemann, G. 109
Heinrich, H. 40, 120, 210, 218
Hempelmann, N. 220
Hernández-Díaz, L. 340
Hewitson, B. 270, 285
Hienola, J. 47
Hirano, J. 187, 189
Hodges, H. 279
Hofstätter, M. 154
Höglund, A. 15, 76
Holtanova, E. 164
Holtslag, A.A.M. 94
Hong, J.-Y. 150
Hong, S.-Y. 236
Hordoir, R. 15
Hourdin, F. 76
Hu, Y. 306
Huang, B. 342
Huard, D. 173
Hughes, M. 10
Hur, J. 221
Huszar, P. 111
Hutjes, R.W.A. 94
Hüttl-Kabus, S. 120, 218
Iba, Y. 378
Iizuka, S. 189
Im, E.-S. 28
Inatsu, I. 376
Iqbal, W. 293
Ishizaki, N.N. 143, 374
Ivanov, V.A. 158
Iyobe, T. 143
Jacob, D. 32, 51, 52, 57, 59, 96, 208, 277
..... 280, 343, 370
Jakacki, J. 36, 114, 133
Jansson, C. 78, 81
Jares, M. 89
Jayanthi, V.R. 49
Jędruszkiewicz, J. 301
Jensen, K.H. 34
Joh, M. 236
Johansson, M. 198
Jonasson, L. 61
Jones, C. 107, 127, 128, 227, 267
Jones, R. 259, 294, 357
Jun, C.-S. 171
Juva, K. 215, 223
Kållberg, P. 162
Kalvova, J. 164
Kaneko, I. 160
Kang, S. 28
Kapitza, H. 26
Katzfey, J. 26
Kawase, H. 143
Kawashima, K. 143
Kayaba, N. 116
Keenlyside, N. 345
Keller, D. 225
Kendon, E.J. 91, 118, 205
Keuler, K. 364
Keune, J. 103
Khodayar, S. 100
Kim, G.-Y. 171
Kim, J. 243, 352
Kimura, F. 143, 382
Kinney, J.-C. 354
Kjellström, E. 127, 128, 227, 229, 267, 364
Klehmet, K. 231
Klein, B. 15, 120, 218
Klein, H. 218
Knist, S. 103
Knutti, R. 225
Kobayashi, H. 160
Koenigk, T. 30
Kollet, S. 103
Konare, E. 233
Kosecki, S. 114, 133
Kotlarski, S. 346, 348
Kouadio, K. 233
Kouakou, K.G. 233
Kriegsmann, A. 208
Kröner, N. 348
Krüzselyi, I. 145
Kulmala, M. 47
Kumar, P. 32
Kuno, R. 376
Kupiainen, M. 227, 234, 267
Kurihara, K. 136, 160
Kurnaz, M.L. 272
Kurths, J. 235
Kusaka, H. 122, 374
Kyselý, J. 240
Laaksonen, A. 47
Lahmers, T. 89
Landelius, T. 162, 229
Landgren, O. 166
Lange, S. 235

Laprise, R. .. 92, 177, 192, 196, 247, 287, 291 ..... 340, 350, 362
Larsen, M.A.D. 34
Le Treut, H. 242
Leduc, M. 350
Lee, D.-K. 171
Lee, H. 243, 352
Lee, J.-W. 236
Lehmann, A. 51
Lelieveld, J. 308
Lenaerts, J. 74
Lenderink, G. 94, 124, 327
Lennard, C. 238, 285
Lenz, C.-J. 325
Lettenmaier, D. 359
Leung, L.R. 126, 359
Lhotka, O. 240
Li, L. 242, 368
Li, S. 242
Liles, S. 203
Lind, P. 127, 128, 229
Lindstedt, D. 127, 128, 229
Liniger, M.A. 225, 386
Lintner, B. 243
Lionello, P. 179
Liu, Y. 15
Loikith, P.C. 243, 352
López-Franca, N. 245
Loriaux, J. 124
Losada, T. 245
Löwe, P. 218
Lucas-Picher, P. 247
Luhamaa, A. 249
Luong, T. 89
Lüthi, D. 346, 348
Lyon, B. 380
Madsen, H. 282
Madsen, K.C. 61
Mailler, S. 19
Mallet, M. 41
Manabottam, M. 264
Männik, A. 249
Marengo, J. 368
Marien, L. 96
Markuszewski, P. 36
Maslowski, W. 10, 354
Mathis, M. 17
Matthes, H. 356
Mattmann, C. 243
Mayer, B. 71, 120
Mayer, S. 251
McGinnis, S. 243
McSweeney, C. 357
Mearns, L.O. 243, 359
MED-CORDEX Group 65, 334
Meier, H.E.M. 15, 22, 38, 56, 76, 120, 389
Mendlik, T. 361, 384
Menéndez, C.G. 304
Meque, A. 253
Mesinger, F. 296
Messmer, M. 105, 255
Mezghani, A. 166
Michaels, S. 359
Mieruch, S. 284
Mikkonen, S. 47
Mikolajewicz, U. 17, 120
Miller, P.A. 81
Mitskevich, Y. 257
Mizuta, R. 374
Möller, J. 40
Moonen, P. 295
Morioka, Y. 49
Moseley, C. 71
Moufouma-Okia, W. 259
Mukherjee, R. 12
Murai, H. 116
Murata, A. 129, 136, 160
Murdock, T.Q. 260
Muys, B. 295
Nabat, P. 41
Nagai, H. 131
Naik, M. 43
Nakamichi, K. 187
Nakano, N. 376
Nakayama, H. 131
Narayan, N. 120
Narisma, G.T. 183, 262
Nayak, S. 264, 266
Neelin, J.D. 243
Nielsen, T.S. 282
Nijssen, B. 10
Nikiéma, O. 177, 340, 362
Nikulin, G. 107, 162, 227, 238, 267, 319
Nosaka, M. 129
Nuissier, O. 204
Obermann, A. 268
Oh, S.-G. 171
Oh'izumi, M. 136
Ohlwein, C. 103
Oikawa, Y. 116

Olesen, M. 321
Olson, R. 331
Omer, F.M. 83
Osima, S.E. 270
Osinski, R. 10, 354
Ozturk, T. 272
PaiMazumder, D. 329
Paquin, D. 273
Parham, P. 220
Partasenok, I. 257
Patarčić, M. 275
Paul, A. 24
Paumann, M. 154
Peltier, W.R. 324
Perroud, M. 213
Petelski, T. 36
Pham, T.V. 8, 45
Pielke Sr., R.A. 189
Pinya, M.A.S. 251
Pietikäinen, J-P 47, 52
Piotrowski, P. 301
Piskozub, J. 36, 133
Pitman, A.J. 84
Podrezova, N. 134
Pohl, B. 200
Pohlmann, T. 71, 120
Polanski, S. 342
Polcher, J. 19, 70
Poulsen, J.W. 61
Prein, A. 141, 364
Preuschmann, S. 277
Pryor, S. 359
Przyborska, A. 114, 133
Qian, Y. 310
Raible, C. 105
Räisänen, J. 366
Raub, T. 51
Rechid, D. 208
Reckermann, M. 389
Redmond, G. 279
Refsgaard, J.C. 34
Remedio, A.R.C. 52, 368
Remke, T. 280
Rinke, A. 291, 356
Roberts, A. 10, 354
Roberts, N.M. 91, 205
Robertson, A. 380
Rockel, B. 26, 231, 313
Romera, R. 245, 334
Ronda, R. 94
Rõõm, R. 249
Rosenhagen, G. 120, 210, 218
Rosgaard, M.H. 282
Rummukainen, M. 78
Rutgersson, A. 69, 79, 389
Ruti, P. 65
Safi, M.J. 200
Sahlée, E. 69, 79
Sain, S. 359
Samuelsson, P. ..... 15, 54, 76, 78, 81, 227 ..... 267, 368
Sánchez, E. 245, 304, 334, 368
Sanchez-Lorenzo, A. 41
Sasaki, H. 129, 136, 160, 183
Sasaki, T. 72
Sasaki, W. 189
Sato, T. 72
Schade, N. 218
Schädler, G. 284
Schär, C. 86, 346, 348
Schefczyk, L. 109
Schimanke, S. 15, 22, 56, 76
Schmidli, J. 86
Schulz, M. 24
Schurgers, G. 78
Scinocca, J. 356
Sedlmeier, K. 284
Seid, H. 285
Sein, D. 32, 57, 59, 71, 120
Sen, O.L. 6
Separovich, L. 287
Seya, H. 187
She, J. 61
Shim, K.-M. 221
Shrestha, P. 103
Sieck, K. 370
Siltberg, J. 78
Simmer, C. 103
Smith, B. 63, 78, 81
Sobie, S.R. 260
Sobolowski, S. 1, 251
Solman, S. 289
Sommerfeld, A. 291
Somot, S. 41, 65, 191, 204, 268
Son, S.-W. 181
Sørensen, P.E. 282
Sörensson, A. 67
Sørup, H.J.D. 251, 321
Sproson, D. 69, 79
Stéfanon, M. 19, 70

Stendel, M. 270
Stepanov, I. 107
Strobach, E. 372
Su, J. 71, 120
Sudarchikova, N. 52
Sugimoto, S. 72
Suh, M.-S. 171
Sulis, M. 103
Suman, M. 264
Sushama, L. 152
Suzuki-Parker, A. 122, 374
Syed, A.A.B. 293
Syed, F.S. 293
Szalai, S. 208
Szépszó, G. 145
Takayabu, I. 139, 160, 185, 374, 378
Takemi, T. 131
Tamaki, Y. 376
Teichmann, C. 52, 208, 343, 364
Termonia, P. 101
Thejll, P. 332
Thiery, W. 295
Tian, T. 61
Tinz, B. 218
Torlaschi, E. 196
Troch, P. 12, 101
Truhetz, H. 141, 343, 364
Tsarev, V. 134
Tsunematsu, N. 187, 189
Tsusilova, K. 169
Tucker, S. 294
Türkes, M. 272
Ueno, G. 185, 378
Undén, P. 162
Uno, F. 143
Van de Berg, W.J. 74
Van den Broeke, M. 74
Van Lipzig, N.P.M. 295
Van Meijgaard, E. 74, 124, 327, 364
Vautard, R. 211, 364
Veljovic, K. 296
Verbist, B. 295
Vereecken, H. 103
Vigaud, N. 380
Villaume, S. 162
Volkholz, J. 235
Von Storch, H. 297
Wakazuki, Y. 382
Waliser, D.E. 243, 352
Walter, A. 169
Wang, S. 15, 76
Wang, Z. 299
Weaver, A.J. 323
Wibig, J. 301
Wiebe, W. 323
Wilcke, R. 162, 384
Wild, M. 41
Winger, K. 247, 340
Wu, G. 299
Wu, L. 69, 79
Wu, M. 78
Xiao, Z. 302
Yamada, T. 116
Yamagata, T. 49
Yamagata, Y. 122, 187
Yan, X. 82
Yang, B. 310
Yang, S. 321
Yang, W. 167
Ylhäisi, Y. 366
Yoshikane, T. 143
Yoshimura, K. 216, 236
Zaninelli, P. 304
Zarghami, M. 20
Zemankova, K. 111
Zeng, X. 10
Zhang, W. 81
Zhang, X. 306
Zhao, D. 82
Zhou, T. 310
Zirk, M. 249
Zittis, G. 308
Zou, L. 301
Zsebeházi, G. 145
Zubler, E. 386

Abstracts

Topic 1

Regional Climate and Earth System Models

Role of atmosphere-ocean coupling in the simulation of a polar low: a case study with the COAWST modeling system

Muralidhar Adakudlu[1,2] and Stefan Sobolowski[1,2]

[1] Uni Climate, Uni Research AS, Bergen, Norway (muralidhar.adakudlu@uni.no)
[2] Bjerknes Centre for Climate Research, Bergen, Norway

1. Introduction

A polar low that formed on 3 March 2008 over the Norwegian Sea is simulated using the Coupled-Ocean-Atmosphere-Wave-Sediment Transport (COAWST) modeling system. COAWST is a high-resolution NWP system involving WRF, ROMS and SWAN models with a fully interactive ice module (CRIM) in ROMS (Warner et al., 2010). It can be run both in coupled and uncoupled modes and is a potential tool to study regional extremes and the associated air-sea-wave interactions. The objective of this study is to assess the importance of atmosphere-ocean coupling in simulating polar lows. The polar low under question provides an ideal platform to carry out such a study given the availability of measurements of its structure and full lifecycle. The observations were taken with dropsondes and wind lidar during the Norwegian IPY-THORPEX field campaign (Kristjannson et al., 2011).

In this work, two simulations are performed, one with a two-way coupling between the atmosphere and the ocean, and the second with an atmosphere-only set-up. The simulations begin at 0000 UTC on 2 March 2008 and are run at a horizontal resolution of ~ 10 km. Initial and boundary conditions are obtained from the NCEP Climate Forecast System Reanalysis (CFSR, Saha et al., 2010).

2. Model set-up

The coupling between WRF and ROMS takes place through surface fluxes and sea-surface temperature (SST). ROMS uses the surface fluxes computed by WRF and feeds back WRF with the SST. Fig. 1 shows the difference in SST between the uncoupled and the coupled simulations at 66 hr. prognosis. It indicates that the SST in the coupled simulation is reduced by ~ 1 – 1.5 ^{0}C in the region of formation and growth of the polar low. This is most likely the result of storm induced surface cooling. The coupled simulation appears to produce a tongue of warmer SST (by ~ 2.5 – 3 ^{0}C) along the ice-edge caused by a northeasterly advection of warm water by the ocean currents simulated by ROMS. This feature was not found in the CFSR forecasts implying that the behavior of ROMS near the ice-edge is suspicious. The exact reason for this is not known, though it is possible that the vertical mixing in ROMS has been inadequate near the ice-edge due to the presence of steep bathymetry. Interestingly, this feature has little or no impact on the characteristics of the polar low.

3. Results

Preliminary results indicate that the polar low becomes

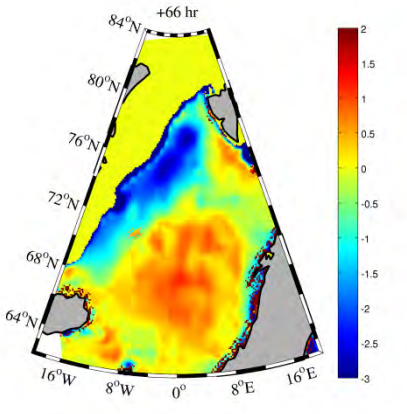


Figure 1. Difference in the SST between the two simulations (uncoupled – coupled) at 66 hr. prognosis.

weaker by ~ 5 hPa in the coupled simulation as a result of the SST cooling. This is evident in the sea level pressure patterns shown in fig. 2. It can also be seen that the horizontal structure and the position of the polar low change to some extent in the coupled simulation. The wind fields associated with the polar low too change correspondingly (not shown here).

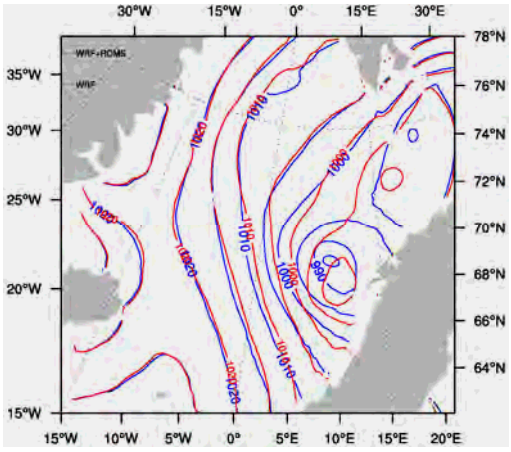


Figure 2. Mean sea level pressure from the uncoupled (blue) and the coupled (red) simulations at 66 hr. prognosis.

A comparison between the simulations and the aircraft observations of the vertical profiles of relative humidity and temperature corresponding to the polar is shown in fig. 3. It suggests that both the simulations capture the temperature profile reasonably well although there are significant changes in the profile of relative humidity. The uncoupled run is too dry in the mid-troposphere whereas the coupled run looks to perform comparatively better but still has large deviations. This hints at considerable differences in the vertical structure of the polar low

between the two simulations as well the with respect to the observations. Investigating these aspects will be our primary focus in the further analysis. Additionally, the present set-up of ROMS does not have the sea-ice that is a very important component in our study domain. It will be interesting to study how does the coupled simulation perform with the inclusion of a sea-ice module.

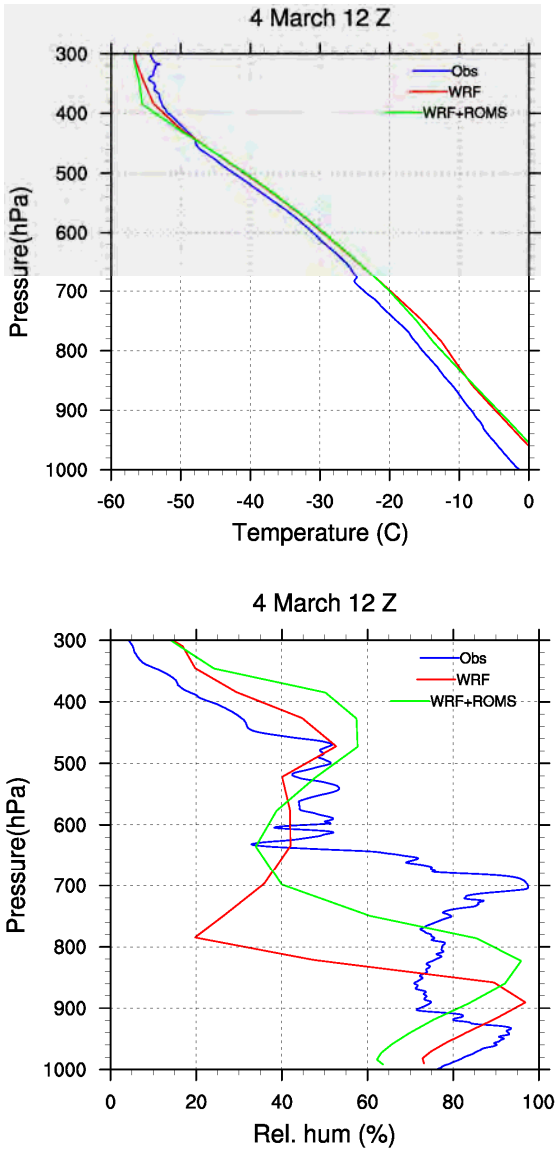


Figure 3. Vertical profiles of temperature and the relative humidity in the observations (blue), uncoupled (red) and the coupled (green) simulations at 66 hr. prognosis.

References

Kristjansson, J. E., Barstad, I., Aspelin, T., Føre, I., Godøy, Ø., Hov, Ø., Ervine, E., Iversen, T., Kolstad, E., Nordeng, T. E., McInnes, H., Randriamampianina, R., Reuder, J., Sætra, Ø., Shapiro, M., Spengler, T., Olafsson, H., 2011, The Norwegian IPY-THORPEX: Polar Lows and Arctic Fronts during the 2008 Andøya Campaign. Bull. Amer. Meteor. Soc., Vol. 92, p. 1443-1466.

Saha, Suranjana., and Coauthors, 2010, The NCEP Climate Forecast System Reanalysis. Bull. Amer. Meteor. Soc., Vol. 91, p. 1015-1057.

Warner, J. C., Armstrong, B., He, R., and Zambon, J. B., 2010, Development of a Coupled Ocean-Atmosphere-Wave-Sediment Transport modeling system: Ocean Modeling, Vol. 35, No. 3., p. 230-244.

Medicanes in an ocean–atmosphere coupled regional climate model

Naveed Akhtar[1,2], Jennifer Brauch[2,3], Andreas Dobler[3], Karine Béranger[4] ,and Bodo Ahrens[1,2]

[1] Institute of Atmospheric and Environmental Science, Goethe University Frankfurt am Main Germany (Naveed.akhtar@iau.uni-frankfurt.de)
[2]Biodiversity and Climate Research Center, Frankfurt am Main, Germany
[3]German Weather Service, Offenbach am Main, Germany
[4]Institute of Meteorology, Freie University Berlin, Germany
[5]Unité de Mécanique, ENSTA-ParisTech, Palaiseau, France

So-called medicanes (Mediterranean hurricanes) are meso-scale, marine, and warm-core Mediterranean cyclones that exhibit some similarities to tropical cyclones. The strong cyclonic winds associated with medicanes threaten the highly populated coastal areas around the Mediterranean basin. To reduce the risk of casualties and overall negative impacts, it is important to improve the understanding of medicanes with the use of numerical models. In this study, we employ an atmospheric limited-area model (COSMO-CLM) coupled with a one-dimensional ocean model (1-DNEMO-MED12) to simulate medicanes. The aim of this study is to assess the robustness of the coupled model in simulating these extreme events. For this purpose, 11 historical medicane events are simulated using the atmosphere-only model, COSMO-CLM, and coupled model, with different setups (horizontal atmospheric grid-spacings of 0.44^o, 0.22^o, and 0.08^o; with/without spectral nudging, and an ocean grid-spacing of $1/12^o$). The results show that at high resolution, the coupled model is able to not only simulate most of medicane events but also improve the track length, core temperature, and wind speed of simulated medicanes compared to the atmosphere-only simulations. The results suggest that the coupled model is more proficient for systemic and detailed studies of historical medicane events, and that this model can be an effective tool for future projections.

1. Introduction

The Mediterranean Sea is known to be one of the main cyclogenetic regions in the world (Pettersen, 1956; Hoskins and Hodges, 2002; Wernli and Schwierz, 2006). A certain type of cyclone in the Mediterranean Sea with physical and structural similarities to tropical cyclones is known as a medicane (Mediterranean hurricane). Medicanes are meso-scale cyclones (the diameter is usually less than 300 km), with a rounded structure and a cloudless area at the center. Other features include a warm-core and intense low sea level pressure, combined with strong cyclonic winds and heavy rainfall (Businger and Reed, 1989). In general, the intensity of medicanes is much weaker than tropical hurricanes (Moscatello et al., 2008); however, a few medicanes have reached tropical hurricane strengths ($33 ms^{-1}$).

2. Experimental Setup

In the present study, a regional COSMO-CLM (Rockel et al., 2008), atmosphere-only and 1-D NEMO-MED12 (Lebeaupin et al., 2011) , coupled model are examined for their robustness and stability in simulating the formation and life cycle of medicanes using different setups (horizontal grid-spacings of 0.44^o, 0.22^o, and 0.08^o and an ocean grid-spacing of $1/12^o$). By applying spectral nudging to the atmospheric model, the same medicane events are also simulated in both coupled and atmosphere-only setups. The primary goal of this study is to investigate the impact of the air–sea interactions in the coupled model on the intensity of medicanes, as compared to the atmosphere-only model and adequate atmospheric grid resolution essential to resolve medicane features For the remainder of this discussion, we used the abbreviations “CPLXX” for the coupled, and “CCLMXX” for the atmosphere-only simulations, where “XX” refers to the resolution (“44” for 0.44^o, “22” for 0.22^o, and “08” for 0.08^o).

3. Results

In the CPL22 simulations, the lengths of the medicane tracks in most cases are shorter than the CCLM22 simulations. However, the lengths of the medicane track in CPL08 are longer than CCLM08. The results show that warm-core structures are also more intense in the CPL08 simulations compared to CCLM08. The wind speed is strongly underestimated in all cases of the 0.22_ simulations. However, the wind speed is significantly improved in the 0.08^o simulations. Compared to CCLM08, the wind speed in CPL08 is more intense and in good agreement with the NOAA dataset. The results show that 0.08^o is an appropriate atmospheric grid resolution to resolve most of the meso-scale characteristics associated with medicanes in coupled and atmosphere-only simulations. The coupled simulations at 0.08^o also improved the results, particularly the medicane’s track lengths, warm-core and wind speed structures compared to atmosphere-only simulations.

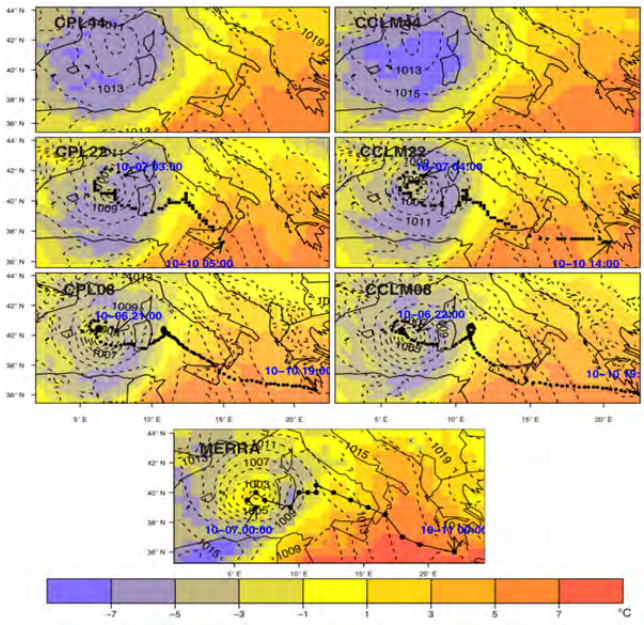


Fig. 1 Mean sea level pressure (hPa; dotted contours lines at 2hPa intervals) and temperature (^{o}C: colored contours at 2 ^{o}C intervals) at 700hPa in coupled and atmosphereonly (0.44^{o}, 0.22 ^{o} , and 0.08 ^{o}) simulations and the MERRA reanalysis data on 7 October 1996 at 18:00UTC.

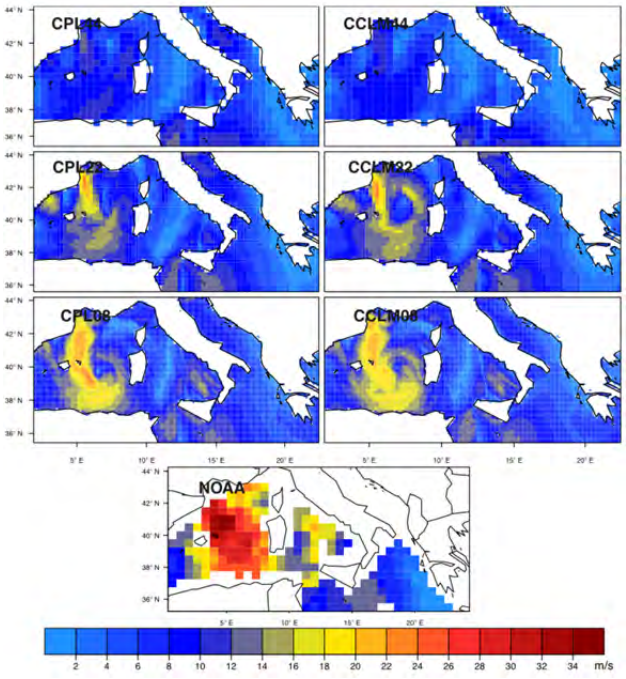


Fig 2. 10m wind speed (ms^{-1}) in coupled and atmosphere-only (0.44^{o}, 0.22 ^{o}, and 0.08 ^{o}) simulations and the NOAA "Blended Sea winds" on 7 October 1996 at 18:00UTC.

4. Conclusion

In this study we examined the ability of the coupled atmosphere–ocean model COSMO-CLM/1-D NEMO-MED12 with atmospheric grid-spacings of 0.44^{o}, 0.22^{o}, and 0.08^{o} (about 50, 25, and 9km, respectively) and an ocean grid-spacing of 1/12^{o} to simulate medicanes. The results show that the model's performance depends strongly on the atmospheric grid resolution. Medicane signals are not observed in the 0.44^{o} simulations. In the 0.22^{o} simulations, the mean sea level pressure and warm-core are captured, and are more intense and finer in the 0.08^{o} simulations. The wind speed is strongly underestimated in the 0.22^{o} simulations compared to the NOAA dataset. Most of the medicane features are well resolved at high-resolution (0.08^{o}) in both coupled and atmosphere-only simulations. Compared to the atmosphere-only simulations, the coupled model did not show any significant improvement at 0.44^{o} and 0.22^{o} resolutions. In most of the 0.22^{o} simulations, the lengths of the medicane tracks in the atmosphere-only simulations are longer than in the coupled simulations. The lengths of the medicane tracks in the 0.22^{o} atmosphereonly simulations are in good agreement with observations. The wind speed and warmcore structures in the 0.22^{o} (both coupled and atmosphere-only) simulations are not well represented. However, the coupled simulations improved significantly compared to atmosphere-only simulations at higher atmospheric grid resolution (0.08^{o}). The characteristic features of medicanes, such as warm-cores and high wind speeds, are more intense in coupled simulations compared to atmosphere-only simulations. In most cases, medicane tracks in the coupled simulations are longer compared to the atmosphere-only simulations, and therefore in good agreement with observations. These results suggest that a 0.08^{o} grid resolution produces accurate detailed results in medicane simulations, particularly with the coupled model. An atmospheric grid resolution higher than 0.22^{o} is vital to simulate the medicanes more realistically in both coupled and atmosphere-only models

References

Rockel, B., Will, A and A. Hense: Rockel B, Will A, Hense A (2008) The regional climate model COSMO-CLM (CCLM). Meteorol Z, 17, 347–348.

Lebeaupin, B. C., Béranger, K., Deltel, C., and Drobinski, P. (2011): The Mediterranean response to diff erent space-time resolution atmospheric forcings using perpetual mode sensitivity simulations, Ocean Model., 36, 1–25.

Pettersen, S. (1956): Weather Analysis and Forecasting, Mac Graw Hills Book Company.

Hoskins, B. and Hodges, K. (2002): New perspectives on the Northern Hemisphere winter storm tracks, J. Atmos. Sci., 59, 1041–1061.

Wernli, H. and Schwierz, C. (2006): Surface cyclones in the ERA–40 dataset (1958–2001), Part I: Novel identification method and global climatology, J. Atmos. Sci., 2486–2507.

Businger, S. and Reed, R. (1989): Cyclogenesis in cold air masses, Weather Forecast., 20, 133–156.

Moscatello, A., Miglietta, M. M., and Rotunno, R. (2008): Observational analysis of a Mediterranean "hurricane" over south-eastern Italy, Mon. Weather Rev., 136, 4373–4397

Use of RCMs, cryosphere, and biosphere models to asses hydrological changes in mountain regions: results from the EU/FP7 "ACQWA" Project

Martin Beniston

Institute for Environmental Sciences, University of Geneva, Switzerland (Martin.Beniston@unige.ch)

1. The ACQWA Project

Future shifts in temperature and precipitation patterns, and changes in the behavior of snow and ice in many mountain regions will change the quantity, seasonality, and possibly also the quality of water originating in mountains and uplands. As a result, changing water availability will affect both upland and populated lowland areas. Economic sectors such as agriculture, tourism or hydropower may enter into rivalries if water is no longer available in sufficient quantities or at the right time of the year. The challenge is thus to estimate as accurately as possible future changes in order to prepare the way for appropriate adaptation strategies and improved water governance.

The ACQWA project aimed to assess the vulnerability of water resources in mountain regions such as the European Alps, the Central Chilean Andes, and the mountains of Central Asia (Kyrgyzstan) where declining snow and ice are likely to strongly affect hydrological regimes in a warmer climate. Based on RCM climate simulations, a suite of cryosphere, biosphere and economic models were then used to quantify the environmental, economic and social impacts of changing water resources in order to assess how robust current water governance strategies are and what adaptations may be needed to alleviate the most negative impacts of climate change on water resources and water use.

2. RCMs simulations within the ACQWA Project

Data from the EU/FP6 "ENSEMBLES" project (www.ensembles-eu.org) were used in ACQWA to drive different impact models. In ENSEMBLES, simulations with different regional climate models were performed with a spatial resolution of 25 km for the European domain. While these simulations currently represent the highest standard of quality in regional climate modeling, their direct application in hydrological modeling or climate change impact research in general is not appropriate due to remaining model errors and the scale gap between climate models with a grid spacing of 25 km (i.e., an effective resolution about 100 km) and most hydrological models (operating at grid-scales of a few 100 meters). Therefore, the ACQWA project had a strong focus on further downscaling and error correction of regional climate simulations. The entire ENSEMBLES multi-model dataset was post-processed using an empirical-statistical technique (quantile mapping, or QM) to remove errors the mean and variability from daily temperature and precipitation time series. This method is capable of removing model biases and of adjusting variability without removing the climate change signal in variability. In addition, QM proved to be very robust over a wide range of applications and to perform equally or better than methods like the analog method, local scaling, or multiple linear regressions.

The impacts of climatic change as simulated by RCMs used in ACQWA show that climate will affect both the natural environment and a number of economic activities. Alpine glaciers may lose between 50 and 90% of their current volume and the average snowline will rise by 150 m for each degree of warming. Hydrological systems will respond in quantity and seasonality to changing precipitation patterns and to the timing of snow-melt in the Alps, with a greater risk of flooding during the spring and droughts in summer and fall. The direct and indirect impacts of a warming climate will affect key economic sectors such as tourism, hydropower, agriculture and the insurance industry that will be confronted to more frequent natural disasters.

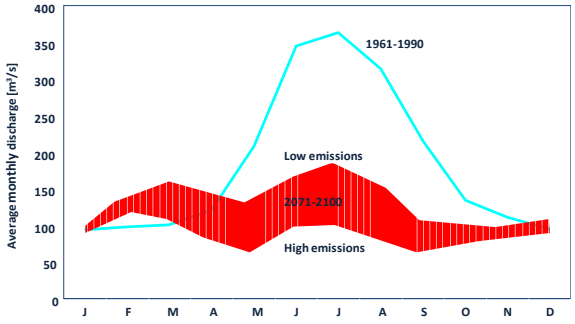


Figure 1. Possible changes in monthly-mean discharge of the Rhone River as it enters Lake Geneva, for IPCC A1B and B2 emission scenarios. The red zone gives the range of responses, taking into account the differences in greenhouse-gas forcings and the uncertainties inherent to model-simulations.

The results from the ACQWA project suggest that there is a need for a more integrated and comprehensive approach to water use and management. In particular, beyond the conventional water basin management perspective, there is a need to consider other socio-economic factors and the manner in which water policies interact with, or are affected by, other policies at the local, national, and supra-national levels.

Forcing a hydrological discharge model with RCM and GCM outputs in the Euphrates-Tigris Basin: Evaluation of the model performance and projected river discharges

Deniz Bozkurt[1,2*], Omer L. Sen[1] and Stefan Hagemann[2]

[1] Istanbul Technical University, Eurasia Institute of Earth Sciences, Istanbul-Turkey
[2] Max Planck Institute for Meteorology, Hamburg-Germany
[*] Permanent address: University of Chile, Department of Geophysics, Center for Climate and Resilience Research, Santiago-Chile (dbozkurt@dgf.uchile.cl)

1. Introduction

The Middle East region, which lies in the east of the Mediterranean Basin, is one of the most vulnerable regions to the global climate change. The Euphrates-Tigris Basin (hereafter ETB) (Fig. 1) hosts two important snow-fed rivers of the Middle East, and its water resources are critical for the hydroelectric power generation, irrigation and domestic use in the basin countries, namely Turkey, Syria, Iraq and Iran (Bozkurt and Sen 2012). In a comprehensive one-way coupling study in the ETB, we forced a state-of-the-art river routing model (the HD model) developed at the Max Planck Institute for Meteorology by Hagemann and Dümenil (1998), with a variety of modeled datasets to investigate the future of the discharges in the basin. These comprise two GCM simulations (ECHAM5/MPIOM following the SRES A1B scenario), hereafter GCM-ECHAM5, and MPI-ESM-LR following the RCP 4.5 scenario), hereafter MPI-ESM, and the dynamically downscaled outputs of ECHAM5/MPIOM (SRES A2 scenario), hereafter RCM-ECHAM5, and NCAR-CCSM3 (SRES A1FI, A2 and B1 scenarios), hereafter RCM-CCSM3. Moreover, dynamically downscaled output of the NCEP/NCAR Reanalysis, hereafter RCM-NCEP/NCAR, data was used to drive the HD model for the reference period. For the downscaling, the RCM, RegCM3 (Pal et al. 2007) was used. Detailed information about the dynamically downscaled reference period simulations and their evaluation with respect to the observations can be found in Bozkurt et al. (2012).



Figure 1. Location and border of the Euphrates-Tigris Basin on a digital elevation map derived from GTOPO30, Global 30 Arc-Second Elevation Data Set. The figure also includes streamflow gauging stations used to validate the HD model

2. Aim and method

The subject of the present study is, twofold: first to present and evaluate the HD model performance in the basin; second to consider the projected river discharges for the basin, which is marked as water-stressed, and the region is notorious for water scarcity Moreover, the GCM forced simulation results provide a comparison between CMIP5 simulations of MPI-ESM and CMIP3 results from its predecessor GCM-ECHAM5 over the ETB.

Hydrological discharge simulations have been carried out by using surface runoff and drainage from the GCM and RCM outputs. Daily surface runoff and drainage from both GCM and RCM outputs are interpolated to the standard HD model grid (0.5^{o} x 0.5^{o}). For all cases, 30-year control climate simulations of present climate are validated against observations. Then, in terms of climate change impacts on the river discharges in the ETB, differences between the future and reference periods are presented.

3. Results

In terms of the HD model evaluation, it is demonstrated that the simulations forced with low resolution GCM outputs are not able to reproduce seasonal cycle of discharge well (Fig. 2).

These results are mostly related with the shortcomings of the GCM fields. Since the surface orography is a major factor in the precipitation distribution over the highlands of the basin, the coarse resolution of the GCMs does not seem to be adequate to represent the spatial distribution of precipitation. It should also be noted that the simulations forced with the MPI-ESM yield better results compared to GCM-ECHAM5 forced simulations. Regarding to this result, in a very recent study, Hagemann et al. (2013) compared MPI-ESM with its predecessor GCM-ECHAM5 in terms of land surface water and energy fluxes. They highlighted that MPI-ESM has an improved simulation of precipitation over central and southern Europe as well as Middle East during the boreal summer. During the boreal winter, MPI-ESM tends to overestimate precipitation over the ETB while GCM-ECHAM5 is underestimating the precipitation. In contrast to GCM forced simulations, high resolution RCM forced simulations reproduce the annual cycle of discharge reasonably well (see Fig. 2).

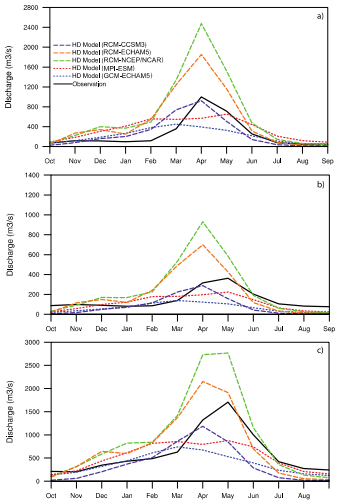


Figure 2. Mean monthly discharges (m3/s) for the Palu (a), Bağıştaş (b) and Hindiya (c) streamflow gauging stations (black solid line) and the HD model simulation results forced by GCM-ECHAM5, MPI-ESM and RCM-NCEP/NCAR, RCM-ECHAM5, RCM-CCSM3 (dashed lines: light blue for GCM-ECHAM5, red for MPI-ESM, orange for RCM-ECHAM5, green for RCM-NCEP/NCAR and dark blue for RCM-CCSM3).

However, overestimation of the discharge during the cold season and a bias in the timing of the springtime snowmelt peak of discharge persist in the RCM-NCEP/NCAR and RCM-ECHAM5 forced simulations. Overestimation of discharge may be attributed to some shortcomings in the simulated RCM precipitation, especially related to the annual cycle of precipitation.

In terms of future river discharge simulations, in general, both GCM forced simulations indicate a striking decrease in discharges of the Euphrates and Tigris Rivers. The MPI-ESM forced simulations yield more decrease in the discharges. Mean annual discharge is projected to decrease by 15-20% in the upper parts of the basin and the main routing paths of the Euphrates and Tigris Rivers for the GCM-ECHAM5 forced simulations, while it is projected to decrease by 20-25% for the MPI-ESM forced simulations (Fig. 3).

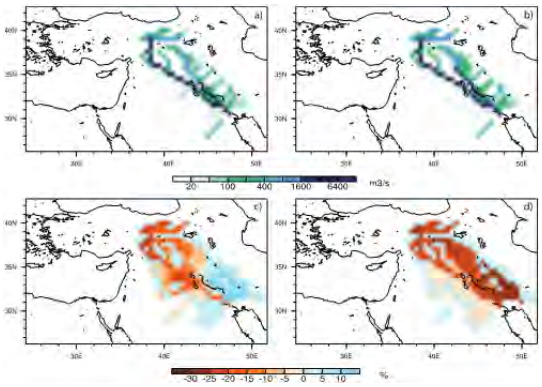


Figure 3. HD model simulations of mean annual discharges (m3/s) for the GCM-ECHAM5 (1961-1990) (a) and MPI-ESM (1971-2000) (b) and annual discharge differences (%) from the reference period (bottom panel). Future projections (2071-2100) of the GCM-ECHAM5 (c) and the MPI-ESM (d) are based on SRES A1B and RCP 4.5 scenarios, respectively.

RCM forced simulations and emission scenarios indicate a striking decrease in mean annual discharge of the Euphrates and Tigris Rivers by the end of the 21st century, ranging from 19% to 58%. In addition, significant temporal shifts to earlier days (3-5 weeks) in the center time of the discharges are projected to occur by the end of the century. Different model and scenario combinations are in agreement with these two main results (Table 1).

	1961-1990	2040-2069		2070-2099	
	CT	CT	Change in Discharge	CT	Change in Discharge
Palu					
RCM- ECHAM5 A2	6 April	19 March	-10%	3 March	-26%
RCM-CCSM3 A2	4 April	12 March	-30%	11 March	-48%
RCM-CCSM3 A1FI	4 April	13 March	-41%	1 March	-58%
RCM-CCSM3 B1	4 April	28 March	-15%	18 March	-36%
Bağıştaş					
RCM-ECHAM5 A2	3 April	16 March	-12%	2 March	-27%
RCM-CCSM3 A2	1 April	9 March	-31%	9 March	-46%
RCM-CCSM3 A1FI	1 April	8 March	-42%	26 February	-58%
RCM-CCSM3 B1	1 April	25 March	-13%	16 March	-37%
Hindiya					
RCM-ECHAM5 A2	10 April	23 March	-6%	4 March	-19%
RCM-CCSM3 A2	11 April	16 March	-27%	18 March	-48%
RCM-CCSM3 A1FI	11 April	20 March	-40%	7 March	-58%
RCM-CCSM3 B1	11 April	6 April	-17%	25 March	-36%

Table 1. Center time dates for both reference and future periods and changes in mean annual discharges from the RCM forced simulations

References

Bozkurt D, Turuncoglu U, Sen OL, Onol B, Dalfes HN (2012) Downscaled simulations of the ECHAM5, CCSM3 and HadCM3 global models for the eastern Mediterranean-Black Sea region: Evaluation of the reference period. Clim Dyn 39(1-2):207-225 DOI:10.1007/s00382-011-1187-x

Bozkurt D, Sen OL (2013) Climate change impacts in the Euphrates-Tigris Basin based on different model and scenario simulations. J Hydrol 480:149-161

Hagemann S, Gates LD (1998) A parametrization of the lateral waterflow for the global scale. Clim Dyn 14:17–31

Hagemann S, Loew A, Andersson A (2013) Combined evaluation of MPI-ESM land surface water and energy fluxes. J Adv Model Earth Syst 5:259-286 doi:10.1029/2012MS000173

Pal JS, Giorgi F, Bi X et al (2007) Regional climate modeling for the developing world: the ICTP RegCM3 and RegCNET. Bull Am Meteorol Soc 88(9):1395–1409

Coupling of COSMO/CLM and NEMO in two regions

Jennifer Brauch[1], Barbara Früh[1], Trang Van Pham[2], Naveed Akhtar[3], Bodo Ahrens[2,3]

[1] Deutscher Wetterdienst, Offenbach am Main, Germany

(jennifer.brauch@dwd.de)

[2] Biodiversity and Climate Research Center, Frankfurt am Main, Germany

[3] Institute of Atmospheric and Environmental Science, Goethe University, Frankfurt am Main, Germany

We have established two coupled regional atmosphere ocean models, one for the Mediterranean Sea and the other for the North and Baltic Seas. The atmosphere model chosen is COSMO/CLM, for the ocean, it is NEMO, which includes the sea ice model LIM. Both models are coupled via the OASIS coupler. This coupler interpolates heat, fresh water, momentum fluxes, sea level pressure and the fraction of sea ice at the interface in space and time.

We will present the individual setups for the two regions and show results of our hindcast experiments. Our main focus is to compare the uncoupled atmospheric model and coupled atmospheric ocean models to study the influence of the active coupled ocean on the atmospheric circulation and especially how far this influence reaches inland. With the Mediterranean Sea setup, we participate in the HYMEX community.

1 Introduction

The Mediterranean region and the region to east of the Baltic Sea have been identified as the two main hot-spots of climate change by Giorgi, 2006, on the base of temperature and precipitation variability. So, our main areas of interest are the Mediterranean Sea with its diverse wind patterns in the atmosphere and deep convection in the ocean and the North- and Baltic Seas with the complex water exchange between them. The development of a regional coupled climate model is a logical step to understand the local interactions between atmosphere and ocean. The complex processes on the interface between atmosphere and ocean are realised with direct flux exchange in a high frequency so the models could react to changes in the other component immediately.

In the region of the North- and Baltic Seas there are already a number of publications with coupled model systems (Schrumm 2003, Kjellstroem 2005, Ho 2012, Dieterich 2013), but so far, the main focus is often on the oceanic variables; air temperature has not been a main topic in assessments of coupled atmosphere-ocean-ice system for the North and Baltic Seas. Our aim is to look at the impact of the North and Baltic Seas on the climate of Central Europe. We want to look at the climate system in a more complete way with an active atmosphere-ocean-ice interaction in order to obtain a model system that is physically more consistent with reality. Somot at al. 2008 have shown, that the Mediterranean Sea is not well represented in AOGCMs (Atmosphere–Ocean General Circulation Models). Recent studies show that high-resolution coupled models over the Euro-Mediterranean region significantly improve the representation of air–sea fluxes (Gualdi 2012; Dubois 2012; Artale 2010). In another study, Sanna et al (2013) have shown that SST simulated through a high-resolution eddy-permitting ocean model has strong and beneficial effects on precipitation and cyclogenesis of medicanes. So we study the representation of the Mediterranean Sea with our coupled ocean-atmosphere model with high resolution. One emphasis is the evaluation of the coupling of the models itself with a focus, another is on the significance of the aerosol forcing over the Mediterranean Sea.

2 Experimental Setup

In the present study, a regional COSMO-CLM (Rockel 2008), atmosphere model is coupled to the ocean model NEMO.

In the North- and Baltic seas, we use the CORDEX-EU setup for COSMO-CLM (Giorgi 2006) which covers the whole of Europe, North Africa, the Atlantic Ocean and the Mediterranean Sea. It is coupled to NEMO-Nordic adapted to the North and Baltic Sea region as described in a technical report by Hordoir 2013. The flux correction for the ocean surface was not applied in our experiments. The coupling mechanism is handled by OASIS3. The coupled model is forced by the ERA-Interim reanalysis (Dee 2011), with a spin up from 1979 to 1984, and evaluation 1985 - 1994.

For the representation of the Mediterranean Sea, COSMO-CLM covers the MED-CORDEX domain, covering southern Europe and the Mediterranean region. NEMO-MED12 (Lebeaupin 2011) is the oceanic component, coupled to the atmosphere with the help of OASIS3-MCT (Akhtar 2014). As a first evaluation of the system, we look at the sea surface temperature in the coupled versus the uncoupled system. Then, we study the influence of the standard COSMO-CLM aerosol data compared to a new monthly MACC and its implication for the coupled system.

3 Results and Conclusion

For the North- and Baltic seas, the coupled run has large biases compared with the E-OBS reference data (Figure 1). However, these biases are in the usual range of biases found in other COSMO-CLM studies. Compared with observations, the coupled model in this study has,

most of the time, smaller biases than the uncoupled atmospheric model.

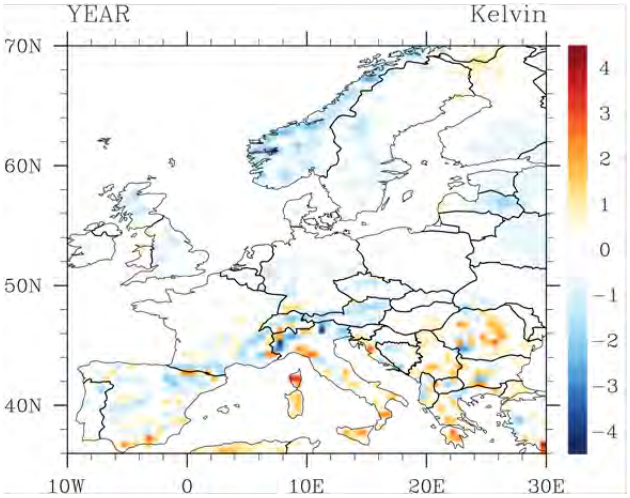


Figure 1. Yearly mean of the differences in 2-m temperature over land between the coupled run and E-OBS data, averaged over the period 1985-1994 (T2MCOUP – T2ME-OBS).

The spatial distribution of temperature biases in spring, summer and autumn (not shown here) resemble the yearly mean distribution; however, the bias magnitudes vary among those three seasons, with summer showing the largest warm bias among the three seasons, up to 3 K in southern Europe.

The simulation of the Mediterranean Sea with the coupled model reveals a cold bias of 2-3°C over the ocean (not shown here). The usage of the monthly MACC aerosol dataset warms Mediterranean Sea in spring and summer by about 40 Watt/m^2 (Figure 2).

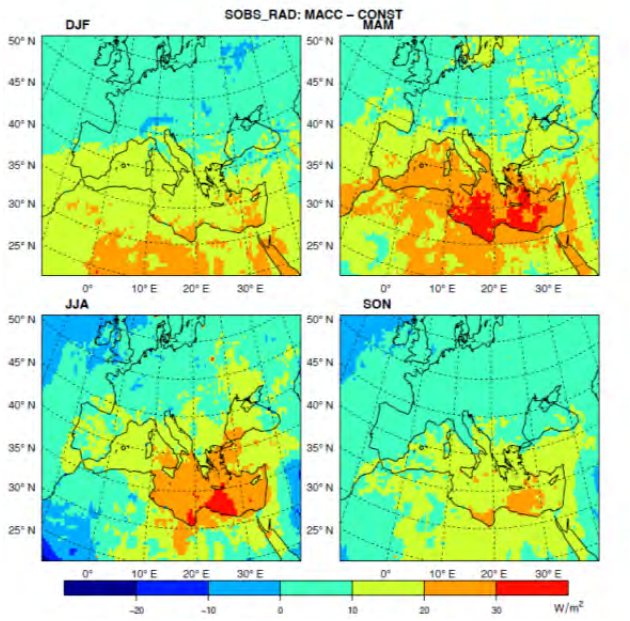


Figure 2. Seasonal mean of the differences of solar irradiance between standard aerosol dataset and MACC monthly values.

This reduces the cold bias of the coupled run by 1-2 °C. A longer simulation is needed to investigate the robustness of these findings.

References

Akhtar N., Ahrens B., and J. Brauch (2014), "Simulation of medicanes in a regional atmospheric model coupled with one dimensional ocean model", Nat. Hazards Earth Syst. Sci., in revision.

Artale, V., Calmanti, S., Carillo, A., Dell'Aquila, A., Herrmann, M., Pisacane, G., Ruti, P. M., Sannino, G., Struglia, M. V., Giorgi, F., Bi, X., Pal, J. S., Rauscher, S., and The PROTHEUS Group (2010), "An atmosphere–ocean regional climate model for the Mediterranean area: assessment of a present climate simulation", Clim. Dyn., 35, 721–740,.

Dee, D.P. et al., (2011), "ERA-Interim reanalysis configuration and performance of the data assimilation system", *Quart. J. Roy. Met. Soc.* 137(656).

Dieterich C., Schimanke S., Wang S., Vaeli G., Liu Y., Hordoir R., Axell L., Hoeglund A., and H. E. M. Meier (2013),"Evaluation of the SMHI coupled atmosphere-ice-ocean model RCA4-NEMO", Report Oceanography No. 47, ISSN: 0283-1112, SMHI.

Dubois, C., Somot, S., Calmanti, S., Carillo, A., Déqué, M., Dell'Aquila, A., Elizalde, A., Gualdi, S., Jacob, D., L'Hévéder, B., Li, L., Oddo, P., Sannino, G., Scoccimarro, E., and Se- vault, F. (2012), "Future projections of the surface heat and water budgets of the Mediterranean Sea in an ensemble of coupled atmosphere–ocean regional climate models", Clim. Dyn., 39, 1859–1884.

Giorgi, F. (2006), "Climate change hot-spots", *Geophys.Res.Lett.* 33(8).

Gualdi, S., Somot, S., Li, L., Artale, V., Adani, M., Bellucci, A., Braun, A., Calmanti, S., Carillo, A., Dell'Aquila, A., Déqué, M., Dubois, C., Elizalde, A., Harzallah, A., Jacob, D., L'Hévéder, B., May, W., Oddo, P., Ruti, P., Sanna, A., Sannino, G., Scoccimarro, E., Sevault, F., and Navarra, A. (2012), "The CIRCE simulations: a new set of regional climate change projections performed with a realistic representation of the Mediterranean Sea", B. Am. Meteorol. Soc., 94, 65–81.

Ho H. T. M., Rockel B., Kapitza H., Geyer B., and E. Meyer, 2012, "COSTRICE – three model online coupling using OASIS: problems and solutions, Geoscientific Model Development Discussions", 5, 3261-3310, doi: 10.5194/gmdd-5-3261-2012.

Hordoir R., An B. W., Haapala J., Dieterich C., Schimanke S., Hoeglund A., and H.E.M. Meier, 2013, "A 3D Ocean Modelling Configuration for Baltic & North Sea Exchange Analysis", Report Oceanography No. 48, ISSN: 0283-1112, SMHI.

Kjellstroem E., Doescher R., and H. E. M. Meier, 2005, "Atmospheric response to different sea surface temperatures in the Baltic Sea: coupled versus uncoupled regional climate model experiments", Nordic Hydrology, 36 (4), 397–409.

Lebeaupin, B. C., Béranger, K., Deltel, C., and Drobinski, P. (2011), "The Mediterranean response to different space-time resolution atmospheric forcings using perpetual mode sensitivity simulations", Ocean Model., 36, 1–25.

Pham, Trang Van, Brauch, J., Dieterich, C, Frueh, B. and B. Ahrens (2014), "New coupled atmosphere-ocean-ice system COSMO-CLM/NEMO: assessing air temperature sensitivity over the North and Baltic Seas", Oceano.Acta, accepted.

Rockel, B., Will, A. and A. Hense, (2008), "Regional climate modeling with COSMO-CLM (CCLM)", *Meteorologische Zeitschrift,* 17(4), pp 347.

Sanna, A., Lionello, P., and Gualdi, S. (2013), "Coupled atmosphere ocean climate model simulations in the Mediterranean region: effect of a high-resolution marine model on cyclones and precipitation", Nat. Hazards Earth Syst. Sci., 13, 1567–1577, doi:10.5194/nhess-13-1567-2013.

Schrum C., Huebner U., Jacob D., and R. Podzun (2003), "A coupled atmosphere/ice/ocean model for the North Sea and the Baltic Sea", Clim. Dyn., 21, 131–151, doi: 10.1007/s00382-003-0322-8.

Somot S., Sevault F., Déqué M., and M. Crépon (2008), "21st century climate change scenario for the Mediterranean using a coupled atmosphere-ocean regional climate model, Global and Planetary Change 63, 112–126, doi: 10.1016/j.gloplacha.2007.10.003.

Modeling Arctic Climate with a Regional Arctic System Model (RASM)

John J. Cassano[1], Alice DuVivier[2], Mimi Hughes[2], Andrew Roberts[3], Michael Brunke[4], Anthony Craig[5], Brandon Fisel[6], William Gutowski[6], Wieslaw Maslowski[3], Bart Nijssen[7], Robert Osinski[8], Xubin Zeng[4]

[1] Cooperative Institute for Research in Environmental Sciences and Department of Atmospheric and Oceanic Sciences, University of Colorado, Boulder, United States (john.cassano@colorado.edu)
[2] Cooperative Institute for Research in Environmental Sciences, University of Colorado, Boulder, United States
[3] Department of Oceanography, Naval Postgraduate School, United States
[4] Department of Atmospheric Sciences, University of Arizona, United States
[5] National Center for Atmospheric Research, Boulder, United States
[6] Department of Geological and Atmospheric Sciences, Iowa State University, United States
[7] Civil and Environmental Engineering, University of Washington, Seattle, United States
[8] Institute of Oceanology, Sopot, Poland

1. Regional Arctic System Model (RASM)

A new regional Earth system model of the Arctic, the Regional Arctic System Model (RASM), has recently been developed. The initial version of this model includes atmosphere (WRF), ocean (POP), sea ice (CICE), and land (VIC) component models coupled with the NCAR CESM CPL7 coupler.

The model is configured to run on a large pan-Arctic domain (Figure 1) that includes all sea ice covered waters in the Northern Hemisphere and all Arctic Ocean draining land areas. The atmosphere and land component models use a horizontal grid spacing of 50 km and the ocean and sea ice components have a horizontal grid spacing of ~9 km. WRF has a total of 40 vertical levels. The lowest WRF level is at ~12 m AGL with 10 levels in the lowest 1000 m to better resolve boundary layer features.

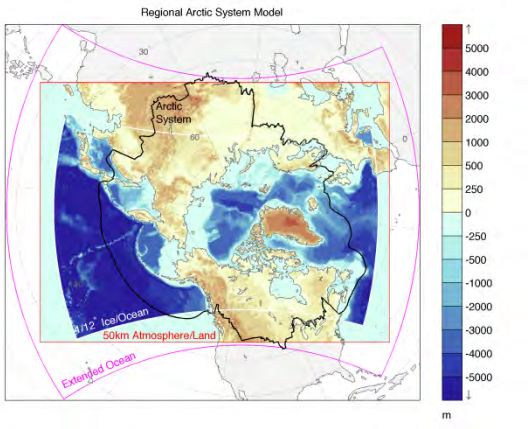


Figure 1. RASM model domain. Atmosphere and land domain shown by red box. Ocean and sea ice domain shown by region with shaded ocean bathymetry. Extended ocean domain shown by purple outline.

ERA-Interim data is used for the WRF initial and lateral boundary conditions. Spectral nudging of temperature and winds for wavenumbers 1 to 4 (WRF x-direction) and 1 to 3 (WRF y-direction) is applied in the top half of the WRF domain using ERA-Interim.

As currently configured WRF in RASM uses Morrison microphysics, CAM longwave and shortwave radiation, YSU boundary layer, Monin-Obukhov surface layer, and Grell-Devenyi cumulus parameterizations. In RASM WRF does not use any of the stand-alone WRF land or sea ice models and instead uses the RASM component models (VIC, POP, and CICE) to represent these portions of the Arctic climate system.

It is expected that RASM will allow for improved simulation of Arctic climate compared to global and non-coupled regional models by simulating features not resolved in these models. It is also expected that RASM will help identify physical and numerical requirements for future generations of global climate models that will be run at resolutions comparable to RASM. Ultimately, we expect that RASM will provide an additional tool for Arctic climate scientistis to gain improved understanding of coupled Arctic climate system processes.

2. RASM decadal simulations

Several decadal length (1989 to present) RASM and stand-alone WRF simulations have been completed.The purpose of these simulations is to assess the baseline climate of RASM and compare it with the climate of stand-alone WRF. These simulations have also been used to assess the impact of changes in the microphysics and radiation parameterizations within WRF. The focus of this presentation will be on the near surface atmosphere, ocean, sea ice, and land state and will emphasize both strengths and weaknesses of the current RASM-simulated climate compared to that from atmosphere-only WRF simulations.

Results from RASM simulations show both areas of improved and degraded results relative to stand-alone WRF. Improvement in the coupled model climate are related to more physically realistic representation of coupled processes such as energy transfer from the ocean to the atmosphere through leads in the sea ice and more realistic representation of sea ice thickness distribution in the coupled model compared to stand-alone WRF. Degraded results come from feedbacks arising from individual model component biases, such as atmospheric circulation biases resulting in incorrect local

sea ice cover that then result in large local atmospheric temperature biases.

In developing RASM it was found that the coupled model sea ice climatology was sensitive to changes in the details of the atmospheric model cloud and radiation parameterizations. As configured in standard WRF the CAM radiation parameterization assumes fixed effective cloud droplet and ice radii that only differ over land and ocean grid points. Sensitivity simulations with RASM in which these parameters were varied over a realistic range of values resulted in decadal sea ice trends that were either increasing, constant, or decreasing.

Given this significant sensitivity to these parameters a major focus of RASM development over the past 6 months has been on the implementation of a more physically realistic coupling between the microphysics and radiation parameterizations in WRF. In the current version of RASM the Morrison microphysics parameterization predicts effective cloud droplet and ice radii at each grid point. These cloud radii are now passed to the CAM (and RRTMG) radiation codes in RASM. Morrison predicted cloud droplet radii have a median value of ~7 μm while the values specified in the standard version of CAM in WRF were 8 and 14 μm over land and ocean grid points respectively.

The smaller cloud droplet radii in the coupled microphysics-radiation version of WRF results in a decrease in monthly mean downwelling longwave radiation of 5 to 20 W m^{-2} with smaller changes in downwelling shortwave radiation (Figure 2). These radiative changes result in a cooling impact at the surface which in turn improves RASM's simulation of sea ice extent and thickness and land snow cover annual cycle. These radiative changes have a minimal impact on the near atmospheric circulation.

Work is now being completed on a thorough analysis of all aspects of RASM's simulated climate for the period 1989 to present. The current version of RASM will be made available for public use once the initial manuscripts describing the model climate have been submitted.

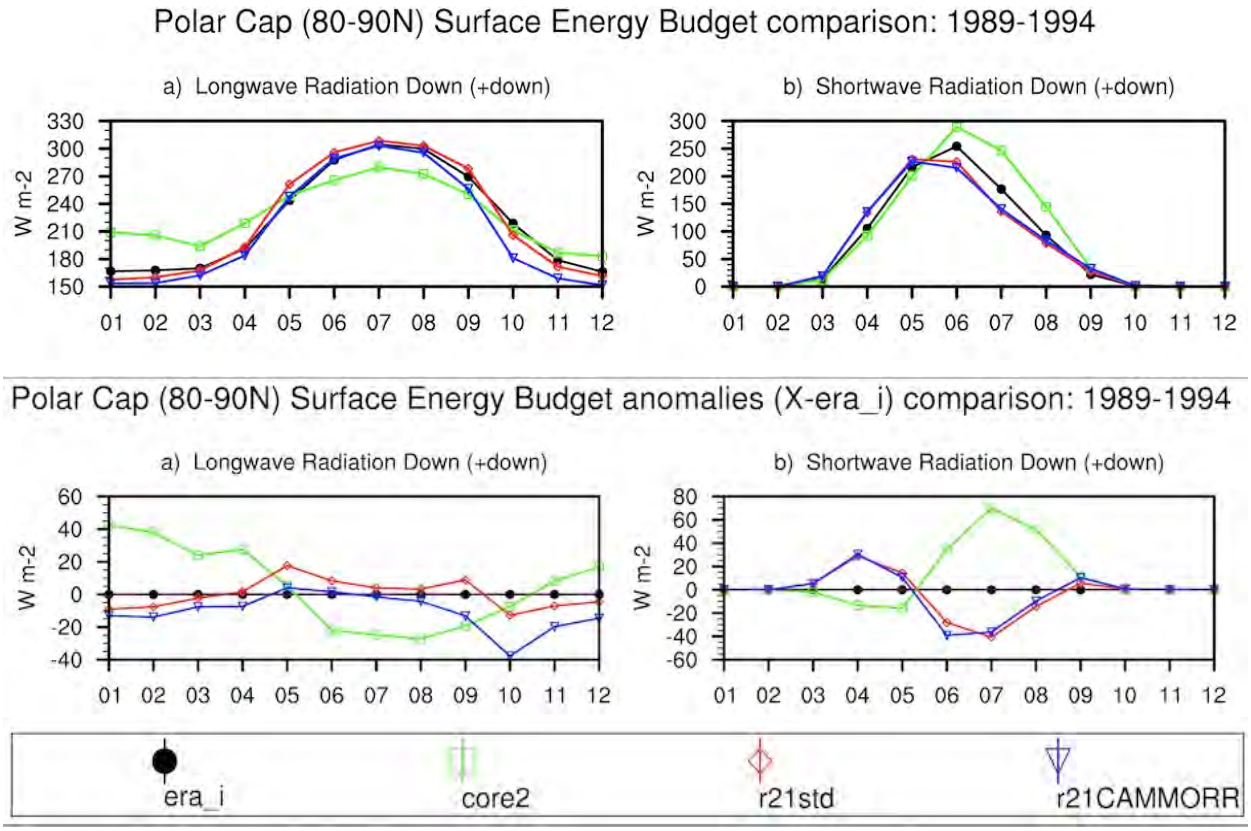


Figure 2. Polar cap (80 to 90 N) monthly surface downward longwave and shortwave radiation for ERA-Interim, CORE2, and two RASM simulations (r21std and r21CAMMORR) for the period 1989 to 1994. Bottom panels show differences in monthly radiative fluxes from ERA-Interim. The r21std RASM simulation uses the standard WRF uncoupled radiation and microphysics parameterizations and the r21CAMMORR RASM simulation uses coupled radiation and microphysics parameterizations as implemented in the current version of RASM.

Regional climate and streamflow projections in North America under IPCC CMIP5 scenarios

Hsin-I Chang[1], Christopher Castro[1], Peter Troch[2], Rajarshi Mukherjee[2]

[1] Department of Atmospheric Sciences, University of Arizona, Tucson, AZ, USA (hchang@atmo.arizona.edu)
[2] Department of Hydrology and Water Resources, University of Arizona, Tucson, AZ, USA

1. Current Global and Regional Climate Trends

Arid to semi-arid regions are projected to experience hotter and drier conditions, according to IPCC assessment reports (e.g. Solomon et al. 2007). These changes reflect two observed trends in the global circulation: the widening of the tropical belt (Seidel et al. 2008, Lu et al. 2009) and a poleward shift of westerly winds (Archer and Caldiera 2008). For the United States, the climatology is found closely related to the sea surface temperature and large scale variability (Castro et al. 2009), especially in the North American monsoon region. Recent climate change studies for the Southwest U.S. region project a dire future, with chronic drought, and substantially reduced Colorado River flows (Seager et al. 2007; Barnett et al. 2008; Rajagopalan 2009; Barnett and Pierce 2009). These regional effects reflect the general observation that climate is being more extreme globally, with areas climatologically favored to be wet getting wetter and areas favored to be dry getting drier (Wang et al. 2012).

2. Western U.S. Climate and Hydrology Projections

The Colorado River system is the predominant source of water supply for the Southwest U.S. and is already fully allocated, making the region's environmental and economic health particularly sensitive to annual and multi-year streamflow variability. Observed streamflow declines in the Colorado Basin in recent years are likely due to synergistic combination of anthropogenic global warming and natural climate variability, which are creating an overall warmer and more extreme climate. Multi-scale downscaling modeling experiments are designed using most recent IPCC AR5 global climate projections to drive regional scale model and future provide finer scale climate forcing to basin-scale hydrology model. The main objective of this project is to characterize how the changing climate of the Southwest U.S. is affecting cool and warm season precipitation in the Colorado River basin.

A physically-based modeling approach has been considered to address the projection of future water resources in the Colorado River basin which incorporates dynamical downscaling and hydrologic modeling components. RCMs add substantial value in the climatological representation of both cool and warm season precipitation in the Southwest (e.g. Dominguez et al. 2012 and Castro et al. 2012). The Weather Research and Forecasting model (WRF) has been selected as the main regional modeling tool; the Variable Infiltration Capacity model (VIC, Liang et al., 1994). will be used to generate streamflow projections for the Colorado River Basin. Recent evaluation of CMIP5 models for North America indicated slight improvement in representing the historical climate, and some models are able to produce a reasonable representation of ENSO and PDO and their atmospheric teleconnection responses (Sheffield et al. 2013a, 2013b). Two IPCC AR5 datasets (MPI-ECHAM6 and HadGEM2-ES) have been selected as RCM forcing based on the climatology and large scale variability in North America.

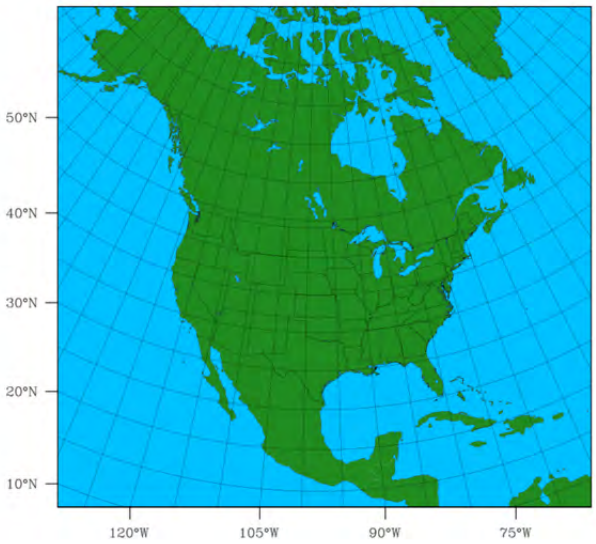


Figure 1. Long-term regional climate modeling domain extended from CORDEX-North America.

Long-term (100 year and longer) WRF regional climate domain is shown in Figure 1, which follows the most recent CORDEX-North America guideline with 25km grid spacing but with extended domain that covers Mexico. The basin-scale streamflow projection is geographically focused to the area of the Colorado River basin with 12.5km grid spacing. An objective methodology has been developed using previously downscaled WRF-CMIP3 data to characterize the natural climate variability in the simulations associated with Pacific SST forcing, based on the dominant spatial modes of precipitation anomalies over the United States. Our analysis shows that climate change is synergistically interacting with ENSO-PDO to intensify extremes of temperature and precipitation in the warm season for the past years of observed record. Further, to preserve the downscaled RCM sensitivity and maintain a

reasonable climatology mean based on observed record, a new bias correction technique is applied when using the RCM climatology to the streamflow hydrology model.

The multi-scale climate and hydrology study aims to characterize how the combination of climate change and ENSO-PDO is changing cool and warm season precipitation. Of specific interest is how droughts associated with La Niña-like conditions may worsen in the future, as these are the times when the Colorado River system is most critically stressed and would define the "worst case" scenario for water resource planning.

References

Archer, C. L., and K. Caldeira (2008) Historical trends in the jet streams, Geophys. Res. Lett., Vol. 35, L08803, doi:10.1029/2008GL033614.

Barnett, T.P, and coauthors (2008) Human-Induced Changes in the Hydrology of the Western United States. Science, Vol. 319, pp. 1080-1083.

Barnett, T. P., and D. W. Pierce (2009) Sustainable water deliveries from the Colorado River in a changing climate, PNAS: 0812762106v1-pnas.0812762106.

Castro, C. L., A. B. Beltrán-Przekurat, and R. A. Pielke, Sr. (2009) Spatiotemporal variability of precipitation, modeled soil moisture, and vegetation greenness in North America within the recent observational record. J. Hydrometeor., Vol. 10, pp. 1355-1378.

Castro, C. L., H. Chang, F. Dominguez, C. Carrillo, J.-K. Schemm, and H.-M.H. Juang (2012) "Can a regional climate model improve the ability to forecast the North American monsoon?" J. Clim., Vol. 25, pp. 8212-8237.

Dominguez, F., E. Rivera, D. P. Lettenmaier, and C. L. Castro (2012) Changes in winter precipitation extremes for the western United States under a warmer climate as simulated by regional climate models, Geophys. Res. Lett., Vol. 39, L05803, doi:10.1029/2011GL050762.

Liang, X., D.P. Lettenmaier, E.F. Wood, and S.J. Burges (1994) A simple hydrologically based model of land surface water and energy fluxes for GCMs. J. Geophys. Res., Vol. 99, pp. 14,415-14,428.

Lu, J., C. Deser, and T. Reichler (2009) Cause of the widening of the tropical belt since 1958. Geophys. Res. Lett., Vol. 36, L03803, doi:10.1029/2008GL036076.

Rajagopalan, B., and coauthors (2009) Water supply risk on the Colorado River: Can management mitigate? Water Resour. Res., Vol. 45, W08201, doi:10.1029/2008WR007652.

Seager, R., and coauthors (2007) Model projections of an imminent transition to a more arid climate in southwestern North America. Science, Vol. 316, pp. 1181–1184.

Seidel, D.J., Q. Fu, W.J. Randel, and R.J. Reichler (2008) Widening of the tropical belt in a changing climate. Nature Geosci., Vol. 1, pp. 21-24.

Sheffield, J. and co-authors (2013a) North American Regional Climate in CMIP5 Experiments: Part I: Evaluation of 20th Century Simulations. J. Clim. Submitted.

Sheffield, J. and co-authors (2013b) North American Regional Climate in CMIP5 Experiments: Part II: Evaluation of 20th Century Intra-Seasonal to Decadal Variability. J. Clim. Submitted.

Solomon, S., D. Qin, M. Manning, Z. Chen, M. Marquis, K. B. Averyt, M. Tignor, and H. L. Miller (eds.) (2008) Climate Change 2007: The Physical Science Basis. Contribution of

Working Group I to the Fourth Assessment Report of the Intergovernmental Panel on Climate Change (2007) Cambridge University Press.

Wang, B., J. Liu, H. J. Kim, P.J. Webster,and S.Y. Yim (2012) Recent change of the global monsoon precipitation (1979–2008). Clim. Dyn., Vol. 39, pp.1123-1135.

Regional Climate and Earth System Models – Added Value Revisited

J.H. Christensen[1], M. Rummukainen[2,3], O.B. Christensen[1], E. Kjellström[3], F. Boberg[1] and M. Drews[4]

[1] Danish Meteorological Institute, Lyngbyvej 100, Copenhagen, Denmark (jhc@dmi.dk)
[2] Lund University, Lund, Sweden
[3] Swedish Meteorological and Hydrological Institute, Norrköping, Sweden
[4] DTU Management Engineering, Danish Technical University, Roskilde, Denmark

1. Internal noise and model evaluation

It has for long been understood that running the same model with slightly different conditions (such as a slightly different initial state) would generate a different trajectory of the model simulation, particularly at the regional scale. To overcome this limitation the solution is to use multiple realizations of otherwise identical simulations or to study simulations covering a very long time span, whether trying to isolate the effect of a new parameterization or assessing climate change due to changes in atmospheric forcings. This insight had important consequences for the strategy to validate global climate models and to determine the response of such models to some prescribed experimental modifications, an area that has not yet fully developed within the regional modeling community. In contrast, many regional modelers, even up to this day, considered one simulation of a short duration sufficient to determine either the quality of the model in reproducing "reality" as well as the sensitivity to changing components of the model. Given the constraint suppressed by the boundary conditions, it is often more or less assumed that internal variability would be over ruled by the large scale forcing. But ensemble-studies from analyzing multiple RCMs have been published since the late 1990s (e.g. Takle et. al., 1999), and the need to address the chaotic nature of regional climate dynamics has been taken up as a central theme in the last decade (e.g. Denis et al., 2003). Both research themes have been leading to considerable insight into fundamental basics of dynamical down scaling.

2. Multi-model approaches

Several large scale collaborative projects have developed (e.g. PRUDENCE, ENSEMBLES and NARCCAP) culminating with the WCRP supported CORDEX (Giorgi et al., 2009). However, there have only been few attempts to capitalize on these efforts in trying to extract the overall information, which scientifically must be addressed by these initiatives; do we actually demonstrate added value to the projections of future climate by applying down scaling? Or more precisely, does the use of ensembles of regional models in climate change research give more credible results to such projections? Figure 1 compares changes in mean annual fields scaled by the change in global mean temperature over Scandinavia. Red and blue dots represent GCM results, while black and green are from downscaling (50km and 25km resp.). As can be seen, the results are comparable. Hence, the challenge is to explain that resolution matters. While it is simple question to ask whether downscaling is adding value, the answers may still prove very difficult to provide with sufficient scientific rigor.

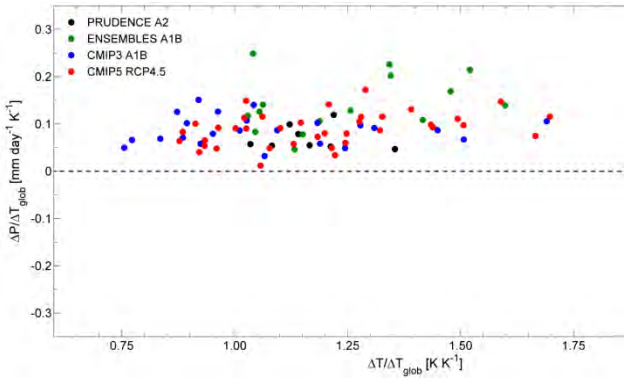


Figure 1. Projected changes in annual mean precipitation vs temperature for Scandinavia, scaled by global mean temperature in the (driving) GCM.

3. The scientific challenge

That the international RCM community still lags behind the GCM one in terms of coordinated experimentation is a keen issue here. In this paper these issues are detailed, building on the results from some of these major community efforts and looking into what may be expected from CORDEX, in particular when dealing with high resolution. It is by no means obvious that we can define simple metrics that are convincingly indicating that projections based on dynamical downscaling are more credible than those based on the suite of GCMs provided in CMIP.

Acknowledgements

We are indebted to our partners in the ENSEMBLES project, who have provided their climate simulation to the ENSEMBLES RCM archive hosted by the DMI. This work benefitted from a grant from the Danish Council for Strategic Research for the project Centre for Regional Change in the Earth System (CRES—www.cres-centre.dk) under contract no: DSF-EnMi 09-066868

References

Denis, B., R. Laprise and D. Caya, 2003: Sensitivity of a regional climate model to the resolution of the lateral boundary conditions. Climate Dynamics, 20, 107-126.

Giorgi, F., C. Jones and G. R. Asrar, 2009: Addressing climate information needs at the regional level: the CORDEX framework. WMO Bulletin, 58, 3, 175 – 183.

Takle, E., S., W. J. Gutowski Jr., R. W. Arritt, et al., 1999: Project to intercompare regional climate simulations (PIRCS): Description and initial results. J. Geophys. Res. 104 D16, 19443-19461.

Surface Heat Budget over the North Sea in Climate Change Simulations

Christian Dieterich[1], Shiyu Wang[1], Semjon Schimanke[1], Matthias Gröger[1], Birgit Klein[2], Robinson Hordoir[1], Patrick Samuelsson[1], Ye Liu[1], Lars Axell[1], Anders Höglund[1], H.E. Markus Meier[1,3]

[1] Swedish Meteorological and Hydrological Institute, Norrköping, Sweden (christian.dieterich@smhi.se)
[2] Federal Maritime and Hydrographic Agency, Hamburg, Germany
[3] Department of Meteorology, Stockholm University, Stockholm, Sweden

An ensemble of RCP scenarios has been conducted with the SMHI coupled regional climate model RCA4-NEMO. The ensemble includes downscaled trajectories of different GCMs and different RCP scenarios. This allows to assess the spread of projected changes for the North Sea and Baltic Sea region. A validation against gridded datasets and station data shows that the ERA40 hindcast of the RCM is in good agreement with observations. Moreover, the historical periods of the scenarios turn out to exhibit the right annual mean and seasonal variability with a 95% confidence level. The scenario solutions show the expected rise in temperature of 2° C to 4° C averaged over the North Sea. During the 21st century an anomalous pattern of high SST and high latent heat flux develops over the western central North Sea that points to changes in the atmosphere-ocean dynamics of the North Sea.

1. Introduction

Global and regional scenario simulations agree on a warming of 2° to 4° C for the North Sea and Baltic Sea region during the 21st century. The increasing temperatures and changes in precipitation have not been studied with respect to their interaction with regional atmosphere-ocean feedbacks. Global models do not resolve important aspects of regional characteristics and ensembles with regional models have been run with either atmosphere or ocean standalone models. By means of a small ensemble of scenario simulations with the coupled regional climate model RCA4-NEMO (Wang et al., 2014) we study the interaction between atmosphere and ocean over the North Sea and how the changing climate affects regional processes and balances.

2. Results

The projected increase in SST averaged over the North Sea amounts to 2° C to 4° C depending on the representative concentration pathway (RCP, Figure 1). In comparison with the downscaled ECHAM5 A1B scenario the RCP4.5 scenarios project a similar increase in SST of 2° C for the North Sea. In the RCP8.5 scenarios the North Sea warms by 4° C to the end of the century. It is interesting to note that in an ensemble of three different RCMs used to downscale the ECHAM5 A1B scenario (Klein et al., 2014) RCA4-NEMO shows the least amount of warming for the North Sea.

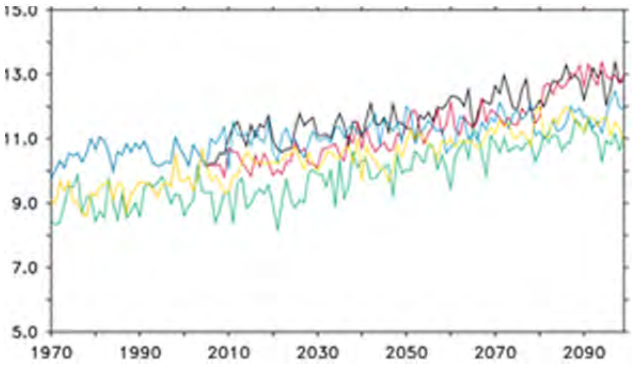


Figure 1. Annual mean SST [° C] averaged over the North Sea for the RCA4-NEMO scenarios MPI-ESM-LR RCP8.5 (black), MPI-ESM-LR RCP4.5 (blue), EC-EARTH RCP8.5 (red), EC-EARTH RCP4.5 (yellow) and ECHAM5 A1B (green), respectively.

The temperature increase is not uniform in space but shows a distinct pattern of more rapid warming in the western central North Sea (Figure 2). It is associated with a reduced net heat uptake compared to the rest of the North Sea where the net heat loss reduces (Figure 3).

The amplitude of the signal is of the order of the radiative forcing caused by a CO_2 doubling (4 W/m^2) and is related to an increased latent heat loss. The increased latent heat loss is due to an atmosphere which will become drier over the western central North Sea. The specific humidity does increase but the 2m temperature increases more rapidly which leads to an increasing dew-point temperature. The decreasing relative humidity allows for extra evaporation and latent heat loss over the North Sea towards the end of the century.

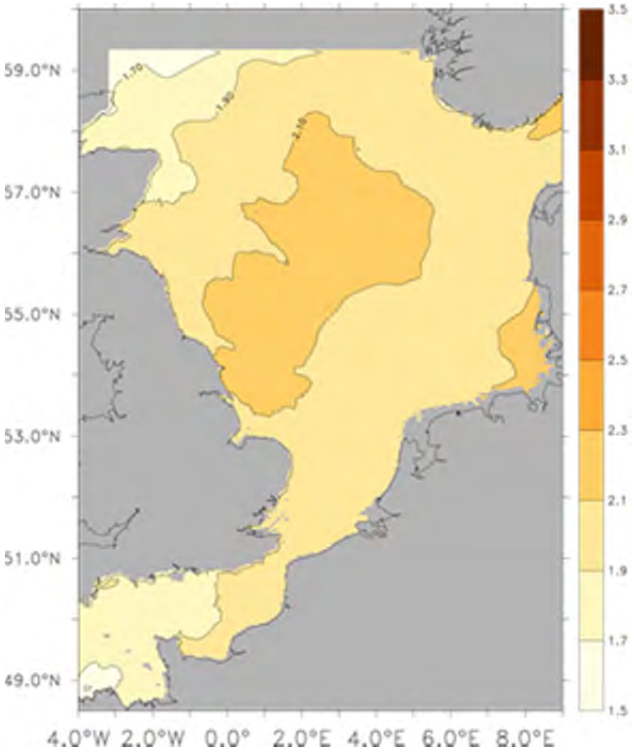


Figure 2. Climatological annual mean changes in SST [° C] in the RCA4-NEMO ensemble mean between periods 2070 to 2099 and 1970 to 1999.

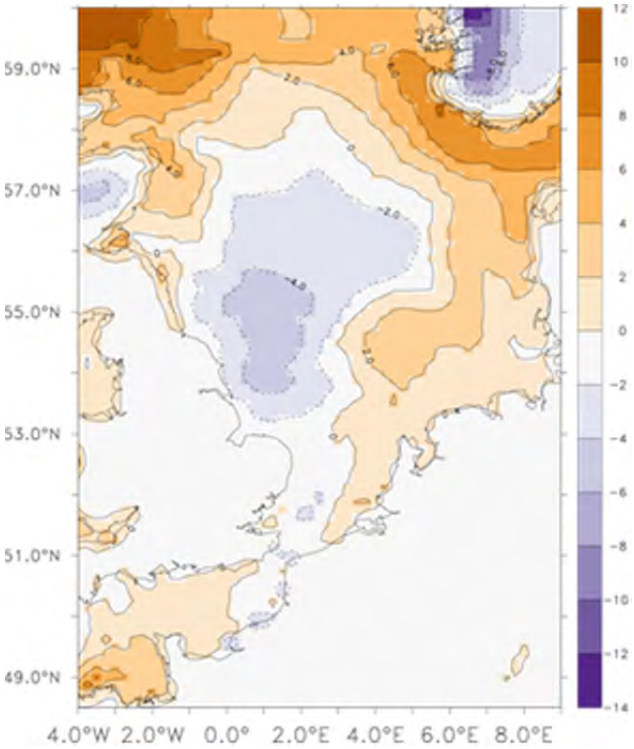


Figure 3. Climatological annual mean changes in net heat flux [W/m^2] in the RCA4-NEMO ensemble mean between periods 2070 to 2099 and 1970 to 1999. Red colors indicate reduced heat loss and blue colors indicate reduced heat gain during period 2070 to 2099.

Acknowledgments

This study was funded by the Swedish Research Council for Environment, Agricultural Sciences and Spatial Planning (FORMAS) within the project "Impact of changing climate on circulation and biogeochemical cycles of the integrated North Sea and Baltic Sea system" (Grant no. 214-2010-1575). The scenario simulations used in this study have been conducted in the framework of "Impacts of Climate Change on Waterways and Navigation" KLIWAS program. KLIWAS is funded by the Federal Ministry of Transport, Building and Urban Development (BMVBS).

References

Shiyu Wang, Christian Dieterich, Ralf Döscher, Anders Höglund, Robinson Hordoir, H.E. Markus Meier, Patrick Samuelsson and Semjon Schimanke (2014) Development and evaluation of a new regional coupled atmosphere-ocean model in the North Sea and the Baltic Sea, Submitted to Tellus A

Birgit Klein, Katharina Bülow, Christian Dieterich, Hartmut Heinrich, Sabine Hüttl-Kabus, Bernhard Mayer, H.E. Markus Meier, Uwe Mikolajewicz, Nikesh Narayan , Thomas Pohlmann, Gudrun Rosenhagen, Dmitry Sein and Jian Su (2014) Climate change projections for the North Sea from three coupled high-resolution models, Submitted to 3rd Lund Regional-scale Climate Modelling Workshop, Lund, Sweden, 16 - 19 June 2014

A new regional climate system model setup for the EuroCORDEX domain

Alberto Elizalde, Moritz Mathis and Uwe Mikolajewicz

Max-Planck-Institute for Meteorology, Hamburg, Germany (alberto.elizalde@mpimet.mpg.de)

1. Introduction

Regional coupled atmosphere-ocean modelling including biogeochemistry is still rather a new approach in earth system sciences and therefore under continuous development. Our regional climate system model has now been made consistent with the EuroCORDEX domain which has become a well reputed and widely used domain for model studies of the European atmosphere (Giorgi et. at. 2006, Jacob et. al. 2013). The standard EuroCORDEX domain has been set for the atmosphere model (Figure 1) with a higher spatial resolution than the previous setup, and the vertical resolution of the ocean model has been increased in the upper layers.

The goal of this development is to perform a comprehensive analysis of the present-day climate as well as of future climate change signals to deepen the understanding of potential climate change impacts on ocean, atmosphere, and ocean biogeochemistry dynamics. The first results of present-day climate simulations in regard of the performance of the new model version are presented.

2. Model Setup

In the new improved model setup the vertical resolution of the global ocean model MPIOM (Marsland et al., 2003) has been increased by 4 vertical levels in the upper 50 m for a better representation of near-surface processes in shallow waters like in the North and Baltic seas. By placing the grid poles on Central Europe and Chicago enhanced spatial resolution for the European seas was obtained, reaching up to 4 km in part of the German Bight. Tides are included by prescribing the full luni-solar ephemeridic tidal potential.

The Hamburg Ocean Carbon Cycle (HAMOCC) (Maier-Reimer, E. 1984) model is embedded in MPIOM to represent ocean biogeochemical processes. It simulates the oceanic cycles of carbon and other biogeochemical elements, including atmosphere-ocean gas exchange.

As an atmospheric domain, the EuroCORDEX domain has been chosen for the setup of REMO (Jacob and Pudzon, 1997). The spatial resolution has been increased to 25 km, which allows for a better representation of the structure and strength of geophysical flows and air-sea-land exchange processes. It covers the northeast Atlantic and entire Europe including the Mediterranean Sea. REMO is interactively coupled to the ocean model MPIOM. Beside the fluxes of heat, mass (freshwater), momentum and turbulent energy, the ocean model is also forced with sea level pressure to be able to capture the full variation of sea level. The hydrological budget in the study domain is closed using the hydrological discharge model HDmodel (Hagemann and Duemenil, 1999).

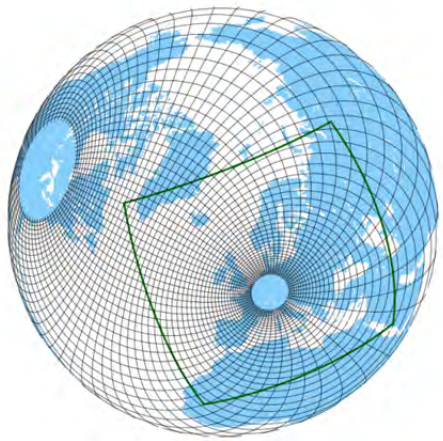


Figure 1. The green line represents the lateral boundaries of the regional atmospheric domain which corresponds to the standard EuroCORDEX domain. The black lines show the non-regular oceanic grid (not all grid lines are plotted)

Outside the coupled region the global model is forced using standard bulk formula. For consistency the atmospheric data are taken from the same data set as is used to drive the regional atmosphere model. In comparison to traditionally used regional ocean models, this approach has the advantage that the ocean component is devoid of open lateral boundaries with prescribed forcing variables, allowing also short-term signals to propagate into the domain of interest.

As a first step, this regionally coupled model is used to perform a dynamical downscaling of present climate simulations. The simulation has been performed using boundary conditions derived from reanalysis data from the European Center of Medium Range Weather Forecast. The simulations will be analyzed for the time slice 1960-2000. Similar analysis will be applied for future climate scenarios from CMIP5 simulations.

This work is funded by the EU project PEARL (Preparing for Extreme And Rare events in CoastaL regions, contract no.603633) and BMBF project RACE project (Regional Atlantic Circulation and Global Change).

References

Hagemann, S. and Duemenil, L. (1999) Application of a global discharge model to atmospheric model simulations in the baltex region. Nordic Hydrology, 30:209–230.

Giorgi, F., Jones, C. and G. R. Asrar, (2006) Addressing climate information needs at the regional level: the CORDEX framework. Bulletin of the World

Meteorologic Organization 58, 175-183.
Maier-Reimer, E. (1984) Towards a global coean carbon model, Progr. Biometeorol., 3, 295-310.
Marsland, S. J., Haak, H., Jungclaus, J. H., Latif, M., and Roeske, F. (2003) The max-planck-institute global ocean/sea ice model with orthogonal curvilinear coordinates. Ocean Modelling, 5(2):91–127.
Jacob, D. and Podzun, R. (1997) Sensitivity studies with the regionalclimate model remo. Meteorology and Atmospheric Physics, 63:119–129.
Jacob, D. Petersen, J. Eggert, B. Alias, A. Christensen, O. Bouwer, L. Braun, A. Colette, A. Déqué, M. Georgievski, G. Georgopoulou, E. Gobiet, A. Menut, L. Nikulin, G. Haensler, A. Hempelmann, N. Jones, C. Keuler, K. Kovats, S. Kröner, N. Kotlarski, S. Kriegsmann, A. Martin, E. Meijgaard, E. Moseley, C. Pfeifer, S. Preuschmann, S. Radermacher, C. Radtke, K. Rechid, D. Rounsevell, M. Samuelsson, P. Somot, S. Soussana, J.-F. Teichmann, C. Valentini, R. Vautard, R. Weber, B. & Yiou, P. (2013) EURO-CORDEX: new high-resolution climate change projections for European impact research Regional Environmental Change, Springer Berlin Heidelberg, 1-16.

Towards a LMD regional Earth simulator with WRF

L. Fita[1] , T. Arsouze[2] , M. Stéfanon[3] , S. Berthou[2] , S. Bastin[4] , J. Polcher[2] , S. Mailler[2] , P. Drobinski[2] , F. Hourdin[1] , and L. Fairhead[1]

[1]Laboratoire de Météorologie Dynamique, UPMC-Jussieu, CNRS, Paris, France (lluis.fita@lmd.jussieu.fr)
[2]Laboratoire de Météorologie Dynamique, IPSL, CNRS, Ecole Polytechnique, CNRS, Palisseau, France
[3]Ecologie, Systématique et Evolution (ESE). Dpt. Ecophysiologie Végétale, Univ. Paris-Sud, Orsay, France
[4]LATMOS/IPSL, Guyancourt, France

1. Introduction

The climate modeling community is putting considerable efforts into developing and using regional climate models (RCMs) because RCMs are seen as better suited for studies of impact and coupled process compared to large-scale resolution General Circulation Models. RCMs can provide smaller spatial scale resolution and account for climatic mechanisms not included GCMs. For example, RCMs do better at reproducing wind patterns and orographic effects on precipitation than GCMs, due to finer spatial resolution and the inclusion of important mechanisms such as non-hydrostatic atmospheric processes. As the base of knowledge of the climate system was growing on time, the complexity of coupled phenomenas has been better understood. In this sense, global climate models have being gaining complexity as they have been incorporating more variety of processes such as: ocean dynamics, dynamic vegetation, criosphere dynamics, chemistry.

2. Methodology

In a way to mimic the GCM complete description, on the scope of the REMEMBER project, we are developing a regional climate model in which, we will combine different components of the climate system developed in the LMD-IPSL such as: atmosphere, ocean, hydrology and dynamic vegetation. Using OASIS-CMT as the linkage between components, we are working for the coupling of the WRF regional atmospheric model with the NEMO ocean mode and the ORCHIDEE land-vegetation-hydrological model. At the same time, LMDZ physical package has been coupled to the WRF model as another set of physical parameterizations. At this stage, we will present some preliminary results of a sensitivity analysis of the WRF-LMDZ integrated model on some severe events at the Mediterranean basin in the scope of the HyMeX (http://www.hymex.org/) project. We will also talk about the design and current state of the coupling.

The study and modeling of rainfall spatial and temporal changes in East Azarbaijan, Iran

Hojjatollah Fouladi Osgouei [1], Mahdi Zarghami [2]

[1] Dept .of Water Eng., Faculty of Civil, University of Islamic Azad, Science and Research Branch - Tehran, Tehran, Iran
[2] Faculty of Civil Eng., University of Tabriz, Tabriz, Iran (mzarghami@tabrizu.ac.ir)

Providing high-resolution spatial rainfall data is one of the most essential needs in the studies of water resources. First part of this paper focuses on the calibration of a climatological *Z-R* relationship for the Sahand radar, located East Azarbaijan, Iran. The calibration method which was used in this study is based on an optimization approach. For this purpose, we consider three rainfall stations located in East Azarbaijan. A climatological *Z-R* relationship in the form $Z = 77.43R^{1.284}$ shows acceptable statistical indicators, making it suitable for radar rainfall prediction for the Sahand station. Second part of study includes testing the suitability of a random cascade model to transform the observed rainfall data in this station. Spatial disaggregation method is based on spatial heterogeneity random cascade. In the Last part, random cascade model has been used to disaggregate the Tabriz rain gage data. Results show that the models proposed in this paper have a good ability to disaggregate the rainfall data.

1. Introduction

Generally, short-term rainfall data is the main factor in many studies such as designing and management of small (especially urban) water resources systems, including continuous flow simulation, evaluation of alternate policies for environmental impact assessment, soil erosion, among others (Pui et al., 2012 ; Jimenez-Hornero et al., 2008; Sivakumar and Shama, 2008). Recently, random cascade models (based on fractal properties of rainfall filed) originate from turbulence theory (Mandelbrot, 1974; Meneveau and Sreenivasan, 1987) have been widely studied (Over and Gupta, 1994). Spatial disaggregation via spatial heterogeneity are proposed by Pathirana and Herathin 2002. Weather radar can potentially provide high-resolution spatial and temporal rainfall data for hydrological applications. The first reporters of measuring rainfall using a radar was reported by Marshall et al. (1947) who suggested the relationship between the reflectivity factor, *Z* and the rainfall rate *R* of the form $Z = AR^b$ (Pedersen and et al., 2010).

2. Case study

This study region is a mountain area located in north-west of Iran. The Sahand radar is a C-band Doppler and located at Sahand. This radar provides maps of the reflectivity factor of rainfall on a cartesiian grid of 500 km by 500 km with a resolution of 1 km in space and 10 min in time (see Fig.1).



Figure 1. The Sahand radar

4. Results

Calibration of Z-R relationship for radar rainfall

The results show that the local *Z-R* relationship ($Z = 77.43R^{1.284}$) can improve the accuracy of the radar rainfall compared to the application of $Z = 200R^{1.6}$. During the calibration process, parameters (*A, b*) were adjusted to minimize four statistical measures. The results finally showed that the $Z = 77.43R^{1.284}$ is suitable for radar rainfall prediction for the Sahand radar (Table 1).

Table 1. Comparisons of the statistical measures obtained from the modified Z-R relationship

Statistical Masures	$Z = 200R^{1.6}$	$Z = 77.43R^{1.284}$
Mean Error(mm)	-0.29663	0.103293
Mean absolute Error(mm)	0.564133	0.440751
Root mean-square Error(mm)	0.745092	0.612367
Bias	1.318949	0.922334

Spatial disaggregation model

The spatial disaggregation method is spatial heterogeneity random cascade model. This disaggregation method depends mainly on parameters values (*β, σ^2*). These two parameters are estimated separately for each season (Table 2). Figure 2 show the Disaggregation rainfall for the East Azarbaijan from a scale of 512 km to a scale of 32 km.

Table 2. Estimated parameters of spatial heterogeneity random cascade for Sahand radar

scale	Seasons	σ^2	β	Mean Rainfall (mm)	Data
15min	Spring	0.109	0.485	0.0186	2011-May-7
15min	Fall	0.098	0.525	0.01814	2011-Oct-26
15min	Winter	0.099	0.5005	0.0229	2011-Feb-20
6h	Fall	0.0931	0.5026	0.416	2010-Oct-3
6h	Winter	0.106	0.469	0.130	2011-Mar-1
24h	Winter	0.097	0.4924	1.28	2013-Jan-29

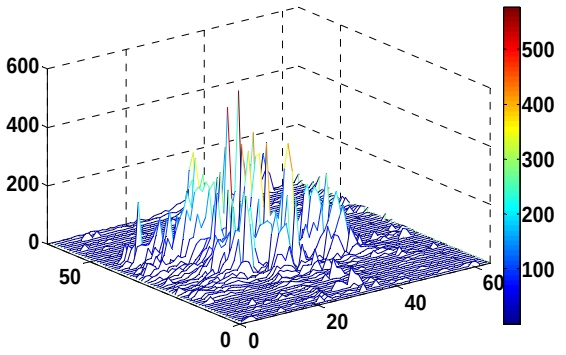


Figure 2. Disaggregation rainfall for the East Azarbaijan from a scale of 512 km to a scale of 32 km.

4.3 Temporal disaggregation model

A temporal rainfall disaggregation model is based on the principles of random multiplicative cascade processes, and the principles of random multiplicative cascade processes is applied in Tabriz rain station (Iran). In the present study, statistical moment scaling function and the log–Poisson distribution. The aim is to convert daily time series to a 6-h resolution. Figure 2 show the Generated time series (6-h) Tabriz rain gage station, East Azarbaijan, Iran. Some conspicuous observations to this end are as follows (see also Table 3): The observed have a maximum value equal to 24, a Mean value equal to 0.169, and over 91.33% of values as zeros. On the other hand, the modeled have a maximum value of 27, a Mean value of 0.178, and over 79.69% of values as zeros. Although the maximum error is concerned with Zeros. The least error is concerned with Maximum.

$\beta = 0.21$ c = 0.703 A = 1.742

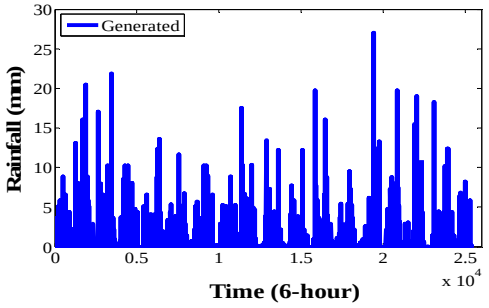


Figure 4. Generated time series (6-h) Tabriz rain gage station, East Azarbaijan, Iran.

Table 3. Comparison between observed data and data generation by model

Statistic	Observed rainfall	Generated rainfall	% Error
Mean	0.1693	0.1781	5.2
Std.Dev	0.9679	0.9765	0.86
Maximum	24.00	27.01	12.54
Zeros	91.33	79.69	12.74

References

Over. T.M, Gupta. V.K., (1996) ,A space-time theory of mesoscale rainfall using random cascades, Journal of Geophysical Research, 101., 26 ., pp.319–331

Pathirana. A, Herath. S, (2002) , Multifractal modeling and simulation of rain fields exhibiting spatial heterogeneity, Hydrology and Earth System Sciences, 6., pp.695–708

Pedersen. L, Jensen. N .E, Madsen. H, (2010) ,"Calibration of local area weather radar—identifying significant factors affecting the calibration" , Atmospheric Research, 97., pp. 129–143

Sivakumar. B, Sharma. A, (2008) ,A cascade approach to continuous rainfall data generation at point locations, Stochastic Environmental Research and Risk Assessment, 22., pp.451-459 .

Pui. A, Sharma. A, Mehrotra. R,Sivakumar.B ,(2012) , A comparison of alternatives for daily to sub-daily rainfall disaggregation, Journal of Hydrology, 470–471 ., pp. 138–157.

Mandelbrot.B, (1974) , Intermittent turbulence in self-similar cascades – divergence of high moments and dimension of carrier, Journal of Fluid Mechanics, 62., pp. 331–358.

Added value of interactive air-sea coupling assessed from hindcast simulations for the North and Baltic seas

Matthias Gröger[1], Christian Dieterich[1] Semjon Schimanke[1], and H.E. Markus Meier[1,2]

[1] Swedish Meteorological and Hydrological Institute, Norrköping, Sweden (matthias.groger@smhi.se)
[2] Meteorological Institute, Stockholm University, Stockholm, Sweden

1. The problem

Nonlinear feedback loops between the ocean and the atmosphere will determine the response to climate change as they regulate the energy transfer between these two compartments. In contrast to global climate simulations where interactive coupling is state of the art, regional ocean and atmosphere models are mostly driven by prescribed forcing fields. In such an idealized setup any change in e.g. the ocean (the atmosphere) like a temperature anomaly is not communicated to the atmosphere (the ocean). Thus, the ocean (atmosphere) lacks an important feedback from the atmosphere (ocean) above (below). We here compare fully coupled with uncoupled hindcast simulations carried out with the recently developed NEMO-Nordic ocean-atmosphere regional model (Dietrich et al., in prep.) and aim to identify air-sea coupling effects and address the question whether interactive coupling introduces an added value to regional modeling.

2. Experimental setup

We here analyze basically two different model setups. In the uncoupled case the oceanic model component NEMO was driven by prescribed atmospheric boundary conditions taken from a downscaled ERA40 hindcast using the regional atmospheric model RCA4. In a second run the ocean model NEMO and the atmospheric model RCA4 were allowed to directly exchange mass and energy fluxes online during the simulation in the RCA4-NEMO model (hereafter coupled run).

The lateral boundary conditions are exactly the same for both the setups. The open boundaries for NEMO are taken from an observed climatology (Janssen, 1999). The atmospheric regional model RCA4 is driven by ERA40 reanalysis data.

Coupling effects operating in the ocean are the main focus here. They are analyzed by comparing the output of the NEMO model from the two setups. Comparison of the two RCA4 outputs give insight to the coupling impact on the atmosphere.

3. Coupling effects in the ocean

In a first step we compare the simulated winter sea surface temperature (SST) with a climatological values derived from observations (Fig. 1). During winter storm activity and wind driven mixing is much stronger than in summer. As a consequence, in most regions the mixed layer deepens considerably during the cold season. Hence, the atmosphere is closer connected to the deeper layers of the ocean. Under these conditions a realistic simulation of ocean-atmosphere heat exchange can be considered important.

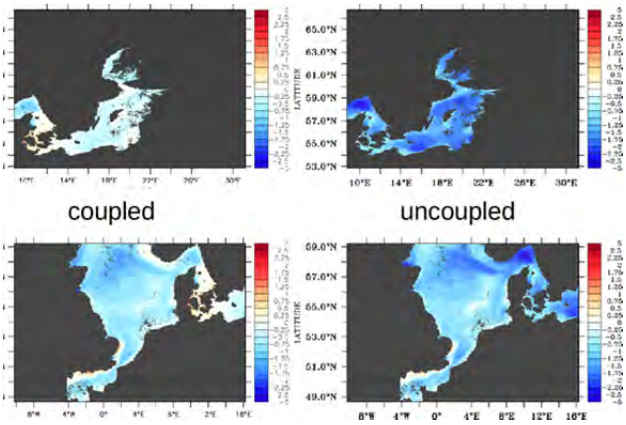


Figure 1. Deviation of simulated sea surface temperature from the observed climatology provided by the Bundesamt fuer Seeschifffahrt und Hydrographie, Hamburg. Shown is the multi-year (1990-2009) winter average (DJF).

Figure 1 clearly shows too cold temperatures both the North Sea, and the Baltic Sea. However, the cold bias is much more pronounced in the model without interactive coupling. We can further conclude that the coupled model performs especially well in highly stratified regions like the Baltic Sea and along the Norwegian cost. In contrast to this, the uncoupled model shows fairly large deviations from the observed climatology. The large difference in performance between the two setups is mainly related to the thermal response of the ocean to atmospheric forcing. During winter the ocean loses heat to the colder atmosphere above which cools the ocean surface. The ocean to atmosphere heat transfer is supported by the deep mixed layer during winter which brings warmer water masses from depth up to the surface. In the coupled model however, the atmosphere considerably warms due to the heat gain from the underlying ocean. In addition the mixed layer is slightly deeper in the coupled model due to stronger wind stress which supports a strong heat transfer to the surface. This results in a warmer SST together with a higher oceanic heat loss at the sea-air interface. However, the oceanic heat loss is damped at the same time by the warming atmosphere. and so the oceanic heat loss is finally controlled by the lateral and vertical advective heat transports in the atmosphere (or in other words) by the atmospheres capability to remove heat).

In the uncoupled model the ocean heat loss leads not to a warming of the atmosphere and so the heat fluxes are controlled by the local processes alone (i.e. air sea temperature difference, wind mixing etc) whereas atmospheric heat transports are neglected. This leads to an unrealistically fast adaption of the ocean's surface to the cold atmosphere resulting in cooler SST compared to the coupled model. Finally the more realistic treatment of air-sea heat fluxes leads to closer match to the observed climatology.

Fig. 1 shows that a realistic coupling is especially important in the highly stratified region like the Baltic. In the well mixed North Sea upward mixing of warmer waters from depth is strong in both models which keeps surface waters warmer and hence, the effective capability of the atmosphere to take up heat is less important (but still the coupled model performs better). In accordance with that, the differences between the coupled and the uncoupled model are much smaller during summer when the atmosphere is much warmer and an intensive thermal stratification develops which damps the effective thermal coupling between the ocean and the atmosphere. Near the surface an strong thermocline develops which strongly weakens the upward mixing of cooler waters to the surface and the thinner mixed layer water can adapt faster to the atmosphere. In this situation an interactive coupling is less essential since heat fluxes are much lower during summer compared to winter.

3. Transient behavior

An important question is, if the two model setups will respond differently to a transient warming as it might be expected in the future. This will depend mainly on the ocean models' capability to absorb and store heat from a warming atmosphere. For the North Sea a recent warming trend has been reported in literature (e.g. Harrison and Carson, 2007; Meyer et al., 2009). Indeed we see this warming trend also in our ERA40 hindcasts and since the ocean model is driven by a fixed mean climatology at the open boundary the only way to warm the North Sea is via the atmosphere. This constitutes an ideal setting to test the different models response in heat uptake/storage.

Fig. 2a shows that the uncoupled model warms much faster than the coupled model which reduces the cold bias of the uncoupled model compared to the coupled model at the beginning of the 21st century. In order to answer whether this different behavior is only due to a different vertical redistribution of heat we have calculated the 3D heat content of the North Sea in the two setups (Fig. 2b)

Indeed, it appears that during the last decade of the simulation the heat content evolves differently indicated by a faster increase in the uncoupled model. Hence the uncoupled model responds faster/stronger to the warming atmosphere. This can be achieved by a lower heat loss during winter and/or by a stronger heat uptake during summer in the uncoupled model. The underlying mechanisms will be presented.

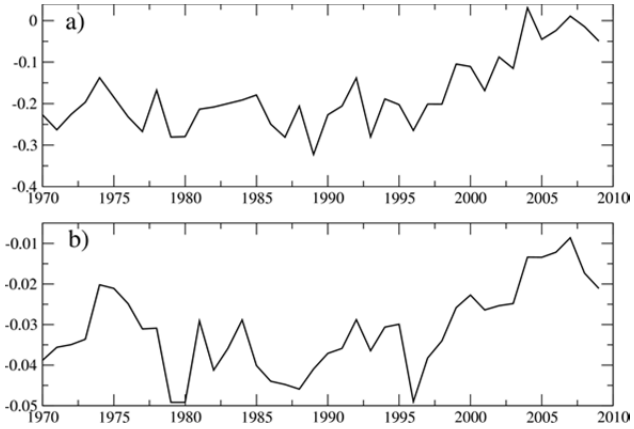


Figure 2: a) Difference in yearly mean North Sea SST (K) uncoupled run minus coupled run. b) Same as a) but for heat content (10^{21} Joule).

References

Dieterich, C., Wang,S., Schimanke,S., Gröger, M., Klein, B., Hordoir, R., Samuelsson, P., Liu, Y., Axell, L., Höglund, A., Meier, H.E.M., and Döscher, R., Surface Heat Budget over the North Sea in Climate Change Simulations, submitted.

Harrison, D. E., Mark Carson, 2007: Is the World Ocean Warming? Upper-Ocean Temperature Trends: 1950–2000. J. Phys. Oceanogr., 37, 174–187. doi: http://dx.doi.org/10.1175/JPO3005.1

Janssen, F., C. Schrum, and J. O. Backhaus, A. 1999, Climatological Data Set of Temperature and Salinity for the Baltic Sea and the North Sea, Hydrographische Zeitschrift, 245 pp.

Meyer, E.M.I., Pohlmann, T., and Weisse, R. (2009) Hindcast simulation of the North Sea by HAMSOM for the period of 1948 till 2007 – temperature and heat content, GKSS reports 2009/3, ISSN 0344-9629, http://www.hzg.de/imperia/md/content/gkss/zentrale_einrichtungen/bibliothek/berichte/2009/gkss_2009_3.pdf

Assessing environmental changes and risks using a regional coupled ocean – atmosphere – sediment model

Alexandra Gronholz, André Paul and Michael Schulz

MARUM – Center for Marine Environmental Sciences and Department of Geosciences, University of Bremen, Bremen, Germany (agronholz@marum.de)

1. Background

Storm events presumably have a strong influence on coastal regions. Regarding western Europe and in praticular the North Sea region, some projections indicate an enhanced occurrence of strong storm events (Haarsma et al., 2013) or a change in the direction of extrem wind events (de Winter et al., 2013) related to global warming.

The aim of this study is to gain an improved understanding of the impacts of historical and future storm events. Interactions between regional atmosphere, ocean circulation and sediment transports are taken into account regarding the questions:

1) How strong is the influence of single extrem storm events compared to atmospherical mean conditions on the sediment transport and distribution in the southern North Sea region?
2) What could be the effects of changing atmospheric conditions in the future on the system?

2. Modeling system

To answer the mentioned questions, a newly available regional Coupled Ocean - Atmosphere – Wave – Sediment Transport (COAWST) modeling system (Warner et al., 2008; Warner et al., 2010) is applied.

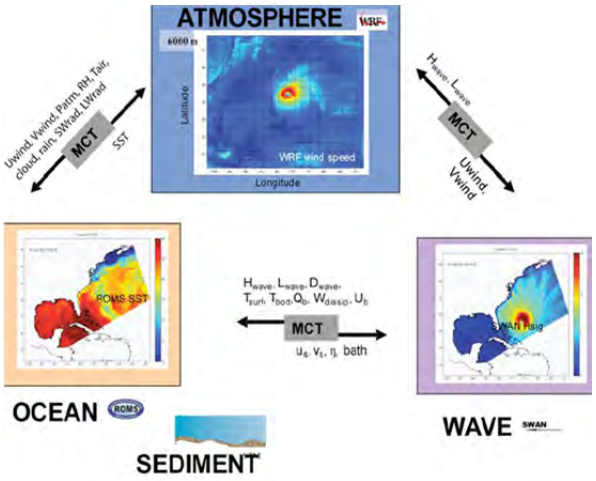


Figure 1. COAWST modeling system (Woods Hole Oceanographic Institution).

The COAWST modeling system includes four components: The atmosphere model WRF (Weather Research and Forecasting model), the ocean model ROMS (Regional Ocean Modeling System), a sediment module and the wave model SWAN (Simulating Waves Nearshore). These components are able to communicate with each other via the Model Coupling Tookit (MCT) which allows an exchange of certain data fields (see Fig. 1).

To set up the coupled system, first the single components are tested separately.

3. ROMS application

The ROMS stand-alone test application includes a horizontal resolution of 1/6° longitude, 1/10° latitude, a vertical resolution of 21 layers and a time step of 400 seconds. The model is initialized and forced with a combination of the following data sets: World Ocean Atlas (WOA; boundary and initial conditions), TPX06 (tides), Comprehensive Ocean-Atmosphere Data Set (surface forcing).

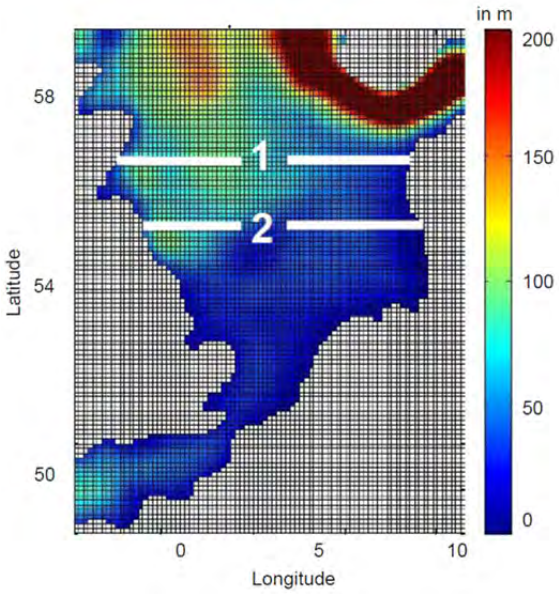


Figure 2. North Sea region with bathymetry data and location of section 1 and 2 for comparison (see Fig. 3 and 4).

Figure 2 illustrates the ROMS grid within the North Sea region and the applied bathymetry data (bathymetry data kindly provided by Christian Winter, MARUM, Bremen). For a test application the model was run for four model years to cover a spin-up period. Figure 3 and 4 show some exemplary model test results regarding temperature distributions for two sections compared to data from WOA.

The comparison between WOA data and the ROMS test results shows two main features. First, the temperatures of the ROMS application and the WOA data generally reach similar ranges and secondly, the mixing during winter (Fig. 3) and the stratification during summer (Fig.

4) are captured. However, this application still includes a nudging for surface temperatures which is planned to be removed in the future.

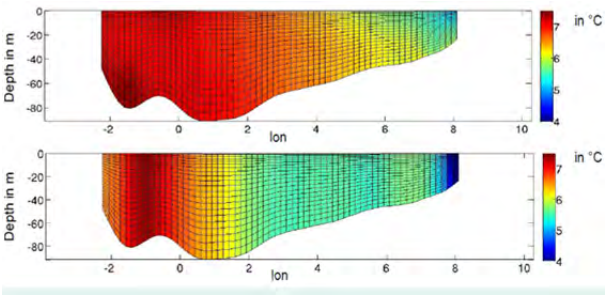


Figure 3. Comparison between WOA data (top) and ROMS results (bottom) for section 1 in January.

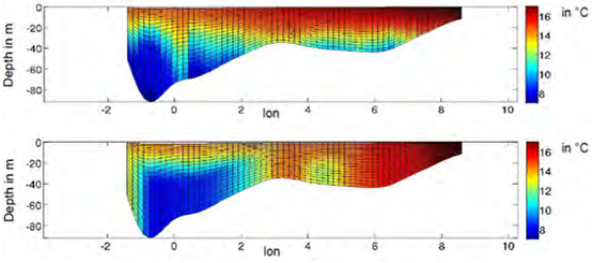


Figure 4. Comparison between WOA data (top) and ROMS results (bottom) for section 2 in August.

4. WRF application

For the WRF stand-alone test application a horizontal resolution of 1/6° longitude, 1/10° latitude, a vertical resolution of 30 layers and a time step of 90 seconds are used.

The model is forced by NCEP Final Analyses (FNL) global data with 1° spatial and 6-hourly temporal resolution.

The aim of the WRF test application is to reproduce a known past strong storm event.

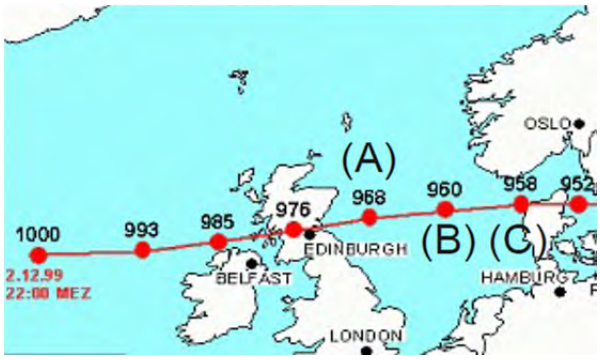


Figure 5. Storm track of storm 'Anatol' and central pressure in hPa in 3-hourly steps (Deutscher Wetterdienst, DWD) showing locations A (03.12.1999, 10:00 MEZ), B (13:00 MEZ) and C (16:00 MEZ) for comparison with WRF test results (see Fig. 6).

Figure 5 shows the pathway of cyclone 'Anatol', which reached the North Sea in December 1999.

The WRF results show a clear signal of the passing cyclone. The conclusion of this test case is, the applied WRF setup combined with NCEP FNL data are most likely able to capture strong and fast storm events. However, more detailed investigations have to be done.

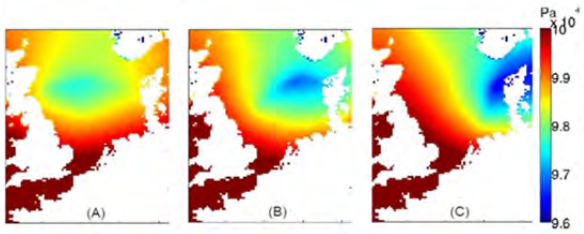


Figure 6. WRF simulation of storm 'Anatol': surface pressure in Pa at time steps A, B and C (compare Fig. 5)

5. Outlook

Further stand-alone tests are planned to validate each model setup. Afterwards, the coupled system will be tested and applied for a period during a strong storm event in the past. Results will be compared with results of a run during atmospheric mean conditions to answer the first mentioned research question. Regarding the second research question, applied wind fields will be adapted according to recent future projections for the end of the 21st century and effects on the sediment distribution and transports will be investigated.

References

De Winter, R.C., Sterl, A., Ruessink, B.G. (2013) Wind extremes in the North Sea Basin under climate change: An ensemble study of 12 CMIP5 GCMs, Journal of Geophysical Research: Atmospheres, 118, 1601-1612

Haarsma, R.J., Hazeleger, W., Severijns, C., de Vries, H., Sterl, A., Bintanja, R., van Oldenborgh, G. J., van den Brink, H. W. (2013) More hurricanes to hit western Europe due to global warming, Geophysical Research Letters, 40, 1783-1788

Warner, J.C., Sherwood, C.R., Signell, R.P., Harris, C., Arango, H.G. (2008) Development of a three-dimensional, regional, coupled wave, current, and sediment-transport model, Computers and Geosciences, 34, 1284-1306

Warner, J.C., Armstrong, B., He, R., and Zambon, J.B. (2010) Development of a Coupled Ocean-Atmosphere-Wave-Sediment Transport (COAWST) modeling system: Ocean Modeling, 35, 3, 230-244

Impacts of different coupling methods on regional atmosphere - ocean simulations

Ha Ho-Hagemann[1], Burkhardt Rockel[1], Hartmut Kapitza[1], and Jörg Behrens[2]

[1] Institute for Coastal Research, Helmholtz-Zentrum Geesthacht, Germany (Ha.Hagemann@hzg.de)
[2] German Climate Computing Centre (DKRZ), Germany

1. Introduction

Coupling between atmosphere and ocean in a coupled climate model system can be done via state variables and/or fluxes. For the atmosphere – ocean – sea ice coupled system COSTRICE, which has been developed for regional climate simulations over the Baltic Sea and North Sea regions, several coupling methods of field exchange are investigated to analyse how these methods impact climate simulations and the interactions and feedback between the atmosphere and ocean.

2. Model and Experiments

The coupled system COSTRICE 2.0 comprises the atmospheric model CCLM (Rockel et al., 2008) version cosmo4.8_clm17, the ocean model TRIMNP (Casulli and Cattani, 1994) version 2.5, and the sea ice model CICE version 5.0 [http://oceans11.lanl.gov /drupal/CICE], which are coupled via the coupler OASIS3-MCT v2.0 (Valcke et al., 2013). COSTRICE is designed to run in parallel on the supercomputing system IBM-power 6 at the German Climate Computing Centre (DKRZ). In this study, CCLM is setup with a horizontal grid mesh size of 50 km and 32 vertical atmosphere layers and is driven by the 6-h ERA-interim reanalysis data (Dee et al., 2011) as initial and boundary conditions. TRIMNP is constructed with a horizontal grid mesh size of 12.8 km and 50 vertical ocean levels. CICE calculates 5 categories of ice and operates with the same horizontal resolution as TRIMNP, but CICE only simulates the Baltic Sea and Kattegat, a part of the North Sea.

Initial and boundary conditions of TRIMNP are updated using ECMWF ORAS-4 monthly reanalysis data. In the two-way coupling setup, TRIMNP and CICE are driven by atmospheric state variables and/or fluxes of CCLM, while CCLM receives skin temperatures which are the combination of the SST from TRIMNP and the sea ice skin temperature from CICE, weighted by the sea ice concentration. For none matching areas between the domains of CCLM and TRIMNP, the ERA-interim reanalysis SST is also used.

In this study, several experiments (EXPs) with different exchange methods were designed for COSTRICE 2.0 to simulate climate over the CORDEX-Europe domain for the period 1979-1990:

(1) **EXP. CPLvar**: State variables, such as mean sea level pressure, temperature, humidity, wind, … are passed from CCLM to TRIMNP, where they are used to calculate surface shortwave incoming radiation, surface longwave downward radiation, latent and sensible heat fluxes. This method is similar as in the coupled setup of the RCAO model used by Döscher et al. (2002). As these fluxes are not given back to CCLM, the surface energy fluxes seen by the atmosphere in CCLM are not consistent to those seen by the ocean in TRIMNP.

(2) **EXP. CPLflx**: All surface radiation and heat fluxes are transferred from CCLM to TRIMNP, except outgoing longwave radiation, that is calculated in TRIMNP using its SST.

(3) **EXP. CPLmix**: Similar to (2) but latent and sensible heat fluxes are determined in TRIMNP using state variables for the bulk formulae.

(4) **EXP. STALN**: Similar to (1) but CCLM and TRIMNP are standlone runs. No sea ice is taken into account.

In the coupled EXPs (1-3), TRIMNP updates sea ice information since Jun 1980, and CCLM gets SST feedback from TRIMNP and CICE since Jun 1985.

For an initial assessment, SSTs of the EXPs are compared to the AVHRR2 reanalysis data [ftp://ftp.cdc.noaa.gov/Datasets/noaa.oisst.v2.highres/]. Simulated 2m temperature (T_2M) and precipitation are compared to CRU data (Harris et al., 2013).

3. Results

Impacts on SST simulations

In general, SST of CPLvar is quite close to AVHRR2 reanalysis data, while CPLflx often has larger biases than CPLvar, especially in the Bothnian Bay, Kattegat and North Sea. The SST difference between CPLflx and CPLvar can be up to 4 degrees before Jun 1985, and decreases after that time. In CPLmix, latent and sensible heat fluxes are calculated by TRIMNP and radiation fluxes are passed from CCLM, which leads to similar results as for CPLvar in both periods.

To understand what may cause the large SST bias in CPLflx, variation of SST and fluxes, such as surface shortwave net radiation, surface longwave downward radiation, latent and sensible heat fluxes (LHFL and SHFL, respectively) of CPLvar and CPLflx are investigated for an ocean grid point near the coastline of Bothnian Bay (see Fig. 1 & 2 for Aug. 1981). The large differences of SST (Fig. 1) occur when fluxes (e.g., SHFL in Fig. 2) from CCLM (pink) differ strongly from those calculated by TRIMNP (orange). As in CPLflx, LHFL and SHFL are kept unchanged during the coupling time step (e.g., 1 hr), TRIMNP cannot update these fluxes at each timestep (e.g. 240s) when SST changes like in CPLvar and CPLmix. However, the changes of the fluxes between timesteps in TRIMNP are relatively small compared to their absolute values. The difference between fluxes of CCLM and TRIMNP is

reduced after the SST feedback is switched on in Jun 1985, as from that on CCLM adjusts its fluxes based on the updated SSTs (due to that the strong warm bias in CPLflx, which is present before the switch, is reduced). Nevertheless, sometime the flux differences between the two models are still present in the three EXPs, especially in CPLflx. Thus, the large differences seem to be caused by the different calculations of heat fluxes applied in the two models.

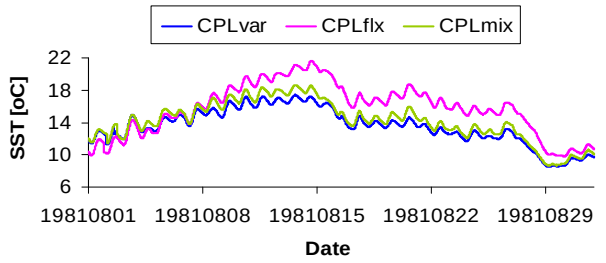


Figure 1. Variation of SST [°C] of CPLvar (blue), CPLflx (pink) and CPLmix (green) for Aug 1981

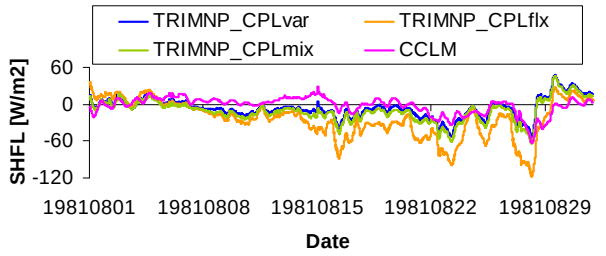


Figure 2. Variation of SHFL [W/m2] of TRIMNP_CPLvar (blue), TRIMNP_CPLflx (orange), TRIMNP_CPLmix (green), and CCLM (pink) for Aug 1981

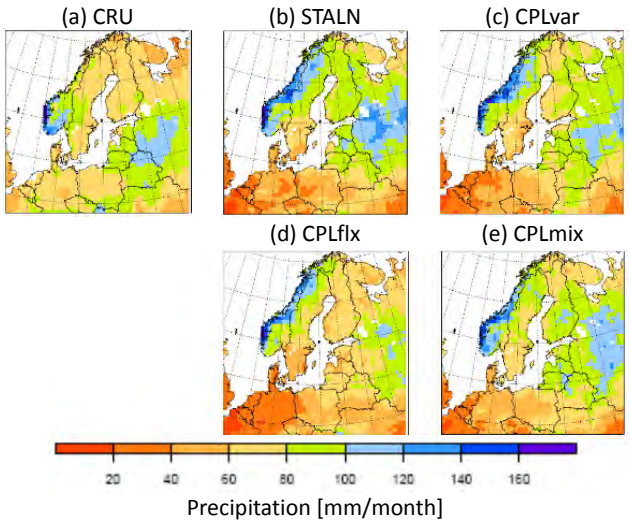


Figure 3. Seasonal precipitation of (a) CRU, (b) STALN, (c) CPLvar, (d) CPLflx, (e) CPLmix for 1986-1990 JJA

Impacts on climate simulations

Impacts of the different coupling methods on the near surface climate are analyzed, especially focusing on T_2M and precipitation. As CPLflx has warm bias of SST over the seas compared to CPLvar and CPLmix, its T_2M is slightly warmer than the others, which makes it a little bit closer to CRU data over north-western Europe, but intensifies the warm bias over the southern part. CPLmix T_2M agrees closely with those of STALN. However, precipitation is different in the three EXPs (Fig. 3). Compared to CRU, the three coupled EXPs (1-3) and the standalone CCLM (STALN) have a wet bias over Scandinavia and a dry bias over southern Europe. EXPs 1-3 improve the wet bias of STALN, especially CPLmix. The dry bias is also reduced in CPLvar and CPLmix but gets worse in CPLflx. Longer runs are needed to yield more robust results.

4. Conclusions

First results show that when TRIMNP calculates latent and sensible heat fluxes by itself in CPLvar (1) and CPLmix (3), SST tends to be reproduced better than when TRIMNP is forced by all fluxes from the atmosphere as in CPLflx (2). Potential reasons are (i) the difference between heat flux calculations of CCLM and TRIMNP, and (ii) when TRIMNP calculates LHFL and SHFL by itself, the fluxes may adapt immediately to the instant changes of SST. Simulations of T_2M and precipitation over Northwest Europe are slightly improved in the coupled EXPs compared to the standalone CCLM. While simulation of T_2M is best in (2), the simulated precipitation is better in (1) and (3). However, longer runs of the EXPs are currently set up to yield more robust results. In addition, an experiment is planned where LHFL and SHFL of TRIMNP are transferred back to CCLM.

References

Casulli, V. and Cattani, E. (1994) Stability, accuracy and efficiency of a semi-implicit method for three dimensional shallow water flow, Computers Math. Applic., Vol. 27, pp. 99–112.

Dee, D.P., et al. (20122) The ERA-Interim reanalysis: configuration and performance of the data assimilation system, Quart. J. Roy. Meteor. Soc., 137, 553–597.

Döscher, R., Willen, U., Jones, C., Rutgersson, A., Meier, H.E.M. and Hansson, U. (2002) The development of the coupled oceanatmosphere model RCAO, Boreal Env. Res., 7, 183-192.

Harris, I., Jones, P.D., Osborn, T.J. and Lister, D.H., 2013: Updated high-resolution grids of monthly climatic observations - the CRU TS3.10 dataset. International Journal of Climatology online doi:10.1002/joc.3711.

Rockel, B., Will, A., Hense, A. (Editorial) (2008) Special issue Regional climate modelling with COSMO-CLM (CCLM), Meteorologische Zeitschrift, Vol. 17, No. 4, pp. 347-348.

Valcke, S., Tony Craig, Laure Coquart (2013) OASIS3-MCT User Guide, OASIS3-MCT 2.0, Technical Report, TR/CMGC/13/17, CERFACS/CNRS SUC URA No 1875, Toulouse, France.

The impact of two land-surface schemes on the characteristics of summer precipitation over East Asia from the RegCM4 simulations

Suchul Kang [1,3], Eun-Soon Im [2] and Joong-Bae Ahn [3]

[1] APEC Climate Center, Busan, Republic of Korea (jbahn@pusan.ac.kr)
[2] Singapore-MIT Alliance for Research and Technology, Environmental Sensing and Modeling, Singapore
[3] Division of Earth Environmental System, Pusan National University, Busan, Republic of Korea (jbahn@pusan.ac.kr)

1. Introduction

RCMs suffer from the large sensitivity and uncertainty of physical parameterizations that directly affect the reliability of model performance. The difficulty of incorporating or modifying physical schemes is the absence of any universally superior physical scheme because its performance varies according to the region, season and combination with other schemes. Therefore, it is important to use appropriate physical parameterizations for the selected target region in order to optimize the model performance. Over East Asia, many studies have attempted to improve the precipitation skill during the summer season based on the cumulus convection schemes (Im *et al.* 2008). Although the precipitation pattern is directly affected by the cumulus convection scheme and its interaction with other physical processes, the land surface scheme can also be important in determining the performance of precipitation over East Asia. In this study, we explored the sensitivity of the East Asia summer monsoon to the land surface scheme by comparing the high-resolution (30 km) multi-decadal (19-year) simulations that implement two different land-surface schemes (BATS vs. CLM3) available in RegCM4, which is considered the state-of-the-art simulation in terms of resolution and period. Our focus is to investigate the impact of the land surface scheme on the characteristics of summer precipitation from the perspective of the convective instability (Kang *et al.* 2014).

2. Data and methods

The regional climate model used in this study is the latest version of the International Centre for Theoretical Physics (ICTP) Regional Climate Model version 4, RegCM4. Among several options for convective parameterization, the MIT Emanuel scheme is selected based on several previous studies that demonstrated its superiority over East Asia (Im *et al.* 2008). RegCM4 incorporates the multiple options of the land surface schemes through the newly coupled CLM3, in addition to the original existing BATS scheme. The simulation domain covers the eastern regions of the huge Asia continent and the Japanese Archipelago with the center on the Korean peninsula. The horizontal resolution is 30 km, while 23 vertical levels are used within the sigma coordinator. The initial and lateral boundary conditions are obtained from the ERA-interim reanalysis with a resolution of 1.5^{o} x 1.5^{o} at 6-hour intervals. The simulations start from 25 May and span 7 days and three months (June-July-August: JJA) in every year of the 19-year period (1989–2007), and the results during the first 7 days are excluded in the analysis as a spin-up period. The two simulation sets are integrated by implementing the BATS and CLM3 land-surface schemes, with all other conditions being identical. To assess the performance of daily precipitation, we use daily precipitation with 0.25^{o} X 0.25^{o} grid provided by the Asian Precipitation Highly Resolved Observational Data Integration Towards the Evaluation of Water Resources project (APHRODITE), as well as 1.5^{o} x 1.5^{o} grid from ERA-interim reanalysis. The daily vertical dataset for the calculation of the convective available potential energy (CAPE) and convective inhibition (CIN) is also extracted from the ERA-interim reanalysis. The simulated latent and sensible heat fluxes are evaluated against the ERA-interim reanalysis on a monthly basis (Kang *et al.* 2014).

3. Results

We begin our analysis with the 19-year climatological aspects of precipitation during the summer season (JJA). The upper panels in Fig. 1 present the spatial distribution of JJA mean precipitation derived from ERA-interim reanalysis, APHRODITE observation, and BATS and CLM3 simulations. Overall, both simulations are in qualitatively good agreement with the observed distribution, capturing some gradient patterns such as more precipitation in the southern China and less precipitation in the northwest China. However, the discrepancy in the quantitative aspect seems to cause the differentiated performance between the two simulations. The biases of the BATS and CLM3 simulations over land areas are 2.5 and 0.8 mm/day, respectively (Fig.1 (g) and (h)). The BATS simulation tends to systematically overestimate the precipitation, leading to a strong wet bias across the whole domain. Replacing BATS with the CLM3 land-surface scheme substantially reduces the wet biases that are seen in the BATS simulation. In particular, a dramatic improvement of CLM3 simulation is found in south China. The large difference between the BATS and CLM3 simulations demonstrates the significant sensitivity in the simulation of precipitation to the choice of land surface scheme. An important feature is that the difference between the two simulations is mostly due to convective precipitation rather than large-scale precipitation.

Given that both simulations show a significant difference of convective precipitation, we attempt to interpret the physical mechanism that controls the convective activity. As an indicator to represent the process of triggering or the strength of the convection, we compare the CAPE and CIN. Using the vertical dataset

with daily time-scale, we calculate θe, CAPE and CIN at the most unstable layer over South China. Figure 2 presents the frequency distribution of θe, CAPE and CIN derived from the ERA-interim reanalysis and BATS and CLM3 simulations. In general, the behaviors differ in both simulations for all three indices. Hence, the comparison of these three indices demonstrates that different land surface schemes can significantly modulate the atmospheric thermodynamic structure, and hence enhance or suppress the triggering of convection. The CLM3 simulation shows considerable improvement in both the general shape of distribution and the relative ratio of each column for all the indices. The basic characteristics of the CIN distribution, such as the peak position and relative ratio of each column, are quite different from those of the CAPE distribution. This is natural because CAPE and CIN are opposite measurements of the atmospheric condition to describe the growth and suppression of the triggering of convection. Contrary to θe and CAPE, the deficiency of the BATS simulation is exposed in the CIN distribution due to the left-side shift of the maximum frequency. Therefore, the relatively larger CAPE and smaller CIN imply a BATS deficiency in both the intensity and the frequency of convective precipitation, which supports the assumption that deep convection intensity is modulated by CAPE while the occurrence frequency is more controlled by CIN (Kang *et al.* 2014).

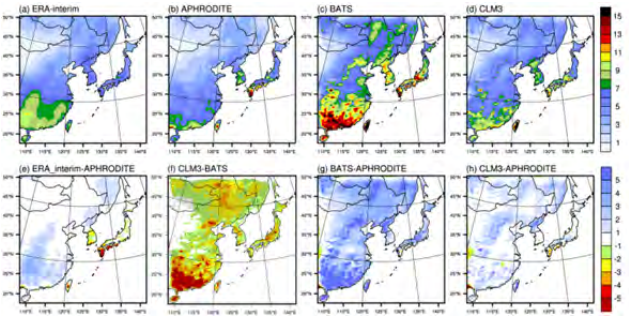


Figure 1. Spatial distribution of JJA mean precipitation derived from ERA-interim, APHRODITE, BATS and CLM3 simulations (a-d) and their differences between ERA-interim and APHRODITE (e), the two simulations (f), and the two simulations and APHRODITE (g-h) (Unit: mm day-1). Here, superimposed dots in (f) indicate the areas where the differences are statistically significant at the 99% confidence level.

4. Conclusion

Overall, the CLM3 simulation offers better agreement of mean, frequency and intensity of daily precipitation with the observed estimates, and presents a substantial reduction in the wet bias seen in the BATS simulation. The improvement in the characteristics of daily precipitation of the CLM3 simulation can be attributed to the improved thermodynamic structure and the resultant convective precipitation. The CLM3 simulation exhibits a more reasonable performance with respect to the frequency distribution of the θe, CAPE and CIN indices. The results presented in this study support the assertion that parameterizations of the land surface are critical for improving model performance (Kang *et al.* 2014).

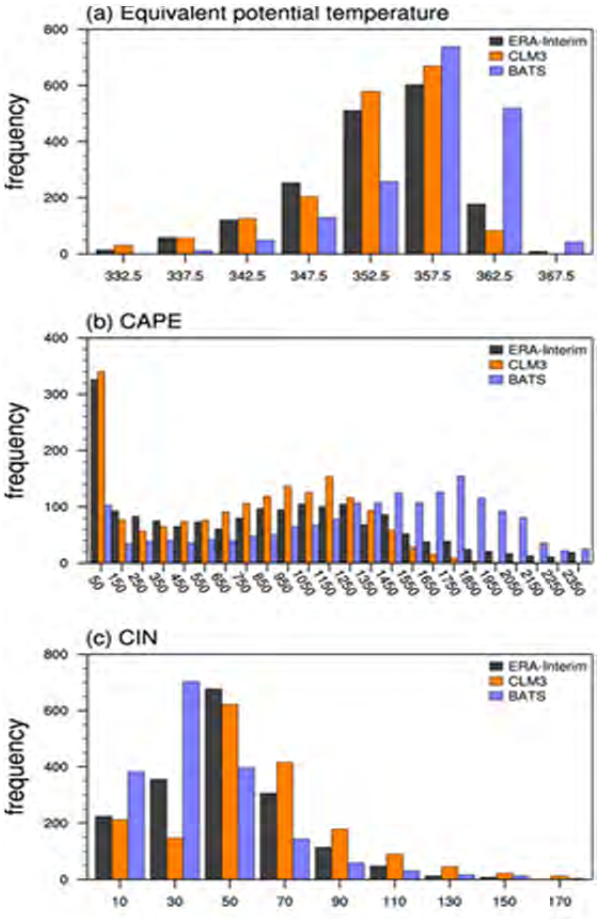


Figure 2. Frequency distribution of equivalent potential temperature (K), CAPE (J/kg), and CIN (J/kg) derived from the ERA-interim reanalysis, BATS and CLM3 simulations over south China.

Acknowledgments

This work was carried out with the support of Korea Meteorological Administration Research and Development Program under Grant CATER 2012-3083 and Rural Development Administration Cooperative Research Program for Agriculture Science and Technology Development under Grant Project No. PJ009353, Republic of Korea.

References

Im, E. S., J. B. Ahn, A. R. Remedio, and W. T. Kwon, 2008: Sensitivity of the regional climate of East/Southeast Asia to convective parameterizations in the RegCM3 modeling system. Part 1: Focus on the Korean peninsula. *Int. J. Climatol*, **28**, 1861- 1877.

Kang, S., E.-S. Im, J.-B. Ahn, 2014: The impact of two land-surface schemes on the characteristics of summer precipitation over East Asia from the RegCM4 simulations. *Int. J. Climatol*, Accepted.

Arctic climate variability and change in the regional models RCA and RCAO

Torben Koenigk[1], Peter Berg[1] and Ralf Döscher[1]

[1] SMHI, Norrköping, Sweden (torben.koenigk@smhi.se)

1. Introduction

Observations show large changes in the Arctic climate system in recent decades. The sea ice cover and volume has dramatically been reduced and temperature increase is amplified compared to the global mean. The atmospheric circulation might already have responded to changes of the Arctic surface with effects for mid-latitude winters.

Model simulations of the future climate indicate an accelerated climate change in the Arctic with a possible total loss of sea ice in the second half of the 21st century.

However, variations among models are still large and biases in air temperature and atmospheric circulation are considerable. Thus, global climate models still show large uncertainties in simulating both today's and future Arctic climate.

2. Simulations

In this study, the Arctic regional atmosphere model RCA and the regional coupled atmosphere – ocean – sea ice model RCAO are used for downscaling ERA-interim data and CMIP5 historical and scenario simulations (Table 1). We analyzed the effect of coupling the ocean-sea ice component to the regional model system. Further, we performed downscaling simulations with and without spectral nudging to assess the effect of constraining the large scale atmospheric circulation to the forcing data. The results are compared to those of the global models to analyze differences and possible added values in the regional simulations.

Table 1: Overview of RCA and RCAO downscaling simulations with and without spectral nudging (RCA-SN, RCAO-SN) using global models and reanalysis as boundary forcing.

	ERA int	EC-Earth	MPI-ESM-LR	Can ESM2	Nor ESM1-M
RCA	yes	hist rcp26 rcp45 rcp85	hist rcp45 rcp85	hist rcp45 rcp85	hist rcp45 rcp85
RCA-SN	yes	hist rcp8.5	hist rcp85		
RCAO	yes	hist rcp85	hist rcp8.5		
RCAO-SN	yes	hist rcp85		hist rcp85	

3. Results

Both RCA and RCAO using ERA-interim as boundary conditions show seasonal SLP biases in the order of several hPa. The biases are strongly reduced using spectral nudging techniques; the bias reduction is more pronounced in RCA compared to the coupled version.

Regional historical simulations using global models as boundaries show similar biases of the large scale atmospheric circulation and temperature patterns as the global models. Often, the large scale bias patterns from the global simulations are reflected in the regional downscalings. However, locally, biases can vary strongly between global models and their regional downscalings. Using spectral nudging towards the global models resulted in a slight reduction of wind biases with positive effects for the sea ice representation in RCAO.

The projected future changes are dominated by strong warming in the Arctic Ocean area, strongly increased precipitation and reduced SLP in most of the year. Temperature and precipitation changes are linearly related to each other (Figure 1).

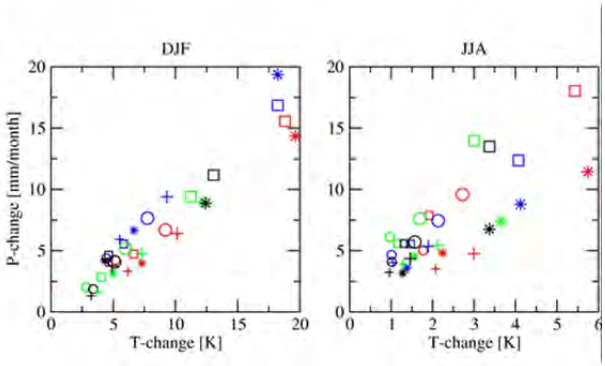


Figure 1: Precipitation and temperature change until 2030-2049 (small symbols) and 2080-2099 (big symbols) averaged over 70-90°N. Circles and quadrates represent RCP4.5 and RCP8.5 of the regional downscalings, plusses and stars represent RCP4.5 and RCP8.5 of the global models. Red, blue, green and black show CanESM2, EC-Earth, NorESM1, MPIESMLR respectively. Reference period is 1980-1999.

The large scale change patterns in RCA are dominated by the simulated changes in the global models but regional differences occur. While, atmospheric circulation changes are also dominated by the lateral boundaries, temperature changes in RCAO differ strongly from both RCA and the global originals, indicating the importance of the surface boundaries. The warming in RCAO is larger in summer but substantially smaller in winter than in RCA. The RCAO downscalings tend to simulate stronger sea ice extent variations and somewhat earlier summer ice free conditions than the global models.

4. Conclusions

The regional Arctic atmosphere stand alone model simulations are to a large degree driven by the lateral and lower boundary conditions from the reanalysis or global models. Coupling of an ocean-sea ice model to the atmosphere shows the importance of the lower boundary conditions in the Arctic. The sea ice representation differs substantially between the coupled regional downscalings and the driving global models with strong impacts on future Arctic temperature changes. However, the large scale atmospheric circulation shows only small changes in the coupled simulations compared to the uncoupled simulations indicating that the lateral boundary conditions are dominating the Arctic circulation.

This study shows also that we can not generally assume that regional model results outmatch their driving global model simulations. It depends strongly on the area and the variable. Furthermore, future projections differ, even if recent climate conditions are represented similarly.

Another interesting fact is that the spatial change patterns in the future scenario simulations are very similar in near and far future periods and across emission scenarios. It is mainly the amplitude of the response, which differs. If reality would behave in a similar way, observed significant change patterns could provide valuable indications for future climate changes.

Improvement of simulated monsoon precipitation over South-Asia with a regionally coupled model ROM

Pankaj Kumar[1,4], Dmitry Sein[2] William Cabos[3], and Daniela Jacob[1,4]

[1,4] Max Planck Institute for Meteorology, Hamburg Germany (pankaj.kumar@mpimet.mpg.de)
[2] Alfred Wegener Institute, Bremerhaven, Germany
[3] University of Alcalà, Spain
[1,4] Climate Service Center, Hamburg, Germany

1. Motivation

A regional coupled atmosphere–ocean model is developed to study the monsoon climate over South Asia. Most of the climate models (both GCM and RCM) underestimate precipitation over South Asia, but overestimate precipitation over the Bay of Bengal and the equatorial Indian Ocean. These systematic differences between the models may be related to a fundamental problem of atmospheric models: the inability to simulate intraseasonal variability. The intraseasonal oscillations of the South Asian monsoon play a major role in influencing the seasonal mean monsoon characteristics and their interannual variability (Goswami and Mohan, 2001). Several GCM studies with focus on the South Asian monsoonal region have concluded that GCMs have difficulties in simulating the mean monsoon climate (Turner and Annamalai, 2012). RCMs do simulate better orographic induced precipitation, but also show limited ability to simulate the land precipitation (Lucas-Picher et al., 2011; Kumar et al., 2013). For this study, differences in coupled and uncoupled simulations are analyzed to investigate the effect of coupling on the simulated climate, especially precipitation spatial patterns.

2. Model Setup

The REgional atmosphere MOdel REMO (Jacob, 2001) with 50km horizontal resolution is coupled to the global ocean – sea ice model MPIOM with increased resolution over the Indian Ocean (up to 20 km). Hereafter this coupled system will be called as ROM. The CORDEX south Asia domain is taken as atmospheric model domain (Fig.1). The models are coupled via the OASIS coupler. The global Hydrological Discharge model HD, which calculates river runoff (0.5° horizontal grid resolution), is coupled to both the atmosphere and ocean components. Exchange of fields between ocean and atmosphere takes place every three hours. Exchange between REMO/MPIOM and HD model is done once per day. Lateral atmospheric and upper oceanic boundary conditions outside the REMO domain were prescribed using ERA40 reanalysis for the two hindcast simulations and using MPI-ESM-LR for two historical runs. The total simulation period is 1958-2005. Results are presented for the period 1988-1997.

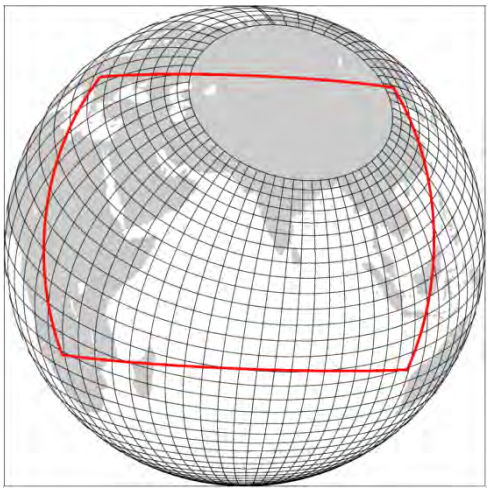


Figure 1. Grid configuration: the red "rectangle" indicates the coupled domain (REMO model) black lines indicate the grid of the MPIOM/HAMOCC. For the ocean/sea ice grid only every 15th line is shown.

3. Hindcast simulations

Fig-2 shows the annual mean SST difference between the two model simulations ROM and REMO [forced with historical simulation of MPI-ESM-LR for the period 1988-1997] with observation (ORSA4) SST. ROM is able to reproduce the SST well over the region of interest. The forcing GCM has a large cold bias (right panel), which the coupled model has reduced (middle panel) despite some enhanced cold biases over the south Indian Ocean.

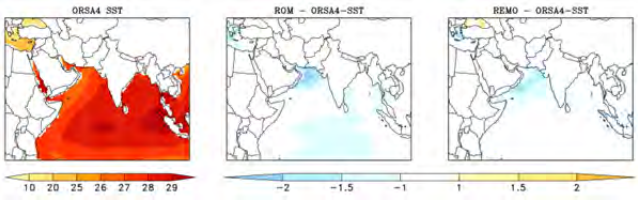


Fig. 2: Left panel, spatial pattern of annual mean observed (ORSA4) SST over the Indian ocean. Middle (ROM) and right (REMO) panels show the SST difference with ORSA4. Period 1988-1997, unit is (°C).

Fig-3 shows the precipitation difference (%) for ROM and REMO with respect to CRU (land)-HOAPS (ocean). Standalone model simulated results (forced with ERA40 and MPI-ESM-LR) show large precipitation biases both over land and ocean.

Over land it is highly underestimating rainfall over plains of South Asia (Bangladesh, India, also over the west coast of Myanmar and India). Keeping in mind that these are key precipitation zones of the monsoon climate (top panel) receiving large annual mean rainfall (6 to 20 mm/d). There is a large overestimation of precipitation over the south Indian Ocean.

However, feedback of ocean SST has a positive influence on the simulated precipitation of ROM both over land and ocean. As evident, compared to REMO, ROM simulations show significant improvement in the annual mean spatial pattern of precipitation both over land and ocean. ROM showed an increase over Bangladesh (~75%), over the plains of northern India (~50%) and decrease over the southern Indian Ocean (~100%) with respect to the uncoupled model. The western part of the domain receives very less amount of rainfall, so small change (< 0.5 mm/d) in magnitude lead to large relative differences (%). The possible mechanisms responsible for such an improvement is still under investigation, results of this analysis may be presented at the conference.

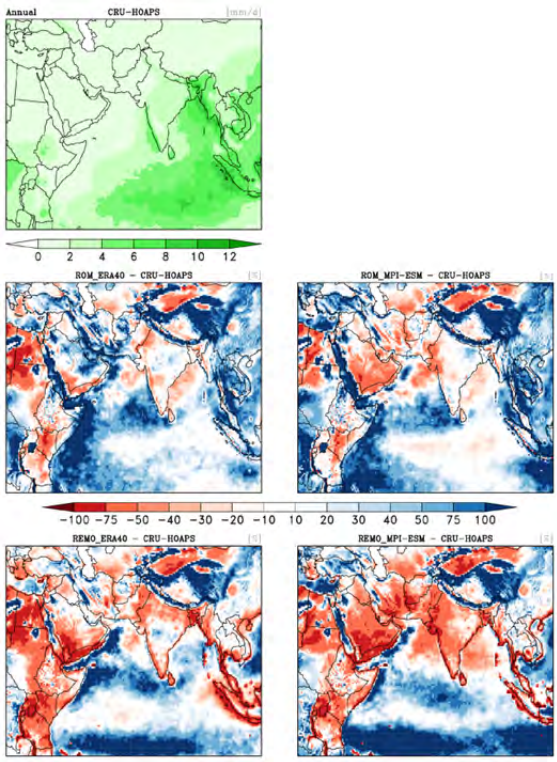


Fig.3: Top panel, annual mean precipitation over south Asia (mm/d). Middle panel shows the ROM (forced with ERA40 and MPI-ESM-LR) precipitation difference (%) with observations CRU-HOAPS. Lower panels is same as middle but for REMO. Period is 1989-2008.

4. Conclusion

REMO coupled with MPIOM (ROM) shows good skill with respect to the REMO standalone model results. ROM shows ability to reproduce SST as well as spatial pattern of monsoon precipitation. The coupling has positive impacts on the simulated precipitation not only over land but also over ocean. However, a more robust conclusion will be made after the assessment of a long term climate simulation.

Reference

Jacob, D. (2001) A note to the simulation of the annual and interannual variability of the water budget over the Baltic Sea drainage basin. Meteorology and Atmospheric Physics, 77, 1-4, 61-73.

Kumar P, Wiltshire A, Mathison C, Asharaf S, Ahrens B, Lucas-Picher P, Christensen JH, Gobiet A, Saeed F, Hagemann S, Jacob D, (2013) Downscaled climate change projections with uncertainty assessment over India using a high resolution multi-model approach.Science of the Total Environment, 468–469, S18–S30

Lucas-Picher P, Christensen JH, Saeed F, Kumar P, Asharaf S, Ahrens B, et al. (2011) Can regional climate models represent the Indian monsoon? J Hydrometeorol;12:849–68.

Goswami B.N., Mohan R.S.A. (2001) Intraseasonal oscillations and interannual variability of the Indian summer monsoon. Journal of Climate 4: 1180 – 1198.

Turner AG, Annamalai H. Climate change and the South Asian summer monsoon (2012) NatClim Change;2:587–95.

Coupled regional climate and hydrology modelling at the catchment scale

Morten Andreas Dahl Larsen[1], Martin Drews[1], Jens Christian Refsgaard[2], Karsten Høgh Jensen[3], Michael Brian Butts[4], Jens Hesselbjerg Christensen[5] and Ole Bøssing Christensen[5]

[1] Technical University of Denmark, Denmark (madla@dtu.dk)
[2] Geological Survey of Denmark and Greenland, Denmark
[3] University of Copenhagen, Denmark
[4] DHI, Denmark
[5] Danish Meteorological Institute, Denmark

1. Introduction

More and more regional climate models are being applied at scales down to even a few kilometres. At these scales the complex interactions between the atmosphere, the land surface, and the subsurface hydrology are crucial for understanding climate feedbacks at the regional to local scales. Many of the current regional climate models, however, have only a limited capability to represent all the parts of the terrestrial water cycle. This is particular true for the interactions between surface water and groundwater dependent ecosystems and surface water and groundwater resources, which in many cases have been shown to play a critical role in the regional earth system.

In the present study we investigate a dynamically coupled version of the DMI-HIRHAM (Christensen et al., 2006) regional climate model and a comprehensive distributed hydrological modelling system, MIKE SHE [Højbjerg et al., 2013], nested inside the regional climate model. A particular challenge in coupling a climate model to a hydrological model resides in in the vastly different philosophies expressed by such codes. While regional climate models generally implement primary physical equations, hydrological models typically are heavily calibrated codes. Likewise, temporal and spatial resolutions are often quite different. Lastly, present versions of MIKE SHE are native only to the Microsoft Windows operating system, necessitating the development of a novel cross-platform model interface based on open-source OpenMI technology (Gregersen et al., 2005 and Gregersen et al., 2007).

The coupled model is evaluated for a groundwater-dominated catchment in the western part of Denmark, Skjern River, covering approx. 2500 km^2 with a grid spacing of 500 m, which is embedded within a 4000 x 2800 km regional climate modelling domain with a horizontal resolution of approx. 11 km (Figure 1). The setup has proven stable and has been used for multi-year simulations.

Inside the shared model domains the coupled model enables two-way interactions between the atmosphere and the groundwater via the river and land surface through an energy-based land surface model (SWET) (Overgaard, 2005). In this manner the simple land surface model embedded in DMI-HIRHAM is effectively replaced by the superior land surface component of the combined MIKE SHE/SWET model, which includes a wider range of processes at the land surface and distributed three-dimensional subsurface flows as well as higher temporal and spatial resolution. Outside the shared domain DMI-HIRHAM utilizes its own embedded land surface model; however, the model nesting makes it possible to detect substantial feedbacks from the improved surface/ subsurface hydrology to the atmosphere even outside the shared domain.

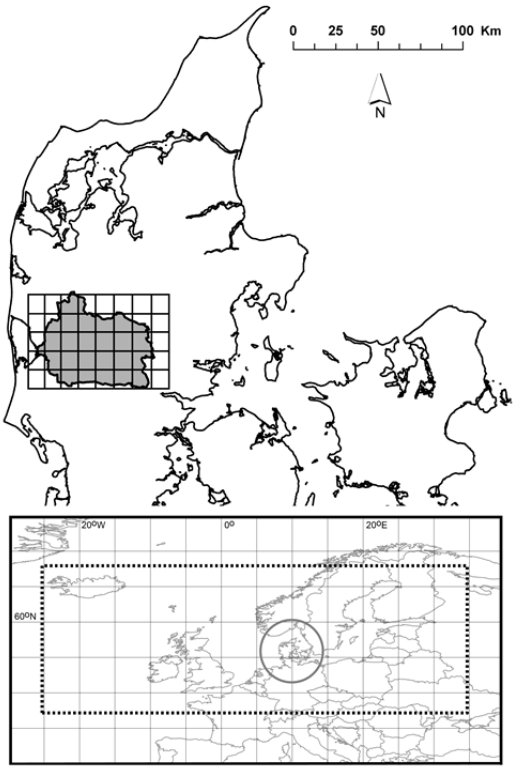


Figure 1. Domain of the DMI-HIRHAM regional climate model and the location of the Skjern River catchment. Grid boxes illustrate the native DMI-HIRHAM grid.

2. Studies

The task of individually calibrating and preparing each of the two modelling systems was performed in two studies preceding the coupled simulations (Larsen et al., 2013a and Larsen et al., *in preparation*). To assess the performance of the coupled simulations, two experiments were carried out.

(i) Using a suite of 26 simulations (e.g. Figure 2), we investigate the overall performance and feasibility of the coupled setup as compared to uncoupled simulations; we further investigate the role of the data transfer interval,

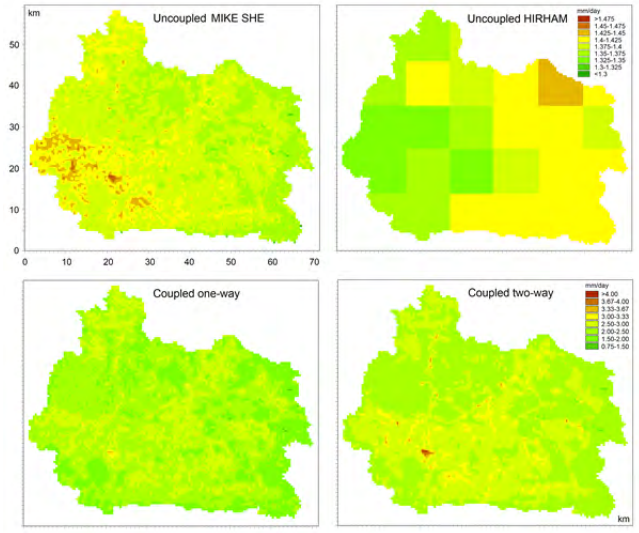


Figure 2. The simulated spatial distribution of mean daily evapotranspiration for the period June 5-11, 2009, from MIKE SHE alone (observed forcing data), DMI-HIRHAM alone, coupled one-way (MIKE SHE simulation with DMI-HIRHAM forcing data and no feedback to DMI-HIRHAM) and fully two-way coupled with dynamic feedback.

i.e. how often the models exchange fields, and of the model variability (Larsen et al. 2013b). The results are tested against ten variables: Six observed atmospheric variables (precipitation, wind speed, air temperature, surface pressure, global radiation and relative humidity) (Figure 3) as well as four ground/surface energy flux and water balance variables (latent-,sensible- and soil- heat fluxes as well as river discharge). Using varied data transfer rates between the models of 12-120 min the coupled results show improvements with an increase in data transfer frequency.

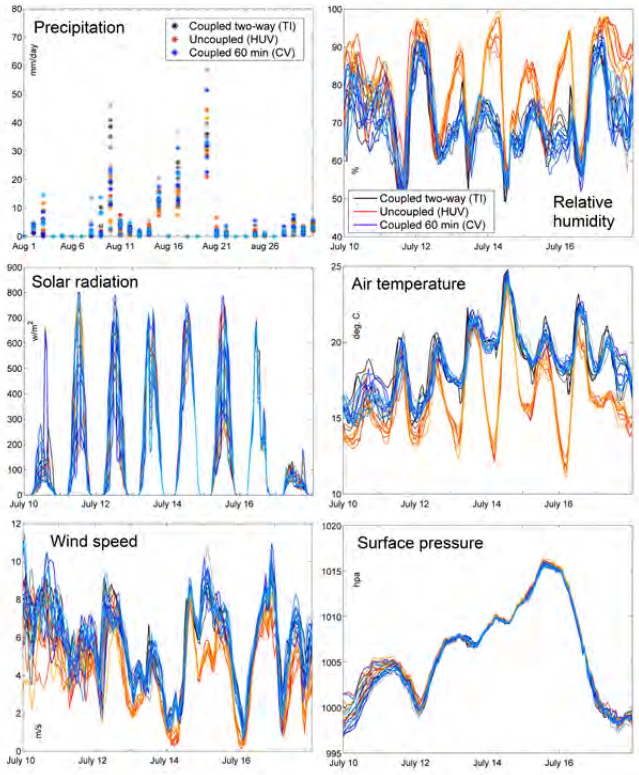


Figure 3. The six climatic variables used in the assessment of the coupled setup for the 10-18 July period, 2009, (precipitation is 1-31 August). The TI, HUV and CV runs each represent groups of eight simulations varying the data transfer interval of 12-120 minutes (TI), assessing DMI-HIRHAM uncoupled variability (HUV) as well as fully coupled variability (CV). The variability is induced by perturbed runs based on starting date.

(ii) The anticipated improvements in the reproduction of land-surface-atmosphere flux exchanges, temporally and geographically, from the MIKE SHE/SWET model as compared to DMI-HIRHAM have been investigated focusing on periods of non-normal weather; in this case we have investigated the model during periods of more pronounced drought/rainfall and temperature minima and maxima.

In general, the performance of the coupled model is poorer as compared to the uncoupled simulations. This was to be expected, however, since the two models as mentioned above were calibrated/set up individually and highlights the need for proper inter-model calibration of the combined modelling system. This will be pursued in future work. Other perspectives include experiments involving larger hydrological domains and in other climatic zones.

References

Christensen, O. B., M. Drews, J. H. Christensen, K. Dethloff, K. Ketelsen, I. Hebestadt and A. Rinke (2006) The HIRHAM regional climate model version 5 (β), Danish Meteorological Institute Technical Report 06-17, Denmark.

Gregersen, J. B., P. J. A. Gijsbers, S. J. P. Westen, and M. Blind (2005) OpenMI: the essential concepts and their implications for legacy software, Adv. Geosci., 4, 37–44, doi:10.5194/adgeo-4-37-2005.

Gregersen, J. B., P. J. A. Gijsbers, and S. J. P. Westen (2007) Open modelling interface, J. Hydroinform., 9, 175–191, doi:10.2166/hydro.2007.023.

Højbjerg, A. L., L. Troldborg, S. Stisen, B. B. S. Christensen and H. J. Henriksen (2013) Stakeholder driven update and improvement of a national water resources model, Environ. Modell. Softw., 40, 202-213.

Larsen, M. A. D., P. Thejll, J. H. Christensen, J. C. Refsgaard, and K. H. Jensen (2013a) On the role of domain size and resolution in the simulations with the HIRHAM region climate model, Clim. Dynam., 40, 2903–2918, doi:10.1007/s00382-012-1513-y.

Larsen, M. A. D., J. C. Refsgaard, M. Drews, M. B. Butts, K. H. Jensen, J. H. Christensen and O. B. Christensen (2013b) Results from a full coupling of the HIRHAM regional climate model and the MIKE SHE hydrological model for a Danish catchment. *Submitted to Hydrol. Earth Syst. Sc.*

Larsen, M. A. D., J. C. Refsgaard, K. H. Jensen, M. B. Butts, S. Stisen, and M. Mollerup (*in preparation*) Calibration of a distributed hydrology and land surface model using uncertain energy flux measurements.

Overgaard, J. (2005) Energy-based land-surface modelling: new opportunities in integrated hydrological modeling, Ph.D. thesis, Institute of Environment and Resources, DTU, Technical University of Denmark, Denmark.

Sea Salt Generation Function in the Baltic Sea region as the important component to regional atmospheric model

Piotr Markuszewski, Tomasz Petelski, Jacek Piskozub, Jaromir Jakacki

Physical Oceanography Department, Institute of Oceanology, Polish Academy of Sciences, Powstancow Warszawy 55, 81-712 Sopot, Poland. (pmarkusz@iopan.gda.pl)

1. Motivation

The Baltic Sea is the very important source of Sea Salt Aerosol (SSA). To improve the quality of regional atmospheric and air-sea interaction models it is necessary to take into account the influence of the Baltic Sea. Constantly improved quality of climatic models contributes to reduction of the uncertainties connected with modelling future climate (Tsigaridis et al. 2013). Marine aerosol significantly influences radiation balance and radiation forcing. There are two effects: direct effect is connected with light extinction (absorption and scattering) on particles, second, the indirect effect, is connected with aerosol influence on cloud microphysics.

Marine aerosols emitted from the sea surface help to clean the boundary layer from other aerosol particles. The emitted droplets do not dry out in the highly humid surface layer air and because of their sizes most of them are deposited quickly at the sea surface. Therefore, marine aerosols have many features of rain i.e. the deposition in the marine boundary layer in high wind events is controlled not only by the "dry" processes but also by the "wet" scavenging.

2. Methodology

During a number of cruises conducted on board r/v Oceania between 2008 and 2012 we collected many data which were further used to calculate sea salt source function over the Baltic Sea. Measurements were carried out using a gradient method. For this method we used a Laser Particle Counter (PMS model CSASP-100_HV) placed on one of the masts of the S/Y Oceania. Measurements were performed on five different levels above sea level: 8, 11, 14, 17 and 20 meters. The vertical aerosol concentration gradient was obtained from a minimum of 4 measurement series. Thus each result consists of a 1 hour series with the average sampling time at each elevation equaling 8 minutes.

Based on the averaged vertical concentration, and using the Monin - Obuchow theory, profiles of vertical sea spray fluxes in the near water layer were calculated (Petelski 2003). Using the results from those experiments the sea spray emission fluxes have been calculated for all particles of sizes in range 0.5 µm to 8 µm, as well as for particles of sizes from fifteen channels of 0.5 µm width. Using these fluxes we calculated the Sea Salt Generation Function (SSGF) over the Baltic Sea. This function provides information on the emission of particles of different sizes, depending on environmental parameters. The emission of sea spray depends on the size of energy lost by the wind waves in the process of a collapse.

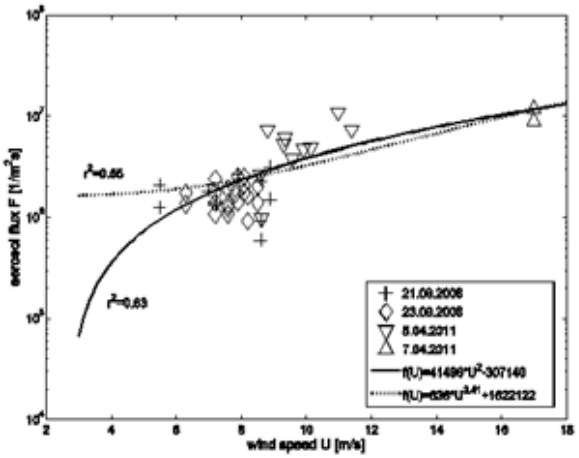


Figure 1 Aerosol flux parameterization based on gradient measurements on board of r/v Oceania

3. The Baltic Sea compared to other basins

The vast majority of the SSA and the SSA flux literature is connected with open ocean measurements. The aerosol measurements in the Baltic Sea region are valuable since the Baltic waters vary substantially from the oceanic waters. The Baltic Sea is one of the largest brackish inland seas by area, where inflows of oceanic waters are rare. Waves in the Baltic Sea surface live relatively short period of time and there are generated by wind friction. The SSA coarse mode is produced by wave crashing and bubble bursting and this mechanisms are strongly correlated with wind speed. Influence of wind speed and air masses on the SSA concentration in the Baltic Sea region have been studied by a number of researchers (Zielinski and Zielinski 2002, Petelski and Piskozub 2006, Lewandowska and Falkowska 2013). In the southern Baltic Sea region western winds dominate. Such circulation determines fresh maritime polar air mass transport (Lepparanta and Myrberg, 2009) and creates strong wind conditions connected with low pressure systems movement from the Atlantic Ocean. There is a strong influence of wind direction on aerosol optical properties in the Baltic Sea region.

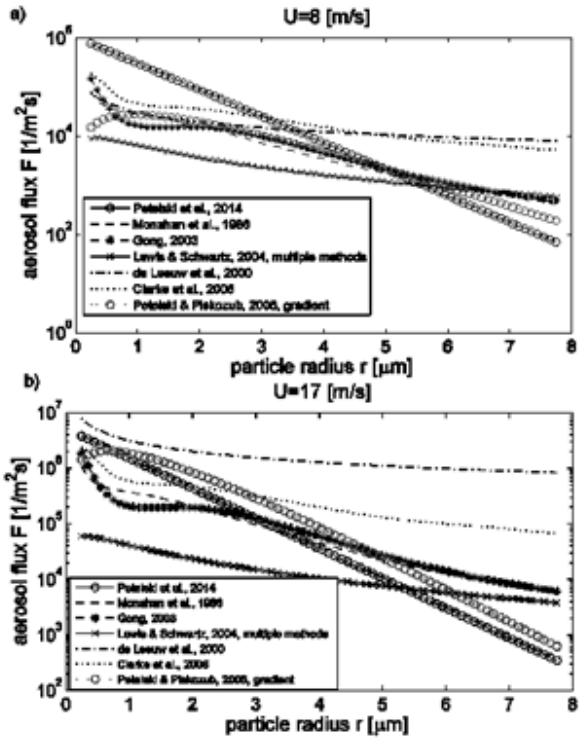


Figure 2 The new Sea Salt Source Function (Petelski et al. 2014) for SSA in the Baltic Sea region from particle radius and wind speed.

References

Clarke A. D., Owens S. R., Zhou J., (2006), An ultrafine sea‐salt flux from breaking waves: Implications for cloud condensation nuclei in the remote marine atmosphere, J. Geophys. Res., 111, D06202, doi:10.1029/2005JD006565.

de Leeuw G., Neele F. P., Hill M., Smith M. H., Vignati E., (2000), Production of sea spray aerosol in the surf zone, J. Geophys. Res., 105(D24), 29397–29409, doi:10.1029/2000JD900549

Gong S. L., 2003, A parameterization of sea-salt aerosol source function for sub- and super-micron particles, Global Biogeochem. Cycles, 17(4), 1097, doi:10.1029/2003GB002079.

Leppäranta M., Myrberg, K., (2009), Physical oceanography of the Baltic Sea, Springer, Chichester, 40 pp.

Lewandowska, A. U., Falkowska, L. M., (2013), Sea salt in aerosols over the southern Baltic. Part 1. The generation and transportation of marine particles, Oceanologia, 55(2), 279-298, doi:10.5697/oc.55-2.279

Lewis E. R., Schwartz S. E., 2004, Sea Salt Aerosol Production: Mechanisms, Methods, Measurements and Models-A Critical Review, Geophys. Monogr. Ser., vol. 152, pp. 413, AGU, Washington, D. C.

Monahan E.C, Spiel D.E., Davidson K.L., 1986, A model of marine aerosol generation via whitecaps and wave disruption. In Oceanic whitecaps and their role in air-sea exchange processes Monahan E.C, MacNiocaill G, pp. 167–174. Eds. Dordrecht, The Netherlands: Reidel.

Petelski, T. (2003), Marine aerosol fluxes over open sea calculated from vertical concentration gradients, J. Aerosol Sci., 34, 359– 371.

Petelski, T., and J. Piskozub (2006), Vertical coarse aerosol fluxes in the atmospheric surface layer over the North Polar Waters of the Atlantic, J. Geophys. Res., 111, C06039, doi:10.1029/2005JC003295.

Tsigaridis K., D. Koch, and S. Menon (2013), Uncertainties and importance of sea spray composition on Aerosol direct and indirect effects, J. Geophys. Res., 118, doi: 10.1029/2012JD018165.

Zielinski T., Zielinski A., (2002), Aerosol extinction and optical thickness in the atmosphere over the Baltic Sea determined with lidar, Journal of Aerosol Science, 33/6, 47-61.

Challenges in regional climate system modeling for the Baltic Sea and North Sea regions

H.E.Markus Meier[1,2] and members of the Baltic Earth Working Group on Regional Climate System Modeling

[1] Swedish Meteorological and Hydrological Institute, Norrköping, Sweden (markus.meier@smhi.se)
[2] Department of Meteorology, Stockholm University, Stockholm, Sweden

1. State-of-the-art

For BALTEX Phase I (1993-2002), one of the major achievements with respect to modelling was the building of high-resolution fully coupled atmosphere – sea-ice – ocean – land-surface models for the Baltic Sea region (Gustafsson et al., 1998; Hagedorn et al., 2000; Döscher et al., 2002; Schrum et al., 2003). For instance, Hagedorn et al. (2000) developed a high resolution fully coupled model based upon a three-dimensional ocean component to investigate and quantify the energy and water cycle in the Baltic Sea region and showed for a three-month period in autumn 1995 that simulated sea surface temperatures (SSTs) are at least as good as the previously used SSTs from operational analyses and in some cases even better. However, Hagedorn et al. (2000) showed also that the improved simulation of surface fluxes in the coupled model affects the atmospheric state variables only during time periods when advective transports in the atmosphere are small. At the end of BALTEX Phase I finally the first coupled models were available that could reproduce even winter conditions including sea ice (Döscher et al., 2002; Schrum et al., 2003) and the first multi-year simulations were performed without artificial drifting (e.g. Döscher et al., 2002; Räisänen et al., 2004).

2. Coupled atmosphere-ocean-land surface models

Whereas the first coupled atmosphere – sea ice – ocean models were developed to improve the short-range weather forecasting (e.g. Gustafsson et al., 1998) or to study processes and the impact of the coupling on the air-sea exchange (e.g. Hagedorn et al., 2000), model development during the second phase of BALTEX was more aligned to perform studies on climate change. Applying the so-called dynamical downscaling approach Regional Climate Models (RCMs) driven with global General Circulation Models (GCMs) at the lateral boundaries were used to assess the changing Baltic Sea in future climate (e.g. Räisänen et al., 2004). These earlier scenario simulations suffered from the fact that only time slices short compared to the Baltic Sea memory of about 30 year have been investigated and that the uncertainties in salinity projections were considerable. Although meanwhile transient simulations for the Baltic Sea for the period 1960-2100 have been performed (e.g. Meier et al., 2011), projections of the future water balance remain still rather uncertain (e.g. Donnelli et al., 2014).

In line with the extended objectives of BALTEX Phase II (2003-2013) (Climate variability and change; biogeochemical cycles) the increase of the degree of complexity and/or the increase of the resolution of the models was the main objective of model development. Coupled atmosphere – sea ice – ocean models were further elaborated by using a hierarchy of sub-models for the Earth system combining regional climate models with sub-models for surface waves, land vegetation, hydrology and land biochemistry, marine biogeochemistry, marine carbon cycle, marine biology and food web modelling. Mostly stimulated by the BONUS+ projects ECOSUPPORT, Baltic-C, INFLOW and AMBER these so-called Regional Climate System Models (RCSMs) have been developed and applied to investigate the impact of climate change on the Baltic Sea ecosystem (Fig. 1).

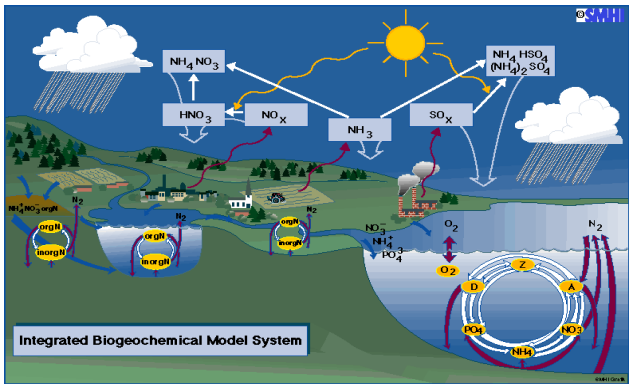


Figure 1: Schematic of relevant processes illustrating the Earth system approach for the Baltic Sea region.

While at the beginning of BALTEX Phase II only two coupled models were available, today several research groups are developing coupled atmosphere – sea ice – ocean models for the Baltic Sea region (e.g. Döscher et al., 2002; Dieterich et al., 2013; Ho-Hagemann et al., 2013; Tian et al., 2013; Van Pham et al., 2014).

3. Modeling of the land-sea continuum

As the Baltic Sea catchment area is four times larger than the Baltic Sea surface, the supply of freshwater from rivers of about 14,000 m^3 s^{-1} is an important factor influencing ocean dynamics in the Baltic Sea. Hence, the coupling of hydrological and ocean models was also in BALTEX Phase II an important activity. In addition, the development of improved hydrological models for water management was a dedicated objective, with an emphasis on more accurate forecasts of extreme events and long-term changes. Recently, a new hydrological model was developed to calculate future river flow and river-borne nutrient loadings, i.e. the HYPE (HYdrological Predictions for the Environment) model (Arheimer et al.

2012). Despite these efforts the uncertainties of runoff in scenario simulations for the end of the 21st century are considerable due to biases in precipitation calculated with regional atmosphere models (Donnelli et al., 2013). Nevertheless, all projections point towards an increased total volume flow into the Baltic Sea as a response to a warmer climate (e.g. Meier et al., 2011). Projections of nutrient loads are perhaps even more uncertain than projections of river flows due to unknown future land use and socioeconomic scenarios (Arheimer et al., 2012).

4. Challenges

What have we learned from these new models? In particular, added values of regional atmosphere models are (1) more detailed orography and improved spatial representation of precipitation, (2) improved land-sea mask, (3) improved sea surface boundary conditions (SST and sea ice) if a coupled atmosphere – sea ice – ocean model is used, (4) more accurate modeling of extremes, e.g. polar lows, typhoons, and (5) more detailed representation of vegetation and soil characteristics (Rummukainen, 2010; Feser et al., 2011 and references therein). Over the sea the added value of the high resolution is limited spatially to the coastal zone. In scenario simulations the differences between uncoupled and coupled models might be considerable due to the ice – albedo feedback. The impact of surface fluxes on summer SSTs is largest when the large-scale flow is weaker and more northerly directed compared to a stronger and more westerly flow over the North Atlantic (high NAO index) causing larger differences between uncoupled and coupled simulations (Kjellström et al., 2005). Hence, for consistent projections applying the dynamical downscaling approach of climate change results from GCMs coupled atmosphere – sea-ice – ocean models are needed. Other feedback mechanisms and their importance in perturbation experiments are currently under investigation. However, in particular the modeling of the water cycling in RCSMs still needs improvements.

In this presentation the challenges in regional climate system modeling for the Baltic Sea and North Sea regions are outlined based upon the discussions within the Baltic Earth Working Group on RCSMs[1].

References

Arheimer, B., J. Dahne, and C. Donnelly (2012). Climate change impact on riverine nutrient load and land-based remedial measures of the Baltic Sea Action Plan. AMBIO 41: 600–612

Dieterich, C., Schimanke, S, Wang, S., Väli, G, Liu, Y, Hordoir, R, Axell, L, Höglund, A, Meier, HEM, 2013. Evaluation of the SMHI coupled atmosphere-ice-ocean model RCA4-NEMO. SMHI Report Oceanography, 47, 80p.

Donnelly, C., W. Yang and J. Dahné (2014) River discharge to the Baltic Sea in a future climate. Climatic Change, Volume 122, Issue 1-2, pp 157-170

Döscher, R., U. Willén, C. Jones, A. Rutgersson, H. E. M. Meier, U. Hansson, and L. P. Graham (2002), The development of the regional coupled ocean-atmosphere model RCAO, Boreal Environ. Res., 7, 183–192.

Feser, Frauke, Burkhardt Rockel, Hans von Storch, Jörg Winterfeldt, Matthias Zahn (2011) Regional Climate Models Add Value to Global Model Data: A Review and Selected Examples. *Bull. Amer. Meteor. Soc.*, **92**, 1181–1192

Gustafsson, N., L. Nyberg and A. Omstedt (1998) Coupling of a High-Resolution Atmospheric Model and an Ocean Model for the Baltic Sea. Monthly Waether Review, 126, 2822-2846

Hagedorn, R., A. Lehmann and D. Jacob (2000) A coupled high resolution atmosphere-ocean model for the BALTEX region. Meteorologische Zeitschrift. 9, 7-20

Ho-Hagemann, H.T.M., B. Rockel, H. Kapitza, B. Geyer, E. Meyer (2013): COSTRICE – an atmosphere – ocean – sea ice model coupled system using OASIS3. HZG Report 2013-5, 26pp

Kjellström, E., R. Döscher and H. E. M. Meier (2005) Atmospheric response to different sea surface temperatures in the Baltic Sea: coupled versus uncoupled regional climate model experiments. 36, 397-409

Meier, H.E.M., H.C. Andersson, K. Eilola, B.G. Gustafsson, I. Kuznetsov, B. Müller-Karulis, T. Neumann, O. P. Savchuk (2011) Hypoxia in future climates: A model ensemble study for the Baltic Sea Geophys. Res. Lett., 38, L24608

Räisänen, J., U. Hansson, A. Ullerstig, R. Döscher, L.P. Graham, C. Jones, H.E.M. Meier, P. Samuelsson, and U. Willén (2004) European climate in the late twenty-first century: regional simulations with two driving global models and two forcing scenarios. Clim. Dyn., 22, 13-31

Rummukainen, M. (2010) State-of-the-art with regional climate models. WIREs Climate Change, 1, 82–96.

Schrum C., Hübner, U., Jacob, D., Podzun, R. (2003). A coupled atmosphere/ice/ocean model for the North Sea and the Baltic Sea, Clim. Dynamics, 21, 131-151

Tian, T., F. Boberg, O. Bøssing Christenssen, J. Hesselbjerg Christenssen, J. She and T. Vihma (2013) Resolved complex coastlines and land-sea contrasts in a high-resolution regional climate model: a comparative study using prescribed and modelled SSTs. Tellus A, 19951

Van Pham, T., J. Brauch, C. Dieterich, B. Frueh, B. Ahrens (2014) New coupled atmosphere-ocean-ice system COSMO-CLM/NEMO: On the air temperature sensitivity on the North and Baltic Seas. Oceanologia, accepted.

[1] http://www.baltic-earth.eu

Sea state projections for the North Sea: Impact of climate change on very high waves?

Jens Möller[1], Nikolaus Groll [2], and Hartmut Heinrich [1]

[1] Bundesamt für Seeschifffahrt und Hydrographie (BSH), Hamburg, Germany, (jens.moeller@bsh.de)

[2] Helmholtz- Zentrum Geesthacht (HZG), Geesthacht, Germany

1. Introduction

The research program KLIWAS of the German Federal Ministry of Transport, Building and urban Development investigates the impacts of climate change on waterways and navigation and provides options for adaptations. One aspect of the research task is to analyse climate scenarios for the sea state, eg. Sea wave height (Hs), wave direction and wave periods for the North Sea. Of particular importance for the safety on waterways is the potential change of frequence and magnitude from severe waves. The scenarios together with the wave climate of the recent years will giver an approximation of projected changes of the sea state in coastal and open sea areas.

2. Data and Models

Here we show the results for projected changes of medium, high and very high waves in the North Sea for the period of 2000-2100 in comparison to 1961-1990, based on the wave model WAM4.5.3. The wave model is driven with wind data from two different regional atmosphere-ocean-models (DMI-HIRHAM and MPI-REMO) in the scenario A1B. The wind data are delivered in a horizontal resolution of about 20 km and a time resolution of one hour, while the wave model provides data of the calculated sea state with a horizontal grid of 5 km and the time resolution of one hour.

3. Results and Discussion

It is seen, that in the eastern North Sea and especially in the German Bight there is a trend to a increasing of the 99^{th} percentile of Hs, while in the western part the 99^{th} percentile of Hs decreases in the future. These changes are mainly caused by changing wind directions in the future, while the wind speed will be mostly unaltered. Supplementary, it was carried out an extreme value analysis with the same data. Although the very high waves (eg. waves with a return period of 1-, 5-, 10-, up to 100 years) displays a similar behavior as the median or 99^{th} percentile, there are regions in the North Sea (eg. the German Bight) with stronger changes of the higher waves. For all waves height a strong decadal variability is detected which superimposes the calculated trends.

References

Grabemann I., N. Groll, J. Möller und R. Weisse 2014: Climate change impact on North Sea wave conditions: a review of ten projections. In preparation

Contribution of anthropogenic aerosols to the Euro-Mediterranean climate trends since 1980 using a regional coupled modelling approach

Pierre Nabat[1], Samuel Somot[1], Marc Mallet[2], Arturo Sanchez-Lorenzo[3] and Martin Wild[4]

[1] CNRM-GAME – Météo-France, Toulouse, France (pierre.nabat@meteo.fr)
[2] Laboratoire d'Aérologie, Toulouse, France
[3] Department of Physics, University of Girona, Spain
[4] Institute for Atmospheric and Climate Science, ETH, Zurich, Switzerland

1. Motivation

Various natural and anthropogenic aerosols observed over the Mediterranean region show a strong spatio-temporal variability and a large variety in aerosol physical-chemical and optical properties (Lelieveld et al., 2002). Their interactions with solar and thermal radiations can cause significant effects on the regional climate (e.g. Nabat et al., 2012; Spyrou et al., 2013). Since the 1980s, sulfur emissions have been considerably reduced, leading to a decrease of sulfate aerosol concentration over the Euro-Mediterranean region (Nabat et al., 2013), probably explaining the increase of incoming solar radiation reaching the surface, observed over the same period (Wild et al., 2005; Sanchez-Lorenzo et al., 2013). On the other hand, global (Allen et al., 2013) and regional (Zubler et al., 2011) models still have trouble in reproducing the all-sky surface solar radiation trends and their consequences on climate.

The present work provides a new approach through the use of a fully coupled regional climate system model (RCSM), in order to investigate the consequences of this aerosol trend on the Mediterranean climate, and its role in the observed changes during the last three decades. This RCSM, namely CNRM-RCSM4 (Sevault et al., 2014; Nabat et al., 2014), includes the atmospheric regional climate model ALADIN-Climate, the regional ocean model NEMOMED8, the land surface model ISBA and the river routine scheme TRIP. This approach enables us to take into account the high-frequency feedback of the sea surface temperature (SST) on the atmosphere, as well as the river-ocean-atmosphere feedback. Aerosols are included in ALADIN-Climate through monthly interannual climatologies, coming from a combination of satellite-derived and model-simulated products (Nabat et al., 2013), and considered as the best possible relevant estimation of the atmospheric aerosol content for the five most relevant species (sea salt, desert dust, sulfates, black and organic carbon aerosols). Two simulations with the forcing of the ERA-INTERIM reanalysis have been carried out over the period 1980-2012, with (TRANS) and without (REF) the trends in sulfate aerosols.

2. Surface radiation trends

The scattering of the incoming solar radiation by sulfate aerosols leads to important changes in the Euro-Mediterranean climate. Comparisons between both simulations and homogenized surface observations (Sanchez-Lorenzo et al., 2013) reveal that our model is able to reproduce the all-sky surface shortwave radiation trends only when the aerosol trend is included (Fig. 1). This improvement in the TRANS simulation is particularly visible in regions where aerosols have been strongly reduced (i.e., Central Europe, Po Valley). Aerosol changes explain 81 per cent of the simulated brightening over the 1980-2012 period, while the direct effect has been found to be the main cause of the simulated brightening.

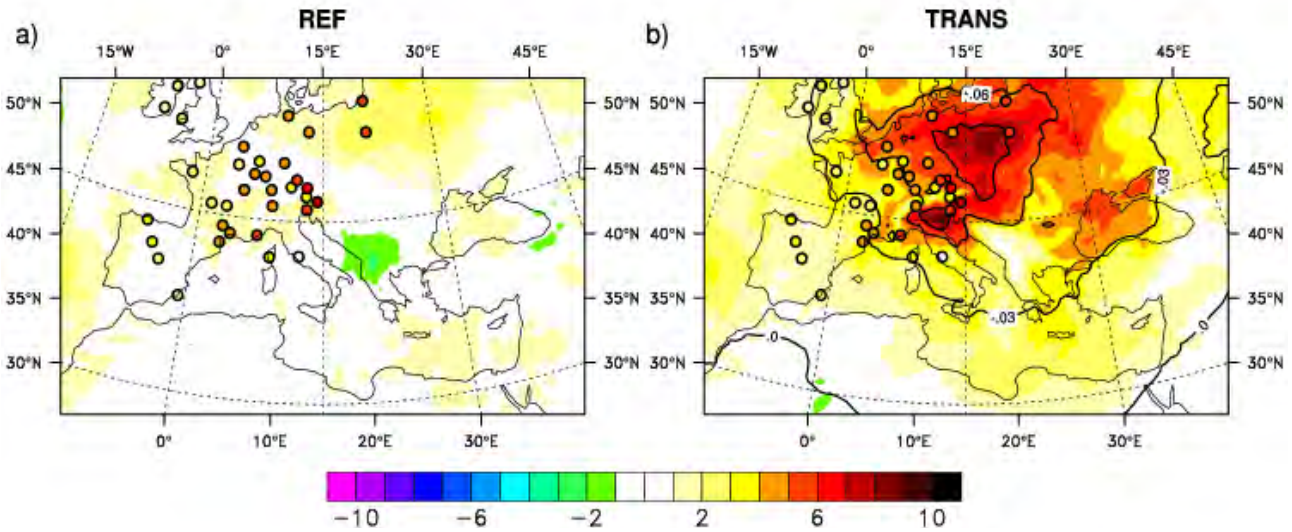


Figure 1. Comparison of surface downward shortwave radiation trends in W.m^{-2}.decade^{-1} for the a) REF and b) TRANS simulations over the period 1980-2009. Homogenized surface observations have been added in colored points; aerosol optical depth trend (decade^{-1}) is indicated in contour lines in b.

3. Consequences on other climate trends

As a result of this brightening effect, the surface temperature trend is also higher in TRANS than in REF. Over Europe, the simulated temperature trend of TRANS (0.35 °C/decade) is closer to homogenized surface observations (0.37-0.40 °C/decade) than REF (0.25°C/decade), indicating that aerosols explain 23% of the observed warming between 1980 and 2012.

The use of an atmosphere-ocean coupled model enables us to show that Mediterranean sea surface temperature changes are also better reproduced using the aerosol trend. Air-sea fluxes have consequently been modified by this evolution in the sulfate aerosol content.

Overall, our results demonstrate the importance of changes in aerosol loads for the understanding of regional climate variability.

References

Allen RJ, Norris JR and Wild M (2013). Evaluation of multidecadal variability in CMIP5 surface solar radiation and inferred underestimation of aerosol direct effects over Europe, China, Japan, and India. J. Geophys. Res. Atmos., 118, 6311–6336.

Lelieveld J, Berresheim H, Borrmann S, Crutzen PJ, Dentener FJ, Fischer H, Feichter J, Flatau PJ, Heland J, Holzinger R, Korrmann R, Lawrence MG, Levin Z, Markowicz KM, Mihalopoulos N, Minikin A, Ramanathan V, de Reus M, Roelofs GJ, Scheeren HA, Sciare J, Schlager H, Schultz M, Siegmund P, Steil B, Stephanou EG, Stier P, Traub M, Warneke C, Williams J, Ziereis H (2002) Global air pollution crossroads over the Mediterranean, Science, 298, 794–799.

Nabat P, Solmon F, Mallet M, Kok JF, Somot S (2012) Dust emission size distribution impact on aerosol budget and radiative forcing over the mediterranean region: a regional climate model approach. Atmospheric, Chemistry and Physics, 12, 10,545–10,567.

Nabat P, Somot S, Mallet M, Chiapello I, Morcrette JJ, Sol mon F, Szopa S, Dulac F, Collins W, Ghan S, Horowitz LW, Lamarque JF, Lee YH, Naik V, Nagashima T, Shindell D, Skeie R (2013) A 4-d climatology (1979–2009) of the monthly tropospheric aerosol optical depth distribution over the mediterranean region from a comparative evaluation and blending of remote sensing and model products. Atmospheric Measurement Techniques, 6, 1287–1314.

Nabat P, Somot S, Mallet M, Sevault F, Chiacchio M and Wild M (in review). Direct and semi-direct effects of aerosol on the Mediterranean climate variability. Clim. Dyn.

Sanchez-Lorenzo A, Wild A, Trentmann T (2013). Validation and stability assessment of the monthly mean CM SAF surface solar radiation dataset over Europe against a homogenized surface dataset (1983–2005). Remote Sensing of Environment, 134, 355–366.

Sevault F, Somot S, Alias A, Dubois C, Lebeaupin-Brossier C, Nabat P, Adloff F, Déqué M and Decharme B (in review). Ocean simulation of the 1980-2012 period for the Mediterranean Sea using a fully coupled atmosphere-land-hydrology-river-ocean regional climate system model: design and evaluation. Tellus.

Spyrou C, Kallos G, Mitsakou C, Athanasiadis P, Kalogeri C, Iacono M (2013) Modeling the radiative effects of desert dust on weather and regional climate. Atmospheric Chemistry and Physics, 13, 5489-5504.

Wild M, Gilgen H, Roesch A, Ohmura A, Long C, Dutton EG, Forgan B, Kallis A, Russak V and Tsvetkov A (2005) From dimming to brightening: decadal changes in solar radiation at Earth's surface. Science, 308, 847-850.

Zubler EM, Folini D, Lohmann U, Lüthi D, Schär C, Wild M (2011) Simulation of dimming and brightening in Europe from 1958 to 2001 using a regional climate model. Journal of Geophysical Research, 116, D18205.

The potential impacts of forestation in mitigating climate change over Southern Africa

Myra Naik and Babatunde J. Abiodun

Climate System Analysis Group, Department of Environmental & Geographical Science,
University of Cape Town, South Africa. (babiodun@csag.uct.ac.za)

1. Introduction

Forestation is generally considered an effective and affordable climate change mitigation option. Large-scale forestation activities can offset current fossil fuel emissions through the sequestration of atmospheric CO_2, a major greenhouse gas. Forestation activities can also generate monetary returns and create economic opportunities through carbon trading initiatives and may also help create more sustainable local livelihoods through increased resource availability. Often overlooked, however, are the biophysical impacts of forestation, such as changes to surface albedo and the hydrological cycle.

Several studies have used regional climate models to investigate biophysical impacts forestation. Climate simulations over Hungary (Gálos *et. al.,* 2011)) and over United States (Chen *et al.,* 2012) show that forestation may successfully mitigate the severity of projected drought and induce a local cooling over these regions in future. But Abiodun *et al.*, (2012) showed that forestation may have both positive and negative effects in West Africa, in that, while it reduces the projected warming over the forested area, it enhances warming outside the forested area. These studies suggest that forest cover can feedback and modify the projected climate change signal at a regional scale. Despite the various ongoing forestation activities in southern Africa, however, limited research has investigated how forestation might feedback to modify regional climate change signal in the future. The present study is in this direction.

2. Data and Method

This study used the International Centre for Theoretical Physics (ICTP) Regional Climate Model version 4 (RegCM4) to simulate the present-day (1970-2000) and future (2031 –2065) climate (under The Representative Concentration Pathway 4.5 scenario) over Southern Africa and test the sensitivity to forestation. The simulations were forced with initial boundary condition data from the European Centre/Hamburg 5 model (ECHAM5). The experimental design considered the effect of an idealized scenario of land cover change, intended to examine the 'upper bounds' of the climate change mitigation potential. The scenario of vegetation change represents an increase in tree density along the eastern and coastal region of South Africa. This is regarded as a plausible change for two reasons. Firstly, the natural occurring phenomenon of bush encroachment has been reported in the mesic and semi-arid savanna regions of The Eastern Cape Province. Secondly, tree density could also increase in the near future as a result of intentional, human forestation efforts. Large areas of land in the Eastern Cape have already been scoped as having good-to-moderate biophysical potential for commercial forestation (DWAF, 2007). In this study, we considered a region of maximum forestation potential based on previous study (by Gush *et.al.*, 2002) which delimited regions of South Africa where the Mean Annual Precipitation exceeded 650 mm as having potential for forestation (Figure 1). The difference between the simulations with and without forestation was used to determine the impact of forest cover on the future climate (2031-2064).

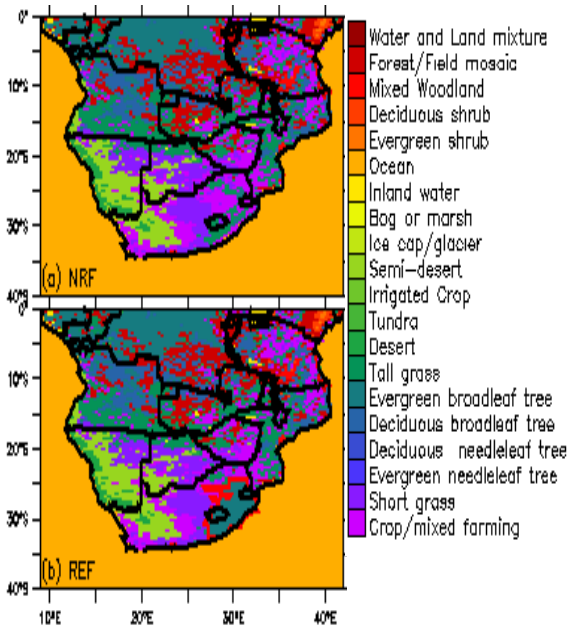


Figure 1: Land cover types used in this study (a) Future scenario (NRF) and (b) forestation (REF). We use previous study by Gush *et al.*, (2002) to delimit the region of maximum forestation potential.

3. Results

A comparison of RegCM4 simulation with observation shows that the model gives a realistic simulation of the present-day climate over much of southern Africa. In agreement with previous studies, RegCM4 projections show a warming across the subcontinent, with a maximum warming of 3.5 ^{o}C the over interior (20 ^{o}E, 28 ^{o}S) and general drying trend (-5%) during the summer season from December—January (DJF) (not shown).

Results from the sensitivity experiments suggest that forest cover may further increase air surface temperatures (+0.3 ^{o}C) over the forested area and much of South Africa during DJF; thereby amplifying the projected warming, rather than mitigating it (Fig. 2a). There is also an increase in the amount of rainfall over

the forested region. These changes are largely due to local changes in the surface energy budget. The darker tree canopy of the forests absorbs more of the incoming solar radiation, relative to pre-existing vegetation cover. The associated decrease in surface albedo (-3%; Fig. 2b) causes an increase in the amount of solar radiation absorbed at the earth's surface. This extra energy in the system increases the amount of sensible (about +5 W/m^2; Fig. 2c) and latent heat (+5 W/m^2; Fig. 2d). Note that while the changes in sensible heat correspond with the region of (peak) increase in temperature, changes in latent heat correspond with the increase in rainfall (+5%; Fig. 2e). Overall, the increase in sensible heat produces a net warming, rather than a net cooling effect. Since, the potential impacts on climate are not limited to the forested area, current work is investigating the changes to the energy balance in adjacent regions.

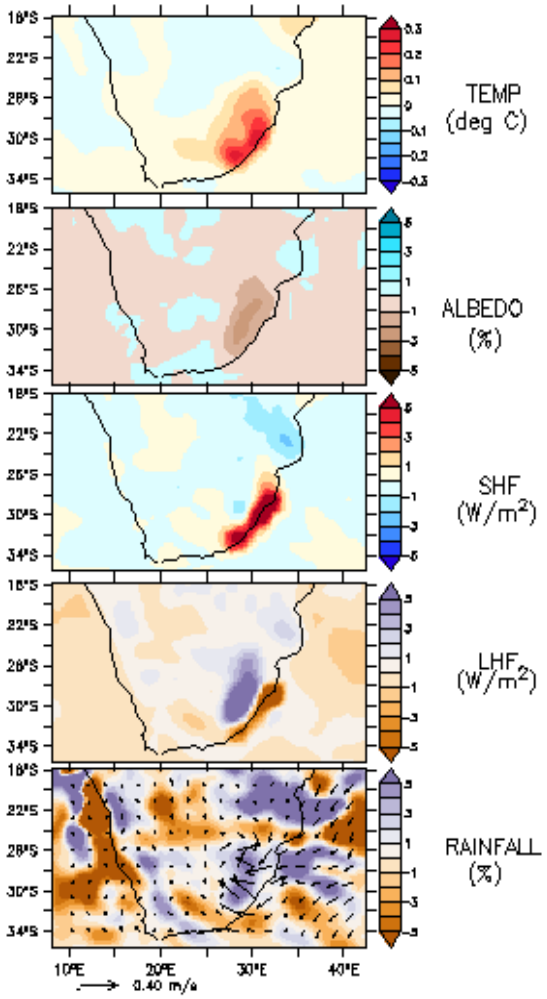


Figure 2: [from top] Difference due to forestation, for the late summer season (DJF) of the future climate (2031—2064), for (a) average 2 m air surface temperature (^{o}C), (b) rainfall (%) and wind speed (m/s), (c) albedo (%), (d) latent heat flux (W/m^2) and (e) sensible heat flux (W/m^2).

4. Discussion

This experiment aimed to provide only an 'upper bounds' of the climate change mitigation potential. While admittedly an idealized scenario of forestation, in South Africa, the impacts of forestation on regional climatic are undoubtedly complex. A more extensive analysis is required in order to determine how factors such as the amount of soil moisture available to plants and/or rooting depth could contribute to the biophysical effects observed in the study. Moreover, the impacts for local hydrology and biodiversity, which have not been considered here, also need to be factored into any assessment before embarking on forestation project. Future work will also assess some of the potential impacts that forestation might have on extreme events such as drought.

Nevertheless, our results suggest that ignoring these potentially adverse biophysical effects could prove unwise. Forestation projects in Southern Africa should not be viewed from the perspective of carbon storage alone. Rather, these biophysical effects need to be carefully weighed out against the biogeochemical benefits of carbon sequestration.

References

Abiodun, B. J., Adeyewa, Z. D., Oguntunde, P. G., Salami, A. T., & Ajayi, V. O. (2012). Modeling the impacts of reforestation on future climate in West Africa. Theoretical and Applied Climatology, 110(1-2), 77–96. doi:10.1007/s00704-012-0614-1

DWAF (2007). Department of Water Affairs and Forestry Eastern Cape Forestry Sector Profile (pp. 1–63).

Chen, G.-S., Notaro, M., Liu, Z., & Liu, Y. (2012). Simulated Local and Remote Biophysical Effects of Afforestation over the Southeast United States in Boreal Summer*. Journal of Climate, 25(13), 4511–4522. doi:10.1175/JCLI-D-11-00317.1

Gálos, B., Mátyás, C., & Jacob, D. (2011). Regional characteristics of climate change altering effects of afforestation. Environmental Research Letters, 6(4), 044010. doi:10.1088/1748-9326/6/4/044010

Gush, M. B., Scott, D. F., Jewitt, G. P. W., Schulze, R. E., & Hallowes, L. A. (2002). A new approach to modelling streamflow reductions resulting from commercial afforestation in South Africa A new approach to modelling streamflow reductions resulting from commercial afforestation in South Africa. South African Forestry Journal, 196, 27–36.

Simulation of snowbands on the Baltic Sea with coupled model COSMO-CLM/NEMO

Trang Van Pham[1,3], Jennifer Brauch[2], Barbara Früh[2] and Bodo Ahrens[3]

[1] Loewe – Biodiversity and Climate Research Center, Frankfurt am Main, Germany
[2] German Meteorological Weather Service, Offenbach am Main, Germany
[3] Institute for Atmospheric and Environmental Sciences, Goethe University Frankfurt, Frankfurt am Main, Germany

1. Introduction

The snowband is a common weather event on the Baltic Sea when the sea surface is much warmer than the atmosphere. This increases the instability of the air mass, enhances convection and finally leads to heavy snow fall often formed in parallel bands.
Six snowband events (Table 1) were simulated using:

- stand-alone atmospheric COSMO-CLM model forced by ERA-Interim (**CCLM**).
- coupled atmosphere-ocean-ice model COSMO-CLM/NEMO over North and Baltic Seas; over other sea areas, COSMO-CLM is forced by ERA-Interim (**CCLM/NEMO**).
- stand-alone atmospheric COSMO-CLM model with monthly average ERA-Interim sea surface temperature (SST) over North and Baltic Seas (the month in that snow bands occurred, Table 1); the rest of the domain is driven by ERA-Interim (**CCLM-MOD**).

Table 1. Dates of snow band events

Dates	Reference	Average SST (K)	Locations
03-07.01.1985	Andersson & Nilsson (1990)	271,93	Gulf of Finland to Kalmar, Sweden
23.12.1986	Andersson & Nilsson (1990)	276,51	Gulf of Finland
11.01.1987	Andersson & Gustafsson (1994) Gustafsson et al. (1998)	269,88	Gulf of Finland
04-07.12.1998	Savijaervi (2012) Vihma & Bruemmer (2002)	276,49	Gaevle, Sweden
17.01.2006	Savijaervi (2012)	274,39	Gulf of Finland
30.11.2010	German Meteorological Service record	279,07	Coast of Germany

2. Heat fluxes

For all events, the daily latent and sensible heat fluxes over the Baltic Sea simulated by CCLM/NEMO are quite close to the fluxes simulated by CCLM.

On the days when snow bands occurred, both simulations yielded noticeably large negative heat fluxes. It means there are enormous upward fluxes released by the ocean to the atmosphere. When average SST is used for CCLM stand-alone (CCLM-MOD), smaller heat fluxes, especially latent heat flux, were observed.

Case 07.12.1998: CCLM/NEMO produced deep negative heat fluxes from Gulf of Bothnia to Gaevle, Sweden where snowbands occurred.

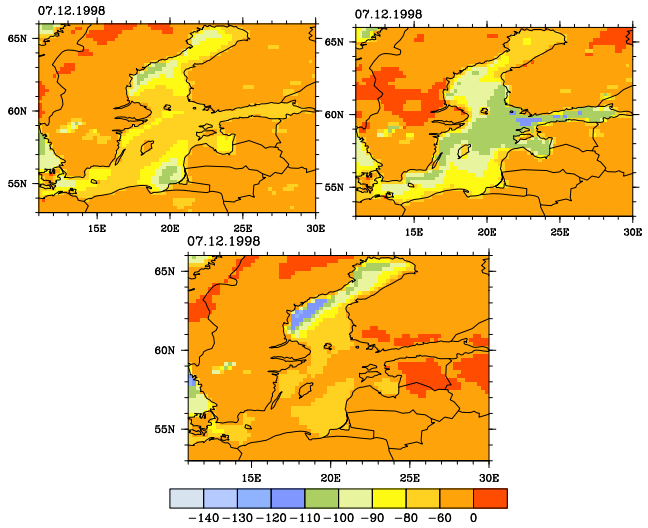


Figure 1. Latent heat flux (Wm-2) over Baltic Sea for the event 1998. Top left: CCLM. Top right: CCLM-MOD. Bottom: CCLM/NEMO.

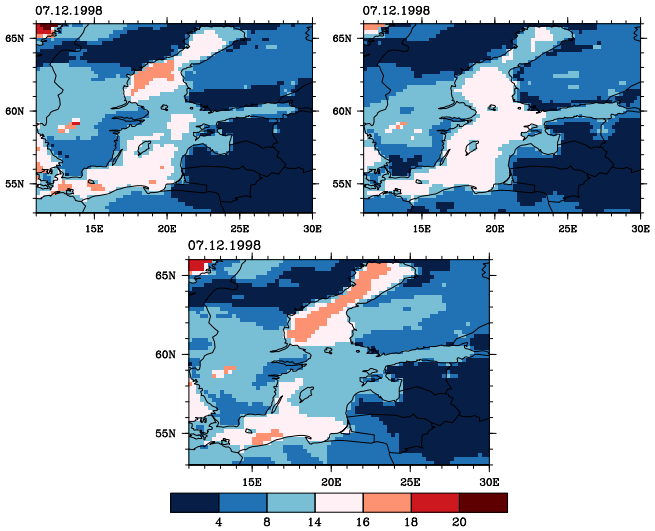


Figure 2. Surface temperature – Temperature at 850hPa (Kelvin) over Baltic Sea for the event 1998. Top left: CCLM. Top right: CCLM-MOD. Bottom: CCLM/NEMO.

3. Instability of the atmosphere

One of the most important criteria for an occurrence of snow bands is the instable atmosphere which could enhance strong convection and leads to heavy snow fall. The instability of the atmosphere is considered by looking at the gradient of temperature from the surface to 850hPa level.

CCLM/NEMO simulated well the high contrast between the surface temperature and temperature at 850 hPa over the Baltic Sea. All temperature differences are larger than 13 K and in good agreement with the CCLM results forced by ERA-Interim.

When CCLM is not coupled to the ocean and does not have good SST from ERA-Interim (CCLM-MOD), the temperature contrast patterns in all cases are different from CCLM and CCLM/NEMO simulations.

4. Pressure system

All experiments produced quite similar pressure systems for all 6 snow band events. It is influenced by the large scale circulation coming from the lateral boundary. Notice that at the lateral boundary, COSMO-CLM is driven by ERA-Interim for all experiments. In most of the cases, high pressure locates at the North of Baltic Sea and low pressure at the South; this allows Easterlies or North-Easterlies to transfer cold air mass from the continent to the warm surface of Baltic Sea.

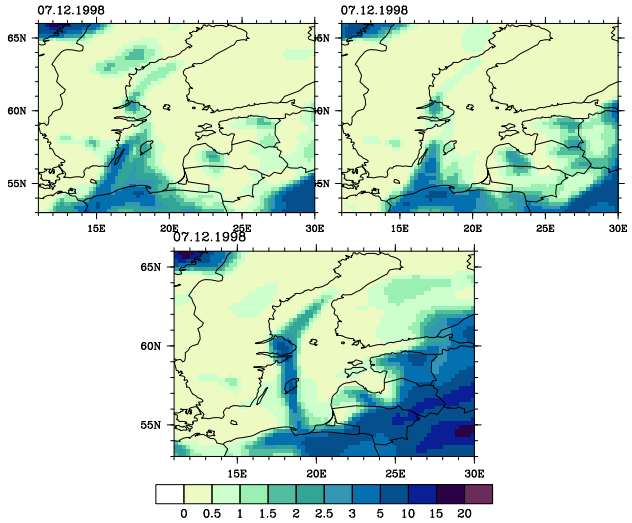


Figure 3. Total precipitation (mm) over Baltic Sea for the event 1998. Top left: CCLM. Top right: CCLM-MOD. Bottom: CCLM/NEMO.

5. Precipitation

When a heavy snow fall event occurs, it is expected that the total precipitation values should be high. The simulated precipitation values on the day when snow bands occurred are up to 10mm.

In all 6 cases, CCLM/NEMO yielded similar total precipitation pattern compared to CCLM. The two simulations agreed well, especially on the precipitation over the Baltic Sea.

In some cases, CCLM-MOD could not produce high enough precipitation. For example, on 11.01.1987, CCLM-MOD simulated too less precipitation in Gulf of Finland. On 07.12.1998, CCLM-MOD also could not produce the precipitation band from Gulf of Bothnia to South Sweden.

6. Conclusion

- Coupled CCLM/NEMO can simulate well a typical extreme event on the Baltic Sea like snow band.
- CCLM/NEMO results are quite close to the results of CCLM forced by ERA-Interim; this implies that when the ocean is coupled to COSMO-CLM, it can be as good as COSMO-CLM driven by a high-resolution re-analysis data such as ERA-Interim.
- However, when a good re-analysis data like ERA-Interim is not available, for example in case of forecast for the future, then COSMO-CLM needs to use the global forcings from a lower resolution source, for example ECHAM. Experiment CCLM-MOD showed that when SST over the North and Baltic Sea is kept as a constant value and there is no update from a global model, COSMO-CLM produced not good results. The temperature contrast and heat fluxes as well as precipitation are different from experiments CCLM and CCLM/NEMO.
- We recommend to use the coupled atmosphere-ocean model to simulate extreme events such as snow bands when high-resolution global data is not available.

References

Andersson T., and S. Nilsson (1990) Topographically induced convective snowbands over the Baltic Sea and their precipitation distribution, American Meteorology Society, 5.

Andersson T., and N. Gustafsson (1994) Coast of Departure and Coast of Arrival: Two Important Concepts for the Formation and Structure of Convective Snowbands over Seas and Lakes, American Meteorology Society, 122, 1036-1049.

Gustafsson N., Nyberg L., and A. Omstedt (1998) Coupling of a High-Resolution Atmospheric Model and an Ocean Model for the Baltic Sea, American Meteorology Society, 126, 2822-2846.

Savijaervi (2012) Cold air outbreaks over high-latitude sea gulfs, Tellus A, 64, 12244, doi: 10.3402/tellusa.v64i0.12244.

Vihma T., and B. Bruemmer (2002) Observations and Modelling of the on-ice and off-ice air flow over the Northern Baltic Sea, Boundary-Layer Meteorology, 103, 1-27.

Analysis of nucleation events in the European boundary layer using the regional aerosol-climate model REMO-HAM

Joni-Pekka Pietikäinen[1], Santtu Mikkonen[2], Amar Hamed[2,†], Anca I. Hienola[1], Wolfram Birmili[3], Markku Kulmala[4] and Ari Laaksonen[1,2]

[1] Finnish Meteorological Institute, Helsinki, Finland (Joni-Pekka.Pietikainen@fmi.fi)
[2] University of Eastern Finland, Kuopio, Finland
[3] Leibniz Institute for Tropospheric Research (IfT), Germany
[4] Department of Physics, University of Helsinki, Finland
[†] Deceased in September 2013

1. Introduction

Atmospheric aerosols influence our quality of life in many different ways from health aspects to changing the climate patterns and the hydrological cycle. Aerosols are directly emitted to the atmosphere, or formed in a gas-to-particle conversion. This conversion, know as aerosol nucleation or new particle formation (NPF), occurs around the world and is an important part of the climate system (Kulmala et al. (2004)). For example, the global and regional cloud condensations nuclei (CCN) concentrations are affected by it (Laaksonen et al. (2005)).

2. Methods

Modelling nucleation and the subsequent growth is a difficult task. Based on the assumption that sulphuric acid (H_2SO_4) is the main driving force in the process of nucleation, several parametrizations have been proposed. In this study the kinetic nucleation scheme for 3 nm particles (in diameter) is used:

$$J_{3\mathrm{nm}} = K \times [\mathrm{H_2SO_4}]^2 \quad (1)$$

where K=1.417*10^{-15} [cm^3/s] is the kinetic coefficient and [H_2SO_4] is the sulphuric acid concentration in molec/cm^3. The equation also show that the nucleation is calculated directly to 3 nm size particles. Earlier, the nucleation rates were calculated for 1 nm size particles (molecule clusters). The formation rates used in the parametrization were based on 3 nm nucleation rate measurements. To get from 3 nm to 1 nm sizes, extrapolation is required, which needs estimates of the cluster growth rates. Using directly the 3 nm formation rates removes the estimation step completely. This approach can be applied if we assume that the only condensing gas is sulphuric acid when particles grow to 3 nm sizes. Since this is the case anyway in HAM-module, direct calculation of 3 nm particles is justified.

In it known that HAM-aerosol module produces too high sulphuric acid concentration (Kazil et al. (2010), Pietikäinen et al. (2012)). The H_2SO_4 concentrations mainly depends on the availability of sulphur dioxide (SO_2) and dimethyl sulphide (DMS), and the oxidative species OH (daytime chemistry, for SO_2 and DMS) and NO3 (night-time chemistry, only for DMS) (Stier et al. (2005)). For H_2SO_4 concentrations, SO2 oxidation by OH during daytime is the most important process.

The OH values are constant 3-D fields over a month in the model. To make this part of the chemistry more realistic without loosing computational time, that is without implementing a more detailed chemistry module, a measurement based OH-proxy was developed.

$$[\mathrm{OH}] = \begin{cases} 3081.0 \cdot \mathrm{Radiation}^{0.8397} & \mathrm{day} \\ 6.033 \times 10^4 & \mathrm{night} \end{cases}, \quad (2)$$

where the units are molec/cm^3 for OH-proxy and W/m^2 for radiation.

In the cloudy part of the grid boxes all the sulfuric acid is removed by condensation. Below clouds the nucleation is active again. The old approach for OH concentrations did not take into account the cloudiness, but the new one does as it is a function of incoming solar radiation (Eg. (2)). This is a big improvement and makes the simple chemistry routine much more realistic.

3. Simulations and results

Simulations are performed for both model versions. The original one is henceforth called REMO-NCH and the new OH-proxy version REMO-OHP. The simulations are conducted for 2003 and 2004 with REMO-OHP and for 2008-2009 with both versions. The results are compared with observations from 13 different European sites.

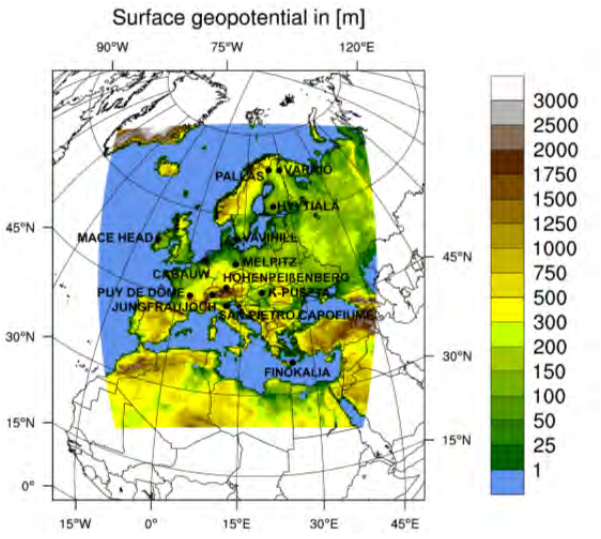


Figure 1. The orography of the REMO-HAM domain and the analysed locations.

The model domain including the analysed locations are presented in Fig. 1. The results are compared with observations in two different ways. For all stations, a literature based observation data is used. In addition, an obervation data for three stations (Hyytiälä, Melpitz and San Pietro Capofiume) is analysed and used. The 3 nm

nucleation rates are validated for these three measurement sites.

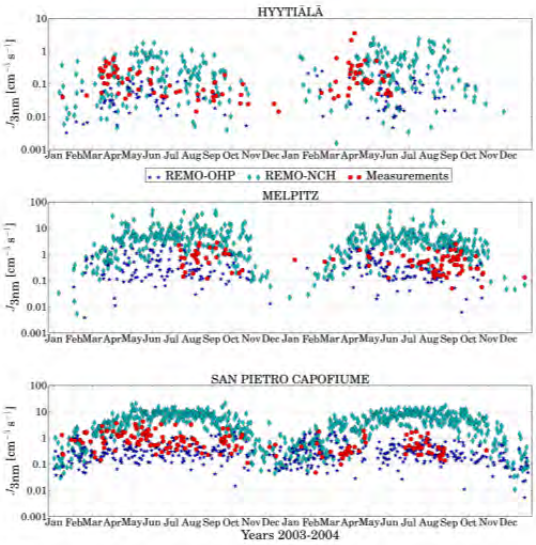


Figure 2. Measured and modelled daily mean J_{3nm} rates for event days at Hyytiälä, Melpitz and San Pietro Capofiume.

The J_{3nm} values in Fig. 2 show that the REMO-NCH overestimates the nucleation rates, especially at San Pietro Capofiume. REMO-OHP show better agreement, although some underestimation can be seen. Nevertheless, the improvement in the nucleation rates is significant and has a big impact on the modelled climate.

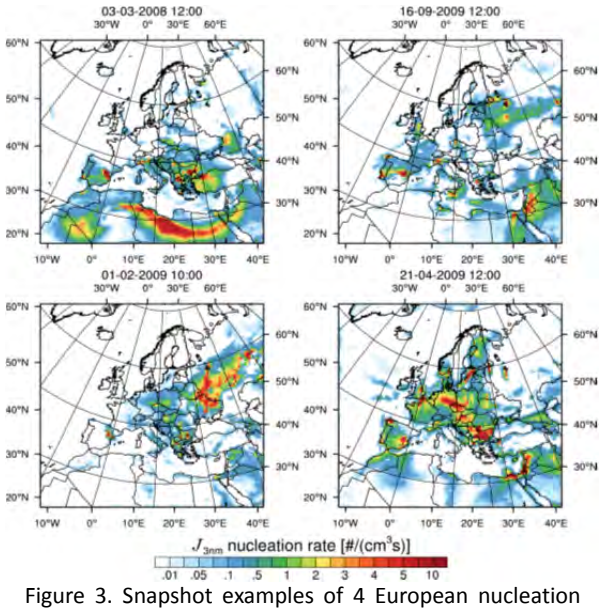


Figure 3. Snapshot examples of 4 European nucleation events.

Figure 3 shows examples of the spatial distribution of nucleation events over Europe. Depending on many variables, the events can be quite local or reach hundreds of kilometres in size. This is in good agreement with with previous studies of the spatial extent of nucleation (Crippa and Pryor (2013)). As an example, Fig. 3 (bottom right panel) also shows how big emission sources from Czech Republic can influence the nucleation over the whole Northern Germany.

4. Conclusions

In this work the underlying chemistry and the calculation of nucleation was improved. The results show better agreement with observations and clearly indicates improved state of the climate.

Many other characteristics of aerosol nucleations are studied in this work, for example the event start time, end time and length, nucleation frequency in terms of days per month, and the vertical extent of events. The analysis of these including more comprehensive comparison against observations will be shown at the Lund conference. The impacts of better presentation of aerosol nucletion related prosesses, mainly the OH-chemistry, will be discussed. Also the challenges related to using the OH-proxy will be shown.

References

Crippa, P. and Pryor, S. C. (2013) Spatial and temporal scales of new particle formation events in eastern North America. Atmos. Environ., 75, 257-264.

Kazil, J., Stier, P., Zhang, K., Quaas, J., Kinne, S., O'Donnell, D., Rast, S., Esch, M., Ferrachat, S., Lohmann, U., and Feichter, J. (2010) Aerosol nucleation and its role for clouds and Earth's radiative forcing in the aerosol-climate model ECHAM5-HAM. Atmos. Chem. Phys., 10, 10733-10752.

Kulmala, M., Vehkamäki, H., Petäjä, T., Dal Maso, M., Lauri, A., Kerminen, V.-M., Birmili, W. and McMurry, P.H. (2004) Formation and growth rates of ultrafine atmospheric particles: A review of observations. J. Aer. Sci., 35, 143-176.

Laaksonen, A., Hamed, A., Joutsensaari, J., Hiltunen, L., Cavalli, F., Junkermann, W., Asmi, A., Fuzzi, S. and Facchini, M. C. (2005) Cloud condensation nucleus production from nucleation events at a highly polluted region. Geophys. Res. Lett., 32, L06812.

Pietikäinen, J.-P., O'Donnell, D., Teichmann, C., Karstens, U., Pfeifer, S., Kazil, J., Podzun, R., Fiedler, S., Kokkola, H., Birmili, W., O'Dowd, C., Baltensperger, U., Weingartner, E., Gehrig, R., Spindler, G., Kulmala, M., Feichter, J., Jacob, D. and Laaksonen, A. (2012) The regional aerosol-climate model REMO-HAM. Geosci. Model Dev., 5, 1323-1339.

On the importance of inclusion of air-sea interactions in the simulation of austral summer precipitation over southern Africa using a regional model

J. V. Ratnam, Yushi Morioka, Swadhin K. Behera and Toshio Yamagata

Application Laboratory, JAMSTEC, Yokohama, Japan (jvratnam@jamstec.go.jp)

1. Introduction

Southern Africa (south of 10^{o}S) receives most of its precipitation during the austral summer season from October to March with peaks in precipitation during January to March (JFM). The intertropical convergence zone (ITCZ) reaches its southern most point in JFM and plays an important role in the precipitation over the tropical countries of southern Africa. The subtropical regions of southern Africa receive precipitation due to the interaction between the tropical processes and the extratropical transients.

The austral summer precipitation and its variations have been modeled using both the global and regional models. Few studies, for example Landman and Beraki (2012), Beraki (2014) have shown the improvement in the spatial and temporal distribution of the simulated precipitation due to inclusion of air-sea interactions in the global models. The studies of Ratnam et al. (2012) and Ratnam et al. (2013) showed that the inclusion of air-sea interactions is also important in the simulation of southern Africa precipitation using a regional model.

In this study, we extend out previous work using a fully coupled regional model with Weather Research and Forecast Model (WRF) as the atmospheric component and Regional Ocean Modelling System (ROMS) as the oceanic component. To bring out the importance of the air-sea interactions, two model runs are performed. The first is a fully coupled run and the second run is with standalone WRF model driven by the sea surface temperature (SST) simulated by the coupled model. The differences between the two runs can be thought to be due to the lack/inclusion of air-sea interactions in the model.

In the following sections, we present the description of the model and the methodology used along with the results of the study.

2. Model and Methodology

The WRF model (Skamarock et al., 2005) ARW Version 3.4.1 is used as the atmospheric component of the regional coupled model. WRF model with 23 vertical levels and a horizontal resolution of 27km covering a domain 47^{o}S-4^{o}S and 0.9^{o}E-67^{o}E is used in the study. The regional ocean model ROMS (Shchepetkin and McWilliams 2005) version 3.6 is used as the oceanic component of the regional model with forty vertical levels and with a horizontal resolution of 9km covering the same domain as the atmospheric model. The models are coupled using the Model Coupling Toolkit (MCT) (Larson et al., 2005; Jacob et al., 2005). The exchange of fluxes between the models takes place every six hours.

The restart file from the ocean model spinup run is used as the initial condition for the coupled model oceanic component and the coupled model runs are performed for a period spanning from 1995 to 2012. The first five years of the model run are considered as spinup and we analyzed the results from 2000 to 2012. The ERA Interim (Dee et al 2012) reanalysis fields are used as the boundary conditions for WRF model for the entire period.

3. Results

Comparison of the SST simulated by the coupled model with observed SST (Figure not given) shows that the oceanic component simulates a realistic distribution of SST with a cool bias of about 0.25 ^{o}C near the east coast of southern Africa. However, the coupled model has difficulty in simulation of SST in the Agulhas retroflection region.

The area averaged precipitation simulated by the model on the southern Africa land mass on comparison with GPCP estimated precipitation shows that the coupled model simulates the annual cycle realistically. Comparison of the annual cycle simulated by the coupled model (WRFC) and the WRF model runs with coupled SST (WRFCSST) shows that the air-sea interactions become important only during the simulation of the JFM precipitation. During other months the precipitation simulated by both the runs are similar.

Figure 1 shows the precipitation simulated by the coupled model. During JFM, ITCZ moves to its southern most point and produces large precipitation over Madagascar and tropical countries of southern Africa (Figure 1a). The precipitation band extending from the tropical region to extratropics through South Africa is due to the interaction between the tropical processes and extratropical transients.

The coupled model due to negative biases in the simulated SST near the east coast of southern Africa simulates less precipitation over most parts of southern Africa landmass compared to GPCP estimates (Figure 1b). The WRF model driven by the coupled model simulated SST also underestimates the precipitation over the landmass (Figure 1c). However, the difference between the simulated precipitation between the experiments shows that the two-tier approach of specifying the SST to an atmospheric model significantly increases the precipitation over the landmass (Figure 1d) showing the importance of including air-sea interactions in the simulation of southern Africa precipitation.

To bring out the importance of air-sea interactions more clearly, we performed WRF model runs with observed SST (WRFO) for the same period. Figure 2a shows the difference between the WRFO runs and GPCP estimated precipitation. From the figure it can be seen that the model significantly overestimates precipitation over southern Africa landmass. Compared to the coupled model simulated precipitation the WRFO runs overestimate the precipitation over southern Africa (Figure 2b).

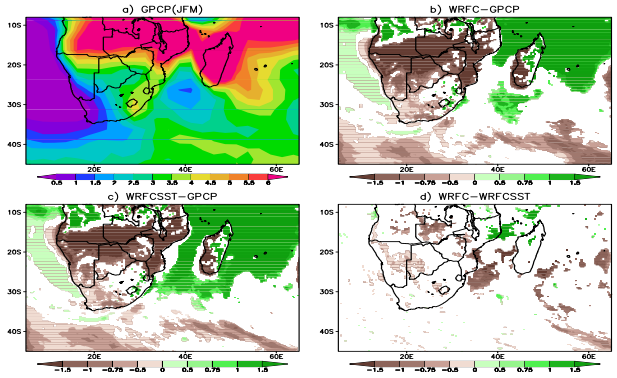


Figure 1. a) GPCP estimated JFM precipitation (mm/day) b) Significant difference between coupled model simulated precipitation and GPCP estimates c) difference in precipitation between WRFCSST and GPCP d) Difference between WRFC and WRFCSST simulated precipitation. Shaded regions in b),c) and d) are significant at 90% using t-test.

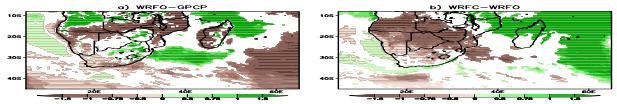


Figure 2. a) Difference between WRFO simulated precipitation and GPCP b) Difference between WRFC and WRFO simulated precipitation. Shaded values significant at 90% using t-test.

4. Conclusions

In this study we tried to understand the importance of inclusion of air-sea interactions in the simulation of austral summer precipitation over southern Africa using a regional coupled model. WRF model coupled to ROMS regional ocean model is used in this study. Two experiments were carried out. The first a fully coupled WRF model and the second was WRF model runs with coupled model simulated SST.

The difference in the precipitation between the two experiments showed that the two tier approach of specifying the SST to a regional atmospheric model tends to increase the precipitation over southern Africa. It may be necessary to include air-sea interactions even in its simple form as in Ratnam et al (2012), Ratnam et al. (2013) to improve the precipitation simulation over southern Africa using regional models.

References

Beraki, A.F, D.G. DeWitt, W.A. Landman and C. Oliver (2014), Dynamical seasonal climate prediction using an ocean-atmosphere coupled climate model developed in partnership between South Africa and the IRI. J. Climate, doi: http://dx.doi.org/10.1175/JCLI-D-13-00275.1

Dee, D. P., Uppala, S. M., Simmons, A. J., Berrisford, P., Poli, P., Kobayashi, S., Andrae, U., Balmaseda, M. A., Balsamo, G., Bauer, P., Bechtold, P., Beljaars, A. C. M., van de Berg, L., Bidlot, J., Bormann, N., Delsol, C., Dragani, R., Fuentes, M., Geer, A. J., Haimberger, L., Healy, S. B., Hersbach, H., Hólm, E. V., Isaksen, L., Kållberg, P., Köhler, M., Matricardi, M., McNally, A. P., Monge-Sanz, B. M., Morcrette, J.-J., Park, B.-K., Peubey, C., de Rosnay, P., Tavolato, C., Thépaut, J.-N. and Vitart, F. (2011), The ERA-Interim reanalysis: configuration and performance of the data assimilation system. Q.J.R. Meteorol. Soc., 137, 553–597. doi: 10.1002/qj.828

Jacob R, J Larson, and E. Ong (2005), MxN Communication and Parallel Interpolation in CCSM3 Using the Model Coupling Toolkit. Int. J. High Perf. Comp. App.,19, 293-307

Landman, W.A, and A. Beraki (2012), Multi-model forecast skill for mid-summer rainfall over southern Africa. Int. J. Climatol., 32, 303-314

Larson, J, R. Jacob, E. Ong (2005), The Model Coupling Toolkit: A New Fortran90 Toolkit for Building Multiphysics Parallel Coupled Models. Int. J. High Perf. Comp. App.,19, 277-292

Ratnam, J.V., S.K. Behera, Y. Masumoto, K. Takahashi, and T. Yamagata (2012), A simple regional coupled model experiment for summer-time climate simulation over southern Africa. Clim Dyn, 39, 2207-2217. DOI: 10.1007/s00382-011-1190-2

Ratnam, J. V., and Coauthors (2013), Dynamical Downscaling of Austral Summer Climate Forecasts over Southern Africa Using a Regional Coupled Model. J. Climate, 26, 6015–6032.

Skamarock, W.C. and Coauthors (2005), A description of the Advanced Research WRF version 2. NCAR Tech. Note TN-468+STR, 88pp

Shchepetkin AF, McWilliams JC (2005), The regional ocean modeling system: a split-explicit, free-surface, topography following coordinates ocean model. Ocean Model, 9, 347–404

Air-Sea Interactions in a Coupled Atmosphere-Ocean Model for the Baltic Sea

Thomas Raub[1,2], Andreas Lehmann[3], Daniela Jacob[1,2]

[1] Max Planck Institute for Meteorology, Hamburg, Germany (thomas.raub@mpimet.mpg.de)
[2] Climate Service Center, Helmholtz-Zentrum Geesthacht, Hamburg, Germany
[3] GEOMAR Helmholtz Centre for Ocean Research, Kiel, Germany

1. Introduction

In this study we investigate the air-sea interactions in a coupled atmosphere-ocean model for the Baltic Sea. We try to identify relevant feedbacks and the time scales they occur.

A potential negative feedback loop is illustrated in figure 1: In summer warm water in the mixed layer is separated by a seasonal thermocline from relatively cold water below. Strong winds can then lead to a deepening of the mixed-layer depth through turbulent mixing lowering the temperature of the mixed layer and thus of the sea surface. The cooler water surface may then lead to an increased stability of the atmospheric boundary layer above. This reduces the vertical momentum transport from the free atmosphere to the surface and thus the near surface wind speed, closing a negative feedback loop.

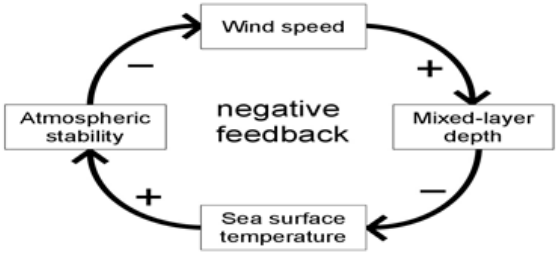


Figure 1. Schematic of a negative feedback loop for near-surface wind speed and SST.

2. Models and Method

The coupled model system is an updated version of BALTIMOS [Hagedorn et al. (2000)]. The atmosphere is represented by the hydrostatic version of the regional model REMO [Jacob (2001)] with a horizontal resolution of 1/6° (~18km) and the ocean by the Baltic Sea ice ocean model BSIOM [Lehmann & Hinrichsen (2000)] with a resolution of 2.5km.

The model is used to simulate a 20-year period from 1989 to 2008 with the ERA-Interim reanalysis from the ECMWF as lateral boundary conditions. The same setup is used to perform an uncoupled atmosphere-only simulation for comparison.

For our analysis we perform lead-lag-correlations for several variables from the coupled and uncoupled simulations on different time scales. Occurring feedback types can be identified via their specific statistical signatures [Frankignoul et al. (1977)].

3. Results

Figure 2 shows the lead-lag covariance of the 10m wind speed and the sea surface temperature (SST) from hourly values in summer (JJA) at a station in the central Baltic Sea, both for the unfiltered time series (solid lines) and for 50-day high-pass-filtered data (dotted lines) from the coupled simulation (black lines) and the atmosphere stand-alone run (red lines).

For the unfiltered data there is a relatively strong negative covariance when the 10m wind leads (positive lags) and very low covariance when the SST leads suggesting that only the wind influences the SST through changes of the mixed layer depth. For time scales shorter than 50 days the covariance shows a more anti-symmetric shape which indicates a closed negative feedback loop.

For the uncoupled simulation we find a similar behavior, however at a lower amplitude, especially when the SST leads. The relatively strong negative covariance for leading 10m winds results from the observed SSTs that contain imprints of wind-induced mixed-layer-depth changes.

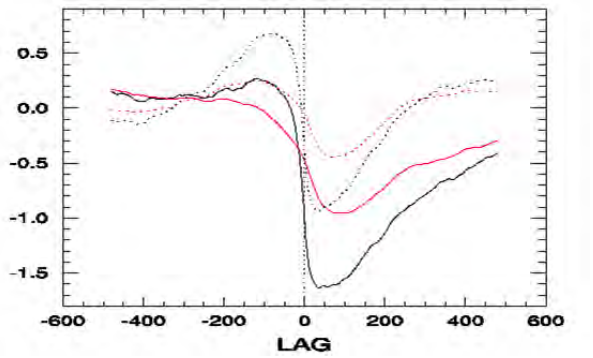


Figure 2. Lag covariance of hourly data of 10m wind and SST at a point in the central Baltic Sea in summer (JJA). Black lines represent results of the coupled model simulation, red lines of the atmosphere-only simulation. Solid lines stand for the covariance of the unfiltered time series and the dotted lines for 50-day high-pass filtered data. The 10m wind leads for positive lags and the SST for negative lags.

References

Hagedorn, R., A. Lehmann, and D. Jacob, (2000) A coupled high resolution atmosphere-ocean model for the BALTEX region. Meteorol. Zeitschrift, 9, pp. 7–20.

Jacob, D. (2001), A note to the simulation of the annual and inter-annual variability of thewater budget over the Baltic Sea drainage basin, Meteorol. Atmos. Phys., 77, pp. 61–73.

Lehmann, A., and Hinrichsen, H.-H. (2000) On the thermohaline variability of the Baltic Sea, J. Mar. Syst., 25, pp. 333–357.

Frankignoul, C., K. Hasselmann (1977) Stochastic climate models. II: Application to sea-surface temperature anomalies. Tellus, 29, pp. 284–305.

Impacts of aerosols in the CORDEX-Europe domain using the regional aerosol-climate model REMO-HAM

Armelle Reca C. Remedio[1], Claas Teichmann[1,2], Joni-Pekka Pietikäinen[3], Natalia Sudarchikova[1], Daniela Jacob[1], and Guy Brasseur[1]

[1] Climate Service Center, Helmholtz Centrum Geesthacht, Germany (armelle.remedio@hzg.de)
[2] Max Planck Institute for Meteorology, Hamburg, Germany
[3] Finnish Meteorological Institute, Helsinki, Finland

1. Introduction

Atmospheric aerosols influence the radiation budget of the Earth directly via scattering and absorption and via their influence on the development of clouds. The regional feedbacks due to aerosol-cloud-precipitation interaction in Europe can be assessed by including an aerosol module in a regional climate model. The aerosol model HAM (Stier et al., 2005) with the aerosol microphysics module M7 (Vignati et al., 2004) has been implemented to the atmospheric general circulation model ECHAM5 (Roeckner et al., 2003). HAM-M7 is an aerosol chemistry and physics model, which predicts the evolution of an ensemble of microphysically interacting internally- and externally-mixed aerosol populations as well as their size-distribution and composition. In order to use the detailed information about the aerosols, a double moment cloud scheme by Lohmann et al., (2007) has been implemented and fully coupled with the aerosol module. In this way, the aerosol information is used when the cloud droplet number concentration is calculated.

The HAM-M7 model has been implemented in the regional model REMO (Jacob and Podzun, 2006), which is called REMO-HAM and is developed by Pietikäinen et al. (2012). In this setup, the aerosol information is only passed to the stratiform (large scale) cloud scheme.

In Pietikäinen et al. (2012), the results from ECHAM5-HAM and REMO-HAM were compared against aerosol measurements from four different measurement sites. Their results indicated that the REMO-HAM were able to represent the observed aerosol concentrations and size distributions. The total number concentration simulated in ECHAM5-HAM showed similar patterns as REMO-HAM. Within the framework of the PEGASOS Project, regional climate simulations with focus on the study of aerosol-cloud-precipitation feedbacks are investigated. The main question that we attempt to address in the project is on how will currently planned air quality regulations affect climate? In this study, we are investigating the effects of aerosols on the European climate. Precipitation, temperature, and cloud cover variables are compared to quantify the changes between REMO-HAM and the standard version of REMO.

2. Methods

Several experiments are planned to investigate the regional feedbacks due to the aerosol-cloud-precipitation interaction using the REMO-HAM. They are listed in Table 1. The simulations are done using the coarse CORDEX Europe domain (Jacob et al., 2012) with spatial resolution of 0.44 degree (~50 km) with 27 vertical levels.

Table 1. List of simulations

Experiment	Description	Period
REMO-CTRL	REMO driven by ERA-Interim, European CORDEX Domain, 0.44°x0.44° horizontal resolution	2005-2009
REMO-HAM	REMO coupled with the HAM-M7 aerosol module driven by ERA-Interim, European CORDEX Domain, 0.44° x.44° horizontal resolution , AEROCOM emission dataset	2005-2009

In order to evaluate the impacts of the aerosol module in the climate conditions over Europe, the simulations of REMO-HAM are compared with the results from the standard model version of REMO, which is without the aerosol module (REMO-CTRL).

3. Results and discussions

The simulations with REMO-HAM are evaluated against the CRU monthly climatic observations (Harris, et al., 2013). Figure 1 shows the precipitation bias during summer for the last two years of the simulation (2008-2009). REMO-HAM has a tendency to produce higher values of total precipitation compared to the observations. Comparing the mean summer temperature, the coupled aerosol-climate simulation has a warm bias compared to observations (figure not shown). This result is similar to the one-year study of Pietikäinen et al. (2012).

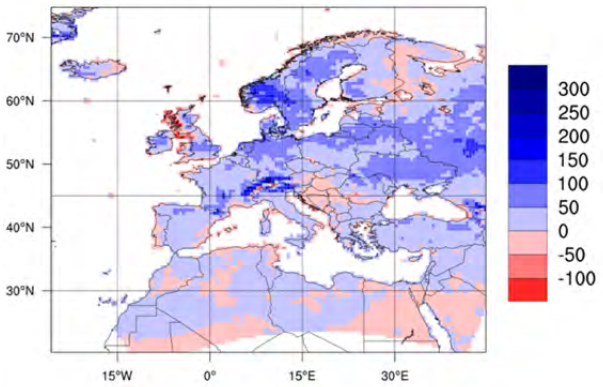


Figure 1. Mean summer total precipitation bias (%) of REMO-HAM against CRU for the summer of 2008-2009. Red (blue) shades indicate dry (wet) bias in REMO-HAM.

To investigate the indirect effect of aerosols, we compare the cloud cover of REMO-CTRL and REMO-HAM simulations. Figure 2 illustrates the difference between the coupled aerosol-climate and standard model. In general, the REMO-HAM simulation has a tendency to produce lower cloud fraction compared to the control simulation during the two-year period.

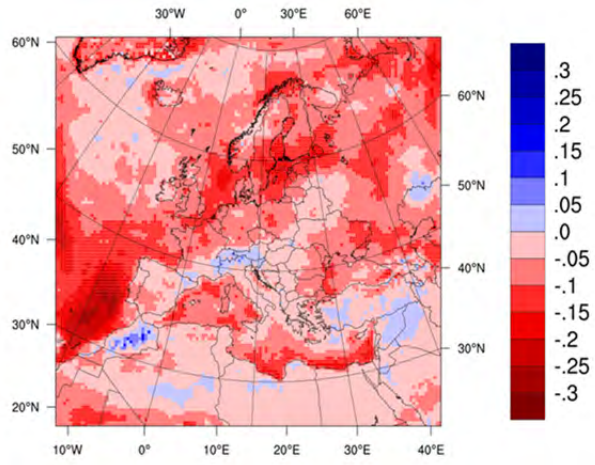


Figure 2. Mean summer cloud cover difference (*fraction*) of REMO-HAM and REMO-CTRL for 2008-2009 period. Red (blue) shades indicate less (more) cloud cover fraction in REMO-HAM than REMO-CTRL.

4. Conclusions and outlook

The impacts of coupling a regional model with an aerosol module is evaluated over the CORDEX European domain at a horizontal resolution of about 50 km. The aerosol-climate coupled model, REMO-HAM, is compared with observations and with the standard REMO model. Precipitation, temperature, and cloud cover fraction changes are detected. REMO-HAM has a tendency to have higher temperature and precipitation values and lower cloud cover fraction than REMO-CTRL during the summer of the last two years of the simulation (2008-2009). Note that the simulations investigated are only in the last two years. Further analysis will be done for the entire five-year simulation period and the changes in the latent and sensible heat fluxes.

References

Harris, I., Jones, P.D., Osborn, T.J., Lister, D.H. 2013. Updated high-resolution grids of monthly climatic observations–the CRU TS3.10 dataset. International Journal of Climatology, DOI: 10.1002/joc.3711.

Jacob, D. and Podzun, R.: Sensitivity Studies with the Regonal Climate Model REMO, Meteorol. Amtos. Phys., 63, 119-129, 1996.

Jacob D., Elizalde, A., Haensler, A., Hagemann, S., Kumar, P., Podzun, R., Rechid, D., Remedio, A. R., Saeed, F., Sieck, K., Teichmann, C., Wilhelm, C. 2012, "Assessing the Transferability of the Regional Climate Model REMO to Different COordinated Regional Climate Downscaling EXperiment (CORDEX) Regions", Atmosphere 3, no.1:181-199.P.

Lohmann, U., Stier, P., Hoose, C., Ferrachat, S., Kloster, S., Roeckner, E., and Zhang, J.: Cloud microphysics and aerosol indi- rect effects in the global climate model ECHAM5-HAM, At- mos. Chem. Phys., 7, 3425–3446, doi:10.5194/acp-7-3425-2007, 2007.

Pietikäinen, J.-P.; O'Donnell, D.; Teichmann, C.; Karstens, U.; Pfeifer, S.; Kazil, J.; Podzun, R.; Fiedler, S.; Kokkola, H.; Birmili, W.; O'Dowd, C.; Baltensperger, U.; Weingartner, E.; Gehrig, R.; Spindler, G.; Kulmala, M.; Feichter, J.; Jacob, D.; Laaksonen, A., 2012. The regional aerosol-climate model REMO-HAM. Geosci. Model Dev. Discuss., 5, 737–779, 2012.

Roeckner, E., Baeuml, G., Bonventura, L., Brokopf, R., Esch, M., Giorgetta, M., Hagemann, S., Kirchner, I., Kornblueh, L., Manzini, E., Rhodin, A.,

Schlese, U., Schulzweida, U., and Tompkins, A.: The atmospheric general circulation model ECHAM5. PART I: Model description, Max Planck Institute for Meteorology report series, Report No. 349, 2003.

Stier, P., Feichter, J., Kinne, S., Kloster, S., Vignati, E., Wilson, J., Ganzeveld, L., Tegen, I.,Werner, M., Balkanski, Y., Schulz, M., Boucher, O., Minikin, A., and Petzold, A.: The aerosol-climate model ECHAM5-HAM, Atmos. Chem. Phys., 5, 1125–1156, doi:10.5194/acp-5-1125-2005, 2005.

Vignati, E., Wilson, J. and Stier, P.: M7: An efficient size- resolved aerosol microphysics module for large-scale aerosol transport models, J. Geophys. Res., 109, D22202, doi:10.1029/2003JD004485, 2004.

Simulated canopy vegetation effects on snow conditions for a forest site using the Multi-Energy Balance option in SURFEX

Patrick Samuelsson[1], Aaron Boone[2] and Stefan Gollvik[1]

[1] Swedish Meteorological and Hydrological Institute, Norrköping, Sweden (patrick.samuelsson@smhi.se)
[2] CNRM -GAME (URA CNRS & Météo-France), Toulouse, France (aaron.a.boone@gmail.com)

1. Introduction

The double-energy balance concept in land-surface models (LSMs), introduced by e.g. Shuttleworth and Wallace (1985), is usually defined as a canopy vegetation layer modelled with a separate energy balance with respect to the energy balance of the underlying surface plus that turbulent fluxes within that canopy-underlying-surface layer relate to conditions in the canopy air space (Figure 1). The double-energy balance concept is used e.g. in the Rossby Centre Regional Climate Model, RCA3 and RCA4 (Samuelsson et al., 2011) and in the NWP model HIRLAM. The same concept is also applied for town energy balance models (TEBs), e.g. in SURFEX (Masson et al., 2013). In coupled climate-vegetation model systems the physical relevance of the coupling depends on how the models interact. RCA-GUESS (Smith et al., 2011) is an example of such a coupled system where the interaction between the models includes the double-energy balance concept.

2. Multi-Energy balance in SURFEX

This abstract describes how the double-energy balance concept in RCA has been generalized and introduced as a Multi-Energy Balance (MEB) concept in the externalized surface model SURFEX (Masson et al., 2013). "Multi" relates to the energy balances of a few possible underlying-surfaces, e.g. bare soil, understory vegetation, snow and inundated water. SURFEX provides an attractive surface model developing platform since it includes many surface physical options and since it can be applied offline, forced by e.g. observations, as well as online coupled to an atmospheric code, e.g. ARPEGE, AROME or ALARO.

MEB is developed to be applicable for any type of vegetation, from tall forest to short grass, in combination with snow. As illustrated in Figure 1, in the presence of snow, a few combinations can appear. As long as any snow does not totally cover the canopy vegetation we model energy fluxes between, in this case, three sub-surfaces, canopy vegetation (v), ground (g) and snow (n), and the lowest model level. When the snow depth is of similar depth as the height of the canopy vegetation the snow energy fluxes relate to both the canopy air space and the lowest model level. When the canopy vegetation is totally covered by snow the snow energy fluxes are disconnected from any remaining canopy air space (snow cover less than 100%). MEB is designed to smoothly and continuously change between these cases as a function of the ratio between snow depth and the height of the vegetation.

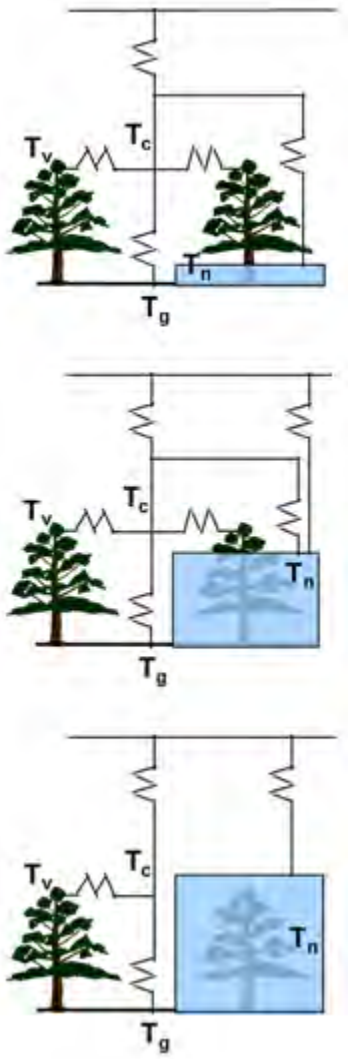


Figure 1. Illustration of three MEB combinations of vegetation and snow. The aerodynamic resistances between the different sub-surfaces and lowest model level are illustrated by zigzag lines. Surface temperatures represent vegetation, T_v, ground, T_g and snow T_n. The canopy air space temperature is represented by T_c. Top panel shows snow well below the canopy vegetation, middle panel canopy vegetation partly covered by snow and bottom panel canopy vegetation totally covered by snow. Snow fraction is lower than 100% in all cases.

The shortwave (SW) and longwave (LW) radiation in the canopy air space is modelled using a one-reflection model. Two wave-length bands are used for SW to account for different surface albedo properties. SW is also treated differently for direct and diffuse radiation since especially the partition of direct SW radiation between the canopy vegetation and the underlying surface is heavily dependent on sun elevation.

Leaf-Area Index (LAI) is one of the crucial physiographic parameters for MEB since LAI decides how the aerodynamic resistances in the canopy-air space relate to each other and how the partition of SW and LW radiation is done between the canopy vegetation and the underlying surface(s). In SURFEX, physiographic parameters are usually provided by ECOCLIMAP (Faroux et al. 2013) but can also be specified for a specific site in offline mode.

MEB is fully implemented in a development version of SURFEX (used for results presented here) and will be officially available as an option in the next release of SURFEX (v8 to be released summer 2014).

3. SURFEX-MEB applied to the Sodankylä site

In Sodankylä, northern Finland, the Finnish Meteorological Institute operates the Artic Research Centre (FMIARC) where plenty of boundary-layer and surface data are measured continuously. For MEB development and evaluation we have used a number of data; temperature, humidity, winds and sensible and latent heat fluxes collected at 18 m height in a tower positioned in the pine forest and radiation components and snow depth collected in nearby forest clearings.

Figure 2 shows how SURFEX-MEB simulated snow depth compares to observed snow depth for the winter season 2008-2009. To make observed and simulated heat fluxes to compare well (not shown) LAI has to be set to 1.5 which is close to the estimated value of 1.2 of the pine forest. However, simulated snow depth does not fit well with observed snow depth in this case. The snow melts too slowly in the spring.

Assuming that the tower meteorological data is representative also for the atmospheric conditions above the forest clearings we can show that a much lower LAI (0.05) is needed to make observed and simulated snow depth to compare better. Area fraction vise such a low LAI corresponds to only 2% forest cover (using the sky-view factor relationship for LW radiation).

4. Comments

In addition to the Sodankylä experiment we have performed a number of offline 2D simulations. The Sodankylä results and the 2D results both give the delayed snow-melt-effect that forest canopy vegetation has on snow conditions. In current official SURFEX this effect is lacking and therefore the simulated river discharge peak for forest dominated drainage basins with snow usually appears too early.

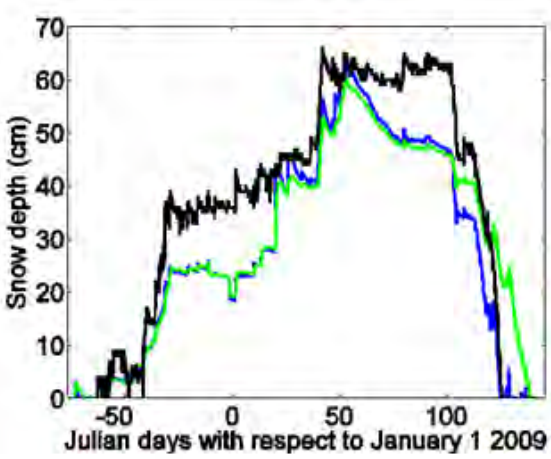


Figure 2. Sodankylä snow depth for the period October 15 2008 – May 26 2009. Blue and green lines represent simulated snow depth for LAI=0.05 and LAI=1.5, respectively. Black line represents observed snow depth.

References

Faroux, S., Kaptué Tchuenté, A. T., Roujean, J.-L., Masson, V., Martin, E., and Le Moigne, P. (2013) ECOCLIMAP-II/Europe: a twofold database of ecosystems and surface parameters at 1 km resolution based on satellite information for use in land surface, meteorological and climate models, Geosci. Model Dev., 6, 563-582, doi:10.5194/gmd-6-563-2013.

FMIARC, http://fmiarc.fmi.fi

Masson, V., et al. (2013) The SURFEXv7.2 land and ocean surface platform for coupled or offline simulation of earth surface variables and fluxes, Geosci. Model Dev., 6, 929-960, doi:10.5194/gmd-6-929-2013.

Samuelsson, P., Jones, C., Willén, U., Ullerstig, A., Gollvik, S., Hansson, U., Jansson, C., Kjellström, E., Nikulin, G. and Wyser, K. (2011) The Rossby Centre Regional Climate Model RCA3: model description and performance, Tellus, 63A, doi: 10.1111/j.1600-0870.2010.00478.x

Shuttleworth, W. J. and Wallace, J. S. (1985) Evaporation from sparse crops-an energy combination theory, Q. J. R. Meteorol. Soc, 111, 839–855.

Smith, B., Samuelsson, P., Wramneby, A. and Rummukainen, M. (2011) A model of the coupled dynamics of climate, vegetation and terrestrial ecosystem biogeochemistry for regional applications, Tellus, 63A, doi: 10.1111/j.1600-0870.2010.00477.x

The sensitivity of major Baltic inflows simulated with the RCM NEMO-Nordic

Semjon Schimanke[1], Christian Dieterich[1], Matthias Gröger[1] and H.E. Markus Meier[1,2]

[1] Swedish Meteorological and Hydrological Institute (SMHI), Norrköping, Sweden (Semjon.Schimanke@smhi.se)
[2] Department of Meteorology, Stockholm University, Stockholm, Sweden

1. Introduction

Major Baltic inflows (MBI) are an important feature to sustain the sensitive steady state of the Baltic Sea. Beside a certain succession of SLP patterns (Matthäus and Schinke, 1994, Schimanke et al., submitted), fluctuations of other factors are known to support or hamper MBIs on different time scales. For instance, part of the preconditioning of the Baltic Sea starts already in late summer long before the inflow season (September to April). On the other hand, prevailing conditions at the time of the (potential) MBI affect the event as well. Here, we will test in a series of sensitivity experiments the importance of contributing circumstances as suggested in the literature, for instance, the occurrence of high pressure areas over the Baltic from late summer to autumn (Schinke and Matthäus, 1998), the role of river runoff and net precipitation (e.g. Meier and Kauker, 2003), and prevailing water masses in the entrance area of the Baltic Sea (Meier et al., 2006).

2. Model and Method

To simulate the intrusion of heavy salt water through the narrow Danish Straits into the deep basins of the Baltic Sea high-resolution models are needed. Here, we use the recently established ocean RCM NEMO-Nordic (Dieterich et al, submitted). NEMO-Nordic is setup with a horizontal resolution of 2 nautical miles (~3.7km) and 56 vertical levels. Atmospheric forcing comes from the atmospheric RCM RCA4 which is driven by ERA40 and ERA-interim, respectively.

Daily output of salinity, temperature, volume and salt transport will be analysed.

3. Sensitivity simulations and working hypotheses

Some of the largest and best-observed MBIs occurred in January 1993 and January 2003. These events will be tested intensely with respect to the previously mentioned factors. For instance, in how far is the occurrence of the MBI dependent on the preconditioning in late summer/autumn of 1992 or 2002, respectively? Does the amount of freshwater input into the Baltic Sea at the time of the occurrence effect the MBI? In general, do factors exist which could have prevented the occurrence of the MBIs independent of the main driving parameters SLP fluctuations and corresponding wind fields?

References

Dieterich, C. and others (submitted): Surface Heat Budget over the North Sea in Climate Change Simulations, submitted to Tellus

Matthäus, W. and Schinke, H. (1994): Mean atmospheric circulation patterns associated with major Baltic inflows, Deutsche Hydrografische Zeitschrift, 46, 321–339, doi:10.1007/BF02226309, http://dx.doi.org/10.1007/BF02226309

Meier, H. E. M. and Kauker, F.: Modeling decadal variability of the Baltic Sea: 2. Role of freshwater inflow and large-scale atmospheric circulation for salinity, Journal of Geophysical Research, 108, 3368, doi:10.1029/2003JC001799, 2003.

Meier, H. E. M., Feistel, R., Piechura, J., Arneborg, L., Burchard, H., Fiekas, V., Golenko, N., Kuzmina, N., Mohrholz, V., Nohr, C., Paka, V. T., Sellschopp, J., Stips, A., and Zhurbas, V. (2006): Ventilation of the Baltic Sea deep water: A brief review of present knowledge from observations and models, OCEANOLOGIA, 48, 133–164

Schimanke, C. Dieterich, H.E.M. Meier (submitted) An algorithm based on sea level pressure fluctuations to identify major Baltic inflow events, submitted to Tellus A

Schinke, H. and Matthäus, W. (1998): On the causes of major Baltic inflows - an analysis of long time series, Continental Shelf Research, 18, 67 – 97, doi:10.1016/S0278-4343(97)00071-X, http://www.sciencedirect.com/science/article/pii/S027843439700071X, 1998.

Regionally coupled modelling of the Tropical Atlantic

Dmitry Sein[1], William Cabos[2] and Daniela Jacob[3]

[1] Alfred Wegener Institute, Bremerhaven, Germany (dmitry.sein@awi.de)
[2] University of Alcala, Alcala, Spain
[3] Climate Service Center, Hamburg, Germany

1. Introduction

Currently, Global Coupled Models (GCMs) have difficulty capturing key phenomena and achieving accurate climate projections on regional and local scales because limitations in computer power do not allow them to reach the necessary horizontal resolutions. Regional climate models (RCMs) provide dynamically downscaled climate information within the region of interest, improving this drawback of current GCMs. At this point, naturally raises the question of how much, if any, the RCM can improve the GCMs results. It has been argued that regional models can reproduce an observed climatology but are not able to predict the change of the climatology in response to a changing climate (e.g. Kerr, 2013). However, Feser et al. (2011) could demonstrate an added value in those parameters that exhibit high spatial variability such as near surface temperature in different regional atmospheric models. They show that the added value originates mainly from the higher resolved orography in the regional models.

2. Regional atmosphere-ocean climate models

However, there are cases when fine scale atmosphere-ocean feedbacks can substantially influence the spatial and temporal structure of regional climate (Li et al., 2012). Recent studies have shown that regional atmosphere-ocean climate models (RAOCMs) are capable of simulating these features of the climate system. Compared to global coupled atmosphere-ocean models, RAOCMs could go for much higher resolution, providing a more accurate representation of the morphological complexity of the land-sea contrasts and relevant mesoscale processes and the associated energy and mass air-sea exchanges. The combination of these factors allows RAOCMs to bring additional added value in those regions where they are important. For instance, Ratnam et al. (2008) found that coupling considerably improved the simulation of the Indian monsoon rain band over both the ocean and land areas.

3. The ROM model

ROM is a RAOCM comprised of the REgional atmosphere MOdel (REMO), the Max Planck Institute Ocean Model (MPIOM), the HAMburg Ocean Carbon Cycle (HAMOCC) model, and the Hydrological Discharge (HD) model which are coupled via OASIS coupler. All the models but REMO are run in a global configuration. MPIOM has high horizontal resolution in the region of interest and its global domain is divided into two different subdomains: coupled, where the ocean and the atmosphere are interacting, and uncoupled, where the ocean model is driven by prescribed atmospheric forcing and runs in a so-called stand-alone mode. Therefore, choosing a specific area for the regional atmosphere we can assume that in that area the ocean-atmosphere system is “free”, whereas in the remaining areas the ocean circulation is driven by prescribed atmospheric forcing.

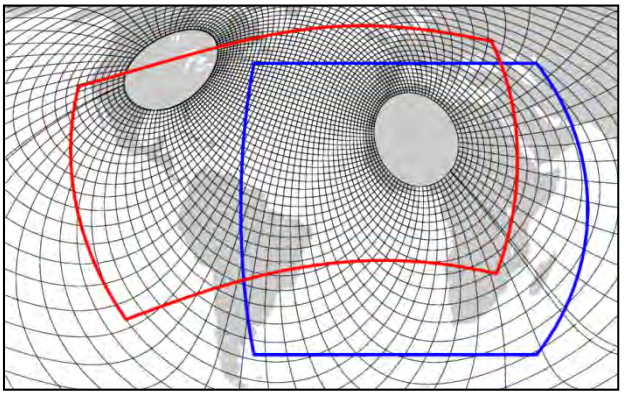


Figure 1. MPI-OM TR04 setup (black lines). REMO-DEP setup (blue line) and REMO-NAT setup (red line). Every 12th grid line is shown.

4. Tropical Atlantic simulations

A set of experiments were carried with different combinations of MPIOM and REMO configurations, as illustrated in Fig 1. The MPI-OM TR04 horizontal resolution reaches 10 km in the North Tropical Atlantic and gradually diminishes, reaching 200 km in the southern oceans The model has 40 vertical levels with increasing level thickness. For REMO we use two different horizontal domains labeled DEP and NAT. Both the domains include the TA region and are defined as follows: 1) DEP extending to the South Atlantic, with Africa and part of the Indian Ocean and Mediterranean region inside the domain and 2) NAT which covers a large portion of North and South America and also the North Atlantic, the Eastern tropical Pacific and the Mediterranean Sea. The model was forced with different realizations of the present day climate with the MPI-ESM Global Circulation Model. Here we present results obtained with the DEP REMO setup.

5. Results

As reported in other studies (e. g. Ratnam et al. 2008), RAOCMs can bring added value not only to near surface temperature, but also to precipitation, as shown by Ratnam et al. (2008) for the Indian Monsoon precipitation. In this work we investigate if our model can

bring added value in the simulation of the Tropical Atlantic (TA) climate. In fig.2 we compare the ROM precipitation with observations, the stand alone REMO and the MPI-ESM realization used to force both ROM and the RCMs.

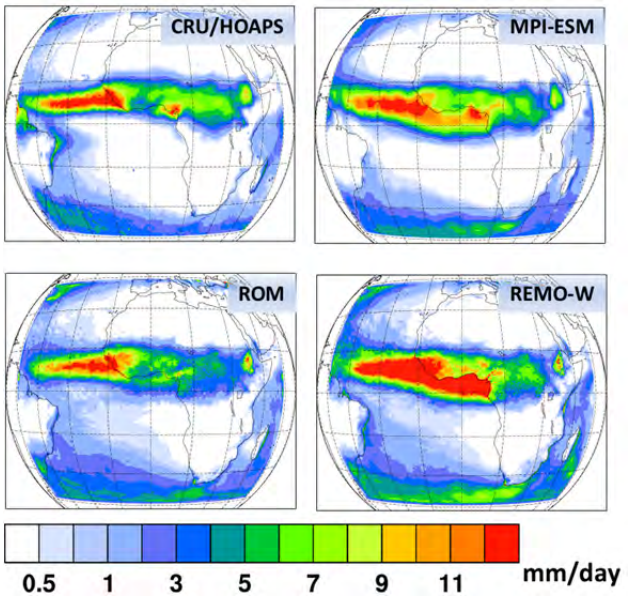


Figure 2. JJA precipitation for the 1966-1975 period. CRU-HOAPS is a blend of HOAPS oceanic and CRU land precipitation data sets. MPI-ESM is the model used to force the ROM and stand-alone REMO configuration. ROM is run in the DEP setup.

ROM precipitation is clearly closer to CRU/HOAPS than MPI-ESM, especially over the ocean. Moreover, ROM simulates the ITCZ better than stand alone REMO. This point to the fact that coupling contributes significantly to the added value in regions where air-sea interaction is important.

The added value from AORCMs is not restricted to the atmosphere. Regional coupled models can also show better results than the forcing GCMs in the ocean component. ROM shows a better representation of the climatology and interannual Tropical Atlantic variability. In figure 3 we represent the correlation of the ORAS4 reanalysis sea surface temperatures with MPI-ESM and ROM forced by MPI-ESM for ensembles of 10 years simulations. ROM shows clearly better SST variability in the Tropical Atlantic region. In particular near the North Africa where the most of the Tropical Cyclones are generated.

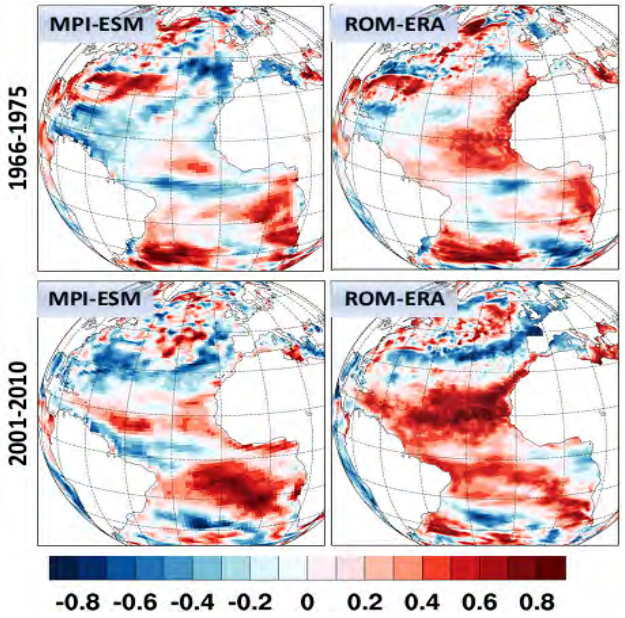


Figure 3. SST correlation between the ORAS4 and MPI-ESM (left column) and ROM-DEP (right column) for the 1966-1975 and 2001-2010 periods.

6. Conclussions

The coupling to an active ocean provides further added value to the REMO RCM when compared to the global MPI-ESM. The smaller-scale air-sea feedbacks resolved in ROM provide a better representation of the precipitation, especially over the ocean and also improve the simulation of oceanic variables, like the SST.

References

Feser, F. , Rockel, B., von Storch, H., Winterfeldt, J., and Zahn, M. (2011) Regional Climate Models add Value to Global Model Data: A Review and selected Examples. Bulletin of the American Meteorological Society, doi: 10.1175/2011BAMS3061.1.

Kerr, R.A. (2013) Forecasting Regional Climate Change Flunks Its First Test, Science, vol. 339, pp. 638-638, 2013. http://dx.doi.org/10.1126/science.339.6120.638

Li, H., M. Kanamitsu, and S.-Y. Hong (2012) California reanalysis downscaling at 10 km using an ocean-atmosphere coupled regional model system, *J. Geophys. Res.*, **117**, D12118, doi:10.1029/2011JD017372

Ratnam, J.V., Giorgi, F., Kaginalkar, A., Cozzini, S. (2008) Simulation of the Indian monsoon using the RegCM3-ROMS regional coupled model. *Clim. Dyn*. **33**, 119-139.

Future climate change RCP4.5 and RCP8.5 scenarios downscaling for the Northern Europe with the focus on the North and Baltic Seas.

Dmitry Sein[1], William Cabos[2] and Daniela Jacob[3]

[1] Alfred Wegener Institute, Bremerhaven, Germany (dmitry.sein@awi.de)
[2] University of Alcala, Alcala, Spain
[3] Climate Service Center, Hamburg, Germany

1. Model setup

The REgional atmosphere MOdel **REMO** (Jacob, 2001) with 37km resolution and 27 hybrid vertical levels is coupled to the global ocean – sea ice – marine biogeochemistry model **MPIOM/HAMOCC** (Marsland et al., 2003) with increased resolution on the North-West European Shelves (up to 4 km in the German Bight). The coupled domain includes Europe, the North-East Atlantic and part of the Arctic Ocean (Fig.1). The models are coupled via the **OASIS** coupler. In addition, the ocean model was run with ocean tides and better representation of the diurnal cycle (one hour coupled time step). The last two modifications make one of the major differences from the MPI-ESM CMIP5 simulations, where the diurnal cycle and tidal dynamics were neglected. The ocean tidal forcing was derived from the full ephemeridic luni-solar tidal potential. The global Hydrological Discharge model **HD**, which calculates river runoff (0.5º horizontal grid resolution), is coupled to both the atmosphere and ocean components.

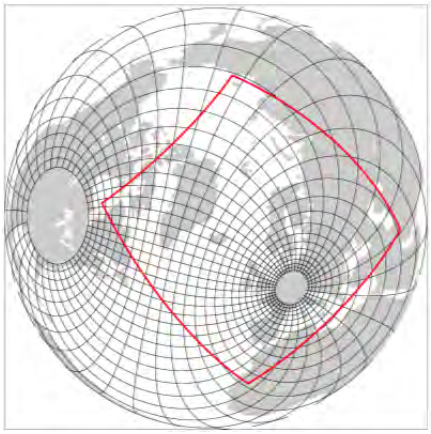


Figure 1. Grid configuration: the red "rectangle" indicates the coupled domain (REMO model) black lines indicate the grid of the MPIOM/HAMOCC. For the ocean/sea ice grid only every 15th line is shown.

Lateral atmospheric and upper oceanic boundary conditions outside the coupled domain were prescribed using MPI-ESM C20 20-th century, RCP4.5 and RCP8.5 scenarios data (the total simulation period was 1920-2005 + 2 x 2006-2100) for corresponding scenarios downscaling. The model was spun-up for the period 1920-2000. Then the **scenario** runs (21st century) and in parallel a **control** run (20th century forcing) were carried out.

2. Hindcast simulations with MPI-ESM forcing

The simulated mean winter 2m temperature (T2M) biases are shown on Fig.2. REMO/MPIOM and driving MPI-ESM show quite different behavior. Whereas MPI-ESM simulates better T2M in the North-eastern Europe, in other European regions, i.e. Central and Southern Europe REMO/MPIOM shows better results.

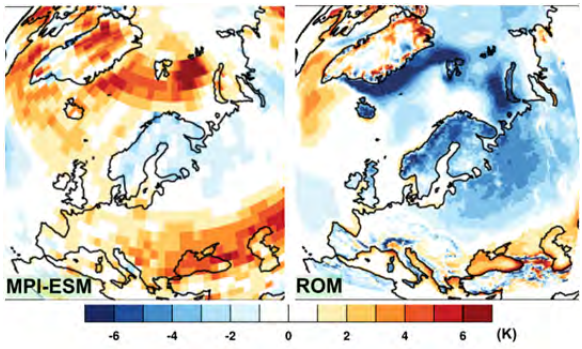


Figure 2. Mean DJF 1980-2000 2m temperature difference (Model – ERA40) Left: MPI-ESM, Right: REMO/MPIOM.

The simulated sea surface temperature (SST) and sea surface salinity (SSS) biases are shown on Fig.3. The Climatology of the North Sea is represented quite well, but the simulated Baltic Sea is to cold (1-2K) and to salty (1-1.5psu). Higher salinity in the Baltic Sea can be explained by the overestimation of the water inflow from the North Sea.

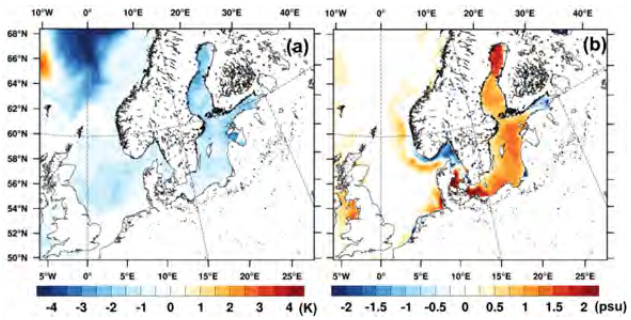


Figure 3. Annual mean 1980-2000 SST (left) and SSS (right) difference (Model – GDEM climatology)

The cold SST bias in both the North Sea and Baltic Seas is mainly caused by the cold atmospheric bias over the North-eastern Europe (Fig.2)

3. Climate change. Atmosphere.

Changes in T2M and total precipitation are presented on the Fig.4. Whereas the Arctic amplification is seen in both the scenarios, the warming signal in RCP4.5 and RCP8.5 is different for the Europe. The stronger warming in case of RCP8.5 enhances the hydrological cycle in the Eastern Europe up to 20-50%.

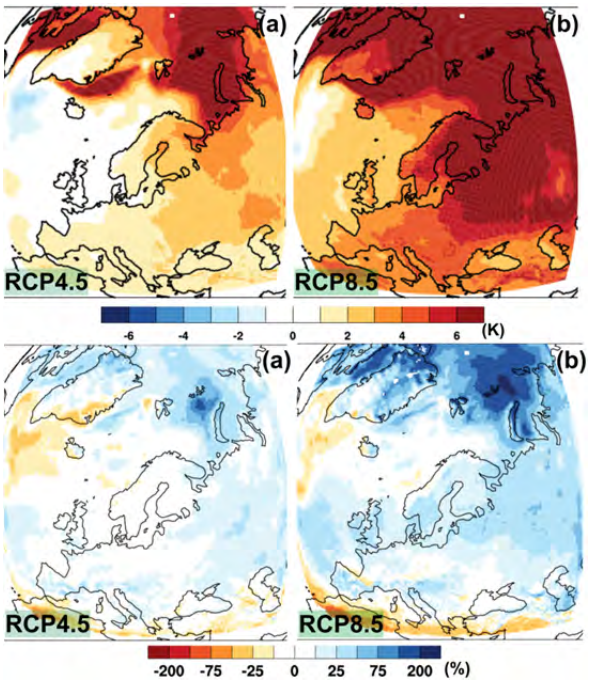


Figure 4. Mean DJF 2m temperature (upper) and relative precipitation (lower) change (2080-2099 – 1980-1999) obtained for RCP4.5 (left) and RCP8.5 (right)

4. Climate change. Ocean

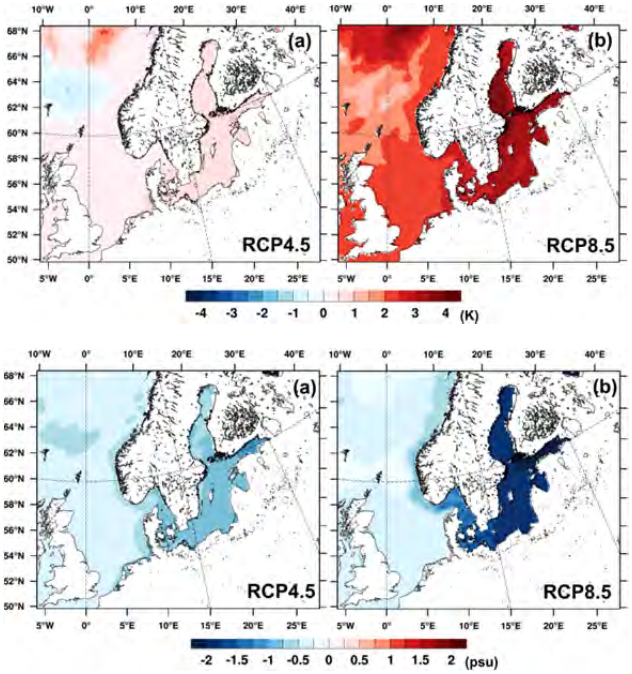


Figure 5. Annual mean SST (upper) and SSS (lower) differences (2080-2099 – 1980-1999) obtained for RCP4.5 (left) and RCP8.5 (right)

To analyze the climate changes in the Baltic and the North Sea regions we provide a comparison between two last decades of the 20th and 21st century for both the RCP4.5 and RCP8.5 scenarios (Fig.5). The warming is substantially different for both the scenarios. In case of RCP4.5 it is in the range of interdecadal variability. The simulated SST change by the end of the 21st century in case of RCP8.5 is much higher reaching up to 4K in the Baltic Sea.

The SSS change in the North Sea is relatively small similar for both the scenarios (Fig.4). In opposite, the changes in the Baltic Sea are much stronger pronounced in the case of RCP8.5. The freshening there reaches more than 2 psu. The main reason for this freshening is the simulated increase of winter precipitation in the Baltic Sea catchment area.

5. Conclusions

The downscaled RCP4.5 scenario shows relatively small changes in the North and Baltic Seas. Both the SSS and SST changes (except of SSS in the Baltic) obtained by RCP4.5 simulations are in the range of interdecadal variability.

The most pronounced changes corresponding to downscaled RCP8.5 scenario projection for the North European shelves were obtained in the Baltic Sea. Global warming will affect the Baltic Sea primarily through an enhancement of the hydrological cycle which delivers more moisture from the tropics towards the poles. The resulting increase of precipitation over the Baltic Sea catchment area leads to substantial increase of the river runoff which is much stronger than in surrounding areas.

References

Aldrian, E., D.V.Sein, D.Jacob, L.D.Gates and R.Podzun (2005) Modelling of Indonesian Rainfall with a Coupled Regional Model. Climate Dynamics **25**, pp. 1–17

Jacob, D. (2001) A note to the simulation of the annual and interannual variability of the water budget over the Baltic Sea drainage basin. Meteorology and Atmospheric Physics, **77**, 1-4, 61-73

Johannessen, J.A., E. Svendsen, S. Sandven, O.M. Johannessen and K. Lygre, (1989) Three-Dimensional Structure of Mesoscale Eddies in the Norwegian Coastal Current. J. of Physical Oceanography, **19**, pp.3-19

Marsland,S.J., H. Haak, J.H. Jungclaus, M. Latif and F. Roeske, (2002) The Max-Planck-Institute global ocean/sea ice model with orthogonal curvilinear coordinates, Ocean Modelling, **5**, No. 2, pp. 91-126

Recent development in regional earth system modelling

Jun She, Tian Tian, Kristine S. Madsen, Jacob W. Poulsen, Per Berg and Lars Jonasson

Centre for Ocean and Ice, Danish Meteorological Institute, Copenhagen, Denmark

1. Hindcasts and projections based on coupled atmosphere-ocean-ice models HIRHAM-HBM for Baltic-North Sea

DMI coupled RCM-ocean-ice model HIRHAM-HBM has been applied in hindcast (Tian et al. 2013) and IPCC AR5 projection studies. The hindcast results show that the system is stable and gives better quality in SST and sea ice in Baltic Sea than ERA-Interim, and suitable for climate projection studies. The projection runs are still on-going and results will be reported in the meeting.

2. Seasonal forecasting experiments in Baltic-North Sea

DMI RCM-ocean-ice-ecosystem model HIRHAM-HBM-ERGOM is applied in a seasonal forecasting experiment in Baltic-North Sea with a dynamic downscaling from ECMWF seasonal forecast. Fig. 1 displays results from a 5-month forecast starting from 1 Jan. 2013.

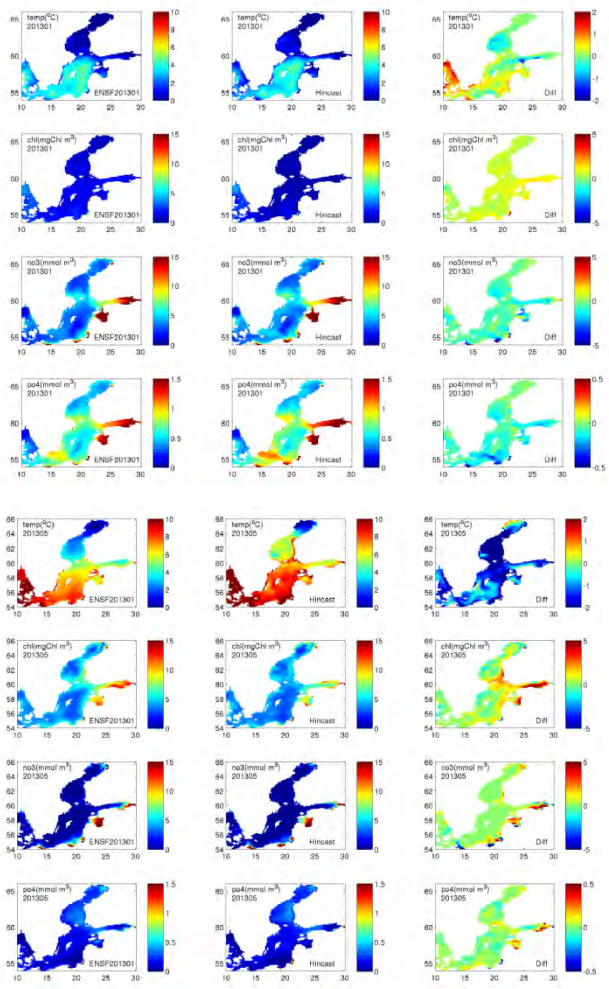


Fig. 1 Five-month prediction of SST, Chl-a, nitrogen and phosphate, starting from 1 Jan. 2013. Upper panel for the first month and lower for the fifth month. The rows (top-down) represent results for SST, Chl-a, Nitrogen and Phosphate with ensemble prediction mean in left column, hindcast in mid-column and difference in right.

It was found that both ocean temperature and nutrients have certain prediction skills in seasonal scale although they decayed with time. Certain areas such as southern Baltic Sea has higher forecast skills than other areas.

3. Coupled system for the Arctic

DMI recently develop a high resolution fully coupled regional model system that describes ocean, atmosphere and sea ice processes in the Arctic Ocean and North Atlantic. The system has been developed using three existing models, the high resolution regional climate model HIRHAM5, the regional ocean model HYCOM and the CICE model that describes sea ice dynamics. These models have been interactively coupled which enables us to perform experiments examining the relative importance of ocean and atmospheric forcing as well as internal dynamics, to explain the recent rapid decline of Arctic sea ice. Analysis of the model results indicates the model can successfully reproduce the interannual and seasonal variability in sea ice extent. This opens up the possibility of a range of process based experiments as well as simulations to project the future of Arctic sea ice that we plan to run using the EC-Earth GCM as boundary forcing. The inclusion of a sophisticated surface snow scheme in the RCM means that we can also examine the impact of sea ice on the surface mass balance of the Greenland ice sheet as well as more generally on the climate of the Arctic region. Future work aims to use the model system to make climate projections for the Arctic.

4. High Performance Computing and next generation pan-European earth system model

To generate more consistent and accurate climate information for climate adaptation and mitigation, high resolution coupled atmosphere-ocean-ice models are needed in large regional scale, e.g., pan-European and Arctic-N. Atlantic scales. The computational load of these models can be hundreds times heavier than current global coupled models (e.g. those used in IPCC AR5). The vision is to make the regional coupled models efficient on both multi- and many-core architecture. To reach this goal, the most challenging part is the ocean model optimization as the model domain is highly irregular with straits of a few hundred meter width to open ocean in a scale of a few thousand kilometres. Based on achievements made in PRACE project ECOM-I (Next generation pan-European coupled climate-ocean model – phase 1), we will show results in optimizing a pan-European two-way nested ocean-ice model, with

focusing on coding standard, I/O, halo communication, load balance and multi-grid nesting. The optimization was tested on different architectures e.g. Curie Thin, CRAY XT5/XT6 and Xeon Phi etc. The results also show that different model setups lead to very different computational complexity. A single real domain setup for Baffin Bay shows scalability to 16000 cores and Amdahl ratio of >99.5% (Fig. 2 and Fig. 3).

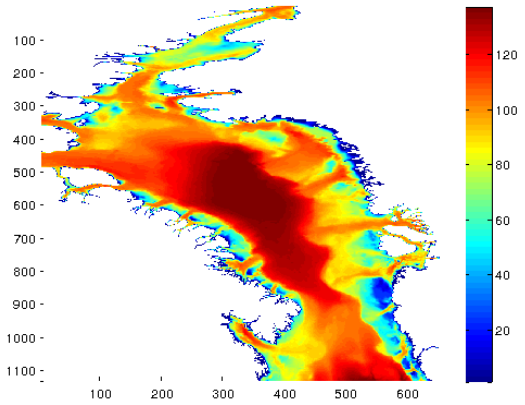


Fig. 2 Baffin Bay Setup with 1nm resolution

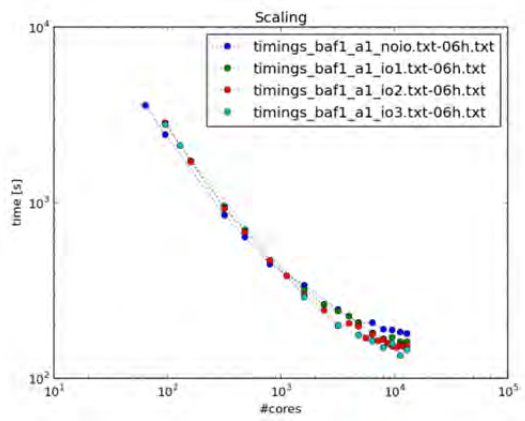


Fig. 3 Scaling and speedup performance of HBM Baffin Bay setup

Preliminary optimization has been made for using HBM (4 nested domain setup) on many-core architecture Xeon-Phi. We have reached a good load balance and Amdahl parallel ration reached 99.5% up to 60 threads and 99-99.25% for 240 cores (Fig. 4).

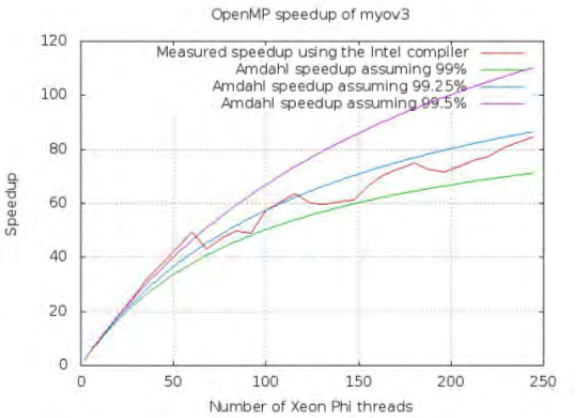


Fig. 4 Threading performance of HBM Baltic-North Sea setup on Xeon-Phil

However, a pan-European setup with nine interconnected nesting domains (Fig. 5) only reaches scalability of less than 2000 cores and an Amdahl ratio 92%. For high resolution (2-5km) pan-European earth system models, significant improvements in HPC have to be made in order to take advantage from next generation architecture. A roadmap for next generation pan-European coupled climate models for many-core architecture will be discussed.

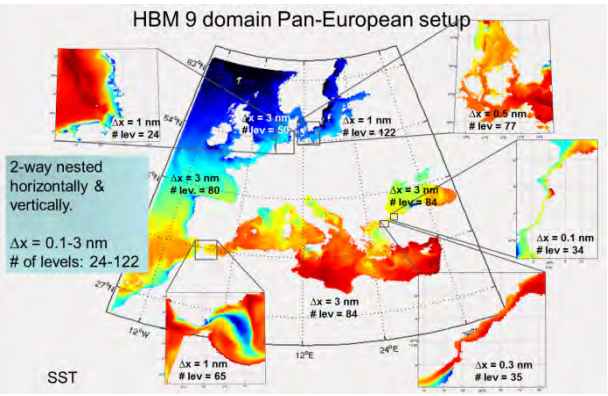


Fig.5 HBM pan-European model setup: horizontal resolution and number of vertical layers are illustrated for each of the nine domains.

References

T. Tian, F. Boberg, O.B. Christensen, J.H. Christensen, J. She, T. Vihma., 2013. Resolved complex coastlines and land-sea contrasts in a high-resolution regional climate model: a comparative study using prescribed and modelled SSTs. Tellus A 2013, 65, 19951, http://dx.doi.org/10.3402/tellusa.v65i0.19951

Poulsen J.W. and P. Berg, 2012. More details on HBM - general modelling theory and survey of recent studies, DMI Technical Report 12-16, pp115. http://www.dmi.dk/dmi/tr12-16.pdf

Poulsen J.W. and P. Berg, 2012. Thread scaling with HBM", DMI Technical Report No. 12-20. www.dmi.dk/dmi/tr12-20.pdf

Land-cover dynamics and feedbacks in RCMs: state-of-the-art, outlook, and lessons learned

Benjamin Smith

Dept of Physical Geography and Ecosystem Science, Lund University, Sweden (ben.smith@nateko.lu.se)

Structural and functional properties of the vegetated land surface influence the climate by controlling energy, water and momentum fluxes, as well as greenhouse gas exchanges and atmospheric chemistry. Land surface changes associated with land use and ecologically-driven vegetation dynamics are thus relevant to consider in climate models. Several IPCC-AR5-generation global Earth system models (ESMs) include vegetation dynamics and biogeochemistry (especially carbon cycle) components, and this will become the standard in the next generation of ESMs. Feedbacks associated with the biogeophysical properties of the land surface are particularly relevant to consider at the regional scale. Studies mainly based on global simulations with GCMs and ESMs have shown that changes in albedo and energy partitioning associated with land use changes such as deforestation (Bala et al. 2007), or climate-driven responses of vegetation such as shrub expansion over Arctic tundra (Bonfils et al. 2012), may influence radiative forcing and surface temperatures over the affected area to a degree comparable with greenhouse gas-driven warming under a future climate scenario. Regional climate models (RCMs), being optimised for application at a grid resolution sufficient to account for the effects of topography and land cover patterns on the atmosphere, constitute attractive tools for the investigation of regional scale land-atmosphere coupling. It is therefore surprising that RCMs have lagged behind the global climate modelling community in incorporating functionality to account for such coupling and the associated Earth system feedbacks.

A number of current RCMs are being developed to incorporate climate-dependent land cover dynamics on time scales longer than a seasonal cycle, and thus may be considered as regional ESMs (Smith et al. 2011; Kraucunas et al. 2014). Exemplifying with results from the RCA-GUESS model (Wramneby et al. 2010), I review the state of progress in the development of such models, and the prospects for their further evolution as tools to study regional-scale Earth system dynamics and the contribution of regional feedbacks to global climate dynamics and radiative forcing.

References

Bala, G., Caldeira, K., Wickett, M., Phillips, T.J., Lobell, D.B., Delire, C., Mirin, A. (2007) Combined climate and carbon-cycle effects of large-scale deforestation, Proceedings of the National Academy of Sciences USA, 104, 6550-6555.

Kraucunas, I., Clarke, L., Dirks, J. et al. (2014) Investigating the nexus of climate, energy, water, and land at decision-relevant scales: the Platform for Regional Integrated Modeling and Analysis (PRIMA), In press, Climatic Change. DOI: 10.1007/s10584-014-1064-9

Bonfils, C.J.W., Phillips, T.J., Lawrence, D.M., Cameron-Smith, P., Riley, W.J., Subin, Z.M. (2012) On the influence of shrub height and expansion on northern high latitude climate. Environmental Research Letters, 7, 015503.

Smith, B., Samuelsson, P., Wramneby, A., Rummukainen, M. (2011) A model of the coupled dynamics of climate, vegetation and terrestrial ecosystem biogeochemistry for regional applications, Tellus 63A, 87-106.

Wramneby, A., Smith, B., Samuelsson, P. (2010) Hotspots of vegetation-climate feedbacks under future greenhouse forcing in Europe. Journal of Geophysical Research 115, D21119.

Med-CORDEX: a first coordinated inter-comparison of fully-coupled regional climate system models (RCSM) for the Mediterranean

Samuel Somot[1], Paolo Ruti[2], and the Med-CORDEX group

[1] Météo-France / CNRM-GAME, Toulouse, France (samuel.somot@meteo.fr)
[2] ENEA, Roma, Italy

1. Motivations

The areas surrounding the Mediterranean basin have quite a unique character that results both from their complex morphology and socio-economic conditions. It is indeed surrounded by various and complex topography channelling regional winds (Mistral, Tramontane, Bora, Etesian, Sirocco) than defined local climates and from which numerous rivers feed the Mediterranean sea. Many small-size islands limit the low-level air flow and its coastline is particularly complex. Strong land-sea contrast, land-atmosphere feedback, intense air-sea coupling and aerosol-radiation interaction are also among the regional characteristics to take into account when dealing the Mediterranean climate modeling. In addition, the region features an enclosed sea with a very active regional thermohaline circulation. It is connected to the Atlantic ocean only by the Gibraltar Strait and surrounded by very urbanized littorals.

The Mediterranean region is consequently a good case study for climate regionalization and was chosen as a CORDEX sub-domain (MED) leading to the Med-CORDEX initiative endorsed by Med-CLIVAR and HyMeX. This initiative has been proposed by the Mediterranean climate research community as a follow-up of previous initiatives. We present here an update of the status of Med-CORDEX as well as some first multi-model results.

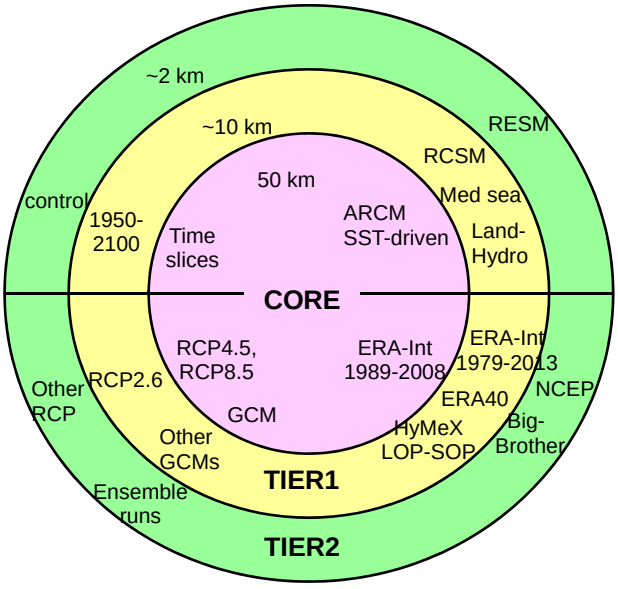


Figure 1. Design of the Med-CORDEX simulation ensemble with the CORE runs following the CORDEX framework and the additional TIER1 and TIER2 runs.

2. Status of the Med-CORDEX inter-comparison

In addition to the CORDEX-like simulations (Atmosphere-RCM, 50 km, ERA-Interim and GCM driven runs), Med-CORDEX proposed TIER1 and TIER2 simulations to experiment some of the regional climate modelling challenges (see Ruti et al. 2014). We present here the status and first results of the TIER1 simulations dedicated to the use of fully coupled Regional Climate System Models (RCSM), coupling the various components of the regional climate: atmosphere, land surface and hydrology, river and ocean. The main goals of this exercise are to:

- define a coordinated framework for a first RCSM inter-comparison
- elaborate an evaluation stragegy for RCSM
- study the potential added-value of RCSM with respect to non-coupled models (ARCM, ORCM, ...)
- understand the coupled regional climate processes and their past climate variability
- make projections of the 21st century Mediterranean regional climate change for the various components
- deliver data for impact studies and climate services

Concerning the Med-CORDEX RCSM simulations, today, Med-CORDEX gathers 20 different modelling groups from 9 different countries (France, Italy, Spain, Serbia, Turkey, Israel, Tunisia, Germany, Hungary) in Europe, Middle-East and North-Africa. It includes 13 atmosphere RCMs including the land-surface models, 4 river models, 10 regional ocean models and 12 different Regional Climate System Models. Evaluation runs use the ERA-Interim reanalysis as lateral boundary conditions. Historical and scenario runs use 6 different GCMs from CMIP5. Most of the ERA-Interim driven runs (1989-2008 minimal period, 1979-2013 advised) are completed as well as the first multi-component RCP8.5 and RCP4.5 scenarios (1950-2100).

The Med-CORDEX data are freely available for non-commercial use through a dedicated database hosted at ENEA at www.medcordex.eu.

3. First multi-model results

The first mono-model studies with the coupled RCSM have been achieved recently for model evaluation for the atmosphere component (e.g. Nabat et al. 2014) and for the river and ocean component (e.g. Sevault et al. 2014).

Following a pioneer work by Dubois et al. (2012)

describing the first Mediterranean Atmosphere-Ocean RCM intercomparison, we present here the first Med-CORDEX multi-model results.

Figure 2 shows the interannual variability of the Sea Surface Temperature and Salinity (SST and SSS) averaged over the whole Mediterranean Sea as simulated by the seven Med-CORDEX RCSM evaluation runs over the 1980-2010 period compared to gridded observations. On the whole the RCSMs capture well the SST behaviour including its interannual variability despite a weak cold bias and an underestimation of the warming trend. Simulating the past variability of the salinity is still a very challenging goal as illustrated in Figure 2 with very diverse behaviours among the 7 simulations. This may have strong impact on the representation of the surface circulation and of the Mediterranean thermohaline circulation.

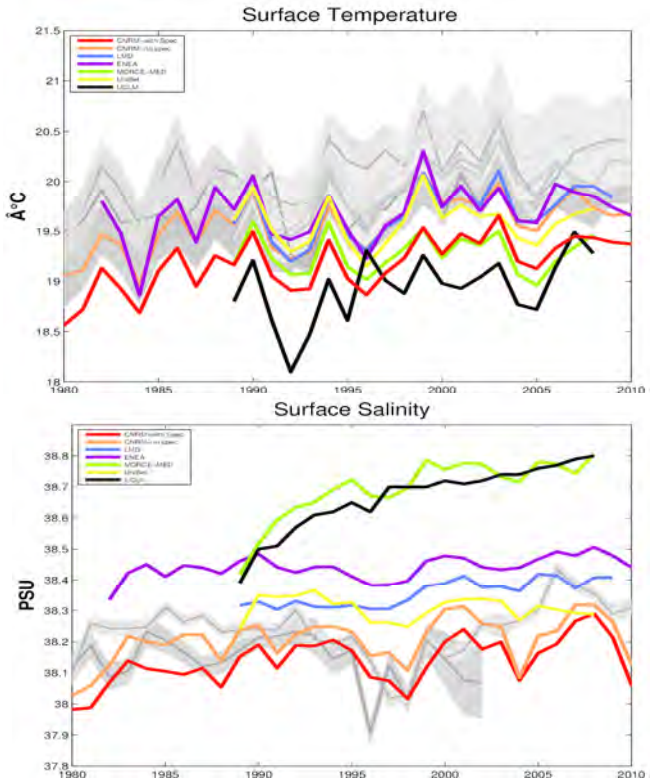


Figure 2. SST and SSS interannual variability hindcast (1980-2010) as simulated by the Med-CORDEX ensemble of RCSM (models from ENEA, CNRM, CNRM-SN, LMD, MORCE-MED, Univ. of Belgrade, UCLM-UPM ; observations from Reynolds OISST, Marullo OISST, Rixen/MedAtlas-II, EN3)

Despite SST and SSS, the following evaluations and analyses are on-going in Med-CORDEX:

- Strong surface wind
- Coastal breeze
- Mediterranean cyclonesis
- Medicanes
- River flow
- Deep water formation
- Mediterranean thermohaline circulation
- Air-sea fluxes
- Strait dynamics
- Coastal and island climate
- Droughts and heat waves
- Heavy precipitation events
- Water vapor, cloud and radiation
- Mediterranean Sea Water and Heat Budgets
- Sea level

4. Towards Med-CORDEX-2

Med-CORDEX demonstrated its capacity to organize the first international inter-comparison of fully-coupled Regional Climate System Models. Up to now, the RCSM includes mainly the following components: atmosphere, land surface, surface hydrology, rivers and ocean.

Next step to be discussed within the international CORDEX framework could be the addition of new relevant components of the regional climate system such as the aerosols, the dynamical vegetation, the lakes or the ocean biogeochemistry to complete the RCSMs or to add the human influence (land-use, irrigation, dam, cities, chemistry) to reach the status of Regional Earth System Models (RESM).

References

Dubois C., S. Somot, S. Calmanti, A. Carillo, M. Déqué, A. Dell'Aquilla, A. Elizalde-Arellano, S. Gualdi, D. Jacob, B. Lheveder, L.Li, P. Oddo, G. Sannino, E. Scoccimarro, F. Sevault (2012) Future projections of the surface heat and water budgets of the Mediterranean sea in an ensemble of coupled atmosphere-ocean regional climate models, Clim. Dyn. 39 (7-8):1859-1884. DOI 10.1007/s00382-011-1261-4.

Nabat P, Somot S, Mallet M, Sevault F, Chiacchio M and Wild M (2014). Direct and semi-direct effects of aerosol on the Mediterranean climate variability. Clim. Dyn. (accepted)

Ruti P., S. Somot, C. Dubois, S. Calmanti, B. Ahrens, A. Alias, R. Aznar, J. Bartholy, S. Bastin, K. Béranger, J. Brauch, J.-C. Calvet, A. Carillo, B. Decharme, A. Dell'Aquila, V. Djurdjevic, P. Drobinski, A. Elizalde-Arellano, M. Gaertner, P. Galan, C. Gallardo, F. Giorgi, S. Gualdi, A. Harzallah, M. Herrmann, D. Jacob, S. Khodayar, S. Krichak, C. Lebeaupin, B. L'Heveder, L. Li, G. Liguro, P. Lionello, B. Onol, B. Rajkovic, G. Sannino, F. Sevault (2014) MED-CORDEX initiative for Mediterranean Climate studies. BAMS (in revision)

Sevault F, Somot S, Alias A, Dubois C, Lebeaupin-Brossier C, Nabat P, Adloff F, Déqué M and Decharme B (2014). Ocean simulation of the 1980-2012 period for the Mediterranean Sea using a fully coupled atmosphere-land-hydrology-river-ocean regional climate system model: design and evaluation. Tellus (submitted)

Soil moisture interaction with surface climate for different vegetation types in the La Plata Basin

Anna Sörensson[1], Hugo Berbery[2]

[1] Centro de Investigaciones del Mar y la Atmósfera, University of Buenos Aires (sorensson@cima.fcen.uba.ar)

[2] Earth System Science Interdisciplinary Center/Cooperative Institute for Climate and Satellites-MD University of Maryland

1. Introduction

The initialization method of employing initial soil moisture interpolated from global reanalysis data or GCMs simulations is still a common practice in regional climate simulations. This inevitably generates initial errors since soil moisture from two different models are not exchangeable. The la Plata Basin in subtropical South America has been identified as a region where the correct representation of interaction between soil moisture and near surface variables as well as precipitation could be important for seasonal prediction skill (e.g. Collini et al. 2008; Barreiro and Díaz 2011; Sörensson et al. 2011; Ruscica et al. 2013).

In this study we examine the hypothesis that, to understand the possible contributions of the soil to the seasonal predictive skill of a model, it is necessary to understand the processes that define the soil moisture memory and the associated uncertainties for different vegetation covers. The specific questions we seek to address are: How does the initialization method affect predictions of surface climate over the basin? Does interaction with the atmosphere depend on the type of land cover? How important is the choice of month of initialization for monthly-to-seasonal climate predictions?

2. Methodology

The main vegetation types of the basin: Savanna (SAV1 and SAV2), Evergreen Broadleaf Forest (EBF), Grassland (GRA) and Dryland Cropland and Pasture (DCP, Fig. 1), are evaluated separately with a focus on the hydrological components and the surface climate. We assess the influence of the initial soil moisture and its memory specifically for the Weather Research and Forecasting model (WRF) coupled with the Noah land surface model and initialized with the NCEP/NCAR reanalysis (Kalnay et al. 1996). 12 experiment simulations of the year 2001 (EXP), starting at the 1st of each month are compared to a longer control simulation (CTL), for which the soil moisture of Noah and the atmosphere of WRF are considered to be in equilibrium.

3. Results

The initial EXP soil moisture is much wetter than the equilibrium CTL values during the dry season (February through August, not shown). The memory is long during this season, especially for the two SAV regions where it is around 2 months for the top soil moisture layer and up to 8 months in deeper layers. During the wet season (September through January) the initial differences are small, indicating higher prediction skill. Evergreen Broadleaf Forest distinguishes from the other vegetation types by having roots in the deepest (fourth) layer, and the water content in this layer influences directly on the on the atmosphere.

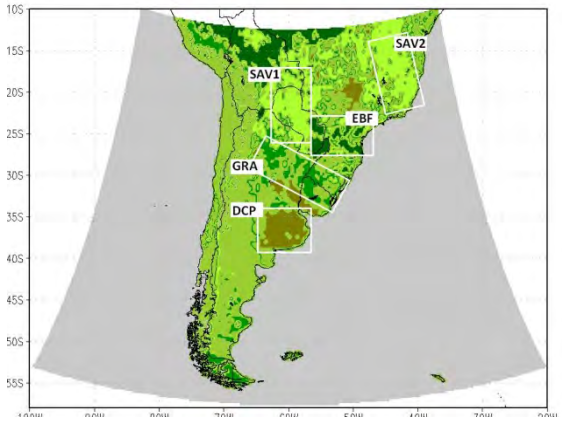


Figure 1. Simulation domain and vegetation types studied. The regions considered are limited by the white rectangles and masked by the corresponding vegetation type. SAV: light green, EBF: dark green, GRA: green and DCP: brown.

The differences in soil moisture cause errors in the surface climate through different partitioning of the surface fluxes. This occurs in particular when fluxes reach their maximum values during daytime and amounts to 2-m maximum temperature errors as large as -5.5°C on the monthly time scale for the SAV1 region. The influence of soil moisture variations on temperature is very high for all vegetation types (Table 1), similarly to the results of Sörensson (2010). Over the GRA and DCP regions the correlations are somewhat smaller suggesting that other factors such as cloud cover and radiation may come into play (e.g. Seneviratne et al. 2010).

Table 1: Correlations of monthly top soil moisture error and monthly mean maximum temperature error on the yearly and the seasonal scale.

	SAV1	SAV2	EBF	GRA	DCP
Yearly	-0,97	-0,96	-0,93	-0,84	-0,73
DJF	-0,97	-0,87	-0,92	-0,76	-0,76
MAM	-0,98	-0,98	-0,94	-0,94	-0,72
JJA	-0,97	-0,97	-0,96	-0,89	-0,66
SON	-0,79	-0,87	-0,84	-0,46	-0,74

The interaction between relevant surface variables of the CTL and EXP simulations for the different vegetation types was assessed by examining the evolution of surface water budget terms, soil moisture, temperature and heat fluxes. For this analysis the EXP simulation initialized on 1 April 2001 was chosen for representing an initial date during the austral autumn where soil moisture initial errors are large. Here the SAV1 region is presented as an example. The CTL and EXP precipitation events are very similar in timing during April-December (Fig. 2a), showing the strong influence of boundary conditions, but they somewhat differ in amplitude due to internal variability and potential soil moisture feedbacks. Fig. 4c shows that the initial soil moisture of EXP of the three upper layers (SM1-3) is 2-3 times the CTL values. This leads to higher evapotranspiration and latent heat flux (Figs. 2b and d) and lower temperatures in EXP (Fig. 2e). Since there are no roots in the deepest layer (SM4), this layer does not contribute to the evapotranspiration, but water amounts that are higher than the equilibrium level of CTL at around 0.26 m3/m3 goes to underground run-off. The extra water in the upper three levels is partitioned between evapotranspiration and drainage, and for SM1 surface run-off. In the CTL simulation, both SM3 and SM4 are constant until late austral spring, and underground run-off is zero, so only the upper two layers interchange water with the atmosphere through infiltration and evapotranspiration. The latent heat flux of CTL (Fig. 4d) follows closely the top soil moisture, while in EXP simulation during the first months, they do not coincide as much and the latent heat depends on other factors such as atmospheric moisture content. The sensible heat flux behaves like a mirror image of the latent heat flux, leading to lower temperatures in the EXP simulation.

4. Conclusions and Discussion

Uncertainty in the simulated surface temperature originates from initial soil moisture errors regardless of vegetation type. The only discernible exception to this is when the deep layer is connected to the atmosphere through deep roots as is the case of the EBF region where this layer influence in the surface temperature through its influence on the partitioning of the surface fluxes.

The impact of a wet initialization depends on the situation, e.g. on the region, season and also vegetation type. When soil moisture is initialized with too high values during a relatively wet season, a vegetation type with limitations on its evapotranspiration (in our case the EBF region) will have a low rate of adjustment to equilibrium values. A situation where soil is initialized too wet during a dry season (in our case the SAV1 region) shows a faster adjustment, which implies higher interaction with the atmosphere, although in this case, initial errors are very high and therefore, the memory is long. In the first case, the impact on heat fluxes and surface temperature is low during the adjustment period, while for the second case the impact is high.

Effects of soil moisture initial differences can be delayed when an initial error persists during a season with limited interaction with the atmosphere. When the soil starts to interact with the atmosphere, this error comes to evidence in surface variables such as evapotranspiration and temperature. The memory and the interaction with the atmosphere depend thus on the deviation of the initial values from equilibrium values and on the moisture/atmospheric regime at the time of initialization. Therefore, wet and dry initializations could be better defined depending of the characteristics of a particular region and season, rather than on a definition that considers a fixed fraction of the soil moisture field for a large simulation domain.

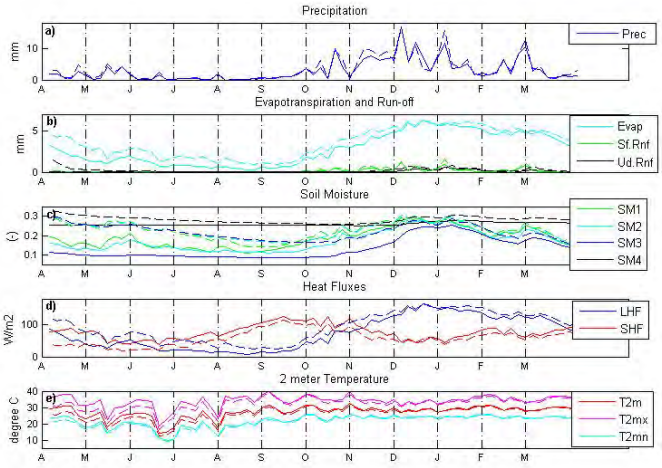


Figure 2: Evolution of 5-day-means of the SAV1 components of the water balance, soil moisture, heat fluxes and temperature at 2 meters for the CTL simulation and the EXP simulation initialized in April. Full lines show CTL results and dashed lines show EXP results.

References

Barreiro, M., N. Díaz (2011) Land–atmosphere coupling in El Niño influence over South America. Atmos. Sci. Lett., 12., pp. 351–355.

Collini, E. A., E. H. Berbery, V. R. Barros, M. E. Pyle (2008): How does Soil Moisture Influence the Early Stages of the South American Monsoon? J. Climate, 2, pp. 195–213.

Kalnay, E., and Coauthors (1996) The NCEP/NCAR 40-year reanalysis project. Bull. Amer. Meteor. Soc., 77, pp 437–471.

Ruscica R, A. Sörensson, C. Menéndez (2013) Hydrological links in South Eastern South America: Soil Moisture memory and coupling within a hot spot. Int. J. Clim, in press.

Seneviratne, S. I., T. Corti, E. L. Davin, M. Hirschi, E. B. Jaeger, I. Lehner, B. Orlowsky, A. J. Teuling (2010) Investigating soil moisture–climate interactions in a changing climate: A review. Earth-Science Reviews, 99, pp 125-161.

Sörensson, A. (2010) Analysis of Land Surface-Atmospheric Feedbacks in South America using a New Regional Climate Model. PhD thesis. University of Buenos Aires.

Sörensson, A. A., C. G. Menéndez (2011) Summer soil–precipitation coupling in South America. Tellus A, 63, pp 56–68.

Coupled atmosphere – wave simulations of high-impact weather systems in the North-Atlantic and Baltic Region.

David Sproson, Erik Sahlée, Lichuan Wu and Anna Rutgersson

Department of Earth Science, Uppsala University, Uppsala, Sweden (David.Sproson@geo.uu.se)

1. Introduction

The exchange of heat, moisture and momentum between the atmosphere and ocean are of fundamental importance in the modelling of the atmosphere in the marine environment. However, these exchanges occur at a very small spatial scale, and their effects must thus be parameterized in numerical models . These parameterizations, however, introduce a significant degree of uncertainty into the models, and to not necessarily capture the full range of physics that control the strength of the air-sea coupling, which includes that state of the surface wave field.

Of particular interest currently is the effect of the feedback of both wind waves and swell on the lower atmosphere (e.g. Rutgersson et al., 2012). In low wind-speed regimes, remotely generated swell may propagate faster than the local wind speed, and thus act as a source of momentum and mixing to the lower atmosphere (Smedman et al., 2009). As wind speeds increase and the wind-sea becomes more dominant, other wave parameters, such as wave age or wave steepness may have to be considered in order to correctly parameterize the drag that the ocean exerts on the atmosphere (Taylor and Yelland, 2001). At even higher wind speeds, breaking waves may become important, and there is evidence that the drag coefficient may stop increasing, or even decrease with increasing wind speeds at wind speeds approaching hurricane force or above (Powell et al., 2003), as a degree of decoupling between the atmosphere and ocean surface takes place (Kudryavtsev and Makin, 2007,2011). At such high wind speeds, the presence of sea-spray in the lower boundary layer is also likely to be important, increasing the drag felt by the lower atmosphere as spray droplets are accelerated to the local wind speed. The dominant height scale for spray processes is likely to be the significant wave height.

2. A coupled WRF-WAM modelling system

In this study we develop a coupled atmosphere-wave modelling system, using WRF-ARW v3.6 for the atmospheric component and WAM 4.5.4 to provide wave data, with inter-process communication provided by OASIS3-MCT. Using this model, we investigate the importance of including wave information in surface flux formulations in a series of simulations of high-impact weather systems in the North Atlantic / Baltic Sea region.

References

Carlsson, B., A. Rutgersson, and A.-S. Smedman (2009), Impact of swell on simulations using a regional atmospheric climate model, Tellus A, 61(4), 527-538.

Kudryavtsev, V. N., and V. K. Makin (2007), Aerodynamic roughness of the sea surface at high winds, Boundary-Layer Meteorology, 125(2), 289-303.

Kudryavtsev, V. N., and V. K. Makin (2011), Impact of Ocean Spray on the Dynamics of the Marine Atmospheric Boundary Layer, Boundary-Layer Meteorology, 140(3), 383-410.

Makin, V. K. (2005), A note on the drag of the sea surface at hurricane winds, Boundary-Layer Meteorology, 115(1), 169-176.

Rutgersson, A., E. O. Nilsson, and R. Kumar (2012), Introducing surface waves in a coupled wave-atmosphere regional climate model: Impact on atmospheric mixing length, J Geophys Res-Oceans, 117.

Smedman, A., U. Hogstrom, E. Sahlee, W. M. Drennan, K. K. Kahma, H. Pettersson, and F. Zhang (2009), Observational Study of Marine Atmospheric Boundary Layer Characteristics during Swell, J Atmos Sci, 66(9), 2747-2763.

Powell, M. D., P. J. Vickery, and T. A. Reinhold (2003), Reduced drag coefficient for high wind speeds in tropical cyclones, Nature, 422(6929), 279-283.

Taylor, P. K., and M. J. Yelland (2001), The dependence of sea surface roughness on the height and steepness of the waves, Journal of Physical Oceanography, 31(2), 572-590.

Testing coupling techniques for a regional climate model: What are the advantages ?

Marc Stéfanon[1], Jan Polcher[2]

[1] Laboratoire d'Ecologie, Systématique et Evolution (ESE), Univ. Paris-Sud, Orsay, France (marc.stefanon@u-psud.fr)
[2] Laboratoire de Météorologie Dynamique,IPSL, CNRS/Ecole Polytechnique/UPMC/ENS, Palaiseau, France

Due to the development of earth system models (ESMs), the integration of the various components within the climate system has been of paramount importance to provide a better understanding for the coupled processes (Drobinski et al. 2012). The comparison of coupled versus uncoupled experiments is the most straightforward way to assess processes that act in a non-linear manner (Seneviratne et al. 2006). The integration of a large number of coupled modules went through the use of two different techniques:

- the components A and B are linked together through a specific software called a "coupler".
- the component B is used as a subroutine of module A.

Each method presents its own feature that induces different assets and drawbacks (Valcke et al. 2012). Coupler have been historically designed to communicate and regrid data between ocean and atmospheric models, however using an additionnal component lead to higher computing time. By calling a subroutine instead of using a coupler, this extra time is avoided but it implies that both models have a similar and tight structure, which precludes an independant development for each module. A coupler offers more flexibility from this point of view,but may decrease the informatic portability.

In this study, we investigate this two techniques by interfacing the ORCHIDEE land surface model with the WRF regional climate model. The strength and weaknesses of the modeled results are discussed in terms of computational performance and specific functionalities added to the coupled model.

References

Drobinski, P., Anav, A., Lebeaupin Brossier, C., Samson, G., Stéfanon; M., et al. (2012) Model of the Regional Coupled Earth system (MORCE): Application to process and climate studies in vulnerable regions, Environmental Modelling & Software 35, 1-18.

Seneviratne, S. I., Lüthi, D., Litschi, M., & Schär, C. (2006). Land–atmosphere coupling and climate change in Europe. Nature, 443(7108), 205-209.

Valcke, S., Balaji, V., Craig, A., DeLuca, C., Dunlap, R., Ford, R.W., Jacob, R., Larson, J., O'Kuinghttons, R., Riley, G.D.,and Vertenstein M. (2012) Coupling technologies for Earth System Modelling. Geosci. Model Dev., 5, 1589-1596, 2012.

Ocean feedback mechanism in a coupled atmosphere-ocean model system for the North Sea

Jian Su[1], Hu Yang[1], Christopher Moseley[2], Alberto Elizalde[3], Dimitry Sein[4], Bernhard Mayer[1], Thomas Pohlmann[1]

[1] Institute of Oceanography, University of Hamburg, Bundesstr. 53, 20146 Hamburg, Germany (Jian.Su@zmaw.de)
[2] Climate Service Center, Fischertwiete 1, 20095 Hamburg, Germany
[3] Max-Planck-Institut f ur Meteorologie, Bundesstrasse 53, 20146 Hamburg, Germany
[4] Alfred Wegener Institute for Polar and Marine Research, Am Handelshafen 12, 27570, Bremerhaven, Germany

1. Coupled model system

Choosing an interactive coupling between atmosphere and ocean models was widely practiced in regional climate study over the last decades. The added value of the coupling is attributed to providing regional details and incorporating the feedback of the ocean in regional climate downscaling. Such coupled model system serves for a variety of purpose, such as detailed process studies, air-sea interaction studies and long-term simulations. However, the necessity of including the ocean component in the regional climate downscaling is still under evaluation. Here we present a coupled model system applied to the North Sea, comprising a regional ocean model HAMSOM (resolution 3 km), an atmospheric model REMO (resolution 37 km) and the coupler OASIS.

2. Results

The assessment presented in this study focused on the reaction of the ocean component. The uncoupled model experiment used the sea surface temperature (SST) from the global model as boundary input for the atmospheric model. The comparison of SST data revealed that spatial pattern of SST in coupled model simulation showed no major deviation from observations (Figure 1). In the uncoupled model simulation, a drift from observations was found when integrating the model for more than 10 years. This led us to revisit the individual years (1997 and 1999) to look for the mechanism of better performance in coupled model. We found that the cloud cover was responsible for correcting the heat flux errors in the uncoupled run. Therefore, we concluded that the local air sea interaction processes are responsible for damping these errors, in particular at the coastal waters, which leads to a better ocean model results.

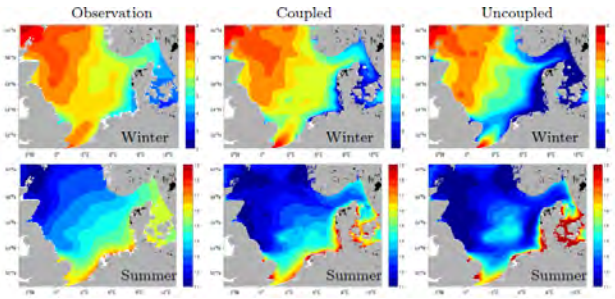


Figure 1. Fourteen years mean SST (^{o}C) of observations (Janssen et al, 1999, left column), coupled (middle column) and uncoupled (right column) experiments in February and August.

3. Summary

The coupled model simulation shows no major deviation from observations, thus it can serve as a tool for a free climate-model run. In the uncoupled model simulation, we found a drift from observations when integrating the model for more than 10 years. This drift is due to the accumulation of latent heat flux errors. The interactive coupling could damp these errors in a long-term simulation. Finally, it provides a better simulation in the coastal waters.

An impact of historical land-cover conversion on regional climate change during winter in Hokkaido Island, Japan

Shiori Sugimoto[1], Tomonori Sato[1] and Tomonori Sasaki[2]

[1] Faculty of Environmental Earth Science, Hokkaido University, Sapporo, Japan (shioris@ees.hokudai.ac.jp)

[2] Hokkaido Government, Sapporo, Japan

1. Introduction

Land surface has significant impact on the Earth's climate system as it alters absorption and reflection of the solar energy and roughness at the surface (Feddema et al. 2005; Pielke 2005). Therefore, a surface modification such as an artificial land-cover conversion is an important topic to attribute the long-term change in regional climate.

The regional climate response to the land-cover conversion differs between the regions and the seasons. In high latitude area, deforestation for agriculture increases snow-covered surface albedo during winter, which significantly decreases regional air temperature because of a reduction of net radiative energy and sensible heat fluxes at the surface (Claussen et al. 2001; Bounoua et al. 2002; Boisier et al. 2013). Although precipitation change during winter is difficult to discuss, latent heat fluxes would also decrease and it has possibility to modify precipitation over the land-cover conversion area. On the other hand, the roughness controls moisture convergence at surface layer (Kanae et al. 2001; Pitman et al. 2004), indicating that a role of the surface roughness in precipitation should be examined during snow-covered season.

In Hokkaido Island, northern area of Japan, forests have been cleared for agriculture and urban growth since the late 19th century. Records of actual vegetation maps in past and current have been remained and they are available for the input data of numerical simulations. In addition, the whole Hokkaido Island is covered by snow during winter; therefore, it is suitable region to examine a regional climate response to the land use change during snow-covered season. In this study, regional temperature and precipitation changes influenced by the land-cover modification are analyzed in the Hokkaido Island during winter.

2. Model and experimental setup

To evaluate regional climate change during winter under the historical land-cover conversion in Hokkaido Island, long-term numerical experiments were conducted using the Weather Research and Forecasting (WRF) model version 3.2.1 with the Advanced Research WRF dynamical core (Skamarock et al., 2008). The first domain was set on the northern Japan area with mesh size of 20km and the second domain was centered on Hokkaido Island with mesh size of 10 km. The 32 vertical layers were set. Time integration was conducted from 0000 UTC 15 October 1982 to 0000 UTC 01 November 2009 every 12 months and was repeated 27 times. The first 15 days were for spin-up.

Two kinds of numerical experiment were conducted; one is the experiment under the past land-cover distribution (Fig. 1a) and other uses the current one (Fig. 1b). These land-use maps were obtained by Nakanishi et al. (2006). For both of experiments, atmospheric initial and boundary conditions and oceanic surface condition were forced by the same reanalysis datasets from 1982 to 2009. The monthly data calculated by hourly output datasets for 27 years, i.e., from 1982/1983 to 2008/2009 winter, were used for analysis.

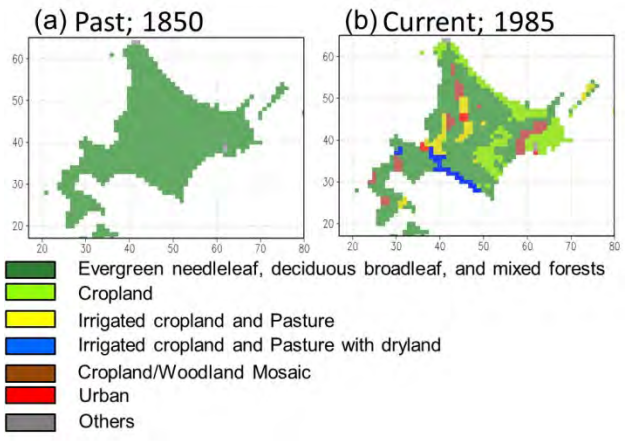


Figure 1. Land-cover in (a) 1850 and (b) 1985 with 10 km grid-spacing for a boundary condition of Domain 2

3. Surface air temperature

In the numerical simulation, the land-cover change from forests to croplands significantly decreases surface air temperature over southern and eastern area (Fig. 2a) because snow cover fraction, which is controlled by a vegetation–dependent parameter of threshold snow depth implying 100 percent snow cover, modifies surface albedo and reduces net radiative energy and sensible and latent heat fluxes. Meanwhile, the urbanization changes the Bowen ratio, i.e., increase of sensible heat fluxes and decrease of latent heat fluxes, which causes a significant warming during daytime. Furthermore, the ground heat storage in the urban area contributes to a weakening of radiative cooling during nighttime.

Observation of surface air temperature showed a difference of long-term warming ratio between forests remaining area and the land-surface modification area to cropland or urban. This long-term variation in the observed air temperature is qualitatively and quantitatively consistent with the simulated temperature change associated with land-cover conversion.

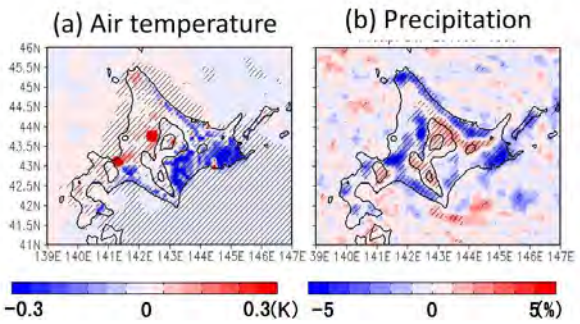


Figure 2. 27-yrs mean anomaly (Current land-use run minus Past land-use run) of (a) surface air temperature and (b) precipitation. Hatching indicates significance with 99% confidence level. Black contour indicates topography at 500 and 1000 m.

4. Precipitation

Simulated precipitation during winter decreases over the area with land use change (Fig. 2b) due to a reduction of evaporation (Fig. 3), which is caused by the decrease of net radiative energy. Surface roughness change intensifies wind speed and moisture divergence over the deforestation area, which also affects precipitation decrease. Meanwhile, precipitation increases over the forests remaining area, i.e., the mountain area, associated with the enhancement of moisture convergence at the leeward boundary of the land-use changed area.

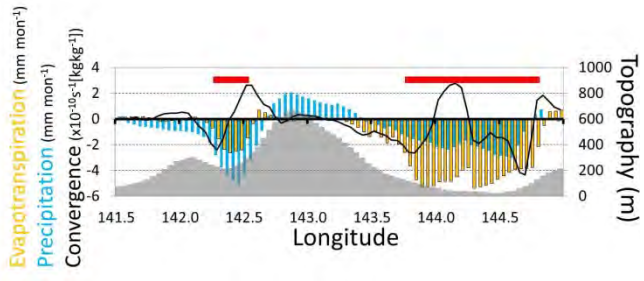


Figure 3. Evapotranspiration anomaly (Current land-use run minus Past land-use run; orange bars), precipitation anomaly (blue bars), and convergence anomaly of surface moisture fluxes (a black line; positive value is convergence anomaly) averaged between 43.75°N to 44.3°N for 27-yrs. Dominant wind direction is west in this region. Gray bars indicates topography. Red bar indicates land-use change zone.

References

Bounoua, L., R. Defries, G. J. Collatz, P. Sellers, and H. Khan (2002), Effects of land cover conversion on surface climate, Climate Change, Vol. 52, No. 1-2, pp. 29-64.

Boisier, J. P., N. de Noblet-Ducoudre, and P. Ciais (2013) Inferring past land use-induced changes in surface albedo from satellite observations: a useful tool to evaluate model simulations, Biogeosciences, Vol. 10, pp. 1501-1516.

Claussen, M., V. Brovkin, and A. Ganopolski (2001), Biogeophysical versus biogeochemical feedbacks of large-scale land cover change, Geophysical Research Letters, Vol. 28, No. 6, pp. 1011-1014.

Feddema, J. J., K. W. Oleson, G. B. Bonan, L. O. Mearns, L. E. Buja, G. A. Meehl, W. M. Washington (2005), The importance of land-cover change in simulation future climates, Science, Vol. 310, pp. 1674-1678.

Kanae, S., T. Oki, and K. Musiake (2001), Impact of deforestation on regional precipitation over the Indochina Peninsula, Journal of Hydrometeorology, Vol. 2, pp. 51-70.

Nishilawa, O., Y. Himiyama, T. Arai, I. Ota, S. Kubo, T. Tamura, M. Nogami, Y. Murayama, and T. Yorifuji (2006), Atlas –Environmental change over Japan-, Asakura-syoten, Japan, 187pp.

Pielke Sr., R. A. (2005), Land use and climate change, Science, Vol. 310, pp. 1625-1626.

Pitman A. J., G. T. Narisma, R. A. Pielke Sr., and N. J. Holbrook (2004), Impact of land cover change on the climate of southwest Western Australia, Journal of Geophysical Research, Vol. 109, D18109, doi:10.1029/2003JD004347.

Skamarock, W. C., J. B. Klemp, J. Dudhia, D. O. Gill, D. M. Barker, X. Y. Huang, W. Wang, and J. G. Powers (2008), A description of the advanced research WRF version 3, NCAR Tech. Note 475+STR, 113 pp., Natl. Cent. for Atmos. Res., Boulder, Colo.

Simulation of the surface mass balance of the ice caps in Arctic Canada and Patagonia with the Regional Atmospheric Climate Model RACMO2

Jan Lenaerts[1], Willem Jan van de Berg[1], Erik van Meijgaard[2] and Michiel van den Broeke[1]

[1] IMAU, Utrecht University, The Netherlands (w.j.vandeberg@uu.nl)

[2] Royal Netherlands Meteorological Institute (KNMI), De Bilt, The Netherlands

1. Motivation

Rising global temperatures have led to a mass loss from nearly all glaciers and ice caps on Earth; their mass loss contributed about 30% of the observed sea level rise for 1993-2010. Mass changes of land-terminating glaciers and ice caps are due a non-zero surface mass balance (SMB), which is dominated by precipitation and melt water runoff.

Although Artic Canada (Figure 1) and Patagonia (Figure 4) have large glaciated areas, their extent is too limited and the topography too rugged to be resolved in a global climate model. However, in a high-resolution RCM the relevant topographic features are retained and the complex delineations of the glaciers and ice caps are captured. Besides resolution, a dedicated surface scheme, included in RACMO2, is essential to estimate the SMB correctly. Such surface scheme represents the temporal evolution of the snowpack in order to physically model the surface albedo, the key factor for snow and ice melt.

2. RACMO2

The RCM RACMO2 consist of the dynamics of the NWP HIRLAM (hydrostatic formulation) and the physical parameterizations from the ECMWF Integrated Forecast Model (IFS). RACMO2 is extended with an interactive 100-layer snow model representing snow and firn processes, i.e., heat conduction, snow compaction, snow grain growth and melt water percolation, retention and refreezing (Ettema and others, 2009). The snow albedo is determined by the snow grain size, cloud cover and solar zenith angle (Kuipers Munneke and others, 2011). RACMO2 has also been applied to the Greenland Ice Sheet (e.g. Van Angelen and others, 2012) and the Antarctic Ice Sheet (e.g. Lenaerts and others, 2012). Simulations of the period 1960-2012 were forced by ERA-40 and ERA-Interim at its lateral boundaries and were run at 11 km resolution for the Canadian Arctic (Lenaerts and others, 2013) and at 5.5 km resolution for Patagonia (Lenaerts and others, 2014).

3. Canadian Arctic Archipelago

The glaciers on the Canadian Arctic Archipelago (CAA) are located in two regions (Figure 1), both characterized by a dry climate with precipitation rates ranging from <300 to >500 kg m^{-2} yr^{-1} and a large amplitude (30-50K) in the seasonal temperature cycle allowing both cold winters and relatively mild summers to occur. In Southern CAA, summer July temperatures can reach well over 10° C due to the proximity of vast areas of snow free land. Modeled SMB by RACMO2 compares favorably with in-situ SMB measurements (Figure 2). The model biases are largely related to elevation differences, with the exception for the Meighen Ice Cap (red dots).

To project the 21st century mass loss of the CAA, RACMO2 was forced at the lateral boundaries with output of HadGEM2-ES using the modest warming scenario RCP4.5. Both RACMO2 and local HadGEM2-ES estimate a much stronger warming in CAA than the global mean, due to regional feedbacks involving a reduction of sea-ice and seasonal snow cover. The projected 21st century warming leads to a 30% increase of precipitation but enhanced melt and runoff cause the CAA to lose about 18% of is mass during this century.

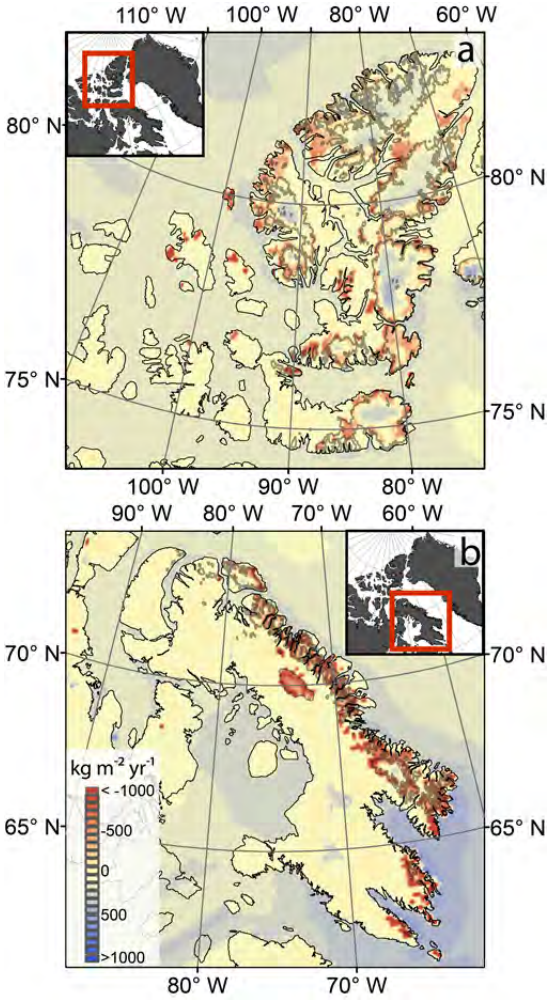


Figure 1. Mean modeled SMB (1960–2011) of the (A) Northern CAA and (B) Southern CAA and its vicinity. Note that SMB is only defined over glaciers (outlined by grey lines) and tundra, whereas over the ocean precipitation-evaporation is presented. The location of the regions is shown on the map inset in red. Figure from Lenaerts and others (2013).

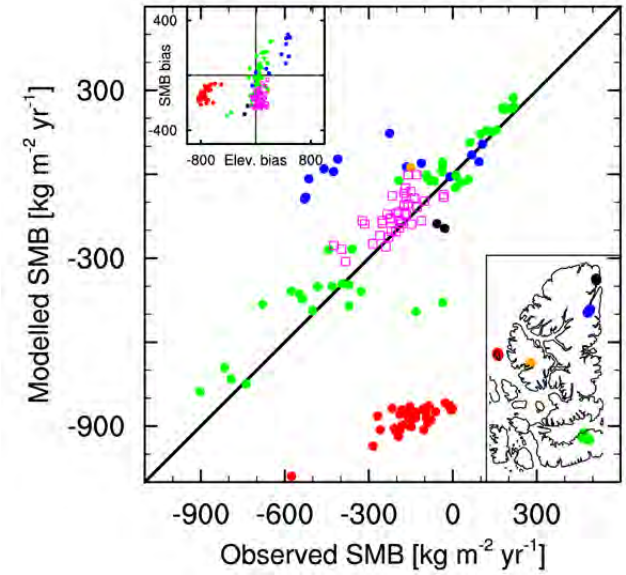


Figure 2. Modeled vs. observed SMB of Northern CAA glaciers for matching time periods. The locations of the measurements are indicated in the lower inset. The purple squares represent measurements on an ice cap outside the inset map. The upper inset shows SMB bias as a function of elevation bias. Figure from Lenaerts and others (2013).

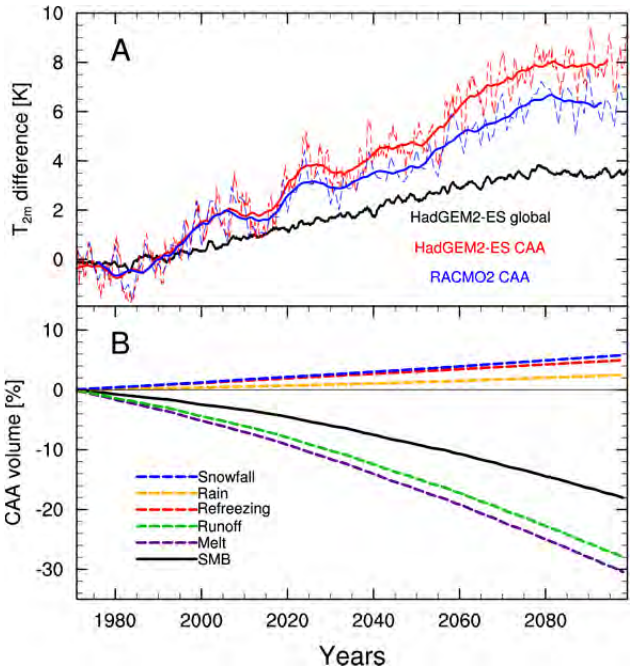


Figure 3: Results of a HadGEM2-ES forced RACMO2 simulation (1971– 2098). (A) Near-surface temperature; global (black) and CAA (red) from HadGEM2-ES directly, and CAA from RACMO2 driven by HadGEM2-ES (blue). Dashed lines are annual mean values; the solid lines are 20-year running averages. (B) Cumulative SMB and its components derived from the RACMO2 simulation, plotted as a relative volume loss of CAA. Figure from Lenaerts and others (2013).

4. Patagonia

The climate of the southern Andes is incomparable with the climate of the CAA. Persistent westerly winds bring massive amounts of moisture to the glaciers, leading to precipitation rates sometimes in excess of 10 m yr^{-1} (Figure 4). East of the mountain ridge, topographic shading and the föhn effect lead to a warmer and dry climate. The SMB-pattern of the Southern Patagonian Ice Field reflects both processes. A sharp gradient separates the moist western side with high accumulation rates from the dry eastern side, where SMB<0. The simulated SMB agrees reasonably well with the few in-situ observations available; the comparison is hampered by the large gradients, which are likely also present on sub-grid scales. Due to the large mass turnover in this ice field, it will respond fast to changes in precipitation or melt, being a good indicator of regional climate change.

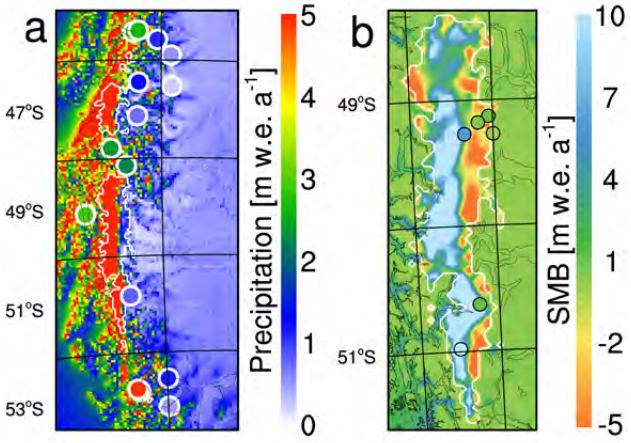


Figure 4. Modeled annual mean (1979-2012) (a) precipitation in the Southern Andes and (b) SMB over the Southern Patagonian Ice Field, along with observations (circles). Figure from Lenaerts and others (2014).

5. Conclusions

The results presented show that RACMO2 is able resolving the near-surface climate and SMB processes of larger ice caps and glaciers. With RACMO2, the SMB and its components can be analyzed and glacier mass loss projections can be performed.

References

Ettema, J. and 6 others (2009) Higher surface mass balance of the Greenland ice sheet revealed by high-resolution climate modelling. Geophys. Res. Lett., 36(12), L12501 (doi: 10.1029/2009GL038110)

Kuipers Munneke, P., and 5 others (2011) A new albedo scheme for use in climate models over the Antarctic ice sheet, J. Geophys. Res., 116, D05114, doi:10.1029/2010JD015113

Lenaerts, J.T.M. and 4 others (2012) A new, high-resolution surface mass balance map of Antarctica (1979–2010) based on regional atmospheric climate modeling. Geophys. Res. Lett., 39(4), L04501 (doi: 10.1029/2011GL050713)

Lenaerts, J.T.M. and 5 others (2013) Irreversible mass loss of Canadian Arctic Archipelago glaciers, Geophys. Res. Lett., 50(1-5), doi:10.1002/grl.50214

Lenaerts, J.T.M. and 7 others (2014) Extreme precipitation and climate gradients in Patagonia revealed by high-resolution regional atmospheric climate modelling. J. Clim., accepted.

Van Angelen, J.H. and 7 others (2012) Sensitivity of Greenland Ice Sheet surface mass balance to surface albedo parameterization: a study with a regional climate model, The Cryosphere, 6, 1175-1186.

Development and evaluation of a new regional coupled atmosphere-ocean model in the North Sea and the Baltic Sea

Shiyu Wang, Christian Dieterich, Ralf Döscher, Anders Höglund, Robinson Hordoir, H.E.Markus Meier, Patrick Samuelsson and Semjon Schimanke

Swedish Meteorological and Hydrological Institute, Norrköping, Sweden (shiyu.wang@smhi.se)

1. Introduction

In recent years, coupled atmosphere-ocean general circulation models are widely used for climate change studies. The concept of ocean-atmosphere coupling has become essential for explaining processes on time scales ranging from seasonal to decadal variability. Due to the coarse resolution of global models, detailed local features, particularly along complex coastlines, cannot be resolved. Hence, for climate change impact and adaptation studies, as well as for climate-process studies of regional importance high-resolution regional coupled models are essential.

As a major tool for regional climate change studies, different regional coupled models have been developed and used to study the climate over Europe during the past two decades. Previous studies either focus only on the Baltic Sea region or the integration period was limited or essential component models like sea ice or river runoff were lacking. The aim of this study is to extent the current scope and to provide an effective tool for climate change studies in Europe which takes regional ocean-atmosphere interaction from the North Sea and the Baltic Sea into account.

2. Description of coupled model and methodology

A new regional coupled Earth System Model (ESM) for the North Sea and the Baltic Sea is developed, which is composed of the regional ocean model NEMO, the Rossby Center regional climate model RCA4, the sea ice model LIM3 and the river routing model CaMa-Flood (Yamazaki, 2011). The regional atmosphere model RCA4 runs in a horizontal resolution of 0.22° on a rotated latitude-longitude grid with 40 vertical levels covering Europe (Figure 1). NEMO runs in a resolution of 2minutes with 56 vertical levels and CaMa-Flood runs in a resolution of 15 minutes. To build up this coupled modelling system, the Ocean Atmosphere Sea Ice Soil Simulation Software (OASIS3) coupler integrates the sub-models simultaneously (Figure 2). This two way coupled system passes heat fluxes, freshwater, momentum fluxes, non-solar heat flux derivative and sea level pressure from the atmosphere to the ocean, and the atmosphere receives SST, sea ice concentration, sea ice surface temperature and sea ice albedo from the NEMO model for the interactively coupled area. The atmosphere-ocean coupling frequency is set to 3 hours. To provide river runoff for NEMO, coastal river runoff from CaMa-Flood is sent to NEMO daily.

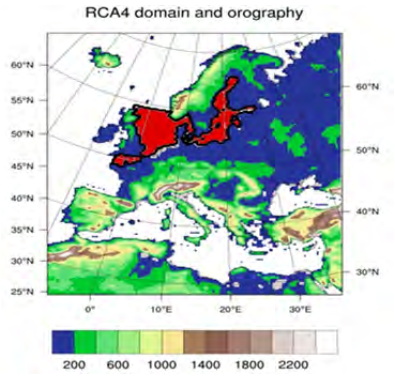


Figure 1 Orography in the RCA4 model domain (Unit: metres) and red region is the ocean domain and active coupling area.

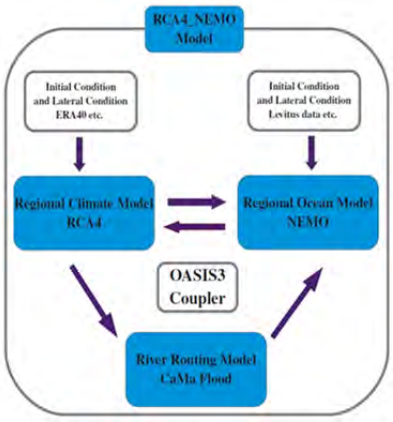


Figure 2 Schematic diagram of the coupled model system

3. Model evaluation

Fig. 3 illustrates the mean seasonal difference of 2m temperature (1981-2010) between the coupled and the uncoupled run and observations for summer and winter. The atmospheric 2m temperature shows biases varying with season. During summer, a negative (positive) bias is found Northern (Southern) Europe. During winter, a negative (positive) bias exists over Southwestern (Northeastern) Europe. The evaluation shows that pronounced atmospheric differences between coupled and uncoupled case usually occur in the North Sea and the Baltic Sea region. We find that the coupled atmosphere is slightly warmer around the Baltic Sea compared to the stand-alone atmosphere run year-round. The North Sea area is slightly warmer during summer and slightly colder during winter. European scale summer temperature biases are slightly reduced in the coupled simulation

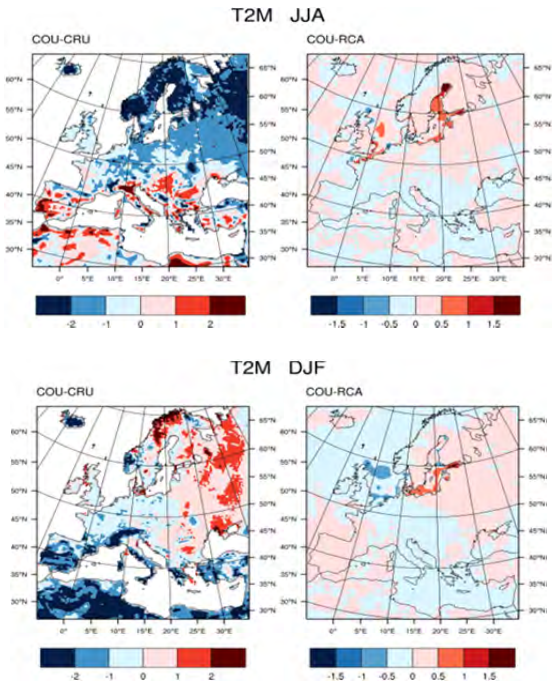


Figure 3 Seasonal mean 2m temperature (T2M) differences between the coupled run (COU) and observations (CRU), the uncoupled run (RCA) for summer (JJA) and winter (DJF) (unit:K)

To evaluate whether the coupled model has produced a valid air-sea relationship, the correlation analysis between the atmospheric variables and SST is used to study the nature of local air-sea interaction (Wu,2006). Figure 4 shows the precipitation-SST correlation in summer and winter for the observations and coupled run. The most pronounced effect of air-sea coupling is seen in summer. High negative correlation reveals that the forcing of the atmosphere on the ocean is strong and this feature is well captured by the coupled model.

4. Summary

The performance of this coupled model system is assessed from a simulation forced with ERA-Interim reanalysis data at the lateral boundaries during the period 1979-2010. Compared to observations, this coupled model system can realistically simulate the present climate. Since the active coupling area covers only the North Sea and the Baltic Sea, the impact of the ocean on the atmosphere over Europe is small. However, we found some local, statistically significant impacts on surface parameters like 2m air temperature and SST. A precipitation-SST correlation analysis indicates that the coupled simulation gives slightly more realistic correlations. A seasonal correlation analysis shows that the air-sea interaction has strong seasonal dependence. Strongest discrepancies between the coupled and the uncoupled simulations occur during summer. In the Baltic Sea in the coupled run the impact of atmospheric forcing on SST is more realistic reproduced. Further, the correlation analysis between heat flux components and SST tendency suggests that the coupled model has a stronger coupling between atmospheric parameters and SSTs than the uncoupled model.

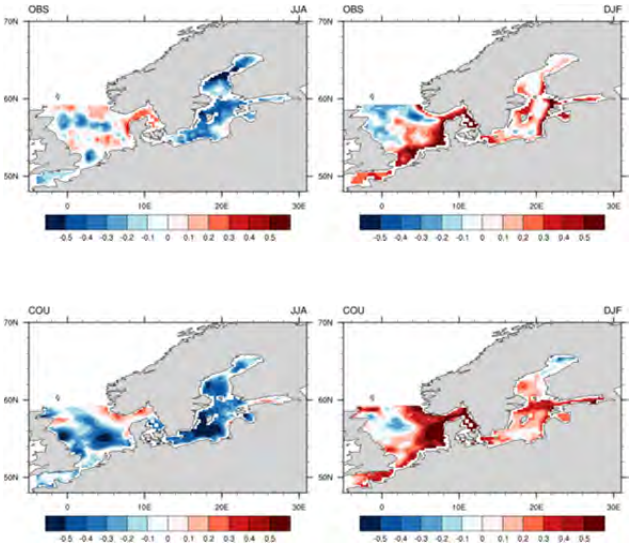


Figure 4 Precipitation-SST correlation of observations (top panel) and coupled simulation (bottom panel) in summer (left column) and winter (right column).

References

Yamazaki D., Kanae S., Kim H. and Oki T. (2011) A physically based description of floodplain inundation dynamics in a global river routing model,Water Resources Research,47, W04501, doi:10.1029/2010 WR009726

Wu, R., Kirtman, B.P. and Pegion, K. (2006). Local air-sea relationship in observation and model simulations. J. Clim.,19:4914-4932

Potential mechanism of vegetation-induced reduction in tropical rainfall in Africa: analysis based on regional Earth system model simulations

Minchao Wu[1], Benjamin Smith[1], Guy Schurgers[1], Joe Siltberg[1], Markku Rummukainen[1], Patrick Samuelsson[2], Christer Jansson[2]

[1] Department of Physical Geography and Ecosystem Science, Lund University, Lund, Sweden (minchao.wu@nateko.lu.se)

[2] Rossby Centre, Swedish Meteorological and Hydrological Institute, Norrköping, Sweden

1. Study aim

In this study the potential impacts of terrestrial vegetation on African precipitation under climate change are assessed, focusing on the role of biogeophysical feedback mechanisms.

2. Methodologies

We applied a coupled regional climate-vegetation model, RCA-GUESS (Smith et al, 2011), over the CORDEX Africa domain at a horizontal grid spacing of 0.44° and forced by boundary conditions from a CanESM2 CMIP5 simulation under the RCP8.5 scenario. The simulations extended from 1961 to 2100. In RCA-GUESS, the dynamic vegetation model GUESS is forced by the regional climate model RCA with 2-meter temperature, precipitation and solar radiation, and simulates changes in the phenology, productivity, relative cover and population structure of up to eight plant function types (PFTs). Such changes feed back to the physical properties of the land surface in RCA and may lead to dynamic adjustments in surface energy fluxes and surface properties, and thus affect the regional climate.

3. Result

We compared simulations with and without vegetation feedback to assess the impact of the vegetation-climate feedback. The study reveals significant changes in tropical rainfall of up to 20% decrease by the end of twenty first century associated with a general growth of African terrestrial vegetation due to CO_2 fertilization effect. Changes in terrestrial vegetation in terms of increased leaf area index in tropics and increased forest cover fraction in subtropics lead to such changes in surface energy fluxes as reduced near surface temperature, and consequently lower temperature gradient between the continent and the ocean and within the continent. This in turn leads to marked changes in the Walker circulation between Eastern Atlantic Ocean and central Africa, as well as the Hadley circulation between tropics and subtropics in the lower troposphere, and hence influences atmospheric moisture transport into the tropics, as well as the convective activity over this region. These effects are especially marked in the boreal spring and autumn, which are important rainy seasons for central Africa.

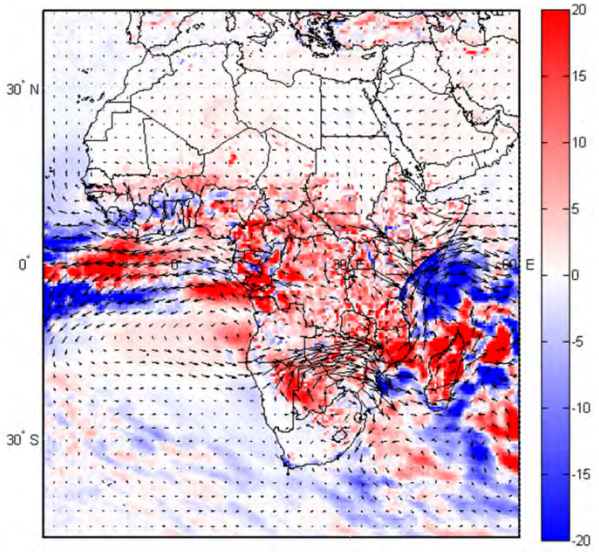


Figure 1. Change in mean (September through November) vertically integrated moisture flux (indicated by the arrows) and change in mean difference between evaporation and precipitation, E-P, between feedback and non-feedback simulation (feedback minus non-feedback) for the period 2071-2100.

4. Conclusion

The results reveal a potential impact of terrestrial vegetation response to climate change on African precipitation, and it suggests that regional vegetation-climate feedbacks may significantly impact the magnitude and character of simulated changes in climate for this region. An implication is that future studies of climate change and its impacts on Africa should make use of models capable of simulating such coupled phenomena.

References

Smith, B., P. Samuelsson, A. Wramneby, and M. Rummukainen (2011), A model of the coupled dynamics of climate, vegetation and terrestrial ecosystem biogeochemistry for regional applications, Tellus A, 63(1), 87-106.

Comparison of air-sea momentum parameterizations in atmosphere-wave coupled system: storm cases study

Lichuan Wu, Anna Rutgersson, David Sproson and Erik Sahlée

Department of Earth Science, Uppsala University, Uppsala, Sweden (lichuan.wu@geo.uu.se)

1. Introduction

The parameterization of wind stress (roughness length or drag coefficient) is very important for the numerical modeling. It can impact on the energy and momentum fluxes. In storm, it can not only influence on the track but also the intensity and the precipitation of the storm. The research about the parameterization of wind stress has last more than forty years, but it still has lots of uncertainties (Taylor and Yelland, 2001), especially, in low wind with swell conditions and extreme wind conditions. It is clear that the drag coefficient is not only depends on the wind speed but also the sea state. Lots of sea state depended parameters are used to parameterize the drag coefficient, e.g., wave age, wave steepness, wave slop.

The presence of swell can modify both magnitude and direction of the wind stress. When the swell presence, there are lots scatter of the wind stress parameterizations. Measurements show that the fast traveling swell in light wind area can make an upward momentum transfer from waves to atmosphere (e.g. Smedman et al., 2009). To take the swell impact into consideration, swell index is included in some wind stress parameterizations (e.g. Hwang et al., 2011).

In extreme wind conditions, measurements show that the drag coefficient will stature and decrease with the increasing wind speed (i.e. Powell et al., 2003; Jarosz et al., 2007). The breaking waves are thought to have a significant contribution to the decreasing drag coefficient. There are some explanations of this reduction, such as, the momentum and energy flux from the wind to short waves will vanish if they are trapped into the separation bubble of breaking longer waves in high wind conditions (Kudryavtsev and Makin, 2007); The droplets form a force called spray force which will direct impact on the airflow momentum forming (Kudryavtsev and Makin, 2011); the air boundary layer near the surface will form a regime of limited saturation by suspended 'light' sea droplets, which contribute to the reduction of the drag coefficient (Makin, 2005).

In this paper, using an atmosphere-wave coupled model (RCA4-WAM), we used several momentum parameterizations to test their performances in two storm cases.

2. Model and parameterizations

To test the performances of momentum parameterizations, we developed an atmosphere-wave coupled model (RCA4-WAM), in which the wave impact on the atmospheric mixing length (ML_W) is included (Rutgersson et al., 2012). The domain used in this study covers Europe. The comparison experiments are shown in table 1.

Table 1. Comparison experiments

No.	ML_W	Momentum parameterizations
Exp1	Without	Original RCA
Exp2	With	Carlsson et al., 2009
Exp3	Without	Carlsson et al., 2009
Exp4	With	Original RCA
Exp5	With	Roughness length from WAM
Exp6	With	Kudryavtsev and Makin, 2011

3. Case study and results

The two wind storms are Erwin/Gudrun in 2005 and Kyrill in 2007. The data (OBS) from [extreme wind storms catalogue, EWSC] is used to evaluate the model results.

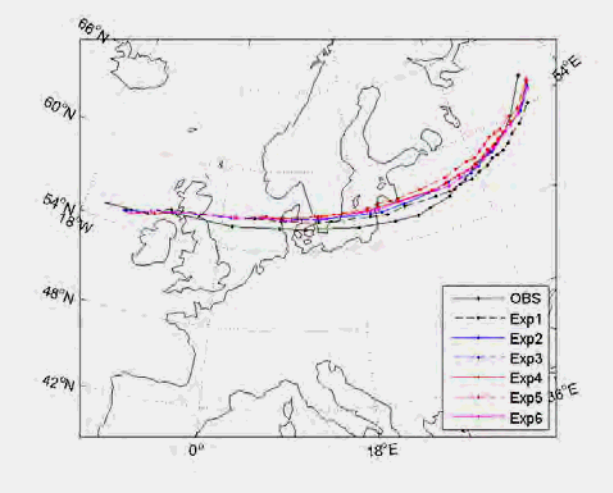


Figure 1. The minimum sea level pressure (SLP) track of Kyrill (every three hours)

Figure 1 shows the track of simulation results of Kyrill using different parameterizations. One can see, Exp2 and Exp1 has better performance in the track compared with other experiments. But their performances in the maximum wind speed and minimum SLP are worse than others (Figure 2 and 3). All the parameterizations with the waves impact improve the model performance, which increase the maximum wind speed at 925hpa and reduce the minimum SLP of the storm center. The roughness length from WAM has the best results in maximum wind speed and minimum pressure in all the six experiments. If both LM_W and the wave impact on roughness are included (Exp2), it will decrease on maximum wind speed and increase the minimum SLP of Exp3 and Exp4. But the wind stress parameterization (Exp6) included the sea spray impact have not significant increase of maximum wind speed as expected. The simulation results of Erwin/Gudrun are similar condition

with Kyrill.

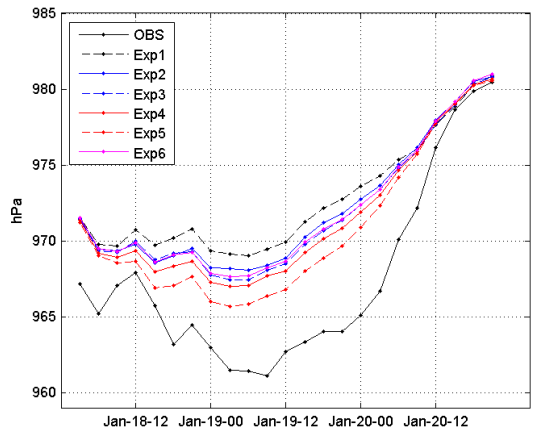


Figure 2. The minimum sea level pressure of Kyrill in different time

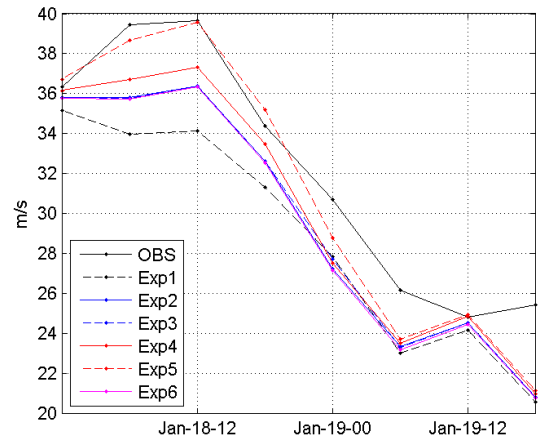


Figure 3. The maximum wind speed of Kyrill at 925hPa at different time

Compared with Exp1, as expected the parameterizations with wave influence have greater impact on the sea and coast area. Compared Exp2 with Exp3 and Exp4, we found that if both impact (ML_W and wind stress parameterization of Carlsson et al., 2009) are added (Exp2), it will reduce their (Exp3 and Exp4) influence. In other words, if Exp3 and Exp4 increase the precipitation (latent and sensible heat fluxes, wind speed) in some area, then Exp2 will reduce their increase amount. The impact area of precipitation are mainly on the banding area which precipitation changes from heavy to light quickly. On the light side, the wave impact will increase the precipitation amount, which means that the wave impact will expand the heavy precipitation area.

4. Conclusions and Discussions

Compared with the original RCA4, all the momentum parameterizations with the wave impact are more or less improve the storm simulation results in maximum wind speed and minimum sea level pressure. The momentum parameterization from WAM are the best one in the all six parameterizations in maximum wind and minimum pressure. The parameterization included sea spray influence (Exp6) did not have the good performance as expected. This maybe because that the intensity of the two storm cases is not high to make the parameterization have a big impact on the results compared with others. The impact on the precipitation of the parameterizations with wave impact will expand the heavy rain area around the storm.

References

Carlsson, B., A. Rutgersson, and A.-S. Smedman (2009), Impact of swell on simulations using a regional atmospheric climate model, Tellus A, 61(4), 527-538.

EWSC, http://www.europeanwindstorms.org/cgi-bin/storms/storms.cgi

Jarosz, E., D. A. Mitchell, D. W. Wang, W. J. Teague (2007), Bottom-up determination of air-sea momentum exchange under a major tropical cyclone, Science, 315(5819), 1707-1709.

Hwang, P. A., H. Garcia-Nava, and F. J. Ocampo-Torres (2011), Dimensionally Consistent Similarity Relation of Ocean Surface Friction Coefficient in Mixed Seas, Journal of Physical Oceanography, 41(6), 1227-1238.

Kudryavtsev, V. N., and V. K. Makin (2007), Aerodynamic roughness of the sea surface at high winds, Boundary-Layer Meteorology, 125(2), 289-303.

Kudryavtsev, V. N., and V. K. Makin (2011), Impact of Ocean Spray on the Dynamics of the Marine Atmospheric Boundary Layer, Boundary-Layer Meteorology, 140(3), 383-410.

Makin, V. K. (2005), A note on the drag of the sea surface at hurricane winds, Boundary-Layer Meteorology, 115(1), 169-176.

Rutgersson, A., E. O. Nilsson, and R. Kumar (2012), Introducing surface waves in a coupled wave-atmosphere regional climate model: Impact on atmospheric mixing length, J Geophys Res-Oceans, 117.

Smedman, A., U. Hogstrom, E. Sahlee, W. M. Drennan, K. K. Kahma, H. Pettersson, and F. Zhang (2009), Observational Study of Marine Atmospheric Boundary Layer Characteristics during Swell, J Atmos Sci, 66(9), 2747-2763.

Powell, M. D., P. J. Vickery, and T. A. Reinhold (2003), Reduced drag coefficient for high wind speeds in tropical cyclones, Nature, 422(6929), 279-283.

Taylor, P. K., and M. J. Yelland (2001), The dependence of sea surface roughness on the height and steepness of the waves, Journal of Physical Oceanography, 31(2), 572-590.

Severity of climate change dictates the direction of biophysical feedbacks of vegetation change to Arctic climate - results from the coupled regional climate-vegetation model CMIP5 simulations

Wenxin Zhang[1], Christer Jansson[2], Paul A. Miller[1], Benjamin Smith[1] and Patrick Samuelsson[2]

[1] Department of Physical Geography and Ecosystem Science, Lund University, SE-223 62 Lund, Sweden (zhang_wenxin2005@hotmail.com)

[2] Rossby Centre, Swedish Meteorological and Hydrological Institute, SE-601 76, Norrköping, Sweden

Vegetation-climate feedbacks induced by vegetation dynamics under climate change alter biophysical properties of the land surface that regulate energy and water exchange with the atmosphere. Simulations with Earth System Models applied at global scale suggest that the current warming in the Arctic has been amplified, with large contributions from positive feedbacks, dominated by the effect of reduced surface albedo as an increased distribution, cover and taller stature of trees and shrubs mask underlying snow, darkening the surface. However, these models generally employ simplified representation of vegetation dynamics and structure and a coarse grid resolution, overlooking local or regional scale details determined by diverse vegetation composition and landscape heterogeneity.

In this study, we perform simulations using an advanced regional coupled vegetation-climate model (RCA-GUESS) applied at high resolution (0.44×0.44°) over the Arctic Coordinated Regional Climate Downscaling Experiment (CORDEX-Arctic) domain. The climate component (RCA4) is forced with lateral boundary conditions from EC-EARTH CMIP5 simulations for three representative concentration pathways (RCP 2.6, 4.5, 8.0). Vegetation-climate response is simulated by the individual-based dynamic vegetation model (LPJ-GUESS), accounting for phenology, physiology, demography and resource competition of individual-based vegetation, and feeding variations of leaf area index and vegetative cover fraction back to the climate component, thereby adjusting surface properties and surface energy fluxes. The simulated 2m air temperature, precipitation, vegetation distribution and carbon budget for the present period has been evaluated in another paper. The purpose of this study is to elucidate the spatial and temporal characteristics of the biophysical feedbacks arising from vegetation shifts in response to different CO_2 concentration pathways and their associated climate change. Our results indicate that the albedo feedback dominates simulated warming in spring in all three scenarios, while in summer, evapotranspiration feedback, governing the partitioning of the return energy flux from the surface to the atmosphere into latent and sensible heat, exerts evaporative cooling effects, the magnitude of which depends on the severity of climate change, in turn driven by the underlying GHG emissions pathway, resulting in shift in the sign of net biophysical at higher levels of warming. Spatially, western Siberia is identified as the most susceptible location, experiencing the potential to reverse biophysical feedbacks in all seasons. We further analyze how the pattern of vegetation shifts triggers different signs of net effects of biophysical feedbacks.

Dynamical downscaling with RIEMS over East Asia

Deming Zhao, Congbin Fu and Xiaodong Yan

Key Laboratory of Regional Climate-Environment for Temperate East Asia, Institute of Atmospheric Physics, Chinese Academy of Sciences, Beijing 100029, China (zhaodm@tea.ac.cn)

1. Model Introduction

RIEMS1.0 (Regional Integrated Environmental Modeling System version 1.0) was developed by researchers from the START (Global change System for Analysis, Research, and Training) Regional Center for Temperate East Asia, IAP/CAS in 1998. The model was built on the thermodynamic frame of PSU/NCAR MM5V2, into which a land surface scheme (BATS1e) and radiative transfer scheme (the revised CCM3) are integrated. The model has been widely used in regional climate studies in the East Asia monsoon system and expresses excellent performance from RMIP (Regional Climate Model Inter-comparison Project). RIEMS2.0 is now being developed starting from RIEMS1.0 by the Key Laboratory of Regional Climate Environment Research for Temperate East Asia, IAP/CAS, and Nanjing University. The new version is built on the thermodynamic framework of nonhydrostatic approximation from MM5V3 with the same land surface model and radiation scheme as RIEMS1.0. To make it an integrated modeling system, the Princeton ocean mode (POM), Atmosphere-Vegetation interaction model (AVIM) and a chemical model are now being integrated.

2. Simulated results

In order to test RIEMS2.0's ability to simulate short-term climate, we perform ensemble simulations with different physics process schemes. The model is used to perform ensemble simulations on two continuous extreme climate events, which is serve drought with high temperature in north China in the summer of 1997 and serve flood in the Yangtze River valley in the summer of 1998 (Zhao et al., 2010). The results show that RIEMS2.0 can reproduce the spatial distribution of the precipitation and surface air temperature (SAT) from two continuous extreme climate events in the summer of 1997/1998, and disclose sub-regional characteristics. Though difference can be found among ensemble members, ensembles can decrease the model's uncertainty and improve the simulation decision in a certain degree. The model's performance on the precipitation and surface air temperature simulation can be improved with suitable physics process schemes.

In order to test RIEMS2.0's ability to simulate long-term climate and climate change, we compare simulated precipitation and SAT from 1980 to 2007 under different cumulus parameterization schemes with the observed data (Zhao et al., 2009). The results show that RIEMS2.0 can also reproduce the spatial distribution of precipitation and SAT, but that the model overestimates precipitation with the rainfall center moving northwestward and underestimates SAT for annual simulations. Annual, interannual variations and the anomalies in precipitation and SAT for different climate subregions are well captured by the model. Although similar distribution can be found between observed data and simulated results under different cumulus parameterization schemes, these show differences in intensity and location.

Further analysis on RIEMS2.0's performance on simulated precipitation compared with observed meteorological data over East Asia show that RIEMS2.0 reproduces the spatial distribution of precipitation in East Asia but that the simulation overestimates precipitation (Zhao, 2013). The simulated 30-year precipitation average is 26％greater than the observed precipitation. Simulated upper and root soil water correlate well with remote sensing derived soil moisture. Annual and interannual variation in the average precipitation and their anomalies are both well reproduced by the model. A further analysis of three subregions representing different latitude ranges shows that there is good correlation and consistency between the simulated results and the observed data. Annual variation, interannual variation of average precipitation, and the anomalies in the three sub-regions are also well captured by the model. The model's performance on atmospheric circulation and moisture transport simulations is discussed to explore the bias between the simulation and observations.

3. Conclusions

RIEMS2.0 shows stability and does well in both simulating long-term climate and climate changes in East Asia. RIEMS2.0 can reproduce the characteristics of the East Asia Monsoon system, as well the rain belt movement. Simulated results and observed data for the monthly mean precipitation and SAT correlate well. There is nice consistency for the anomalies between the simulation and observation. RIEMS2.0 can also disclose regional climate characteristics over East Asia in a certain degree.

References

Zhao Deming, Congbin Fu, Xiaodong Yan, 2009: Testing the ability of RIEMS2.0（Regional Integrated Environment Modeling System）to simulate multi-year precipitation and air temperature in China. Chinese Science Bulletin, 54(17): 3101-3111, doi: 10.1007/s11434-009-0178-3

Zhao Deming, Congbin Fu, 2010: The analysis on the ability of RIEMS2.0 (Regional Integrated Environment Modeling System) to simulate two extreme climate events in the summer of 1997/98 in China. Acta Meteorologica Sinica, 68(3):325-338 (in Chinese)

Zhao Deming, 2013: Performance of Regional Integrated Environment Modeling System (RIEMS) in precipitation simulations over East Asia. Climate Dynamic, 40:1767-1787, DOI: 10.1007/s00382-012-1660-1.

Topic 2

Very high-resolution RCMs

Using High Resolution climate Modelling to Study the Effect of Climate Change on Lylan Valley Ground Water Characteristic in Kirkuk City in Iraq

Sameer S. Al-Juboori , Fawzi M. Omer

Kirkuk Technical College, Iraq

Laylan Valley is one of the main food crop baskets in Kirkuk city in Iraq. In this study, 40 years data were used to build a model for the variation of some ground water properties like Ec, TDs …… Ca++ using Milkankovich cycle pattern repetition of the discrete in the rainfall in the study area.

Amplified climate change signal due to urban expansion at local scales from a regional climate model.

Daniel Argüeso[1,2], Jason P. Evans[1,2], Lluís Fita[2,3], Andrew J. Pitman[1,2] and A. Di Luca[2]

[1] ARC Centre of Excellence for Climate System Science, University of New South Wales, Sydney, Australia (d.argueso@unsw.edu.au)
[2] Climate Change Research Centre, University of New South Wales, Sydney, Australia
[3] Laboratoire de Météorologie Dynamique, UPMC-Jussieu, CNRS, Paris, France

1. Introduction

The climate in the city is clearly different than in neighboring rural areas. Urban structures alter the local atmosphere in a breadth of ways creating an environment with its own climate characteristics. In a future where rapid population growth, changing urban landscapes and climate change will pose enormous challenges to our society, understanding the different response of the urban and rural areas to changes in climate is crucial.

Quantifying the effect of urban structures in the local climate requires that the cities be explicitly represented in the model and, for most studies, that the regional climate model resolution be as high as possible to resolve the urban scales. Computational limitations and model structure have often limited research of future urban climate.

This study examines the role of urbanization under climate change conditions. For that purpose, a regional climate model was configured at unparalleled spatial resolution in the context of climate runs to investigate the climate in a plausible future scenario. The model outputs were analyzed to determine to which extent urban expansion could modify the local climate change signal.

2. Methodology

The Weather Research and Forecasting (WRF) modeling system was selected to simulate the climate over Greater Sydney Area at very high spatial resolution (2km) spanning 20-year periods (Argueso et al. 2013). The finest domain was embedded in a 10km domain that was in turn nested in a 50km domain (Figure 1).

The WRF default land use dataset was replaced with data from the New South Wales (NSW) state government to better describe the Sydney area and the extension of the city. A future scenario of the urban expansion was derived from the NSW urban development planning.

Three simulations were completed. A first run spanning the period 1990-2010 and using present climate land use was performed to represent as closely as possible the present climate. A second run covering the period 2040-2060 and using the future scenario of urban development was completed to study the combined effect of climate change and city sprawl. Finally, a third simulation over the period 2040-2060 was performed using the present land use to separate the effects of climate change alone. All three runs were driven by the CSIRO-MK3.5 Global Climate Model and the A2 scenario was adopted for the future climate runs. Rather than a formal projection where a number of ensembles is required, this experiment is aimed at quantifying the impact of urbanization for a given climate change signal.

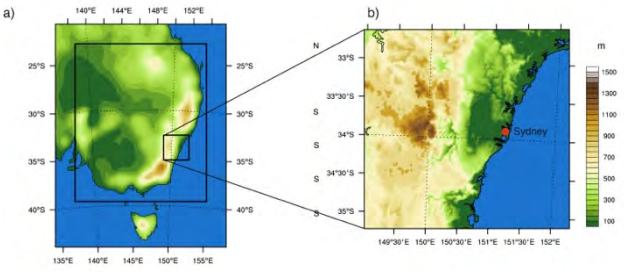


Figure 1. a) Location of the WRF domains at 50-km, 10-km and 2-km spatial resolution. The 10-km and 2-km domains are defined by black rectangles. b) Topography of the 2-km domain.

Mean projected changes in daily maximum and minimum temperature, as well as humidity were investigated. The combined changes in both variables were aggregated into a heat stress index to measure impact on human comfort within the city.

In addition to changes in the annual mean values, seasonal changes were also calculated to determine whether the effect of urban expansion varies across the year.

A set of thresholds was also chosen for the heat stress index (Sherwood and Huber, 2010) to measure the effect of urban growth on the frequency of particularly adverse conditions in a future climate.

Finally, changes in the daily cycle of the surface energy budget were analyzed to identify processes responsible for these changes at different times of the day.

3. Results

Figure 2b shows the daily minimum temperature climatology for the present climate from the model. The effects of the urban areas on minimum temperature can be observed in the present climate, when the urban areas tend to cool less during the nights than rural counterparts.

However, it is for the future projected changes when the impact of urban development is better observed. Urban expansion has major influence on minimum temperature changes and its contribution is comparable to the effect of climate change alone. In areas where the city is expected to grow, the combined effect of climate change and urbanization is approximately twice the

projected changes without urban expansion. While the domain will be subjected to relatively homogeneous changes according to this particular simulation using current land use (Figure 2d), the footprint of urban development is clear in the spatial patterns of minimum temperature changes using the future land use (Figure 2c).

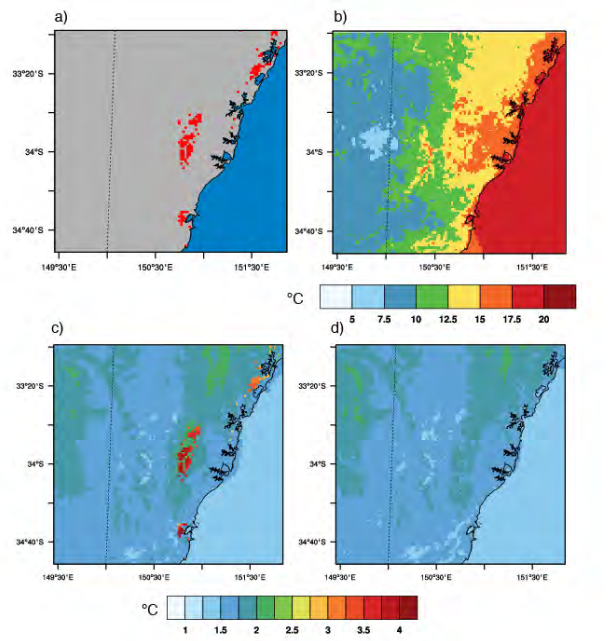


Figure 2. a) Areas of changes projected urban expansion in Greater Sydney Area (red), b) Daily minimum temperature annual climatology (1990-2010) from WRF, c) Mean changes in daily minimum temperature (2040-2060 minus 1990-2010) with c) land use changes and d) the present land use.

On the other hand, changes in daily maximum temperature are driven by large scale forcing only and no effect of urban development could be seen.

In terms of seasonal changes, urbanization seems to have a particularly strong contribution during winter and spring, although the footprint of land use changes in minimum temperature is clearly noticeable during all seasons.

Impervious surfaces hinder evaporation in the urban areas and thus near surface humidity is affected. Changes in humidity and temperature were aggregated into the wet-bulb globe temperature (WBGT) as a measure of heat stress. Projections of WBGT were examined and they reveal that, despite the fact that humidity reduction partly compensates temperature increases in the city in terms of human comfort, thresholds of adverse to dangerous WBGT values will be exceeded more frequently in the new urban areas.

The daily cycle of surface energy budget is not projected to change using the present city extension. However, when the urban expansion is incorporated, latent heat exchanges at the surface are significantly reduced in the new urban areas. During the central hours of the day, net radiation (incoming) is reduced. The latent heat is now channeled into sensible heat, which increases. Overall, the new partition has no effects on maximum temperature. Around sunset, the signs of net radiation and sensible heat reverse. Radiation from the surface increases and sensible heat uptake is reduced, which leads to higher near surface minimum temperatures.

References

Argueso D., Evans J.P, Fita L. and Bormann K.J. (2013) Temperature response to future urbanization and climate change, in press.

Sherwood S. and Huber M. (2010) An adaptability limit to climate change due to heat stress, PNAS, 107, 21, pp 9552-9555.

Cloud-resolving regional climate modeling approach in decade-long simulations

Nikolina Ban[1], Jürg Schmidli[1] and Christoph Schär[1]

[1] Institute for Atmospheric and Climate Science, ETH Zurich, Zurich, Switzerland (nikolina.ban@env.ethz.ch)

1. Introduction

The uncertainties in current global and regional climate model integrations are partly related to the representation of clouds, moist convection, and complex topography. Reducing the grid spacing down to some few kilometers and switching off the convection parameterization (as is done in cloud-resolving models; CRM) is thus an attractive approach. On climate time scales, cloud-resolving methods have been used for process studies (e.g., Hohenegger et al., 2008, Langhans et al., 2012, Froidevaux et al. 2014), and for extended validation studies on relatively small domains (e.g., Kendon et al., 2012, Prein et al., 2013). The application to long-term scenario simulations has been very limited. Here we present cloud-resolving simulations for a 10-year-long periods over an extended Alpine domain (1100 km x 1100 km). It is one of the first cloud-resolving climate simulations covering such a large domain for such a long time period. The set of simulations includes a validation period (driven by reanalysis), as well as control and scenario periods driven by a CMIP5 GCM. The summary presented here is largely based on the validation period and follows a submitted manuscript (Ban et al., 2014).

2. Model setup and observations

The simulations are integrated with the COSMO-CLM model and driven by ECMWF interim reanalysis data (for present day climate) and a global climate model (control and scenario run). Two one-way nested grids are used with horizontal resolutions of 2.2 km for a cloud-resolving model (CRM2) over an extended Alpine domain (1100 km x 1100 km), and 12 km for a cloud-parameterizing simulation (CPM12) covering Europe. The CRM2 is driven by lateral boundary conditions from the CPM12 run, while the CPM12 run is driven by lateral boundary conditions from ERA-Interim reanalysis and the Earth-System Model of the Max-Planck-Institute (MPI-ESM-LR).

Validation of simulations is conducted against high-resolution surface observations: this includes daily precipitation analysis from a high-resolution station data set over the Alpine region (Isotta et al., 2013), radar-disaggregated hourly precipitation analysis over Switzerland (Wüest et al., 2010), and conventional European-scale precipitation data (EOBS, Haylock et al., 2008).

3. Results

The CRM2 model strongly improves the simulation of the diurnal cycles of precipitation (Figure 1) and temperature, despite a slightly enhanced warm bias and a tendency for the overestimation of precipitation over the Alps. The CPM12 model has a poor diurnal cycle associated with the use of parameterized convection (Figure 1).

The assessment of precipitation statistics reveals that both models adequately represent the frequency-intensity distribution for day-long events (not shown).

Larger differences occur for the frequency distribution of daily maximum hourly precipitation sums (Figure 2). The CPM12 model underestimates the frequency of wet events, while CRM2 shows good agreement with observations for weak and moderate precipitation, but overestimates the frequency of heavy hourly events, which is consistent with the overestimation of the 90th percentile of hourly precipitation (not shown). However, this overestimation gets smaller if one qualitatively accounts for the underestimation in observations due to gauge-undercatch.

We also present results on the scaling of precipitation extremes with local daily-mean temperatures following Berg et al. (2013). In accordance with observations, CRM2 exhibits adiabatic scaling for intermediate hourly events (90th percentile) and super-adiabatic scaling for extreme hourly events (99th and 99.9th percentiles) during the summer season. The CPM12 model has difficulties in obtaining the observed scaling for high temperatures.

The excellent performance of CRM2 in representing hourly precipitation events in terms of intensity and scaling is highly encouraging, as this addresses a previously untested (and thus untuned) model capability.

4. Outlook

We will also present preliminary results on the scenario simulations using projections driven by a GCM for control and validation periods. Particular consideration will be given to extreme precipitation events.

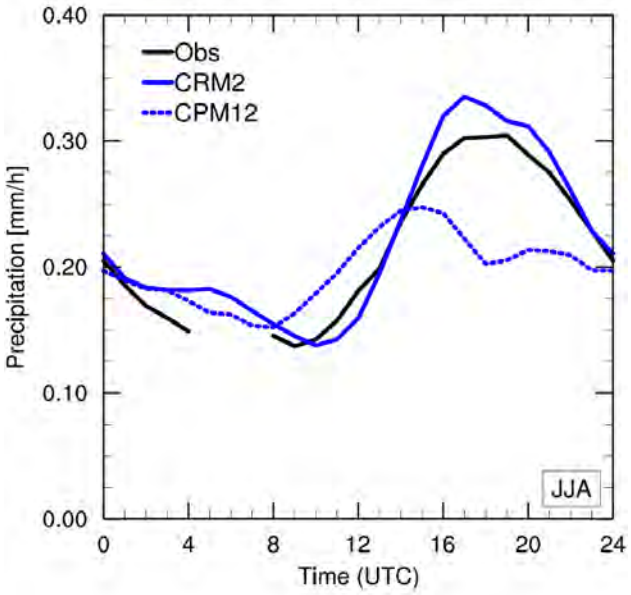


Figure 1. Mean diurnal cycle of summer (JJA) precipitation (mm/h) for observations (black line), CRM2 (solid blue) and CPM12 (dashed blue). The observations use an objective analysis based on radar and rain gauge data. The precipitation has been averaged over the area of Switzerland, and for the time period 2004-2007 when hourly precipitation observations were available.

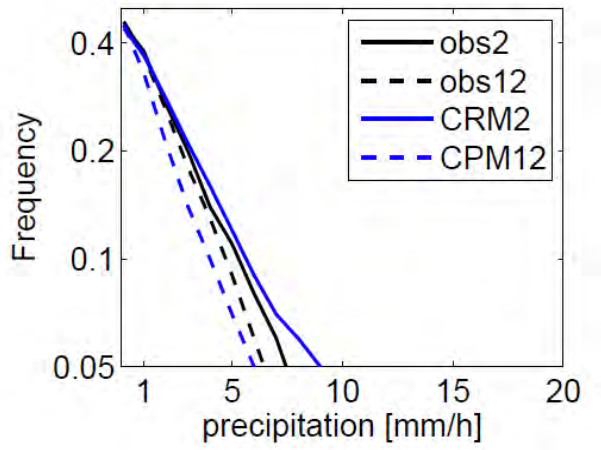


Figure 2. Cumulative distributions of daily maximum hourly precipitation as a function of threshold expressed relative to the total number of days. For observations, the frequency distribution is calculated on the original 2 km grid (obs2) and on an upscaled 12 km grid (obs12). The distributions have been calculated for the summer (JJA) season in the period 2004-2007 over Switzerland.

References

Ban, N., J. Schmidli and C. Schär (2014) Evaluation of the cloud-resolving regional climate modelling approach in decade-long simulations, Submitted to JGR.

Berg, P., C. Moseley and J.O. Haerter (2013), Strong increase in convective precipitation in response to higher temperatures, Nature Geoscience, &, 181-185.

Froidevaux, P., L. Schlemmer, J. Schmidli, W. Langhans and C. Schär (2014), Influence of the background wind on the local soil moisture-precipitation feedback, J. Atmos. Sci., 71, 782-799

Haylock, M., N. Hofstra, A. K. Tank, E. Klok, P. Jones, and M. New (2008), A European daily high-resolution gridded dataset of surface temperature and precipitation, J. Geophys. Res. (Atmospheres), 113, D20119, doi:10.1029/2008JD10201

Hohenegger, C., P. Brockhaus and C. Schär (2008), Towards climate simulations at cloud-resolving scales., Meteorol. Z., 17, 383-394

Isotta, F., C. Frei, V. Weilguni, M. P. Tadic, P. Lassegues, B. Rudolf, V. Pavan, C. Cacciamani, G. Antolini, S. M. Ratto, M. Munari, S. Micheletti, V. Bonati, C. Lussana, C. Ronchi, E. Panettieri, G. Marigo, and G. Vertaµcnik (2013), The climate of daily precipitation in the Alps: development and analysis of a high-resolution grid dataset from pan-Alpine rain-gauge data, Int. J. Climatol., doi:10.1002/joc.3794.

Kendon, E. J., N. M. Roberts, C. A. Senior and M. J. Roberts (2012) Realism of rainfall in a very high resolution regional climate model, J. Climate, 25, 5791-5806

Langhans, W., J. Schmidli and C. Schär (2012) Bulk convergence of cloud-resolving simulations of moist convection over complex terrain, J. Atmos. Sci., 69, 2207-2228

Prein, A. F., A. Gobiet, M. Suklitsch, H. Truhetz, N. K. Awan, K. Keuler and G. Georgievski (2013) Added value of convection permitting seasonal simulations, Climate Dyn., 41 (9-10), 2655-2677

Wüest, M., C. Frei, A. Altenho, M.Hagen, M. Litschi, and C. Schär (2010), A gridded hourly precipitation dataset for Switzerland using rain-gauge analysis and radar-based disaggregation., Int. J. Climatol., 30, 1764-1775

Downscaling of precipitation for the Himalayas using WRF model

Bhuwan Chandra Bhatt

Uni Climate, Uni Research AS and the Bjerknes Center for Climate Research, Norway (bbh081@uni.no)

1. Introduction

The Himalayas are believed to be hotspot of climate change (IPCC 2013), but little is known in detail about region`s current climate. The effect of climate change on the regional characteristics of Himalayan precipitation is unclear, but likely very important given the large precipitation totals. The enhanced warming due to climate change is likely to alter the diurnal heating cycles that modulate atmospheric processes and hence, the precipitation. So, precipitation projections at high resolution are essential to assess potential future climate change impacts on the Himalayas.

In this research, we use dynamic downscaling technique and the Weather Research and Forecasting (WRF) model is nested inside the Norwegion Earth System Model (NorESM). The main objective of this study is to emphasize the diurnal cycle of precipitation and also to discuss any projected future change of precipitation patterns around the Himalayas.

2. Data and Method

A large domain, encompassing the Himalayas is chosen for downscaling (not shown). Two experiments are performed using WRF as: the present day simulations for 2000-2010 and future simulations under RCP8.5 for the period 2030-2050. The model is run at a spatial resolution of 12 km x 12 km with 4 hourly output. The observed precipitation data used are the 4 hourly TRMM radar data averaged for 2000-2010. Other data used include TRMM 3B43, Aphrodite, GSMap_MVK precipitation products.

Precipitation is assessed over selected sub-regions over the Himalayas. The patterns of diurnal precipitation are obtained by averaging over selected sub-regions and performing an EOF analysis, in order to extract the dominant modes of variability. The first two EOF`s are used to reconstruct the diurnal cycle in order to highlight the most robust signals.

3. Results

The diurnal precipitation features in GSMap observations and WRF model are encapsulated within the first tow EOF`s, which explain over 75% of the variance in GSMap and 90% in the WRF model (not shown). There are difference between modeled and GSMap percentage variance for EOF1, however, EOF2 is essentially identical. This is similar to results shown by Kikuchi and Wang (2008).

A different perspective on the diurnal cycle is presented in terms of peak local time in precipitation. The TRMM radar data shows midnight-early morning rainfall maxima over the Himalayas and daytime maxima over northern India, the Tibetan Plateau and at higher elevations over the Himalayas. The model also shows similar features. The major deficiencies of the model are the too large amplitude and too early initiation of precipitation seen in most of sub-regions.

Projected changes in precipitation in model simulations from 2030-2050 are also investigated.

4. Summary

The present precipitation simulations are first evaluated against observations to establish model credibility and the results indicate that model simulates the present diurnal cycle of precipitation reasonably well.

The differences in the dynamics behind the two EOF`s can give insight as to which processes the model represents well.

The future precipitation projections are evaluated to determine the regional patterns of climate change. The future simulations do not indicate a shift in the diurnal cycle. Although the projected future changes of precipitation presented in this article are within of the expected range of precipitation changes caution must be exercised when interpreting single-model experiments.

References

IPCC (Intergovernmental Panel on Climate Change), 2013. Climate change 2013: The physical science basis: contribution on working group I to the Fifth assessment report of the IPCC. [Stocker, T. F., D. Qin, G.-K. Plattner, M. Tignor, S. K. Allen, J. Boschung, A. Nauels, Y. Xia, V. Bex, and P. M. Midgley (eds.)]. Cambridge University Press, Cambridge, United Kingdom and New York, NY, USA (in press).

Kikuchi, K. and B. Wang (2008), Diurnal precipitaton regimes in the global tropics, J. Climate, 21, 2680-2696.

Ensuring a robust regional model experimental design for future projection of extreme weather during the North American monsoon in the Southwest U.S.

Christopher L. Castro, Hsin-I Chang , Thang Luong, Megan Jares, Timothy Lahmers, and Carlos Carrillo

Department of Atmospheric Sciences, University of Arizona, Tucson, Arizona, USA (castro@atmo.arizona.edu)

1. Motivation and Overview

The North American Monsoon (NAM) occurs in late summer and is the principal driver of severe weather events in the Southwest U.S. Formation of ridge of high pressure (or monsoon ridge) over western North America facilitates the transport of moisture from the Gulf of California, Gulf of Mexico, and eastern Pacific and the passage of synoptic-scale transient disturbances. With sufficient atmospheric instability and moisture, convection over high terrain initiates in the early afternoon and later may organize into mesoscale convective systems (MCSs). Most monsoon-related severe weather occurs in association with this organized convection, including microbursts, dust storms, flash flooding, and lightning.

Our ultimate objective is to project how monsoon severe weather is changing due to anthropogenic global warming. We first consider a dynamically downscaled reanalysis, generated with the Weather Research and Forecasting (WRF) model, to evaluate identified severe weather events during the period 1948-2010. Changes in the character of severe weather events within this period likely reflect long-term climate change driven by anthropogenic forcing. Next, we apply the identical model simulation analysis procedures to dynamically downscaled CMIP3 and CMIP5 models, to assess how monsoon severe weather may change in the future and if these change correspond with what is already occurring per the downscaled reanalysis and real observational data. Our current emphasis is on developing a robust regional model experimental design that is suitable for severe weather event projection, which reasonably accounts for the known thermodynamic and dynamic prerequisites for severe monsoon weather and appropriately simulates convective organization and propagation. Results from this project will be used for climate change impacts assessment for U.S. military installations in the Southwest.

2. Regional modeling approach

Two sources of boundary forcing to the regional atmospheric model are considered. The NCEP-NCAR global reanalysis (1950-2010) retrospectively considers the previous approximately 60 year historical period and defines the “perfect” boundary forcing. Several “well performing” CMIP3 and CMIP5 global climate models for the Southwest, per an objective evaluation, are dynamically downscaled for the approximate period 1950-2100. Either the A2 or RCP 8.5 greenhouse gas emission scenarios are respectively considered. The specific CMIP3 models are MPI-ECHAM5 and UKMO-HadCM3. To explore the potential effect of global model improvement, the next generations of models from these same research centers are being utilized for CMIP5 data (MPI-ECHAM6 and UMKO-HadGEM). The Weather Research and Forecasting (WRF) model is used as a regional climate model to dynamically downscale all of these sources of data over North America with a grid spacing of 10s of kilometers Model domain and parameterizations that are somewhat similar to the NARCCAP experiment for CMIP3 data and CORDEX compliant for CMIP5 data. From the long-term WRF regional climate model simulations, days conducive to severe weather are identified considering the known thermodynamic and dynamic criteria for monsoon severe weather. The severe weather events are then simulated in a numerical weather prediction mode for 24h periods with convective-resolving grid spacing of 2km for a domain that covers just the Southwest U.S. This yields projection results that consider changes in extreme monsoon weather in a physically-based way, using a robust regional modeling paradigm that has been established for weather forecasting.

3. Criteria for identifying severe weather event days

Atmospheric instability and moisture are the necessary thermodynamic prerequisite conditions for monsoon thunderstorms, and can be respectively quantified in WRF data by the metrics of most unstable CAPE and column-integrated PW. The maximum daily values of CAPE and PW can be used to determine favorable days for severe weather. We define favorable days as those that fall within both the top 30% and 25% of the PW and CAPE distributions, respectively (Fig. 1). This selection method yields high correspondence with U.S. National Weather Service severe weather reports, using the WRF dynamically downscaled global reanalysis during the last twenty years, with a hit rate of approximately 67.7% in the vicinity of Tucson, Arizona. Using daily station data of the maximum values of CAPE and PW from seven rawinsonde deployment sites, an empirical orthogonal function (EOF) analysis, linear regressions and correlations are used to determine if spatial coherency is present in the severe weather condition across monsoon region. We found that CAPE and PW exhibit a high degree of spatial coherence across the Southwest during the monsoon, so one set of criteria can be effectively used to define the severe weather event days for the region.

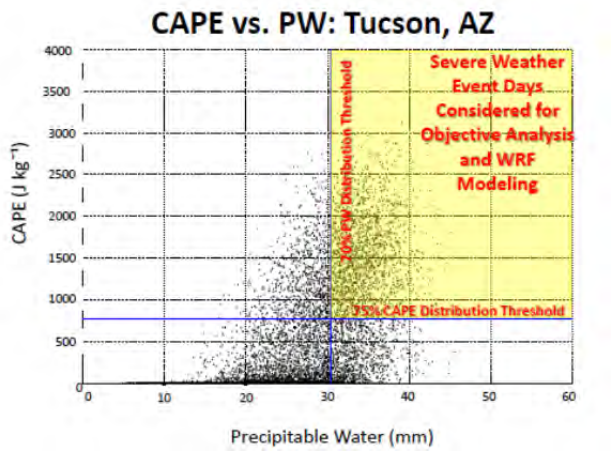


Figure 1: Scatter plot of CAPE (J kg^{-1}) versus PW (mm) in Tucson, Arizona, considering all days during the monsoon period (JJAS) from 1948-2010 , derived from dynamically downscaled reanalysis data. The thresholds at the 70th percentile for PW and 75th percentile for CAPE are used to select severe weather event days to be used for further analysis.

There are several dynamic criteria we then use to further classify severe weather event days. An EOF analysis of large-scale circulation patterns of the days determines the dominant orientations of the monsoon ridge over the Southwest. We look to see if the statistically dominant orientations of the monsoon ridge correspond to well-known atmospheric circulation patterns for severe monsoon weather. Surges of moisture from the Gulf of California are identified using wind direction and dew point temperature thresholds in the vicinity of Yuma, Arizona. Transient inverted troughs are identified with an objective vortex tracking approach. If the necessary thermodynamic and dynamic criteria are lacking in dynamically downscaled CMIP3 and CMIP5 models, then it would be inappropriate to consider them for severe weather event projection with convective-resolving simulations. Our work thus far promisingly indicates that the dynamically downscaled CMIP3 data do reasonably satisfy these metrics.

4. Convective-resolving severe weather simulations

We have performed the convective-resolving NWP-simulations on the identified monsoon severe weather events in the dynamically downscaled reanalysis for the period 1993-2010. To account for the episodic, or bust and break character of the convection, an extra day was added to the beginning and end of the event. Convective-resolving simulations are compared to the NCEP/EMC Stage IV radar-derived precipitation data to verify whether the model correctly exhibits the proper diurnal cycle and organization and westward propagation of monsoon convection. The convective resolving warm simulations show that monsoon convection appears to be reasonably well captured with the use of the dynamically downscaled reanalysis, in comparison to Stage IV data (Fig. 2). WRF tends to initiate convection too early, though correctly simulates convective maximum and propagation into the afternoon and evening. We are presently considering severe weather events in the dynamically downscaled CMIP3 and CMIP5 data.

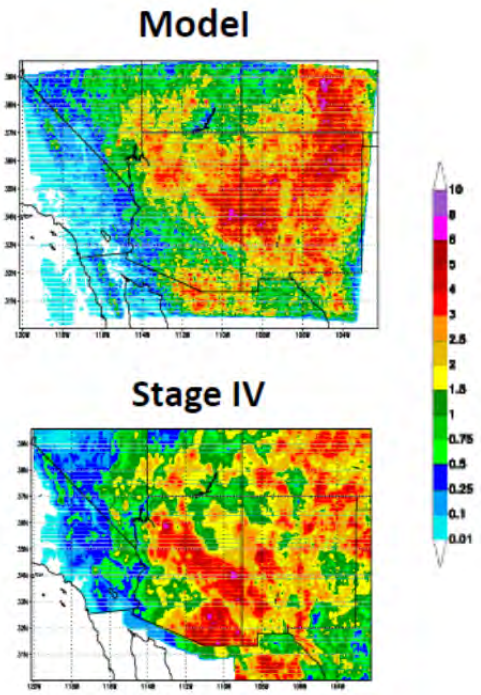


Figure 2: Composite daily mean of precipitation (mm) of all selected event days during 1993-2010 produced from WRF model simulation (top) compared to Stage IV precipitation data (bottom). There is high correspondence of the precipitation means of both the model and the Stage IV data.

Acknowledgments: This work is funded by the Strategic Environmental Research and Development Program (SERDP), Project RC-2205.

Precipitation intensity and return level change projections by a convective-permitting regional climate model

Steven C Chan[1], Elizabeth J Kendon[2], Hayley J Fowler[1], Nigel M Roberts[3], and Stephen Blenkinsop[1]

[1] Newcastle University, Newcastle-upon-Tyne, United Kingdom (steven.chan@metoffice.gov.uk)
[2] Met Office Hadley Centre, Exeter, United Kingdom
[3] Met Office@Reading, Reading, United Kingdom

Extreme precipitation intensities and return levels projections for the end-of-21st-century are simulated by the GCM-driven Met Office 1.5-km very-high-resolution convective permitting ("explicit convection") limited-area regional climate model. Such explicit convection models avoids known physical issues that are caused by convective parameterisation (Kendon et al 2012). Apart from that, these simulations are continuous over multiple years (i.e. not seasonal slices), so that land-surface feedbacks are reasonably captured.

Summer (JJA) extreme precipitation intensities are projected to increase by about 30%. Air temperatures for extreme wet days are projected to increase by approximately 4-5 degrees Kelvin. Hence the temperature increases are consistent with the 30% increase in precipitation intensity as according to the Clausius-Clapyeron relation (Trenberth et al 2003). However, we note that the higher temperature days in the future climate simulation have suppressed precipitation intensities, and this phenomenon is actually noted in observations (Hardwick Jones et al 2010). These high temperature days are poorly sampled in the control climate simulation.

The frequency of summer extreme and non-extreme precipitation is projected to decline substantially (by as much as 50%) in the future climate, and this leads to a smaller but still significant (~10%) increase in future summer return levels. The large event frequency decline is also found with coarser RCMs which give different intensities and return level projections (Kendon et al 2014). Hence, the summer model guidance can be summarised as "less frequent precipitation, but harder if it does".

A much larger increase (50+%) of winter (DJF) return levels are projected by the future climate simulation. Unlike the summer, no significant changes in precipitation frequencies are found. Similar Clausius-Clayeron scaling relationship is found with the winter increases.

References

Kendon, E J, N M Roberts, C A Senior, and M J Roberts (2012) Realism of rainfall in a very high resolution regional climate model, J. Climate, 25, 5791-5806.

Kendon, E J, N M Roberts, H J Fowler, M J Roberts, S C Chan, and C A Senior (2014) Heavier summer downpours with climate change revealed by weather forecast resolution model, Nature Clim. Change, submitted.

Hardwick Jones, R, S Westra, and A Sharma (2010) Observed relationships between extreme sub-daily precipitation, surface temperature, and relative humidity, Geo. Phys. Res. Lett., 37, L22805.

Trenberth, K E, A Dai, R M Rasmussen, and D B Parsons (2003) The changing character of precipitation, Bull. Am. Meterol. Soc., 84, 9, pp. 1205-1217.

Feasibility Study of Very High Resolution Regional Climate Modelling Through Grid Telescoping Applied to the Canadian Regional Climate Model (CRCM5)

Mélissa Cholette and René Laprise

Centre ESCER, Département des sciences de la Terre et de l'atmosphère, Université du Québec à Montréal, Montréal (Québec) Canada (cholette.melissa.2@gmail.com)

1. Introduction

Today General Circulation Models (GCMs), with grid spacing generally around 250 to 100 km, have too coarse resolution to adequately resolve many important mesoscale processes. The alternative approach with nested Regional Climate Models (RCMs) using finer grid spacing (25 to 50 km) partly resolves some of these processes, but the resolution still too coarse for a proper representation of several important weather and climate features that may be relevant for impacts studies. Seek effective ways to produce higher resolution climate simulations at an affordable computational cost, this study proposes to apply the grid telescoping method (or cascade) to fifth-generation Canadian Regional Climate Model (CRCM5; Hernández-Díaz et al. 2013) and to perform a feasibility study of very high resolution simulations.

This paper pursues two goals. One is illustrating the potential usefulness and interest for climate impact studies of kilometer-scale climate simulations by showing specific samples of simulated results. The other is demonstrating the computational affordability of such simulations performed with telescoping domains and time slices of events. The cascade is based on a suite of nested-grid simulations, with larger domain coarse-mesh simulations successively driving smaller domain simulations with finer meshes. Hence each nested model uses lateral boundary conditions (LBCs) provided by the previous coarser grid simulation's outputs.

2. A Pragmatic Cascade Strategy

The proposed grid telescoping strategy aims at obtaining very high-resolution climate integrations at an reasonable computational cost. Starting from the computing time for a global model:

$$C_{GCM} = K * N_x * N_y * N_z * N_t \qquad (1)$$

where K is the average cost per grid point, N_x and N_y are the numbers of grid points along horizontal x- and y-axes, respectively, N_z is the number of levels in the vertical, and N_t is the number of time steps required to complete the simulation. It is well known that the computational cost of a GCM is an inverse function of third power of grid spacing. With an RCM, if one accepts to keep the same number of grid points (hence reducing the physical domain size with increasing resolution), the cost is simply inversely proportional to the first power of the grid spacing. If one were to further accept to reduce the period of integration as the resolution increases, then the theoretical computational cost would remain constant for each step of the cascade, independent of the mesh size.

3. The Model Domains and Grids Description

A suite of five one-way nested CRCM5 simulations has been performed with horizontal grid mesh of 0.81°, 0.27°, 0.09°, 0.03° and 0.01° (hereinafter referred to as d81, d27, d9, d3 and d1, respectively). The respective domains are shown in Fig. 1. The time steps, the archival times and the lengths of integrations are decreased as the resolution is increased in the cascade.

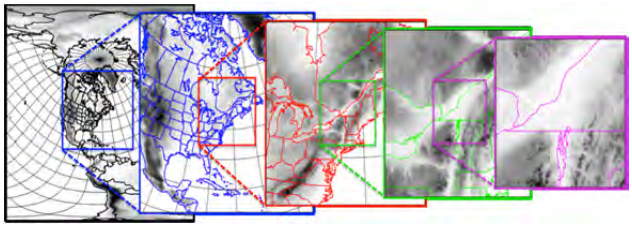


Figure 1. The computational domains used for the CRCM5 cascade: d81 (black contours) for the 0.81° mesh, d27 (blue) for the 0.27°, d9 (red) for the 0.09°, d3 (green) for the 0.03° and d1 (pink) for the 0.01° simulations. The domains are square and centred on Montréal (Québec, Canada: 45°30'N, 73°35'W). The grey tones represent the topography in each of the domains. [Source: Cholette and Laprise (2014), submitted to Climate Dynamics.]

The d81 simulation was driven at 6-hourly intervals by the ERA-Interim data, the d81 outputs are used to drive d27 at 3-hourly intervals, the d27 samples are driving the d9 simulation at hourly interval, the d9 simulation provided driving data for d3 at 20-min intervals, and the d1 simulation was driven by d3's data at 5-min intervals. A major change of model formulation was operated in CRCM5 with grid meshes finer than 9 km: for these convection-permitting simulations, the non-hydrostatic option and the prognostic cloud and precipitation microphysics of Milbrandt and Yau (2005) were turned on, and the deep convection parameterization turned off. The 3-km simulation with prognostic cloud and precipitation microphysics requires LBCs for the six types of hydrometeors' masses and concentrations; such information is not available from the diagnostic schemes used at larger scales (d81, d27 and d9).

4. Results

We will show here some examples of the added value associated with increased resolution afforded by the cascade method: (1) low-level winds intensity, frequency and direction, (2) kinetic energy spectra, and (3) precipitation patterns and intensity distributions.

The channelling effect in the St Lawrence River Valley (SLRV) plays an important role in the occurrence of freezing rain in southern Québec. Carrera et al. (2009)

have documented that the low-level winds in the SLRV can become very strong, especially under stable atmospheric conditions, blowing in the direction along the valley, roughly from high to low surface pressure. The results show that CRCM5 meshes of 9 km or finer are required for realistic simulation of wind channelling in the SLRV (Fig. 2). Wind roses diagrams of the grid point nearest to Québec City also show changes in the winds directions (from North-West for d81 to North-East/South-West for d9 and d3) and intensities (low for d81 to high for d9 and d3) as the grid is refined (not shown).

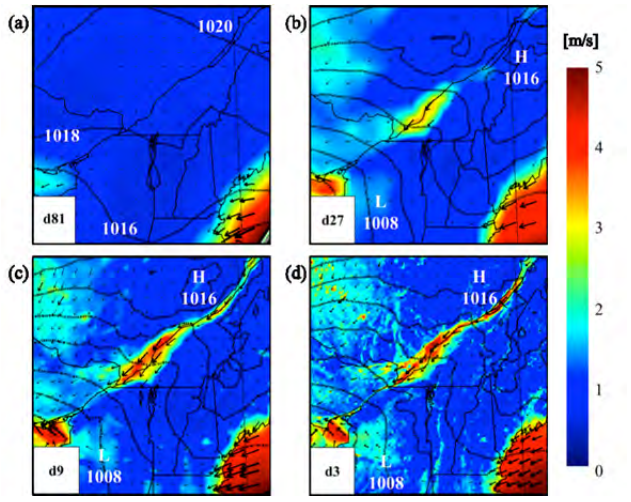


Figure 2. Typical situation for northeast winter winds channelling in the SLRV. Speed [m/s] and directions (background colors and black arrows, respectively) of the 1000hPa wind and the mean sea level pressure (black lines) for d81 (a), d27 (b), d9 (c) and d3 (d) simulations, at 1200 UTC 26 February 2002. [Source: Cholette and Laprise (2014), submitted to Climate Dynamics.]

Variance spectra are useful tools to analyse dynamical equilibrium in fine scales. Kinetic energy variance spectra can be computed over limited-area domain using the Discrete Cosine Transform (DCT; Denis et al. 2002). The spectra are analysed in term of spin-up time and effective resolution. The spin-up time is the time needed for the simulation to develop fine-scale variance starting from the coarser-mesh driving data. The spin-up times decrease with finer mesh, varying from roughly 12 h for d81 and d27, 10 h for d9, 2 h for d3 and 50 min for d1 (not shown). These results are in general agreement with those obtained by Skamarock (2004) with the WRF model. Variance spectra provide a first measure of the necessary condition to be fulfilled for declaring a scale as resolved: length scales shorter than the effective resolution have to be considered as suspect in model simulations. The results showed that the effective wavelengths are 571, 190, 63 and 21 km for d81, d27, d9 and d3, respectively, which corresponds to roughly seven times the grid spacing, i.e. 3.5*(2*Δx). This finding is also consistent with the result obtained by Skamarock (2004).

Finally, precipitation intensity distributions of the five domains have been computed and compared. The three- and one-hourly precipitation intensity distributions exhibit systematic changes as a function of resolutions: the frequently occurring weaker intensity precipitations in low-resolution simulations are shifted towards higher intensity with finer mesh (not shown). This shift goes in the right direction to correct a long-standing bias of most coarse-mesh models. The results showed that the overall patterns are similar, reflecting the control exerted by the LBCs during the cascade (Fig. 3).

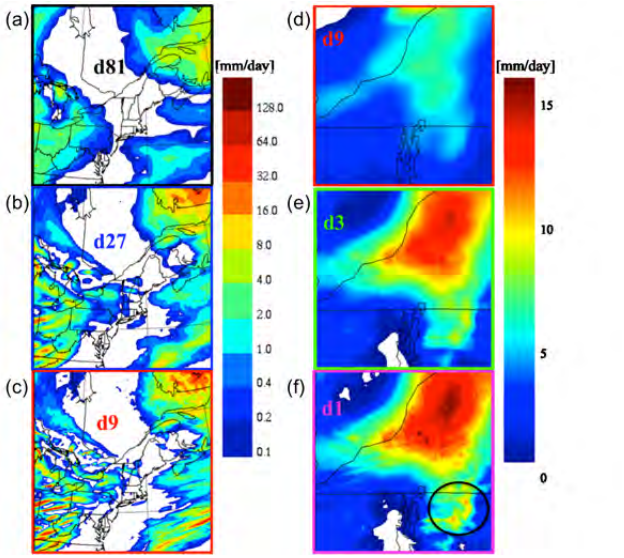


Figure 3. Precipitation rates [mm/day] for d81 (a), d27 (b), d9 (c and d), d3 (e) and d1 (f). The maps are for the 0300 UTC 13 February 2002 time step for (a), (b) and (c), and the computation domain is d9. The maps are for the 0000 UTC 17 February 2002 time step for (d), (e) and (f) computed on the d1 domain. It can easily be seen that the general pattern are well preserved and that the intensity is enhanced with the refinement of the mesh. [Source: Cholette and Laprise (2014), submitted to Climate Dynamics.]

5. Conclusion

This paper aimed mostly at proposing the cascade method with telescoping grids as a pragmatic approach for achieving very high-resolution climate simulations and projections at a computationally affordable cost, and demonstrating its feasibility using the CRCM5. The evaluation of the simulations over a rather short period focussed mainly on establishing the plausible nature of the results, rather than a verification of their real quantity and accuracy. Future work is needed to evaluate the quality of simulations with available observations and to quantify the added value afforded by the cascade method.

References

Cholette M, Laprise R (2014) Feasibility study of very high resolution regional climate modelling through grid telescoping applied to the Canadian Regional Climate Model (CRCM5). Submitted to Climate Dynamics (December 19th 2013).

Denis B, Côté J, Laprise R (2002) Spectral decomposition of two-dimensional atmospheric fields on limited-area domains using the Discrete Cosine Transform (DCT), Mon Weather Rev 130, pp. 1812-1829

Hernández-Díaz L, Laprise R, Sushama L, Martynov A, Winger K, Dugas B (2013) Climate simulation over CORDEX Africa domain using the fifth-generation Canadian Regional Climate Model (CRCM5), Clim Dyn 40(5-6), pp. 1415-1433

Milbrandt JA, Yau MK (2005) A multimoment bulk microphysics parameterization. Part II: A proposed three-moment closure and scheme description, J Atmos Sci 62(9), pp. 3065-3081

Roebber PJ, Gyakum JR (2003) Orographic influences on the mesoscale structure of the 1998 ice storm, Mon Weather Rev 131, pp. 27-50

Skamarock WC (2004) Evaluating mesoscale NWP models using kinetic energy spectra, Mon Weather Rev 132, pp. 3019-3032

Land surface feedbacks on spring precipitation in the Netherlands

E.E Daniels[1], G. Lenderink[2], R.W.A.Hutjes[1], R. Ronda[3] and A.A.M. Holtslag[3]

[1] Earth System Science group, Wageningen University and Research center (WUR), the Netherlands (emma.daniels@wur.nl)
[2] Royal Netherlands Meteorological Institute (KNMI), De Bilt, the Netherlands
[3] Meteorology and Air Quality group, Royal Netherlands Meteorological Institute (KNMI), De Bilt, the Netherlands

1. Introduction

Land surface processes affecting the amount of evapotranspiration have substantial influence on both large-scale and mesoscale circulation (Chen; Dudhia 2001). Evaporation of (soil) moisture directly feeds back on temperature and precipitation (Seneviratne et al. 2010). The resulting soil moisture-precipitation feedback can be positive or negative. In addition, large urban areas have been shown to influence temperature and precipitation amounts, area, and triggering (e.g. Kalnay; Cai 2003; Shepherd 2005). However, little research has been conducted on the influence of urbanization within Europe (only Trusilova et al. 2009; Trusilova et al. 2008) although Even though 50% increase in urban area in 2040 compared to 2000 (Dekkers et al. 2012) is expected in the Netherlands.

2. Methods

The Weather Research and Forecasting (WRF) model is used to investigate the impact of soil moisture and urban areas on precipitation in the Netherlands. on a single domain of about 1000 x 1000 km. The domain is centered around the Netherlands (see Fig 1) and has a horizontal grid spacing of three kilometers. We analyze the average output of a four day event from 10-13 May 1999 for which the individual days had similar synoptical forcing. Four simulations (SM_...) are conducted to test the sensitivity of precipitation to soil moisture. We execute two additional experiments in which urban areas in the Netherlands are expanded and one in which urban areas are completely removed (URB_...).

3. Effects on precipitation

In the sensitivity experiments we conduct, local water availability is altered in two different ways: directly, through changes in soil moisture, and indirectly, through the evaporative fraction in urban areas. In our simulations a consistent reduction of precipitation under reduced soil moisture and increased urban coverage is found (see Fig **Fehler! Verweisquelle konnte nicht gefunden werden.**2). Meaning we find a positive soil moisture-precipitation feedback, i.e. wet soils increase the amount of precipitation. We quantify the strength of this feedback using the ratio of evaporation to precipitation and find an average of more than 65% in the soil moisture sensitivity experiments. Precipitation over land is in our case simply triggered by the instable air over land due to the large temperature and associated moisture contrast between the sea and the land.

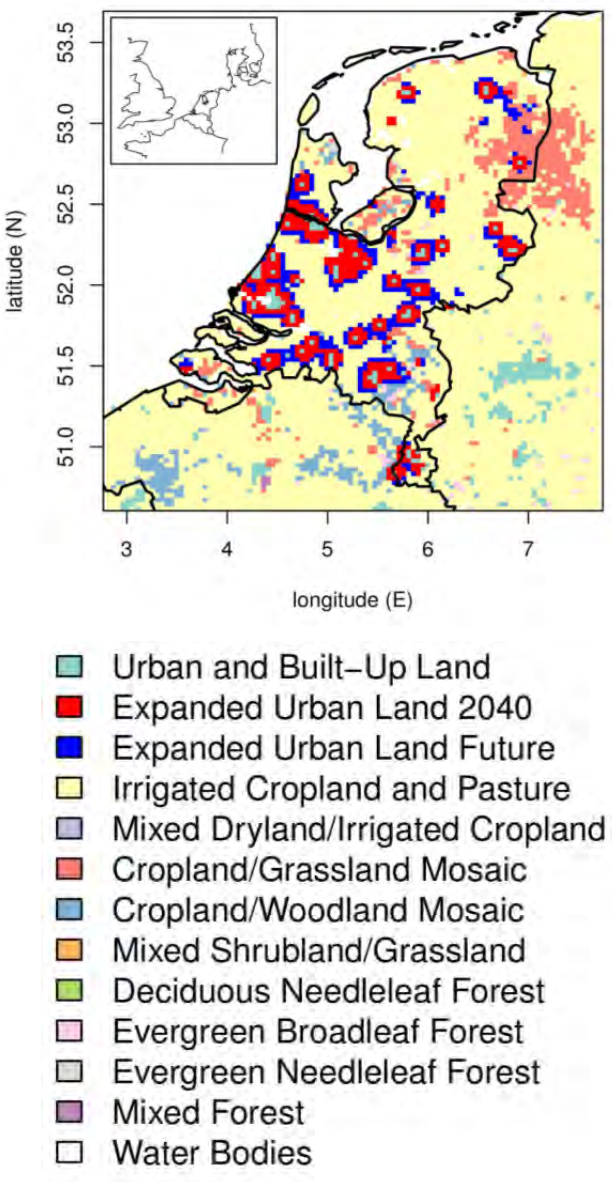


Fig.1: Dominant land cover data in the Netherlands with the expanded urban areas in red and blue. The inlay plot in the top left corner shows the full model domain.

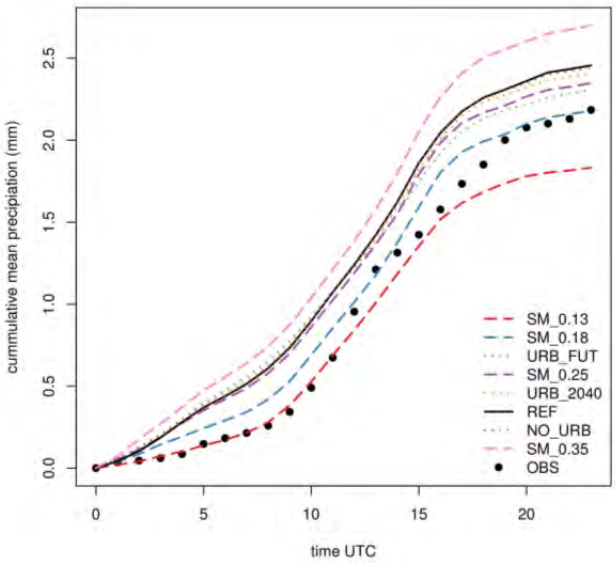


Fig 2: Cumulative mean precipitation in the Netherlands for the reference simulation (REF), and soil moisture (SM_...) and urbanization (URB_...) sensitivity experiments for the period 10-13 May 1999.

4. Impact of urbanization

The temperature in urban areas is higher due to the changes in the energy partitioning (LH and HFX), but also due to the increased surface roughness and higher heat storage capacity in urban areas. The heat trapped by buildings during daytime is returned during the night. Fig 3 shows the spatial and temporal difference in temperature between URB_2040 and NO_URB. Comparing URB_2040 to REF (not shown here) shows the mean diurnal UHI will increase with more than 0.4 K within existing urban areas. The maximum diurnal UHI under urban coverage plausible in 2040 will increase with 1 K within existing urban areas and the maximum UHI can be up to 2.3 K higher.

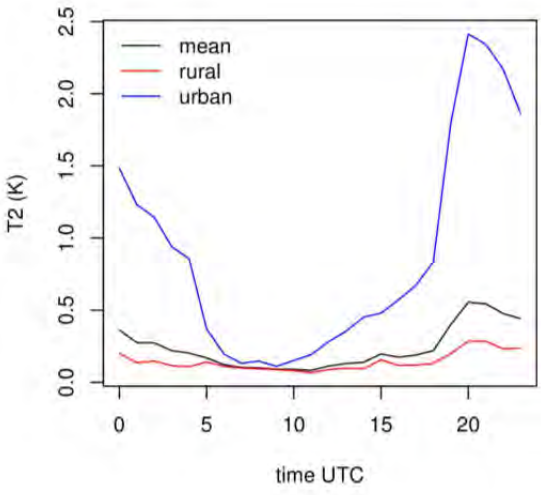


Fig 3: Difference in 2 meter temperature in the Netherlands for the period 10-13 May between a simulation with urban coverage comparable to that expected in 2040 and a simulation with urban areas removed, averaged over the entire country (mean) within urban areas (urban) and non-urban areas (rural) throughout the day

5. Conclusions

In general, in both the soil moisture and urbanization experiments, we find a positive soil moisture-precipitation feedback. The experiments with more moisture lead to higher total precipitation amounts. Increased precipitation results from both the increase in evaporation as well as enhanced triggering. The ratio of evaporation to precipitation is almost three times as large in the soil moisture experiments compared in the urbanization experiments. The relatively high reduction of LH in the urban expansion experiments is countered by a relatively small reduction in triggering. These combined effects result in a reduction of precipitation similar to what would be expected based on the soil moisture and evaporative fraction in urban areas. On the whole, the heating of the air is key for the triggering of precipitation, while the evaporation over land is crucial for the amount of precipitation that occurs.

References

Chen, F., and Dudhia, J. (2001). "Coupling an advanced land surface-hydrology model with the Penn State-NCAR MM5 modeling system. Part I: Model implementation and sensitivity." Monthly Weather Review, 129(4), 569-585.

Dekkers, J., Koomen, E., Jacobs-Crisioni, C., and Rijken, B. (2012). Scenario-based projections of future land use in the Netherlands: A spatially-explicit knowledge base for the Knowledge for Climate programme. Department of Spatial Economics/ Spatial Information Laboratory (SPINlab), Amsterdam, the Netherlands.

Kalnay, E., and Cai, M. (2003). "Impact of urbanization and land-use change on climate." Nature, 423(6939), 528-531.

Seneviratne, S. I., Corti, T., Davin, E. L., Hirschi, M., Jaeger, E. B., Lehner, I., Orlowsky, B., and Teuling, A. J. (2010). "Investigating soil moisture-climate interactions in a changing climate: A review." Earth-Science Reviews, 99(3-4), 125-161.

Shepherd, J. M. (2005). "A review of current investigations of urban-induced rainfall and recommmendations for the future." Earth Interactions, 9(12), 1-27.

Trusilova, K., Jung, M., and Churkina, G. (2009). "On Climate Impacts of a Potential Expansion of Urban Land in Europe." Journal of Applied Meteorology and Climatology, 48(9), 1971-1980.

Trusilova, K., Jung, M., Churkina, G., Karstens, U., Heimann, M., and Claussen, M. (2008). "Urbanization Impacts on the Climate in Europe: Numerical Experiments by the PSU–NCAR Mesoscale Model (MM5)." Journal of Applied Meteorology and Climatology, 47(5), 1442-1455.

High-resolution sensitivity studies over Crete with the non-hydrostatic regional climate model REMO-NH

Bastian Eggert[1], Lennart Marien[1], Daniela Jacob[1,2]

[1] Climate Service Center, Helmholtz-Zentrum Geesthacht, Hamburg, Germany (Bastian.Eggert@hzg.de)
[2] Atmosphäre im Erdsystem, Max-Planck-Institut für Meteorologie, Hamburg, Germany

1. Introduction

A non-hydrostatic version of the regional climate model REMO-NH has been used to downscale extreme precipitation events that occurred over Crete. As lateral boundary data a "poor-man's" reanalysis[1] has been used, that was conducted earlier with REMO. This study shows the performance of the regional climate model REMO-NH simulated at a 2x2 km^2 horizontal resolution. Only small changes in the physical parameterizations were implemented to adapt to the cloud resolving scale. The objective of this study is to assess whether REMO-NH is able to reproduce these extreme events.

2. The regional climate model REMO-NH

REMO (Jacob and Podzun (1997), Jacob (2001), Göttel (2009)) is a three-dimensional, non-hydrostatic atmospheric circulation model. It is based on the 'Europa-Modell' of the German Weather service (Majewski, 1991). The physical parameterizations are taken from the global climate model ECHAM-4 (Roeckner et al., 1996). Important modifications to the ECHAM-4 physics are the following: A subgrid scale tile approach for land, water and sea ice surfaces by Semmler (2004), a cloud microphysics scheme by Pfeifer (2006) following Lohmann and Röckner (1995), the land surface scheme related to surface runoff (Hagemann and Gates 2003), land surface parameters (Hagemann 2002) and background surface albedo (Rechid et al. 2009).

Prognostic variables of REMO-NH are the wind components, surface pressure, temperature, specific humidity and cloud liquid water. For temporal integration a leapfrog scheme with semi-implicit correction and time filtering after Asselin (1972) is used. In the vertical, variations of the prognostic variables (except surface pressure) are represented by a hybrid vertical coordinate system (Simmons and Burridge, 1981). For horizontal discretization REMO-NH uses a spherical Arakawa-C grid (Arakawa 1988).

3. Adapting the model to the cloud resolving scale

For this study only a few changes have been made to the model code to adapt the physical parameterizations to the cloud resolving resolution.

1. The convection parameterization is turned off so that convection may be resolved explicitly.
2. Sensitivity studies have been conducted for the relative humidity threshold (a threshold that has to be reached before cloud condensation starts), and for the maximum mixing length, which is used for the calculation of the vertical turbulent fluxes.

4. The case study region

Crete is a semi-arid island with a complex orography. The highest elevation is 2.456 m. The considered domain expanse from 22.4° to 27.7° longitude W and from 34° to 37.2° latitude N. Using a horizontal grid cell size of 2x2 k, the highest captured elevation in REMO-NH is 2.236 m.

5. Results

The REMO-NH results of the different sensitivity studies will be evaluated against observations and compared to the driving data. As an example we show the daily precipitation sums for the 16th to 18th Oct. 2006 (Fig. 1 a,c,e). In this time a frontal depression crossed the island of Crete and caused an intensive precipitation event that led to a flash flood in the Almirida basin (Tsanis et al., 2008). This event is well captured in the "poor-man" reanalysis (Fig. 1,3 b,d,f). REMO-NH was able to represent the event and to add small-scale details due to the higher resolution (fig. 1,3 a,c,e). In some grid points REMO-NH overestimated the extreme precipitation intensities (Fig. 2).

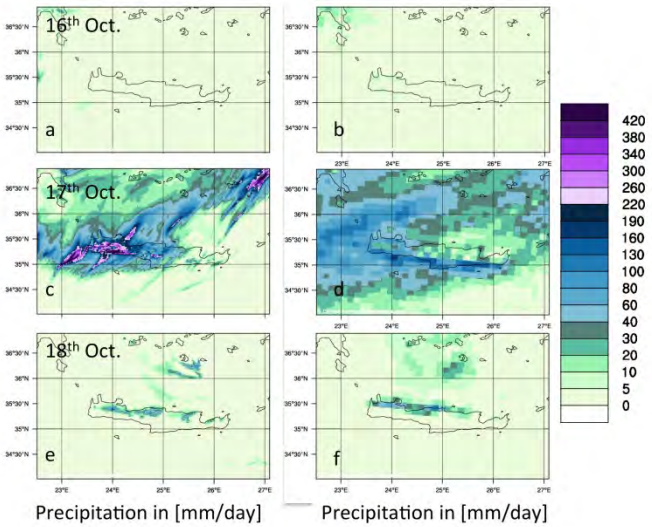


Figure 1. Precipitation in mm/day over the Crete island as simulated by REMO-NH (a, c, e) and in the REMO poor-man simulation (b, d, f) 16th (top) - 18th (bottom) Oct. 2006.

[1]"poor-man's" reanalysis: ERA-Interim (Dee et al., 2011) reanalysis downscaled with REMO to 12x12 km^2 horizontal resolution covering the period 1989-2008 with a frequent re-initialization towards its driving fields.

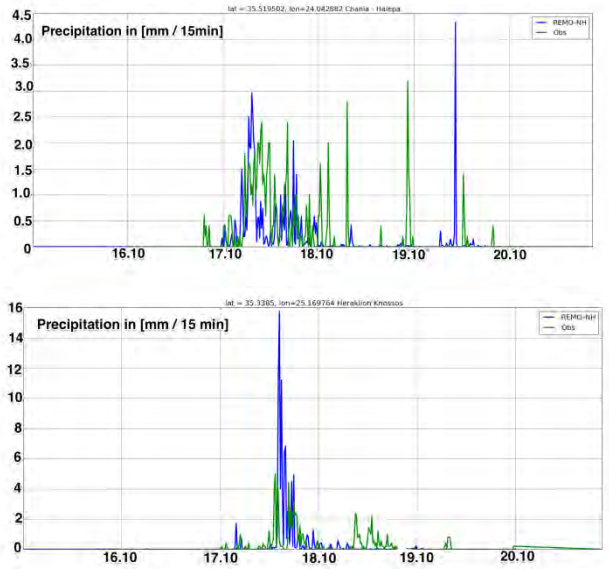


Figure 2. Precipitation in mm/15 min for the grid box closest to the observational site in Chania-Helepa (top) and Heraklion Knossos (bottom) as simulated by REMO-NH. The green line shows the corresponding precipitation measurement from the rain gauge.

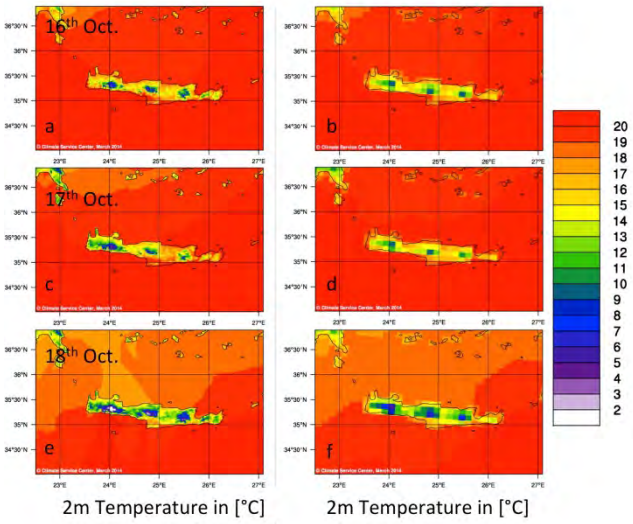


Figure 3. Temperature in °C over the Crete island as simulated by REMO-NH (a, c, e) and in the REMO poor-man simulation (b, d, f) 16th (top) - 18th (bottom) Oct. 2006.

References

Arakawa A (1988) Finite-Difference Methods in Climate Modeling. Proceedings of the NATO Advanced Study Institute on Physically-Based Modeling and Simulation of Climate and Climate Change (Part 1), Erice, Italy, 11-23 May 1986.

Asselin R (1972) Frequency Filter for Time Integrations. Mon. Wea. Rev., 100, 487–490.

Dee DP, Uppala SM, Simmons AJ, Berrisford P, Poli P, Kobayashi S, Andrae U, Balmaseda MA, Balsamo G, Bauer P, Bechtold P, Beljaars ACM, van de Berg L, Bidlot J, Bormann N, Delsol C, Dragani R, Fuentes M, Geer AJ, Haimberger L, Healy SB, Hersbach H, Hólm EV, Isaksen L, Kållberg P, Köhler M, Matricardi M, McNally AP, Monge-Sanz BM, Morcrette J-J, Park B-K, Peubey C, de Rosnay P, Tavolato C, Thépaut J-N and Vitart F (2011) The ERA-Interim reanalysis: configuration and performance of the data assimilation system. Q.J.R.M.S., 137: 553–597. doi: 10.1002/qj.828.

Göttel H (2009) Einfluss der nichthydrostatischen Modellierung und der Niederschlagsverdriftung auf die Ergebnisse regionaler Klimamodellierung. Berichte zur Erdsystemforschung, 60, Max- Planck-Institute for Meteorology, Hamburg.

Hagemann S (2002) An improved land surface parameter dataset for global and regional climate models. Report 336, Max-Planck-Institute for Meteorology, Hamburg.

Jacob D, Podzun R(1997) Sensitivity studies with the regional climate model REMO. Meteorology and Atmospheric Physics, 63 (1-2), 119-129.

Jacob D (2001) A note to the simulation of the annual and inter-annual variability of the water budget over the Baltic Sea drainage basin. Meteorology and Atmospheric Physics, 77 (1-4), 61-73.

Lohmann U, Roeckner E (1995) Introduction of a prognostic cloud ice scheme in the ECHAM general circulation model: Impact on climate and climate sensitivity. Max-Planck-Institut f• ür Meteorologie, Report No. 179.

Majewski D (1991) The Europa-Modell of the Deutscher Wetterdienst. ECMWF Seminar on Numerical Methods in Atmospheric Models, 2, 147-191.

Pfeifer S (2006) Modeling Cold Cloud Processes with the Regional Climate Model Remo. Reports on Earth System Science 23, Max-Planck-Institute for Meteorology, Hamburg.

Rechid D, Raddatz TJ, Jacob D (2009) Parameterization of snow-free land surface albedo as a function of vegetation phenology based on MODIS data and applied in climate modelling. Theor. Appl. Climatol. 95, 245–255.

Roeckner E, Arpe K, Bengtsson L, Christoph M, Claussen M, Dümenil L, Esch M, Giorgetta M, Schlese U, Schulzweida U (1996) The atmospheric general circulation model ECHAM-4: Model description and simulation of present-day climate. Report No. 218, Max-Planck-Institute for Meteorology, Hamburg.

Semmler T, Jacob D, Schlünzen KH, Podzun R (2004) Influence of sea ice treatment in a regional climate model on boundary layer values in the Fram Strait region. Mon Weather Rev, 132, 985-999.

Simmons AJ and Burridge DM (1981) An energy and angular-momentum conserving finite-difference scheme and hybrid vertical coordinates. Mon. Wea. Rev., 109, 758-766.

Tsanis, I.K., Koutroulis, A., Daliakopoulos, I., Michaelides, S., “Storm analysis and precipitation distribution of the flash flood in Almyrida basin, Crete", EGU2008 Session IS31-Flash floods: observations and analysis of atmospheric and hydrological controls, Vol. 10, EGU2008-A- 09498, Vienna, Austria, 13-18 April 2008.

Pursuing high resolution downscaling for hydrological applications in the Victorian Climate Initiative (VicCI)

Marie Ekström

Commonwealth Scientific and Industrial Research Organisation (CSIRO), Land and Water Flagship, Australia
(marie.ekstrom@csiro.au)

1. Background

The Victorian Climate Initiative (VicCI) is a State funded initiative that follows the South Eastern Climate Initiative (SEACI) (CSIRO 2012). SEACI was formed to improve the understanding of the nature and causes of climate variability in southeast Australia, following years of sustained drought conditions in the region. It proved a successful project, both in terms of research outcomes and also in terms of strengthening collaboration between the climate and hydrological research community.

VicCI builds on both successes, this time with a focus on the State of Victoria to assess trends and patterns in the variability of regional drivers of rainfall in current and plausible future climates.

2. Hydrological context

The main objective of VicCI is to provide an improved understanding of the risks climate change poses to water supplies to inform water resource planning decisions. Previous assessments in this region have been hampered by the lack of breadth in downscaling methods and, in particular, by the lack multiple dynamical downscaling data (Chiew et al., 2009; Frost et al., 2011). As revealed in SEACI, a general weakness in the methods applied in this region is the underestimation of 3-5 day rainfall totals and the magnitude of extremes (e.g. the persistence of rainfall events and their intensity), which leads to underestimation in the high runoff events and the mean annual runoff.

Recent experiments by the UK MetOffice have shown that improved spatial and temporal characteristics of rainfall can be obtained when using convective resolving high resolution regional climate models (RCMs) (Kendon et al., 2012). Whilst their high resolution version (1.5 km) tended to produce too intense heavy events compared to observed data, overall it provided much better representation of the duration and spatial extent of heavy events compared to the coarse resolution model (12 km). In particular, the heavy rainfall in the coarser resolution model was found to be too persistent and widespread. Further, commonly known RCM problems, such as too much persistent light rain and errors in the diurnal cycle, were much reduced in the high resolution models.

In VicCI a convection permitting set-up of the Weather Research and Forecasting (WRF) modeling system (Skamarock and Kemp, 2008) is implemented to investigate the potential for high-resolution experiments to improve on spatio-temporal characteristics of rainfall, as simulated in previous dynamical downscaling exercises in southeast Australia (Evans et al., 2012, Evans and McCabe, 2010). This, in turn, has the potential to inform the development of improved methodologies for future runoff projections and, potentially, assessments of future flood risk.

3. Planned experiments

Because the multiple configuration options possible for WRF, some initial testing is conducted to ensure that choices of physics parameter schemes are suitably chosen for the region of interest. Choices are based on peer-review literature (foremost Evans et al., 2012) and WRF support documentation. Of particular interest is the performance of application-relevant microphysics (mp) schemes. All in all, 10 set-ups of WRF are identified, representing unique combinations of 5 mp schemes and 2 boundary layer schemes.

The 10 models will be deployed for three case study periods: 7th-21st of August 2010, 5th-19th October 2010 and 30th January to 13th of February 2013. These three events occur during a period noted for several heavy rainfall events – as detailed in the Final Report of the Review of the 2010-2011 Flood Warnings and Response commissioned by the Victorian Government (Comrie, 2011).

A three nested configuration of WRF is used for all 10 physics ensembles focusing on a number of catchments of interest in Victoria and the transition from the great dividing range in the east towards the plains in the west (Figure 1 and 2).

Key research questions, initial results and discussion thereof will be provided on the poster.

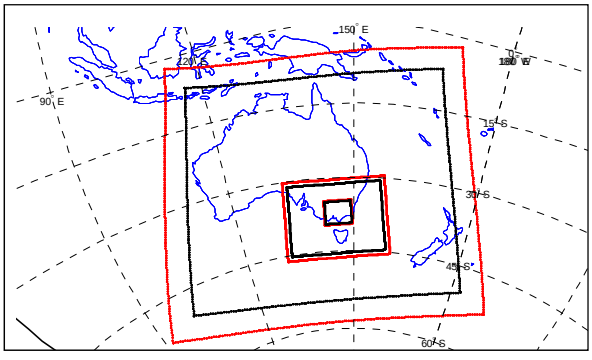


Figure 1. Outline of three nests in Lambert conformal projection. Distance between black and red lines indicate relaxation zone.

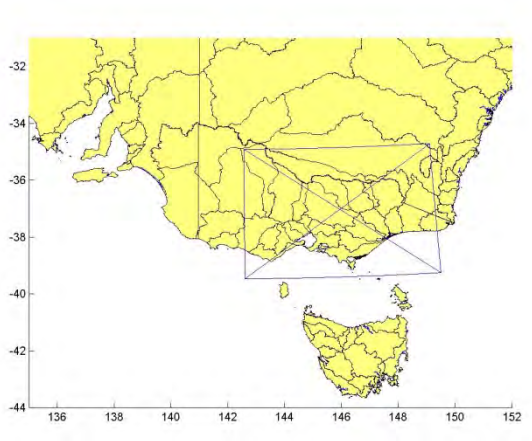


Figure 2. Outline of the innermost nest (excluding relaxation zone) and river basins in southeast Australia.

References

Chiew F.H.S., Teng J., Vaze J., Post D.A., Perraud J.M., Kirono D.G.C., Viney, N.R. (2009) Estimating climate change impact on runoff across southeast Australia: method, results, and implications of the modeling method. Water Resources Research, 45, DOI: 10.1029/2008WR007338

Comrie N. (2011) Review of the 2010–11 Flood Warnings & Response Melbourne, Victoria, Australia

CSIRO (2012) Climate and water availability in south-eastern Australia: A synthesis of findings from Phase 2 of the South Eastern Australian Climate Initiative (SEACI), CSIRO, Australia, 41pp.

Evans J. P., Ekstrom, M., Ji F. (2012) Evaluating the performance of a WRF physics ensemble over South-East Australia. Climate Dynamics, 39**,** 1241-1258.

Evans J.P., McCabe M.F. (2010) Regional climate simulation over Australia's Murray-Darling basin: A multitemporal assessment, Journal of Geophysical Research- Atmospheres, 115, DOI: 1 0.1029/2010JD013816

Frost A.J., Charles S.P., Timbal B., Chiew F.H.S., Mehrotra R., Nguyen K.C., Chandler R.E., McGregor J.L., Goubin F., Kirono D.G.C., Fernandez E., Kent D.M. (2011) A comparison of mulit-site daily rainfall downscaling techniques under Australian conditions, Journal of Hydrology, 408, pp.1-18

Kendon E.J., Roberts N.M., Senior C.A., Roberts M.J. (2012) Realism of rainfall in a very high-resolution regional climate model. Journal of Climate, 25, DOI: 10.1175/jcli-d-11-00562.1

Skamarock W.C., Kemp J.B. (2008) A time-split nonhydrostatic atmospheric model for weather and forecasting applications, Journal of Computational Physics, 227, pp. 3465-3485.

Climate change signal of convective precipitation through convection permitting climate model simulations

Fosser G.[1,2], Khodayar S.[1] and Berg P.[3]

[1] Institute for Meteorology and Climate Research (IMK-TRO), Karlsruhe Institute of technology, Germany (giorgia.fosser@kit.edu)
[2] Now at CNRM-GAME, Météo France & CNRS, Toulouse, France
[3] Swedish Meteorological and Hydrological Institute, Norrköping, Sweden

1. Introduction

Climate change is a global phenomenon but its impact differs substantially on local and regional scales. Regional climate models (RCMs) are crucial in bridging the spatial gap between global climate models (GCMs) and smaller scale impact modelling. Moreover, increasing horizontal resolution enables a more detailed representation of topographical features and may lead to a better representation of the precipitation field (Berg et al. 2012) and thus help in reducing uncertainties (Giorgi 2006).

Recent literature underlines the advantages of convection permitting models (CRMs) versus coarser resolution especially in the representation of convective precipitation (Prein et al. 2013, Fosser et al. under review). In terms of climate change, higher spatial resolution could allow gaining more information on the precipitation changes and the responsible processes especially in summer, when the uncertainties related to the parameterisation of convection are higher.

2. Methodology

Long-term simulations (30 years) were performed at 7 km and 2.8 km resolution with RCM COSMO-CLM driven with both ERA40 reanalysis data and ECHAM5 for the recent past (1971-2000) and with ECHAM5 (A1b scenario) for the near future (2021-2050). The investigation area, known for its significant orographically induced convective precipitation, is located in the state of Baden-Württemberg in southwestern Germany (Figure 1).

3. Results

Our results clearly show the added value of using convection permitting scale especially when simulating convective events, with significant improvements in e.g. the diurnal precipitation cycle and the more realistic representation of atmospheric conditions leading to convection. These advantages are only weakly dependent on the lateral boundary forcing, as convection is mainly controlled by local processes.

In general, the convection permitting scale agrees well with the coarser resolution on both the sign and the relative magnitude of the changes for long term averages. However, the more physical representation of convective precipitation at higher resolution makes CRMs more reliable to investigate climate change. The study highlights the importance of using different temporal scales to evaluate the future changes in the precipitation pattern in order to avoid false conclusions on the climate change signal.

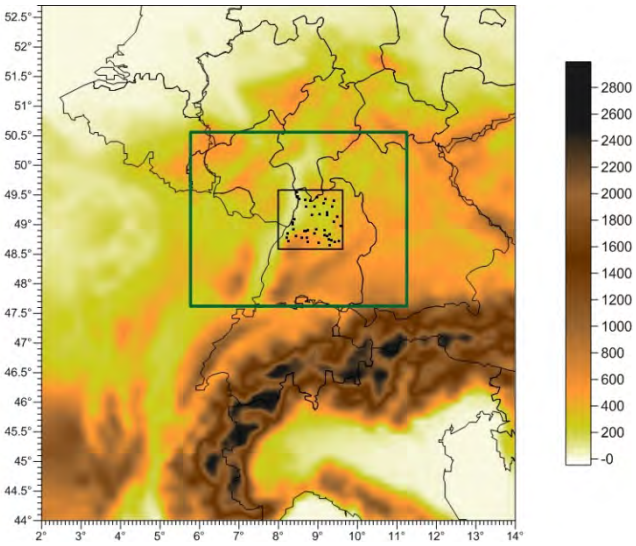


Figure1: Topographical map of the simulation domain at 7 km resolution over Germany and surrounding areas. The green box represents the simulation domain at 2.8 km resolution. The inner black frame indicates the investigation area common to all simulations. The black dots indicate the locations of the precipitation gauges

References

Berg P, Wagner S, Kunstmann H, Schädler G (2012) High resolution regional climate model simulations for Germany: part I—validation, Climate Dynamics, 40, 401–414. doi: 10.1007/s00382-012-1508-8

Giorgi F (2006) Regional climate modeling: Status and perspectives. Journal de Physique IV, 139, 101–118. doi: 10.1051/jp4

Fosser G, Khodayar S, Berg P (under review) Improving physical consistency for convective precipitation through convection permitting climate model simulations, Climate Dynamics

Prein AF, Gobiet A, Suklitsch M, Truhetz H, Awan NK, Keuler K, Georgievski G (2013) Added value of convection permitting seasonal simulations, Climate Dynamics, 41, 2655-2677. doi: 10.1007/s00382-013-1744-6

Impact of using the surface scheme SURFEX within ALARO-0 for the ERA-Interim high-resolution dynamical downscaling over Belgium

Olivier Giot[1,2], Rozemien De Troch[1,3], Rafiq Hamdi[1], Alex Deckmyn[1] and Piet Termonia[1,3]

[1] Royal Meteorological Institute of Belgium, Belgium (olivier.giot@meteo.be)
[2] Plant and Vegetation Ecology, University of Antwerp, Belgium
[3] Department of Physics and Astronomy, Ghent University, Belgium

1. Introduction

Recent studies by Hamdi et al. (2012) and De Troch et al. (2013) on the evaluation of 30 year summer maximum temperature and precipitation (1961-1990) over Belgium with the ALARO-0 model, have demonstrated that the new parameterizations within the model which are centered around an improved convection and cloud scheme, are responsible for a correct simulation of extreme daily maximum temperatures and extreme daily precipitation events at various horizontal resolutions of 40 km, 10 km and 4 km (see Fig. 1 for extreme daily summer precipitation). While previous studies used a simple surface scheme within ALARO-0, another study by Hamdi et al. (2013) has showed that local climate phenomena such as the Urban Heat Island effect (UHI) are very well simulated with the use of a more sophisticated surface scheme called SURFEX (SURface Externalisée).

Therefore, the aim of this work is to compare both approaches, namely with and without the use of SURFEX within the ALARO-0 model. Such a comparison allows to asses in a consistent and profound way the impact of using a more sophisticated surface scheme such as SURFEX for high-resolution regional climate modelling.

2. Experimental design

The recent ERA-Interim reanalysis (1981-2010) is dynamically downscaled using the ALARO-0 model at 4 km resolution with and without the surface scheme SURFEX. SURFEX is an externalized surface scheme developed by Météo-France and in this work it is run in a coupled mode in such a way that the atmospheric forcing is provided by the host atmospheric model (ALARO-0 in our case).

In SURFEX, each grid box consists of four adjacent surfaces: vegetation, urban areas, sea or ocean and lake, which are each associated with a specific parameterization. Vegetated areas are parametrized with the interactions between soil, biosphere and atmospheric (ISBA) model and for the parameterization of urban surfaces the Town Energy Balance (TEB) single-layer urban canopy model is used.

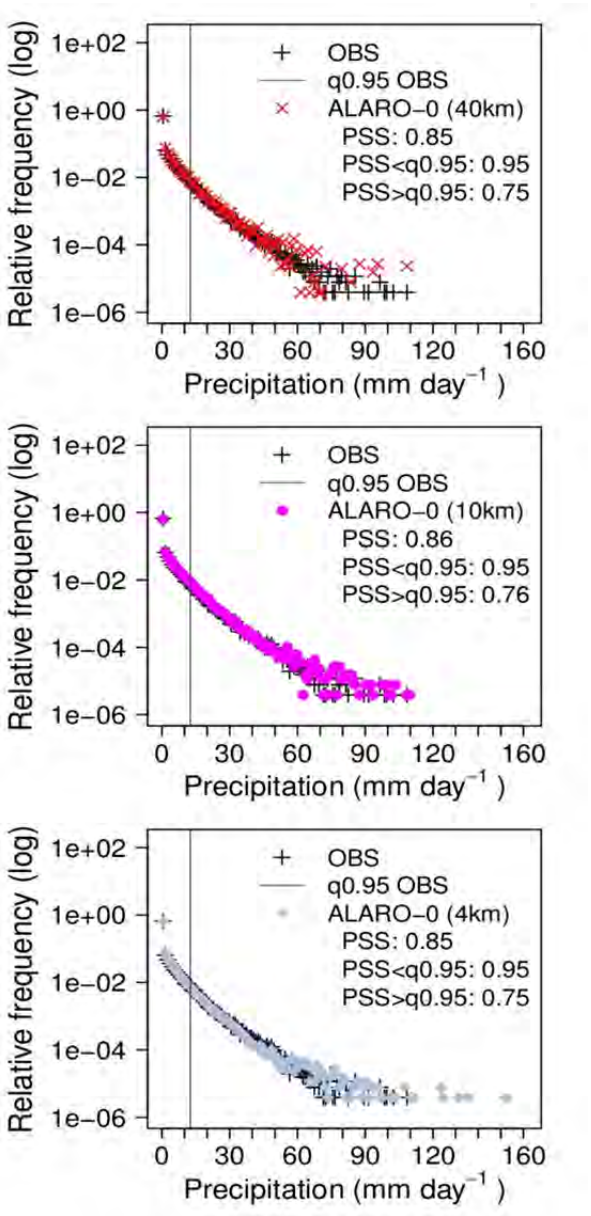


Figure 1. Relative frequencies of daily cumulated summer precipitation from observations and model simulations from ALARO-0 at 40 km (top), 10 km (middle) and 4 km (bottom) resolution. The black vertical line indicates the 0.95th quantile of the observations (Figure adapted from De Troch et al. 2013).

3. Preliminary results, conclusions and outlook

Figure 2 shows the mean daily maximum temperature, minimum temperature and precipitation amounts for the period 2001-2010 produced using SURFEX as the surface scheme coupled to ALARO-0. The inclusion of the TEB module in SURFEX allows for a clear reproduction the UHI effect, especially visible in the minimum temperature. Cities such as Brussels, Ghent, Antwerp, Mons, Charleroi, Liège, Lille and most notably Paris and London can be clearly discriminated in the figures. Precipitation on the other hand seems to be less dependent on urbanization and more on orography, although a more thorough study should give a more definite answer.

Computations for the remaining ERA-Interim years and computations with the default surface scheme ISBA are planned for March 2014.

The analysis will focus on how the different surface schemes impact both mean climatological properties (biases, variability) as extremes (heat waves, UHI effect, extreme precipitation).

References

De Troch, R., R. Hamdi, H. V. de Vyver, J.-F. Geleyn, P. Termonia (2013) Multiscale performance of the ALARO-0 model for simulating extreme summer precipitation climatology in Belgium, Journal of Climate, 26, 8895–8915, doi:10.1175/JCLI-D-12-00844.1.

Hamdi, R., H. Van de Vyver, P. Termonia (2012) New cloud and microphysics parameterisation for use in high-resolution dynamical downscaling: Application for summer extreme temperature over Belgium, International Journal of Climatology, 32, 13, 2051–2065, doi: 10.1002/joc.2409.

Rafiq Hamdi, H. Van de Vyver, R. De Troch, P. Termonia (2013) Assessment of three dynamical urban climate downscaling methods: Brussels's future urban heat island under an A1B emission scenario, International Journal of Climatology, In press, doi: 10.1002/joc.3734.

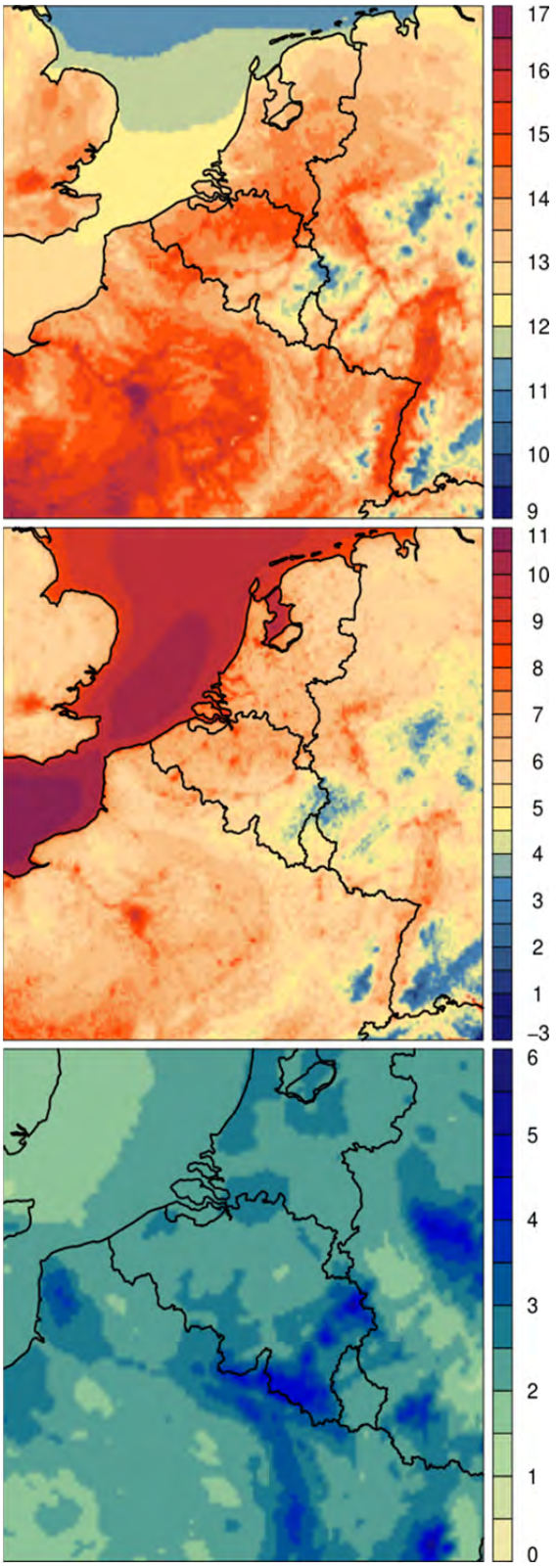


Figure 2. Mean daily maximum temperature (top, °C), minimum temperature (middle, °C) and precipitation amounts (bottom, mm/day) for the period 2001-2010 computed by downscaling ERA-Interim with ALARO-0 coupled to SURFEX.

Implementation and initial results of convection-permitting Pan-European TerrSysMP and WRF simulations

Klaus Goergen[1,2,4], Jessica Keune[2,4,5], Fabian Gasper[3,4], Prabhakar Shrestha[2], Mauro Sulis[2], Sebastian Knist[1,2,4], Christian Ohlwein[2,5], Stefan Kollet[3,4], Clemens Simmer[2,4] and Harry Vereecken[3,4]

[1] SimLab TerrSys, Jülich Supercomputing Centre, Jülich Research Centre, Jülich, Germany (k.goergen@fz-juelich.de)
[2] Meteorological Institute, University of Bonn, Bonn, Germany
[3] Agrosphere (IBG-3), Jülich Research Centre, Jülich, Germany
[4] Centre for High Performance Scientific Computing in Terrestrial Systems, Geoverbund ABC/J, Jülich, Germany
[5] Hans-Ertel-Centre for Weather Research, Climate Monitoring Branch, Meteorological Institute, University of Bonn, Bonn, Germany

1. Background and motivation

Convective processes and the effects of land-use patterns, topography, and coastlines on exchange processes between atmosphere, surface and subsurface are decisive features for the evolution of the terrestrial system. Its representation in numerical models requires spatial resolutions of at least 5 km in order to replicate dominat interaction processes like atmospheric boundary-layer variability, local wind systems, and related convection initiation and precipitation.

Continent-wide model domains offer the potential to investigate processes and their variances across multiple spatial scales and watersheds. Such model runs are however technically and computationally demanding. Here we primarily show the feasibility of such model runs for continental model domains and give an indication of a possible added value of these simulations.

2. Experiment design

The experiment design consists of two simulations with the Weather Research and Forecasting model (WRF) and the fully coupled Terrestrial Systems Modelling Platform (TerrSysMP) that are run on a common grid for a 3 km European model domain (more than 2.3 Mio. grid elements) for two months, January and July 2010. The model domain is inscribed into the official Coordinated Regional Downscaling Experiment (CORDEX) EUR-11 model grid (about 12 km) (Giori et al., 2009).

3. Model systems

The WRF model is used with the Noah LSM and a climate mode setup similar to runs performed for the EURO-CORDEX project (Vautard et al., 2013; Kotlarski et al., 2014). Its forcing is derived from these 3-hourly 50-level validation runs on the EUR-11 grid.

The relatively new TerrSysMP has been developed in the Transregional Collaborative Research Centre 32 (Patterns in Soil-Vegetation-Atmosphere Systems - Monitoring, Modelling and Data Assimilation). It is a fully coupled integrated model system where the NWP model COSMO, the LSM CLM and the variably saturated subsurface flow model ParFlow (Shrestha et al., 2012). These component models are externally coupled with the OASIS3 coupler (Valcke, 2013). It allows for a complete simulation of the hydrologic cycle from the bedrock across the land surface into the atmosphere. TerrSysMP is driven by a high-resolution regional re-analysis based on the COSMO NWP model at about 6.2 km resolution, also nested into the EUR-11 domain from research groups of the Hans Ertel Centre for Weather Research (HErZ) branch on Climate Monitoring and Diagnostics of the German Weather Service (DWD).

4. Analyses

We show results of January and July 2010 simulations with a focus on precipitation events and boundary layer processes. A comparison is done to different observations, e.g. the HYRAS (Rauthe et al., 2013) or Fluxnet (Agarwal et al., 2010) datasets, and in case of WRF also to coarser resolution simulations to derive the added value.

In simulations for Alpine model domains Prein et al. (2013) e.g. give evidence for an added value in the reproduction of the diurnal cycle of convective precipitation during summer as well as precipitation intensity and the spatial distribution.

5. Computational environment and scaling results

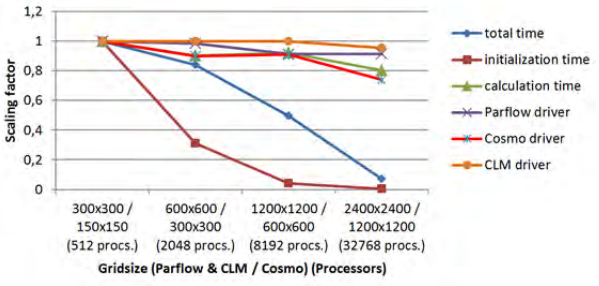


Figure 1. Example of fully coupled TerrSysMP weak scaling behaviour in an idealized experiment on JUQUEEN: scaling factor vs. problem size. COSMO 1 km, ParFlow, CLM 0.5 km, optimum static load balancing via Scalasca, OASIS-MCT coupler. The unit problem size of 300x300 (ParFlow, CLM) and 150x150 (COSMO) is overall increased by factor 64. The initialisation behaviour of CLM can be improved.

The models run on the massively parallel 28-rack 5.9 PFLOP IBM Blue Gene/Q system JUQUEEN of the Jülich Supercomputing Centre (JSC). A substantial effort in terms of application porting, tuning and optimisation is needed to efficiently operate geoscience codes on such highly scalable low-memory architectures. Only with

large model domains and/or high spatial resolutions a good scaling behaviour seems achievable. TerrSysMP can meanwhile efficiently be run using the OASIS3-MCT coupler (Valcke et al., 2013) with over 32k processes (see Figure 1).

References

Agarwal, D. A., Humphrey, M., Beekwilder, N. F., Jackson, K. R., Goode, M. M. and van Ingen, C. (2010) A data-centered collaboration portal to support global carbon-flux analysis, Concurrency and Computation: Practice and Experience, 22, 17, pp. 2323–2334

Giorgi, F., Jones, C., and Asrar, G. R. (2009) Addressing climate information needs at the regional level: the CORDEX framework, Bulletin of the World Meteorological Organization, 58, pp. 175-183

Kotlarski, S., Keuler, K., Christensen, O. B., Colette, A., Déqué, M., Gobiet, A., Goergen, K., Jacob, D., Lüthi, D., van Meijgaard, E., Nikulin, G., Schär, C., Teichmann, C., Vautard, R., Warrach-Sagi, K., and Wulfmeyer, V. (2014) Regional climate modeling on European scales: a joint standard evaluation of the EURO-CORDEX RCM ensemble, Geoscientific Model Development Discussions, 7, pp. 217-293

Prein, A. F., Gobiet, A., Suklitsch, M., Truhetz, H., Awan, N. K., Keuler, K. and Georgievski, G. (2013) Added value of convection permitting seasonal simulations, Climate Dynamics, 41, 9-10, pp. 2655-2677

Shrestha, P., Sulis, M., Masbou, M., Kollet, S. and Simmer, C. (2012) Development of a scale-consistent soil-vegetation-atmosphere modeling system using COSMO, Community Land Model and ParFlow, in: AGU Fall Meeting, H32E Patterns in Soil-Vegetation-Atmosphere Systems: Monitoring, Modeling, and Data Assimilation I, San Francisco, USA, 3-7 December 2012

Valcke, S. (2013) The OASIS3 coupler: a European climate modelling community software, Geoscientific Model Development, 6, pp. 373-388

Valcke, S., Craig, T. and Coquart, L. (2013) OASIS3-MCT User Guide, OASIS3-MCT 2.0, Technical Report, TR/CMGC/13/17, CERFACS/CNRS SUC URA No 1875, Toulouse, France

Vautard, R., Gobiet, A., Jacob, D., Belda, M., Colette, A., Déqué, M., Fernández, J., García-Díez, M., Goergen, K., Güttler, I., Halenka, T., Karacostas, T., Katragkou, E., Keuler, K., Kotlarski, S., Mayer, S., Meijgaard, E., Nikulin, G., Patarčić, M., Scinocca, J., Sobolowski, S., Suklitsch, M., Teichmann, C., Warrach-Sagi, K., Wulfmeyer, V. and Yiou, P. (2013) The simulation of European heat waves from an ensemble of regional climate models within the EURO-CORDEX project, Climate Dynamics, 41, 9-10, pp. 2555-2575

Simulating historical wind storms in Switzerland with WRF: identification of the optimal setup and its performance in high-resolution simulations

Juan Jose Gomez-Navarro[1,2], Martina Messmer[1,2], Christoph Raible[1,2]

1 Climate and Environmental Physics, Physics Institute, University of Bern, Switzerland
2 Oescher Centre for Climate Change Research, University of Bern, Switzerland (gomez@climate.unibe.ch)

1. Introduction

A prominent feature of the North Atlantic and European climate is the appearance of cyclonic disturbances, which have lead a number of severe wind storms in Central Europe during the last decades (Etienne, 2013). These situations, although rare, produce great economical cost and forest damage, and indeed they are listed as an important natural hazard in Europe.

The proper assessment of the risks related to such extreme events demand a deep knowledge of the wind climatology. However, this variable has not been as extensively investigated as temperature or precipitation. This is partly due to the inherent complexity of this variable, which is very sensitive to geographical features. This precludes its realistic simulation with coarse-resolution models, but also hampers the extrapolation of local observation onto regular grids which could be used for impact studies or wind power assessments. Finally, the general lack of reliable and widely available measurements of this variable does not ease its climatic characterization.

This study aims at tackling this gap of knowledge. A number of simulations have been performed to evaluate the skill of the WRF model to reproduce the wind characteristics, as well as identifying the optimal model setup for this purpose. The focus of this analysis is on Switzerland. This region has several characteristics that makes it suitable for this kind of analysis. First, it has a complex orography which renders the use of regional models of major relevance and it grants a rich wind behaviour. Second, the Swiss meteorological office is running a dense and homogeneous network of automatic stations which record wind with hourly resolution for several decades. The combination of a challenging orography for the model plus reliable observations to compare with, creates a promising environment for the evaluation of model performance regarding wind.

2. Model Setup

This study aims at identifying the most suitable model setup for the reliable simulation of wind, with a special focus on extreme events. For this task a number of historical storms have been simulated with the Weather Research and Forecasting model (WRF). The catalogue of 24 storms analysed by Etienne (2013) has been chosen as starting point. ERA-Interim has been used to provide the initial conditions and to drive the regional model at the boundaries. The model implements 4 one-way nested domains, with the inner one covering entirely the Alps at a horizontal resolution of 2 km and 42 eta levels in the vertical, as shown in Fig. 1. The analysis hereafter focuses on the inner domain.

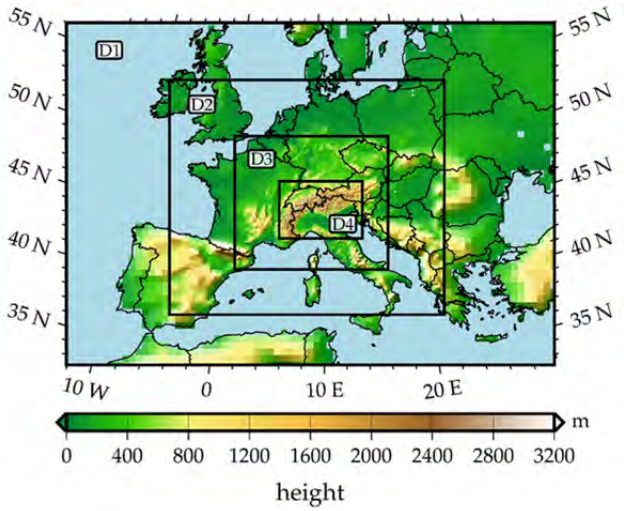


Figure 1. 4 nested domains setup used for all the simulations. The domains have a resolution of 54, 18, 6 and 2 km, respectively.

For analysing the sensitivity of the model performance to the parametrized Planetary Boundary Layer (PBL), an ensemble of four simulations has been performed for each storm changing only these schemes. They consist of a non-local scheme (YSU), a local approach (MYJ) and an hybrid approximation (ACM2). Finally, a modification of the YSU parametrization, specifically developed for surface wind characterization, has also been tested (Jimenez, 2012).

The sensitivity of the model skill to the nesting strategy has also been explored. In this respect, a run without any kind of nudging has been performed for each storm, and compared to the results of analysis and spectral nudging, respectively. Finally a re-forecast approach has been tested, where the simulation is initialized for each day separately and then merged, instead of performing a continuous run.

In total, each storm has been simulated with 8 different setups, leading to a total of 24 x 8 simulations of 6 days. Hence, a total of 1152 days are analysed and compared to measures of surface wind speed.

3. Results

All the simulations have been evaluated against surface wind speed observations of available for Switzerland. For this, only the closest grid point to the

station location has been considered. The comparison focuses on the ability of the model to reproduce the temporal evolution of the storm, as well as the proper characterization of the spatial structure of mean values. Skill is based on correlation, root mean square error (RMSE) and bias.

Figure 2 shows the results for the Lothar storm (26 December 1999). The boxplots indicate the spatial distribution of the three aforementioned skills calculated in the temporal series, whereas diamonds represent spatial skill of mean temporal value. Columns #1 to #4 show the skill of the four tested PBL schemes when no nudging strategy is implemented. Configuration #2 outperforms in several aspects. First, it presents significantly fewer bias (note that a general aspect of the model performance is that it generally overestimates wind speed). More notably, this setup also reproduces more accurately the spatial structure of the mean wind. This configuration corresponds to the YSU scheme modified by Jimenez et al. (2012).

The role of the nesting strategy is analysed in the next setups. #5 and #6 represent the same as #1 and #2, respectively, but when analysis nudging is employed. As before, the Jimenez (2012) scheme performs better in terms of reducing the bias. Nudging seems not to be able to improve the spatial structure of the mean wind, but it has a notable impact on the temporal correlation. Thus, the use of analysis nudging slightly narrows differences with observations. #7 and #8 represent re-forecast and spectral nudging, respectively. The skill of spectral and analysis nudging is hardly noticeable, whereas the re-forecast seems to produce lower correlations and higher RMSE. Given that re-forecast is more expensive in computational terms (the spin-up period in each chunk is discarded), our results suggest that it is not an optimal approach for wind evaluation.

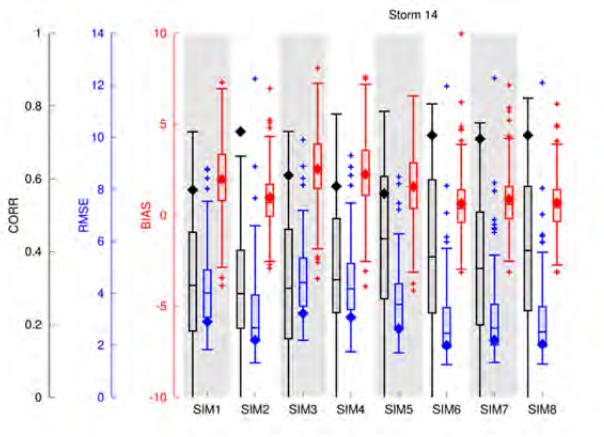


Figure 2. Statistics of the model performance for the Lothar storm. Each column represents the skill for a different setup (see main text for details). The distribution of temporal skill for each location is shown in the boxplot, whereas the diamonds represent the spatial skill. Correlation (black), root mean square error (blue) and bias (red) are shown.

4. Conclusions and Outlook

Although Fig. 2 shows the results for just one out of 24 simulations, the other simulated storms (not shown) allow to draw similar conclusions. They are:

1. The model reproduces the spatial structure of the mean wind with notable skill (correlations above 0.6).
2. The temporal correlation is lower. This could be due to errors in the RCM itself, but also to disagreements between the driving conditions and the observational dataset.
3. WRF generally overestimates wind.
4. The parametrization scheme developed by Jimenez et al (2012) clearly outperforms in this aspect by removing great part of the bias, but also improving the spatial structure of the mean wind.
5. Nudging strategies generally improve the temporal correlation, which suggest that not all of the disagreement between the results and observations are due to the driving conditions. Particularly analysis nudging seems to be the optimal approach in this situation.

In the next steps, a longer period will be simulated with the aim of establishing a reliable wind climatology for Switzerland and the Alpine area in general.

References

Jiménez, P. And Dudhia, J. (2012) Improving the Representation of Resolved and Unresolved Topographic Effects on Surface Wind in the WRF Model, Journal of Applied Meteorology, Vol.51, pp. 300-316

Etienne, C., Goyette, S. and Kuszli, C.A. (2013) Numerical investigations of extreme winds over Switzerland during 1990-2010 winter storms with the Canadian Regional Climate Model, Theor. Appl. Climatol., Vol. 113, pp. 529-547

Precipitation in complex orography simulated by the regional climate model RCA3

Ivan Güttler[1], Igor Stepanov[2], Grigory Nikulin[3], Colin Jones[4], Čedo Branković[1]

[1] Meteorological and Hydrological Service of Croatia (DHMZ), Zagreb, Croatia (ivan.guettler@cirus.dhz.hr)
[2] TU Delft Climate Institute, Delft, The Netherlands
[3] Rossby Centre, Swedish Meteorological and Hydrological Institute, Norrköping, Sweden (grigory.nikulin@smhi.se)
[4] School of Earth and Environment, University of Leeds, Leeds, UK

1. Introduction

The aim of this study is to evaluate the improvement in simulated precipitation of the third version of the Rossby Centre Climate model (RCA3), when run at horizontal resolutions of 50, 25, 12 and 6 km.

The analysis is focused on the countries of Switzerland and Norway, where complex orography can play a dominant role in precipitation formation. Observation data sets used for model validation were for Switzerland, the RhiresD dataset, an approximately 2-km resolution product of the Swiss National Meteorological Service (MeteoSwiss), and over Norway, the KLIMAGRID dataset (Mohr, 2007), a 1-km resolution product of the Norwegian Meteorological Institute (METNO), is used. The range of horizontal resolutions in experiments facilitates a systematic analysis of the impact of increasing the horizontal resolution on precipitation, in two different climate regimes.

2. Methodology

We analyse the RCA3 (Jones et al. 2004, Samuelsson et al. 2011) simulations for the period 1987-2008 with horizontal grid resolutions of approximately 50 km, 25 km, 12 km and 6 km. In all simulations the model was forced by ERA-40 re-analysis (Uppala et al. 2005) from January 1987 to August 2002, followed by ECMWF operational analysis from September 2002 to December 2008 over the whole Europe. The geographical domain, the RCA3 model version and 24 vertical levels remain unchanged in all simulations. No double nesting procedure was applied in the dynamical downscaling for the highest RCA3 resolution(s) used here; for all four resolutions considered, a direct downscaling from ERA-40 and ECMWF operational analysis was carried out.

From the same set of experiments Walther et al. (2013) evaluated precipitation diurnal cycle over Sweden and Pryor et al. (2012) studied wind climate over the northern parts of Germany and Denmark. They showed that the increase in spatial resolution down to 6 km improved the simulation of the afternoon peak in the convective precipitation during summer (Walther et al., 2013) and increased wind variability at the synoptic time scales (Pryor et al. 2012).

3. Results and discussion

At all model resolutions, the simulated mean winter precipitation is generally higher in central Switzerland and lower compared to the observations, in both the southern and northern parts of the country (Fig. 1). The largest overestimation is seen in the eastern mountainous regions where small precipitation amounts of 1-3 mm day^{-1} are doubled; the largest underestimation is approximately -40%.

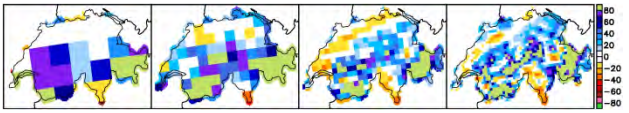


Figure 1. Winter mean seasonal total precipitation relative errors over Switzerland in the 50, 25, 12 and 6 km RCA3 simulations when compared to MeteoSwiss RhiresD data (units 10%).

In the mountainous regions, part of the overestimation could be coming from the undercatch potentially present in RhiresD dataset which were not corrected as for the case of the KLIMAGRID dataset. The undercatch occurs for both solid and liquid precipitation during windy episodes because of the wind flow deformation near the observational field gauge (e.g. Neff 1977, Adam and Lettenmaier 2003). Frei and Schär (1998) found that the undercatch can reduce the total winter precipitation by up to 40%. Such an uncertainty in observations implies that some of the biases in modelled precipitation amount in the mountainous regions may not be as significant as they appear to be.

From Fig. 1 it could not be explicitly inferred that the increased horizontal resolution generally yields an improvement, i.e. a reduction of error, in the winter seasonal climatology.

The RCA3 precipitation over the southern Norway in winter (Fig. 2) is mostly underestimated in the coastal regions (typically about -50%) but also well into the land. On the other hand, it is overestimated over high orography and in the easternmost parts for high resolution runs (an overestimation of about 30%). The precipitation overestimation on the lee side of the Scandinavian mountains in RCA3 was also documented in Samuelsson et al. (2011). The underestimation on the windward side of the mountains was also detected in few very high-resolution simulations over Norway (Heikkilä et al. 2011) and Portugal (Soares et al. 2012) where the simulated precipitation by the WRF model was compared directly with the rain gauge station data.

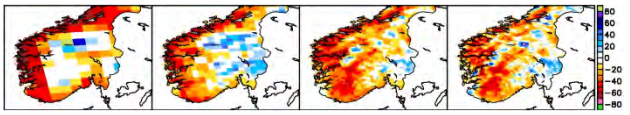


Figure 2. Winter mean seasonal total precipitation relative errors over southern Norway in the 50, 25, 12 and 6 km RCA3 simulations when compared to METNO KLIMAGRID data (units

10%).

Annual cycle analysis of the RhiresD area-mean shows that the total precipitation for Switzerland domain peaks at near 5 mm day^{-1} in the summer (Fig. 3a). This recorded amount reflects the maximum in convection activity and its significance over the continental Europe. The minimum of around 3 mm day^{-1} is reached in the month of January (Fig. 3a). The annual cycle is generally overestimated by the model with the largest errors emerging at the 50-km resolution, in the spring season. The 6-km simulation, however, does not always offer the best match with observations. From the month of June to August, the highest resolution model experiment consistently produces much too intense summer precipitation. The 6-km simulation is outperformed by both 12-km and 25-km simulations, whereas the 50-km simulation output is not far from these results either. Nevertheless, 6-km (and 12-km) RCA3 simulation over Switzerland seems to capture well month-to-month precipitation amount variability, compared to the observation.

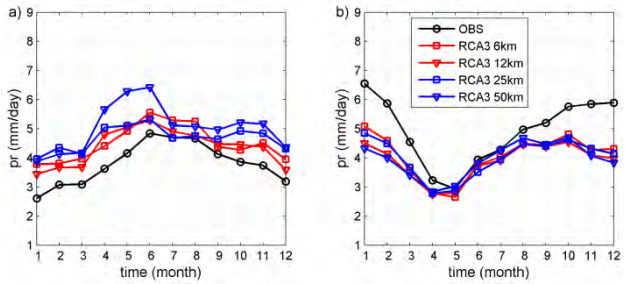


Figure 3. Annual cycle of the total precipitation over a) Switzerland, b) southern Norway. Observations at 6 km in black and marked by circles. RCA3 simulations at 6 km and 12 km are in red and marked by squares and triangles, while RCA3 simulations at 25 km and 50 km are in blue and marked by squares and triangles.

The maximum values of the annual cycle of the precipitation in the southern Norway, region characterized by the dominant high mountains, peak in January, around 6 mm day^{-1} (Fig. 3b). The peak extends throughout the cold season as well, degrading to its minimum in the month of April. (Fig. 3b). This is the time of the year when strong north Atlantic westerlies are blasting over the northern European shores. Decrease of precipitation intensity from the late spring into the summer is associated with the weaker westerlies. The shape of the annual cycle curve is simulated well by the model at all resolutions, however, the winter and autumn maxima are underestimated. This is in contrast with the results for the Switzerland area. The 6-km resolution model simulates the annual cycle with slight improvement, when compared to lower resolutions.

References

Adam, J. C., Lettenmaier, D. P. (2003) Adjustment of global gridded precipitation for systematic bias, J. Geophys. Res., 108, doi: 10.1029/2002JD002499

Frei, C., Schär, C. (1998) A precipitation climatology of the Alps from high-resolution rain-gauge observations, Int. J. Climatol., 18, pp. 873–900

Heikkilä, U., Sandvick, A., Sorteberg, A. (2011) Dynamical downscaling of ERA-40 in complex terrain using the WRF regional climate model, Clim. Dyn., 37, pp. 1551–1564

Jones, C., Willén, U., Ullerstig, Hansson, U. (2004) The Rossby Centre regional atmospheric climate model part I: model climatology and performance for the present climate over Europe, Ambio, 33, pp. 199–210

Mohr, M. (2008) New Routines for Gridding of Temperature and Precipitation Observations for "seNorge.no", Met.No Note, 43 pp

Neff, E. L. (1977) How much rain does a rain gage gage? J. Hydrol., 35, pp. 213–220

Uppala, S. M., 46 co-authors (2005) The ERA-40 re-analysis, Q. J. R. Meteorol. Soc., 131, pp. 2961–3012

Pryor, S. C., Nikulin, G., Jones, C. (2012) Influence of spatial resolution on regional climate model derived wind climates, J. Geophys. Res., 117, doi: 10.1029/2011JD016822

Samuelsson, P., Jones, C. G., Willén, U., Ullerstig, A., Gollvik, S., Hansson, U., Jansson, C., Kjellström, E., Nikulin, G., Wyser, K. (2011) The Rossby Centre Regional Climate Model RCA3: Model description and performance, Tellus, 63A, pp. 4–23

Soares, P. M. M., Cardoso, R. M., Miranda, P. M. A., de Medeiros, J., Belo-Pereira, M., Espirito-Santo, F. (2012) WRF high resolution dynamical downscaling of ERA-Interim for Portugal, Clim. Dyn., doi: 10.1007/s00382-012-1315-2

Walther, A., Jeong, J.-H., Nikulin, G., Jones, C., Chen, D. (2013) Evaluation of the warm season diurnal cycle of precipitation over Sweden simulated by the Rossby Centre regional climate model RCA3, Atmos. Res., 119, pp. 131–139

Impact of the horizontal resolution on extremes investigated with convection-resolving COSMO-CLM simulations

Gutjahr O., Heinemann G. and Schefczyk L.

Environmental Meteorology, University of Trier, Germany (gutjahr@uni-trier.de)

1. Introduction

The horizontal resolution of General Circulation models (GCMs) is much too coarse to represent local extremes adequately. To overcome this problem and to provide regional information, downscaling techniques are widely used.

In this study we dynamically downscale reanalysis data (1993-2000) with the regional climate model (RCM) COSMO-CLM (CCLM, Rockel et al., 2008) over 18 km (CCLM18, Hollweg et al.,2008, Keuler et al., 2012) down to 4.5 km (CCLM4.5, Gutjahr & Heinemann, 2013) and 1.3 km (CCLM1.3).

Then we compare the extremes of these hindcasts with the observational data sets REGNIE (REG1.3, DWD: German Weather Service) for precipitation and INTERMET (IMET1.3, Dobler et al., 2004) for precipitation and maximum/minimum 2 m temperature. Both data sets are products of interpolated station data with a native resolution of about 1 km. In order to compare the CCLM results with the observations, we have interpolated the observations to 1.3 km. It is investigated which impact the gradually increased horizontal resolution does have on the estimation and simulation of extremes. We calculate return levels (RL) for precipitation and 2 m minimum/maximum temperature by applying "peak-over-threshold" (POT) models for return periods of 2, 5 and 10 years of summer (JJA) and winter (DJF).

The investigation area is the state of Rhineland-Palatinate in Western Germany. In the 1.3 km resolution the Tiedtke scheme for moist convection parameterization is switched off, only a shallow convection scheme is retained. This explicitly allows the simulation of deep-convection, which is expected to improve the simulation of precipitation extremes.

2. Estimation of the return levels and their uncertainty

The fitting of “Peak-over-threshold” (POT) models (Coles, 2001) require independent and identical distributed time series. Therefore every time series of a grid box of the observations and the CCLM was linearly detrended and declustered prior to the fitting of a General Pareto Distribution (GPD). The declustering was done, following Knote et al. (2010), with the “run-length” method after Leadbetter et al. (1989) where the run-length was determined by the annual average of the maximum significant lag of the auto-correlation function (ACF), here denoted as *rd*. As a threshold we used the local 95% percentile.

Confidence intervals for the return levels were constructed by a block-bootstrapping approach (500 repetitions) on the basis of Zwiers & Kharin (1998). The block-length was set to the run-length *rd* in order to sample extreme events, which would be destroyed if no block-bootstrap would be used. From these bootstrapped return levels the 90% confidence interval is calculated. Finally we calculate the sampling uncertainty following Früh et al. (2010) as a signal-to-noise ratio (SNR). The SNR is calculated by dividing the bootstrapped-mean return levels by the range of the 90% confidence interval.

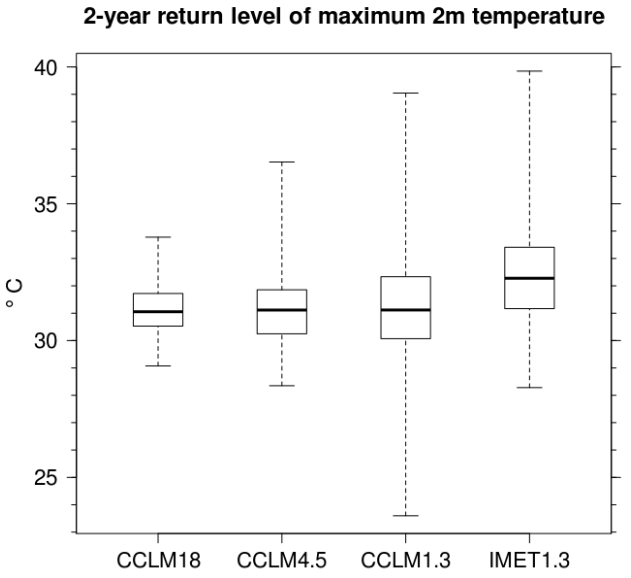


Figure 1. Spatial boxplot of the estimated 2-year return level of maximum 2 m temperature in summer (JJA) for the period 1993-2000 of the observational data set INTERMET (IMET1.3) in 1.3km resolution and from the COSMO-CLM simulations in 18 km (CCLM18), 4.5 km (CCLM4.5) and 1.3 km (CCLM1.3) resolution. The black horizontal bar denotes the median.

3. Effect of an increased resolution on the return levels

The 2, 5 and 10 year return levels have been calculated for every grid box of the observations and the COSMO-CLM simulations.

In Fig.1 the spatial variability of the 2-year RL of 2 m maximum temperature is shown as boxplots. By comparing the RL of CCLM18 with IMET1.3 there is a clear underestimation of spatial variability visible and a slight underestimation in the median. The spatial variability increases with a higher resolution and the hottest observed extremes are matched in case of CCLM1.3. However, some extremes are colder than

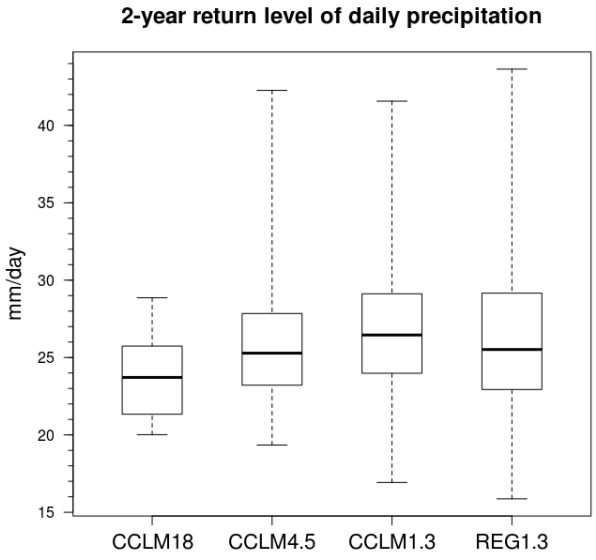


Figure 2. As in Fig.1 but for daily precipitation and that the observational data set is REGNIE in 1.3 km resolution.

observed, in particular at mountain ridges (not shown) but the median remains approximately constant for CCLM4.5 and CCLM1.3. One explanation for these stronger cold extremes in the COSMO-CLM simulations is that in these particular regions the density of observational stations is low, which may result in too warm temperatures after a spatial interpolation but is better simulated in COSMO-CLM.

In case of precipitation (Fig. 2) the spatial variability increases as well with the resolution and CCLM1.3 matches the observations. However, the median rises gradually with the resolution so that extremes are likely higher in CCLM1.3 than in the observation REG1.3. Similar overestimations of precipitation extremes on a scale < 2 km were also found by Kendon et al. (2012).

4. Conclusion

Although these are preliminary results, there is evidence that increasing the horizontal resolution of a regional climate model may result in a more realistic representation of extremes. In case of temperature this is clearly related to the better representation of the orography. Precipitation extremes are a result of a much more complex process and thus more difficult to interpret. The effect of increasing the horizontal resolution and switching off the parameterization of deep-convection increases precipitation extremes and their spatial variability. This indicates that there is a transition from too widespread and too low extremes (18 km and 4.5 km) to more localized and more intense extremes (1.3 km).

References

Dobler L., Hinterding A., Gerlach N. (2004) INTERMET – Interpolation stündlicher und tagesbasierter meteorologischer Parameter. Gesamtdokumentation. Institut für Geoinformatik der Westfälischen Wilhelms-Universität Münster i.A. Landesamt für Wasserwirtschaft Rheinland-Pfalz.

Früh B., Feldmann H., Panitz H.-J., Schädler G., Jacob D., Lorenz P., Keuler K. (2010) Determination of precipitation return values in complex terrain and their evaluation, J. Climate, 23, 2257-2274.

Hollweg H., Böhm U., Fast I., Hennemuth B., Keuler K., Keup-Thiel E., Lautenschlage M., Legutke S, Radtke K., Rockel B., Schubert M., Will A., Wildt M., Wunram C. (2008) Ensemble simulations over Europe with the Regional Climate Model CLM foced with IPCC AR4 Global Scenarios, Tech. Report, Max-Planck-Institut für Meteorologie, Gruppe: Modelle & Daten.

Gutjahr O., Heinemann G. (2013) Comparing precipitation bias correction methods for high-resolution regional climate simulations using COSMO-CLM, Theor Appl. Climatol., 114, 511-529.

Kendon E.J., Roberts N.M., Senior C.A., Roberts M.J. (2012) Realism of rainfall in a very high-resolution regional climate model, J. Climate, 25 (17), 5791-5806.

Keuler K., Radtke K., Georgievski G. (2012) Summary of evaluation results for COSMO-CLM version 4.8.clm13 (clm17): Comparison of three different configurations over Europe driven by ECMWF reanalysis data ERA40 for the period 1979-2000, Tech. Report, Brandenburg University of Technology, Cottbus.

Knote C., Heinemann G., Rockel, B. (2010) Changes in weather extremes: Assessment of return values using high resolution climate simulations at convection-resolving scale, Met. Z., 9, 11-23.

Leadbetter, M.R., Weissmann, I., de Haan, L., Rootzén, H. (1989) On clustering of high values in statistically stationary series, Tech. Report, Center for Stochastic Processes, University of North Carolina, Chapel Hill.

Rockel, B., Will, A., Hense, A. (2008) The Regional Climate Model COSMO-CLM (CCLM), Met. Z., 17, 4, 347-348.

Zwiers F.W., Kharin V.V. (1998) Changes in extremes of the climate simulated by CCC GCM2 under CO2 doubling, J. Climate, 11(9), 2200-2222.

Air quality and climate interaction within urban environment

Tomas Halenka[1], Peter Huszar[1], Michal Belda[1] and Katerina Zemankova[2]

[1] Dept. of Meteorology and Environment Protection, Fac. of Mathematics and Physics, Charles University, Prague, Czech Republic (tomas.halenka@mff.cuni.cz)

[2] LATMOS, IPSL, Paris, France

1. Introduction

Big cities or urban aglomerations can significantly impact both climate and environment. Due to the emissions of large amount of gaseous species and aerosols, which affect the composition and chemistry of the atmosphere (Timothy et al., 2009) and thus it can have adverse effect on the environment in the cities and their vicinity. Moreover, this can negatively impact the population (Gurjar et al., 2010). In addition, this pathway can result in indirect impact on the meteorology and climate, due to radiation impact of the atmospheric composition on the thermal balance, the temperature, especially within the canopy layer in the cities, can change.

However, the primary reason for temperature increase within the cities or large urbanized areas with respect to the rural vicinity, is the effect of so called urban heat island (UHI, Oke, 1973), which is mainly due to construction elements within the urban environment. This kind of surface clearly differs from natural surfaces by mechanical, radiative, thermal, and hydraulic properties, therefore, these surfaces represent additional sinks and sources of momentum and heat, affecting the mechanical, thermodynamical and hydrological properties of the atmosphere (Lee et al., 2010). Moreover, the changes of meteorological conditions within the urban areas due to UHI can further affect the air-quality. This has been studied recently by e.g. Ryu et al. (2013), they found significant impact on the ozone day and night-time levels especially due to circulation pattern changes for the Seoul metropolitan area.

In this study, we will focus on the aspects of climate conditions changes in urban environment, yet especially on those with strong potential to impact the air-quality. For the region of Central Europe, we will investigate the impact of the urban environment by means of its introducing into the regional climate model. As the spatial scale of the meteorological influence due to the cities is much smaller than the scale resolved by the mesoscale model, inclusion of urban land-surface requires additional parameterizations. The approach covering three dimensional character of the effects is provided using urban canopy models (single layered – SLUCM, or multi-layered MLUCM) coupled to the driving mesoscale model (Chen et al. 2011). Our study describes in more details the implementation of such a SLUCM into our regional climate chemistry modelling system using the couple of RegCM and CAMx.

2. Urban parameterization and experimental setup

Cities affect the boundary layer properties thus having direct influence on the meteorological conditions and therefore on the climate. The urban surface is covered by large number of artificial object with complex 3 dimensional structure and considerable vertical size. Specific characteristics in urban morphology can be involved in complicated physical processes such as increased momentum drag, radiation trapping between buildings (effect of vertical surfaces), and heat conduction by the artificial surfaces. There had been many field measurements in cities that found characteristic features of mean flow, turbulence and thermal structures in the urban boundary layer (e.g. Allwine et al., 2002; Rotach et al., 2005).

Although there is a trend (enabled by the faster computational resources) to increase the spatial resolution of the mesoscale models, regional weather prediction and climate models still fail to capture appropriately the impact of local urban features on the mesoscale meteorology and climate without special sub-grid scale treatment. This accelerated the implementation and application of urban canopy sub-models (Chen et al., 2010 or Lee et al., 2010). For the regional climate model RegCM4 we have chosen the SLUCM developed by Kusaka et al. (2001) and Kusaka and Kimura (2004); this scheme is proven to perform well in simulating the urban environment and it is less demanding in computational resources unlike its multi-layer counterparts (Lee et al., 2010).

RegCM4.1 (Giorgi et al., 2012) includes a two land-surface models: BATS (Giorgi et al., 2003b) and the CLM model (Oleson et al., 2008). Both land-surface models can work in mosaic-type mode where the model grid is divided into sub-grid boxes for which the calculation of fluxes is carried out separately and the fluxes are then aggregated back to the large scale model gridbox (for BATS scheme reffered as SUBBATS, see Pal et al., 2007). An improvement can be achieved by implementing more sophisticated urban parameterizations lying under these land-surface models that better represent for the urban land-use type most urban features like building morphology, street geometry, variability of the properties of artificial surfaces, as well as the description of radiation trapping in the street canyon. For this purpose, a Single Layer Urban Canopy Model (SLUCM), originally developed by Kusaka et al. (2001) and applied in Kusaka and Kimura (2004) has been implemented into RegCM4.1 by linking it to the BATS surface scheme, applying SUBBATS with 2 km x 2 km sub-grid resolution. SLUCM is called within SUBBATS wherever urban land-use categories are recognized in the land-use data supplied. The scheme returns the total sensible heat flux from the roof/wall/road to BATS, as well as the total momentum

flux. The total friction velocity is aggregated from urban and non-urban surfaces and passed to RegCM's boundary layer scheme. However, as RegCM4.1 by default does not consider urban type land-use categories, we extracted the urban land-use information from the Corine 2006 (EEA, 2006) database and we have added this information to the RegCM4.1 land-use database. In those parts of the domain where this was not available in Corine data, the GLC2000 (GLC, 2000) database was used. We considered two categories, urban and suburban.

3. Results

Fig. 1 presents the change of surface temperature as an example of meteorological parameters changes between experiments SLUCM (the urban canopy model turned on) and NOURBAN (urban canopy not considered) averaged over years 2005-2009. Shaded areas represent significant changes on the 95% confidence level. We show only summer season, actually, the effect is well expressed in spring and autumn as well, but summer signal is stronger, while the winter one is rather small.

For temperature, there is an evident increase with urban canopy introduced in summer, for winter only slight signal can be seen for big cities like Berlin and Vienna, similarly for urban and industrial areas like Rhine-Ruhr region and Po-valley. In summer, this temperature increase can be of 1K over urbanized areas (effect of cities like Budapest, Vienna, Prague, Berlin are well seen), but it is statistically significant elsewhere with up to 0.4K increase even over non-urban areas. Opposite effect can be seen for specific humidity. Urban surfaces can absorb less water vapor than other surfaces and they represent a sink for the precipitated water as well. Therefore the evaporation from the urban surfaces is reduced as well which leads to the lower humidity over urban areas. Again, this decrease is highest above cities (up to -0.8 g/kg), but significant decrease is simulated over non-urbanized areas as well, up to -0.3 – -0.4 g/kg. Signal is quite strong in summer, but similar patterns, although much slighter, can be seen in winter. Finally, we assess the effect of urban canopy parameterization on the height of planetary boundary layer from the model, which leads to statistically significant increase in summer above most of the domain, with quite strong signal above the cities and industrial regions of about 100-150 m, mostly negligible and not significant in winter.

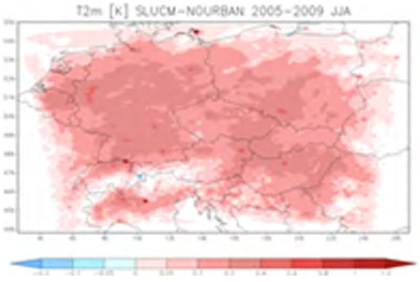


Figure 1. The mean differences of temperature at 2 m (K) between experiments with SLUCM against NOURBAN averaged over 2005-2009 for summer. Shaded areas represent significant changes on the 95% level of confidence.

Acknowledgements

The presented work was funded by the project of Czech Grant Agency No. 13-19733P and by the project UHI supported in the framework of EC OP NN (No. 3CE292P3). Partial support is provided through program PRVOUK “Environmental Research” No. 02 of the Charles University.

References

Giorgi, F., E. Coppola, F. Solmon, F., L. Mariotti, M. Sylla, X. Bi, N. Elguindi, G. T. Diro, V. Nair, G. Giuliani, S. Cozzini, I. Guettler, T. A. O’Brien, A. Tawf k, A. Shalaby, A. Zakey, A. Steiner, F. Stordal, L. Sloan and C. Brankovic, 2012: RegCM4: Model description and preliminary tests over multiple CORDEX domains, Clim. Rev., 52, 7–29.

GLC, 2000: Global Land Cover 2000 database. European Commission, Joint Research Centre, 2003. http://bioval.jrc.ec.europa.eu/products/glc2000/glc2000.php

Gurjar, B. R. et al., 2010: Human health risks in megacities due to air pollution, Atmos. Environ., 44, 4606-4613.

Huszar, P., T. Halenka, M. Belda, and K. Zemankova, 2013: Air-quality changes induced by urban land surface forcing in Central Europe. HARMO 2013 Proceedings.

Huszar, P., K. Juda-Rezler, T. Halenka, H. Chervenkov and others, 2011: Effects of climate change on ozone and particulate matter over Central and Eastern Europe, Clim. Res., 50,51–68.

Huszar, P., J. Miksovsky, P. Pisoft, M. Belda and T. Halenka, 2012: Interactive coupling of a regional climate model and a chemistry transport model: Evaluation and preliminary results on ozone and aerosol feedback, Clim. Res., 51, 59-88.

Kusaka, H. H. Kondo, Y. Kikegawa and F. Kimura, 2001: A simple singlelayer urban canopy model for atmospheric models: comparison with multi-layer and slab models, Boundary-Layer Meteorol., 101, 329–358.

Kusaka H. and F. Kimura, 2004: Coupling a single-layer urban canopy model with a simple atmospheric model: impact on urban heat island simulation for an idealized case, J. of the Met. Soc. of Japan, 82, 67–80.

Lee, S.-H. et al., 2010: Evaluation of urban surface parameterizations in the WRF model using measurements during the Texas Air Quality Study 2006 field campaign, Atmos. Chem. Phys. Discuss., 10, 25033-25080.

Oke, T.R., 1973: City size and the urban heat island. Atmospheric Environment (1967) 7(8):769–779.

Pal, J. S., F. Giorgi, X. Bi, N. Elguindi, F. Solomon, X. Gao, R. Francisco, A. Zakey, J. Winter, M. Ashfaq, F. Syed, J. L. Bell, N. S. Diffenbaugh, J. Karmacharya, A. Konare, D. Martinez, R. P. da Rocha, L. C. Sloan and A. Steiner, 2007: The ICTP RegCM3 and RegCNET: Regional Climate Modeling for the Developing World, B. Am. Meterol. Soc., 88, 1395–1409.

Ryu,Y.-H., J.-J. Baik, K.-H. Kwak, S. Kim and N. Moon, 2013: Impacts of urban land-surface forcing on ozone air quality in the Seoul metropolitan area, Atmos. Chem. Phys., 13, 2177-2194.

Timothy, M. et al., 2007: The influence of megacities on global atmospheric chemistry: a modeling study, Environ. Chem., 6, 219–225.

Assessment of three dynamical urban climate downscaling methods: application for Brussels and Paris

Rafiq Hamdi

Royal Meteorological Institute, Brussels, Belgium (rafiq.hamdi@meteo.be)

Abstract

Today, scientists, urban planners and policy makers are beginning to work together to understand and monitor the interaction between urban areas and climate change and to consider adaptation and mitigation strategies. To maintain or improve the quality of living in cities, urban planners need detailed information on future urban climate on residential scale. Such information is provided by climate models. However, because impervious surfaces cover only less than one percent of the world's land area, most of the global circulation models that are utilized for climate change research do not account for urban surfaces. In fact, cities affect the local weather by perturbing the wind, temperature, moisture, turbulence, and surface energy budget field. One very known phenomena is the so-called urban heat island (UHI) effect where urban air temperatures are substantially higher than corresponding temperatures in the surrounding rural areas.

Therefore, in order to provide detailed climate change projections to the regional scale required for impact studies over urban areas, we developed a new high-resolution dynamical downscaling strategy to examine how rural and urban areas respond to change in future climate (Hamdi et al. 2013). The regional climate simulations have been performed with a new version of the limited-area model of the ARPEGE-IFS system running at 4-km resolution coupled with the Town Energy Balance scheme (TEB). In order to downscale further the regional climate projections to a urban scale, at 1km resolution, a stand-alone surface scheme is employed in offline mode.
We performed downscaling simulations according to three model set-ups: (i) reference run, where TEB is not activated neither in 4-km simulations nor in 1-km urban simulation, (ii) offline run, where TEB is activated only for 1-km urban simulation and (iii) inline run, where TEB is activated both for regional and urban simulations. As a first step, the applicability of the method is demonstrated for the period 1961-1990. Then, the evolution of the urban climate of Brussels and Paris for the period 2046-2055 and 2071-2100 will be studied in the context of climate scenarios that was proposed by the IPCC. Particular attention will be given to the interaction between UHI and heat waves under current and future climate and to the assessement of urban mitigation strategies.

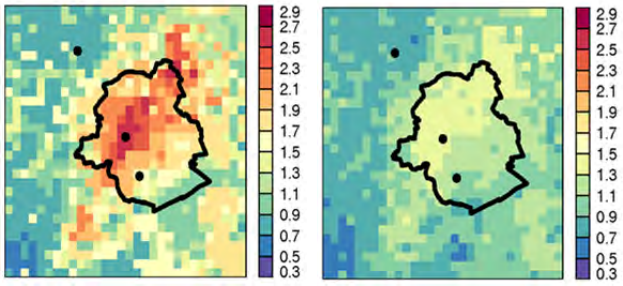


Figure 1. The nocturnal UHI of Brussels averaged over 30 years [1961-1990]. Left using the Town Energy Balance (TEB) scheme and right without TEB. The three black dots represent the city center of Brussels and two RMI observation stations: the Uccle station situated some 6km south of the center of the capital in a suburban area, and the rural Brussegem station situated 13 km far away from the center of Brussels where the model output has been verified with respect to observations.

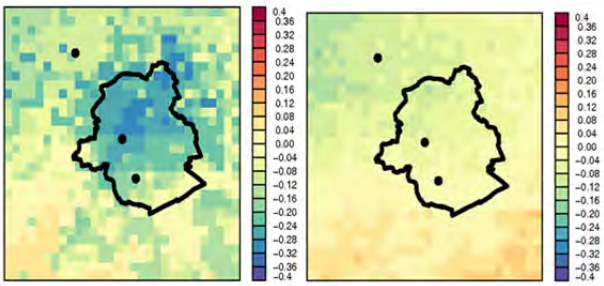


Figure 2. 2071-2100 minus 1961-1990 spatial distribution of 30-year average nocturnal UHI [°C]. Left using the Town Energy Balance (TEB) scheme and right without TEB.

References

Rafiq Hamdi, H. Van de Vyver, R. De Troch, P. Termonia (2013) Assessment of three dynamical urban climate downscaling methods: Brussels's future urban heat island under an A1B emission scenario, International journal of climatology, In press, DOI: 10.1002/joc.3734.

Implementation of the tidal forces into the models of the selected Svalbard fjords

Jaromir Jakacki, Anna Przyborska and Szymon Kosecki

Institute of Oceanology, Polish Academy of Sciences, Sopot, Poland (jjakacki@iopan.gda.pl)

1. Abstract

Svalbard fjords represent the inlets of the archipelago that the General Circulation Models (GSM) does not take into account or they are represented in the models only as a few model cells. Also, the bottom topography of the inlets does not suggest to use GCM models for such area. In our work commercial software MIKE 3D (developed by Danish Hydraulics Institute (DHI)), which is unfortunately not plug-and-play system, was implemented for the following Svalbard fjords: Kongsfiorden, Krosfiorden and Hornsund.

2. Model domain and resolution

Mesh grid with variable resolution, which is best option for such basins, was applied for these areas. The first picture presents example of implemented mesh grid for the Kongsfiorden and Krosfiorden (Figure 1), color scale represents the model bathymetry. Horizontal resolution strongly depends on variability of the bottom topography and also on the depth. Shallow waters and areas with larger gradients of the depths have higher horizontal resolution. The horizontal resolution starts from the hundreds of meters.

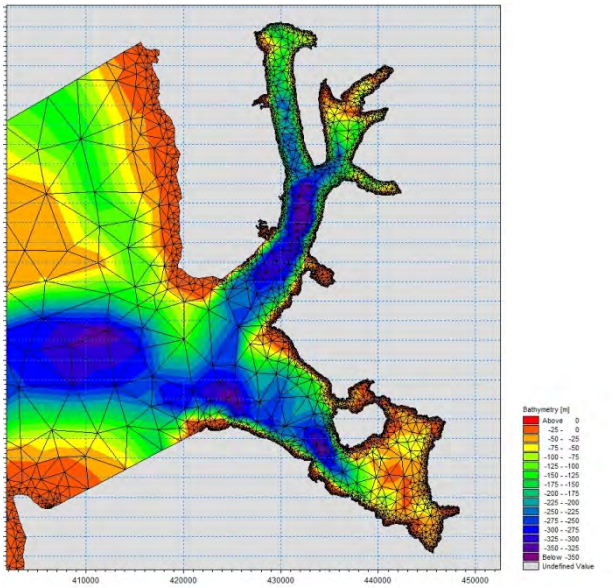


Figure 1. Kongsfiorden and Krosfiorden domain and bathymetry. Variable resolution mesh grid was also added.

3. Lateral boundary conditions

Important part of the regional model is lateral boundary. In our case, as a first approximation, sea level from the global tidal model was implemented (data represents the major diurnal (K1, O1, P1 and Q1) and semidiurnal tidal constituents (M2, S2, N2 and K2) with a spatial resolution of 0.25 ° × 0.25 ° based on TOPEX / POSEIDON altimeters data). One-year simulation (2011) has been done with implemented boundary conditions. Because of lack of data for the fjords, sea level from the Ny Alesund for the year 2002 was compared with the modeled sea level (2011). If we will not take into account low frequencies, there should be only phase shift between modeled and measured data.

3. Results

The comparison of the sea levels from Ny Alesund station and model is presented on the Figure 2. Horizontal axis of this picture represents sea level from the model, vertical axis represents data from the station. Black points are for all every hour saved data.

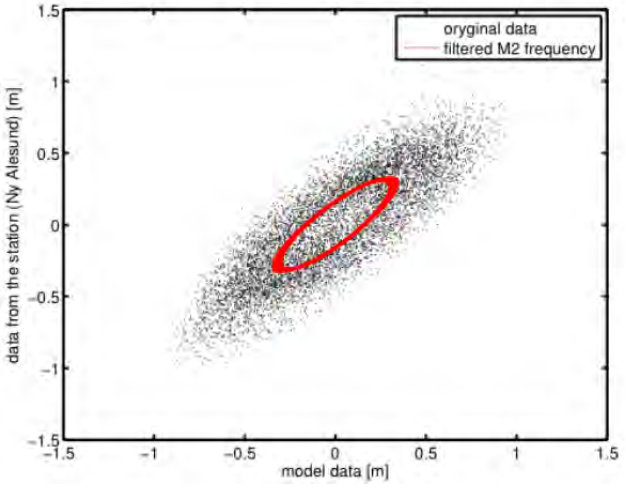


Figure 2. Measured versus modeled sea level (black points) for Ny Alesund.

On the Figure 3, power spectrum densities are presented for each time series. The upper one is for data from Ny Alesund station (black line) and the lower one is for modeled sea level. For clean presentation horizontal axis of the spectrum is presented as the period of the signal and amplitude was normalized to the maximum (maximum of both spectral densities).

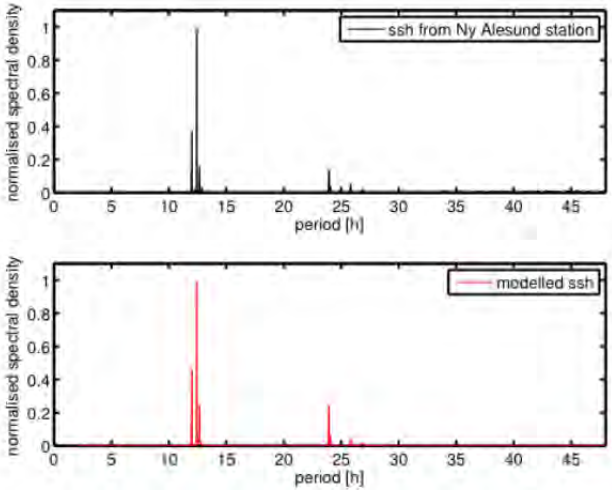


Figure 3. Power spectrum density calculated for signal from Ny Alesund station (upper image, black line) and for modeled sea level (lower image, red line)

4. Summary

The pictures show very good agreement between modeled and measured sea level. Spectral density shows similar components (tidal constituents) with comparable amplitudes. Also signal that represents M2 tidal constituent was filtered using pass band filter from both signals and is presented as a red line on the picture 2.

References

Lakshmi H. Kantha, Carol Anne Clayson (2000) Numerical Models of Oceans and Oceanic Processes, International Geophysics Series Volume 66

Z.Kowalik, T.S.Murty (1993), Numerical Modeling of Ocean Dynamics, Advanced Series on Ocean Engineering, Volume 5

Application of High-resolution RCM to Climate Change Projection and Urban Climatology Research

Nobuyuki Kayaba[1], Masashi Harada[2], Takashi Yamada[1], Hirokazu Murai[1], Satoshi Hagiya[3], Yoshinori Oikawa[1]

[1] Climate Prediction Division, Japan Meteorological Agency (n-kayaba@met.kishou.go.jp)

[2] Environment and Energy Division, Ministry of Education, Culture, Sports, Science and Technology

[3] Aerological Observatory, Japan Meteorological Agency

1. Introduction

The applicability of a convection-permitting non-hydrostatic model (NHM), developed by the Meteorological Research Institute (MRI) of the Japan Meteorological Agency (JMA), has evolved recently from daily weather forecasting to regional climate change projection (NHRCM) and urban climatology assessment (NHUCM). The latest developments from research efforts at JMA using these derivative versions of NHM are presented.

2. Climate Change Projection

Future changes in extreme weather events towards the end of this century relative to the end of the 20th century are examined for across the Japanese Archipelago using NHRCM run at 5km horizontal resolution (JMA, 2013a) under the IPCC SRES A1B emissions scenario (IPCC, 2000).

To feed the lateral boundary conditions into NHRCM, an atmospheric general circulation model is driven by future sea surface temperatures generated from the averaged anomalies of CMIP3 multi-model dataset superimposed over the observed 20th-century SSTs. This experimental design is adopted to prevent the spatial pattern of SST anomalies from drifting in a spurious way whereby model biases and internal variability obscure the climate change signals on a regional scale.

The results indicate that by the end of the 21st century Japan might be exposed to substantial increase in frequency of temperature extremes represented in terms of statistics such as the average annual number of days with maximum temperature 35 deg C or above. Precipitation extremes, represented in terms of statistics such as hourly rainfall exceeding 50mm or 20-year return value of annual maximum daily precipitation, are projected to increase all across Japan in response to rising temperature (Figure 1).

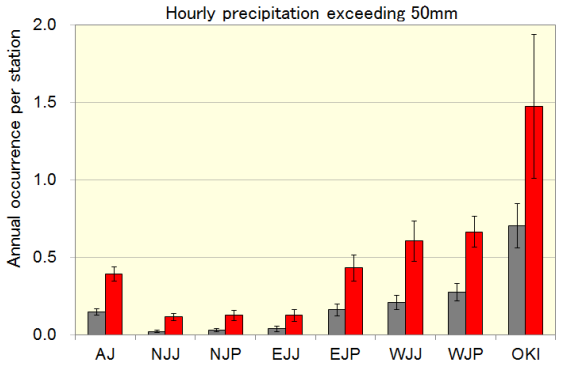


Figure 1. Projected changes in annual frequency of hourly precipitation over 50 mm for all Japan (AJ) and seven climatological regions. The grey (red) bars show frequency around the end of the 20th century (the end of the 21st century), and the thin black lines indicate the standard deviation of interannual variability.

3. Urban Climatology Assessment

Annual variability of impacts of urban heat island (UHI) on temperatures experienced in the Kanto Plain (KP) is investigated (JMA, 2013b). The observed monthly mean temperatures were the highest on record since the end of the 19th century for August 2010 at all seven meteorological observatories in KP, and were the second highest for August 2012 at the four inland observatories.

A comparison between the two NHUCM experiments for the August average temperatures from 2009 to 2012, one under actual urban ground conditions and the other under hypothetical pristine ground conditions, shows that in the extremely hot summers of 2010 and 2012, the effects of UHI were significantly enhanced both in intensity and in extent across KP (Figure 2).

Extremely hot summer conditions in Japan are closely associated with the intensity, extent and persistency of the Northwestern Pacific High. In summers when this high-pressure system dominantly influences the eastern part of Japan, daylight hours are longer, southerly winds prevail and temperatures soar. These synoptic weather conditions also happen to be factors that contribute to the evolution of UHI intensity in KP. This result suggests the UHI acts like a type of positive feedback, exacerbating scorching heat in summers when the synoptic atmospheric circulation pattern favors extremely high

temperatures.

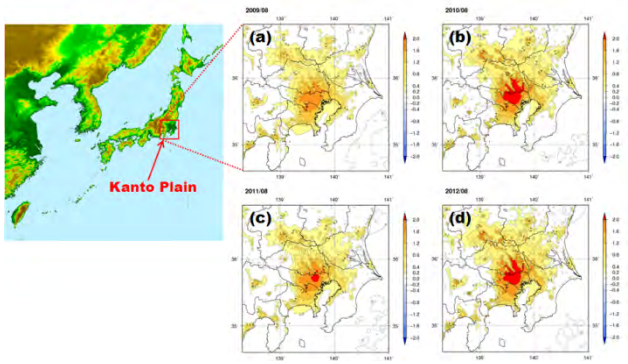


Figure 2. The spatial distribution of UHI intensity over the Kanto Plain for August 2009(a), 2010(b), 2011(c), and 2012(d). The UHI intensity is defined as differences in monthly mean temperature between the simulations under urban ground conditions and under pristine ground conditions.

References

IPCC (2000), Emission Scenarios, Cambridge University Press, UK. pp 570

Japan Meteorological Agency (2013a), Global Warming Projection Vol.8 (in Japanese)

Japan Meteorological Agency (2013b), Heat Island Monitoring Report for 2012 (in Japanese)

Very high resolution regional climate modeling – benefits and future prospects

Elizabeth J. Kendon

Met Office Hadley Centre, Exeter, UK (elizabeth.kendon@metoffice.gov.uk)

1. Introduction

Global and regional climate models, with typical grid spacings of 60-300km and 10-50km respectively, rely on a convective parameterization scheme to represent the average effects of convection. This leads to deficiencies in the diurnal cycle of convection (Brockhaus et al., 2008) and the inability (by design) to represent hourly precipitation extremes (Hanel and Buishand, 2010; Gregersen et al., 2013). The representation of complex topography and land-surface properties is also limited by the model grid size.

Very high resolution models (order 1km grid spacing) can represent convection explicitly without the need for a parameterization scheme (Hohenegger et al., 2008). Such models are termed 'convection-permitting' because larger storms and meso-scale convective organization are permitted but convective plumes and small showers are still not resolved.

2. Benefits of very high resolution models

Convection-permitting models are commonly used in short range weather forecasting, where they give a much more realistic representation of convection and are able to forecast localized extreme events not captured at coarser resolutions (Lean et al., 2008). This is illustrated in Figure 1, where the forecast from a 1.5km model for a recent convective storm over the UK is much more realistic than from a 12km model.

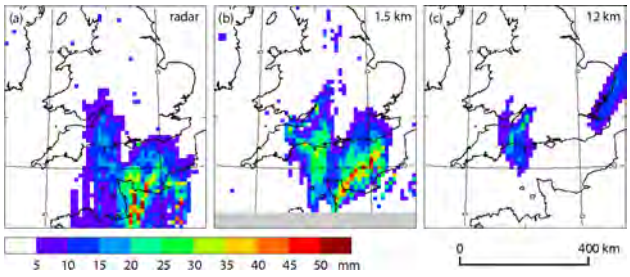


Figure 1. Rainfall accumulations (mm) for 5h period 13-18 UTC on 27th July 2013 for (a) radar, (b) 1.5km forecast model and (c) 12km forecast model. The improvement in the 1.5km model is typical for convective storms.

There are few examples of convection-permitting models being applied in climate studies, due to their high computational cost. These studies are often limited to a single season and small domains, although continuous multi-year climate simulations at convection-permitting scales are now becoming available (e.g. Kendon et al., 2012). These studies have shown improvements due to the explicit treatment of convection, in particular there are improvements in:

- Diurnal cycle of convection (Hohenegger et al., 2008; Kendon et al., 2012; Langhans et al., 2013)
- Hourly precipitation extremes (Wakazuki et al., 2008; Prein et al., 2013; Chan et al., in press)
- Duration and extent of heavy rain (Kendon et al., 2012)
- Precipitation-soil moisture feedbacks (Hohenegger et al., 2009)

There are also improvements due to the higher resolved orography, for example in summer temperature fields and precipitation maxima over mountains (Prein et al., 2013; Warrach-Sagi et al., 2013).

3. Climate change at convection permitting scales

Due to model deficiencies, we have low confidence in projections of sub-daily rainfall from coarse resolution climate models. Sub-daily observations are also sparse, but there is increasing evidence that sub-daily rainfall extremes may increase with temperature faster than daily extremes; above the Clausius-Clapeyron (CC) rate in some regions (Lenderink and van Meijgaard, 2008). This appears to be a property of convective precipitation (Berg et al., 2013) and may be explained by latent heat released within storms invigorating vertical motion.

Convection-permitting models simulate realistic hourly rainfall characteristics, unlike coarser resolution climate models, giving us confidence in their ability to project future changes on hourly timescales (Kendon et al., 2012). Super CC scaling of hourly precipitation extremes is seen in idealized warming experiments with a convection-permitting model (Attema et al., 2014). Long climate simulations at 1.5km resolution for a future scenario have recently been completed for a region of the UK. Initial results will be presented, which suggest that accurate representation of the local storm dynamics is essential for predicting changes to convective extremes.

The few other studies available examining future changes at convection-permitting scales reveal regionally dependent results. A comprehensive assessment of future changes in sub-daily rainfall is not yet possible, but it is hoped this will change as more convection-permitting climate simulations become available.

4. Future prospects

With more powerful computers, it will likely become common-place to run regional kilometre-scale climate models over increasingly large domains over different parts of the world. Such models, however, are still deemed to be in the convective 'grey-zone' (convective cells approach the model grid scale so equilibrium convection scheme assumptions are invalid, but convection is not fully resolved either) and can suffer

from biases due to under-resolved convective cores and uncertainties in microphysical processes. New approaches in convective parameterization are being developed to alleviate the grey zone problem, but they do not eliminate it.

Regional climate modeling should keep up-to-date with research into weather forecast model developments at convection-permitting resolutions. It is hoped that improvements in the quality and availability of sub-daily precipitation observations will continue and facilitate these model developments in the future.

References

Attema, J. J., Loriaux, J. M. & Lenderink, G. (2014) Extreme precipitation response to climate perturbations in an atmospheric mesoscale model, Environ. Res. Lett., 9.

Berg, P., Moseley, C. & Haerter, J. O. (2013) Strong increase in convective precipitation in response to higher temperatures, Nature Geosci., 6, 181 – 185.

Brockhaus, P., Luthi, D. & Schar, C. (2008) Aspects of the diurnal cycle in a regional climate model, Meteorol. Z., 17 433-443.

Chan, S. C. et al (in press) The value of high-resolution Met Office regional climate models in the simulation of multi-hourly precipitation extremes, J. Climate.

Gregersen, I. B. et al (2013) Assessing future climatic changes of rainfall extremes at small spatio-temporal scales, Clim. Change, 118, 783-797.

Hanel, M. & Buishand, T. A. (2010) On the value of hourly precipitation extremes in regional climate model simulations, J. Hydrol., 393, 265-273.

Hohenegger, C., Brockhaus, P. & Schar, C (2008) Towards climate simulations at cloud-resolving scales, Meteorol. Z., 17, 383-394.

Hohenegger, C., Brockhaus, P., Bretherton, C. S. & Schar, C (2009) The soil moisture-precipitation feedback in simulations with explicit and parameterized convection, J. Climate, 22, 5003-5020.

Kendon, E. J., Roberts, N. M., Senior, C. A. & Roberts, M. J. (2012) Realism of rainfall in a very high resolution regional climate model, J. Climate, 25, 5791-5806.

Langhans, W., Schmidli, J., Fuhrer, O., Bieri, S. & Schar, C. (2013) Long-term simulations of thermally driven flows and orographic convection at convection-parameterizing and cloud-resolving resolutions, J. Appl. Meteorol. Clim., 52, 1490-1510.

Lean. H. W. et al (2008) Characteristics of high-resolution versions of the Met Office Unified Model for forecasting convection over the United Kingdom, Mon. Weather Rev., 136, 3408-3424.

Lenderink, G. & van Meijgaard, E. (2008) Increase in hourly precipitation extremes beyond expectations from temperature changes. Nature Geosci., 1, 511-514.

Prein, A. F. et al (2013) Added value of convection permitting seasonal simulations, Clim. Dyn., 41, 2655-2677.

Wakazuki, Y., Nakamura, M., Kanada, S. & Muroi, C. (2008) Climatological reproducibility evaluation and future climate projection of extreme precipitation events in the Baiu Season using a high-resolution non-hydrostatic RCM in comparison with an AGCM, J. Meteorol. Soc. Jpn., 86, 951-967.

Warrach-Sagi, K., Schwitalla, T., Wulfmeyer, V. & Bauer, H.-S. (2013) Evaluation of a climate simulation in Europe based on the WRF-NOAH model system: precipitation in Germany, Clim. Dyn., 41, 755-774.

Climate change projections for the North Sea from three coupled high-resolution models

Birgit Klein[1], Katharina Bülow[1], Christian Dieterich[2], Hartmut Heinrich[1], Sabine Hüttl-Kabus[1], Bernhard Mayer[3], H.E. Markus Meier[2], Uwe Mikolajewicz[4], Nikesh Narayan [1], Thomas Pohlmann[3], Gudrun Rosenhagen[5], Dmitry Sein[6], and Jian Su[3]

[1] Bundesamt für Seeschifffahrt und Hydrographie, Operationelle Ozeanographie, Hamburg, Germany, (birgit.klein@bsh.de)
[2] SMHI, Norköpping, Sweden
[3] Institute of Oceanography, University Hamburg, Hamburg, Germany
[4] Max-Planck-Institut für Meteorologie, Hamburg, Germany
[5] Seewetteramt, DWD, Hamburg, Germany
[6] Alfred-Wegener Institute, Bremerhaven, Germany

1. Introduction

Most of the common global climate models (coupled ocean atmosphere models) have too large spatial scales to be suitable in the North Sea area. Therefore, either high-resolution global models have to be run or dynamical downscaling of the model-output has to be employed using regional models.

Regionalized climate change simulations for the North and Baltic Seas were carried out with coupled ocean atmosphere models (Dietrich et al. (2013); Jacob, (2001); Marsland et al. (2003); Pohlmann (2006)) in the framework of the research program KLIWAS The numerical simulations of the A1B scenario were performed by the Max-Planck Institute for Meteorology (MPI), the Swedish Meteorological and Hydrological Institute (SMHI) and the Institute of Oceanography (IfM Hamburg).

Output from the models is analyzed jointly with the Federal Maritime Service (BSH) and the German Weather Service (DWD/SWA).

2. Temperature changes

The three models are showing a large scale temperature increase in the order of 2- 2.5 °C at the end of the 21 century, but differ seasonally at smaller horizontal scales. The largest warming is found in the central North Sea, while inflowing waters of Atlantic origin from the north and through the English Channel show slightly reduced warming (Figure 1).

Two of the three models (HAMSOM and MPIOM) additionally indicate changes in the annual cycle in the future with larger warming rate in late spring and early winter.

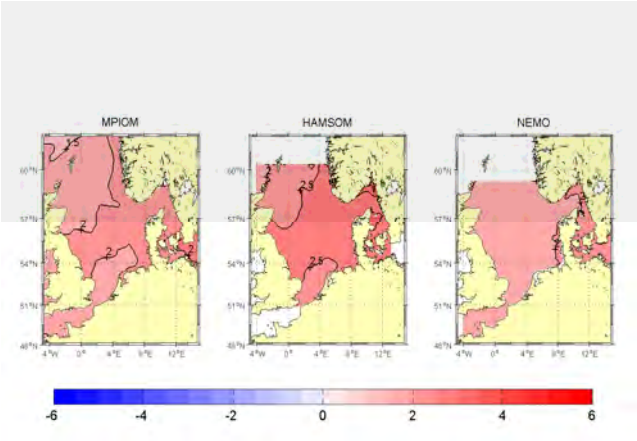


Figure 1. Annual mean SST changes from 1970-1999 to 2070-2099 in [°C].

3. Salinity changes

The enhanced hydrological cycle and moister climate of the A1B scenario leads to a freshening of North Sea proper. The strongest decreases in the North Sea at the end of the 21 century are associated with the Baltic outflow, where salinity decreases by more than 2 psu.

This signal does not seem to mix substantially with surrounding waters and is confined to the narrow band of the Norwegian Coastal Current. In the southern North Sea, two of the three models indicate slightly larger freshening, mostly associated with changes in the surface fresh water flux.

The detection of the anthropogenic climate change signal is impeded by a low signal-to-noise ratio caused by the large multi-decadal variability. All simulations show pronounced 30-40 year oscillations in salinity with the same order of magnitude as the long-term trends.

4. Sea level changes

The three models give similar rise of the steric component of sea level in the North Sea in the order of 28-30 cm at the end of the 21 century. The sea level rise signal is spatially mostly homogeneous and indicates only small dynamic changes.

Sea level time series are dominated on inter-annual

time scales by large natural variability associated with the North Atlantic Oscillation with similar representation in the three models.

The contributions from glacial melt (ice shields and glaciers) and terrestrial sources have to be estimated from other sources and have to be added offline since the simulations only provide the steric part of the sea level budget.

The vertical land movement due to glacial isostatic adjustment has to be considered in order to translate simulated geocentric sea level into a reference frame based on land. Land movement rates are particularly large around the North Sea, and the uncertainties in GIA (glacial isostatic adjustment) models need to be considered.

References

Dieterich, C., S. Schimanke, S. Wang, G. Väli, Y. Liu, R. Hordoir, L. Axell, A. Höglund, H.E.M Meier (2013): Evaluation of the SMHI coupled atmosphere-ice-ocean model RCA4_NEMO SMHI-Report, RO 47, ISSN 0283-1112.

Jacob, D. 2001: A note to the simulation of the annual and interannual variability of the water budget over the Baltic Sea drainage basin. Meteorology and Atmospheric Physics, 77, 61–73.

Marsland, S. J., Haak, H., Jungclaus, J. H., Latif, M., and Röske, F. 2003: The Max Planck Institute global ocean/sea ice model with orthogonal curvilinear coordinates. Ocean Modelling, 5(2), 91–127.

Pohlmann, T., 2006: A meso-scale model of the central and southern North Sea: Conse-quences of an improved resolution. Continental Shelf Research, 491 26 (19), 2367-2385.

Urban Climate Projection in Tokyo for the 2050's August: Impact of Urban Planning Scenarios and RCMs

Hiroyuki Kusaka[1], Asuka Suzuki-Parker[2], Toshinori Aoyagi[3], Sachiho A. Adachi[4], and Yoshiki Yamagata[5]

[1] Center for Computational Sciences, University of Tsukuba, Tsukuba, Japan (kusaka@ccs.tsukuba.ac.jp)
[2] Graduate School of Life and Environmental Sciences, University of Tsukuba, Tsukuba, Japan
[3] Meteorological Research Institute, Japan Meteorological Agency, Tsukuba, Japan
[4] Japan Agency for Marine-Earth Science and Technology, Yokohama, Japan
[5] National Institute for Environmental Studies, Yokohama, Japan

1. Introduction

Greater Tokyo is the world's largest metropolitan area, with a population of about 32.5 million. Due to Urban Heat Island (UHI) and Global Warming (GW), heat stroke mortality rate has been increasing in Tokyo, and has exceeded the fertilities from other weather disasters in Tokyo. With continuing UHI and GW, how worse will the urban environment be in the future?

For urban climate projections, Kusaka et al. (2012a) conducted downscaling from three GCMs. However, there are other sources of uncertainties for urban climate projection. In particular, urban planning scenarios and selection of regional models (in which local processes are treated differently) may have significant impacts. This study presents urban climate projection for the 2050's Augusts in Tokyo. Projection is conducted using dynamical downscaling from a single GCM (MIROC5) under the RCP4.5 scenario, by two RCMs (namely WRF and NHRCM). Furthermore, three different urban scenarios are considered, (i) status-quo city, (ii) compact city, and (iii) spread city, created by Yamagata et al. (2011).

2. Experimental Design

The WRF includes a single-layer urban canopy model (UCM) developed by Kusaka et al. (2001), Kusaka and Kimura (2004a, b). The NHRCM is a regional climate model version of the Non-hydrostatic Model by the Japan Meteorological Agency. This model includes another single-layer UCM developed by Aoyagi et al. (2012). Both UCMs consider the urban geometry, green fraction, and anthropogenic heat emission with diurnal variation at the urban grid. Model performances of WRF and NHRCM, each coupled with their UCM, have been validated for current climate urban climatology (Kusaka et al. 2012b and Aoyagi et al. 2012).

The model uses the nested domains. The larger domain with 20km horizontal grid spacing covers entire Japan islands and the smaller domain with the 4km horizontal grid spacing covers central Japan including Tokyo.

3. Results

We compare Impacts of RCM and urban scenario differences on August mean temperature increase in Tokyo and its rural town Tsukuba. The impact of RCM difference is 0.25 K and 0.37 K for Tokyo and Tsukuba, respectively. On the other hand, the impact of urban scenario difference is 0.16 K and 0.31 K for Tokyo and Tsukuba, respectively. These results indicate that impacts of RCM and urban scenario differences are comparable.

Acknowledgment

This work was supported by the SOUSEI Program of the Ministry of Education, Culture, Sports, Science, and Technology.

References

Aoyagi, T., N. Kayaba, and N. Seino, 2012: Numerical simulation of the surface air temperature change caused by increases of urban area, anthropogenic heat, and building aspect ratio in the Kanto-Koshin area. J. Meteor. Soc. Japan, 90B, 11–31.

Kusaka, H., Kondo, H., Kikegawa, Y., Kimura, F., 2001: A simple single-layer urban canopy model for atmospheric models : Comparison with multi-layer and slab models. Bound. -Layer Meteor., 101, 329-358.

Kusaka, H., Kimura, F., 2004: Thermal effects of urban canyon structure on the nocturnal heat island. J. Appl. Meteor. Clim., 43, 1899-1910.

Kusaka, H., Hara, M., Takane, Y., 2012a: Urban climate projection by the WRF model at 3-km horizontal grid increment: Dynamical downscaling and predicting heat stress in the 2070's August for Tokyo, Osaka, and Nagoya metropolies. J. Meteor. Soc. Japan., 90B, 47-63.

Kusaka, H., Chen, F., Tewari, M., Dudhia, J., Gill, D. O., Duda, M. G., Wang, W., Miya, Y., 2012: Numerical Simulation of Urban Heat Island Effect by the WRF Model with 4-km Grid Increment: An Inter-Comparison Study between the Urban Canopy Model and Slab Model. J. Meteor. Soc. Japan., 90B, 33-45.

Yamagata, Y., H. Seya, and K. Nakamichi, 2011: Scenario analysis of the future urban land use in the Tokyo metropolitan area. Journal of Society of Environmental Science, 24(3), 169-179. (in Japanese).

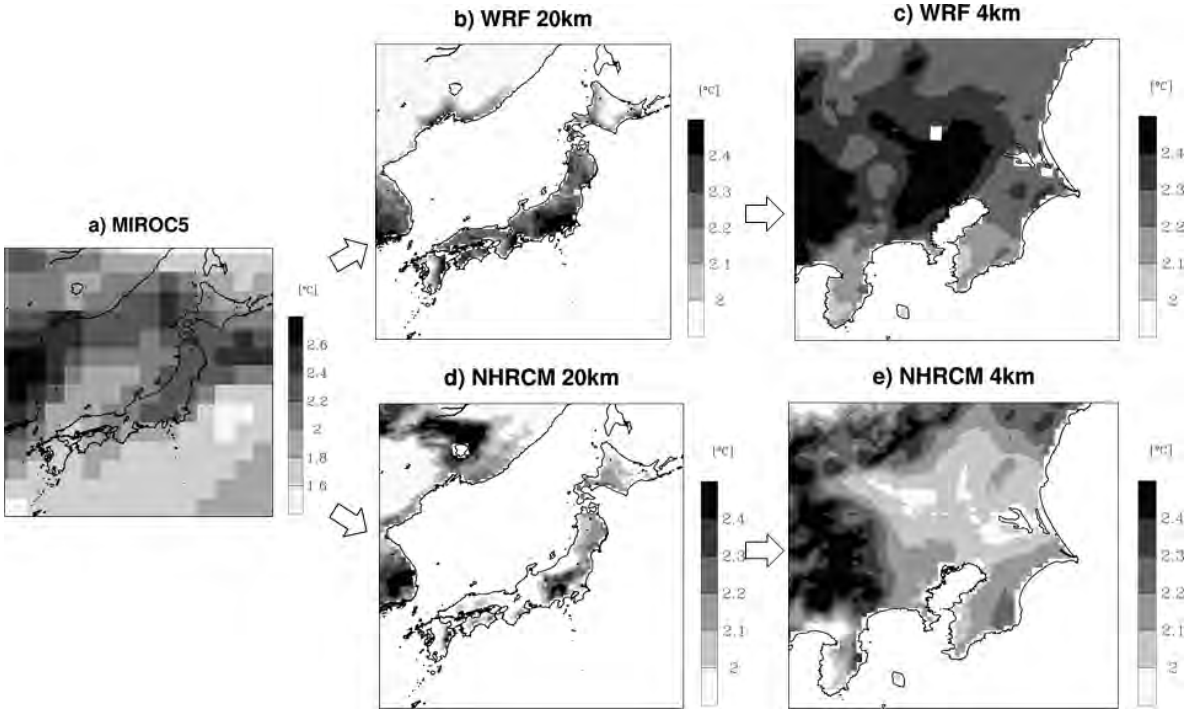


Figure 1. Projected increase of August mean surface air temperature by (a) MIROC5, (b) WRF with 20km resolution, (c) WRF with 4km resolution, (d) NHRCM with 20km resolution, and (e) NHRCM with 4km resolution.

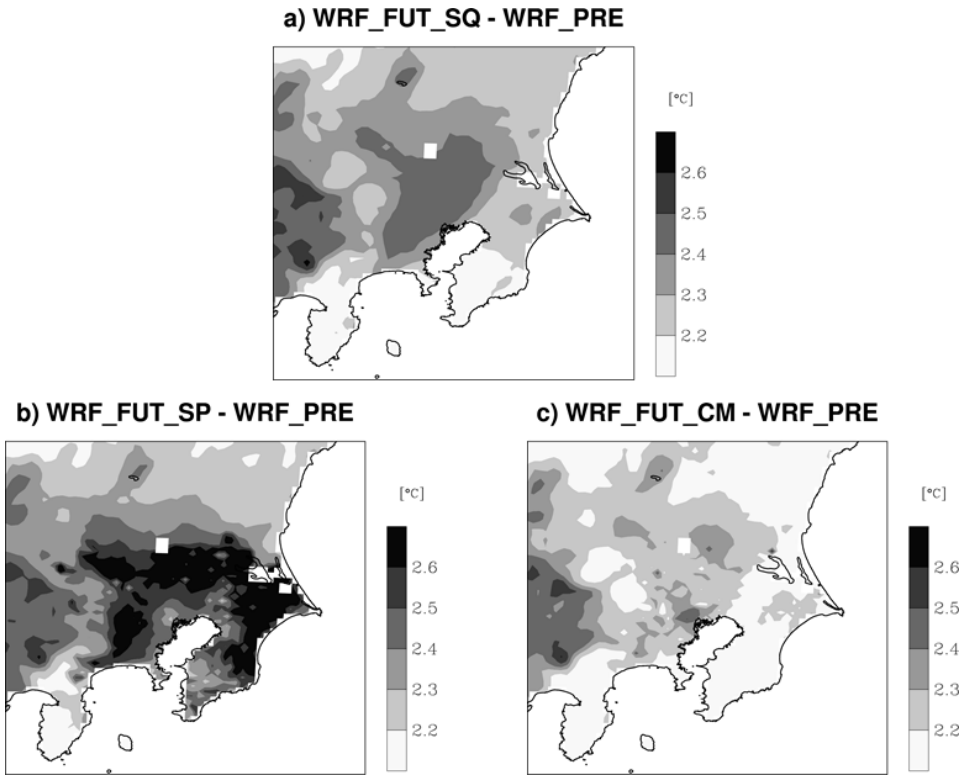


Figure 2. Projected increase of August mean surface air temperature by WRF (a) with status-quo urban scenario, (b) with spread city urban scenario, and (c) with compact city scenario.

Response of hourly precipitation extremes to temperature and moisture perturbations: results from a mesoscale model.

Geert Lenderink[1], Jisk Attema[1], Jessica Loriaux[1,2] and Erik van Meijgaard[1]

[1] Regional Climate Research Division, Royal Netherlands Meteorological Institute, De Bilt, The Netherlands (lenderin@knmi.nl)

[2] Technical University Delft, Delft, The Netherlands

1. The Clausius-Clapeyron relation and precipitation extremes

Observations of extreme (sub-)hourly precipitation at mid-latitudes show a large dependency on the dew point temperature often close to 14% per degree, which is 2 times the dependency of the specific humidity on dew point temperature as given by the Clausius–Clapeyron (CC) relation (e.g. Lenderink et al. 2011). In literature, it is argued that this 2CC scaling is linked to the response of convective precipitation to temperature and moisture increases (Moseley et al. 2013; Loriaux et al. 2013).

2. Modeling setup and analysis

By simulating a selection of 11 cases over the Netherlands characterized by intense showers, we investigate this hypothesis in the non-hydrostatic weather prediction model Harmonie at a resolution of 2.5 km. First, for each case a reference simulation representing present-day climate conditions is performed. Then, the experiments are repeated using perturbations of the atmospheric profiles of temperature and humidity: (i) using an idealized approach with a 2 warmer (colder) atmosphere, uniform with height, assuming constant relative humidity, and (ii) using changes in temperature and humidity derived from a long climate change simulation at 2 degrees global warming. The climate perturbation reveals a warming that is non- uniform with height. In general, the warming near the tropopause is largest, indicating a small increase in stability of the atmosphere. Also, the warming near the surface is ~0.5 °C larger than the global average temperature rise of 2 °C, and the relative humidity near the surface decrease with a few percent.

Here, we will discuss the sensitivity of precipitation extremes to local dew point temperature changes; see Lenderink et al. (2011) for why the dew point temperature is used. All perturbations have a difference in the local dew point temperature compared to the reference of approximately 2 degrees.

3. Results of one case

Results of one case (based on 11 August 2004) are shown in Figure 1, for both the reference experiment and the plus 2 degrees idealized warming experiment. It is shown that the broad features of the accumulated precipitation field are in both experiments very similar. Yet, the warmer experiment shows considerably higher precipitation amounts, in particular for the southern part of the domain. Likewise, the experiment with a 2 degree colder atmosphere reveals a decrease in precipitation amounts.

Results obtained with the climate perturbation are generally close to results of the plus 2 degrees idealized perturbation for areas with high precipitation amounts. However, the areas with lighter precipitation show a decrease for the climate perturbation, whereas in the idealized plus 2 degrees perturbation they generally reveal an increase. Apparently, this is due to the decrease in relative humidity for the climate perturbation.

The other 10 cases give comparable results. Except for one case, all cases show an increase in precipitation amounts with temperature, although the actual increase varies from experiment to experiment.

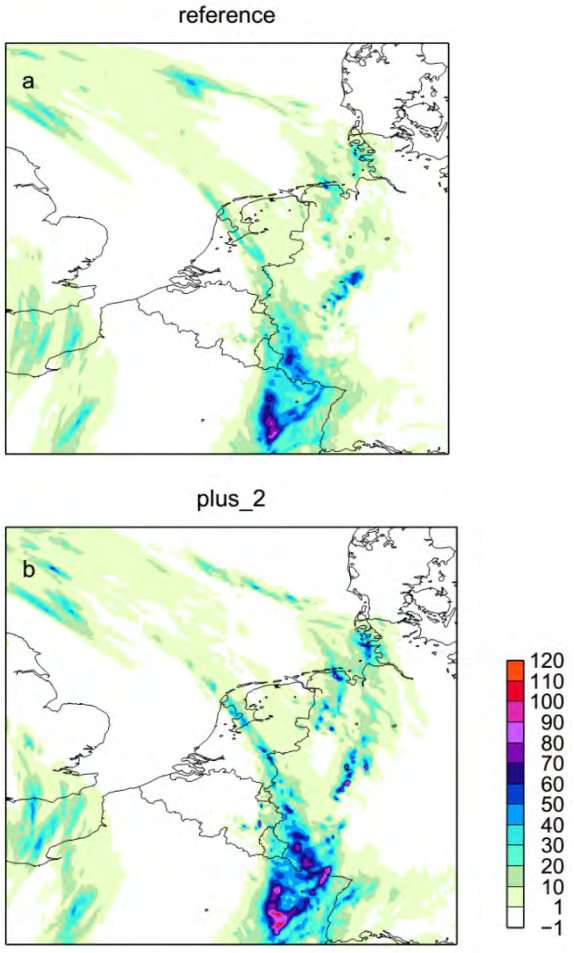


Figure 1. Daily precipitation sum for the reference experiment (upper panel) and the future experiment (lower panel) under a idealized two degree uniform warming and unchanged relative humidity perturbation.

4. Changes in hourly precipitation extremes

Next, we look at changes in the statistics of hourly precipitation extremes. We pooled all data from all grid boxes, all hours and all 11 cases together, and computed precipitation amounts for different values of the Probability of Exceedance (PoE).

Results as shown in Figure 2 reveal a remarked increase in precipitation extremes with (dew point) temperature derived from comparing different set of perturbed experiments to the reference experiment. For the most extreme events (right side of the plot) hourly precipitation increase with more than 10 % per degree rise in dew point temperature. The sensitivity to the temperature perturbation is rather constant with PoE for the two uniform perturbation experiments, but shows a remarked dependency on the PoE for the climate perturbation; that is, less extreme events show smaller increases.

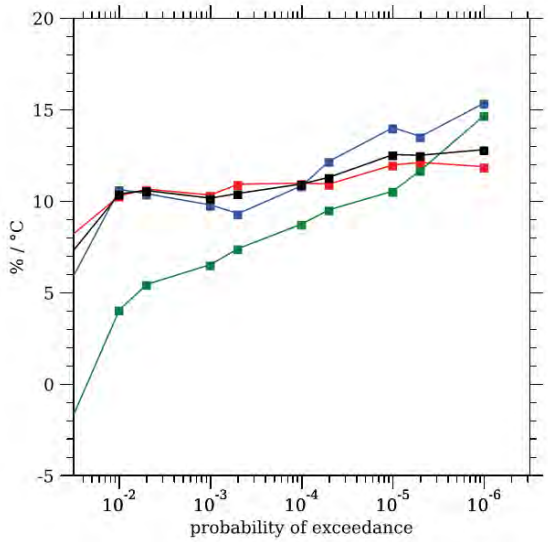


Figure 2. Change in extreme precipitation for different values of the Probability of Exceedance (PoE) with respect to the reference simulation. Changes are normalized per degree rise in dew point temperature. Colors are: red, derived from +2 °C perturbation; blue derived from -2 °C; black, derived from -2 and +2 °C perturbations; green, derived from climate perturbation.

Results for the individual cases separately display different sensitivities of hourly precipitation extremes to the perturbations, with values between 7 and 17 % per degree derived from the uniform perturbation (combined sensitivity from the -2 and +2 °C perturbations), and 0 and 15 % per degree for the climate perturbation. Considering the statistics of individual events it appears that for some events a positive temperature perturbation does not results in considerable increase in precipitation intensity, suggesting a possible limit on precipitation intensity. We note that the same cases do show a considerable reduction in precipitation intensity with the -2°C perturbation. On the other hand, the poor statistics of these individual runs, and the chaotic behavior of the atmosphere in convective conditions, may play a role as well.

5. Conclusion

We simulated a selection of 11 cases with extreme convective precipitation under present-day climate conditions and modified colder and warmer climate conditions with a mesoscale model (Harmonie). This model explicitly resolves the largest convective motions, in contrast to regional (and global) climate model in which convection is parameterized. In general, a considerable increase of hourly precipitation extremes – in the tail of the distribution averaging to 10-14 % per degree – was found. This is larger than expected based on moisture availability, predicting an increase of 6-7 % per degree. Yet, also the differences between the results of the cases were substantial. This, and the suggestion of a possible limit of the increase of precipitation intensity with temperature, needs to be investigated further.

References

Attema, J. J., J. M. Loriaux, and G. Lenderink (2014), Extreme precipitation response to climate perturbations in an atmospheric mesoscale model, Environ. Res. Lett., 9(1), 014003, doi:10.1088/1748-9326/9/1/014003.

Lenderink, G., H. Y. Mok, T. C. Lee, and G. J. van Oldenborgh (2011), Scaling and trends of hourly precipitation extremes in two different climate zones – Hong Kong and the Netherlands, Hydrol. Earth Syst. Sci., 15(9), 3033–3041, doi:10.5194/hess-15-3033-2011.

Loriaux, J. M., G. Lenderink, S. R. De Roode, and a. P. Siebesma (2013), Understanding Convective Extreme Precipitation Scaling Using Observations and an Entraining Plume Model, J. Atmos. Sci., 70(11), 3641–3655, doi:10.1175/JAS-D-12-0317.1.

Moseley, C., P. Berg, and J. O. Haerter (2013), Probing the precipitation life cycle by iterative rain cell tracking, J. Geophys. Res. Atmos., 118(November), n/a–n/a, doi:10.1002/2013JD020868.

A Review of Very High Resolution Climate Modeling

L. Ruby Leung

Pacific Northwest National Laboratory, Richland, WA, USA (ruby.leung@pnnl.gov)

Climate is influenced by physical and dynamical processes that occur over a wide range of spatial and temporal scales. Climate models discretize each earth system component using computational grids to solve the dynamical and thermodynamical equations, but processes not resolvable by the computational grids must be parameterized using conceptual theories, physical laws, or closure assumptions that relate their influence on the grid scale processes to quantities explicitly resolved by models. Ideally climate models may be more skillful when more processes are resolved explicitly with increasing model resolution, as this reduces their dependence on model parameterizations, which arguably are incomplete in their representations of the physical world. In practice, however, improvements in model skill with increasing resolution have been illusive partly because most physics parameterizations include some assumptions of scale separation so their range of applicability may be limited to that for which they were intended. Furthermore, different processes have more dominant influence at different scales, so with increasing model resolution, processes that may have been ignored or simplified in coarse resolution models must be included to represent variability that is resolved, which also have upscaled influences. As computing resources allow regional climate models to go beyond the hydrostatic limit, more studies have begun to investigate model skill in convection permitting simulations, as they address one of the key limitations in climate models related to cumulus convection. This presentation will provide a review of previous and ongoing efforts on understanding resolution effects in both regional and global climate modeling, with more emphasis on efforts towards “very high” resolution climate modeling with grid resolutions between 25 and a few kilometers.

Simulating extreme precipitation in the island of Crete with non-hydrostatic high-resolution RCMs

Petter Lind[1,2], David Lindstedt[1,2], Colin Jones[3] and Erik Kjellström[1]

[1] Rossby Centre, Swedish Meteorological and Hydrological Institute, Norrköping, Sweden (petter.lind@smhi.se)
[2] Meteorological institution, Stockholm University, Stockholm, Sweden
[3] Hadley Centre, Met Office, Exeter, United Kingdom

Due to its dependence on a wide range of processes and scales, accurate model projections of precipitation distribution, especially the frequency and intensity of wet (and dry) extremes, still remains one of the largest challenges in the climate model community. Meanwhile, appropriate risk management in the context of climate change adaptation requires local scale knowledge in order for society to act appropriately to reduce vulnerability and exposure. Accordingly, user communities have needs that are highly dependent on accurate simulation of both the spatial distribution and intensity of precipitation, at daily or even sub-daily timescales and often in areas of complex terrain.

Here, a set of experiments with high-resolution non-hydrostatic (NH) regional climate models (RCMs), NHRCMs, was conducted for the island of Crete. The experiments were designed to take advantage of the convection resolving capabilities of this class of models and as such three recent episodes exhibiting extreme precipitation and catastrophic flooding were chosen. The main question we seek to answer in this study is:

- Are convection-permitting resolutions (< 4km) able to capture intense convection and thus accurately represent extreme precipitation events over Crete?

The models were run at horizontal resolutions of ~2km and thus required high resolution lateral boundary conditions. These were derived through a "poor-man's reanalysis" procedure, whereby ERA-Interim (Dee et al., 2011) was downscaled with an RCM using frequent re-initializations towards its driving fields at a horizontal resolution of approximately 12 km over a domain covering Europe. The benefit of re-initializing the three-dimensional atmospheric fields is to generate a climate data set of high resolution retaining the weather events inherent to the forcing data (in this case of ERA-Interim).

High temporal resolution precipitation model output from the three extreme events were compared to precipitation station observations for a first order evaluation of the models' performance (Fig. 1). These first results indicates that the NHRCMs generally do well, showing spatial details and capturing peaks, timing, magnitude and location. However, there were notable differences between the simulations indicating that structural differences between the models and microphysical processes are likely important contributors to uncertainty at these scales.

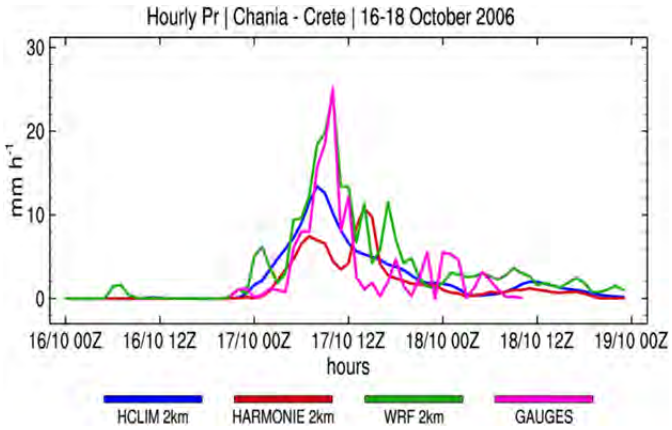


Figure 1. Precipitation amount (mm h^{-1}) for the grid box closest to the observational site in Chania (Crete) as simulated by the HCLIM, HARMONIE and WRF NHRCMs. The pink line shows the corresponding precipitation measurement from the rain gauge.

To address this, further analysis will be undertaken to evaluate a wider range of the meteorological aspects of these events (e.g. 3D wind fields, temperature and humidity vertical stratification) and how these are represented in the various models. While such an analysis is necessary to understand model differences, the initial outcomes of these experiments illustrates that the NHRCM model setup can be used to study localized extreme precipitation events and are likely suitable as tools to be used in impacts studies within the context of climate services.

References

Dee, D., Uppala, S. M., Simmons, A. J., Berrisford, P., Poli, P., Kobayashi, S., Andrae, U., Balmaseda, M. A., Balsamo, G., Bauer, P., Bechtold, P., Beljaars, A. C. M., Van De Berg, L., Bidlot, J., Bormann, N., Delsol, C., Dragani, R., Fuentes, M., Geer, A. J., Haimberger, L., Healy, S. B., Hersbach, H., Hólm, E. V., Isaksen, L., Kållberg, P., Köhler, M., Matricardi, M., McNally, A. P., Monge-Sanz, B. M., Morcrette, J. J., Park, B. K., Peubey, C., De Rosnay, P., Tavolato, C., Thépaut, J. N., and Vitart, F. (2011). The ERA-Interim reanalysis: configuration and performance of the data assimilation system. Quarterly Journal of the Royal Meteorological Society, 137, 656, pp. 553-597.

A new regional climate model operating at the meso-gamma scale; performance over Europe

David Lindstedt[1,2], Petter Lind[1,2], Colin Jones[3] and Erik Kjellström[1]

[1] Rossby Centre, Swedish Meteorological and Hydrological Institute, Norrköping (david.lindstedt@smhi.se)
[2] Meteorological Institution, Stockholm University, Sweden
[3] Hadley Centre, Met Office, Exeter, UK

1. Background

Current generation climate models struggle to accurately capture the observed intensity and frequency of precipitation (Wehner et al., 2013), where one reason is the low resolution used in climate models. As grid sizes reach below ~10 km in RCM's, referred to as the "grey-zone" scale, parametrizations start to violate underlying statistical assumptions. Arakawa et al (2011) advocates a unified cloud parametrization, enabling a continuous transition from coarse meshes to finer scales. Gerard et al (2009) approached the scale dilemma with a more unified parametrization which is here used in a climate setting.

2. Models

A new model system has been employed; HCLIM which we compare to observations and to state-of-the-art Regional Climate Model; RCA4 (Samuelsson et al., 2011). HCLIM is the climate configuration of the numerical weather prediction model HARMONIE (Hirlam Aladin Regional Mesoscale Operational NWP In Europe) which is built and used by several national meteorological services. The model system contains a suite of physical parameterization packages that are developed to be applicable to different resolutions. This is the first time HCLIM has been used as a climate model and also one of the first times an RCM has been run in climate mode at grey-zone resolution.

3. Conclusion

This study describes the performance of a new model system in a climate configuration, with a resolution within the "grey-zone" scale.

Main findings include:

i. The large scale climate is very well represented
ii. For the very rare, high precipitation events, HCLIM reproduces the frequency and intensity compared to high-resolution observed data
iii. Compared to a coarser resolution model setup we see some improvement with the too frequent low-to-moderate events ("drizzle") in the model

This leads us to conclude that HCLIM is a suitable tool for investigating future projections over Europe.

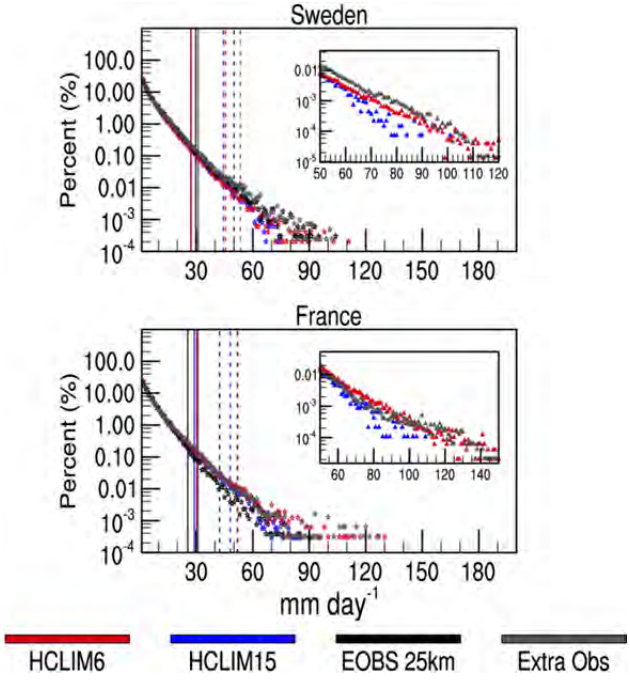


Figure 1. PDF of summer daily mean precipitation for Sweden and France. All data in large figure are aggregated to E-OBS grid and for the inset all data are on the HCLIM6 (6km) grid. Grey dots are high-resolution regional data sets. Vertical lines are 99th (solid) and 99.9th (dashed) percentiles.

References

A. Arakawa, J.-H. Jung and C.-M. Wu (2011). Toward unification of the multiscale modeling of the atmosphere. Atmospheric Chemistry and Physics, Vol 11(8)., pp. 3731-3742

Luc Gerard, Jean-Marcel Piriou, Radmila Brožková, Jean-François Geleyn, and Doina Banciu. (2009) Cloud and Precipitation Parameterization in a Meso-Gamma-Scale Operational Weather Prediction Model. Monthly Weather Review, Vol., 137., pp. 3960–3977

Patrick Samuelsson, Colin G. Jones, Ulrika Willén, Anders Ullerstig, Stefan Gollvik, Ulf Hansson, Christer Jansson, Erik Kjellström, Grigory Nikulin, and Klaus Wyser (2011) The Rossby Centre regional climate model rca3: model description and performance. Tellus A, Vol., 63(1)., pp 4–23

Michael F. Wehner (2013) Very extreme seasonal precipitation in the NARCCAP ensemble: model performance and projections. Climate Dynamics, Vol., 40(1-2)., pp 59–80

Convection permitting regional climate simulations of precipitation over a southwestern region of Japan

Akihiko Murata, Hidetaka Sasaki, Mizuki Hanafusa and Masaya Nosaka

Meteorological Research Institute, Tsukuba, Japan (amurata@mri-jma.go.jp)

1. Introduction

The horizontal resolution of regional climate models (RCMs) has recently been improved. RCMs with resolution of a few kilometers have been employed in simulations of regional climates. Such high-resolution models do not need convective parameterization because the models have the ability to represent cumulus convection.

It is necessary to evaluate the performance of convection permitting RCMs over Japan. In the field of mesoscale numerical models, a number of studies have shown that the switching off of a convection scheme has a great impact on simulation results. However, few studies have investigated the performance of a convection permitting RCM from the viewpoint of regional climate. In particular, no studies have, so far, examined the reproducibility of regional climate over Japan in all seasons using such a high-resolution model.

In this study, we investigate precipitation climatology over a southwestern region of Japan reproduced by a convection permitting regional climate model.

2. Numerical Model and Experimental Design

The regional climate model used is called the non-hydrostatic regional climate model (NHRCM), which was developed by Sasaki et al. (2008). NHRCM is the climate version of the Japan Meteorological Agency Nonhydrostatic Model (JMA-NHM) (Saito et al. 2006). JMA-NHM is operationally used in numerical weather prediction. NHRCM has successfully been used for previous studies (e.g., Sasaki et al. 2011, Hanafusa et al. 2013, Murata et al. 2013).

Nesting strategy for numerical simulations is as follows. The model domain (251 × 251 grid points) of NHRCM with a grid spacing of 2 km (NHRCM02) was set to cover a southwestern region of Japan. Boundary conditions for NHRCM02 were derived from a simulation using NHRCM with a grid spacing of 5 km (NHRCM05) that covered Japan. Similarly, boundary conditions for NHRCM5 were provided by a simulation using NHRCM with a grid spacing of 15 km (NHRCM15) that covered East Asia. Boundary conditions for NHRCM15, on the other hand, were derived from a simulation using an atmospheric general circulation model with 20-km horizontal resolution (Mizuta et al. 2012).

Simulations for the present climate were performed for 19 years, from September 1981 to August 2000. For each year, the simulation was started in August and was run through August of the following year. The first month of the simulation was discarded as model spinup.

3. Annual Precipitation

It is found that the annual precipitation is reasonably well reproduced by NHRCM02 by comparing with data based on observations: Data from Global Precipitation Climatology Project (GPCP) and from Climate Prediction Center Merged Analysis of Precipitation (CMAP). Table 1 reveals that the domain-averaged annual precipitation reproduced by NHRCM02 is in good agreement with that derived from the GPCP data. The magnitude of bias is within interannual variations, measured by the standard deviation, of the observed precipitation. As for the CMAP data, on the other hand, the magnitude of bias is larger than the standard deviation, suggesting that bias is not negligible. These results might reflect a negative bias in the simulated precipitation over the southwestern region of Japan.

Table 1. Annual precipitation averaged over the model domain and its standard deviation (as an index of interannual variability) obtained from GPCP and CMAP data. Bias represents difference between modeled and observed precipitation (model minus observation).

	GPCP	CMAP
Annual precipitation [mm]	1695	2022
Standard deviation [mm]	213	252
Bias [mm]	-91	-418

4. Monthly Precipitation

The time evolution of monthly precipitation is reasonably well reproduced by NHRCM02 although the simulated precipitation seems to be underestimated for several months. Figure 1 shows the time series of the simulated and observed monthly precipitation. The overall evolution of monthly precipitation represented by NHRCM02 is similar to that obtained from the GPCP and CMAP data. For example, both the modeled and observed precipitation is larger in June and smaller in December and January, compared with precipitation in other months. However, another peak in summer (i.e., in August and September) is not well represented by NHRCM02.

Biases in the simulated precipitation are relatively large from late summer to mid-autumn. Figure 2 shows the time series of biases in monthly precipitation

reproduced by NHRCM02. Also shown is the standard deviation of observational precipitation, index of interannual variation. It is found that the magnitude of bias is within the standard deviation of the observed precipitation most months of the year. However, the magnitude of bias in several months is comparable to the standard deviation. In particular, biases from September to October are relatively large and comparable to the standard deviation, suggesting that precipitation associated with tropical cyclones is not well represented by NHRCM02. Closer inspection of precipitation simulated by NHRCM05, the driving model for NHRCM02, reveals that NHRCM05 also has a similar magnitude of bias during this period. We therefore conclude that the performance of the driving model greatly affects that of NHRCM02 and leads to the relatively large bias in precipitation from late summer to mid-autumn.

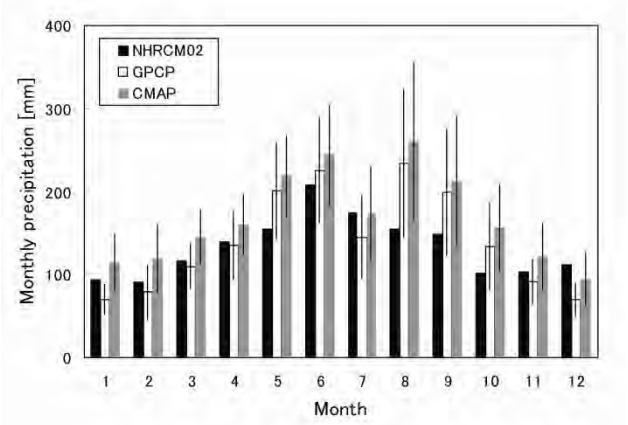


Figure 1. Time series of the simulated (NHRCM02) and observed (GPCP and CMAP) monthly precipitation averaged over the southwestern region of Japan. A solid line on a bar for GPCP and CMAP denotes the standard deviation of monthly precipitation, as an index of interannual variability.

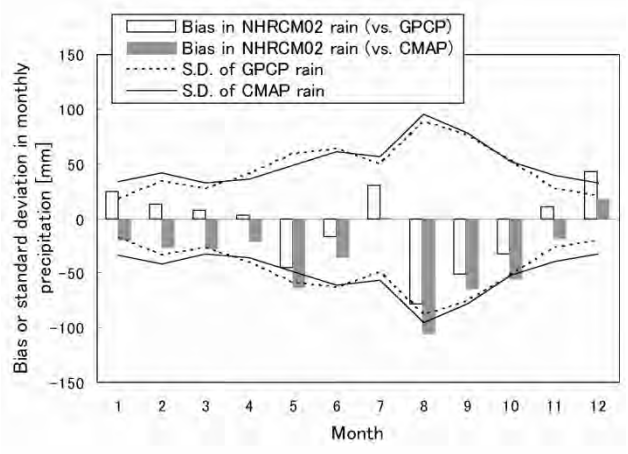


Figure 2. Time series of bias in the simulated precipitation (NHRCM02), averaged over the southwestern region of Japan, measured by GPCP and CMAP. The standard deviation of the observed precipitation, as an index of interannual variability, for each observation is also shown for comparison.

5. Hourly precipitation

The frequency of intense precipitation tends to be overestimated in the NHRCM02 results. Figure 3 shows the relative frequency of hourly rainfall rate derived from the NHRCM02 results and observational data, where the automated meteorological data acquisition system (AMeDAS) administered by JAM are used for the observational data. The distribution reveals that the modeled precipitation is larger than the observed one in the range over 40 mm h^{-1}. This overestimation tends to arise in autumn. On going research is under way to examine thermodynamic structures of the environment.

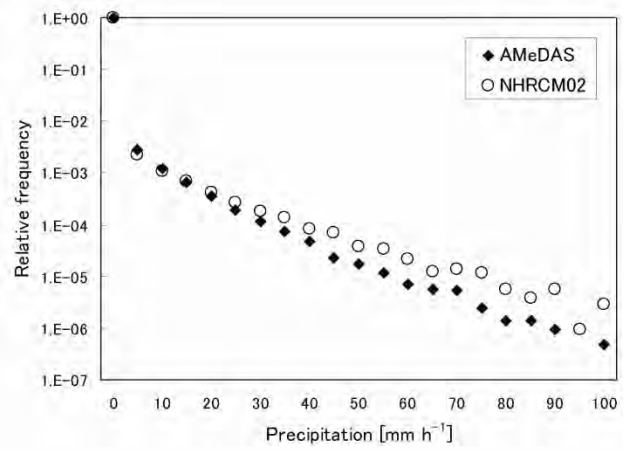


Figure 3. Relative frequency of hourly rainfall rate reproduced by NHRCM02 and observed by AMeDAS. Extraction of the modeled precipitation is based on selecting the nearest land grid point to the location of each AMeDAS station.

References

Hanafusa, M., H. Sasaki, A. Murata, K. Kurihara (2013) Projection of changes in future surface wind around Japan using a non-hydrostatic regional climate model, SOLA, 9, pp. 23–26

Mizuta, R., H. Yoshimura, H. Murakami, M. Matsueda, H. Endo, T. Ose, K. Kamiguchi, M. Hosaka, M. Sugi, S. Yukimoto, S. Kusunoki, A. Kitoh (2012) Climate simulations using the improved MRI-AGCM with 20-km grid, J. Meteor. Soc. Japan, 90A, pp. 233–258

Murata, A., H. Sasaki, M. Hanafusa, K. Kurihara (2013) Estimation of urban heat island intensity using biases in surface air temperature simulated by a nonhydrostatic regional climate model, Theor. Appl. Climatol., 112, pp. 351–361

Saito, K., T. Fujita, Y. Yamada, J. Ishida, Y. Kumagai, K. Aranami, S. Ohmori, R. Nagasawa, S. Kumagai, C. Muroi, T. Kato, H. Eito, Y. Yamazaki (2006) The operational JMA nonhydrostatic mesoscale model, Mon. Wea. Rev., 134, pp. 1266–1298

Sasaki, H., K. Kurihara, I. Takayabu, T. Uchiyama (2008) Preliminary experiments of reproducing the present climate using the non-hydrostatic regional climate model, SOLA, 4, pp. 25−28

Sasaki, H., A. Murata, M. Hanafusa, M. Oh'izumi, K. Kurihara (2011) Reproducibility of present climate in a non-hydrostatic regional climate model nested within an atmosphere general circulation model, SOLA, 7, pp. 173−176

Evaluation of the coupling between NWP and LES-based CFD models for simulating urban boundary layer flows

Hiromasa Nakayama[1], Tetsuya Takemi[2] and Haruyasu Nagai[1]

[1] Japan Atomic Energy Agency, Tokai, Ibaraki, Japan (nakayama.hiromasa@jaea.go.jp)

[2] Disaster Prevention Research Institute, Kyoto University, Uji, Kyoto, Japan

1. Introduction

For understanding a wind system over urban areas, a numerical modeling is a useful tool. To simulate atmospheric flows in real meteorological settings, numerical weather prediction (NWP) models are commonly used. Although the accuracy of NWP models for daily weather is continuously improving, it is difficult to reproduce wind fluctuations due to the effects of urban buildings that are not explicitly represented in NWP models. On the other hand, for simulating wind flows over urban areas composed of a diverse, random arrangement of buildings and obstacles with various shapes and sizes, a computational fluid dynamics (CFD) technique is helpful. In CFD models, urban surface geometries can be explicitly represented at high resolutions. Especially, with the rapid development of computational technology, CFD models based on Large-eddy simulation has come to be regarded as effective tools.

In order to simulate wind flows within and over urban areas under real meteorological conditions, coupling technique between NWP and LES-based CFD models is considered to be promising. Therefore, in coupling between both models, we applied a recycling technique (Kataoka and Mizuno, 2002) to a strong wind event in Tokyo owing to the landfall of a major typhoon and compared with the observed data of time series of wind speed at a certain height (Nakayama et al. 2012). Although the observed ranges of wind fluctuations and gust factors were well reproduced in the LES, the effectiveness of this coupling approach has not been fully evaluated.

In this study, we apply to the field experiments, the Joint Urban 2003 (Allwine and Flaherty, 2003) held at the central district of Oklahoma City on July 2003, and examine the coupling approach in comparison to the observed data in detail.

2. Field experimental dataset and Numerical method

Outline of Joint Urban 2003

The field experiment Joint Urban 2003 was conducted in the central district of Okalhoma City from June 28 through July 31, 2003 (Allwine and Flaherty, 2003). Participating organizations are many U.S. government institutes, U.S. universities, other U.S. federal agencies and private companies. Wind velocity was measured by sonic anemometers, meteorological stations, and a variety of remote sensing instruments during the 10 main IOPs (intensive observation periods). In this study, we compare with the data of wind velocity on 16th July in the IOP6.

Mesoscale meteorological simulation model

The model used for a mesoscale meteorological simulation is the Weather Research and Forecasting (WRF) model, the Advanced Research WRF Version 3.3.1 (Skamarock et al. 2008). We use a nesting capability to resolve the Oklahoma City region at a fine grid spacing by setting two-way nested, three computational domains (with the top being at the 50-hPa level). The three domains cover areas of 2700 km^2 at 4.5 km grid, 600 km^2 at 1.5 km grid, and 150 km^2 at 500-m grid, respectively. The number of vertical levels is 53, with 12 levels in the lowest 1-km depth.

The terrain data used are the global 30-second data (GTOPO30) from the U.S. Geological Survey. The land-use/land-cover information is determined by the 30-second resolution Global Land Cover Characterization dataset. To determine the initial and boundary conditions for the atmospheric and surface variables, we use 6-hourly Final Analysis (FNL) data of the U.S. National Centers for Environmental Prediction. The horizontal resolution is 1 degree. Full physics processes are included in the present simulation in order to reproduce real meteorological phenomena. A physics parameterization closely relevant to the simulation of wind fields is a planetary boundary layer (PBL) mixing parameterization. We choose a Mellor-Yamada Level 2.5 scheme of Janjic (2002) in which mixing is done vertically between the adjacent vertical levels. A single-moment, 6-category water- and ice-phase microphysics scheme is employed for cloud and precipitation processes in all the domains. No cumulus parameterization is used for all the domains.
In order to simulate the atmospheric conditions of IOP6, the simulated period is from 0000 UTC 15 July to 0000 UTC 17 July 2003. The nested inner domains are initialized at 0000 UTC 16 July for the first inner domain and at 1200 UTC July 16 for the second inner domain. The simulated outputs of the innermost domain at 1-min interval are used as the inputs of a CFD model.

LES-based CFD model

The CFD model is based on the LES model developed by Japan Atomic Energy Agency (Nakayama et al., 2014). A digital surface model dataset at 4-m resolution is used to explicitly resolve urban buildings and obstacles. The LES domain covers an area of 8km by 8km by 1.5km with the

grid spacing of 20m by 20m by 2-20m stretched in the streamwise, spanwise and vertical directions, respectively.

The governing equations of the LOHDIM-LES are the filtered continuity equation, the Navier–Stokes equation, and the scalar conservation equation. The subgrid- scale turbulent effect is represented by the standard Smagorinsky model (1963) with a constant value of 0.1. The building effect is represented by the immersed boundary method proposed by Goldstein et al. (1963). The time step interval is 0.1s.

Coupling approach

In this study, in coupling between NWP and LES-based CFD models, the recycling technique of Kataoka and Mizuno (2002) is applied. Figure 1 shows schematic diagram of coupling between both models. First, the WRF wind velocity is imposed at the main inlet of the LES domain. The inlet boundary condition of a special region intended to drive turbulent flows is formulated as follows:

$$u_{inlt}(y,z,t) = \langle u \rangle_{WRF}(y,z,t) + \phi(z)\{u_{recy}(y,z,t) - [u](y,z)\} \quad (1)$$

$$v_{inlt}(y,z,t) = \langle v \rangle_{WRF}(y,z,t) + \phi(z)\{v_{recy}(y,z,t) - [u](y,z)\} \quad (2)$$

$$w_{inlt}(y,z,t) = \langle w \rangle_{WRF}(y,z,t) + \phi(z)\{w_{recy}(y,z,t) - [u](y,z)\} \quad (3)$$

where, u, v, and w are the wind components of the streamwise (x), spanwise (y), and vertical (z) directions, respectively, and the suffixes of inlt and recy indicate the instantaneous wind components at the inlet and the downstream position (i.e. the recycle station), respectively. $\langle u \rangle$, $\langle v \rangle$, and $\langle w \rangle$ are wind components of the WRF model at the inlet location; [u], [v], and [w] are horizontally averaged winds over the driver domain; ϕ(z) is a damping function.

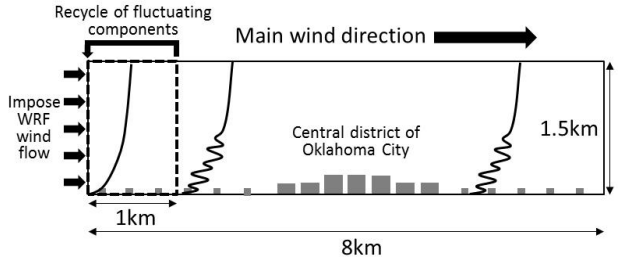


Figure 1. Schematic diagram of the LES numerical model for simulating turbulent winds over an urban area under a real meteorological condition.

3. Results

Figure 2 shows the vertical profiles of observed data, WRF, and LES of vertical profiles of wind speed and wind direction in the central district of Oklahoma City obtained at the LES domain for 13:45 UTC 16 July 2003. It is seen that the LES winds maintain the structure of mean flow and fluctuate around the WRF winds. It is shown that our approach to produce turbulent winds within urban areas under real meteorological conditions is effective.

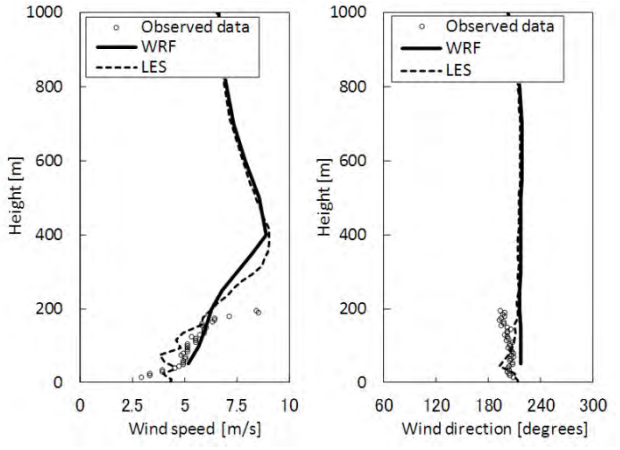


Figure 2. Vertical profile of wind speed and wind direction obtained at the LES domain.

4. Conclusion

We performed LESs of turbulent flows in an actual urban area under a real meteorological condition. In coupling with a mesoscale meteorological simulation model, the existing recycling technique is applied to produce turbulent inflows at the inlet of the LES domain. The LES winds are successful in maintaining the structure of mean flow and fluctuating around the WRF winds. It can be concluded that the proposed coupling approach is effective.

References

Allwine, K. J., Flaherty, J. E. (2003) Joint Urban 2003 Study Overview and Instrument Locations. PNNL-15967, Pacific Northwest National Laboratory, Richland, WA.

Goldstein, D., Handler, R., and Sirovich, L. (1993) Modeling a no-slip flow boundary with an external force field, J. Comput. Phys., 105: 354-366.

Kataoka, H., and Mizuno, M. (2002) Numerical flow computation around aeroelastic 3D square cylinder using inflow turbulence. Wind and Structures, **5**, 379-392.

Nakayama, H., Takemi, T., and Nagai, H. (2012) Large-eddy simulation of urban boundary-layer flows by generating turbulent inflows from mesoscale meteorological simulations, Atmospheric Science Letters, 13: 180–186

Nakayama, H., Leitl, B., Harms, F., and Nagai, H. (2014) Development of Local-Scale High-Resolution Atmospheric Dispersion Model Using Large-Eddy Simulation. Part 4: Turbulent Flows and Plume Dispersion in an actual urban area, Journal of Nuclear Science and Technology (in press).

Skamarock, W. C., Klemp, J. B., Dudhia, J., Gill, D.O., Barker, D.M., Duda, M, G., Huang, X, Y., Wang, W., and Powers, J, G. (2008) A description of the Advanced Research WRF Version 3, NCAR Tech. Note, NCAR/TN-475+STR, 1 pp.

Smagorinsky, J. (1963) General circulation experiments with the primitive equations, Monthly Weather Review: 91: 99-164.

The GAME project: challenges in modeling circulation of Svalbard fjords

Jacek Piskozub, Jaromir Jakacki, Szymon Kosecki and Anna Przyborska

Institute of Oceanology, Polish Academy of Sciences, Sopot, Poland (piskozub@iopan.gda.pl)

1. The Project

The research is performed as apart of the GAME (Growing of the Arctic Marine Ecosystem) three year project funded in Poland by Narodowe Centrum Nauki as a MAESTRO grant. Its aim is to study the ecosystem changes caused by climate change in two Svalbard fjords: Kongsfjorden and Hornsund and in adjacent shelf sea areas. The fjords are influenced by, respectively, warm West Spitsbergen Current and cold Sørkapp current. This difference should enable better understanding of biological changes driven by climate variability in a warming world.

2. The modelling

The ecological changes studied in the project ore driven by physical forcings. Therefore it is very important to learn as much as possible about the physical processes in the studied are. One of the most important is the circulation in the fjords themselves and in their foreground. Therefore one of the main scientific tasks in the project is modeling of the circulation. Because of the spatial scales of the fjords, this needs to be based on a high resolution model. We decided to use Mike 3 model developed by DHI, Denmark. This required preparing the bathymetry and model grids for both the fjords and a large area of adjacent continental shelf.

3. The data

We use all available data, including oceanographic data from cruises and moorings and meteorological data from available stations. We use also atmospheric reanalysis for geostrophic winds. Part of the data available comes from Polish sources: the Polish Polar Station in Hornsund operated by Institute of Geophysics PAS in Warsaw and data from R/V Oceania, the ship of Ocean of Oceanology PAS in Sopot. Oceania cruises provide summertime data series of over 20 years for the region of West Spitsbergen Current and Hornsund fjord. For the project an additional measurement campaign in Kongsfjorden has been performed in 2013.

4. The challenges

High resolution modeling of Arctic fjords surrounded by mountains and glaciers needs to overcome many challenges. Some of the most important we met so far are:

- The available oceanographic data come mostly from summers. Only some mooring data are all-year.
- The model domain needed a very large domain to be able to simulate the eddies on the West Spitspergen Current which influence strongly the fjords themselves.
- Limited data on fresh water inflow from the glaciers and their seasonality makes it difficult to realistically model in-fjord stratification, a crucial parameter for the ecological part of the project.
- There is not enough data on tides, especially in Hornsund to verify whether the model bathymetry if good enough.
- There are only a few meteorological stations in Svalbard which makes it difficult to model atmospheric forcings.
- Reanalysis data are available but very coarse for the purposes of high resolution modeling.
- The presence of mountains all around the fjords creates very strong orthographic effects which most atmospheric models are unable to reproduce.

This poster presents some of the problems the GAME project tries to overcome. The successes we have achieved are the subject of separate presentations.

Simulation of salty bottom water penetration in a Deep

Podrezova Nadezda and Tsarev Valeriy

Russian State Hydrometeorological University, 98, Malookhtinsky Ave., 195196, St.Petersburg, Russia,(podrezova@rshu.ru)

1. Introduction

Bottom density flows play an important role in the formation of many sea processes. Such processes as salinity dynamics of seas, water masses formation, update and aeration of bottom and deep waters are closely related with bottom density flows. Specific features of density flows are there episodic character, small vertical and horizontal size, and an important role of non-hydrostatic effects in their formation. In this study it is investigated the possibility of application of hydrostatic model for their simulation.

2. Model

It is sumulated a bottom salt water spreadding in rectangular basin with bottom depth as presented at the fig.1. The vertical salinity distribution in the area is excepted to be homogeneous and equal to 29 pml. At the side boundary salt flux was equal to 0. It is assumed that there is some source of salt that retain salinity of some nere bottom water volume qual to 30 pml. Salinity difference and bottom inclination generate bottom saline water flow. A set of the model governing equations describing bottom water flow from the local source involves tree-dimensional non-stationary non-linear hydrostatic equations of motion. It also includes equations of mass and salinity conservation and equation of the state.

The vertical and horizontal viscosity coefficients were accepted equal $k_z = 10^{-4}$ м^{2}с$^{-1}$, k_l = 10 м^{2}с$^{-1}$. The vertical and horizontal diffusivity were as follows $k_{sz} = 10^{-5}$ м^{2}с$^{-1}$, k_{sl} = 10 м^{2}с$^{-1}$. The domain was covered by 117x49x40 grid with 40 levels in vertical direction. The spatial steps are 1 km. In a vertical direction first ten steps from the bottom are 2 м, and above are equal to (H-20м) /19, where H bottom depth in meters.

3. Model results

From the model run initially saline bottom water spreads in the Basin in form of narrow flow (Fig.1). The bottom salt water moves from the source along the isobars basically right on the direction of slope of the bottom. In the area from the source to the middle of the left lateral border the water movement is accompanied by an increase in slope of the bottom. There the water movement is in the form of a narrow stream of width about 30 km. Flow velocity in the vicinity of the source is 20-cm.s^{-1}. It then increases due to increased slope of the bottom. The calculated currents velocity in the flow corresponds to the value obtained from the Nof equation (Nof, 1983).

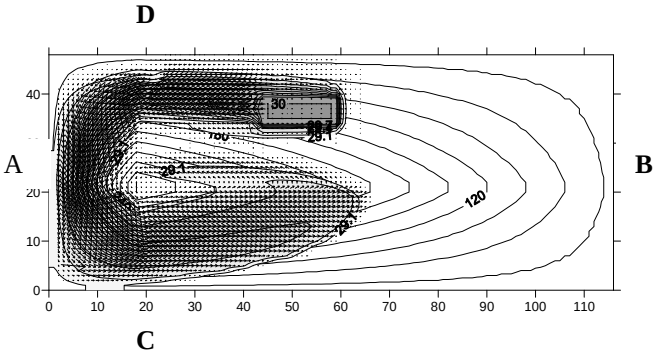


Figure1: Bottom water salinity and currents velocity in 16 days. Thin lines are isobaths.

When the flow moves further from the left side of the boundary it is influenced by decreasing slope of the bottom. The result is a decrease in flow velocity, an increase of its thickness and horizontal size (Fig.2-3).

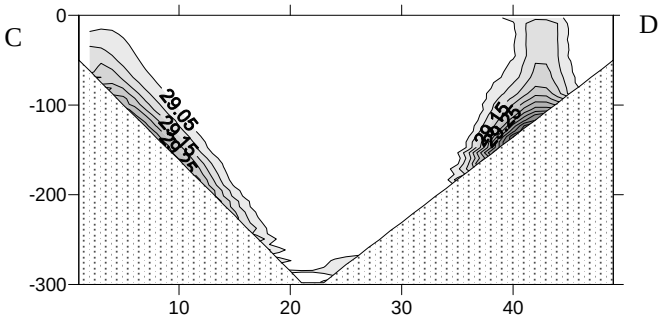


Figure 2. Salinity distribution at CD section in 16 days

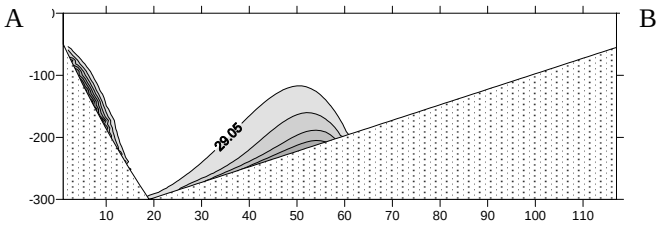


Figure 3. Salinity at AB section in 16 days

Under the influence of bottom friction the flow movement deviates from the direction of flow along the isobars in the direction of the bottom inclination. As a result, the trajectory of the bottom flow takes the form of a spiral rotating around maximum depths. The water does not reach the area of the greatest depths. It teaming up with the upstream part of the stream. This forms a ring of salt water around the greatest depths. When moving of salt water its salinity decreases due to the outflow of salt in the upper layers. Simultaneously salinity of overlying water increases, which reduces the

outflow of salts coming from the bottom salt water which comes later and reduces its freshening. Over time, therefore salinity of spreading bottom water increases. Bottom salt water that spread later displaces the previously transformed bottom water to overlying horizons and to the lateral border (fig.4-6). Thus takes place increasing of thickness and horizontal dimensions of bottom salt water volume accumulating in the vicinity of the area of maximum deepness. This process determines the pattern of accumulation of salt water in the basin and its filling.

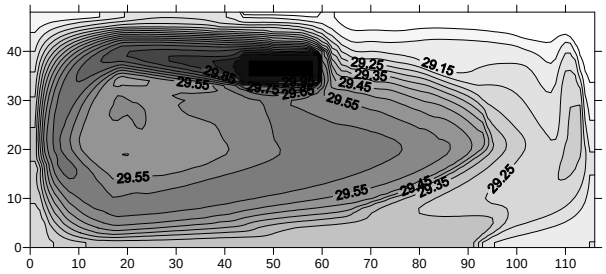


Figure 4. Bottom water salinity and currents velocity in 100 days

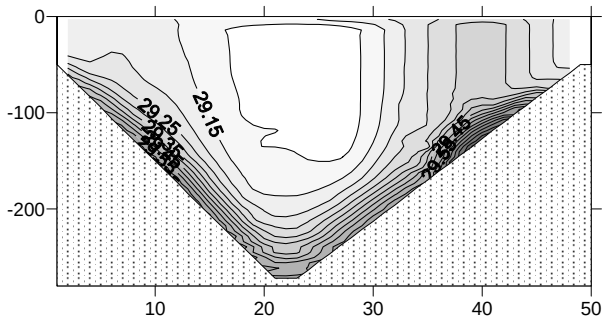


Figure 5. Bottom water salinity and currents velocity in 32 days

A B

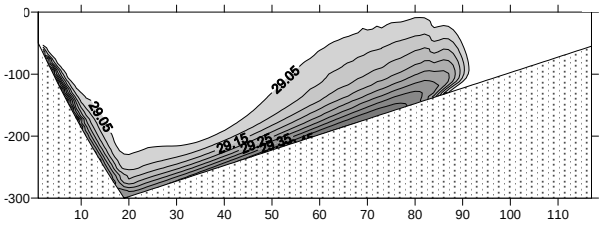


Figure 6. Bottom water salinity and currents velocity in 32 days

4. Conclusions

Calculated bottom saline water spreads in form of narrow flow. That is consistent with data of observation (Zoccolotti L., Salusti E. 1991; Bignami F., Solusti E., Schiarini S.1990). Model simulation made it possible to study different features of saline bottom water inflow into the Basin. It shown main way of bottom water spreading, its evolution and interaction with upper layer.

Reference

Nof D. The translation of isolated cold eddies on a sloping bottom. Deep-Sea Res. 1983. V.30, P.171-182

Zoccolotti L., Salusti E. Observation a very dense marine water in the southern Adriatic sea. Cont. Shelf. Res. 1991, N7. P.535-551.

Bignami F., Solusti E., Schiarini S. Observations on a bottom vein of dense water in the southern Adriatic and Ionian seas. J. Geophys. Res., 1990 N0 C5, P.7249-7259.

Projection of Future Climate Change around Japan in a Non-hydrostatic Regional Climate Model

Hidetaka Sasaki [1], Akihiko Murata [1], Mitsuo Oh'izumi [2] and Kazuo Kurihara [1]

[1] Meteorological Research Institute, Tsukuba, Japan (hsasaki@mri-jma.go.jp)
[2] Meteorological College, Kashiwa, Japan

1. Introduction

That warming of the climate system is unequivocal is stated in the Fifth Assessment Report (AR5) of the Intergovernmental Panel on Climate Change (IPCC 2013). As there is a strong likelihood that global warming will have many impacts on, for example, disaster prevention, agriculture, water resources, and human health, countermeasures are required. Therefore, climatologists need to project future climate changes at a fine scale. To cope with these demands, Sasaki et al. (2008) developed a non-hydrostatic regional climate model (NHRCM) having a grid spacing of 4 km, and carried out a simulation for 5 years with perfect boundary conditions. They showed that the model performed well in reproducing climatic temperature and precipitation fields. In this study, the NHRCM is used for projecting the future (the end of the 21st century) climate change around Japan under the SRES A1B scenario for greenhouse gas concentrations. We also show the effect of bias correction on the future climate projection.

2. Nesting method

A multiple nesting method is used in this study as shown in Fig. 1. Outer most data is results of climate experiments using an AGCM whose grid spacing is 20km (Kitoh et al. 2009). The AGCM is based on the operational model for numerical weather prediction of the Japan Meteorological Agency (JMA) (Mizuta et al, 2006). A regional model, the first NHRCM, with a grid spacing of 15 km, is nested within the AGCM. The AGCM does not have variables of cloud water, cloud ice, and other cloud properties, so the 15-km NHRCM grid is included to generate such variables for the lateral boundary of a smaller domain having a 5 km grid spacing. Sasaki et al. (2008) describes the specifications of the NHRCM used in this study. The domain of the 5-km inner grid is slanted from northeast to southwest. By skewing the inner domain, calculations are reduced, and the inner domain still covers almost all of the Japanese Archipelago.

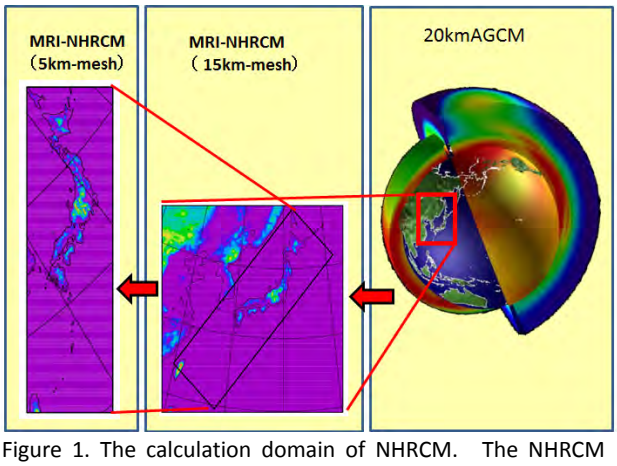


Figure 1. The calculation domain of NHRCM. The NHRCM having a grid spacing of 15 km is nested in an AGCM. Moreover, another NHRCM having a 5-km grid is nested in it.

3. Reproducibility of Present Climate

We verified the NHRCM by comparing the observed data of the Automated Meteorological Data Acquisition System (AMeDAS) to the results at the closest model grid point on land to each observation station. The differences of annual mean temperature between the climate variables in the NHRCM and AMeDAS climate are shown in the upper panel of Fig. 2. In mountainous regions, the NHRCM calculated surface temperatures 2–3 °C lower than AMeDAS observations at several points. The differences of annual precipitation between the NHRCM and AMeDAS are shown in the lower panel of Fig. 2. The differences are less than 20% at almost all the points. However, along the coast of the Japan Sea and the Nansei Archipelago, the NHRCM underestimated precipitation from 20% to 40% compared with observed amounts. At some steep slope areas, the NHRCM overestimated precipitation by more than 40%.

The AGCM underestimated the frequency of hourly precipitation, especially when precipitation was heavy. The NHRCM underestimated it slightly but reproduced the observed frequencies better. It reproduced intense precipitation (more than 80 mm/h) much better than the

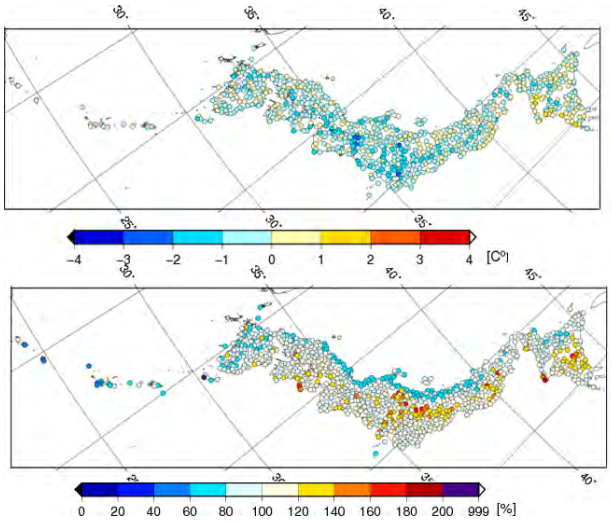


Figure 2. Station plots of the differences between the NHRCM's values and AMeDAS observations: the upper panel shows the annual mean surface temperature and the lower panel shows the ratio of NHRCM/observed annual precipitation expressed as a percentage.

AGCM. It is necessary for reproducing the heavy rain to use the fine grid spacing. The basic performance of the NHRCM is good enough to be used for downscaling from the AGCM.

The NHRCM simulated well the daily change of snow depth, and the inter-annual variability of snow depth, except on the western coast of northern Japan. The NHRCM did not correctly locate the point of maximum snow depth (situating it in the center of Hokkaido rather than on the west coast, the AMeDAS location). Although there remain some defects, the NHRCM otherwise well reproduced the distribution of snow depth around Japan.

4. Projection of Future Climate Change

The left panel of Fig.3 shows the monthly mean temperature simulated by the NHRCM in the present and the future. Surface air temperature averaged over Japan was projected to increase by about 3 °C throughout the year, with especially large increases projected in February. In general, the warming is greater in northern than in southern regions.

The right panel of Fig.3 shows the monthly precipitation simulated by the NHRCM in the present and the future. Future precipitation is projected to increase from winter to spring and decrease in autumn. However, only in February, the change is statistically significant at the 5% level in two-sided test. Future precipitation is projected to increase in February almost everywhere in Japan, and the projected increase is remarkable along the Pacific coast. We attribute this large projected increase to the weakening of the northwesterly monsoon, which will allow storm tracks over the Pacific Ocean to approach the Japanese Archipelago. In addition, the annual frequency of heavy precipitation is projected to increase, which means that we should be prepared for natural disasters such as floods and landslides, which may become more common.

The future maximum snow depth is projected to decrease almost everywhere. As future precipitation is projected to increase, the snow depth reduction is due to rising temperatures. However, the reduction in high mountains and in northern Japan, where even under the future climate the temperatures will remain below the melting point, is projected to be small.

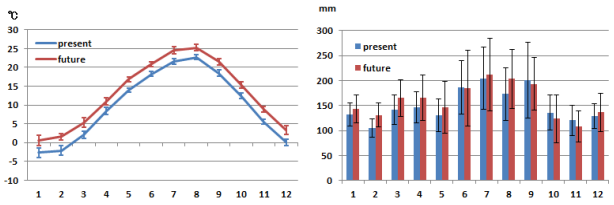


Figure 3. Monthly mean surface temperatures (left) and monthly precipitation (right) in the present and future climate. Error bars indicate standard deviations.

5. Bias Correction

The simulated monthly mean snow depths at the present time were generally more accurate when estimated with the NHRCM than with the AGCM. However, on the Japan Sea side of northern Japan, the NHRCM underestimated snow depths compared to AMeDAS. To improve the accuracy of simulated monthly mean snow depths, we examined two methods to correct for bias. Because 20 samples are insufficient to conduct a statistical correction for bias with the cumulative distribution function of monthly mean snow depths, we applied regional frequency analysis introduced by Hosking and Wallis (1997) to correct for bias on Hokkaido. After application of the bias correction, the biases were small at almost every AMeDAS site in the western part of Hokkaido. Without a bias correction (left panel of Fig. 4), the monthly mean snow depths were projected to decrease by less than 40 cm at almost all AMeDAS sites in Hokkaido. In contrast, with the bias correction (right panel of Fig. 4), snow depths were projected to decrease even more along the western part of Hokkaido. Because the bias correction greatly reduces the bias and RMSE of simulated monthly mean snow depths compared to the original NHRCM simulations.

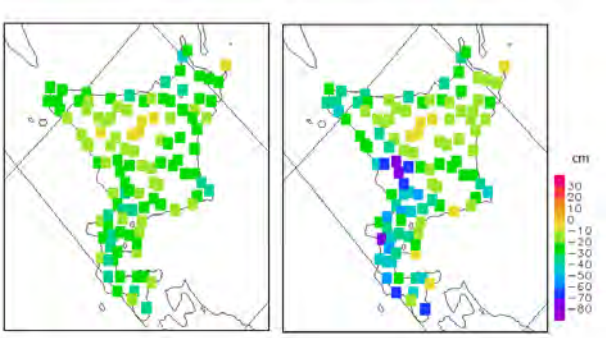


Figure 4. Future changes of monthly mean snow depths simulated by the NHRCM without using a bias correction (left) and with it (right).

References

Hosking J. R. M, and J. R. Wallis (1997) Regional Frequency Analysis: An Approach based on L-moments. Cambridge University Press, Cambridge, 224 pp.

Kitoh, A., T. Ose, K. Kurihara, S. Kusunoki, M. Sugi, and KAKUSHIN Team-3 Modeling Group (2009) Projection of changes in future weather extremes using super-high resolution global and regional atmospheric models in the KAKUSHIN Program: Results of preliminary experiments. Hydro. Res. Lett., 3, 49–53.

Mizuta, R., K. Oouhi, H. Yoshimura, A. Noda, K. Katayama, S. Yukimoto, M. Hosaka, S. Kusunoki, H. Kawai and M. Nakagawa (2006) 20 km-mesh global climate simulations using JMA-GSM model. –model mean climate state-, J. Meteor. Soc. Japan, 84, 165-185.

Sasaki, H., K. Kurihara, I. Takayabu and T. Uchiyama (2008) Preliminary experiments of reproducing the present climate using the non-hydrostatic regional climate model, SOLA, 4, 25-28

Usage of high-resolution dynamical downscaling around East and South-East Asia

Izuru Takayabu

Meteorological Research Institute, Tsukuba, Ibaraki, Japan (takayabu@mri-jma.go.jp)

1. Introduction

Impact study researchers request to dynamical down-scaler, detailed climate projections useful for risk management, which could not be got from AO-GCM's data directly. In such a case, their requests are divided into the following two kinds.

(1) Probability density function useful for disaster prevention.

(2) Worst case scenario useful for disaster reduction

For (1), we need to do the ensemble experiment, and its need a lot of computer resources. On the other hand, for (2), we need a high resolution sophisticated model, and need to clarify the developing mechanisms of the disturbances. In this paper, we focus on (2).

2. Important phenomena around Asian region

There are three important phenomena which have much influence on our lives in Asian monsoon region. They are,

(1) Tropical depressions or Typhoons
(2) Heavy precipitation related with the Asian Monsoon
(3) Urban climate of mega-cities

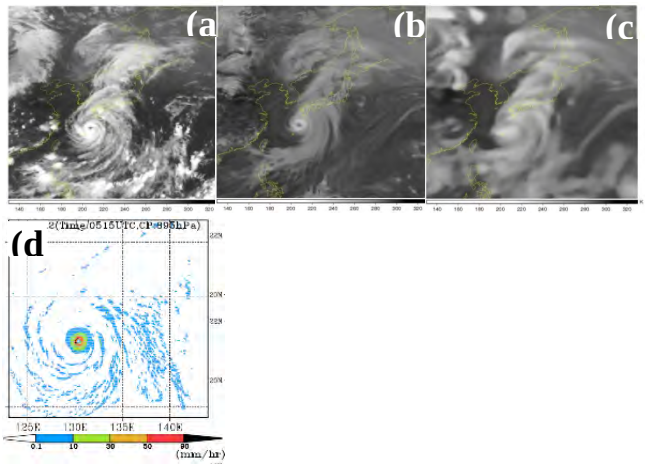


Figure 1. (a) Satellite image of a real typhoon. (b) Radiation temperature image of a typhoon represented by 20km grid model. (c) Same as (b) but for 55km grid model. (Murakami, 2005). (d) Horizontal distributions of hourly precipitation amounts in the one hour preceding the most intense phase of a Typhoon simulated by a 2km grid regional model. (Kanada et., al, 2012)

(1) Though spiral rain-bands elongate for several hundred kilometers from cyclone center, the main engine of the disturbance is the eye-wall cloud, which has the radii of only several tens of kilometers. Thus a tropical cyclone is a kind of meso-scale phenomenon and need high resolution model to represent the structure realistically (e.g. Kanada et. al., 2012, 2014). In Fig. 1, the structural change of the tropical cyclone depending on the model's gird size is shown. It is easily found that 2km grid size is needed to represent the fine structure of the tropical cyclones.

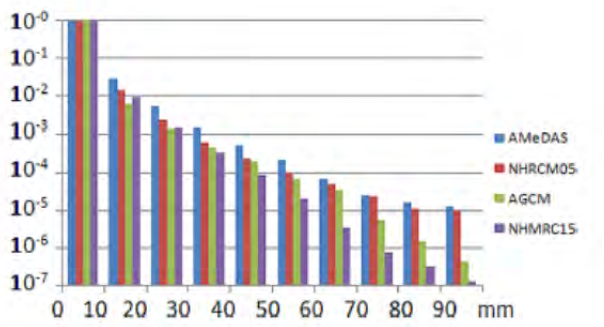


Figure 2. Probability density functions of hourly precipitation intensity of Japan Islands. Blue: Observation data from automated data acquisition system (AMeDAS) of JMA, with the horizontal resolution of around 15km. Green: 20km resolution AGCM. Purple: 15km grid NHRCM. Red: 5km grid NHRCM. (Sasaki et . al., 2011)

(2) Fig. 2 indicates validation results of the frequency distribution of the hourly precipitation intensity around Japan Islands (Sasaki et. al., 2011). 20km resolution GCM or 15km grid RCM underestimate precipitation intensity stronger than 50mm/hour. Only 5km grid RCM (NHRCM05) can successfully represent the frequency of the heavy precipitation intensity. Though we can correct bias for such heavy precipitation by ESD (empirical statistical down-scaling), for clarify the mechanism of it, we need to represent such heavy precipitation explicitly in RCMs (Kanada et. al., 2010, Sasaki et. al., 2011).

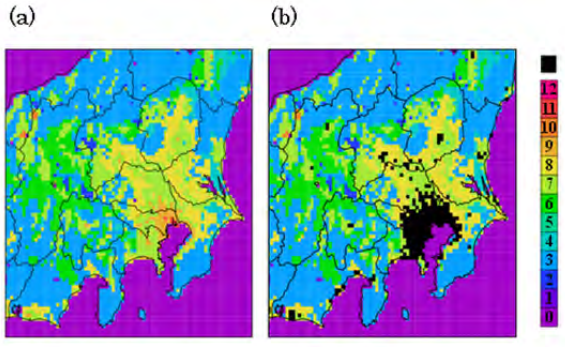


Fig. 3. Distributions of land surface in 4km grid RCM. Left: Without an urban canopy model. Right: With an urban canopy model. Black rectangle in the right hand figure represents the urban area. (Aoyagi, 2014)

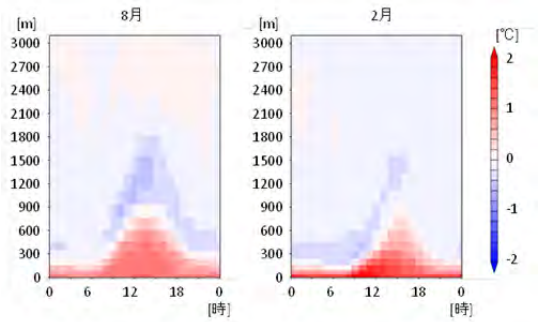


Fig.4. Difference of temperature between with and without urban canopy model. Monthly mean values among the urban area of Tokyo metropolitan area (Aoyagi, 2014).

(3) It is believed that the population of many mega-cities in Asia increase within these several tens of years, so downscale the area around the cities become more important. To represent mega-cities, we need to drive high resolution RCM coupled with the urban canopy model. Fig. 3 indicates the distribution of land surface around Tokyo metropolitan area, by using 4km grid RCM (NHRCM04). We use such high resolution models to represent urban canopy area. The climate around the city is controlled with heat island and land-sea breeze, which have about the same horizontal scale with the city's size itself, and makes it easier to apply a rather smaller scale RCMs. As indicated in Fig. 4, we can find the influence of the urban canopy, up to about 1800m above Tokyo metropolitan area.

3. Concluding remarks

Thus, for analyzing such important phenomena in Asian region, we need to drive high resolution RCM, though we could hardly drive it for many cases.

4. Acknowledgement

This presentation has supported by the SOUSEI program of the Ministry of Education, Culture, Sports, Science, and Technology.

References

Aoyagi, T., (2014) Urban canopy model installed into NHRCM04, Annual report of the SOUSEI program, MEXT, Japan (in Japanse)

Kanada, S., M. Nakano, and T. Kato (2010) Climatological characteristics of daily precipitation over Japan in the Kakushin regional climate experiments using a non-hydrostatic 5-km mesh model: Comparison with an outer global 20-km mesh atmospheric climate model, SOLA, 6, 117-120

Kanada, S., M. Nakano, A. Wada, and T. Kato (2012) Effect of PBL schemes on the development of intense tropical cyclones using a cloud resolving model, J. Geophys Res., 117, D3, doi:10.1029/2011JD016582

Kanada, S., A. Wada, and M. Sugi (2013) Future changes in structures of extremely intense tropical cyclones using a 2-km mesh nonhydrostatic model, J. Clim., 26, 9986-10005

Sasaki H., A. Murata, M. Hanafusa, M. Oh'izumi, and K. Kurihara (2011) Reproducibility of present climate in a non-hydrostatic regional climate model nested within an atmospheric general circulation model, SOLA. 7, 173-176

Convection permitting climate simulations (CPCS) – lessons learned at the Wegener Center

Heimo Truhetz, Andreas Prein and Andreas Gobiet

Wegener Center for Climate and Global Change, University of Graz, Graz, Austria (heimo.truhetz@uni-graz.at)

1. Introduction

Thanks to the general progress in computing technology, continent wide climate simulations on the 10 km scale became feasible and are now internationally accepted (e.g., Jacob et al., 2013). However, a further increase of the resolution towards convection permitting scales (grid spacing <4 km) is not straightforward: (1) RCMs (originally developed for coarser resolutions) need significant reconsideration, because relevant processes on former unresolved (parameterized) scales become resolved, (2) highly resolved surface information is required for lower boundary conditions, (3) highly resolved observational data for model evaluation only exists in exceptional cases (e.g. special observation campaigns) and hence alternative reference data have to be found, and (4) the demand of computational resources increases exponentially when grid spacing is reduced. A further difficulty lies in model evaluation techniques: at high resolution the misplacement of modeled and observed processes (like convective cells) is stronger penalized (double penalty problem) which asks for special statistical methods and highly resolved reference data.

Nonetheless, so-called convection-permitting climate simulations (CPSCs) are becoming more and more established (e.g. Argüeso et al., 2013; Gutjahr and Heinemann, 2013), because they have two major advantages: (1) deep moist convection, which is an important process in the majority of extreme precipitation events, becomes resolved and (2) the representation of orography and surface fields, which interact closely with precipitation, is improved.

The Wegener Center for Climate and Global Change (WEGC) operates non-hydrostatic regional climate models (RCMs) in the European Alpine region in convection permitting mode (3 km and 1 km grid spacing) since seven years. This manuscript provides a review on the key results collected during the project "Non-Hydrostatic Climate Modelling, Part I (NHCM-1)", funded by the Austrian Science Fund (FWF) (number P19619-N10), and the EU-FP7 project ACQWA (www.acqwa.ch) (number 212250) and outlines next steps to be taken.

2. Model sensitivities

There are four categories of factors that determine the model configuration: (1) model formulation (numerical core, parameterizations), (2) surface boundary conditions, (3) lateral boundary conditions, and (4) model resolution (horizontal and vertical grid spacing and time step).

Statistical analysis of 62 one-year and 35 seasonal multi model (COSMO-CLM, MM5, WRF, and REMO) ensemble simulations with 10 km grid spacing in the European Alpine region have shown that the models react differently when their configurations are perturbed. For instance, for COSMO-CLM it was found that the impact of perturbing the parameterization schemes is not as large as the choice of the model domain (Suklitsch et al., 2008; Suklitsch et al., 2011). In contrast, WRF and MM5 are much more sensitive to the choice of parameterizations than to the domain size (Awan et al., 2011). Soil moisture initialization has been found to have significant impact on climatological means of near surface temperature and precipitation. For heavy precipitation events, the models' ability to capture the synoptic dynamics is of vital importance and hence the influence of the models' degree of freedom (determined by domain size and nudging techniques) is larger than the choice of specific parameterizations (Awan, 2011).

When the grid spacing is reduced to convection permitting scales, such (model specific) sensitivities remain.

There exists neither a best model nor a best model configuration (also on convection permitting scales). Hence, well balanced (model specific) model configurations need to be derived in advance to long-term climate simulations. This also implies the continuation of the multi model ensemble concept in both, climate simulations and model based investigations of (climate) processes.

3. Added value in CPCSs

In order to detect added value in CPCSs with 3 km grid spacing, Prein et al. (2013) used highly resolved (1 km grid spacing) data from a nowcasting system as reference data and adopted fuzzy and object oriented evaluation techniques (usually used in numerical weather prediction) for model evaluation. By means of that, the authors analyzed summer/winter seasons in CPCSs in the Eastern Alpine region from a small multi model (WRF, MM5, and COSMO-CLM in two versions) ensemble. In summary, it was found that CPCSs (1) decrease spatial error ranges of temperature in summer, but not in winter or other parameters, (2) improve the diurnal cycle of precipitation in summer (onset and intensity), and (3) generate more realistic precipitation patterns. In addition, the CPCSs also showed higher (+14% in summer) domain averaged seasonal means of global radiation probably cause by a shift in the diurnal cycle and by smaller clouds. However, the models react in different ways on this surplus of incoming energy.

The impact of a further increase of resolution to 1 km

grid spacing with regard to extreme precipitation events in the European Alpine region simulated with COSMO-CLM indicate only structural improvements (see Figure 1).

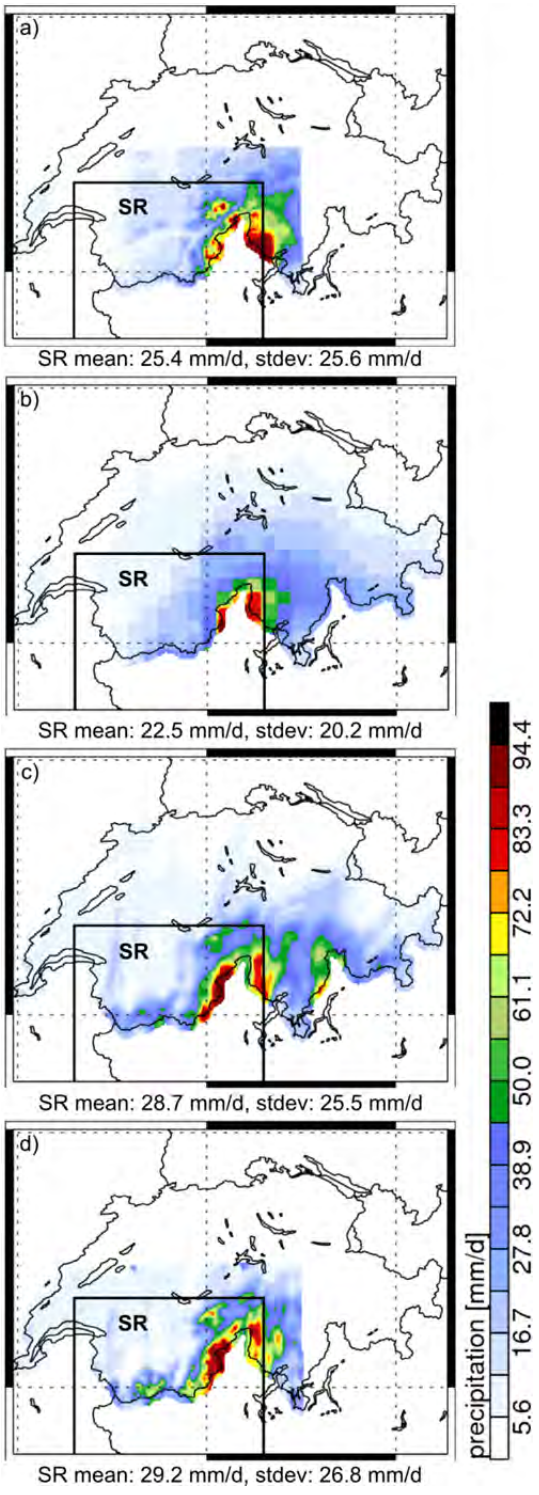


Figure 1. (a) Observed mean precipitation of the period September 19 to 21, 1999, and their counterparts simulated with COSMO-CLM with (b) 12.5 km, (c) 3 km, (d) 1 km grid spacing. Area mean and standard deviation of the study region (SR) are given.

The reduction of the grid spacing from 10 km to 3 km bears the largest benefit, although biases are not necessarily improved. Since convection/cumulus parameterizations are switched off or loose their functionality, other model components (e.g. the radiation or microphysics scheme) also need to be adopted to stay consistent with coarser resolutions.

5. Outlook

In the upcoming years, we will focus on the CPCSs' ability to capture the shielding effect of the Alps within the project "Non-Hydrostatic Climate Simulations II (NHCM-2)" (www.nhcm-2.eu), funded by the Austrian Science Fund (FWF). This includes: (1) extending the multi-model CPCSs ensemble in both, model domain and simulation period, (2) process oriented analysis of error characteristics with respect to orographic forcing, (3) continuing the adaptation of object oriented techniques for model evaluation in a climate research context, and (4) deriving well balanced model configurations for long-term CPCSs in the Alpine region based on systematically perturbed model components.

References

Argüeso, D., J. P. Evans, L. Fita (2013) Precipitation bias correction of very high resolution regional climate models, Hydrol. Earth Syst. Sci., 17, 11, pp. 4379-4388

Awan, N. K. (2011), Performance of state of the art high resolution Regional Climate Models in the European Alpine region, Ph.D. Thesis, 138 pp., University of Graz, Austria

Awan, N. K., H. Truhetz, A. Gobiet (2011) Parameterization-Induced Error Characteristics of MM5 and WRF Operated in Climate Mode over the Alpine Region: An Ensemble-Based Analysis, J. Climate, 24, 12, pp. 3107-3123

Gutjahr, O., G. Heinemann (2013) Comparing precipitation bias correction methods for high-resolution regional climate simulations using COSMO-CLM, Theor. Appl. Climatol., 114, 3-4, pp. 511-529

Jacob, D., J. Petersen, B. Eggert et al. (2013) EURO-CORDEX: new high-resolution climate change projections for European impact research, Reg. Environ. Change, published online

Prein, A. F., A. Gobiet, M. Suklitsch, H. Truhetz, N. K. Awan, K. Keuler, G. Georgievski (2013) Added value of convection permitting seasonal simulations, Clim. Dyn., 41, 9-10, pp. 2655-2677

Suklitsch, M., A. Gobiet, A. Leuprecht, C. Frei (2008) High Resolution Sensitivity Studies with the Regional Climate Model CCLM in the Alpine Region, Meteorol. Z., 17, 4, pp. 467-476

Suklitsch, M., A. Gobiet, H. Truhetz, N. K. Awan, H. Göttel, D. Jacob (2011) Error Characteristics of High Resolution Regional Climate Models over the Alpine Area, Clim. Dyn., 37, 1-2, pp. 377-390

Reproducibility of Regional difference of Altitudinal Dependence of Snow Depth using 1.5km High Resolution Experiments

Fumichika Uno[1], Hiroaki Kawase[1], Noriko N. Ishizaki[1], Takao Yoshikane[1], Masayuki Hara[1], Fujio Kimura[1], Tsutomu Iyobe[2], Katsuhisa Kawashima[2]

[1] Research Institute for Global Change, Japan Agency for Marine-Earth Science and Technology, Japan. (f.uno@jamstec.go.jp)
[2] Research Institute for Natural Hazards and Disaster Recovery, Niigata University, Japan.

1. Introduction

Understanding the snow cover distribution is important to improve prediction of snow related disasters. The primary factors that affect snow cover distribution are related to the horizontal scale (Clark et al. 2011). The predominant elements of snow cover depend on the horizontal precipitation gradients on a regional scale (10-1000 km). Previous studies have reported a simple proportionality relation between altitude and snow depth (e.g., Peck and Brown 1962). Hereafter, we refer to the proportionality relation between altitude and snow depth as the altitudinal dependency of snow depth (ADSD).

ADSD is used to estimate the snow cover distribution (e.g., Lundquist et al. 2010). Iyobe et al. (2007) showed the ADSD using high-density surface observational data including the high-altitude area in the coastal areas of the Japan Sea and reported regional differences of ADSD in a prefecture scale. The ADSD was a simple proportional relation in Toyama, Ishikawa and Fukui prefectures, while the gradient and variation of ADSD changed at altitudes higher than 300 m A.S.L. in the Niigata prefecture. The regional differences of ADSD were evident over a number of years. They speculated that the regional difference of ADSD was caused by snow density and precipitation forms. However, as discussed previously, ADSD on a regional scale was dominated by precipitation distribution; for instance, ADSD is complicated by topographic reduction of precipitation (well known as a rain-shadow effect) in the mountainous area.

The purpose of this study is to clarify the main factors causing regional difference of ADSD using high-density surface observational data and numerical experiments. We perform sensitivity experiments to investigate the orography effect on the regional difference of ADSD. We also discuss the applicable range of ADSD for estimating the distribution of snow cover.

Table 1. Configurations of numerical experiments

Configurations	Scheme
Microphysics	WSM6
Cummulus convection	KF on domain 1
Bondary layer	MYMM 2.5
Surface layer	MYMM
Land surface	Noah LSM

2. Data and design of numerical experiment

We used the high-density observational data of snow depth collected by Iyobe et al. (2007). The numerical experiments were carried out using the Advanced Research Weather Research and Forecasting (WRF) modeling system Version 3.4. Two-way nested grid systems were adopted; the grid intervals were 18, 4.5 and 1.5 km (Fig. 1a). The initial and lateral boundary conditions for the coarse grid system were interpolated from the European Centre for Medium Range Weather Forecasts (ECMWF) Interim reanalysis (ERA-interim) dataset. The simulation was executed from August 1, 2005 to April 1, 2006. We also executed the simulation focusing on two heavy snow winter seasons (1980/1981 and 2005/2006) and one light snow winter season (2006/2007). We mainly analyzed in 2005/2006 winter season.

3. Observed and estimated regional difference of ADSD

Figure 2a shows the position of the observation sites. We divided these observation sites between windward (open circle) and leeward (filled circle) areas on the coastal mountains. We define the windward (leeward) area as the front (behind) area of coastal mountain over 1000 m A.S.L by the predominant northwest wind direction. Figure 2b shows ADSD using surface observational data on Region A (see Fig. 1b). ADSD shows a high gradient and low variation in the windward area. Inversely, it shows low gradient and high variation in the leeward area. This result indicates the regional difference of ADSD is also influenced by the coastal mountains. Figure 2c shows ADSD simulated by WRF model (CTL-run). The observed regional difference of ADSD was reproduced by CTL-run. The correlation coefficient and root mean square error of the snow depth were 0.82 and 102 cm, respectively.

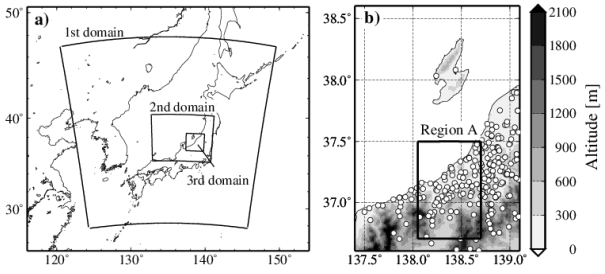


Figure 1. (a) Experimental domain and (b) orography at third domain. The shade indicates altitude and open circles indicate observation points by Iyobe et al. (2007)

4. Main factor in the regional difference

From the analysis of observational data and results of the CTL-run, we have confirmed that ADSD was different between the windward and leeward areas (see Fig. 2). These results indicate that the regional difference of ADSD is influenced by orography. Hence, we performed a sensitivity experiment (Alter-run) to clarify the impact of orography on regional difference of ADSD. The sensitivity experiment was performed under the condition in which the altitude of the specific single mountain at an altitude about 1000 m A. S. L. (see Fig. 2a) was eliminated and treated as a plain area.

Figure 3 shows ADSD simulated by the CTL-run and Alter-run. ADSD has a different gradient between Region B and C in CTL-run. However, there are no apparent the regional differences of ADSD between Region B and C in the Alter-run. It is noted that the altitude in Region B was decreased less than 500 m A. S. L., because the altitude in this area was modified in the Alter-run.

These results indicate that ADSD differs between the windward and leeward areas because ADSD is primarily controlled by the spatial distribution of snow depth and snowfall affected by orographic precipitation. ADSD is complex in the mountainous areas. In particular, the spatial variation of ADSD is reinforced in the leeward area. It is considered that the snow depth and snowfall are affected by several mountains in the leeward area in Niigata prefecture. On the other hand, ADSD appeared a simple proportional relation in Toyama, Ishikawa, and Fukui prefectures (Iyobe et al. 2007) where the orography is simpler than that in Niigata prefecture. It is considered that the snow depth and snowfall are affected by several mountains in the leeward area in Niigata prefecture. Therefore, it should be noted that the estimation method for the spatial distribution of snow depth using the ADSD has limitation.

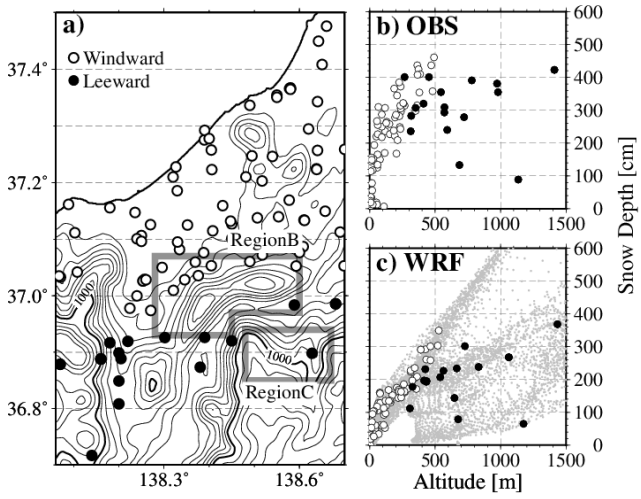


Figure 2. The regional difference of ADSD in Region A (Fig. 1b). (a) The location of observation sites. The right figures show the ADSD on (b) observation results, and (c) WRF estimation in Region A. The open (filled) circles indicate the data of windward (leeward) sites. The data of WRF estimation is nearest grid values of observation site, and gray small dots indicate all grid data on Region A. The contour indicates the orography drawn at a 100 m interval. Over 1000 m A.S.L., the interval changes to 200 m. The enclosed areas with gray thick line represent Region B and Region C in Fig. 3.

5. Acknowledgements

This research was supported by the Research Program on Climate Change Adaptation (RECCA) Fund by Ministry of Education, Culture, Sports, Science and Technology (MEXT) of Japan.

References

Clark P. M., J. Hendrikx, A. G. Slater, D. Kavetski, B. Anderson, N. J. Cullen, T. Kerr, E. Ö. Hreinsson, and R. A. Woods, 2011: Representing spatial variability of snow water equivalent in hydrologic and land-surface models: A review. Water Resour. Res., 47, W07539, doi:10.1029/2011WR010745.

Iyobe T., K. Kawashima, and K. Izumi, (2007), Characteristics of snow-depth distribution in Japan during heavy snowfall of 2005-2006 winter. Seppyo, 69, 45-52 (in Japanese with English abstract).

Lundquist J. D., J. R. Minder, P. J. Neiman, and E. Sukovich, 2010: Relationships between Barrier Jet Heights, Orographic Precipitation Gradients, and Streamflow in the Northern Sierra Nevada. J. Hydrometeor., 11, 1141-1156.

Peck L.E., and M. J. Brown, 1962: An Approach to the Development of Isohyetal Maps for Mountainous Areas. J. Geophys. Res.. 67, 681-694.

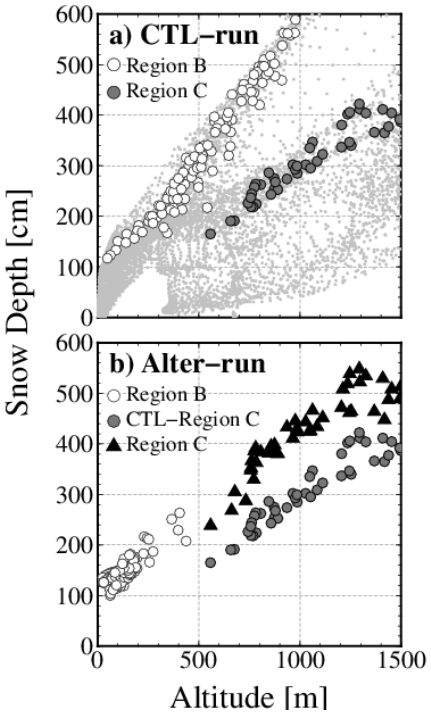


Figure 3. The ADSD of WRF estimation on Region B and C (see Fig. 2a). The plots show regional difference of ADSD on (a) CTL-run and (b) Alter-run. (a) The open and filled circles indicated the ADSD on Region B and Region C, respectively. Gray dots show the ADSD on Region A. (b) The open circles and filled triangles indicate the ADSD on Region B and C, respectively. The CTL-Region C in (b) is the same as Region C in (a).

Investigations of urban climate characteristics with SURFEX/TEB model: preliminary results for Budapest city

Gabriella Zsebeházi, Ilona Krüzselyi and Gabriella Szépszó

Climate and Atmospheric Environment Department, Hungarian Meteorological Service, Budapest, Hungary (zsebehazi.g@met.hu)

1. Introduction

Climate change can have more serious impacts over urban areas (e.g., they have to face with higher temperature rise) than its surroundings. Since majority of mankind is affected by these enhanced changes, investigating the impact of future climate change on cities is essential.

Climate models are sufficient tools for estimating future climate change, although most of them cannot represent urban climate characteristics, because their spatial resolution is too coarse (to date 10-50 km) and they characterize the urbanized areas as natural surfaces.

In our study we applied the SURFEX land surface scheme including the TEB urban canopy model to describe the processes over urban areas. TEB is coupled to the ALADIN-Climate atmospheric model and tested for a shorter 10-year period over the capital of Hungary, Budapest.

The objectives of this work are to validate the temperature results of the ALADIN-Climate and SURFEX models against station measurements and to investigate the added value of SURFEX to ALADIN-Climate regional climate model over Budapest.

2. Models and methods

SURFEX is a detailed externalised surface model, which is suitable for describing the surface-atmosphere interactions over four tiles (sea, nature, lake and town). In the model the processes are calculated by the ISBA scheme (*Noilhan and Planton,* 1989) over natural covers and by the TEB scheme (*Masson*, 2000) over built-up surfaces.

In our experiment the physiographical information was obtained from the ECOCLIMAP database (*Masson et al.*, 2003). The atmospheric forcing was provided by the 10 km resolution results of ALADIN-Climate v5.2 regional climate model (*Csima and Horányi*, 2008) driven by ERA-40. We applied the 5.1 version of SURFEX, which was integrated between January 1990 and December 2000, at a horizontal resolution of 1 km, on a 61x61 gridpoint sized domain covering Budapest (Fig. 1).

In the analysis we regarded the temperature fields for the period of 1991–2000. The model results were validated against data of two meteorological stations, either of them represents the urban conditions (located in the vicinity of the downtown); the other represents the suburban conditions (located in the south-east region of Budapest). The choice was based largely on the availability of long term observational data.

In this work, on the one hand we investigated the added value of SURFEX to the ALADIN-Climate through monthly and seasonal temperature biases in the ALADIN-Climate and SURFEX results over the reference points. On the other hand we calculated the mean urban heat island intensity (UHI; temperature difference between the inner and outer points) on different time scales and analysed its temporal and spatial characteristics.

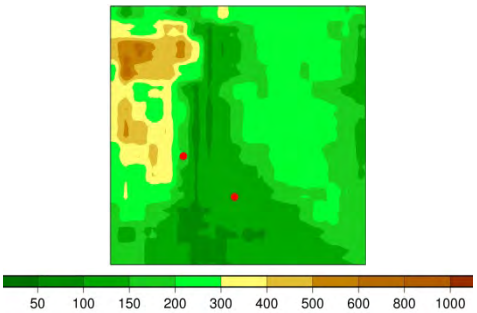


Figure 1. Integration domain of SURFEX. Red markers indicate the validation points (left: inner point; right: outer point).

3. First results

Fig. 2 shows the spatial distribution of the summer mean temperature in the 10 km resolution ALADIN-Climate and 1 km resolution SURFEX. As a result of the finer resolution and TEB scheme, the SURFEX presents much more detailed temperature field compared to the ALADIN-Climate. The urban heat island effect can be clearly noticed, since the highest temperature (23 °C) occurs in the centre of Budapest. Similar results are found in other seasons and on monthly time scale as well. The diurnal and annual characteristics of UHI (the most robust UHI occurs in the summer months at night time; in winter the daily cycle of UHI is more flat) are also reflected in the results (not shown).

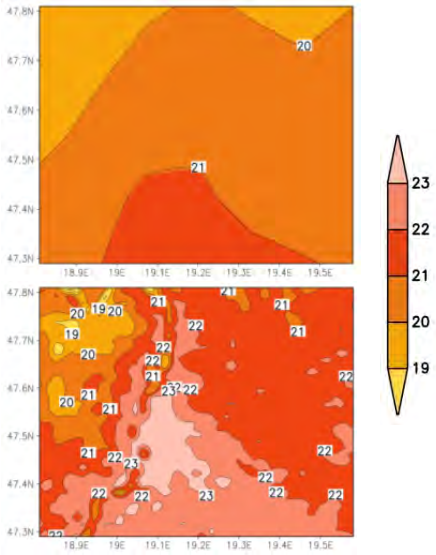


Figure 2. Summer mean temperature (in °C) in Budapest simulated by the ALADIN-Climate (top) and SURFEX (bottom) in 1991–2000.

Fig. 3 presents the bias in the ALADIN-Climate and SURFEX results at the two reference points. The ALADIN-Climate produces relatively large negative bias in January, April and October in both sites; this feature can be discovered in the SURFEX results as well. SURFEX adds extra heating to the ALADIN-Climate results in every month, and this temperature surplus varies within the annual cycle and differs amongst the two locations. From May to September the heating rate is bigger in the outer than in the inner point, but from November to March the inner point gains larger surplus.

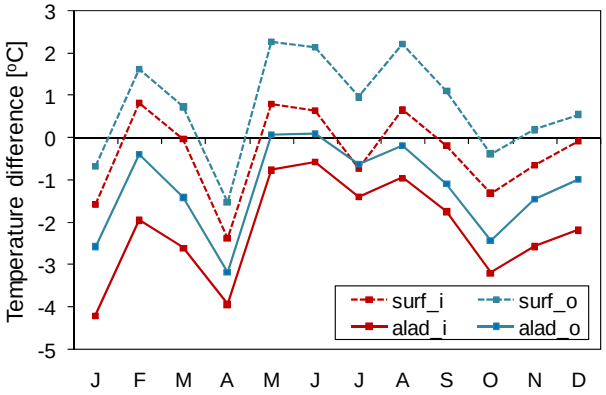


Figure 3. Monthly mean temperature difference (in °C) between the ALADIN-Climate (solid lines), SURFEX (dashed lines) and observations in the inner (red) and outer (blue) points in 1991–2000.

Regarding the simulated and real annual cycle of the UHI intensity between the two selected sites (Fig. 4) – as a consequence of the abovementioned results –, in winter a positive, but underestimated UHI intensity is revealed in the SURFEX, while large negative bias appears in summer (i.e., the simulated temperature in the outer point is higher than in the inner point).

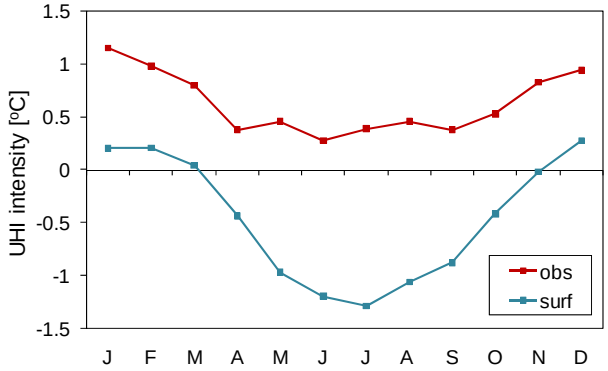


Figure 4. Monthly mean urban heat island Intensity (in °C) according to the measurements (red) and simulated by the SURFEX (blue) in 1991–2000.

4. Conclusion remarks and future plans

It is found that SURFEX is able to detect the spatial characteristics and diurnal and annual cycle of the urban heat island effect over Budapest. However, it cannot cure the shortcomings inherited from the ALADIN-Climate forcing. At the investigated two reference points (located in the centre and in the suburban region) large bias in the summer UHI appears which can be explained by the differing bias in the ALADIN-Climate and the different heating rate of the SURFEX at the two sites. Note that both points are described with the same cover-type (gridpoint cover is composed of 60% town and 40% nature) in the ECOCLIMAP database.

In the next step we intend to continue the validation and analyse the results deeply in order to better understand our findings. Moreover we will carry on some sensitivity analyses with urban surface parameters (e.g. albedo, building height) to correct ECOCLIMAP parameters and improve the results.

References

Csima, G., and Horányi, A. (2008). Validation of the ALADIN-Climate regional climate model at the Hungarian Meteorological Service. *Időjárás,* **112**, 3–4, 155–177.

Masson, V. (2000). A Physically-based scheme for the Urban Energy Budget in atmospheric models. *Bound.-Lay. Meteorol.*, **94**, 3, 357–397. doi:10.1023/A:1002463829265

Masson, V., Champeaux, J.-L., Chauvin, F., Meriguet, C., and Lacaze, R. (2003). A global database of land surface parameters at 1-km resolution in meteorological and climate models. *J. Climate*, **16**, 9, 1261–1282. doi:10.1175/1520-0442-16.9.1261

Noilhan, J., and Planton, S. (1989). A simple parameterization of land surface processes for meteorological models. *Mon. Wea. Rev.,* **117**, 3, 536–549. doi:10.1175/1520-0493(1989)117<0536:ASPOLS>2.0.CO;2

Topic 3

Challenges for RCM Evaluation and Adaptation

Objective Type Comparison And Classification Of Precipitation Variability Over Ethiopia Based On Cordex Simulations And Gpcp Datasets

Nigus Hiluf Abay

Agriculture Department Saint merry College,Wukro ,Tigray,Ethiopia

In this study, quantitative validation of regional climate model simulation and classification of homogeneous precipitation regions have been performed based on better resolution precipitation datasets. The simulated datasets are generated in the framework of CORDEX project for the African domain from Royal Netherlands Meteorological Institute (KNMI) regional climate model, RACMO2. They are evaluated against observational datasets produced by the Global Precipitation Climatology Project (GPCP). The analysis domain covers the area bounded by latitudes 3°N to 15°N and longitudes 33°E to 48°E. The results show that rainfall from RACMO2 is as good as GPCP rainfall in describing the seasonal cycle, as well as simulating the spatial distribution of precipitation. Assessing the performance of the model to determine extremes, it is found that RACMO2 has the tendency to overestimate precipitation over highlands and underestimate over eastern lowlands of Ethiopia in relation to GPCP precipitation. Principal components (PCs), empirical orthogonal functions (EOFs), and associated spectra for both datasets are in good agreement with GPCP. The leading four PCs explain 75% and 80% of the variances in RACMO2 and GPCP respectively while the corresponding EOFs describe homogeneous precipitation regions. Spectra of the PCs exhibit dominant peaks at a period of 6 and 12 months, that is, equivalent to monomodal and bimodal rainfall types.

How well do regional climate models simulate extreme rainfall events in South Africa?

Babatunde J. Abiodun and Sabina Abba Omar

Climate System Analysis Group, Department of Environmental & Geographical Science,
University of Cape Town, South Africa. (babiodun@csag.uct.ac.za)

1. Introduction

The socio-economic impacts of extreme rainfall events are severe in South Africa, where the events often lead to massive floods that destroy infrastructure and human lives. Skillful seasonal predictions from regional climate models (RCMs) can help reduce these impacts, but simulating extreme rainfall events over South Africa, expecially over Western Cape, remains a big challenge for most regional climate models. Hence, there is need to investigate and improve the capability of RCMs in simulating extreme rainfall events and in reproducing the synoptic patterns that induce the events. Lennard et al. (2013) showed that 58% of the extreme rainfall events over Western Cape in winter are caused by the passage of mid-latitude cyclones to south of South Africa and a high pressure over the interior of the country; cut-off lows accounted for the extreme rainfall event in autumn, while Tropical Temperate Troughs (TTTs) produced about 35% of extreme rainfall in autumn, 46% in spring, but almost all extreme rainfall in summer. The present study investigates how well the RCMs can simulate the characteristics of extreme rainfall events over Western Cape, focussing on widespread extreme rainfall events.

2. Data and Method

We analyzed observation, reanalysis, and simulation datasets for the study. The observation data are from the Global Precipitation Climatology Project (GPCP; Huffman et al.,2001) and from the Tropical Rainfall Measuring Mission (TRMM; Huffman et al., 2007), but GPCP dataset the dataset. The reanalysis dataset is from the European Centre for Medium-Range Weather Forecasts (ECMWF) ERA-Interim (ERAINT; Dee et al., 2011) reanalysis. The simulation datasets are from seven of the RCMs (CCLM, REMO, PRECIS, CRCM5, CCLM, ARPEGE and RCA) that participated in the Regional Climate Downscaling Experiment (CORDEX; Nikulin et al., 2012). The RCMs simulations were driven by the ERAINT dataset. All the simulations datasets were obtained from the Swedish Meteorological and Hydrological Institute (SMHI).

We defined an extreme rainfall at any grid point as the 95th percentile of daily rainfall over the point, and defined a synoptic or widespread extreme rainfall event (WERE) as a simultaneous occurrence of an extreme rainfall event over at least 50% of Western Cape region in a day. We applied Self Organizing Maps (SOM) analysis to classify WEREs from all datasets and examine each dataset to the SOM's nodes.

3. Results and Discussion

The extreme rainfall threshold over Southern Africa

ERAINT simulates a lower threshold than both GPCP and TRMM. Only four RCMs (CRCM5, RAC35, REMO and WRF) perform better than ERAINT in simulating the threshold pattern. Other RCMs (ARPEGE, CCLM, RACMO PRECIS and RegCM3) perform worst than ERAINT in simulating the threshold pattern.

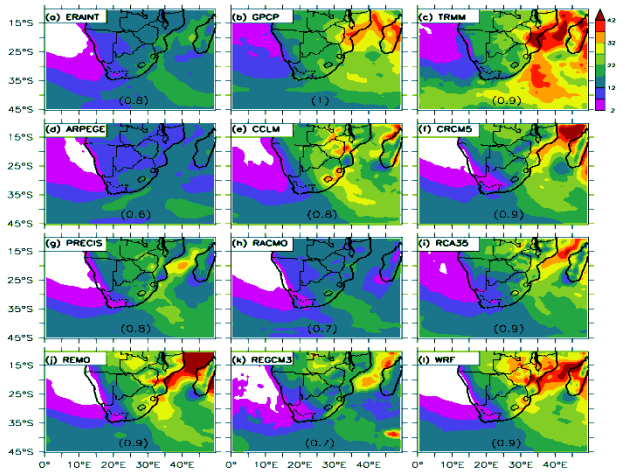


Figure 1: The threshold of the extreme rainfall over Southern Africa in 1998-2008. The correlation between the pattern in each panel and that of GPCP is indicated in the bracket.

Seasonal variation of extreme rainfall in Western Cape

ERAINT report 27 WERE in total and agrees with GPCP that the maximum frequency of WERE is in MAM. Only two RCMs (PRECIS and RACMO) report higher numbers of WERE than ERAINT, other RCMs report lower number. This implies that downscaling ERAINT datasets with RCMs may not necessarily increase the number of WERE over Western Cape. None of the RCMs reproduces the seasonal variation of WERE as GPCP, but most RCMs reproduce the maximum frequency of WERE in MAM.

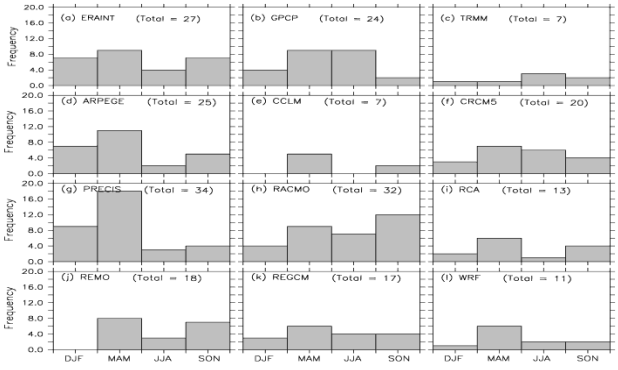


Fig 2: The seasonal variation of WERE over Western Cape (1998-2008).

The classification of widespread extreme rainfall evenvt in Western Cape

Figure (3) presents the SOMs classification of the WEREs into 12 nodes (Fig 3) while figure (4) shows the contibution of each dataset to the nodes. A visual inspection of figure (3) suggests that the nodes can be broadly grouped into four categories. In the first group (i.e. nodes 1, 2, and 5; hereafter, TRW), WEREs are well linked with tropical rainfall activities over the continent. In the second group (i.e. nodes 6, 9 and 10; hereafter, ISW), WEREs are isolated (or weakly linked with tropical rainfall activities). In the third group (i.e. nodes 3, 4 and 7; hereafter, MLW), WEREs are linked with the mid-latitude rainfall activities over the South Indian Ocean. In the fourth group (i.e. nodes 8, 11 and 12; hereafter, ACW), WEREs are influenced by Agulhas Current (which is located south of the continent), though they are still the mid-latitude rainfall.

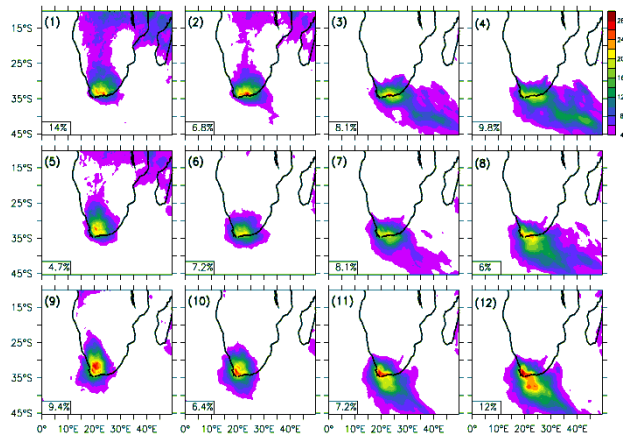


Figure 4: The SOMs classification (nodes 1 - 12) of widespread extreme rainfall events (WEREs) in Western Cape (1998-2008), obtained using both observed and simulated datasets. The percentage contribution of each node to the total WEREs are indicated at the lower left corner of each panel.

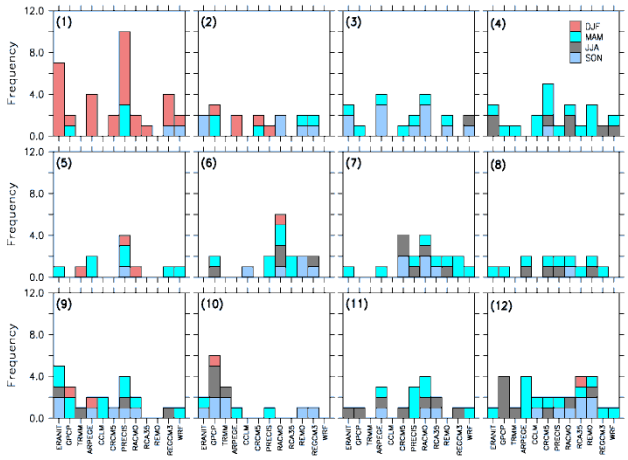


Figure 3: The frequency of the SOMs nodes (shown in Fig. 7) in the observed (GPCP and TRMM) and in simulated (ERAINT and CORDEX RCMs) datasets.

Figure (4) shows that all RCMs (except CCLM) simulate TRW events, but PRECIS simulates the higher frequency of TRW events than any dataset; in fact, most of WERE in PRECIS simulation are in TRW group. All the RCMs simulate at least one event in ISW group; however, only three models (i.e. RACMO, PRECIS and REGCM3) simulate the number of ISW event that is comparable with that of GPCP. Other RCMs (especially WRF and CRCM5) grossly underestimate the number of ISW events. Nevetheless, only one model (i.e. RACMO) agrees with GPCP that ISW events can occur in any season; other datasets (except ARPEGE) fail to report the occurrence of ISW events in summer (DJF), while ARPEGE fails to report the events in winter (JJA). All RCMs simulate MLW events, but CCRM5 and RACMO simulate the highest occurrence of the events (i.e., 11 events) in this group. There is a general consensus among the datasets that MLW events mainly occur in MAM, JJA and SON, but never in DJF. All the RCMs simulate at one ACW event; among the datasets, ARPEGE simulates the highest frequency (i.e. nine events) ACW events; RACMO, RCA35, PRECIS and REMO also simulate higher frequency of the events than observed in GPCP. However, GPCP and TRMM reports ACW events only in winter (JJA), but ERAINT and the RCMs also report them in the shoulder seasons (MAM and SON). Only except RCA reports the events in summer (DJF).

4. Conclusion

This study has CORDEX evaluated the capability of used evaluated the capability nine regional climate models in simulating the characteristic of extreme rainfall events over Western Cape. The RCMs reproduce the four patterns of synoptic pattern associated with widespread extreme rainfall events over Western Cape. However, some RCMs underestimate the frequency of the patters were other RCM over estimate the patterns.

Reference

Lennard, C. J., Coop, L., Morison, D., & Grandin, R. (2013). Extreme Events: Past and future Changes in the Attributes of Extreme Rainfall and the Dynamics of their Driving Processes. South African Water Research Commission report 1960/1/12.

Huffman, G. J., Adler, R. F., Bolvin, D. T., Gu, G., Nelkin, E. J., Bowman, K. P., Hong, Y., Stocker E. F., & Wolff, D. B. (2007). The TRMM Multisatellite Precipitation Analysis (TMPA): Quasi-global, multiyear, combined-sensor precipitation estimates at fine scales. Journal of Hydrometeorology, 8(1).

Huffman, G. J., Adler, R. F., Morrissey, M. M., Bolvin, D. T., Curtis, S., Joyce, R., McGavock , B. & Susskind, J. (2001). Global precipitation at one-degree daily resolution from multisatellite observations. Journal of Hydrometeorology, 2(1), 36-50.

Nikulin, G., Jones, C., Giorgi, F., Asrar, G., Büchner, M., Cerezo-Mota, R., ... & Sushama, L. (2012). Precipitation Climatology in an Ensemble of CORDEX-Africa Regional Climate Simulations. Journal of Climate, 25(18).

Dee DP, and co-authors (2011) The ERA-Interim reanalysis: configuration and performance of the data assimilation system. Q J R Meteorol Soc **137**:553–597. doi:10.1002/qj.828.

Climate projection over the East Asia based on RCP scenarios using WRF

Joong-Bae Ahn and Ja-Young Hong

Division of Earth Environmental System, Pusan National University, Busan, South Korea (jbahn@pusan.ac.kr)

1. Introduction

The mean temperature of the Korean Peninsula rose by 1.5℃ during the 20th century, due to global warming as well as rapid urbanization (Kwon, 2005). Recently, Intergovernmental Panel on Climate Change (IPCC) has adopted new scenarios of potential future anthropogenic climate change, Representative Concentration Pathways (RCPs) based on Coupled Model Intercomparison Project phase 5 (CMIP5). Thus it is necessary to project the regional climate changes over the East Asia based on the RCPs. In this study, the detailed climate changes over the East Asia based on the Historical, RCP4.5 and RCP8.5 were simulated by using regional climate model, Weather Research and Forecasting (WRF) version 3.4.

2. Data and Methods

For this study, WRF system was set-up at "Haebit", one of the early portions of the Korea Meteorological Administration (KMA) Supercomputer Unit-3. Using the system, dynamical downscaling was performed over East Asia centered on the Korean Peninsula (117°E-138°E, 29°N-46°N) with 12.5km-horizontal resolution over the period of 1979-2010 for the Historical and over the periods of 2019-2100 for the RCPs simulations. Initial and lateral boundary conditions are obtained from the Hadley Centre Global Environmental Model version 2 - Atmosphere and Ocean (HadGEM2-AO) from National Institute of Meteorological Research / KMA (NIMR/KMA) which is a model participates in CMIP5. To evaluate the simulation ability of WRF Historical, Climatic Research Unit (CRU) time series (TS) 3.2 (Harris et al., 2013) is used over the period 1981-2010.

3. Results

The simulated results of HadGEM2-AO and WRF are presented in terms of 2m-temperature (Figure 1) and precipitation (Figure 2) during boreal summer and winter of Historical for the period 1981-2010, compared with observation. As for the mean 2m-temperature, the general patterns of HadGEM2-AO and WRF are similar with observation although WRF showed lower values than observation due to the systematic model bias. The WRF reproduced a feature of the terrain-following characteristics reasonably well owing to the increased horizontal resolution. Both of the models simulated the observed precipitation pattern for DJF than JJA reasonably, while the rainfall over the Korean Peninsula in JJA is less than observation. HadGEM2-AO in DJF 2m-temperature and JJA precipitation has warm and dry biases over the Korean Peninsula, respectively. WRF showed cold bias over JJA 2m-temperature and wet bias over DJF precipitation. The larger bias in WRF was attributed to the addition of HadGEM2-AO's bias to WRF's systematic bias.

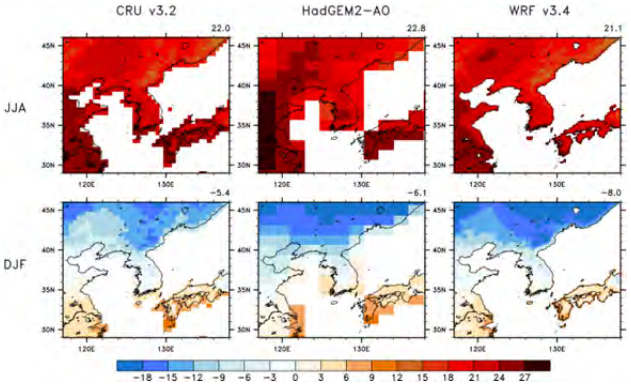


Figure 1. From June to August (JJA) and from December to next year February (DJF) mean climatologies of temperature at 2m [℃] for the 1981-2010 periods for observation, HadGEM2-AO and WRF Historical simulations.

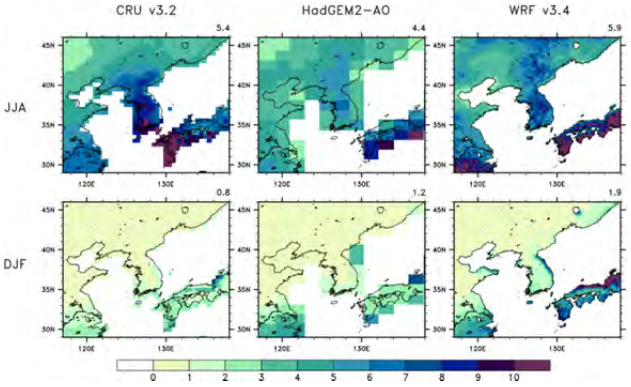


Figure 2. Same as Figure 1 except for precipitation [mm/day].

In differences between RCPs (2071-2100) and Historical (1981-2100), summer mean surface temperature (2.5-4.5℃) and precipitation (1.5-3.5 mm/day) are projected to be risen over the Korean Peninsula. Sea level pressure increases mainly over the northwestern Pacific (NP) area implying the strengthening of the NP High, while relatively weak increase over the East Sea and the Yellow Sea. As a result, enlarged pressure gradient and anomalous warm and wet air might contribute to the increased surface temperature and precipitation. Under RCP8.5, more anomalous 850 hPa moisture flux from low latitude is expected to be flowed into the Korean Peninsula than under RCP4.5. The decrease of 200 hPa zonal wind over the Korean Peninsula is also simulated in both RCPs.

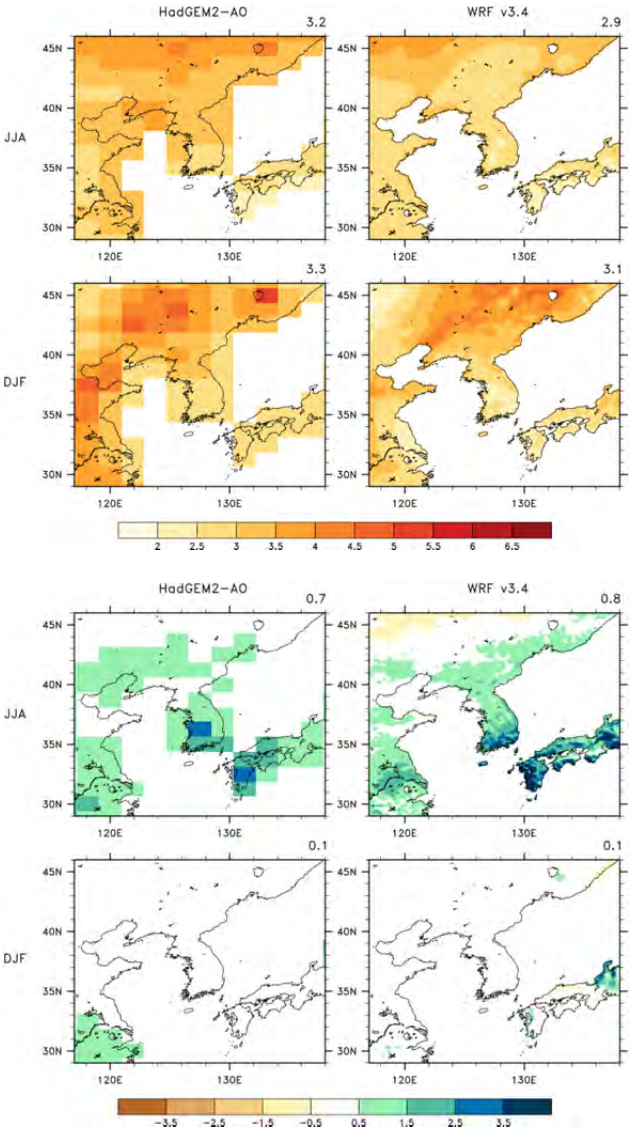


Figure 3. Differences between RCP4.5 (2071-2100) and historical (1981-2010) of seasonal temperature at 2m [℃] and precipitation [mm/day] for HadGEM2-AO and WRF.

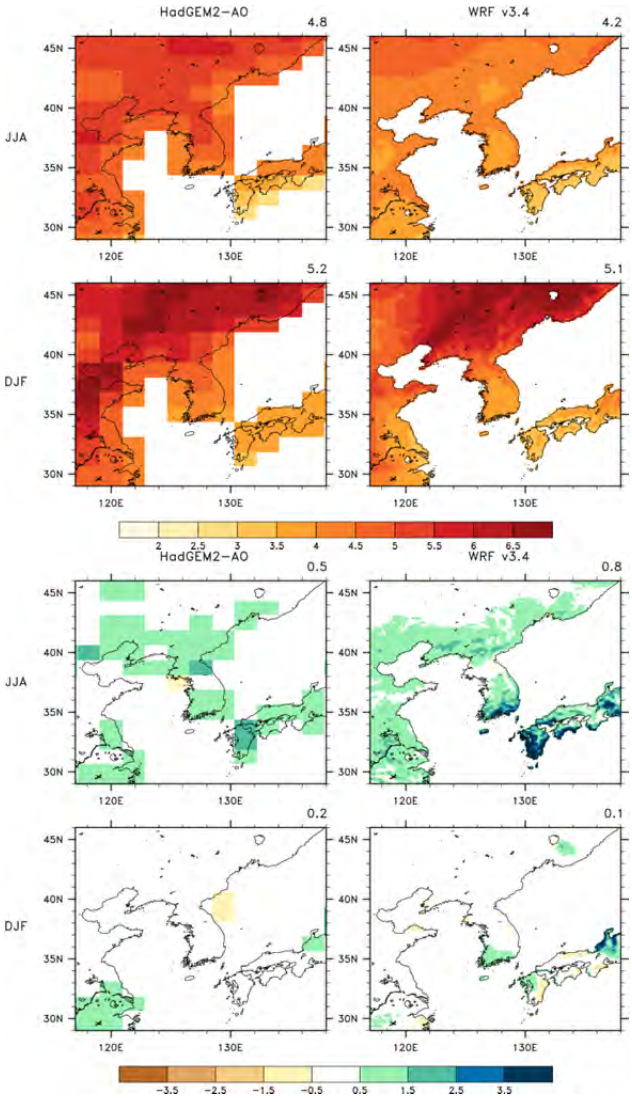


Figure 4. Same as Figure 3 except for RCP8.5.

4. Future work

The high resolution data covering whole the East Asia (e. g. Coordinated Regional Climate Downscaling Experiment East Asia) will be simulated and analyzed for the projection of climate change based on RCP scenarios.

Acknowledgments

This work was funded by the Korea Meteorological Administration Research and Development Program under grant CATER 2012-3083. We thank KMA's supercomputer management division for providing us with the supercomputer resource and consulting on technical support.

References

Harris, I., P. D. Jones, T. J. Osborn, and D. H. Lister (2013) Updated high-resolution grids of monthly climatic observations - the CRU TS3.10 Dataset, International Journal of Climatology, doi: 10.1002/joc.3711

Kwon, W.-T. (2005) Current status and perspectives of climate change sciences, Asia-Pacific Journal of Atmospheric Sciences, 41, 2-1, 325-336

CRCM5: performance errors, boundary forcing errors and climate projections over India

Adelina Alexandru and Laxmi Sushama

Centre ESCER, Département des sciences de la Terre et de l'atmosphère, Université du Québec à Montréal, Montréal (Québec) Canada (adelina@sca.uqam.ca)

1. Introduction

This study aims to provide new insights on the ability of the fifth generation of the Canadian Regional Climate Model (CRCM5) in simulating, for the very first time, the monsoon climate over India. In addition to commonly considered variables such as temperature, precipitation, sea level pressure etc, variables such as soil moisture and total runoff, that are extremely important for a number of impact and adaptation studies, are analysed in both current and future climates, for all four seasons (pre-monsoon, SW-monsoon, post-monsoon and winter). More specifically, this study provides (1) assessment of CRCM5 performance errors, (2) assessment of boundary forcing errors in GCM-driven CRCM5 simulations, and (3) assessment of projected changes to selected climate variables for various seasons over India – a non-native domain for CRCM5. The simulations performed in this study will also contribute to the CORDEX (Coordinated Regional Climate Downscaling Experiment) project, which aims to build an improved generation of regional climate change projections over India.

2. CRCM5 Simulation setup

Three CRCM5 simulations were performed: a reanalysis-driven control simulation for the period 1959–2008 and two CGCM-driven transient climate-change simulations for the period 1950–2100 forced with two independent GCMs, CanESM2 and MPI-ESM-LR; the future climate simulations were based on the RCP 4.5 radiative forcing scenario. The ERA-40/ERA Interim-driven simulation was used to assess, against various observational datasets, the CRCM5 performance over India for the 1971–2000 period. Boundary forcing errors, i.e. errors in CRCM5 simulations due to errors in the driving GCM data, were assessed by comparing CRCM5 simulations driven by CanESM2 and MPI-ESM-LR with the CRCM5 simulation driven by ERA-40/ERA-Interim for the 1971–2000 period.

3. Results and discussion

Results show that CRCM5 driven by ERA-40/ERA-Interim is able to capture well the current climate patterns of precipitation, wind, sea level pressure, total runoff and soil moisture over most part of India in comparison with available reanalysis and observations. However, some noticeable differences between the model and observational data were found during the SW monsoon season within the domain of integration. CRCM5 is 1°C to 2°C colder than CRU observations and generates more precipitation over the Western Ghats and central regions of India and not enough in north, northeast India and along the Konkan west coast in comparison with the observed precipitation. The monsoon onset occurs earlier in CRCM5 simulations while the monsoon withdrawal occurs too late in comparison with observations. Boundary forcing errors are generally of the same magnitude or larger for the southwest monsoon seasons and smaller for the other seasons when compared to performance errors.

For the two future 30-year time slices (2041–2070 and 2071–2100) analysed here, both CRCM5 climate projections imply a general warming over India in the 21st century, especially in the pre-monsoon and winter seasons. However, for precipitation and other related variables, such as the total soil moisture and total runoff, the two GCM-driven CRCM5 simulations give conflicting signals with reference to the 1971–2000 baseline, mostly due to the differences between the two GCM-driven simulations in representing the 1971–2000 baseline precipitation. This highlights the need for multi-model ensembles to better represent the uncertainties related to future projections. Results also suggest a change in the timing of monsoon onset and withdrawal in future climate, with both onset and withdrawal likely to occur later than for the 1971-2000 period.

4. Conclusion

Though this study shows reasonable performance of the CRCM5 over the India domain, more model improvements are required. Further studies will focus on the suitability of the convection scheme. Another important aspect, that is currently being investigated, is to bias correct SSTs, which could have influence on the simulated climate over India as indicated by other studies (i.e., Levine et al. 2012). In the long term, the plan is to have coupled simulations (i.e. CRCM5 coupled to an ocean model) that will be able to better represent ocean-atmosphere interactions and feedbacks.

Currently, the model does not include irrigation, which is important to consider as it has huge impacts on the energy and water partitioning at the surface. The role of irrigation in modifying the local climate of India through feed back mechanisms has been already demonstrated in many studies (e.g. Saeed et al.2009) and it is also planned to introduce irrigation in CRCM5. Also, the projected changes presented in this study are based on a single RCM and RCP scenario. A multi RCM-GCM ensemble, for various RCP scenarios, is required to better quantify uncertainties, which hopefully will be achieved through the CORDEX program.

References

Levine, R. C. and Turner, A. G., 2012 : Dependence ofIndian monsoon rainfall on moisture fluxes across the Arabian Sea and the impact of coupled model sea surface temperature biases. Clim. Dyn., 38 (11-12). pp. 2167-2190.

Saeed F, Hagemann S, Jacob D., 2009: Impact of irrigation on the South Asian summer monsoon. Geophys Res; 36 (20).

Impacts of using spectral nudging on COSMO-CLM simulations of single Vb-events

Ivonne Anders[1], Manuela Paumann[2], Barbara Chimani[1] and Michael Hofstätter[1]

[1] ZAMG - Central Institute for Meteorology and Geodynamics, Vienna, Austria (Ivonne.Anders@zamg.ac.at)
[2] University of Vienna, Department of Meteorology and Geophysics, Vienna, Austria

1. Introduction

Mid-latitude cyclones play an essential role in maintaining the global atmospheric energy balance, by the exchange, transport and transformation of mass and energy. Moreover these weather systems are associated with different, local weather phenomena affecting every day's life, especially in the case of related extremes as windstorms or extreme precipitation. As early as 1891 W.J. van Bebber has recognized and described the importance of certain cyclone types for the risk of heavy, large-scale precipitation or winter storms in Central Europe (Van Bebber, 1891). He attributed most of these events to cyclones which are propagating from Northern Italy to the northeast, leaving the Alps on the left. Especially this specific type of cyclones named as "Vb" is still well known, since some of the most devastating European floods have been associated either with type Vb in Central Europe like in Aug 2002 (Ulbrich et al., 2003) or in May/June 2013 (Blöschl et al., 2013 - under review), as well as with the similar type Vc in Eastern Europe (Apostol, 2008).

A recent study (Hofstätter et al., submitted) revealed that Atlantic and Polar type cyclones are typically the most intense when crossing Central Europe (CE), but very closely followed by Van Bebber's type Vb. This underlines speculations about the relevance of the latter for causing certain weather extremes in CE. Another study by Hofstätter and Chimani (2012) demonstrated that Vb cyclones are most frequent in early spring, but show a pronounced activity in autumn when restricting to the most intense cyclones only.

In this contribution we investigate the influence of spectral nudging in a RCM on the development of certain Vb events and related precipitation amounts and pattern in Austria, Germany and the Czech Rebublic.

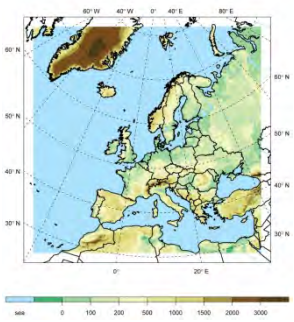


Figure 1. Model domain

2. Experimental setup

The state-of-the-art regional climate model COSMO-CLM is applied in a hindcast-mode forced by NCEP reanalysis data to the case of several individual Vb-events in August 2002 and Mai/June 2013. All simulations have been started out of a stable simulation starting 1950, carried out within the coastDat framework. (cf. http://www.coastdat.de) This simulation covers Europe (248x254 grid points) (cf. Figure 1.) with a spatial resolution of 25km.

Besides the conventional forcing of the regional climate model at its lateral boundaries a spectral nudging technique following Storch et al. (2000) is applied. This means that inside the model area the regional model is forced to accept the analysis for large scales whereas it has no effect on the small scales. The simulations for the Vb-events mentioned above have been varied systematically by changing nudging factor - *alpha_sn*, number of nudged waves – *isc_sn* and *jsc_sn*, nudged variables - *yvarsn*, uppermost pressure threshold - *pp_sn*, and the number of model time steps after that the spectral nudging module is applied again – *nincsn* (cf. Table 1).

Table 1. Experimental design (description of parameters see text)

ID	alpha_sn	isc_sn	jsc_sn	yvarsn	pp_sn	nincsn
sn000	0.5	5	5	U,V	850	5
sn010	0.05	5	5	U,V	850	5
sn011	0.1	5	5	U,V	850	5
sn012	0.2	5	5	U,V	850	5
sn013	0.3	5	5	U,V	850	5
sn014	0.4	5	5	U,V	850	5
sn015	0.6	5	5	U,V	850	5
sn016	0.7	5	5	U,V	850	5
sn017	0.8	5	5	U,V	850	5
sn018	0.9	5	5	U,V	850	5
sn019	1.0	5	5	U,V	850	5
sn020	0.5	2	2	U,V	850	5
sn021	0.5	3	3	U,V	850	5
sn022	0.5	4	4	U,V	850	5
sn023	0.5	6	6	U,V	850	5
sn024	0.5	7	7	U,V	850	5
sn030	0.5	5	5	U,V	800	5
sn031	0.5	5	5	U,V	900	5
sn040	0.5	5	5	U,V,PP	850	5
sn041	0.5	5	5	PP	850	5
sn042	0.5	5	5	U,V,T	850	5
sn043	0.5	5	5	T	850	5
sn044	0.5	5	5	U,V,PP,T	850	5
sn050	0.5	5	5	U,V	850	2
sn051	0.5	5	5	U,V	850	8
sn052	0.5	5	5	U,V	850	12
sn053	0.5	5	5	U,V	850	24
sn054	0.5	5	5	U,V	850	72
sn055	0.5	5	5	U,V	850	144
sn901	0.9	7	7	PP	850	2
sn902[1)]	0.5	5	5	U,V	850	5
sn903[2)]	0.5	5	5	U,V	850	5
sn904[1)]	1.0	7	7	U,V,PP	900	2
sn905[1)]	1.0	7	7	U,V,PP,T	900	2
sn906[2)]	0.5	5	5	U,V,T	850	5
snFALSE	.FALSE.	.FALSE.	.FALSE.	.FALSE.	.FALSE.	.FALSE.

3. Methods

The resulting precipitation amounts over whole of Europe, the area of Austria/Germany/Czech Republic and the upper Danube catchment have been compared separately to E-OBS gridded European precipitation data set, a recent high spatially resolved precipitation data set for the countries mentioned before (HYRAS combined with GPARD-6) and to river runoff data of the river Danube at the Vienna observation site.

We analysed on one hand the amount and pattern of mean, minimum and maximum precipitation accumulated over the days of the individual strong precipitation events. On the other we compared the location of the cyclone tracks.

4. Results

The results show that increasing the number of nudged waves from 1 to 7 as well as the choice of the variables used in the nudging process (cf. Figure 2) have a large influence on the development of the low pressure system and the related precipitation patterns. On the contrary, the nudging factor or the definition of the uppermost pressure level for the nudging is of low impact on the results.

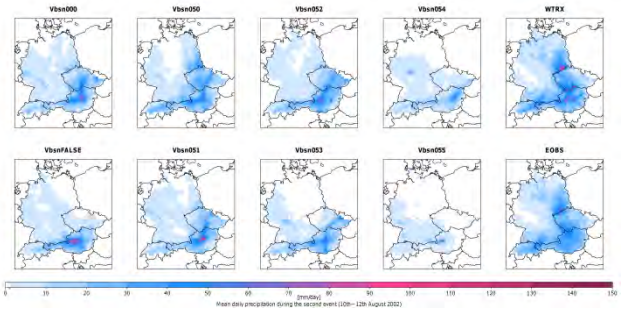


Figure 2. Precipitation amounts accumulated from 10.08.2002 to 12.08.2002 from simulations (1st to 4th column) compared to observations (last column) from EOBS and WTRX (HYRAS combined with GPARD-6).

Looking at the time series of daily precipitation amounts it can be seen that in August 2002 the second event 10th-12th of August can be better captured by the models than the event a few days before from 6th to 7th of August (not shown). The very high precipitation amount occurred related to these Vb events are underestimated by the models.

Figure 3 shows the Vb cyclone tracks detected in sn000 and ERAinterim reference data (cf. Table 1), derived from mean sea level pressure (black) and 700hPa geopotential height (red). The location of the track can be well captured by the model simulation. In the simulation with no spectral nudging the cyclone cannot be tracked at the level of mean sea level pressure due to low pressure intensities.

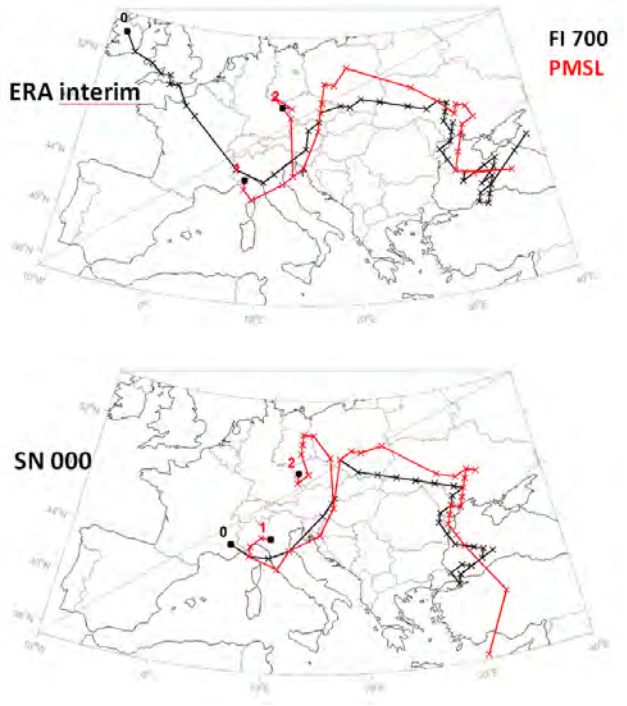


Figure 3. Vb cyclone tracks detected in ERAinterim reference data and sn000 simulation (cf. Table 1) 10.08.-12.08.2002, derived from mean sea level pressure (black) and 700hPa geopotential (red).

References

Apostol L. (2008) The Mediterranean cyclones -- The role in ensurig water resources and their potential of climatic risk in the East of Romania, Editura Edit. Univ. ,,Al. I. Cuza", Iaşi.

Bebber, W.J. van, (1891) Die Zugstrassen der barometrischen Minima nach den Bahnkarten der Deutschen Seewarte für den Zeitraum 1875-1890. Meteorlogische Zeitschrift 8, pp 361-366

Blöschl G., Nester T., Komma J., Parajka J., and Perdigão R.A.P: The June 2013 flood in the Upper Danube basin, and comparisons with the 2002, 1954 and 1899 floods. Hydrol. Earth Syst. Sci. Discuss.,10,9533-9573

Hofstätter M., Chimani, B., Steinacker, R. and G. Blöschl, (2013) A stream-based classification of cyclone tracks over Europe (submitted)

Hofstätter M., Chimani B. (2012) Van Bebber's cyclone tracks at 700 hPa in the Eastern Alps for 1961–2002 and their comparison to Circulation Type Classifications. – Meteorol. Z. 21, No. 5, 489-503.

Storch H.v., Langenberg H., and F. Feser (2000) A Spectral Nudging Technique for Dynamical Downscaling Purposes , Monthly Weather Review 128(10) 3664-3673.

Ulbrich U., Brücher T., Fink A.H., Leckebusch G.C., Krüger A., J.G. Pinto (2003) The Central European Floods in August 2002 , Part II: Synoptic causes and considerations with respect to climatic change. Weather 58, 434--441.

The Indian Summer Monsoon Projections: Climate variability or Climate Change?

Shakeel Asharaf[1,2], and Bodo Ahrens[1]

[1] Institute for Atmospheric and Environmental Sciences, Goethe University, Frankfurt, Germany
[2] Deutscher Wetterdienst, Offenbach, Germany

1. Introduction

Indian summer monsoon rainfall was investigated in two different greenhouse gas emission scenarios: Special Reports on Emissions Scenario (SRES; B1) and the new Representative Concentration Pathways (RCPs; RCP4.5). For this purpose, the regional climate model (RCM) COSMO-CLM (CCLM) and its driving global coupled atmospheric-ocean model (GCM) MPI-ESM-LR were used. The scenario B1 simulation with CCLM showed a small decreasing trend for all-Indian monsoon rainfall in contrast to increasing trends in the driving GCM simulation. Contrary, the trend increased slightly in the RCP4.5 during the CCLM experiment, which was consistent with the driving GCM simulation.

Given the mixed results, it is important to address how the resulting monsoonal rainfall trends originate within the framework of a modeled future climate. Understanding the driving processes will bring more robust information for the projected inter-annual precipitation variability and associated trends in uncertainty. Possible causes behind the changes in the monsoonal precipitation on the basis of regional and global climate model projections will be addressed in the current study.

2. Data and Model

The simulations were performed with the non-hydrostatic, limited-area climate model CCLM (Steppeler et al., 2003; Asharaf et al. 2012). More details about the model are given on the community website (www.clm-community.eu).

We used data from three different climate simulations: two with the green house gas scenarios SRES B1 and RCP4.5, and one from an unperturbed control (CTL) experiment. The downscaled and the driving model data are hereafter referred to with suffixes linked to the names of the experiments CCLM and EC, respectively (CCLM_B1, CCLM_RCP45, CCLM_CTL for the downscaled, and EC_B1, EC_RCP, and EC_CTL for their forcing data). The initial and lateral boundary conditions were taken from simulations with the coupled atmospheric (ECHAM)-ocean (MPIOM) general circulation model MPI-ESM-LR.

Following Schär et al. (1999) and Asharaf et al. (2012), changes in three different year slices (2006–2035, 2041–2070, and 2071–2100) of the scenario experiments with respect to the present day climate (1971–2000) were analyzed to determine whether the precipitation results were derived primarily from changes in local evapotranspiration (surface effect) or whether the results were driven by external sources (remote effect) or were due to the efficiency effect.

3. Results and discussion

Figure 1 shows the summer monsoon rainfall trends that were computed from the linear fitting method on normalized (*i.e.*, data divided by the present day summer inter-seasonal mean) rainfall data. Significant decreasing rainfall trends were detected in some areas, such as in northwestern and central India, with the CCLM_B1 in contrast to their driving EC_B1 model data. It was explained in a previous study that the westward propagation of an attenuated number of depressions and frequent (compared to the driving model) heavy rainfall events were the major factors behind the decreasing rainfall trend in CCLM_B1 (Dobler and Ahrens, 2011). Both CCLM_B1 and EC_B1 simulations formed an increasing trend pattern over the southern part of India (including the Southern Ocean); however, the trend magnitude was more intense with CCLM. Over land, CCLM_RCP yielded somewhat similar positive trends to those from EC_RCP and EC_B1 with the exception of the CCLM_B1 simulated trends.

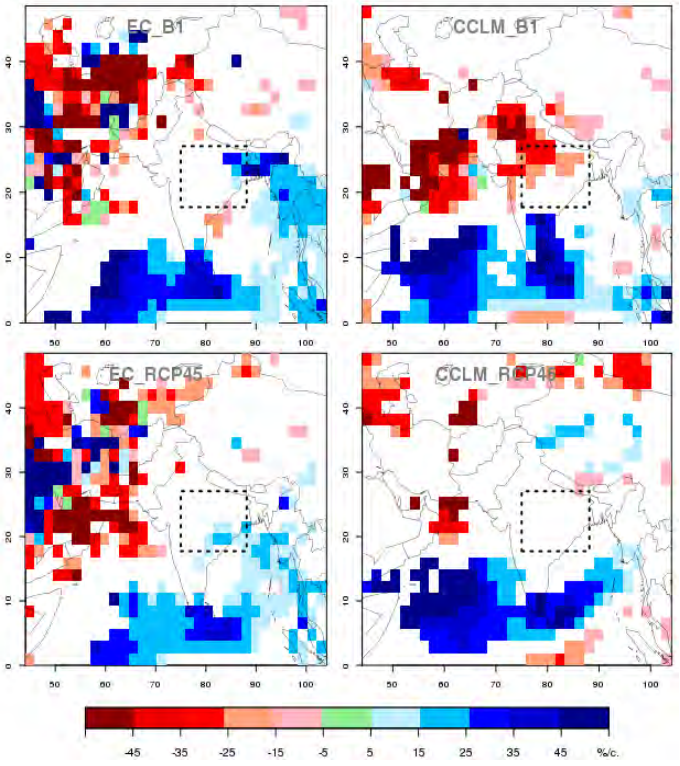


Figure 1 Linear trends in monsoon rainfall (%/century) during the time period 1971–2100. Dotted rectangle is the analysis region for changes in precipitation.

It was inferred from the analysis results (figure not shown) that changes in the efficiency generated precipitation will show decreasing trends throughout future time periods in CCLM and the driving EC models. But at the same time the remotely driven precipitation increased with time.

A comparison of the projections against the unforced steady state CTL simulations provides information about whether the trends in projections were drawn from external sources or due to internal variability in the model. Our results showed that the simulated increasing trends of the remote effect in the projections B1 and RCP4.5 were statistically significant (tested with Mann-Kendall at a 5% significance level) relative to the unperturbed CTL remote effect trends. The remote signal was more robust in RCP4.5 than in B1 simulations. On the contrary, decreasing trends in the efficiency effects of the projections were confined within the range of the CTL efficiency effect trends (figure not shown).

4. Conclusions

A comparison of the projected rainfall with rainfall in an unperturbed pre-industrial greenhouse gas control (CTL) simulation revealed the statistical significance of the increases in remotely induced precipitation under the future scenarios. The decreasing precipitation efficiency (in both GCM and RCM scenario simulations) varied within the range of the CTL variability and thus the interpretations of changes in precipitation. Hence, the projected rainfall trends for the Indian summer monsoon season remain uncertain and ambiguous since the remote effect and efficiency effect are the leading factors that drive changes in monsoonal precipitation (Asharaf et al., 2012).

References

Asharaf, S., A. Dobler, B. Ahrens (2012) Soil Moisture–Precipitation Feedback Processes in the Indian Summer Monsoon Season, J. Hydrometeor, 13, pp. 1461–1474

Dobler, A., and B. Ahrens (2011) Four climate change scenarios for the Indian summer monsoon by the regional climate model COSMO-CLM, J. Geophys. Res., 116, D24104

Schär, C., D. Lüthi, and U. Beyerle (1999) The soil-precipitation feedback: A processes study with a regional climate model, J. Climate, 12, pp. 722-741

Steppeler, J., G. Dom, U. Schattler, H. W. Bitzer, A. Gassmann, U. Damrath, and G. Gregoric (2003) Meso-gamma scale forecasts using the non-hydrostatic model LM, Meteorol. Atm. Phy., 82, pp. 75-96

Submesoscale hydrodynamic response of the Black Sea coastal zone to the surface forcing provided by the regional climate model

Bagaiev A.V., Ivanov V.A. and Demyshev S.G.

Marine Hydrophysical Institute of National Academy of Sciences of Ukraine, Sevastopol, Ukraine (bagaiev.andrii@gmail.com)

1. Introduction

Mixing processes on the shelf and continental slope at the scale of 1-10 km make an important contribution to the energy transfer (so called 'cascade') and transport of various tracers including oxygen and methane, which are relevant in the Black Sea. Since the issue of adequate representation of these processes is on the cutting edge in the modern high-res hydrodynamic modelling, the appearance of submesoscale oscillations have to be quantified and parameterized in order to be included in the regional models.

Thus, the subject of this study is developing a regional model of very-high-resolution capable of adequate representation of processes which occur on the Black Sea shelf and continental slope, and using the model simulations for analysing different appearances of the ocean waves.

2. Methods

An operational Black Sea forecasting system (Demyshev and Dymova, 2012) has been developed at Marine Hydrophysical Institute (Sevastopol, Ukraine) and is used to simulate mesoscale and submesoscale oscillations of the thermohydrodynamic fields.

The system is based on a three-dimensional finite-difference numerical free-surface model based on the primitive equations with Boussinesq and hydrostatic approximations. The governing equations for non-compressible fluid are written in the Cartesian coordinates using Lamb-Gromeka form. The problem is set up with respect to the three components of the ocean current, temperature, salinity and turbulent kinetic energy. Finite difference approximation on the 1.6 x 1.6 km horizontal Arakawa C-grid and 27 non-uniformly distributed vertical levels are implemented.

Horizontal turbulent mixing has been parameterized as a biharmonic Laplacian operator. The vertical mixing coefficients for momentum and tracers are calculated using the Pacanowski and Philander (1981) turbulence closure scheme.

The model is driven by the 12-hour wind stress field and thermohaline fluxes at the sea surface obtained via local (2.5 km) atmospheric model ALADIN (Farda et al., 2010). Zero fluxes of heat and salt and no-slip conditions as well as zero normal flux for the velocity field are applied at the bottom and lateral solid boundaries. Lateral open boundary conditions are defined through Dirichlet condition (for the inflow boxes), while momentum/heat/salt fluxes for the outflow boxes and prescribed on the annual basis.

To avoid the time-layer divergence the explicit second-order accuracy 'leap-frog' scheme with intermittent Matsuno scheme are used for the equations of motion. The equations for tracers are solved using the Total Variation Diminishing scheme (Fomin, 2006).

3. Results and Discussion

The present research is focused on the Southern Crimean Coastal area (from 32.9°–35.9° E to 44.0°–45.0° N) due to its recreation significance and anthropogenic overloading (Fig. 1). Additionally, an oceanographic platform located there, in Katsiveli, provides the data on interdisciplinary monitoring for calibration and validation of the regional models.

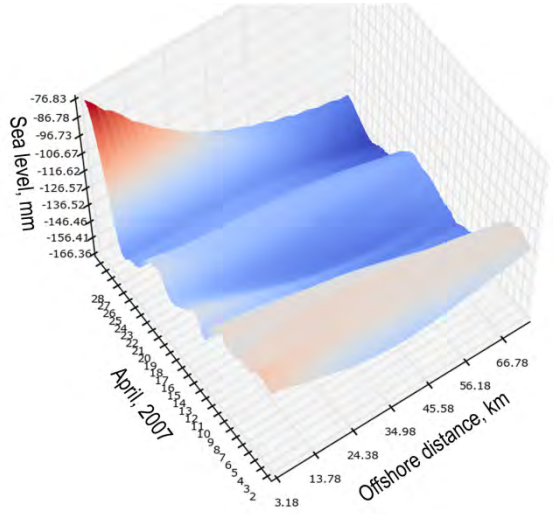


Figure 1. Sea surface height along an orthogonal to the Southern Crimean Coast section (modelling).

The period of April, 2007 is chosen to analyze the fluctuations of sea surface height (an example is shown in Fig. 1), kinetic energy, temperature and salinity. The simulations reveal that dynamics of the domain is controlled by the basin-scale Rim Current, that encounters the continental slope, and modulated by the regional high frequency currents.

Thermohaline profiles (Fig. 2) indicate the high vertical gradients, beginning of the seasonal thermocline formation at the depths of 25–30 m and the permanent halocline at the depth of 50 m. Pronounced asymmetry with a relatively thin layer of desalinated water at the top and a thick quasi-homogeneous high-saline bottom layer is a feature of the Black Sea as a strongly stratified basin. In the upper part of the halocline, the other feature takes place: cold intermediate layer (CIL) with the temperature below 8°C. CIL plays a key role in the heat transfer in the Black Sea and is extremely sensible to the regional climate change. Vertical profiles of the kinetic energy are under the direct influence of the wind stress.

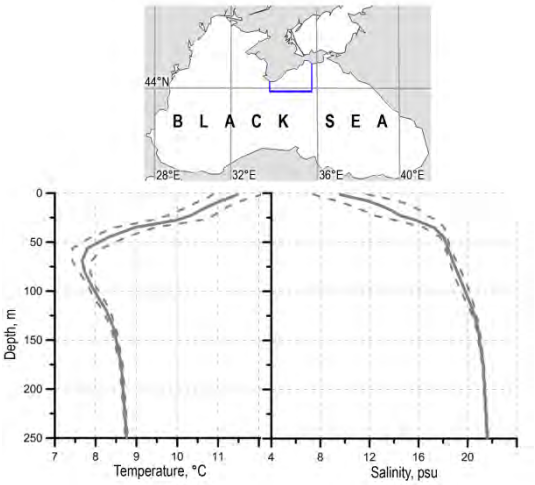


Figure 2. Model domain and the area of interest in blue (top panel) and the averaged profiles of temperature (bottom left) and salinity (bottom right) in April, 2007 (modelling).

During April 2007, Rim Current is located extremely close to the shore, feeding the oscillations by energy. A narrow shelf and abrupt continental slope serves as an efficient waveguide. Analysis of sea surface height has shown that the maximal period of oscillations exceeds 15 days (360 hr), which coincides with the variability of wind stress at synoptic scale. It was found that the oscillations of kinetic energy tend to gradually decrease seaward.

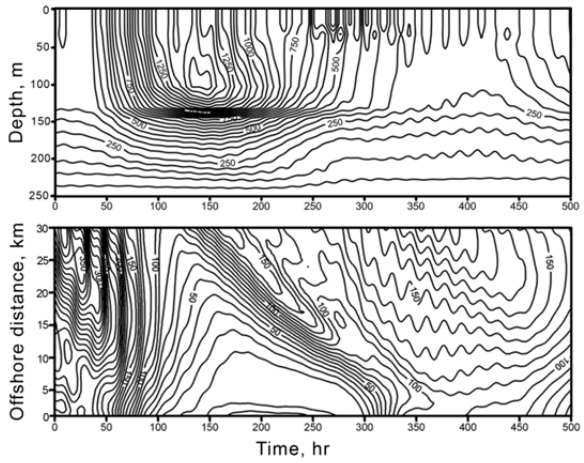


Figure 3. Hovmöller diagram for variation of the vertical profile of kinetic energy (top panel) and for kinetic energy along an orthogonal to the Southern Crimean Coast section at the depth of 20 m (bottom panel) (modelling).

Temporal evolution of the kinetic energy up to the depth of 250 m is clearly shown in the Hofmöller diagrams (Fig. 3, top panel), which allowed us to trace both the intensive higher frequency fluctuations and long-term ones with the period of 15 days.

Spatial and temporal evolution of the kinetic energy at the depth of 20 m (Fig. 3, bottom panel) demonstrates the oscillation with a period of 300 hr at open sea and mainly cyclonic propagation. Short-period oscillations with a period of about 150 hr are obtained near the coastline, exponentially shading seaward.

By means of FFT more than 50 frequencies and wavenumber PSDs are distinguished in the scalar fields including:

- barotropic seiches with the period of 2–10 hr that are typical of the observations in Southern Crimean Coastal area;
- inertial oscillations;
- baroclinic Poincaré waves with the periods of 9–16 hr;
- Kelvin waves with the period of 50 hr;
- coastaltrapped waves with the period of 30–70 hr.

The longest periods of the trapped waves, caused by the geostrophic adjustment to the regional wind forcing, vary from 120 hr to 220 hr. Oscillation parameters obtained with the high-resolution model are compared with the observations on oceanographic platform indicating quite a good quantitative agreement.

4. Conclusion

Development of the numerical models of very-high-resolution gives a powerful tool to investigate the interconnections among ocean circulation, stratification and various oscillations at different scales including meso- and sub-mesoscales. The high-resolution model is used to simulate circulation and thermohaline structure in the Black Sea.

A wide spectrum of meso- and submesoscale oscillations in sea surface height, temperature, salinity, and kinetic energy is found and verified by the observations. Wave patterns obtained demonstrate consistency with stratification and currents. Poincaré, Kelvin waves and trapped shelf waves has manifested itself as a part of mesoscale and submesoscale dynamical oscillations. That allows us to involve well known theoretical dispersion relations to estimate their parameters. Substantial increase in the amplitudes of barotropic seiches due to interaction with bottom topography in the coastal area is confirmed, which is relevant for the diagnostic skill assessment of the numerical model in the Black Sea. Inventory of all the barotropic and baroclinic oscillations, which were obtained in the model and observations on the oceanographic platform, is performed.

The similar researches are planned in the Southern Crimean Coastal area on a regular basis. The methodology worked out will be applied to the Caucasian Coastal area in the Black Sea.

References

Demyshev S.G., Dymova O.O. (2012) Energy analysis of mesoscale variability of the Black Sea water circulation based on hydrophysical fields numerical modeling for January – September 2006, Marine Hydrophysical Journal, No 5, pp. 40-49 (in Russian)

Pacanowski R.C., Philander S.G.H. (1981) Parameterization of vertical mixing in numerical models of tropical oceans, J. Phys. Oceanogr, Vol. 11., No 11, pp. 1443-1451.

Farda A., Déué M., Somot S., Horányi A., Spiridonov V., Tóth H. (2010) Model ALADIN as regional climate model for Central and Eastern Europe, Studia Geophysica et Geodaetica, Vol. 54, No 2, pp 313-332

Fomin V.V. (2006) Use of TVD schemes for numerical modeling of frontal zones of salinity in a shallow sea, Meteorology and hydrology, No 2, pp. 59-68.

Capitalizing on high resolution projections in application on regional climate change adaptation planning in Japan

Yingjiu Bai[1], Ikuyo Kaneko[1], Hikaru Kobayashi[1], Hidetaka Sasaki[2], Mizuki Hanafusa[2], Kazuo Kurihara[2], Izuru Takayabu[2], and Akihiko Murata[2]

[1] Graduate School of Media and Governance, Keio University, Fujisawa, Japan (bai@sfc.keio.ac.jp)

[2] Meteorological Research Institute, Tsukuba, Japan

1. Introduction

The Working Group I Contribution to the Fifth Assessment Report, a new report by the Intergovernmental Panel on Climate Change (IPCC 2013), noted that global mean surface temperature change for the period 2016–2035 relative to 1986–2005 will likely be in the range of 0.3–0.7 °C (medium confidence), and the increase of global mean surface temperature for 2081–2100 relative to 1986–2005 will be 0.3–0.7 °C (RCP2.6), 1.1–2.6 °C (RCP4.5), 1.4–3.1 °C (RCP6.0), or 2.6–4.8 °C (RCP8.5) (Representative Concentration Pathway: RCP). These projections highlight the need for immediate action, especially the development of substantive adaptation policies and measures on the local scale. The local governments have an increasing need to take measures locally to adapt to regional climate change; however, they have difficulty in accessing and understanding reliable information from climate experts, such that these governments lack the capability of producing local, community-based actionable policies. User-friendly tools to support decision making by non-expert government authorities are vital for the comprehension of high-resolution climate change information with documented uncertainties.

As mentioned above, a platform for providing "high-resolution reliable, timely, accurate, and appropriate" regional climate change data and local information is essential, as part of the local decision-making processes for adaptation planning on the local (community) scale. The principal objectives of this paper are: 1) to promote a platform for climate projection services and to construct a science-based database for empowering local people to learn and practice how they can respond individually to climate change; 2) to provide a tool based on a Geographic Information System (GIS) that allows the exchange of high-quality climatic data (observed and projected data) in an easily understandable and usable form for local policy makers; and 3) to address the adjustment of projection bias and quantify the uncertainty in future outcomes to transcribe regional climate projections into valuable forms for a wide variety of users. Kurihara (population 74,149 as of 31 August 2013; area 804.93 km^2) in Miyagi Prefecture, Japan was chosen for a pilot study. The region, in northwestern Japan, is an active volcanic and seismogenic area.

2. Data and Methods

In this study, we used a high-quality daily data set based on observations from the Japan Meteorological Agency and projections (5-km resolution) from the Non-Hydrostatic Regional Climate Model (NHRCM-5 km), following the SRES-A1B scenario developed by the Meteorological Research Institute (MRI) with JMA data. The NHRCM-5 km is a dynamic downscaling of results from the MRI-AGCM3.2S (20-km resolution). The MRI-AGCM3.2S output is successful in simulating characteristic features of the seasonal cycle of the East Asian summer monsoon and topographically regulated precipitation data and it has good agreement with observations.

Since the 1990s, GIS statistical analyses have been conducted stepwise for local governments in Japan. Similarly, we reproduced the GIS statistics from the Ministry of International Affairs and Communications, Japan and conducted them stepwise for local governments. Use of a common data set of information, including the topography and other key data sets (environmental, socio-economic, financial statistics) can be effective in fostering integrated local governments.

The mapping tool uses GIS to present the observed (station data) and projected (grid mesh data) data together. Mapping the observed and projected data on the same GIS domain allows the user to link other GIS data directly, such as societal and biological impact data as well as climate change data. Climate change mapping is a vehicle for readily depicting specific distribution changes and trends across temporal and geographic scales. This allows the projected information to become available to multiple users and encourages national and subnational governments to work closely with local authorities. Furthermore, vulnerability assessment by GIS includes an analysis of natural, social, and economic vulnerabilities, which are intended to inform decision makers by analyzing current and potential impacts of global change and by recognizing the pressures from other stresses. All data are computed and analyzed for regional tasks in the GIS domain and output is saved as a GIS database. Moreover, the user can transform all output easily into a KML/KMZ file, which is available for presentation in Google Earth. This capability is of great benefit to local (community) governments in depopulated regions in developed countries and undeveloped (poor) areas in developing countries, for obtaining information via the World Wide Web (WWW).

3. Regional climate change and adjusting bias of projections: a case study of Kurihara, Miyagi Prefecture

The climate informatics module comprises the spatial

distribution of projected climatic indices and their change, using daily, monthly, and annual weather data (focusing on temperature and precipitation) from three study periods. These are the present period (September 1980–August 2000), near-future period (September 2016–August 2036, and future period (September 2076–August 2096). As an example, Fig. 1 indicates the mean temperature changes and percentage changes in monthly precipitation in February and August in Kurihara, Miyagi Prefecture in both the near-future and future periods based on the NHRCM-5 km output.

It can be seen by comparing the near-future and future conditions that temperatures in Kurihara will increase by more than 0.7–1.8 °C and 0.7–3.1 °C (summertime), and 2.5–3.3 °C and 2.8–4.3 °C (wintertime), respectively. The increases in mean temperature in July and November are higher than in other months in Kurihara during the near-future and future periods, respectively. The level of statistical significance test of changes in monthly mean temperature is more than 99% ($p \leq 0.01$) except for August and January, more than 95–99% ($p \leq 0.05$) in August, and more than 90–95% ($p \leq 0.1$) in January during the near-future period. Moreover, the level of statistical significance test of changes in monthly mean temperature is more than 99% ($p \leq 0.01$) during the future period.

Percentage changes of monthly precipitation in the summer and winter are −15% to 23% and 9% to 2% in the future period, respectively. Moreover, maximum snow depth in February will decrease by 6–16 cm and 12–45 cm during the near-future and future periods, respectively. However, that depth in April will increase little in the near-future period. The level of statistical significance test of changes in monthly precipitation is more than 90% ($p \leq 0.1$) in January, February, and March only during the near-future period, and in January, February, April, and November only during the future period. One of the reasons for this is the topographic complexity, where the highest peak reaches 1,627.4 m.

To estimate and reduce possible structural modelling uncertainty, root mean square (RMS) errors and bias of monthly mean temperature and monthly precipitation were calculated. Observed data were available from 26 observation stations covering Kurihara. Twenty years of data in the present period were analyzed. Additionally, statistical analyses of correspondence were estimated between the model simulations and observations during the present period. Both monthly mean temperature and monthly precipitation indicate a significant correlation between model simulations and observations (r = 0.60 to 0.92; 520 samples). As an example, Fig. 2 indicates spatially strong correlation between the observations and NHRCM 5-km outputs of monthly mean temperature (February $R^2 = 0.77$; August $R^2 = 0.79$) and monthly precipitation (February $R^2 = 0.71$; August $R^2 = 0.60$) in February and August, respectively. These demonstrate the model experiments' ability to obtain probabilistic projections in the present period.

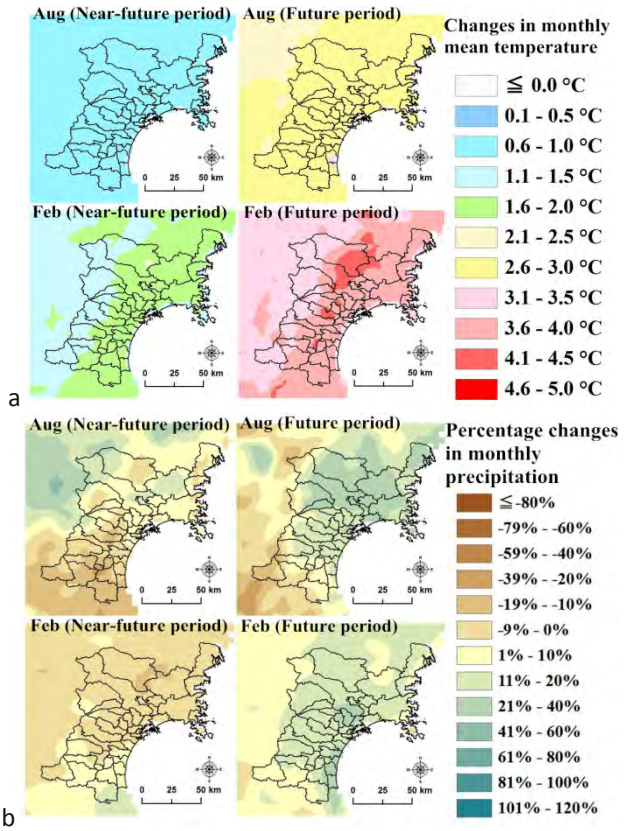


Figure 1. Mean temperature changes (a) and percentage changes in monthly precipitation (b) in February and August over Miyagi Prefecture in the near-future (2017–2036) and future (2077–2096) periods based on the NHRCM-5 km output

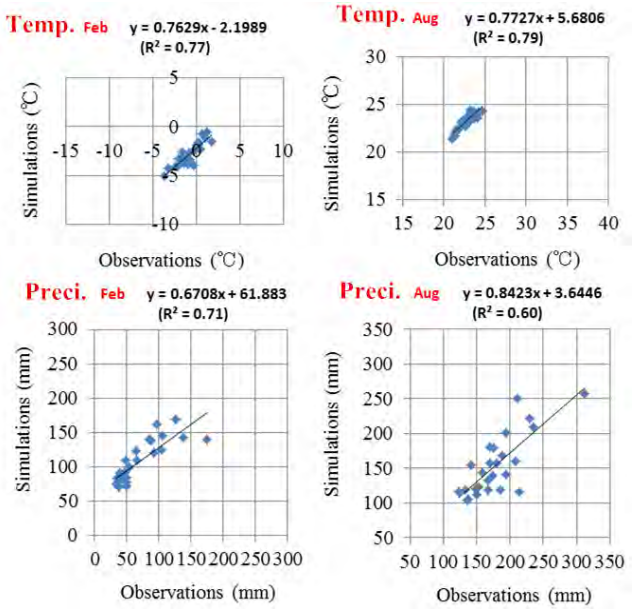


Figure 2. Samples of good correlation between observations and NHRCM-5 km outputs of monthly mean temperature (February $R^2 = 0.77$, August $R^2 = 0.79$) and monthly precipitation (February $R^2 = 0.71$, August $R^2 = 0.60$) in February and August (520 samples)

References

IPCC The Fifth Assessment Report "Climate Change 2013" (online versions) Working Group I: The Physical Science Basis. Summary For Policymakers. http://www.climatechange2013.org/images/uploads/WGI_AR5_SPM_brochure.pdf

A new high-resolution European region reanalysis dataset for RCM evaluation and calibration – first tests and comparison to other datasets

Lars Bärring[1,3], Tomas Landelius[2], Renate A.I. Wilcke[1], Per Dahlgren[2], Grigory Nikulin[1], Sèbastien Villaume[2], Per Undén[2], Per Kållberg[2]

[1] Rossby Centre, Swedish Meteorological and Hydrological Institute, Norrköping,, Sweden (lars.barring@smhi.se)
[2] Meteorological Analysis and Prediction Group, Swedish Meteorological and Hydrological Institute, Norrköping,, Sweden
[3] Centre for Environment and Climate Research, Lund University, Sweden

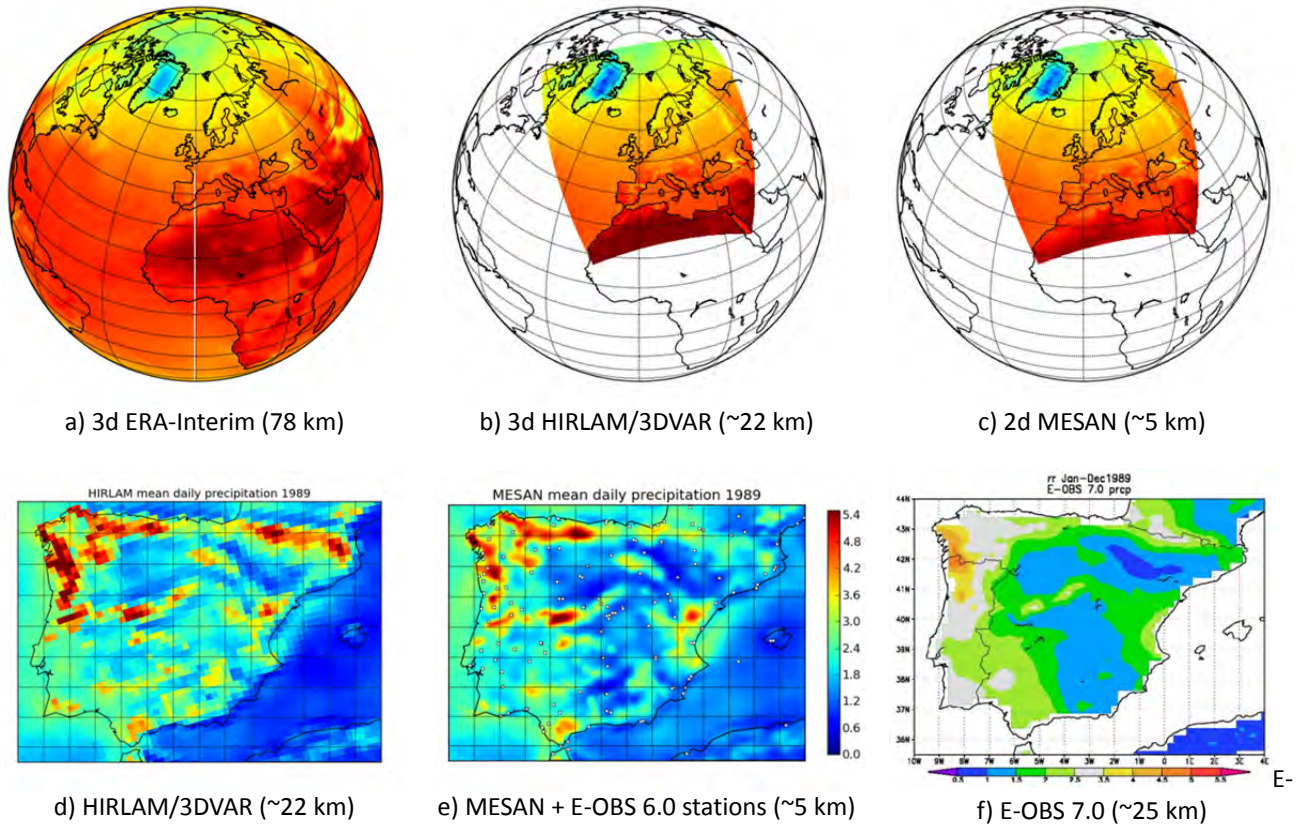
1. Introduction

As the resolution of regional climate models (RCMs) increases it becomes increasingly more difficult – and important – to find new evaluation and calibrations data-sets. In Europe there are several high-resolution (i.e. better than 10 km) datasets covering individual countries and European sub-regions. But for a consistent evaluation of the whole CORDEX or Ensembles domains the E-OBS datasets (Haylock et al, 2008) having a spatial resolution of ~25 km is, in practice, the only one.

Within the just recently concluded European project EURO4M (http://www.euro4m.eu/) new high-resolution datasets have been produced through regional reanalysis. Here we present a first test of how these datasets can be used to evaluate and bias-correct RCM simulations.

2. EURO4M reanalysis setup and output data

A version of the operational forecasting system HIRLAM was used is the key component fo the system. At the lateral boundaries the HIRLAM was forced by ERA-Interim data. Moreover, the large-scale flow was introduced into the variational assimilation by an additional term representing the ERA-Interim vorticity in the cost function (Dahlgren and Gustafsson, 2012). Within the domain observational data from the ERA-Interim observational database was ingested into the model using 3-dimensional variational assimilation. Through this



a) 3d ERA-Interim (78 km) b) 3d HIRLAM/3DVAR (~22 km) c) 2d MESAN (~5 km)

d) HIRLAM/3DVAR (~22 km) e) MESAN + E-OBS 6.0 stations (~5 km) f) E-OBS 7.0 (~25 km)

Figure 1. Upper row give and overview of the EURO4M regional reanalysis steps: (a) ERA-Interim is used as the large scale forcing of (b) the HIRLAM 3-dimensional variational assimilation system, which is (c) downscaled to ~5 km by 2-dimensional interpolation and analysis using MESAN. Lower row: Iberian Peninsula mean daily precipitation for year 1989 as an example of the high-resolution datasets:, (d) HIRLAM/3DVAR, (e) MESAN 2d optimum interpolation of E-OBS 6.0 daily station data, (f) E-OBS 7.0 gridded data a comparison.

system, HIRLAM/3DVAR, (Fig. 1a-b) the 3-dimensional state of the atmosphere, as well as relevant surface variables are saved for every 3 hours for the period 1981-2012 at a spatial resolution of 0.2° (rotated latitude/ longitude), or about 22 km.

From this dataset surface fields were extracted for downscaling using the MESAN system (Häggmark et al., 2000). The downscaling was done in two steps, first the HIRLAM 0.22°field was interpolated to the MESAN 0.05° (rotated latitude/longitude) grid (Fig. 1b-c). This was then used by MESAN as first guess in an optimum interpolation in which available surface observations were analysed. The data (Table 1) consists of 1286 x 1361 gridcells at a spatial resolution of ~5.5 km. Example results for precipitation is shown in Fig. 1d-f, and an evaluation of MESAN and other EUR4M reanalysis products carried out by Jermey & Renshaw (2014). They comcluded that MESAN compared favourably almost all aspects. Further technical documentation can be found at the EURO4M web site (http://www.euro4m.eu/).

Table 1. List of MESAN output variables. 24h data are valid for 00UTC to 24UTC.

2 m	Temperature	3 h
2 m	Minimum temperature	24 h
2 m	Maximum temperature	24 h
2 m	Relative humidity	3 h
2 m	Minimum relative humidity	24 h
2 m	Maximum relative humidity	24 h
surface	Accumulated precipitation	24 h
sea level	Pressure	3 h
10 m	U-component of wind	3 h
10 m	V-component of wind	3 h

4. Bias correction of CORDEX EUR-11 scenario data

We use the MESAN data as reference for bias-correcting RCA4 (Samuelsson et al., 2011) scenarios of the CORDEX EUR-11 domain (spatial resoultion ~12.5 km) and compare with corresponding bias corrections using E-OBS as reference as well as the regional Swedish high-resolution (4 km) dataset "PTHBV" based on the methodology developed by Johansson & Chen (2005). We use two variants of the quantile-mapping approach to bias-correction; the DBS methods which is a parametric variant, and a non-parametric empirical variant (Wilcke et al., 2013). Focus is on daily (24h) precipitation and daily mean temperature (i.e. average of the 3h temperatures).

Acknowledgements

This work has been supported by the European projects EURO4M and CLIP-C. Additional support has been provided by the Swedish research programme Mistra-SWECIA and from the Swedish University of Agricultural Sciences. We acknowledge the E-OBS dataset from the European project ENSEMBLES and the data providers in the ECA&D project (http://www.ecad.eu)

References

Dahlgren,P. & N. Gustafsson, 2012. Tellus A, 64, 15836,

Häggmark, L. et al. 2000. Tellus, 52A, 2-20.

Haylock, M.R. et al. 2008. J. Geophys. Res. (Atmos.), 113.

Jermey P. & R. Renshaw, 2014. Evaluation of precipitation in EURO4M reanalyses and downscalers. UK Met Office Forecasting Research Technical Report 589. EURO4M Deliverable D2.8. http://www.euro4m.eu/Deliverables.html

Johansson, B. & Chen, D. 2005: Climate Research, 29, 53-61.

Samuelsson, P.,et al., 2011. Tellus A, 63, 4-23.

Wilcke, R. A. I., et al. 2013. Climatic Change, 120(4), 871-887

Yang, W., et al., 2010: Hydrology Research, 41(3–4), 211-228.

On the integrated climate assessment using climate classification

Michal Belda, Tomas Halenka, Jaroslava Kalvova and Eva Holtanova

Dept. of Meteorology and Environment Protection, Fac. of Mathematics and Physics, Charles University, Prague, Czech Republic (tomas.halenka@mff.cuni.cz)

1. Motivation

The analysis of climate patterns can be performed for each individual climate variable separately, or the data can be aggregated, for example, using some kind of climate classification that integrates more climate characteristics. These classifications usually correspond to vegetation distribution in the sense that each climate type is dominated by one vegetation zone or eco-region. Thus, climate classifications can also represent a convenient, i.e., integrated, but still quite simple tool for the validation of climate models and for the analysis of simulated future climate changes.

New global simulations were performed for CMIP5 (Taylor et al., 2012) in framework of IPCC activity to assess climate change and huge amount of data available can be used for application and tests of further validation methods as well as the analysis of the future development of climate change. The use of climate clasifications can bring new, integrated view on the future development of individual regions around the world, and contribute to validation of the models when comparing the eco-regions location and area.

The same procedure can be used on the regional simulations (e.g. CORDEX activity) providing more detailed insight into the eco-regions development in different continents. Clearly, our main interest is in Europe, where two resolutions 0.44 and 0.11 degree of these experiments are available, which enable to assess the benefit of higher resolution.

2. Climate classification

The first quantitative classification of Earth's climate was developed by Wladimir Köppen in 1900 (Kottek et al. 2006). Even though various different classifications have been developed since then, those based on Köppen's original approach and its modifications, still belong to the most frequently used systems. For application on climate model outputs the Köppen-Geiger system (Köppen 1936, Geiger 1954) or Köppen-Trewartha modification (e.g., Trewartha & Horn 1980) are usually utilized.

The first digital Köppen-Geiger world map for the second half of 20th century was created by Kottek et al. (2006). They used the Climate Research Unit (CRU) TS2.1 dataset (Mitchell & Jones 2005) and the VASClim0v1.1 precipitation data (http://gpcc.dwd.de) for the period of 1951–2000. Prior to this, many textbooks reproduced a copy of one of the historical hand-drawn maps from Köppen (1923, 1931, or 1936) or Geiger (1961). The work of Kottek et al. (2006) was followed by Rubel & Kottek (2010) with a series of digital world maps covering the extended period of 1901–2100. These maps are based on CRU TS2.1 and on GPCC Version 4 data, and Global Climate Model (GCM) outputs for the period 2003–2100 were taken from the TYN SC 2.0 dataset (Mitchell et al. 2004). A new high-resolution global map of the Köppen-Geiger classification was produced by Peel et al. (2007). Climatic variables used for the determination of climate types were calculated from 4279 stations of the Global Historical Climatology Network (Peterson and Vose, 1997) and interpolated onto a 0.1° × 0.1° grid.

One of the first attempts to use the Köppen climate classification (KCC) to validate GCM outputs was presented in Lohmann et al. (1993). The observed climate conditions were represented by temperature data from Jones et al. (1991) and precipitation data from Legates & Willmott (1990). In Kalvová et al. (2003), the KCC was applied to CRU gridded climatology (New et al. 1999) for the periods of 1961–1990 and 1901–1921.

The modifications to the KCC proposed by Trewartha (Trewartha & Horn 1980) adjust both the original temperature criteria and the thresholds separating wet and dry climates (for details see Section 3). The resulting classification is usually denoted as the Köppen-Trewartha classification (KTC). Fraedrich et al. (2001) applied KTC to CRU data (New & Hulme 1997) with 0.5° × 0.5° resolution (excluding Antarctica). They analyzed the shifts of climate types during the 20th century in relation to changes in circulation indices (Pacific Decadal Oscillation and North Atlantic Oscillation). KTC types were also used by Guetter & Kutzbach (1990) who studied atmospheric general circulation model simulations of the last interglacial and glacial climates (126 and 18 thousand years before present). Furthermore, Baker et al. (2010) compared KTC types over China for historical (1961–1990) and projected future climates (2041–2070) simulated by the HadCM3 model for the SRES A1F1 scenario (Nakicenovic & Swart 2000). The KTC types were obtained by applying classification criteria for each grid box of the 30-year PRISM climatology (Daly et al. 2002) and to eco-regions defined through the Multivariate Spatio-Temporal Clustering algorithm. Feng et al. (2012) used the KTC to evaluate climate changes and their impact on vegetation for the area north of 50° N and the period of 1900–2099 focusing on the Arctic region. In addition to the observed data, the outputs of 16 AR4 GCMs (Meehl et al. 2007) under SRES scenarios B1, A1B, and A2 were used. de Castro et al. (2007) used the KTC for validation of nine regional climate models (RCMs) from project PRUDENCE (http://prudence.dmi.dk) over Europe for the period of 1961–1990 and for the analysis of simulated climate change for 2071–2100 under scenario SRES A2. They used the CRU climatology as the observed dataset (New et al. 1999). Wang & Overland (2004) quantified historical changes in vegetation cover in the Arctic (1900–2000) by applying the KTC to NCEP/NCAR reanalysis and CRU TS2.0 (New et al. 1999, 2000). Gerstengarbe &

Werner (2009) studied how global warming in the period of 1901–2003 influenced Europe by using the KTC types on the data with spatial resolution of 0.5° × 0.5° produced at the Potsdam Institute for Climate Impact Research.

3. Results

These results provides background for further validation of the new generation of CMIP5 GCMs (Taylor et al. 2012), analysis of recent climate change, and for the evaluation of simulated future climate change. Moreover, the classification is further used to the results of RCMs from EuroCORDEX activities.

Fig. 1 presents the example based on CMIP5 experiment, the overall areas of KTC types in Europe based on GCM forced simulations (1971-2000) are shown.

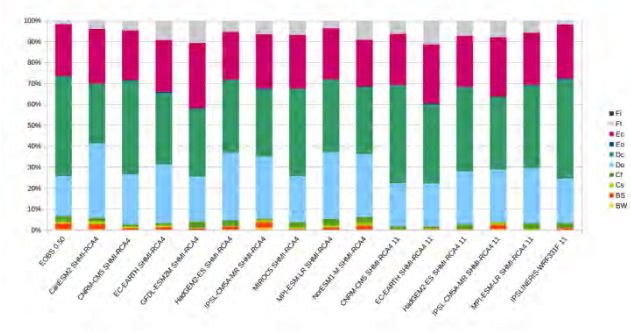


Figure 1. Overall areas of KTC types in Europe based on GCM forced simulations (1971-2000) of CMIP5 experiment.

Acknowledgements

Partial support is provided through program PRVOUK "Environmental Research" No. 02 of the Charles University.

References

Baker B, Diaz H, Hargrove W, Hoffman F (2010) Use of the Köppen – Trewartha climate classification to evaluate climatic refigia in statistically derived ecoregions for the People`s Republic of China. Clim Change 98:113–131

Daly C, Gibson WP, Taylor GH, Johnson GL, Pasteris P (2002) A knowledge-based approach to the statistical mapping of climate. Clim Res 22:99–113

de Castro M, Gallardo C, Jylha K, Tuomenvirta H (2007) The use of a climate-type classification for assessing climate change effects in Europe form an ensemble of nine regional climate models. Clim Change 81:329–341

Feng S, Ho CH, Hu Q, Oglesby RJ, Jeong SJ, Kim BM (2012) Evaluating observed and projected future climate changes for the Artic using the Köppen – Trewartha climate classification. Clim Dyn 38:1359–1373

Fraedrich K, Gerstengarbe FW, Werner PC (2001) Climate shifts during the last century. Clim Change 50:405–417

Geiger R (1954) In: Landolf-Börnstein-Zahlenwerte und funktionen aus Physik, Chemie, Astronomie, Geophysik und Technik, alte serie vol.3, Ch. Klassifikationen der Klimate nach W.Köppen. Springer, Berlin. pp. 603–607

Geiger R (1961) Überarbeitete neuausgabe von Geiger, R: Köppen-Geiger/Klima der Erde. (Wandkarte 1:16 Mill.) – Klett-Perthes, Gotha

Gerstengarbe FW, Werner, PC (2009) A short update on Koeppen climate shifts in Europe between 1901 and 2003. Clim Change 92:99–107

Guetter PJ, Kutzbach JE (1990) A modified Koeppen classification applied to model simulation of glacial and interglacial climates. Clim Change 16:193–215

Jones PD, Wigley TML, Farmer G (1991) Marine and land temperature data sets: a comparison and a look at recent trends. In: Schlesinger, M.E. (ed.) Greenhouse-gas-induced climatic change: a critical appraisal of simulations and observations, vol.19. Elsevier, Amsterdam, pp. 153–172

Kalvová J, Halenka T, Bezpalcová K, Nemešová I (2003) Köppen climate types in observed and simulated climates. Stud Geophys Geod 47:185–202

Kottek M, Grieser J, Beck Ch, Rudolf B, Rubel F (2006) World map of the Köppen-Geiger climate classification. Meteorol Z 15:259–263

Köppen W (1936) Das geographische System der Klimate. In: Köppen W, Geiger R (eds) Handbuch der Klimatologie, Gebrüder Borntraeger, Berlin, pp. C1–C44

Legates DR, Willmott CJ (1990) Mean seasonal and spatial variability in gauge-corrected, global precipitation. Int J Climatol 10:111–127

Lohmann U, Sausen R, Bengtsson L, Perlwitz J, Roeckner E (1993) The Köppen climate classiffication as a diagnostic tool for general circulation models. Clim Res 3:177–193

Meehl GA, Covey C, Delwort T, Latif M, McAvaney B, Mitchell JFB, Stouffer RJ, Taylor KE (2007) The WCRP CMIP3 multi-model dataset: A new era in climate change research, Bull Am Meteorol Soc, 88:1383–1394

Mitchell TD, Carter TR, Jones PD, Hulme M, New M (2004) A comprehensive set of high-resolution grids of monthly climate for Europe and the globe: the observed records (1901-2000) and 16 scenarios (2001-2100). Tyndall Centre of Climate Change Research, Norwich, working paper 55

Mitchell TD, Jones PD (2005) Improved method of constructing a database of monthly climate observations and associated high-resolution grids. Int J Clim. 25:693–712

Nakicenovic N, Swart R (eds.) (2000) Emission Scenarios. Cambridge University Press, p. 612

New M, Hulme M (1997) Development of an observed monthly surface climate dataset over global land areas for 1901-1995. In: Physics of Climate Conference, Royal meteorological Society, London, 29-30 October 1997

New M, Hulme M, Jones P (1999) Representing twentieth–century space-time climate variability. Part I: Development of a 1961-1990 mean monthly terrestrial climatology. J Clim 12:829–856

New M, Hulme M, Jones P (2000) Representing twentieth–century space-time climate variability. Part II: Development of a 1901-96 monthly grids of terrestrial surface temperature. J Clim 13:2217–2238

Peel MC, Finlayson BL, McMahon TA (2007) Updated world map of the Köppen-Geiger climate classification. Hydrol Earth Syst Sci 11:1633–1644

Peterson TC, Vose RS (1997) An overview of the Global Historical Climatology Network temperature database, Bull Am Meteorol Soc 78:2837–2849

Rubel F, Kottek M (2010) Observed and projected climate shifts 1901 – 2100 depicted by world maps of the Köppen-Geiger climate classification. Meteorol Z 19:135–141

Taylor K, Stouffer RJ, Meehl GA (2012) Overview of CMIP5 and the Experiment Design. Bull Am Meteorol Soc 93:485–498

Trewartha GT, Horn LH (1980) Introduction to climate. 5th edition. McGraw Hill, p. 416

Wang M, Overland JE (2004) Detecting arctic climate change using Köppen climate classification. Clim Change 67:43–62

Statistical downscaling for assessing GCMs, RCMs and vice versa

R.E. Benestad[1], A. Mezghani[1], O. Landgren[1], J-E.Haugen[1], H. Haakenstad[1]

[1] The Norwegian Meteorological Institute (rasmus.benestad@met.no)
[2] Institute for Regional Climate, University of Gdynia, Poland

1. Proposition

Regional climate models (RCMs) and empirical-statistical downscaling (ESD) are both tools for downscaling global climate model (GCM) results to locations and regions of interest. Often there is a tacit dichotomy between the different methods, with little overlap between the approaches. For instance, initiatives such as ENSEMBLES and CORDEX seem to have been dominated by the RCM community. However, ESD and RCMs offer more than just a description of the local climate characteristics.

2. Demonstration

We show how these tools can be used to assess models and increase our general understanding. For instance, ESD is a suitable tool for studying teleconnection patterns and we present results showing how it can be used to compare those found in the GCM or RCM results to those found in the reanalyses. Furthermore, the flexibility of ESD makes it attractive to assess ensembles of runs in a robust statistical framework. Finally, we show how GCM and RCM results are well-suited for providing 'pseudo-reality' data for testing ESD methods.

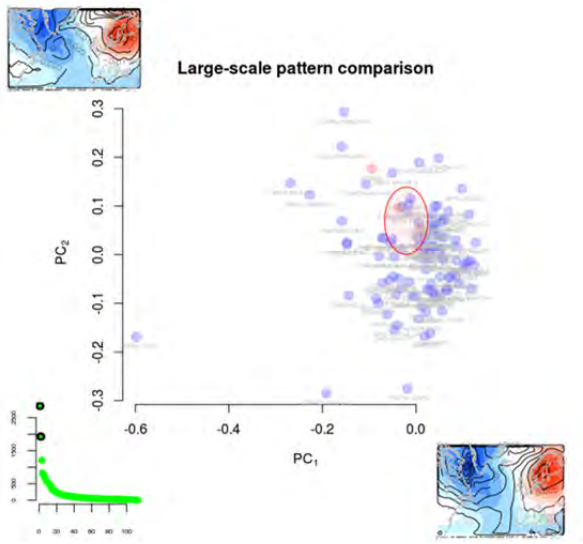


Figure 1. Example of a comparison between the teleconnection patterns in annual mean temperature associated with the local temperature in southern Norway between 5 reanalyses and 108 GCMs from CMIP5. Red symbols represent reanalyses and blue the GCMs. The maps shown at the axes are the two leading EOFs associated with the principal component predicted along the x and y axes. Lower left panel shows the eigenvalues. Red circle marks the mean ± 1 standard deviation of the reanalyses.

Figure 1 shows one example where ESD was used to identify teleconnection patterns in reanalyses and in GCM results. The teleconnection pattern is taken to be the large-scale predictor patern computed from ESD, based on a common interval. The predictor patterns from each reanalysis and GCM are stacked together into a new data matrix, after having been regridded to a common grid. An empirical orthogonal function (EOF; Lorenz, 1956)) analysis is then applied to the matrix containing the stack of patterns, and the different models are subsequently compared in terms of the two leading principal components (PCs; Figure 1).

The null-hypothesis is that the model results and the reanalyses follow the same statistical distribution, here qunatified in terms of the two leading PCs. The example shows that ERA40 gives a slightly different teleconnection pattern to the other reanalyses, and that the majority of the CMIP5 GCMs give results that are broadly consistent with the reanalyses (similar scatter). Three GCMs, however, are outliers, which may suggest that they are less suitable for downscaling temperature over southern Norway.

Figure 1 serves as just one example for how ESD can be used to assess RCMs and GCMs.

2. Open-source philosophy

All the results presented here are produced by an open-access and open-source R-package 'esd', which can provide an additional resource for the RCM community.

References

Lorenz, E.N., (1956). Empirical Orthogonal Functions and Statistical Weather Prediction (Sci. rep. No. 1). Department of Meteorology, MIT, USA. Journal

Creating a model consistent reference data set for bias correction applications

Peter Berg, Thomas Bosshard and Wei Yang

Swedish Meteorological and Hydrological Institute, Norrköping, Sweden (peter.berg@smhi.se)

1. Introduction

Bias correction of regional climate model (RCM) data has evolved over the last decade from simple corrections of mean values to highly detailed corrections of higher moments of the distribution (Yang et al. 2010; Berg et al., 2013a). This higher detail requires good observational reference data. However, with increasing spatial (and temporal) resolution of RCMs, there is less support from observational data over larger domains to make such corrections.

Pseudo observational data sets can be constructed by correcting e.g. monthly means in a reanalysis simulation to that observed, as was performed for the WFD (WATCH Forcing Data; Weedon et al. 2011). This is feasible, since the reanalysis data can be assumed sufficiently well synchronized with observational data on such coarser temporal scales. The finer temporal resolution in the WFD is scaled to have the observed monthly means, and can be used for applications at sub-daily resolutions, however, with underlying assumptions on the quality of the reanalysis model.

Here, we present an application of an extended version of the Weedon et al. (2011) method to produce a pseudo observational reference based on a spectrally nudged RCA4 Euro-CORDEX simulation at 0.11 degree resolution. The reference data is evaluated with existing high resolution observational data sets for Sweden, and applied for bias correction of additional members of the RCA4 Euro-CORDEX ensemble.

2. Model and Data

We apply the RCM RCA4, with a newly implemented spectral nudging method of constraining large scale circulation in the inner domain (Berg et al., 2013b). This is applied for temperature and horizontal winds at all model levels above the boundary layer with increasing nudging strength with height. The effect of the spectral nudging is that the internal variability of RCA4 is reduced and the atmospheric circulation over Europe remains closer to the driving data. Here, the ERA-Interim reanalysis product is applied as forcing data in order to be as closely synchronized with observations as possible (EUR11SN).

As observational reference, we use the PTHBV data set (Johansson and Chen, 2005) of 4 km resolution gridded temperature and precipitation observations for Sweden. This is a daily data set, and allows a detailed evaluation of the model at different timescales. The data set was remapped to the 0.11 degree grid of RCA4.

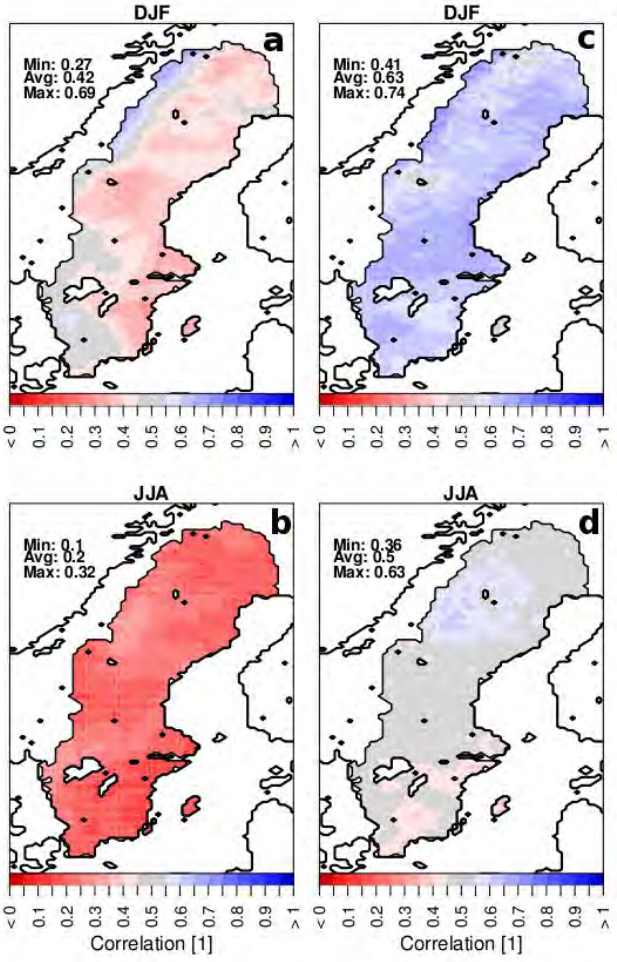


Figure 1. Temporal correlations of precipitation between RCA4 and PTHBV for a standard ERA-Interim downscaling simulation (a, b) and for a simulation with spectral nudging (c,d) for winter (top) and summer (bottom).

3. Method

The method of Weedon et al. (2011) is applied for corrections of precipitation and temperature of the spectrally nudged RCA4 simulation toward monthly means of the PTHBV data set (EUR11SNCORR). Briefly, the method is to scale all time steps of the model within a given month by the ratio of the observed and modeled monthly means.

Albeit the high spatial resolution of the original PTHBV grid, the actual resolution is not that high, due to coarse station density. We therefore make the assumption that the RCM is superior to the observational data set in describing the finer spatial details. Thus, before correcting the RCM simulation, we perform a spatial smoothing of the correction factors, such that spurious regional details are removed.

For bias correction, we use the DBS (Distribution Based Scaling; Yang et al., 2010) system and apply this to different RCA4 Euro-CORDEX simulations at 0.11 degree resolution. The standard approach is to apply the observational gridded data set as reference data for the corrections. Instead, we apply the newly constructed pseudo reference data. Because this data set is closer to the model in most aspects besides the monthly mean climatology, this means that finer spatial and temporal variability of the RCM remain similar to the original simulation after bias correction, whereas the coarser information is corrected towards observations.

4. Results

The spectrally nudged simulation shows significantly increased daily temporal correlations for precipitation with the PTHBV data set, compared to a standard simulation with lateral boundary forcing (Figure 1).

The EUR11SN simulation produces an average wet bias of 13% across Sweden. It shows good performance regarding the intensity distribution on wet days compared to PTHBV, besides an overestimation of extreme values (Figure 2). This overestimation is reduced after the correction towards PTHBV, which is however a result of the wet bias. Compared to station observations, the extreme intensities are within the observational uncertainty. Note that we do not strive to reproduce the PDF of the observations in high detail, although our trust in the model for making the new reference data set depends on similarity in such characteristics.

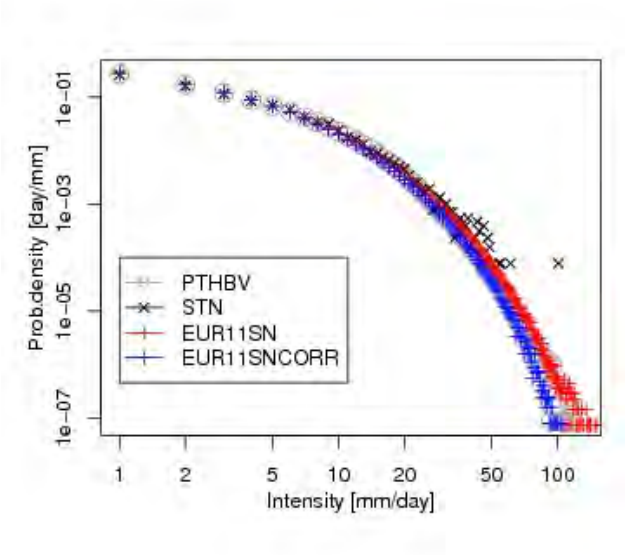


Figure 2. Precipitation intensity PDFs for PTHBV, stations observations (STN) and the spectrally nudged simulations with (EUR11SN) and without (EUR11SNCORR) monthly mean corrections.

5. Discussion

We will present further results from the analyses of the constructed RCA4 pseudo observational reference regarding also sub-daily statistics, and more details about the variability and performance of the updated correction algorithm. Furthermore, we will present results for a sub-set of the RCA4 Euro-CORDEX ensemble and their bias corrections with DBS for Sweden, using the new reference data set as well as corrected directly with the PTHBV data set.

References

Berg P., H. Feldmann, H.-J. Panitz (2013a) Bias correction of high resolution regional climate model data, Journal of Hydrology, 448, pp. 80-92

Berg P., R. Döscher, T. Koenigk (2013b) Impacts of using spectral nudging on regional climate model RCA4 simulations of the Arctic, Geoscientific Model Development, 6, pp. 849-859

Johansson B., D. Chen (2005) Estimation of areal precipitation for runoff modelling using wind data: a case study in Sweden, Climate Research, 29, pp. 53-61

Weedon G., S. Gomes, P. Viterbo, W.J. Shuttleworth, E. Blyth, H. Österle, J.C. Adam, N. Bellouni, O. Boucher, M. Best (2011) Creation of the WATCH forcing data and its use to assess global and regional reference crop evaporation over land during the twentieth century, Journal of Hydrometeorology, 12, 5, pp. 823-848

Yang W., J. Andréasson, L.P. Graham, J. Olsson, J. Rosberg, F. Wetterhall (2010) Distribution-based scaling to improve usability of regional climate model projections for hydrological climate change impacts studies, Hydrology Research, 41, 3/4, pp. 211-229

Evaluation of regional climate model simulations over Central Europe using the new high-resolution HYRAS precipitation climatology

Susanne Brienen, Barbara Früh, Andreas Walter, Kristina Trusilova and Paul Becker

Deutscher Wetterdienst, Offenbach, Germany (susanne.brienen@dwd.de)

1. Introduction

As regional climate model simulations are run on constantly increasing horizontal grid spacings, also observational data at corresponding resolution are required for the evaluation of the model performance at this scale. The aim of this paper is to investigate the added value of using the new HYRAS data set compared to coarser gridded observations for the evaluation of simulations with the COSMO-CLM model.

2. Data

A new high-resolution precipitation climatology (HYRAS version 2.0) is available covering the river catchments in Germany and neighbouring countries at 5km grid spacing (Rauthe et al., 2013). The data cover the period of 1951-2006 at daily resolution. The interpolation is based on a multiple linear regression considering orographical conditions and an inverse distance weighting.

Simulations with the COSMO-CLM model (Rockel et al., 2008) have been made for Europe for three years (2002, 2003 and 2006, corresponding to a wet, dry and normal year) and with three different grid spacings: 7, 14 and 28 km (referred to as CLM7, CLM14, CLM28). Initial and boundary conditions come from the global model GME (Majewski et al., 2002).

In addition, we compare our results with three other data sets with different resolution:

- E-OBS gridded observations version 8.0 (Haylock et al., 2008): 28 km
- ERA-Interim reanalysis data (Dee et al., 2011): 79 km
- The driving model GME: 60 km (2002/2003)/ 40 km (2006)

Note that the GME output was remapped to the E-OBS grid as the model uses an icosahedral-hexagonal grid.

3. Methods

Different precipitation characteristics are analyzed over ten river catchment areas in Central Europe (Fig 1). The difference in resolution representing the areas between the HYRAS and E-OBS data set is visible. As precipitation indices we selected the total precipitation on wet days (TOT; threshold for wet days: 1mm), number of wet days (nwet), maximum number of consecutive dry days (CDD), 95th quantile (Q95), number of days with precipitation >10mm (R10mm) and maximum precipitation amount on 5 consecutive days (RX5day). The analysis is done for the whole year as well as for summer (JJA) and winter (DJF). General evaluation metrics include bias, RMSE, correlation and quantiles. Also the spatial variability is discussed using Taylor diagrams.

To estimate the error which would be made by a too coarse observational grid we compare the original HYRAS data set at 5 km grid spacing with an aggregated version of 5x5 grid cells (i.e. 25 km resolution) by means of linear regression.

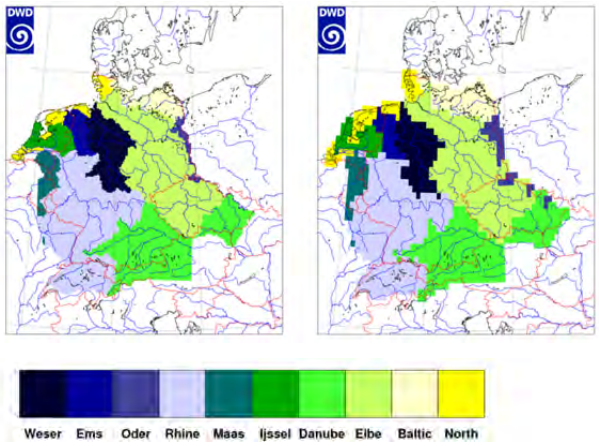


Figure 1. The analyzed river catchments in the resolution of HYRAS (left) and E-OBS (right).

4. Results

In the larger river catchments (Rhine, Elbe, Danube, Weser) we can compare all the data sets. We find that the variability between the data sets is very large (Table 1). This can be seen also when looking at the different indices. The different resolutions of the COSMO-CLM simulations seem to have less impact compared to the differences between types of data sets. On a seasonal basis, the COSMO-CLM simulations exhibit contrasting deviations to HYRAS in JJA and DJF, whereas for ERA-Interim they are very similar in both seasons. The indices calculated from E-OBS are in good agreement with those from HYRAS in DJF, but show some deviations between 5 and 10% in JJA.

Table 1. Grid spacing (ΔX), mean annual precipitation (P) averaged across the whole HYRAS domain, its deviation to HYRAS (ΔP), spatial variability (maximum – minimum precipitation, var) and its deviation to HYRAS (Δvar).

Data set	ΔX (km)	P (mm/a)	ΔP (%)	var (mm/a)	Δvar (%)
HYRAS	5	821	0	1971	0
E-OBS	28	792	-3	1342	-32
GME	60/40	711	-13	2802	+42
ERA-Int.	79	891	+9	820	-58
CLM7	7	940	+14	2355	+19
CLM14	14	991	+21	2489	+26
CLM28	28	919	+12	1786	-9

For the smaller catchment areas, a comparison of all data sets is not possible due to the low number of grid points representing the region. Thus, the comparison is made only for a subset of the data; for the smallest catchments only for CLM7 and HYRAS.

For the comparison of the original and upscaled HYRAS data we find that the upscaled version underestimates daily precipitation amounts with a regression slope of 1.04 in summer and 1.03 in winter (explained variance: 0.94 in JJA and 0.96 in DJF). Also the RMSE is higher in summer. The regression slope does not show any spatial structure, whereas the RMSE is higher in mountain areas. For the different precipitation indices we see also underestimation, in particular an underestimation of spatial maximum values by 5-20% depending on index and season (mostly larger in JJA).

5. Conclusions

The new precipitation climatology HYRAS is suitable for the evaluation of high-resolution regional climate model simulations. In the larger catchment areas, a large variability of different data sets is found. If interested in smaller catchments, a comparison with coarser-resolved observations is not always possible due to low number of grid points. The added value of a high-resolution data set such as HYRAS is seen also in the underestimation of different precipitation characteristics by the upscaled 25 km version by up to 20%.

The results of this study are in preparation to be published in Brienen et al. (2014).

References

Brienen, S., B. Früh, A. Walter, K. Trusilova, P. Becker (2014) A Central European precipitation climatology – Part II: Added value of the high-resolution HYRAS climatology for COSMO-CLM evaluation, in preparation

Dee, D. P., with 35 co-authors (2011) The ERA-Interim reanalysis: configuration and performance of the data assimilation system. Quart. J. R. Meteorol. Soc., 137, pp. 553-597

Haylock, M.R., N. Hofstra, A.M.G. Klein Tank, E.J. Klok, P.D. Jones, M. New (2008) A European daily high-resolution gridded dataset of surface temperature and precipitation. J. Geophys. Res (Atmospheres), 113, D20119, doi:10.1029/2008JD10201

Rauthe, M., H. Steiner, U. Riediger, A. Mazurkiewicz, A. Gratzki (2013) A Central European precipitation climatology – Part I: Generation and validation of a high-resolution gridded daily data set (HYRAS), Meterologische Zeitschrift, 22, pp. 235-256, doi: 10.1127/0941-2948/2013/0436

Rockel, B., A. Will and A. Hense (eds.), 2008: Regional climate modeling with COSMO-CLM (CCLM), Meteorologische Zeitschrift, 17(4), pp. 347

Climate Change Projections over CORDEX East Asia Domain using Multi-RCMs

Dong-Hyun Cha[1], Ga-Young Kim[1], Chun-Sil Jin[1], Dong-Kyou Lee[2], Seok-Geun Oh[3] and Myoung-Seok Suh[3]

[1] Ulsan National Institute of Science and Technology, Ulsan, Korea (dhcha@unist.ac.kr)
[2] Seoul National University, Seoul, Korea
[3] Kongju National University, Kongju, Korea

1. Introduction

High-impact weather and climate events associated with recent climate change have occurred more frequently and their intensities tend to increase. Detailed estimates of future climate change have been become much important to reduce the societal impact of climate change. The Korean Meteorological Administration (KMA) and 4 universities in Korea have conducted the experiments using multi-RCMs to generate regional climate change estimations for CORDEX East Asia domain (Suh et al., 2012). In this study, we evaluate the results from historical runs and estimate future projections for a RCP emission scenario.

2. Model and Data

In this study, global climate change scenario by KMA HadGEM2-AO is dynamically downscaled using 5 RCMs (i.e., HadGEM3-RA, RegCM4, MM5, WRF, and RSM). All RCMs have 50km horizontal resolution and reproduce continuous 70-year regional climate over CORDEX East Asia domain (Giorgi, 2009). RCP 4.5 and 8.5 scenarios are downscaled using multi-RCMs. We evaluate 25-year (1981-2005) historical runs against observations and analyze 25-year (2025-2049) future projections only for RCM 8.5 by comparing with historical runs to estimate future changes. In the evaluation of historical runs, GPCP and CRU data are used for precipitation and surface air temperature, respectively.

3. Result

In the evaluation of historical runs, all RCMs overestimate precipitation over the subtropical western North Pacific, while they underestimate precipitation around the Bay of Bengal (Fig. 1 left panels). In contrast, all models have relatively small biases for the precipitation over the mid-latitudes. In general, RegCM4 and WRF have better statistics in the simulation of precipitation over CORDEX East Asia domain. One possible reason for large precipitation biases over the tropical and subtropical oceans can be uncoupled air-sea interactions in all RCMS.

For the simulation of surface air temperature, all models have cold biases over China continent compared with the CRU observation (Fig. 1 right panels). RegCM4 has significant warm bias in the high-latitudes and RSM has the largest cold bias in the mid-latitudes. RegCM4 and MM5 have better statistics in the simulation of surface temperature.

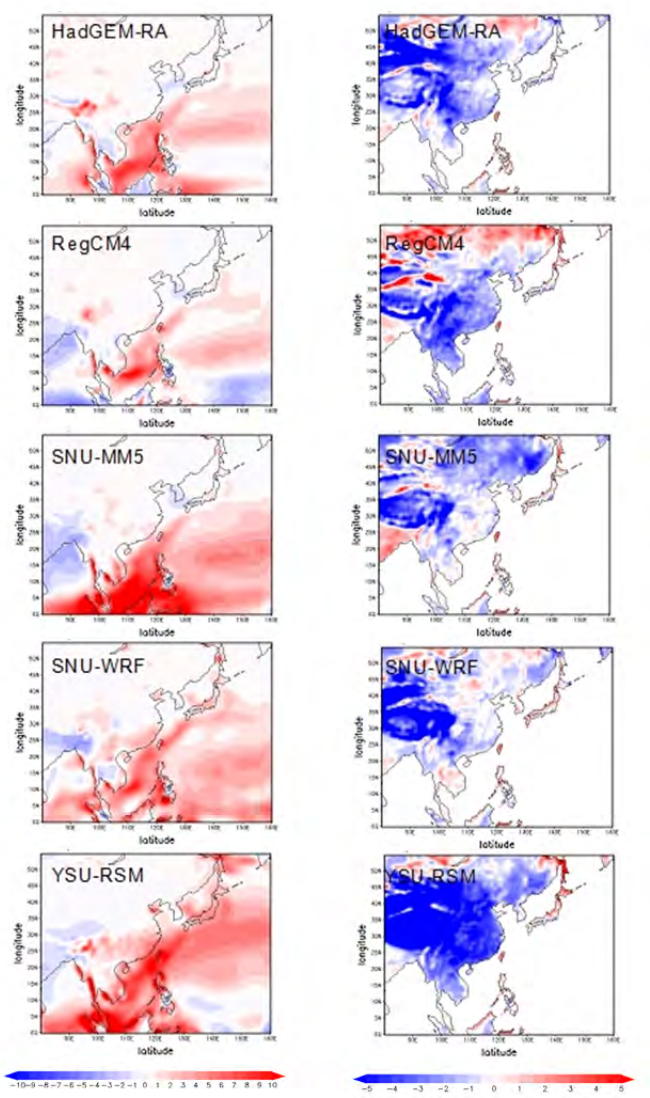


Fig. 1. Difference in 25-year mean annual precipitation (mm day^{-1}, left panels) and surface air temperature (^{o}C, right panels) between simulations and observations.

In the future projections, all models have similar changes in precipitation such as increasing precipitation over the tropical oceans and slightly decreasing precipitation over the East China Sea (Fig. 2 left panels). In the mid-latitudes, convective precipitation tends to increase due to the enhanced convective instability, while non-convective precipitation tends to decrease slightly due to the changes in subtropical high and monsoon circulation.

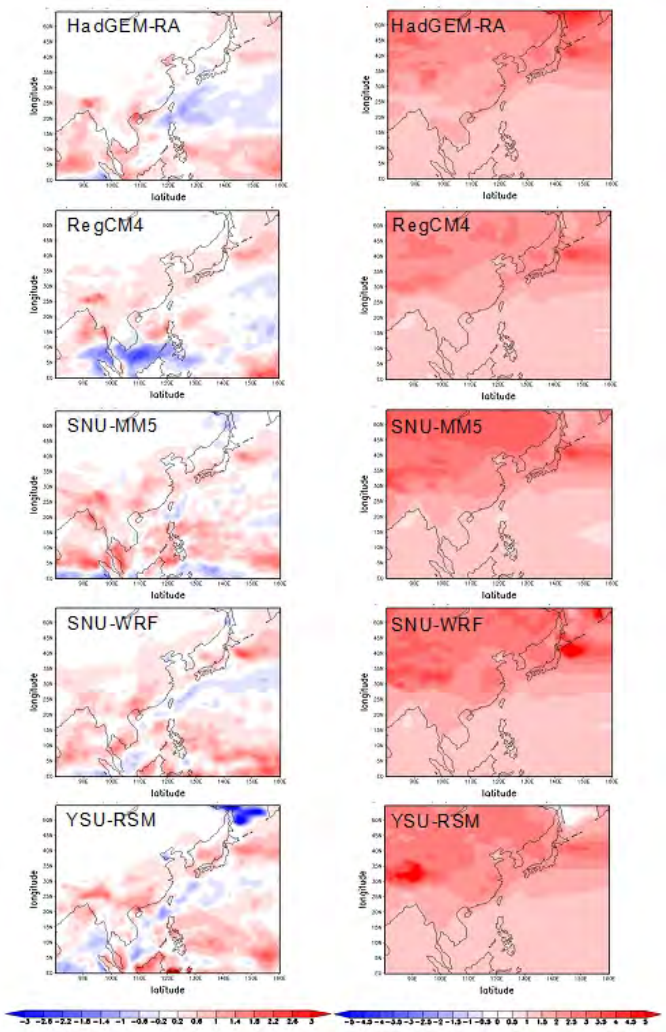


Figure 2. Difference in precipitation (mm day^{-1}, left panels) and surface air temperature (^{o}C, right panels) between present 25-year mean and future 25-year mean.

For surface air temperature, warming tendency is captured by all models and the tendency is larger in higher latitude regions. The warming surface air temperature is related to the increase in longwave radiation, which leads to prominent increase in minimum surface air temperature.

References

Giorgi Filippo, Colin Jones and Ghassem R. Asrar (2009) Addressing climate information needs at the regional level: the CORDEX framework.

Suh, M. S., S. G. Oh, D. K. Lee, D. H. Cha, S. J. Choi, C. S. Jin, and S. Y. Hong (2012) Development of new ensemble methods based on the performance skills of regional climate models over South Korea. *J. Clim*., doi:10.1175/JCLI -D-1100457.1.

Climate information for decision making – the challenge of responding to user needs

Diane Chaumont, David Huard and Isabelle Charron

Ouranos, Montréal, Canada (chaumont.diane@ouranos.ca)

1. Introduction

Planning and adapting to a changing climate requires credible information about the magnitude and rate of projected changes. The *Climate Scenarios and Services Group* at Ouranos specializes in the development and production of climate scenarios adapted to users' needs based on state-of-the-art methodologies, climate models and observational data. The group works in a multidisciplinary environment, in close collaboration with the Climate Simulations and Analysis group, dedicated to the production of regional simulations with the CRCM, and the VI&A group, which acts as a network hub and liaison officers with stakeholders and project managers. The proximity to users has the advantage of helping us adequately identify climate information needs, anticipate requests and proactively research new climate products.

2. Scenario generation

Over a period of several years, Ouranos has developed a consistent method to develop scenarios and to communicate them effectively (Huard et al., 2014). First, an objective approach is applied in order to select representative sub-sets of a projection ensemble that include the model and emission-based uncertainties without over-burdening the user with information. Second, Ouranos has developed a suite of empirical post-processing approaches appropriate to each particular variable and to the needs of impact and adaptation studies (Themeßl et al. 2010). Finally, major efforts have been devoted to developing effective ways to communicate scenarios. Our method of scenario generation aims at being transparent and rigorous (i.e. by taking into account the major sources of uncertainty), while at the same time remaining simple enough that results can be readily understood by end-users.

3. Requirements for climate simulations

The fact that these end-users work with different physical contexts, have varying requirements in terms of climate information complexity, and come with uneven levels of climate expertise has led Ouranos to tailor climate information through a case by case approach. Charron (2014) published the resulting framework linking the diverse needs of users and the type of useful climate information. Among the choices that must be made is the development of scenarios based on regional climate models versus/or in addition to those based on global climate models. Hence, although there is high confidence that regional climate simulations add values compared to global simulation in complex terrain and for mesoscale phenomena (Flato et al. 2013), the benefits of including RCM simulations in the climate scenarios produced at Ouranos are not always obvious or straightforward from a climate service perspective. In particular, the restricted size of regional ensembles available over North America does not allow us to capture the uncertainty from the driving GCM, which is typically the leading source of uncertainty.

3. Anticipating needs for the coming decade

Climate service providers will face a number of challenges ahead over the coming years. Our users, many of which are in the engineering community, are increasingly asking for robust information about projected climate extremes. Being by definition rare and, often localized events, extremes are considerably harder to estimate reliably than mean values, and call for scenarios built from very large ensembles of high-resolution simulations.

Another challenge is that the most rigorously crafted scenarios may very well never be used by stakeholders in their day-to-day operations or strategic planning. Indeed, many of our past projects, while methodologically sound, have had little impact on how industries or government manage their assets. The gap between climate scenarios and adaptation action will need to be bridged for climate science to have an effective impact on decision-making. The anticipated needs will undoubtedly pose certain challenges for the regional modeling community.

References

Charron, I. (2014). A Guidebook on Climate Scenarios: Using Climate Information to Guide Adaptation Research and Decisions. Ouranos. Copies of this guidebook can be downloaded from http://www.ouranos.ca.

Flato, G., Marotzke J., Abiodun B., Braconnot P., Chou S.C., Collins W., Cox P., Driouech F., Emori S., Eyring V., Forest C., Gleckler P., Guilyardi E., Jakob C., Kattsov V., Reason C., Rummukainen M. (2013) Evaluation of Climate Models. In: Climate Change 2013: The Physical Science Basis. Contribution of Working Group I to the Fifth Assessment Report of the Intergovernmental Panel on Climate Change [Stocker, T.F., D. Qin, G.-K. Plattner, M. Tignor, S.K. Allen, J. Boschung, A. Nauels, Y. Xia, V. Bex and P.M. Midgley (eds.)]. Cambridge University Press, Cambridge, United Kingdom and New York, NY, USA

Huard D., Chaumont D., Logan T., Sottile M.F., Brown R.D., Gauvin-St-Denis B., Grenier P., Braun M. (accepted) A Decade of Climate Scenarios – The Ouranos Consortium Modus Operandi, BAMS.

Themeßl M.J., Gobiet A., Leuprecht A. (2010) Empirical-statistical downscaling and error correction of daily precipitation from regional climate models. International Journal of Climatology, doi:10.1002/joc.2168.

Potential Added Value of COSMO-CLM in Simulating Extreme Precipitation over East Africa

Bedassa R. Cheneka, Barbara Früh, Susanne Brienen, Fröhlich Kristina and Shakeel Asharaf

Deutscher Wetterdienst, Offenbach, Germany (beregassa@gmail.com)

Small scale features often resolve by a regional climate model (RCM). In this study, we investigate the potential added value of the RCM COSMO-CLM (CCLM) for two extreme rainfall years (1987 and 1999) in East Africa. The RCM simulations are derived from the global coupled atmospheric ocean model MPIESM, while the models were initialized at the beginning of May month. For investigating the potential added values, four regions (viz., North Ethiopia (EN), South Ethiopia (ES), South Sudan (SS), and Sudan(S)) are considered and the analysis is done for daily and eight days aggregated precipitation value, covering from June to September (JJAS) months. Results show that the RCM has potential to capture the regional meso-scale features over East Africa. RCM has added value over East Africa at 95% and 90% extreme precipitation which is more dominant over North Ethiopia a region where high mountainous influences moderate local precipitation. The

1. Introduction

Uncertainties associated with the model physics or domain geometry (size and vertical resolution) (B.Pohl et al., 2011) are a serious concern over East Africa. Local processes and internal model physics are the key elements in determining the precipitation change signal simulated by nested regional model in large domain (Africa CORDEX)experiment, especially over equatorial and tropical regions (Mariotti et al., 2011). Recent modeling study suggests that COSMO-CLM Regional Climate Model (CCLM) is generally able to reproduce the overall features of the African climate, although some deficiencies are evident (Pantiz, 2013).

2. Added Value Concept

The potential advantage of an RCM over a GCM is representation of small scale features (both in horizontal and temporal scales), which are often missed in GCMs (Di Luca, 2011).

RCMs added value in climate variability in scales that are not explicitly resolved in GCMs simulation (AV1), (Di Luca, 2011). A necessary condition for RCM to produce AV1 is that the contribution of the simulated fine-scale details on climate statistics is not negligible.

3. Data and Methods

COSMO-CLM is applied in order to simulate JJAS precipitation over East Africa for the two years (1987 and 1999) extreme precipitation. The simulated precipitation is aggregated spatially and temporally to filter the scale separation approach (Giorgi, 2002 and Di Luca, 2011). Up-scaling high resolution regional climate model to coarse resolution regional climate model is called virtual general climate model (vGCM) is done by aggregating precipitation $pr^{n,m}$ where n, represents spatial scale at (0.22°, 0.44°, 0.88°, 1.66°, 3.52° and 7.04°) and m represents temporal scale (1, 2, 4, and 8 days). Cumulative frequency, local maximum, potential and relative potential precipitation is computed over each region (EtN, EtS, S and SS).

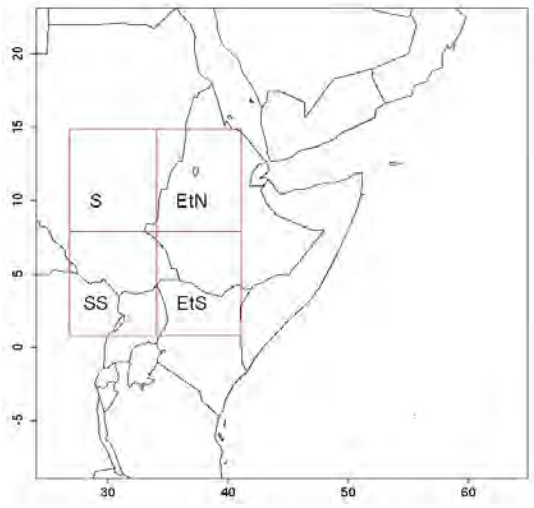


Figure 1. East Africa with COSM CLM simulation domain and areas where different potential and relative potential added value is tested

4. Frequency Distribution of Precipitation

The relative frequency of precipitation was calculated for different binned spatial precipitation over the different regions of East Africa.

From the figure (2), over all regions we observe that high frequency distributions of lowest precipitation (<4mm) occur at the high resolution 0.22^0, whereas low to moderate precipitation (8-32 mm/day) frequency occurs at vGCM scale. High precipitation (>32mm/day) frequency is simulated in high resolution scale.

The observation of the gap between the cumulative frequency of high resolution and vGCM over the course helps us decide where mesoscale is more prominent. The cumulative frequency range between high resolution precipitation and coarse resolution (vGCM) precipitation is shown in Fig. 2. Figure 2a and Figure 2b shows that the increase of the range of the spread between different grid resolutions is directly proportional to added value of RCM. The range between different grid resolution is decreases in figure 2c and 2d where this is an indication that relative to other regions of the study domain the added value of RCM less. We will see in detail in section 5.3. We aggregated the precipitation temporal similar to what we have done for spatial aggregation from daily scale to eight day. In eight day we find out that due to

temporal arithmetic mean compute RCM added value is decreased relative to daily RCM added value.

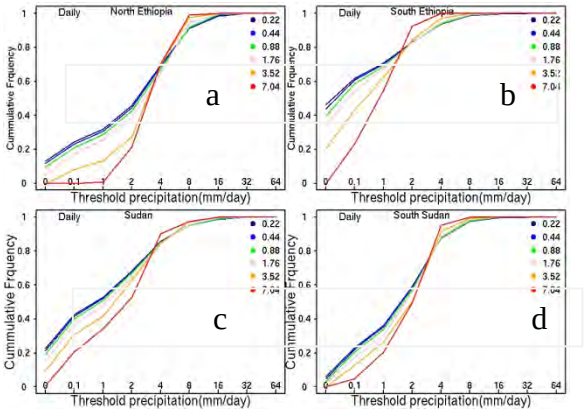


Figure 2. Daily cumulative frequency of precipitation over different spatial scales over East Africa

Spatial Maximum Precipitation

The local maximum precipitation at 95% and 90% is computed over different grid resolutions for two years 1987 and 1999 for the main rainy season (JJAS) over Ethiopia. Di Luca, 2011 concluded that local maximum precipitation in coarse resolution is smaller than the high resolution precipitation. This sue to the truth that RCMs has a potential to resolve small scale dynamics and physical parameters. Figure 3 shows that the extreme precipitation at 95% and 90% is decreased as the RCM coarse goes from high to coarse resolution. Figure3a and 3b is for normal year 1987 while figure 3c and 3d is for wet year 1999. Instead of differ in precipitation magnitude the slope from high to coarse resolution is similar.

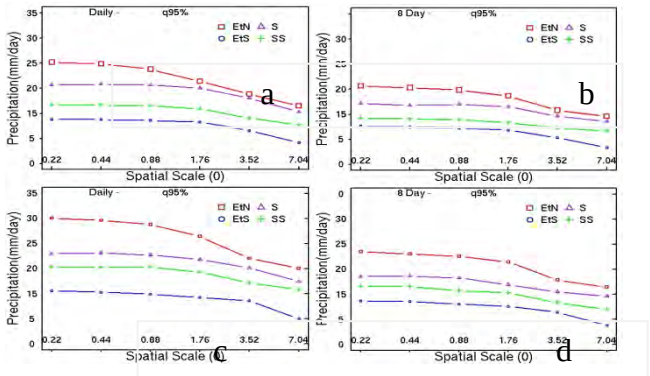


Figure 3. Local Maximum Precipitation at 95% for daily and eight day top (1987) and bottom (1999)

Potential and Relative Added Value

From Fig 3 we have observed that the range of the spread in the simulated precipitation is increased as the grid resolution is virtually increased. Based on this fact we adopted Di Luca, 2011 method to define the potential and relative potential added value of RCMs.

The difference between small spatial scale and large spatial scale climatic statistics can be highlighted as PAV measures

$$PAV^{m} = q_{95,mean}^{0,m} - q_{95,mean}^{3,m}$$

Where $q_{95,mean}^{0,m}$, the spatial mean at 95% at 0.22 and $q_{95,mean}^{3,m}$, the spatial mean at 3.52 which is the vGCM scale. The superscript 0 and3 and m represents spatial and temporal resolution respectively. PAV^{m} is used as quantity to measure the difference between the high resolution in RCMs scale and the coarse resolution GCM. $PAV^{m} \neq 0$ is necessary but not sufficient condition adding value to lower resolution (Di Luca, 2011).

A relative potential of spatial-mean PAVm is defined as

$$rPAV^{m} = \frac{PAV^{m}}{q_{95,mean}^{0,m}} = 1 - \frac{q_{95,mean}^{3,m}}{q_{95,mean}^{0,m}}$$

The $rPAV^{m}$ is between 0 and 1. The $rPAV^{m}$ ~0 indicates that RCMs has no added value.

Figure 4 shows that PAV and rPAV over different regions of East Africa for two years (1987 and 1999), two extremes precipitation (95% and 90%) and two temporal resolutions (daily and 8 day) aggregated. Figure 4a and Figure4b is potential and relative potential added value for daily temporal scale, respectively. Potential and relative potential added value is dominant over EN (North Ethiopia) than the other regions and less RCM added value over S (sudan) and SS (South Sudan). Figure 4c and Figure 4d is the same as Figure 4a and 4b but for eight day temporal scale respectively.

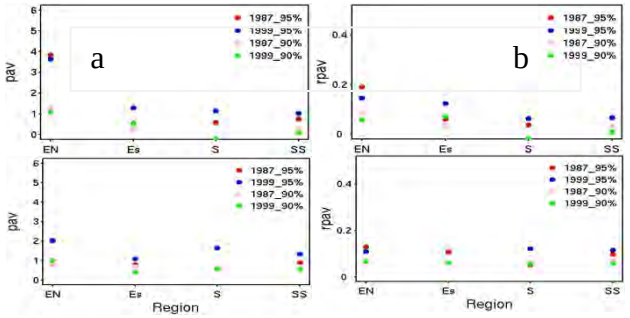


Figure 4. Potential and Relative Potential added value precipitation over different regions of East Africa top (daily) and bottom (eight day)

References

Benjamin Pohl, Julien Cre´tat, Pierre Camberlin(2011), Testing WRF capability in simulating the atmospheric water cycle over Equatorial East Africa, Clim Dyn, 37:1357–1379 DOI 10.1007/s00382-011-1024-2

Di Luca, R. de Elı´a, R. Laprise (2011): Potential for added value in precipitation simulated by high-resolution nested Regional Climate Models and observations, Clim Dyn (2012) 38:1229–1247, DOI 10.1007/s00382-011-1068-3

Giorgi F (2002): Dependence of the surface climate interannual variability on spatial scale. Geophys Res Lett 29(23):16.1–16.4

H. Panitz, A. Dosio, M. Bu¨chner, D. Lu thi, K. Keuler (2013): COSMO-CLM (CCLM) climate simulations over CORDEX Africa domain: analysis of the ERA-Interim driven simulations at 0.44_ and 0.22_ resolution, Clim Dyn, DOI 10.1007/s00382-013-1834-5

L. Mariotti, E. Coppola, M. B. Sylla,F. Giorgi, and C. Piani (2011),Regional climate model simulation of projected 21st century climate change over an all-Africa domain: Comparison analysis of nested and driving model results, JOURNAL OF GEOPHYSICALRESEARCH,VOL.116,D15111,doi:10.1029/2010JD015068

Limited-Area Energy Budget for the Canadian RCM

Marilys Clément, René Laprise and Oumarou Nikiéma

Centre ESCER, Département des sciences de la Terre et de l'atmosphère, Université du Québec à Montréal, Montréal (Québec) Canada (clement.marilys@courrier.uqam.ca)

1. Introduction

The study of atmospheric energetics provides fundamental information on the physical behaviour and maintenance of the general circulation. Lorenz (1967) proposed two forms of energy suitable for the global atmosphere: the available potential energy (APE) and the kinetic energy (K). APE is generated by the horizontal temperature gradient caused by the differential heating by the Sun. APE is converted into K by the weather systems (eddies) that transport heat from low to high latitudes, thus reducing the temperature gradient and associated APE, and K is ultimately dissipated by friction. The cycle goes on infinitely as the horizontal temperature gradient is constantly replenished by differential heating by the Sun.

To understand the physical processes and the underlying energy conversions responsible for the formation and development of individual weather systems, it is important to develop an atmospheric energetics approach suitable for limited regions, and applicable to high-resolution regional atmospheric analyses and model simulations.

The goal of this study is to carry a limited-area energy cycle calculation. The formalism developed by Pearce (1978) and Marquet (2003), and exploited by Nikiéma and Laprise (2013; hereinafter NL13) for inter-member variability budget, will here be used to compute a limited-area energy budget. The abstract is organised as follows. The next section will summarise the mathematical formulation of the energy equations. Section 3 will describe the energy cycle and its components, while section 4 will present some results obtained for one specific month. Finally, section 5 will briefly review the findings.

2. Tendency equations for available enthalpy and kinetic energy

Following NL13, available enthalpy (A) is approximated as:

$$A \approx \frac{C_p}{2T_r}\left(T - T_r\right)^2$$

where T_r is a constant reference temperature.

Starting from the basic field equations (the momentum, thermodynamics and continuity equations and the hydrostatic equilibrium and state law for ideal gas), the equations for available enthalpy (A) and kinetic energy (K) are established. A is better suited than APE for limited-domain energetics.

Each atmospheric variable $\Psi \in \{T, u, v, \omega, \Phi, \ldots\}$ can be decomposed as $\Psi = \langle\Psi\rangle + \Psi'$, where $\langle\Psi\rangle$ is the time mean and Ψ' is the time variability (deviation from the time mean).

Following a similar approach as NL13, approximate equations for the time mean available enthalpy (A_{TM}) and kinetic energy (K_{TM}) and for the time variability available enthalpy (A_{TV}) and kinetic energy (K_{TV}) are derived, valid for a limited-area domain. A fifth term (B) arises because the mass is not constant over a limited-area domain.

The prognostic equations for the atmospheric energy reservoirs are as follows:

$$\frac{\partial A_{TM}}{\partial t} = G_{TM} + I_{AB} - C_{TM} - C_A - F_{A_{TM}} - H_{A_{TM}} \quad (1)$$

$$\frac{\partial K_{TM}}{\partial t} = C_{TM} - C_K - D_{TM} - F_{K_{TM}} - H_{K_{TM}} \quad (2)$$

$$\frac{\partial A_{TV}}{\partial t} = G_{TV} - C_{TV} + C_A - F_{A_{TV}} - H_{A_{TV}} \quad (3)$$

$$\frac{\partial K_{TV}}{\partial t} = C_{TV} + C_K - D_{TV} - F_{K_{TV}} - H_{K_{TV}} \quad (4)$$

$$\frac{\partial B}{\partial t} = -F_B - I_{AB} \quad (5)$$

For brevity, only the terms appearing in Eq. 3 for A_{TV} are detailed:

$$\begin{aligned}
A_{TV} &= \frac{C_p}{2T_r}\left\langle T'^2\right\rangle \\
G_{TV} &= I\left\langle \frac{T'}{T_r}Q'\right\rangle \\
C_{TV} &= -\left\langle \omega'\alpha'\right\rangle \\
C_A &= -\frac{\left\langle \vec{V}'T'\right\rangle}{T_r}\cdot\vec{\nabla}\left\langle C_pT\right\rangle - \frac{\left\langle \omega'T'\right\rangle}{T_r}\frac{\partial\left\langle C_pT\right\rangle}{\partial p} \\
F_{A_{TV}} &= \vec{\nabla}\cdot\left(\left\langle \vec{V}\right\rangle A_{TV}\right) + \frac{\partial\left(\left\langle \omega\right\rangle A_{TV}\right)}{\partial p} \\
H_{A_{TV}} &= \frac{C_p}{2T_r}\left\langle \vec{\nabla}\cdot\left(\vec{V}'T'^2\right) + \frac{\partial\left(\omega'T'^2\right)}{\partial p}\right\rangle
\end{aligned} \quad (6)$$

3. Energy cycle

The five energy reservoirs are linked together, resulting in the diagram presented in Fig. 1, where the different transfers between reservoirs and with the environment are shown with arrows. G are generation terms produced by covariance of diabatic heating and temperature, acting as sources of energy for A_{TM} and

A_{TV}. D are dissipation terms, mainly due to friction, acting as sinks of energy for K_{TM} and K_{TV}. C and I are conversion terms, transferring energy from one reservoir to another. F are transport terms, carrying energy in or out of the domain. These terms only exist locally; they would disappear on the global scale. H are boundary terms, also arising due to the fact that the region is limited.

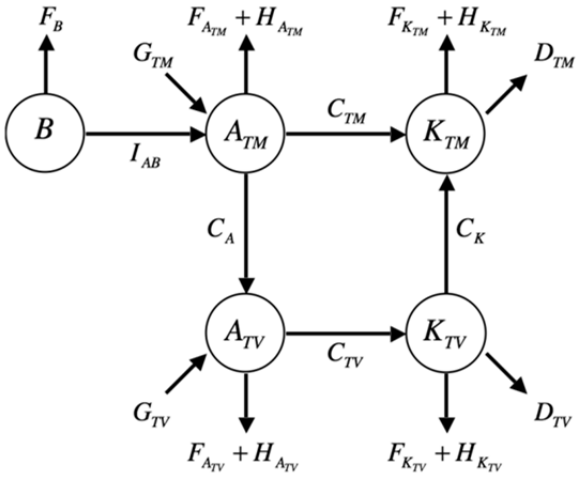
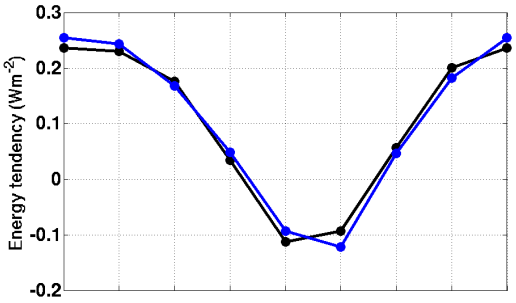


Figure 1. Energy cycle for a limited-area domain.

4. Results and discussion

The above equations characterizing the energy cycle have been computed for the month of February 2005, for a 45-km mesh simulation of the fifth-generation Canadian Regional Climate Model (CRCM5) driven by reanalyses over a domain covering the east of the North American continent and a part of the Atlantic Ocean.

For Eq. (1) to (5), the left-hand sides of the equations (the energy tendency) is compared to the right-hand side of the equations (the sum of all the sources and sinks terms, using archived samples of variables). Despite many approximations, there is a very good correspondence between the left- and right-hand side terms, as shown in Fig. 2 for a daily cycle of A_{TV} and K_{TV}.



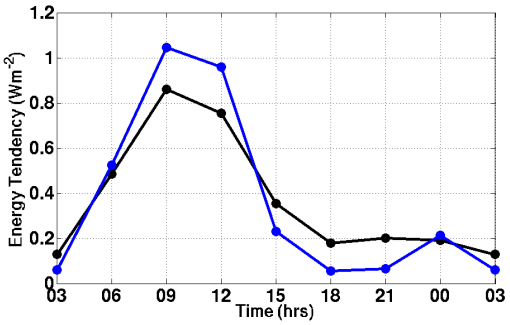


Figure 2. Daily evolution of the left-hand (blue line) and right-hand (black line) sides of the A_{TV} (upper panel) and K_{TV} (lower panel) energy tendencies.

The baroclinic conversion C_{TV} between reservoirs A_{TV} and K_{TV} is illustrated in Fig. 3. This conversion represents the covariance of vertical motion and density: $-\langle \omega' \alpha' \rangle$.

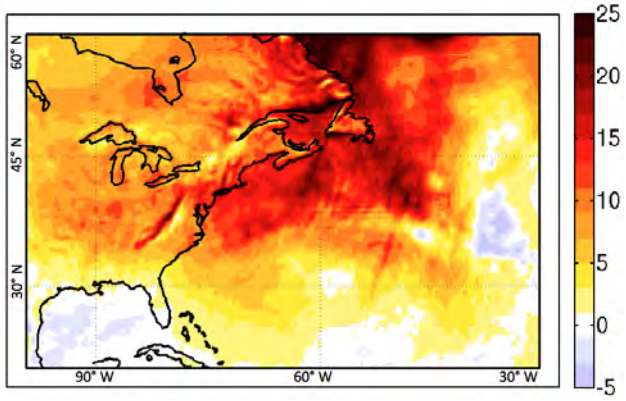


Figure 3. Map of the baroclinic term C_{TV} (in Wm^{-2}).

5. Conclusion

The purpose of this work is to study the atmospheric energetics over a limited-area domain. The set of prognostic equations for K and A, approximated and decomposed into contributions from time mean and time variability, were used to generate an approximate energy cycle.

The various terms of source and sink of energy will be studied in order to gain physical understanding of the processes acting at regional scale.

References

Lorenz E N (1967) The nature and theory of the general circulation of the atmosphere, World Meteorol Organ, Tellus, 7, 161 pp.

Marquet P (2003a) The available-enthalpy cycle. I: introduction and basic equations, Q J R Meteorol Soc, 129, 593, pp. 2445-2466

Marquet P (2003b) The available-enthalpy cycle. II: Applications to idealized baroclinic waves, Q J R Meteorol Soc, 129, 593, pp. 2467-2494

Nikiéma O, Laprise R (2013) An approximate energy cycle for inter-member variability in ensemble simulations of a regional climate model, Clim Dyn, 41(3), pp. 831-852

Pearce R P (1978) On the concept of available potential energy, Q J R Meteorol Soc, 104, pp. 737-755

Role of domain size and grid resolution on the accuracy of regional climate simulations with the COSMO-CLM model over the Mediterranean region

Dario Conte[1] and Piero Lionello[2,1]

[1] CMCC (euroMediterranean Center on Climate Change), Lecce, Italy (dario.conte@cmcc.it)
[2] DiSTeBA, Univ ersity of Salento, Lecce, Italy

1. Introduction and motivations

Large scale European projects such as PRUDENCE and ENSEMBLES (and now CORDEX with its European and Mediterranean domain) have extensively explored sources of uncertainty in RCM (Regional Climate Model) projections and shown that boundary forcing plays generally the most important role (in fact greater than the role of the RCM), in particular for temperature (Déqué et a., 2007). The set of simulations that are carried out in this study adopt boundary conditions that are extracted always from the same global data set (ERA-Interim, Dee et al., 2011), but different model domains are used. The aim is to explore the dependence of model results on the relative importance of RCM dynamics inside the domain (which increases with the domain size and drives the RCM results away from ERA-Interim) and boundary forcing (which constrains the RCM simulation to ERA-Interim).

The RCM resolution is another source of uncertainty in climate simulations and it is generally agreed that higher resolution determines more realistic features especially above complex topography and along coastlines (e.g. Li et al. 2012). This study aims to explore the relative importance of resolution and model domain for the accuracy of the RCM results. At difference with a previous study based on HIRHAM and focused on Denmark (Larsen et al., 2013), our contribution focuses on a different region (The Mediterranean Region) and uses a different model (COSMO-CLM).

2. Data and methods

All simulations have been carried out with COSMO-CLM 4.8-19 (Rockel et al., 2008), which is jointly developed by the COnsortium for Small-scale Modelling (COSMO) and the Climate Limited-area Modelling Community (CLM-Community). In this study we describe the results of 4 different simulations, all driven by the ERA-Interim reanalysis (Dee et al., 2011). Three simulations cover the 1979-2011 period on a rotated grid at 0.44 degs resolution adopting three different domains denoted as EU GRID+, MEDCORDEX GRID, EAST EU GRID (fig.1). The MEDCORDEX grid corresponds to the recommended domain of the MEDCORDEX experiment. The EU GRID+ enlarges (mainly northward) the MEDCORDEX GRID and it represents an eastward extension of the EU GRID domain, which is recommended by the EuroCORDEX experiment. The EAST EU GRID is a restriction centered on the Balkan peninsula of the MEDCORDEX GRID. These three grid are meant to explore the effect of the choice of the integration domain on model results. A fourth experiment (MEDCORDEX GRID HR) covers a shorter 5-year long period (1979-1983) on the MEDCORDEX GRID at higher resolution (0.11degs). Model validation is based on the EOBS dataset (Haylock et al. 2008, van den Besselaar et al. 2011) with a 0.25degs resolution.

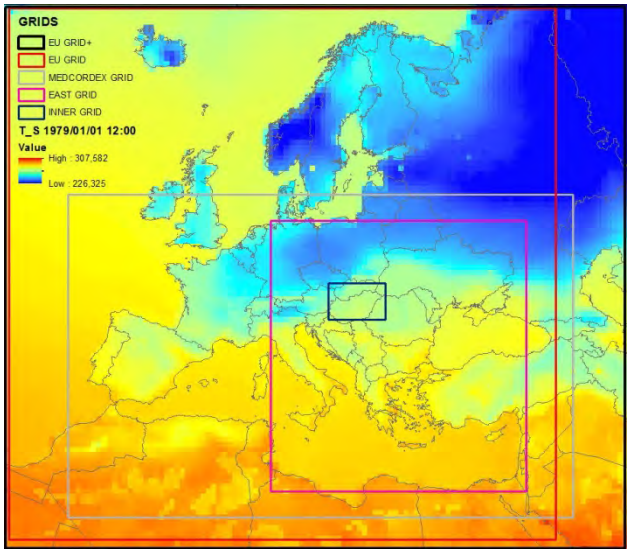


Figure 1. Domains used for the model simulations: EU GRID, MEDCORDEX GRID, EAST EU GRID. The EU GRID+ corresponds to the whole map. The EU GRID representing the recommended domain of the EuroCORDEX experiment is also shown. Grid resolution is 0.44degs but for a further MEDCORDEX GRID HR simulation resolution (0.11 degs). The INNER GRID box shows the area analyzed in section 3 and figure 2.

3. Results

The discussion here focuses on comparing the 4 simulation to the EOBS observational dataset considering the small INNER GRID box shown in figure 1.

For temperature results show a clear dependence on the model domain with the EAST EU GRID producing the smallest bias. In fact, COSMO CLM introduces a systematic negative bias inside the INNER GRID (and over most of Europe), which is not present in the ERA-Interim simulation. Results with high and low resolution grid are very similar, but high resolution generally improves the standard deviation.

Precipitation behaves similarly to temperature considering differences among the three domains, but the high resolution simulation has a systematically larger standard deviation with respect to the other simulations.

MSLP (Mean Sea Level Pressure) has the strongest dependence on model domain among the three EOBS variables, with the EU GRID showing systematically the

worst results. Increasing the resolution has always a negative effect, increasing both mean error and standard deviation.

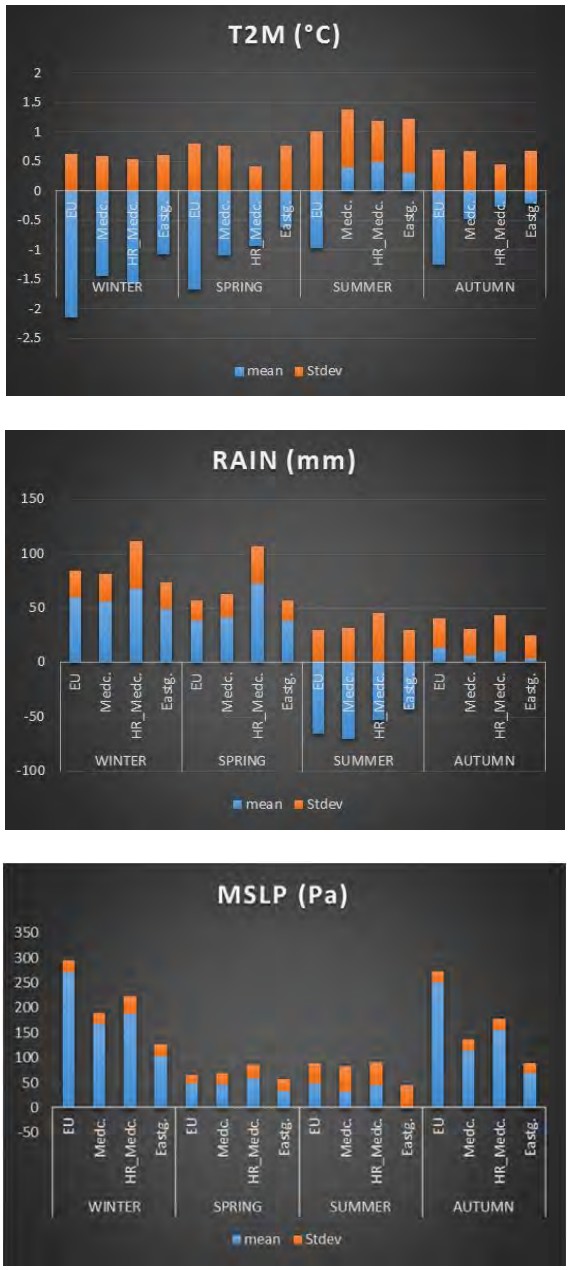


Figure 2. Mean error (blue bars) and standard deviation (orange bars) for the 4 different simulations (EU GRID, MEDCORDEX GRID, MEDCORDEX GRID HR, EAST EU GRID) in the INNER GRID box. Top, middle and bottom panels refer to 2m temperature (K), total precipitation (mm per season), MSLP (Pascal), respectively. Results are grouped according to season, (WINTER, SPRING, SUMMER, AUTUMN) from left to right in each panel)

4. Conclusions

These results show that caution should be used when considering high resolution as a necessary improvement of model results. In fact, the fine features that it introduces do not improve the match with observations in the considered area but for temperature. In this case, the improvement is likely due to a better reproduction of the topography and, consequently, of the dependence of temperature on the terrain level. However, model resolution is higher than the resolution of the observational data set used and validation of precipitation against a dense network of rain gauges could lead to different conclusions.

Results further show that in this specific and small area COSMO-CLM introduces errors whose size increases with the domain size. In this case, it might concluded that the dynamical downscaling would have spoiled the area average results of the global model providing the boundary conditions for the simulation.

However, this result should not be generalized without further analysis. Considering an INNER GRID differently located and with a different size might have brought to different conclusions.

References

van den Besselaar, E.J.M., M.R. Haylock, G. van der Schrier and A.M.G. Klein Tank (2011) A European Daily High-resolution Observational Gridded Data set of Sea Level Pressure. J. Geophys. Res., 116, D11110, doi:10.1029/2010JD015468

Dee D. P., Uppala S. M., Simmons, [… 33 authors …] and Vitart, F. (2011) The ERA-Interim reanalysis: configuration and performance of the data assimilation system, Q. J. Roy. Meteor. Soc., 137, 553–597, doi:10.1002/qj.828.

M. Déqué, D. P. Rowell, D. Lüthi, F. Giorgi, J. H. Christensen, B. Rockel, D. Jacob, E. Kjellström, M. de Castro and B. van den Hurk (2007): An intercomparison of regional climate simulations for Europe: assessing uncertainties in model projections. Climatic Change, 81, 53-70. DOI: 10.1007/s10584-006-9228-x.

Haylock, M.R., N. Hofstra, A.M.G. Klein Tank, E.J. Klok, P.D. Jones, M. New (2008) A European daily high-resolution gridded dataset of surface temperature and precipitation. J. Geophys. Res (Atmospheres), 113, D20119, doi:10.1029/2008JD10201

Larsen, M.A.D., Thejll, P., Christensen, J.H., Refsgaard, J.C. and Jensen, K.H. (2013) On the role of domain size and resolution in the simulations with the HIRHAM region climate model. Clim Dyn, Vol 40, 2903-2918, doi:10.1007/s00382-012-1513-y.

Li L., A. Casado, L. Congedi, A. Dell'Aquila, C. Dubois, A. Elizalde, B. L' Hévéder, P. Lionello, F. Sevault, S. Somot, P. Ruti, M. Zampieri (2012) Modeling of the Mediterranean Climate System in Lionello P. (Ed.) The Climate of the Mediterranean Region. From the Past to the Future , Amsterdam: Elsevier (NETHERLANDS), 419-448, ISBN:9780124160422

Rockel B, Woill A., Hense A. (eds) (2008) The Regional Climate Model COSMO-CLM (CCLM), Meteorologische Z., 4, Vol. 17

Challenges of tracking extratropical cyclones in regional climate models

Hélène Côté[1], Kevin M. Grise[2], Seok-Woo Son[3], Ramón de Elía[1,4] and Anne Frigon[1]

[1]Consortium Ouranos on Regional Climate and Adaptation to Climate Change (cote.helene@ouranos.ca)

[2]Lamont-Doherty Earth Observatory, Columbia University, Palisades, New York

[3]School of Earth and Environmental Sciences, Seoul National University, Seoul, South Korea

[4]Centre ESCER, Université du Québec à Montréal, Montreal, Canada

1. Introduction

Climate models' ability to reproduce the extratropical cyclones characteristics (ETCs) is of great importance. ETC tracking algorithms are sophisticated diagnostic tools that have been developed and extensively applied on coarse resolution global datasets such as GCMs and reanalyses.

Using ETC tracking algorithms on higher resolution RCM datasets is attractive, even though it introduces additional factors that do not need to be considered for global datasets. Therefore, all stages of the tracking procedure that require a different treatment between the global reanalysis dataset and RCM-produced dataset are investigated. It will be done by comparing the ETC tracking results of a simulation produced by the Canadian Regional Climate Model (CRCM V4) driven by ECMWF ERA-Interim, with those obtained directly from the driving reanalyses. Winter ETC tracks climatology over a large portion of North America is analyzed. It will be shown that the mere existence of boundaries in the CRCM regional domain affects the tracking results not only near the boundaries but also well within the domain.

2. Methodology and data description

Following Hoskins and Hodges (2002) and Grise et al. (2013), the tracking algorithm is applied to the 6-hourly 850-hPa relative vorticity field, which is low-pass filtered to retain synoptic spatial scales. Additional criteria were used (lifetime > 2 days, track length > 1000 km with a peak vorticity > 3.0 x 10^{-5} s^{-1}, growth rate > 2.0 x 10^{-5} s^{-1}, decay rate > 2.0 x 10^{-5} s^{-1}).

The ERA-Interim data are handled in three different ways to see how a limited domain impacts the tracking algorithm outputs: (1) the vorticity field is smoothed with a global spectral filter followed by applying the Hodges ETC tracking algorithm to the global data before extracting the limited domain, hereafter called the SHE method ("S" for spectral filtering, "H" for Hodges tracking algorithm, and "E" for extraction of limited domain, applied in this order); (2) the SEH method consists of applying the spectral filter to the global dataset then extracting the RCM's subregion, before applying the ETC tracking algorithm; (3) the ECH method first isolates the regional domain, then a Cressman filter ("C") with a radius of 600 km is used since a global technique is ruled out, and finally the ETC tracking algorithm is applied. This last approach emulates the way any RCM dataset is treated.

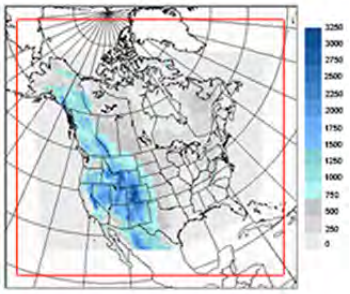


Figure 1. The grid of the CRCM simulation at a 45-km resolution (200x192 gridpoints) in its native polar-stereographic projection (true at 60° N). The red line defines the 10-points sponge zone that is excluded from the analysis. The shaded area corresponds to the CRCM topography (m), contoured every 250m and located within the effective tracking zone which encompasses the gridpoints poleward of 25°N that are at least 600 km (Cressman filter) away from the sponge zone.

The regional climate dataset is produced with the CRCM V4.2.4, a version very similar to that described in De Elía and Côté (2010). The domain appears on the Figure 1. LBCs are provided by ERA-Interim using the one-way nesting method. Spectral nudging is applied to large-scale winds for wavelengths > 1400 km and above 500 hPa. Sea-ice concentration and SSTs are prescribed from ERA-Interim data.

3. ETC tracking results for ERA-Interim

Figure 2 shows the November–March 1991-2009 ETC track climatology. The units correspond to the average number of cyclones per month that pass (top row), develop (middle row), or decay (bottom row) within 500 km of a given grid point. ERA-Interim results obtained from the SHE, SEH and ECH methods appear in the 1st, 2nd and 3rd columns respectively. The 4th column shows CRCM results that are discussed in the next section.

The results of the SHE method (Figures 2a-c) applied to ERA-Interim data shows well-known patterns of the various North American storm tracks. They correspond well with other studies.

Figures 2d-f show the effect of extracting the subdomain before performing the tracking (SEH method). The minimum duration and length thresholds strongly affect the pattern and frequency of the ETC tracks and the regions of cyclone development and decay, along both Pacific and Atlantic coasts, since numerous cyclones are not accounted for. The Rockies lee-side cyclones are the least affected by shrinking the domain.

Figures 2g-i show that modifying the filtering technique in the ECH method is responsible for an additional, although modest, reduction in the number of

tracks, development and decay patterns.

4. ETC tracking for the CRCM

Figures 2j-l display the ETC tracking results of the CRCM simulation. They are compared with ERA-Interim results obtained using an equivalent treatment (ECH; Figure 2, 3rd column) to avoid methodological artifacts. The overall CRCM track pattern in Figure 2j is very similar to its ERA-Interim driver in Figure 2g. The CRCM's ETC frequency is also higher directly over the Rockies. This is consistent with the fact that the CRCM 45-km-resolution topography acts as a weaker barrier than the real-world Rockies detected by the ERA-Interim assimilation.

There is an obvious CRCM underestimation of developing cyclones compared to the ECH ERA-Interim (Figure 2k vs Figure 2h) but also for the decaying cyclones (Figure 2l vs Figure 2i). Possible causes to these underestimations are investigated in Côté et al. (2014).

5. Conclusions

By using a perfect-prog approach, we found that the ETC tracks on a regional domain produce quantitatively different results to those on the global domain. The underestimation of the cyclone tracks, development, and decay regions is mostly caused by the effect of extracting the regional grid from the global domain with a smaller additional contribution from adopting a new filtering technique. This method provides a useful tool for studying the potential drawbacks of a selected domain. It could help to find the optimal regional domain (size and position) required for studying a given cyclone track in a RCM.

By applying the same methodology (ECH) to both global and regional datasets, we are able to compare the results of CRCM with those of its ERA-Interim driver. It is important to state that comparison against SHE or SEH would have been an unfair test for the regional model. For the ETC tracking statistics studied here, CRCM4 does a good job of reproducing the cyclone-track patterns found in the ERA-Interim. Nevertheless, CRCM4 still produces a noticeable underestimation of cyclone track numbers.

Due to the importance of mesoscale processes during their life cycle, high-resolution modeling offers interesting perspectives for studying ETC characteristics. Very high resolution GCMs are extremely attractive because they encompass the cyclogenesis and cyclolysis regions of any cyclone track, but their computation costs are still prohibitive, especially for climate change experiments. In the meantime, RCMs offer a suitable alternative when handled carefully and used over large domains targeting the cyclone track of interest.

References

Côté H., K.M. Grise, S.-W. Son, R de Elía and A. Frigon (2014) Challenges of tracking extratropical cyclones in regional climate models, *submitted to Climate Dynamics*.

De Elía R., H. Côté (2010) Climate and climate change sensitivity to model configuration in the Canadian RCM over North America. Meteorol Zeitschrift 19:325–339. doi: 10.1127/0941-2948/2010/0469

Grise K.M., S.-W. Son, J.R. Gyakum (2013) Intraseasonal and Interannual Variability in North American Storm Tracks and Its Relationship to Equatorial Pacific Variability. Mon Weather Rev 141:3610–3625. doi: 10.1175/MWR-D-12-00322.1

Hoskins B.J., K.I. Hodges (2002) New Perspectives on the Northern Hemisphere Winter Storm Tracks. 1041–1061.

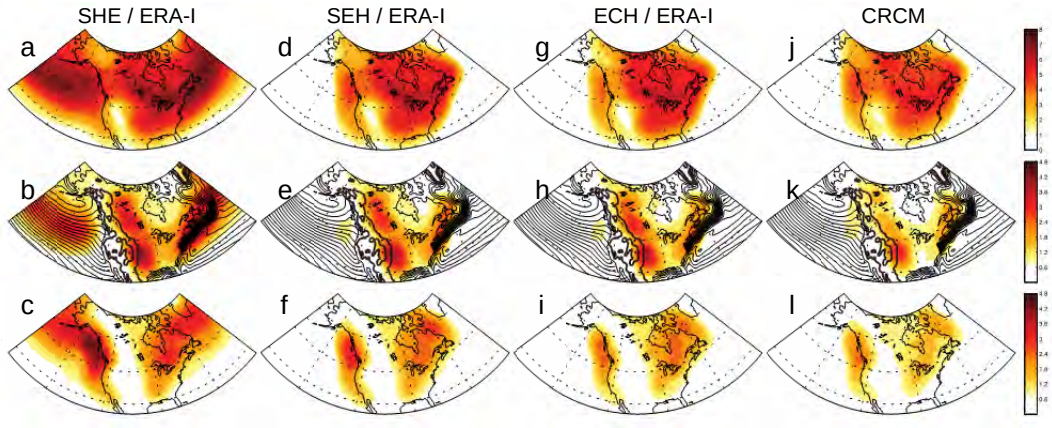


Figure 2. 1991-2009 November-March ETC climatology. (Top) Average number of cyclones per month. (Middle) Average number of developing cyclones per month. (Bottom) Average number of decaying cyclones per month. Storm tracks are defined using the 850 hPa relative vorticity field and Hodges' algorithm. Individual tracks are assigned to a 500-km radius region surrounding the vorticity maximum and must have a lifetime > 2 days and a length > 1000 km. First column shows results from the SHE treatment on ERA-Interim, second column presents results from SHE on ERA-Interim, third column shows results from ECH on ERA-Interim. Fourth column shows results from the CRCM4.

Sensitivity of the NHRCM simulation of the southwest monsoon rainfall over the Philippines to model resolution

Faye T. Cruz[1], Hidetaka Sasaki[2] and Gemma T. Narisma[1,3]

[1] Regional Climate Systems Program, Manila Observatory, Quezon City, Philippines (faye.cruz@gmail.com)
[2] Atmospheric Environment and Applied Meteorology, Meteorological Research Institute, Tsukuba, Japan
[3] Atmospheric Science Program, Physics Department, Ateneo de Manila University, Quezon City, Philippines

1. Introduction

Global climate models (GCM) have been useful tools in providing climate information, but their low resolution does not capture some features, such as the local climate effects of topography, land use and coastlines. Thus, downscaling methods, whether statistical or dynamical (i.e. using a regional climate model (RCM)), are implemented to obtain higher resolution climate information from GCMs for a particular region, e.g. the Philippines (Robertson et al. 2012). Studies have shown RCMs can provide added value to GCMs, especially for areas with complex topography and coastlines (Feser et al. 2011). However, using a high spatial resolution for an RCM can be computationally expensive. It is therefore critical to find an adequate resolution such that both large- and fine-scale features are still represented well.

In this study, the non-hydrostatic regional climate model (NHRCM) developed at the Meteorological Research Institute of Japan (Saito et al. 2006) is used to simulate the southwest monsoon (SWM) rainfall in the Philippines at two horizontal resolutions. The rainfall brought about by the SWM is important for the Philippines since it contributes to about 43% of its mean annual rainfall (Cayanan et al. 2011). However, the heavy rainfall of the SWM can also lead to intense flooding, which was recently experienced over metropolitan Manila in August 2012 and 2013. There have been earlier attempts to study the SWM rainfall using another RCM with some degree of success (Francisco et al. 2006). This study examines the performance of NHRCM for a tropical climate, particularly its sensitivity to spatial resolution in capturing the magnitude, seasonality and spatial distribution of the SWM rainfall over the Philippines.

2. Methodology

Simulations have been conducted with NHRCM centered over the Philippines at 50 km resolution from 1998 to 2007 using boundary conditions from the 2° resolution ECMWF ERA-Interim dataset (Dee et al. 2011). In order to account for local-scale features, the 50 km model output is further downscaled to a finer resolution of 10 km. In this case, only the months of May to September were simulated to focus on the SWM season from June to September.

Rainfall from the model is evaluated with observed datasets, such as from the Asian Precipitation – Highly-Resolved Observational Data Integration Towards Evaluation (APHRODITE) project (Yatagai et al. 2012) and from the Tropical Rainfall Measuring Mission (TRMM 3B43 ver.7; Huffman et al. 2007). Observational records are also obtained from selected stations of the Philippine Atmospheric, Geophysical and Astronomical Services Administration (PAGASA) over the northwestern part of the country where rainfall is high during the SWM season. Other key features to be examined in the model simulation include the seasonal shifts in the direction of the monsoon and in the spatial distribution of rainfall.

3. Results and Discussion

Initial results indicate that the seasonal changes in the prevailing wind flow (monsoon) from southwest in June to August to northeast in December to February are well represented in the model. During the SWM season, the model is also able to capture the spatial distribution of rainfall in both 50 and 10 km resolutions, particularly the seasonal high rainfall over the northwestern side of the country (Figure 1). However, rainfall tends to be underestimated elsewhere in the 50 km run (Figure 1b). In the case of the 10 km run, more rainfall is generated over areas with high elevation (Figure 1c). This is likely because the topographic effects on rainfall are captured by the model due to a better representation of the topography at this resolution. However, the dry bias in the 50 km output is still evident in the 10 km result since the 10 km run uses boundary conditions from the 50 km output.

Comparison of the simulated monthly rainfall with observed station data indicates the model's ability to reproduce the seasonality. Generally, the model tends to underestimate rainfall regardless of the model resolution, e.g. Dagupan (Figure 2a). However, this model sensitivity to resolution can vary across the sites. In some areas, the increase in the model resolution from 50 km to 10 km may still improve the magnitude, e.g. Iba (Figure 2b). On the other hand, the 50 km output can be closer to observed values than the 10 km result at other sites, e.g. Coron (Figure 2c). This model behavior will therefore need to be explored further.

4. Conclusion

Initial results show that the SWM and its associated rainfall are simulated reasonably well by NHRCM. However, rainfall is generally underestimated in the model. Improvements in the magnitude may be obtained using a higher model resolution but it depends on the site. These preliminary results indicate the potential of the model to be used in further studying the SWM rainfall over the Philippines.

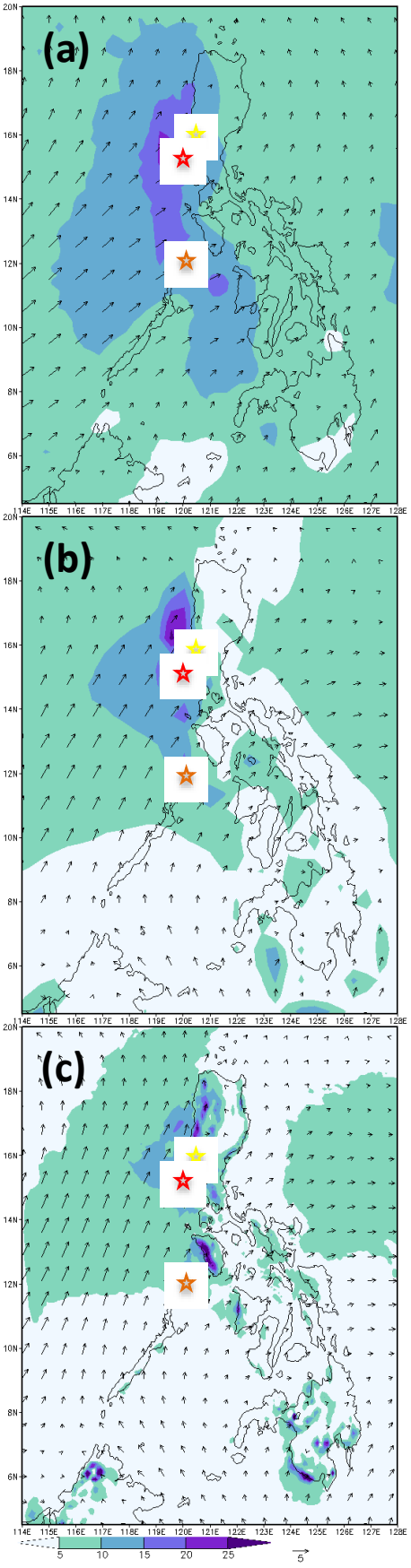


Figure 1. The mean rainfall (mm/day) and surface winds (m/s) from June to September from 1998 to 2007 from (a) TRMM and ERA-Interim, (b) NHRCM at 50 km resolution, and (c) NHRCM at 10 km resolution. Stars indicate the location of stations in Figure 2 (Dagupan (yellow), Iba (red), and Coron (orange)).

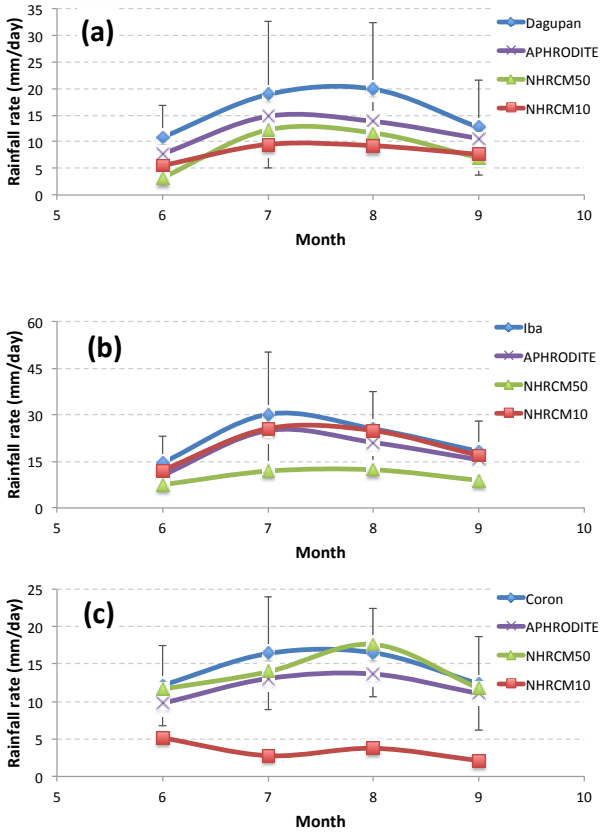


Figure 2. The mean rainfall (mm/day) from PAGASA station, APHRODITE, and NHRCM model at 50 km and 10 km resolutions at (a) Dagupan, (b) Iba, and (c) Coron. Error bars indicate observed variability from 1998 to 2007.

Acknowledgement

This work was partly supported by SOUSEI program of MEXT Japan.

References

E. Cayanan et al. (2011) The effect of tropical cyclones on southwest monsoon rainfall in the Philippines, J. Meteorol. Soc. Japan, 89A, pp. 123-139

D. Dee et al. (2011) The ERA-Interim reanalysis: configuration and performance of the data assimilation system, Quart. J. R. Meteorol. Soc., 137, pp. 553-597

F. Feser et al. (2011) Regional climate models add value to global model data: A review and selected examples, Bull. Amer. Meteor. Soc., 92, pp. 1181-1192

R. Francisco et al. (2006) Regional model simulation of summer rainfall over the Philippines: Effect of choice of driving fields and ocean flux schemes, Theor. Appl. Climatol., 86, pp. 215-227

G. J. Huffman et al. (2007) The TRMM Multi-satellite Precipitation Analysis: Quasi-Global, Multi-Year, Combined-Sensor Precipitation Estimates at Fine Scale. J. Hydrometeor., 8, pp. 33-55

A. Robertson et al. (2012) Downscaling of seasonal rainfall over the Philippines: Dynamical versus statistical approaches, Mon. Wea. Rev., 140, pp. 1204-1218

K. Saito et al. (2006) The operational JMA Nonhydrostatic Mesoscale Model. Mon. Wea. Rev., 134, pp. 1266–1298

A. Yatagai et al. (2012) APHRODITE: constructing a long-term daily gridded precipitation dataset for Asia based on a dense network of rain gauges, Bull. Amer. Meteor. Soc., 93, pp. 1401–1415

Probabilistic climate scenarios for risk assessment in Japan

Koji Dairaku[1], Genta Ueno[2], Izuru Takayabu[3]

[1] Department of Integrated Research on Disaster Prevention, National Research Institute for Earth Science and Disaster Prevention, Tsukuba, Japan.

[2] The Institute of Statistical Mathematics, Research Organization of Information and Systems, Tachikawa, Japan

[3] Meteorological Research Institute, Japan Meteorological Agency, Tsukuba, Japan

1. Introduction

Climate information and services for Impacts, Adaptation and Vulnerability (IAV) Assessments are of great concern. In order to develop probabilistic regional climate information that represents the uncertainty in climate scenario experiments in Japan, we compared the physics ensemble experiments using the 60km global atmospheric model of the Meteorological Research Institute (MRI-AGCM) with multi-model ensemble experiments with global atmospheric-ocean coupled models (CMIP3) of SRES A1b scenario experiments

2. Results

The MRI-AGCM shows relatively good skills particularly in tropics for temperature and geopotential height. The skills are dependent on the region and variable. Variability in surface air temperature of physical ensemble experiments with MRI-AGCM was within the range of one standard deviation of the CMIP3 model in the Asia region. On the other hand, the variability of precipitation was relatively well represented compared with the variation of the CMIP3 models. Models which show the similar reproducibility in the present climate shows different future climate change. We couldn't find clear relationships between present climate and future climate change in temperature and precipitation.

3. Probabilistic climate scenario

We develop a prototype of probabilistic climate scenario using the multi-model ensemble experiments. An appropriate combination of statistical methods and optimization of climate ensemble experiments are discussed.

Acknowledgment

This study was supported by the SOUSEI Program, funded by Ministry of Education, Culture, Sports, Science and Technology, Government of Japan.

References

Gleckler, P. J., K. E. Taylor, and C. Doutriaux(2008): Performance metrics for climate models, *J. Geophys. Res.*, 113, D06104, doi:10.1029/2007JD008972.

Reichler, T., and J. Kim(2008): How Well do Coupled Models Simulate Today's Climate?, *Bull. Amer. Meteor. Soc,* 89, 303-311.

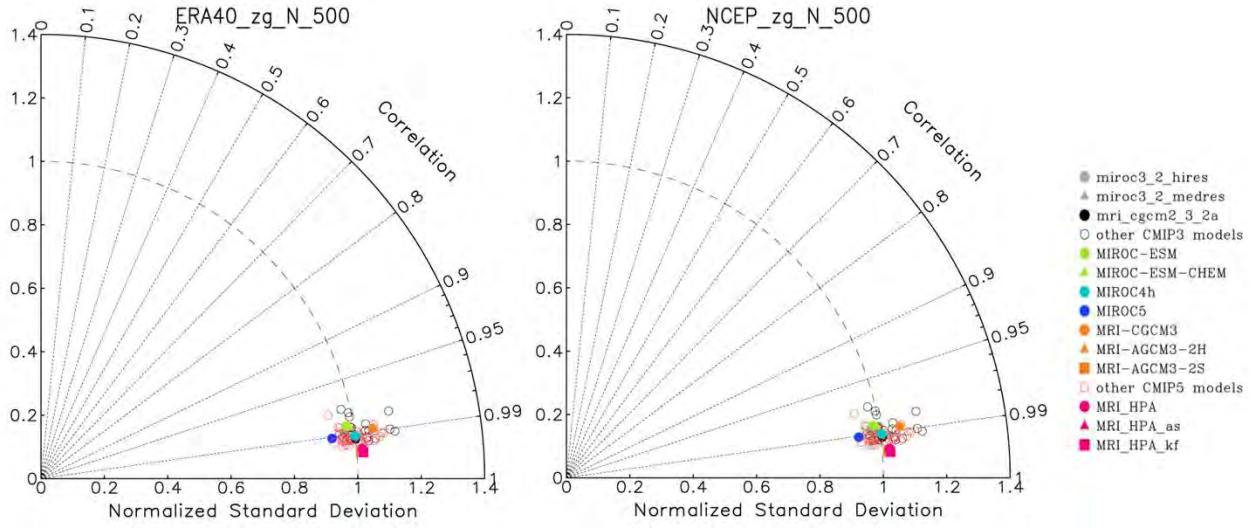


Figure 1. 500hPa Geopotential Height in Northern hemisphere. Left panel uses ERA40 as reference. Right panel uses NCEP.

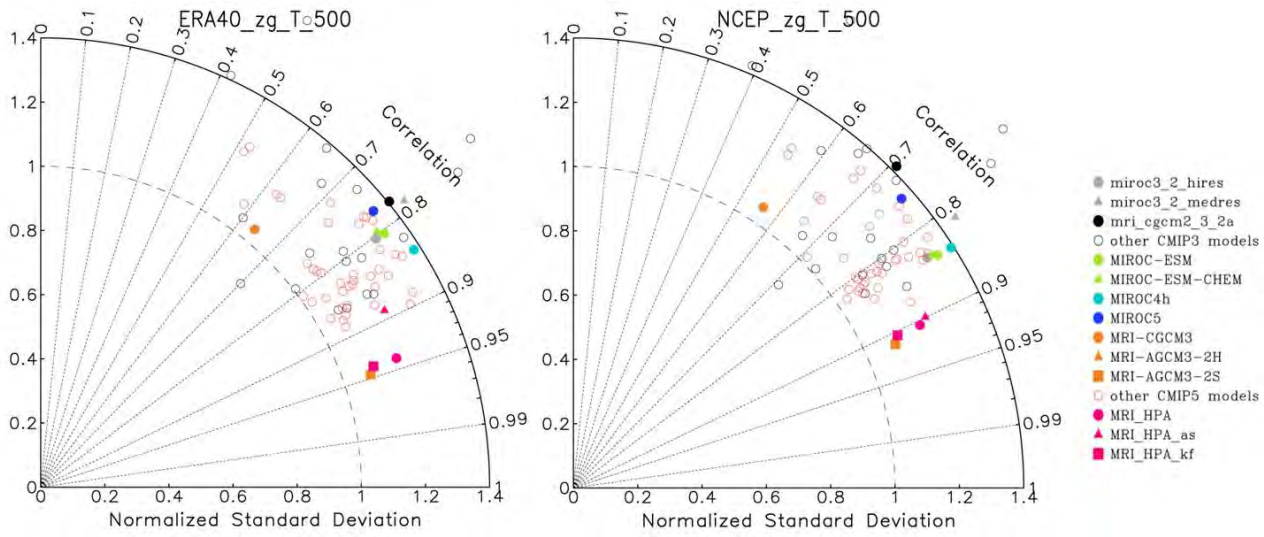


Figure 2. Same as Figure 1 but in Tropical region.

Dynamical downscaling and socio-economic land use scenarios for regional scale adaptation to climate change in Tokyo metropolitan area

Koji Dairaku[1], Yoshiki Yamagata[2], Junpei Hirano[1], Hajime Seya[2], Nobumitsu Tsunematsu[3], Kumiko Nakamichi[4]

[1] Department of Integrated Research on Disaster Prevention, National Research Institute for Earth Science and Disaster Prevention, Tsukuba, Japan.

[2] National Institute for Environmental Studies(NIES), Tsukuba, Japan.

[3] Tokyo Metropolitan Research Institute, Koto, Japan.

[4] Tokyo Institute of Technology, Meguro, Japan.

1. Introduction

Because regional responses of surface hydrological and biogeochemical changes to increases in carbon dioxide concentrations and to changes in land use/land cover are particularly complex, climate information and services for Impacts, Adaptation and Vulnerability (IAV) Assessments are of great concern. Climate scenarios produced by global climate models with coarse grid-spacing involve an inadequate mismatch of spatial scale. It is necessary to develop assessment tools for regional scale adaptation to climate change.

2. Development for regional climate change adaptation

We develop 1) dynamical downscaling method using socio-economic land use scenarios in Tokyo Metropolitan Area to add spatial resolution to accurately assess critical interactions within the regional climate system for vulnerability assessments to climate change for regional scale adaptation, 2) regional-scale assessment of the impacts of climate and socio-economic change on flood with the bottom-up perspective and landuse scenarios in Tokyo Metropolitan Area using an urban economic model.

We will present our current progress on water-related hazard and risk assessment in Tokyo Metropolitan Area and on cost/benefit analyses on adaptation measures to mitigate the disaster risk and reduce the CO2 emission toward producing useful climate assessments for decision-making for regional scale adaptation to climate change.

Acknowledgment

This study was conducted as part of the research subject "Vulnerability and Adaptation to Climate Change in Water Hazard Assessed Using Regional Climate Scenarios in the Tokyo Region" (National Research Institute for Earth Science and Disaster Prevention; PI: Koji Dairaku) of Research Program on Climate Change Adaptation (RECCA), and was supported by the SOUSEI Program, funded by Ministry of Education, Culture, Sports, Science and Technology, Government of Japan.

References

Tsunematsu, N., K. Dairaku, and J. Hirano(2013): Future changes in summertime precipitation amounts associated with topography in the Japanese islands, Journal of Geophysical Research, 118, doi:10.1002/jgrd.50383

Pielke, R.A. Sr., R. Wilby, D. Niyogi, F. Hossain, K. Dairaku, J. Adegoke, G. Kallos, T. Seastedt, K. Suding(2013): Dealing with Complexity and Extreme Events Using a Bottom-up, Resource-based Vulnerability Perspective, Extreme Events and Natural Hazards: The Complexity Perspective Geophysical Monograph Series 196, 10.1029/2011GM001086

Hirano, J, K. Dairaku(2013): Climate change adaptation and flood risk assessment in Tokyo Metropolitan Area, Impacts World 2013, International Conference on Climate Change Effects, pp.1-6

Yamagata Y., H. Seya(2013): Simulating a future smart city: An integrated land use-energy model, Applied Energy, 112, pp. 1466–1474

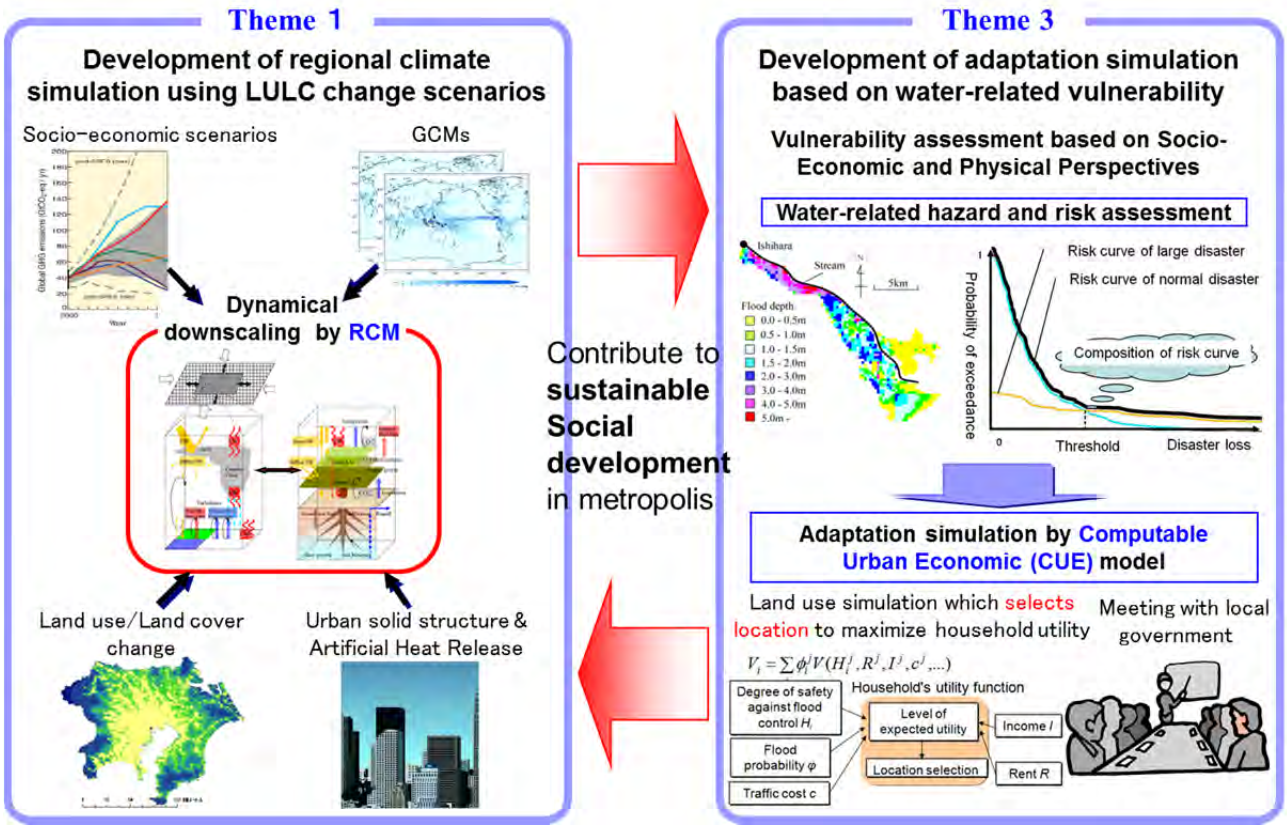


Figure 1. Overview of the research project “Vulnerability and Adaptation to Climate Change in Water Hazard Assessed Using Regional Climate Scenarios in the Tokyo Region”.

Assessment of add-value of ensemble dynamical downscaling in Japan

Koji Dairaku[1], Satoshi Iizuka[1], Nobumitsu Tsunematsu[2], Junpei Hirano[1], Wataru Sasaki[3], Roger A. Pielke Sr.[4]

[1] National Research Institute for Earth Science and Disaster Prevention, Tsukuba, Japan.
[2] Tokyo Metropolitan Research Institute, Koto, Japan.
[3] Japan Agency for Marine-Earth Science and Technology, Yokohama, Japan.
[4] University of Colorado, Boulder, USA.

1. Introduction

Climate effects caused by human activities will continue for centuries and natural climate influences have always been a risk. Mitigation is a complex, uncertain approach and will need at least several decades. It is necessary, therefore, to put adaptation together immediately. The impacts and potential applications of interest to the stakeholders are mostly at regional and local scales as the essential resources of water, food, energy, human health, and ecosystem function respond to regional and local climate. Users of climate scenarios produced by global climate models with coarse grid-spacing involve an inadequate mismatch of spatial scale. Downscaling technique is used to obtain the regional climate scenarios, especially in regions of complex topography, coastlines, and in regions with highly heterogeneous land surface covers where those results are highly sensitive to fine spatial scale climate processes.

2. Add-value of ensemble dynamical downscaling

Dynamical and statistical downscaling techniques are available for generating regional climate information. We investigated the respective strengths and weaknesses using multi-regional climate model (NHRCM, NRAMS, TWRF) ensemble experiments in Japan.

As a test for predictability, statistical downscaling from the parent model was used as the benchmark (control) with which dynamic downscaling would have to improve on. Though all downscaling models successfully improve the quality of daily precipitation data relative to reanalysis, no best downscaling model for all aspects exist. Each downscaling models have own strengths and weaknesses.

Multi-regional climate model ensemble experiments reasonably simulate the Tropical cyclone (TC) tracks and reduced TC track errors for about 60% of the TCs.

We assessed the value (skill) added by the ensemble downscaling to a global climate simulation in Japan for regional future changes. Future changes in summertime precipitation amounts over the Japanese islands and their relations to the topographical heights were investigated. The results indicate that increases in June-July-August (JJA) mean daily precipitation are noticeable in the west and south sides (windward sides) of the mountainous regions, especially in western Japan where heavy rainfall is frequently observed in the recent climate. The intensification of southwesterly moist air flows in the lower troposphere is considered to be one of the main causes of the orographic precipitation changes. These results indicate strong influences of topography and prevailing wind direction on future precipitation changes.

3. Summary

Based on the lesson learning from the multi-model ensemble downscaling project in Japan (S5-3), “added value” and "predictability" of downscaling are discussed for developing a probabilistic climate scenario and regional climate adaptation.

Acknowledgment

These works were supported by the Environment Research and Technology Development Fund (S5-3) of the Ministry of the Environment, Research Program on Climate Change Adaptation (RECCA), Program for Risk Information on Climate Change (SOUSEI) funded by Ministry of Education, Culture, Sports, Science and Technology, Japan.

References

Iizumi, T., M. Nishimori, K. Dairaku, S. A. Adachi, and M. Yokozawa (2011), Evaluation and intercomparison of downscaled daily precipitation indices over Japan in present-day climate: Strengths and weaknesses of dynamical and bias correction-type statistical downscaling methods, J. Geophys. Res., 116, D01111, doi:10.1029/2010JD014513.

Sasaki, W., S. Iizuka, and K. Dairaku (2012): Capability of Regional Climate Models in Simulating Coastal Winds and Waves around Japan, Journal of the Meteorological Society of Japan, Vol. 90, No. 5, pp. 603−615, 2012 DOI: 10.2151/jmsj.2012-502

Iizuka, S., K. Dairaku, W. Sasaki, S. A. Adachi, H. Kusaka, N.N. Ishizaki, and I. Takayabu: Assessment of Ocean Surface Winds and Tropical Cyclones around Japan by RCMs, JMSJ, 90B, 91-102.

Ishizaki, N.N., I. Takayabu, M. Ooizumi, H. Sasaki, K. Dairaku, S. Iizuka, F. Kimura, H. Kusaka, S.A. Adachi, K. Kurihara, K. Murazaki, and K. Tanaka(2012): Improved Performance of Simulated Japanese Climate with a multi-model ensemble, JMSJ, 90, 235-254.

Izumi, T., I. Takayabu, K. Dairaku, H. Kusaka, M. Nishimori, G. Sakurai, N.N. Ishizaki, S.A. Adachi, and M.A. Semenov(2012): Future change of daily precipitation indices in Japan: A stochastic weather generator-based bootstrap approach to provide probabilistic climate information, J. Geophys. Res., 117, D11114, doi:10.1029/2011JD017197

Tsunematsu, N., K. Dairaku, and J. Hirano(2013): Future changes in summertime precipitation amounts associated with topography in the Japanese islands, Journal of Geophysical Research, 118, doi:10.1002/jgrd.50383

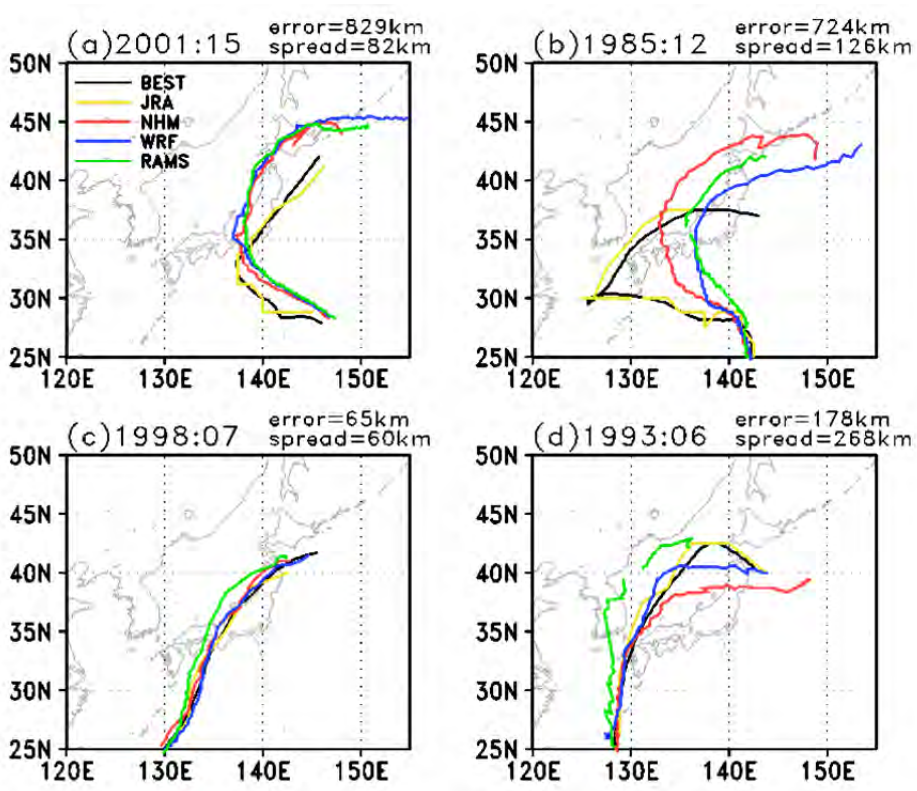


Figure 1. Examples of Tropical cyclone tracks simulated by three RCMs (NHRCM, NRAMS, TWRF).

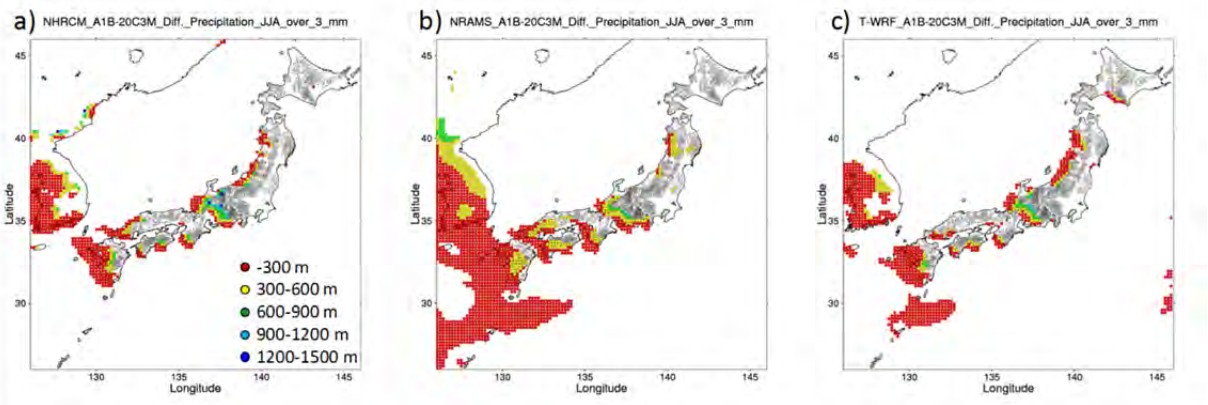


Figure 2. Differences in the JJA average daily precipitation amounts (mm day-1) between 2081-2100 and 1981-2000, derived from the regional climate scenarios simulated by a) NHRCM, b) N-RAMS, and c) T-WRF. The shadings represent the future precipitation increases greater than 3 mm day-1 at an interval of 300 m of topographical heights.

Some sources of bias in the Eurocordex historical runs

Michel Déqué, Antoinette Alias, Clotilde Dubois and Samuel Somot

Météo-France/CNRM, CNRS/GAME, Toulouse, France (michel.deque@meteo.fr)

1. Motivation

Contrary to FP5-PRUDENCE, and, to some extent, to FP6-ENSEMBLES, the CORDEX protocol prescribes that the RCM should be driven directly by the CMIP5 simulations. This has two practical consequences :

- a jump in resolution from 100-200 km to 12 m
- an SST with systematic errors

As a consequence, the bias obtained in the ERA-interim driven simulations, which is used to evaluate the RCM, has nothing to do with the bias in the historical period. However, impact studies (e.g. hydrological model driving) will be concerned by the latter bias. In order to investigate possible ways of improving this bias, four Eurocordex-12 km experiments with ALADIN (Colin et al., 2010) driven by CNRM-CM5 (Voldoire et al., 2013) have been produced:

1) standard CORDEX protocol
2) bias-corrected SST
3) double nesting with an intermediary 50-km resolution AGCM
4) combination of both

2. Results

The results shows that improved SST and improved lateral boundary conditions do not address the same biases. Figure 1 shows the summer precipitation bias in the ERA-interim driven and in the historical run for the same period. Due to the GCM lateral boundary conditions, a wet bias is evidenced in the West and South of Europe. Figure 2 shows the bias with corrected SST and with double nesting (uncorrected SST). The improvement comes clearly from the lateral boundary conditions. When combining the two techniques (not shown) there is a further improvement by correction of the wet bias over Greece.

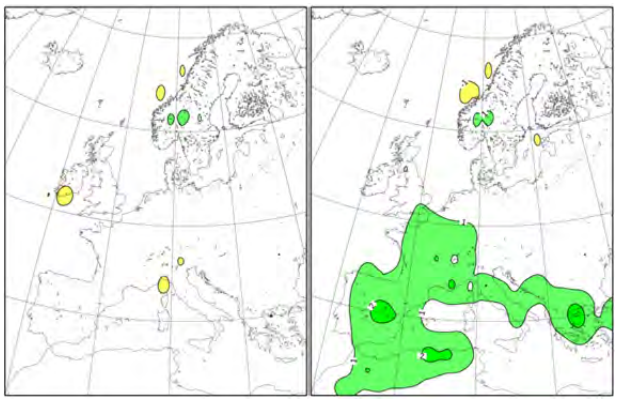


Figure 1. Summer precipitation bias in ERA-interim driven (left) and CMIP5-driven (right) reference simulations. Contours ±1 and ±2 mm/day.

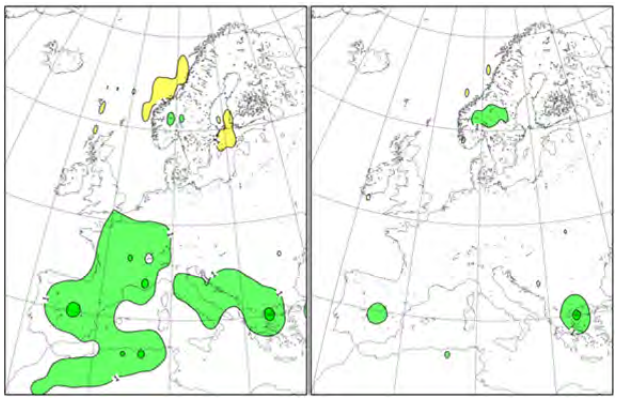


Figure 2. As Figure 1 with SST correction (left) and double nesting (right)

RCP8.5 snapshots for 2071-2100 with the four experimental designs described above indicate that the wet biases induce a less dry response over Europe: the error cancellation between scenario and reference does not fully work.

3. Conclusions and perspectives

The double nesting technique (as in PRUDENCE) reduces the systematic errors in the historical period.
In addition, it modifies in a non-negligible way the climate response with respect to the standard CORDEX experiment.

References

Colin J., M. Déqué, R. Radu, S. Somot (2010) Sensitivity study of heavy precipitations in Limited Area Model climate simulation: influence of the size of the domain and the use of the spectral nudging technique. Tellus SERIES A, Vol. 62, No. 5, pp. 591-604

Voldoire A., E. Sanchez-Gomez, D. Salas y Mélia, B. Decharme, C. Cassou, S.Sénési, S. Valcke, I. Beau, A. Alias, M. Chevallier, M. Déqué, J. Deshayes, H. Douville, E. Fernandez, G. Madec, E. Maisonnave , M.-P. Moine, S. Planton, D. Saint-Martin, S. Szopa, S. Tyteca, R. Alkama, S. Belamari, A. Braun, L. Coquart, F. Chauvin (2013) The CNRM-CM5.1 global climate model : description and basic evaluation. Clim. Dyn., Vol. 40, No. 9-10, pp. 2091-2121

A framework to study the potential benefits of using high-resolution regional climate model simulations

Alejandro Di Luca[1,3,4], Ramón de Elía[2,3] and René Laprise[1,3]

[1] Université du Québec à Montréal (UQAM), Montréal, Canada;
[2] Consortium Ouranos, Montréal, Canada;
[3] Centre pour l'Étude et la Simulation du Climat à l'Échelle Régionale (ESCER), Montréal, Canada;
[4] Climate Change Research Centre, Faculty of Science, University of New South Wales, Sydney, Australia (a.diluca@unsw.edu.au)

1. Introduction

Added value (AV) is generally defined as the ability of RCM simulations to improve some particular aspect of the driving fields compared to observations, e.g., Feser et al. (2011). The necessary use of observed data in order to identify this AV restricts its study to only recent past RCM simulations. The scarceness of fine-scale observations and the limited number of variables available for validation limit even more those cases where AV can be evaluated.

In order to circumvent these limitations, Di Luca et al. (2013a,b) have developed a framework, nicknamed "potential added value" (PAV), that uses the presence of fine-scale structures in RCM-derived climate statistics as a prerequisite condition for an RCM to generate some real fine-scale AV. The objective of this paper is twofold. First, to describe the PAV framework and, second, to apply it to quantify the fine-scale part of the RCM-derived climate change (CC) signal and its relative importance compared to either the large-scale CC part or present climate statistics. The analysis concentrates here on time-averaged seasonal temperature and precipitation.

2. Potential added value framework

Using the delta approach, a future climate statistics X can be expressed as:

$$X^{future} = X_{OBS}^{present} + CC_{simulated}, \quad (1)$$

where $CC_{simulated}$ is computed in the usual form as the difference between *X* in future and present climates, using either RCM or GCM simulations. The CC signal added value (AV_{CC}) can then be defined as:

$$AV_{CC} = \left(X_{GCM}^{fut} - X_{true}^{fut}\right)^2 - \left(X_{RCM}^{fut} - X_{true}^{fut}\right)^2, \quad (2)$$

where the subscript "true" denotes the still unknown climate statistics that will arise in future climate conditions. Defined in this way, an RCM generates some AV if its error in the CC signal estimation is smaller than the GCM one, i.e. if AV_{CC} is positive. Replacing Eq. (1) in Eq. (2) gives:

$$AV_{CC} = \left(CC_{GCM} - CC_{true}\right)^2 - \left(CC_{RCM} - CC_{true}\right)^2. \quad (3)$$

Eq. (3) shows that, when using the delta method, the AV of RCMs in future climate statistics does not depend directly on the future climate statistics, but on the CC signal. Replacing the total CC signal in Eq. (3) according to the contribution of large (CC_{ls}) and small (CC_{ss}) scales, and neglecting covariance terms we obtain,

$$AV_{CC} \approx AV_{CC}^{ls} + AV_{CC}^{ss} \quad (4)$$

with

$$AV_{CC}^{ss} = \left(CC_{true}^{ss}\right)^2 - \left(CC_{RCM}^{ss} - CC_{true}^{ss}\right)^2. \quad (5)$$

Eq. (5) suggests that a few conditions must be satisfied for the RCM to add value in the fine-scale CC signal: first, the true and the RCM CC fields (CC_{true} and CC_{RCM}) must contain non-negligible fine-scale information; second, the error of the fine-scale RCM-derived CC information must be smaller than the signal itself. Eq. (5) also suggests that the term AV^{ss}_{CC} can potentially increase as CC^{ss}_{true} increases, justifying the idea of using the increase in the CC signal fine-scale variance as a proxy of an increase in AV_{CC}.

A simple way to quantify the importance of fine scale in the high-resolution CC signal can be done by defining

$$PAV_{CC}^{ss} = var\left(CC_{RCM}^{ss}\right) \quad (6)$$

where $var(CC_{RCM})$ denotes the spatial variance of the high resolution CC field over a 300-km side region. Relative PAV quantities can then be defined for temperature as:

$$rPAV_{CC}^{ss} = var\left(CC_{RCM}^{ss}\right) / CC_{300}^{2}, \quad (7)$$

and for precipitation as:

$$rPAV_{CC}^{ss} = var\left(CC_{RCM}^{ss}\right) / pr_{300}^{present^2}, \quad (8)$$

where CC_{300} and $pr^{present}_{300}$ represent the spatial-mean CC signal and present precipitation over 300-km side regions respectively.

3. PAV in 2-m temperature

Fig. 1 shows the RCM ensemble-mean value of the *rPAV* quantity for temperature (see Eq. 7) in summer. The RCM ensemble consists of five RCM-AOGCM pairs

from the North American Regional Climate Change Assessment Program (NARCCAP) simulations made with horizontal grid spacing of about 50 km.

Fig. 1 shows values that are always smaller than 0.6, suggesting that fine-scale mean-temperature changes are smaller than the large-scale ones. The domain-averaged in winter (summer) is 0.086 (0.093) with a maximum value of 0.31 (0.58). That is, averaged over continental North America, the contribution of the fine scales to the total climate-change signal is of the order of 10%, although it can attain 60% in specific regions. The largest ensemble-mean $rPAV_{CC}$ values appear along the Pacific, Atlantic and Hudson Bay coasts, due to the differential heating between land and ocean surfaces (Di Luca et al. 2013b).

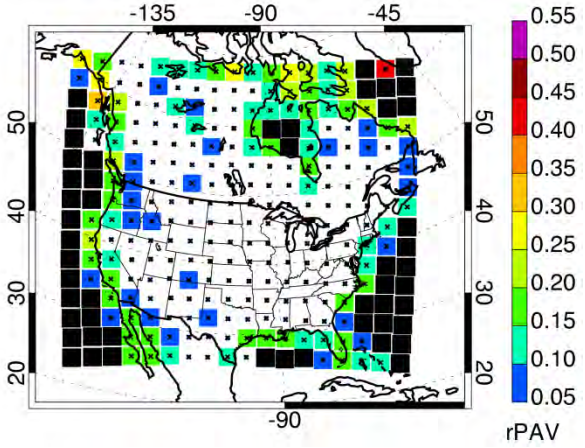


Figure 1. Ensemble mean ratio between the small scale variance and the square of the large scale CC signal for 2-m temperature in summer.

4. PAV in precipitation

Fig. 2 shows the ensemble-mean *rPAV* quantity for the CC signal of summer precipitation. Domain-average values are about 0.045 and 0.048 in winter and summer seasons respectively, suggesting that fine scales induce a precipitation change of about 5% compared to the present time-averaged precipitation. In summer, the largest values appear in the south-western part of the continent with values attaining 0.3 in some regions. These regions, however, appear to be non-robust according to a sampling uncertainty criterion (black crosses in Fig. 2) indicating that in these regions the uncertainty is quite large. In winter (not shown), the largest changes in mean precipitation (~10%) seem to arise related with the presence of fine-scale topographic features along the Rocky Mountains.

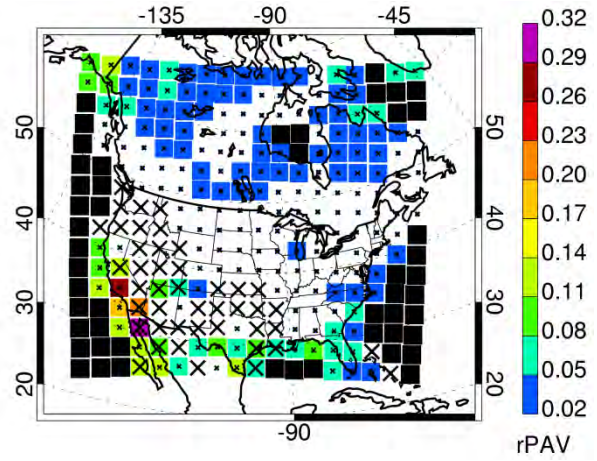


Figure 2. Ensemble mean ratio between the variance of the CC small scale mean signal and the present mean precipitation in summer.

5. Summary

In this paper, the importance of fine scales in the climate change signal is studied using the potential added value framework as presented in Di Luca et al. (2013a,b).

For temperature, the largest PAV appears in coastal regions mainly related with differential heating in land and oceanic surfaces. In northern regions along the Hudson Bay and the Canadian Archipelago, this seems to be related with a differential snow-sea-ice albedo feedback. Fine-scale features can account for nearly 60% of the total CC signal in some coastal regions, although for most regions the fine scale contributions to the total CC signal are only ~5%.

For precipitation, fine scales contribute to a change of generally less than 15% of the seasonal-averaged precipitation in present climate, with a continental North American average of ~5% in both summer and winter. In winter, the largest PAV appears in mountainous regions, possibly related with the interaction between large-scale precipitation changes in mid-latitudes and the fine-scale topography of the Rocky Mountains.

The analysis also shows that the sampling uncertainty associated with fine-scale features in the CC signal is much larger in precipitation than in temperature.

References

Di Luca A, de Elía R, Laprise R (2013a) Potential for added value in RCM-simulated surface temperature. Clim Dyn, 40, pp. 443-464

Di Luca A, de Elía R, Laprise R (2013b) Potential added value of RCM's downscaled climate change signal. Clim Dyn, 40, pp. 601-618

Feser F, Rockel B, von Storch H, Winterfeldt J, Zahn M (2011) Regional climate models add value to global model data: A review and selected examples. Bull Am Meteorol Soc., 92, pp. 1181-1192

Identifying cyclones in high-resolution RCM simulations and reanalysis

Alejandro Di Luca[1], Jason P. Evans[1,2] and Daniel Argüeso[1,2]

[1] Climate Change Research Centre, Faculty of Science, University of New South Wales, Sydney, Australia (a.diluca@unsw.edu.au)
[2] ARC Centre of Excellence for Climate System Science, University of New South Wales, Sydney, Australia.

1. Introduction

Cyclones are key meteorological phenomena that strongly influence the day-to-day weather and the climate of most regions around the world. In particular, the eastern seaboard of Australia is strongly influenced by the passage of low pressure systems over the adjacent Tasman Sea (i.e., East Coast Lows (ECLs)). ECLs can cause significant amount of damage along the coast due to strong winds, large ocean waves and/or heavy rains (Speer et al. 2009). They are also a major source of water for the reservoirs serving coastal communities and thus are both vital to, and dangerous for, human activities in the region.

Mainly motivated through the Eastern Seaboard Climate Change Initiative (ESCCI) on ECLs, a number of projects are currently underway to better understand the development and impacts of ECLs and how their frequency and intensity may change in the future. In particular, in order to quantify likely future changes in ECL statistics, two issues must be carefully addressed: first, simulations need to be performed at relatively high spatial resolution to properly capture the development and intensification of ECLs which have sizes ranging from 50 to 1000 km; and second, an automatic algorithm is needed to objectively identify ECLs in present and future simulations.

The objective of this study is double: first, to quantify the uncertainty arising from the use of various reanalysis and, second, to evaluate the performance of three RCM simulations to represent the statistics of ECLs over the Tasman Sea.

2. Data

RCM simulations are provided by the New South Wales and Australian Capital Territory Regional Climate Modelling Project (NARCliM; Evans et al., 2014) project and were performed using the Weather Research and Forecasting (WRF) model at 50 km grid spacing. NCEP/NCAR reanalysis are used as boundary conditions and the domain of integration is shown in Fig. 1. Differences between RCMs are related with the use of different physical parameterizations to represent subgrid-scale processes (see Evans et al. (2014)) and simulations are here identified simply as versions R1, R2 and R3.

The evaluation and uncertainty estimation is conducted using three reanalysis products available at a similar resolution as the RCM simulations: the NCEP CFSR, the ECMWF ERA Interim and the NASA MERRA.

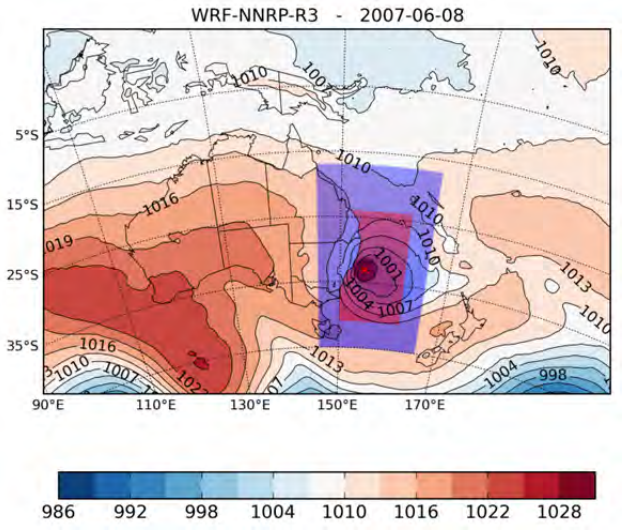


Figure 1: MSLP field as simulated by the version R3 of the WRF RCM. Also shown are the region where lows are identified (blue shaded) and where the analysis is performed (red shaded).

The analysis is performed using the 30 year period between 1980 and 2009.

3. Methodology

The methodological approach distinguishes a number of steps. First, time-varying mean sea level pressure fields from any given dataset (simulation or reanalyses) are re-gridded into a range of common grid meshes differing only in their horizontal grid spacing (ranging from 50 to 300 km). Second, the cyclone detection and tracking algorithm developed by Browning and Goodwin (2013) is applied to all the datasets derived in the first step. The identification is based on a presure gradient threshold and is applied over the blue shaded region in Fig. 1. Third, the identified cyclones are grouped into events based on their timing and relative positions. Finally, a number of metrics characterizing the intensity, duration, frequency and evolution of events are estimated for each ECL dataset over the region of analysis (red shaded in Fig. 1).

4. Intensity of ECL events

Fig. 2 shows the mean intensity across all ECL events as a function of the spatial scale for the various datasets (different colors). The intensity is measured here using the pressure gradient averaged over a 200-km region around the center of the cyclone. Fig. 2 shows that all reanalysis present a similar spatial scale dependence that tends to follow closely the linear spatial scale dependence imposed to the pressure gradient threshold

(see blue light dashed line in Fig. 2). Versions R1 and R3 of the WRF RCM show somewhat higher mean pressure gradient values compared to reanalysis results but a similar spatial scale dependence with only some discrepancies when considering changes between the 100 and 50-km spatial scale.

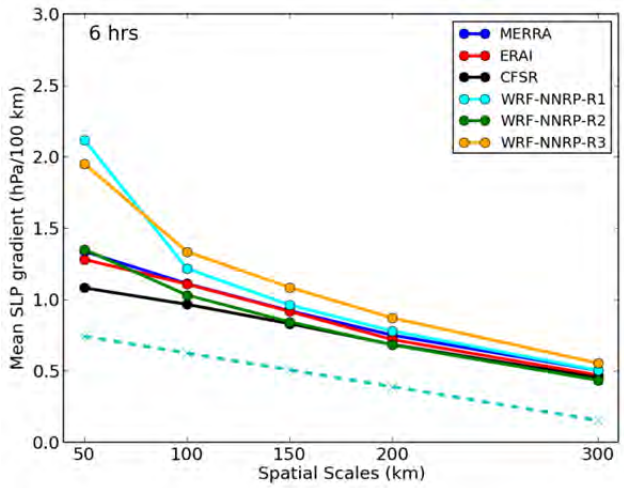


Figure 2: Mean pressure gradient as a function of the spatial scale for reanalysis and simulated datasets.

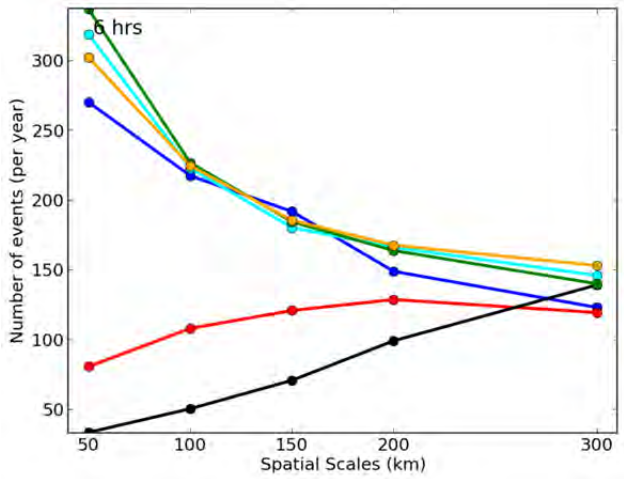


Figure 3: As in Fig. 2 but for the number of events per year.

5. Number of ECL events

Fig. 3 shows the number of events per year for each datasets as a function of the spatial scale. Clearly, differences between datasets are very important. Results obtained at the 50-km grid mesh (original grid) show about 270, 100 and 30 events for the MERRA, the ERAI and the CFSR reanalyses respectively. That is, there is almost a factor of 10 between the number of events in MERRA and CFSR. All WRF versions produce a similar number of events that is closer to the number of events in the MERRA reanalyses.

Differences between reanalysis and simulated datasets tend to be much smaller as the spatial scale of the data increases. At the 300-km scale, the number of events per year vary between 120 in ERAI reanalyses to 155 in the version R3 of the WRF RCM. Interestingly, reanalysis datasets showing the largest number of events also show the shortest mean duration of events (not shown) and thus the total number and mean duration of events tend to compensate for different datasets to lead to a better agreement on the total number of ECL days across datasets.

5. Summary

Our results show that the identification of cyclones can be strongly dependent on the dataset (either reanalysis or simulation) when looking at phenomena near the truncation limit of mean sea level pressure fields. The large sensitivity on the number of events is probably related with particular physical parameterizations and the method used to assimilate observations in reanalysis data.

We also find that, when performing the identification and tracking over smoother MSLP fields (~300 km spatial scales), results tend to be very similar across reanalysis and the WRF RCMs perform well regarding the intensity, number and duration of events.

References

Browning, Stuart A. and Ian D. Goodwin, 2013: Large-Scale Influences on the Evolution of Winter Subtropical Maritime Cyclones Affecting Australia's East Coast. Mon. Wea. Rev., 141, 2416–2431.

Evans, J.P., F. Ji, C. Lee, P. Smith, D. Argüeso and L. Fita, 2014. A regional climate modelling projection ensemble experiment – NARCliM, Geoscientific Model Development. Accepted.

Speer MS, Wiles P and Pepler A. 2009. Low pressure systems off the New South Wales coast and associated hazardous weather: establishment of a database. Australian Meteorological and Oceanographic Journal, 58 (1), 29-39.

Evaluation of fifth-generation Canadian Regional Climate Model (CRCM5) simulations using Stage IV precipitation analyzes over the eastern United States

Mamadou Insa DIOP, René LAPRISE and Enrico TORLASCHI

Centre ESCER, Université du Québec à Montréal (UQAM), Montréal (Québec) Canada (diop.mamadou_insa@courrier.uqam.ca)

1. Introduction

In recent years, projecting future climate has become a great challenge for the scientific community. Scientists have invested a lot of efforts in developing climate models, and in particular Regional Climate Models (RCMs), so they can be more efficient and reliable to assess realistically the anticipated climate changes. For this purpose, verification tests continue to be necessary to evaluate and improve the performance of RCMs. Several projects have been carried out over North America, such as those of Takle et al. (1999) under the Project to Intercompare Regional Simulations (PIRCS), Gutowski et al. (2010) and Mearns et al. (2012) under the North American Regional Climate Change Assessment Program (NARCCA), and Martynov et al. (2013) and Šeparović et al. (2013) under the Coordinated Regional Climate Downscaling EXperiment (CORDEX). These studies show that RCMs used can provide useful information on present climate and future climate changes.

Here we use Stage IV precipitation analyses (Lin and Mitchell, 2005) at high spatiotemporal resolution to assess CRCM5 simulations over North America.

2. Data and analysis method

Stage IV hourly analyzes are available on polar stereographic projection with a grid mesh of 4 km across the continental United States. Radar data and rain gauge measurements are merged at 12 regional River Forecast Centers that produce regional analyzes of precipitation for their jurisdictional areas. These regional products are then mosaicked into a national product at NCEP.

The CRCM5, as described by Martynov et al. (2013), uses deep convection following Kain and Fritsch (1990), shallow convection based on a transient version of Kuo (1965) and Bélair et al. (2005) scheme, large-scale condensation scheme of Sundqvist et al. (1989). It also uses the version 3.5 of Canadian land-surface scheme (CLASS3.5) of Verseghy (1991, 2009).

Simulations were performed on a rotated latitude-longitude grid, with a grid spacing of 0.11° across North America. They were driven by ERA-Interim reanalyses that were available to us on pressure levels on grid meshes of 2° and 0.75°, depending on the period.

Stage IV data were first aggregated by combining four elements of the original grid, and then linearly interpolated to the model grid. Simulations assessment is performed by comparing the seasonal-mean precipitations, the average number of wet days, and the average duration of hourly rainfall events over the entire domain, and the diurnal cycle and frequency distribution of hourly precipitation in different sub-regions. For this abstract, results are only shown for the summer season (June-July-August).

3. Seasonal mean precipitations

Figure 1 shows the relative bias of seasonal-mean precipitation of CRCM5, compared to Stage IV data. Results show that CRCM5 overestimates rainfall in adjacent regions of east coast and underestimates it in northwest regions, with relative biases of the order 20-60 %. Overall CRCM5 reproduces the main features of the spatial distribution of observed precipitation, but with events that, on average, are much more intense and more widespread.

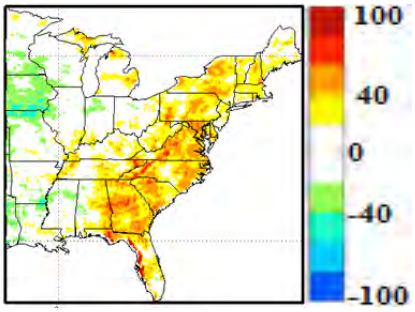


Figure 1. Relative biases (in %) of CRCM5 compared to Stage IV, normalised by their mean.

4. Frequency distributions of hourly precipitations and diurnal cycle

Figure 2 shows the frequency distribution of hourly precipitations over a sub-region in the South of the domain. The peak intensity in CRCM5 is shifted slightly towards lower intensities, but overall the model reproduces rather well the distribution. While previous studies such as Martynov et al. (2013) could only analyze daily precipitation intensity distribution because of the lack of high temporal resolution data, Stage IV data allow quantifying the high intensities contributions in total precipitation accumulations that are lost when analyzing daily means.

The main features of the observed diurnal cycle of precipitation are relatively well reproduced in CRCM5 simulations (not shown). Diurnal variations are generally weak in winter and very pronounced during summer. In JJA, maximum precipitations occur over night in the Centre and the Great Lakes, and in late afternoon in the East and Southeast. However, the heavy nocturnal precipitations in the Centre remain problematic for the model.

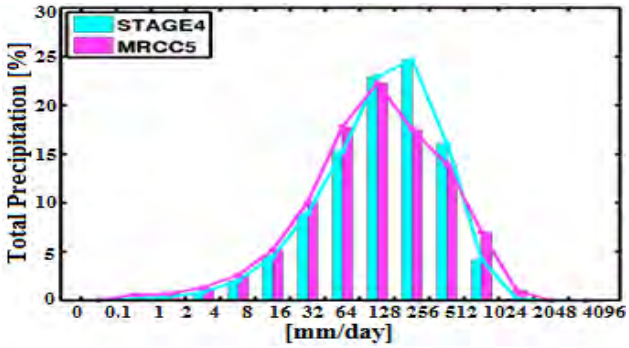


Figure 2. Frequency distribution of hourly precipitations of Stage IV and CRCM5 simulation in the south sub-region, as defined by Martynov et al. (2013)

5. Average number of wet days

Analysis of the average number of wet days with a threshold of 1 mm shows rather good agreement between simulation and observations. Figure 3 shows that relative biases are less than 20% over most the domain. With a threshold of 3 mm, biases are somewhat larger, with wet biases in southeast and dry biases in northwest regions.

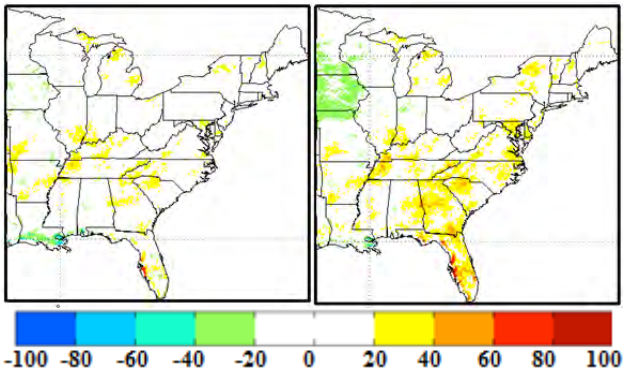


Figure 3. Normalised relative biases (in %) between CRCM5 and Stage IV for threshold 1 mm (left) and 3 mm (right).

6. Average duration of rainfall events

Figure 4 shows statistics relating to the average duration of hourly rainfall events. In general CRCM5 shows good skills, with relative biases less than 20 % over most of the area for a threshold 1 mm. A generalized positive bias becomes more widespread with an increase of the threshold to 3 mm.

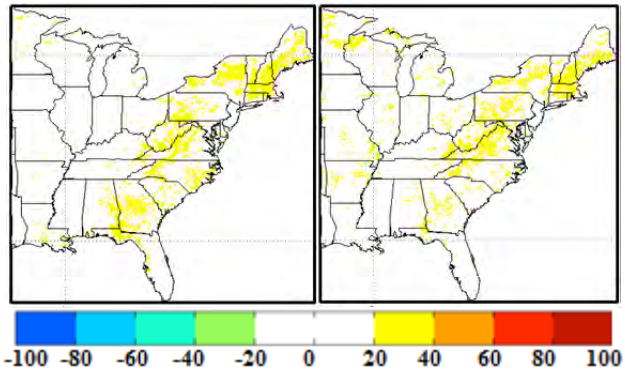


Figure 4. Normalised relative biases (in %) between CRCM5 simulation and Stage IV data for thresholds 1 mm (left) and 3 mm (right).

7. Conclusion

In general the model succeeded in reproducing several aspects of the precipitation statistics. However, CRCM5 simulations overestimate rainfall in the adjacent regions of the eastern coast and underestimate it in northwest regions. Overestimation in the simulation results from the contribution of high intensities, the high frequency of rainy days and the slightly longer duration of hourly rainfall. Some dry biases are associated with the low frequency of rainy days. CRMC5 performance errors might be associated with parameterization schemes despite the use of “perfect” driving boundary conditions provided by reanalyses data.

This study was also done for the others seasons, and CRCM5 shows generally good skills.

References

Bélair S, Mailhot J, Girard C, Vaillancourt P (2005) Boundary layer and shallow cumulus clouds in a medium-range forecast of a large-scale weather system, Mon Weather Rev, 133(7), pp. 1938-1960

Gutowski WJ Jr, Arritt RW, Kawazoe S, Flory DM, Takle ES, Biner S, Caya D, Jones RJ, Laprise R, Leung LR, Mearns LO, Moufouma-Okia W, Nunes AMB, Qian Y, Roads JO, Sloan LC, Snyder MA (2010) Regional extreme monthly precipitation simulated by NARCCAP RCMs, J Hydrometeorol, 11(6), pp. 1373-1379

Kain JS, Fritsch JM (1990) A One-Dimensional Entraining / Detraining Plume Model and Its Application in Convective Parameterization, J Atmos Sci, 47(23), pp. 2784-2802

Kuo HL (1965) On Formation and Intensification of Tropical Cyclones Through Latent Heat Release by Cumulus Convection. J Atmos Sci, 22(1), pp. 40-63

Lin Y, Mitchell KE (2005) The NCEP Stage II/IV precipitation analyses: Development and applications, Preprints, 19th Conf. on hydrology, Amer Meteor Soc, San Diego, CA. Paper 1.2

Martynov A, Laprise R, Sushama L, Winger K, Šeparović L, Dugas B (2013) Reanalysis-driven climate simulation over CORDEX North America domain using the Canadian Regional Climate Model, version 5: Model performance evaluation, Clim Dyn, 41(11-12), pp. 2973-3005

Mearns LO, and Coauthors (2012) The North American Regional Climate Change Assessment Program: Overview of Phase I Results. Bull Amer Meteor Soc, 93(9), pp. 1337-1362

Šeparović L, Alexandru A, Laprise R, Martynov A, Sushama L, Winger K, Tete K, Valin M (2013) Present climate and climate change over North America as simulated by the fifth-generation Canadian Regional Climate Model (CRCM5), Clim Dyn, 41(11-12), pp. 3167-3201

Sundqvist H, Berge E, Kristjansson JE (1989) Condensation and cloud parameterization studies with a mesoscale numerical weather prediction model, Mon Weather Rev, 117(8), pp. 1641-1657

Takle ES et al. (1999) Project to intercompare regional climate simulations (PIRCS): Description and initial results, J Geophys Res, 104(D16), pp. 19443-19461

Verseghy DL (1991) CLASS — A Canadian land surface scheme for GCMs: I. Soil model. Int J Climatol, 13(11), pp. 347-370

Verseghy DL (2009) CLASS — The Canadian Land Surface Scheme (Version 3.4) — Tech. Docum. (version 1.1). Internal report, Climate Research Division, Science and Technology Branch, Environment Canada, 183 pp.

Exploiting regional climate modeling in the Arctic

Ralf Döscher[1], Torben Königk[1], Peter Berg[2] and Margareta Johansson[3]

[1] Swedish Meteorological and Hydrological Institute of Meteorology (SMHI), Rossby Centre, Norrköping, Sweden
[2] Swedish Meteorological and Hydrological Institute of Meteorology (SMHI), Hydrology Research, Norrköping, Sweden
[3] Lund University, Dept of Physical Geography and Ecosystem Science, Lund, Sweden

1. The challenge

Climate modeling of the Arctic as a special case of regional climate modeling is a challenge due to the dominant role of sea ice and due to the Arctic amplification. The rapid decrease of Arctic sea ice shows an integrated action of various processes, which need to be explored to understand the fate of the sea ice and consequences of its variability and change.

As for all regional climate models (RCMs), Arctic RCMs, when run under real-world forcing, can potentially perform better than Global climate models (GCMs) due to higher resolution and the possibility for regional tuning of parameterizations. The chances to realize that improvement potential is lowered by the dominating circumpolar atmospheric circulation, providing weak forcing over the boundaries and allowing for model-specific equilibrium. Mathematical ill-posedness of most lateral boundary condition formulations worsens the problem.

2. Tasks for Arctic RCMs

Despite existing challenges, coupled ocean-sea ice-atmosphere models and uncoupled atmosphere-standalone models have been shown to give reasonable performance for e.g. sea ice cover and surface temperatures. Arctic RCMs have been shown to be well suited

- to address questions on the relative impact of large scale versus Arctic internal processes,
- to study processes supporting rapid sea ice drop events and strong year-to-year variability,
- to perform regional downscaling of climate change scenarios,
- to study processes related to uncertainty of future projections,
- to serve as basis for climate change impact studies on e.g. vegetation and permafrost.

The presentation reviews examples from the fields above, focusing on SMHI's and partners regional studies with the coupled regional model RCAO. Special emphasis is given to uncertainty of sea ice projections in relation to wind forcing.

3. The atmosphere as the major driver of sea ice change

The atmospheric circulation and its variability in the Arctic appears to be the major driver of sea ice extent change. Under recent climate conditions, sea ice extent and its trend since 1980 can be simulated well with coupled RCMs (Döscher et al. 2010). After year 2000, the observed accelerated sea ice decline can be simulated only if the atmospheric circulation is represented realistically. Circulation biases in simulations can be remedied by a spectral nudging technique (Berg et al. 2013) as a workaround. Figure 1 shows an example for the effect of weakly forcing the coupled model to observed atmospheric circulation conditions without interfering with thermal or radiative fluxes. The shape record the sea ice minimum in September 2007 can be simulated very close to the observed picture.

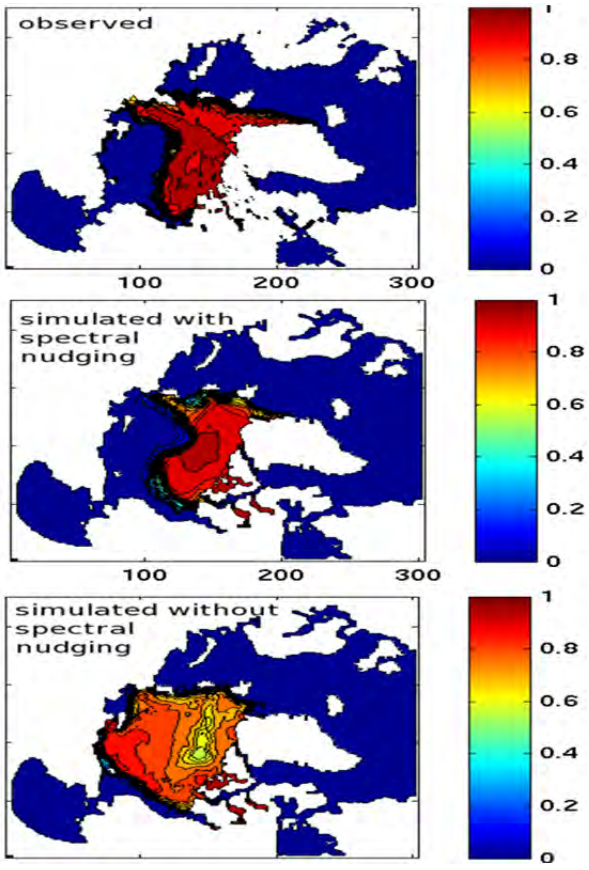


Figure 1. Sea ice concentration in the Arctic during September 2007 as (a) observed, (b) simulated with spectral nudging and (b) simulated without spectral nudging.

Coupled Arctic downscaling of GCM future climate projection gives generally increased variability of sea ice extent, which in the light of recent observed sea ice drops and variability appears more realistic than a smooth decline. Spectral nudging techniques applied to RCM future scenarios, enforce the GCMs atmospheric circulation on the RCM's circulation. This leads to a smoother development of the sea ice extent (Berg et al. 2014), which again points out the large scale atmospheric circulation as a major driver of sea ice development under the conditions of thinning ice.

4. A case study of Arctic land conditions

While the projection of future sea ice is afflicted by large uncertainties, air temperatures over land rise monotonously centered over the ocean, often independent of specific model configuration (Koenigk et al. 2014).

As a case study, a RCM future climate scenario has been used to assess possible future change in soil conditions in the Arctic location of the Torneträsk valley around the Abisko research station in northern Sweden (Johansson et al. 2014). The study area has a unique long term climate record extending back to 1913, which allows for establishing empirical relations between changes of valley-wide temperature and local conditions on scales less than 100 m.

A permafrost model (GIPL 2.0) has been utilized to simulate past and to project future permafrost changes. It is important to model the permafrost distribution at a high resolution so that the model output can be used by local people to help mitigate future climate change, as the effects from warming and thawing permafrost in this region will mainly have local impacts. Results show a decrease in permafrost extension from 70% in 1920 to 13% in 2000 to 1% in 2080 at 5 meter depth. The largest changes in permafrost distribution have and will be in the mountains.

The case study serves as an example for possibilities of translating regional downscaling into local practical use.

References

Berg P, Döscher R, Koenigk T (2013) Impacts of using spectral nudging on regional climate model RCA4 simulations of the Arctic. Geoscientific Model Development Discussions 6:495–520, DOI 10.5194/gmdd-6-495-2013

Döscher R, Wyser K, Meier H, Qian M, Redler R (2010) Quantifying Arctic contributions to climate predictability in a regional coupled ocean-ice-atmosphere model. Climate Dynamics 34:1157–1176, DOI 10.1007/s00382-009-0567-y

Johansson, M., J. Bengtsson, Z. Yang, Oregon, T. V. Callaghan, R. Döscher, S. Marchenko (2014): Past, present and future permafrost development in the Torneträsk catchment. Presentation at the 4th European Conference on Permafrost (18-21 June - Évora, Portugal)

Koenigk, T., P. Berg and R. Döscher, (2014): Arctic climate change in an ensemble of regional CORDEX simulations , to be submitted.

Evaluation of a surface temperature simulation over Tunisia using the WRF model

Bilel Fathalli[1], Benjamin Pohl[2], Thierry Castel[2] and Mohamed Jomaa Safi[1]

[1] Ecole Nationale d'Ingénieurs de Tunis, Université de Tunis El Manar, Tunisie (bilelfathalli@yahoo.fr)

[2] Centre de Recherches de Climatologie, CNRS/Université de Bourgogne, France

1. Introduction

According to a recent World Bank study (Verner 2013), Tunisia is and will continue be impacted by climate variability and change mainly through the adverse effects resulting from increasing temperatures, sea level rise, reduced and variable precipitation. Meteorological records and observations show that mean annual temperatures rose by about 1.4°C in the twentieth century.

In this context, the need for climate information at the regional scale by using regional climate models (RCMs) seems to be so necessary in order to examine Tunisian present climate and prepare illustrative scenarios for the future.

In this study, we aim to evaluate the Weather Research and Forecasting (WRF) model for regional climate application over Tunisia, focusing in simulated surface temperature.

2. Methods and data

The model used in this study is the Weather Research and Forecasting/Advanced Research WRF (ARW) model, version 3.4 (WRF here- after, Skamarock et al. 2008). WRF simulation was setup with two nested domains, one at 60 km and a second at 12 km horizontal grid spacing. The coarse grid (120 x 60 grid points) extends over the Mediterranean basin (Southern Europe and North Africa) while the high-resolution nest (46 x 71 grid points) covers Tunisia (Figure 1), both grids have 28 vertical levels.

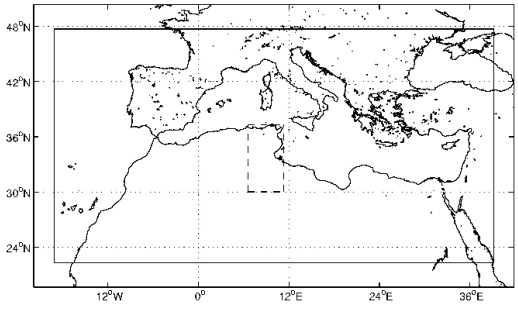


Figure 1. Model domains (continuous line for the parent domain and dashed line for the fine nest)

Initial and lateral boundary conditions for the outermost domain are provided at 6h interval by ECMWF ERA-interim (ERAI) reanalysis (Dee et al. 2011). SST for both grids are also provided every 24 h, at monthly resolution, from ERAI. Surface data are derived from the 20-category MODIS-based land use data with inland water bodies (Friedl et al. 2002). WRF physics options include the WRF Single-Moment 6-class (WSM6) for cloud microphysics, the Yonsei University (YSU) parameterization of the planetary boundary layer, the Rapid Radiative Transfer Model (RRTM) scheme for long wave radiations and Dudhia scheme for short wave radiations. Over the continent, WRF is coupled with Noah LSM 4-layer soil temperature, soil and canopy moistures model (Chen and Dudhia, 2001). The WRF run started at 0000 UTC 1 January 1991 and ended at 2400 UTC 31 December 2011. The first year was considered as model spin-up.

To assess the accuracy of our simulation, WRF surface (2m) temperature is compared (using the nearest grid point of the model to the observations) against an observational dataset belonging to the Tunisian National Institute of Meteorology. Available observations were checked for continuity, retaining 18 surface temperature stations. A variety of statistical verification techniques (Bias, Root Mean Square (RMSE), correlation coefficient (R) and Standard Deviation of the difference (SD)) are also used to evaluate the model. Comparisons are carried out at annual and seasonal time scales

3. Results

Long term means (1992-2011) of annual and seasonal simulated surface temperatures are given by figures 2 and 3. Spatial pattern of temperature is heterogeneous and significantly superimposed with regional topographic features. Indeed, the minimum of temperature is observed along the Tunisian Saharan Atlas while the maximum is obtained in the Tunisian salt depressions : “Chott el Djerid”, “Chott El Gharsa” (particularly visible during SON season, see frame in figure 3D).

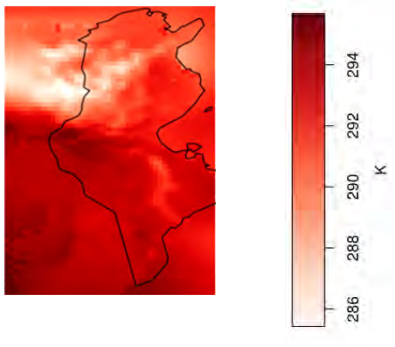


Figure 2. The 20-years mean annual simulated temperature

Spatial distributions of averaged annual and seasonal temperature biases are showed in figures 4 and 5. WRF underestimates mean annual temperature and only few (1 to 2) stations show hot seasonal biases. The south stations always record the highest values of bias. Error

measures computed by pooling together all the weather stations are summarized in table 1. The best correlation (0.92) between the simulated and observed temperatures is obtained during spring (MAM). Time averaged biases are cold and always inferior to -1°C.

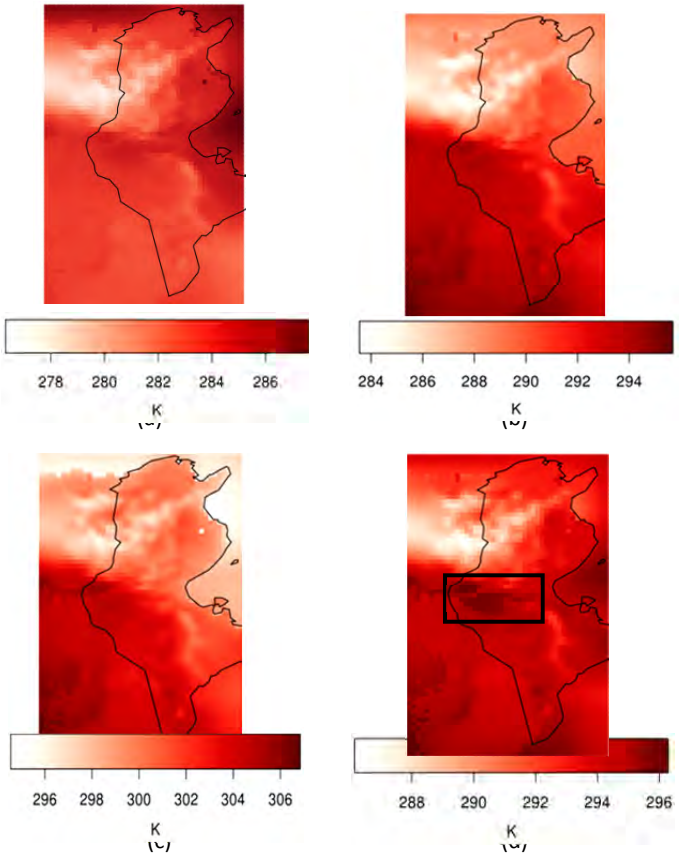


Figure 3. The 20-years mean seasonal simulated temperature (a: DJF, b: MAM, c: JJA and d: SON)

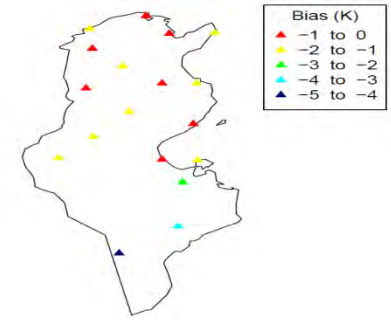


Figure 4. Spatial distribution of 20-years biases of annual temperature

3. Conclusion

WRF temperature simulation shows significant topographic signatures as the model uses finer surface parameters and more elaborated parameterization schemes allowing good representation of local processes. Simulated temperature is colder than the observations, especially in the south of the country where the model underestimates temperature higher than other regions. Although the systematic cold bias, WRF reproduces well the interannual variability and annual cycle (not shown) of Tunisian temperatures. Unlike results for the first domain (not shown) where simulations were compared to some observational gridded datasets, the few number of available stations cannot allow a robust evaluation of the model in addition to the lack of similar regional climate application performed over the country and allowing comparisons.

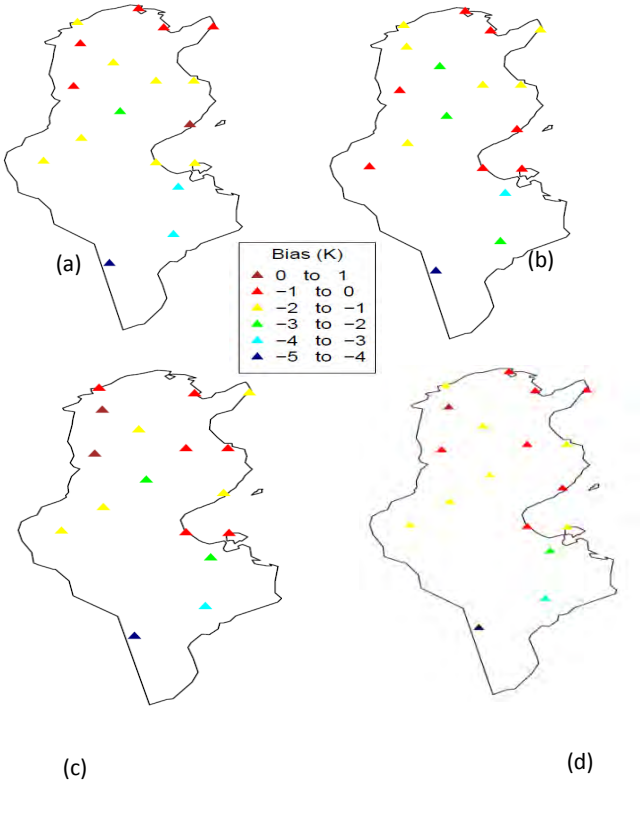


Figure 5. Spatial distribution of 20-years biases of seasonal temperatures (a :DJF, b: MAM, c: JJA and d : SON)

Table 1. Annual and seasonal temperature errors

	BIAS (°C)	RMSE (°C)	SD (°C)	R
Annual	-1,5	1,84	1,10	0,88
DJF	-1,6	1,93	1,09	0,80
MAM	-1,6	1,92	1,08	0,92
JJA	-1,3	1,90	1,40	0,89
SON	-1,4	1,83	1,22	0,85

Acknowledgments Calculations were performed using HPC resources from DSI-CCUB, Université de Bourgogne.

References

Chen, F., Dudhia, J. (2001) Coupling an advanced land-surface/hydrology model with the Penn State/NCAR MM5 modeling system. Part II: Preliminary model validation, Monthly Weather Review, 129., pp. 587-604

Friedl, M.A., McIver, D.K., Hodge,s J.C.F., Zhang, X.Y., Muchoney, D., Strahler, A.H., Woodcock, C.E, Gopal,S., Schneider, A., Cooper, A., Baccini, A., Gao, F., Schaaf, C. (2002) Global land cover mapping from MODIS: algorithms and early results, Remote Sens Environ, 83., pp. 287–302.

Dee, D.P et. al. (2011) The ERA-Interim reanalysis: configuration and performance of the data assimilation system, Q. J. R. Meteorol. Soc, 137., pp. 553–597. DOI:10.1002/qj.828

Skamarock, W. C., J. B. Klemp, J, Dudhia, D. O. Gill, D. M. Barker, M. Duda, X.-Y. Huang, W. Wang and J. G.Powers (2008) A Description of the Advanced Research WRF Version 3 NCAR Technical Note., 125p.

Verner, Dorte (2013) Tunisia in a Changing Climat : Assessment and Actions for Increased Resilience and Development. Washington, DC: World Bank. https://openknowledge.worldbank.org/handle/10986/13114 License: CC BY 3.0 IGO."

Typhoons in regional climate model simulations

Frauke Feser [1] and Monika Barcikowska [2]

[1] Institute for Coastal Research, Helmholtz-Zentrum Geesthacht, Geesthacht, Germany (Frauke.Feser@hzg.de)

[2] Princeton Environmental Institute, Princeton University, Princeton, U. S. A.

1. Typhoons and Best Track Data

Tropical cyclones like typhoons lead to large damages due to high wind speeds, rain falls, waves, and storm surges. A realistic reconstruction of the past state is needed to answer the question whether typhoons did become more frequent or stronger in order to deduce future trends.

Changes in typhoon frequency and intensity for the last decades can be derived from 'Best Track Data' sets. These data sets are provided by several meteorological institutes, which compile reanalyzed in-situ- and satellite-based measurements. Sea level pressure and near-surface wind speed along the cyclone's track are given. But, the individual best track data differ, especially for tropical cyclone intensities (Barcikowska et al., 2012).

Weather services have their own subjective approach in estimating TC intensity (i.e. different definitions of extreme intensity, measurement sources, and algorithms to estimate tropical cyclone intensity). This leads to severe inconsistencies in derived typhoon activity trends for the last decades, which makes it difficult to decide which data set is more realistic.

2. Regional Typhoon Simulations

A different approach to obtain homogenous long-term data is dynamical downscaling of reanalysis data with a regional climate model (RCM) (Feser and von Storch, 2008a, b). NCEP/NCAR reanalyses are spectrally nudged (von Storch et al., 2000) within the entire model domain in addition to the usual forcing via the lateral boundaries. The regional model used is CCLM.

A number of simulations were computed to test the influence of model settings and spectral nudging on typhoon formation (Feser and Barcikowska, 2012). The simulations with and some without spectral nudging differ only in their starting date. The overall number of simulated typhoons decreased by about a factor of two when spectral nudging was applied. But, the number of typhoon tracks which resembled observations, clearly increased. This is shown in Figure 1, which depicts three different typhoon tracks for ensemble simulations with and without spectral nudging. The spectrally nudged tracks converge soon after their appearance and are then very similar, while tracks without nudging are quite diverse and the typhoon was not found in each simulation. This improved TC climatology in the spectrally nudged simulation results from a more realistic representation of the mean climate state.

Some tests were performed to check if spectral nudging would inhibit typhoon formation at higher model levels. Vertical temperature profiles show that this was not the case. Large-scale circulations like the Madden–Julian Oscillation and monsoonal precipitation were also analyzed.

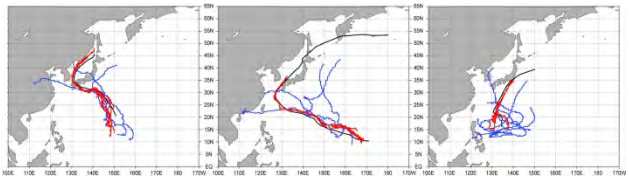


Figure 1. Tracks of Typhoon Namtheun 200410 (left), Songda, 200418 (middle) and Ma-on 200422 (right), as given by best track data of JMA (black), RCM simulations with (red) and without (blue) spectral nudging

3. Long-Term Typhoon Climatology

A regional climate simulation for Southeast Asia and the Northwest Pacific was computed for the last decades. The RCM CCLM was forced with either NCEP/NCAR or ERA-40 reanalyses. Intense tropical cyclone numbers show large similarity to observed ones, especially for the last three decades. But, TC frequency trends of all intensities differ. Both reanalyses indicate an increase in TC numbers, but Best Track Data exhibit decadal variability. The RCM run presumably reflects inhomogeneities of the forcing reanalyses. An upward shift in TC intensities as well as in the magnitude of its variability in 1978 was detected in both regional simulations. At this time satellite measurements were introduced to the atmospheric reanalyses that drive the RCM. This seems to be responsible for the detected shift, and may partly explain the increase in TC activity measures.

References

Barcikowska, M., F. Feser, and H. von Storch, 2012: Usability of best track data in climate statistics in the western North Pacific, Mon. Weather Rev., 140, pp 2818-2830, doi: 10.1175/MWR-D-11-00175.1.

Feser, F. and M. Barcikowska, 2012: The Influence of Spectral Nudging on Typhoon Formation in Regional Climate Models. Environ. Res. Lett., 7, 014024, doi:10.1088/1748-9326/7/1/014024

Feser, F. and H. von Storch, 2008b: Regional modelling of the western Pacific typhoon season 2004. Meteorolog. Z., 17 (4), 519-528.

Feser, F. and H. von Storch, 2008a: A dynamical downscaling case study for typhoons in SE Asia using a regional climate model. Mon. Weather Rev., 136 (5), 1806-1815.

von Storch, H., H. Langenberg, and F. Feser, 2000: A Spectral Nudging Technique for Dynamical Downscaling Purposes. Mon. Weather Rev. 128(10) 3664-3673.

Exploring new evaluation methods for RCM exercises. Using Australian soundings for the NARCliM experiment

L. Fita[1,2] , S. Liles[2] , J. P. Evans[2] , and D. ArgÜeso[2]

[1]Laboratoire de Météorologie Dynamique, UPMC-Jussieu, CNRS, Paris, France (lluis.fita@lmd.jussieu.fr)
[2]Climate Change Research Center – ARC CoECCS, UNSW, Sydney, Australia

1. Introduction

Regional Climate Model (RCM) simulations are commonly evaluated by comparison of the control period run with observed present day climatologies. Most frequently this involves daily precipitation and surface temperature (minimum and maximum) using either direct station based values or gridded datasets of these. These measured quantities are accessible, have long-time series and dense observational networks. At the same time, they directly impact many facets of human activity and hence are key focus on most of the experiments.

2. Methodology

In this talk we will present the results of an exploratory exercise using radiosondes to evaluate RCMs. Radiosondes often have a long period of record but with a sparser spatial distribution. Balloon records have the advantage that they provide vertical information of the state of the atmosphere and they record information of all the state variables. Thus, they offer a distinctly different way to evaluate RCM experiments.

The NARCliM experiment (http://www.ccrc.unsw.edu.au/NARCliM/) is a dynamical downscaling exercise performed in Australia. An ensemble of simulations is produced using 3 different conf gurations of a regional model (WRF v3.3), with 4 different GCMs over 3 time-windows: 1989-2009, 2020-2040, 2060-2080. We present a series of statistical analyses for the control period run (1950-2009) using the NCEP/NCAR re-analyses as the boundary and initial conditions. Bureau of Meteorology soundings data is used as the observational data-set and the RCM simulations are evaluated at different locations in order to capture the richness of climates existing in Australia.

3. Results

Preliminary Results show a variety of results depending on the station, the variable and the height illustrating the potential of such an evaluation.

Representation of Heavy Precipitation Events over the western Mediterranean region in regional climate models

Fosser G[1], Roehrig R[1], Nuissier O[1], Dubois C[1] and Somot S[1]

[1] CNRM-GAME, Météo France & CNRS, Toulouse , France (giorgia.fosser@meteo.fr)

Heavy Precipitation Events (HPEs) often cause in autumn devastating flash-floods over the western Mediterranean region (Ducrocq et al. 2008; Nuissier et al. 2008). Regional Climate Models (RCMs) are often used to determine the effect of climate change at regional level and to elaborate effective adaptation strategies. Thus, it is crucial to investigate the reliability of RCMs in representing these type of events, in order to deliver informative and relevant messages to end-users.

The present study is based on RCM simulations of the recent period driven by ERA-Interim reanalysis, which were performed within the CORDEX (Med-CORDEX, Euro-CORDEX) framework. The aim is to evaluate the skill of several RCM atmospheric components in capturing the physics and dynamics of HPEs.

The investigation area covers the south of France, where a dense rain gauge network is available (Figure 1).

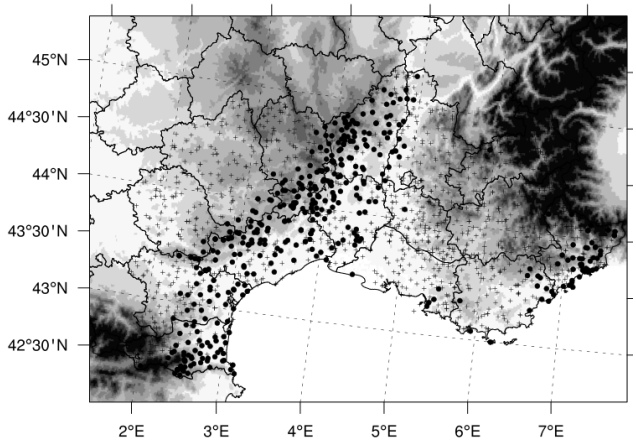


Figure 1. Topographical map of the south of France. The black crosses indicate the available precipitation gauges. The black dots represent the rain gauges selected for the analysis of HPEs.

The observational dataset is first used to evaluate the main features of extreme precipitation over the region. Then, an objective selection of the most extreme HPEs is performed, based on two criteria: an intensity constraint using the 99.9% quantile at the station level and a scale constraint of the system to eliminate local convective events. These HPEs can be further clustered according to the associated large-scale and synoptic situation. The ability of RCMs to reproduce the chronology and structure (location, intensity) of these events is then evaluated, using new statistical methods such as Fraction Skill Score (Roberts and Lean 2008). The link with the large-scale situation is also assessed to better identify model weaknesses. The analysis then focuses on the atmospheric conditions associated with HPEs (e.g. instability, vertical profiles of temperature and humidity, moisture and radiation budgets, orography, cold pools generated by evaporation of convective precipitation and other triggering/maintenance mechanisms), in order to identify which types of events are best represented in RCMs, which are not and why. Particular attention is given to the influence of parameterisations on the representation of HPEs, as well as to the potential added value of increased horizontal resolution (from ~50km to ~10km).

References

Nuissier O, Ducrocq V Ricard, D, Lebeaupin C and Anquetin S (2008) A numerical study of three catastrophic precipitating events over southern France. I: Numerical framework and synoptic ingredients, Q.J.R. Meteorol. Soc., 134, 111–130. doi: 10.1002/qj.200

Ducrocq V, Nuissier O, Ricard D, Lebeaupin C and Thouvenin T (2008) A numerical study of three catastrophic precipitating events over southern France. II: Mesoscale triggering and stationarity factors, Q.J.R. Meteorol. Soc., 134, 131–145. doi: 10.1002/qj.199

Roberts N M and Lean H W (2008) Scale-Selective Verification of Rainfall Accumulations from High-Resolution Forecasts of Convective Events, Mon. Wea. Rev., 136, 78–97

Challenges for RCM evaluation and application when moving to high resolutions

Hayley J Fowler[1], Elizabeth J. Kendon[2], Stephen Blenkinsop[1], Steven C. Chan[1,2], Nigel Roberts[3], Christopher A. T. Ferro[4]

[1] School of Civil Engineering and Geosciences, Newcastle University, UK (h.j.fowler@ncl.ac.uk)

[2] Met Office Hadley Centre, Exeter, UK.

[3] MetOffice@Reading, Reading, UK.

[4] University of Exeter, Exeter, UK.

Very high resolution Regional Climate Models of 4km or less are now more commonplace within climate modelling groups and a number of simulations have now been run as full decadal length integrations. However, appropriate observed datasets and analysis methods are not necessarily available with which to evaluate these new simulations. This presentation will evaluate methods and datasets that have been developed and are being developed in further projects to allow the evaluation of very high resolution RCMs.

1. Very High Resolution Regional Climate Modelling

Convection-permitting models are commonly used for short-range weather forecasting, and they have benefits in terms of representing convection. The added value of convection-permitting resolutions has also been seen in longer seasonal simulations. Improvements are found in the diurnal cycle of convective rainfall [e.g. Hohenegger et al., 2008], the spatial structure of rainfall [Warrach-Sagi et al., 2013] and the intensity of the most extreme rainfall [Prein et al., 2013]. Kendon et al. [2012] carried out a continuous (20 year) length climate simulation with a 1.5 km model over a region of the UK. They showed improved realism in the representation of hourly rainfall, including the duration-intensity characteristics and the spatial extent of heavy rain. Evaluation of the same 1.5 km simulation also revealed an improved realism in the representation of hourly extremes compared to a 12 km resolution model [Chan et al., 2014].

However to be confident in a regional climate model's projections of sub-daily rainfall extremes, the model must be able to represent the physical processes responsible for future changes. Convection-permitting models in particular have shown a high degree of realism in the representation of rainfall (including the spatial and temporal characteristics of rainfall across a range of space and time scales, as a function of the meteorological situation). This provides a good indication of their skill in representing the underlying physical processes [Kendon et al., 2012]. This model evaluation step has proven difficult, particularly for precipitation, as observations of sub-daily rainfall are typically short, have been subject to changes in instrumentation technology over time, and are only available at a small number of locations worldwide.

2. High Resolution Observed Datasets for Model Assessment

The lack of long, homogenous, high-quality extreme rainfall data at sub-daily timescales represents a significant barrier for further progress in assessing whether sub-daily extremes are intensifying under climate change. The absence of comprehensive international repositories for sub-daily data, instrumental limitations in the capacity to measure high-intensity short-duration rainfall, inhomogeneities in the instrumentation technology used over time, and inconsistent approaches for quality assessment and control have all acted to hamper progress in this area. Potential approaches for better using the available sub-daily record will be described in the next section; however, it is clear that climate models at different spatial and temporal resolutions will be required to supplement instrumental data in assessing how sub-daily extremes can be expected to change under a future climate.

3. Recent assessment of a Very High Resolution RCM over the UK

In Kendon et al. (in press) we have recently compared future changes in hourly rainfall in the 1.5km RCM with results from a 12km RCM over the southern UK. The models were run for 13-year present-day (1996-2009) and 13-year future (2100), under the Intergovernmental Panel on Climate Change RCP 8.5 scenario) periods, driven by a 60km global climate model (GCM). Model biases for the present-day were assessed by comparison with gridded hourly observations from radar, available for 2003-2012.23 Since radar tends to systematically underestimate heavy rain, we applied a bias correction using daily gauge observations. This was used as an alternative to hourly observations from ~300 stations across England and Wales processed from TBR gauges due to its spatial consistency.

Remotely sensed data remains under-utilized in studies of sub-daily rainfall. However, there are many issues with radar data (clutter, anaprop, bright band, beam attenuation), and in particular radar data are known to systematically underestimate heavy rainfall amounts. Despite this, Berne and Krajewski [2013] recently suggested that radar can be used to analyse the dynamics and variability of extreme events, and to understand the spatial variability of extreme rainfall and a bias-corrected radar product has been developed to assess high resolution regional climate model simulations of short-duration precipitation extremes [Kendon et al., in press].

The UK Met Office calibrates radar against rain gauges

and employs algorithms to take account of known issues but some problems cannot be fully rectified. One of these is that the hourly gauges used in the calibration are relatively sparse, and thus are not able to fully correct for locally-varying effects such attenuation. Despite possible large measurement errors, daily rainfall extremes from the radar were found to be comparable to those from gridded daily gauge data. Additionally, the rate of increase of return levels with increasing return period (the 'growth curve' commonly used in hydrology) is comparable between radar data and hourly gauge station estimates. This suggests that radar data can provide useful information for assessing model-simulated precipitation extremes. However, bias correction (simple scaling) was applied to the radar data to account for errors due to beam attenuation. Although this product is far from perfect, blended radar and observation datasets are need to assess the ability of very high resolution RCMs to simulate sub-daily rainfall patterns.

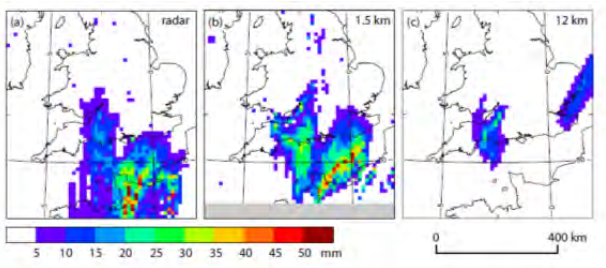


Figure 1. Rainfall accumulations (mm) for the 5 hour period 13 to 18 UTC on 27th July 2013 for the (a) radar, (b) 1.5km UKV forecast model and (c) 12km forecast model. Forecasts were initiated at 21 UTC on the 26th (UKV) and 18 UTC on the 26th (12km). From Kendon et al. (in press).

Novel methods must also be developed for model assessment. One such method may be to examine comparable events in observations, historical, control and future runs and their environmental controls to see if the models are able to reproduce these factors. We assessed the ability of the models to simulate heavy rainfall events. Looking at the heaviest 50 events (averaged to the 12km grid) in the 1.5km model in summer in the future simulation, about half of these are larger-scale storms (embedded convection within a front, Mesoscale Convective Systems or squall lines) with the remainder being individually smaller storms (often clustered). The events appear physically plausible, with realistic evolution and the model responding to the environment in a sensible way. In particular, nearly all events are associated with cyclonic flow and hot humid conditions (high 850hPa wet-bulb potential temperature). A recent observed event (27th July 2013) with similar conditions is shown in Figure 1 (from Kendon et al., in press), illustrating the ability of the 1.5km model to capture rainfall accumulations associated with an intense squall-line, for example.

4. Conclusions and Recommendations

A recent review of changes to sub-daily rainfall extremes by a team of international authors (Westra et al., submitted) concludes that a focused international research effort is needed to better understand future changes to sub-daily extreme rainfall, and should focus on: (1) improving both gauge-based and remotely-sensed observing networks; (2) developing and applying extreme value techniques that can handle a diversity of artefacts particularly prominent in sub-daily rainfall data; (3) applying kilometre-scale models to climate change studies, and improved assessment of the performance of these models in simulating short time-scale rainfall; and (4) strengthening the link between climate science and impact science, focusing on understanding how extreme rainfall leads to flood risk.

To aid this endeavor a cross-cutting activity has been set up by GEWEX to coordinate the collection, evaluation and processing of global sub-daily rainfall observations to supplement the HadISD product developed by Dunn et al. (2012). This group will also try to set standard evaluation methods for sub-daily rainfall products and methods for a global analysis. Additional efforts should also be concentrated on a coordinated assessment of very high resolution RCM outputs from different groups worldwide using standard assessment methods and datasets. This will be ad hoc but could then lead to coordinated experiments like CORDEX, NARCCAP or ENSEMBLES but at very high resolutions, when observations can be made available with which to evaluate these simulations.

References

Berne, A., and W. F. Krajewski (2013), Radar for hydrology: Unfulfilled promise or unrecognized potential? , Advances in Water Resources, 51(0), 357-366.

Chan, S. C., E. J. Kendon, H. J. Fowler, S. Blenkinsop, N. M. Roberts, and C. A. T. Ferro (2014) The value of high-resolution Met Office regional climate models in the simulation of multi-hour precipitation extremes, Journal of Climate, In press.

Dunn, R. J. H., K. M. Willett, P. W. Thorne, E. V. Woolley, I. Durre, A. Dai, D. E. Parker, and R. S. Vose (2012), HadISD: A quality-controlled global synoptic report database for selected variables at long-term stations from 1973-2011, 8(1649-1679).

Hohenegger, C., Brockhaus, P. & Schar, C. (2008) Towards climate simulations at cloud-resolving scales. Meteorol. Z. 17, 383–394.

Kendon, E. J., N. M. Roberts, C. A. Senior, and M. J. Roberts (2012), Realism of rainfall in a very high resolution regional climate model, Journal of Climate, 25(5791-5806).

Kendon, E. J., N. M. Roberts, H. J. Fowler, M. J. Roberts, S. C. Chan, and C. A. Senior (in press), Heavier summer downpours with climate change revealed by weather forecast resolution model, Nature Climate Change.

Warrach-Sagi, K., T. Schwitalla, V. Wulfmeyer, and H.-S. Bauer (2013) Evaluation of a climate simulation in Europe based on the WRF-NOAH model system: precipitation in Germany, Climate Dynamics, 41, 755-774.

From high-resolution simulations to the client

Anne Frigon [1], Sébastien Biner [1], Ramon de Elia [1,2]

[1] Ouranos Consortium on regional climatology and adaptation to climate change, Climate Simulation and Analysis Group, Montreal, Canada (frigon.anne@ouranos.ca)

[2] Centre pour l'étude et la simulation du climat à l'échelle régionale, Université du Québec à Montréal (UQAM), Montréal, Canada

1. A new Regional Climate Model at Ouranos

Over the last few years, the Climate Simulation and Analysis Group at Ouranos has started the operationalization of the new Regional Climate Model (RCM), developed by Environment Canada and Université du Québec à Montréal. This new model contains many new features that make it a better tool to be driven by the latest generation of Earth System Models. Thanks to its parallel computing capabilities and physics scaled to high resolution, it allows us to plan the production of an ensemble of climate projections at a 25-km resolution over a large North American domain. Results of the first simulations will be presented and compared with those performed with the previous generation RCM (the Canadian Regional Climate Model version 4).

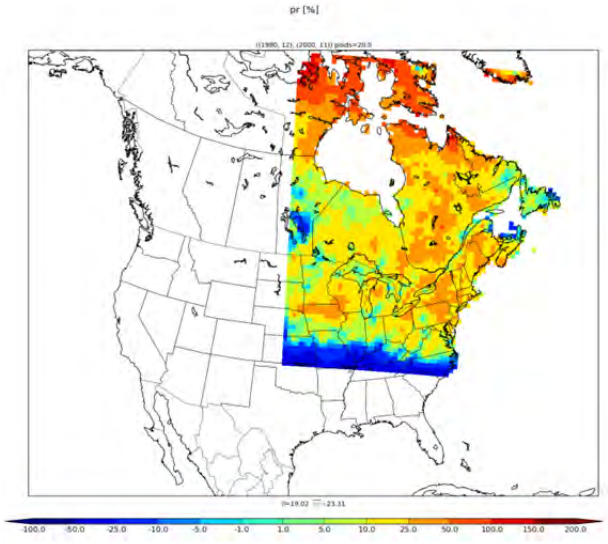


Figure 1. Preliminary validation results from the new RCM for fall (SON) precipitation over the 1981-2000 period, compared to the CRU TS 3.2 [relative error in %]. In this case, the historical simulation was driven by ERA-interim over a sub-domain.

2. An RCM-generated historical database to circumvent insufficient observational data

An integrative approach to the handling of observations in the model validation process will also be presented, along with the associated uncertainty, showing large differences between datasets. This approach brought us to develop a new project aimed at producing a high-resolution (15 km) historical database over the recent past covering the province of Quebec. This project addresses a need expressed by many users at Ouranos in the last few years, and constitutes a promising solution to the problem of missing data over the territory, which represents a major impediment to impact and adaptation studies. The database is also planned to provide information on the uncertainty associated to each available meteorological variable.

3. Providing usable information to the users

In addition, we will present new analysis techniques that help us transform climate change simulation outputs into usable information for Ouranos' members and clients. A key issue for climate change information users relates to the rate of change of the variables of interest and their vulnerability associated to this change. Results from this technique (de Elia et al. 2013, 2014), that relates to the Time-of-Emergence approach, already in use by some researchers (Giorgi and Bi 2009, Hawkins and Sutton 2012, Maraun 2013), will be presented.

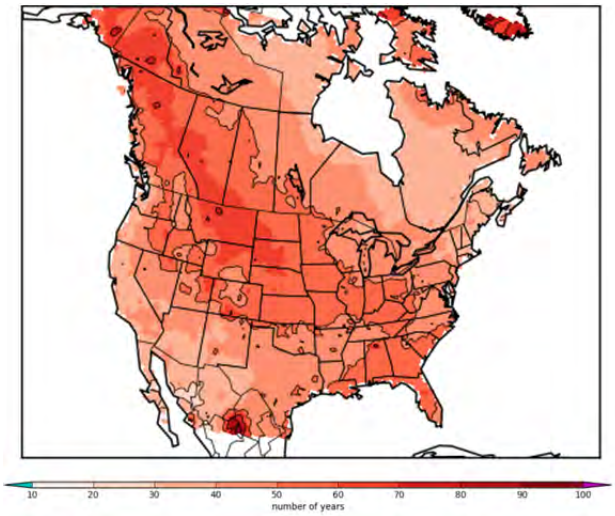


Figure 2. Number of years needed for detecting the climate change trend projected by NARCCAP models (winter). Regions of large trends as well as small inter-annual variability are affected earlier (see de Elia et al. 2013).

References

de Elia, R, S Biner, A Frigon, H Côté (2014) Timescales associated to climate change and their relevance in adaptation strategies. Climatic Change. Submitted March 2014.

de Elia, R, S Biner, A Frigon (2013) Interannual variability and expected regional climate change over North America. Climate Dynamics. Vol. 41(5-6), pp. 1245-1267. DOI: 10.1007/s00382-013-1717-9.

Giorgi, F, X Bi (2009) Time of emergence (TOE) of GHG-forced precipitation change hot-spots. GRL, Vol. 36, DOI:10.1029/2009GL03759.

Hawkins E, RT Sutton (2012) Time of emergence of climate signals. Geophys Res Lett, Vol. 39, pp. 1–6. DOI:10.1029/2011GL050087.

Maraun, D (2013) When will trends in European mean and heavy daily precipitation emerge? Environ. Res. Lett., Vol. 8 DOI:10.1088/1748-9326/8/1/014004.

Evaluation of CORDEX-REMO simulations applying a new high-resolution gridded dataset for the Carpathian region

Borbála Gálos[1], Sándor Szalai[2], Diana Rechid[3,4], Claas Teichmann[3,4], Arne Kriegsmann[4], and Daniela Jacob[4]

[1] Institute of Environmental and Earth Sciences, University of West Hungary, Sopron, Hungary (bgalos@emk.nyme.hu)
[2] Szent István University, Faculty of Agricultural and Environmental Sciences, Gödöllő, Hungary
[3] Max-Planck-Institute for Meteorology, Hamburg, Germany
[4] Climate Service Center – eine Einrichtung am Helmholtz-Zentrum Geesthacht, Hamburg, Germany

1. Background

For evaluation and validation of high-resolution RCM simulations as well as for applied regional climatological studies, cross-border harmonized datasets are essential in fine temporal and spatial structure. In the frame of the CarpatClim project a fine-scale gridded database has been developed for the Carpathian region (Szalai et al. 2013). The 0.1° x 0.1° grid dataset is based on station data of the national meteorological services and is freely available in the form of a digital Climate Atlas (www.carpatclim-eu.org). It includes harmonized and spatially interpolated data for 16 basic meteorological parameters in daily temporal resolution, as well as several climate indicators (primarily drought indices) from 1961 to 2010.

The CarpatClim database is the best available validation dataset for Hungary, so far. In this study, we use this new dataset to evaluate historical climate simulations of a GCM-RCM model chain, which serve as baseline climate simulations for climate change studies with the same model chain. The aim of our study was to evaluate, how the mean annual cycle of temperature and precipitation as well as the frequency distribution of daily values are represented at the increased horizontal resolution of a regional climate model.

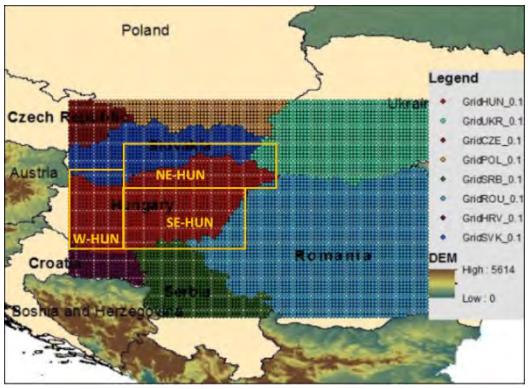


Figure 1. The target area and the countries of the CarpatClim project. The investigated sub-regions are marked with rectangles.

2. Data and methods

For the time period 1971-2000 the EURO-CORDEX results (Jacob et al. 2013) of the GCM-RCM model chain MPI-ESM / REMO have been analysed. The global climate simulations of MPI-ESM had been downscaled with REMO using double nesting technique, first to 0.44°, then to 0.11° horizontal resolution.

Simulated temperature and precipitation values of REMO on 0.44° and on 0.11° resolution were compared to gridded observational data from the CarpatClim database. The 0.1° x 0.1° grid daily dataset covers the area between latitudes 44°N and 50°N, and longitudes 17°E and 27°E. In this study 3 sub-regions in Hungary have been selected and investigated (Fig. 1).

3. Mean annual cycle of temperature and precipitation

From March to July the simulated monthly temperature means are close the observations on 0.44° resolution, but they are overestimated by up to 0.5-1.5 °C on finer resolution. Consequently, REMO results in 0.44° horizontal resolution show better agreement with the CarpatClim data than the 0.11° simulation in the investigated regions (Fig. 2).

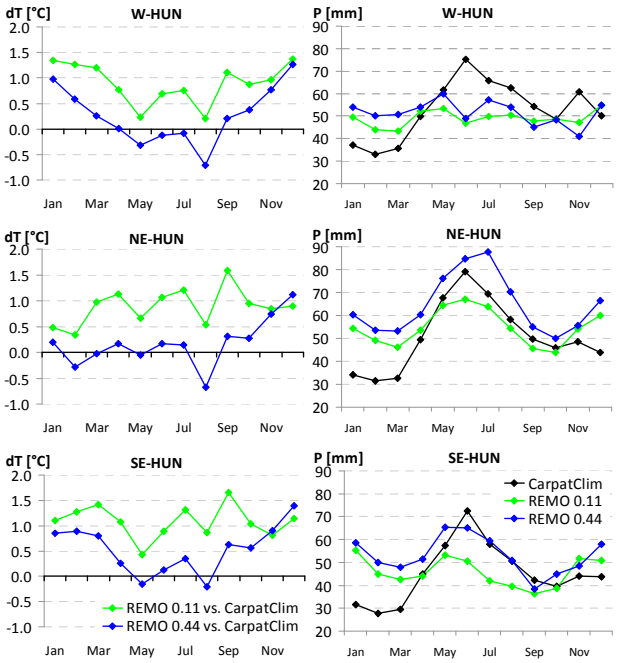


Figure 2. Model biases with respect to the CarpatClim observational dataset for the montly temperature means (dT; left panel) and the simulated and observed annual cycle of precipitation (P; right panel) for the selected Hungarian sub-regions in the time period 1971-2000.

Precipitation sums in winter and early spring are overestimated in both REMO simulations. Except of the summer months, the model bias is improved by the higher resolution (fig. 2). Variability of the sign and

magnitude of the model bias among the selected regions is the largest in summer.

4. Frequency distribution of daily temperature and precipitation

The simulated distribution of daily temperatures can be characterized by less cold values compared to the CarpatClim data. For the 0.11° simulation the frequency of extreme warm temperature means is overestimated (Fig. 3). The value of the 90th percentile is 1 °C higher than observed in all regions (not shown). For warm days the model biases are larger at high resolution than at low resolution. A possible reason for it could be the drying out of soil, which needs further investigations.

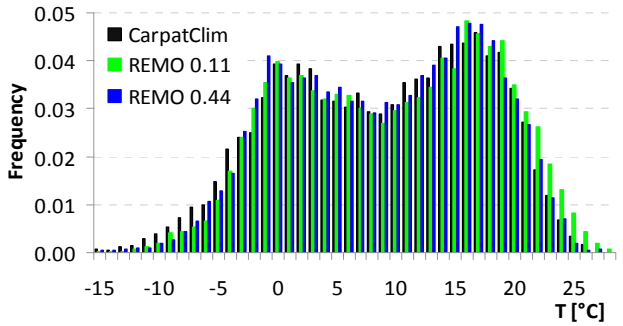


Figure 3. Frequency distribution of the daily mean temperatures for the Norteast-Hungarian sub-region in the time period 1971-2000.

REMO simulates less dry days compared to the observational dataset on both horizontal resolutions. The frequency of higher daily precipitation intensities is overestimated for eastern Hungary, in case of the 0.44° simulation. On 0.11° resolution the total number of days above 20 mm precipitation is underestimated, it is 51-62 % of the observed amount (Fig. 4).

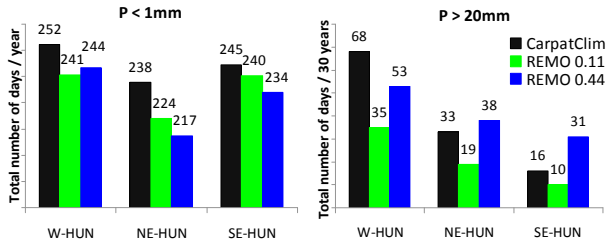


Figure 4. Total number of dry days/year (left) and heavy rainfall events/30 years (right) in the time period 1971-2000, for the selected sub-regions.

5. Conclusions

The effects of the increased resolution on the model bias have been evaluated applying the new high-resolution observational dataset CarpatClim. Results of the 3 sub-regions can be summarized and concluded as follows:

- For the annual cycle, the 0.11° simulation show warmer and dryer conditions compared to the 0.44° simulation.
- Monthly precipitation sums (except of summer months) are better represented in the 0.11° simulation.
- However, for monthly temperature means and daily extremes the increase of resolution does not improve the model bias in the analyzed regions (this is similar to the findings of Vautard et al. 2013).
- The possible reasons of the larger frequency of the simulated extreme warm temperatures as well as the underestimation of the high daily precipitation amounts on finer resolution will be further investigated.
- In depth analyses are essential for other regions, models and extreme indices. The CarpatClim data are planned to be compared to other observational datasets.

Long-term time series of harmonized, good quality climatological data over large regions can effectively support model validation and evaluation. Therefore it is suggested to extend the CarpatClim dataset for whole Europe that could also serve as basis for climate impact research.

References

Jacob D., et al. (2013) EURO-CORDEX: new high-resolution climate change projections for European impact research, Reg Environ Change, DOI 10.1007/s10113-013-0499-2

Szalai S., Auer I., Hiebl J., Milkovich J., Radim T. Stepanek P., Zahradnicek P., Bihari Z., Lakatos M., Szentimrey T., Limanowka D., Kilar P., Cheval S., Dea, Gy., Mihic D., Antolovic I., Mihajlovic V., Nejedlik P., Stastny P., Mikulova K., Nabyvanets I., Skyryk O., Krakovskaya S., Vogt J., Antofie T., Spinoni J. (2013) Climate of the Greater Carpathian Region, Final Technical Report, www.carpatclim-eu.org

Vautard R., et al. (2013) The simulation of European heat waves from an ensemble of regional climate models within the EURO-CORDEX project, Clim Dyn, 41, 2555-2575, DOI 10.1007/s00382-013-1714-z

Climate model results for wind speed and direction over the North Sea

Anette Ganske[1], Gudrun Rosenhagen[2] and Hartmut Heinrich[1]

[1] Federal Maritime and Hydrographic Agency, Hamburg, Germany (Anette.Ganske@bsh.de)
[2] Deutscher Wetterdienst, Hamburg, Germany

1. Introduction

The most affecting climate element at sea is the wind Wind speed and direction influence the currents, surges, waves and the probability and strength of storm floods. Changes in the wind fields may have severe impact for the safety of the coasts, the navigation. The analysis of these consequences is the aim of the project KLIWAS of the German Federal Ministry of Transport and Digital Infrastructure (BMVI).

Wind speed frequency distributions and wind direction frequencies of 10 m wind over the North Sea from an ensemble of Regional Climate Model (RCM) runs were examined for subareas of the North Sea. The chosen subareas are identical with those used for operational forecasts of wind speed over the North Sea, see Figure 1. Hence it was assumed, that wind speed and direction at all grid points within each respective area are highly correlated.

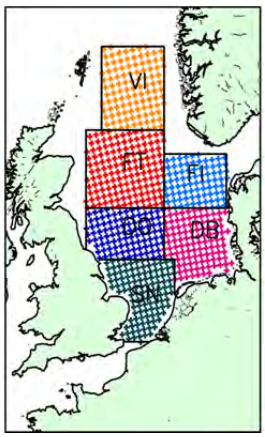


Figure 1: The North Sea subareas and the RCM grid points over sea of each area.

2. Frequency distributions of wind speed

Yearly wind speed frequency distributions were calculated by concatenation of daily values for all grid points of each subarea of the North Sea. Percentiles of the distributions were evaluated for 8 RCM runs based on the A1B scenario and for the time period 1961 – 2099. All percentile time series showed strong yearly fluctuations and minor trends, which were often statistically insignificant. Running 30-year means of yearly percentiles for the whole period also displayed decadal fluctuations.

3. Frequency distributions of wind directions

To examine changes in wind direction high frequency data are required because a temporal resolution of daily means is not sufficient. Investigations of past storm surges at the German coasts have shown that the wind direction causing the highest surges only lasted for a few hours. For this reason, only sub-daily results can be used for the analysis of wind direction causing storm surges. Those were only available from six of the eight RCM runs. Wind direction data were sampled in eight classes and yearly frequencies calculated for each North Sea subarea by concatenation over all grid points. Time series of yearly frequencies of the wind direction classes showed inter-annual as well as decadal fluctuations. However, significant trends were found for few wind directions and RCM runs, only.

Is it possible to separate model calibration and evaluation? A multi-physics study with modern radiation and soil datasets

Markel García-Díez[1], Jesús Fernández[1] and Robert Vautard[2]

[1] Department of Applied Mathematics and CC, University of Cantabria, Santander, Spain (garciadm@unican.es)

[2] Laboratoire des Sciences du Climat et de l'Environnement, Institute Pierre-Simon-Laplace, CEA, CNRS, UVSQ, Gif sur Yvette, France

1. Introduction

Over the last years, a large effort has been put in developing Regional Climate Models capable to accurately represent the physical processes behind regional-scale climate and climate change. However, the evaluation process is still facing important challenges. Climate models are complex programs that manage many variables and are adjusted with many parameters, some of which are difficult or impossible to measure (Mauritsen et al. 2012). In most evaluation studies, only a few variables are used, being precipitation and temperature the most popular ones. Furthermore, there is not a clear enough discrimination between the calibration and evaluation processes. This can lead to reduce the bias by balancing out errors, instead of improving physical realism.

In this context, multi-physics ensembles (MPEs) appear as an interesting methodology. These ensembles are built by perturbing a model changing the physical parameterizations used to represent unresolved phenomena (e.g., microphysics, cumulus, etc). In this work, our goal is to show how a multi-variable analysis of an MPE can be used to improve the understanding of the physical realism of a model, and of the sources of uncertainty. With this aim, a MPE is analysed looking not only P&T, but also at radiation fluxes, cloud cover, soil moisture and albedo.

2. Model configuration

A new 8 member multi-physics ensemble has been produced with the Weather Research and Forecasting (WRF) model. The parameterization combinations are based in those used by the WRF contributions to Euro-CORDEX evaluation simulations in Vautard et al. (2013), and are summarized in table 1. ERA-INTERIM reanalyses have been used as boundary data and the domain used is the CORDEX-compliant domain for Europe at 0.44 deg. horizontal resolution. The period covered is 5 year long (2002-2006) leaving one year (2001) as spin up. The RCM used is the (WRF) model version 3.3.1, which is an open source model described in detail in Skamarock et al. (2008). Thus, the present results are directly relevant for the WRF community involved in CORDEX. Moreover, the multi-physics methodology can be used with any model, and some of the problems detected in WRF are also present in other RCMs (Samuelsson et al. 2011).

3. Observations

Observations from different sources have been gathered. For temperature and precipitation the well-known E-OBS dataset has been used. For radiation data the Cloud and Earth's Radiant Energy System (CERES) has been chosen as reference dataset. Finally, for soil moisture the Global Land Data Assimilation System (GLDAS) data have been used. These are not observations, but a reanalysis produced by forcing a land surface model (Noah-LSM) with observations. This is the LSM used in our simulations, so GLDAS provides a good reference as essentially is WRF soil with unbiased forcing.

4. Results

The analysis involves 8 different simulations and 10 variables. In summer, similar patterns were found between temperature (not shown) and short wave downward radiation biases (figure 1) Some simulations (MPE-C, MPE-A), compensate too cold temperatures with excessive radiation.

Two main biases have been identified in the model. One is the overestimation of precipitation, which occurs in almost in all seasons and ensemble members, except MPE-M, and specially in the eastern half of the domain. The second bias is the pronounced cold bias appearing in the NE quarter of the domain during winter, which is related to the treatment of the snow cover. It was found that this bias propagates by affecting the albedo in the beginning of the spring.

Sensitivity to parameterizations is found to be very large for cloud cover and radiation, explaining the ensemble spread found in the temperatures. Simulations using the M-2M microphysics are found to remove the winter cold bias in the NE by producing an unrealistic cloud cover. RRTMG is generally warmer than CAM thanks to an enhanced downward long wave radiation flux. Spatial correlations amongst the biases found for the different variables are summarized using dendrograms computed with correlation distance.

5. Conclusions

A new multi-physics ensemble has been produced and analysed with observations from different sources. The analysis extends beyond precipitation and temperature (P&T) and spans other key variables in the climate system, such as radiation fluxes and soil moisture. It is shown how, when abandoning the limited perspective of P&T, a rich and complex picture emerges, where the good performance in some variables is often related to compensation of errors and not to improved realism. It is generally assumed that observations used for model calibration cannot be also used for evaluation and ensemble weighting. In the present study, distinguishing

these two processes is shown to be crucial, as important variables as temperature are very easy to tune. Thus, a large effort is needed to improve the documentation and transparency of the model calibration process.

Table 1: Parameterization combinations used in the multi-physics ensemble. Legend: KF is Kain-Frisch scheme, BM is Betts-Miller-Janjic, GD is Grell-Devenyi, WSM is WRF Single Moment (3, 5 or 6), M-2M is Morrison-2 Moment, CAM is the Community Atmosphere Model radiation scheme and RRTMG an improved version of the Rapid Radiative Transfer model.

Label	Cumulus	Microphysics	Radiation
MPE-A	KF	WSM6	CAM
MPE-C	KF	WSM3	CAM
MPE-D	BM	WSM6	RRTMG
MPE-F	GD	WSM5	RRTMG
MPE-G	GD	WSM6	CAM
MPE-H	KF	M-2M	CAM
MPE-M	GD	M-2M	CAM
REFOR	GD	WSM6	CAM

References

Mauritsen, T., B. Stevens, E. Roeckner, T. Crueger, M. Esch, M. Giorgetta, H. Haak, J. Jungclaus, D. Klocke, D. Matei, U. Mikolajewicz, D. Notz, R. Pincus, H. Schmidt, and L. Tomassini (2012), Tuning the climate of a global model, Journal of Advances in Modeling Earth Systems, 4 (3), doi: 10.1029/2012MS000154.

Samuelsson, P., C. G. Jones, U. Willen, A. Ullerstig, S. Gollvik, U. Hansson, C. Jansson, E. Kjellstr om, G. Nikulin, and K. Wyser (2011), The rossby centre regional climate model rca3: model description and performance, Tellus A, 63(1), 4-23.

Skamarock, W., J. Klemp, J. Dudhia, D. Gill, D. Barker, M. Duda, W. Wang, and J. Powers (2008), A description of the advanced research wrf version 3, Tech. rep., NCAR.

Vautard, R., A. Gobiet, D. Jacob, M. Belda, A. Colette, M. Deque, J. Fernández, M. García-Díez, K. Goergen, I. Güttler, and others (2013), The simulation of european heat waves from an ensemble of regional climate models within the euro-cordex project, Climate Dynamics, p. 1-21, doi:10.1007/s00382-013-1714

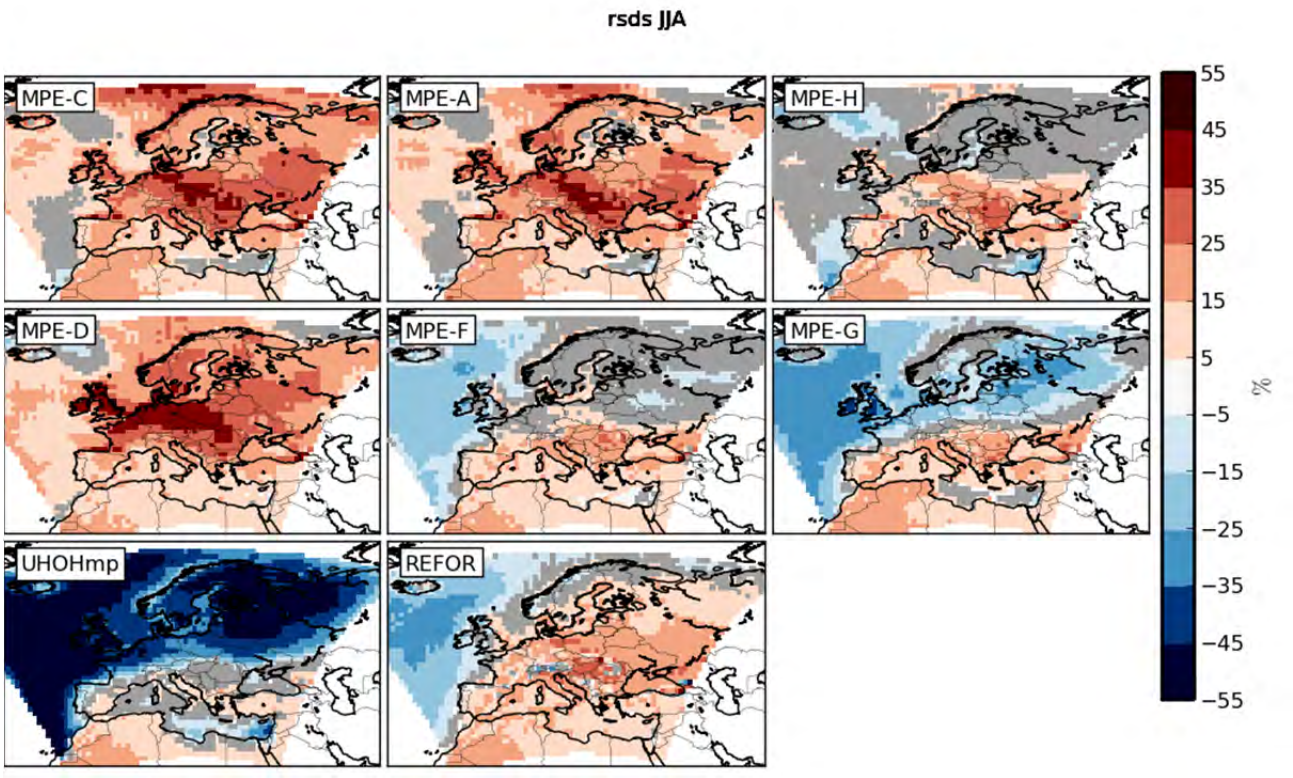


Figure 1: Relative bias for surface short wave downward radiation flux in JJA. The points which were not found to be significantly different from zero with a t-test are grayed out.

Development, validation and application of a single-column atmosphere model in the framework of the Canadian RCM with an application to deep Lake Geneva

Stéphane Goyette and Marjorie Perroud

C[3]i, Institute for Environmental Sciences, University of Geneva, Switzerland (stephane.goyette@unige.ch)

This study investigates the potential of an atmospheric single-column model, SCM, developed in the framework of the Canadian Regional Climate Model, C-RCM. This SCM, termed FIZC, is embeddable in the C-RCM computational grid, and intended to be run separately but with a numerical structure similar to that developed for the C-RCM. FIZC, offers interesting prospects as the resolution of regional models is ever increasing. Its usefulness is undeniable and potential applications are numerous due to the low computational cost and the versatility of this approach to realize specific case studies, as well as longer term simulations. Ad hoc parameterizations are avoided as far as possible to distinguish this model from others SCMs published so far in the literature. Results from sensitivity studies to some structural parameters are first described. Here the C-RCM driven by reanalysis provides necessary inputs to FIZC. Impacts following a change of lower boundary conditions are then analyzed over Western Switzerland. Finally, an application to deep-Lake Geneva is presented where FIZC is coupled to a lake model.

1. The FIZC approach and experimental setup

The atmospheric numerical modeling approach is basically the same column model as that described in Goyette and Perroud (2012). The main difference with the previous application is that this SCM is a column version of the C-RCM (e.g. Caya and Laprise, 1999), driven by NCEP-NCAR reanalysis (Kalnay et al., 1996). The simplified prognostic equation for the main atmospheric variables Ψ = (u, v, T, q) in FIZC, as is the case for most GCMs and RCMs, can be written symbolically as follows:

$$\frac{\partial \Psi}{\partial t} = D_\Psi + P_\Psi \qquad (1)$$

This formulation includes the equations for momentum, thermodynamic energy, and vapor continuity where u, v, T and q, function of space and time have their usual definitions. These partial differential equations allows for a forward integration in time when initial and boundary conditions are provided, and the contributions to the dynamics tendencies, D_Ψ, and these to the physics, P_Ψ, are available at each time step. During numerical integrations with the C-RCM, the multi-level atmospheric prognostics, Ψ, and the cumulative contributions to the physics tendencies, $\overline{P}_\Psi$, have been saved at regular time intervals. Consequently, mean contributions to the dynamic tendencies can be derived as follows:

$$\overline{D}_\Psi = \frac{\partial \Psi}{\partial t} - \overline{P}_\Psi \qquad (2)$$

These time-averaged values serve to compute the evolution of atmospheric profiles. A stochastic component is introduced to parameterize D_Ψ in Eq. (1) as follows:

$$D_\Psi = (1 + R_\Psi)\overline{D}_\Psi \qquad (3)$$

The prescribed dynamics computed on the basis of C-RCM archives in a specific column is then linearly interpolated at each time step in FIZC and superimposed on some noise, $R_\Psi = S_\Psi R^*$, with S_Ψ, scaling parameters allowed to vary in the vertical for each prognostic variable, and R^*, random numbers ranging from -1 to +1. This parameterization is intended to re-inject the unresolved variability in the dynamical processes that is present in the real atmosphere, but lost in Eq. (2). In Eq. (1), the term P_Ψ is computed on the basis of the C-RCM physics package. A practical FIZC option allows nudging the vertical profiles of Ψ towards the C-RCM archived profiles. The prognostic variables computed in FIZC may somehow be ''relaxed'' at specified intervals toward the C-RCM values found in the corresponding column. These coefficients are required for preventing FIZC from diverging from the C-RCM prognostics but carefully chosen small enough to stay close to these in addition to allow feedbacks in the vertical dimension. In what follows, FIZC is interfaced with a version of the 60-km C-RCM with 29 vertical levels driven by NCEP-NCAR reanalysis for the year 1990 over a domain covering the North Atlantic Ocean and continental Europe as in Goyette et al. (2001). In FIZC, the column overlies a solid surface of Western Switzerland. The scaling parameters S_Ψ have been fixed to 1, and the C-RCM archival periods varied from 10 min (i.e., the model timestep), to 6 h, and 24 h; the nudging may then be applied and the contributions to the dynamic tendencies averaged over the 6- and 24 h periods. In a second step, the surface is changed into a freshwater body whose evolving thermal profiles are computed by a buoyancy-extended k–ε model termed SIMSTRAT described in Burchard et al., (1995) where an application to Lake Geneva is described with many details in Perroud et al. (2009).

2. Preliminary sensitivity analysis

When full nudging and D_Ψ are prescribed every 10 min, FIZC reproduced trivially the results of the C-RCM at this location. Decreasing the nudging parameters allows more interactions in the vertical. Sensitivity tests have shown that small nudging values are required to reproduce atmospheric profiles “close” to these in the corresponding C-RCM column, while leaving enough feedbacks to operate. However, when the nudging frequency is increased once every 6 and 24 h, an increase

of its intensity is somewhat required to ensure a better reproduction of the atmospheric prognostics and surface fluxes. A summary of some results is given in Table I. In practice, 6-hourly for $\overline{D}_\Psi$ and a weak nudging would be a suitable trade-off between feedbacks and accuracy. Also, this is a standard and practical RCM archival period to save model field variables and tendencies over long time periods.

4. Application to deep Lake Geneva, Switzerland

The coupling between the atmosphere and a 309 m-deep open-water body modifies the surface fluxes as a result of the higher heat capacity and water availability, the lower albedo, surface emissivity and roughness height. Yearly averages of surface air temperature, wind speed, evaporation, sensible heat flux are higher while surface stress is smaller. Impacts differ due to positive and negative feedbacks subsequent to weakening the nudging values. A run using a strong nudging shows for instance that a complete turnover takes place in March in the lake (Fig. 1a). Inversely, weak nudging increases the the windspeed and the surface energy budget. Consequently, the lake remains slightly stratified over the winter season (Fig. 1b). If a low nudging seems to be more accurate in winter, a high nudging simulates better the profiles in summer. The nudging values thus need to be carefully chosen.

Table I: Annual averages (avg) and standard deviations (std) of simulated screen-level temperature (T_{2m}), humidity (q_{2m}), anemometer-level windspeed (v_{10m}), precipitation (P), surface sensible (H_s), evaporation (E_s) fluxes, and wind stress magnitude (τ_s). Run labels without a lake are R1: 10 min archives with full nudging; R2: 6 h min archives with full nudging; R3: 24 h archives with full nudging; run using a lake model R4: 10 min archives with full nudging and; R5: 10 min archives with weak nudging.

Runs\var		T_{2m} (°C)	q_{2m} (g kg^{-1})	v_{10m} (m s^{-1})	P (mm d^{-1})
R1	avg	8.4	8.4	3.9	0.17
	std	7.0	4.0	2.8	0.63
R2	avg	8.5	8.5	3.9	0.15
	std	7.1	4.1	2.8	0.55
R3	avg	8.6	8.6	3.6	0.14
	std	7.0	4.1	2.5	0.37
R4	avg	11.0	9.3	5.3	0.17
	std	6.2	4.0	4.0	0.63
R5	avg	11.0	9.3	6.6	0.17
	std	5.7	3.7	4.5	0.60
Runs\flux		H_s (W m^{-2})	E_s (mm d^{-1})	τ_s (N m^{-2})	
R1	avg	38.4	0.079	0.57	
	std	78.3	0.120	0.63	
R2	avg	38.4	0.082	0.57	
	std	78.8	0.121	0.62	
R3	avg	38.8	0.085	0.50	
	std	74.9	0.125	0.54	
R4	avg	43.0	0.100	0.07	
	std	38.6	0.082	0.10	
R5	avg	40.3	0.087	0.09	
	std	45.2	0.076	0.13	

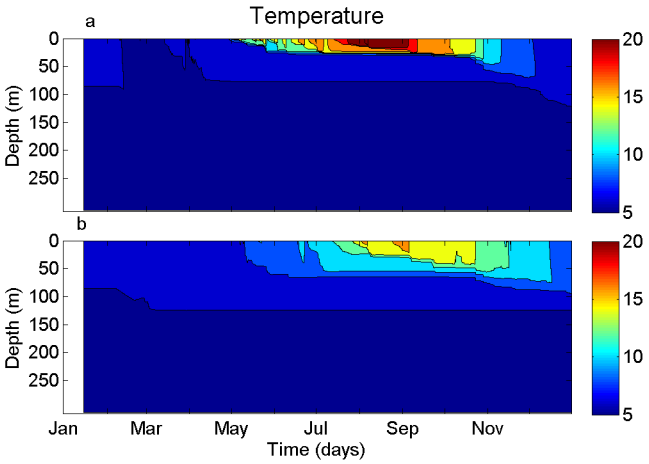


Figure 1: Lake water temperatures simulated for 1990 from the surface down to 309 m with (a) a full nudging, and (b) a weak nudging. The initial profile is given by the measurements of 15 January.

5. Future work

The FIZC approach has been successfully embedded in the C-RCM. However, further tests and sensitivity analysis are required to assess its versatility and full potential. These will aim at running this model over various spatial and temporal resolution and locations in order to benchmark results as a function of structural parameters. Also, work is underway to improve the parameterization of D_Ψ in Eq. (3). FIZC is intended be interfaced with other model physics package thus allowing testing different parameterizations against a number of different case studies.

References

Burchard, H., and H. Baumert (1995): On the performance of a mixed layer model based on the k–e turbulence closure. J. Geophys. Res. 100, 8523–8540.

Caya, D., and R. Laprise (1999), A semi-implicit semi Lagrangian regional climate model: the Canadian RCM. Mon. Wea. Rev., 127, 341-362.

Goyette, S., and M. Perroud (2012): Interfacing a one-dimensional lake model with a single-column atmospheric model : Application to the deep Lake Geneva, Switzerland. Water Resour. Res., 48, W04507, doi:10.1029/2011WR011223.

Goyette, S., M. Beniston, D. Caya, J. P. R. Laprise, and P. Jungo (2001): Numerical investigation of an extreme storm with the Canadian Regional Climate Model : The case study of windstorm VIVIAN, Switzerland, February 27, 1990. Clim. Dyn., 18, 145 - 178. DOI 10.1007/s003820100166.

Kalnay, E., Kanamitsu M, Kistler R, Collins W, and others (1996): The NCEP/NCAR 40-year reanalysis project, Bull. Amer. Meteor. Soc., 77, 437-470.

Perroud, M., S. Goyette, A. Martynov, M. Beniston, and O. Anneville (2009): Simulation of multiannual thermal profiles in deep Lake Geneva: A comparison of one-dimensional lake models. Limnol. Oceanogr., 54, 1574–1594.

Estimation of future temperature and sea ice extremes of the Baltic Sea

Jari Haapala, Byoung Woong An and Katriina Juva

Finnish Meteorological Institute, Helsinki, Finland (jari.haapala@fmi.fi)

1. Introduction

Natural variability of the Baltic Sea temperature and sea ice conditions is very large and consequently ecosystem and society obey rather large tolerance for climate variations. However, in addition to the general warming trend, extremes in the Baltic Sea temperature regime are expected to be changed (BACC-2, 2014).

For a winter stage, a main interest is to know would probabilities of the extreme sea ice conditions, i.e mild or severe ice seasons, change in future, since marine species and coastal erosion are very vulnerable for changes in extremes conditions. Also long term planning of ice breaker fleets and other offshore activities need this information.

Changes in summer stage sea surface temperatures become to be important if the temperature will exceed certain threshold. Temperature threshold is very much depend on the species considers. A modest increase during a summer would enhance growth of some fish species, but very warm summer temperatures would enhance also harmful blue-green algae blooms.

In this study, we analyses changes of the SST in the Baltic Sea and calculate return periods using extreme value distributions.

2. Experiments

We utilize an advanced Baltic Sea model, BaltiX (Hordoir et al, 2012), for numerical investigations. The model is based on the NEMO/LIM3 ice-ocean circulation model. Horizontal resolution of the model is two nautical miles with 56 vertical layers. It includes also the North Sea and tides. The sea -ice component is a multicategory viscous-plastic sea-ice model. Hindcast simulations cover period from 1961 to 1997 and climate projections from 1950 to 2100. The model was forced by the SMHI dynamic downscaled RCAO simulations of the IPCC SRES A2 emission scenario.

3. Results

Modelled trends of SST manifest large regional differences. Locally, negative trends in 20-30 year time scales are found regardless of a positive trend in a Baltic Sea scale. Regional differences are expected due to changes in circulation and upwelling/downwelling intensity.

Under SRES A2 scenario, results indicate that the warm extremes (e.g. 10- and 30-year return values) will occur more frequently than those for the current condition, and there seems to be a gradual increase of warm extremes from the southern to the northern Baltic Sea, while cold extremes will almost disappear in the future.

References

BACC-2, 2014. Second Assessment of Climate Change for the Baltic Sea basin, in preparation.

R. Hordoir, B. W. An, J. Haapala, C. Dieterich, S. Schimanke, A. Höglund and H.E.M. Meier (2012) BaltiX: A 3D Ocean Modelling Configuration for Baltic & North Sea Exchange Analysis. SMHI-Report, Oceanography 115, 2013, ISSN 0283-7714

Future Climate Changes over East Asia by the RCP scenarios downscaled using the Regional Spectral Model

Suryun Ham, and Kei Yoshimura

Atmosphere and Ocean Research Institute, The University of Tokyo, Kashiwa, Japan (suryun01@gmail.com)

1. Introduction

It is well known that climate change has great impacts on human activities. Feasible future climate scenarios has been developed and analyzed. These scenarios reflect plausible future climate, which have been constructed for explicit use in investigating the potential consequences of anthropogenic climate change and natural climate variability.

In climate research communities, global climate models (GCMs) are used to primary tools for the future climate assessment by producing future simulations. Although GCMs can resolve synoptic-scale disturbances, they are unable to adequately resolve anomalous surface forcing due to their coarse spatial resolution. The dynamical downscaling approach has a potential to better reproduce meso-scale disturbances that play important roles in the regional scale, which cannot be resolved in low-resolution GCMs. Many studies demonstrated the importance of model resolution in reproducing the extreme event or monsoon precipitation in future projections. However, their studies were designed independent domain configuration. To develop an inter-comparable downscaling protocol with future scenarios, the Coordinated Regional Climate Downscaling Experiment (CORDEX) project has launched to provide unified framework for the downscaling researches (Giorgi et al. 2009).

In this study, the future climate changes over East Asia as well as extreme weather conditions over Japan are investigated by Regional Spectral Model (RSM; Juang et al. 1997).

2. Experimental Setup

This study assesses future climate change over East Asia using the RSM. The RSM is forced by three-types of future climate scenarios produced by the Hadley Center Global Environmental Model version 2; the representative concentration pathways (RCP) 2.6, 4.5, and 8.5 scenarios for the intergovernmental panel on climate change fifth assessment report (AR5).

The domain includes East Asia, India, the Western Pacific Ocean, and the northern part of Australia, as shown in Fig. 1. These regions have been reported to have significant direct and remote effects on the East Asian monsoon system. This configuration of the model domain follows a protocol of the CORDEX for East Asia (Giorgi et al. 2009). The number of grid points in Cartesian coordinates is 200 (west-east) by 165 (north-south), with a horizontal resolution of 50 km. A 28-level terrain-following (sigma) vertical grid is used.

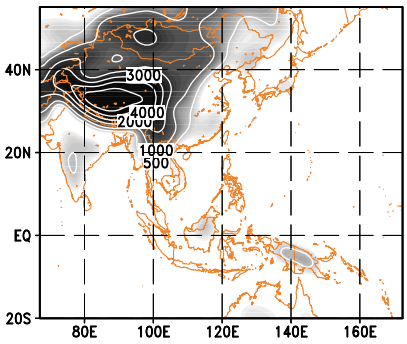


Figure 1. Regional model domain and orography (m)

Analyses for the current (1980-2005) climate are performed to evaluate the RSM's ability to reproduce precipitation and near surface temperature. Three different future (2020-2050) simulations are compared with the current climatology to investigate the climatic change over East Asia. The boundary condition is used from the historical run of the HadGEM2-AO (hereafter, HG2) simulation of National Institute of Meteorological Research of Korea Meteorological Administration (Back et al. 2013). The HG2 is composed by an atmospheric GCM with N96 (1.875° × 1.25°) horizontal and 38 vertical levels with 38 km of top altitude and an ocean GCM with 1° horizontal and 40 vertical levels.

To prevent the distortion of large-scale fields, the scale selective bias correction (SSBC) method has been applied (Hong and Chang 2012). The method allows more freedom in the RSM by nudging only the large-scale vorticity component with a vertical weighting which permits the lower troposphere component to be more ageostrophic.

3. Preliminary Results

The RSM satisfactorily reproduces the observed seasonal mean and variation of precipitation (Fig. 2) and near surface temperature. The spatial distribution of the simulated large-scale features and precipitation by RSM shows generally improved pattern compared to that is given by the HG2. In addition, their inter-annual variations and probability distribution for intensity of precipitation over Japan are better captured by the RSM. Assessment of future climate changes over the East Asia will be presented at the workshop. Also, regional ocean-atmosphere coupled and uncoupled model simulations are compared

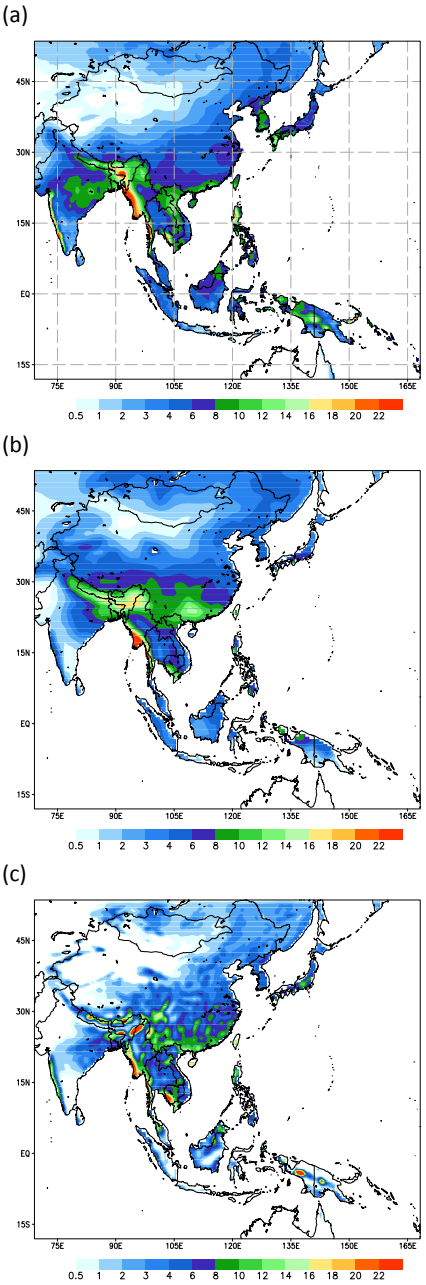


Figure 2. Seasonally averaged precipitation (mm d^{-1}) during 1980-2005 from the (a) CRU observation, (b) HG2, and (c) RSM for June-July-August (JJA).

References

Baek HJ and Coauthors (2013) Climate change in the 21st century simulated by HadGEM2-AO under representative concentration pathways. Asia Pac J Atmos Sci, 49(5), 603-618

Giorgi F, Jones C, Asrar GR (2009) Addressing climate information needs at the regional level: the CORDEX framework. World Meteorological Organization (WMO). Bulletin, 58, 175-183

Hong S-Y, Chang E-C (2012) Spectral nudging sensitivity experiments in a regional climate model. Asia Pac J Atmos Sci, 48(4), 345-355

Juang HH, Hong S, Kanamitsu M (1997) The NCEP regional spectral model: An update. Bull Amer Meteor Soc 78, 2125-21

The KLIWAS Project: Adapting Shipping and Waterways to Climate Change – The North Sea Case -

Hartmut Heinrich[1], Birger Tinz[2], Gudrun Rosenhagen[2], Birgit Klein[1], Holger Klein[1], Anette Ganske[1], Katharina Bülow[1], Nils Schade[1], Jens Möller[1], Sabine Hüttl-Kabus[1], Peter Löwe[1] , Lydia Gates[2]

[1] Bundesamt für Seeschifffahrt und Hydrographie, Operationelle Ozeanographie, Hamburg, Germany,

[2] Seewetteramt, DWD, Hamburg, Germany (birger.tinz@dwd.de)

1. Introduction

KLIWAS is a 5-year research project awarded by the German Ministry of Transport and Digital Infrastructure (BMVI). It was carried out by the Ministry's four research institutions concerned with water with the goal to identify vulnerabilities from climate change and to explore options for adaptation of shipping and waterways in Germany and the open North Sea. Here we report on the North Sea part of the project.

The North Sea part of the project was originally based on the examination of existing future climate projections (A1B) for their suitability to extract information relevant for shipping; especially those that were produced within the EU project ENSEMBLES. However, tests and products showed that these projections were of limited value, because the re-analysis used (ERA 40) and the reference period model simulations showed remarkable deviations from in-situ data of the North Sea that were available to us. The problems identified pointed to the fact that the ENSEMBLES projections originate from regional atmosphere-only models.

As a consequence, KLIWAS initiated co-operations with several research institutions to provide a range of regional coupled ocean-atmosphere models with a focus on the North Sea area. The results of these simulations verified well and will be presented here in Lund in a presentation by Klein et al.

2. Methods and Outcomes

The project identified several challenges of regional model validation. The ERA-40 re-analysis was compared against meteorological and oceanographic data from the North Sea. For some important parameters, e.g. air temperature during the wintertime, deviations from in-situ data were identified to be larger than 2K. As a consequence, a completely new climatological ocean-atmosphere data set for the North Sea was developed on the basis of high quality data. The climatology is provided as an open access dataset.

In order to facilitate the validation of the ocean state, a climatology of oceanographic fronts in the North Sea based on satellite data was developed for future dynamic oceanic analyses. This new method is now in operation as a marine core service in the Copernicus Programme.

Water level data of the Cuxhaven tide gauge was analyzed to separate tidal from meteorological influences on the past sea level. Such time series can act as a sophisticated identifier of storms and as a basis for future sea level rise predictions.

A new method for the identification of storms in future climate projections that can lead to storm surges was developed and successfully tested. It now can be applied in the analyses of projections studied in the project.

The ENSEMBLES projections were also analyzed for wind and air parameters. The results showed clearly the importance of the decadal variability rather than trends until the year 2100.

Investigations of sea state derived from uncoupled projections revealed information on the regional development of the significant wave height, extreme waves and the influence of a rising sea level on the sea state in the North Sea.

In order to overcome the deficits identified in the uncoupled regional ENSEMBLES projections, three regional coupled ocean-atmosphere models were developed (MPIOM/REMO, HAMSOM/REMO, NEMO/RCA) and an ensemble of simulations was provided for present day and future climate. All three members of the ensemble compared better to validation data and provided more reliable projections of parameters relevant to shipping, other economic activities and the North Sea ecology (see presentation Klein et al.).

3. Results

According to our investigations, in the medium or long term greenhouse gas scenario A1B will not lead to higher levels of adverse conditions to shipping than at present. Sea level rise in combination with a more intense sea state in the western North Sea could put some risk to coastal protection and the use of estuaries. Increasing water temperatures in conjunction with circulation changes in the North Sea as well as in the Northeast Atlantic might lead to modifications in the ecology of the North Sea environment. Salinity changes are minor (decrease). However, there are still large uncertainties in precipitation and freshwater discharges. In general, until the end of the century decadal variability seems to play a more important role rather than trends. The KLIWAS studies mainly focused on average situations and climatological means. Studies on extreme conditions and more extreme GHG scenarios remain necessary. Such investigations including a broadening of the ensemble of coupled regional climate models are planned for the

coming five year period of the project.

4. Acknowledgements

KLIWAS research was carried out in co-operation with:

- SMHI Norrköping
- Max-Planck Institut für Meteorologie Hamburg
- ZMAW at Hamburg University
- ICDC at Hamburg University
- Climate Service Center Hamburg
- Helmholtz Gesellschaft Geesthacht
- Freie Universität Berlin, Institut für Meteorologie
- Universität Siegen
- Brockmann Consult

Web Processing Services for Climate Data – with Examples for Impact Modelers

Nils Hempelmann[1], Carsten Ehbrecht[2], Wolfgang Falk[3], and Paul Parham[4]

[1] Climate Service Center (CSC), Helmholtz-Zentrum Geesthacht, Hamburg, Germany, (nils.hempelmann@hzg.de)
[2] German Climate Computing Centre (DKRZ), Hamburg, Germany
[3] Bavarian State Institut of Forestry (LWF), Freising, Germany
[4] Grantham Institute for Climate Change, Dept of Infectious Disease Epidemiology, Imperial College London, London, UK

1. Introduction

Impact modeling forced by climate data is often connected with big data processing, but a frequent problem is that impact modelers are not optimally-equipped with appropriate hardware (computing and storage facilities) nor programming experience for software develoment.

Web Processing Services (WPS) can close this gap and offer impact modelers a valuable practical tool to process and analyse big data. WPS represents an interface to perform processes over the HTTP network protocol, enabling users to trigger processes over a website.

The appropriate processes are predefined, together with access to the relevant data archives where appropriata data are stored.

In case of the WPS we present here, the data archive of the earth system grid federation (ESGF) is connected with a search process, allowing the processing of all data stored in the ESGF, including data resulting from the Coordinated Regional Climate Downscaling Experiment (CORDEX) programme.

Furthermore, the WPS we present here conforms with the standartisation defined by the Open Spatial Consortium (OGC), allowing combination with WPS from other institutions to establish a network of computing providers.

2. WPS for impact modelers

Besides several general processing operations realised with climate operator commands (CDO), a range of specific processes can also be performed within a WPS. Here, we present two more complex impact models: a population dynamics model of *Anopheles gambiae s.s.*, one of the three principal vectors of human malaria in Africa, and a model to project the distribution of tree species. Results can be stored in personal folders for further processing, visualisation or downloading for local postprocessing.

Population dynamics model for *Anopheles gambiae* s.s.

As a more complex example, we present a model to calculate the abundance and distribution of adult *Anopheles gambiae* s.s. mosquitoess in Africa using the WPS interface. The lifecycle of *Anopheles gambiae* from egg, larvae, pupae to adult is strongly influenced by climatic conditions including air temperatures, rainfall and relative humidity. Based on empirical data on the dependence of parameters such as daily survival probabilities, stage durations and gonotrophic cycle duration on climatic factors, and the model of Parham *et al.* (2012), the WPS gives a netCDF file with the simulated number of adult mosquitoes as the output. The user has the option to select the input variablls from any CORDEX Africa data experiment to assess the impact on the resultant mosquito population dynamics.

Species distribution model

For a second example, we realized a method to calcuate the favourability of climatic conditions for the distribution of trees. Based on geographical information (single points) on the presence or absence of the appropriate species, the distribution favourability can be calculated based on climatic conditions. Once this is preference is calculated based on historical runs, future projections are performed. In the WPS, each process is realized twice; once for the historical run to calculate the distribution dependency on climatic conditions and then to perform the required projection.

The user has the oportunity to select several climate indices to calculate the climatic distribution limits, as well as temperature and precipitation datasets from the CORDEX project stored in the ESGF.

This process is realized with R and shows the software independency of the WPS.

3. Summary

This presetation in an introduction to an early stage of the ClimDaPs project. ClimDaPs uses WPS for climate data processing. It is based on the PyWPS implementation of WPS and additionally provides a simple web-based user-interface to access and combine climate data processes.

It provides access to the climate data archive of the Earth System Grid Federation (ESGF) for CMIP5 and CORDEX data. Performing simple processes on climate data up to the implementation of complex impact models are already available within ClimDaPs. One can also visualize climate data and the processed results.

References

Falk, W. and N. Hempelmann, 2013: Species favourability shift in Europe due to climate change: a case study for fagus syvatica L. and picea abies (L.) Karst. Based on an ensemble of climate models. J.Climatology, Vol. 2013, ID787250, 18 pp.

Parham PE, Pople D, Christiansen-Jucht C, Lindsay S, Hinsley W, Michael E, 2012, Modeling the role of environmental variables on the population dynamics of the malaria vector Anopheles gambiae sensu stricto, *Malaria Journal*, Vol:11, ISSN:1475-2875, 13 pp.

The Change of Cherry First-flowering Date over South Korea Projected from Downscaled IPCC AR5 Simulation

Jina Hur[1], Joong-Bae Ahn[1] and Kyo-Moon Shim[2]

[1] Division of Earth Environmental System, Pusan National University, Busan, Republic of Korea (jbahn@pusan.ac.kr)

[2] National Academy of Agricultural Science, RDA, Suwon, Republic of Korea

1. Introduction

Rapid warming has been observed over South Korea for the last several decades, as in other mid- and high-latitudinal areas, particularly during winter and spring (Kwon, 2005). The flowering date for deciduous trees in mid- and high-latitude, in particular, depends strongly on the temperature of winter and early spring among several climate factors (Menzel and Fabian, 1999; Wielgolaski, 2003). Accordingly, many studies have been performed to project the changes of spatial distribution of the flowering time for certain fruit trees in association with regional climate change. Among deciduous trees, the cherry tree (*Prunus yedoensis*), which flowers in early spring, is widely distributed throughout the Korean Peninsula. The flowering time of the cherry blossom has been observed by Korean meteorological observation sites since 1922 and these flowering data have, therefore, been usefully applied by many phenological studies (Jeong *et al.*, 2011; Chung *et al.*, 2009). Therefore, in this study, based on the AR5 climate scenarios, the first-flowering date (FFD) of the cherry blossom in South Korea is newly estimated using daily temperature data obtained from six different climate models. In order to reduce uncertainties (Ahn *et al.*, 2012; Krishnamurti *et al*., 1999), multi-model ensemble (MME) results are used after removing the mean bias of individual models (Hur *et al.*, 2013).

2. Data and methods

The data used are daily Historical (1986-2005), RCP4.5 (2071-2090), and RCP8.5 (2071-2090) gridded temperature data for early spring (February-April, FMA) from six models participating in the Coupled Model Intercomparison Project 5 (CMIP5). The gridded data having relatively coarse resolution simulated by the global climate models are statistically downscaled to in-situ meteorological observation sites in South Korea. For the statistical downscaling, we use a hypsometric method that considers both inverse distance weighting and the lapse rate correction factor based on elevation difference (Daly *et al.*, 2003).

The simulated temperatures over the Northern Hemisphere and Northeast Asia are compared with the National Centers for Environmental Prediction/National Center for Atmospheric Research (NCEP/NCAR) reanalysis 2 (hereafter NCEP2) data. The mean bias of each model downscaled to the observation sites is estimated and eliminated using daily temperature during the 20-year period from 1986 to 2005 obtained from the 59 in-situ observations over South Korea. In addition, MME is performed using the Simple Composite Method in order to produce a representative value for each scenario and to reduce uncertainties contained in individual models (Ahn *et al.*, 2012; Krishnamurti *et al.*, 1999).

The cherry FFD data observed by the Korean Meteorological Administration are used to analyze the current characteristics of cherry FFD and to verify the capability of FFD simulation. The number of days transformed to standard temperature (DTS) phenological model is applied to the downscaled climate model output for cherry FFD estimation in the study models (Hur *et al.*, 2013).

3. Results

First, the temperature over Northeast Asia derived from the six climate models and the reanalysis data are investigated and compared (Fig. 1). The general patterns of the historical simulations are similar to the NCEP2 reanalysis, although they differ from the analysis by between -0.5K and 1.6K, which is attributed to systematic bias (Ahn et al., 2012). The average temperatures over Northeast Asia simulated under the RCP4.5 and RCP8.5 scenarios are expected to increase by 2090 by about 2.0K and 3.5K, respectively, compared to the Historical simulation, which is lower than the Northern Hemisphere average increase of 2.8K and 4.9K, respectively.

Systematic biases in individual models are estimated and eliminated based on the method suggested by Ahn et al. (2012). The estimated mean biases for early spring are 1.2K, 1.3K, 1.8K, 1.3K, 0.1K, and 2.7K for BCC-CSM1-1M, CCSM4, CMCC-CM, EC-EARTH, MIROC5, and MRI-CGCM3, respectively. By applying MME to the downscaled data after bias removal, ensemble data representing each scenario are produced and examined. The temperatures over South Korea at RCP4.5 and RCP8.5 are expected to increase by about 2.0K and 3.5K by 2090 compared to the Historical simulation (279.7K), respectively.

Cherry FFD is estimated by applying the DTS phenological model to the simulated temperature. The average current FFD is JD 96.1, indicating that the cherry blossom generally flowers at the beginning of April. On the other hand, the cherry blossoms from the RCP4.5 and RCP8.5 simulations are expected to flower at the end of March by moving forward about 6.3 and 11.2 days, respectively, compared to the present. In other words, the increased temperature in February and March accelerates the growth rate of the cherry blossom and thereby advances the phenological spring. The spatial distributions of cherry FFD derived from the observation and simulations are also investigated (Fig. 2). In

qualitative terms, the Historical simulation can capture the spatial pattern of the observation, but in quantitative terms, the estimate is an average of 1.2 days later than the observation. The FFDs from the RCP4.5 and RCP8.5 simulations are uniformly advanced in time over all stations compared with the Historical simulation. Especially, FFD under the RCP8.5 scenario is advanced by 11.6 days compared to the Historical simulation. The current cherry FFD under the RCP4.5 and RCP8.5 scenarios moves north at a speed of 0.01 and 0.03° Nyear-1, respectively models (Hur et al., 2013).

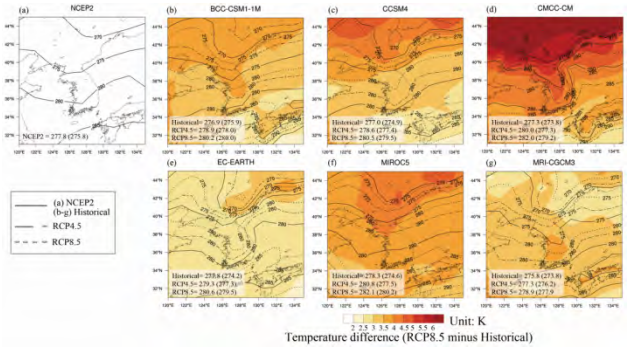


Figure 1. Average temperature (K) derived from NCEP reanalysis-2 data (for 1986-2005, a), Historical (for 1986-2005, solid line), RCP4.5 (for 2071-2090, dash-dotted line), and RCP8.5 (for 2071-2090, dotted line) simulations (b-g) for the flowering period (February-April). Here shading indicates the temperature difference between the Historical and RCP8.5 simulations.

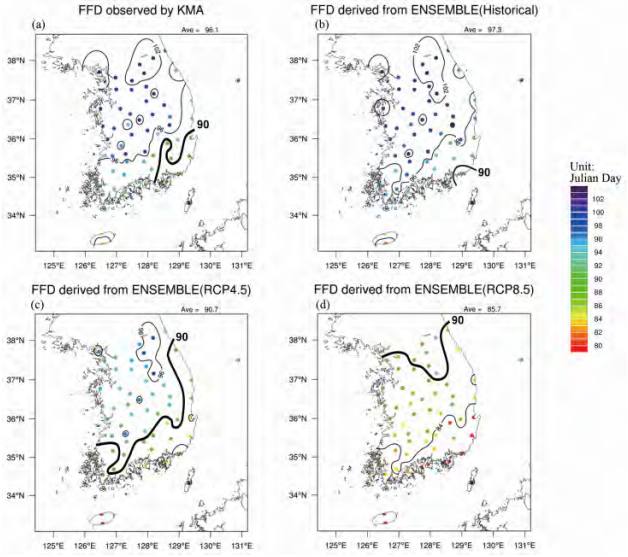


Figure 2. Spatial distribution of cherry first-flowering date derived from observation (for 1986-2005, a) and Historical (for 1986-2005, b), RCP4.5 (for 2071-2090, c), and RCP8.5 (for 2071-2090, d) simulations for the flowering period (February-April).

4. Conclusion

Although plant growth cannot be perfectly estimated using only temperature information due to the influence of many other environmental factors such as day length, precipitation, and solar radiation, this method can help to project potential variations of the local ecosystem in the present era of anthropogenic climatic change. The methodology used in this study to estimate cherry FFD can be applied to many different plants and crops in various aspects of growth response. For estimating regional warming, our results demonstrate the importance of eliminating the systematic bias inherently contained in the model simulation results in order to improve the prediction of future global climate changes models (Hur *et al.*, 2013).

Acknowledgments

This work was carried out with the support of Korea Meteorological Administration Research and Development Program under Grant CATER 2012-3083 and Rural Development Administration Cooperative Research Program for Agriculture Science and Technology Development under Grant Project No. PJ009353, Republic of Korea.

References

Ahn J-B, Lee J, Im E-S. 2012. The reproducibility of surface air temperature over South Korea using dynamical downscaling and statistical correction. J. Meteorol. Soc. Jpn. **90**: 493–507.

Chung U, Jung J-E, Seo H-C, Yun JI. 2009. Using urban effect corrected temperature data and a tree phenology model to project geographical shift of cherry flowering date in South Korea. Clim. Change **93**: 447–463.

Daly C, Helmer EH, Quinones M. 2003. Mapping the climate of Puerto Rico, Vieques and Culebra. Int. J. Climatol. **23**: 1359–1381.

Hur J, Ahn J-B, Shim K-M. 2013. The change of cherry first-flowering date over South Korea projected from downscaled IPCC AR5 simulation. Int. J. Climatol. DOI: 10.1002/joc.3839

Jeong J-H, Ho C-H, Linderholm HW, Jeong S-J, Chen D, Choi Y-S. 2011. Impact of urban warming on earlier spring flowering in Korea. Int. J. Climatol. **31**: 1488–1497.

Krishnamurti TN, Kishtawal CM, LaRow TE, Bachiochi DR, Zhang Z, Williford CE, Gadgil S, Surendran S. 1999. Improved weather and seasonal climate forecasts from multimodel superensemble. Science **285**: 1548–155.

Kwon W-T. 2005. Current status and perspectives of climate change sciences. J. Korean Meteorol. Soc. **41**: 325–336(English Abstract).

Menzel A, Fabian P. 1999. Growing season extended in Europe. Nature **397**: 659.

Wielgolaski FE. 2003. Climatic factors governing plant phonological phases along a Norwegian fjord. Int. J. Biometeorol. **47**: 213–220.

Model based analysis of decade scale variability of Baltic Sea hydrography

Katriina Juva, Byoung Woong An and Jari Haapala

Finnish Meteorological Institute, Helsinki, Finland (katriina.juva@fmi.fi)

1. Introduction

Our understanding of changes and variability of the physical state of the Baltic Sea mostly based on the in-situ or satellite measurements (BACC-2, 2014). In-situ timeseries are superior in determing long term changes, but their spatial and temporal resolution is rather poor. This shortage can be complemented with the sea surface satellite measurement, but with numerical experiments we can obtain more representative overview of the changes in the Baltic Sea hydrography.

In this study, we utilize hindcast simulation conducted with the Baltic Sea community model, BaltiX (Hordoir et al, 2012), based on the NEMO/LIM-3 code. The model domain includes Baltic and North Seas with two nautical mile resolution. Numerical simulations covers period from 1961 to 2007. In order to find optimal parameters, we conducted several simulation and use the coastal station data in model validation.

2. Experiments and validation

Three experiments of BaltiX configuration used in this study vary in the number of vertical layers, barotropic time step, bottom drag coefficient and initial conditions. The variability in the number of vertical layers caused the main difference between experiments' results. The hindcast experiments were created to time period from 1961 to 2007, but since it takes about 10 years to experiments to stabilize, the time period of 1971-2007 was used to analysis.

5 Finnish coastal stations and 12 HELCOM stations located in the northern Baltic Sea were used for validation. In this study we focused on the coastal stations, since no previous studies including the coastal stations have been done. Coastal stations have long and continuous time series through the year whereas in the HELCOM station's measurements are more random and concentrated on the open water season. The monthly means were compared to experiments and the seasonal trends for surface and bottom layer were calculated.

3. Results and future work

The temperature derived from the experiments is well representative in all experiments. The representativeness of salinity varies more with station's depth and location.

Experiments present the interannual variability well (fig. 1). The more problematic is the exact level of temperature and of salinity values and the vertical mixing (fig.2). For the future work the best estimation is used for long-time analysis in the hydrographic changes in the Baltic Sea. The study includes for example the heat content changes in the water column and hydrographic changes in the bottom layer.

References

BACC-2, 2014. Second Assessment of Climate Change for the Baltic Sea basin, in preparation.

R. Hordoir, B. W. An, J. Haapala, C. Dieterich, S. Schimanke, A. Höglund and H.E.M. Meier (2012) BaltiX: A 3D Ocean Modelling Configuration for Baltic & North Sea Exchange Analysis. SMHI-Report, Oceanography 115, 2013, ISSN 0283-7714

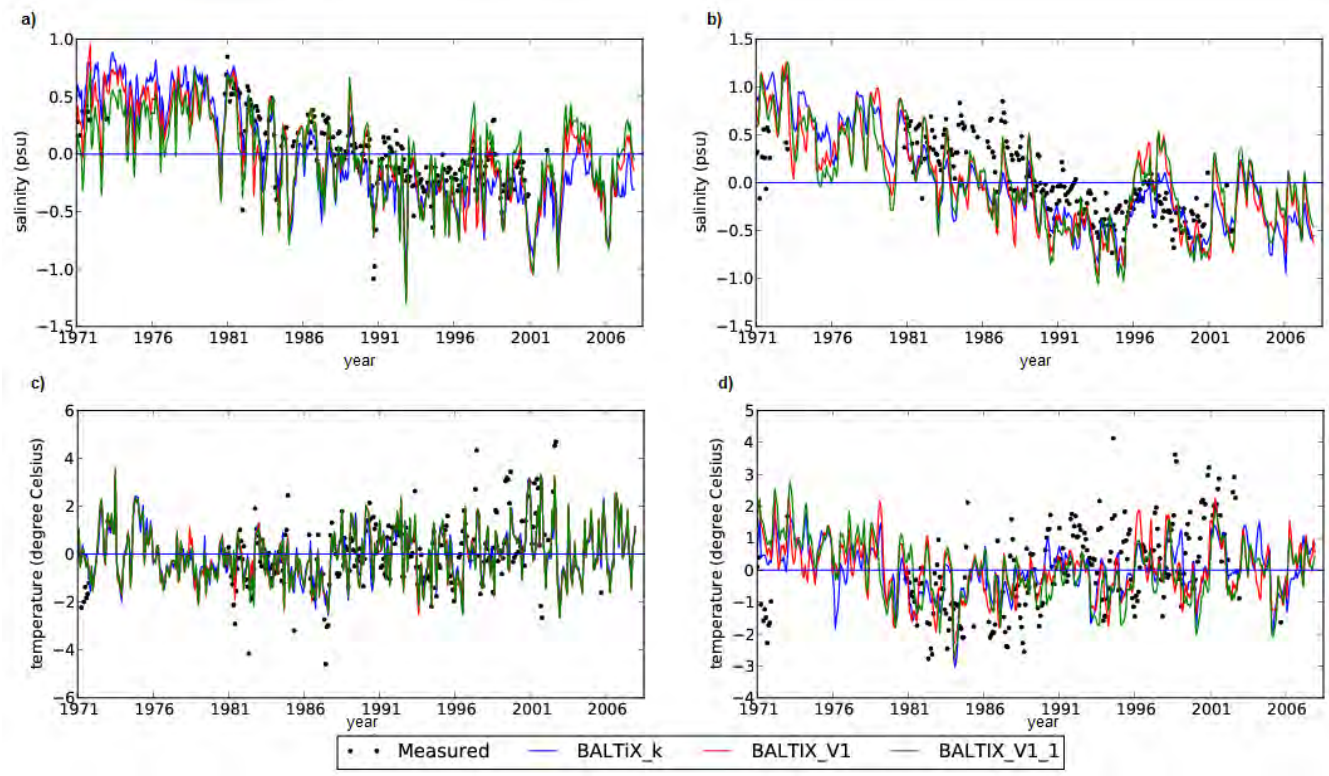


Figure 1. Interannual hydrographical variability in the Utö station from experiments and measured values for the period 1971-2007. a) Salinity at the surface, b) Salinity at the bottom c) Temperature at the surface d) Temperature at the bottom

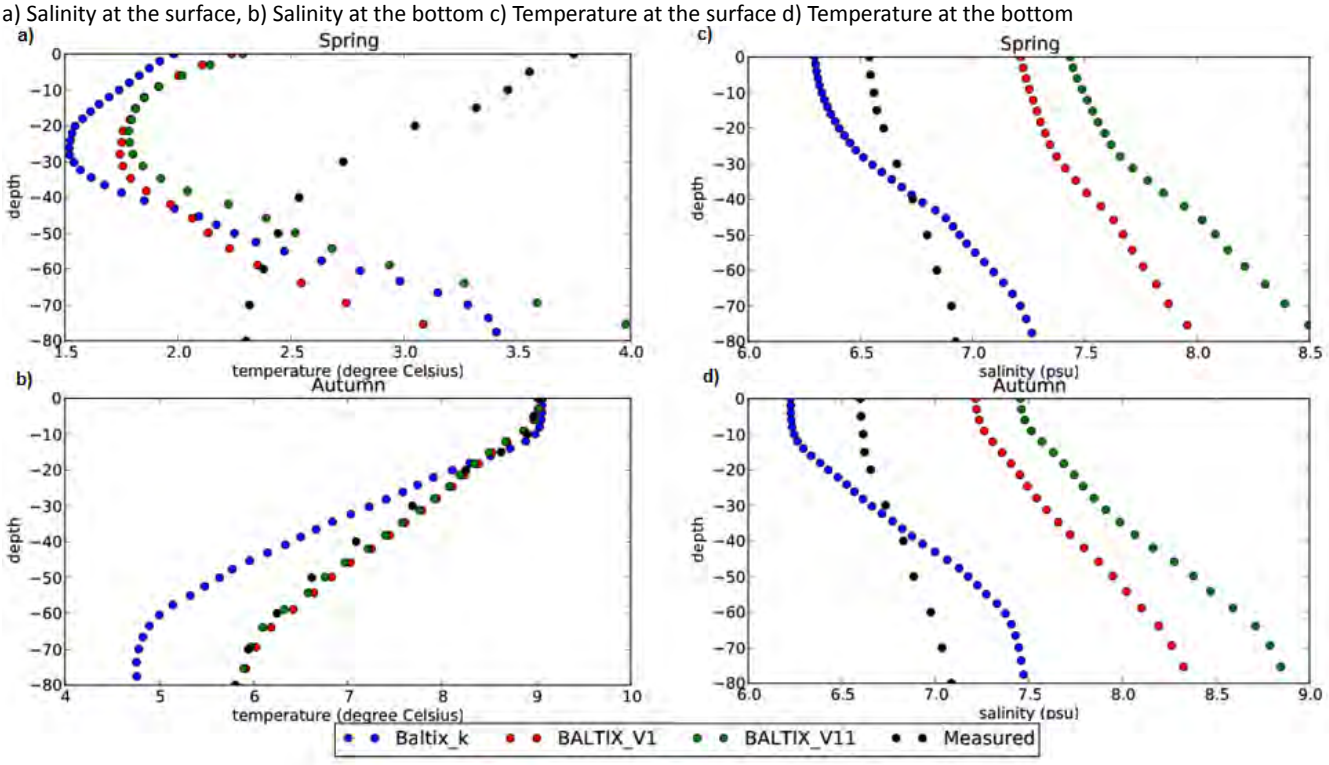


Figure 2. Mean spring and autumn profiles in the Utö station from experiments and measured values for the period 1971-2007 a) spring, temperature b) autumn, temperature c) spring, salinity d) autumn, salinity.

Stochastic modelling of future daily weather in consistency with RCM projections and the observed spatio-temporal structure

D.E. Keller[1,2,3], A.M. Fischer[1], C. Frei[1], M.A. Liniger[1,3], C. Appenzeller[1,3] and R. Knutti[2,3]

[1] Federal Office of Meteorology and Climatology MeteoSwiss, Zurich, Switzerland (denise.keller@meteoswiss.ch)
[2] Institute of Atmospheric and Climate Science, ETH, Zurich, Switzerland
[3] Center for Climate Systems Modeling C2SM, Zurich, Switzerland

1. Introduction

Given the expected changes in the climate system over the 21st century, the need for reliable and quantitative projections is continuously growing. Climate adaptation and risk management, impact modelers, end-users and decision makers need reliable high-resolution future climate data in order to evaluate and respond to the potential threats of climate change.

Regional climate models (RCMs) typically provide information about possible future climate change at a spatial resolution of 10-50 km. This resolution is often too coarse for direct use of the simulated variables in climate impact studies. Further statistical downscaling becomes relevant in particular over complex topography such as the Alps, where unresolved local-scale dynamics and processes are of great importance.

Over recent years, various statistical and dynamical methods have been proposed to bridge the scale discrepancy between the meso- and local-scale. In this context, stochastic models, such as weather generators (WGs) are an appealing downscaling method due to their computational cheapness and their straightforward way to allow for multiple weather variables. Another advantage is their ability to simulate unlimited realisations of synthetic weather time-series consistent with both current and future monthly weather statistics. However, a major constraint of most WGs is the lack of spatial consistency, i.e. series for different locations are uncorrelated on a day-to-day basis.

Here, we present first results of simulated future daily pseudo weather with a realistic spatio-temporal correlation structure based on (a) a recently developed multi-site WG that has been tested for current climate over a catchment within Switzerland (Keller et al., 2014) and based on (b) expected changes derived from RCM projections from the ENSEMBLES project.

2. Data & Method

Core of the multi-site WG by Keller et al. (2014) is a Richardson-type WG (Richardson, 1981): First, daily precipitation is simulated based on a first-order two-state Markov chain for precipitation occurrence and a mixture model of two exponential distributions for wet day intensity. Second, conditioned on the wet or dry state of each day, minimum and maximum daily temperature are simulated with a multivariate first-order auto-regression model. For both, precipitation and temperature, the WG by Keller et al. (2014) takes into account the spatial dependencies between different sites in the weather generation process (Wilks, 1998).

The multi-site WG is applied to a network of Swiss stations maintained by MeteoSwiss. The WG is calibrated at each station separately by a set of parameters comprising: transition probabilities (dry-wet and wet-wet), distributional parameters of wet day intensity, the lag-0 and lag-1 cross-correlation matrices for minimum/maximum temperature and parameters describing the spatial structure. The set of WG parameters is chosen so that the generated series are consistent with the observed monthly statistics at the stations. To simulate daily future weather for the same station network, some of these parameters are perturbed by change factors derived from coupled RCM-GCM projections from the ENSEMBLES project (van der Linden & Mitchell, 2009). This is again done in a way so that the monthly statistics of expected future climate is preserved.

3. Results

Under current climate conditions, the evaluation of the developed multi-site WG by Keller et al. (2014) reveals that the observed spatio-temporal correlation structure, distributional characteristics and the precipitation- temperature relationship are realistically reproduced. It turns out that the incorporation of inter-station dependencies in the stochastic process brings substantial added value over multiple single-site WGs regarding for instance area-averaged precipitation sums over several days. This is especially the case when the precipitation regime is subject to a large spatial and temporal heterogeneity such as over the Swiss Alps (Keller et al.,2014).

To adapt our multi-site WG to future climate conditions, we first investigate changes in precipitation occurrence over north-eastern Switzerland projected by the ENSEMBLES climate models. Figure 1 shows the relative model changes in monthly wet day frequency over north-eastern Switzerland at the end of the 21st century relative to the reference period 1980-2009. The ENSEMBLES models consistently project a decrease in summer wet day frequency, while the sign of change can be both for other seasons.

Based on the changes in wet day frequency and changes in monthly statistics, further WG-relevant parameters such as transition probabilities can be deduced. To derive future estimates in these WG

parameters, we adjust the parameters for current climate conditions by the change between current and future climate simulations. As an example of current and future WG parameters Figure 2 and Figure 3 show the annual cycle of the wet-wet and dry-wet probabilities together with the inter-annual variability derived from observations (boxplots) for a representative station in north-eastern Switzerland. Largest changes between current and future transition probabilities are expected during the warm season. The chances for two consecutive wet days is reduced in the future and the precipitation system favours increased likelihood to remain in a dry state given a preceding dry day. As a consequence, multi-day dry spells are expected to increase over Switzerland (Fischer et al., 2014). It is interesting to note that these expected changes in mean still lie within the range of today's inter-annual variability. This in turn means that present-day dry summers resemble normal summer days at the end of the 21st century.

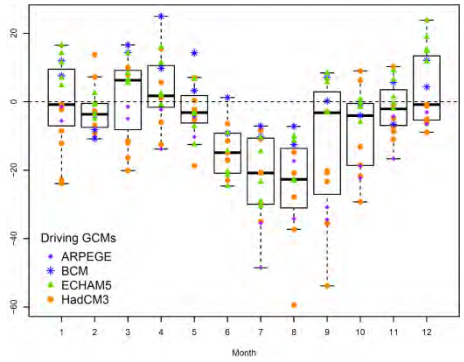


Figure 1. Expected relative changes in monthly wet day frequency over north-eastern Switzerland at the end of the 21st century relative to the reference period 1980-2009. Shown are the individual model projections (symbols, colour-coded according to driving GCM) and boxplots of the multi-model summary statistics. The changes are given in percent.

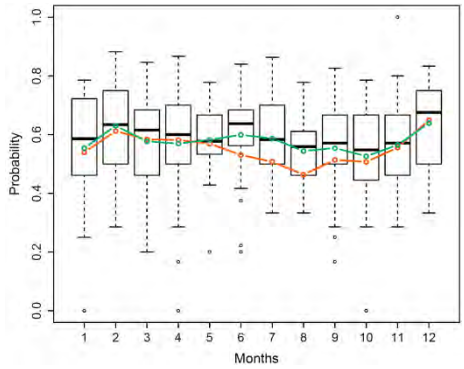


Figure 2. Annual cycle of observed and projected wet-wet probability for a station in north-eastern Switzerland. The green line indicates the observed mean transition probability under current climate (1980-2009) the orange line for the future climate (2070-2099) based on the multi-model mean changes. The boxplots illustrate the inter-annual variability of the transition probability based on observations within 1980-2009.

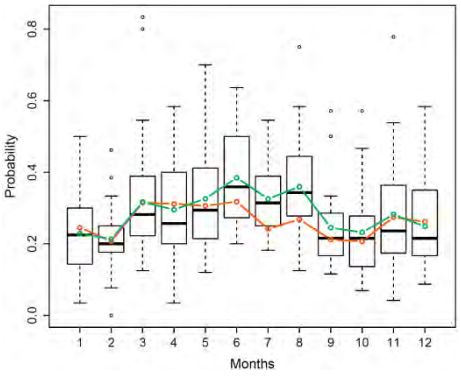


Figure 3. Same as figure 2, but for the dry-wet probability.

4. Summary

First results of our attempt to generate future daily weather time-series for the Swiss station network have been shown. Changes in WG parameters for modelling precipitation occurrence have been analysed in the ENSEMBLE multi-model and used to adjust observed values. Largest differences in the so-generated future time-series compared to a simple delta change method can be expected during the summer seasons which are marked by a substantial change in the dry-wet temporal structure.

References

Fischer A.M, Keller D.E, Liniger M.A, Rajczak J, Schär C, Appenzeller C (2014) Projected changes in precipitation intensity and frequency in Switzerland: a multi-model perspective, International Journal of Climatology, submitted

Keller D.E, Fischer A.M, Frei C, Liniger M.A, Appenzeller C, Knutti R (2014) Stochastic modelling of spatially and temporally consistent daily precipitation time-series over complex topography, in preparation

Richardson C.W (1981) Stochastic Simulation of Daily Precipitation, Temperature, and Solar Radiation, Water Resources Research, 17,1,182-190

Van der Linden P, Mitchell J.F.B (2009) ENSEMBLES: Climate Change and its Impacts: Summary of research and results form the ENSEMBLES project, Met Office Hadley Centre, Exeter, 160 pp

Wilks D.S (1998) Multi-site generalization of a daily stochastic precipitation generation model, Journal of Hydrolgy, 210, 178-191

Differences in future European climate change between an RCM ensemble and the underlying GCMs

Erik Kjellström[1,2], Grigory Nikulin[1], Patrick Samuelsson[1], Marco Kupiainen[1], Ulf Hansson[1] and Colin Jones[1]

[1] Rossby Centre, Swedish Meteorological and Hydrological Institute, Norrköping, Sweden (erik.kjellstrom@smhi.se)

[2] Department of Meteorology, Stockholm University, Sweden

1. Introduction

As part of the Coordinated Regional Downscaling EXperiment (CORDEX, Jones et al., 2011), the Rossby Centre has produced a large number of RCM simulations at 50km resolution for Europe. Here, a total of 18 different climate change simulations are used. This relatively large RCM ensemble can be used to address uncertainties at the local to regional scale due to choice of GCM (in total 9) and external forcing (2 emission scenarios).

The objective of the study is to assess differences in the simulated climate between the underlying GCMs and the RCM.

2. The RCA4 model

Since RCA3 (Samuelsson et al., 2011), RCA has undergone both technical and physical changes. The technical changes have led to improved capabilities of using lateral boundary conditions from different GCMs. A brief summary of the changes in the physical parameterisations in the atmosphere and in the land surface treatment is given in Kjellström et al. (2013).

3. The RCA4 ensemble

In the simulations used here RCA4 has been forced by nine different GCMs under two different emission scenarios.

Table 1. List of CMIP5 GCMs that have been used to provide boundary conditions for the RCA4 runs presented here.

No	Modelling Centre	Model name
1	Canadian Centre for Climate Modelling and Analysis	CanESM2
2	Centre National de Recherches Météorologiques / Centre Européen de Recherche et Formation Avancée en Calcul Scientifique	CNRM-CM5
3	EC-EARTH consortium	EC-EARTH
4	NOAA Geophysical Fluid Dynamics Laboratory	GFDL-ESM2M
5	Met Office Hadley Centre	HadGEM2-ES
6	Institut Pierre-Simon Laplace	IPSL-CM5A-MR
7	Atmosphere and Ocean Research Institute (The University of Tokyo), National Institute for Environmental Studies, and Japan Agency for Marine-Earth Science and Technology	MIROC5
8	Max Planck Institute for Meteorology	MPI-ESM-LR
9	Norwegian Climate Centre	NorESM1-M

The GCM runs are from the CMIP5 (Coupled Model Intercomparison Project Phase 5) as listed in Table 1. Apart from different formulation the GCMs have been operated at different horizontal resolution, ranging from c. 125 to 300 km at the equator.

For all GCMs two emission scenarios were downscaled. These are the RCP (Representative Concentration Pathway) scenarios RCP4.5 (Thomson et al., 2011) and RCP8.5 (Rihai et al., 2011).

In addition one simulation with RCA4 with boundary conditions from the reanalysis ERA-Interim (Dee et al., 2011) has been used.

4. The simulated control climate

The results clearly indicate that the simulated control climate is most often in less good agreement with observations when RCA4 is forced by boundary conditions from coarse-scale GCMs than when forced by reanalysis data from ERA-Interim. Furthermore, many of these larger biases can be attributed to errors in the large-scale circulation in the GCMs. Typically, too zonal conditions leads to too mild and wet winter climate in large parts of southern and central Europe in winter. However, biases differ between RCA4 and the underlying coarse-scale GCMs in several areas of Europe implying that errors in the large-scale circulation is not the only explanation for the biases. As an example Fig. 1 shows biases in seasonal mean temperature and precipitation for an area in Eastern Europe. For this particular case the ensemble mean bias does not differ much between the GCMs and the RCM. However, biases in the different GCM-RCM pairs are quite different where RCA4 sometimes amplifies errors and sometimes reduces them compared to the GCMs.

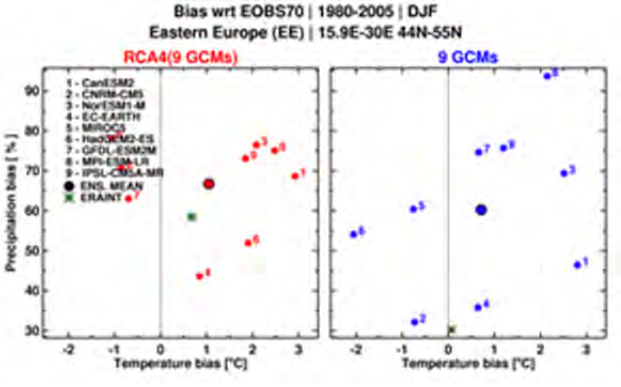


Figure 1. Winter (December-February) biases in temperature and precipitation with respect to E-OBS (Haylock et al., 2008) for an area in Eastern Europe. The numbering refers to the GCMs in Table 1.

5. Simulated climate change

Figure 2 shows the simulated changes in wintertime temperature and precipitation for three different time periods in the future compared to the reference period 1971-2000 for the same region in Eastern Europe as in Figure 1. It is clear that the signal in RCA4 largely follows that in the GCMs with a gradual increase in both temperature and precipitation over time. However, it is also evident that RCA4 to some extent modifies the signal. The ensemble mean indicate that the relative increase in precipitation is slightly larger in RCA4 than in the GCMs while for temperature it is the other way with a weaker increase in RCA4. In some other regions and seasons it is clear that RCA4 significantly reduces the spread between the different members. A more detailed look at the individual simulations shows that RCA4 can even change the relative ordering of the simulations, i.e. a GCM showing the strongest warming can - when downscaled by RCA4 - show only modest warming and vice versa.

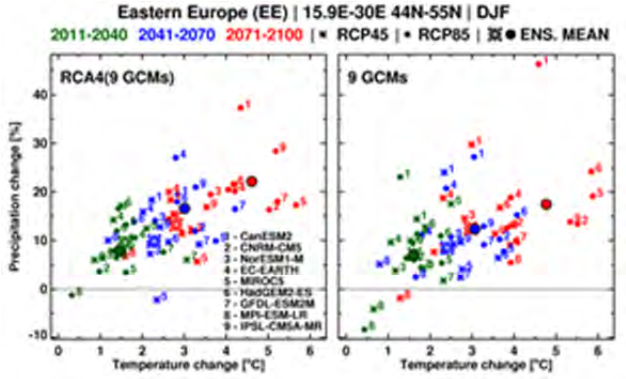


Figure 2. Winter (December-February) changes in temperature and precipitation for an area in Eastern Europe relative to the reference period (1971-2000). The numbering refers to the GCMs in Table 1.

6. Conclusions

A large ensemble of RCM scenarios with one RCM forced by different GCMs shows robust climate change signals in temperature and precipitation for Europe. In many aspects the climate change signal is dictated by the GCMs but the results also indicate that the RCM has a strong influence on the actual amplitude of the climate change signal. In some areas and seasons the spread between the ensemble members is significantly reduced in RCA4 compared to the underlying GCMs. We stress that this result does not imply that the RCM reduce the uncertainty. Rather, it is a manifestation of the fact that all ensemble members are run through one set of physical parameterisations in RCA4 compared to the nine different ones in the underlying GCMs. Other RCMs may show different results.

7. Acknowledgements

Part of the simulations and subsequent analysis work has been done in the Swedish Mistra-SWECIA programme funded by Mistra (the Foundation for Strategic Environmental Research) and in the European FP7 projects IMPACT2C (Grant agreement no. 282746) and ECLISE (Grant agreement no. 265240). We acknowledge the World Climate Research Programme's Working Group on Coupled Modelling, which is responsible for CMIP, and we thank the climate modeling groups (listed in Table 1 of this paper) for producing and making available their model output.

References

Dee DP et al. (2011) The ERA-Interim reanalysis: configuration and performance of the data assimilation system. Q.J.R. Meteorol. Soc., 137: 553–597. doi: 10.1002/qj.828

Haylock MR et al. (2008) A European daily high-resolution gridded dataset of surface temperature and precipitation. J Geophys Res 113, :D20119 doi:10/1029/2009JD011799

Jones C et al. (2011) The Coordinated Regional Downscaling Experiment: CORDEX, An international downscaling link to CMIP5: CLIVAR Exchanges, No 56, Vol 16, No 2, 34-40.

Kjellström E et al. (2013) A new generation of regional climate model scenarios for the Baltic Sea area. 7th Study Conference on BALTEX, Borgholm, Island of Öland, Sweden, 10 to 14 June 2013.

Riahi K et al. (2011) RCP 8.5—A scenario of comparatively high greenhouse gas emissions. Climatic Change 109, 33–57.

Samuelsson P et al. (2011) The Rossby Centre Regional Climate Model RCA3: Model description and performance. Tellus, 63A, 1, 4-23.

Thomson AM et al. (2011) RCP4.5: a pathway for stabilization of radiative forcing by 2100. Climatic Change 109,77–94.

Evaluating temperature distributions in a high-resolution RCM at 6 km horizontal resolution over Europe

Erik Kjellström[1,2], Petter Lind[1,2], David Lindstedt[1,2] and Tomas Landelius[1]

[1] Rossby Centre, Swedish Meteorological and Hydrological Institute, Norrköping, Sweden (erik.kjellstrom@smhi.se)

[2] Department of Meteorology, Stockholm University, Sweden

1. Introduction

High-resolution regional climate models (RCM) require high-resolution reference data for their evaluation. To date, one of the data sets most used for evaluating RCMs in Europe is the E-OBS data set (Haylock et al. 2008). E-OBS is a product based on observations of climate parameters gridded to a horizontal resolution of 25 km grid spacing. E-OBS is high-resolution also in time as it contains daily data. However, the most recent high-resolution RCMs operate at even higher horisontal resolution as in EURO-CORDEX at 12 km (Jacob et al., 2013). Next-generation RCMs operate at even higher resolution. An example is the 6 km long-term integrations with the HARMONIE-climate model (e.g. Lindstedt et al., 2014). These high-resolution simulations add value as the representation of local details are improved but to date the evaluation of these models is limited to the local scale due to lack of high-resolution pan-european evaluation data (e.g. Lindstedt et al. 2014).

This study combines efforts in the RCM community to produce high-resolution simulations with progress in the production of high-resolution reference data sets. We compare output from the regional HARMONIE-climate model run at 15 and 6 km horizontal resolution for all of Europe with a gridded data reference data set based on regional reanalysis combined with objective interpolation in a mesoscale analysis resulting in new a high-resolution reference data set for all of Europe. In this case high-resolution means 6-hourly temporal resolution and 5 km spatial resolution.

Changes in temperature variability at daily time scales have been reported both in climate change simulations (Kjellström, 2004) and in studies based on observations (Stainforth et al. 2013). A good representation of higher-order statistics like daily (or sub-daily) variability is essential for a model that is intended to use for climate change studies. The objective of this study is therefore to investigate if a new high-resolution RCM can represent the observed PDFs of 2m-temperature for Europe during the last decade.

2. The HARMONIE-climate model

The HARMONIE-climate model is based on the operational NWP model HARMONIE used at several national meteorological institutes in Europe. Here, it is used in a climate setting at two different resolutions (6km and 15km) for the ten-year period 1998-2007. Among its different features this model has a convection scheme particularly designed to operate in the ”grey-zone” regime, which increase the realism and accuracy of the time and spatial evolution of convective processes compared to more traditional parameterizations. See Lindstedt et al. (2014) for a more elaborate description of the model and the experiment.

A first study showing results from the HARMONIE-climate model indicates that the model reproduces many of the observed features of the climate. The study also points out that the 6 km run shows added value compared to the 15 km one in areas where high-resolution observations were available. As an example of model performance probability distributions for daily temperature in winter and summer is shown in Figure 1.

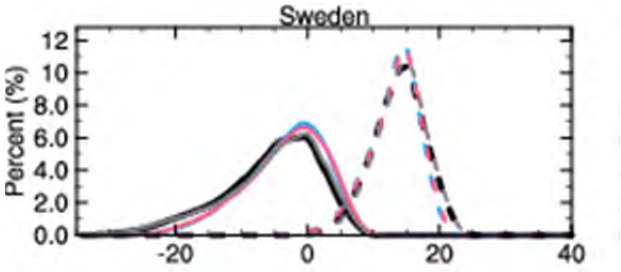


Figure 1. Probability density function for winter (December-February, solid) and summer (June-August, dashed) two meter temperature for Sweden. The grey lines are from high-resolution observations (Johansson, 2002) and the black lines are E-OBS data (Haylock et al. 2008). Blue (15km) and red (6km) represents the HARMONIE-climate simulations. Adapted from Lindstedt et al. (2014).

3. Evaluation data

In this study we use a new data set from the EURO4M (European Reanalysis and Observations for Monitoring) FP7 project. In EURO4M observations from satellites, ground-based stations and results from comprehensive model-based regional reanalyses are combined. As a high-resolution product the mesoscale analysis system MESAN (Häggmark et al., 2000) is used to produce gridded information at 5 km horisontal resolution for all of Europe by use of optimal interpolation. The temporal resolution of this data set is 3 or 6 hours depending on variable. An example of the data is shown in Figure 2 where 2m-temperature from the high-resolution regional reanalysis (25 km resolution) and the MESAN analysis (5 km) are shown for a region in eastern Sweden.

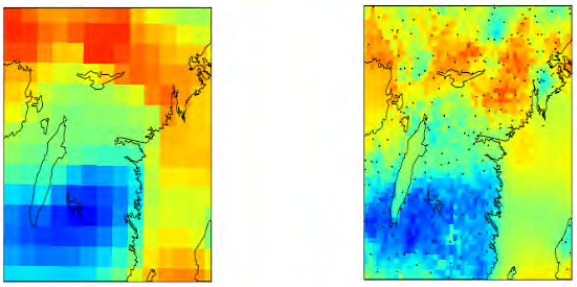


Figure 2. 2m-temperature for one occasion as simulated by the regional reanalysis from the NWP 6 hour forecast with 0.2 degree resolution (left) and from the optimal interpolation MESAN at 0.05 degree resolution (right).

In addition to the new EURO4M-dataset we also use the E-OBS data as it is a standard data set used for model evaluation (e.g. Kjellström et al., 2010). We use the two-metre air temperature from the EURO4M high-resolution data set and from E-OBS to compare with the output from the HARMONIE-climate model.

4. Results and outlook

The results show that the model reproduces many of the observed features of the observed climate including the asymmetry in winter with a long tail at cold temperatures (e.g. Fig. 1). Differences between the different data sets are discussed and it is assessed how the new EURO4M-dataset can be used to add information about the performance of high-resolution RCMs.

5. Acknowledgements

Part of the simulations and subsequent analysis work has been done in the Swedish Mistra-SWECIA programme funded by Mistra (the Foundation for Strategic Environmental Research) and in the European FP7 project IMPACT2C (Grant agreement no. 282746). The high-resolution MESAN analysis has been produced within the European FP7 project EURO4M (Grant agreement no. 242093).

References

Haylock MR et al. (2008) A European daily high-resolution gridded dataset of surface temperature and precipitation. J. Geophys. Res., 113, D20119, doi:10.1029/2008JD10201

Häggmark L, Ivarsson K-I, Gollvik S and Olofsson P-O (2000) MESAN, an operational mesoscale analysis system, Tellus, 52A, 2-20.

Jacob D et al (2013) EURO-CORDEX: new high-resolution climate change projections for European impact research. Regional Environmental Change. Doi: 10.1007/s10113-013-0499-2

Johansson B (2002) Estimation of areal precipitation for hydrological modelling in Sweden. PhD thesis, Earth Sciences Centre, Dept. Phys. Geog., Gothenburg University, Sweden.

Kjellström E (2004) Recent and future signatures of climate change in Europe. Ambio, 33(4-5), 193-198.

Kjellström E, Boberg F, Castro M, Christensen JH, Nikulin G, and Sanchez E (2010) On the use of daily and monthly temperature and precipitation statistics as a performance indicator for regional climate models. Climate Research, 44(2-3), 135-150. Doi: 10.3354/cr00932.

Lindstedt D, Lind P, Jones C and Kjellström E (2014) A new regional climate model operating at the meso-gamma 2 scale; performance over Europe. Submitted to Tellus.

Stainforth, DA, Chapman, SC and Watkins NW (2013) Mapping climate change in European temperature distributions Environ. Res. Lett. 8 (2013) 034031 (9pp)

The representation of recent Siberian snow cover in the regional climate model COSMO-CLM

Katharina Klehmet, Beate Geyer and Burkhardt Rockel

Institute of Coastal Research, Helmholtz-Zentrum Geesthacht, Geesthacht, Germany (Katharina.Klehmet@hzg.de)

1. Introduction

Snow cover is an important feature of terrestrial landscape in Siberia. It has profound implications for surface energy and water balance due to its high short-wave albedo, low heat conductivity, control on evaporation, water storage, soil moisture and river discharge (Vavrus, 2007, Troy et al., 2012). Snow properties affect moreover soil temperature and thus thermal state of permafrost and biogeochemical cycles (Zhang et al., 2005).

Monitoring of Siberian climate parameters, including those for snow cover, is complicated by the lack of in situ measurements (Khan et al., 2008; Serreze et al., 2003). The sparse station density makes it difficult to obtain a detailed regional overview of past and ongoing changes. The need of long-term climate information with less spatial and temporal gaps has motivated the effort to generate a model-based reconstruction of recent Siberian climate using the regional model COSMO-CLM (CCLM).

This study analyzes the representation of recent snow cover for Siberia derived by a regional climate model hindcast. The focus is on snow water equivalent (SWE) as one important parameter within the hydrological cycle determining e.g. snowmelt runoff.

2. Model and Datasets

The reconstruction of Siberian climate was obtained by means of dynamical downscaling of NCEP-R1 reanalysis data using the regional climate model CCLM (http://www.clm-community.eu, Rockel et al., 2008). Reconstructed fields are available over a period of 1948-2010 at 50km grid spacing.

First test simulations over Siberia indicated a strong winter warm bias of 2m air temperature in the arctic and central parts of the model domain which was only partly related to the driving fields (not shown here). Therefore, the application of CCLM over Siberia implied some changes in the model configuration, e.g., the reduction of the minimal heat diffusion coefficient, which leads to reduced vertical mixing and to a better representation of the stable conditions predominant in the Siberian High pressure system and thus winter temperatures. In addition, the multilayer snow model, introduced in a preliminary version by the Deutscher Wetterdienst (DWD), was used. To account for the distribution of energy within the deep reaching permafrost soils in that region, three more soil layers were added from the standard 13m up to a total soil depth of 92m.

To evaluate the model output in a larger scale, the satellite-derived SWE estimate provided by ESA GlobSnow is used as reference for the years 1987-2010 in combination with the SWE products of several reanalyses (NCEP-R2, NCEP-CFSR, ERA-Interim).

3. Results

Figure 1 presents the spatial distribution of mean SWE during 1987-2010 for January and April for GlobSnow, CCLM and ERA-Interim. The SWE hindcast is in good agreement with GlobSnow in January (mid-winter), whereas it overestimates SWE during the melting season compared to GlobSnow. During January and April, CCLM is able to locate the peaks of SWE as shown by ESA GlobSnow. It is evident that CCLM can add spatial detail compared to the very smooth patterns of SWE in GlobSnow despite the 25km original resolution.

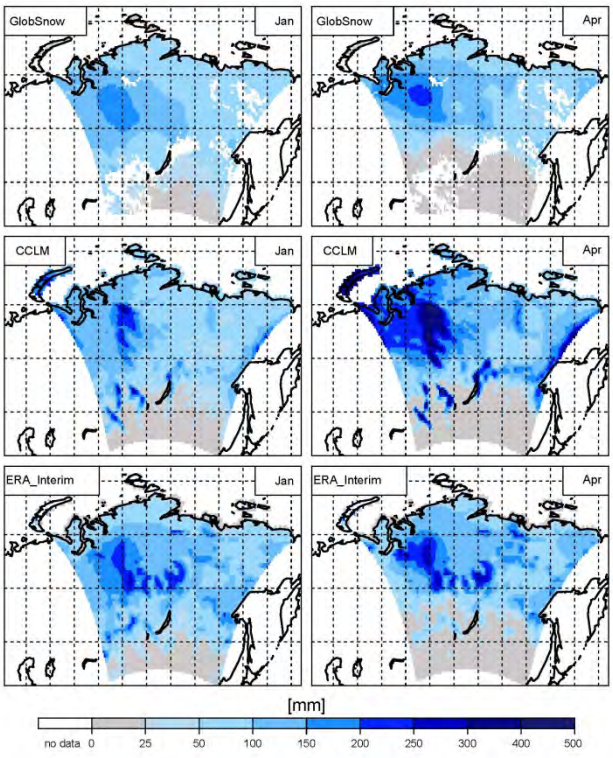


Figure 1. Long-term mean of SWE [mm] (1987–2010) of GlobSnow, CCLM and ERA-Interim for January and April. White boxes within the model domain indicate missing values of GlobSnow.

In terms of the temporal consistency, SWE of the regional model hindcast is more homogeneous in time than ERA-Interim that presents a spurious jump in 2003, obvious in certain subregions as shown here e.g. for a central subregion Mid-Mid (MM) in Figure 2. A temporal inconsistency is also evident in NCEP-R2 in 1999-2001. The CCLM can also compete with the newest generation of NCEP reanalysis (CFSR). NCEP-R1 shows no interannual variation of SWE and is outside the uncertainty range of

GlobSnow.

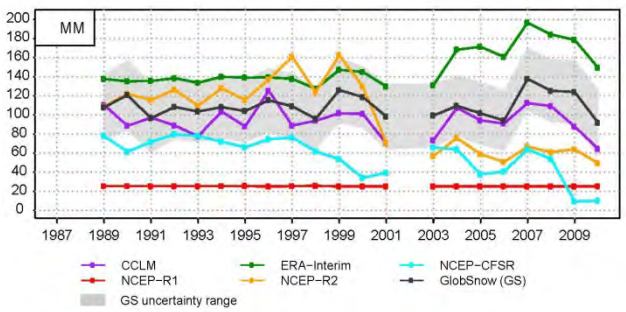


Figure 2. Time series mean January SWE [mm] (1987–2010) for the central subregion Mid-Mid (MM). The gray shaded area represents the uncertainty range of GlobSnow. Years are excluded when GlobSnow provides SWE with more than 3 missing days per month.

4. Conclusion

This study shows that the regional CCLM climate reconstruction can deliver more realistic information in terms of SWE than the global product of NCEP-R1 and provide a better quality in temporal consistency compared to many further reanalyses for the years after 1987. The SWE product of NCEP-R1 does not represent any of the regional and temporal variation. However, this added value was not unexpected because of the errors of the SWE fields of NCEP-R1 already documented. Nevertheless, it was possible to illustrate that the technique of dynamical downscaling of atmospheric forcing fields provided by NCEP-R1 can be used to derive historical SWE fields with more realistic information than the driving reanalysis product itself can present. As shown by the SWE overestimation of CCLM in April, there is still an obvious model deficiency. However, the results are dependent on the quality of the reference data of ESA GlobSnow. In general, a multi-decadal dataset at regional scale is necessary in the data-sparse region of Siberia. This may help to improve the understanding of snow–climate relations.

References

Khan, V., Holko, L., Rubinstein, K., and Breiling, M. (2008) Snow Cover Characteristics over the Main Russian River Basins as Represented by Reanalyses and Measured Data, J. Appl. Meteor. Clim., 47, 1819–1833

Rockel, B., Will, A., and Hense, A. (2008) The Regional Climate Model COSMO-CLM (CCLM), Meteorol. Z., 17, 347–348

Serreze, M. C., Clark, M. P., and Bromwich, D. H. (2003) Monitoring Precipitation over the Arctic Terrestrial Drainage System: Data Requirements, Shortcomings, and Applications of Atmospheric Reanalysis, J. Hydrometeorol., 4, 387–407

Troy, T. J., Sheffield, J., and Wood, E. F. (2012) The role of winter precipitationand temperature on northern Eurasian streamflow trends, J. Geophys. Res., 117

Vavrus, S. (2007) The role of terrestrial snow cover in the climate system, Clim. Dynam., 29, 73–88

Zhang, T., Frauenfeld, O. W., Serreze, M. C., Etringer, A., Oelke,C., McCreight, J., Barry, R. G., Gilichinsky, D., Yang, D., Ye, H.,Ling, F., and Chudinova, S. (2005) Spatial and temporal variability inactive layer thickness over the Russian Arctic drainage basin, J.Geophys. Res., 110, D16101

Validation of Cordex data over Cote d'Ivoire (Prepared to be submitted)

Kouadio K[1, 4]. , A. KONARE[2] , K. GJE Kouakou[3], and A. Diedhiou[4]

[1] University Felix Houphouet-Boigny, Cote d'Ivoire (Kouadio.kouakou@ird.fr)
[2] National Meteorology, Cote d'Ivoire
[3] LTHE-IRD, Université de Grenoble, France

[4] WASCAL Graduate Research Program on West African Climate System (WACS)/Federal University of Technology Akure (FUTA), Nigeria

It is well known that West Africa is one of the poorest regions in terms of the global economy and scientific information. Its agriculture is exclusively depending on the monsoon rains which occur between June and September. The region is thus one of the most vulnerable to the climate change and variability. This situation is aggravated by the interaction of 'multiple stresses'(drought frequency and duration, frequency of extreme events…), occurring at various levels, and low adaptive capacity. In spite of several campaigns and various platforms to collect information, it's still a lack of appropriate observational datasets. Thus, models constitute a real occasion to understand the features of the West African Monsoon (WAM), specially the Coordinated Regional Downscaling Experiment (CORDEX) program. According to CORDEX Africa, "this program presents an unprecedented opportunity to advance knowledge of regional climate responses to global climate change and for these insights to feed into on-going climate adaptation and risk assessment research and policy planning in the region. Rainfall in this region is one of the closest parameter to the WAM regime. In this work, we assessed the performance of six models (HadRNM3, ICTP-REGCM3, METHNO, SMHIRCA, DMI-HIRHAM5, KNMI-RACMO2) used in the CORDEX experiment over Cote d'Ivoire throughout the rainfall from five (5) stations (Abidjan, Bondoukou, Daloa, Dimbokro, Gagnoa and Tabou). We first focused on the period 1995-2005 which is the historical period and secondly the period 2010-2013. In the second period we assess the capacity of this experiment in the projection of WAM. The method consisted to the comparison of the variability using the Taylor diagram to assess how close the models output are to the observation data. The results showed that the performance of the models varied from one station to another and are also related to the season. Any models presented a high performance over the entire country and the seasons. In general the computed Ensemble has a good accuracy with the observation and offers an improvement of the representation of the climate compared to a single model. These results suggest that the models may not well perform for the representation of rainfall pattern over Cote d'Ivoire during any period. It's seemed from this study that the choice of any model for an efficient focus on climate over the country may be done according to the period and the area of interest.

Accurate Boundary Conditions for Regional Climate Modeling

Marco Kupiainen

Rossby Centre, Swedish Meterological and Hydrological Institute (SMHI)

An accurate treatment of boundary conditions is a central issue in Regional Climate Modeling (RCM) and non-global Numerical Weather Prediction (NWP). The science of computational mathematics has evolved significantly since the publication of boundary relaxation, Davies (1976) , and can nowdays treat the setting of boundary conditions accurately, e.g. Funaro et. al. (1988), Carpenter et. al. (1993), Hesthaven et. al. (1996), Nordström et. al. (2005). As far as the author knows, this knowledge has not been used by the RCM/NWP community. The commonly used boundary relaxation leads one to believe that the boundary value problem is ill-posed e.g. Hong et. al. (2014), and that other various methods, e.g. spectral nudging, Storch et.al. (2000) are necessary to use in order to have reliable results.

The emphasis is on deriving lateral boundary conditions that ensure that the continuous problem is well-posed, work already published by others, e.g. Hesthaven et. al. (1996), Nordström et. al. (2005), in the field of computational mathematics. Further it is shown how to construct a semi-discrete energy-stable scheme for imposing these conditions, Hesthaven et. al. (1996), Svärdh et. al. (2007) . The relation between the stability of the semi-discrete and the fully discrete scheme is discussed by Kreiss et. al. (1993).

References

Davies (1976) A lateral boundary formulation for multi-level prediction models, Quart. J. Roy. Meteor. Soc., 102, pp 405-418

Carpenter, Gottlieb, Abarbanel (1993), Time-stable boundary conditions for finite-difference schemes solving hyperbolic systems: Methodology and applications to high-order compact schemes, ICASE Report no.93-9

Funaro, Gottlieb (1988), A new method of imposing boundary conditions in pseudospectral approximations of hyperbolic equations, Math. Comp., 51, pp.599-613

Hesthaven, Gottlieb (1996), A stable penalty method for the compressible Navier-Stokes equations: I. Open boundary conditions, J. Comp. Phys. 17,3 pp. 579-612

Hong, Kanamitsu (2014) Dynamical Downscaling: Fundamental Issues from an NWP Point of View and Recommendations, Asia-Pac. J. Atmos. Sci., 50(1), pp. 83-104

Kreiss, Wu (1993), On the stability definition of difference approximations for the initial boundary value problem, Appl. Numer. Math., 12 pp. 213-227

Nordström, Svärdh (2005), Well-posed boundary conditions for the Navier-Stokes equations, SIAM J. Numer. Anal. Vol 43, No 3,pp.1231-1255

Storch, Langenberg, Feser (2000) A Spectral Nudging Technique for Dynamical Downscaling Purposes, Mon. Wea. Rev. 128,pp 3664-3674

Svärdh, Carpenter, Nordström (2007), A stable high-order finite-difference scheme for the compressible Navier-Stokes equations, far-field boundary conditions, J. Comp. Phys. 225,pp.1020-1038

Spatially explicit climate model evaluation with complex networks

Stefan Lange[1,2], Jonathan F. Donges[2,3], Jan Volkholz[2], Jan H. Feldhoff[1,2], and Jürgen Kurths[1,2,4]

[1] Department of Physics, Humboldt University, Berlin, Germany
[2] Potsdam Institute for Climate Impact Research, Germany (slange@pik-potsdam.de)
[3] Stockholm Resilience Center, Stockholm University, Sweden
[4] Institute for Complex Systems and Mathematical Biology, University of Aberdeen, United Kingdom

In this study we introduce three local difference measures on complex networks which allow for a spatially explicit network-based evaluation of climate models. The utility of this approach is exemplified by the analysis of statistical vs. dynamical regional climate simulations of the South American monsoon system. Networks are constructed on precipitation time series in three ways to represent different aspects of general as well as extreme rainfall dynamics. An evaluation against daily satellite data from the Tropical Rainfall Measuring Mission 3B42 V7 demonstrates the distinct levels of difficulty the models have reproducing the observations. While they perform comparably well in simulating the network of positive correlations between common rain events, especially the statistical model struggles with networks based on anticorrelations of common and synchronizations of extreme rain events, in particular in the Amazon basin. Performances of a suitable random network model attribute greater a-priori complexity factors to the reproductions of these latter two networks but on their own cannot explain all performance differences between climate models and network types.

Evaluation of River Discharge Simulated by Regional Climate Modeling over the Korean Region and Sensitivity on Resolution of River Routing Scheme

Ji-Woo Lee[1,2], Song-You Hong[2,3], Jung-Eun Esther Kim[4], Kei Yoshimura[5], Suryun Ham[5], and Minsu Joh[1]

[1] Supercomputing Service Center, Korea Institute of Science and Technology Information, Daejeon, Korea (jiwoolee@kisti.re.kr)
[2] Department of Atmospheric Sciences, Yonsei University, Seoul, Korea
[3] Korea Institute of Atmospheric Prediction System, Seoul, Korea
[4] Cooperative Institute for Research in the Atmosphere, Colorado State University, Fort Collins, and National Oceanic and Atmospheric Administration / Earth System Research Laboratory, Boulder, Colorado, USA
[5] Atmosphere and Ocean Research Institute, University of Tokyo, Kashiwa, Japan

1. Introduction

Fresh water discharge from land to oceans (i.e. river discharge at estuaries) is one of the most important components in the hydrological cycle, which provides a chain connection for the movement of water quantities from the atmosphere to oceans via river routing process on the land surface. It is known to have sensitive response on climate change (Sperna Weiland et al. 2012).

In terms of numerical modeling, river discharge is important for the evaluation of models' land surface processes and for linking the hydrological cycle between the land and ocean. Since station observations measure the amount of river discharge at fixed points, conversion from grid runoff to point discharge is essential for the comparison. It is generally simulated by river routing scheme, which horizontally advects the model-simulated surface and sub-surface runoff along river channels (Oki and Sud 1998).

Traditionally, the river discharge has been diagnosed by applying result of global climate models (GCMs) to hydrological models, as reviewed by Fowler et al. (2007) and Praskievicz and Chang (2009); however, the coarse resolution of GCMs limits describing details in regional scale, whereas many of water strategies are planned in that spatial scale. The regional climate models (RCMs) are introduced as an alternative approach to overcome the resolution problem of GCMs, as reviewed by Leung et al. (2003), Laprise (2008), and Hong and Kanamitsu (2014).

The river discharge has been focused in recent RCM studies due to its importance on planning regional water strategies in changed climate condition, as reviewed by Teutschbein and Seibert (2010). Furthermore, developments of RCMs for elaborate coupling of atmosphere and ocean models strengthen importance of river routing scheme in RCM frameworks. Ham et al. (2012) confirmed that the freshwater discharge into ocean has feedback to atmosphere by changing sea surface temperature using coupled GCM frameworks. Li et al. (2013) and Samala et al. (2013) studied ocean coupled RCMs and their applications; however, the simulation of river discharge was not considered yet in those studies. The roles of river discharge will be more important in RCM frameworks in the future as coupling of atmosphere and ocean becomes more elaborate. Nevertheless, its accurate estimation is still challengeable due to strewn uncertainties crossing observation and model components.

As a prerequisite of implementation of river routing scheme in coupled RCM frameworks, it is essential to find proper resolution of river routing scheme that can provide reasonable temporal variation of river discharge at given RCM resolution. It is conceptually obvious that river routing scheme would show better performance as its resolution becomes higher; however, there should be computational limitation at increasing the resolution for the online coupling of atmosphere, river, and ocean in the RCM frameworks.

In this study, we selected the Korean region, where RCMs were rarely introduced for river discharge studies, to find proper resolution of river routing scheme for reasonable representation of river discharge variation at given RCM resolution. The possibility of the reproduction of river discharge from a dynamically downscaled dataset obtained by a RCM simulation is first accessed, and sensitivity experiments are conducted varying RCM resolution, river maps, and resolution of river routing model.

2. Data and Methodology

For the RCM, we adapted the Regional Model Program (RMP) of the Global/Regional Integrated Model system (GRIMs; Hong et al. 2013), which has been successfully employed for regional climate studies, especially for East Asian monsoon and scenario projection studies (e.g. Kang and Hong 2008; Lee et al. 2014). To prevent distortion of large-scale fields, the vertically weighted spectral nudging method, namely the Revised Scale Selective Bias Correction (Hong and Chang 2012), was applied. The ERA-Interim global atmospheric reanalysis produced by the European Centre for Medium-Range Weather Forecasts was employed as external forcing from 2000 to 2010. The model domain covers Korea (Fig. 1a), and a 28-level terrain-following (sigma) vertical grid was used with spatial horizontal resolutions of 50 km and 12.5 km. Two different spatial resolution RCMs experiments were designed to examine effect of atmospheric forcing on the river routing process.

For the river routing process, the Total Runoff Integrate Pathway (TRIP; Oki and Sud 1998) was coupled with the GRIMs-RMP in one-way interaction. The total runoff (i.e., sum of surface and subsurface runoffs) calculated by the land surface module of the RMP is

provided to TRIP, and it aggregates runoff along the stream-flow network, i.e., river map.

The basins of three main river systems in Korea (i.e. Han, Nakdong, and Geum rivers) were selected for the evaluation of simulated river discharge at the river mouth by comparison with corresponding Station observations (Fig. 1a). The default TRIP river map is too simplified to describe rivers and the basins' areas were inaccurately estimated (Fig. 1b). To overcome this problem, revised river maps were created in two ways: 1) the river direction map was revised (Fig. 1c), and 2) the river map resolution was enhanced to 0.25° (Fig. 1d). The revised river maps showed much more closely fitted basin areas with those from the real world. The river direction maps were upscaled from HydroSHEDS.

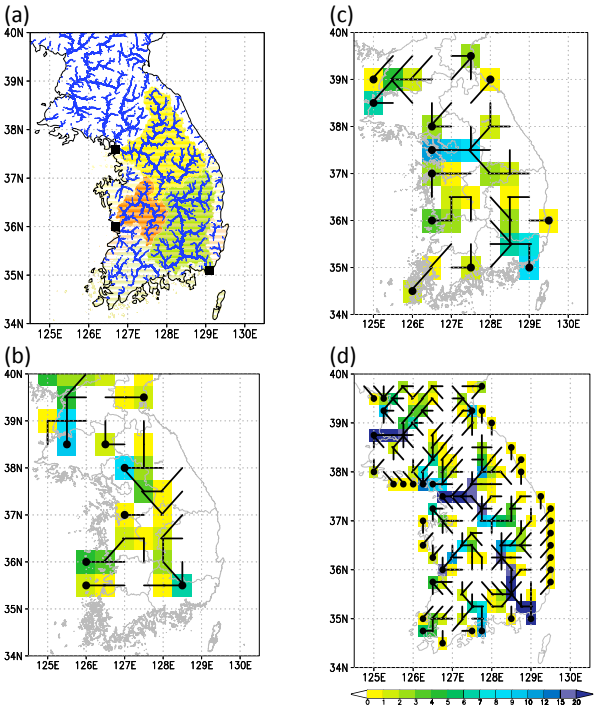


Figure 1. (a) Han (yellow), Nakdong (green), and Geum (orange) river basins obtained from the HydroSHEDS dataset. River sequences (i.e. number of upstream grid; shaded) and drainage streams (black) obtained from the (b) TRIP default map, (c) revised 0.5°, and (d) 0.25° resolution maps upscaled from HydroSHDES. Closed circles denote river mouths.

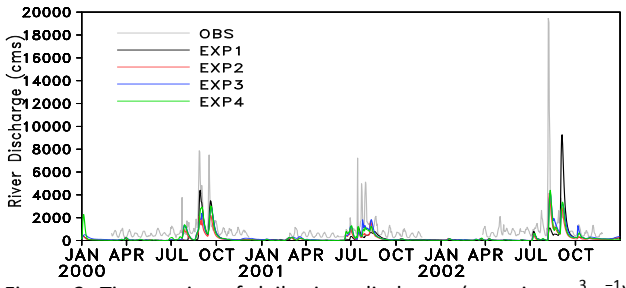


Figure 2. Time series of daily river discharge (cms; i.e. m^3 s^{-1}) from 2000 to 2002 at mouth of Han River.

3. Preliminary Results

Four different experiments were conducted varying (1) resolution of RCM, (2) river stream map, and (3) resolution of river routing scheme. In the preliminary analysis, it is roughly shown that the river discharge tends to be captured better as RCM resolution increases, basin area becomes closer to measured, and resolution of river routing model increases (Fig. 2).

The detailed results and discussions about remained issues will be presented at the workshop.

References

Fowler HJ et al. (2007) Linking climate change modelling to impacts studies: recent advances in downscaling techniques for hydrological modelling. Int. J. Climatol., 27, pp. 1547–1578

Ham S et al. (2012) Effects of freshwater runoff on a tropical pacific climate in the HadGEM2. Asia-Pacific J Atmos Sci, 48, pp. 457-463

Hong S-Y, Chang E-C (2012) Spectral Nudging Sensitivity Experiments in a Regional Climate Model. Asia-Pacific J Atmos Sci 48, pp. 345-355

Hong S-Y, Kanamitsu M (2014) Dynamical downscaling: Fundamental issues from an NWP point of view and recommendations, Asia-Pacific J Atmos Sci, 50, pp. 83-104

Hong S-Y et al. (2013) A Multi-Scale Atmospheric/Oceanic Modeling System: The Global/Regional Integrated Model system (GRIMs). Asia-Pacific J Atmos Sci 49, pp. 219-243.

Kang H-S, Hong S-Y (2008) An assessment of the land surface parameters on the simulated regional climate circulations: The 1997 and 1998 east Asian summer monsoon cases. J Geophy Res 113, D14121

Laprise R (2008) Challenging some tenets of Regional Climate Modelling. Meteorol Atmos Phys, 100, pp. 3-22

Lee J-W et al. (2014) Assessment of Future Climate Change over East Asia Due to the RCP Scenarios Downscaled by GRIMs-RMP. Clim Dyn, 42, pp. 733-747

Leung R, Mearns LO, Giorgi F, Wilby RL (2003) Regional climate research: Needs and opportunities. B Am Meteorol Soc, 84, pp. 89–95

Li H et al. (2013) A high-resolution ocean-atmosphere coupled downscaling of the present climate over California. Clim Dyn, 42, pp.701-714

Oki T, Sud YC (1998) Design of Total Runoff Integrating Pathways (TRIP)—A Global River Channel Network. Earth Interact 2, pp. 1–37

Praskievicz S, Chang H (2009) A review of hydrological modelling of basin-scale climate change and urban development impacts. Progress in Physical Geography, 33, pp. 5650-671

Samala BK et al. (2013) Study of the Indian summer monsoon using WRF–ROMS regional coupled model simulations. Atmosph. Sci. Lett., 14, pp. 20–27

Sperna Weiland FC et al. (2012) Global patterns of change in discharge regimes for 2100, Hydrol. Earth Syst. Sci. 16, pp. 1047-1062

Quantifying uncertainty in observed rainfall datasets across Africa: A probabilistic history

Chris Lennard[1], Alessandro Dosio[2] and Grigory Nikulin[3]

[1] Climate System Analysis Group, University of Cape Town, Cape Town, South Africa (lennard@csag.uct.ac.za)
[2] EC JRE, Institute for Environment and Sustainability, Climate Risk Management Unit, Ispra, Italy
[3] Swedish Meteorological and Hydrological Institute, Norrkoping, Sweden

1. Observational rainfall data in CORDEX Africa

The CO-ordinated Regional Downscaling Experiment (CORDEX) has to date seen the publication of at least eight journal papers that examine the African domain during 2012 and 2013. Five of these papers consider Africa generally (Nikulin et al. 2012, Kim et al. 2013, Hernandes-Dias et al. 2013, Laprise et al. 2013, Panitz et al. 2013) and five have regional foci: Tramblay et al. (2013) on Northern Africa, Mariotti et al. (2014) and Gbobaniyi el al. (2013) on West Africa, Endris et al. (2013) on East Africa and Kalagnoumou et al. (2013) on southern Africa. There also are a further three papers that the authors know about under review.

These papers all use an observed rainfall and/or temperature data to evaluate/validate the regional model output and often proceed to assess projected changes in these variables due to climate change in the context of these observations. The most popular reference rainfall data used are the CRU, GPCP, GPCC, TRMM and UDEL datasets. However, as Kalagnoumou et al. (2013) there are many other rainfall datasets available for consideration, for example, CMORPH, FEWS, TAMSAT & RIANNAA, TAMORA and the WATCH & WATCH-DEI data. They, with others (Nikulin et al. 2012, Sylla et al. 2012) show that the observed datasets can have a very wide spread at a particular space-time coordinate (Fig. 1).

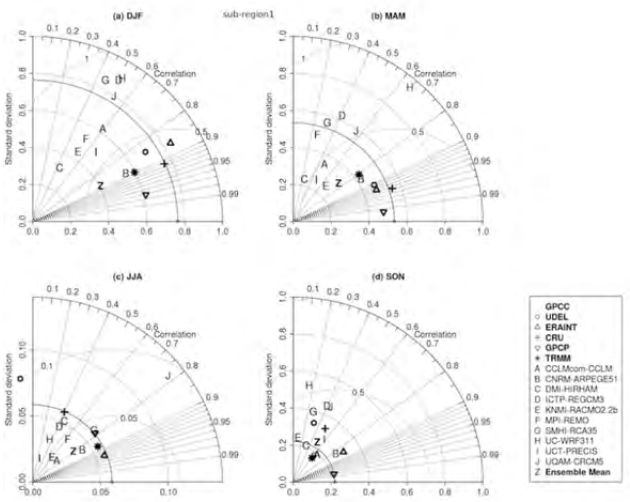


Figure 1. Taylor diagrams per season for a) DJF, b) MAM, c) JJA, d) SON, based on the interannual variation of seasonal mean precipitation for the period 1990-2006 in a tropical region over southern Africa. Ten RCM results, the multi-model ensemble, four observational data sets (UDEL, CRU, GPCP and TRMM) and one reanalysis data set (ERAINT) are compared against GPCC observational data. The radial coordinate gives the magnitude of total SD [mm/day] (the solid radial highlights the SD of GPCC), the angular coordinate gives the correlation with observations (GPCC) and the distance between the observed point on the x-axis and any other point is proportional to the RMSE [mm/day] (gray radials). Note the scales of the SD and RMSE radials are not constant in all the images to allow for assessment of the correlation coefficient where SD and RMSE are small. From Kalagnoumou et al. (2013).

2. Quantifying uncertainty of observed rainfall data

As more ground, space and reanalysis-based rainfall products become available, all which use different methods to produce precipitation data, the selection of reference data is becoming an important factor in model assessment. A number of factors can contribute to a uncertainty in terms of the reliability and validity of the datasets. For satellite-based rainfall one source of uncertainty between different datasets are the algorithims that that produce the rainfall product. Additionally, for mixed gauge-satellite products the quantity and quality of available station data, the different interpolation techniques or (in the case of satellite data) the gauge analysis products used in the adjustments contribute to the observational uncertainty. However, to date no comprehensive study has been performed to evaluate the uncertainty in all of these observational datasets.

In this paper we present all the rainfall datasets available over Africa and assess the spatial and temporal differences that exist between these. We use Taylor diagrams to quantify these differences based on Cordex-Africa homogenous rainfall regions and spatial maps to highlight hotspots of regional uncertainty. We then try to diagnose the reasons behind the differences based on the how the dataset was produced. We finally recommend that, in the context of the quantified observational uncertainty, a probabilistic view of historical rainfall be adopted in rainfall studies over Africa.

References

Endris, H. S., P. Omondi, S. Jain, C. Lennard, B. Hewitson, L. Chang'a, J. L. Awange, A. Dosio, P. Ketiem, G. Nikulin, H-J. Panitz, M. Büchner, F. Stordal, and L. Tazalika (2013) Assessment of the Performance of CORDEX Regional Climate Models in Simulating East African Rainfall. J. Climate, 26, 8453–8475. DOI: 10.1175/JCLI-D-12-00708.1

Gbobaniyi, E., A. Sarr, M. B. Sylla, I. Diallo, C. Lennard, A. Dosio, A. Dhié diou, A. Kamga, N. A. B. Klutse, B. Hewitson, and B. Lamptey (2013) Climatology, annual cycle and interannual variability of precipitation and temperature in CORDEX simulations over West Africa. Int. J. Climatol., DOI: 10.1002/joc.3834

Hernández-Díaz, L., R. Laprise, L. Sushama, A. Martynov, K. Winger, and B. Dugas (2013) Climate simulation over CORDEX Africa domain using the fifth-generation Canadian Regional Climate Model (CRCM5). Clim. Dyn. 40, 1415-1433. DOI: 10.1007/s00382-012-1387-z

Kalognomou, E., C. Lennard, M. Shongwe, I. Pinto, A. Favre, M. Kent, B. Hewitson, A. Dosio, G. Nikulin, H. Panitz, and M. Büchner (2013) A diagnostic evaluation of precipitation in CORDEX models over southern Africa. Journal of Climate, 26, 9477-9506. DOI:10.1175/JCLI-D-12-00703.1

Kim, J., D. E. Waliser, C. A. Mattmann, C. E. Goodale, A. F. Hart, P. A. Zimdars, D. J. Crichton, C. Jones, G. Nikulin, B. Hewitson, C. Jack, C. Lennard, and A. Favre (2013) Evaluation of the CORDEX-Africa multi-RCM hindcast: systematic model errors. Clim. Dyn. 42:1189-1202. DOI: 10.1007/s00382-013-1751-7

Laprise, R., L. Hernández-Díaz, K. Tete, L. Sushama, L. Šeparović, A. Martynov, K. Winger, and M. Valin (2013) Climate projections over CORDEX Africa domain using the fifth-generation Canadian Regional Climate Model (CRCM5). Clim. Dyn. 41:3219-3246. DOI:10.1007/s00382-012-1651-2

Mariotti, L., I. Diallo, E. Coppola, and F. Giorgi (2014) Seasonal and intraseasonal changes of African monsoon climates in 21st century CORDEX projections. Climatic Change, 1-13. DOI: 10.1007/s10584-014-1097-0

Nikulin, G., C. Jones, F. Giorgi, G. Asrar, M. Büchner, R. Cerezo-Mota, O. Bøssing Christensen, M. Déqué, J. Fernandez, A. Hänsler, E.van Meijgaard, P. Samuelsson, M. Bamba Sylla, and L.Sushama (2012) Precipitation Climatology in an Ensemble of CORDEX-Africa Regional Climate Simulations. J. Climate, 25, 6057–6078. 10.1175/JCLI-D-11-00375.1

Panitz, H.-J., , A. Dosio, M. Büchner, D. Lüthi, and K. Keuler (2013) COSMO-CLM (CCLM) climate simulations over CORDEX Africa domain: analysis of the ERA-Interim driven simulations at 0.44 degree and 0.22 degree resolution. Clim. Dyn., DOI:10.1007/s00382-013-1834-5

Sylla, M. B., F. Giorgi, E. Coppola, and L. Mariotti (2012) Uncertainties in daily rainfall over Africa: assessment of gridded observation products and evaluation of a regional climate model simulation. Int. J. Climatol., 33:1805-1817. DOI: 10.1002/joc.3551

Tramblay Y., D. Ruelland, S. Somot, R. Bouaicha, and E. Servat (2013) High-resolution Med-CORDEX regional climate model simulations for hydrological impact studies: a first evaluation of the ALADIN-Climate model in Morocco. Hydrol. Earth Syst. Sci. Discuss., 10, 5687-5737. DOI:10.5194/hessd-10-5687-2013

Atmospheric circulation and precipitation in regional climate models during major heat waves in Central Europe

Ondřej Lhotka[1,2] and Jan Kyselý[1]

[1] Institute of Atmospheric Physics AS CR, Prague, Czech Republic (ondrej.lhotka@ufa.cas.cz)
[2] Faculty of Science, Charles University, Prague, Czech Republic

1. Introduction

Heat waves are important phenomena of the European climate that have major impact on the natural environment and society. Due to expected rise in global air temperature and projected strengthening of atmospheric blocking over the Euro-Atlantic region due to Arctic Amplification (Francis and Vavrus, 2012) there are concerns that the losses caused by heat waves will be increasing.

Changes in heat wave characteristics in the future climate over Europe were analyzed by many authors. Using an ensemble of regional climate models (RCMs), Fischer and Schär (2010) demonstrated that heat waves will become more frequent and severe at the end of the 21st century. These results are in concordance with Ballester et al. (2010), who used several RCMs to analyze changes in European heat waves under global warming conditions.

To verify the credibility of these projections, outputs of RCMs for the recent climate have to be evaluated against observed data. Vautard et al. (2013) analyzed a large ensemble of RCM simulations and showed that they tend to overestimate the strength and persistence of European heat waves, which might cause inaccuracies in simulations of heat waves in the future climate.

The aim of the present study is to evaluate atmospheric circulation and precipitation in individual RCMs during major Central European heat waves. Such analysis contributes to better understanding of sources of errors when reproducing these extreme events.

2. Data and methods

We examined 7 RCM runs driven by the ERA-40 reanalysis from the ENSEMBLES project (van der Linden and Mitchell, 2009). The list of the RCMs is given in Table 1.

Table 1. Examined RCMs driven by ERA-40 reanalysis.

Acronym	Institute	Model
C4IRCA3	Community Climate Change Consortium for Ireland	RCA ver. 3
ETHZ-CLM	Federal Institute of Technology in Zurich	CLM ver. 2.4.6
KNMI-RACMO2	Royal Netherlands Meteorological Institute	RACMO ver. 2.1
METNOHIRHAM	Norwegian Meteorological Institute	HIRHAM ver. 2
METO-HC_Had	Hadley Centre	HAD ver. 3.0
MPI-M-REMO	Max-Planck Institute	REMO ver. 5.7
SMHIRCA	Swedish Meteorological and Hydrological Institute	RCA ver. 3

The analysis was performed over Central Europe defined by 1,000 grid points (40×25) covering an area of 625,000 km^2. This region is located approximately between 47-53 N and 8-22 E (Figure 1).

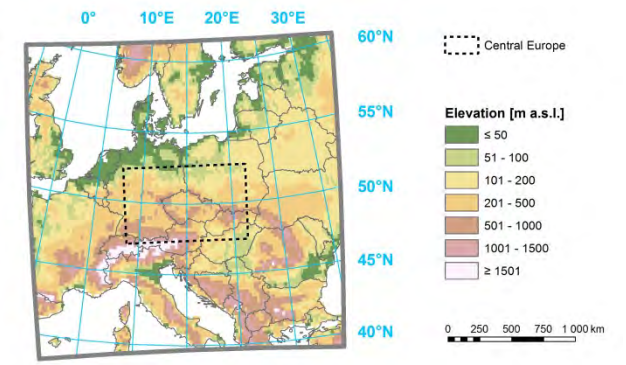


Figure 1. Definition of Central Europe (black dashed polygon), and the elevation model (GTOPO30) used in the majority of RCMs (colour scale).

The definition of heat wave (HW) was based on the persistence of hot days. Daily maximum air temperature (T_{max}) in each grid point over Central Europe was transformed into T_{max} deviation by subtracting the grid point specific 95% quantile of summer T_{max} distribution. A hot day occurred when the average of these T_{max} deviations over Central Europe was greater than zero. HW was defined as a period of at least three consecutive hot days. For this period, the grid maps of positive Tmax deviations were summed up into a cumulative map. In order to remove T_{max} bias present in the RCMs, the quantiles were calculated individually for each RCM.

To describe severity of individual HWs, we used a heat wave extremity index (I_{hw}) that utilizes positive T_{max} deviations over Central Europe. I_{hw} is calculated as a sum of positive T_{max} deviations from the 95% quantile of summer T_{max} distribution in a cumulative map (TSmax') scaled by the total number of grid points in Central Europe (1,000):

$$I_{hw} = \sum_{i=1}^{n} (TSmax')_i \Big/ 1{,}000 \ [°C]$$

where n is the number of grid points with a positive Tmax deviation in a cumulative map.

This index uses summed up deviations over the whole period when a HW persists, and hence captures joint effects of temperature magnitude, spatial extent and also duration of a HW over the area of Central Europe.

3. Differences in simulations of the 1994 heat wave

In observed data (E-OBS), the most severe HW in Central

Europe over 1950-2012 occurred between July 23 and August 6, 1994 (15 consecutive days). Cumulative maps of positive temperature anomalies in the RCMs and E-OBS during this event are depicted in Figure 2.

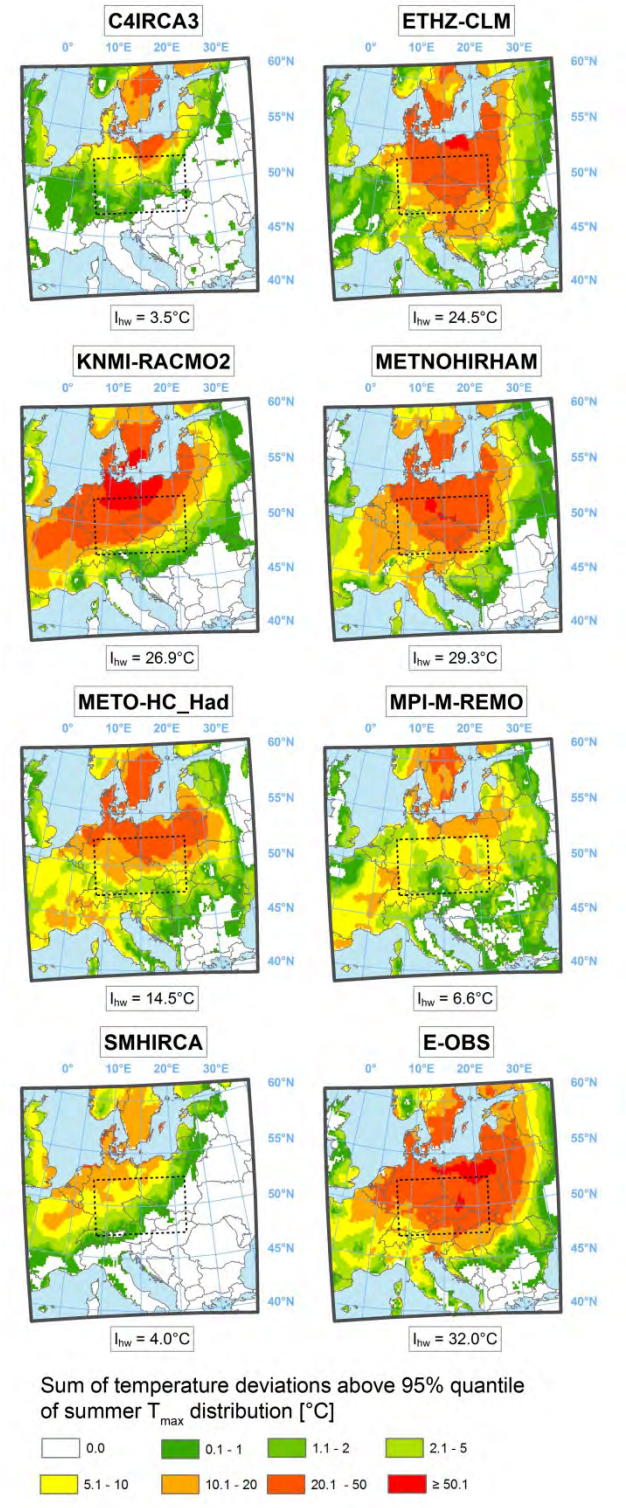


Figure 2. Cumulative maps of positive Tmax deviations between July 23 and August 6 for each RCM and E-OBS.

Relatively good reproduction of the major 1994 HW was found in ETHZ-CLM and METNOHIRHAM. These RCMs simulated the spatial distribution of cumulative temperature deviations quite well; however, the I_{hw} was slightly reduced. In KNMI-RACMO2, a distinct area of extreme hot anomalies (sum of temperature deviations above the 95% quantile of summer Tmax distribution greater than 50°C) was detected over north-eastern Germany, north-western Poland and southern Sweden. On the contrary, the south-eastern part of Central Europe was only little affected resulting in relatively low I_{hw}. In the rest of the RCMs, the severity of the 1994 HW was substantially underestimated. Especially C4IRCA3, MPI-M-REMO and SMHIRCA simulated weak temperature anomalies that resulted in low values of I_{hw} (Figure 2).

4. Ongoing research

In order to determine causes of these large differences among the RCMs during the 1994 HW, the atmospheric circulation and precipitation are being evaluated.

The large-scale flow is analyzed based on circulation indices (Blenkinsop et al., 2009) as modified by Plavcová et al. (2013) for Central Europe. The evaluation of precipitation focuses on reproduction of precipitation amounts during and before the HW.

Finally, analogous analyses will be performed for other major heat waves over Central Europe.

Acknowledgement: The RCM data were obtained from the ENSEMBLES project (EU-FP6, contract number 505539). The study is supported by the Czech Science Foundation under project P209/10/2265.

References

Ballester J, Rodó X, Giorgi F (2010) Future changes in Central Europe heat waves expected to mostly follow summer mean warming, Clim Dyn, 35, pp. 1191–1205

Blenkinsop S, Jones PD, Dorling SR, Osborn TJ (2009) Observed and modelled influence of atmospheric circulation on central England temperature extremes, Int J Climatol, 29, pp. 1642–1660

Fischer EM, Schär C (2010) Consistent geographical patterns of changes in high-impact European heatwaves, Nat Geosci, 3, pp. 398–403

Francis JA, Vavrus SJ (2012) Evidence linking Arctic amplification to extreme weather in mid-latitudes, Geophys Res Lett, 39, L06801

Plavcová E, Kyselý J, Štěpánek P (2013) Links between circulation types and precipitation in Central Europe in the observed data and regional climate model simulations, Int J Climatol, doi: 10.1002/joc.3882

van der Linden P, Mitchell JFB (2009) ENSEMBLES: Climate Change and its Impacts: Summary of research and results from the ENSEMBLES project, Met Office Hadley Centre, Exeter, pp. 160

Vautard R, Gobiet A, Jacob D, et al. (2013) The simulation of European heat waves from an ensemble of regional climate models within the EURO-CORDEX project, Clim Dyn, 41, pp. 2555–2575

Studies of scale interaction in a two-way nesting climate model

Laurent Li, Shan Li and Hervé Le Treut

Laboratoire de Météorologie Dynamique, IPSL/CNRS, Université Pierre et Marie Curie, Paris, France (laurent.li@lmd.jussieu.fr)

1. Objective

Climate downscaling performed with limited-area regional climate models suffers from a design imperfection. That is, the global climate is insensitive to any information coming from the region, that may ultimately affect the regional climate when the outside global climate changes. This problem of scale interaction is addressed here with a few purposely designed simulations done in a two-way nesting climate model.

Our investigated region is the geographic sector of Europe-Mediterranean, extended to North Africa and the Western North Atlantic.

2. Model and simulations

The model used is a two-way nesting system coupling interactively LMDZ-regional and LMDZ-global, two versions of the LMDZ climate model. LMDZ-global is a comprehensive global climate model with a regular grid of 3.75° and 2.5° over the globe. LMDZ-regional covers an extended region of Europe-Mediterranean. Its spatial resolution is about 100 km. The two models share the same physics package and the same dynamical framework, only their spatial configuration is different. They are interactively coupled together with information exchanged every two hours.

This two-way nesting system is run with climatological sea-surface temperature and sea-ice cover as lower boundary conditions. A long simulation was run for 150 years. To fully appreciate the added value of this two-way nesting system, a second run was performed with no up-scaling information from the regional model to the global model. The latter simulation also lasts 150 years. It is similar to a classic downscaling experiment with the global model running prior to the regional model. In our case, however, information from the global model enters into the regional model every two hours (instead of the generally-admitted frequency of every 6 hours).

3. Results

The two long simulations are analyzed and compared to each other, in terms of surface air temperature, rainfall and other relevant climate variables. Differences between the two global runs indicate the up-scaling effects from the regional climate in Europe-Mediterranean when the region is solved with a higher-resolution model instead of its coarse resolution. Significant results are obtained with either colder or warmer surface temperature over the globe. Rainfalls show also significant responses. We also examine differences between the two regional runs to show added value of the two-way nesting system in terms of regional climate downscaling.

Large Scale Meteorological Patterns Associated with Temperature Extremes in the North American Regional Climate Change Assessment Program Hindcast Experiment

Paul C. Loikith[1], Duane E. Waliser[1,2], Jinwon Kim[2], Huikyo Lee[1], J. David Neelin[3], Seth McGinnis[4], Benjamin Lintner[5], Chris Matmann[1,2], and Linda O. Mearns[4]

[1] Jet Propulsion Laboratory, California Institute of Technology, Pasadena, CA, USA (paul.c.loikith@jpl.nasa.gov)
[2] Joint Institute for Regional Earth System Science and Engineering, University of California Los Angeles, CA.
[3] University of California Los Angeles, Department of Atmospheric and Oceanic Sciences, Los Angeles, CA.
[4] Institute for Mathematical Applications to the Geosciences, National Center for Atmospheric Research, Boulder, CO.
[5] Rutgers, The State University of New Jersey, Department of Environmental Sciences, New Brunswick, NJ.

1. Introduction

Changes in temperature extremes are expected to be associated with some of the most severe impacts of anthropogenic climate change (IPCC 2012). In order for climate models to produce realistic changes in temperature extremes, they must be able to reproduce the key physical and meteorological processes associated with extreme temperature events in the current climate. In addition to being the dynamical mechanisms for extreme temperatures, large-scale meteorological patterns (LSMPs) may also influence the shape of the tails of the temperature probability distribution function (PDF). Ruff and Neelin (2012) demonstrate the importance of the shape of PDF tails in anticipating changes in temperature extremes due to global warming with locations exhibiting long tails being less sensitive to changes in extremes than locations with short or near Gaussian tails.

Systematic evaluation of LSMPs associated with temperature extremes across an entire RCM domain is challenging given that the spatial configuration of the LSMPs may vary from point to point. Using relatively coarse resolution observations, Loikith and Broccoli (2012, 2014) identified, described, and evaluated several features of LSMPs associated with extreme temperature days over North America in global climate models (GCMs). Their findings suggest that current generation GCMs are capable of reproducing many features of LSMPs associated with temperature extremes; however, at coarse resolution it is difficult to resolve temperature extremes at scales relevant to end-users of climate information.

The increasingly fine spatial resolutions of state-of-the-art regional climate models (RCMs) provide more detailed information about temperature extremes than most current generation GCMs, especially in places with complex topography and along coastlines. However, the large-scale features associated with this local-scale phenomenon are still key to RCMs being able to realistically simulate extreme events and the shape of the tails of the temperature PDFs. Here we present an observationally based evaluation of the LSMPs associated with extreme daily temperatures across the entire North American Regional Climate Change Assessment Program (NARCCAP) domain. This work is a process-based extension of the evaluation of daily temperature PDF shape presented in Loikith et al. (2014) and further aims to explore the link between fidelity in simulating the shape of PDF tails and the underlying meteorological dynamics.

2. Data and Methodology

Hindcasts from a suite of five NARCCAP RCMs, driven by NCEP Reanalysis II and originally produced at 50 km spatial resolution, covering most of the North American continent for the period 1980-2002 (Mearns et al. 2012), are evaluated. Data from the 32 km North American Regional Reanalysis (NARR; Messinger et al 2006) are used as the evaluation reference. All data have been interpolated to a common 0.5^{o}x0.5^{o} latitude longitude grid. For analysis of individual cases, station observations of daily temperature are obtained from the National Climate Data Center Global Surface Summary of the Day product.

The LSMPs evaluated in this work consist of spatial patterns of anomalies in surface temperature, 500 hPa geopotential height (Z500), sea level pressure (SLP), and surface wind speed and direction. Each pattern is computed by compositing the anomaly field for all days above the 95^{th} (for warm extremes) and below the 5^{th} (for cold extremes) percentiles of the daily temperature anomaly distribution. Extremes are defined relative to the individual climatology of each dataset. This results in one LSMP for each variable for extreme warm days, and one LSMP for each variable for extreme cold days at each grid point. Analysis is performed on summer (June, July, August) and winter (December, January, February) seasons separately.

3. Sample results

LSMPs are evaluated for individual cases, selected to represent different climatological conditions and a range of NARR-RCM agreement. Figure 1 shows an example for extreme cold temperatures at the grid cell closest to Chicago, Illinois during the winter. The temperature PDF

for Chicago is characterized by a long cold tail, with the RCMs exhibiting strong agreement with NARR and station data (not shown). The LSMPs for SLP (Fig 1a) for NARR show a large area of positive anomalies extending from Alaska to the Gulf of Mexico, indicative of a large, cold high pressure system associated with the extremely cold airmass advecting south and eastward. At Z500, a large area of negative anomalies span the majority of the domain with the center of the anomalous trough just to the east of Chicago. Both of these patterns are well reproduced by the RCM ensemble mean, however some differences in the magnitude of the SLP patterns are apparent. Chicago in winter is an example of a case where the RCMs reproduce observations well.

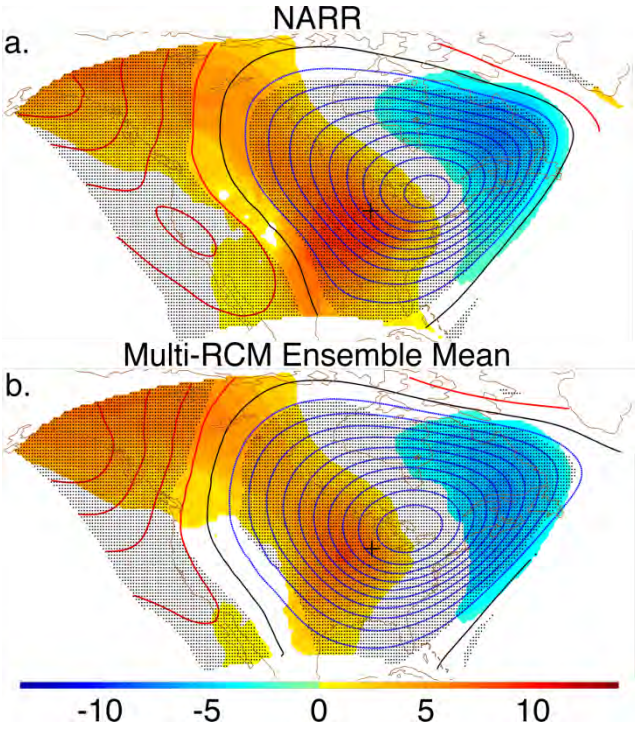


Figure 1. Composites of SLP (color shading in mb) and Z500 contoured every 20 m for (a) NARR and (b) multi-RCM ensemble mean. Blue (red) contours are negative (positive) Z500 anomalies and the black line is the 0 m contour. For NARR, statistically significant SLP anomalies are shaded and Z500 anomalies are stipled. For the multi-RCM mean shading/stipling indicates where at least three out of the five RCMs show both the same sign anomaly as NARR and statistical significance.

This analysis can be expanded beyond just individual cases to evaluate the LSMPs for the entire domain. One approach is to compute the spatial pattern correlation between the NARR LSMP and the multi-RCM ensemble mean LSMP at each grid cell. The correlation coefficients for SLP and Z500 are plotted in Figure 2 for extreme cold winter days. While most of the domain shows high correlation coefficients indicative of strong RCM-NARR agreement, relatively small values are found over the complex terrain of the southwestern United States and northern Mexico for both SLP and Z500. Over portions of northern Canada, values close to and even less than zero suggest lower fidelity in the simulation of LSMPs associated with extremes here.

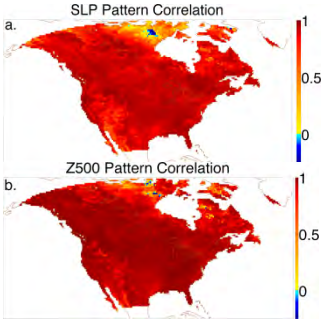


Figure 2. Pattern correlation coefficients between the NARR (a) SLP composite pattern and (b) Z500 pattern for each grid cell for extreme cold winter temperature days.

4. Summary and Conclusions

Large-scale meteorological patterns associated with temperature extremes are simulated with reasonable fidelity in the winter over most of the NARCCAP domain while summertime patterns are characterized by greater RCM-NARR disagreement for both PDF shape and LSMPs. This suggests more difficulty in simulating temperature extremes over much of the domain in summer compared with winter in the NARCCAP RCMs; however, other factors that have been associated with extreme temperatures in the summer, e.g. anomalous soil moisture, are not captured in this analysis. Additional analysis will focus on intra-composite variability and investigate mechanisms behind areas of large RCM-NARR disagreement.

References

IPCC (2012), Managing the Risks of Extreme Events and Disasters to Advance Climate Change Adaptation. A Special Report of Working Groups I and II of the Intergovernmental Panel on Climate Change, edited by C. B. Field, V. Barros, T. F. Stocker, D. Qin, D. J. Dokken, K. L. Ebi, M.D. Mastrandrea, K. J. Mach, G.-K. Plattner, S. K. Allen, M. Tignor, and P. M. Midgley, 582 pp.

Loikith, P. C., and A. J. Broccoli (2012) Characteristics of Observed Atmospheric Circulation Patterns Associated with Temperature Extremes over North America, Journal of Climate, 25, 7266-7281.

Loikith, P. C., and A. J Broccoli (2014), Comparison between Observed and Model Simulated Atmospheric Circulation Patterns Associated with Extreme Temperature Days over North America, under revision for Journal of Climate.

Loikith, P. C., D. E. Waliser, J. Kim, H. Lee, B. R. Lintner, J. D. Neelin, S. McGinnis, C. A. Mattmann, and L. O. Mearns (2014), under revisions for Journal of Climate.

Mearns, L. O. and coauthors (2012), The North American Regional Climate Change Assessment Program: Overview of Phase 1 Results, Bulletin of the American Meteorological Society, 93, 1337-1362.

Messinger, F., and co-authors (2006), North American Regional Reanalysis, Bulletin of the American Meteorological Society, 87, 343-360.

Ruff, T. W., and J. D. Neelin (2012), Long tails in regional surface temperature probability distributions with implications for extremes under global warming, Geophysical Research Letters, 39, LA4704, doi:10.1029/2011GL050610.

Markovian behaviour of dry spells over the Iberian Peninsula using ESCENA regional climate models

N. López-Franca[1,2], E. Sánchez[3], M. Domínguez[1], T. Losada[1,4] and R. Romera[1]

[1] Instituto de Ciencias Ambientales (ICAM), UCLM, Toledo, Spain.
[2] Centro de Investigaciones del Mar y la Atmósfera (CIMA), CONICET- UBA, Buenos Aires, Argentina.
[3] Facultad de Ciencias Ambientales y Bioquímica, UCLM, Toledo, Spain (E.Sanchez@uclm.es).
[4] Departamento de Física de la Tierra I, UCM, Madrid, Spain.

1. Introduction

The persistence of dryness is considered as an indicator of drought, being useful to plan mitigation and adaptation strategies (Steinemann, 2003). It is studied as an isolated parameter or considered into the study of occurrence of dry spells probabilities. This last concept allows to know what dry spells duration of a region are more and less probable. Thus, the second order of Markov Chain concept is used to characterize the temporal structure of dry spells, and it has been applied along 20th century observational data (Singh et. al 1986, Lana & Burgueño, 1998). This theoretical model considers persistence as the conditional probabilities that a present day being dry depends on the two previous days that also have been dry (Wilks, 2005). Its study under future conditions could be useful to anticipate the possible impacts on the society.

The Regional Climate Models (RCM) have demonstrated to be a adequate tool in the dry spells analysis, specially at local or regional scale in climatic complex areas as the Iberian Peninsula (IB).

The aim of this work is to present the markovian features of dry spells studying the IB region under present and future climate conditions from the ESCENA project RCMs.

2. Data and Methods

Daily precipitation is the variable used in the analysis. First, a two states second order markov chain (MC2) model is applied on Spain02 observational (0.2°) dataset for baseline period (1989-2007) to inspect the markovian characteristics over the domain. Then, it is applied for five RCM-forced simulations (0.25) of ESCENA Spanish project (Jiménez-Guerrero et al, 2013). These RCMs are forced by ERA-Interim reanalysis in the baseline period to validate the RCMs performance. Finally the ECHAM5r2 GCM RCMs-forced are used to analyse the markovian dry spells behaviour in present period (1970-2000) under 20C3M SRES and future (2021-2050) changes under A1B SRES.

3. The markovian process application

A 1 mm/day is chosen to define a dry day. The empirical frequencies are computed from the datasets outputs, while the theoretical ones are resulting to apply MC2 model. The computations are on annual basis at each grid point. The probability of occurrence of a dry spell lengths of *n* days (Qn) from MC2 is computed following Wilks (2005):

$$Qn = p100 \cdot (p000)(n-2) \cdot p001 \text{ , for } n \geq 2$$

$$Q1 = p101$$

where, *p* is the probability of occurrence of the sequence of dry (0) and wet (1) days. For example *p101* is the probability of rainy day following a dry day when the day before is a wet one. The goodness-of-fit of empirical frequency distribution to the theoretical model is made by the χ^2 test at the significance level of 0.05 (Wilks, 2005) for all of the datasets. Discrete classes imposed by this test are obtained from Spain02. Three classes are defined, grouping adjacent spells:

- Short dry spells length (SDSL): 1-6 days.
- Medium dry spells length (MDSL): 7-12 days.
- Long dry spells length (LDSL): > 12 days.

4. Observational markovian behaviour of dry spells features

The Figure 1 shows that all the points of Spain02 dataset fit the empirical dry spells distribution with the MC2 model over almost all the domain. A latitudinal gradient is found in all of the classes, with the maximum values in the North and the minimum in the South for the SDSL, while MDSL and LDSL present a inverse spatial pattern. The SDSL reach 0.85 of probability of occurrence in the North decreasing to the South with the lowest values in the South East (0.40). The MDSL pattern is influenced by the Cantabrian and Mediterranean seas. The maximum probabilities of LDSL are located in the South East (0.50) and the minimum in the North (0.05 to 0.10).

5. RCMs performance (1989-2007)

RCMs-ERA-Interim reanalysis model simulations (not shown) follow the same spatial pattern of each dry spell classes. With just some unfitted points located in the North for some of the models.

6. Changes in the markovian characteristics in the future

The analysis of the present period under SRES 20C3M scenario of RCMs-ECHAM5r2 forced simulations present also similar pattern than RCMs-ERA-Interim forced simulations with an overall agreement among them.

The projected future changes (figure 2, for one

RCM) maintain the empirical distribution fitting to MC2 process all over the domain. Just some points are then unfitted in the IB south-eastern coast. A general decrease of the SDSL probability is observed, still showing the N-S gradient. The maximum decreases are located in the South East. Negligible changes are shown in the Atlantic area. In the MDSL, the RCMs agree in the regions with significant changes. LDSL depicts a general increase over the domain. The orographic effect is kept under future conditions.

7. Conclusions

The dry spells over IB from the observational dataset present a second order markovian process characteristics. That is the occurrence of a dry day depends on the two preceding days had also been dry, implying persistence of the dryness.

A N-S decreasing gradient of the probability obtained in the SDSL is reversed in MDSL and LDSL. The North of IB is characterised by SDSL, while the South, especially the South East, by LDSL. A strong effect of the main orography over the markovian process of dry spells is shown, specially in the SDSL and LDSL.

The ESCENA RCMs reproduce successfully those observational spatial MC2 patterns. Thus, they can be used to analyse projected changes in the markovian future characteristics under different SRES.

A large agreement among the RCMs is obtained in climate change projections. The IB maintains present MC2 characteristics in the future except in just some points of the South East of IB. This fact can be due to great increases in the dry spell length. The SDSL project a N-S decrease of their probability of occurrence. In contrast, a increase of long lengths is showed over the domain, specially in the highest orographic points, except in the North West. MDSL exhibit some discrepancies between the simulations, while PROMES and MM5 display a general increase all over the domain, the rest project increases in the North and decreases in the South of IB.

References

Jiménez-Guerrero P, Montávez JP, Domínguez M, Romera R, Fita L, Fernández J, Cabos WD, Liguori G, Gaertner MA (2013) Mean fields and interannual variability in RCM simulations over Spain: the ESCENA project. Clim Res 57:201–220

Lana X, Burgueño A (1998) Daily dry–wet behaviour in Catalonia (NE Spain) from the viewpoint of Markov chains. Int J Climatol 18(7): 793–815

Singh SV, Kripalani RH, Shaha P, Ismail PMM, Dahale SD (1981) Persistence in daily and 5-day summer monsoon rainfall over India. Arch Meteor Geophy A 30(3):261–277

Steinemann A (2003) Drought indicators and triggers: A stochastic approach to evaluation. J Am Water Resour As 39(5):1217–1233

Wilks D (2005) Statistical Methods in the Atmospheric Sciences. International Geophysics, Elsevier Science.

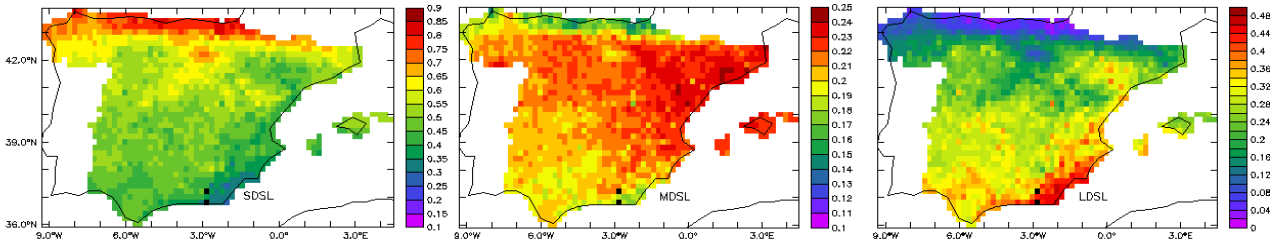


Figure 1. Probability of occurrence of SDSL, MDSL an LDSL dry spell classes by Spain02 in baseline period (1989-2007). The points where the fitting does not occur are marked as black.

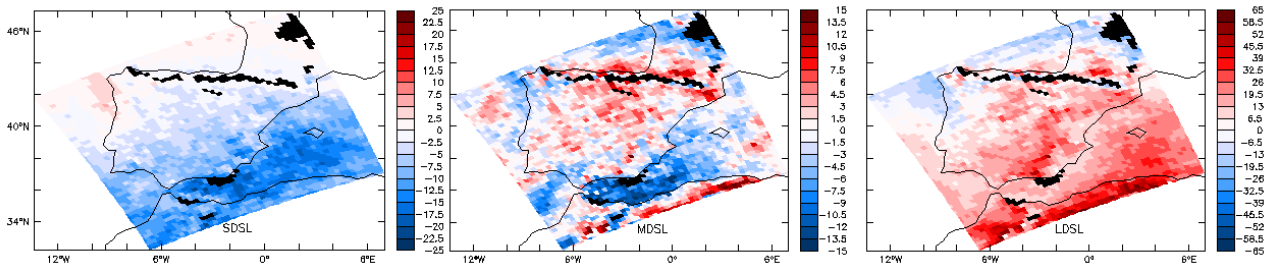


Figure 2. Change (%) in the probability of occurrence of SDSL, MDSL an LDSL dry spell classes by PROMES in the future (2021-2050) under A1B SRES respect to present climate conditions (1971-2000). The points where the fitting does not occur are marked as black.

Comparison of North-American CORDEX simulations with the Canadian Regional Climate Model (CRCM5) at 0.44°, 0.22° and 0.11°: Does the simulated climate get better with higher resolution?

Philippe Lucas-Picher, René Laprise and Katja Winger

Centre ESCER, Dept. of Earth and Atm. Sciences, Univ. du Québec à Montréal, Montréal (Québec), Canada (plp@sca.uqam.ca)

1. Introduction

In the CORDEX project, climate modelling centres around the world are invited to perform regional climate model (RCM) simulations over specific domains. The horizontal resolution of the simulations is fixed to a relatively coarse resolution of 0.44° in order to give the opportunity to centres with less computer power to participate to the project. However, centres with strong computing capabilities are invited to perform higher resolution simulations to investigate the added value of higher resolution simulations. In this work, we compare three RCM simulations with grid meshes of 0.44°, 0.22° and 0.11°, driven by ERA-Interim, for the period 1979-2012 over the North-American CORDEX domain. The analysis will focus on added value of higher resolution simulations using the following climatic features: The Great Lakes snowbelt, and the following North American Monsoon precipitation characteristics: spatial pattern, annual cycle and intensity distribution.

2. Methodology

The RCM used in this study is the fifth-generation Canadian RCM (CRCM5), developed at Université du Québec à Montréal (Martynov et al. 2013). In the CRCM5, lakes are represented by the 1-D FLake model and the surface scheme is the Canadian land-surface scheme (CLASS3.5). Three simulations were performed from 1979 to 2012 with horizontal grid meshes of 0.44°, 0.22° and 0.11°. The simulations are driven at their lateral boundaries by the ERA-Interim reanalysis. The free domains of these simulations respect the minimum North American CORDEX requirements and have the exact same lateral boundaries, except the eastern boundary, which changes a little. No large-scale spectral nudging was applied. Sea surface temperature and sea ice fraction from ERA-Interim are prescribed once per day. All simulations use 56 levels in the vertical and the same parameterization; only the time step was shorten with increasing resolution.

3. Snowbelt next to the Great Lakes

The snowbelt describes a region near the Great Lakes where heavy snowfall is common due to a lake effect that occurs when a cold and dry continental air mass passes over a relatively mild lake in winter. Turbulent fluxes of heat and moisture destabilize the air mass and increase its moisture content, enhancing cloudiness and precipitation on the lee side of the lakes. This mesoscale feature has been simulated by some RCMs and it is recognized as an added value of higher resolution simulations (Notaro et al. 2013). Fig. 1 shows the mean snow water equivalent (SWE) in February in the Great Lakes region for the three simulations and the National Snow Analysis (NSA) from the NOAA, which is only available over the USA. The snowbelt next to the Great Lakes has higher SWE in the simulation at 0.11° compared to those at 0.22° and 0.44°. The spatial distribution of the snowbelt at 0.11° also matches better the NSA dataset.

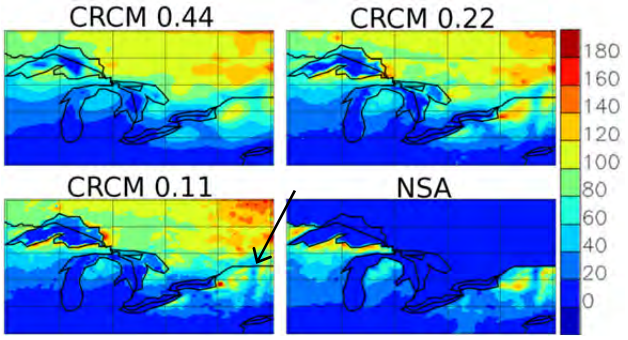


Figure 1. Mean 2004-2012 February snow water equivalent (mm) for the 0.44°, 0.22°, 0.11° CRCM5 simulations, and the National Snow Analysis (NSA), available over the USA only.

Another feature that is improved in the higher resolution simulation is the distribution of SWE around the Champlain Valley located between the Adirondacks on the West and the Green Mountains on the East. The Adirondacks force the frequent westerly winds to rise, initiating condensation, which then generates snowfall. Consequently, snow accumulates and remains on the ground due to the cold conditions on the mountains. The Champlain Valley, on the lee side of the Adirondacks, receives comparatively little snow. Also, with the warmer conditions due to the lower elevation, little snow remains in the valley. East of the valley, the Green Mountains also generate orographic lifting and have high amount of SWE. With sharper mountains due to the higher resolutions, the orographic effect is more realistic in the 0.11° simulation. This leads to a better SWE spatial distribution, which matches closely the NSA dataset.

4. Precipitation in the North American monsoon region

The North American monsoon (NAM) induces a large increase of rainfall from July to mid-September in southwestern USA and northwestern Mexico. This phenomenon is a consequence of many factors such as warm land surfaces in low land areas and atmospheric moisture supplied by nearby maritime sources. The large spatial variability of the topography in southwestern USA is also an important factor contributing to the NAM. Even though Bukovsky et al. (2013) concluded that RCMs from

NARCCAP perform reasonably well in simulating the NAM, they recognized that 50-km resolution may be too coarse to resolve adequately the terrain, coastline and mesoscale circulation features in this region.

Fig. 2 shows the spatial distribution of precipitation in August for the three simulations and three gridded observations datasets in southwestern North America. The large-scale pattern of the CRCM5 simulations and the observations is similar. However, in detail, the precipitation is higher over the west coast of Mexico and lower in the interior of Mexico with the higher resolutions. Over Colorado and New Mexico, the precipitation is also higher in the 0.11° and 0.22° simulations than in the 0.44° one. The 0.11° simulation matches better CONUS than the 0.22° and 0.44° ones. The CONUS dataset, only available in the USA on a mesh of 0.06°, has more small-scale details than TRMM and CRU that use grid meshes of 0.25° and 0.5°, respectively.

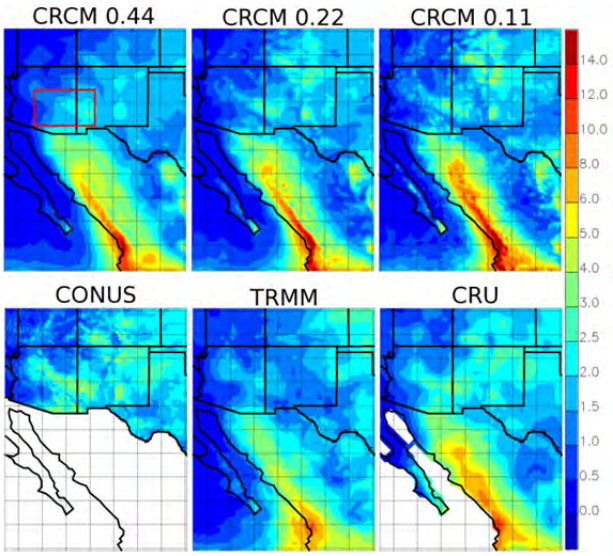


Figure 2. Mean 1981-2010 August precipitation (mm/d) in southwestern North America for the simulations at 0.44°, 0.22° and 0.11°, and three gridded observation datasets (CONUS, TRMM and CRU). TRMM only covers the period 1998-2009.

5. Mean annual cycle of precipitation and distribution of precipitation intensities in the NAM region

Fig. 3a shows the mean annual cycle of precipitation over a region in Arizona and New Mexico that has been used in previous studies to evaluate the NAM. In general, the mean annual cycle between the CRCM5 simulations and the observations is similar. The CRCM5 precipitation is lower in summer during the monsoon than the observations (CRU and CONUS), which are close to each other. However, the 0.11° and 0.22° simulations have higher precipitation in July than the 0.44° one. Fig. 3b shows the contribution of each daily intensity bin to the total precipitation in summer for the CRCM5 simulations and CONUS. The contribution of the higher intensities is more important for the CRCM5 simulations with higher resolutions. However, CONUS shows higher contributions for the medium intensities (between 4 and 16 mm/d) and lower contributions for the high intensities (> 32 mm/d) than the CRCM5 simulations. These differences could be explained by the dry bias of the CRCM5 simulations. Also, it is likely that high precipitation intensities in CONUS are underestimated due to the interpolation algorithm used to get a gridded product from the sparsely distributed stations in this region.

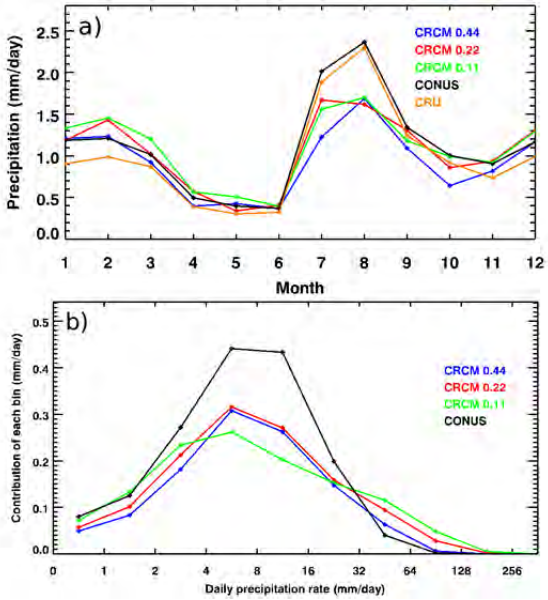


Figure 3. a) 1981-2010 mean annual cycle of precipitation (mm/d) for the three simulations (0.44°, 0.22° and 0.11°) and CONUS over the region indicated in red on Fig. 2. b) 1981-2010 distribution of daily JJA precipitation intensities over the same region.

6. Conclusions

In general, the CRCM5 simulations show similar features at the large scales. At smaller scales, however, the spatial distribution of the snowbelt and the precipitation in southwestern USA in the higher resolution CRCM5 simulations at 0.11° and 0.22° matches better the gridded observation datasets than the lower resolution simulation at 0.44°. The mean annual cycle of precipitation over a region in New Mexico and Arizona for the three simulations is also very similar, except that the monsoon precipitation is slightly higher for the 0.11° and 0.22° simulations. Finally, the 0.11° simulation shows higher precipitation intensities than the 0.22° and 0.44° ones. The comprehensive evaluation of the CRCM5 simulations is challenged by the lack of a high-resolution station network, which likely reduces high precipitation intensities and small-scale details that would be required to show added value and to fully determine the extent to which higher resolutions give better climate simulations.

References

Bukovsky, M.S., D.J. Gochis, L.O. Mearns (2013) Towards Assessing NARCCAP Regional Climate Model Credibility for the North American Monsoon: Current Climate Simulations. J. Climate, 26, pp. 8802–8826.

Martynov, A., R. Laprise, L. Sushama, K. Winger, L. Šeparović, B. Dugas (2013) Reanalysis-driven climate simulation over CORDEX North America domain using the Canadian Regional Climate Model, version 5: model performance evaluation. Clim. Dyn., 41, pp. 2973-3005.

Notaro, M., A. Zarrin, S. Vavrus (2013) Simulation of heavy lake-effect snowstorms across the Great Lakes basin in RegCM4: Synoptic climatology and variability. Mon. Wea. Rev., 141, pp. 1990-2014.

A regional climate model hindcast downscaling study of screen level temperature and precipitation for Estonia and the Baltic Sea region

Aarne Männik[1,2], Andres Luhamaa[1,2], Marko Zirk[1] and Rein Rõõm[1]

[1] Institute of Physics, University of Tartu, Tartu, Estonia (aarne.mannik@ut.ee)
[2] Estonian Environmental Agency, Tallinn, Estonia

1. Introduction

In 2012, a project "Estonian environmental and climate change impact assessment based on dynamic atmospheric- marine- and catchment models" was launched with the aim to obtain the scientific basis for assessment of future climate change in Estonia using complex approach by the dynamical modelling of atmospheric, land, sea, river and coastal water processes. Current presentation focuses on atmospheric modelling results for the basic climate parameters of screen level temperature and precipitation performed in the hindcast regime to assess the model quality and specific properties in the region of interest.

2. Models and domains

The Rossby Centre regional atmospheric model version 4 (RCA4) with 11 km horizontal resolution was used to downscale the global Earth System Model EC-Earth calculations. The modelling study was performed in the hindcast regime over the period 1961 – 2005. EC-Earth fields were used as boundary conditions for RCA4 and were provided by Met Eireann. The hindcast study was conducted in the Coordinated Downscaling Experiment - European Domain (EURO-CORDEX) region shown on Figure 1 while the statistical analysis of results has been performed in the much smaller regions of interest.



Figure 1. The modelling domain and the domains of statistical analyses for the Baltic Sea region and Estonia.

3. Methods

The usual methods of spatial and temporal averaging and linear trend calculations are applied over the Baltic Sea region and Estonia. The hindcast modelling results are evaluated against the Baltic Sea region reanalysis database BaltAn65+ covering years 1965 – 2005 (Luhamaa et al., 2010) for the screen level temperature and against the database of observations E-OBS (Haylock et al. 2008) for the total precipitation. The linear trends in hindcast dataset are compared to similar results from the BaltAn65+ and E-OBS databases as calculated for the period 1965 – 2005 by Männik et al (2014).
Measurements from Tõravere meteorological station present good general characteristics of the Estonian climate and are used as verification of hindcast quality.
Downscaled modelling results are compared to global model estimates to assess an added value of the regional climate model application.

4. Results

The seasonal and annual averaged maps and time series of screen level temperature and total precipitation are computed, presented and compared to the measurement or reanalysis based maps and time series. The climatological trends of time series and the trend maps of screen level temperature and total precipitation are presented and compared to the observation based results.
The temporal and spatial characteristics of the screen level temperature bias are presented. RCA4 exhibits a cold bias over the land areas and a warm bias over the lakes in the Baltic Sea region. Strong wintertime cold bias is evident in arctic region of the White Sea. Total precipitation is overestimated in simulations in general by RCA4 but downscaled model fields show better seasonal cycle representation compared to the global model results.

5. Bias correction

To improve the applicability of downscaled model fields in the region of interest and as the input to other models, a simple bias correction is applied for the screen level temperature fields. The analysis of the temporal and spatial pattern of the bias suggests that seasonal average bias correction would be most appropriate.

7. Acknowledgments

This work was supported by research grant No. 9140 and targeted financing grant SF0180038s08 of the Estonian Science Foundation and research project No. SLOOM12144T (EstKliima) under the Environmental

Protection and Technology Programme KESTA and the institutional research grant IUT20-11 of the Estonian Research Council. The BaltAn65+ database was created with the support of the Estonian Environmental Investment Centre. We acknowledge the provision of EC-Earth global model data by Met Eireann. We acknowledge the provision of the E-OBS dataset by the EU-FP6 project ENSEMBLES (http://ensembles-eu.metoffice.com) and the data providers in the ECA&D project (http://www.ecad.eu). We also thank the developers of the free and open-source software packages GrADS and R for their excellent work in providing these indispensable scientific tools.

References

Haylock M.R., N. Hofstra, A.M.G. Klein Tank, E.J. Klok, P.D. Jones, M. New (2008) A European daily high-resolution gridded data set of surface temperature and precipitation for 1950-2006, Journal of Geophysical Research, **113**, Issue 20 DOI DOI:10.1029/2010JD015468

Luhamaa, A., K. Kimmel, A. Männik, R. Rõõm (2011) High resolution re-analysis for the Baltic Sea region during 1965-2005 period,Climate Dyn., **36**, pp. 727-738

Männik, A., M. Zirk, R. Rõõm, A. Luhamaa (2014) Climate parameters of Estonia and the Baltic Sea region derived from the high-resolution reanalysis database BaltAn65+ (submitted to Theoretical and Applied Climatology)

Identifying added value in two high-resolution climate simulations over Scandinavia

Stephanie Mayer[1], Cathrine Fox Maule[2], Stefan Sobolowski[1], Ole Bøssing Christensen[2], Hjalte Jomo Danielsen Sørup[2,3], Maria Antonia Sunyer Pinya[3], Karsten Arnbjerg-Nielsen[3], Idar Barstad[4]

[1] Uni Climate, Uni Research AS, 5007 Bergen, Norway (stephanie.mayer@uni.no)
[2] Danish Climate Centre, Danish Meteorological Institute, 2100 Copenhagen, Denmark
[3] DTU Environment, Technical University of Denmark, 2800 Lyngby, Denmark
[4] Uni Computing, Uni Research AS, 5008 Bergen, Norway

1. Introduction

Recent developments in high-performance computer technology allow for high resolution climate simulations of limited areas on the order of 10 km and even down to cloud resolving scales (< 4 km). Very high resolution may be needed in impact models that are employed to address particular societal needs and risks, such as future storm surge protection of coastlines and low-level lands or drainage systems in urban areas. The purpose of this study is to analyze the properties of high-resolution climate simulations over Scandinavia by testing a hypothesis that dynamic simulations are better at retaining the properties of precipitation, notably precipitation extremes than coarser simulations. When compared to statistical methods the dynamical downscaling has the advantage of retaining the full set of atmospheric variables as well as a physically more realistic description of e.g. complex terrain (e.g. mountain ranges and coastlines) and when the representation and behavior of extremes are important to be captured in a realistic manner. Here, we present a set of two high-resolution dynamical downscaling simulations on an 8 km grid.

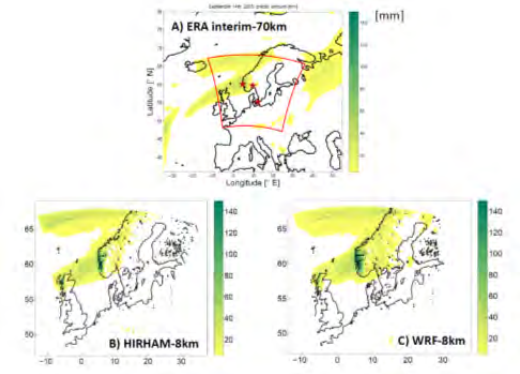


Figure 1. A) 24-hour precipitation amount in mm on September 14th, 2005 as represented in the ERA interim data product. The red box indicates the domain used to perform dynamical downscaling. The locations of Bergen, Oslo and Copenhagen are indicated with red stars. The maps below show the same variable as simulated in the RCMs B) HIRHAM5 and C) WRF.

Very heavy precipitation (> 100 mm day^{-1}) impacted the Norwegian southwest coast on September 14th, 2005. This event was caused by an atmospheric river, which was formed by the transport of subtropical and tropical moisture due to the extra-tropical transition of two hurricanes over the North Atlantic (Stohl et al., 2008). This caused a 600-year event in the city of Bergen, Norway (156 mm in 24 hours). The accumulated 24-hour rainfall simulated in the two high-resolution models (≈8 km) and in the lower resolution ERA interim reanalysis product (≈70 km) is shown in Figure 1. The latter produces a smooth precipitation pattern, underestimating the actual precipitation amount over the Norwegian west coast by 50-100 %, while the RCM simulations add much greater detail in the precipitation pattern and precipitation amount both over sea and over land areas. In fact, the atmospheric river which caused these extreme precipitation amounts becomes visible in the high-resolution simulations (Figure 1 B) and C)).

Before performing climate simulations under future emission scenarios, it is crucial to validate the model performance under present-day climate conditions to identify systematic biases within the models (Jacob et al., 2007) and to evaluate to what degree the models simulate observed weather. This is done by performing a so-called 'perfect boundary experiment' by dynamically downscaling ERA interim data.

2. Data

The atmospheric models WRF and HIRHAM5 were used as regional climate models (RCMs) in this study. Both models were initialized and driven at their lateral boundaries with ERA-interim data. The simulation period covers 1989-2010 with the first year considered spin-up and discarded. As observational reference we have used both gridded data (E-OBS, Haylock et al., 2008) as well as station observations.

3. Method

To measure the performance of the RCMs various methods are employed to examine seasonal to sub-daily time scales. Maps of seasonal biases and frequency skill scores are used to identify systematic biases and their spatial distribution. To investigate the models' ability to reproduce extreme precipitation, we show the upper percentiles for selected locations. Spatio-temporal correlation measures as well as a statistical moments scaling relationship are employed to evaluate the models' ability to reproduce localized and short duration extremes, respectively.

4. Results

Overall both models suffer a wet bias of 50-100 % (1-3 mm) in seasonal mean precipitation. This bias is most pronounced during winter and this feature is likely inherited from the ERA interim input data. For example, ERA interim shows a strong wet bias over parts of Poland and Belarus during winter, which also appears clearly within both simulations. This bias is also reflected in skill score maps as these regions show relatively low values ranging between 0.6 and 0.75, whereas the bulk of the study area exhibits skill scores ≥ 0.75. During summer the wet bias in simulated precipitation is less pronounced and frequency skill scores are in general higher in these regions compared to winter.

Table 1. Seasonal biases of wet-day mean precipitation in % were calculated for selected locations. A wet day is defined as a day when the precipitation amount exceeds 1 mm.

	DJF	MAM	JJA	SON
Bergen				
ERA interim	-23.2	-28.8	-36.3	-33.6
WRF	+10.5	-0.6	-16.6	-1.4
HIRHAM	+14.1	+0.2	-28.9	-6.2
Oslo				
ERA interim	-15.0	-18.6	-17.0	-26.5
WRF	+18.8	+7.8	+7.3	+9.7
HIRHAM	+66.6	+24.4	+1.2	+14.8
Copenhagen				
ERA interim	-13.0	-26.6	-32.0	-25.5
WRF	+1.3	-7.2	-11.6	-12.6
HIRHAM	+7.6	-6.1	-1.7	+5.3

ERA interim underestimates wet-day mean precipitation in all four season by 13-36 % over selected cities Bergen, Oslo and Copenhagen (Table 1). The RCM simulations show quite large reductions in this negative bias and even indicate a sign change in some seasons/locations. Precipitation extremes can be caused by varying types of weather regimes, depending on season. During winter most extreme precipitation is caused by advective systems, i.e. low-pressure systems and storms that originate over the North Atlantic and impact the north European continent. In contrast, most summer precipitation extremes are caused by more localized convective systems. For example, in Copenhagen, the most extreme rainfall with up to 70 mm day^{-1} occurs during summer when convective systems are more active. In Oslo the difference in precipitation amounts is not as clear as for Copenhagen and during winter and summer extreme precipitation ranges between 15-55 mm day^{-1}. However, in Bergen most extreme precipitation is caused by storms during fall and winter that impinge the Norwegian west coast causing extremes as high as 100 mm day^{-1}. The ERA interim data set considerably underestimates extreme precipitation in all locations in both seasons. Both models either agree very well with the observations or even lie above them. This is a clear improvement compared to the ERA interim data product. As a further step to validate the models with respect to the high temporal and spatial resolution needs required of urban hydrology, a spatio-temporal evaluation of downscaled precipitation extremes was performed. In Figure 2 a sharp exponential decay in the 3-hourly observational correlation structure (blue line) indicates that these events are highly localized, while this behavior is not reflected within the ERA interim data. Both RCM downscalings are much closer to the observational behavior and therefore we can state that short duration extreme precipitation is better simulated within both models. For daily precipitation extremes, the RCM simulations are even closer to the observational structure.

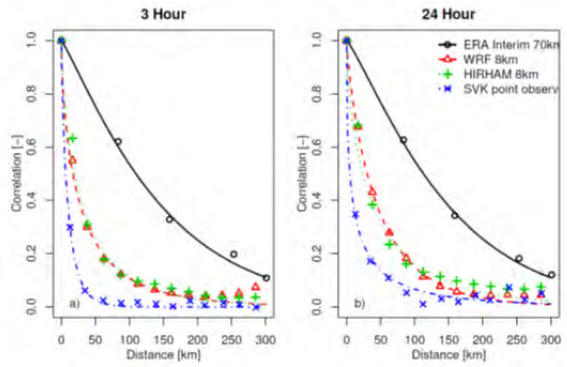


Figure 2. Spatio-temporal correlation structure of observed (SVK), ERA interim (70 km) and downscaled (8 km) mean intensities of extreme precipitation for 3 hour (a) and 24 hour (b) duration. To highlight the tendencies an exponential function is used for fitting by using least square method (Gregersen et al., 2013).

5. Outlook

Within the RiskChange project (http://riskchange.dhigroup.com/) the models are currently employed to dynamically downscale the global climate models NorESM and EC-Earth for future time slices 2021-2050 and 2071-2100 under the assumption of climate change with the representative concentration pathways rcp4.5 and rcp8.5.

References

Gregersen, I.B., Sørup, H.J.D., Madsen, H., Rosbjerg, D.,Mikkelsen, P.S., and Arnbjerg-Nielsen, K. (2013) Assessing future climatic changes of rainfall extremes at small spatio-temporal scales. Climatic Change, 118, 3-4, 783-797

Haylock, M.R., Hofstra, N., Klein Tank, A.M.G., Klok, E.J. Jones, P.D. and New, M. (2008) A European daily high-resolution gridded dataset of surface temperature and precipitation. J. Geophys. Res (Atmospheres), 113, D20119

Jacob, D., Bärring, L., Christensen, O. B., Christensen, J. H., de Castro, M., Déqué, M., Giorgi, F., Hagemann, S., Hirschi, M., Jones, R., et al. (2007) An inter-comparison of regional climate models for Europe: model performance in present-day climate. Clim. Change, 81(1), 31-52

Rummukainen, M. (2010) State-of-the-art with regional climate models. Wiley Interdiscip. Rev. Clim. Change, 1(1), 82-96

Stohl, A., Forster, C., and Sodemann, H. (2008) Remote sources of water vapor forming precipitation on the Norwegian west coast at 60°N-a tale of hurricanes and an atmospheric river, J. Geophys. Res., 113(D05102), 1-13

The link between El Niño Southern Oscillation (ENSO) and the Southern African rainfall in a Regional Climate Model

Arlindo Meque and Babatunde J. Abiodun

Climate System Analysis Group, Department of Environmental & Geographical Science,
University of Cape Town, South Africa. (babiodun@csag.uct.ac.za)

1. Introduction

Southern Africa is a region with the economy largely dependent on water resources. It is characterized by a high degree of variability in rainfall at different time scales (e.g, Richard et al 200). As a consequence of this variability, extreme weather events as well as drought episodes are recurrent issues in the region (Jury and Mwafulirwa, 2002). For instance, the region was impacted by a number of droughts during early 1990's and devastating floods in 2000. Such high vulnerability of Southern Africa to climate hazards is expected to increase in the future due to the changes in the hydrological cycle as direct consequence of global warming. Hence, a good understanding of the current climate as well as in the future would help governments in the region to better prepare. Several studies have shown that El Niño Southern Oscillation (ENSO) plays a crucial role in the rainfall variability in the region. Typically, its negative phase leads to wetter conditions while its positive phase leads to widespread drought across the region. Therefore, a better simulation of the climate anomalies associated will ENSO may improve the seasonal forecast and the reliability of the climate projections. Regional Climate Models (RCMs) have shown a significant improvement in simulating the regional climate scale features by dynamically downscaling the outputs from Global Climate Model. Here we investigate the ability of a suite of ten RCMs from the Coordinated Regional Climate Downscaling Experiment (CORDEX, Jones et al., 2011) project in simulating the link between ENSO and rainfall over Southern Africa.

2. Data and Method

We used a set of ten RCMs simulations from the CORDEX project. All the RCMS were driven by the ERA-INTERIM Reanalysis for the 1989-2008 period and cover the entire African continent. All the RCMs were integrated on a horizontal grid resolution of approximately 44 km. Observed precipitation data used in this study are taken from the Climate Research Unit (CRU,Mitchell and Jones, 2005) and have 50km horizontal resolution. The Multivariate ENSO Index (MEI, Wolter and Timlin, 2011) was used as surrogated for ENSO. Correlation analysis between MEI and rainfall was performed for the December-January-February period. Composites analysis for negative and positive phase of ENSO is performed in both observed and simulated rainfall.

Modeling Center	Model Name
Centre National de Recherches Meteorologiques ARPEGE	
Danmarks Meterologiske Institut	HIRHAM
Abdus Salam Internation Centre for Theor. Physics	RegCM3
CCLM community	CCML
Koninklijk Nederlands Meteorologisch	RAMCO
Max Planck Institute	MPI
Sveriges Meteorologiska och Hydrologiska Institute	RCA
University of Cape Town	PRECIS
Universidad de cantabria	WRF
Université du Québec á Motréal	CRCM

Table1: List of the RCMs used in the study

3. Results

Correlation Between ENSO and rainfall

The correlation between ENSO and precipitation over Southern Africa is shown in figure (1). There is a dipole pattern in the correlation, with negative values over a bulk of southern Africa and positive correlation coefficient over the northeastern part of our study domain. All the RCMs capture the overall pattern. The ARPEGE model outperforms other RCMs and the CRCM model seems to have the lowest ability in simulating the link.

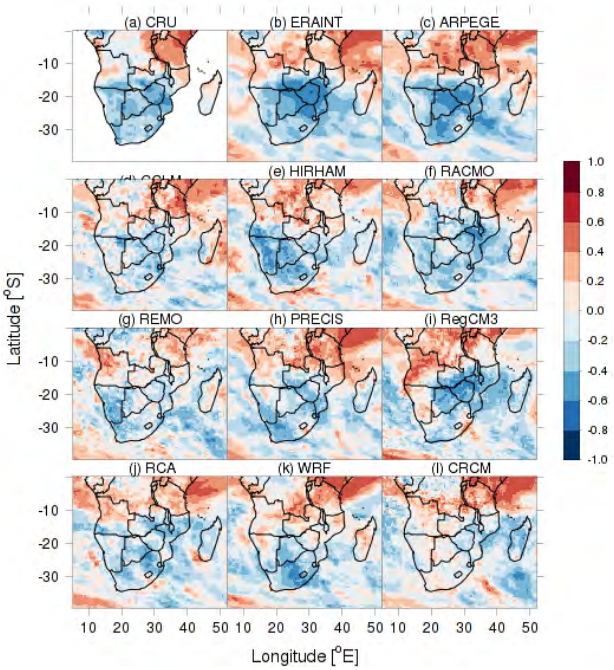


Figure1. Correlation coefficient between ENSO and precipitation over southern Africa during summer (December-january-February).

Composite anomalies during El Niño years

To further understand the link between ENSO and rainfall in the region composite analysis were performed for the positive (El Niño) and negative phase (La Niña) of ENSO. During El Niño years (Figure 2) negative rainfall anomalies dominate over a large part of Southern Africa with the exception of north of the 10˚S latitude were positive anomalies are more common during an El Niño event. This result is in agreement with previous results that concluded that during El Niño event a high pressure center dominates over central Southern Africa which leads to suppression of rainfall (Mulenga et al., 2003). All the RCMs have also captured the pattern, though the CRCM model portrays week anomalies. Again, the ARPEGE model performs better than the remaining models.

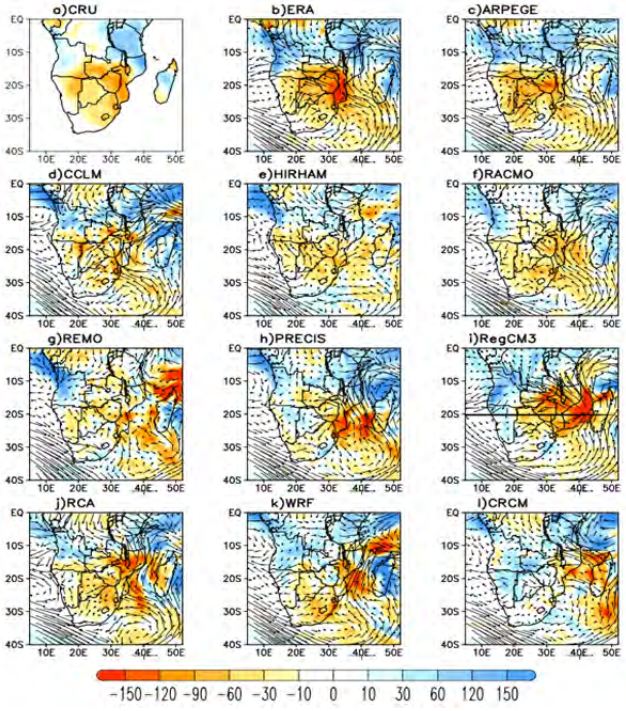


Figure 2. Composite rainfall anomalies during El Niño Years

Composite anomalies during La Niña years

During la Niña years (Figure 3) the situation is reversed. The Southern African region south of 10°S is characterized by positive rainfall anomalies while north of 10°S negative rainfall anomalies are dominating. Overall the RCMs capture the pattern, though similar to El Niño years, the CRCM model seems to not perform well south of 10°S latitude. The good performance in the CRCM model is confined over the southeastern part of our study domain. The ARPEGE model is in a good agreement with the CRU data as well as the ERAINT reanalysis data.

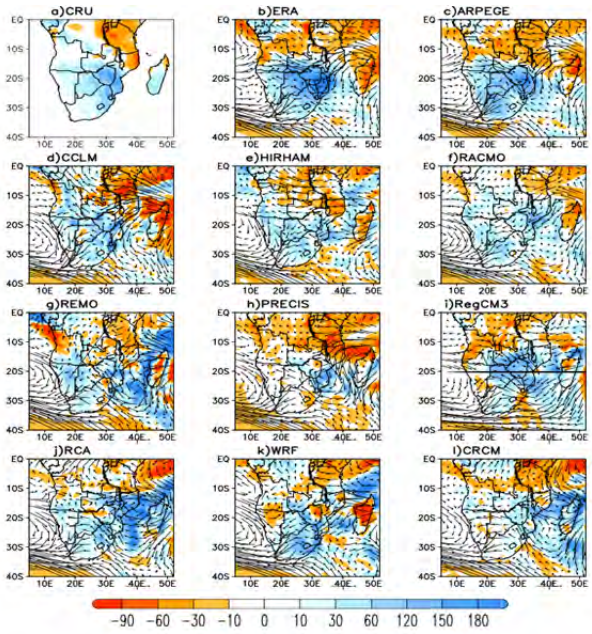


Figure 3. Composite rainfall anomalies during la Niña Years

4. Conclusions

This study examines the ability of ten regional climate models in simulating the link between ENSO and rainfall over Southern Africa. ENSO is the main rainfall driver in the region. A comparison between the RCM simulations with observations reveals that the ARPEGE model outperforms the remaining models in the CORDEX set of models in simulating the link between ENSO and rainfall. On the other hand, CRCM models exhibits the lowest capability in simulating the link.

References

Jury MR and Mwafulirwa ND (2002) Climate variability in Malawi, part 1: Dry summers, statistical associations and predictability. Int. J. Climatol. 22: 1289–1302.

Mitchell TD, Jones PD (2005) An improved method of constructing a database of monthly climate observations and associated high-resolution grids. Int. J. Climatol., 25: 693–712.

Mulenga HM, Rouault M, Reason CJC (2003) Dry summers over northeastern South Africa and associated circulation. Clim Res, 25: 29-41.

Richard Y, Trzaska S, Roucou P, Rouault M (2000) Modification of Southern African Rainfall Variability/ENSO relationship since the late 1960s. Climate Dynamics 16:883-895.

Wolter K, Timlin MS (2011) El Niño/Southern Oscillation behavior since 1871 as diagnosed in an extended multivariate ENSO index (MEI.ext). Int. J. Climatology, 31:1074-1087.

Using WRF to analyse the role of Vb-events in extreme precipitations over Central Europe

Martina Messmer[1,2], Juan José Gómez-Navarro[1,2] and Christoph Raible[1,2]

[1] Climate and Environmental Physics, Physics Institute, University of Bern, Switzerland (messmer@climate.unibe.ch)

[2] Oeschger Centre for Climate Change Research, University of Bern, Switzerland

1. Introduction

Extreme weather situations are of major relevance for society, since they lead to disastrous events reporting great economical and personal damage. This is especially relevant under a climate change scenario, where shifts in frequency and severity of these events are expected to occur (IPCC SREX, 2012). This poses not only a challenge for current but also for future societies.

Particularly for Central Europe, one important source of extreme precipitation accompanied by large floodings is the so-called Vb-events. They were identified in earlier studies by W. J. Van Bebber (1891). Vb-events are defined as cyclones following particular pathways. The cyclones often arise from a cold air outbreak and develop over the Genoa region, where they take up a large amount of moisture. This moist air is then transported towards the Alps and Central Europe. Under these circumstances, the cycling air masses are potentially blocked by the northern face of the Alps, which then leads to heavy precipitation events and even floodings over wide regions of Central Europe.

However, despite being recognized long time ago and its major relevance in floodings in Central Europe, this kind of events are rare (only once every 3 to 4 years) and its relevant triggering processes are not yet fully understood. In particular it is unknown how the frequency and severity of these events could react to climate change.

A better understanding of these events and their impact in extreme precipitation requires the use of reliable observations and realistic simulations. Regarding the latter, the complex orography of the Alps poses a challenge. The interactions between the cyclones and the sharp orography of the Alps is fundamental to reproduce the large precipitations events related to Vb situations. Resolving this interaction demands the use of high-resolution simulations. For this task, Regional Climate Models (RCM) represent a valuable tool, which allows performing high-resolution simulations at an affordable computational cost.

This study consists of two main parts. First, reanalysis data is analysed with an automatic tracking tool to identify the most prominent Vb situations during the last few decades. Second, the WRF regional model (Skamarock et al. 2005) has been used to downscale the reanalysis. We analyse the model skills in reproducing such events compared to a set of observational data, and identify the drawbacks of the simulations.

2. Methods and Simulations

For identifying Vb-events, a cyclone tracking tool (Blender et al. 1997) has been applied to the geopotential height at 850 hPa from ERA-Interim (1979-2013, 1.5°x1.5°). In order to keep the total number of tracks as low as possible, cyclones are only detected over a box from 0°-35° E and 20°-60° N. The ERA-Interim data set has been previously low-pass filtered with a Hann window of 9x9 grid points (approximately 13.5 degrees). This filter removes small-scale features, secondary low pressure centres and noise that might have been introduced into this field by friction along the Alps.

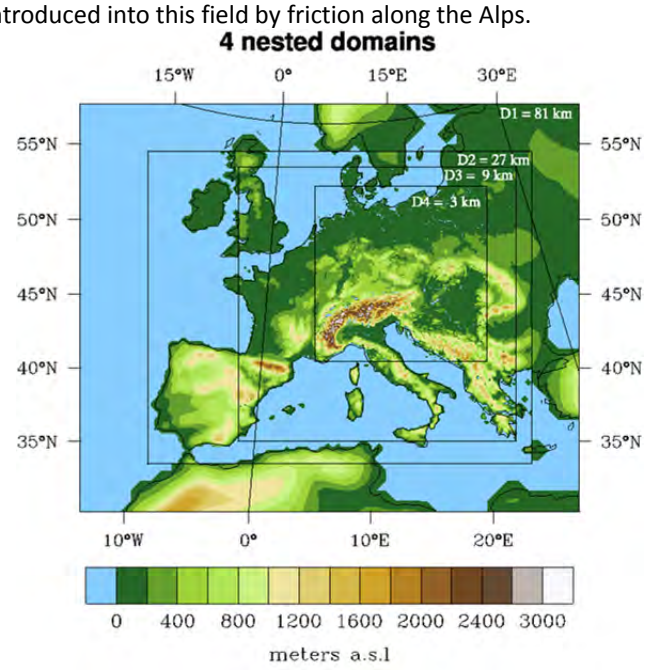


Figure 1. The four domains setup used in the nested WRF runs. The inner domain implements a resolution of 3 km, which allows to reproduce some of the high complex orography of the Alpine region.

The tracked cyclones where then automatically filtered with a criterion based on the origin and end of the track to discard those paths which can not be associated with Vb-events. This procedure is similar to the one used by M. Hofstätter and B. Chimani (2012).

The detected events were later simulated using the WRF regional model, driven by ERA-Interim at the boundaries. For this, a four nested domains setup is chosen, where the finest one has a resolution of 3 km, as depicted in Fig. 1. This domain covers Switzerland, Austria, Germany and Poland. It is the domain where our analysis focuses hereafter.

3. Results

A first manual review of the results shows that several Vb-events can be found among the cyclone pool produced by the tracking tool. Nevertheless the number

of non Vb situations is dominant. Hence, it is necessary that the Vb-events are filtered out from this pool. This is a challenging task, since they do not follow just one prescribed pathway. The filtering is constrained by somewhat subjective criteria e.g., the pathway range that is tolerated in order to be accepted as Vb-track. Also the level at which the tool is applied, influences the number and pathways of the events. The 850 hPa level has been chosen, as it allows to recognize the shallow young lows over the Mediterranean Sea, whereas it is not strongly influenced by topographic disruptions introduced by the Alps.

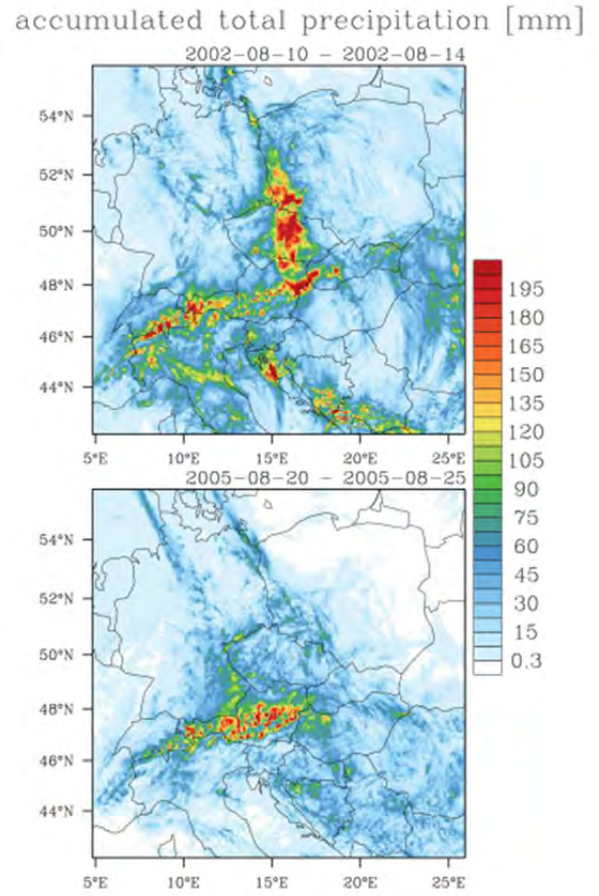


Figure 2. Accumulated precipitation (in mm) over a period of 4 and 5 days, respectively, of the two prominent Vb-events of August 2002 and 2005.

In contrast to what might be expected, no clear statement about the seasonality of Vb situations can be drawn. This is, because the tracks appear evenly distributed through the annual cycle.

Regarding the dynamic downscaling step, preliminary results show that the regional model is able to reproduce the main characteristic of the Vb-events and its impact in extreme precipitation. For this evaluation, well-known events such as the Europe wide floods in August 2002 and 2005 have been analysed in detail. Figure 2 depicts the accumulated precipitation of both events during the whole persistence of the respective Vb-event. A maximum in the accumulated total precipitation can be observed over Austria in both cases with 459 (417) mm in four (five) days for the 2002 (2005) event. The results from the model output have been compared with observational data over Switzerland, and an overall good agreement in the amount and spacial structure of precipitation is found. This approves the ability of the regional model to capture the precipitation patterns correctly.

In the future further situations will be analysed, and the model performance will be established over a broader area, as this kind of phenomenon is not restricted to Switzerland. The main goal of this research is to understand the dynamics of the past events and to provide a reliable climatology`, which allows to provide a first guess for future behaviour of these potentially disastrous situations.

References

Blender R., K. Fraedrich, and F. Lunkeit (1997) Identification of cyclone-track regimes in the North Atlantic, Quart. J. Roy. Meteor. Soc., 123, pp. 727–741

IPCC (2012) Managing the Risks of Extreme Events and Disasters to Advance Climate Change Adaptation. A Special Report of Working Groups I and II of the Intergovernmental Panel on Climate Change [Field, C.B., V. Barros, T.F. Stocker, D. Qin, D.J. Dokken, K.L. Ebi, M.D. Mastrandrea, K.J. Mach, G.-K. Plattner, S.K. Allen, M. Tignor, and P.M. Midgley (eds.)]. Cambridge University Press, Cambridge, UK, and New York, NY, USA, 582 pp

Skamarock, W. C., J. B. Klemp, J. Dudhia, D. O. Gill, D. M. Barker, W. Wang, and J. G. Powers (2005) A description of the Advanced Research WRF Version 2, NCAR Tech Notes-468+STR

Van Bebber, W. J. (1891) Die Zugstrassen der barometrischen Minima nach Bahnenkarten der Deutschen Seewarte für den Zeitraum von 1870 – 1890, Meteor. Z., 8, pp. 361 – 366

Simulation of high-altitude frontal zones in the tropopause and their role in the formation of the synoptic situation and climatic variability in the Northern Hemisphere and Europe region

Yaroslav Mitskevich[1] and Irina Partasenok[2]

[1] Belarus State University, Minsk, Belarus (yaroslav.mitskevich@gmail.com)

[2] Republic Hydrometeorological Center, Minsk, Belarus (irina-danilovich@yandex.ru)

1. Introduction

The importance of this study is connected with our trying to find dependencies of trajectories of barometrical systems and Altitude Frontal Zone (AFZ). It would allow to determine initial parameters for numerical weather forecasting and explore climate with applying of AFZ estimation. It makes possible to compare the parameters with Global Pressure Systems and elementary circulation mechanisms. We used the schemes of macro atmospheric processes which are clearly presented in classification of circulation mechanisms of Northern hemisphere by Dzerdzeevsky et. al. (1946) and such following like Kononova et. al. (2009).

There are several methods which could be used for synoptic fronts reconstruction. The problem of objective reconstruction and plotting of fronts on the maps is in application of different software described by Hewson (1998). The present study is directed to define the location of AFZ on the tropopause level and development of technical tools for their automatic constructions.

Localization of AFZ at tropopause level, on the boundary interaction between troposphere and the upper atmosphere, determines the relevance of the study. Stratosphere is characterized by its own atmosphere circulation system, different processes of energy exchange, variability. Thus, the particular geographical location of global AFZ should in theory affect the trajectory of the active pressure systems (cyclones). Also, AFZ influences indirectly passive atmospheric centers within circulating cells, as they are closure zones of global cells, which realize energy exchange between low and high latitudes, regional cells.

3. Main goals of study:

1. to Define main characteristics of AFZ at tropopause level;
2. to Create software (program) for frontal zones calculating and plotting;
3. to Create functionalities for other additional maps;
4. to Implement in the software possibility of practical comparison of the location of fronts and the synoptic situations over the Northern hemisphere (in particular - over the Europe and Belarus);
5. to Compare the locations of fronts with the synoptic situations, elementary circulation mechanisms;
6. to Find dependences which can be used in numerical modelling for parameterization choosing.

3. Data and methods

The Tropopause frontal zones program (TrFZ) was used for automated processing of Global Forecast Model data and construction of AFZ at tropopause level for the present study. Than, we provided comparison of fronts location and synoptic situation within the territory of Belarus.

We used geopotential height, vertical wind speed, sea level pressure, the maximum and minimum air temperature values for frontal zones research. Reanalysis data of the Global Forecast Model (in initialization moments - 00:00, 06:00, 12:00, 18:00) was applied for the whole of Northern Hemisphere. Additional maps were plotted for Northern Atlantic and European regions. Data was received from The National Oceanic and Atmospheric Administration (NOAA).

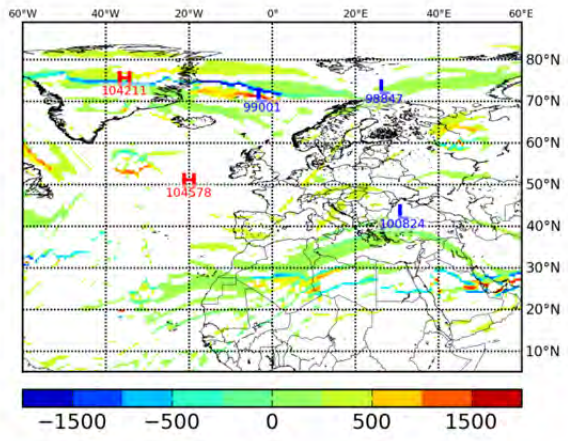


Figure 1. Altitude Frontal Zones example, created in TrFz

3. Results

Figure 1 illustrates plotted AFZ using calculated data based on gradients calculating of tropopause geopotential height and several masks. The figure represents the distribution of AFZ during the 14-15th of February 2012. The territory of East Europe on the 13th of February was under the impact of high pressure ridge which extended from Siberian anticyclone to the whole region of West Europe. Over the next few days deep cyclone came to this region. The cyclone trajectory completely corresponds with AFZ, which extended from

East Greenland to Scandinavia. Few small AFZ were present before the cyclone and they moved athwart of the main AFZ during this period.

We developed the program which was an automatic tool connected with some ready modules and applicable for work with large data massifs and interface construction. To develop the program we used mathematical resources presented in the open access. First of all, we applied computer language Python (version 3) with various available modules. We used Numpy module for numerical operations with data massifs, Pygrib module to manage file with machine code of WMO (grb.2), Tkinter module was implicated for the construction of interface, Matplotlib module we applied to plot data on the maps. We used Fedora 19 operational system for the study. We added the calculation function and function of local cyclones and anticyclones plotting. It simplified the process of representation and analyzing of barometric systems' directions in correspondence of AFZ location. According to the visual testing, the mask, providing clearer and more accurate reflection of AFZ, was constructed and implicated.

As a first result, we obtained the following:

1) If there are any powerful frontal zones at the tropopause level, trajectories of active cells are often traced to match with its configuration.

2) Deep cyclones (SLP<1000 hPa) often move to frontal zones, which appear above passive circulation cells.

3) The height of the tropopause is a very variable value; additional studies must be conducted to check the data oscillations.

4) The scheme of general circulation is an idealized system (with distinct global circulation cells), which is not always true. But in some cases it can be quite useful to explain the observed phenomena.

5) It is necessary to use additional tools for more accurate research of the observed processes.

References

Dzrdzeevsky B.P., Kurganskaya E.M. and Vitvitskaya E.M. (1946) Classification of circulation mechanisms in the Northern hemisphere and characteristics of synoptic seasons. Works of GUHMS, Hydrometeoizdat, Leningrad. 80p.

Kononova N.K. (2009) Classification of circulation mechanisms of northern hemisphere by B.L. Dzerdzeevskii. Under edit. A.B. Shmakin. Russian academy of Science, Instit. of Geography, Voentechizdat, Moscow. 372 p.

Hewson T. B. (1998) Objective fronts. Meteorological Applications. Volume 5, Issue 1. P. 37–65 Joint Centre for Mesoscale Meteorology, Department of Meteorology, University of Reading, UK

Simulation of the African hydroclimate using the HadGEM3-RA regional climate model: Resolution versus parametrisation dependence

Wilfran Moufouma-Okia and Richard Jones

Met Office Hadley Centre, Exeter, United Kingdom (wilfran.moufouma-okia@metoffice.gov.uk)

1. Introduction

As computing power steadily increases with time and running higher resolution RCM simulations become more affordable, addressing the need for more accurate climate predictions over Africa may necessitate a unified modelling approach that explicitly resolve key climate processes and mechanisms across a range of time and space scales. The results from the first sets of CORDEX-Africa simulations indicate substantial biases in individual model depending on the region and seasons (Kim et al. 2013, Nikulin et al. 2012). RCMs show generally higher fidelity for Western rather than Eastern part of Africa. This raises questions on the robustness of the model formulation and appropriateness of the horizontal resolution used.

This study documents the relative effects of horizontal resolution and physical formulation on the ability of the Met Office third-generation Global Atmosphere Regional Climate Model, a regional atmospheric configuration of the HadGEM3 model, to simulate present-day features of rainfall variability over the CORDEX-Africa domain.

2. Methodology and key results

First, we examine the influence of the horizontal resolution through a set of 20-year long ERA-Interim reanalysis driven RCM simulations performed separately at 12km, 25km, 50km, 70km, 90km, and 150km. Secondly, we explore the model sensitivity to parametrisation of aerosols, dust, and convection. To provide further insight on the model behaviour, HadGEM3-RA performance is also compared to RCM outputs from the CORDEX data archive and to results from the parent Global Climate Model simulations using three different spatial resolutions (70km, 100km, and 150km), as well as to HadRM3P – the current Met Office regional climate model.

3. Key results

The 50km resolution configuration of HadGEM3-RA reproduces reasonably well the spatial and temporal features of rainfall variability across regions and seasons including the seasonal progression of the tropical rainbelt, its extent and location, the annual cycle and interannual variability (Fig. 1). Although model biases vary across seasons and locations, a prominent feature is the over-prediction of rainfall totals over Central Africa, and the underestimation of rainfall in coastal areas of the Guinea Gulf during boreal spring and autumn seasons. Simulation improves with increased horizontal resolution, but some model errors persist.

The Comparison with the parent global model simulations demonstrates generally consistent behaviour over large scales but confirms the benefit of increasing the model horizontal resolution. Simulated precipitation from the regional climate models systematically outperforms that from the ERA-Interim and MERRA reanalysis datasets. Compared to the resolution dependence, HadGEM3-RA results are far more sensitive to the parametrisation of aerosols and convection. This work also highlights the challenges for evaluating climate models in data sparse regions where satellite derived rainfall and gridded observational datasets often diverge.

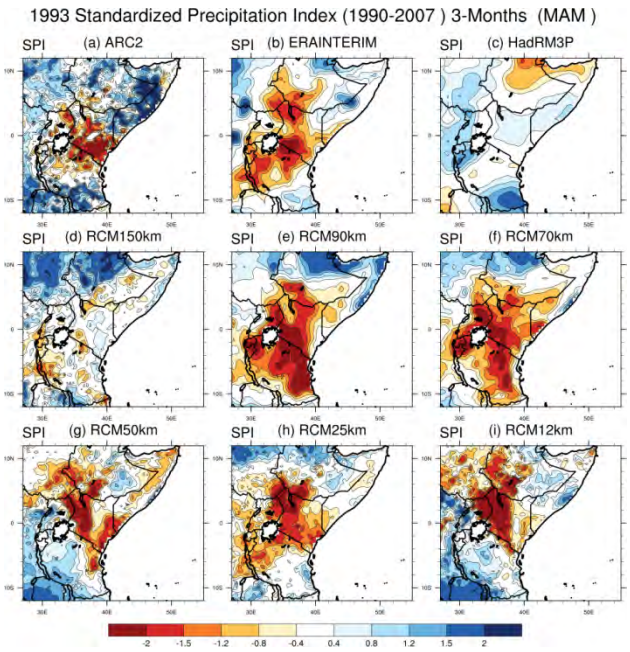


Figure 1. The 3-Month Standardized Precipitation Index for May 1993 (relative to 1990-2007) over East Africa for ARC2 satellite estimates, ERA-Interim, HadRM3P, and HadGEM3-RA experiments using different grid-spaces.

References

Kim S., D. Luthi, and B. Ahrens (2013) Analysis of the West African Monsoon system in the regional climate model COSMO-CLM,. *Int. J. Climatol.,* doi:10.1002/joc.3702.

Nikulin G., et al. (2012), Precipitation climatology in an Ensemble of CORDEX-Africa regional climate simulations,. *J. Climate,* 25, 6057–6078. doi:10.1175/JCLI-D-11-00375-1.

Evaluation of projected changes in extreme precipitation with increasing spatial resolution

Trevor Q. Murdock, Stephen R. Sobie and Alex J. Cannon

Pacific Climate Impacts Consortium, University of Victoria, Canada (tmurdock@uvic.ca)

1. Introduction

Changes in precipitation extremes are occurring and information about future projections is required for planning (IPCC, 2012). Projected changes in extremes from Global Climate Models (GCMs), while useful for understanding the future evolution of climate in general, have spatial resolution too coarse to provide information specific to regions and local communities that decision-making requires.

Higher resolution is achieved via statistical and/or dynamical downscaling. A strength of dynamical downscaling with Regional Climate Models (RCMs) is that it resolves processes physically that occur at scales smaller than the driving GCM (Murphy, 1998). A disadvantage is that biases from the driving GCM can influence results and RCMs demand considerable computational power (Plummer et al. 2006).

What is rarely considered, however, is the effect of downscaling methods themselves on projected changes in extremes. Our objective is to explore whether or not projected changes simulated by GCMs are preserved after downscaling.

To determine this, downscaled precipitation fields were re-aggregated to initial model resolution and results are compared. This approach allows us to address the following questions:

1. Does statistical downscaling preserve the large-scale patterns from the GCMs and RCMs?
2. How do distributions of GCM/RCM precipitation and extreme precipitation indices differ from re-aggregated statistically downscaled projections?
3. How do differences in distributions compare to other sources of uncertainty?

2. Downscaling technique

We build upon previous downscaling evaluations (Bürger et al. 2013) in which five different statistical techniques were evaluated based on ability to reproduce historical climate extremes. Evaluation criteria included daily sequencing of events, similarity of distributions, and spatial variation.

Subsequent to these studies, a Bias Correction Constructed Analogues Quantile mapping method (BCCAQ) was developed. BCCAQ is a field-based model output statistic downscaling method that shows superior skillful performance over North America compared with other methods (Cannon et al. in prep).

3. Scenarios selection

We carry out our analysis using a subset of 12 GCM simulations for Representative Concentration Pathway (RCP) 4.5 from the most recent Coupled Model Intercomparison Project (CMIP5; Taylor et al. 2012). Ensemble members were chosen based on an objective set of selection criteria that included hemispheric skill assessment based on the CLIMDEX indices (Sillmann et al. 2013; http://www.climdex.org/) and refinement based on a modified clustering algorithm (Cannon et al. in prep).

RCM simulations used include all 11 runs from the North American Regional Climate Change Assessment Program (NARCCAP, Mearns et al. 2012).

4. Target dataset

The ANUSPLIN gridded daily dataset (McKenney et al. 2011) was used as a statistical downscaling target. It uses interpolation of station data based on thin-plate splines to a gridded resolution of 300 arc-seconds (~10 km).

5. Indices

We consider three climate indices:

1. Total annual precipitation (P).
2. Annual extreme precipitation (R95ptot from CLIMDEX) is the total annual precipitation on days wetter than the 95th percentile during the historical period.
3. The 10-year return period value (RP10) is the precipitation intensity with a likelihood of occurrence on average once every 10 years.

6. Experimental design

As shown in Figure 1, we calculate the three precipitation indices using model output directly as well as from BCCAQ downscaled results. As our intent is to assess robustness of downscaled output in comparison to the driving model, we re-aggregate downscaled fields to the original GCM or RCM resolution. To eliminate differences between model grids, we first re-grid model simulations to common grids: 1.5° (~150km) for GCMs and 0.5° (~50km) for RCMs.

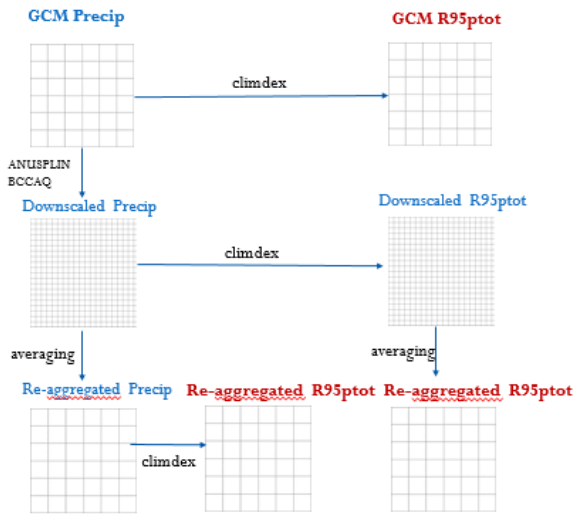


Figure 1. Experimental design: coarse resolution fields are used to calculate R95ptot. Downscaled GCM output (middle left) is re-aggregated to the original resolution in two ways: after (middle row) and before (bottom row) computing R95ptot. Both of these are compared to indices computed from the GCM directly (top row). This approach is also applied to RP10, and repeated using statistical downscaling of RCM simulations.

7. Statistical tests

The re-aggregated output from the different approaches and indices are analyzed using several statistical tests. The anomaly fields from the GCM and downscaled output are simply correlated and significance tested (at a 5% level). Distributions are compared using the Kolmogorov-Test of similarity, which compares the cumulative distribution function of each index to determine if the distributions are the same or not. This test is useful if we have either small or large differences between the distributions, but it is not sensitive for distributions with slight differences.

Therefore, the Energy-Test is also considered, which has minimum energy if both samples show the same distribution (Aslan & Zech, 2005).

We also consider the spatial distribution of results using the Walker field significance test (Wilks, 2006).

Finally, we estimate the uncertainties in re-aggregated output and compare to the uncertainty from using different models, climatological periods, and for different regions within the study area.

8. Results and applications

Results will be presented including an application to provide guidance on the use of projections of extreme precipitation to the British Columbia Ministry of Transportation and Infrastructure (Murdock et al. 2013).

9. Acknowledgments

The authors acknowledge Dr. Francis Zwiers and Martha Vogel for collaboration on project design as well as funding from the British Columbia Ministry of Transportation and Infrastructure.

References

Aslan, B., & Zech, G. (2005). Statistical energy as a tool for binning-free, multivariate goodness-of-fit tests, two-sample comparison and unfolding. Nuclear Instruments and Methods in Physics Research Section A: Accelerators, Spectrometers, Detectors and Associated Equipment, 537(3), 626–636.

Bürger, G., Sobie, S.R., Cannon, A.J., Werner, A.T., & Murdock, T.Q. (2013). Downscaling Extremes: An Intercomparison of Multiple Methods for Future Climate. Journal of Climate, 26(10), 3429–3449.

Cannon, A.J., Sobie, S.R., and Murdock, T.Q., (in prep.) Downscaling extremes - an intercomparison of multiple gridded methods, to be submitted to J. of Climate

IPCC (2012). Managing the Risks of Extreme Events and Disasters to Advance Climate Change Adaptation. A Special Report of Working Groups I and II of the Intergovernmental Panel on Climate Change. (C. B. Field, V. Barros, T. F. Stocker, & Q. Dahe, Eds.) (p. 582). Cambridge: Cambridge University Press.

McKenney, D. W., Hutchinson, M. F., Papadopol, P., Lawrence, K., Pedlar, J., Campbell, K., … Owen, T. (2011). Customized Spatial Climate Models for North America. Bulletin of the American Meteorological Society, 92(12), 1611–1622.

Mearns, L. O., Arritt, R., Biner, S., Bukovsky, M. S., McGinnis, S., Sain, S., … Snyder, M. (2012). The North American Regional Climate Change Assessment Program: Overview of Phase I Results. Bulletin of the American Meteorological Society, 93(9), 1337–1362.

Murdock, T.Q., Cannon, A.J., and Sobie, S.R., (2013), Downscaling extremes – a new set of climate change projections for Canada, American Geophysical Union poster #GC43C-1069, San Francisco.

Murphy, J. (1998). An Evaluation of Statistical and Dynamical Techniques for Downscaling Local Climate. Journal of Climate, 12, 2256–2284.

Plummer, D. A., Caya, D., Frgion, H., Côté, H., Giguère, M., Paquin, D., … De Elia, R. (2006). Climate and Climate Change over North America as Simulated by the Canadian RCM. Journal of Climate, 19, 3112–3132.

Sillmann, J., Kharin, V. V., Zhang, X., Zwiers, F. W., & Bronaugh, D. (2013). Climate extremes indices in the CMIP5 multimodel ensemble: Part 1. Model evaluation in the present climate. Journal of Geophysical Research: Atmospheres, 118(4), 1716–1733. doi:10.1002/jgrd.50203

Taylor, K. E., Stouffer, R. J., & Meehl, G. a. (2012). An Overview of CMIP5 and the Experiment Design. Bulletin of the American Meteorological Society, 93(4), 485–498.

Wilks D S. (2006). On “Field Significance” and the False Discovery Rate. Journal of Applied Meteorology and Climatology, 45, 1181–1189.

Climate-type based analysis of RegCM4 model performance over the Philippines

Gemma T. Narisma[1,2] and Arnold Discar[2,1]

[1] Regional Climate Systems Program, Manila Observatory, Quezon City, Philippines (narisma@observatory.ph)
[2] Atmospheric Science Program, Physics Department, Ateneo de Manila University, Quezon City, Philippines

1. Introduction

Regional climate models (RCMs) are essential tools for downscaling coarse climate change projections from global climate models into higher resolutions that may be more useful for local impacts and adaptation studies. In assessing the performance of RCMs, the ability of the models to capture historical climate variability, changes, and extremes are often analyzed.

In this study, we investigate the performance of a regional climate model, RegCM4 (Giorgi et al., 2012), over the Philippines within the context of the different climate types that dominate in the different regions of the country. According to the Modified Coronas Classification (Kintanar, 1994), there are four climate types in the Philippines, which are based on the annual distribution and amount of rainfall (see Figure 1). These climate types also reflect the influence of synoptic scale systems that are dominant over the Philippines at particular times of the year. Climate Type 1 along the western regions, for example, has a pronounced wet season from June to September, which is the period when the southwest monsoon system is most dominant. Regions on the eastern parts of the country, on the other hand, are of Climate Type 2 that has pronounced maximum rain from December to February, signaling the influence of the northeast monsoon.

A climate-type based analysis of model performance determines the models ability to capture seasonal variability and, hence, can also be indicative of the capability of the model in simulating the influence of large scale systems that affect the climate of different regions in the Philippines vis a vis local climatic influences.

2. Methodology

RegCM4 simulations at 50 km resolution were done over the Philippine region, covering a 17-year period from 1989-2005, and using the 2° resolution ECMWF ERA-Interim dataset (Dee et al. 2011) as boundary conditions. Running the model with different parameterization schemes showed that the Kuo convective scheme with the Zeng ocean flux parameterization best captured, in general, local historical climate.

Model results were validated using observation station datasets from the Philippine Atmospheric, Geophysical and Astronomical Services Administration (PAGASA). For each climate type, five representative stations, shown in Figure 1, were chosen for comparison with the model output. Model performance in terms of capturing precipitation variability, changes, and extremes will be analyzed.

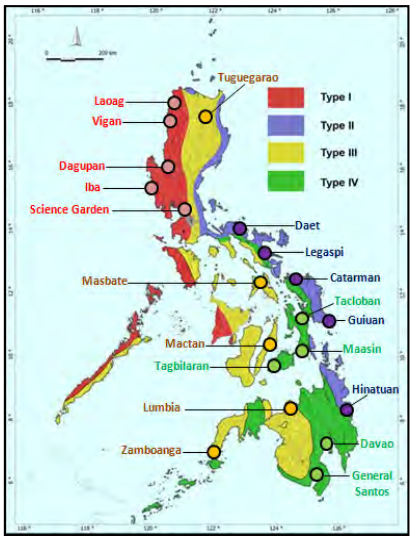


Figure 1. The different climate types in the Philippines based on the Modified Coronas Classification. The circles denote locations of PAGASA observation stations used in this study.

3. Results and Discussion

Comparison of the annual average daily rainfall between observed and modeled data for the five stations in each of the four climate types shows that the model performs best in capturing climate type 2 average daily rainfall with an r2 value of 0.73. Climate type 3 daily precipitation, on the other hand, was poorly simulated giving a very low r2 value of 0.04198.

The ability of the model to represent well climate type 2 rainfall is highlighted when comparing the monthly average daily rainfall for the different climate types with observed data (Figure 2). For climate type 2, Figure 2b, the model is able to simulate the pronounced maximum rainfall from December to February, although with a slight overestimation, and it also captured the drier conditions from April to September. The wet season of climate type 1 during the southwest monsoon season in the west regions of the country was underestimated by the model and the dry season rainfall was overestimated especially for the months of November and December (Figure 2a).

For climate types 3 and 4, RegCM4 fails to capture the seasonal variability of rainfall and reproduces instead seasonal profiles similar to that of climate type 2 (see Figures 2c and 2d). High precipitation amounts were simulated during the dry months of January to March. For climate type 3, the modeled variability of the daily rainfall values in the different months are also much

higher than the observed station data variability as denoted by the error bars.

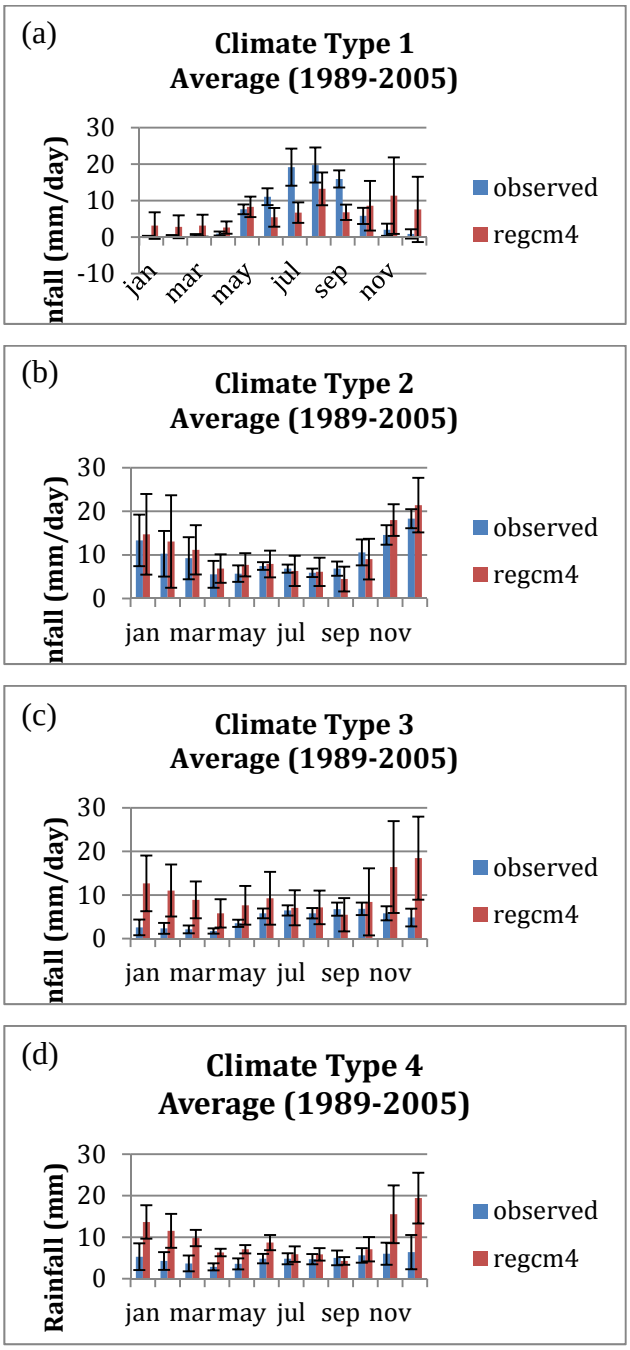


Figure 2. Comparison between observed station data (blue bars) and modeled monthly averaged daily rainfall (red bars) for the different climate types in the Philippines. Both observed and modeled variability are also indicated by the error bars.

4. Conclusion

Preliminary results on assessing the performance of RegCM4 according to climate types in the Philippines show that the model performs best in climate type 2 regions and poorly simulates the seasonal rainfall profile of climate types 3 and 4. The underlying possible mechanisms behind the inability of the model to simulate certain climate types will be analyzed. Climate extremes and changes will also be investigated in the context of climate type characteristics and behavior. This study will help determine and/or establish the suitability of the model for future climate change studies, especially since climate types can play an important role in determining future climate change impacts on various sectors, including water and agriculture. Agriculture planting calendars for example are location specific and follow local historical seasonal climate characteristics. The potential shifting of climate types in the Philippines due to a globally warmer world can have serious consequences and hence, establishing the ability of the model to simulate the different climate types is a critical step.

References

D. Dee et al. (2011) The ERA-Interim reanalysis: configuration and performance of the data assimilation system, Quart. J. R. Meteorol. Soc., 137, pp. 553-597

Giorgi et al. (2012) RegCM4: model description and preliminary tests over multiple CORDEX domains, Clim Research, 52, pp7-29, doi:10.3354/cr01018

Kintanar, R.L. (1984) Climate of the Philippines, PAGASA report, 38 pp.

Performance evaluation of Regional Climate Model (RegCM4) in simulating the climate over Indian region

Sridhara Nayak, Manabottam Mandal, and Suman Maity

Centre for Oceans, Rivers, Atmosphere and Land Sciences (CORAL), Indian Institute of Technology Kharagpur, India
(sridhara@coral.iitkgp.ernet.in)

1. Introduction

The regional climate modeling system RegCM, in last few decades, is widely used in seasonal as well as multi-decadal climate simulation and a number of studies (e.g., Halenka et al., 2006; Sylla et al., 2012) already demonstrated its suitability in reproducing the climate over their regions. Few studies are also conducted over Indian region towards the simulation of summer monsoon, but the performance of the modeling system towards multi-decadal climate simulation is not evaluated over the region so far. In the present study an attempt is made to evaluate the performance of RegCM4 in simulating the regional climate (30 years climate, 1981-2010) over Indian region and is presented in this study.

2. Methods

The RegCM4 is integrated over Indian region (30E-120E and 15S-45N) at 30km grid resolution with NNRP1 reanalysis forcing. The 30 years climatology of annual and seasonal surface temperature and precipitation are prepared from model simulation for the period 1981-2010 and those of from the UDel and GPCC observation. The standard error and the correlation between the model simulation and observation for the period are calculated to analyze the model performance. Inter-annual and inter-decadal variability in annual means of surface temperature and precipitation over India and its five homogeneous regions (Figure 1) are also estimated during this period. Inter-annual variability is computed with respect to their 30 years climatic mean and inter-decadal variability is estimated with respect to their decadal mean.

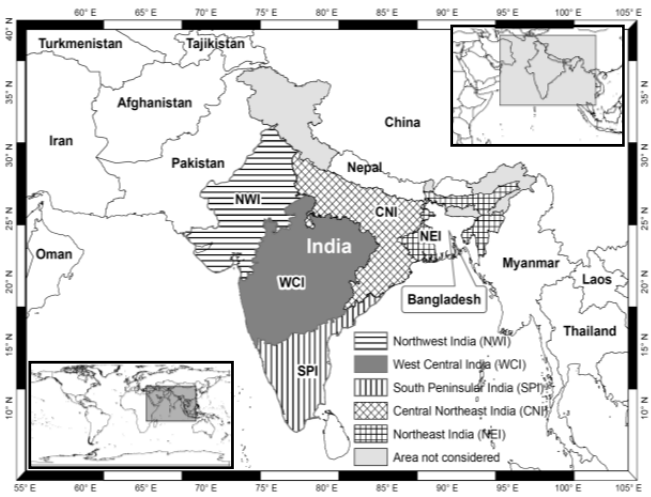


Figure 1: Domain of the Study.

3. Results and Discussions

The results over India indicate that the model has cold bias in simulating the 30 years temperature climatology and dry bias in simulating the annual, monsoon and autumn precipitation climatology. The model showed wet bias in simulating winter and summer precipitation climatology. The model has cold bias of the order of ~2 °C in simulating surface temperature climatology over India and the same is in the order of 1.5 °C over CNI, NEI, NWI and WCI, while over SPI is more than 2.5°C.

The spatial correlation between the model and observation in simulating the temperature climatology over India is 0.979 with a standard error of ~3 °C. The performance of the model in representing the spatial variability of temperature varies from region to region and is reasonably well simulated (Figure 2).

The model shows dry bias of 0.66-0.90mm/d over India and its five homogeneous regions. The bias is less over CNI, NWI, SPI and more over WCI. The spatial correlation between the model and observation in simulating the precipitation climatology over India is 0.611-6.46 with a standard error of 1.84-1.89 mm/d.

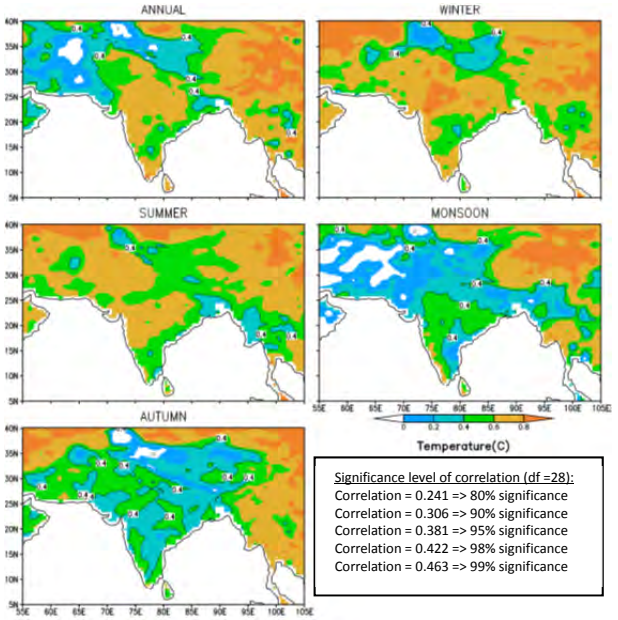


Figure 2: Time correlation between RegCM4 and UDel in simulating the temperature climatology.

4. Conclusions

The performance of the modeling system is

evaluated towards the multi decadal climate simulation over Indian region. The bias and standard error in the model climatology, and the correlation between the model and observations are computed. The results indicate that the model has cold bias in the 30 years temperature climatology and dry bias in the precipitation climatology over India and its five homogeneous regions. Inter-annual and inter-decadal variability of temperature and precipitation over India and its five homogeneous regions are well simulated by the model (Figure 3 & 4).

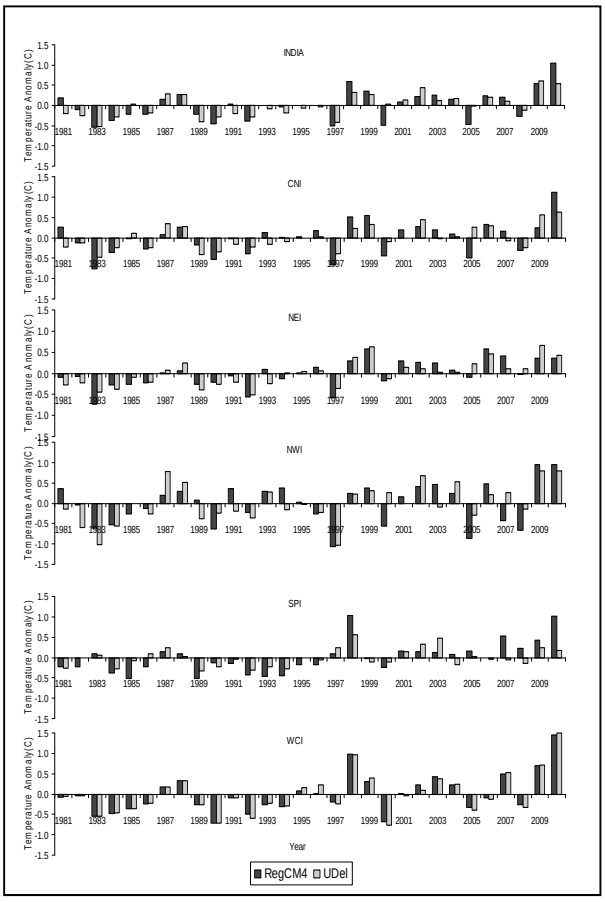


Figure 3: Inter-annual variability of surface temperature anomalies over India and its five homogeneous regions during 1981-2010

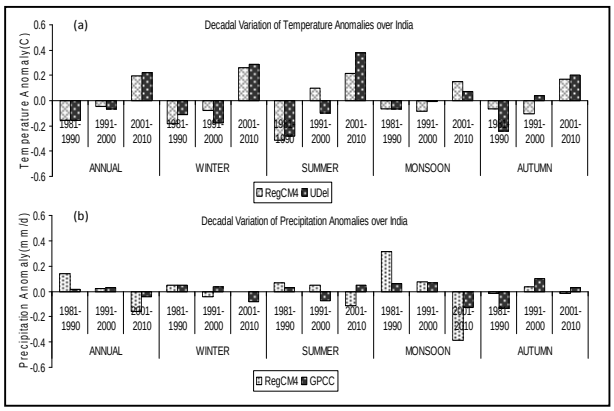


Figure 4: Inter-decadal variability of (a) Temperature and (b) precipitation anomalies over India for the whole years and all the four seasons during 1981-2010.

Overall the model could able to reproduce the temperature over Indian region though the precipitation over the region, particularly, in the monsoon season is not well simulated.

Acknowledgement

The authors gratefully acknowledge ICTP, Triesty, Italy for providing the RegCM. Authors also gratefully acknowledge GPCC and UDel for providing observed precipitation and temperature datasets respectively. Authors also gratefully acknowledge the RegCM4 data web (http://users.ictp.it/~pubregcm/RegCM4) for providing all the required datasets used in the model. Centre for Development of Advanced Computing (C-DAC), Pune, India is acknowledged providing the computing facility. Indian Institute of Technology Kharagpur is acknowledged for providing the required facilities for conducting the research work.

References

Halenka, T., Kalvova, J., Chladova, Z., Demeterova, A., Zemankova, K. and Belda, M (2006), On the capability of RegCM to capture extremes in long term regional climate simulation – comparison with the observations for Czech Republic, Theoretical and Applied Climatology, Vol. 86, pp. 125-145, DOI: 10.1007/s00704-005-0205-5

Sylla, M. B., Giorgi, F. and Stordal, F. (2012), Large-scale origins of rainfall and temperature bias in high-resolution simulations over southern Africa, Climate Research, Vol. 52, pp. 193-211, DOI: 10.3354/cr01044

An analysis of Precipitation-Temperature relationship: Responses from Multiple RCM simulations over Japan

Sridhara Nayak, and Koji Dairaku

Department of Integrated Research on Disaster Prevention, National Research Institute for Earth Science and Disaster Prevention, Tsukuba, Japan (sridharanayakiitkgp@gmail.com)

1. Introduction

It is well accepted that temperature and precipitation are two most important factors in determining our climate. Though there are other factors such as topography, winds, surface currents etc. still play major roles, but most of climate studies focus on the study of temperature and precipitation trends over a region and their distributions and future changes. Thus a number of studies have been conducted over various regions to analyze their inter-relationship/ dependence which may facilitate to prepare various strategies. Lenderink and Meijgaard (2008) analyzed the relationship between them over Netherland. Buishand and Brandsma (1999) analyzed the dependence between them over Florence and Livorno, Italy. Similarly, Adler et al. (2008) investigated the relationships between global precipitation and surface temperature on inter-annual and longer timescales. Portmaan et al. (2009) also made an analysis over United States to find out the relationship between daily temperature and average daily precipitation. But the studies over Japan, in this context, mainly have been conducted to investigate the future changes in precipitation and temperature (e.g., Iizumi et al., 2012; Ishizaki et al., 2012). Recently, Tsunematsu et al. (2013) investigated the future changes in summertime precipitation amounts over Japan and analyzed the relationship of changes in precipitation with the topography. In the present study, an attempt has been made to analyze the how the hourly and daily extreme precipitation varies with temperature over Japan.

2. Methods

The future changes in summertime (JJA) precipitation and temperature over Japan will be estimated from the deviations of the recent climate (1981-2000) from the future climate (2081-2100) using three different RCM products viz. NHRCM, NRAMS, TWRF. Then, the daily extremes in the change precipitations will be stratified based on daily mean temperature in bins of 2 or 3 °C width and the 90th, 95th and 99th percentiles of wet events will be computed. Using these data values the interrelation between the change in precipitation and temperature will be analyzed and finally compared with the Clausius-Clapeyron relation. The discussions will be based on the responses from the each of the said RCM simulations.

3. Expected Outcome

Results are expected to get an indication that how changes in extreme precipitation is related with temperature, which will be useful information for risk assessment and adaptation strategies.

Acknowledgement

This study is be conducted as part of the research subject "Vulnerability and Adaptation to Climate Change in Water Hazard Assessed Using Regional Climate Scenarios in the Tokyo Region" (National Research Institute for Earth Science and Disaster Prevention; PI: Koji Dairaku) of Research Program on Climate Change Adaptation (RECCA), and was supported by the SOUSEI Program, funded by Ministry of Education, Culture, Sports, Science and Technology, Government of Japan.

References

Adler, R. F., G. Gu, J.-J. Wang, G. J. Huffman, S. Curtis, and D. Bolvin (2008), Relationships between global precipitation and surface temperature on interannual and longer timescales (1979 – 2006), Journal of Geophysical Research, 113, D22104, doi:10.1029/2008JD010536

Buishand, T. A., & Brandsma, T. (1999). Dependence of precipitation on temperature at Florence and Livorno (Italy). Climate Research, 12(1), 53-63.

Ishizaki, N. N., H. Shiogama, K. Takahashi, S. Emori, K. Dairaku, H. Kusaka, T. Nakaegawa and I. Takayabu (2012), Air Temperatures Derived from Dynamical and Statistical Downscaling Models, Journal of the Meteorological Society of Japan, Vol. 90B, pp. 75-82, doi:10.2151/jmsj.2012-B06

Lenderink, G. and E. V. Meijgaard (2008), Increase in hourly precipitation extremes beyond expectations from temperature changes, Nature Geoscienes, Vol. 1. doi:10.1038/ngo262

Portmann, R. W., Solomon, S., & Hegerl, G. C. (2009). Spatial and seasonal patterns in climate change, temperatures, and precipitation across the United States. Proceedings of the National Academy of Sciences, 106(18), 7324-7329.

Tsunematsu, N., K. Dairaku, and J. Hirano (2013), Future changes in summertime precipitation amounts associated with topography in the Japanese islands, Journal of Geophysical Research: Atmospheres, 118, doi:10.1002/jgrd.50383

Contradicting projected changes in precipitation over West Africa from the CMIP5 and CORDEX simulations

Grigory Nikulin[1], Erik Kjellström[1], Colin Jones[2], Patrick Samuelsson[1], Marco Kupiainen[1], Ulf Hansson[1] and the CORDEX-Africa Team

[1] Rossby Centre, Swedish Meteorological and Hydrological Institute, Norrköping, Sweden (grigory.nikulin@smhi.se)
[2] School of Earth and Environment, University of Leeds, UK

During last years more and more regional climate simulations for the CORDEX-Africa domain became available and the first analysis of the CORDEX-Africa results shows that regional simulations and their respective driving global ones may project contradicting climate change signals in precipitation. In addition, it was also found that different RCMs downscaling the same AOGCMs may also produce contradicting future projections in precipitation. Interpretation of such contradicting signals in global and regional ensembles of climate simulations is a challenging task and a detailed and process-oriented analysis is required.

Figure 1 (right panel) shows July-September (JAS) projected changes in temperature and precipitation averaged over West Africa (10°W-10°E, 7.5°N-15°N) for 4 CMIP5 AOGCMs (CNRM-CM5, EC-EARTH, HadGEM2-ES and MPI-ESM-LR) under the RCP8.5 scenario and for 3 subsequent 30-yr periods (2011-2040, 2041-2070 and 2071-2100). 3 of 4 AOGCMs project no changes in precipitation at the end of the century (2071-2100) while one global model (CNRM-CM5) projects an increase. Taking this small global ensemble, one can conclude that no changes in precipitation are projected in West Africa with the raising global temperature.

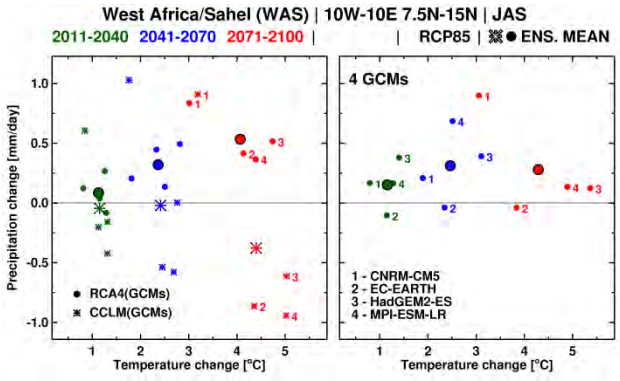


Figure 1. July-September projected changes in temperature and precipitation over West Africa for (right) 4 CMIP5 AOGCMs and (left) corresponding downscaling by two RCMs – SMHI-RCA4 and CLMcom-CCLM4-8-17.

When the global models are downscaled by two different RCMs (SMHI-RCA4 and CLMcom-CCL4-8-17) interpretation of future projections in precipitation becomes more complex. All four RCA4 simulations (Fig. 1, left panel) show an increase in precipitation even if 3 of the 4 global driving models show no changes. In contrast to the RCA4 results 3 of the 4 CCLM ensemble members project drier conditions and only one member driven by CNRM-CM5 shows wetter conditions.

Such contradiction between the global and regional ensembles and between two regional ensembles driven by the same AOGCMs raises a reasonable question: "What simulations should be taken for assessment of possible future climate changes in West Africa?" From one side it can be expected that the regional simulations with higher resolution and better resolved local processes are more reliable compared to the global simulations. However, the difference found between the regional ensembles clearly shows that local-scale process defined by RCM physical formulation can be more important than large-scale signals from the driving AOGCMs. The main focus in this study is on an attempt to identify key processes, which can be responsible for contradicting changes in precipitation between regional and global models and between different regional models driven by the same AOGCMs.

Mistral and its Siblings in RCMs

Anika Obermann[1], Samuel Somot[2] and Bodo Ahrens[1]

[1] IAU, Goethe University Frankfurt, Germany (obermann@iau.uni-frankfurt.de)
[2] Meteo France/CNRM Toulouse, France

1. Motivation

Mistral is a regional cold and dry north to northwesterly wind following the lower Rhône Valley. It causes deep water formation in the Mediterranean Sea. Therefore it is important for modeling of the circulation in the Mediterranean Sea. Its sibling Tramontane blows in the valley between Pyrenees and Massif Central. Another similar wind is the Cierzo along Ebro Valley south of Pyrenees.

These regional winds are influenced by processes occurring in valleys (e.g. channeling) and deceleration at the valley exit as well as the surface roughness. Above water, the surface roughness varies with wind speed. In RCMs, the friction velocity dependend Charnock formula is used to determine surface roughness of the Mediterranean Sea.

We investigate the quality of RCMs in terms of surface winds with emphasis on Mistral and its siblings and study the processes that influence the 10-meter wind speed over land and sea surface.

2. Data

We compare daily mean wind speed in ERA-Interim driven RCM runs on the Med-CORDEX domain in the HyMeX framework to gridded scatterometer data of ocean winds from QuikSCAT at 0.25° resolution and SAFRAN (e.g. Vidal et al. 2010) daily mean wind speed over France.

The investigated RCMs are:

- COSMO-CLM (e.g. Doms et al. 2011) on 0.44° and 0.088° resolution.
- ALADIN-climate (e.g. Herrmann et al. 2011) on 0.44° and 0.11° resolution.

3. 10-Meter Wind Speed

As shown in figure 1 for a Mistral event on February 9th 2000, Mistral and Tramontane accelerate rapidly when reaching the Mediterranean Sea. A deceleraton occurs after the wind has travelled some distance above water. We investigate the differences in location, shape and amount of wind speed gain and loss in models and observations. Emphasis is on days when Mistral and Tramontane occur in contrast to days without Mistral or Tramontane.

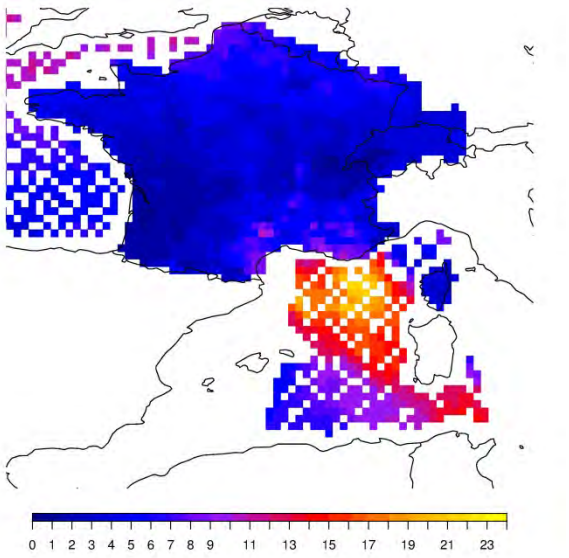


Figure 1. Daily mean wind speed (m/s) on February 9th, 2000. SAFRAN data over France, QuikSCAT data over sea.

Furthermore, we discuss the spatial distribution and fetch dependence of wind speed. Therefore, the average fetch is estimated for each grid cell and wind direction taking into account shading by coastal grid cells and uncertainties in wind direction. As a first result we find the RMSE to decrease with increasing fetch (figure 2).

4. Outlook

Wind speed over water is influenced by local effects (e.g. roughness length) as well as fetch and error propagation from land to sea. We want to do further studies on these effects. Thus, modifications of the Charnock formula and topographic effects will be investigated as the next step. Additionally, we plan to study other winds e.g. Cierzo and Bora.

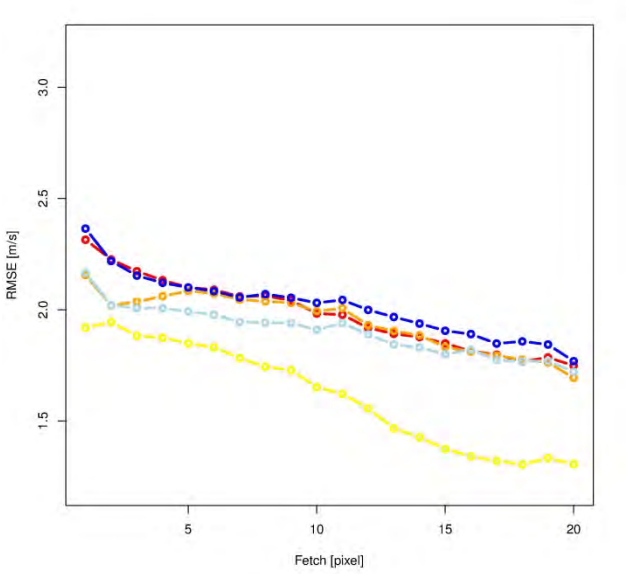


Figure 2. RMSE in Tramontane and Mistral region as function of fetch (pixel size: 0.25°). Red: COSMO-CLM 0.44°, orange: COSMO-CLM 0.088°, blue: ALADIN 0.44°, light blue: ALADIN 0.11°, yellow: ERA-Interim.

References

J.-P. Vidal, E. Martin, L. Franchistéguy, M. Baillon, J.-M. Soubeyroux (2010): A 50-Year High-Resolution Atmospheric Reanalysis Over France with the Safran System, INT J CLIMATOL, 30, 11, 1627-1644

G. Doms, J. Foerstner, E. Heise, H.-J. Herzog, D. Mironov, M. Raschendorfer, T. Reinhardt, B. Ritter, R. Schrodin, J.-P. Schulz, G. Vogel (2011): A Description of the Nonhydrostatic Regional COSMO Model, Part II: Physical Parameterization

M. Herrmann, S. Somot, S. Calmanti, C. Dubois, F. Sevault (2011): Representation of daily wind speed spatial and temporal variability and intense wind events over the Mediterranean Sea using dynamical downscaling: impact of the regional climate model configuration, Nat. Hazards Earth Syst. Sci., 11, 1983-2001

How well does HIRHAM5 model simulate East Africa climate.

Sarah Emerald Osima, Bruce Hewitson and Martin Stendel

Climate System Analysis Group, Department of Environmental & Geographical Science, University of Cape Town, South Africa, Danish Meteorological Institute (sarah.osima@gmail.com)

1. Introduction

Earlier studies has shown that, East Africa climate is highly variable due to its surrounding topography, such as the highest peak of Africa (Mount Kilimanjaro), Great Lakes (Lake Victoria), Great Rift Valley and boarded to Indian Ocean in the east (Nicholson 1996; Mutai et al. 1998). Therefore, it is important to use more reliable regional climate models which will be able to resolve such complex climate. High resolution regional climate models are proven to have essential property that they demonstrate good skill in capturing environmental variability (complex topography) which are either difficult/partially captured by the coarser resolution models (Kattsov et al. 2013).

This study will focus on evaluating how well HIRHAM5 regional model is capable in reslving East Africa climate.

2. Data and Method

This study used the output of the downscaled HIRHAM5 model from Danish Metrological Institute. HIRHAM5 was downscaled under lateral boundary forcing of ECHAM5 (European Centre/Hamburg 5 model) at 50km and 10km resolution. The first resolution covered 1950 to 2100 while the later is in three time slices (1980-1999, 2046–2065 and 2080–2099). Moreover, we used 20 year HIRHAM5 under boundary forcing of ERA Interim (CORDEX data) for the purpose of comparison and evaluation of the model. We also used the boundary forcing ECHAM5 (as GCM) in the comparison and evaluation. The model domain covers tropical East Africa between the longitudes 15.956 ^{o}W and 52.056 ^{o}E and between the latitudes 28.035 ^{o}S and 5.035 ^{o}N with grids points about 362 x 332 at 10km, 38grid points with elevation about and above 3000m which covers the height of Mount Kilimanjaro and Kenya (Figure 1). However, this study focus on three countries: Tanzania, Kenya and Uganda part of the domain (longitude: 29 °E–43 °E; and latitude:11 °S–5°N) (Anyah & Semazzi 2007). The observation datasets for CRU and FEWS are used as reference in the evaluation of the model.

The experimental design considered the HIRHAM5 model representation of the inter-annual variability of rainfall and surface temperature over East Africa. Moreover, the projected changes of the mean climatology and extreme climatic events, and the dynamic s these change.

This study focuses on three main regions namely Kenya, Uganda and Tanzania (Figure 1). However, for the purpose of details in the model validation, the bimodal and unimodal regions were selected where there were possibilities of getting observed stations data during this study.

3. Results

HIRHAM5 model demonstrate good skill in representing East Africa current climate over large part of East Africa. Moreover a model shows good skill in representing the inter-annual variability of rainfall during OND season. For future projection, a model also showed good agreement in the projection of mean and extreme rainfall and temperature changes over East Africa. Both of these variables are changing (whether positive or negative) in the future (IPCC, AR4, and AR5). The surface temperature is projected to increase in the near and far future. The coastal belts are projected to have less warm than the mainland of East Africa. A model also projects increase in very heavy rainfall (Shongwe et al. 2011)(Shongwe et al. 2009) and this is more confined over the western portion of East Africa In this summary only we present model representation of the inter-annual variability of rainfall over the study domain, composites of rainfall anomalies in El Niño Southern Oscillation (ENSO) and the extreme rainfall and surface temperature in the 90th percentile.

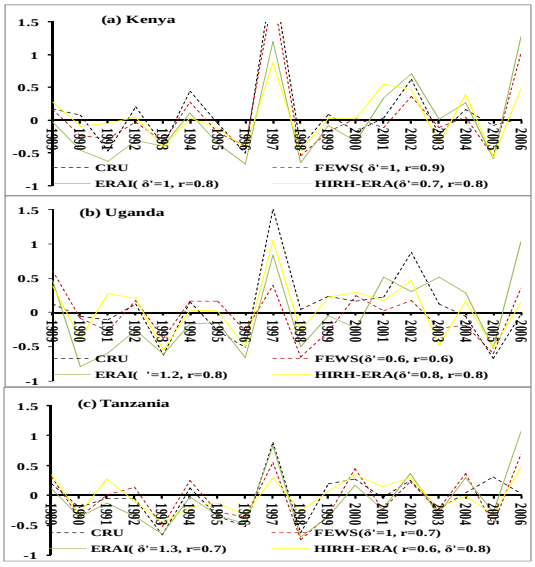


Figure 1: Inter-annual variability of standardised anomalies of MAM rainfall season over East Africa for (a) Kenya(-3.6^{o} S – 4.8^{o} N, 34^{o}E –41.7^{o} E), (b) Uganda (-1.8^{o} S – 4.035^{o} N, 29.5^{o}W – 35^{o} E) and (c) Tanzania (29^{o} W – 41^{o} E, -11^{o} S – -1^{o} S) from 1989 to 2006 as simulated by HIRHAM5-ERAI, ERA Interim (ERAI), and observations from CRU and FEWS.

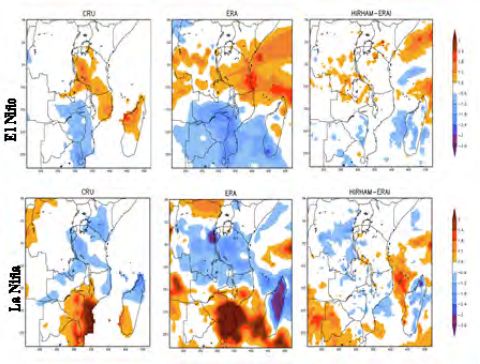


Figure 2: Composite of rainfall anomalies during El Niño (first row) and La Niña (second row)

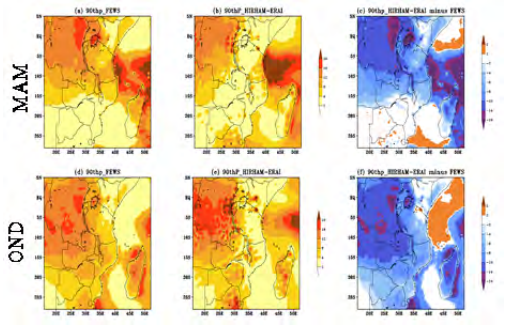


Figure 3: The 90th percentile of daily rainfall (mm/day) as presented by the (a) observations from FEWS (b), HIRHAM5-ERA and (c) their differences (HIRHAM-ERAI minus FEWS).

4. Discussion

Figure 1 shows that, HIRHAM5 is able to capture the patterns of rainfall variability over East Africa. The model shows strong correlation with the observation ($r \geq 0.7$) over the study domain. The model also captured well the anomalies of rainfall during the strongest El Niño Southern Oscillation (ENSO). For example, 1997/98 (El Niño) and 1999/2000 (La Niña) are well captured by the model. this is also evident in the composites of rainfall anomalies (Figure 2).

Figure 3 presents the results of the extreme heavy rainfall over East Arica in the present day climate as simulated by HIRHAM5 driven by ERAI. HIRHAM5 shows good representation of the geographical pattern of extreme heavy rainfall, however with some differences. A model underestimate rainfall over large portion of East Africa, and overestimate over high ground. In further details of evaluation of HIRHAM5 in annual cycles of rainfall (not shown here), a model also found to have wet bias over large portion the domain. Mean extreme of surface temperature are also overestimated (not shown here).

5. Conclusion

This study investigates the ability of HIRHAM5 model in simulating inter-annual variability of East Africa rainfall. A model was evaluated using two different observation datasets (CRU and FEWS) for more realization of the present day climate. The comparison of the two observation datasets with the model output shows that HIRHAM5 can be used in the simulation of East Africa climate.

References

Anyah, R.O. & Semazzi, F.H.M., 2007. Variability of East African rainfall based on multiyear Regcm3 simulations. *International Journal of Climatology*, 27(3), pp.357–371. Available at: http://doi.wiley.com/10.1002/joc.1401 [Accessed November 12, 2013].

Kattsov, V. et al., 2013. Evaluation of Climate Models 9.

Mutai, C.C., Ward, M.N. & Colman, a. W., 1998. Towards the prediction of the East Africa short rains based on sea-surface temperature–atmosphere coupling. *International Journal of Climatology*, 18(9), pp.975–997. Available at: http://doi.wiley.com/10.1002/(SICI)1097-0088(199807)18:9<975::AID-JOC259>3.0.CO;2-U.

Nicholson, S.E., 1996. A Review of climate dynamics and variability of East Africa climate. In *The Limnology, Climatology and Paleoclimatology of the East African Lake*. Amsterdam: Gordon and Breach, pp. 25–56.

Shongwe, M.E. et al., 2009. Projected Changes in Mean and Extreme Precipitation in Africa under Global Warming. Part I: Southern Africa. *Journal of Climate*, 22(13), pp.3819–3837. Available at: http://journals.ametsoc.org/doi/abs/10.1175/2009JCLI2317.1 [Accessed March 11, 2013].

Shongwe, M.E. et al., 2011. Projected Changes in Mean and Extreme Precipitation in Africa under Global Warming. Part II: East Africa. *Journal of Climate*, 24(14), pp.3718–3733. Available at: http://journals.ametsoc.org/doi/abs/10.1175/2010JCLI2883.1 [Accessed March 11, 2013].

Projected Changes in Air Temperature and Precipitation Climatology in Central Asia CORDEX Region 8 by Using RegCM4.3.5

Tugba Ozturk[1,3], Murat Türkeş[2] and M. Levent Kurnaz[1]

[1] Department of Physics, Faculty of Science and Arts, Bogazici University, 34342, Istanbul, Turkey (tugbaozturkt@gmail.com)
[2] Affiliated Faculty at the Department of Statistics, Middle East Technical University (METU), 06800, Ankara, Turkey
[3] Department of Physics, Faculty of Science and Arts, Isik University, 34980, Istanbul, Turkey

In this work, projected future changes for the period of 2071-2100 in mean surface air temperature and precipitation climatology and variability over the large Central Asia region with respect to present climate (1971 to 2000) were studied based on the RCP4.5 and RCP8.5 emission scenarios. Regional Climate Model (RegCM4.3.5) of the International Centre for Theoretical Physics (ICTP) was used for projections of future and present climate conditions. Hadley Global Environment Model 2 (HadGEM2) of the Met Office Hadley Centre was downscaled for the Cordex Region 8. We investigated the seasonal time-scale performance of RegCM4.3.5 in reproducing observed climatology over the domain of Central Asia by using 2 different emission scenario datasets for three future periods. The regional model is capable of reproducing the observed climate with few exceptions which are due to the meteorological and physical geographical complexities of the domain. For the future climatology of the domain, the regional model predicts relatively high warming in the warm season and northern part of the domain at cold season with a decrease in precipitation almost all part of the domain. The results of our study show that surface temperatures in the region will increase from 3°C up to more than 7°C on average according to the emission scenarios for the period of 2071-2100 with respect to past period of 1971-2000. In the future, a decrease in the amount of precipitation is also expected for the region. The projected warming and decrease in precipitation for the domain might strongly affect the ecological and socio-economic systems of this region, which is already a mostly arid and semi-arid environment.

This work was supported by the BU Research Fund under the project number 7362. One of the authors (MLK) was partially supported by Mercator-IPC Fellowship Program.

.

Regional climate model evaluation of atmospheric conditions leading to severe weather and large precipitable water events.

Dominique Paquin[1], Ramon de Elia[1,2] and Anne Frigon[1]

[1] Ouranos, Montréal, Québec, Canada (paquin.dominique@ouranos.ca)

[2] Centre pour l'étude et la simulation du climat à l'échelle régionale (ESCER), Université du Québec à Montréal (UQAM), Montréal, Québec, Canada

1. Introduction

The Vulnerability, Impact and Adaptation (VIA) community is using RCMs outputs more and more frequently to elaborate their adaptation strategies. In the case of the Ouranos consortium, the existence of a climate simulation team within the organization ensures the close collaboration with climate scenario and VIA teams. As part of our mandate we are focusing on evaluating the model's ability to simulate phenomenon and variables of particular interest for some users. This presentation will show two examples of such evaluation: one finished study on severe weather and one just in the first phase on precipitable water.

2. Severe weather

This study (Paquin et al. 2014) aims to investigate the possibility of a future increase of severe weather related to deep convective events over North America due to the evolution of favorable atmospheric conditions. Twelve CRCM4 (Canadian Regional Climate Model) climate simulations at 45 km over North America are used, some driven by reanalysis (NCEP/NCAR, ERA40, ERA-interim), some by GCMs (MPI-ECHAM5, CCCma-CGCM3 and CNRM-CM3.3), and some sensitivity simulations by GCMs with perturbed humidity fields at the lateral boundaries. The climate change evaluation is made from 1960 to 2100 with four simulations (two members for ECHAM5 and CGCM3) and for one 2-time slices simulation (CNRM-CM3.3). To determine the favorable atmospheric conditions for severe weather, we are using covariables that the severe weather community has identified as indicators in two distinct formulations: CAPE and wind shear between the surface and 6 km (S6). We are also looking at direct precipitation output from the convective scheme.

We begin by assessing the possibility of using standardized wind shear output by comparing S6 calculated on model levels with the approximation obtained using standard pressure levels. This equivalence confirmed, we are using the 500-850 hPa wind shear for the rest of the study. We compute the Number of Archives of SEVere weather (NASEV) from every 6-hour archive in the dataset. For the 1960-1999 period, common in simulations both driven by reanalysis and GCMs, we show that the NASEV is influenced by the driving model but does not show any tendency over the 40 year period. However, in accordance with other studies on this subject, we find that for over a longer time period, from 1960 to 2100, the number of severe events is increasing significantly. We have also calculated the number of convective precipitation events greater than 25 mm/day, and the same results are found, with increase from 1960 to 2100 and a large dependence on the driving model. Studying the covariables separately, we found that from 1960 to 2100, CAPE increases significantly, leading the NASEV increases, while the wind shear is in fact decreasing slightly. Through the analysis of the CRCM's convective precipitation outputs, we show that severe convective liquid precipitation events become both more frequent and slightly more intense. We have used the four transient simulations driven by ECHAM and CGCM3 to look at the source of instability. It appears that even if the temperature is increasing from 1960 to 2100, the lapse rate between 500 and 850 hPa is decreasing. For the humidity however, both the values and the vertical gradients are increasing, being the main driver of the instability and thus CAPE and NASEV increases.

In order to explore the sensitivity to the driving data, experiments conducted with reduced humidity input (75% and 50%) at the lateral boundaries are carried out for a 10-year period for simulations driven by ECHAM5 and CGCM3. These experiments show the significant role that the driving GCM's humidity inflow has on simulated extreme events, even when boundaries are located over the ocean and very far from the region of interest. The reason behind this dependence on the driving model humidity occurs is still unclear and would need further study.

To complete our study, we have done analysis at the regional level. For those smaller regions, results are in general consistent with those found at the continental scale, but large inter-regional variations exist, as can be seen in Figure 1, showing the regional decadal trend (in number of events per decade) for 13 North American regions.

3. Precipitable water

The second topic of interest focuses on precipitable water, once again in the context of extreme events in general, but this time for probable maximum precipitation (PMP) in particular. Such an interest is coming from the hydrology community that is using the PMP for dam regulations. In this study, we begin the evaluation of the CRCM4 at 45km driven by ERA-interim precipitable water by comparing with the National

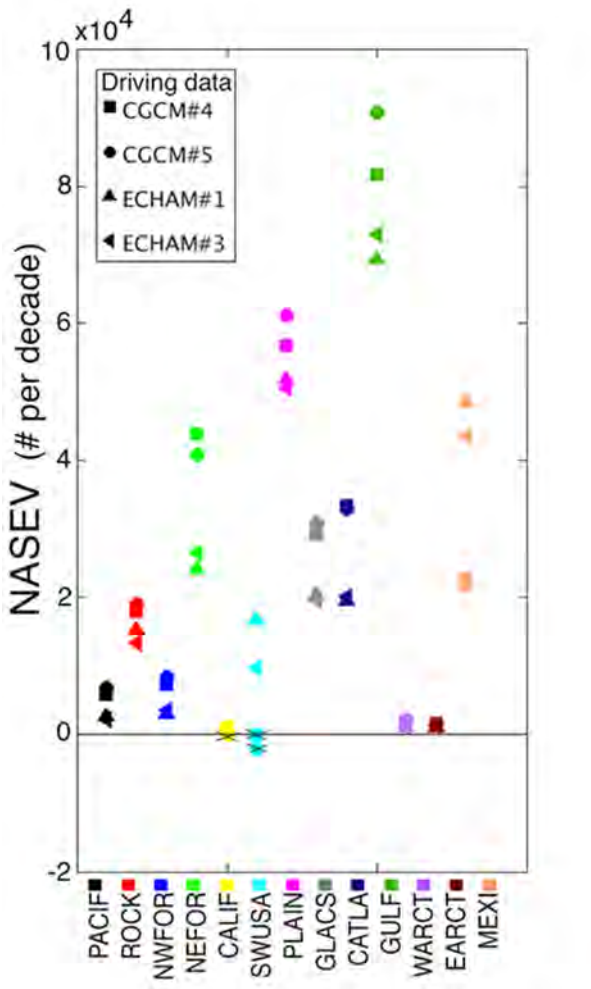


Figure 1. CRCM simulated 140-year (1961-2100) regional decadal trends of NASEV (number of events per decade) for simulations CRCM_CGCM#4 (squares), CRCM_CGCM#5 (circles), CRCM_ECHAM#1 (upward triangles) and CRCM_ECHAM#3 (left-pointing triangles). The different regiona of North America are CALIF (California), CATLA (coastal Atlantic), EARCT (east Arctic), GLACS (Great Lakes), GULF (Gulf of Mexico), MEXI (Mexico), NEFOR (north-east forest), NWFOR (north-west forest), PACIF (Pacific coast), PLAIN (Great Plains), ROCK (Rocky mountains), SWUSA (south-west USA) and WARCT (west Arctic). Statistically non-significant trend values are crossed off.

Aeronautics and Space Administration (NASA) Water Vapor Project –MEaSUREs (NVAP-M) global water vapor dataset, available from 1988-2009. Both observed and simulated extreme annual values for different Canadian regions will be compared and will allow evaluating the model performance prior to engage in a climate change study. The same evaluation will also be carried out for the CRCM4 at 15km, and for CRCM5.

4. Conclusion

In order for the regional climate community to be relevant to VIA projects, it is imperative to do model evaluation of topics and variables that are of interest for the users. By inspecting the changing conditions associated with deep convection and severe weather, we are able not to only assess their increase, but also to explain physically why they occur. By looking at the precipitable water and probable maximum precipitation, we can explore the nature of events that have very large impacts for some users, while in addition increasing our model understanding.

References

Paquin, D., R. de Elia and A. Frigon, 2014. Change of North American atmospheric conditions associated with deep convection and severe weather using CRCM4 climate projections. *Atmosphere-Ocean. DOI*: *10.1080/07055900.2013.877868*

Sensitivity of ERA-Interim driven RegCM4 precipitation to horizontal resolution

Mirta Patarčić, Ksenija Cindrić and Čedo Branković

Meteorological and Hydrological Service (DHMZ), Zagreb, Croatia (mirta.patarcic@cirus.dhz.hr)

1. Introduction

As a part of the EURO-Cordex project, two 20-yr integrations (1989-2008) of the Regional Climate Model RegCM4 (Giorgi et al. 2012) over Europe were performed at the Meteorological and Hydrological Service of Croatia (DHMZ). Both simulations were driven with ERA-Interim (Dee et al. 2011) data but at different horizontal resolutions: 50 km and 12.5 km.

In this study we validate simulated precipitation from both experiments against observed gridded data over Europe. The next step will be to focus on the Croatian mountain areas where largest precipitation amounts occur. High and steep orography and proximity of the Adriatic Sea play a major role in precipitation formation, making these regions suitable to evaluate simulated local precipitation from both experiments and assess the potential improvements in the high resolution experiment.

2. Experimental setup and observations

The domain of both RegCM4 simulations corresponds to the EURO-Cordex domain, covering Europe and parts of Greenland, northern Africa and Asia (Fig. 1). There are 142×142 grid cells in the 50 km simulation and 573x573 in the 12.5 km simulation. In the vertical, atmosphere is divided into 23 σ-levels and the model top is set to 50 hPa. Convective precipitation is computed using the Emanuel (1991) parameterisation scheme.

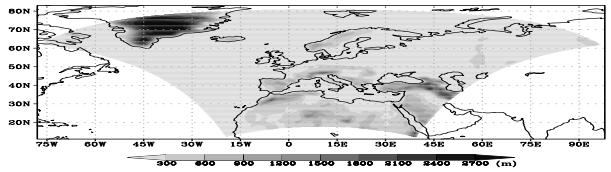


Figure 1. RegCM4 domain and topography at 50 km horizontal resolution.

Over Europe, model is validated against CRU (Harris et al. 2013) and EOBS (Haylock et al. 2008) gridded observed precipitation. RegCM4 precipitation from both experiments was interpolated to the CRU 0.5x0.5 deg and EOBS 0.25x0.25 deg regular grids. Validation is performed for simulated seasonal values with respect to both CRU and EOBS data, and for percentiles of the wet day precipitation distribution (i.e. when daily precipitation $R_d \geq 1.0$ mm) against those from EOBS.

3. RegCM4 evaluation over Europe

Fig. 2 shows the winter (December-February; DJF) and summer (June-August; JJA) systematic errors for both experiments against corresponding CRU precipitation seasonal means. RegCM4 generally overestimates seasonal precipitation except over western coastal regions of northern Europe in the winter and over the Alps in summer. Systematic errors are larger for the 12.5 km than for the 50 km simulation, particularly in the winter over mountainous regions, possibly indicating a too coarse resolution of the observed dataset for validation of the 12.5 km experiment. However, in JJA when local circulation regimes prevail, precipitation errors over the Alps are smaller in the 12.5 km simulation. Similar results, in terms of the magnitude and spatial distribution of errors, were obtained when RegCM4 was compared to the EOBS 0.5 deg seasonal precipitation (not shown).

When compared to the EOBS data at 0.25 deg, the biases of the 12.5 km simulation (Fig. 3) exhibit similar values to those in Fig. 2, bottom panels. The underestimation of precipitation over the Alps in summer is reduced, and the model slightly overestimates precipitation in this region. Over the Dinaric Alps and the Apennine peninsula, systematic errors in the summer are even larger than when compared to CRU data.

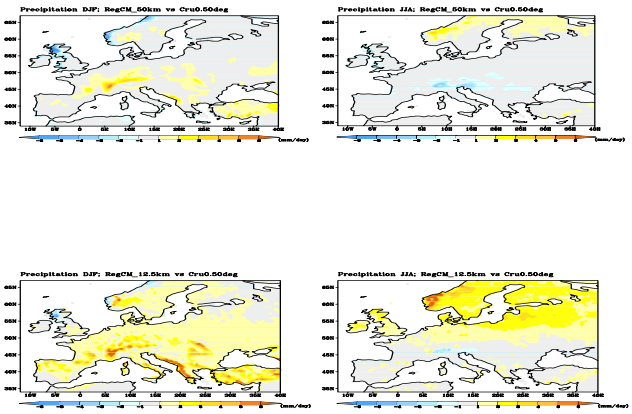


Figure 2. RegCM4 systematic errors relative to the CRU precipitation in the winter (left panels) and summer (right panels) for 50 km (top panels) and 12.5 km (bottom panels) simulation.

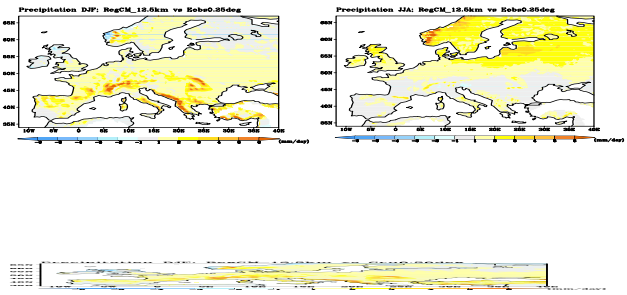


Figure 3. RegCM4 12.5 km simulation systematic errors relative to the EOBS precipitation at 0.25 deg regular grid in the winter (left panel) and summer (right panel).

For the 50 km simulated daily precipitation, biases against the EOBS data are largest in the summer when precipitation is underestimated across all but first percentiles of the daily precipitation distribution (Fig. 4). In other seasons, daily precipitation is also underestimated for most of percentiles but the magnitude of the bias is smaller than in summer. For the extreme percentiles of daily precipitation, overestimation of up to 10% is seen.

For 12.5 km simulation, underestimated daily precipitation in summer is also seen (except for the lowest and highest percentiles), but it is smaller in magnitude when compared to that for 50 km experiment. Bias is also reduced for lower percentiles in the spring and autumn. However, daily precipitation above 50th percentile is overestimated in all seasons except summer, and these biases are larger than for the 50 km simulation.

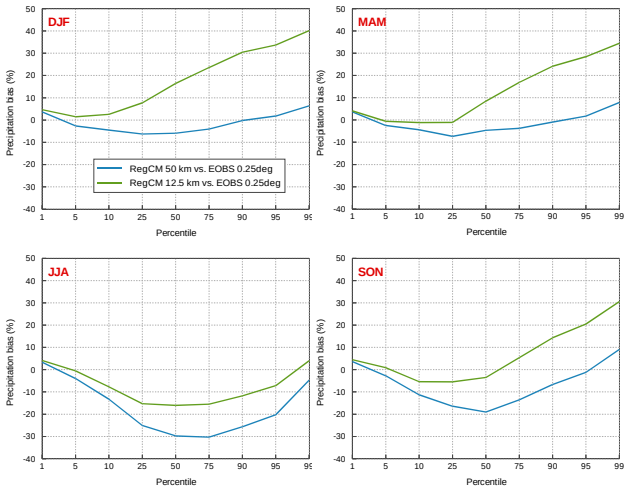


Figure 4. Seasonal RegCM4 precipitation biases, with respect to the EOBS data at 0.25 deg regular grid, for percentiles of daily precipitation distribution at wet days averaged over the area in Fig. 3. Bias is expressed in percentages of the observed values.

4. Future work

The further work is to evaluate RegCM4 precipitation against observations from stations that belong to the DHMZ station network. Additionally, model results will be evaluated against the high resolution (5 km) gridded precipitation dataset over the Alpine region (Isotta et al. 2013) which also covers a large part of Croatia. These two datasets are more suitable for evaluation of the 12.5 km experiment.

7. Acknowledgment

We thank Ivan Güttler and Lidija Srnec for their contribution in performing the RegCM4 simulations.

References

Dee DP et al. (2011) The ERA-Interim re-analysis: configuration and performance of the data assimilation system, Q J R Meteorol Soc 137, pp. 553–597

Emanuel KA (1991) A scheme for representing cumulus convection in large-scale models, J Atmos Sci 48, pp. 2313-2335

Giorgi F et al. (2012) RegCM4: model description and preliminary tests over multiple CORDEX domains, Clim Res, 52, pp. 7-29

Harris I, Jones PD, Osborn T.J and Lister DH (2013) Updated high-resolution grids of monthly climatic observations - the CRU TS3.10 dataset, Int J Climatol, 34, pp. 623-642

Haylock MR, Hofstra N, Klein Tank AMG, Klok EJ, Jones PD, New M (2008) A European daily high-resolution gridded dataset of surface temperature and precipitation, J Geophys Res (Atmospheres) 113, D20119, DOI: 10.1029/2008JD10201

Isotta FA et al. (2013) The climate of daily precipitation in the Alps: development and analysis of a high-resolution grid dataset from pan-Alpine rain-gauge data, Int J Climatol, DOI: 10.1002/joc.3794

Character analysis of observation data for model evaluation and land use changes

Swantje Preuschmann and Daniela Jacob

Climate Service Center, Helmholtz-Zentrum Geesthacht, Hamburg, Germany (swantje.preuschmann@hzg.de)

1. Introduction

This study addresses the question of validating land surface parameters in a climate model; here the REgional climate MOdel (REMO) [Jacob 2009] is considered. In this work an analysis concept exemplarily for land surface albedo is presented, revealing relevant characteristics of albedo observations. It could be proven that land use types have unique seasonal albedo curves, however, still depending on the region.

Based on this analysis, a new method is introduced, which uses observations to derive albedo characteristics for different land use types. The scheme, called Land Use CHaracter Shifts (LUCHS) allocates land use characters on considered areas for land use change. Using this method enables regional climate models to describe land use changes on an empirical basis also for future scenario conditions.

2. The concept of albedo characteristics

Due to the complex retrieval algorithms, albedo data and also vegetation indices from different satellite products are not necessarily comparable in their absolute values. Since the annual cycle of albedo is observable, this can be used for comparison. If one instrument observes an increasing albedo for one location, another instrument will also observe an increase for the same location, though the absolute values might differ substantially. One can assume that the shape of the albedo's annual cycle for one vegetation cover is similar for different satellite instruments. The characteristic information can be used like a fingerprint for the observed vegetation cover.

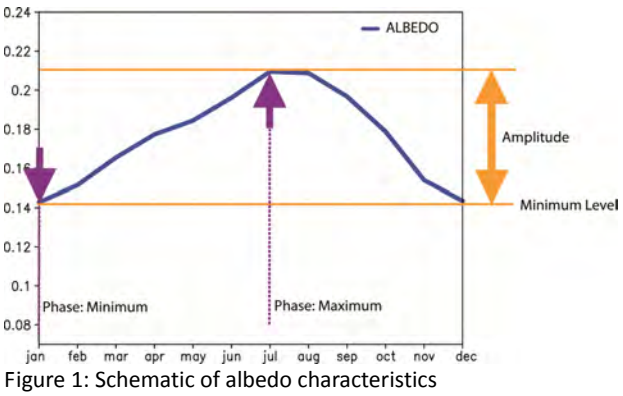


Figure 1: Schematic of albedo characteristics

An annual cycle has three main characteristic features: amplitude, phase, and minimum level. The amplitude is seen as a peak-to-peak amplitude and reflects the seasonal variability. The phase refers to the shape of the annual cycle. The dates for the minimum and maximum are important for the radiation budget. The absolute minimum level is important for a categorical classification. Summarizing these three aspects for the albedo, the expression "albedo characteristics" is used in this work. All three aspects are schematically demonstrated in Figure 1.

3. Albedo characteristics for evaluation

For model evaluation the albedo characteristics can be used for simple comparison. Within this study two albedo satellite data sets are used for showing the principals of the analysis method. Here the annual albedo amplitude, phase and albedo minimum level of REMO (α_SL4R) is compared to Albedomap (α_amap) [Fischer et al, 2007] and to MODIS (α_modis) [Schaaf et al. 2000 & Liang et al. 1999] in different horizontal resolutions, shown in figures 2, 3 and 4.

The mean amplitude in both observation data sets is about 2%. The result for the parameterized albedo from SL4R is with 0.06% almost by a factor of three smaller.

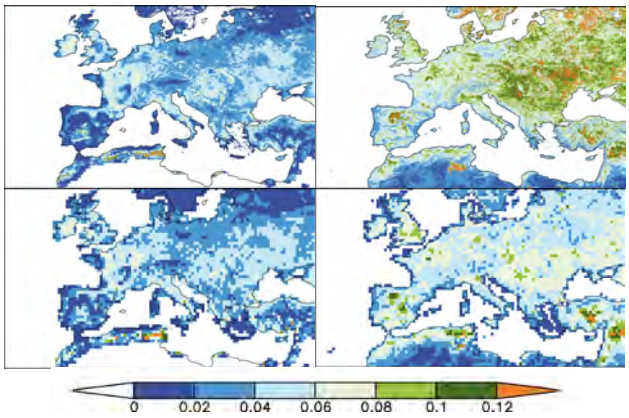


Figure 2: Horizontal visualization of amplitude per grid box. Comparison for: α_SL4R in 0.088° resolution (upper left), α_SL4R in 0.5° (bottom left), α_amap in 0.05° (upper right), α_modis in 0.5° (bottom right).

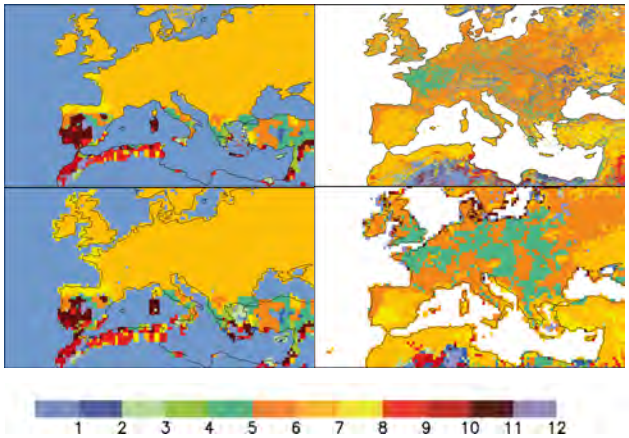


Figure 3: Same as figure 2 but appearance of month with albedo maximum. Jan=1,...,Dec=12], colors are attached to seasons: bluish (DFJ), greenish (MAM), yellowish (JJA), reddish (SON).

An occurring albedo difference at one time step due to a shift in the appearances of the albedo maxima is in the same range as the annual variability of the albedo.

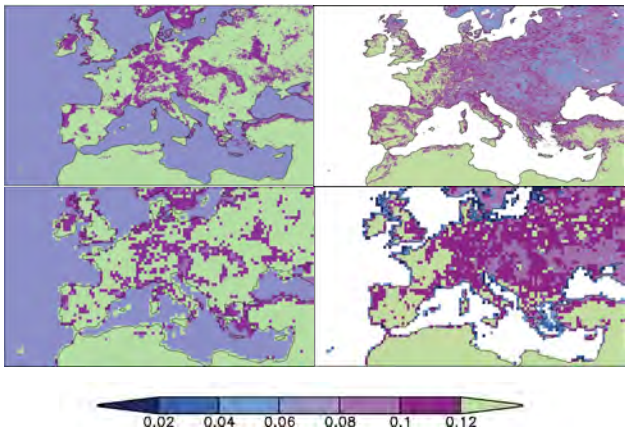


Figure 4: Same as figure 2 but for albedo minimum level.

The minimum level shows lowest observed albedo values in areas in the north of the Black Sea. This matches with the distribution of Chernozem (black soil), whereby Kondratyev et al. (1981) are reporting of albedo values of 4% for ploughed Chernozem.

5. Albedo characteristics for Land Use Change

While applying GLC2000 [Bartholome et al. 2005] masks for different land cover types of the Iberian region on α_amap, shown in figure 5, characteristic shapes in the climatologies are observable, as can be seen in figure 6. Albedo differences for different land covers are often as small as the annual cycle of albedo. The seasonal variability in albedo is varying averagely from 0.01 to 0.05 albedo percent points.

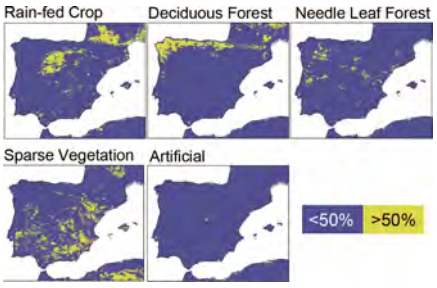


Figure 5: GLC masks for fractional coverage per grid box in 0.05° horizontal resolution. Yellow indicates more than 50% of assigned land use type.

6. Land Use Character Shifts

Land Use CHaracter Shifts (LUCHS) is the name of the new method, which uses an extracted recent annual albedo cycle for a certain land cover class in one region. This information can further on be used for spatial transfers, in case of an extension of this land cover class.

It is based on the assumption that the courses of mean seasonal albedo cycles are transferable on neighboring areas, by assuming persistence in floral, pedological and cultural conditions. LUCHS may transfer albedo characteristic information on land use classes in space and very probably also in time.

7. Conclusion

To investigate regional aspects of land-atmosphere interactions, the lower boundary description for climate models should be able to represent a realistic annual cycle of the parameters albedo, Leaf Area Index and vegetation ratio. For the annual cycle of albedo a new approach is developed in order to provide

- realistic annual cycle of albedo
- realistic regional specification of the albedo
- transfer of observed albedo information in space
- transfer of observed albedo information in time

The transfer of information for future is speculative; also LUCHS is limited onto information which is observable. The transfer for land use change scenarios is an empirical, grid based re-allocation on the highest resolution possible.

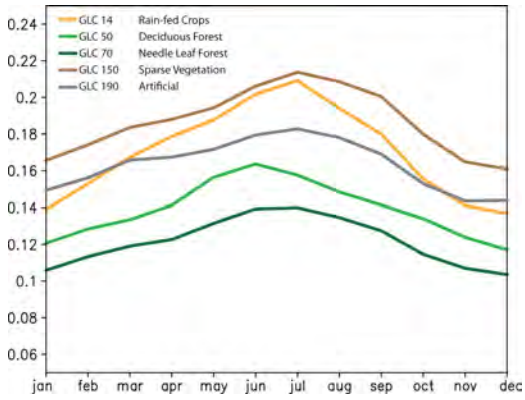


Figure 6: Iberian Peninsula annual cycles of α_amap for areas with more than 50% fractional contribution per grid box of GLC-types 14 (Rain-fed Crop), 50 (Deciduous Forest), 70 (Needle Leaf Forest), 150 (Sparse Vegetation), 190 (Artificial).

References

Bartholome, E. and A. S. Belward (2005): GLC2000: a new approach to global land cover mapping from Earth observation data. International Journal of Remote Sensing, 26(9), 1959–1977.

Fischer, J., R. Preusker, J.-P. Muller and M. Zühlke (2007): ALBEDOMAP-Validation Report - ESA AO/1-4559/04/I-LG. online.

Jacob, D. (2009): Regional Climate Models: Linking Global Climate Change to Local Impact. In: Encyclopaedia of Complexity and Systems Science, pp. 7591–7602. Springer Verlag.

Kondratyev, K. Y., V. I. Korzov, V. V. Mukhenberg and L. N. Dyachenko (1981): The Shortwave Albedo and the Surface Emissivity, pp. 463 – 514, in: Eagleson, P. S. (ed.): Land surface processes in atmospheric general circulation models. Cambridge University Press.

Liang, S., A. H. Strahler and C. W. Walthall (1999): Retrieval of land surface albedo from satellite observations: A simulation study. Journal of Applied Meteorology, 38, 712–725.

Preuschmann (2012): Regional surface albedo characteristics – analysis of albedo data and application to land-cover changes for a regional climate model. Reports on Earth System Science, 117, ISSN 1614-119.

Schaaf, C. B., F. Gao, A. Strahler, T. Tsang, W. Lucht, N. Strugnell, X. Li, J.-P. Muller, P. Lewis, M. Barnsley, P. Hobson, M. Disney, M. Dunderdale and G. Roberts (2000): The MODerate Resolution Imaging Spectroradiometer (MODIS) BRDF and Albedo Product: Preliminary Results,. Proc. Int. Geosci. Remote Sens. Symp., IGARSS 00.

Examining the impact of domain size on tropical cyclone simulations and projections over Vietnam in a regional climate model downscaling of a 5 member GCM ensemble.

Grace Redmond[1], David Hein[1] and Kevin Hodges[2]

[1] The Met Office Hadley Centre, Exeter, UK (grace.redmond@metoffice.gov.uk)
[2] Department of Meteorology, University of Reading, UK

1. Introduction

The regional climate modelling system PRECIS (Jones et al. 2004), was run at 25km horizontal resolution over two domains for 150 years (1949-2100). Global data from a five member perturbed physics ensemble (based on the coupled global climate model HadCM3) were used to drive the model. Output from these simulations are used to investigate the impact of regional model domain size on projected changes in tropical cyclones (TCs) over Vietnam and the South China Sea due to global warming (under SRES scenario A1B).

Dynamical downscaling is computationally expensive; one way to reduce this cost is to reduce the size of the domain over which the regional model is run. However, by using a smaller domain, we may not be able to capture all of the key processes relevant to the region's climatology. In this study we use two domains, the larger spanning 90-138 degrees east and -8-32 degrees north and including the majority of the TC genesis region (for those TCs which impact Vietnam), and the smaller, 92-122 degrees east and 5-35 degrees north, which only includes the western part of the TC genesis region.

When examining projected changes in TCs generated by regional models, there are a number of sources of uncertainty of which we must be aware, and, where possible, take account of. In this study, by using different domain sizes, we consider the uncertainty which comes from the regional model domain used; and, by using a perturbed physics ensemble, uncertainty which comes from the model parameterization schemes used. There are other sources of uncertainty which are not considered in this study, for example that which comes from the choice of tracking algorithm and that which comes from the choice of regional model.

By comparing results from these two domains we will firstly establish the sensitivity of tropical cyclone projections to changes in domain size, and whether using a smaller domain can produce similar results at a reduced computing cost. Also, by using a perturbed physics ensemble, we are not only able to sample an important source of uncertainty, but we are also able to examine whether changes in domain size affect the results from all ensemble members in a similar way.

2. Tracking Method

The TC tracking algorithm employed is an object based tracking (described in detail in Hodges 1995, 1999). The algorithm uses 6-hourly instantaneous 850hPa relative vorticity fields, spectrally filtered to T42 resolution (which minimises noise) to identify vortices, which appear as maxima (minima) in the Northern (Southern) hemispheres. This vorticity feature is then isolated from the background field and tracked coherently in space and time. To identify a track as a tropical cyclone a number of filters are used.

3. Initial results

Firstly the models ability to realistically simulate present day TCs over Vietnam was evaluated with 30-year present day simulations compared to IbTRACS observations (A full description of this dataset can be found in Kruk et al. 2010.) Both the smaller and larger domain are able to capture the spatial distribution and timing of October-December (OND) TCs which mostly impact the central and southern parts of Vietnam; however, too few June-September (JJAS) TCs are generated in both domains. Contrary to initial assumptions, JJAS TCs are simulated better in the small domain.

All ensemble members and both domains project that by the end of the century (2070-2099) the number of TCs will decrease by 20-44%, but the amount of precipitation associated with TCs will increase by 27-53%. Changes in intensity are unclear in the larger domain, but all ensemble members in the smaller domain project a small increase of 3-9% in maximum 10m wind speed.

The somewhat unexpected result that JJAS TCs are better reproduced in the smaller domain will be investigated further.

References

Hodges, K. I. 1995. Feature tracking on the unit-sphere. Monthly Weather Review, 123, 3458-3465.

Hodges, K. I. 1999. Adaptive constraints for feature tracking. Monthly Weather Review, 127, 1362-1373.

Jones, R. G., M. Nouger, D. C. Hassell, D. Hudson, S. S. Wilson, G. J. Jenkins, and J. F. B. Mitchell, 2004: Generating high resolution climate change scenarios using PRECIS. Met Office Hadley Centre Rep., 40 pp.

Kruk, Michael C., Kenneth R. Knapp, David H. Levinson, 2010: A Technique for Combining Global Tropical Cyclone Best Track Data. J. Atmos. Oceanic Technol., 27, 680–692.

On the variability in a regional climate model using dynamical downscaling with frequent reinitializations

Thomas Remke and Daniela Jacob

Climate Service Center (CSC), Helmholtz-Zentrum Geesthacht, Hamburg, Germany (thomas.remke@hzg.de)

1. Introduction

Regional climate models are extensively used to dynamical downscale large-scale climate information to generate small-scale and fine-scale detail. An alternative procedure to the common continuous downscaling approach is to frequently reinitialize the three-dimensional atmospheric driving fields. This procedure retains the sequence of meteorological events inherent to the forcing data. Certain model applications, such as land-surface models, impact models or tools for identifying and assessing hydrological extremes, or impact studies rely on such high resolution data.

Lucas-Picher et al. (2013) evaluated this procedure with respect to the hydrological cycle and extreme events. They reported reduced systematic errors and generated reliable added value while providing a sequence of meteorological events matching with observations, compared to a standard continuous regional climate model simulation. Furthermore, they conclude high resolution data sets generated with regional climate models using frequent reinitializations to better suit the needs of impact studies, since they reproduce observation-based weather events in space and time when driven with an atmospheric reanalysis.

Besides these benefits, the method of dynamical downscaling with frequent reinitializations could bear disadvantages. The reinitialization of the entire model-atmosphere is a strong forcing towards its driving data. Preventing drift could result in a reduction of model generated variability. Until now, just few studies addressing dynamical downscaling with frequent reinitializations have been carried out in a climate context. The impact of frequent reinitializations on the simulated long-term climate and climate variability have not been assessed extensively.

2. Experiment Design

The regional climate model REMO (e.g. Jacob and Podzun, 1997) is capable of simulating climate for various regions over the globe without any additional tuning necessary. In addition, it can be used in a climate as well as in a forecast mode (Jacob, 2001). The former one implies a continuous simulation, starting with initial conditions and updated lateral boundary conditions every six hours as well as updated lower boundary conditions once per day, allowing for simulations of several decades. The latter one depicts consecutive simulations over a fixed forecast period, e.g. 24 hours, starting with initial conditions and being restarted again with initial conditions after this period.

To investigate the impact of frequent reinitializations on the simulated long-term climate and climate variability, a standard continuous and a frequent (daily) reinitialized model simulation with the regional climate model REMO are analysed. Both simulations are using the same configuration, except for the treatment of the driving fields. Thus, the direct effect of frequent reinitializations on the simulation with the regional climate model REMO can be assessed. In this manner, the ERA-Interim reanalysis is downscaled over the European CORDEX domain at a horizontal resolution of 0.11 degree for the period from 1989 to 2008.

Analysed is the direct effect of frequent reinitializations on the simulation of climate with the regional climate model REMO focussing on the temporal variability. Therefore, the spatial distribution as well as the time series for different regions over Europe representing regional climate are analysed. The analysis is based on three different parameters being characterised by processes acting on different spatial and temporal scales, namely the wind speed, the temperature and the mean sea level pressure. Two reanalyses data sets, ECMWF's ERA-Interim reanalysis and NASA's MERRA reanalysis, serve as reference to the model simulations.

3. Results

Overall, REMO is able to reproduce the mean climate over Europe generating small-scale and fine-scale detail, despite of the treatment of the driving fields. Additionally, the temporal evolution, the annual cycle and the diurnal cycle of all three variables are well simulated by both simulations. Thus, the simulated long-term climate does not get affected significantly.

Nonetheless, the reinitialized simulation is staying closer to the driving data in the majority of cases. This is expressed in relatively lower deviations present for, especially, the mean sea level pressure (Figure 1) and the temperature (Figure 2), visible in their spatial patterns throughout the year as well as in their time series at all temporal scales. This is in agreement to a higher spatial and temporal correlation of the reinitialized simulation.

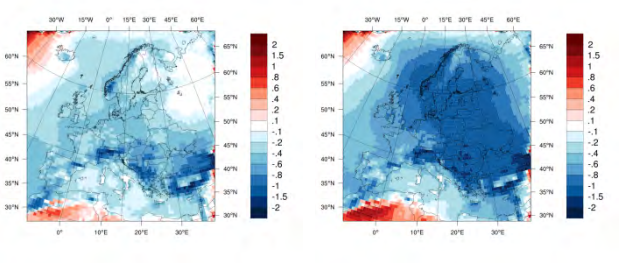


Figure 1. Multi-year annual mean differences of mean sea level pressure between the REMO simulations (left: reinitialized, right: continuous) and the ERA-Interim reanalysis for the period

1989 to 2008. The colors indicate mean sea level pressure differences in hPa. Red colors denote a positive, blue colors a negative deviation of the REMO simulation.

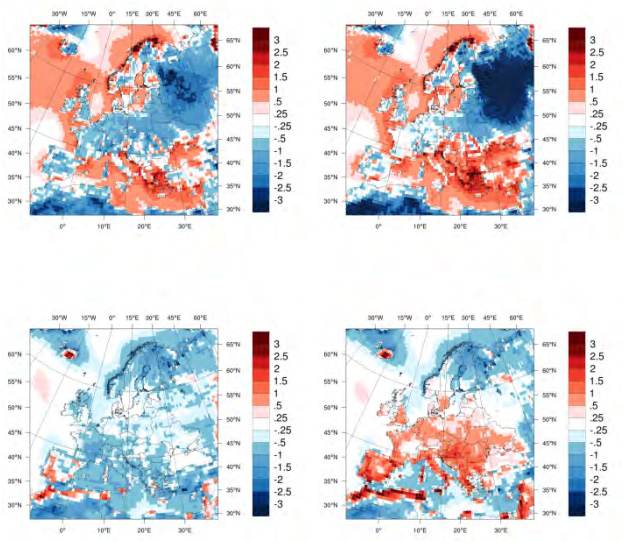


Figure 2. Multi-year winter (DJF, top row) and summer (JJA, bottom row) mean differences of 2 m temperature between the REMO simulations (left column: reinitialized, right column: continuous) and the ERA-Interim reanalysis for the period 1989 to 2008. The colors indicate 2 m temperature differences in K. Red colors denote a positive, blue colors a negative deviation of the REMO simulation.

Contrary to the temperature and the mean sea level pressure, the wind speed does not seem to be significantly closer to the driving data when being reinitialized, even though its temporal correlation is slightly higher. Nonetheless, deviations between both REMO simulations are present on a seasonal scale (Figure 3), which are most likely associated to local wind systems. These are mainly located over the Mediterranean Sea. The diurnal cycle over designated areas indicates discrepancies in the occurrence of wind speeds at an early stage of the simulated 24-hour slices of the reinitialized simulation. This could be an indicator for a local enhancement or dampening of wind speeds through reinitializing the atmospheric fields.

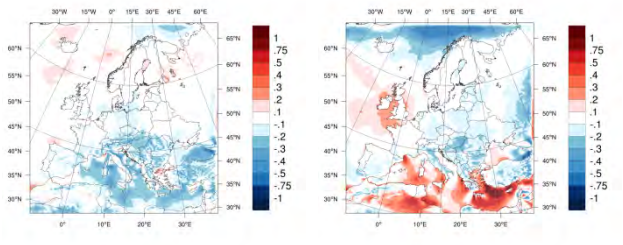


Figure 3. Multi-year winter (DJF, left) and summer (JJA, right) mean differences of 10 m wind speed between both REMO simulations for the period 1989 to 2008. The colors indicate 10 m wind speed differences in ms^{-1}. Red colors denote a positive, blue colors a negative deviation of the REMO reinitialized simulation.

Despite of staying closer to the driving data in the majority of cases, the deviations between both REMO simulations are comparably smaller than the deviations between both simulations and the reanalyses. Also similar deviation-patterns between the REMO simulations and the reanalyses occur. Even though, they might differ in their amplitudes, this reveal systematic inherent to the REMO simulations.

Preventing drift through reinitializing the atmospheric fields is associated with a dampening in its standard deviation for all analysed parameters and on all temporal scales. Thus, there is clear evidence that frequent reinitializations generate less variability on all temporal scales.

4. Conclusions

Dynamical downscaling with frequent reinitializations towards its driving fields prevents drift. Thus, this method potentially corrects for systematic errors inherent to the model. However, this is at the expense of model generated variability on all temporal scales compared to a standard continuous simulation.

Overall, dynamical downscaling with frequent reinitializations is a beneficial tool to increase the spatial and temporal resolution, while retaining the sequence of meteorological events inherent to the forcing data. Because atmospheric reanalysis products or other methods do not provide climate information to this extent, the procedure of dynamical downscaling with frequent reinitializations has potential. Nonetheless, the constraints in terms of generated variability might be a limitation to certain applications, according to their individual requirements on the data.

5. Outlook

A validation with observations is necessary to clarify the quality of this climate data set. Furthermore, the analysis should be extended for additional parameters and their extremes.

When this quality control is successfully completed, this climate data set could serve as forcing data for certain model applications or impact studies as well as be used for investigating and identifying processes accounting for systematic errors inherent to the model.

References

Jacob, D. and R. Podzun (1997) Sensitivity studies with the regional climate model REMO, Meteorology and Atmospheric Physics, Vol. 63, No. 1-2 , pp. 119–129

Jacob, D. (2001) A note on the simulation of the annual and inter-annual variability of the water budget over the Baltic Sea drainage basin, Meteorology and Atmospheric Physics, Vol. 77, No. 1-4, pp. 61–73

Lucas-Picher, P., F. Boberg, J.H. Christensen and P. Berg (2013) Dynamical downscaling with reinitializations: a method to generate fine-scale climate data sets suitable for impact studies, Journal of Hydrometeorology, Vol. 14, No. 4, pp. 1159-1174

Evaluation of Dynamical Downscaling Resolution Effect on Wind Energy Forecast Value for a Wind Farm in Central Sweden

Martin Haubjerg Rosgaard[1], Andrea Noemí Hahmann[2], Torben Skov Nielsen[1], Gregor Giebel[2], Poul Ejnar Sørensen[2] and Henrik Madsen[3]

[1] ENFOR A/S, Denmark (mhr@enfor.dk)

[2] Department of Wind Energy, Technical University of Denmark

[3] Department of Applied Mathematics and Computer Science, Technical University of Denmark

1. Introduction

For any energy system relying on wind power, accurate forecasts of wind fluctuations are essential for efficient integration into the power grid. Increased forecast precision allows end-users to plan day-ahead operation with reduced risk of penalties which in turn supports the feasibility of wind energy.

The present study aims to quantify value added to wind energy forecasts in the 12-48 hour leadtime by downscaling global numerical weather prediction (NWP) data from the National Centers for Environmental Prediction Global Forecast System (GFS) using the limited-area NWP model described in Skamarock et al. (2008).

2. Performance metric

For leadtimes beyond six hours ahead NWP input is needed for statistical wind power forecasting tools, see e.g. Giebel et. al. (2011). Typical performance metrics are mean absolute error or root mean square error for predicted against observed wind power production, and these metrics are closely related to wind speed forecast bias and correlation with observations. Wind speed bias can be handled in a statistical wind power forecasting model, though it is entirely up to the NWP input to describe the timing of wind speed fluctuations correctly. Correlation between observed and forecasted values is one metric addressing this aspect of model performance.

3. The dataset

Forecasts from global and limited-area NWP models, together covering five different horizontal computational grid spacings of ~50km down to ~1km, are studied for a yearlong, continuous time period. The basis of comparison for forecasts is farm-averaged data from the 40 turbines of the Stor-Rotliden wind farm in central Sweden. The surrounding forest and uneven terrain adds to the forecasting challenge, thus motivating the downscaling experiment as potential for wind power forecast improvement is higher in complex terrain.

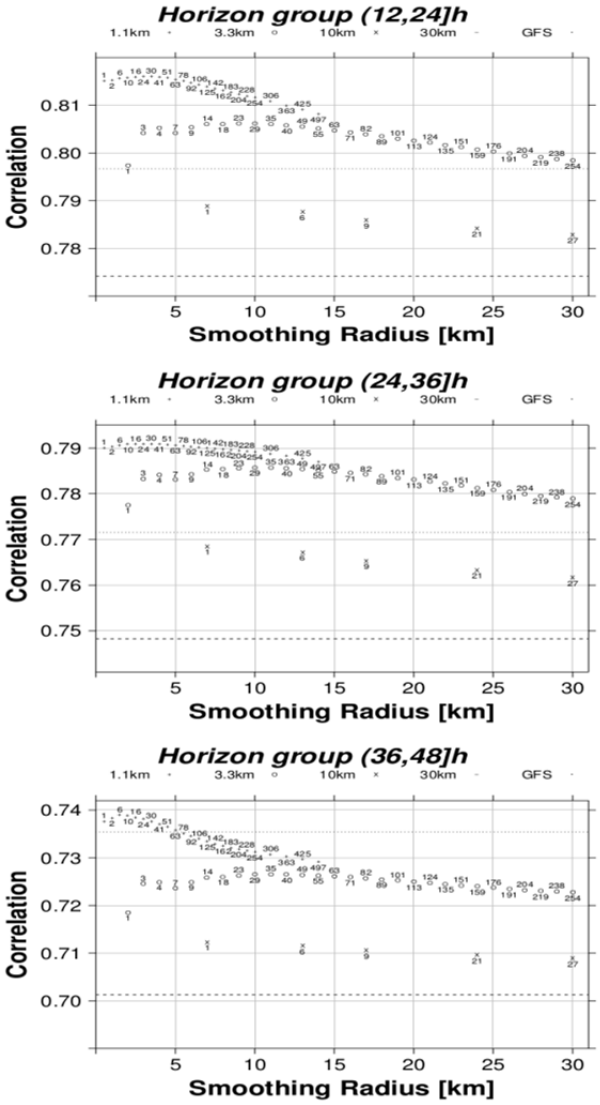


Figure 1. Correlation between observed and forecasted wind speed vs. the distance bounding the half-tricube weighting function used for spatially smoothing wind speed values at high-resolution NWP model grid points. Above/below datapoints are noted the number of computational grid points with non-zero weight.

4. Results

In Fig. 1 correlation dependence on spatial smoothing radius is shown along with the number of computational grid points within a given radius. Each of these grid points are assigned a weight determined by a half-tricube

function that decreases from maximum near the wind farm centre to zero at the radius.

In Fig. 2 the 1.1km computational grid points covering the spatial extent of the Stor-Rotliden wind farm are sketched.

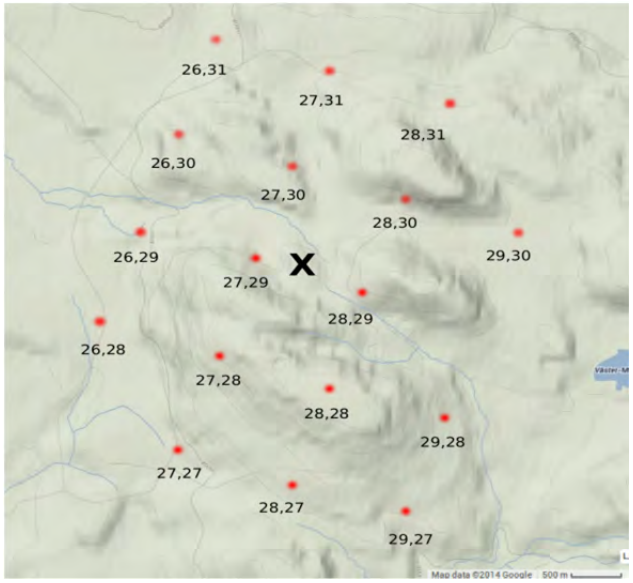


Figure 2. High-resolution computational grid points covering the Stor-Rotliden wind farm. **X** is the average of turbine coordinates and marks the reference point for smoothing radii.

Fig. 3 shows the correlation of each grid point sketched in Fig. 2, ordered according to distance from the wind farm centre **X**.

5. Conclusion

The optimal smoothing radius for the 1.1km computational grid decreases as a function of forecast leadtime, as shown in Fig. 1. This can be explained by increased phase errors which cause grid points in the vicinity of the wind farm to be less likely to capture in space the wind speed observed at turbine hub height. A similar effect is not observed for the 3.3km grid for which the curve appears to be parallel shifted for different horizon groups. Perhaps not surprisingly, no performance gain is detected from smoothing 10km data.

Fig. 3 shows that the three 1.1km grid points closest to the average of the 40 turbine coordinates – the **X** in Fig. 2 – are also the ones best correlated with the farm-averaged wind speed observations for all three horizon groups. Also, there is a constant ~0.05 difference between best and worst correlation.

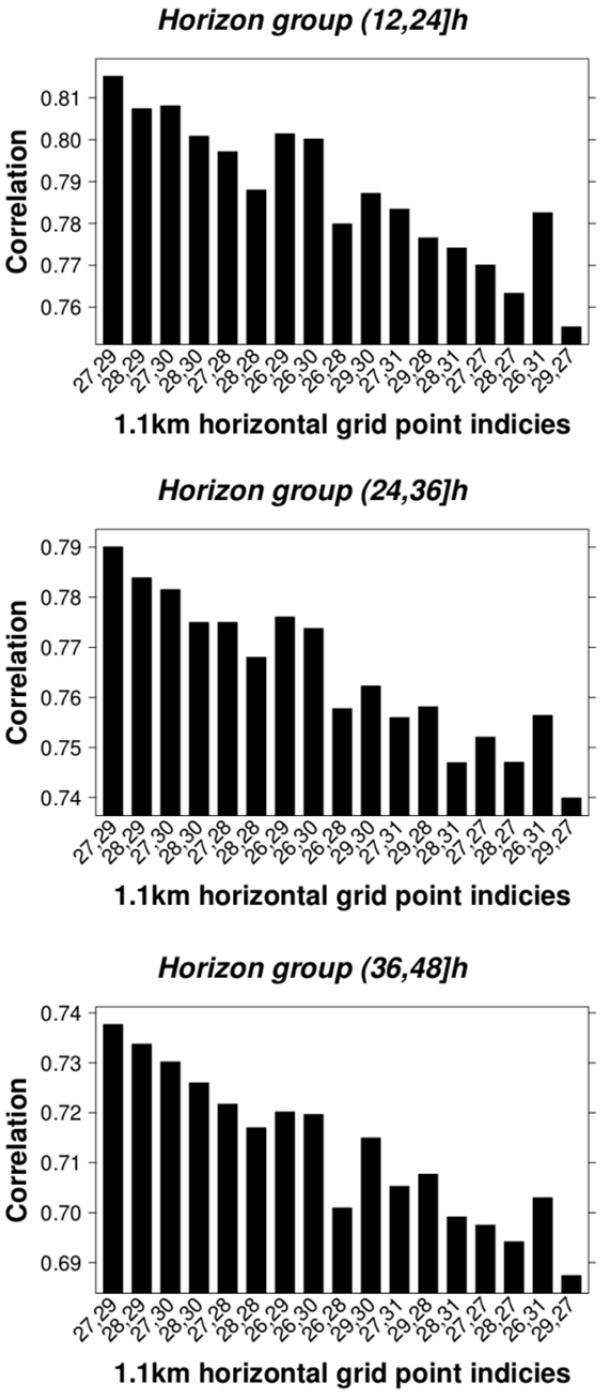


Figure 3. Correlation between observed wind speed and 1.1km grid forecasts for individual points covering the spatial extent of the Stor-Rotliden wind farm. Indices are relative to the 60km by 60km horizontal 1.1km grid at turbine hub height extracted from the raw forecast data for use in the present analysis.

References

William C. Skamarock, Joseph B. Klemp,Jimy Dudhia, David O. Gill, Dale M. Barker, Michael G. Duda, Xiang-Yu Huang, Wei Wang Jordan G. Powers (2008) A Description of the Advanced Research WRF Version 3, NCAR Technical Note

Gregor Giebel et al. (2011) The State-Of-The-Art in Short-Term Prediction of Wind Power, ANEMOS.plus deliverable D-1.2

A Markov chain method to determine the dynamic properties of compound extremes and their near future climate change signal

Katrin Sedlmeier, Sebastian Mieruch, Gerd Schädler
Institute for Meteorology and Climate Research, KIT, Karlsruhe, Germany (katrin.sedlmeier@kit.edu)

1. Introduction

Reliable knowledge of the change signal of extreme events is an important issue for studies related to climate change. In recent years compound extremes (in the sense of two or more extremes occurring simultaneously or consecutively) are receiving more and more attention in the scientific world because of their great impact on society. It is therefore of great interest how well state-of-the-art regional climate models can represent the dynamics of multivariate extremes. Furthermore, the near future climate change signal of compound extremes is interesting, especially on the regional scale because high resolution information is needed for impact studies and mitigation and adaptation strategies. Based on a work by Mieruch et al. (2010), we use a Markov Chain method to assess these two questions.

2. Data and Methods

We use an ensemble of high resolution (7km) regional climate simulations for Central Europe with the COSMO-CLM regional climate model (Doms and Schättler, 2002; Rockel et al., 2008). The ensemble currently consists of 10 members, with different global climate models, some with different realizations, as driving data. Furthermore, we used the Atmospheric Forcing Shifting Method (Sasse and Schädler 2013). The time periods considered are a control period (1971-2000) and the near future (2021-2050) and running windows within these time periods. For comparison, E-Obs and HYRAS gridded observational datasets are used.

The method we use is based on the representation of multivariate climate anomalies by first order homogeneous Markov Chains. A first order Markov Chain is a time-discrete stochastic process where the present state only depends on the preceding one. The conditional probability with which a state i is followed by a state j can be summarized in a transition probability matrix which is time independent for homogeneous Markov Chains. From the transition matrix several descriptors such as persistence (how long does the system stay in the current state?), recurrence time (how long does it take until the system comes back to the state?) and entropy (measure of predictability) are derived, which characterize the dynamic properties of the multivariate system.

We partition our dataset into extreme and non-extreme regimes and reduce the multivariate dataset to a univariate symbolic sequence which can then be described as a discrete stochastic process, a Markov Chain.

3. First Results

The Markov Chain method is currently applied to temperature and precipitation data. Analysis of other combinations of variables is planned. By comparing the descriptors for model and observation data, the representation of the dynamics of the climate system by different models is evaluated and the representation by the ensemble mean assessed. This is done for each grid point, thus regional differences can be investigated. Near future shifts or changes of the dynamics of compound extremes are detected by using regional climate projections and comparing the descriptors for different time periods. First results show that the representation of the climate dynamics differs between variables and regions.

References

Doms G, Schättler U (2002) A Description Nonhydrostatic Regional Model LM, Part I: Dynamics and Numerics, Consortium for small-scale modelling, Deutscher Wetterdienst, Offenbach, Germany

Mieruch S, Noel S, Bovensmann H, Burrows JP, Freund JA (2010) Markov chain analysis of regional climates, Nonlin. Processes Geophys., Vol17, pp.651-661

Sasse R, Schädler G (2013) Generation of regional climate ensembles using Atmospheric Forcing Shifting, Int.MetZ, Climatol. doi: 10.1002/joc.3831

Rockel B, Will A, Hense A (2008) The Regional Climate Model COSMO-CLM (CCLM), MetZ, Vol17, No.4, pp.347-348

Evaluating teleconnection responses of the CORDEX models: A case study over Eastern Africa

Hussen Seid, Christopher Lennard and Bruce Hewitson

Climate System Analysis Group, University of Cape Town, Cape Town, South Africa (hussen.seid1@gmail.com)

1.Introduction

Rainfall variability associated with sea surface temperature (SST) anomalies is known to largely affect the economy of many regions of the globe particularly regions that are depend on rain-fed agriculture. Regional climate models(RCMs) are presently one of the fundamental tools used to study recent and future climate variability and change(Giorgi, et al., 2009). However, accurate simulation of rainfall still remains a major challenge in regional climate models. Thus, a process based comparison of models with observation is required to understand the limitation of the models and to provide guidance for model improvement.

This study examines the ability of COordinated Regional climate Downscaling EXperiment (CORDEX) models, with lateral and surface boundary conditions drived from Coupled Ocean-atmosphere General Circulation Models (AOGCMs), in simulating rainfall teleconnection patterns over Eastern Africa region.

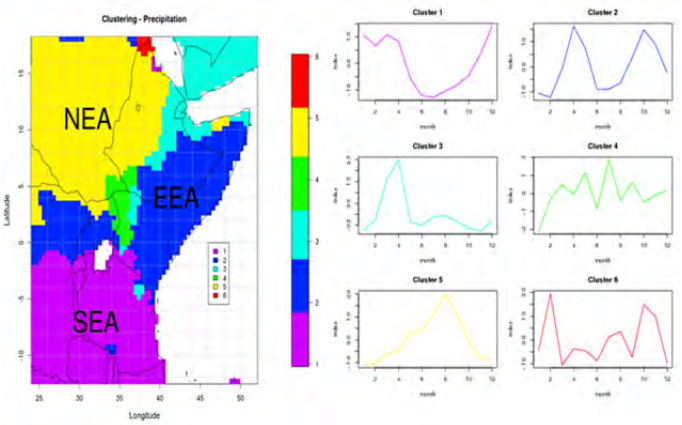


Fig 1: Study region. The left side show the homogeneous rainfall regions and the right side indicate the corresponding annual cycles as categorized using Ward's hierarchical clustering technique. The area of analysis are Northern part of Eastern Africa (NEA-yellow), Equatorial part of Eastern Africa (EEA-blue) and Souther part of Eastern Africa (SEA-pink).

2. Data and methodology

The models that we used for this study are Rossby Centre regional atmospheric model(RCA4) driven by 8 CMIP5 GCMs(CanESM2, CNRM-CM5, EC-EARTH, GFDL-ESM2M, HadGEM2-ES, MIROC5, MPI-ESM-LR and NorESM1-M) and COSMO Climate Limited-area Modelling(CCLM4) driven by four the same CMIP5 GCMs(CNRM-CM5, EC-EARTH, HadGEM2-ES and MPI-ESM-LR). In order to investigate the source of the errors, data from the parent GCMs are also analyzed. Additionally, GCM-driven RCM results are compared with the results Era-Interim driven results.

Teleconnection patterns are examined using regression and correlation analysis. It would be important to note that for CORDEX Africa simulations, the first member from the CMIP5 GCMs is used to force the RCMs(except EC-EARTH model). Therefore, for our analysis, we used the SST from the parent GCM (1st member) and rainfall from the RCMs(1st member) to compute SST-rainfall teleconnection.

The focus of this study is at seasonal time scale. The seasons used are JJAS for NEA, and OND for EEA and SEA. Since the main focus of this study is to look at the model response on the teleconnection signals, we filtered any long-term changes/trend in both observed and simulated time series. Thus, all seasonal time series have been detrended linearly at each grid point. Then SST at a grid-point is correlated against a spatially averaged rainfall time series in order to identify oceanic regions which have strong relationship with the regional seasonal rainfall. Once we have identified these regions that have strong relation with regional rainfall, precipitation at a grid-point is regressed against a spatially averaged SST time series (results not shown). Appropriate t-tests are used in both the rank and linear methods to resolve grid-points that meet or pass 95% confidence levels.

3. Results and Discussion

Figure 2 shows the spearman's rank correlations between JJAS rainfall area averaged over NEA, against concurrent grid-point SSTs. As it has been mentioned above in data and methodology section, RCA4 model was driven by 8 GCMs, whereas CCLM was driven by 4 GCMs. For direct inter-comparison of GCM and downscaled results, fig.2 contains two panels (top and bottom). The top panel show the 4 driving GCMs(left), 4 GCMs downscaled by RCA4(middle) and 4 GCMs downscaled by CCLM4(right), whereas the bottom panel shows the remaining 4 GCMs and the downscaled RCA4 results.

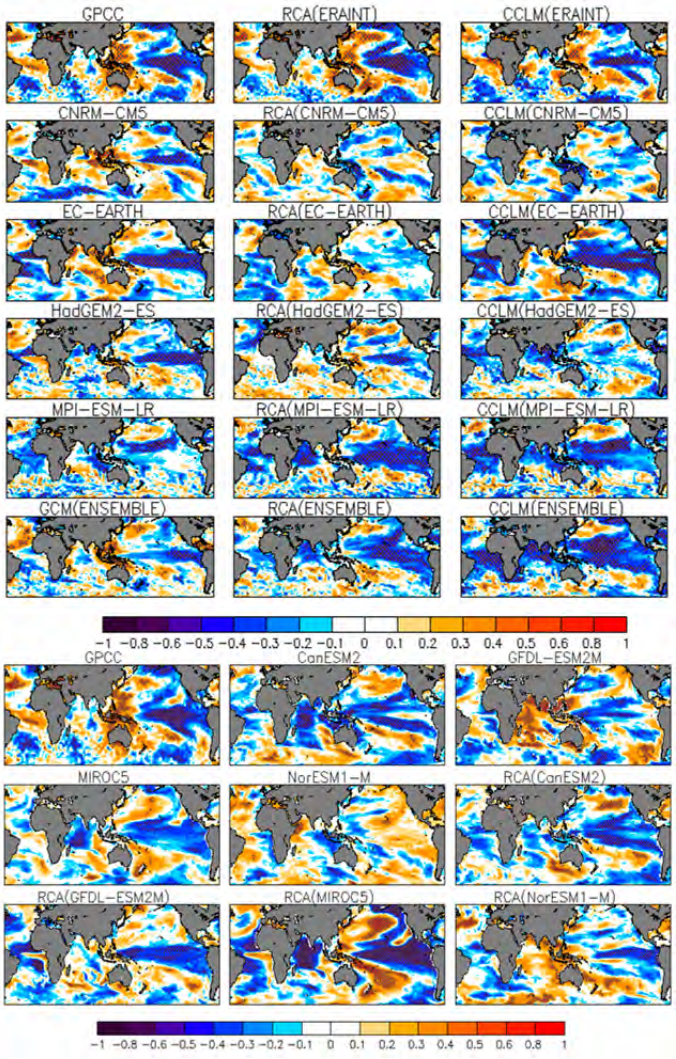


Fig 2: Correlations of JJAS rainfall averaged over NEA, against concurrent grid-point SSTs. Patterns indicate statistically significant correlations at 95% confidence level

The observed dataset GPCC (top left) shows that JJAS rainfall in the northern part of the region has significant correlation with SSTs in Eastern equatorial Pacific, with a positive rainfall anomaly tends to occur during the cold phase of ENSO, while dry conditions prevail during the warm phase ENSO. This signal is well captured by Era-Interim driven RCMs. But there is a wide disagreement in capturing the teleconnections when these two RCMs were driven by GCMs and as well as in the parent GCMs. Meant that some models reproduces number of observed features, while others show the opposite signal. For example, CanESM2, MIROC5, RCA(MIROC5), and RCA(CanESM2) show strong negative correlation, while GFDL-ESM2M shows strong positive correlation with central Indian Ocean which is not observed with our reference dataset(see fig2 lower panel). In addition, NorESM1-M show positive correlation with eastern equatorial pacific which is opposite to the observed signal.

4. Summary and conclusions

This study examines the ability of CORDEX models to represent the main teleconnections between the Eastern Africa rainfall and the tropical sea surface temperatures. Simulated seasonal rainfall teleconnection patterns are compared to observations for the period 1982-2005. In general, our analysis indicated that most of the errors in simulating the teleconnection patterns are coming from the GCMs/drivers. The RCMs driven by reanalysis (nearly perfect boundary conditions) are well captured the rainfall teleconnections in most of the subregions and seasons. Concerning to individual models, RCMs driven by HadGEM2-ES, MPI-ESM-LR and GFDL-ESM2M are relatively performed better than RCMs driven by other GCMs. It's also showed that these three GCMs performed consistently better than other GCMs. The paper concluded that the boundary conditions given to the RCMs is the most important parameter in simulating the teleconnection patterns, and therefore more work has to be targeted towards improving the boundary forcing given to the regional climate models.

5. References

Giorgi, F., Jones, C. and Asrar, G. R., 2009: Addressing climate information needs at the regional level: the CORDEX framework. World Meteorological Organization bulletin, 58, 175-183.

Simulation Strategies for Optimal Detection of Regional Climate Model Response to Parameter Modifications

Leo Separovic[1], Ramón de Elía[2] and René Laprise[1]

[1] Université du Québec à Montréal (presently at Environment Canada, leo.separovic@ec.gc.ca)
[2] Consortium Ouranos

1. Introduction

When assessing the impact of Regional Climate Model (RCM) modifications on the downscaled information, the issue the researcher faces is the detection of the model response to modifications (signal) among the noise originating from the intrinsic variability of the system. A distinct feature of RCM-simulated variability is that it is contributed from two sources: (1) sensitive dependence to arbitrary small modifications, such as perturbations in the initial conditions, and (2) variability forced through the lateral and lower boundary conditions (LLBC). Sensitive dependence can represent a nuisance in RCM testing and development if large ensembles are needed in order to obtain statistically significant responses to modifications. In Separovic et al. (2012) the application of spectral nudging (SN; von Storch et al. 2000) at upper atmospheric layers reduced the RCM sensitive dependence in single-year integrations, thus helping to increase the statistical significance of the estimated difference of mean response to perturbations of physics parameters.

In our present study a more general framework for quantifying RCM intrinsic variability is employed, in order to account for effects of both sensitive dependence and variability enforced through the LLBC on model response to parameter modifications.

2. RCM intrinsic variability

In order to account for sensitive dependence on small inaccuracies in the initial conditions, it is convenient to think of an RCM variable ψ at a given grid point as a random variable that depends on ensemble member m and time t_k, which can be summarized as follows:

$$\psi_{km} = \mu + f_k + \varepsilon_{km}. \quad (1)$$

Here, μ is the overall expectation of ψ, while $\mu+f_k$ is the expectation of ψ at specific times t_k. The reproducible part of the anomaly, f_k, represents the components of time variations common to all ensemble members. It arises in response to the specific LLBC that all ensemble members share at time t_k. The irreproducible part of the anomaly, ε_{km}, originates in the sensitive dependence and it is distinct in every ensemble member.

Since the ensemble members are statistically indistinguishable, they all have the same mean and reproducible anomalies f_k, as well as other statistics, in the limit of sufficiently long integrations. The expected members' temporal (or so called transient-eddy; TE) variance can be decomposed as

$$\sigma_{TE}^2 = \sigma_f^2 + \sigma_\varepsilon^2, \quad (2)$$

where σ_f^2 and σ_ε^2 are the variances of the reproducible and irreproducible components (Separovic et al. 2008). The TE variance is an observable; when an RCM is driven by reanalyses, one hopes that the temporal variability of the simulations is close to that of the true atmosphere. Unlike the sum of the reproducible and irreproducible variances, however, there are no general recommendations about the relative magnitude of the reproducible and irreproducible variances in RCM simulations. In RCM simulation configurations characterized with small ensemble variance, such as in spectrally nudged simulations, the small irreproducible variance component has to be compensated by a larger reproducible variance in order to conserve the sum of the two components.

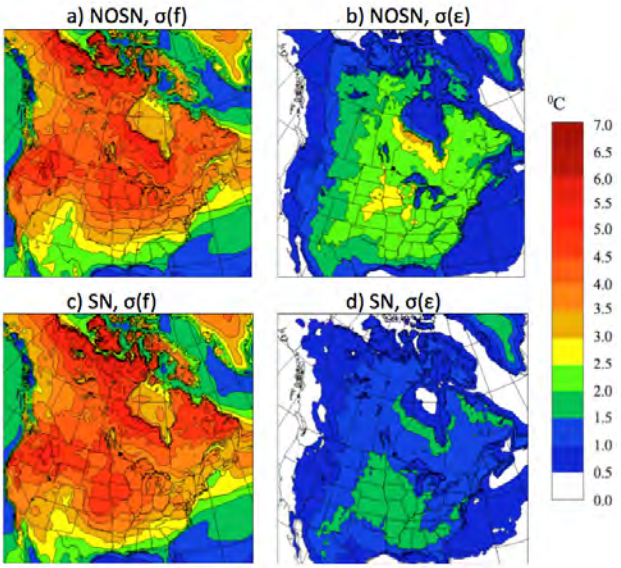


Figure 1 Reproducible (a, c) and irreproducible (b, d) components of the TE variance in CRCM5-simulated summer daily screen-level temperature in no-SN (a, b) and SN configurations (c, d).

Figure 1 displays the reproducible and irreproducible variance components in two 10-member ensembles of 1993-2002 ERA40-driven integrations with the Canadian RCM, version 5 (CRCM5; Zadra et al. 2008), for summer (JJA) daily screen-level temperatures (SLT). The upper (bottom) row in Fig. 1 displays results from non-SN (SN) ensemble, respectively. The SN setup is described in Separovic et al. (2012). The reproducible (irreproducible) components are shown in the left (right) columns, respectively. It can be seen in Fig. 1 that the reproducible TE variance is considerably larger than the irreproducible component, even without spectral nudging (Fig. 1a, b) for SLT.

3. Variability of RCM response to modification

In what follows, we present the CRCM5 1993-2002 JJA daily-averaged SLT response to an increased threshold parameter in the Kain-Fritsch deep convection parameterization, estimated from 10-member ERA40-driven ensemble integrations with the control and modified model, conducted within identical setup. This parameter modification results in increased mean JJA SLT by 1-2 °C over land (see Separovic et al. 2012 for details). Here we focus on the second-order statistics.

Difference $\Delta\psi$ between the values obtained from control and modified model versions, ψ_1 and ψ_2, respectively, can be also decomposed into the difference of means, reproducible and irreproducible time anomalies, similarly as in Eq. (1). This permits decomposition of the TE mean-square difference (MSD) into reproducible and irreproducible components as

$$msd = \sigma^2_{\Delta f} + \sigma^2_{\Delta\varepsilon}, \qquad (3)$$

where

$$\sigma^2_{\Delta f} = \sigma^2_{f_1} + \sigma^2_{f_2} - \sigma_{f_1}\sigma_{f_2} r_{f_1,f_2} \qquad (4)$$

$$\sigma^2_{\Delta\varepsilon} = \sigma^2_{\varepsilon_1} + \sigma^2_{\varepsilon_2} \qquad (5)$$

Here, r is the time correlation between the reproducible anomalies f_1 and f_2 in the two CRCM5 versions. This correlation must be accounted for because the control and the modified ensemble simulations are driven with the same LLBC. The irreproducible anomalies ε_1 and ε_2 are, however, independent and their correlation vanishes. The TE MSD quantifies the variability in the sample of differences between two models; reduction of the variability in the sample of differences increases the statistical significance of estimates of RCM response to modification.

Figure 2 shows the estimated temporal correlation r between the reproducible anomalies f_1 and f_2 for daily-averaged SLT in no-SN (a) and SN (b) simulations' configurations. It can be seen that r is very close to one, except in the North American monsoon region, where it has lower values, implying that timing of the monsoon onset and bursts is highly sensitive to the deep-convection parameter modification.

Figure 3 displays the reproducible (left) and irreproducible (right) components of TE MSD, for no-SN (top) and SN (bottom) configurations. It can be seen that, unlike in the single-model case (Fig. 1), the variability in the model response to the parameter modification is dominated by the irreproducible components originating in the sensitive dependence and not by the variability enforced through the LLBC. Hence, for minor RCM modifications, ensemble members can efficiently sample variability in the difference, even over shorter integration periods. Furthermore, the application of SN considerably reduces the irreproducible MSD component while the reproducible MSD component is not changed considerably. The reproducible part does not increase because the high correlation r allows for the cancelation of terms in Eq. (4). In fact, the efficiency of SN in reducing the TE MSD essentially depends on the correlation r between the reproducible anomalies in the control and modified model simulations. If they are not correlated ($r=0$), then from Eq. (2-5) we obtain:

$$msd = \sigma^2_{TE_1} + \sigma^2_{TE_2}, \qquad (6)$$

i.e., the TE MSD becomes the sum of the control and modified-model TE variances. This quantity, if the model skilfully reproduces the TE variance, cannot considerably change upon the application of SN.

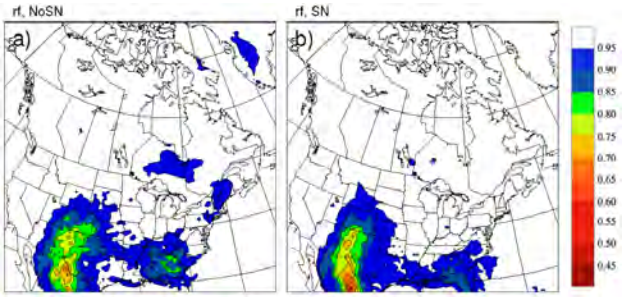


Figure 2 Correlation between the reproducible components of transient-eddy variability of perturbed-parameter and control CRCM5 screen-level temperatures for no-SN (a) and SN configurations (b).

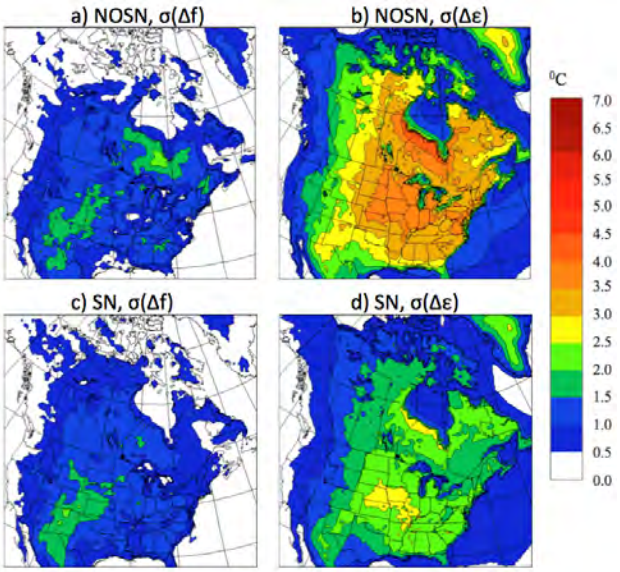


Figure 3 Reproducible (a, c) and irreproducible (b, d) components of the TE MSD between perturbed-parameter and control CRCM5 screen-level temperatures in no-SN (a, b) and SN configurations (c, d).

References

Separovic L., de Elía R., and Laprise R. (2008) Reproducible and Irreproducible Components in Ensemble Simulations with a Regional Climate Model. Mon. Wea. Rev., 136, pp. 4942-4961.

Separovic L., de Elía R., and Laprise R. (2012) Impact of Domain Size and Spectral Nudging in Studies of RCM Response to Parameter Modification. Clim. Dyn., 38, 7-8, pp. 1325-1343.

Von Storch H., Langenberg H., and Feser F. (2000) A Spectral Nudging Technique for Dynamical Downscaling Purposes. Mon. Wea. Rev., 128, pp. 3664–3673.

Zadra A., Caya D., Côté J., Dugas B., Jones C., Laprise R., Winger K., and Caron L.-P. (2008) The Next Canadian Regional Climate Model. Phys. Canada, 64, pp. 74-83.

Systematic temperature and precipitation biases in the CLARIS-LPB ensemble simulations over South America and possible implications for climate change projections

Silvina A. Solman

CIMA , CONICET-UBA – DCAO, FCEyN-UBA, Buenos Aires, Argentina (solman@cima.fcen.uba.ar)

1. Introduction

Within the framework of the CLARIS-LPB EU Project, a suite of 7 coordinated Regional Climate Model (RCM) simulations over South America were performed. The ability of this set of RCMs (driven by the ERA-Interim reanalysis) in reproducing the observed climate conditions was evaluated in a recent study (Solman et al. 2013) and several systematic biases were identified. In particular, most of the RCMs showed a systematic temperature overestimation and precipitation underestimation over the La Plata Basin (LPB) region. These systematic biases were shared by every RCM, suggesting a common shortcoming of the models. In this study we analyze the bias in the mean climate but for the present climate simulations driven by CMIP3 GCMs. We demonstrate that these systematic model errors are more dependent on the RCMs rather than on the driving GCMs. Moreover, we demonstrate that model biases are not invariant, but a temperature-dependent temperature bias and a precipitation-dependent precipitation bias were identified for the LPB region. A similar behavior was also found for other regions of the world (e. g. Christensen and Boberg, 2012). Under warmer and wetter climate conditions for the future, these biases may amplify the climate change signal. A bias correction method based on a quantile-based mapping was applied to model projections in order to account for the identified systematic biases.

2. Data and methods

The RCM simulations used in this analysis are the results of the coordinated experiment in the framework of the CLARIS-LPB EU project. A suit of 7 ERA-Interim driven RCM simulations covering the period 1981-2008 and 10 GCM-driven RCM simulations under the A1B emission scenario were used. The GCM-driven simulations cover the period 1961-1990 and 2071-2100. The RCM models were run on a 50 km grid resolution. All model data were interpolated onto a common grid. Monthly mean temperature and precipitation as simulated by the RCMs were used, together with observational monthly data from the Climate Research Unit (CRU). Temperature and precipitation biases were identified for the LPB region using modeled vs. observed ranked data.

The bias correction methodology applied to the GCM-driven RCM simulations is based on the quantile mapping method, which maps the distribution of monthly-simulated variables (precipitation and temperature) onto that of gridded observed data. The method is a relatively simple approach that has been successfully used in hydrologic and many other climate impact studies (Wood et al., 2004). However, is has some limitations, such as not allowing changes in the shape of the distribution.

3. Results and discussion

The systematic overestimation of the mean temperature over the LPB region has been identified in previous analysis. In order to identify the temperature-dependent temperature bias, the ranked monthly mean simulated temperature vs. observed, averaged for the LPB region is depicted in Figure 1.

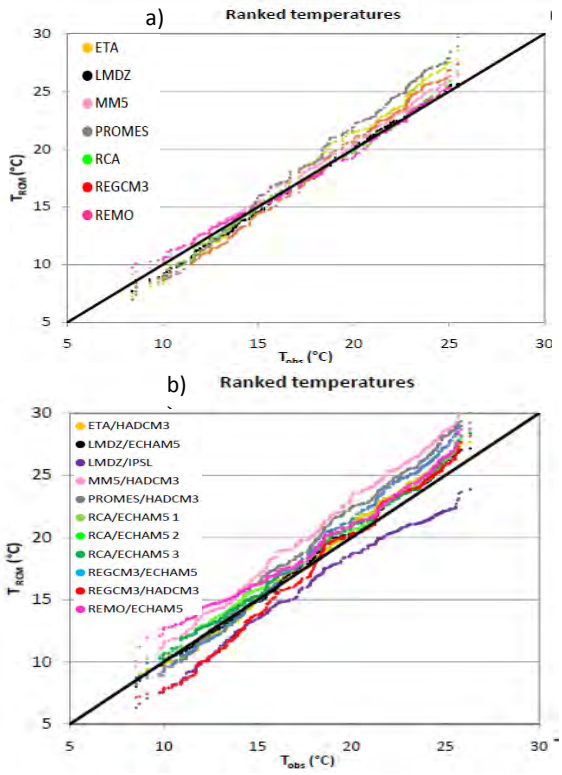


Figure 1: Ranked monthly mean temperature modeled versus observed for the LPB region. (a) ERA-Interim driven RCMs for 1981-2008. (b) GCM-driven RCMs for 1961-1990.

For both ERA-Interim and GCM driven simulations most of the RCMs show a warm bias, with the exception of some RCMs for the cold months. Moreover, the warm bias is even larger for warmer climate conditions (in this case for summer months). Accordingly, the mean temperature bias for summer was found to be larger than for winter months for both the ERA-Interim and the GCM driven simulations.

Results for monthly mean precipitation are depicted in Figure 2, which highlights the systematic dry bias in every

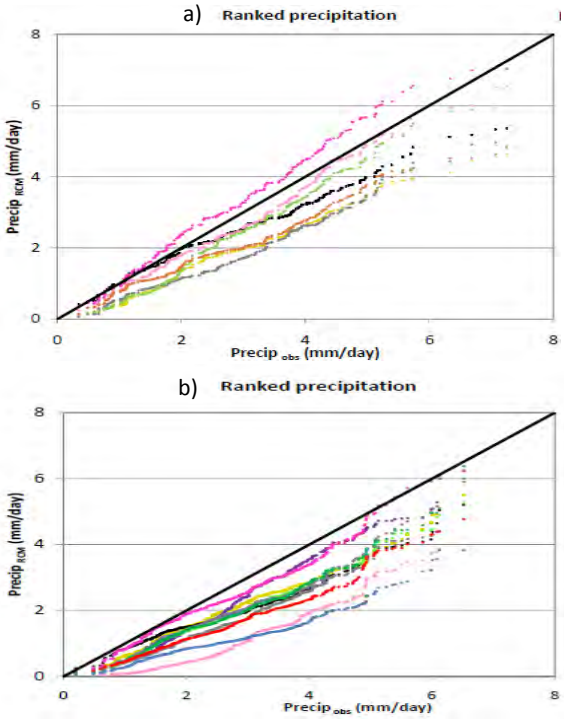


Figure 2: Same as Fig. 1 but for monthly precipitation.

RCM independently of the driving model. With the exception of the REMO RCM, which overestimates rainfall over the LPB region when driven by the ERA-Interim reanalysis, all the RCMs show large deficiencies in reproducing the observed rainfall amount. Moreover, note that the dry bias becomes even larger for wetter conditions.

Figures 1 and 2 suggest than the model biases are not invariant, but depend on both temperature and precipitation, respectively. This model behavior may have serious implications in the interpretation of the future climate projections. As warm biases are amplified under warmer climate conditions (summer months), and dry biases are amplified under wetter climate conditions (rainy season), climate change projections due to increased greenhouse gas concentrations may also be amplified, taking into account that most RCMs project increased temperature and precipitation for the LPB region under the A1B emission scenario. Moreover, as noted in the figures displayed above, the amplitude of the biases is model dependent. This implies that the models with larger warm biases may amplify the projected temperature change. As for temperature, it is expected that the models with the driest biases could be even drier for wetter climate conditions in the future. With this in mind, we have applied a correction methodology for the monthly mean temperature and precipitation from the GCM-driven simulations. The quantile-based approach was applied to a calibration period (1961-1975) and then evaluated for an independent validation period. Finally, the correction was applied to the projected climate for the period 2071-2100. The projected changes for temperature and precipitation over the LPB region from the uncorrected and corrected model outputs are displayed in Figure 3 for 6 RCMs (more models will be included in the analysis).

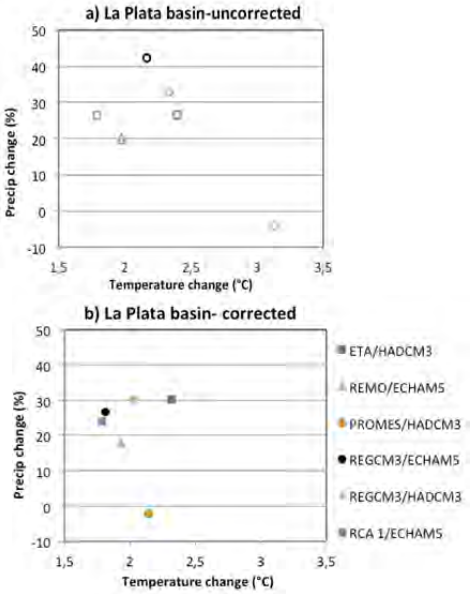


Figure 3: Temperature change versus precipitation change for the LPB projected for the period 2071-2100 relative to 1976-1990 from a suite of RCMs under A1B scenario. a) from uncorrected RCMs; b) from bias corrected RCMs.

Projected temperature changes after bias correction are systematically reduced and as well as the spread among RCMs. Note that for the PROMES model, which showed the largest temperature bias, the uncorrected change was much larger compared with the rest of the RCMs. However, after bias correction, the temperature change was reduced lying within the signal of the other RCMs. For precipitation, almost all models project wetter conditions, and, as for temperature, both the magnitude and the spread are reduced after bias correction. Though applying bias correction methodologies to projected climate conditions is controversial, this study demonstrates that bias correction methodologies should be considered in order better interpret climate change signals.

References

Christensen, J. H., F. Boberg (2012) Temperature dependent climate projection deficiencies in CMIP5 models, Geophys. Res. Lett., 39, L24705, doi:10.1029/2012GL053650.

Solman S. and co-authors (2013) Evaluation of an ensemble of regional climate model simulations over South America driven by the ERA-Interim reanalysis: Model performance and uncertainties, Clim Dyn, 41, pp. 1139-1157.

Wood AW, Leung LR, Sridhar V, Lettenmaier DP (2004) Hydrologic implications of dynamical ad statistical approaches to downscaling climate model outputs. Climate Change, 62, pp. 189-216.

Diagnostic Budget Study of the Internal Variability of Ensemble Simulations of HIRHAM5 for the Arctic

Anja Sommerfeld[1], Oumarou Nikiema[2], Annette Rinke[1], Klaus Dethloff[1] and René Laprise[2]

[1] Alfred-Wegener-Institute, Helmholtz Centre for Polar and Marine Research, Potsdam, Germany (anja.sommerfeld@awi.de)
[2] Université du Québec à Montréal, Montreal, Canada

1. Introduction

The challenge in evaluating and applying regional atmospheric models is the poorly understood non-linear behavior of atmospheric processes. The non-linearities lead to an internal variability in the model. Therefore an ensemble of un-nudged simulations with different initial conditions and a diabatic budget study for potential temperature which accounts diabatic and dynamical contributions is applied on ensemble simulations to investigate the internally generated variability. Hence, the physical processes inducing inter-member variability (IV) in ensemble simulations can be analyzed and understood.

The study is applied over the Arctic with the regional model HIRHAM5 from July 6th 2012 to September 30th 2012. This time period is of particular importance because of the melting sea ice and its influence on atmospheric circulations and the resulting effect on the IV. In summer 2012 a strong sea ice melting occurred.

2. Model Setup

The hydrostatic regional atmospheric model HIRHAM5 (Christensen et al. 2007) was first applied on a circum-Arctic region by Klaus et al. 2012. The dynamical core of HIRHAM5 is provided by the regional weather forecast model HIRLAM7 (Undén et al. 2002), the physical parameterizations by ECHAM5 (Roeckner et al. 2003). The model is driven by ERA-Interim (Dee et al. 2011) and runs with a spatial resolution of 25 km covering 218x200 grid cells and 40 vertical levels up to 10 hPa.

The ensemble consists of 20 members, running with the same lateral boundary conditions, but differs in their atmospheric initial conditions. Therefore the initialization time of each simulation shifts by six hours. The first simulation starts on July 1st 2012 at 0000 UTC and the last on July 5th 2012 at 1800 UTC. Each simulation is performed until September 30th 2012. The budget study is applied for the period that is covered by all ensemble-members from July 6th to September 30th 2012.

3. Method

The applied equations of IV budget study for potential temperature was developed and described in detail by Nikiema et al. 2010 and 2011. IV of a variable φ is defined as the inter-member variance (σ^2) of the 20 ensemble-members (n) (Eq. 1). The initial equations are the first law of thermodynamics and the mass-continuity equations in vertical pressure coordinates for potential temperature and they can be combined to Eq. 2, where Θ_n is the potential temperature, V_n is the horizontal wind, ω_n is the pressure vertical motion and J_n is the diabatic heating rate combining temperature tendency due to radiation, vertical diffusion, convection and condensation. Applying the Reynolds decomposition (Eq. 3) leads to a variable φ_n split in the ensemble mean $\langle\varphi\rangle$ and its deviation from the ensemble mean φ'_n. Further transposing and combining of the equations lead to seven contributions of the potential temperature IV budget study (Eq. 4).

$$\sigma_\varphi^2 \approx \langle \varphi_n'^2 \rangle \quad \text{Eq. 1}$$

$$\frac{\partial \theta_n}{\partial t} + \vec{\nabla}\cdot\left(\theta_n \overrightarrow{V_n}\right) + \frac{(\theta_n \omega_n)}{\partial p} = J_n \quad \text{Eq. 2}$$

$$\varphi_n = \langle\varphi\rangle + \varphi'_n \quad \text{Eq. 3}$$

$$\underbrace{\frac{\partial \sigma_\theta^2}{\partial t}}_{L_\theta} = \underbrace{-\vec{\nabla}\cdot\left(\langle\vec{V}\rangle\sigma_\theta^2\right)}_{A_h} \underbrace{-\frac{\partial(\langle\omega\rangle\sigma_\theta^2)}{\partial p}}_{A_v} \underbrace{-2\langle\theta'_n\overrightarrow{V'_n}\rangle\cdot\vec{\nabla}\langle\theta\rangle}_{B_h} \underbrace{-2\langle\theta'_n\omega'_n\rangle\frac{\partial\langle\theta\rangle}{\partial p}}_{B_v}$$

$$\underbrace{+2\langle\theta'_n J'_n\rangle}_{C} \underbrace{-2\langle\theta'_n\vec{\nabla}\cdot\left(\theta'_n\overrightarrow{V'_n}\right)\rangle}_{E_h} \underbrace{-2\langle\theta'_n\frac{\partial}{\partial p}(\theta'_n\omega'_n)\rangle}_{E_v} \quad \text{Eq. 4}$$

The left-hand side of Eq. 4 is the diagnostic potential temperature IV tendency (L_Θ) and on the right-hand side are the local changes of the inter-member spread variance in the ensemble simulations (Nikiema et al. 2010). The right-hand side consists of seven parameters contributing to IV and describing different atmospheric processes. The terms A_h and A_v are the horizontal and vertical transport terms. The terms B_h and B_v are the horizontal and vertical baroclinic terms and are linked to synoptic events. C is the diabatic source and sink term. The terms E_h and E_v are the third-order-terms.

4. Results

The amplitude of potential temperature IV of the HIRHAM5 ensemble simulations fluctuates in time (Fig. 1, left) and depends on the height in the atmosphere (Fig. 1, right). During the analyzed time period IV reaches high values between July 27th and August 7th with an absolute maximum on August 5th 2012 at 0600 UTC. The vertical profile shows strongest IV at 500 hPa. A smaller maximum is observed at 925 hPa and the lowest values of IV are found at the surface and at 300 hPa.

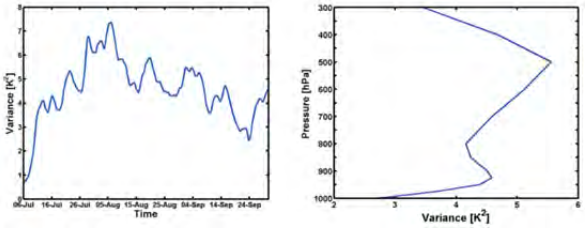


Figure 1. Time evolution (left) and vertical profile (right) of the domain averaged inter-member variability of potential temperature.

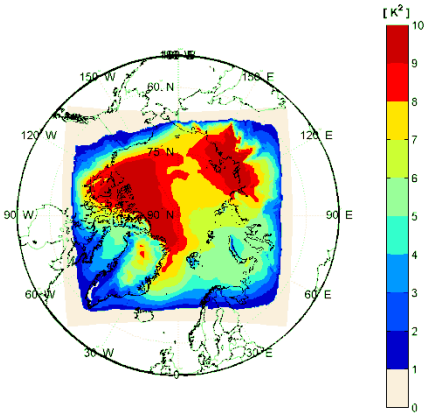


Figure 2. Spatial distribution of the time averaged inter-member variability of potential temperature at 925 hPa.

The temporal (July - September) and vertical average of IV shows the spatial distribution and highlights locations with high and low IV. From the boundary toward the center of the model domain IV increases at each level. A detailed view on the 925 hPa level (Fig. 2) points two centers of high IV out, at the Laptev Sea and Beaufort Sea/North America.

The time evolution of the seven contributions (Fig. 3) indicates that the horizontal and vertical baroclinic terms exert the strongest influence on IV. The positive values of B_h represent a generation and the negative values of B_v a reduction of IV. The other terms fluctuate around zero, because their contribution to IV in general is small (A_v, E_v and C) or they are balanced over the model domain with regions where they contribute to an increase and where they contribute to a decrease of IV (A_h and E_h).

The centers of high IV observed in Fig. 2 are mostly induced by B_h which reaches values of more than $20*10^{-5}$ K^2/s (Fig. 4, left). However B_v (Fig. 4, right) has a negative influence in these regions leading to a reduction of IV but with a weaker contribution, so that there is a strong baroclinic contribution to IV.

These results for the Arctic are different to those Nikiema et al. 2010 and 2011 found for North America using the Canadian RCM. They obtain that the diabetic term C, followed by B_h contribute to a generation of potential temperature IV and B_v, followed by A_h are responsible for the reduction of potential temperature IV.

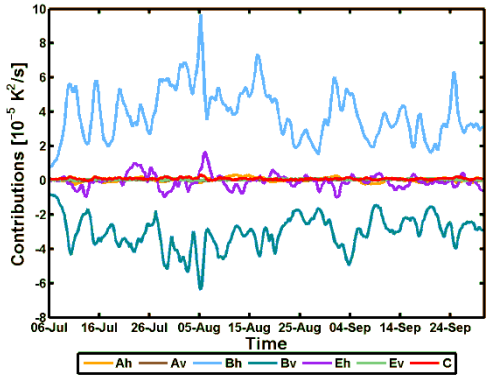


Figure 3. Time evolution of the vertical and domain averaged contributions to the inter-member variability of potential temperature.

5. Summary and Outlook

In this study a budget equation for potential temperature is applied to investigate IV generated in a regional arctic atmospheric model HIRHAM5 with ensemble simulations differing in their initial conditions for the period from July 6th 2012 to September 30th 2012. IV fluctuates strongly in time and reaches its maximum at 500 hPa. IV is mainly generated by horizontal (B_h) and reduced by vertical baroclinicity (B_v).

Further subjects will be analysis of IV and its contributions by investigating shorter time periods and individual events of high and low IV depending on sea ice melting. A further aim will be the application of the budget study for other years.

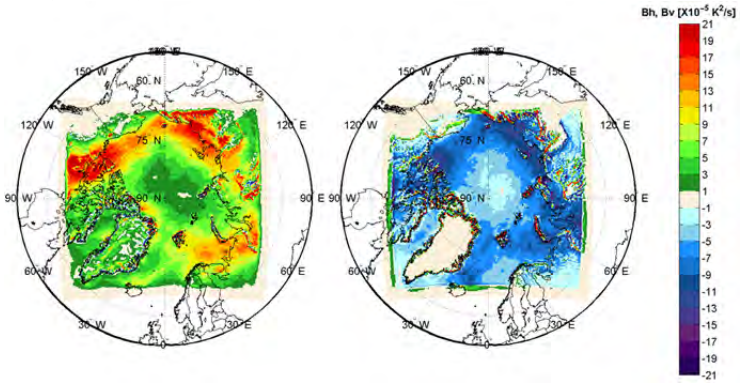


Figure 4. Spatial distribution of the time averaged horizontal baroclinic term B_h (left) and vertical baroclinic term B_v (right) contributing to the inter-member variability of potential temperature at 925 hPa.

References

Christensen O.B., Drews M., Christensen J.H. (DMI); Dethloff K., Ketelsen K., Hebestadt I., Rinke A. (AWI) (2007) The HIRHAM Regional Climate Model Version 5 (β), Technical Report 06-17, Danish Meteorological Institute (DMI): Copenhagen, Denmark

Dee D.P., Uppala S.M., Simmons A.J., Berrisfort P., Poli P., Kobayashi S., Andrae U., Balmaseda M.A., Balsamo G., Bauer P. (2011) The ERA-Interim reanalysis: Configuration and performance of the data assimilation system, Q.J.R.Meteorol.Soc., 137, pp. 553-597

Nikiema O., Laprise R. (2010) Diagnostic budget study of the internal variability in ensemble simulations of the Candian RCM, Clim Dyn, 36, pp. 2313-2337

Nikiema O., Laprise R. (2011) Budget study of the internal variability in the ensemble simulations of the Canadian Regional Climate Model at the seasonal scale, Journal of Geophysical Research, 116, pp. 1-18

Roeckner E., Bäuml E., Bonaventura L., Brokopf R., Esch M., Giorgetta M., Hagemann S., Kirchner I., Kornblueh L., Manzini E., Rhodin A., Schlese U., Schulzweida U., Tompkins A. (2003) The Atmospheric General Circulation Model ECHAM5-Part 1: Model Description, Technical report 349, Max-Planck-Institut (MPI) for Meteorology: Hamburg, Germany

Undén P., Rontu L., Järvinen H., Lynch P., Calvo J., Cats G., Cuxart J., Eerola K., Foortelius C., Garcia-Moya J.A. (2002) HIRHLAM-5 Scientific Documentation., In HIRHAM-5 Project, Swedish Meteorological and Hydrological Institute (SMHI): Norrköping, Sweden

Uncertainties in the regional climate models simulations of South-Asian summer monsoon and climate change

Faisal Saeed Syed[1], Waheed Iqbal[2], Ahsan Ali Bokhari Syed[2]

[1] Comsats Institute of science and technology, Islamabad (faisalsaeed@comsats.edu.pk), Pakistan.

[2] Research and Development Division, Pakistan Meteorological Department, Islamabad, Pakistan.

The uncertainties in the regional climate models (RCMs) are evaluated by analyzing the driving global data of ERA40 reanalysis and ECHAM5 GCM, and the downscaled data of two RCMs (RegCM4 and PRECIS) over South-Asia for the present day simulation (1971-2000) of South Asian summer monsoon. The differences between the observational datasets over South-Asia are also analyzed. The spatial and the quantitative analysis over the selected climatic regions of South-Asia for the mean climate and the inter-annual variability of temperature, precipitation and circulation show that the RCMs have systematic biases which are independent from different driving datasets and seems to come from the physics parameterization of the RCMs. The spatial gradients and topographically-induced structure of climate are generally captured and simulated values are within a few degrees of the observed values. The biases in the RCMs are not consistent with the biases in the driving fields and the models show similar spatial patterns after downscaling different global datasets. The annual cycle of temperature and rainfall is well simulated by the RCMs, however the RCMs are not able to capture the inter-annual variability. ECHAM5 is also downscaled for the future (2071-2100) climate under A1B emission scenario. The climate change signal is consistent between ECHAM5 and RCMs. There is warming over all the regions of South-Asia associated with increasing greenhouse gas concentrations and the increase in summer mean surface air temperature by the end of the century ranges from 2.5 to 5ºC, with maximum warming over north western parts of the domain and 30% increase in rainfall over north eastern India, Bangladesh and Myanmar.

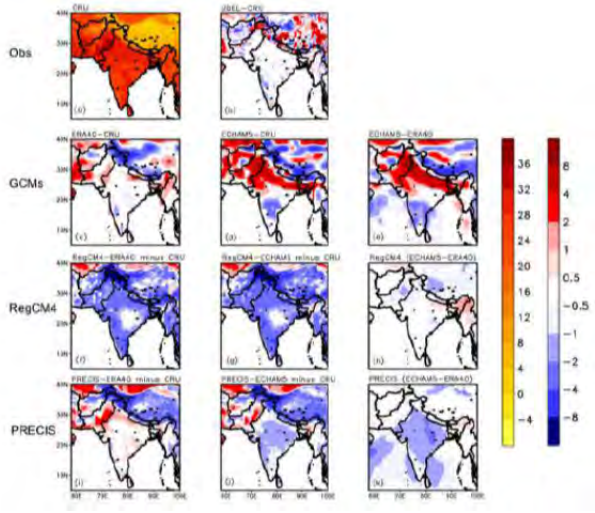


Fig 1. Mean (1971-2000) surface temperature (◦C).

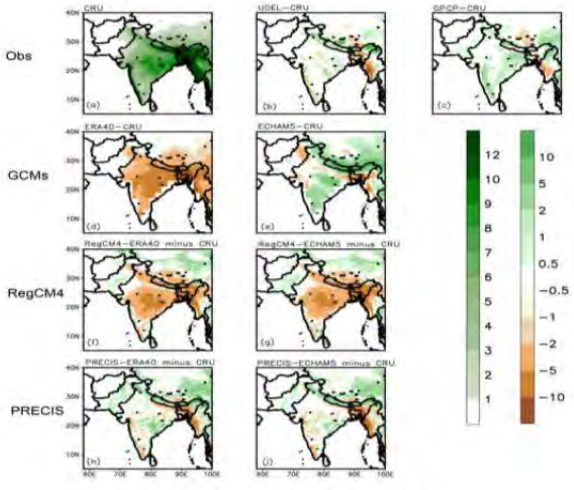


Fig 2. Mean (1971-2000) precipitation (mm/day).

References

Adler RF, Huffman GJ., Chang A, Ferraro R, Xie P, Janowiak J, Rudolf B, Schneider U, Curtis S, Bolvin D, Gruber A, Susskind J, Arkin (2003) The Version 2 Global Precipitation Climatology Project (GPCP) Monthly Precipitation Analysis (1979-Present). J. Hydrometeorology 4: 1147-1167

Almazroui M (2012) Dynamical downsca4ling of rainfall and temperature over the Arabian Peninsula using RegCM4. Climate Research 52: 49–62

Assessment of methods for downscaling European wind storms

Simon Tucker, Erasmo Buonomo and Richard Jones

Met Office Hadley Centre, Fitzroy Road, Exeter, Devon, UK (simon.tucker@metoffice.gov.uk)

1. Background

The ACRE facilitated 20th century reanalysis (20CR) is a 140 year (1871 - 2011) reconstruction of the evolution of the Earth's atmosphere over this period. See Compo et al. (2011). Dynamical downscaling produces a more realistic and detailed description of weather systems that are not well resolved at the resolution of the 20CR data, including storms. Hence downscaling 20 CR enables us to:

- Study specific past weather events.
- Gain a better understanding of the long-term natural variability of such weather events.

2. Description of this study

In this study, we investigate the most suitable method to downscale European wind storms in order to produce the most accurate representation of such events. We select around 30 of the biggest storms in the period 1990-2013 and downscale the ERA-INTERIM reanalysis (Dee et al (2011)) using various methods. The methods we consider are:

1. A multi-year regional climate model initialised at the start of the simulation and driven only by lateral boundary conditions, i.e. so that the simulation has been 'spun up' and hence the results are independent of the initial conditions and the only constraint is from the lateral boundary conditions.
2. A regional climate model as in 1 but where the solution is 'nudged' in the interior of the domain towards the driving data. The strength of the nudging applied is also investigated (i.e. by changing the relaxation parameter).
3. Downscaling in 'weather forecasting mode' where every 24 hours a new limited area model is initialised with both lateral boundary and initial conditions coming from the driving model. The model is run for 36 hours and output from the last 24 hours of this run is used.

The assessment is made using mean sea level pressure, 10 metre winds and precipitation. We look at

- The location and timing accuracy of the storm.
- The intensity and spatial extent of the storm.

Finally once we determine the most appropriate method we use it to downscale the same storms from 20CR and compare the results with the ERA – INTERIM driven results.

3. At the conference

At the conference results from the comparison of the different downscaling strategies will be discussed.

References

Compo, G.P., J.S. Whitaker, P.D. Sardeshmukh, N. Matsui, R.J. Allan, X. Yin, B.E. Gleason, R.S. Vose, G. Rutledge, P. Bessemoulin, S. Br�nnimann, M. Brunet, R.I. Crouthamel, A.N. Grant, P.Y. Groisman, P.D. Jones, M. Kruk, A.C. Kruger, G.J. Marshall, M. Maugeri, H.Y. Mok, Ø. Nordli, T.F. Ross, R.M. Trigo, X.L. Wang, S.D. Woodruff, and S.J. Worley, 2011 The Twentieth Century Reanalysis Project. Quarterly J. Roy. Meteorol. Soc., 137, 1-28. DOI: 10.1002/qj.776

Dee, D. P., Uppala, S. M., Simmons, A. J., Berrisford, P., Poli, P., Kobayashi, S., Andrae, U., Balmaseda, M. A., Balsamo, G., Bauer, P., Bechtold, P., Beljaars, A. C. M., van de Berg, L., Bidlot, J., Bormann, N., Delsol, C., Dragani, R., Fuentes, M., Geer, A. J., Haimberger, L., Healy, S. B., Hersbach, H., Hólm, E. V., Isaksen, L., Kållberg, P., Köhler, M., Matricardi, M., McNally, A. P., Monge-Sanz, B. M., Morcrette, J.-J., Park, B.-K., Peubey, C., de Rosnay, P., Tavolato, C., Thépaut, J.-N. and Vitart, F. (2011), The ERA-Interim reanalysis: configuration and performance of the data assimilation system. Quarterly Journal of the Royal Meteorological Society, 137: 553–597. doi: 10.1002/qj.828

A realistic land cover change trajectory, including re-vegetation, reveals substantial climate impact of deforestation in the Congo basin

Nicole P.M. van Lipzig, Tom Akkermans, Wim Thiery, Pieter Moonen, Bruno Verbist, Bart Muys

Department Earth- and Environmental Sciences, KU Leuven, Belgium (Nicole.vanlipzig@ees.kuleuven.be)

The demand for agricultural land in the Congo basin (tropical Africa) is expected to yield large deforestation over the coming decades. Such deforestation significantly alters the surface energy and water balance, and hence the climate of this region. Although several studies exist on the climatological impact of deforestation in the Congo basin, existing scenarios of deforestation rates and successional land cover, that are used in climate models, are generally crude. In this study, we aim to refine existing impact assessments by replacing the primary forest by a typical combination of successional fallow vegetation types observed for the Congo Basin. This is done within the COSMO-CLM regional climate model at 25 km grid spacing coupled to a state-of-the-art soil-vegetation-atmosphere transfer model (Community Land Model). An evaluation of the model shows good performance compared to in-situ and satellite observations. Model integrations indicate that the deforestation, expected for the middle of the 21th century, induces a warming of 0.7°C, which is about half of the greenhouse gas-induced surface warming in this region. This shows the necessity of taking into account deforestation in order to obtain realistic future climate projections. Precipitation is also affected: As a consequence of surface warming due to deforestation, a regional heat low develops above the rainforest. Resulting low-level convergence causes a dynamical redistribution of moisture in the boundary layer, thereby weakening atmospheric instability, convection intensity and hence precipitation, which decreases by 5 to 10% in the heat low region.

References

Akkermans, T., Thiery, W., Van Lipzig, N. (2014). The regional climate impact of a realistic future deforestation scenario in the Congo Basin. Journal of Climate, 27(7), 2714-2734

Can an RCM improve on large scales within its domain – how much to this end does the resolution help?

Katarina Veljovic[1] and Fedor Mesinger[2]

[1] Institute of Meteorology, Faculty of Physics, Belgrade, Serbia, (katarina@ff.bg.ac.rs)

[2] Serbian Academy of Sciences and Arts, Belgrade, Serbia

There have been results in operational use and various tests and experiments done with the Eta model indicating that the Eta was successful in improving on large scales within its domain compared to those of the driver global model. Perhaps the most conspicuous among those is the result of Fennessy and Altshuler (Veljovic et al., 2010) achieving a rather accurate depiction of the summer precipitation difference between the flood year of 1993 and the drought year of 1988 over the U.S. Midwest, in spite of the failure of the driver global model to do so. For a direct investigation of the issue we have run 26 ensemble membrs of the Eta driven by ECMWF 32-day ensemble members (loc. cit.). Verification of 250 hPa winds looking at two skill measures seemed to offer a convincing confirmation that the large scales of the Eta have indeed been most of the time somewhat more skillful that those of the driver ECMWF ensemble members.

Trying to identify the reason for this apparent advantage of the Eta we have rerun 10 members of the Eta using the Eta model switched to use sigma. The same two verification measures however failed to indicate an advantage of the Eta members over their sigma counterparts. What we did notice however is that what looked like a crucial feature of the situation at about the 12-day time, a tilt of the 250 hPa wind speed trough as it was crossing the Rockies, was by three Eta members done visibly more accurately than by their sigma counterparts (Fig. 1). One member showed the opposite result.

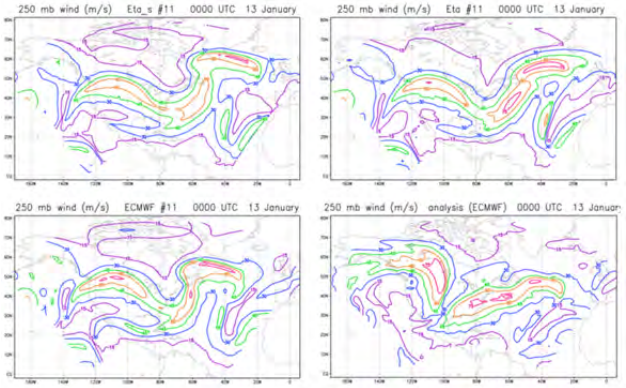


Figure 1. Contours of the 250 hPa wind speeds of 12-day forecasts of the Veljovic et al. (2012) Eta member 11 runs using sigma coordinate, top left; same, but using the tea, top right; same but of the ECMWF ensemble member 11 used to drive these Eta forecasts, bottom left. Same except ECMWF analysis verifying at the same time, bottom right.

To look into the possible resolution impact of this Eta favorable result we have subsequently rerun these same 10 members with the resolution reduced from 31 to 80 km. This is about the resolution of the ECMWF driver ensemble members after the 10-day time. Looking at the scores averaged over 5 and 5.5 day periods (Fig. 2), very minor impact of resolution could be noticed, and not always in the direction of the scores being improved with higher resolution. Our conclusion is that the Eta favorable result, of the Eta members showing large scale skill generally not inferior to that of their ECMWF driver members in spite of absorbing the lateral boundary condition error, was not due to higher resolution. Thus, it must be due to another model feature or a combination of features, maybe its near finite-volume design with a conservation of numerous properties.

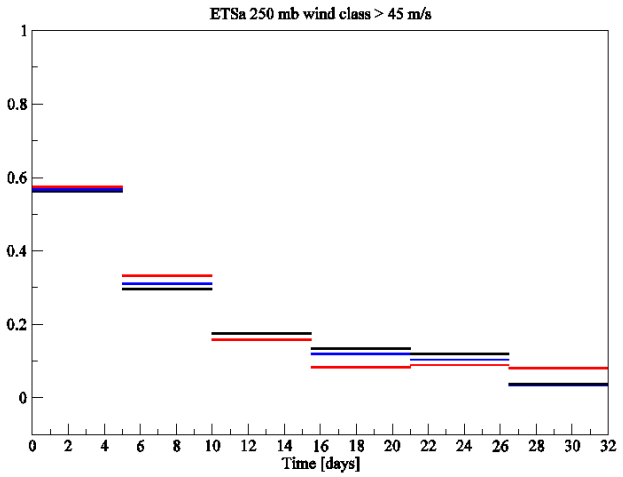


Figure 2. Averaged Bias adjusted Equitable Threat Scores of the 32-day ensemble forecasts of the position of 250 hPa wind speeds greater than 45 m s^{-1}, each done by three models or model versions: driver ECMWF ensemble model (red), Eta with the resolution 31 km (blue), and Eta with the resolution 80 km (black). Scores are averaged over 5 day periods (from day 0 to day 10) and over 5.5 day periods (from day 10 to 32).

References

Veljovic K., B. Rajkovic, M. J. Fennessy, E. L. Altshuler, F. Mesinger, 2010, Regional climate modeling: Should one attempt improving on the large scales? Lateral boundary condition scheme: Any impact? – Meteorologische Zeitschrift, 19: 237-246.

Strategies and measures for determining the skill of dynamical downscaling

Hans von Storch

Institute of Coastal Research, Helmholtz-Zentrum Geesthacht, Germany (hvonstorch@web.de)

1. Dynamical Downscaling

The basic idea of downscaling is that a link X_s = f(X_l,p_s) exists, with X_s representing the small-scale dynamics, X_l the large scale dynamics and p_s the physiographic forcing on small scales; f is supposed to be a transfer function, which may be stochastic. If such a link exists, then one can determine the small-scale dynamics if the large-scale dynamics and the small-scale forcing are known. In the present case we consider only the case of atmospheric dynamics.

The presence of such an f implies that details of the small scale dynamics do not matter for the large-scale dynamics; indeed, all full climate models implicitly employ such an assumption, when parameterizations of sub-grid scale "physics" are applied. Parameterizations are physically motivated but semi-empirical closures, which specify a suitable effect of the considered processes on the resolved scales – conditional upon the large state. This suitable effect can be the conditional mean effect, or a randomly chosen effect from an ensemble of effects available for the prevailing large-scale state.

The existence of f implies that through regional modeling an improvement of the representation of large-scale states cannot be achieved by doing a better job with describing the details the small-scales. Instead, misrepresentations in the large-scales will inevitably lead to misrepresentations in the small scales, no matter how good the regional atmospheric model is. Improvement of the large-scales needs improvements of the global models, in particular the paramterizations.

One could argue that in some cases, in particular in the tropics, such an f does not exist, because the details of the small-scale processes, for instance convection, has an effect around the world, i.e., on all scales. However, at mid-latitudes, where the weather regime is typically flushing every limited area in relatively short time, the assumption of an existing f is plausible – when X = X_l+X_s is a realization of the real world.

One may also argue that the downscaling mechanism with such an f would not work in case of purely GCM-generated states, when, X = X_l and X_s = 0. While one may use the same method to construct an f, no hard testing has been devised to test the plausibility of the existence of such an f.

The practical problem is to determine f. One way is to use a dynamical limited area model; another to use in the spirit of "perfect prog" an empirical downscaling approach. The former returns complete and space-time detailed atmospheric states, while the empirical calculates mostly realizations of weather streams at some sites or fields of statistical descriptors such as mean, variances or extremes. In the talk, only the dynamical approach will be discussed.

2. Indeterminacy

Formally, the limited area simulations generate solutions of an instationary boundary value problem, where values at the lateral and lower boundaries determine what is going on in the interior. The problem is that the latter assertion is simply false – mathematically, the boundary value problem is not well posed, and given the lateral and lower boundary values different weather streams can emerge – and they do. This problem can be overcome by adding forcing terms in the interior so that the solution is not deviating too strongly from the large scale state prescribed by observations or coarse grid simulations.,

Another problem is that the phase speeds of waves in the interior would not fit the phase on the coarse grid, from which the lateral boundary values are taken. This problem has been long solved by an ad-hoc measure, namely the so-called sponge zone, which enforces as smooth transfer from the interior to the outside and vice versa.

When no large-scale constraint is applied, different weather streams will emerge in different simulations with the LAM, and differences between observations and a simulation may reflect the indeterminacy of the mathematical problem and not errors, as was naively believed in the early years of regional modelling. Thus, in this case ensembles of model runs need to be done, to determine the significance of changes and differences – just as with global climate models

3. Added Value

As outlined above, the added value is expected in the small-scale dynamics. One would hope that the model is improving the description of these dynamics – first of all it should have higher variability on these scales than the driving analyses or simulations. To determine this, a method is needed to separate the scales – Thus a decision is needed about what is "large". Usually "small" is everything that is "not large". The separation can be done by expansion into orthogonal functions, such as spherical harmonics or trigonometric's, or by using digital filters.

When comparing with observed states, then sometimes (operational forecast or satellite) data is available, which describe for a shorter time and maybe

limited regions high-resolution dynamics. Then again, after filtering, it may be worthwhile to compare with the model output.

Finally, one would expect added value in regions, where the physiographic detail p_s matters, near coasts, near mountain ranges and the like. Also, certain dynamical processes, such as polar lows may be better described and therefore may undergo a more realistic dynamic within the LAM when the grid resolution is improved. In that case, specific algorithms to determine such events are needed, so allow if the downscaling returns better and useful statistics of such events.

Impacts of boundary layer parameterization schemes and air-sea coupling on WRF simulation of East Asian summer monsoon

Ziqian Wang[1,2], Anmin Duan[1] and Guoxiong Wu[1]

[1] The State Key Laboratory of Numerical Modeling for Atmospheric Sciences and Geophysical Fluid Dynamics, Institute of Atmospheric Physics, Chinese Academy of Sciences, Beijing, China (wzq@lasg.iap.ac.cn)

[2] University of Chinese Academy of Sciences, Beijing, China

1. Introduction

The regional climate model (RCM) has higher resolution that can represent the more accurate topography and reasonable land surface process, and it is a useful tool in the study of weather and climate change over East Asia. However, there are still large uncertainties in the East Asia summer monsoon (EASM) simulation using the RCM, particularly the simulation of monsoon precipitation (Fu et al., 2005). The uncertainties from the model physical parameterization schemes are one of the primary causes to the systemic error in RCM, such as the schemes of cumulus convection, land surface process, and planetary boundary layer (PBL). Most previous studies focused on the evaluation of the impacts from cumulus convection parameterization schemes on the simulated results (e.g., Wang et al., 1997; Emori et al., 2001; Lee et al., 2005; …..). Except for the cumulus convection, the imperfect PBL scheme can also cause large systematic biases; this is because the PBL scheme in RCM has a significant impact on the interactions of moisture, momentum, and energy between land, ocean, and atmosphere.

This study will investigate the impacts of four widely used PBL parameterization schemes in Weather Research and Forecasting (WRF) model on EASM simulation in the period of 2000-2009, and discuss the possible reason for the simulated biases. The four PBL schemes include two nonlocal closure schemes YSU (Yonsei University scheme) and ACM2 (Asymmetric Convective Model version 2), and two local turbulent kinetic energy (TKE) schemes BouLac (Bougeault-Lacarrere) and MYJ (Mellor-Yamada-Janjic).

2. Experimental design

Four ensemble experiments were performed with the above four different WRF PBL schemes respectively, while the model's other physical parameterization schemes were same. Each of the ensemble experiments has ten summers (2000-2009) with the initial modeling conditions at 0000UTC April 22, and ends at 1800UTC August 31. The simulation domain covers most parts of Asia and adjacent oceans (Figure 1). A Lambert projection is adopted and the domain is centered at 30°N, 102.5°E. The model has a 45 km horizontal resolution and 35 vertical layers with a prescribed model top at 10 hPa.

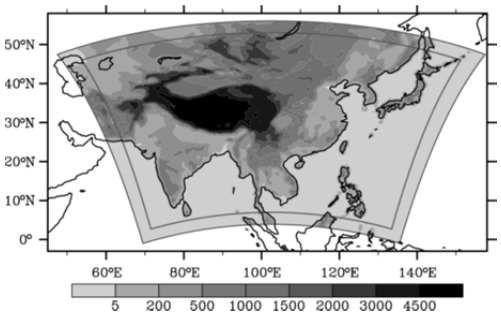


Figure 1. The WRF model domain and topography map (m); the area lapped by the solid lines at the boundary is the buffer zone.

3. Results

Based on the four different PBL schemes (YSU, ACM2, Boulac, and MYJ) in WRF model, the impacts of these schemes on the simulation of circulation and precipitation during the EASM are investigated. The simulated results of the two local TKE schemes, Boulac and MYJ, are more consistent with the observations than those in the two nonlocal closure schemes, YSU and ACM2. The former simulate more reasonable low-level southwesterly flow over East China and west pacific subtropical high (WPSH) than the latter (Figure 2). As to the modeling of summer monsoon precipitation, both the spatial distributions and temporal evolutions from Boulac and MYJ are also better than those in YSU and ACM2 schemes (Figure 3).

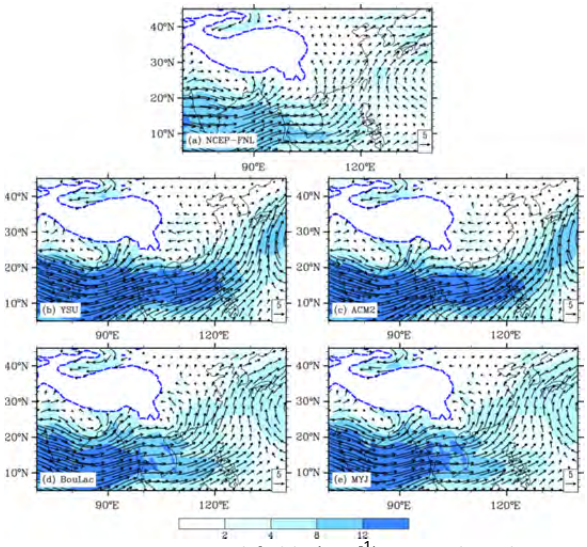


Figure 2. JJA mean wind fields (m s^{-1}) at 850 hPa during 2000-2009 from (a) NCEP-FNL; (b) YSU; (c) ACM2; (d) BouLac; (e) MYJ. The shaded indicates the wind speed, and the dash line marks the terrain height of 2000 m (same in the following figures).

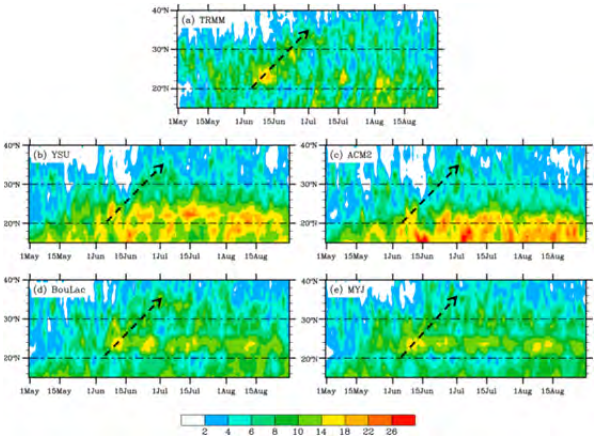


Figure 3. The latitude-time cross-sections of daily precipitation (mm day^{-1}) over East China (105-122°E) for May to August. (a) TRMM (Observation); (b) YSU; (c) ACM2; (d) BouLac; (e) MYJ.

In addition, through the comparison between YSU and Boulac experiments, the differences from the results of EASM simulation are more obvious over the oceanic area (Figure 4). In the experiments with the nonlocal schemes YSU and ACM2, the boundary layer mixing processes are much stronger, which lead to produce more sea surface latent heat flux and enhanced convection, and finally induce the overestimated precipitation and corresponding deviation of monsoon circulation.

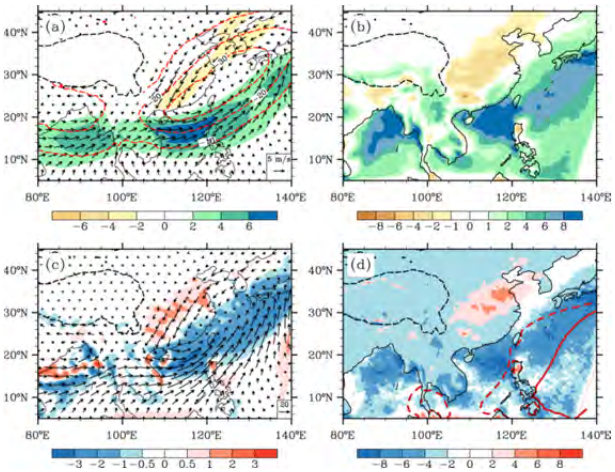


Figure 4. The differences of simulated results between YSU and BouLac in JJA. (a) wind (m s^{-1}) and potential height (contour, m) at 850 hPa; (b) precipitation (mm day^{-1}); (c) total moisture flux (10^{-5} kg m^{-1} s^{-1}) and its divergence (shaded, 10^{-5} kg m^{-2} s^{-1}) from the surface to 300 hPa; (d) vertical velocity (10^{-2} Pa s^{-1}) at 500 hPa, the red solid line is the 5880 gpm potential height in YSU scheme, and the dashed is in BouLac scheme.

With the further study, it is found that the absence of air-sea interaction in WRF may amplify the biases caused by PBL scheme over the oceanic region. Then, we coupled an ocean mixed layer model into WRF, and this coupled model can improve the WRF's performance on the simulation of typhoon (Wang et al., 2012). Through the comparison between the coupled and uncoupled runs with YSU scheme, the process of cloud-radiation feedback in the air-sea coupled model can cool the sea surface. The reduced SST weakens the upward latent heat flux and convective activity that are caused by the stronger PBL mixing, and then improves the simulation of monsoon circulation and precipitation (Figure 5).

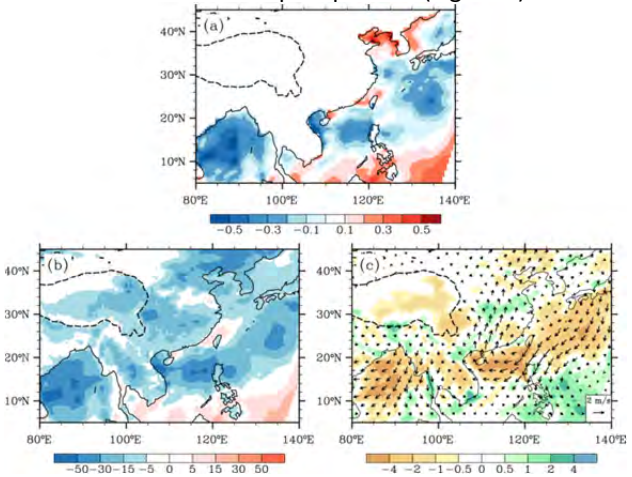


Figure 5. The differences of simulated results between coupled and uncoupled experiments with YSU scheme in JJA. (a) SST (℃); (b) latent heat flux (W m^{-2}); (c) precipitation (shaded, mm day^{-1}) and wind at 850 hPa (m s^{-1}).

4. Summary

Here we investigated the impacts of four widely used PBL schemes (YSU, ACM2, Boulac, and MYJ) and air-sea interaction on the EASM simulation with WRF model. We found that the modeling circulation and precipitation in the nonlocal closure scheme YSU are similar to another nonlocal scheme ACM2; and the results in the other two local TKE schemes (BouLac and MYJ) are also close to each other. But the simulated results of the Boulac and MYJ schemes are more consistent with the observations than those in the YSU and ACM2 schemes. Through the comparison between the YSU and Boulac experiments, the main reason for the obviously differences in the results of EASM simulation is the different intensity of PBL mixing process, particularly over the oceanic area. We further found that the absence of air-sea interaction in WRF may amplify the biases caused by PBL scheme over the ocean.

References

Emori, S., Nozawa, T., Numaguti, A., et al. (2001) Importance of cumulus parameterization for precipitation simulation over East Asia in June. J. Meteorol. Soc. Jpn., 79, 939-947

Fu, C. B., S. Y. Wang, Z. Xiong, et al. (2005) Regional climate model intercomparision project for Asia. Bull Amer. Meteorol. Soc., 86, 257-266

Lee, D-K, D-H Cha, S-J Choi (2005) A sensitive study of regional climate simulation to convective parameterization scheme for 1998 East Asian summer monsoon. J. Terr. Atmos. Ocean Sci., 16, 989-1015

Wang, W., N. L. Seaman (1997) A comparison study of convective parameterization schemes in a mesoscale model. Mon. Weather Rev., 25, 252-278

Wang, Z. Q., A. M. Duan (2012) A new mixed-layer model coupled into WRF. Atmos. Oceanic Sci. Lett., 5, 170-175

Future of precipitation in Poland – Projections for XXI century

Joanna Wibig, Joanna Jędruszkiewicz and Piotr Piotrowski

Department of Meteorology and Climatology, University of Lodz, Lodz, Poland (zameteo@uni.lodz.pl)

1. Introduction

At the moment there is a consensus concerning global warming and the increase of temperature. According to 5th IPCC report the globally averaged combined land and ocean surface temperature data as calculated by a linear trend, show a warming of 0.85 [0.65 to 1.06] °C, over the period 1880–2012 (Hartmann et al, 2013). However the changes in precipitation are not uniform over the globe. Since the beginning of twentieth century it has increased in middle latitudes of the Northern Hemisphere but the increase since 1950 is not significant. Even less is known about trends in precipitation extremes (Hartmann et al., 2013). However even in the regions where precipitation totals are not supposed to increase, the highest daily totals can become more extreme, because of the higher water holding capacity of the warmer air.

Because precipitation can occur in large scale frontal systems or be of convective origin, their future changes should be analysed in relation to changes in large scale atmospheric circulatrion and changes in temperature (Maraun et al., 2010).

The aim of present study is to make projections of precipitation in a future climate in Poland analysing separately changes in large scale and convective precipitation.

2. Data and Methods

Outputs of several RCMs are used in this study. The daily values of large scale and convective precipitation over Poland from the period 1971-2100 are analysed as well as daily SLP data. In each season (winter – DJF, spring – MAM, summer – JJA and autumn SON) the values of large scale and convective precipitation are divided into groups of days with precipitation in selected intervals. The atmospheric circulation on days from each group is analysed.

The above described analysis is done separately for four 30-year subperiods 1971-2000, 2011-2040, 2041-2070 and 2071-2100. The comparison between circulation types accompanying to different groups of precipitation is conducted in two aspects:

- temporal evaluation of precipitation on days with similar ciculation types,
- temporal evaluation of circulation types accompanying similar groups of precipitation.

In the second part of work the projections of precipitation for three scenario periods (2011-2040, 2041-2070 and 2071-2100) will be prepared as an ensemble projection with equal weights. The projection will be done separately for large scale and convective part of precipitation and for each season. The statistical significance of changes will be analysed on the basis of bootstrap methods (Chernick, 2008).

3. Acknowledgements

The work is supported by grant 2012/05/B/ST10/00945 founded by Polish National Science

References

Chernick, M.R. (2008) Bootstrap Methods: A guide for practictioners and researchers, A John Wiley & Sons, Inc., Publication, 369 pp.

Hartmann, D.L., A.M.G. Klein Tank, M. Rusticucci, L.V. Alexander, S. Brönnimann, Y. Charabi, F.J. Dentener, E.J. Dlugokencky, D.R. Easterling, A. Kaplan, B.J. Soden, P.W. Thorne, M. Wild and P.M. Zhai, (2013) Observations: Atmosphere and Surface. In: Climate Change 2013: The Physical Science Basis. Contribution of Working Group I to the Fifth Assessment Report of the Intergovernmental Panel on Climate Change [Stocker, T.F., D. Qin, G.-K. Plattner, M. Tignor, S.K. Allen, J. Boschung, A. Nauels, Y. Xia, V. Bex and P.M. Midgley (eds.)]. Cambridge University Press, Cambridge, United Kingdom and New York, NY, USA.

Maraun, D., F. Wetterhall, A.M. Ireson, R.E. Chandler, E.J. Kendon, M. Widmann, S. Brienen, H.W. Rust, T. Sauter, M. Themessl, V.K.C. Venema, K.P. Chun, C.M. Goodess, R.G. Jones, C. Onof, M. Vrac and I. Thiele-Eich (2010) Precipitation Downscaling under climate change. Recent developments to bridge the gap between dynamical models and the end user, Rev. Geophys. 48, RG3003, DOI: 10.1029/2009RG000314

Impact of BOB tropical storms on Tibetan Plateau precipitation and soil moisture

Zhixiang Xiao[1,2], Anmin Duan[1,3]

[1] State Key Laboratory of Numerical Modeling for Atmospheric Sciences and Geophysical Fluid Dynamics, Institute of Atmospheric Physics, Chinese Academy of Sciences, Beijing 100029, China (xiaozhixiang@lasg.iap.ac.cn)

[2] University of Chinese Academy of Sciences, Beijing 100049, China

[3] Key Laboratory of Meteorological Disaster of Ministry of Education, Nanjing University of Information Science and Technology,210044,China

1. Abstract

This study investigates the impact of Bay of Bengal (BoB) Tropical Storms (TSs) on Tibetan Plateau (TP) by observation data analysis and Regional Climate Model (RCM)-Weather Research and Forecasting (WRF). Climatologically, 1.35 tropical storms influence TP each year and they most happen in May and October, the BoB TSs genesis in the spring and early summer(April-June, AMJ) influence on TP with larger extension and higher latitude than those in autumn and winter(September-December, SOND). The maximum regional precipitation induced by BoB TSs accounts for more than 50% for the genesis month and about 20% for the season. Moreover, the surface soil moisture (SM) anomalies induced by BoB TSs persist 20-25 days in AMJ, and the same as for the snow depth (SD) induced by BoB TSs in SOND. The RCM (WRF) reveals that the deeper layer the SM anomalies persist longer, i.e. about 20 days for the surface and 2 month for sub-surface, while several months for the deep layers, which is agree with the observation analysis. Finally, the effect of preceding BoB TSs on TP cannot last to summer, and there is no clear connection between the BoB TSs and the summer precipitation anomaly over the East China.

2. DATA

The best-track data from Joint Typhoon Warning Centre (JTWC) is used in this study, including 6 hourly TSs center latitude and longitude, the lowest sea surface pressure and the maximum wind speed near the surface. And daily station rainfall and snow depth data at 756 stations over China are used for 1981-2011.

The Global Land Data Assimilation System Version1 (GLDAS-1) soil moisture data is used to study the soil moisture anomaly over TP, with a spatial resolution of $1^{o}\times1^{o}$.

3. TSs selected in this study

We assume that the TSs rain rate depends only on the distance from the TSs center as used by Kubota and Wang (2009). And the relationship between the distance from TSs center and rainfall rate is showed in Figure. 1a. when the distance is greater than 1000-km, the precipitation varies slowly and nearly independent of the distance and the 1000-km is considered as the threshold distance of TSs impact on TP. Figure 1b shows the selected TSs during 1981-2011.

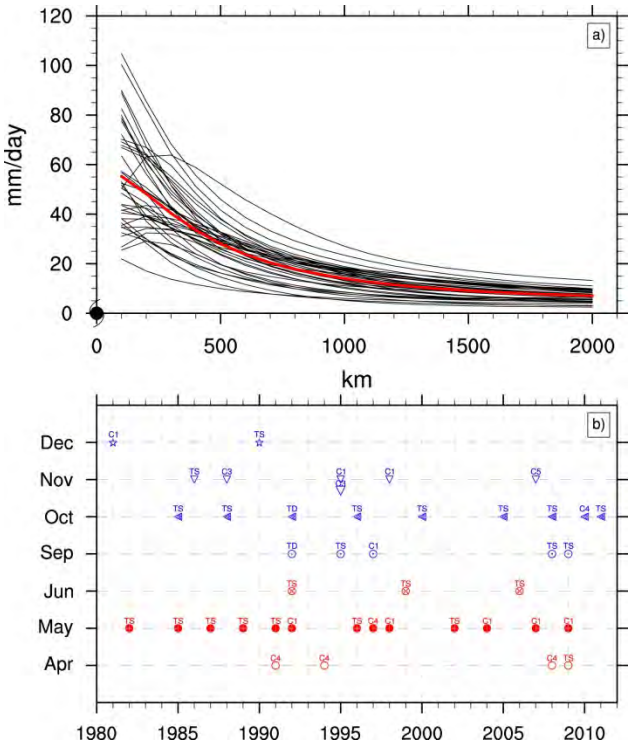


Figure 1. Mean radial distribution of the 38 BoB tropical storms rainfall from the TSs center to 2000-km radius based on TRMM during 1998-2011(a, units:mm/day, red line means the average value), and the selected TSs which have an influence on TP (b, the labels(TD, TS, C1, C2, C3, C4, C5)represent the corresponding TSs intensity).

4. SM anomaly induced by TSs

Basically, the TSs move to the northernmost on the decay day and closest to the TP, making largest rainfall on that day and the maximum SM occurs. The SM begins to reduce after that and rise when another raining event happens (Fig. 2).

A simple mathematical method is employed to reveal SM memory; it's calculated from its 1-day lag autocorrelation coefficients using the autocorrelation function of a first-order Markov process (Jones 1975):

$$\tau=-t/\ln(r(t)),$$

where τ means the SM memory in days, r(t) is the autocorrelation coefficient at decay time t.

The SM memory ranges from the least 5.5 to the maximum 50 days, and 21 days for total average; while the sub-surface SM memory shows from 14.5 days to 141.5 days, with an average of 40.7 days.

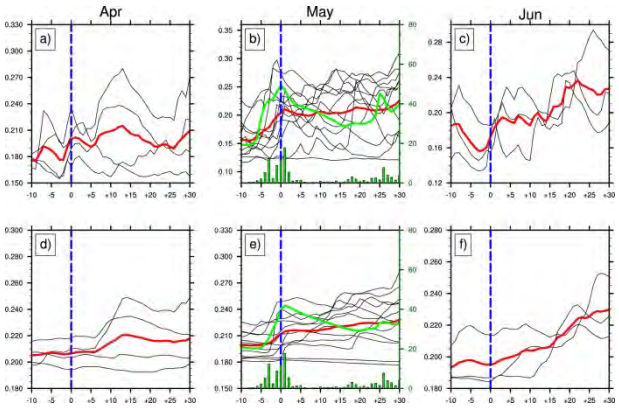


Figure 2. The average surface (a, b, c) and sub-surface (d, e and f) soil moisture evolution before and after the TS dissipate. The negative x axis means before and positive means after (units: day), separated by the blue dash lines. The red line in each panel represents the average value of each month and the green lines in b) and e) represents the soil moisture anomaly persistence the longest after the TS dissipate and there are little precipitation(green bars) in 20-25 days after that(0 day). The first column for the month of April (a and d), the second for May (b and e) and the third for June(c and f).

5. RCM Simulation study

Two experiments are designed, control and sensitivity experiment. The SM over central and east TP (CETP) is specified to 150% of control run in sensitivity experiment, and the rest options are the same as control. Each experiment starts at 3000UTC April 30, 1991 and ends at 00UTC August 31, 1991. Parameterizations are showed in Table 1.

Table 1. The main options of WRF3.5

Model feature/Parameter	Option used
Model core	ARW
Microphysics scheme	Lin
Longwave radiation scheme	RRTM
Shortwave radiation scheme	Dudhia
Cumulus parameterization scheme	GD
Planetary boundary layer scheme	MYJ
Land surface scheme	Noah

The sensitivity run initial SM over CETP declines rapidly in the first few days. The surface layer(0-10cm) SM (Fig. 3, red solid line) is the most violent decrease layer and becomes comparable with control experiment after WRF model running about 20 days, and keeps stable after that. The sub-surface (Fig. 3, red dash line, 10-40cm) SM persists about two months, and SM lasts longer in deep layers. The model results consistence with the observations above.

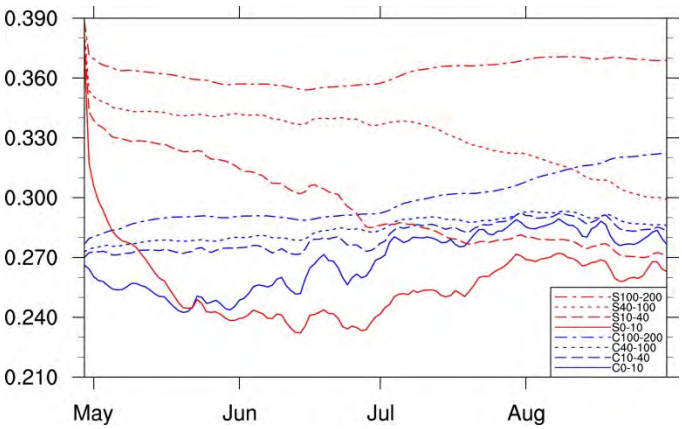


Figure 3. The four layers soil moisture evolution of control experiment (blue) and sensitivity experiment (red).units: m^3/m^3.

6. Conclusions

The characteristics of BoB TSs influencing TP are investigated using data diagnostic analysis during 1981-2011 and a case study of WRF model simulation. Though BoB TSs are weaker and less than typhoons in northwest Pacific Ocean, they also have a comparable influence radius of 1000-km. There are only 3.48 storms formation in BoB each year and only 1.35 storms have impacts on TP; May and October are the two peak month that BoB TSs influence TP, exhibiting a notable bimodal character. And the maximum rainfall induced by BoB TSs occupies more than 50% of the TS genesis month. Due to the southward and northward oscillation of equatorial troughs, the BoB TSs move to higher latitude in May than October and influence larger areas on TP. What's more, TP surface SM anomaly induced by BoB TSs precipitation only persists 20-25 days and SD caused by BoB TSs will melt over after 20 days. The RCM results reveal that the SM anomaly depends on soil depth (e. g. deeper layers, longer persistence), from 20 days in the surface layer to several months of the deep layers.

References

Kubota, H., and B. Wang, 2009: How much do tropical cyclones affect seasonal and interannual rainfall variability over the western North Pacific? J. Climate, 22(20), 5495-5510.

Jones, R. H., 1975: Estimating the variance of time averages. J. Appl. Meteorol., 14, 159-163.

Dry spells: RCMs performance to simulate present climate and projections for future climate in South America

Pablo Zaninelli[1,2], Andrea F. Carril[1,2], Claudio G. Menéndez[1,2,3] and Enrique Sánchez[4]

[1] Centro de investigaciones del mar y la atmósfera (CIMA/CONICET-UBA), Buenos Aires, Argentina (pzaninelli@cima.fcen.uba.ar)
[2] Instituto Franco-Argentino para el Estudio del Clima y sus Impactos (UMI IFAECI/CNRS-CONICET-UBA), Buenos Aires, Argentina
[3] Departamento de Ciencias de la Atmósfera y los Océanos, Facultad de Ciencias Exactas y Naturales, Universidad de Buenos Aires, Buenos Aires, Argentina
[4] Universidad Castilla – La Mancha, Física de la Tierra, Envirnomental Sciences, Toledo, Spain

1. Introduction

Dry spells can generate significant economic lost in activities related to land use (e.g. agriculture and forestry), cause deficit in water resources and occasionally damage the health of the population (Magrin et al. (2007)), making it important to study.

Typical definitions of dry spells imply the use of fixed thresholds, both to define dry days as to define dry spells (Lana et al. (2008), Sánchez et al. (2011), Rivera et al. (2012)), which serve to relatively small regions or regions with similar climatological characteristics. But when we need to study large domains with different climate characteristics the use of fixed thresholds could result inappropriate.

In this work our aim is to study the ability of regional climate models (RCMs) to capture the present-day dry spells over South America and the projected changes based on a variable-threshold approach.

2. Data and Methodology

The dataset used is an ensemble of five RCMs: LMDZ, PROMES, RCA, REMO and RegCM3, which were integrated in the framework of CLARIS-LPB project (A European-South America Network for Climate Change Assessment and Impact Studies in La Plata Basin; European Commission 7th Framework Programme). These RCMs were forced by different Coupled General Circulation Models (IPSL, ECHAM5 and HadCM3) from the CMIP3 and integrated at about 50km of horizontal resolution for two 30-year periods: recent climate (1960-1990) and distant future (2070-2100). Integrations of these RCMs have been previously evaluated when forced by ERA-Interim reanalysis for the South America domain (Solman et al. (2013)).

A dataset of gridded precipitation data (CPC-UNI, NOAA Climate Prediction Center Unified Precipitation) (Chen et al. (2008)) is used to evaluate the model simulations.

Definitions of dry days and dry spells are based on a variable-threshold approach. A dry day is defined as a day with accumulated daily precipitation below a threshold calculated as the percentile 25 of the series of accumulated daily precipitation for CPC-UNI dataset. In addition, because CPC data overestimate the number of days with light precipitation (Carvalho et al. (2012)) in regions with few precipitation gauges (as., e.g., vast areas of South America), we consider only days with precipitation above 0,2 mm for computing the percentile.

On other hand, the threshold defined as the number of consecutive dry days plus two standard deviations is used to determine a dry spell. Then, a dry spell is indicated as the number of consecutive dry days (N) larger than the above described threshold. This threshold is both, grid point -dependent and model-dependent.

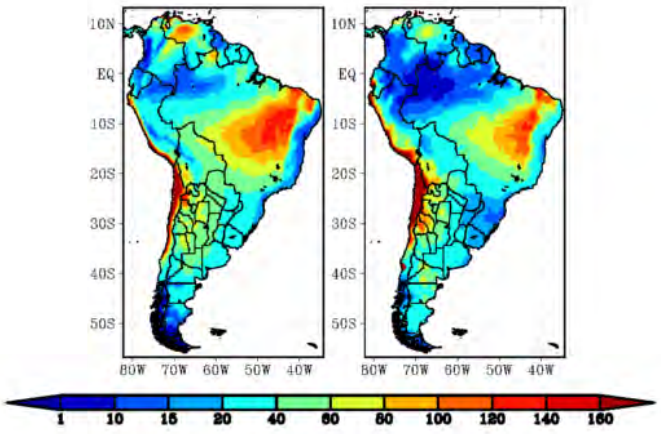


Figure 1. Mean length of dry spells for recent climate. Ensemble of models (left) and CPC-UNI (right). Units are in days.

3. Skill of RCMs to simulate present climate

As shown in Figure 1, in general the ensemble captures appropriately the spatial patterns with the maximum and minimum values well localized, although the mean length of dry spells tends to be overestimated. This can be seen mainly in the Mato Grosso Plateau, in South Eastern South America (SESA) and in the Amazon basin where the overestimation is about 20 days. However, the length of dry spells is underestimated along the Pacific coasts. Similar results were found by Marengo et al. (2009) with the regional climate model HadRM3P.

In SESA this overestimation could be associated with inaccuracies to simulate the intensity of daily precipitation and the frequency of wet days. The RCMs tend to overestimate the frequency of wet days and underestimate the intensity of daily precipitation in SESA (e.g., Menéndez et al. (2010) and Carril et al. (2012)). Moreover, the ensemble of models underestimates the annual mean precipitation but reproduces relatively well the percentage of dry days (not show). This could lead to an overestimation of the number of consecutive days with light precipitation which contributes to increment the length of dry spells.

In western Amazon basin RCMs also overestimate the

mean length of dry spells (models tend to cluster dry days in that region). Unlike what is happening in SESA, in western Amazon the models underestimate the percentage of dry days and reproduce acceptably the annual mean precipitation (not shown); however the effect over the dry spells simulations is the same that in SESA.

4. Future climate

The changes projected by the ensemble of RCMs are shown in Figure 2. The major increases in the mean length of dry spells for future climate (2071-2100) are expected over northeastern quadrant of South America, Chile and northwestern Argentina, with typical increases of 10-30% with respect to the base period (1961-1990). Over the northwestern quadrant of the continent the projections show local reductions (up to the 20%) in the mean length of dry spells.

The increase projected by the RCMs in the eastern side of the Amazon basin (which ranges from 10% to 50%) was also documented by Marengo et al. (2009) for two possible emission scenarios (A1 and B1) and using a different definition of dry spells.

The uncertainty is large in central Argentina and La Plata basin where two models project an increase (LMDZ and PROMES) meanwhile the others two a reduction (RCA and RegCM3) of the dry spells length (not shown), with no changes in the ensemble mean (REMO does not project changes). These different responses may be due to the influence of the global circulation models that have been used to force the RCMs (RCA and RegCM3 have been forced by the same global model and LMDZ and PROMES by different models). Of course, the manner in which models simulate the significant local or regional processes, such as convective precipitation and land-atmosphere interaction, can also influence the results.

5. Conclusions

Based on a variable-threshold approach we have documented the ability of an ensemble of RCMs to simulate present-day dry spells.

The ensemble mean reproduce appropriately the main spatial pattern of the dry spells length. Deficiencies are mainly associated with an overestimation of the mean length of dry spells caused by an overestimation of the persistence of dry days.

For future climate, the major increases in the mean length of dry spells are projected over northeast of South America, Chile and north of Argentina, meanwhile some decreases are expected over the western Amazon basin. In other regions like SESA the uncertainty makes it difficult to identify a signal of change.

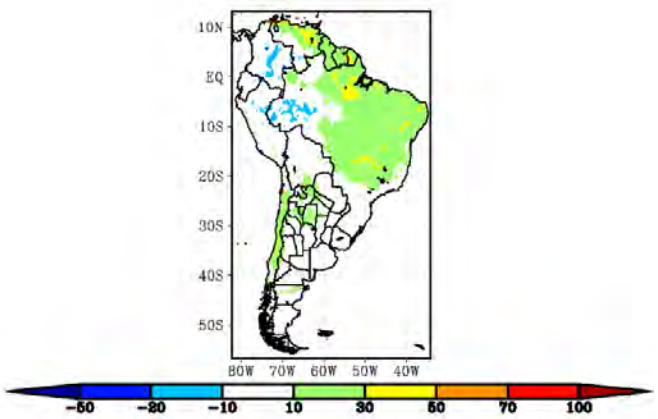


Figure 2. Response to the climate change of mean length of dry spells for the ensemble of models. Units are in percentage of change respect to the recent climate (1961-1990).

References

Carril, A.F. et al., 2012. Performance of a multi-RCM ensemble for South Eastern South America. Clim. Dyn., 39(12): 2747-2768.

Carvalho, L.M. et al., 2012. Precipitation characteristics of the South American monsoon system derived from multiple datasets. Journal of Climate, 25(13): 4600-4620.

Chen, M. et al., 2008. Assessing objective techniques for gauge-based analyses of global daily precipitation. J. Geophys. Res. D, 113(4).

Lana, X. et al., 2008. Spatial and temporal patterns of dry spell lengths in the Iberian Peninsula for the second half of the twentieth century. Theor. Appl. Climatol., 91(1): 99-116.

Magrin, G. et al., 2007. Latin America. Climate Change 2007: Impacts, Adaptation and Vulnerability. Contribution of Working Group II to the Fourth Assessment Report of the Intergovernmental Panel on Climate Change. Cambridge University Press: 581-615.

Marengo, J.A., Jones, R., Alves, L.M. and Valverde, M.C., 2009. Future change of temperature and precipitation extremes in south america as derived from the precis regional climate modeling system. Int. J. of Climatol., 29(15): 2241-2255.

Menéndez, C.G. et al., 2010. Downscaling extreme month-long anomalies in southern South America. Clim. Change, 98(3): 379-403.

Rivera, J.A., Penalba, O.C. and Betolli, M.L., 2012. Inter-annual and inter-decadal variability of dry days in Argentina. Int. J. Climatol.

Sánchez, E. et al., 2011. Regional modeling of dry spells over the Iberian Peninsula for present climate and climate change conditions. Clim. Change, 107(3): 625-634.

Solman, S.A. et al., 2013. Evaluation of an ensemble of regional climate model simulations over South America driven by the ERA-Interim reanalysis: model performance and uncertainties. Clim. Dyn.: 1-19.

Comparisons of simulated climate changes of Eastern China using WRF with Noah and Noah-MP land surface scheme

Xuezhen Zhang[1] and Yang Hu[2]

[1] Institute of Geographic Sciences and Natural Resources Research, Chinese Academy of Sciences, Beijing 100101, China (xzzhang@igsnrr.ac.cn)

[2] State Key Laboratory of Earth Surface Processes and Resource Ecology, Beijing Normal University, Beijing, 100875, China

1. Background

Land surface provide heat and moisture to atmosphere. The land surface scheme plays very important role on determining the performance of the coupled climate model. Jin *et al.* (2010) reported WRF model with CLM3 land surface scheme has more excellent performance than with other land surface schemes through one-year simulation. Here, we compared the simulations of WRF model with Noah land surface model and Noah-MP land surface model respectively. We didn't only compare the ability of capturing climatology pattern but also the ability of representing the climate variations.

2. Experimental design

Our simulation domain covers the eastern China with the central point of (37N, 115E) and has 155 grids in east-west direction and 168 grids in south-north direction with grid size of 30 km by 30 km (Figure 1).

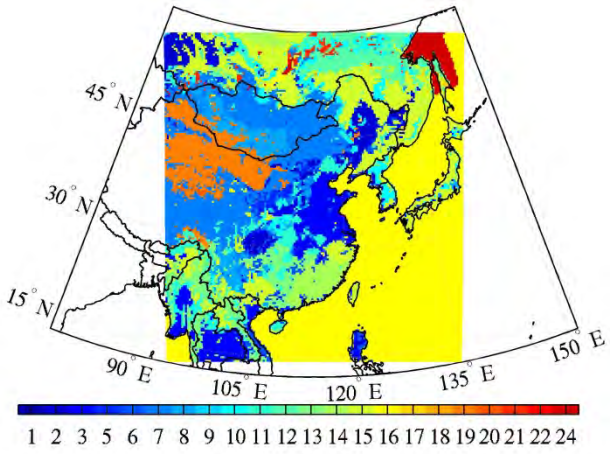


Figure 1. Simulation domain (color bar represents the land use following the USGS category).

We carried out two 21-years (1980-2000) simulations. Both of simulations used exactly same settings and physical parameterizations except for the land surface scheme. One simulation used Noah land surface scheme (Exp0, hereafter) and the other one used Noah-MP land surface scheme (Exp1, hereafter).

3. Results

As shown by Figure 2 and Figure 3, the simulation with Noah-MP land surface scheme is generally warmer than the simulation with Noah land surface scheme. For winter, the largest overestimation mainly occurs across the North China, particularly for the Northeast China and Mongolia area, with the largest values higher than 5℃ (Figure 2). For the summer, the overestimation is also prevailing across the eastern China. The overestimation is cut off and the largest values is no more than 3℃. It is obvious that there is a large area with underestimation in the Mongolia area with the large value of about 1.5℃ (Figure 3).

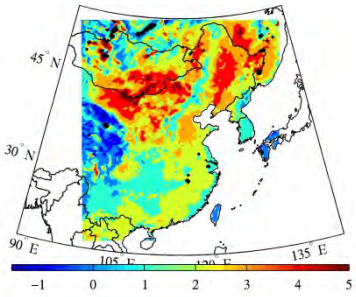


Figure 2. Differences of simulated T 2m for DJF from 1981 to 2000 (Exp1 minus Exp0).

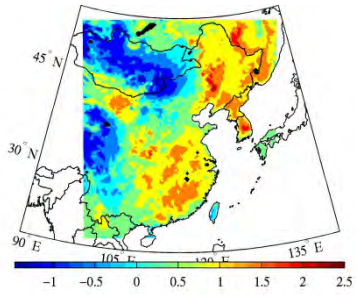


Figure 3. Same as Figure 2, but for JJA

Figure 4 and Figure 5 illustrate the variations of simulated temperature. Generally, both of the two simulations are significantly correlated with each other. The significant correlations could be detected in both of winter and summer.

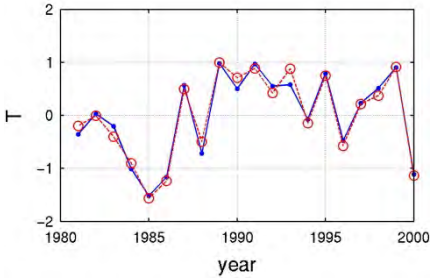


Figure 4 Simulated variations of regional mean T 2m of land area for DJF from 1981 to 2000 (blue: Exp0; red: Exp1)

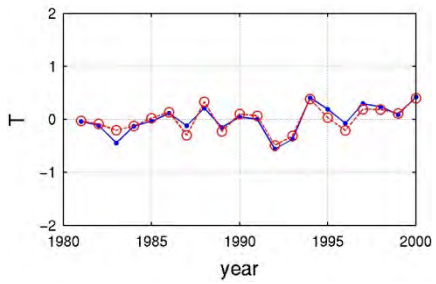


Figure 5 Same as Figure 4, but for JJA

4. Discussion and Conclusion

Above findings demonstrate that the simulated climatology temperature with Noah and Noah-MP has large differences. The difference is larger in winter than that in summer. And, the differences have large spatial variability. Such complex differences might be derived from the surface flux. More diagnose is being done.

Besides, we could found the simulated inter-annual variations with Noah and Noah-MP has little differences. The consistent inter-annual variations may imply the land surface scheme in the WRF model have poor ability to regulate the variation from the lateral boundary.

References

Jin, J., N. L. Miller, and N. Schlegel (2010) Sensitivity Study of Four Land Surface Schemes in the WRFModel,

WRF sensitivity to physics parameterizations over the MENA-CORDEX domain

George Zittis[1], Panos Hadjinicolaou[1] and Jos Lelieveld[1,2]

[1] Energy, Environment and Water Research Center, The Cyprus Institute, Nicosia, Cyprus (g.zittis@cyi.ac.cy)
[2] Department of Atmospheric Chemistry, Max Planck Institute for Chemistry, Mainz, Germany

1. Introduction

According to climate projections, the Middle East and North Africa (MENA) region will be greatly affected by climate change. Significant decreases in precipitation, more pronounced during winter and strong warming, especially during summer, will likely induce strong socioeconomic impacts in the region. The need for timely design and implementation of adaptation strategies is pressing. However, the coarse resolution of the current global climate models ($\approx$ 100 km) is not sufficient for impact studies on a regional or national level and higher spatial resolution is required.

Climate studies focusing on the MENA are so far limited and not well coordinated. The World Climate Research Program through the Coordinated Regional Climate Downscaling Experiment (CORDEX) and the establishment of the MENA-CORDEX domain aims to fill this gap. CORDEX provides the required guidelines for experiments and coordination between research groups interested in the region. The already changing climate, the increasing population of the region, the large potential for renewable energy production are only some of the factors that highlight the need for regional studies focused over MENA.

Besides the rapid development of computers over the last decades, computational limitations still exist. During the design of long-term climate simulations guidelines regarding what parameterization schemes should be used or avoided could probably reduce computational power requirements, storage space and time for analysis. Under this framework, with this study we try to provide a point of reference for potential users of the climate mode of WRF in the MENA region.

2. Regional Climate Modeling with WRF

One of the widely used techniques of obtaining high-resolution information relevant for regional-scale studies is dynamical downscaling. Data derived from global models are used as initial and boundary conditions to drive the higher resolution limited-area models. Such a model is the Weather Research and Forecasting (WRF) model (Skamarock et al., 2008). It is a meso-scale numerical weather prediction model, originally designed to serve atmospheric research and operational forecasting. Over the last years it is also widely used as a dynamical downscaling tool (Salathè et al. 2010, Nikulin et al. 2012, Soares et al. 2012, Warrach-Sagi et al. 2013a). Regional climate modeling with WRF is not widespread in this region, and most of the relevant studies focus either on Europe or Africa.

Parameterization of subgrid-scale phenomena persists as one of the most challenging problems in numerical modeling of the atmosphere (García-Díez et al. 2013). In the WRF system users have the flexibility to select from a range of different physics parameterizations. However, this choice can be a question of the type of application, the location of interest or the horizontal and time resolutions. This type of uncertainties related to the physics parameterizations has received much attention over the last years.

3. Model configuration - Data

The CL-WRF (Fita et al., 2010) set of modifications to the version 3.5.1 of WRF model was used for the simulations of this study. The length of each simulation is 2 years (December 1988-Nomber 1990). We have used a horizontal resolution of 0.44° ($\approx$50km) in 30 vertical levels. The ERA-Interim reanalysis dataset was used to provide initial and boundary conditions. The latter were updated every six hours.

All possible combinations between two Planetary Boundary Layer (PBL), three Cumulus (CUM) and two Microphysics (MIC) schemes were tested. Namely, the Yonsei University and Mellor-Jamada-Janjic (MYJ) PBL schemes, the Kain-Fritz (KF) and Betts-Miller-Janjic (BMJ) CUM schemes and the Grell-Devenyi (GD), the WRF Single-Moment 6-class (WSM6) and the Goddard (GCE) MIC schemes were used. The CAM short and long wave radiation schemes and the Noah land-surface model were used for all simulations.

Surface meteorological variables (maximum/ minimum temperature and precipitation) extracted from the model output were compared with the roughly same resolution (0.50°) CRU gridded observational dataset, version TS3.10 (Harris et al., 2013). Additionally, daily ECA&D observations (Klein Tank, 2002) were used for 12 selected locations of MENA.

4. Methods and metrics

In order to isolate the effect of each physics scheme from the total configuration, we have calculated the mean differences between simulations that only differ in one type of physical parameterization (PBL, MIC or CUM) each time. Relevant plots of these differences can indicate how sensitive each of the tested surface variables is to the parameterization of the selected physical processes within the WRF model and for the MENA region.

As mentioned above, in this WRF physics inter-comparison we focus on three surface variables. In order to explore the performance of each simulation in an objective way, we used a range of statistical metrics after

calculating the monthly values of the model output and CRU data. These metrics are the correlation coefficient, the mean absolute error, the modified index of agreement and the mean absolute difference of the standard deviations of the two samples.

The statistical metrics described in the previous paragraph, were applied between the monthly values of CRU data and each of the 12 CL-WRF simulations. Every grid point of the MENA domain was independently analyzed. For each grid point the 12 runs were ranked according to their metrics performance for all of the three variables. Finally, the total number of grid points where each run was ranked first was recorded. The runs with the highest number of corresponding ranking-first grid points are considered as the best performing ones over the region.

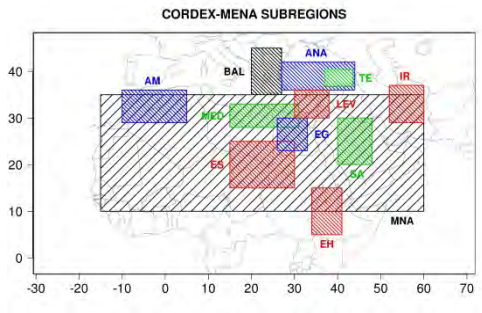


Figure 1. Definition of the 12 sub-regions in the CORDEX-MENA domain.

Because of the large extent of the MENA domain, the selection might be biased from the performance over grid points not necessarily relevant for studies over the traditional MENA definition territories, especially near the tropics. To avoid this, we repeated the analysis including only grid points over sub-domains of special interest (Fig. 1). Similar type of analysis between the ECA&D station data and the closest model grid points was conducted.

5. Results and discussion

Our findings show that maximum and minimum temperature are most sensitive to the selection of the microphysics parameterization. In more detail, runs that resolve the WSM6 scheme are in closer agreement to the gridded CRU observations and station data. This is mainly connected to the more realistic cloudiness produced by this scheme. In contrast the GCE scheme overestimates cloud amounts and thus strongly underestimates temperature. Temperature sensitivity to the cumulus parameterization is minor since convection mainly occurs during the evening hours, after maximum and well before minimum temperatures are recorded within the daily cycle. PBL is critical only for minimum temperature and mainly over parts of the domain influenced by desert but is of less significance comparing to the selection of microphysics.

As expected, precipitation is more difficult to be modeled. The scores of the statistical metrics are in general lower than for temperature; nevertheless, for the dry region of interest (MNA subdomain in Fig. 1) the model performs better and seems to be able to adequately capture the annual precipitation cycle. Precipitation is found to be sensitive mainly to the selection of cumulus and microphysics schemes. This is particularly evident in the tropics, which is a part of the domain less relevant for impact studies over the traditional definition of MENA region.

An objective ranking based on four statistical metrics between the 12 experiments and the observational data was performed. The configuration of the best-performing simulation includes the YSU boundary layer, the KF cumulus and WSM6 microphysics schemes in addition to the CAM long and shortwave radiation and NOAH land surface models that were used in all simulations.

These results should be considered representative for climate modeling studies for the MENA domain and not necessarily for other regions. A more extensive evaluation, including longer simulations that will allow the calculation of trends, will follow.

References

Fita L, Fernández J, Gracia-Diez M (2010) CLWRF: WRF modifications for regional climate simulation under future scenarios. 11th WRF User's Workshop, NCAR, Boulder, Colorado.

García-Díez M, Fernández, J, Fita, L, Yagüe C (2013) Seasonal dependence of WRF model biases and sensitivity to PBL schemes over Europe. Quarterly Journal of the Royal Meteorological Society 139(671): 501-514.

Harris I, Jones PD, Osborn TJ, Lister DH (2013) Updated high-resolution grids of monthly climatic observations. In press, Int. Journal of Climatology.

Klein Tank, AMG et al. (2002) Daily dataset of 20th-century surface air temperature and precipitation series for the European Climate Assessment. International Journal of Climatology 22: 1441-1453.

Nikulin G, Jones C, Giorgi F, Asrar G, Büchner M, Cerezo-Mota R, Christensen OB, Déqué M, Fernandez J, Hänsler A, van Meijgaard E, Samuelsson P, Sylla MB, Sushama L (2012) Precipitation climatology in an ensemble of CORDEX-Africa regional climate simulations. Journal of Climate 25(18): 6057-6078.

Salathé EP, Leung LR, Qian Y, Zhang Y (2010) Regional climate model projections for the state of Washington. Climatic Change 102(1): 51-75. DOI: 10.1007/s10584-010-9849-y

Skamarock WC et. al. (2008) A description of the Advanced Research WRF version 3. NCAR Tech. Note NCAR/TN-4751STR.

Soares, P, Cardoso R, Miranda P, Medeiros J, Belo-Pereira M, Espirito-Santo F (2012) WRF high resolution dynamical downscaling of ERA-interim for Portugal. Climate Dynamics 39(9-10): 2497-2522.

Warrach-Sagi K, Schwitalla T, Wulfmeyer V, Bauer HS (2013) Evaluation of a climate simulation in Europe based on the WRF-NOAH Model System: precipitation in Germany. Climate Dynamics 41: 755-774.

Parameter tuning and calibration of RegCM3 with MIT-Emanuel cumulus parameterization scheme over CORDEX East Asian domain

Liwei Zou[1], Yun Qian[2], Tianjun Zhou[1], and Ben Yang[3]

[1] LASG, Institute of Atmospheric Physics, Chinese Academy of Science, Beijing China (zoulw@lasg.iap.ac.cn)
[2] Pacific Northwest National Laboratory, Richland, Washington, USA
[3] School of Atmospheric Sciences, Nanjing University, Nanjing China

1. Introduction

Previous studies have attempted to customize the RegCM3 with MIT-Emanuel cumulus parameterization scheme by designing sensitivity experiments through three different aspects. Such type of sensitivity experiments is effective for the selection of the model physics, while it is a little difficult to identify the optimal values of the tunable input parameters in the model physics, because there are too many possible combinations to be exhaustively enumerated.

Identifying a set of the optimal values from the tunable input parameters space could be regarded as the problem of "global optimization". The multiple very fast simulated annealing (MVFSA) algorithm has been shown to be a practical method that can progressively and efficiently move toward regions of the parameter space that minimize model errors.

In this study, based on the previous sensitivity studies, we apply the MVFSA technique to calibrate the RegCM3 with MIT-Emanuel cumulus parameterization scheme over CORDEX East Asian domain.

2. Model and experimental design

These selected seven parameters can be divided into three categories:

1) Convection suppression criteria. We choose the relativity humidity (RH) criteria in this study. The convection is activated when the RH averaged from the cloud top to cloud base is larger than a critical value;

2) Two parameters in MIT-Emanuel cumulus parameterization scheme: a) the relaxation rate, α b) the warm cloud autoconversion threshold, l_0;

3) RHmin (the gridbox relative humidity threshold for cloudiness) and Cacs (the autoconversion scale factor) in SUBEX. RHmin and Cacs can be defined separately for land and ocean;

The RegCM3 experiments are performed one by one with a set of perturbed parameters sampled by the MVFSA technique. To obtain the global optimal values, we repeat VFSA procedure three times with different starting parameter set (three chains). There are 80 experiments in each chain. Each simulation is integrated starting from 1 May through 31 August of 1998. The first month is regarded as the "spin-up" time of simulation.

3. Results

The parameter "relative humidity criteria (RH)" has significant effects on the model results (Figure 1). Around 75% of the good simulations are found when the RH is set from 0.65 to 0.85. There is highest probability for obtaining a good simulation when the RH is set around 0.75. The second important parameter is the l_0. The frequency of good simulations is about 30% when the l_0 is set around 0.040. The rest parameters have weaker effects on the model results, especially RHmin_land, RHmin_ocean and relaxation rate α, whose frequency distributions are rather uniform.

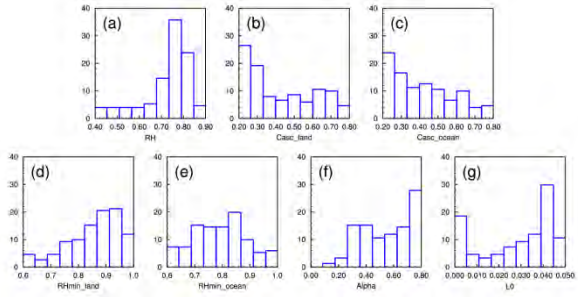


Figure 1 Frequency (%) distributions of good simulations, which have better model skill than the simulation with default parameters, as a function of each parameter.

The spatial distribution of precipitation averaged from June to August of 1998 with optimal parameters is shown in Figure 2 along with that with default parameters and the observation. The observed precipitation is characterized with major rainband over tropics, the Bay of Bengal, and the Meiyu front region. The above-normal Meiyu rainfall caused severe flooding over East Asia. In the simulation with default parameters, however, the simulated precipitation over the Bay of Bengal, the northern South China Sea, and the Western North Pacific is highly overestimated, while that over the northern equatorial western Pacific is significantly underestimated. This simulated pattern was also found in Chow et al. (2006), whose simulated domain was smaller than CORDEX East Asian domain. The spatial correlation coefficient (SCC) is 0.29, and the model skill with default parameters is 2.02. The simulation with optimal parameters significantly improves the model performance, with the model decreasing from 2.02 to 1.60. In particular, the overestimated rainfall is reduced over the Bay of Bengal, the northern South China Sea, and the Western North Pacific, while the increased rainfall over northern equatorial western Pacific is evident, approaching the observation. The SCC is increased to 0.50.

The responses of rainfall over different regions to the seven parameters are shown in Figure 3. The sensitivity responses are shown as the correlation coefficients

between the regional rainfall averaged over seven regions and the perturbed seven parameters from the total 240 simulations. Among the seven parameters, overall, the parameter "relative humidity criteria (RH)" is the most important parameter, with high influence on the rainfall over all the regions except that over Yangtze River valley and over tropical Indian Ocean. The parameter RHmin_land (RHmin_ocean) has more effects on the rainfall over the Yangtze River valley (tropical Indian Ocean).

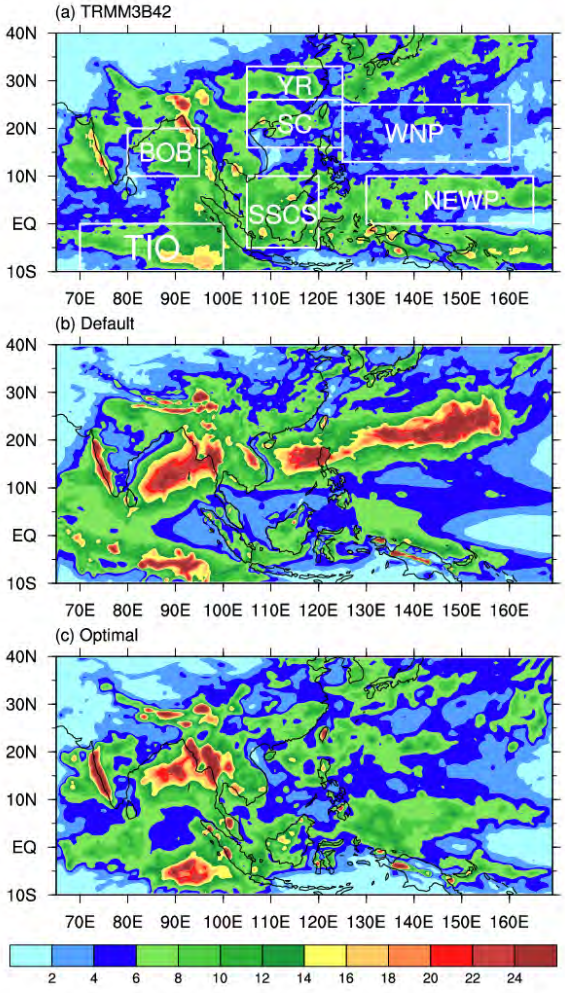


Figure 2 Spatial distributions of precipitation (mm/day) averaged from June to August of 1998 derived from (a) TRMM3B42, (b) the simulation with default parameters, and (c) the simulation with the identified optimal parameters. Boxes illustrate the seven subregions of the simulated domain: Tropical Indian Ocean (TIO; –10°S–0°, 70°E–100°E); Southern South China Sea (SSCS; –5°S–10°N, 105°E–120°E); northern equatorial western Pacific (NEWP; 0°–10°N, 130°E–165°E); Bay of Bengal (BOB; 10°N–20°N, 80°E–95°E); South China (SC; 16°N–26°N, 105°E–125°E); Yangtze River (YR; 26°N–33°N, 105°E–125°E); and Western North Pacific (WNP; 13°N–25°N, 125°E–160°E).

4. Summary

In this study, we calibrated the performance of regional climate model RegCM3 with Massachusetts Institute of Technology (MIT)-Emanuel cumulus parameterization scheme over CORDEX East Asia domain by tuning the selected seven parameters through multiple very fast simulated annealing (MVFSA) sampling method. The seven parameters were selected based on previous studies, which customized the RegCM3 with MIT-Emanuel scheme through three different ways by using the sensitivity experiments. The responses of model results to the seven parameters were investigated. Since the monthly total rainfall is constrained, the simulated spatial pattern of rainfall and the probability density function (PDF) distribution of daily rainfall rates are significantly improved in the optimal simulation. Sensitivity analysis suggest that the parameter "relative humidity criteria" (RH), which has not been considered in the default simulation, has the largest effect on the model results. The responses of total rainfall over different regions to RH were examined. Positive responses of total rainfall to RH are found over northern equatorial western Pacific, which are contributed by the positive responses of explicit rainfall. Followed by an increase of RH, the increases of the low-level convergence and the associated increases in cloud water favor the increase of the explicit rainfall. The identified optimal parameters constrained by the total rainfall have positive effects on the low-level circulation and the surface air temperature. Furthermore, the optimized parameters based on the extreme case are suitable for a normal case and the model's new version with mixed convection scheme.

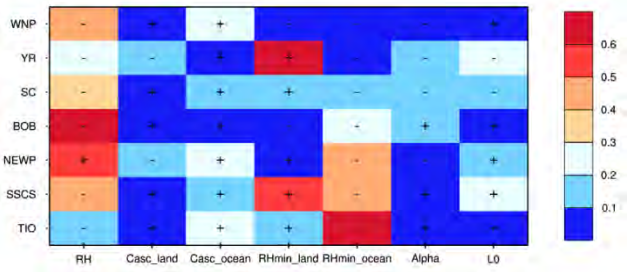


Figure 3 Responses of total rainfall (mm/day) over the selected regions shown in Figure 2a to the seven parameters. Sensitivity ranking is shown as the correlation coefficients between the regional rainfalls averaged over seven regions and the perturbed seven parameters from the total 240 simulations. Positive and negative correlation coefficients are represented as "+" and "-" symbols, respectively.

Topic 4

RCM Ensembles

Regime-dependent validation of simulated surface wind speed in coastal areas of the North Sea

Ivonne Anders[1], Burkhardt Rockel[2]

[1] Central Institute for Meteorology and Geodynamics, Vienna, Austria (Ivonne.Anders@zamg.ac.at)
[2] Helmholtz-Zentrum Geesthacht – Centre for material and coastal research, Geesthacht, Germany

1. Introduction

The knowledge of the wind climate at specific locations is of vital importance for risk assessment, engineering, and wind power assessment. Results from regional climate models (RCM) are getting more and more important to enlarge the investigation from local to regional scale.

With help of GCM- and RCM-simulations Leckebusch and Ulbrich (1994) investigate the relationship between cyclones and extreme windstorm events over Europe. It is clearly visible that with the higher temporal and spatial resolution, especially in coastal areas the RCM lead to an improvement in simulating the extreme wind speeds compared to the GCM. For open ocean areas Winterfeldt and Weisse (2009) show no adding value for RCM modeling compared to reanalysis forcing in the wind speed frequency distributions, whereas in coastal regions RCM results - especially for higher wind speed percentiles - are closer to the observations than the forcing data. Rockel and Woth (2007) focused on near-surface wind speed over Europe and identified that most of the RCMs have not been able to simulate wind velocities above 8 Bft.

In this study we investigate the simulated near surface wind speed by a regional climate multi model ensemble carried out in the EU funded project ENSEMBLES based on two different regime classifications one for Europe and the other for the North Sea.

2. Wind observation data and Multi Regional Climate Model Ensemble

Within the ENSEMBLES project several participating European institutions run their regional climate models (RCM) for the same European domain (including the Mediterranean and Island) with the same grid size of 0.44 and in a second simulation 0.22. The simulations use ERA40 reanalysis as forcing data and cover at least the time period from 1961 to 2000. To verify the near surface wind speed simulated by all participating models we compared not only daily mean of simulated 10m-wind speed but also daily maximum values to observation data. The station data for wind speed and direction has been provided by the German and the Dutch Weather Services DWD and KNMI. With the help of a change detection algorithm and together with the provided stations histories we defined two time windows where as many as possible of the measurements are less disturbed. For the Netherlands we choose obser- vation data of 10 stations for the time period 1971-1983 and 5 stations from 1971 to 2000, for the German coast it is 11 and 8 stations respectively.

3. Weather regime classifications for Europe and the North Sea

For Europe Sanchez-Gomez et al (2008) used the simulation results from the regional climate model ensemble introduced above to investigate the models ability to reproduce the large-scale atmospheric circulation of the driving field the ERA40 Reanalysis data. Four weather regimes (Blocking (BL), Zonal (NAO+), Atlantic Ridge (AR) and Greenland Anticyclone (NAO-)) have been analysed for every day in the summer months (from June to September) and the winter months (from December to March) seperatly for the period 1961 to 2000.

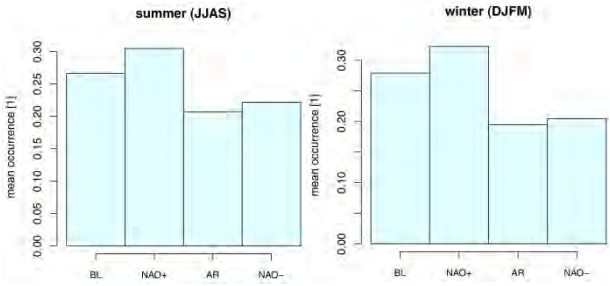


Figure 1. Frequency of the occurence of the four weather regimes Blocking (BL), Zonal (NAO+), Atlantic Ridge (AR) and Greenland Anticyclone (NAO-) derived from geopotential height at 500 hPa pressure level for the summer months (JJAS) and winter months (DJFM) in 1961-2000 by Sanchez-Gomez et al (2009)

The objective procedure to classify the atmospheric circulation near the surface for the North Sea goes back to investigations of Jenkinson and Collison (1977). This simple and efficient method is based on the areal pressure distribution at the mean sea level (MSLP) and the derivation of two representative indices for wind and velocity at 16 grid points covering the North Sea and the surrounding with a spatial resolution of 10 by 5 (longitude by latitude) (cf. Figure 1). The definition of the circulation type, but also the identification of storm events are finally based on empirical relations between the two indices.

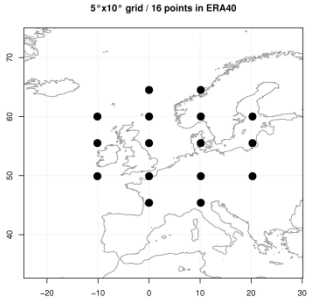


Figure 2. Visualization of the grid point locations used in weather type classification for the North Sea

If In this way 27 different weather types can be distinguished. Beside the predefined 8 prevailed wind directions and the two possibilities on cyclonic or anticyclonic turbulences, 2x8 hybrid weather types can be defined. Additionally there is an unclassifiable type (UNC), which mainly occurs in combination with weak pressure gradients. With respect to a robust investigation of wind speed depending on their directional component all hybrid types have been grouped to one of the pure directional types.

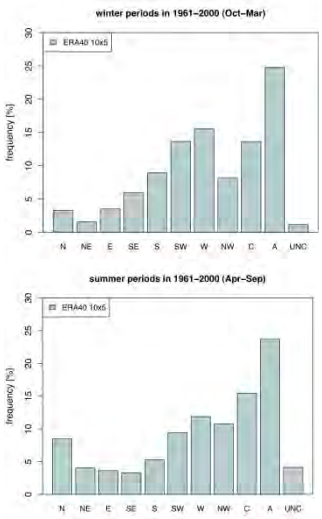


Figure 3. Relative occurrence frequency (%) of the 11 weather regimes based on ERA40 daily mean sea level pressure fields at the different 16 grid points (cf. Figure 2) within the time period 1961 to 2000.

4. Results

Based on the weather classification provided by Sanchez-Gomez et al. (2008) a regime-dependent validation of the simulated surface wind speeds has been carried out. Several measures and skill scores have been applied to analyse the RCMs performance compared to the driving field and to evaluate accuracy gain by including higher spatial resolution of the grid cell. Results for bias, RMSE, standard deviation but also for Brier Skill Score and Perkins adapted skill score have been calculated.

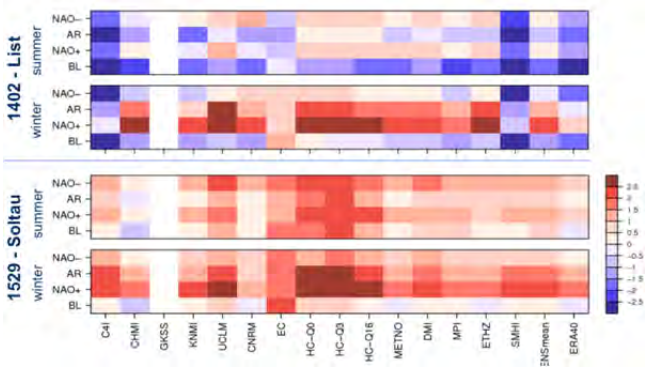


Figure 4. Bias between simulated wind speed by the different regional climate models separated by the regimes at certain locations in the DWD network for the spatial resolutions of 25km within the time period 1971-2000.

Blocking in the winter season shows often better results than the other regimes in the same season (cf. Figure 4). For Perkins score an added value of 25km compared to 50km simulations can be detected (cf. Figure 5). NAO+ and AR regimes indicate a stronger bias in wintertime at all stations. At few stations, e.g. Helgoland, RCMs show an added value concerning the quantiles assessment of daily mean surface wind speed compared to the driving field.

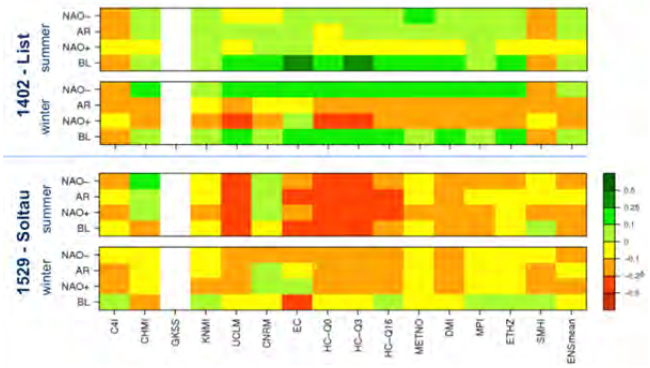


Figure 5. Extended Perkins score of simulated wind speed by the different regional climate models separated by the regimes at certain locations in the DWD network for the spatial resolutions of 25km within the time period 1971-2000.

5. Discussion and Outlook

Several measures and skill scores were applied to analyse the RCMs performance compared to the driving field and to evaluate accuracy gain by including higher spatial resolution of the grid cell

Analysis based on the regime classification by Sanchez-Gomez et al. (2009) shows a diverse behavior and vary from station to station but they cannot be addressed to the different large scale atmospheric conditions. The reason is, that the regimes do not represent the wind conditions at the area of interest.

All analysis will be repeated based on the regime classification for the North Sea described above.

References

Jenkinson A, Collison F (1977) An initial climatology of gales over the north sea. Synoptic Climatology Branch Memorandum 62:18pp, UK Met Office

E. Sanchez-Gomez, S. Somot and M. Déqué (2008): Ability of an ensemble of regional climate models to reproduce weather regimes over Europe-Atlantic during the period 1961-2000. Climate Dynamics, Vol.33(5), 723-736.

Leckebusch, G.C. and Ulbrich, U. (1994), On the relationship between cyclones and extreme windstorm events over Europe under climate change, Global and Planetary Change, No. 4, pp. 181-193

Perkins S.E. et.al (2007), Evaluation of the AR4 Climate Models' Simulated Daily Maximum Temperature, Minimum Temperature, and Precipitation over Australia Using Probability Density Functions, J. Clim., Vol. 20, pp. 4356–4376

Rockel, B. and Woth, K. (2007) Extremes of near-surface wind speed over Europe and their future changes as estimated from an ensemble of RCM simulations, Climate Change, pp. 267-280

Uppala, S.M., et al. (2005) The ERA-40 re-analysis. Quart. J. R. Meteorol. Soc., No. 131, pp. 2961-3012

Winterfeldt, J. (2008), Comparison of measured and simulated wind speed data in the North Atlantic, GKSS Report, No. 2

Use of a multiple GCM and mixed physics ensemble of regional climate simulations to evaluate trends in extreme precipitation

Raymond W. Arritt[1], Pavel Ya. Groisman[2] and Ariele R. Daniel[3]

[1] Department of Agronomy, Iowa State University, Ames, Iowa 50011 USA (rwarritt@bruce.agron.iastate.edu)
[2] Hydrology Science and Services Corporation, Asheville, North Carolina 28804 USA
[3] Department of Agronomy, Iowa State University, Ames, Iowa 50011 USA

1. Problem statement

The shift of precipitation intensity toward heavy rates has been one of the most pronounced climate change signals observed for central and eastern North America (Groisman et al. 2012). We investigate this trend by using the RegCM4 regional climate model to dynamically downscale CMIP5 projections for 1950-2100 over the CORDEX North America domain. We examine the robustness of this signal by driving the regional model with output from a range of CMIP5 global models, and by using several physics parameterizations in the regional model.

2. Methodology

Our long-term goal is to perform regional climate simulations with most or all CMIP5 global models having output available at 6 hourly time resolution suitable for use as RCM boundary conditions. The first three global models we are using sample the range of climate sensitivity produced by the CMIP5 models. The UK Met Office model HadGEM2-ES has the highest equilibrium climate sensitivity of the CMIP5 models; the NOAA GFDL-ESM2M has one of the lowest; and the Canadian Earth System Model CanESM2 is near the middle of the range (Andrews et al. 2012). Six-hourly output fields from the RCP 8.5 scenario were used for each global model. Simulations began on 1 January 1950 and continue through 31 December 2099 (or the latest date available from the global model). Results for 1950 are discarded to allow partial adjustment between the atmosphere and land surface.

Each of the global models was downscaled using the International Centre for Theoretical Physics regional climate model RegCM4.4. The regional model was configured using 50 km horizontal grid spacing over the CORDEX North America domain. This is somewhat coarse in comparison to the current state of the art in regional climate modeling, but its lower computational demands reduce the compromises sometimes required for fine-resolution simulations. In particular this allows fairly large ensembles to be generated and makes it more practical to perform long transient simulations instead of relatively short time slices.

In addition to using different CMIP5 global models, RegCM4.4 is being executed with various convective parameterizations in order to examine the sensitivity of our results to the RCM configuration. Here we show results for the hybrid convective parameterization that uses the Emanuel scheme over water grid points and the Grell scheme with Fritsch-Chappell type closure (constant rate of release of convective instability) over land grid points. Sensitivity experiments using the ERA-Interim reanalysis for initial and lateral boundary conditions showed this scheme produced the highest domain-wide spatial correlation with observed monthly precipitation.

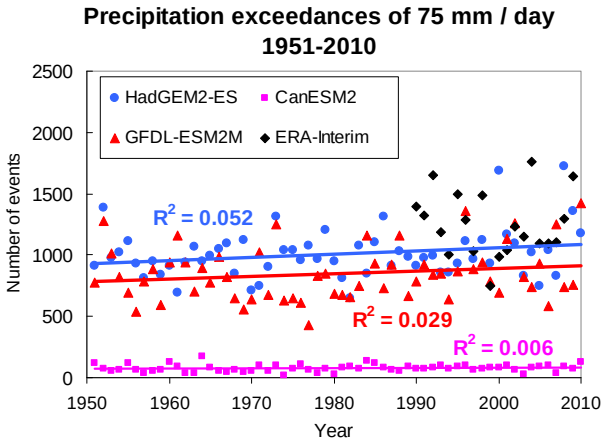


Figure 1: Annual incidence of precipitation exceeding 75 mm per day for a region of the central and eastern United States, produced in RegCM4.4 results using the indicated sources for initial and lateral boundary conditions. See text for details.

3. Preliminary results

We examine the trend in annual number of heavy precipitation events, defined as precipitation rate exceeding 75 mm per day at one grid point. This statistic is evaluated for land grid points east of longitude 100 W and latitudes between 23 and 47 N, corresponding approximately to the eastern half of the continental U.S. and adjacent parts of Canada.

Results for 1951-2010 show increasing incidence of heavy precipitation in RegCM4.4 simulations using HadGEM2-ES and GFDL-ESM2M global models for initial and lateral boundary conditions (Figure 1). The annual number of events for these two simulations during 1990-2009 is comparable to results from an ERA-Interim driven RegCM4.4 simulation for that period. Simulations using CanESM2 for initial and lateral boundary conditions produced far fewer heavy precipitation events.

The trend is mainly attributable to increases during the latter part of the period. Performing the analysis separately for 1951-1990 and 1971-2010 shows that the correlation vanishes for the earlier period (R^2 for the linear trend is < 0.01 for all simulations) and is higher for the later period (R^2 = 0.06 for the RegCM4.4.simulation

driven by HadGEM2-ES and R^2 = 0.08 for the one driven by GFDL-ESM2M). For both of these simulations the linear trend for 1971-2000 corresponds to an increase of about 5% per year, which is comparable to the trend found by Groisman et al. (2012) for the trend in observed precipitation rate exceeding 76.4 mm/day over the central United States.

4. Summary

Preliminary results from dynamically downscaled CMIP5 projections using RegCM4.4 show that simulations driven by the HadGEM2-ES and GFDL-ESM2M global models produce incidence of heavy precipitation (> 75 mm/day) comparable to that obtained when using ERA-Interim reanalysis for initial and boundary conditions. The trend over the period 1951-2010 is broadly similar to the observed trend reported by Groisman et al. (2012). A simulation driven by the CanESM2 global model produced much lower incidence of heavy precipitation. Keeping in mind that the sample of CMIP5 models considered here is very small, it is not clear that there is a relationship to equilibrium climate sensitivity of the global model. Although the global model with the highest sensitivity (HadGEM2-ES) produced the greatest number of heavy precipitation events in the regional model, the global model with medium sensitivity (CanESM2) produced far fewer events than the one with intermediate sensitivity (GFDL-ESM2M). There is a possibility that CanESM2 is an outlier and that a relationship to equilibrium climate sensitivity may emerge when a larger sample of CMIP5 models is used.

These results are very preliminary and it is obvious that much more needs to be done to confirm their robustness and to diagnose the physical mechanisms at work. Of particular interest is the reason for the very low incidence of heavy precipitation when using the CanESM2 global model to drive the regional model. Among the hypotheses we will explore are deficiencies in the CanESM2 representation of dynamical features such as storm tracks, and differences in the thermodynamic environment leading to convective precipitation. Updated results will be presented at the workshop.

Acknowledgments

This research was sponsored by the U.S. Department of Agriculture (USDA) under the Earth System Modeling program, Award No. 2013-67003-20642.

References

Andrews, T., J.M. Gregory, M.J. Webb and K.E. Taylor, 2012: Forcing, feedbacks and climate sensitivity in CMIP5 coupled atmosphere-ocean climate models. Geophys. Res. Lett. 39, L09712, doi:10.1029/2012GL051607.

Groisman, P. Y., R.W. Knight and T.R. Karl, 2012: Changes in intense precipitation over the central United States. J. Hydrometeorology, 13, 47-66.

Seasonal forecasting: Opportunities and challenges for use of regional climate models

Raymond W. Arritt[1], Christopher L. Castro[2]

[1] Department of Agronomy, Iowa State University, Ames, Iowa, USA (rwarritt@bruce.agron.iastate.edu)

[2] Department of Atmospheric Sciences, University of Arizona, Tucson, Arizona, USA (castro@atmo.arizona.edu)

1. Overview

Skillful seasonal forecasts are potentially of value for applications as diverse as agriculture, transportation, and insurance. Yet the use of regional climate models for seasonal forecasting has received far less attention than their use for climate change. Seasonal forecasts impose unique challenges that differ from both shorter-term numerical weather prediction and longer-term climate projections. In particular, the seasonal time scale is beyond the horizon for deterministic predictability, yet the goal is still to provide forecasts that are valid for specific periods (weeks to months) rather than long-term statistical tendencies.

We provide an overview of past and ongoing efforts in the use of RCMs to downscale global seasonal forecasts, with a focus on activities within the United States. We discuss both practical and scientific challenges to using RCMs for this problem, such as availability of driving data, the need for large ensembles, and constraints on the skill of global seasonal forecasts on which the skill of regional seasonal forecasts ultimately depend.

2. Winter seasonal forecasts: The MRED project

The Multi-RCM Ensemble Downscaling of Global Seasonal Forecasts (MRED) project was designed to test the usefulness of downscaling winter seasonal forecasts from global models using an ensemble of regional models. In MRED, seven RCMs downscaled 23 years of winter (December- April) reforecasts from the NOAA CFS Version 1 global seasonal forecast model (T62L64, ~1.9° degrees latitude/longitude), initialized in November. The MRED domain spans the coterminous U.S. at 32 km grid spacing. Each regional model downscaled 10 members from a CFS ensemble for each cool season 1982-2004. The MRED team consisted of participants from institutions throughout the United States, including universities, research laboratories, and the National Center for Environmental Prediction (NCEP) within the National Oceanic and Atmospheric Administration.

MRED confirmed that for seasonal forecasts as for global projections, regional model skill ultimately depends on the skill of the driving global model. CFS has highest precipitation skill in the southwest and southeastern U.S., both regions with strong ENSO-forced signals. The regional models tend to enhance global model forecast skill mostly in areas where there is already some skill in the global model. Individual RCMs mostly track CFS precipitation and temperature predictions, with each RCM having a consistent offset relative to the CFS (Figure 1). Though the MRED ensemble does not appear to increase the seasonal forecast skill for 2m air temperature over CFS, there is higher precipitation skill over the central and western U.S. tied to the terrain features (Yoon et al. 2012). Even for strongly forced ENSO events, there is large spread among global ensemble members, and dynamical downscaling has little effect on the ensemble spread. Benefits of ensemble size begin to decline with the inclusion of more than five ensemble members and increasing ensemble size improves skill only if there is skill with a small ensemble.

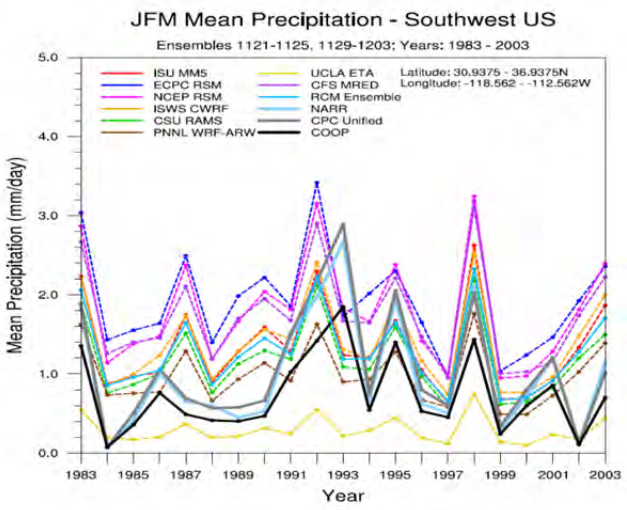


Figure 1. Seasonal (January-February-March) mean precipitation rate for the southwestern U.S. from the NOAA CFS global model, MRED regional models, and observations, illustrating the consistent offset of regional model predictions from the global model.

MRED participants also developed a measure of value added by the regional models that is particularly well-suited to seasonal forecasts, termed the Added Value Index (AVI; Kanamitsu and DeHaan, 2011). The AVI differs from some other measures of RCM value by considering the spatial distribution of skill rather than mean values over a given domain.

3. Warm season forecasts

In addition to MRED, we will review some parallel work to dynamically downscale CFS warm season seasonal forecasts, albeit with just one regional model (the Weather Research and Forecasting Model, or WRF). Regional models may be even more useful in terms of adding value during the warm season, because convective precipitation is so poorly represented in global models. Very similar to the cool season, the

regional model appears to add value in those regions where there already is some skill in the global model (Castro et al. 2012). CFS and regional model forecast skill ultimately depend on the ability of CFS to deterministically represent warm season atmospheric teleconnection patterns. CFS-WRF at least appears to statistically represent the atmospheric teleconnection response related to Pacific SST forcing and the corresponding dominant mode of early warm season precipitation in North America reasonably well, but not in a deterministic sense.

4. The way forward

Current operational seasonal forecasts in North America are based on the National Multimodel Ensemble (NMME). We are in the process of trying to organize a new coordinated research effort that would follow on from MRED, in which all the NMME models with would be downscaled with multiple regional models. This approach mirrors existing community strategies to dynamically downscale global climate model projections (e.g. CORDEX). We will briefly discuss some of the scientific and logistical challenges that currently exist in the pursuit of such an effort.

Acknowledgments

This research was sponsored by U.S. National Oceanic and Atmospheric Administration grant NA08OAR4310578 (RWA) and by U.S National Science Foundation grant ATM-813656 (CLC).

References

Castro, C.L., H-I. Chang, F. Dominguez, C. Carrillo, J. Kyung-Schemm and H. H.-M. Juang, 2012. Can a regional climate model improve warm season forecasts in North America? J. Climate, 25, 8212-8237.

Kanamitsu, M. and L. DeHaan, 2011: The Added Value Index: A new metric to quantify the added value of regional models. J. Geophys. Res. 116, DOI: 10.1029/2011JD015597.

Yoon, J.H., L.R. Leung and J. Correia Jr., 2012: Comparison of dynamically and statistically downscaled seasonal climate forecasts for the cold season over the United States. J. Geophys. Res. 117, DOI: 10.1029/2012JD017650.

Seasonal Ensemble Simulations in East Africa

S. Asharaf[1], Cheneka R. Bedassa[1], S. Brienen[1], K. Fröhlich[1], G. Nikulin[2], B. Früh[1] and the EUPORIAS East Africa Team

[1] Deutscher Wetterdienst, Offenbach, Germany (shakeel.asharaf@dwd.de)

[2] Rossby Centre, Swedish Meteorological and Hydrological Institute, Norrköping, Sweden

Seasonal forecasting over East Africa is a challenging concern. Towards the goal to achieve a reliable and trusted forecast system for impact assessments and decision supports, the European Provision of Regional Impact Assessment on a seasonal to decadal timescale (EUPORIAS) program provides a common framework to understand model uncertainties through the use of multi-member simulations. The participated regional climate model (RCMs) are driven by the atmospheric-only version of EC-EARTH global climate model (GCM). An ensemble of five months (May to September) long hindcast has already been produced by EC-EARTH taking into account the bias corrected sea surface temperature from ECMWF System-4 hindcast. As a first step, the performance of one of the engaged RCM, COSMO-CLM (COSMO model in climate mode) is evaluated in capturing the observed regional features over East Africa for the dry year 2009. For investigating this, we incorporated the 15 ensemble members as simulated by CCLM and EC-EARTH models. The accuracy of the model simulations for the chosen year (June to September) is assessed using the global reanalysis data with satellite and ground-based observations. Preliminary results reveal the potential usefulness of improved ensemble simulations, especially in sub-seasonal to seasonal rainfall forecasting, that indicates the importance of RCM simulations in predicting the precipitation extremes in East Africa.

Availability of CORDEX output through the ESGF network

Ole B. Christensen

Danish Climate Centre, Danish Meteorological Institute, Copenhagen, Denmark (obc@dmi.dk)

It is an essential part of the WCRP CORDEX project (http://wcrp-cordex.ipsl.jussieu.fr/; http://cordex.dmi.dk/) that regional climate model output data should be well defined and should be made easily available for users. In the initial planning of the CORDEX project, it was imagined that this aim could be achieved through very simple web services in the style of the prior PRUDENCE (http://prudence.dmi.dk) and ENSEMBLES RT3/RT2b (http://ensemblesrt3.dmi.dk) archives. As the project grew, it was realized that such an approach would not be able to work efficiently due to a larger expected data amount in combination with limitations in bandwidth on individual servers. It was decided to follow the distributed archiving strategy employed in the CMIP5 global data archive (http://cmip-pcmdi.llnl.gov/cmip5/) using the so-called ESGF software. This approach has been implemented, and data have been stored and made available, e.g. at http://cordexesg.dmi.dk/

In this poster, a status overview will be given of the CORDEX data specifications, of the status of CORDEX simulations, and of European CORDEX ESGF nodes, their data availability and features.

The support from the EU FP7 IS-ENES2 project, in particular from Prashanth Dwarakanath (Linköping U), has helped considerably towards achieving the goal of integrating CORDEX simulations into ESGF and making it possible to have an index- and data-node at the DMI.

Europe in a 6 Degrees Warmer Climate

Ole B. Christensen[1], S. Yang[1], F. Boberg[1], C. Fox Maule[1], M. Olesen[1], M. Drews[2], H. J. D. Sørup[1,2] and J. H. Christensen[1]

[1] Danish Climate Centre, Danish Meteorological Institute, Copenhagen, Denmark (obc@dmi.dk)
[2] Danish Technical University, Lyngby, Denmark

1. Introduction

There is no doubt that a world with an average temperature 6 degrees above pre-industrial climate will be very different from what we currently know; but what will it look like? With the help of a simulation with the ECEARTH global model, downscaled over Europe with the regional model HIRHAM5 in 25km grid point distance, we investigate such a climate.

Through a complementary analysis of CMIP5 GCM results we also study the time at which such a condition may be reached.

One simulation is normally insufficient for a robust analysis of climate change effects. Therefore some work is devoted to an analysis of the extent to which various climate parameters exhibit pattern scaling, i.e. that the change in the relevant parameter is proportional to the change in global temperature. We analyse simulations with the same regional model under weaker climate change, and examine whether the 6-degree simulation scales the same way as these simulations.

2. Method

In this study, targeted simulations have been performed with the HIRHAM5 regional climate model (RCM) for time slices corresponding to around 6 degrees of global warming and for an RCP4.5 scenario, and finally a transient RCP8.5 experiment; these simulations have been driven by the EC-EARTH global circulation model (GCM) and have used the same integration domain as was employed in the ENSEMBLES project (http://ensembles-eu.metoffice.com). In this study, data from these simulations are being compared to the ENSEMBLES RCM database.

To establish the 6-DEG scenario, we performed the benchmark CMIP experiment of idealized 1% per year CO2 increase using the EC-EARTH model (Hazeleger, 2012). The run initialized from the pre-industrial control, and the atmospheric CO2 concentration was prescribed to increase at 1% per year from the pre-industrial value (i.e., 285 ppm) until five times the initial level had been reached, and then kept constant afterwards. The simulation was 250 years with all other forcings kept at the pre-industrial level. As long as the CO_2 increases, the simulated global mean surface temperature rises. It continues to slowly increase for several decades even after the CO2 stops growing, and gradually stabilizes at a level of about 6.5 K warmer than the preindustrial level towards the end of the simulation.

3. Results

Figure 1 shows the absolute changes in seasonal mean temperature and the relative changes in seasonal mean precipitation compared to the 1976-2005 level for a global mean temperature change of about 6K for both summer (JJA) and winter (DJF). We find that the winter temperatures increase from about 5 K in western and southern Europe (British Isles, Iberian Peninsula, France) to more than 9K in the northeast (northern Finland, western Russia). In summer the largest temperature change of more than 9K is found in the Iberian Peninsula and southern France; large changes of 7-8 K are also found along the northern coast of the Scandinavian Peninsula. The lowest temperature increases of about 5-6 K are found in most of Northern Europe, centered on the Baltic Sea, and also including the British Isles. The geographical pattern of these changes is very similar to the changes projected in a 2 K warmer Europe (Vautard et al, 2014), just with a much higher amplitude.

For precipitation we find that in winter the seasonal mean precipitation increases in large parts of Europe, primarily north of 47°N, with the largest changes of more than 60% increase north and east of the Baltic Sea. The largest decrease of 30-50% occurs in the Iberian Peninsula and along the Mediterranean coastline. In summer the line dividing wetting from drying shifts northward; increases of about 20-40% are only found on the Scandinavian Peninsula, in Finland, the Baltic countries and in Russia, with the highest values being in the Norwegian mountains. The largest decreases of 50-60% in seasonal mean precipitation occur in the Iberian Peninsula, southern Italy, Albania, Greece and Turkey. In summary, EC-EARTH-HIRHAM5 projects that particularly in winter, northeastern Europe will get a much warmer and wetter climate, whereas in summer the largest changes will occur in the Iberian Peninsula and along the Mediterranean coast with a much warmer and drier climate. The noticeable changes in winter of much warmer and wetter conditions in northeastern Europe are also visible in a just 2K warmer Europe for the ensemble mean of 14 ENSEMBLES models (Vautard et al., 2014), indicating that this feature is very robust.

4. Scaling with Global Temperature Change

In order to investigate to which extent the climate signals shown here are compatible with pattern scaling, we show in Fig. 2 the average change of several quantities over Scandinavia as a function of the global warming of the driving GCM. All ENSEMBLES regional model results as well as a transient RCP8.5 simulation and time-slice simulations for 6 degrees warming and for RCP4.5 are shown, all with HIRHAM5 for the ENSEMBLES domain, driven by EC-EARTH. It can be seen that pattern scaling

works quite well, and we therefore conclude that the 6-degree-warming simulation presented here is not implausible.

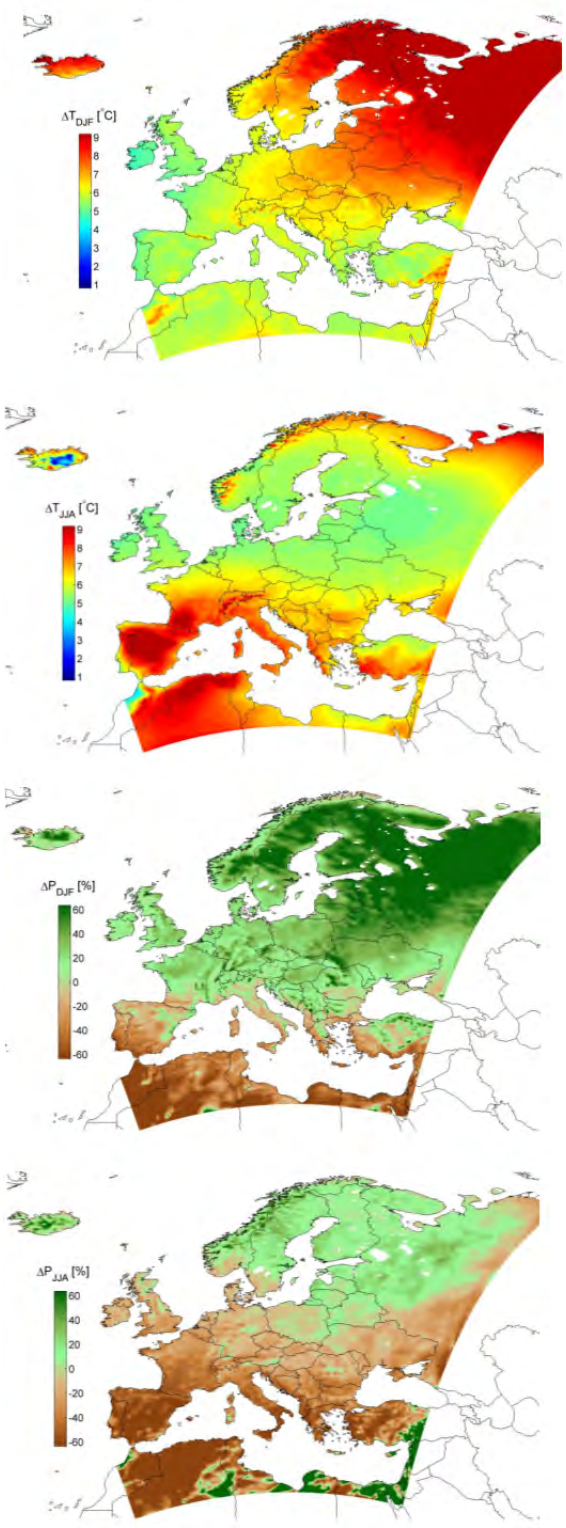


Figure 1 Absolute changes in seasonal mean temperature and relative changes in seasonal mean precipitation compared to the 1976-2005 level for a global mean temperature change of about 6K for summer (JJA) and winter (DJF).

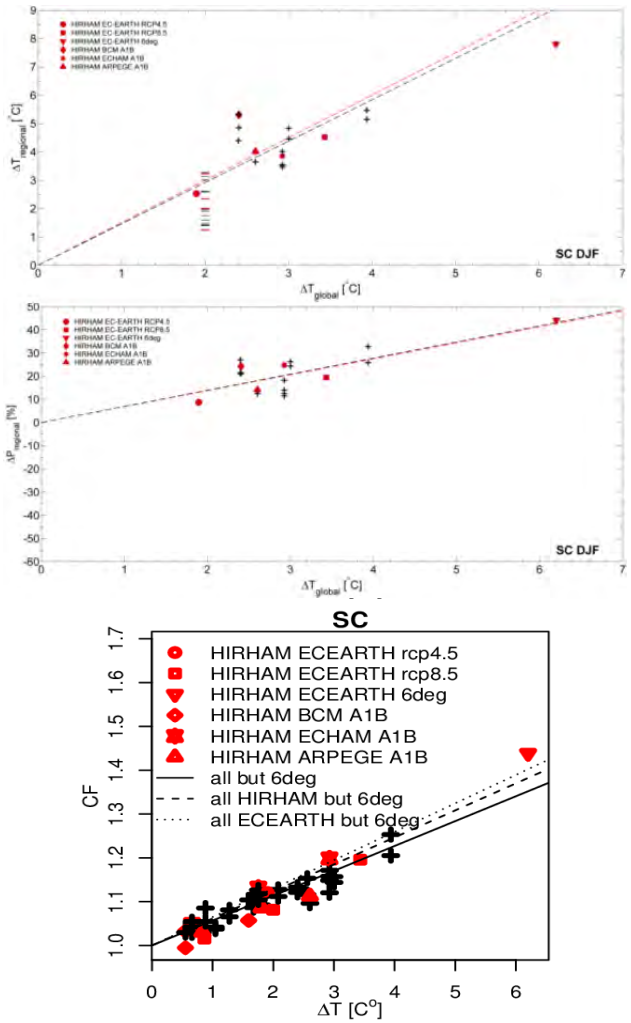


Figure 2 Scaling of climate signal with global temperature change for ENSEMBLES plus several HIRHAM5 simulations. Top panel: Scandinavia winter temperature (K). Middle panel: Scandinavia winter precipitation (%). Bottom panel: 99.9 percentiles of daily precipitation for Scandinavia (roughly 3-year return values; shown as climate factor, scenario divided by control). Red symbols: HIRHAM5. Black crosses: Other ENSEMBLES simulations.

References

Hazeleger, W., X. Wang, C. Severijns, S. Ştefănescu, R. Bintanja, A. Sterl, K. Wyser, T. Semmler, S. Yang, B. van den Hurk, T. van Noije, E. van der Linden, K. van der Wiel (2012): EC-Earth V2.2: description and validation of a new seamless Earth system prediction model. Clim Dyn., 39, 2611–2629, doi:10.1007/s00382-011-1228-5.

Vautard, R., A. Gobiet, S. Sobolowski, E. Kjellström, A. Stegehuis, P. Watkiss, T. Mendlik, O. Landgren, G. Nikulin, C. TheicmannTeichmann, D. Jacob (2014) The European climate under a 2°C warming, Environment Research Letters, 9, 034006 doi:10.1088/1748-9326/9/3/034006

Quantifying uncertainty in regional climate model projections over Western Canadian watersheds

Charles L. Curry[1], Andrew J. Weaver[1], Daniel Caya[2] Michel Giguère[2] and Edward Wiebe[1]

[1] School of Earth and Ocean Sciences, University of Victoria, Canada (cc@uvic.ca)

[2] Ouranos Consortium, Montréal, Canada

1. Goals of this work

Uncertainty in model projections of future climate change presents a key challenge for adaptation policy. In particular, the uncertainty inherent in models' unforced internal variability is irreducible, and of a different character to the uncertainty in future emissions or in the differences between different model representations of climate processes. At the regional scale, and for a projection horizon shorter than a few decades, model internal variability can dominate these other uncertainties in specific sub-continental regions.

In this study, the role of model internal variability is studied using an ensemble of 10 climate model simulations over Western Canada with a single regional climate model (RCM), the Canadian Regional Climate Model, CRCMv.4.3. Eight ensemble members are driven at the large (i.e. continental) scale by a different global climate model (GCM) simulation over the period 1950-2100, while the remaining two members are driven by global reanalyses up to 2005 only.

Of particular interest is the spread amongst model projections of hydrological variables at subregions within the RCM domain corresponding to specific watersheds. We focus on three British Columbia watersheds: the Peace, Nechako and Upper Columbia River basins. While the ensemble members agree reasonably well with respect to present-day climatology over these watersheds, projected changes of climate variables vary widely across the ensemble, especially with respect to fall and winter temperature and precipitation, snowpack, and spring runoff. When expressed in terms of the projected "time of emergence" of the climate change signal relative to the noise of interannual and interensemble variability in these quantities, the results exhibit a sensitive dependence on the specific subregion and the variable of interest. These results imply that relying on only a few realizations of climate model response over watershed-scale regions is often not sufficient to capture the uncertainty associated with hydroclimatic variability.

2. Example: Model-simulated snowpack

Figure 1 demonstrates the large degree of variation amongst different ensemble member projections of snowpack over a particular watershed, the Columbia River Basin. The results in the lower two panels were generated by the *same* RCM with boundary forcing provided by the *same* GCM; the only difference being the initial state at 1950. Nevertheless, one sees a drastic difference in the predicted snowpack change in future.

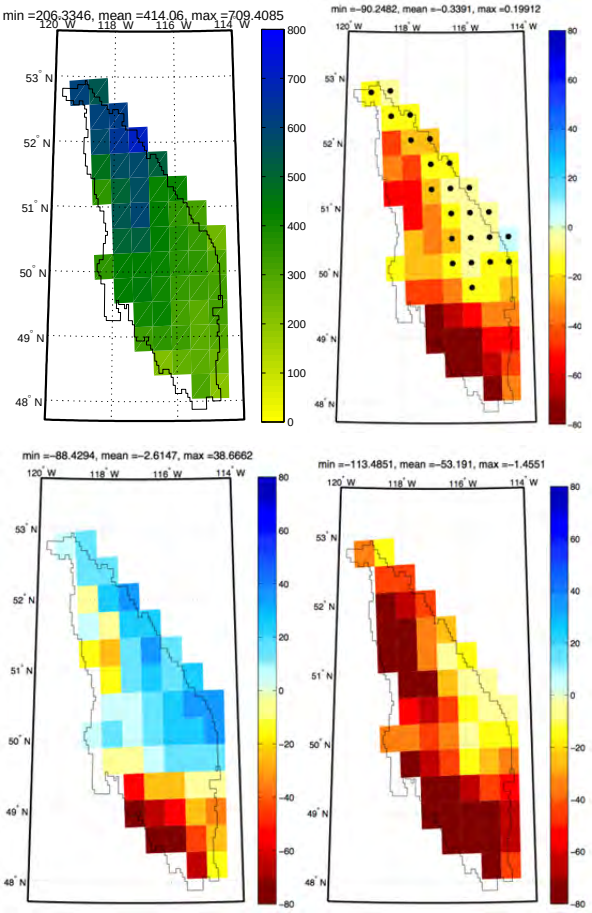


Figure 1. Model-simulated snowpack in the Upper Columbia River Basin, situated along the western Rocky Mountains straddling the British Columbia-U.S. border. *Top left panel:* Multi-ensemble mean simulated April snowpack (in mm H_2O equiv.) for the 1979-2000 period. *Top right:* Multi-ensemble mean change in snowpack (mm H_2O) between April 1979-2000 and April 2039-2060. Black dots signify changes that are indistinguishable from zero at the 5% significance level, based upon inter-ensemble variability. *Bottom panels:* Projected change in April snowpack from two single ensemble members exhibiting the smallest (*left*) and largest (*right*) area-averaged change.

Global Warming Impacts on Great Lakes Basin Precipitation Extremes

Marc d'Orgeville,[1,2] W. Richard Peltier,[1] and Andre R. Erler[1]

[1] Department of Physics, University of Toronto, Toronto, Ontario, Canada. (marcdo@atmosp.physics.utoronto.ca)
[2] Canadian Research and Development Centre, IBM, Toronto, Ontario, Canada.

A physics-based mini-ensemble of dynamically downscaled WRF model simulations of global warming over the Great Lakes Basin has been constructed based upon a single CESM1 global climate reconstruction. The analysis pipeline is successfully verified by comparison with observations for the historical period (1979-1994) and then applied to produce future projections (2045-2060).

By mid-century, the annually averaged rainfall is expected to experience a median increase of between 13 and 19%, while, on the basis of extreme value analysis, the amplitude of extreme rainfall event characterized by a 50 year return period would see a median increase of between 14 and 29%. Since both average and extreme rainfall changes are shown to accurately follow the thermodynamically expected 7% increase per degree of warming, independently of the physics ensemble members, we provide a detailed examination of the physical processes responsible for the predicted fattening of the tail of the precipitation distribution.

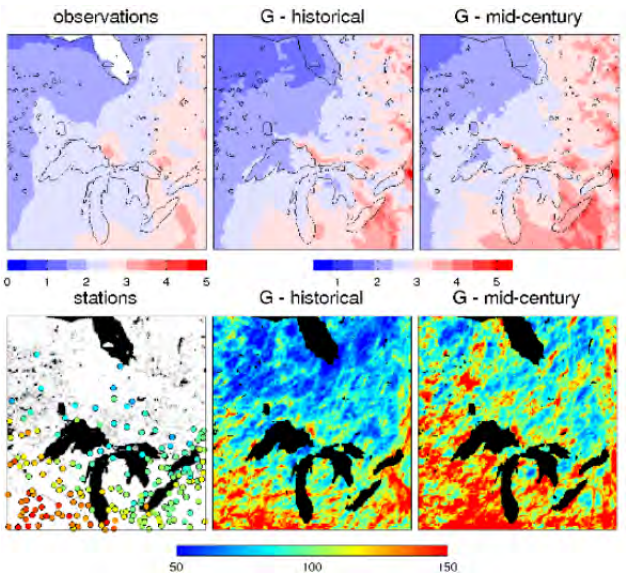


Figure 1. Yearly average of daily precipitation ($Rain_{tot}$, top row) and the extreme 50 year return value of daily precipitation distribution (X^{50}, bottom row) for historical observations (left), one historical simulation (center) and one future simulation (right). Both simulations are for the same physics configuration for years 1979-1994 and 2045-2059. Observation for the average are from years 1979-1994 of the CRU monthly dataset. Observations for the extreme values are from the extreme value analysis of daily precipitation timeseries of 193 Canadian and US weather stations. Unit is mm/day.

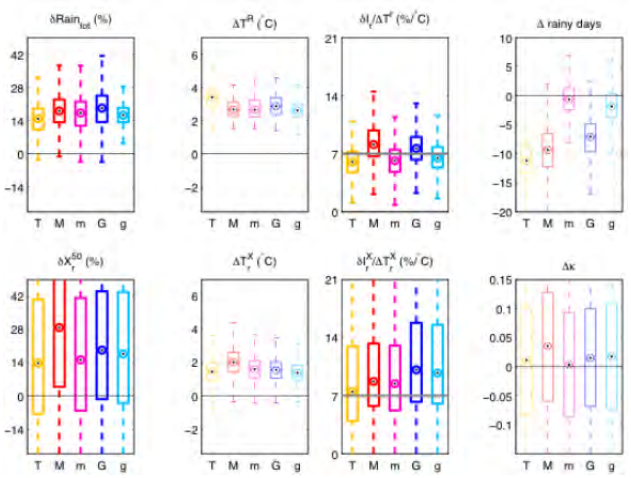


Figure 2. Boxplots of the distribution over all grid cell points of future changes. Each box corresponds to one physics configuration. Median changes are highlighted with black dots. Top row: change in yearly average rainfall ($\delta Rain_{tot}$), in surface temperature and rainfall of the average rainy day composite (ΔT_r and $\delta I_r/\Delta T_r$), and in number of rainy days per year (Δ rainy days). Bottom row: change in X^{50}, in surface temperature and rainfall of the extreme composite (ΔT_r^X and $\delta I_r^X/\Delta T_r^X$), and in the shape parameter ($\Delta\kappa$) of the GP distributions used to compute X^{50}. Notations δ and Δ correspond to relative changes (in %) and absolute changes (unit in the plot title) respectively.

On Reliability of Regional Decadal Ensemble Prediction for Europe

Fatemeh Davary Adalatpanah, Barbara Früh, Claus-Jürgen Lenz and Paul Becker

Deutscher Wetterdienst, Offenbach, Germany (fatemeh.davary-adalatpanah@dwd.de)

1. Overview

Within the BMBF-funded programme MiKlip one main focus is on the decadal climate prediction on the regional scale. The general goal of the project LACEPS (A Limited-Area Climate Ensemble Prediction System) within MiKlip is the development of an ensemble climate prediction system for the decadal forecast for the region of Europe employing the regional climate model COSMO-CLM.

2. Data

The ensemble is created using three strategies, the perturbation of initial conditions, model physics, and boundary conditions and data. The regional downscaling has been done using different driving MPI-ESM datasets, baseline0 (Müller et al., 2012) and baseline1 in low resolution (respectively b0-LR and b1-LR). The MPI-ESM hindcast experiments were downscaled to the CORDEX-Europe domain with a horizontal grid resolution of 0.22° using COSMO-CLM.

By using driving data from hindcasts starting on different days, the "initial conditions" perturbation strategy is implemented. The ensemble with "model physics" perturbation is generated varying one tuning parameter in COSMO-CLM.

As observational basis, for the evaluation of the MPI-ESM as well as the COSMO-CLM hindcasts, the gridded observational E-OBS data in version 8.0 (Haylock et al., 2008) were used.

3. Parameters and Skill Scores

In this study, the evaluation has been done for five parameters including 2-m temperature, total precipitation, maximum and minimum temperature and mean sea level pressure, based on daily value for observational data as well as all hindcasts)

The focus of the presentation is on the 2-m temperature, the number of wet days with ≥ 1 mm/day precipitation and simple daily intensity index, SDII (the mean precipitation amount of wet days) by the Ensemble Mean Bias (EMB), ensemble spread score (ESS), β-Score and β-Bias maps and time series as well as Talagrand (Analysis Ranked Histogram, ARH) diagrams (Hamill, 2001) to have a much more reliable estimation of the ensemble system.

The β-Score and β-Bias are respectively a score and a bias representing reliability and bias of the given ensemble forecast by assuming that the ARH is distributed according to a β-distribution (Keller, 2011). These results have been provided for two time periods, 2002-2005 and 2006-2009 (Goddard, 2013), by implementation of two perturbation strategies: initial conditions and model physics.

4. Results

The main part of the presentation is focused on the evaluation of the COSMO-CLM simulations and the reliability of the ensemble achieved until present.

The ESS in Figure 1 is around one indicating that the spread (standard deviation) of the 2-m temperature due to the perturbation of initial conditions is in the order of the mean forecast error. Hence, the ensemble generated by the perturbation of initial conditions can be considered to be reliable in both models for decade 2000 (Palmer, 2006). The β-Score (with perfect value of zero) shows that its temporal development is quite similar to the ESS.

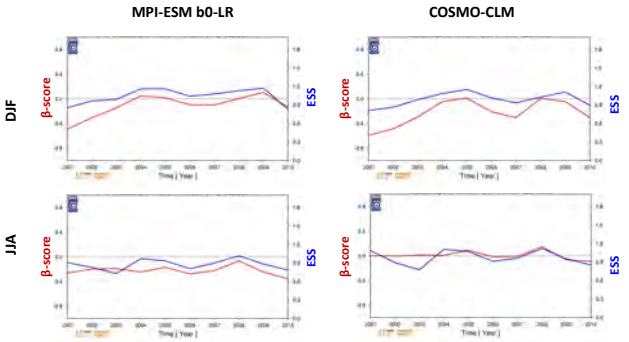


Figure 1: Time series of ESS (ensemble spread score, blue lines, right axis) and β-score (red lines, left axis) for 10 MPI-ESM b0-LR (left column) and COSMO-CLM (right column) hindcasts in DJF (top row) and JJA (bottom row) for the decade 2001–2010 in Europe by implementation of initial condition perturbation.

Figure 2 illustrates the added value of 2-m temperature reliability by downscaling in most part of Europe. While in the COSMO-CLM results, the only marginal differences between MPI-ESM b0-LR and b1-LR driven hindcasts show an added value in the b1-LR driven simulations where the ESS is nearer to the optimal value of 1 for most parts of southern and central Europe.

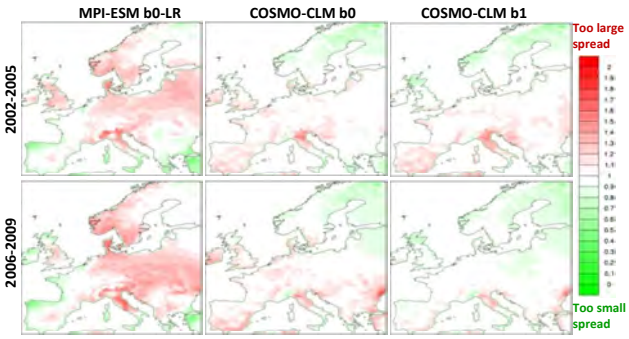


Figure 2: ESS (ensemble spread score) for the 2-m temperature in the MPI-ESM b0-LR ensemble for decade 2001-2010 (10 members, left column), the COSMO-CLM ensemble driven by the 10 MPI-ESM b0-LR hindcasts (middle column) and by the corresponding 10 MPI-ESM b1-LR hindcasts (right column) in DJF

The results of EMB show less overestimation of the number of wet days in COSMO-CLM than in MPI-ESM in most parts of Europe by “initial condition” perturbation strategy. For both perturbation strategies, “initial conditions” and “model physics”, the corresponding Talagrand diagrams of SDII show overestimation of SDII indicated by the inverse J-shape (positive β_B) for all considered periods and seasons (not shown).

5. Conclusions

The results of initial conditions perturbation show a sufficiently large spread of 2-m temperature. Also for most parts of Europe, the EMB of 2-m temperature shows positive bias in winter (DJF) and negative in summer (JJA) leading to a too small annual cycle of 2-m temperature in both models: the driving MPI-ESM and COSMO-CLM.

Perturbation of “model physics” represents a very small ensemble spread in the 2-m temperature, which is much smaller than in the “initial conditions” perturbation strategy.

Implementation of both “initial conditions” and “model physics” perturbation lead to a positive bias of SDII. This overestimation is higher in winter than in summer when convective conditions prevail and a decoupling of COSMO-CLM from the driving MPI-ESM is supported.

Furthermore, the results show that the large percentages of observational data of SDII are outside the range spanned by the ensemble resulting in an inadequate spread. Therefore, a change in the strategy of “model physics” may be necessary, e.g. perturbing more than one tuning parameter.

References

Goddard, L., Kumar, A., Solomon, A., Smith, D., Boer, G., Gonzalez, P., Kharin, V., Merryfield,W., Deser, C., Mason, S., Kirtman, B., Msadek, R., Sutton, R., Hawkins, E., Fricker, T., Hegerl, G., Ferro, C., Stephenson, D., Meehl, G., Stockdale, T., Burgman, R., Greene, A., Kushnir, Y., Newman, M., Carton, J., Fukumori, I., and Delworth, T. (2013) A verification framework for interannualto-decadal predictions experiments, Climate Dynamics, 40, 245–272

Hamill, T.M. (2001) Interpretation of rank histograms for verifying ensemble forecasts, Mon. Wea. Rev., 129, 550-560

Haylock, M. R., Hofstra, N., Klein Tank, A. M. G., Klok, E. J., Jones, P. D., and New, M. (2008) A European daily high-resolution gridded data set of surface temperature and precipitation for 1950–2006, Journal of Geophysical Research, Atmospheres, 113, n/a–n/a

Keller, J.D., A. Hense (2011) A new non-Gaussian evaluation method for ensemble forecasts based on analysis rank histograms, Meteorol. Z., 20, 107–117

Keller, J.D., A. Hense (2011) A new non-Gaussian evaluation method for ensemble forecasts based on analysis rank histograms, Meteorol. Z., 20, 107–117

Müller, W. A., Baehr, J., Haak, H., Jungclaus, J. H., Kröger, J., Matei, D., Notz, D., Pohlmann, H., von Storch, J. S., and Marotzke, J. (2012) Forecast skill of multi-year seasonal means in the decadal prediction system of the Max Planck Institute for Meteorology, Geophysical Research Letters, 39, n/a–n/a

Palmer, T., Buizza, R., Hagedorn, R., Lawrence, A., Leutbecher, M., Smith, L. (2006) Ensemble prediction: a pedagogical perspective, Newsletter n. 106, ECMWF, Shinfield Park, Reading RG2-9AX, UK, 10-17

Future snowfall in western and central Europe projected with a high-resolution regional climate model ensemble

Hylke de Vries, Geert Lenderink and Erik van Meijgaard

Royal Netherlands Meteorological Institute (KNMI), De Bilt, The Netherlands (vanmeijg@knmi.nl)

1. Introduction

Snowfall is expected to be strongly influenced by climate change. In a warmer climate substantial changes can be expected in both the number of potential snowfall-days (i.e. days cold enough to permit snowfall to occur), as well as the actual snowfall amounts on such days. Here we report on the future changes in mean and extreme snowfall amounts in western and central Europe as projected from an 8-member ensemble of regional climate model simulations (de Vries et al., 2014). This ensemble also forms the basis of the new KNMI climate scenarios for the Netherlands to be issued in 2014.

2. Data and Methodology

Simulations (1950-2100) have been carried out with the regional climate model KNMI-RACMO2 at 0.11 degree resolution (van Meijgaard et al., 2012) forced by realizations obtained with the EC-EARTH2.3 GCM (Hazeleger et al., 2012). An 8-member ensemble was generated by perturbing the GCM initial atmospheric state in 1850. Beyond 2005 the RCP8.5 emission scenario (Meinshausen et al., 2011) was assumed.

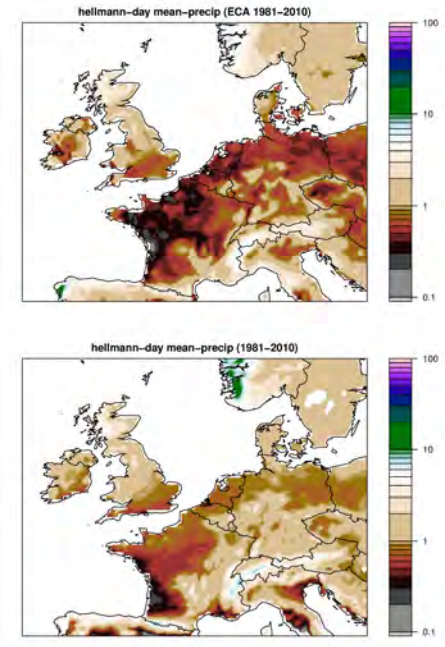


Figure 1. H-day precipitation (mm/day) in the current climate (1981-2010) derive from the ECA&D observations (top) and from the 8-member RACMO ensemble.

Observations were taken from the gridded E-OBS data set provided by ECA&D (Haylock et al., 2008). Prior to analysis all data were mapped on a 0.25 degree regular grid.

Because snowfall itself is not a parameter in the E-OBS data set, the concept of H-day precipitation (de Vries et al., 2012) is used as a proxy, where H-day refers to a Hellmann day, being a day with a mean temperature below freezing. Note that mean H-day precipitation implies an average over the number of H-days.

3. Current Climate

Figure 1 shows the observed and simulated H-day precipitation in the current climate. Largest values are found in the mountains (the Alps and, in particular, Norway), while lowest amounts are seen in SW-France There, H-days are rare and when they occur conditions are dry. In general mean DJF-precipitation is much larger than H-day precipitation (not shown), although in cold regions differences tend to be smaller. Nearly everywhere, the RACMO ensemble produces more precipitation on H-days than is observed, which might in part be the consequence of a model cold bias in winter (Kotlarski et al., 2014)

4. Future trend

Figure 2 shows future projections of snowfall in terms of changes in local temperature relative to the current-climate snowfall. While reductions can be as large as 20% per degree warming in many areas, the outcome in cold, mountainous, regions indicate a non-negligible positive trend.

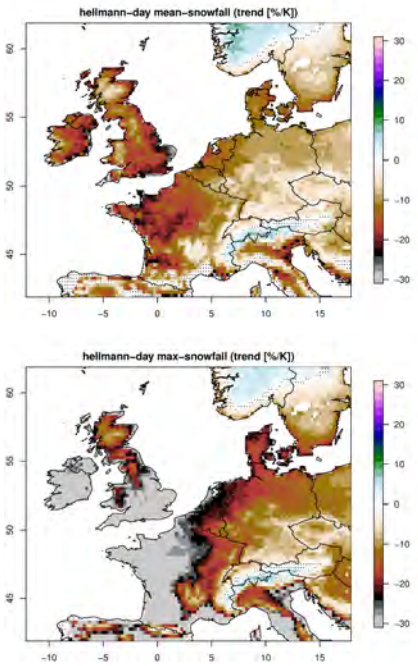


Figure 2. Relative linear trend (% per degree local warming) in H-day mean snowfall (top) and maximum snowfall (bottom) inferred from the RACMO ensemble. Dots denote regions where the trend is not significant at the 95% confidence level.

5. Local trend in extreme daily snowfall linked to mean winter temperature

Figure 3 shows the trend in seasonal-maximum H-day snowfall in relation to the current-climate mean winter temperature at each land grid point and the current-climate winter H-day frequency of occurrence. Evidently, where mean winter temperatures are below -8^{o} C or H-day frequency is close to 100%, projections in extreme snowfall display positive trends, while everywhere else trend projections are negative down to -60%. It is also noticed that both relationships are non-linear in nature, with absolute slopes increasing in magnitude for current-climate mean temperatures already above the freezing point, or current-climate H-day frequencies already below 40%.

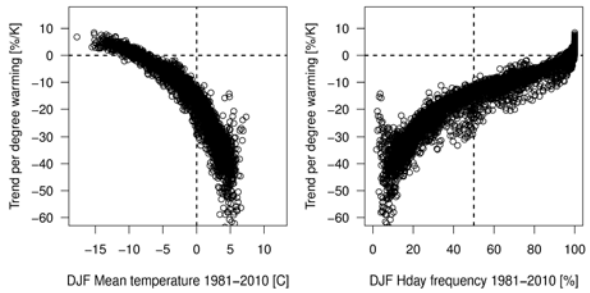


Figure 3. Scatterplot of local trend in seasonal-maximum H-day snowfall (% per degree warming) versus present-day winter (DJF) temperature (left), and present-day winter H-day frequency (right plot).

6. Joint probability distributions per region

An interesting contrast is posed by the comparison of two regions displaying opposite future trends in snowfall: Netherlands (NL, negative trend), and the Alps (positive trend). Snowfall amount and projected trend are analyzed in relation to region averaged temperature with resulting pdf's shown in Figure 4. For region NL the pdf-center is above the freezing point, indicating that the most significant snowfall events occur at melting conditions. In future, the pdf-center displaces to higher temperatures but also to much lower snowfall amounts. In the Alps the current-climate pdf is at much lower temperature, while the future trend is a displacement to higher temperatures, but still well below zero, and higher snowfall amounts. An explanation for this contrast might be that for region-NL the total number of H-days in the current climate consists of a sample of cold and dry days on the one hand, and a sample of less cold and wet days on the other hand, and that in future as a result of warming a considerable part of the latter sample drops out from the H-day number. This is not seen in the Alps because conditions there are much colder.

7. Conclusions

Mean and extreme snowfall in most parts of western and central Europe are projected to have strongly reduced by the end of this century. The reduction is not only caused by a reduction in the frequency of cold days, but also by a reduction in snowfall on the cold days that are left. These findings are derived on the basis of an 8-member ensemble of simulations with a single RCM forced by a single GCM. It would be very interesting to extend this analysis to a multi-model ensemble including different RCMs and/or forcings provided by different GCMs. For this to achieve, Euro-CORDEX is expected to provide a very suitable framework.

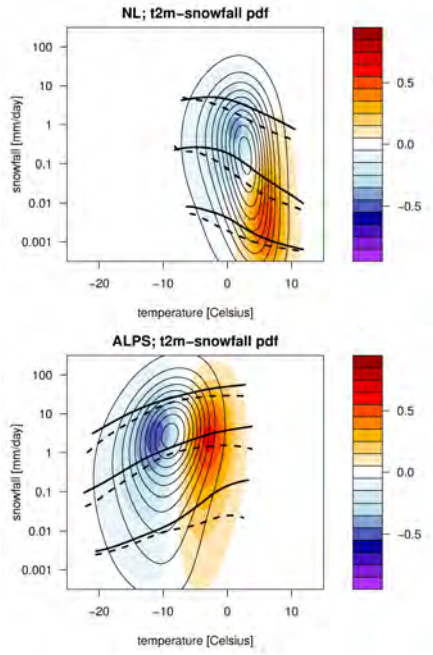


Figure 4. Probability density estimate in (2-meter temperature) x (snowfall) space for NL (top) and the Alps (bottom). Note the log-scale on the vertical axis. Contours designate current-climate pdf-isolines (normalized to unit maximum, levels 0.05, 0.15,…,0.95). Color shading display the difference between future (2071-2100) and current climate (1981-2010). Quasi-horizontal lines denote the temperature-binned snowfall percentiles P10, P50, and P90 (solid for present-day, dashed for future.)

References

Haylock, M., et al. (2008) A European daily high-resolution gridded dataset of surface temperature and precipitation for 1950-2006, J. Geophys. Res., 113, D20119

Hazeleger, W., et al. (2012) EC-Earth V2.2: description and validation of a new seamless earth system prediction model, Clim. Dyn., 39, pp 2611-2629

Kotlarski, S., et al. (2014) Regional climate modeling on European scales: a joint standard evaluation of the EURO-CORDEX RCM ensemble, Geosci. Model Dev. Discuss., 7, 217-293, doi:10.5194/gmdd-7-217-2014

van Meijgaard, E., et al. (2012), Refinement and application of a regional atmospheric climate model for climate scenario calculations of Western Europe, KvR 054/12, Climate change Spatial Planning, pp 44

Meinshausen, M. et al. (2011). The RCP greenhouse gas concentrations and their extensions from 1765 to 2300, Climate Change, 109, pp 213-241,

de Vries, H., et al. (2012) On the future reduction of snowfall in western and central Europe, Clim. Dyn., 41, pp 2319-2330

de Vries, H., G.Lenderink and E. van Meijgaard et al. (2014) Future snowfall in western and central Europe projected with a high-resolution regional climate model ensemble, submitted to Geophys. Res. Lett.

Weather Extremes in Regional Climate Ensembles

James M Done and Debasish PaiMazumder

National Center for Atmospheric Research Earth System Laboratory, Boulder Colorado, US (done@ucar.edu).

1. Introduction

The representation and predictability of high-impact weather and climate events in regional climate ensembles is explored with particular focus on (i) the role of domain size, (ii) the role of different cumulus, boundary layer and microphysical schemes and their synergy and (iii) the relative importance of internal variability uncertainty versus model physics uncertainty. Results have important implications for both the design of coordinated regional ensemble experiments and seasonal to decadal ensemble forecasting.

2. Data

An initial condition ensemble and a model physics ensemble are generated using the Weather Research and Forecasting (WRF) model at 36 km grid spacing over a limited area domain (the region shown in Fig. 1) driven by European Centre for Medium-Range Weather Forecasts (ECMWF) Re-Analysis Interim (ERA-I, Simmons et al. 2006) data at the lateral and lower boundaries.

The initial condition ensemble has 16 members and was created using combinations of lagged start times and stochastic backscatter to generate initial condition perturbations. The ensemble runs for a single year from May 1 through Dec 1. Further details can be found in Done et al. (2014).

The physics ensemble has 24 members and comprises of strategically chosen combinations of cumulus, microphysical, boundary-layer and radiation parameterization schemes. The ensemble runs for a 15-month period from September 1 through Dec 1 the following year. These ensembles driven by reanalysis data represent the best-case scenario to explore regional model ensemble performance.

3. The Importance of Large Domains

Weller et al. (2013) showed that simulated extreme events from reanalysis-driven NARCCAP models exhibit strong one-to-one correspondence to extreme events in the observational record. However, the observed sequence of extreme events is itself a single realization of a range of possibilities, and we argue that the value of an ensemble is not in reproducing the observed sequence of extreme events but rather in providing information on a range of possible scenarios consistent with the large-scale conditions. This requires the ensemble members to generate different solutions to the boundary conditions and this can be achieved through the use of large domains.

The value of large domains is assessed using the initial condition ensemble and the reproducible fraction (RF, defined by Crétat et al. 2011) that quantifies the fraction of day-to-day variability that occurs in phase between ensemble members. RF is defined as the ratio of the daily variance of the ensemble mean to the variance of the ensemble members. Figure 1 shows RF of 500hPa height across the initial condition ensemble for the late summer months August-September-October. Values equal to 1 indicate variability is in phase between ensemble members and values closer to zero indicate a lack of phase agreement. As expected, RF is highest at the domain boundaries decreasing towards the domain interior, demonstrating the changeover from boundary forced constancy (little benefit of running an ensemble since the variance is strongly constrained) to internally generated variability (the added value of running an ensemble). An ensemble domain that is smaller than the main modes of variability is therefore too closely coupled to the driving data thereby constraining the range of possible solutions.

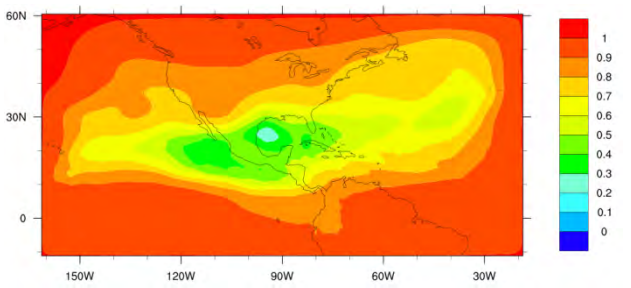


Figure 1. Reproducible fraction of 500hPa height for August-September-October for the initial condition ensemble. Warm colors indicate a high degree of phase agreement (a constrained ensemble) and cool colors indicate low phase agreement (added value of the ensemble).

4. The Role of Different Physical Parameterization Schemes and Their Synergy

Several numerical studies show that the representation of cumulus convection, vertical mixing in the boundary layer, and cloud microphysical processes all play important roles in the spatial and temporal variability of precipitation and temperature and the development of weather extremes (e.g. Prein et al. 2013; Wang and Seaman 1997). Furthermore, non-linear interactions between schemes further complicates assessment of the associated uncertainties. Using indices of weather extremes, this study explores the sensitivity of the intensity and frequency of the extremes to combinations of physical parameterization schemes and provides increased understanding of the role of model physics uncertainty.

5. The Relative Importance of Internal Variability Uncertainty Versus Model Physics Uncertainty

The relative importance of internal variability uncertainty versus model physics uncertainty in the representation and predictability of weather extremes is explored for the case of seasonal tropical cyclone frequency. For the initial condition ensemble, the simulated internal variability of annual tropical cyclone frequency for the case study year is approximately 0.4 times of the inter-annual variability of observed tropical cyclone frequency (Done et al. 2014). This contrasts with variability across the physics ensemble of 1.1 times the observed inter-annual variability. However, we caution that the initial condition ensemble and the physics ensemble were run for different years.

These initial results suggest that both internal variability uncertainty and physics uncertainty are important with physics uncertainty dominating the total uncertainty. This result agrees with Villarini and Vecchi (2012) who found both internal variability uncertainty and model uncertainty to be important for tropical cyclone frequency on seasonal to decadal timescales.

6. Implications for Co-ordinated Ensemble Experiments and Seasonal Prediction

The value of an ensemble is in providing information on the range of possible solutions to the large-scale climate conditions. A large domain appears to be essential for a regional model ensemble to freely generate spread in day-to-day weather and extreme events and to minimize constraints of the boundary conditions. The size of the domain needs to be sufficiently large to contain the dominant modes of variability to enable upscale interaction to occur. A large domain is therefore relevant to ensemble simulations of current climate driven by reanalysis data and ensemble simulations of future climate driven by global climate model data.

The simulation of weather extremes is characterized by large internal variability uncertainty, at least on seasonal timescales. Physics uncertainty is also significant, perhaps even more so, and is likely to extend on far longer timescales than initial condition uncertainty. It is therefore desirable for coordinated ensemble experiments to fully explore both initial condition and physics uncertainties.

The large internal variability uncertainty and large model physics uncertainty have important implications for the interpretation of seasonal forecasts of weather extremes. Seasonal forecasts usually make the implicit assumption that the externally forced component is far larger than the components from internal variability uncertainty or model physics uncertainty. Ensemble based forecasts, as explored by Chen and Lin (2013) for the case of tropical cyclones, are therefore critical to both isolate the predictable component and provide information on the range of possibilities.

References

Chen, J.-H., and S.-J. Lin (2013) Seasonal Predictions of Tropical Cyclones Using a 25-km-Resolution General Circulation Model. J. Climate, 26, pp 380–398, doi:10.1175/JCLI-D-12-00061.1

Crétat, J., C. Macron, B. Pohl, and Y. Richard (2011) Quantifying internal variability in a regional climate model: a case study for Southern Africa. Climate Dyn., 37, 7-8, pp 1335-1356, doi:10.1007/s00382-011-1021-5.

Done, J.M., Bruyère, C.L., Ge, M., and A. Jaye (2014) Internal Variability of North Atlantic Tropical Cyclones. Submitted to JGR Atmospheres.

Prein, Andreas F., Gregory J. Holland, Roy M. Rasmussen, James Done, Kyoko Ikeda, Martyn P. Clark, Changhai H. Liu, 2013: Importance of Regional Climate Model Grid Spacing for the Simulation of Heavy Precipitation in the Colorado Headwaters. J. Climate, 26, 4848–4857.

Simmons, A., S. Uppala, D. Dee, and S. Kobayashi (2006) ERA-Interim: New ECMWF reanalysis products from 1989 onwards. ECMWF Newsletter, No. 110, ECMWF, Reading, United Kingdom, 26–35.

Villarini, G., and G. A. Vecchi (2012) Twenty-first-century projections of North Atlantic tropical storms from CMIP5 models. Nat. Climate Change, 2, pp 604–607.

Wang, W., and N. L. Seaman, 1997: A comparison study of convective schemes in a mesoscale model. Mon. Wea. Rev., 125, 252–278

Weller, G.B., Cooley, D., Sain S.R., Bukovsky, M.S., and L.O. Mearns. 2013: Two case studies on NARCCAP precipitation extremes. JGR Atmospheres, doi: 10.1002/jgrd.50824

Including model performance and independence in ensemble design

J.P. Evans[1], D. Argüeso[1], A. Di Luca[1], R. Olson[1] and L. Fita[2]

[1] Climate Change Research Centre, University of New South Wales, Sydney, Australia (jason.evans@unsw.edu.au)
[2] Laboratoire de Météorologie Dynamique, IPSL, Université Pierre et Marie curie, Paris, France

NARCliM (NSW/ACT Regional Climate Modelling project) is a regional climate modelling project for the Australian area. It will provide a comprehensive dynamically downscaled climate dataset for the CORDEX-AustralAsia region at 50km, and South-East Australia at a resolution of 10km. NARCliM data will be used by the NSW and ACT governments to design their climate change adaptation plans.

Given computational limitations a small set of GCMs and RCMs must be chosen to perform the downscaling. With this selection we aim to satisfy the following criteria

1. The chosen models perform adequately for the recent past compared to observations.
2. The chosen models do not exhibit the same strengths and weaknesses in their representation of the climate (i.e. they are independent).

And for the GCMs

3. The chosen models span the plausible future change space.

In order address these criteria in the selection of RCMs we investigated 36 different configurations of WRFv3.3. They were all run for eight 2-week periods that contained representative events for the region and model performance was assessed using observations and analysis of five climate variables and multiple performance metrics. A subset of six models were found to perform consistently worse than the others and were excluded from possible selection. Model independence was quantified using a method based on the covariance of model errors (Bishop and Abramowitz 2013). Models whose errors varied most differently (independently) from the rest of the ensemble were then chosen.

For GCM selection the model performance was assessed based on previously published evaluations relevant for the region. These were combined through a fractional demerit score where a score of 0.5 or above indicates poor performance and these models are removed from the selection process. The same independence measure that was applied to the RCMs is then applied to the GCMs in order to identify GCMs whose errors are most different from others in the ensemble. This method has been found to produce desired ensemble characteristics such as minimizing error and maintaining ensemble variance (Evans et al. 2013). This independence ranking can then be placed within the GCMs future climate change space, here defined in terms of the change in temperature and precipitation, and the highest rankings that span the space were chosen in a subjective manner.

Using this process an ENSEMBLE of 12 simulations for each period is obtained (Evans et al. 2014). Additionally to the GCM-driven simulations, 3 control run simulations driven by the NCEP/NCAR reanalysis for the entire period of 1950-2009 are also performed in order to validate the RCMs performance in the area. In this talk, we will present the initial evaluation results of the long control period simulations of the project. The focus of the analysis is the models ability to capture the influence of large scale oceanic modes on the regional climate.

References

Bishop, C. H., and G. Abramowitz, 2013: Climate model dependence and the replicate Earth paradigm. Clim Dyn, 41, 885–900, doi:10.1007/s00382-012-1610-y.

Evans, J. P., F. Ji, G. Abramowitz, and M. Ekström, 2013: Optimally choosing small ensemble members to produce robust climate simulations. Environ. Res. Lett., 8, 044050, doi:10.1088/1748-9326/8/4/044050.

Evans, J. P., Ji, F., Lee, C., Smith, P., Argüeso, D., and Fita, L.: A regional climate modelling projection ensemble experiment – NARCliM, Geosci. Model Dev. Discuss., 6, 5117-5139, doi:10.5194/gmdd-6-5117-2013, 2013.

Selection of a best subset of GCM-RCMs from an ensemble for impact studies.

Cathrine Fox Maule, Ole B. Christensen and Peter Thejll

Danish Climate Centre, Danish Meteorological Institute, Copenhagen, Denmark (cam@dmi.dk)

1. Introduction

During the past decade it has repeatedly been shown that when dealing with climate modelling working with ensembles is a must (Christensen et al. 2010, Annan and Hargreaves 2011). So the general message from the climate modeling community to other communities is; do not use a single model, always look at ensembles with the ensemble median as the best representation of reality and the variance of the ensemble as an estimate of uncertainty and spread.

As beautiful as this thought is, it is in many cases often not realistic for the users of climate model output to fully embrace this. In many impact studies the amount of data from a full ensemble of RCM output may be overwhelming and the calculation time of running an impact model with data from 10-15 different RCMs too long. Therefore in practice one often ends in the situation of having to select a relevant subset of a few GCM-RCMs from a larger ensemble (e.g. Madsen et al. 2013). A general issue to consider is then, how to select a few GCM-RCMs, such that they represent the ensemble in the best possible way. One should of course always select the best GCM-RCM, however, many studies have shown that the "best" model depends on which parameter(s) that is being considered and that it may vary from region to region (e.g. Christensen et al. 2010, Maule et al. 2012). So a general selection once and for all cannot be made as different parameters are relevant for different impact studies; therefore selections have to be made on a case-by-case basis.

2. The MODEXTREME project

One of these cases is the FP7 project MODEXTREME. The primary aim of this project is to improve crop and yield models for cases of extreme weather as drought, heat waves and heavy precipitation events. As particularly the extreme weather is expected to change in the furture, experiments using RCM output as input into crop and yield models for future climate will be carried out. Within this project the wish is to apply 3-4 different realizations, i.e. GCM-RCMs, of the future climate with particular focus on different changes in future precipitation patterns. Here we will focus on Europe, but the MODEXTREME project also looks at areas in China, South America (Brazil and Argentina), South Africa and USA.

3. Selection of EUR-11 simulations for MODEXTREME

The focus time-slices of the MODEXTREME project are 1991-2000 (present-day), 2021-2040 (near-future) and 2041-2060 (far-future). No preference is given to the choice of RCP scenario. As our aim is to explore extremes, we will be investigating changes in the precipitation pattern of the far-future time-slice compared to the present-day time-slice, for as many simulations as possible, preferably for the RCP8.5 scenario, as we expect more extreme events in this compared to RCP4.5. At the moment of writing seven different GCM-RCMs are available:

- CNRM-CERFACS-CNRM-CM5—SMHI-RCA4
- ICHEC-EC-EARTH—SMHI-RCA4
- IPSL-IPSL-CM5A-MR—SMHI-RCA4
- MOHC-HadGEM2-ES—SMHI-RCA4
- MPI-M-MPI-ESM-LR—SMHI-RCA4
- IPSL-IPSL-CM5A-MR—IPSL-INERIS-WRF331F (RCP4.5)
- ICHEC-EC-EARTH—DMI-HIRHAM5

This ensemble has a clear over-representation of the RCM SMHI-RCA4. The IPSL-IPSL-CM5A-MR—IPSL-INERIS-WRF331F is only available for RCP4.5.
Figure 1 shows the relative changes in seasonal mean precipitation of the seven models and of the ensemble median from 1991-2010 to 2041-2060.

Two selection approaches can be considered. One in which selection is made by choosing different, (assumed) independent models, and one in which only the change in precipitation patterns is considered. The first approach, from the point of view of using independent models, the two simulations not using RCA4 (namely IPSL-INERIS-WRF331F and DMI-HIRHAM5) should be part of the selected models. This leaves two models to be selected from the group of RCA4 simulations; here we should rule out the ICHEC-EC-EARTH and the IPSL-IPSL-CM5A-MR driven simulations as these GCMs already are represented amongst our selected models. Then the simulations driven by MOHC-HadGEM2-ES, MPI-M-ESM-LR and CNRM-CERFACS-CNRM-CM5 are left. As these GCMs presumably are independent, one can chose as one likes.

The second approach to selecting the subset of three to four simulations out of the seven is based solely on comparison of the seven simulations with the ensembles median shown in Figure 1. Based on a first glance, particularly the IPSL-IPSL-CM5A-MR-SMHI-RCA4 is quite unique and an obvious representative of the span of the ensemble, but should possibly be considered an outlier. The model CNRM-CERFACS-CNRM-CM5-SMHI-RCA4 stands out by having wet conditions over Ukraine in autumn, but in general it is not possible to make the selection based on visual inspection of the maps. To

make an objective selection of the models we evaluate which model that constitutes the ensemble median in each grid point. From this we find the model which most often is the median in the five European study areas in MODEXTREME; Spain, France, Switzerland, Italy and Ukraine in each season. Based on this, we can identify the model, which is the best representative of the ensemble median. By also evaluating which models that rarely are the median we can identify the models which span the extremes.

Based on the first observations presented here, it is clear that it matters which selection procedure one chooses.

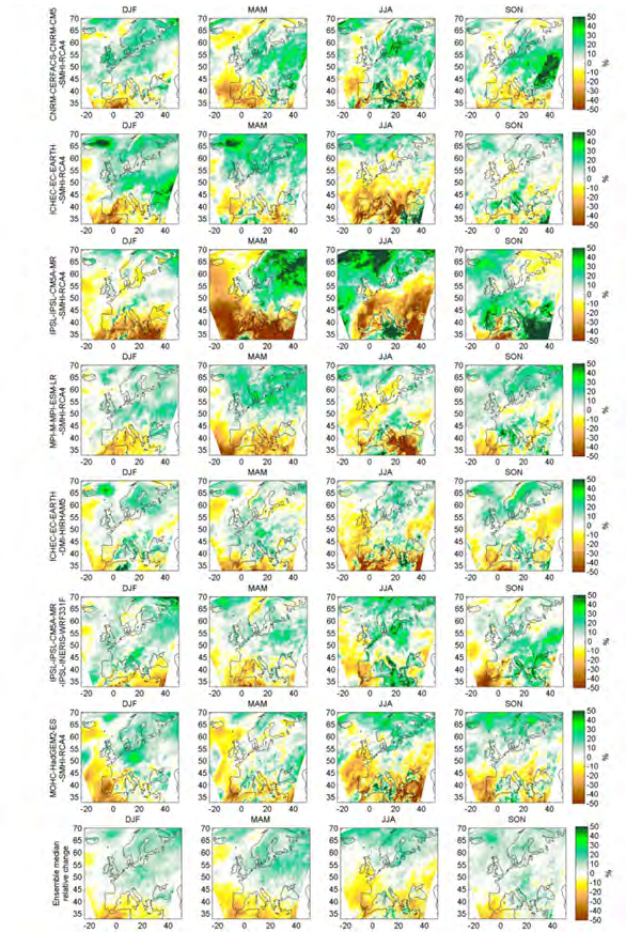


Figure 1. Relative change in seasonal mean precipitation from 1991-2010 to 2041-2060 for the seven 0.11 Euro-CORDEX simulations as well as their median.

4. Outlook

Based on the ideas outline above, we will present the subset of GCM-RCMs most relevant to the MODEXTREME project in its European study areas, as well as describe the selection procedure used to identify the optimal subset.

References

Annan, JD., JC. Hargreaves (2011) Understanding the CMIP3 Multimodel Ensemble, Journal of Climate, 24, pp. 4529-4538

Christensen, JH., E. Kjellström, F. Giorgi, G. Lenderik, M. Rummukainen (2010) Weight assignment in regional climate models, Climate Research, 44, pp. 179-194

Madsen, MS., CF. Maule, N. MacKellar, JE. Olesen, JH. Christensen (2012) Selection of climate change scenario data for impact modelling, Food Additives and Contaminants: Part A, 29, 10, pp. 1502-1513

Maule, CF., P. Thejll, JH. Christensen, SH. Svendsen, J. Hannaford (2012) Improved confidence in regional climate model simulations of precipitation evaluated using drought statistics from the ENSEMBLE models, Climate Dynamics, 40, pp. 155-173

Simulation of medicanes over the Mediterranean Sea: multi-model analysis of the impact of high resolution and ocean-atmosphere coupling

Miguel Ángel Gaertner[1], Marta Domínguez[2], Raquel Romera[2], Victoria Gil[2], Enrique Sánchez[1], Clemente Gallardo[1], EURO-CORDEX and Med-CORDEX teams

[1] Faculty of Environmental Sciences and Biochemistry, University of Castilla-La Mancha, Toledo, Spain (Miguel.Gaertner@uclm.es)
[2] Institute of Environmental Sciences, University of Castilla-La Mancha, Toledo, Spain

1. Motivations

Medicanes (Mediterranean tropical-like cyclones) are a special kind of cyclones that are observed sporadically over the Mediterranean Sea. They have a rather small diameter, tipically less than 300 km and a generally symmetrical cloud structure around a cloudless eye (Tous and Romero, 2013), which points to tropical characteristics like a warm core and a predominant role of air-sea fluxes in its development and maintenance. They form from baroclinic cut-off lows, and their distribution area lies to the south of the more frequent extratropical Mediterranean cyclones. Some studies indicate the possibility of more intense medicanes under future climate change conditions (Gaertner et al, 2007; Romero and Emanuel, 2013).

The simulation of medicanes with regional climate models is challenging due to its small size and the importance of air-sea fluxes. The regional climate simulations from EURO-CORDEX and Med-CORDEX projects are particulary valuable for the analysis of such cyclones, as they include high-resolution (0.11º) and atmosphere-ocean coupled runs.

2. Method and data

We use pairs of evaluation runs (nested in ERA-Interim reanalysis) from EURO-CORDEX and Med-CORDEX:

- Low/high resolution simulations
- Uncoupled/coupled simulations

Multi-model ensembles of such simulation pairs are used to analyse the impact of high resolution and atmosphere-ocean coupling on the simulation of medicanes.

The cyclone detection and tracking method of Picornell et al. (2001) is applied for detecting cyclones. The cyclone intensity is measured by the daily maximum wind. The existence of tropical characteristics is tested with the cyclone phase space (CPS) method of Hart (2003), by which a cyclone is classified as tropical if it's thermally symmetric (no fronts) and it has a full-tropospheric warm core. This method is also applied to observed medicanes.

3. Results

Figure 1 shows the comparison of cyclone intensity extremes for low (.44º) and high (.11º) resolution simulations on the left part. Two of the three models shown simulate a clear increase of the intensity extremes in the high resolution simulations. On the right part of this figure, intensity extremes are compared for uncoupled and coupled simulations. Most models show a small extreme intensity decrease in the coupled runs.

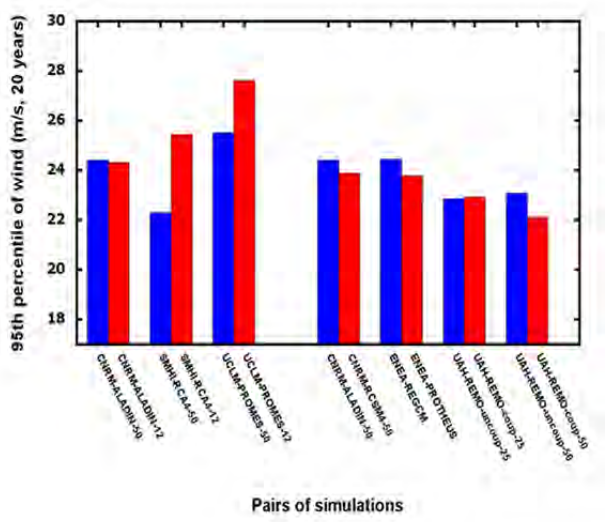


Figure 1. Cyclone intensity extremes for pairs of low resolution (blue) and high resolution (red) runs (left part) and pairs of uncoupled (blue) and coupled (red) runs (right part). Extreme values of cyclone intensity are measured by the 95th percentile of daily maximum wind.

The CPS analysis is applied to the most intense cyclones, in order to detect possible changes in tropical characteristics for the most intense cyclones. Several of the most intense cyclones show at least partially tropical characteristics. The increase of resolution is associated to deeper or more intense warm cores. The effect of atmosphere-ocean coupling is not clear with respect to changes in tropical characteristics. The analysis of a set of observed medicanes indicates that most of them show indeed at least partially tropical characteristics.

References

Gaertner, M.A., Jacob D., Gil, V., Domínguez, M., Padorno, E., Sánchez, E., and Castro, M. (2007). Tropical cyclones over the Mediterranean Sea in climate change simulations. Geophysical Research Letters, 34(14).

Hart, R. E. (2003). A cyclone phase space derived from thermal wind and thermal asymmetry. Monthly Weather Review, 131(4).

Picornell, M. A., Jansa, A., Genovés, A., and Campins, J. (2001). Automated database of mesocyclones from the HIRLAM (INM)-0.5° analyses in the western Mediterranean. International Journal of Climatology, 21(3), 335-354.

Romero, R. and Emanuel, K. (2013). Medicane risk in a changing climate. Journal of Geophysical Research: Atmospheres, 118(12), 5992-6001.

Tous, M. and Romero, R. (2013). Meteorological environments associated with medicane development. International Journal of Climatology, 33(1), 1-14.

Acknowledgements: this work is being funded by the Spanish Economy and Competitivity Ministry, through grant CGL2010-18013.

Assessing the sensitivity in the ensemble building from RCMs for hydrological applications

García Galiano, S. G.[1], Olmos Giménez, P.[2] and Giraldo Osorio, J.D.[1]

[1] Universidad Politécnica de Cartagena, R&D Group of Water Resources, Department of Civil Engineering, Cartagena, Spain (sandra.garcia@upct.es)

[2] Pontificia Universidad Javeriana, Bogotá, Colombia

1. Introduction

Several studies suggest trends of increasing temperature and decreasing rainfall, mainly for the Iberian Peninsula, due to climate variability and change. The multi-model ensemble approach allows the quantification and reduction of uncertainties in the predictions (Giraldo and García, 2013).

In this work, the latest-generation Regional Climate Models (RCMs) from ENSEMBLES European Project, and observed gridded meteorological dataset (rainfall, maximum, minimum and mean temperatures), are considered for building robust ensembles of meteorological variables over Spain, as input to hydrological models.

The evaluation of goodness-of-fit for the building of RCMs ensemble is based on empirical probability density functions (PDF) at each site analyzed (906) for the period 1961-1990 from both datasets (observed and simulated).

A PDF ensemble is built at grid site, based in the reliability and skills of RCMs for represent the interest variable. Therefore, by adjusting PDF to time series of variables, the assessment of patterns of regional changes and trends considering the scenarios 1961-1990 and 2021-2050, were assessed.

The hydrological modelling for supporting decision taking processes in planning and management of water resources at basin scale, are requiring more robust meteorological variables ensemble maps from RCMs. In this work, a novel approach is presented.

2. Methodology

The method is based in the Reliability Ensemble Averaging (REA) method (Giorgi and Mearns, 2002). Xu et al. (2010) in order to address some limitations of the original approach are eliminating the convergence-based reliability factor from the definition of the overall weight. The proposed approach is considering the impact of seasonal and annual PDF on PDF ensemble, as follows:

$$R_i = (Winter^a * Spring^b * Summer^c * Autumn^d * Year^e)^{1/(a+b+c+d+e)}$$

where R_i are REA for each RCM, and the parameters *a*, *b*, *c*, *d* and *e* are the criterion weights.

Finally, the likelihood P_m for each RCM is defined as follows (Giorgi and Mearns 2003):

$$Pm_i = \frac{R_i}{\sum_1^N R_j}$$

The Figure 1 presents the REA estimated from each RCM, according the methodology proposed.

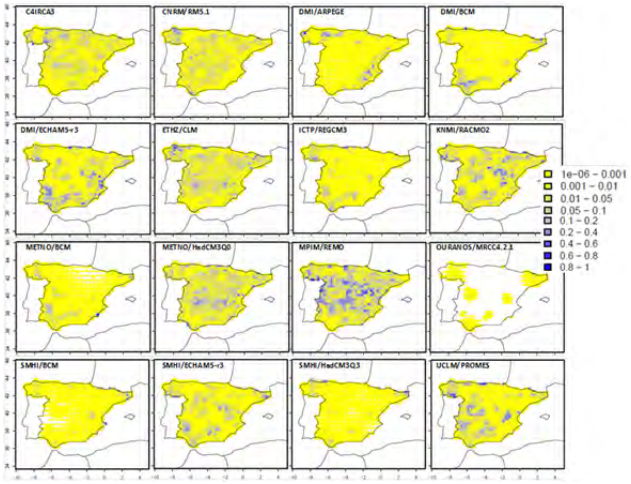


Figure 1. Map of REA for each RCM.

As an example, the Figure 2 presents the CDFs of rainfall from each RCMs, observed dataset and ensemble, estimated for the site 732 (South East of Spain), for 1961-1990 time period.

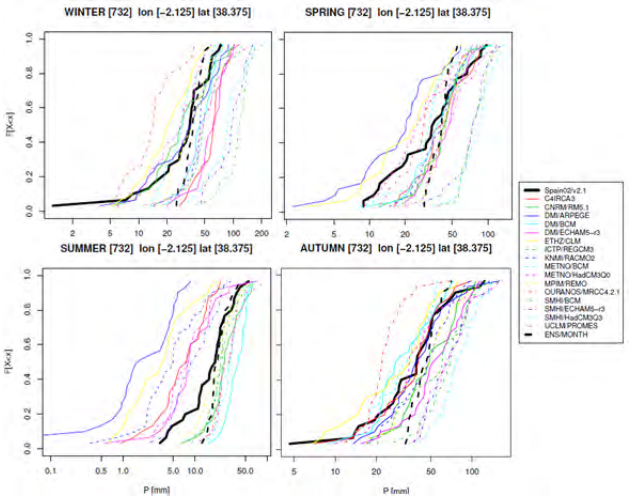


Figure 2. CDFs of rainfall from observed dataset (in black), ensembles (dashed black) and RCMs, for 1961-1990 period.

The sensitivity of PDF ensemble to selection of criterion weights, was evaluated considering several combinations of parameters. The assessments were

mainly based on the analysis of p value of the goodness of fit Kolmogorov-Smirnov test.

6. Conclusions

This paper presents a novel approach based on REA method, to compute the RCM weighting factors (the normalized reliability factor Pm), which allow to build ensemble for several meteorological variables as input to hydrological models.

The sensitivity of ensemble PDF to selection of criterion weights, was assessed considering the goodness of fit Kolmogorov-Smirnov test.

In conclusion, the combination of RCMs generally increases the reliability of the predictions although there are different weighting methodologies. The evaluation of the sensitivity of the methodologies for building RCMs ensembles, as proposed in this work, allows a better understanding of uncertainties involved.

References

Giorgi F, Mearns LO (2002). Calculation of average, uncertainty range, and reliability of regional climate changes from AOGCM simulations via the ‘‘reliability ensemble averaging’’ (REA) method. J Clim 15(10), pp. 1141–1158.

Giorgi F, Mearns LO (2003). Probability of regional climate change based on reliability ensemble averaging (REA) method. Geophys Res Lett 30(12), pp. 311–314.

Giraldo Osorio J. D., Garcıa Galiano S. G. (2013). Assessing uncertainties in the building of ensemble RCMs over Spain based on dry spell lengths probability density functions. Clim Dyn 40. pp. 1271–1290. DOI 10.1007/s00382-012-1381-5

Xu Y, Gao X, Giorgi F (2010) Upgrades to the reliability ensemble averaging method for producing probabilistic climate-change projections. Clim Res 41, pp. 61–81.

COSMO-CLM and RCA4 Multimodel ensemble Projections for the West African Monsoon

Emiola O. Gbobaniyi[1,2], Ivonne Anders[3]

[1] Swedish Meteorological and Hydrological Institute (bode.gbobaniyi@smhi.se)
[2] Centre for Atmospheric Research, Anyigba, Nigeria
[3] Central Institute for Meteorology and Geodynamics (ZAMG), Vienna, Austria

We intercompare two regional climate simulation ensembles to see how they reproduce the main features of the West African Monsoon (WAM) under future conditions. Four CMIP5 coupled atmosphere ocean general circulation models (AOGCMs), namely, CNRM-CM5, HadGEM2-ES, EC-EARTH, and MPI-ESM-LR are downscaled separately by RCA4 and COSMO-CLM regional models in the ongoing CORDEX-Africa activities to create the ensembles. The spatial resolution of the driving AOGCMs varies from about 1° to 3° while all regional simulations are at the same 0.44° resolution.

Future climate projections from the RCP8.5 scenario are analyzed and inter-compared for both ensembles in order to assess deviations and uncertainties. The main focus in our analysis is on the projected WAM rainy season statistics. We look at projected changes in onset and cessation, total precipitation and temperature toward the end of the century (2071-2100) for different time scales spanning seasonal, annual and interannual variability, and a number of spatial scales covering the Sahel, the Gulf of Guinea and the entire West Africa. Differences in the ensemble projections are linked to the parameterizations employed in the regional models and the associated influences discussed.

Keywords: CORDEX, Regional climate Models, West African Monsoon, ensembles.

Use of RCM ensembles to produce regional climate projections: Key issues and the CORDEX perspective

Filippo Giorgi

Abdus Salam International Centre for Theoretical Physics, Trieste, Italy

Regional climate projections produced with the use of dynamical (e.g. Regional Climate Model, RCM) and statistical downscaling (SD) techniques are characterized by a range of different sources of uncertainty, such as: greenhouse gas emission and concentration scenarios; response of global climate models (GCMs) used to drive the regionalization tools; response of different RCMs to the driving conditions; response of different regionalization techniques (e.g. RCMs vs. SD); internal variability of the climate system and of the regionalization tools; application of the regionalization tools to different regions; systematic biases in the climate models. The characterization of uncertainty in regional projections is a key element of the provision of climate information usable for vulnerability, impact and adaptation (VIA) studies. A full exploration of this multi-dimensional uncertainty space requires the completion of large ensembles of simulations with multiple models and methods, which is clearly beyond the capabilities of individual laboratories. This calls for a coordination effort of the RCM and broader downscaling community which has lacked in the past (except for some targeted regional intercomparison projects) and has in fact prevented the systematic use of RCM information in VIA applications and in major assessments (e.g. by the Intergovernmental Panel of Climate Change). Because of these reasons, the downscaling community, under the auspices of the World Climate Research Program (WCRP), has designed and implemented the COordinated Regional Downscaling EXperiment, or CORDEX.

The primary goal of CORDEX is to provide a general and common framework to i) evaluate and improve different downscaling techniques (RCM, SD); ii) produce a new generation of climate change projections over regions worldwide based on multi-model, multi-method ensembles in order to characterize uncertainties; and iii) facilitate the interaction between the climate and VIA communities towards teh application of regional climate information. A Phase I of the CORDEX project has been designed and implemented (Giorgi et al. 2009), with many groups participating and completing the first set of projections. For example, the RegCM (Giorgi et al. 2012) community has completed initial projections over different CORDEx domains, such as Europe, Mediterranean, Africa, Central and South America, South and East Asia. In the first part of this presentation I will review the status of the CORDEX Phase I experiments, highlighting with a set of illustrative examples the main issues emerging from this first experience. Among them are the inhomogeneity of the efforts across regions; the need to better explore the behaviour of the models in terms of added value and representation of regional processes; the distillation of useful information from the ensembles produced; the collection and dissemination of large amounts of data.

In the second part of the presentation I will elaborate on the lessons learned from the Phase I activities to date in order to illustrate the main aspects of the ongoing discussion on the next phase of the project. In particular, I will call for the need to design flagship pilot regional studies that would allow us to explore in depth the potential of downscaling tools for providing actionable climate information along with some of the key scietific issues still being debated within this community (e.g. added value, effects of resolution, uncertainty characterization). These pilot studies would also allow us to make use of high quality regional observations produced as part of special observing programs, which is another key issue for the in depth analysis of regionalization products.

References

Giorgi F, Jones C, Asrar GR (2009) Addressing climate information needs at the regional level: The CORDEX framework. WMO Bulletin 58:175-183.

Giorgi F, et al. (2012) RegCM4: Model description and preliminary tests over multiple CORDEx domains. Climate Research 52:7-29.

Exploring a three-stage dynamical downscaling with empirical correction of sea-surface temperature using CRCM5 over the CORDEX-Africa domain

Leticia Hernández-Díaz, René Laprise, Oumarou Nikiéma and Katja Winger

Centre ESCER, Université du Québec à Montréal, Montréal (Québec) Canada (leticia@sca.uqam.ca)

1. Introduction

The use of Regional Climate Models (RCMs) for the dynamical downscaling of climate projections over a limited-area domain is nowadays a common technique. It has been shown that RCMs can add value to climate simulation in regions with complex topography (orography, coastlines) and for mesoscale phenomena and extremes, e.g. Di Luca et al. (2012), Feser et al. (2011).

Climate projections by dynamical downscaling with atmosphere-only RCM use 2 types of boundary conditions (BC) interpolated from Coupled Global Climate Model (CGCM) simulations: atmospheric lateral BC and ocean surface BC. It is well documented that biases in CGCM simulations have detrimental impacts in nested RCM simulations. While the quality of CGCMs has steadily been improving, BC from state-of-the-art CGCMs are not yet as good as one would like. For example, strong sea surface temperature (SST) biases are still present in most of the CMIP5 CGCMs.

Previous work using the fifth-generation Canadian Rcm (CRCM5) for climate simulations over the CORDEX-Africa domain has shown for example that, when driven by ERA-Interim reanalyses, the CRCM5 is capable of reproducing the double rainy seasons in the region of the Guinea Coast; see Hernández-Díaz et al. (2012). On the other hand, two CGCM-driven CRCM5 simulations failed in this respect, similarly to the CGCMs themselves; see Laprise et al. (2013). It is worth mentioning that both CGCMs suffered from strong SSTs biases in tropical and equatorial Atlantic Ocean (Fig. 1).

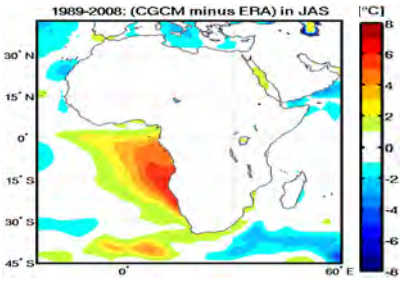


Figure 1. Sea-surface temperature bias of MPI-ESM-LR for current climate (1989-2008) in boreal summer (JAS). (Reproduced from Laprise et al. © 2013 Climate Dynamics).

In an attempt to improving BC used to drive the RCM simulations, an empirical correction of SSTs biases from a CGCM simulation has been done, inspired by the studies of Rowell (2005) and Katzfey et al. (2009). Here we present a 3-step approach in which the SST from a CGCM simulation are empirically corrected and used as ocean lower BC for an Atmosphere-only GCM simulation, which in turn will provide the BC to drive an RCM simulation.

2. Experimental framework

Fig. 2 shows a flowchart describing the proposed 3-step dynamical downscaling technique. Using the assumption of a persisting bias, the first step is to empirically correct the CGCM-simulated SST by subtracting the biases identified in simulating a historical period. The second step is to run an atmosphere-only GCM (AGCM) using these corrected SST as BC. The final step is to use the atmospheric fields from the AGCM simulation, together with the corrected SST fields, as BC for driving an RCM simulation over the region of interest: in the present case, the CORDEX-Africa domain.

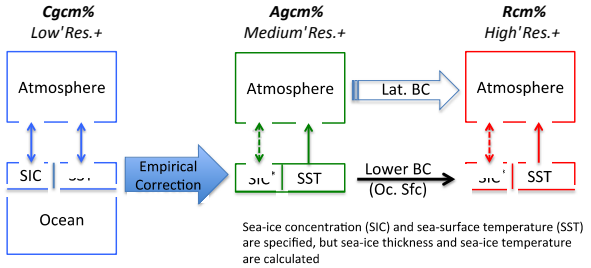


Figure 2. Three-stage dynamical downscaling: Cgcm-Agcm-Rcm.

Note also that the present technique of correcting the SST by removing systematic bias corrects the climatological bias, but retains the CGCM-simulated temporal variability and its evolution in future time.

3. Simulations configuration

The CGCM used in this study is MPI-ESM-LR, the Low-Resolution version of the *Max-Planck-Institut für Meteorologie* Earth System coupled global climate model (http://www.mpimet.mpg.de/en/science.html) with the atmospheric component operating at T63 with a linear transform grid of approximately 2.85°, and 47 levels in the vertical. The MPI_ESM_LR simulation covers the period 1950 to 2100, under historical and RCP4.5 emission scenario. The period 1979-2008 was chosen to calculate the SST biases of the CGCM with respect to ERA reanalyses. The bias correction is applied to the fields of SST and sea-ice cover of MPI-ESM-LR for the whole period (historical and RCP4.5).

The corrected ocean surface fields are then used as BC for the AGCM simulation from 1950 to 2100 under historical and RCP4.5 emission scenario. Here the AGCM is a global version of the Canadian Global Environment Multiscale (GEM) model (Zadra et al. (2008)) in its AMIP-type configuration, with a regular latitude-longitude grid at a resolution of 1.4°, and 64 levels in the vertical (top level at 2 hPa). Model physics as well as the land-surface

scheme are the same of those of CRCM5. This simulation provided the atmospheric lateral BC for the RCM (CRCM5) simulation.

CRCM5 is based on the limited-area model (LAM) configuration of GEM; a detailed description can be found in Hernández-Díaz et al. (2012). CRCM5 was integrated over the CORDEX-Africa domain (Fig. 1) with a horizontal grid spacing of 0.44°, with a 20-min. time step. The computational domain has 216 x 221 grid points, including a 10-grid-point wide sponge zone around the perimeter; hence the free domain is 196 x 201 grid points. In the vertical, 56 levels were used, with the top level near 10 hPa and the lowest level at 0.996* p_s where p_s is the surface pressure.

4. Preliminary results

Figure 3 displays the mean annual cycle of precipitation for the West Africa-South region (WA-S) of the CORDEX-Africa domain for the period (1998-2008). The observed annual cycle from three different datasets (CRU, UDEL, GPCP, TRMM), as well as from the ERA-driven RCM simulation, are shown in addition to those from the CGCM- and AGCM-driven RCM simulations and from the CGCM and AGCM simulations themselves. The WA-S region has a bimodal distribution of precipitation that represents the double passage of the tropical rainbelt in the equatorial regions. This feature is well accounted for only in the ERA-driven RCM simulation (cyan) and the AGCM-driven RCM simulation (black), but it is absent in the CGCM-driven simulation (green), as well as in the CGCM (blue) and AGCM (red) simulations. This reflects the importance of the BC, in the nested simulations.

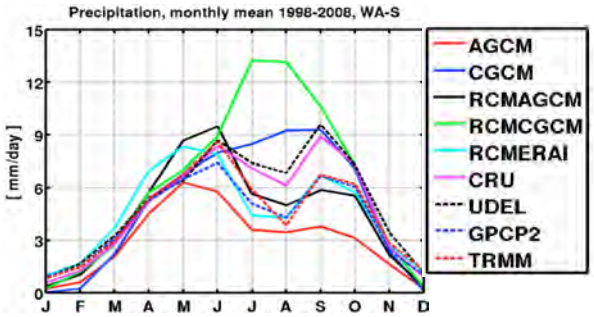


Figure 3. Mean (1998-2008) annual cycle of precipitation (mm/day) for the West Africa-South (WA-S) region of the CORDEX-Africa domain from observations and models.

Figure 4 shows the combined effect of changing the atmospheric driving model as well as the ocean surface conditions on the RCM simulations.

5. Conclusions

Despite its relative simplicity, the proposed three-step dynamical downscaling technique shows that substantial improvements can be afforded in simulating present-day climate with empirically corrected SST. The bimodal distribution of precipitation over WA-S region was only obtained in the high-resolution CRCM5 simulation driven by AGCM using empirically corrected SST. This illustrates the importance of the combination of high resolution and BC for successful simulation of this phenomenon.

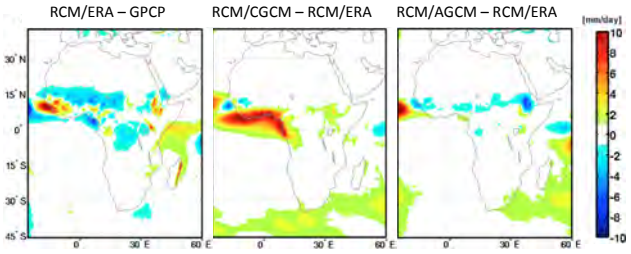


Figure 4. JAS mean precipitation biases (mm/day) of (left) the ERA-driven RCM simulation with respect to GPCP dataset, (centre) the CGCM-driven RCM and (right) the AGCM-driven RCM simulations with respect to the ERA-driven RCM simulation.

For the choice of the AGCM in the intermediate step, there can be two possibilities: (1) to use the atmosphere-only version of the CGCM that provides the sea surface conditions, or (2) to use a global version of the RCM, as was the case here. Option (2) facilitates the nesting since the AGCM shares identical formulation with the RCM. However, if the intent is to downscale several CGCM simulations, the use of the same AGCM may reduce the spread across the ensemble of driving data, despite the use of sea surface conditions from different CGCMs.

An interesting technical advantage of proposed three-tier approach using an intermediate AGCM is that there is no need to import 3D atmospheric fields from a (foreign) CGCM to provide the lateral BC to the RCM. One-dimensional surface fields of SST and sea-ice cover suffice.

References

Di Luca A, de Elía R, Laprise R (2012) Potential for added value in precipitation simulated by high-resolution nested Regional Climate Models and observations. Clim Dyn. 38(5-6), pp. 1229-1247. doi:10.1007/s00382-011-1068-3

Feser F, Rockel B, von Storch H, Winterfeldt J, Zahn M (2011) Regional climate models add value to Global Model data. Bull Am Meteorol Soc 92, pp. 181-1192.

Hernández-Díaz L, Laprise R, Sushama L, Martynov A, Winger K, Dugas B (2012) Climate simulation over the CORDEX-Africa domain using the fifth generation Canadian Regional Climate Model (CRCM5). Clim Dyn. 40, pp. 1415-1433. doi:10.1007/s00382-012-1387-z

Katzfey JJ, McGregor J, Nguyen K, Thatcher M (2009) Dynamical downscaling techniques: Impacts on regional climate signals. 18th World IMACS/MODSIM Congress, Cairns, Australia. http://mssanz.org.au/modsim09

Laprise R, Hernández-Díaz L, Tete K, Sushama L, Šeparović L, Martynov A, Winger K, Valin M (2013) Climate projections over CORDEX-Africa domain using the fifth-generation Canadian regional Climate Model (CRCM5). Clim Dyn 41, pp. 3219-3246.

Rowell DP (2005) A scenario of European climate change for the late twenty-first century: seasonal means and interannual variability. Clim Dyn 25, pp. 837–849.

Zadra A, Caya D, Côté J, Dugas B, Jones C, Laprise R, Winger K, Caron LPh (2008) The next Canadian Regional Climate Model. Phys Canada 64, pp. 75-83.

Evaluation of the Performance of Regional Climate Models from CORDEX-East Asia

Bo Huang, Stefan Polanski and Ulrich Cubasch

Institute of Meteorology, Free University of Berlin, Germany (huangb@zedat.fu-berlin.de)

This study investigates the performance of 5 Regional Climate Models, that participated in the Coordinated Regional Climate Downscaling Experiment East Asia (CORDEX-East Asia), driven by ERA-Interim reanalysis (1989-2008). We analyses the ability of RCMs and the multi ensemble model (MME) to reproduce the spatio-temporal characteristics of present-day Asian monsoon system. We focus on precipitation and temperature to evaluate the performance of the models. We find that the individual RCMs show acceptable skill in simulating the main spatio-temporal precipitation and temperature patterns in agreement with observation (GPCP). However, most of the RCMs tend to simulate a weakened monsoon in East Asia and enhanced monsoon in West Pacific Ocean. MME is improves the representation of the monsoon system compared to individual RCMs, but still underestimate monsoon precipitation intensity in East China Sea.

The Euro-CORDEX initiative: A new generation of regional climate scenarios for Europe

Daniela Jacob[1], Andreas Gobiet[2], Claas Teichmann[1,3], Heimo Truhetz[2]

[1] Climate Service Center, Hamburg, Germany (daniela.jacob@hzg.de)
[2] Wegener Center for Climate and Global Change, University of Graz, Austria
[3] Max-Planck-Institut für Meteorologie, Hamburg, Germany

1. EURO-CORDEX within the CORDEX framework



The WCRP Coordinated Regional Downscaling Experiment (CORDEX, Giorgi et al., 2006) provides an internationally coordinated framework to improve regional climate scenarios. This includes harmonization of model evaluation activities and the generation of multi-model ensembles of regional climate projections for the land-regions worldwide.

As part of the global CORDEX framework the EURO-CORDEX initiative (http://www.euro-cordex.net) provides regional climate projections for Europe at 50 km (EUR-44) and 12.5 km (EUR-11) resolution, thereby complementing coarser-resolution data sets of former activities like PRUDENCE (Christensen et al., 2007) and ENSEMBLES (Hewitt and Griggs, 2004, van der Linden and Mitchell, 2006).

2. The EURO-CORDEX community

EURO-CORDEX is a voluntary effort of many of the leading and most active institutions in the field of regional climate research in Europe and is coordinated by D. Jacob and A. Gobiet . EURO-CORDEX (similar to the entire CORDEX initiative) is not providing funding to any participant, but is fully relying on the enthusiasm of the participating researchers and institutions (see www.euro-cordex.net for details). This enthusiasm is based on the aim to improve climate projections, in order to enable the European society to better adapt to unavoidable climate change and to design more efficient mitigation strategies.

3. EURO-CORDEX simulations

The regional simulations are based on the new CMIP5 global climate projections and the new representative concentration pathways (RCPs). EURO-CORDEX is actively supported by 29 modelling groups contributing with 10 different regional climate models, partly in different model versions. In total, 38 evaluation simulations and 90 scenario simulations have been conducted or are currently being produced (38 of them in high resolution), based on the RCP2.6, RCP4.5 and RCP8.5 pathways (Moss et al., 2010).

In its initial phase EURO-CORDEX mainly focuses on the construction of a simulation matrix that covers uncertainty in emission scenarios, the driving global climate model, and the downscaling method in the best affordable manner. Recently, also the first analysis of future climate simulations started and the construction of an extended simulation matrix by joining empirical-statistical methods is discussed. As an example, Figure 1 illustrates which of the General Circulation Models (GCMs) are downscaled within EURO-CORDEX at a resolution of 12.5km for RCP4.5. It also shows the spread of the multi-annual mean temperature and precipitation climate change signal of the GCMs and how it is sampled by the RCMs. The spread of the GCMs by the RCMs looks reasonable, but could still be improved to rather warm and wet GCMs.

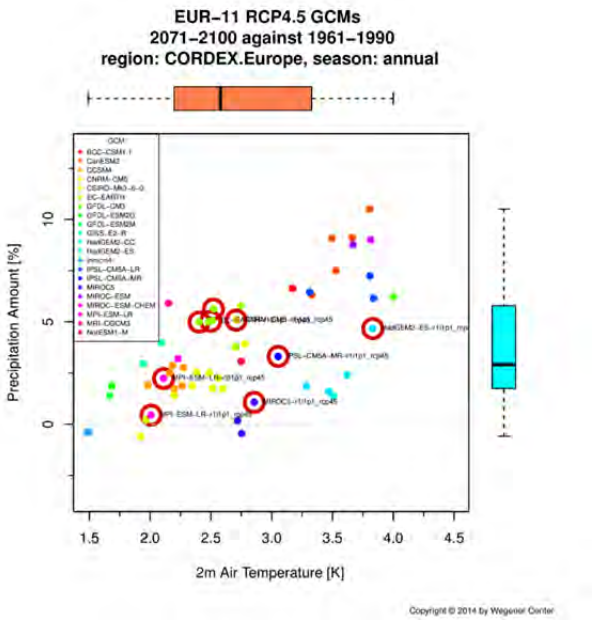


Figure 1. Precipitation amount and temperature of CMIP5 GCMs. GCMs downscaled by RCMs within EURO-CORDEX are marked with a circle.

4. EURO-CORDEX research

In the beginning of the EURO-CORDEX effort, the focus lies on the evaluation of various aspects of the regional simulations in present-day climate. In Vautard et al. (2013), the ability of the EURO-CORDEX ensemble (EUR-11 and EUR-44) to accurately simulate heat waves at the regional scale of Europe was evaluated. They found that despite some improvements, especially along coastlines, the analyses conducted in the paper did not

allow us to generally conclude that a higher resolution is clearly beneficial for a correct representation of heat waves by regional climate models. Even though local-scale feedbacks should be better represented at high resolution, combinations of parameterizations have to be improved or adapted accordingly.

Kotlarski et al. (2014) documents the performance of the EURO-CORDEX models in representing the basic spatio-temporal patterns of the European climate, with respect to near-surface air temperature and precipitation for the period 1989–2008. Overall, the analysis confirms the ability of RCMs to capture the basic features of the European climate, including its variability in space and time, while it also identifies non-negligible deficiencies of the simulations for selected metrics, regions and seasons.

In many research activities within EURO-CORDEX, future climate change is investigated. In Jacob et al. (2013) the first set of high-resolution simulation (EUR-11) is presented. They found that compared to the ENSEMBLES simulations, the large-scale patterns of changes in mean temperature and precipitation are similar in all three scenarios, but they differ in regional details, which can partly be related to the higher resolution in EURO-CORDEX.

5. EURO-CORDEX data in impact research

Further, in order to facilitate the application of the EURO-CORDEX results in climate impact research, suitable bias correction techniques are applied and guidance documents are prepared. Additionally, one of the EURO-CORDEX objectives is to foster the interaction with the users of EURO-CORDEX data.

This presentation provides an overview on the status and on current research activities within the EURO-CORDEX framework.

References

Christensen, J. H.; Carter, T. R.; Rummukainen, M. & Amanatidis, G. (2007), Evaluating the performance and utility of regional climate models: the PRUDENCE project, Climatic Change 81, 1-6.

Giorgi, F.; Jones, C. & Asrar, G. (2006), Addressing climate information needs at the regional level: the CORDEX framework, Bulletin World Meteorolgical Organization 58, 175-183.

Hewitt, C. & Griggs, D. (2004), Ensembles-based predictions of climate change and their impacts (ENSEMBLES), Eos (AGU) 85(52), 566.

Jacob, D.; Petersen, J.; Eggert, B.; Alias, A.; Christensen, O. B.; Bouwer, L. M.; Braun, A.; Colette, A.; Déqué, M.; Georgievski, G.; Georgopoulou, E.; Gobiet, A.; Menut, L.; Nikulin, G.; Haensler, A.; Hempelmann, N.; Jones, C.; Keuler, K.; Kovats, S.; Kröner, N.; Kotlarski, S.; Kriegsmann, A.; Martin, E.; van Meijgaard, E.; Moseley, C.; Pfeifer, S.; Preuschmann, S.; Radermacher, C.; Radtke, K.; Rechid, D.; Rounsevell, M.; Samuelsson, P.; Somot, S.; Soussana, J.-F.; Teichmann, C.; Valentini, R.; Vautard, R.; Weber, B. & Yiou, P. (2013), EURO-CORDEX: new high-resolution climate change projections for European impact research, Regional Environmental Change, 1-16.

Kotlarski, S.; Keuler, K.; Christensen, O. B.; Colette, A.; Déqué, M.; Gobiet, A.; Goergen, K.; Jacob, D.; Lüthi, D.; van Meijgaard, E.; Nikulin, G.; Schдr, C.; Teichmann, C.; Vautard, R.; Warrach-Sagi, K. & Wulfmeyer, V. (2014), Regional climate modeling on European scales: a joint standard evaluation of the EURO-CORDEX RCM ensemble, Geoscientific Model Development Discussions 7(1), 217--293.

van der Linden, P. & Mitchell, J. F. B.van der Linden, P. & Mitchell, J. F. B., ed., (2009), ENSEMBLES: Climate Change and Its Impacts: Summary of Research and Results from the ENSEMBLES Project, Met Office Hadley Centre, Exeter.

Moss, R. H.; Edmonds, J. A.; Hibbard, K. A.; Manning, M. R.; Rose, S. K.; van Vuuren, D. P.; Carter, T. R.; Emori, S.; Kainuma, M.; Kram, T.; Meehl, G. A.; Mitchell, J. F. B.; Nakicenovic, N.; Riahi, K.; Smith, S. J.; Stouffer, R. J.; Thomson, A. M.; Weyant, J. P. & Wilbanks, T. J. (2010), The next generation of scenarios for climate change research and assessment, Nature 463(7282), 747--756.

Vautard, R.; Gobiet, A.; Jacob, D.; Belda, M.; Colette, A.; Déqué, M.; Fernández, J.; García-Díez, M.; Goergen, K.; Güttler, I.; Halenka, T.; Karacostas, T.; Katragkou, E.; Keuler, K.; Kotlarski, S.; Mayer, S.; Meijgaard, E.; Nikulin, G.; Patarčić, M.; Scinocca, J.; Sobolowski, S.; Suklitsch, M.; Teichmann, C.; Warrach-Sagi, K.; Wulfmeyer, V. & Yiou, P. (2013), The simulation of European heat waves from an ensemble of regional climate models within the EURO-CORDEX project, Climate Dynamics, 1-21.

Decadal prediction and new opportunities for downscaling in the North Atlantic Sector

Noel Keenlyside

Geophysical Institute, University of Bergen and Bjerknes Centre

Decadal changes in sea surface temperature (SST) the North Atlantic sector can be skilfully predicted through accurate initialisation of the ocean, while radiative forcing changes are of secondary importance. Although North Atlantic SST changes may influence the atmosphere, only a limited amount of predictability has been demonstrated for climate of the region.

In this presentation I will argue that decadal predictions provide an exciting opportunity for skilful downscaling of oceanic and atmospheric variability in the North Atlantic sector. I will discuss the mechanisms for oceanic predictability and how the links to the Nordic Seas and the Arctic could extend predictability of the ocean to higher latitudes. Dynamical downscaling could further enhance predictions with applications to marine ecosystem and fisheries.

New studies show that resolving oceanic fronts and stratosphere-troposphere interaction are important to capturing the atmospheric response to extra-tropical SST variations. Remotely forced climate variations, for example from the tropics and Eurasian snow cover, may also impact climate in the North Atlantic sector. The potential for these mechanisms to enhance predictability of climate in this region will be discussed. As will the impact of model bias and approaches to mitigate their detrimental impact.

The elevation dependency of 21st century European climate change in a multi-RCM ensemble

Sven Kotlarski, Daniel Lüthi , Christoph Schär

Institute for Atmospheric and Climate Science, ETH Zurich, Switzerland (sven.kotlarski@env.ethz.ch)

1. Introduction

Observed past and projected future climate change are subject to an important variability in space and exhibit distinct three-dimensional patterns. Spatial variability includes the horizontal pattern of climate change signals as well as their height dependency in the free troposphere. A hybrid form of such variability is the elevation dependency of near-surface climate change, i.e., the relation between the change of a near-surface quantity and the topographic height of the respective location. Its origin lies in both predominantly horizontal variability (caused, e.g., by large-scale changes in circulation patterns) and in variations in the vertical undisturbed atmospheric profile. Further contributing factors are fundamental geometrical effects responsible for the influence of orography on precipitation patterns, diabatic processes in the mid- and high troposphere and elevation-dependent surface forcings. The existence of an elevation-dependent variability in near-surface climate change has major implications for climate impact assessment in mountainous terrain as it can be associated with amplifications or attenuations of large-scale climate change signals at specific elevations.

The present study transfers the work of Kotlarski et al. (2012) who analyzed the elevation dependency of 21st century European climate change in a transient scenario of the regional climate model (RCM) COSMO-CLM into a multi-model framework. Elevation dependencies of near-surface climate change are investigated in an ensemble of 15 regional climate scenarios provided by the ENSEMBLES project (van der Linden and Mitchell 2009). These experiments were carried out by 11 different RCMs which are, in turn, driven by 6 different general circulation models (GCMs). For the future period, all simulations assume greenhouse gas concentrations according to the IPCC SRES A1B emission scenario. The analysis focuses on near-surface air temperature and precipitation, i.e., two parameters that are particularly relevant for climate impact analysis, and is carried out separately for four distinct sub-domains of the European continent (namely the European Alps (AL), Eastern Europe (EA), the Iberian Peninsula (IP) and Scandinavia (SC)), for four seasons (winter: DJF, spring: MAM, summer: JJA, autumn: SON) and for mean values over 100m elevation bins. Before investigating climate change signals, the experiments are evaluated with respect to their ability to represent the observed elevation dependency of temperature and precipitation in the historical period. As observational reference the gridded E-OBS dataset is used (Haylock et al. 2008).

2. Model Evaluation

Figure 2 compares the simulated vertical profile of annual mean 2m temperature (1961-2000) in each analysis domain against the E-OBS reference (upper panels). Additionally, the monthly mean lapse rate (based on linear least-squares regression) is analyzed (lower panels). In all sub-domains the E-OBS reference indicates a close-to-linear elevation dependency of annual mean values. The RCMs are able to capture the broad characteristics of this temperature-elevation relationship. This includes deviations from a linear dependency for individual elevation bands (e.g., elevations around 150 m in EA). However, in AL, IP and SC most experiments show an increasing cold bias towards high elevations, leading to a pronounced overestimation of the temperature lapse rate in most months (lower panels). For AL, EA and IP the variability of the temperature lapse rate throughout the year is approximately reproduced. For precipitation (not shown) elevation dependencies in the historical climate are reproduced less accurately, but the general increase of precipitation sums with elevation is captured.

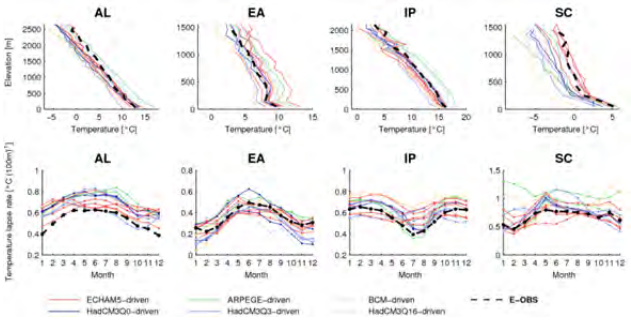


Figure 1. Upper row: Elevation dependency of mean annual 2 m temperature for the period 1961-2000 in the 15 RCM experiments (colored) and in E-OBS (dashed black) in the four analysis domains. Lower row: Mean annual cycle of the temperature lapse rate in the period 1961-2000 as obtained by linear regression for the 15 RCM experiments (colored) and for E-OBS (dashed black).

3. Climate Scenarios

For the case of 2m temperature, the analysis of the vertical pattern of climate change signals until the end of the 21st century indicates a high inter-model agreement in most sub-domains and most seasons, despite considerable differences in the general warming magnitude (Figure 2). The latter is strongly controlled by the driving GCM. In the European Alps (AL) maximum warming typically occurs at upper elevations. The same is true for EA in spring and summer and for IP in winter and spring. Conversely, winter and spring warming

magnitudes in SC are largest at low elevations. In the Alps, the anomalous high elevation warming leads to a decrease of temperature lapse rates in most experiments and throughout most parts of the year. Except for EA, largest warming rates typically occur at elevations of strongest losses of snow days (not shown).

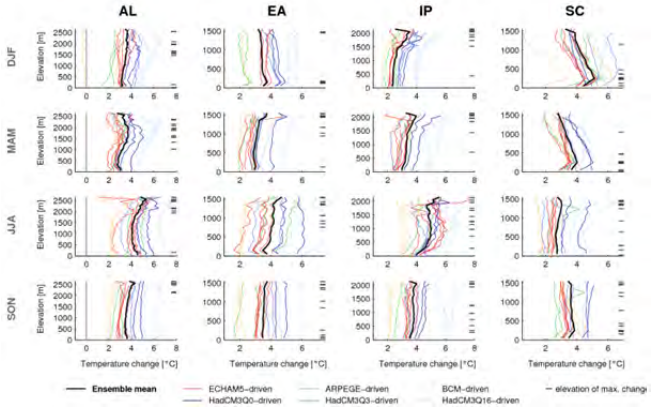


Figure 2. Simulated change of mean seasonal 2m temperature between 1961-1990 and 2070-2099 [°C] in each 100 m elevation band for all seasons (rows) and for all analysis domains (columns). The colors denote the driving GCM, the bold black line indicates the ensemble mean change. For each model experiment, the elevation of maximum temperature change is indicated by a horizontal bar at the right hand side of the respective panel.

For the vertical pattern of relative precipitation changes (Figure 3) model agreement is less pronounced but can be identified for some domains and some seasons. In summer, precipitation decreases are obtained for all sub-domains except SC. In the Alps, most models agree on largest relative JJA precipitation decreases at low elevations, while relative changes are largest at high elevations in sub-domain EA. In Scandinavia, a large spread of model responses is obtained. As for temperature, an influence of the driving GCM on the sign and the magnitude of precipitation changes can be identified in many case.

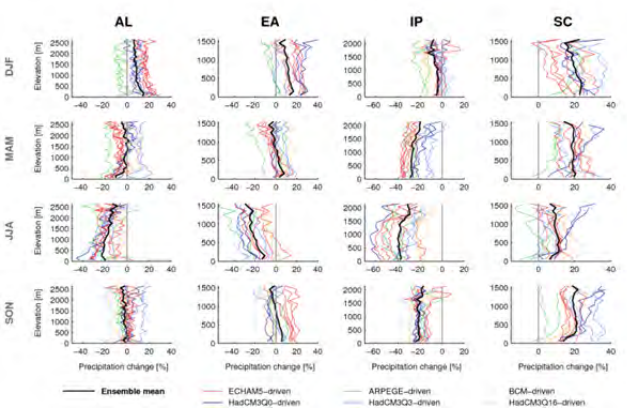


Figure 3. Simulated change of mean seasonal precipitation between 1961-1990 and 2070-2099 [%] in each 100 m elevation band for all seasons (rows) and for all analysis domains (columns). The colors denote the driving GCM. The bold black line indicates the ensemble mean change.

4. Summary and Conclusions

The elevation dependency of 21st century near-surface climate change over Europe has been analyzed in an ensemble of RCM experiments. Results indicate a good model agreement on the vertical pattern of 2m temperature changes, despite considerable differences in the general warming magnitude. Vertical anomaly profiles of mean warming rates can therefore be considered as comparatively robust. In many cases strongest warming occurs at elevations of important decreases of snow cover, suggesting an important contribution of the snow albedo feedback to the elevation dependency of temperature changes. Model agreement is typically less pronounced for the vertical pattern of precipitation changes, although common features can be identified.

References

Kotlarski S, Bosshard T, Lüthi D, Pall P, Schär C (2012) Elevation gradients of European climate change in the regional climate model COSMO-CLM, Climatic Change, 112, pp. 189-215

Haylock MR, Hofstra N, Klein Tank AMG, Klok EJ, Jones PD, New M (2008) A European daily high-resolution gridded data set of surface temperature and precipitation for 1950–2006. Journal of Geophysical Research, 113, D20119

van der Linden P, Mitchell JFB (2009) ENSEMBLES: Climate Change and its Impacts: Summary of research and results from the ENSEMBLES project, Met Office Hadley Centre, Exeter, UK, 160 pp

The European summer climate in a surrogate experiment

Nico Kröner, Sven Kotlarski, Erich Fischer, Daniel Lüthi and Christoph Schär

Institute for Atmospheric and Climate Science, ETH Zurich, Switzerland (nico.kroener@env.ethz.ch)

1.Introduction

The record-breaking summer heatwaves in 2003 and 2006 raised the interest of the scientific community in the European summer climate (Schär et al. 2004, Vidale et al. 2007; Rebetez et al. 2009). Different observational studies showed that European summer temperatures were rising in the last decades especially in the upper percentiles (e.g. Parey et al. 2010). Projections into the future provide strong evidence for this trend to continue (Kjellstrom et al. 2007, Fischer et al. 2009). However, the processes responsible for the observed and projected changes in European summer climate and variability are still not fully understood. Different mechanisms were proposed including changes in soil moisture regime (Seneviratne et al. 2006, Vidale et al. 2007), cloud cover changes, or altered large-scale circulation patterns (e.g., Lenderink et al. 2007; Andrade et al. 2012, Fischer et al. 2012). Until now most studies focused on individual aspects of the driving mechanisms, but could not quantify their respective contribution. The objective of the present work is to gain more insight into the processes responsible for the variability of the European summer climate and their quantitative contribution to its future changes. For this purpose we apply a suite of surrogate climate change experiments.

2.The Surrogate Scenario Approach

The idea of the surrogate technique is to apply certain aspects of future climate change, e.g. a large-scale warming, onto a present-day reference simulation (Schär et al. 1996).

The first experiment suite includes six runs of the regional climate model COSMO-CLM carried out at a horizontal resolution of 50km. The first two runs are used as reference and encompass a control (1971-2000) (CTRL) and scenario (2070-2099) (SCEN) run driven by the global climate model MPI-ESM-LR under the RCP8.5 scenario. The third and fourth run are surrogate experiments in which only the large-scale warming signal from the reference scenario run is imposed onto the boundary conditions of the control period (1971-2000), without changing the circulation characteristics. The fifth and the sixth run, in contrast, use the boundary conditions of the scenario reference run (2071-2100) subtracted by the mean warming signal of the reference simulation, yielding a control temperature climate, but with the projected large-scale circulation pattern of the future. Analyzing this surrogate experiment suite we can disentangle large-scale thermodynamic effects (warming and moistening) and dynamical effects (changes in the large-scale circulation).

We used two different approaches to apply the warming, respectively cooling, onto our simulations. In the simpler approach we calculated the mean annual cycle of the mean warming signal at 850 hPa and applied it homogeneously over the entire atmospheric column (homogeneous warming, HW). In a more complex approach we calculated the mean annual cycle of the warming signal for every model level separately and applied a vertically dependent warming (VW). SSTs were raised by the same amount as atmospheric temperatures (HW) or by the same amount as temperatures of the lowest atmospheric level (VW). This approach resulted in the following 6 Simulations: 1. CTRL, 2. SCEN, 3. CTRL+HW, 4. CTRL+VW, 5. SCEN-HW, 6. SCEN-VW.

Figure 1 shows a schematics of the 6 experiments.

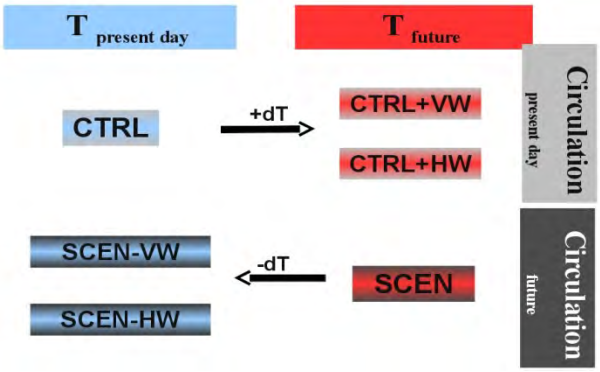


Figure 1. Experiment matrix.

3.Results and Discussion

Figure 2a shows the climate change signal due to large-scale circulation changes, i.e. (SCEN-VW)-CTRL. One can see that a considerable fraction of the north-south gradient in 2m-temperature changes (Figure 3b) originates from large-scale circulation changes. Figure 2b shows that without changes in large-scale circulation and vertical stratification the warming is expected very homogeneous over Europe. Figure 3a shows the sum of those two and figure 3b shows the full climate change signal as the difference SCEN-CTRL. Our methodology is based on the assumption that the separate surrogate experiments represent different parts of the climate change signal and should approximately sum up to the full climate change signal. a) and b) in Figure 3 show a very similar pattern, confirming that our experimental setup allows to approximately reconstruct the full climate change signal from the two surrogate experiments. Note that temperature change patterns over sea surfaces are similar by design.

4. Conclusions

The results provide some evidence that the thermodynamic and circulation effects are additive and can be distinguished with our approach. Another interesting opportunity is the comparison between the HW and VW approaches. For the HW approach the warming over the Mediterranean is much less pronounced (not shown), indicating that the change in the vertical stratification of the atmosphere is likely an important factor for the warming over the Mediterranean.

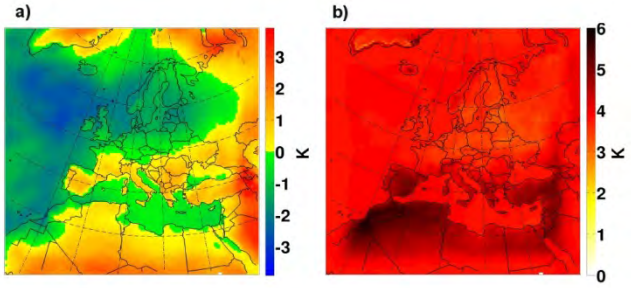
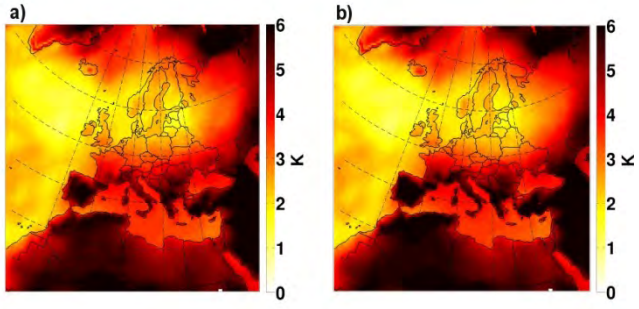


Figure 2. Shows 2m temperature [K] differences for the summer season JJA. (a) Shows a measure of the circulation effects i.e. (SCEN-VW)-CTRL, (b) shows the warming-only effect in the VW surrogate experiment, i.e. (CTRL+VW)-CTRL.

Figure 3. Shows 2m temperature [K] differences for the



summer season JJA. (a) Shows the sum of the circulation effect (Figure 2a) and the warming-only effect (Figure 2b): [(SCEN-VW)-CTRL] + [(CTRL+VW)-CTRL], (b) shows the full climate-change signal between SCEN and CTRL, i.e. (SCEN-CTRL).

References

Andrade, C., S. M. Leite, and J. A. Santos (2012) Temperature extremes in Europe: overview of their driving atmospheric patterns, NATURAL HAZARDS AND EARTH SYSTEM SCIENCES, 12, doi:10.5194/nhess-12-1671-2012., pp. 1671–1691

Fischer, E.M. and C. Schär, 2009: Future changes in daily summer temperature variability: driving processes and role for temperature extremes. Clim. Dyn., 33 (7), 917-935, DOI 10.1007/s00382-008-0473-8

Fischer, E. M., J. Rajczak, and C. Schär (2012) Changes in European summer temperature variability revisited, GEOPHYSICAL RESEARCH LETTERS , 39, doi:10.1029/2012GL052730.

Kjellstrom, E., L. Barring, D. Jacob, R. Jones, G. Lenderink and C. Schär (2007) Modelling daily temperature extremes: recent climate and future changes over Europe, CLIMATIC CHANGE, 81, 10.1007/s10584-006-9220-5, pp. 249-265

Lenderink G, A. van Ulden, B. van den Hurk, E. van Meijgaard (2007) Summertime inter-annual temperature variability in an ensemble of regional model simulations: analysis of the surface energy budget. Climate Change 81:233–247

Parey, S., D. Dacunha-Castelle, and T. T. H. Hoang (2010) Mean and variance evolutions of the hot and cold temperatures in Europe. CLIMATE DYNAMICS , 34, doi:10.1007/s00382-009-0557-0. pp. 345–359

Vidale, P. L., D. Luethi, R. Wegmann, and C. Schär, 2007: European summer climate variability in a heterogeneous multi-model ensemble. CLIMATIC CHANGE , 81, doi:10.1007/s10584-006-9218-z. pp. 209–232

Rebetez, M. and Dupont, O. and Giroud, M. (2009) An analysis of the July 2006 heatwave extent in Europe compared to the record year of 2003. THEORETICAL AND APPLIED CLIMATOLOGY, 95, doi: 10.1007/s00704-007-0370-9, pp. 1-7

Schär, C., C. Frei, D. Luthi, and H. Davies, (1996) Surrogate climate-change scenarios for regional climate models. GEOPHYSICAL RESEARCH LETTERS , 23, doi:10.1029/96GL00265. pp. 669–672

Schär, C., P. Vidale, D. Luthi, C. Frei, C. Haberli, M. Liniger, and C. Appenzeller (2004) The role of increasing temperature variability in European summer heatwaves. NATURE , 427, doi:10.1038/nature02300. pp. 332–336

Seneviratne, S. I. and R. D. Koster, Z. Guo, P. A. Dirmeyer, E. Kowalczyk, D. Lawrence, P. Liu, C-H. Lu, D. Mocko, K. W. Oleson and D. Verseghy, (2006) Soil moisture memory in AGCM simulations: Analysis of global land-atmosphere coupling experiment (GLACE) data. JOURNAL OF HYDROMETEOROLOGY, 7, doi: 10.1175/JHM533.1, pp: 1090-1112

Investigating structural dependencies between AOGCM models and their impact on regional-scale climate-change projections

Martin Leduc[1], René Laprise[1] and Ramón de Elía[1,2]

[1] ESCER Centre, Université du Québec à Montréal, Montréal, Canada (leduc@sca.uqam.ca)

[2] Ouranos Consortium, Montréal, Canada

1. Introduction

Scientists share knowledge about the climate system through literature, congresses and other types of communication. As a result, climate models are not expected to be independent from one another, and neither their climate-change projections. An important drawback from this lack of independence is that contemporary multi-model ensembles can't be analyzed using classical statistical frameworks but rather involve experts' judgment to overcome the lack of a widely accepted metric for assessing model independence (Bishop and Abramowitz, 2013).

The latter issue can be approached whether from the ''model'' or the ''output'' point of view. The former consists in investigating dependencies in model structures and parameterizations. The second approach holds to the definition of statistical independence assuming minimized error correlation (Pennell and Reichler, 2011). While the second method is more straightforward, it can't be directly applied to climate-change projection without using the debatable assumption that independent estimates of the current climate necessarily lead to independent realizations of the future climate.

In the following, we show how the structural similarities between the CMIP3 climate models may induce non-informative agreements in the resulting climate-change projections.

2. Multi-model data

We focus on small groups of Atmosphere-Ocean General Circulation Models (AOGCMs) developed by a same modelling centre within the CMIP3 multi-model ensemble. This preselection leads to a collection of 35 simulations performed by 15 models sharing different levels of structural dependencies. We consider the climate-change projections following the A1B emission scenario, for the North-American continent with seasonal averages over 20-year time periods. All model results are linearly interpolated over a common grid of 4°x5°.

3. Results

Fig. 1 provides a general view on the selected ensemble by showing the domain-averaged climate-change projections of surface air temperature for the summer season. Each colour represents a modelling centre and the line styles refer to the individual models. Each model may provide several realizations (or members) differing only by slight perturbations in the initial conditions.

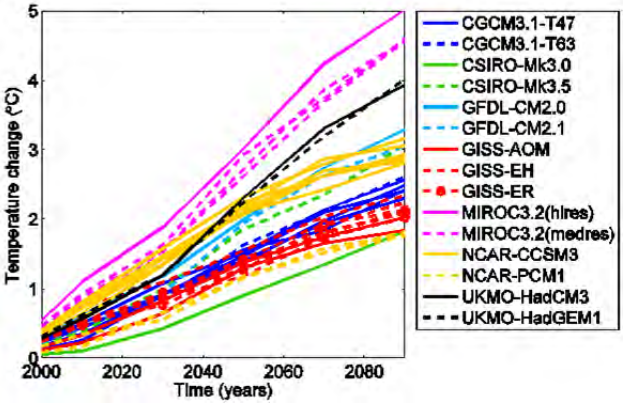


Figure 1. Domain averaged climate change projections as function of model name and centre.

AOGCMs from a same modelling centre may differ at any structural level. The CGCM (blue) and MIROC (magenta) pairs of models both differ in spatial resolution and the CSIRO (green) and GFDL (cyan) pairs consist in different versions of same models. Model versions generally differ by minor modifications in the code, for instance according to parameterizations or numerical approximations. The three GISS models (red) are characterized by higher-level structural differences: EH and ER use the same atmosphere but different ocean models, while AOM use a different atmosphere with a newer version of the ER ocean model. The NCAR and UKMO model pairs consist in seemingly independent models developed by a same institute.

It is clearly seen from Fig. 1 that models developed by nearby actors tend to agree by their climate-change projections. Striking examples are CGCM, GFDL, GISS and UKMO. Depending on the number of available members, model agreement often appears as inter-model differences falling within the magnitude of the internal variability (inter-member variance).

In order to quantify the degree of model agreement over the regional domain, the statistical significance of the differences between climate-change signals is assessed by using a measure of the internal variability as the noise level in the test. In Fig. 2 is shown the mask of the 5% significance level where red and blue areas mean positive and negative differences respectively. For GISS models differing in ocean component only (EH-ER, upper row in Fig. 2), significant differences mainly appear over the Hudson Bay. This area enlarges with time since the

models diverge from each other due to different climate sensitivities. For the GISS models differing in both their atmosphere and ocean components (AOM-EH, bottom row in Fig. 2), significant differences are again detected over the Hudson Bay with an extent over the continental region. Different signs over the Hudson Bay between the two model pairs is simply due to the order of operations.

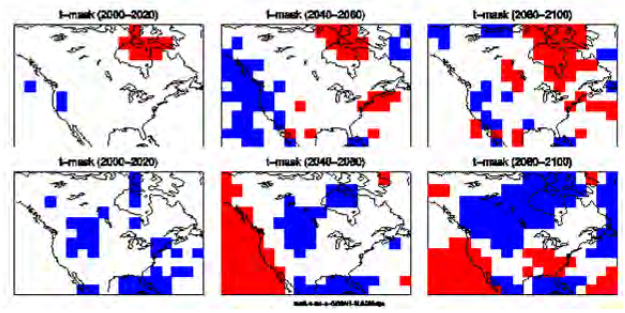


Figure 2. Mask of the statistical significance at the 5% level for climate-change differences between for pairs of GISS models: EH-ER (upper row) and AOM-EH (bottom row).

4. Conclusions

Agreements between climate models' projections are often interpreted as predictors of confidence. However, such an inference may be ill-posed when structural dependencies exist between the considered models (Pirtle et al. 2010). While studies about model independence often focus on the global domain (Knutti et al. 2013), we showed that the general message of the lack of model independence may also holds at the regional scale. Because our analysis focused on North America, conclusions might however be different for other variables and domain locations. Taking example with the GISS models, we also showed how coherency may exist between the nature of the structural changes (i.e. atmosphere or ocean) and the patterns of significance of inter-model differences between climate-change signals.

In the context of downscaling experiments where Regional Climate Models (RCMs) are used to refine coarse-resolution information from projects such as CMIP3 or CMIP5, a small fraction of these ensembles is generally considered due to limited human and computational resources. An efficient selection criteria for reducing the size of such ensembles if to consider a single realization per AOGCM model for being downscaled. While this reduces significantly the number of simulations to the number of available AOGCMs, about twenty CMIP3 models is still relatively large for the processing capability of a single modelling centre. Supplementary criteria may influence the choice of driving models such as the availability of the fields necessary for driving an RCM or potential compatibility issues between the RCM and AOGCM parameterizations and resolutions.

Our results suggest that using a single model per institute constitutes a cautious selection criterion for reducing the size of an ensemble. This technique aims at limiting potential degradation of the climatic information in the resulting ensemble by filtering model agreements that are due to model similarities rather than to the likelihood of a given climatic outcome (Leduc 2013, Leduc et al. in preparation).

References

Bishop C H, and Abramowitz G (2013). Climate model dependence and the replicate earth paradigm. Climate Dynamics, 41(3-4), pp. 885–900.

Knutti R, Masson D, and Gettelman A (2013). Climate model genealogy: Generation CMIP5 and how we got there. Geophysical Research Letters, 40(6), pp. 1194–1199.

Leduc M (2013) Characterisation of multi-model ensembles of climate-change projections regarding sampling, treatment and interpretation. PhD Thesis, Université du Québec à Montréal , 190pp.

Leduc M, Laprise R, de Elía R and Separovic L (in preparation) On the nature of non-informative agreements between the CMIP3 multi-model climate-change projections.

Pennell C, and Reichler T (2011). On the effective number of climate models. Journal of Climate, 24, pp. 2358–2367.

Pirtle Z, Meyer R, Hamilton A (2010) What does it mean when climate mod-els agree? A case for assessing independence among general circulation models. Environmental Science & Policy 13(5), pp. 351–361. DOI 10.1016/j.envsci.2010.04. 004.

Bayesian model averaging to combine surface temperatures simulated in the North America Regional Climate Change Assessment Program

Huikyo Lee[1], Amy Braverman[1], Chris Mattmann[1], Duane Waliser[1], Paul Loikith[1] and Jinwon Kim[2]

[1] Jet Propulsion Laboratory, California Institute of Technology, Pasadena, USA (huikyo.lee@jpl.nasa.gov)

[2] Joint Institute for Regional Earth System Science and Engineering, University of California, Los Angeles, USA

1. Introduction

In recent years, there have been many coordinated experiments evaluating climate models. Many models show improvement over previous versions, and this improvement could help reduce uncertainty in future climate projections. However, as more observational and model data are included in model intercomparison projects, the spread of some key variables among models becomes large. This raises important issues for combining multiple model outputs: for such ensembles to be useful for reducing uncertainty, it is necessary to account for similarity among models. As Solazzo et al. (2013) point out, many previous studies assume independence of the ensemble members, and this may compromise the validity of conclusions drawn from a simple arithmetic average of model outputs.

Bayesian Model Averaging (BMA) (Raftery et al., 2005) is a statistical approach for combining simulation results from multiple models in a way that accounts for uncertainty and dependence. BMA has been used to find the best combination of weather forecast models (e.g., Raftery et al., 2005; Wilson et al., 2007), and to evaluate globally averaged temperatures from global climate models (Min, 2006).

In this study, we apply BMA to temperatures simulated by the regional climate models (RCMs) in the North American Regional Climate Change Assessment Program (NARCCAP). The main objective of this evaluation is to obtain an ensemble whose probability distribution is similar to the observed temperature distribution. We evaluate spatially averaged temperature time series in fourteen sub-regions over the contiguous United States (Figure 1). BMA produces a time series that is the optimally weighted average of the individual model time series for each sub-region. We compare the BMA time series, individual model outputs, a simple arithmetic average of them with observational time series, using Taylor diagrams.

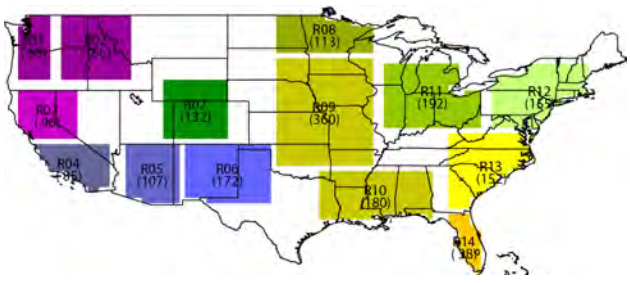


Figure 1. 14 sub-regions in the conterminous U.S. The numbers inside the parenthesis are number of grid points over the land in sub-regions.

2. Data

The observational data used in this study are monthly average temperatures from the Climate Research Unit (CRU) at University of East Anglia. RCM simulations are from the NARCCAP hindcast experiment [Mearns et al., 2012] forced by data from NCEP/DOE Reanalysis II. Here, we used 23 years of data from six models (CRCM, ECP2, HRM3, MM5I, RCM3, and WRFG) spanning the time period March 1980 and February 2003. We form four time series for each model consisting of 23 time points for each of four seasons.

3. Methodology

For a given location, BMA produces a weighted average of k model outputs for each time point, t =1, 2, …, T=23. We denote this by

$$BMA(t) = \sum_{k=1}^{K} \omega_k M_k(t), \qquad K=6,$$

where $M_k(t)$ is the t-th time point of the spatially-averaged time series from the k-th model's output for the sub-region. Let the t-th time point of the spatially-averaged observational time series for the same sub-region be denoted by $D(t)$. Further, assume that all $M_k(t)$ and $D(t)$ have been pre-processed to remove their respective time-mean values.

Following Raftery et al. (2005), we assume that differences between $M_k(t)$ and $D(t)$ are time independent. Then, the weighting factor for the k-th model's output, ω_k is the time-average of model k's relative posterior probabilities, given the observed data:

$$\omega_k = \frac{1}{T}\sum_{t=1}^{T} \frac{P(D(t)|M_k(t))}{\sum_{k=1}^{K} P(D(t)|M_k(t))},$$

where $P(D(t)|M_k(t))$ is the Gaussian probability density with model-specific mean $M_k(t)$, and model-specific variance, σ_k^2. The latter must be estimated from the full time series, $M_k(1), \cdots, M_k(T)$. In order to compute the BMA weights, we use the Expectation-Maximization (EM) algorithm (Dempster et al., 1977) to estimate the 12 unknown parameters,

$$\hat{\sigma}_1^2, \cdots \hat{\sigma}_K^2, \omega_1, \cdots \omega_K.$$

If outputs from models are independent of each other, the ω's can be viewed as metrics measuring models' performance against observations. However, in the NARCCAP hindcast experiment, the independence

assumption does not hold because the same boundary forcings are used to drive all simulations. Wilson et al. (2007) show that when two model output time series are highly correlated, BMA favors the better model and ignores the other. For example, Figure 2(a) shows two model time series (MM5I and RCM3) and the CRU observational time series for Northern California (sub-region1) in summer. The two model time series exhibit high correlation (r = 0.9), and the BMA time series derived from them (Figure 2(b)) is similar. MM5I shows slightly better agreement with the observed time series, but the BMA weighting factors for the two models are 0.9 and 0.1 respectively after more than 100 EM iterations (Figure 2(c)). The simple arithmetic average of two model time series has a standard deviation (over time) of 0.95, while the standard deviation (over time) of the BMA time series is 0.86. This is closer to the standard deviation (over time) of the observational time series (0.67), and this shows that BMA filters out redundant information among ensemble members.

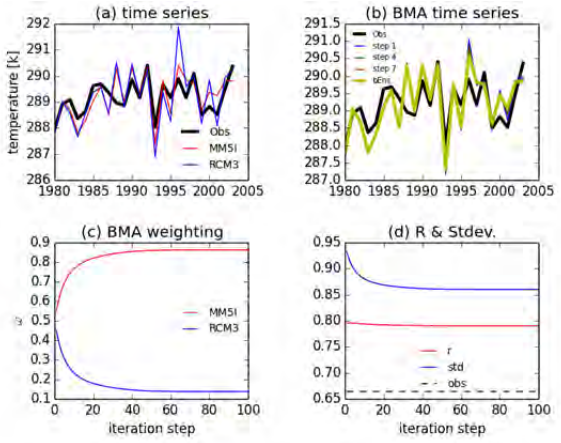


Figure 2. (a) Time series of surface air temperature from CRU 3.1 observations (black), MM5I (red) and RCM3 (blue), all averaged over sub-region1 in summer. (b) Time series of CRU 3.1 observations (black) and the BMA ensemble generated at the first (blue), fourth (green), seventh (red) and 300th (yellow) iteration of the EM algorithm. (c) BMA weighting factors for the two models versus the number of EM iterations. (d) Changes in linear correlation between BMA and observed time series (red) and the standard deviation of the BMA time series (blue) and observed time series (dotted line) as a function of EM iteration.

4. Preliminary results

We applied BMA to the time series of CRU observations and model-simulated data for six models in all 14 sub-regions, and for all four seasons. Because of the dependence among the models, their BMA weighting factors are not proportional to models' performance. However, the BMA weighting factors can be used to identify which model provide results closest to observations and to generate a future projection constrained by observations.

In Figure 3, the BMA time series (bENS) is compared with six individual models, and with their simple arithmetic average (aENS), for Arizona (sub-region5) in summer. bENS reflects information mostly from the three models (CRCM, ECP2 and WRFG) with relatively high weighting factors. The largest weighting of 0.46 is given to CRCM. The CRCM time series has the largest correlation coefficient with the CRU observational time series, and standard deviation that is closest to that of CRU. As a result, CRCM has the smallest root mean square error:

$$RMSE = \sqrt{\frac{1}{T}\sum_{t=1}^{T}(D(t) - M_k(t))^2} \ ,$$

between model and observational time series, which is proportional to the distance between the observation and CRCM in Figure 3. This indicates that BMA weighting factors are qualitatively consistent with the three metrics displayed in Taylor diagrams. In some sub-regions, the RMSE of bENS is larger than that of CRCM. In addition, bENS is almost same as the CRCM time series whose BMA weighting factor is 0.95.

Our evaluation shows that the performance of bENS is always better than aENS in every sub-region and season.

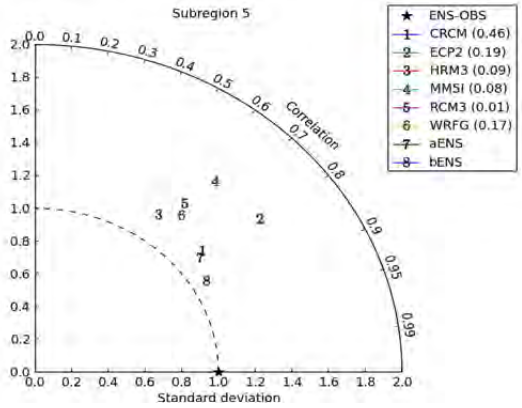


Figure 3. Taylor diagram displaying statistical comparisons of surface temperature time series between six RCMs (1-6), aENS (7) and bENS (8) with CRU 3.1 observation (star symbol). The temporal correlation coefficients and standard deviations are computed for Arizona (sub-region5) in summer. The numbers in parentheses are the BMA weighting factors.

References

Dempster, A. P., N. M. Laird, and D. B. Rubin (1997): Maximum likelihood from incomplete data via the EM algorithm, J. Roy. Stat. Soc., 39B, 1-39.

Mearns, L. O., et al. (2012), The North American Regional Climate Change Assessment Program Overview of Phase I Results, B Am Meteorol Soc, 93(9), 1337-1362.

Min, S. K. (2006), A Bayesian assessment of climate change using multimodel ensembles. Part I: Global mean surface temperature (vol 19, pg 3237, 2006), Journal of Climate, 19(16), 4134-4134.

Raftery, A. E., T. Gneiting, F. Balabdaoui, and M. Polakowski (2005), Using Bayesian model averaging to calibrate forecast ensembles, Mon Weather Rev, 133(5), 1155-1174.

Solazzo, E., A. Riccio, I. Kioutsioukis, and S. Galmarini (2013), Pauci ex tanto numero: reduce redundancy in multi-model ensembles, Atmos Chem Phys, 13(16), 8315-8333.

Wilson, L. J., S. Beauregard, A. E. Raftery, and R. Verret (2007), Calibrated surface temperature forecasts from the Canadian ensemble prediction system using Bayesian model averaging, Mon Weather Rev, 135(12), 4231-4236.

Regional Arctic Climate System Model (RASM): An overview and selected results on sea ice sensitivity to variable parameter space

Wieslaw Maslowski[1], Robert Osinski[2], Andrew Roberts[1], Jaclyn Clement Kinney[1], John Cassano[3]

[1] Naval Postgraduate School, Monterey California, USA (maslowsk@nps.edu)
[2] Institute of Oceanology, Polish Academy of Sciences, Sopot, Poland
[3] University of Colorado, Boulder, Colorado, USA

1. Introduction

The Arctic is undergoing rapid climatic change (Jeffries et al. 2013), as indicated by the retreat of the perennial sea ice, increasing surface temperatures, the retreat of spring snow extent, warming oceans, coastal erosion associated with thawing permafrost, accelerating ice-sheet outflow, increasing freshwater runoff and oceanic circulation changes. These are some of the most coordinated changes currently occurring anywhere on Earth, with arctic sea ice cover changes exceptional in at least the last 1400 years (Kinnard et al. 2011) and related surface temperature extremes unusual in at least the past 600 years (Tingley and Huybers 2013).

Reconstructions of the high north past from Global Climate and Global Earth System Models (GC/ESMs) are in broad agreement with these changes; however, the rate of change in the GC/ESM forecasts remains outpaced by observations (Stroeve et al. 2012). There are a number of reasons why models may not be able to simulate rapid change in the Arctic, including: (i) poorly resolved clouds and cloud processes impacting net surface radiation, (ii) boundary layer and bulk surface flux parameterizations, (iii) unresolved oceanic currents, eddies and tides that affect the advection of heat into and around the Arctic Ocean, (iv) crudely represented sea ice mechanics, surface snow processes, sea ice melt ponds, and surface roughness which affect ocean-ice-atmosphere surface momentum and energy transfer, and (v) poorly resolved land surface processes such as albedo effects of snow/vegetation interactions, permafrost and active layer development, the evolution of seasonal melt water lakes and wetlands, and the accumulation and melt of mountain glaciers and snow fields, all of which affect the freshwater flux to the Arctic Ocean and the energy and momentum exchange at the land-atmosphere interface. These shortcomings stem from a combination of coarse model resolution, inadequate parameterizations, unrepresented processes, and a limited knowledge of physical interactions.

2. The Regional Arctic System Model (RASM)

Regional climate models allow high spatiotemporal coverage and focus on processes typically not resolved in GC/ESMs. They are part of a model hierarchy important for improving climate predictions: from simple, 1D process-based models, to regionally constrained simulations, and ultimately to fully coupled GC/ESM codes (Knutti 2008).

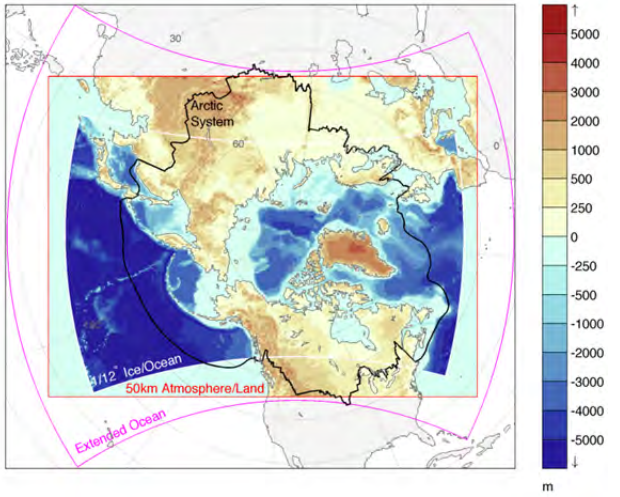


Figure 1. The RASM configuration and model topobathymetry. An extended ocean domain provides boundary surface state to WRF outside the POP/CICE domain.

Regional models have been configured for the Arctic as stand-alone limited area atmospheric models with ice-ocean boundary conditions (e.g. Cassano et al. 2011), ice-ocean models with atmospheric forcing (e.g. Maslowski et al. 2014), and fully coupled ice-ocean-atmosphere-land models (Roberts et al. 2010; Maslowski et al. 2012), in both hindcast and assimilation modes.

We use the Regional Arctic System Model (RASM), which is a limited-area, coupled ice-ocean-atmosphere-land model (Maslowski et al. 2012). It includes the Weather Research and Forecasting (WRF) atmospheric model, the Los Alamos National Laboratory (LANL) Parallel Ocean Program (POP) and Community Ice Model (CICE) and the Variable Infiltration Capacity (VIC) land hydrology model configured for the pan-Arctic region (Figure 1). The ocean and sea ice models are regionally configured versions of those used in the Community Earth System Model (CESM). A streamflow routing model (RVIC) has been developed and implemented to transport the freshwater flux from the land surface to the Arctic Ocean. These components are coupled using a regionalized version of the CESM flux coupler (CPL7).

RASM's domain (Figure 1) covers the entire Northern Hemisphere marine cryosphere, terrestrial drainage to the Arctic Ocean, and major inflow and outflow pathways, with optimal extension into the North Pacific and Atlantic oceans to account for the passage of cyclones into the Arctic. WRF's standard configuration uses a polar stereographic grid at a resolution of 50 km and 40 levels, with the finest vertical resolution in the boundary layer. WRF uses spectral nudging in the upper

half of the model atmosphere to constrain large-scale features (wavenumbers less than 4) to be similar to the driving reanalysis data. VIC shares the WRF horizontal grid. Flows generated at the grid cell level are assumed to reach a channel within each horizontal cell. These flows are routed by RVIC runoff model coupled to CPL7, delivering freshwater to POP at all coastal grid cells.

The standard POP configuration in RASM uses 45 vertical z-coordinate levels with 7 ocean layers in the upper 42 m to resolve Ekman layer dynamics. It the horizontal, a 1/12º rotated sphere mesh yields minimal area distortion near the boundaries. CICE uses the same horizontal grid as POP. It is configured with five sea-ice thickness categories plus an open water division to represent the ice thickness distribution within each grid cell. It currently uses eastic-viscous-plastic (EVP) rheology with incremental remapping for advection and between ice thickness categories for vertical growth, deformation and melt. Surface shortwave albedo is calculated using the Delta-Eddington scheme for two bands partitioned at 700nm and subsequently used by WRF to calculate dual-band net downward surface shortwave radiation. The RASM CICE implementation also includes a variable surface roughness length. CPL7 is the CESM flux coupler adapted for RASM as flux/state variable coupler and synchronization manager.

3. Selected Results

We investigate sensitivity of simulated sea ice states to scale dependence of model parameters controlling ice dynamics, thermodynamics and coupling with the atmosphere and ocean (Osinski et al. 2014). For this study we use a subset of the fully coupled Regional Arctic System Model (RASM), where the atmospheric and land components are replaced with the Common Ocean Reference Experiment database version 2 (CORE2) for 1948-2009.

To evaluate results from each ensemble we are utilizing satellite-based observations of sea ice extent and volume to compare with model results. For the former, the Scanning Multichannel Microwave Radiometer (SMMR) and Special Sensor Microwave / Imager (SSM/I) observations calculated with bootstrap algorithm are used. For the latter, data from the five fall Ice, Cloud, and land Elevation Satellite (ICESat) campaigns (Kwok et al. 2009) were employed.

This approach allows direct comparison of model results with observations and reduces computational costs. The parameters examined here include the sea ice strength, surface roughness length scale, ice-ocean drag, and oceanic mixing parameterization. Model outputs from twenty multi-decadal ensembles are compared against each other and against basin-wide estimates of sea ice extent and volume. Our results confirm that many sub-grid parameterizations of physical processes currently used in climate models are scale-dependent. We provide further details on fine-tuning required for some of them when changing model spatial resolution. We also show that while sea ice extent in many runs compares well against observations, sea ice thickness distribution is acceptable only in a few cases. Hence, we conclude that the use of observed sea ice extent only to validate the skill of sea ice models is not a sufficient model constraint.

References

Cassano, E. N., J. J. Cassano, and M. Nolan (2011), Synoptic weather pattern controls on temperature in Alaska, *J. Geophys. Res., 116*, D11108, doi:10.1029/2010JD015341.

Kinnard, C., C. M. Zdanowicz, D. A. Fisher, E. Isaksson, A. de Vernal, and L. G. Thompson (2011), Reconstructed changes in Arctic sea ice over the past 1,450 years, *Nature*, *479*(7374), doi:10.1038/nature10581.

Knutti, R. (2008), Should we believe model predictions of future climate change?, *Philos. Trans. R. Soc. A Math. Phys. Eng. Sci.*, *366*(1885), doi:10.1098/rsta.2008.0169.

Jeffries, M. O., J. A. Richter-Menge, and J. E. Overland, Eds. (2013), Arctic Report Card 2013, http://www.arctic.noaa.gov/reportcard.

Kwok, R., G. F. Cunningham, M. Wensnahan, I. Rigor, H. J. Zwally, and D. Yi (2009), Thinning and volume loss of the Arctic Ocean sea ice cover: 2003–2008, *J. Geophys. Res.*, *114*(C7).

Maslowski W., J. Clement Kinney, M. Higgins, and A. Roberts (2012), The future of arctic sea ice, *Ann. Rev. of Earth and Plane. Sci.*, *40*, 625-654.

Maslowski, W., J. Clement Kinney, S. Okkonen, R. Osinski, A. Roberts, and W. Williams (2014), The Large Scale Ocean Circulation and Physical Processes Controlling Pacific-Arctic Interaction, in *The Pacific Arctic Region: Ecosystem Status and Trends in A Rapidly Changing Environment*, eds. J. Grebmeier and W. Maslowski, Springer, in press.

Osinski R., W. Maslowski, A. Roberts, J. Clement Kinney, and A. Craig (2014), On the sensitivity of sea ice states to variable parameter space in the Regional Arctic System Model (RASM), Ann. Glaciol., submitted.

Roberts, A. et al. (2010), A Science Plan for Regional Arctic System Modeling, A report to the National Science Foundation from the International Arctic Science Community, *International Arctic Research Center Technical Papers 10-0001*. University of Alaska Fairbanks, 47pp.

Stroeve, J. C., V. Kattsov, A. Barrett, M. Serreze, T. Pavlova, M. Holland, and W. N. Meier (2012), Trends in Arctic sea ice extent from CMIP5, CMIP3 and observations, *Geophys. Res. Lett.*, *39*(16), doi:10.1029/2012GL052676.

Tingley, M. P., and P. Huybers (2013), Recent temperature extremes at high northern latitudes unprecedented in the past 600 years, *Nature*, *496*(7444), doi:10.1038/nature11969.

Regional climate modeling of Arctic temperature extremes and their variability

Heidrun Matthes[1], Annette Rinke[1], Torben Königk[2], John Scinocca[3], Ralf Döscher[2], Klaus Dethloff[1]

[1] AWI, Alfred Wegener Institute Helmholtz Centre for Polar and Marine Research, Potsdam, Germany (Annette.Rinke@awi.de)
[2] SMHI, Rossby Center, Norrköpping, Sweden
[3] CCCma, Canadian Centre for Climate Modelling and Analysis, University of Victoria, Victoria, Canada

1. Motivation

The Arctic has widely been accepted as a region of high climate variability as well as high sensitivity to climate change. Changes in climate extremes present an important aspect of global warming and are of particular importance, as they directly impact the society and people in the affected regions. Within the scope of the WCRP CORDEX program, various regional climate models were applied over the Arctic, using a common domain (roughly everywhere north of 65 degrees North) and the same horizontal resolution (approximately 50 km). In a first step, the models are used for downscaling the ERA-Interim reanalysis data from 1979-2012, to allow an initial intercomparison of the models as well as an evaluation with reanalysis and observational data. Additionally, an intercomparison of different models offers the possibility to highlight regions of high (or low) model uncertainties.

2. Analysis

We analyzed the available model output (from HIRHAM5, RCA4, CanRCM4) concerning temperature extremes and their variability, using climate extreme indices. We calculate intra-seasonal extreme temperature range (ETR) as a first measure of temperature variability, warm and cold spell days (WSDI, CSDI) as a measure for lasting warm and cold periods, and growing degree days (GDD) as a measure for potential plant growth. We present an evaluation of the RCM derived indices with the forcing ERA-Interim data for spatial comparison and with observational station data from the NCDC dataset Global Summary of the Day in the form of time series (averaged over Arctic sub-regions). The focus of our analysis is on the models' ability to reproduce the mean values of the temperature extreme indices, but also on its temporal evolution and decadal variability.

3. Results

For ETR, we find that both reanalysis data and observations show no significant trends (exception: spring over Eastern Russia), a development which is well reproduced by almost all models. However, the model performance depends on the considered region and specific indices. For example, the comparison with station data over the Canadian Arctic shows that CanRCM4 and RCA4 fit the station data for ETR better than HIRHAM5 and the reanalysis, while for CSDI, the opposite is true. Generally, the spatial patterns of ETR and CSDI are well captured by the analyzed models. For GDD, trends and their significance depend on the region and season. While in the western Arctic, trends are mostly positive and not significant, the eastern Arctic shows significant positive trends. The models seem to capture the temporal development of GDD well, however an offset from the station data can frequently be found, especially over the western Arctic. WSDI show non-significant trends over all seasons and regions (except, again, eastern Russia in spring). The associated model biases show no clear season and region dependent behavior.

In general, we find that the model performance is highly dependent on the geographical region and analyzed season, for both temperature extreme indices means as well as their variability.

Strategic sub-selection of CMIP5 GCMs for dynamical downscaling

Carol McSweeney[1] and Richard Jones[1,2]

[1] Met Office Hadley Centre, Exeter, UK (carol.mcsweeney@metoffice.gov.uk)
[2] School of Geography and Environment, Oxford University, UK

1. The resource requirements of dynamical downscaling mean that most regional modelling groups will have to select sub-sets of Global Climate Models (GCMs) for downscaling in order to design manageable experiments.

The unprecedented availability of 6-hourly data from GCMs made available via the fifth coupled model inter-comparison project (CMIP5) for use in regional climate modelling experiments creates a wealth of opportunities to develop high-resolution downscaled climate projections relevant to detailed assessment of climate vulnerability and climate change impacts. High-resolution climate projections can now be derived from the same set of models that are used to characterise the range of future climate changes within Intergovernmental Panel on Climate Change (IPCC) assessment reports, allowing consistency between headline information on global and large-scale regional climate change and detailed downscaled climate change projections. Here we explore how those using Regional Climate Models (RCMs) to downscale CMIP5 projections might select from the GCMs available in order to design efficient and manageable experiments that sample GCM uncertainty effectively.

2. We propose a strategy for sub-selecting GCMS from the CMIP5 ensemble

The strategy that we demonstrate for sub-selecting GCMs from the CMIP5 ensemble identifies 8-10 models that are most suitable across three continental scale regions – Europe, Africa and Southeast Asia. The selection process (a) avoids the inclusion of the least realistic models for each region and (b) simultaneously captures the maximum possible range of changes in surface temperature and precipitation for the three regions. This methodology is described fully in McSweeney et al (*Submitted*).

3. The model performance criteria used include the assessment of key large-scale climatological features

These include key features of circulation (e.g. the southwest and northeast monsoon circulations for southeast Asia), annual cycles of mean precipitation and temperature for sub-regions within each region and indices describing inter-annual variability where available (e.g. indices relating to representation of African teleconnections described in Rowell, 2013).

We find that, of the GCMs with 6-hourly fields available, there are several which simulate the key aspects of regional circulation so poorly that we consider the projections from those models 'implausible', and choose to exclude these from our subset. A number of other models are found to have 'biases' or 'significant biases' – we exclude these models only if another model with better performance has future projections with similar characteristics.

4. We identify the optimal subset of models from those that have not been excluded

From the remaining models, we demonstrate a method for identifying the sub-set that optimally samples the range of changes in mean temperature and precipitation for the different seasons and regions.

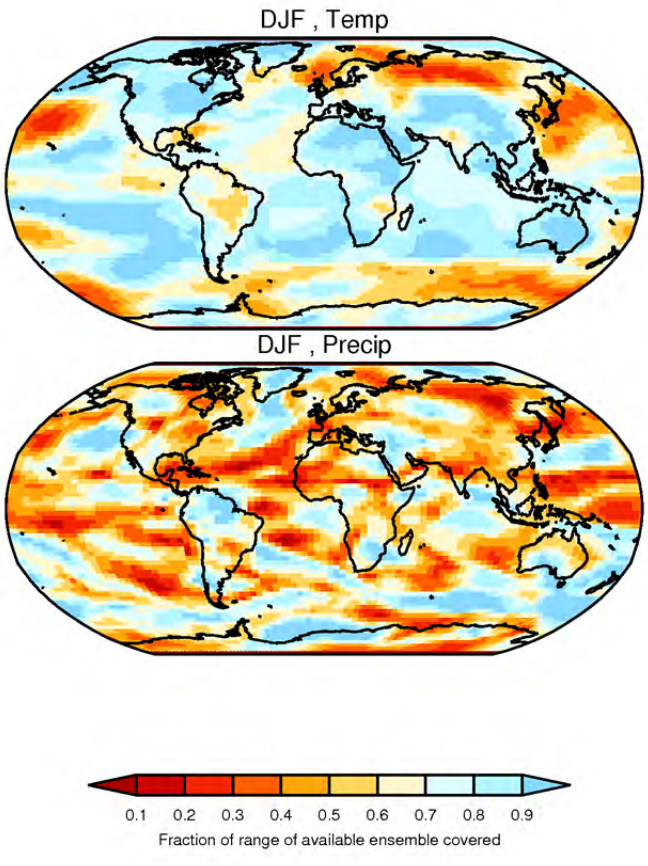


Figure 1. How well does a set of 5 from 38 CMIP5 GCMs , which have not been strategically selected, span the range of changes in future projections in DJF (a) mean temperature (Top) and (b) mean precipitation (bottom)?

5. Representative sampling of future projections in a sub-set of models has significant implications for the interpretation of uncertainty

There are many situations when users of future climate information may only have available to them a restricted sub-set of the CMIP5 projections which may not have been selected strategically (for example, where regional climate modelling groups have downscaled GCMs for which data were first available from CMIP5). We explore the implications of using an 'ad-hoc' subset by exploring how well randomly sampled sets of *n* models from CMIP5 can be expected to sample GCM uncertainties (see Fig 1.).

References

McSweeney C.F., Jones, R.G., Lee, R.W. and Rowell, D.P. (*Submitted*). Sub-selecting CMIP5 GCMs for downscaling over multiple regions. Submitted to Climate Dynamics.

Rowell, D.P. (2013) Simulating SST Teleconnections to Africa: What is the State of the Art?, Journal of Climate, 26, pp.5397-5417.

Establishing the value of multiple GCM-RCM simulation programs

L. O. Mearns[1], F. Dominguez[2], W. Gutowski[3], D. Hammerling[1], D. Lettenmaier[4], R. Leung[5], S. Michaels[6], S. Pryor[7], S. Sain[1]

[1] National Center for Atmospheric Research
[2] U. Arizona
[3] Iowa State U.
[4] U. Washington
[5] Pacific Northwest National Labs
[6] U. Nebraska
[7] Indiana U.

1. Introduction

There have been a number of multiple GCM-RCM programs, covering Europe, North America, and now, through CORDEX, most regions of the world. Standard metrics of success for these programs include number of publications, number of users of the data, and number of citations to the program. However, these metrics do not necessarily reflect the scientific value of the program, for example, what new scientific knowledge has been developed. Partially motivated by an effort to encourage greater interest within US funding agencies to support a North American CORDEX program, we began to carefully consider how one does establish the scientific value of such programs. We thought that establishing the scientific value of NARCCAP would be a good way to examine this issue. We present in this paper our thinking so far on this issue and demonstrate how we are proceeding. We hope that our analysis will prove useful for explicitly establishing the value of such programs throughout the world.

2. Basics of NARCCAP

The North American Regional Climate Change Assessment Program (NARCCAP) was developed to: 1) explore and characterize the uncertainties regarding future climate based on combinations of global and regional climate model simulations, and 2) provide to the climate impact and adaptation communities relatively high-resolution (50 km) climate change scenarios (for numerous variables) with sub-daily (3 hourly) output frequency for use in assessing the impacts of climate change (Mearns et al., 2009). Four different global climate models (GCMs) (from the CMIP3 set of simulations) provided boundary conditions for six different regional climate models (RCMs) using a particular matrix sampling design (balanced fractional factorial) for 30 years of a current period (1971-2000) and 30 years of the future (2041-2070) using the SRES A2 emissions scenario. In addition, 30 years of simulation with each RCM was produced using boundary conditions from the NCEP R2 reanalysis. In all, 11 different sets of current and future climate scenarios were produced, covering nearly half the 4 X 6 matrix. A large volume of data was produced and made available to the larger climate research community (~ 40 TB).

3. How to Assess a Scientific Program

Perhaps the most direct indication of a program's value is whether the goals set out for the program have been met. In the case of NARCCAP, this is relatively straightforward. We can point to the research papers published that quantify the uncertainty based on the global and regional climate simulations (e.g., Mearns et al., 2013), and we can point to the number of data users and the number of papers published by the impacts community using the NARCCAP data. There is also any number of more general quantitative metrics available for evaluating a scientific program. Some of the simpler ones include: number of journal articles produced that used the generated data sets (for NARCCAP, about 110 articles and reports), citations of the program (960 citations), and number of users registered on the program web site (over 1,000). While these are all useful indicators of value, we are interested in probing more deeply to determine what new climate and impacts science has been generated through this program. Of particular interest is to determine what we have learned about future climate projections and their impacts based on the use of higher resolution dynamically generated future climate information. Of course to do this one must evaluate all the material published using NARCCAP data, a non-trivial task.

4. Article/Report Typologies

We divided the publications into different groups based on fairly standard categories in climate and climate change research, and in relation to the number of articles in each group: climate analysis (including validation and projections of future climate); precipitation extremes (on various time scales), statistical methods (use of the extensive NARCCAP dataset to develop statistical methods using multi-model simulations), impacts (using NARCCAP output to determine the effect of climate change on various resource systems); and other (including educational value – masters' theses and dissertations, and use of NARCCAP as a test bed for developing evaluation systems or tools).

5. Evidence of Scientific Value

One of the most important issues regarding regional modeing is establishing that the simulations produce added value. This is critical in terms of establishing the value of regional climate modeling experiments for providing additional insight into likely climate changes and also thus in establishing the value of using these results for projecting impacts of climate change and the value of running regional climate models for projecting climate change. We reviewed the relevant papers that focuses explicitly on the issue of added value. Two papers (Di Luca et al., (2012, 2013)) explored the potential added value (PAV) of the NARCCAP simulations. Their approach defines PAV based on the prospects of adding spatial details over what can be resolved by GCMs, with the latter estimated by aggregating the RCM simulations to the coarse scales of the GCMs. They found that PAV is stronger at short temporal scales and in the warm season. Furthermore, PAV is mostly associated with the RCM stationary and transient response to stationary forcing, particularly related to orography, and spatial variability related to weather disturbances, which are stronger in winter and the high latitudes. Elguindi and Grundstein (2010) used a revised Thornthwaite climate classification to evaluate the NARCCAP RCM and GCM simulations compared to climate types derived from observations based on the same method. They found significant added value by RCMs over GCMs in topographically diverse regions. More specifically, RCMs produced climate types closer to those derived from observations and the spatial gradients of the climate types are more realistic than that of the GCMs over mountainous areas.

Another common type of analysis performed with RCM simulations is of extreme precipitation events. An important motivation for the precipitation extremes analysis is engineering and water resources impacts, so precipitation analyses most often focus on intensity-duration-frequency curves or return periods of extreme events. Partly for this reason, analyses typically look at subregions of the NARCCAP domain, such as specific watersheds, or just a few selected locations. In general the models better reproduce extremes than do the NCEP Reanalys or the driving GCMs. This has been domnstrated in a number of studies. A few analyses also evaluate the underlying physical processes leading to extreme precipitation. The models often show more consistency with observations of features leading to extremes, such as synoptic circulation and atmospheric rivers, than for the extreme precipitation itself, highlighting the strengths of the models to capture regional circulation features well. As is common with the GCMs, the projections of the RCMs show intensification but with important spread across members of the ensemble.

The availability of the NARCCAP data set has motivated a number of new statistical approaches to analyzing the model results. At least 20 different statistical methods papers have been produced as of this date. Topics include new methods for combining model output across the ensemble (e.g., Christensen and Sain, (2012)) and new methods in extreme value theory (e.g., Cooley and Sain, 2010).

Research regarding impacts of climate change using NARCCAP output covers numerous areas: hydrology/water resrouces, human health, forest fires, ecosystems, and agriculture. Common reasons given for using NARCCAP include the higher spatial resolution, the availability of a wide range of variables (not just temperature and precipitation), and the high temporal frequency of the data. The high-resolution argument obviously relies on the notion that the RCM results are more credible than those of the driving GCMs, and this harkens back to the importance of establishing added value. While some of the results of the impacts articles do not break new ground per se, the availability of the high frequncy data makes certain impacts calculations possible that hitherto were not.

The NARCCAP results were widely used in the recently released US National Climate Assessment. The dataset was one of the three sources of material used for information about future climate change in the report.

6. Discussion

It is not a simple task to demonstrate the scientific value of this kind of scientific program beyond the usual quantitative metrics. To date we have demonstrated particular added scientific value in a number of arenas, particularly climate science, statistics, and impacts.

References

Christensen, W.F. and Sain, S.R. (2012) Spatial latent variable modeling for integrating output from multiple climate models Mathematical Geosciences, 44, 395-410.

Cooley, D. and S. Sain (2010) Spatial hierarchical modeling of precipitation extremes from a regional climate model, J. of Agric., Biol., and Environ. Statistics, 15, 381-402.

Di Luca, A. et al. (2012) Potential for added value in pre cipitation simulated by high-resolutuion nested Regional Climate Models and observations. Clim. Dyn. 38, 1229.

DiLuca, A. et al. (2013) Potential for added value in present temperature simulated by high-resolution nested RCMs in climate and in the climate change signal. Clim. Dyn. 40, 443.

Elguindi, N. and A. Grudnstein (2013) An integrated approach to assessing 21st century climate change over the continguous US using the NARCCAP RCM output. Climatic Change 117, 809-827.

Mearns, L. O., W. J. Gutowski, R. Jones, et al. (2009) A regional climate change assessment program for North America. EOS 90, 311-312.

Mearns, L. O., S. Sain, R. Leung, M. Bukovsky, et al. (2013) Climate change projections of the North American Regional Climate Change Assessment Program (NARCCAP). Climatic Change Letters DOI 10.1007/s10584-013-0831-3.

Selecting climate simulations for impact studies based on multivariate patterns of climate change

Thomas Mendlik and Andreas Gobiet

Wegener Center for Climate and Global Change, University of Graz, Austria (thomas.mendlik@uni-graz.at)

1. Introduction

Climate scenarios generated with general circulation models (GCMs), often refined with regional climate models (RCMs) and empirical-statistical post-processing methods (e.g., Maraun et al., 2010) are often used as basis for investigating the impacts of climate change on society and ecosystemys. The selection of climate simulations as input for the impact investigation is mostly based on subjective expert judgment. However, a more sophisticated objective approach should consider the fact that these climate simulations stem from an ensemble lacking a proper expermintal design, which might lead to model inter-dependencies and an underestimation of the model spread. It is just until recently that such objective methods for selecting climate simulations received attention in scientific literature (e.g. Evans et al. (2013)).
Here we present a framework to aid users selecting climate simulations for their impact studies by accounting for their similarity structure. The method is illustrated using RCMs from the ENSEMBLES project for spatial and seasonal changes of 5 meteorological parameters.

2. Methods

The method for model selection is set-up in two steps. First, a principal component analysis is applied to identify common spatial patterns of climate change for meteorological variables of interest. Second, based on these climate change patterns, a similarity measure is defined using cluster analysis, resulting in a tree-like structure as depicted in Figure 1. It allows the user to partition the ensemble into groups of relatively similar simulations and to select representative models out of each cluster.

3. Results and Conclusions

The most dominant common regional patterns of climate change In the ENSEMBLES dataset are twofold: A temperature increase over the European continent and an increase of humidity as well as precipitation with a decrease of global radiation mainly in the northern and eastern parts of Europe.

We identify 5 groups of RCMs with similar behavior, which is mainly determined by the choice of the driving GCM. This means, regarding the common patterns of climate change until mid-century, the driving GCMs have a bigger influence on the uncertainty spread than the choice and parametrization of RCMs.

The proposed method generalizes the approach to select simulations by exploring the model spread for parameters as temperature and precipitation (IPCC-TGICA (2007)) in two ways. First, by extending the amount of parameters to a multivariate spatial setting for impact-relevant climate indicators. Second, by accounting for the similarity structure of the models, which allows to select representative simulations from the ensemble. This leads to a more independent sub-sample while conserving the main climate change characteristics of the original ensemble.

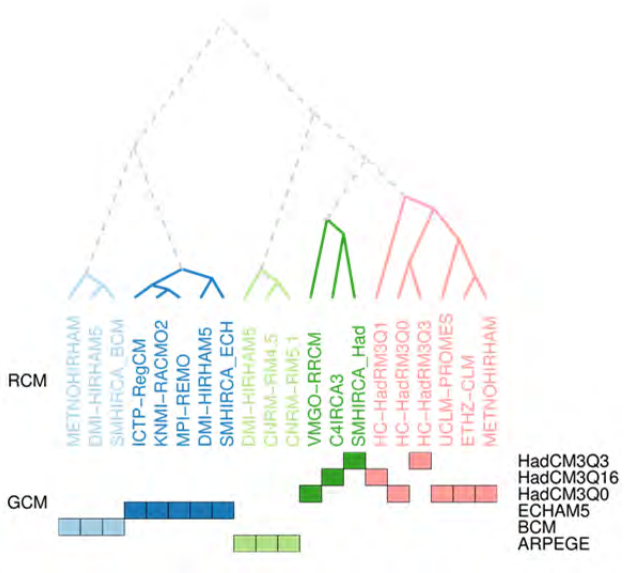


Figure 1. Similarity of RCMs (ENSEMBLES) based on their climate change patterns from 1971-2000 to 2021-2050 over several subregions of the European continent.

References

Evans JP, Ji F, Abramowitz G, Ekström M (2013) Optimally choosing small ensemble members to produce robust climate simulations, Environmental Research Letters, Vol. 8, No. 4, pp. 044-050

IPCC-TGICA (2007) General guidelines on the use of scenario data for climate impact and adaptation assessment. Version 2,. Tech. Rep.

Maraun D, Wetterhall F, Ireson AM, Chandler R, Kendon E, Widmann M, Brienen S, Rust H, Sauter T, Themeßl MJ et al (2010) Precipitation downscaling under climate change: recent developments to bridge the gap between dynamical models and the end user, Rev Geophys, Vol. 48, No. 3, pp. 1–34

Energy cycle associated with Inter-member Variability in a large ensemble of simulations of the Canadian RCM (CRCM5)

Oumarou Nikiéma and René Laprise

ESCER Centre, Earth and Atmospheric Sciences Dept., UQAM, Montréal (Québec) Canada (nikiema.oumarou@sca.uqam.ca)

1. Introduction – Inter-member Variability

In an ensemble of high-resolution Regional Climate Model (RCM) simulations where different members are initialised at different times, the individual members provide different, but equally acceptable, weather sequences. In others words, RCM simulations exibit a kind of uncertainty called Internal Variability (or Inter-member Variability, IV), defined as the inter-member spread between members of the ensemble of simulations.

Previous studies showed that the RCM's IV greatly fluctuates in time, with episodes of large growth associated with strong synoptic events in the simulations, as mentioned by Alexandru et al. (2007). Nikiéma and Laprise (2011, 2012) showed that IV has physical interpretation, and is not associated with a numerical artefact due to the nesting technique (for instance). Nikiéma and Laprise (2013, hereafter referred to as NL13) proposed a formulation of an energy cycle for IV. In this paper, we present an analysis of some results of IV energy cycle based on a large ensemble of simulations run with the Canadian RCM (version 5).

The paper is structured as follows. Section 2 recapitulates briefly the IV energy cycle, and results are presented in Section 3. The main conclusions are summarized in Section 4.

2. Inter-member variability energy cycle

Expanding upon previous studies on global atmospheric energetics of pioneered by Lorenz (1955, 1967), Pearce (1978) and Marquet (1991) established a formulation of an energy cycle that is applicable to study weather systems over limited-area domains. NL13 applied similar approach to IV energy cycle. Noting by n the simulation index in an ensemble of N members, each atmospheric variable $\Psi_n \in \{T_n, u_n, v_n, \omega_n, \Phi_n, \ldots\}$ can be split in two components: an ensemble-mean (EM) part $\langle\Psi\rangle$ and deviation thereof Ψ':

$$\Psi = \langle\Psi\rangle + \Psi' \tag{1}$$

where the EM is calculated as:

$$\langle\Psi\rangle = \frac{1}{N}\sum_{n=1}^{N}\Psi$$

Note that the index *n* is left out without ambiguity. The IV is estimated as the EM of the deviation square:

$$\sigma_\Psi^2 \approx \frac{1}{N}\sum_{n=1}^{N}\Psi'^2 \equiv \langle\Psi'^2\rangle \tag{2}$$

The quadratic form of the kinetic energy (*K*) leads to decompose the mean K in two components as:

$$\langle K\rangle = K_{EM} + K_{IV} \tag{3}$$

where $K_{EM} = \langle\vec{V}\rangle\cdot\langle\vec{V}\rangle/2$ and $K_{IV} = \langle\vec{V}'\cdot\vec{V}'\rangle/2$ are the kinetic energy of the EM wind and the EM kinetic energy of the deviation winds, respectively. Similarly, the mean available enthapy *A* is decomposed, as

$$\langle A\rangle = A_{EM} + A_{IV} \tag{4}$$

where $A_{EM} = \frac{C_p}{2T_r}\langle T - T_r\rangle^2$ and $A_{IV} = \frac{C_p}{2T_r}\langle T'^2\rangle$; T_r is a constant reference temperature.

From the basic field equations, prognostic equations have been established for A_{IV}, K_{IV}, A_{EM} and K_{EM}. For instance, the A_{IV} equation is written as follows:

$$L_{A_{IV}} = R_{A_{IV}} = G_{IV} + C_A - C_{IV} - F_{A_{IV}} - H_{A_{IV}} \tag{5}$$

where $L_{A_{IV}} = \partial A_{IV}/\partial t$ and $R_{A_{IV}}$ is the sum of all contributions to the A_{IV} tendency.

Figure 1 shows schematically the IV energy cycle for an ensemble of RCM simulations. It is composed of five reservoirs linked together with energy conversion terms (*C* and *I*). The external reservoir (*B*) linked to A_{EM} is due to the fact that mass is not constant over limited-area domain. The *G* term act as generation term for A_{EM} and A_{IV}, whereas kinetic energy is destroyed by dissipation term *D*. Because the energy cycle is computed locally over a regional domain, additional terms *F* and *H* are present, representing boundary fluxes; they would vanish upon integration over the entire globe.

This energy cycle can be extended to a further decomposition in horizontal average on pressure surfaces and deviation thereof. In this case, the IV energy cycle takes another shape with additional reservoirs and conversion terms (see NL13).

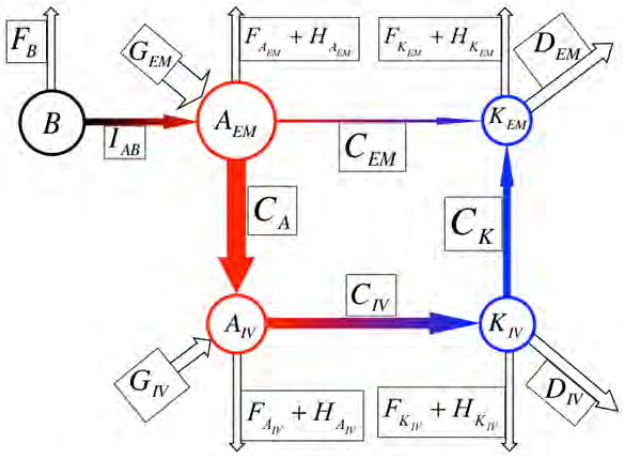


Figure 1. Inter-member variability energy cycle (NL13).

3. Inter-member variability energy cycle in a large ensemble of simulations of the CRCM5

This study uses a 50-member ensemble of simulations carried out on a 260 by 160 grid-point computational domain, with a grid mesh of 0.3°. The study domain covers eastern North America and part of the Atlantic Ocean. All the simulations use the same Lateral Boundary Conditions (LBC) for atmospheric fields from Era-Interim, and prescribed sea-surface temperature (SST) and sea-ice coverage. The only difference between simulations is the initial time to start the MRCC5. Each member starts at 0000 UTC on different days from October 12th 2004 to November 30th 2004. Thus, fifty simulations were run for one year, and they were archived at 3 h intervals, from December 1st 2004 to December 1st 2005.

Before going further, we verified that the budget closes, by comparing for example the terms $L_{A_{IV}}$ and $R_{A_{IV}}$ in Eq. 5. We verified that the sum of incoming arrows for each IV energy reservoir corresponds (approximately) to the sum of outgoing arrows, on average. For each prognostic equation, results denote fairly good agreement between L and R terms, with correlations coefficient up to 0.95.

Figure 2 shows the maps of different contributions to IV available enthalpy (A_{iv}) and kinetic energy (K_{iv}). We notice that K_{iv} is around 5 times A_{iv}, which we believe is reasonable considering the thermal-wind relationship. We note that individual contributions tend to act systematically as either a positive or a negative contribution to IV energies. The same findings are noted for the other seasons (results not shown). The terms C_A and C_K have positive contributions to A_{IV} and K_{IV} tendencies, respectively, corresponding to energy transfers from EM to IV. Due to diabatic processes such as condensation, convection and radiation, G_{iv} also acts to increase A_{iv}. The C_{iv} pattern shows that the available enthalpy is lost at the expense of IV kinetic energy. As in weather systems, IV kinetic energy is lost through dissipation processes in term D_{iv}.

For both A_{IV} and K_{IV}, the F terms act as sink terms, transporting IV energy out of the regional domain by the EM flow. The term H_{Kiv} also contributes to decreasing K_{IV} because of the divergence of the covariance of geopotential and horizontal wind fluctuations (see the formulation of H_{Kiv} in NL13). At the seasonal time scale, the third-order term H_{Aiv} is negligible in the A_{iv} budget.

4. Conclusion

In a 50-member ensemble that differ only in their initial conditions, we evaluated the various energy reservoirs of IV and exchange terms between reservoirs in one-year (2005) simulations performed with the fifth-generation Canadian RCM (CRCM5) over an eastern North American domain. Results show a remarkably close parallel between the energy conversions associated with IV in ensemble simulations and the energy conversions in weather systems. Indeed, the energy conversions associated to IV perturbations appear to behave similar fashion to those of transient-eddy energy [e.g., Lorenz 1955, 1967], with fluctuations of available enthalpy being generated by some physical processes, and this energy being converted to fluctuation kinetic energy. Our results indicate that RCM's IV is a natural phenomenon arising from the chaotic nature of the atmosphere.

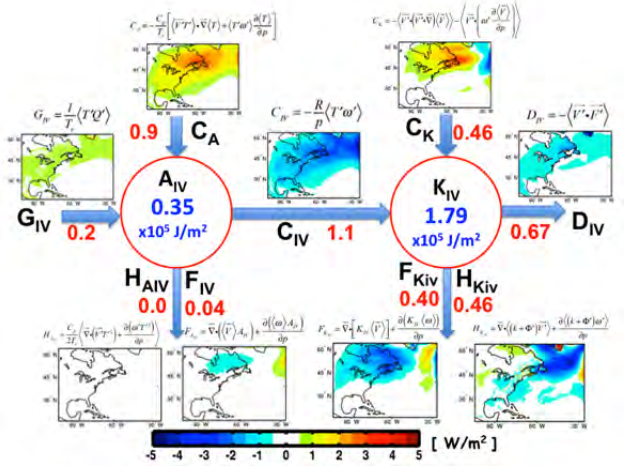


Figure 2. Maps of contributions to IV available enthalpy (A_{iv}) and kinetic energy (K_{iv}) computed in 50-member simulations for summer 2005. Values in red colour indicate the domain-averaged for various fluxes (in W/m^2). See NL13 for the mathematic formulations of the various terms.

References

Alexandru A, de Elía R, Laprise R (2007) Internal Variability in regional climate downscaling at the seasonal scale. Mon Weather Rev 135, pp. 3221-3238.

Lorenz E N (1955) Available potential energy and the maintenance of the general circulation. Tellus 7, pp. 157–167.

Lorenz E N (1967) The nature and theory of the general circulation of the atmosphere. World Meteorological Org. 218 TP 115, 161 pp.

Marquet P (1991) On the concept of exergy and available enthalpy: Application to atmospheric energetics. Q J R Meteorol Soc, 117, pp. 449–475

Nikiéma O, Laprise R (2011) Budget study of the internal variability in ensemble simulations of the Canadian RCM at the seasonal scale. J Geophysical Res, 116(D16112), 18 pp., doi:10.1029/2011JD015841.

Nikiéma O, Laprise R (2012) Diagnostic budget study of the internal variability in ensemble simulation of Canadian Regional Climate Model. Clim Dyn, DOI:10.1007/s00382-010-0834-y.

Nikiéma O, Laprise R (2013) An approximate energy cycle for inter-member variability in ensemble simulations of a regional climate model. Clim Dyn, 22 pp., doi:10.1007/s00382-012-1575-x.

Pearce RP (1978) On the concept of available potential energy. Q J R Meteorol Soc 104, pp. 737–755.

Precipitation in the EURO-CORDEX 0.11° and 0.44 simulations: High resolution, High benefits?

A. F. Prein[1], A. Gobiet[1], H. Truhetz[1], K. Keuler[2], K. Görgen[3], C. Teichmann[4], C. Fox Maule[5], E. Van Meijgaard[6], M. Déqué[7], G. Nikulin[8], R. Vautard[9], E. Kjellström[8], A. Colette[10]

[1] Wegener Center for Climate and Global Change (WEGC), University of Graz, Austria (andreas.prein@uni-graz.at)

[2] Brandenburg University of Technology (BTU), Germany

[3] Institute for Advanced Simulation (IAS), Jülich Supercomputing Centre (JSC), Germany

[4] Max-Planck-Institut for Meteorology (MPI), Hamburg, Germany

[5] Danish Climate Centre (DKC) Danish Meteorological Institute, Copenhagen, Denmark

[6] Royal Netherlands Meteorological Institute (KNMI), De Bilt, Netherlands

[7] Météo-France/CNRM, CNRS/GAME, Toulouse, France

[8] Swedish Meteorological and Hydrological Institute (SMHI), Norrköping, Sweden

[9] Institut Pierre-Simon Laplace (IPSL), CEA-Orme des Merisiers, France

[10] French National Instiute for Industrial Environment and Risks (INERIS), Toulouse, France

1. Introduction

Precipitation is a key variable in the climate system and influences most ecosystems, agriculture, hydro-electric power production, or drinking water supply. However, simulating precipitation with climate models is challenging because precipitation patterns and intensities are influenced by processes on various scales (synoptic to micro-scale) and are highly variable in space and time. Additionally, parameterizations like microphysics and deep convection can introduce large errors to simulated precipitation (e.g., Molinari and Dudek 1993, Liu et al. 2011). Increasing the horizontal grid-spacing of climate models is expected to improve simulated precipitation, because orography and other land surface characteristics become more realistic and small-scale dynamical processes are better resolved (e.g., Chan et al. 2013). It is expected that especially simulated extreme precipitation is improved because of its small scale nature.

The European branch of the COordinated Regional climate Downscaling Experiment (CORDEX) called EURO-CORDEX (Jacob et al. 2013) is the first initiative where multiple regional climate models are used to simulate transient climate change with 0.11° horizontal grid-spacing for an entire European continent. In this study we investigate, if the 0.11° (12,5 km grid spacing) hindcast simulations are able to add value to simulated extreme and mean precipitation compared to their 0.44° (50 km grid spacing) counterpart simulations.

2. Data and Methods

Daily precipitation from 8 climate models from the EURO-CORDEX ensemble is investigated. With each model one pair (0.11°/0.44° grid-spacing) of ERA-Interim driven simulations is performed within the period 1989 to 2008. The simulated precipitation is compared to high resolution gridded regional observations in Spain, the Alps, Germany, Sweden, and Norway (grid-spacings smaller or equal to 0.11°). The analyses where carried out on two different spatial scales: on the grid of the coarser 0.44° simulations and on the grid of the high resolution 0.11° simulations. All statistics where performed for mean and extreme precipitation (events above the 97.5 percentile).

3. Results

No or only small added value can be found in seasonal mean and extreme precipitation biases of regionally averaged precipitation. Generally, the 0.11° simulations tend to produce more precipitation than the 0.44° runs in all regions and seasons.

Comparing biases on a 0.44° grid-cell basis, however, reveals that for many areas the 0.11° simulations decrease biases consistently meaning that more than 6 out of the 8 0.11° simulations have smaller biases than their 0.44° counterparts. Figure 1a depicts consistently improved (red) and deteriorated (blue) grid points for mean precipitation in MAM. Large areas are improved especially in Spain, Norway, and Sweden whereas only in small parts of the regions biases are deteriorated by higher model resolution. Figure 1b pictures an overview of consistently improved minus deteriorated regions for extreme and mean precipitation. Improved areas are always larger than deteriorated areas (except for Germany during JJA). The highest improvements can be found in Spain, followed by the Alps, Scandinavia, and Germany. The improved grid-cells are majorly located in mountainous areas or are influenced by those. Added value is not restricted to extreme precipitation but can also be found in mean precipitation. Partly, added value is even larger for mean precipitation like in Scandinavia during MAM. Added value is even more pronounced when statistics are performed on an 0.11° evaluation grid, especially in Germany. This indicates that the 0.11° models are able to improve precipitation biases on scales beyond the resolution of the 0.44° models.

In addition to biases we analyzed spatial correlation

coefficients for different horizontal scales from 50 km to 800 km. The 0.11° simulations tend to improve the spatial correlation coefficients of extreme precipitation in most seasons and regions and for all spatial scales. No improvements can be found in Germany during DJF and JJA and in Sweden during JJA. Strongest spatial dependences are found in JJA where small scales (below ~200 km) are improved while larger scales are hardly affected. For mean precipitation the improvements tend to be more robust but generally smaller.

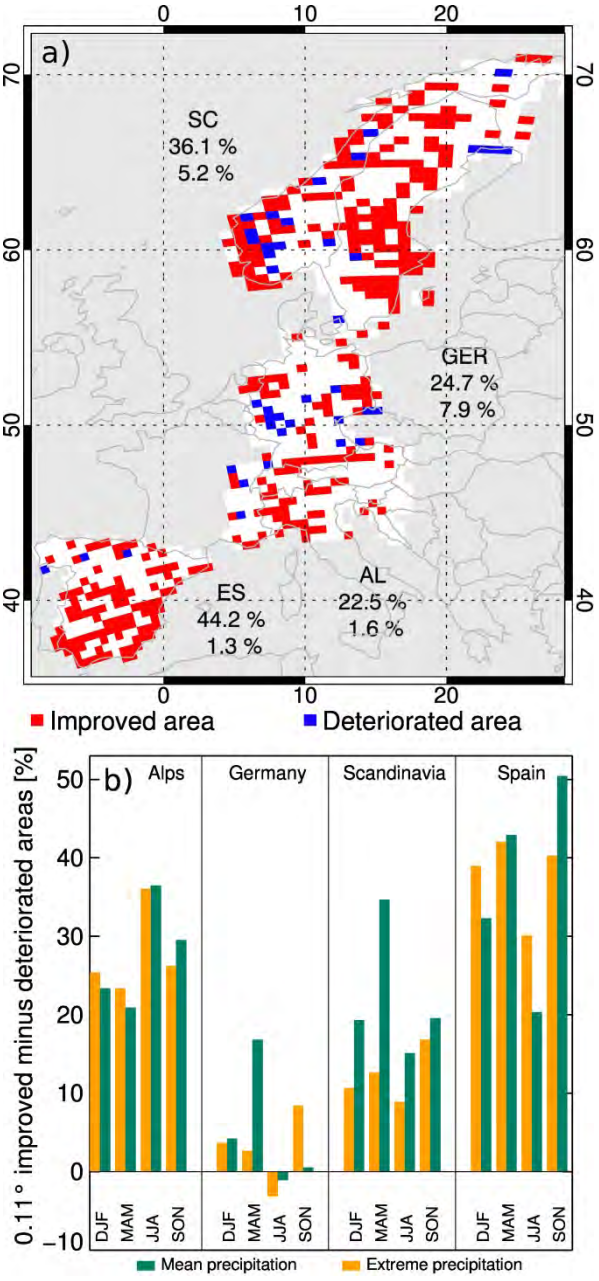


Figure 1. Consistently improved (red boxes) and deteriorated (blue) mean precipitation biases in the 0.11° simulations in MAM compared to 0.44° biases on a 0.44° evaluation grid (panel a). Numbers under the region acronym show the fraction of consistently improved and deteriorated areas. Panel b displays fractions of consistently improved minus deteriorated areas in all seasons and regions and for mean and extreme (above 97.5 %) precipitation.

Calculating spatial correlation coefficients for different precipitation percentiles also shows clear advantages of the 0.11° simulations. In the Alps and Spain, events above the ~90th percentile are stronger improved than low intensities (except for JJA) while in Germany, Sweden, and Norway correlation coefficients of percentiles below ~80 % are stronger improved. On a common 0.11° evaluation grid the improvements of correlation coefficients are getting larger. This means that the 0.11° models are able to simulate skillful precipitation patterns beyond the resolution of the 0.44° models.

4. Conclusion

By evaluating precipitation of 16 EURO-CORDEX hindcast simulations (8 with 0.11 ° and 0.44 ° grid-spacing) with high resolution gridded datasets we were able to demonstrate that increasing model resolution from 0.11° to 0.44° creates added value in simulated mean and extreme precipitation. The 0.11° models are able to decrease biases in large areas of the investigated regions and improve spatial correlation coefficients. Improvements can not only be found in extreme but also in mean precipitation and on 0.44° and 0.11° evaluation grids. The main driver of added value is the improved representation of orography. Improvements are however not restricted to mountainous areas but can also be found in regions which are downstream or influenced by mountains.

The added value can have benefits for small scale climate change impact investigations, because particularly regional and local scales are improved. Further research is needed to find out whether such added value is also visible in GCM driven simulations.

References

Chan, S. C., Kendon, E. J., Fowler, H. J., Blenkinsop, S., Ferro, C. A., Stephenson, D. B. (2013) Does increasing the spatial resolution of a regional climate model improve the simulated daily precipitation?. Climate dynamics, 41, 5-6, pp. 1475-1495.

Liu, C., Ikeda, K., Thompson, G., Rasmussen, R., Dudhia, J. (2011) High-Resolution Simulations of Wintertime Precipitation in the Colorado Headwaters Region: Sensitivity to Physics Parameterizations. Monthly Weather Review, 139, 11

Molinari, J., Dudek, M. (1992) Parameterization of convective precipitation in mesoscale numerical models: A critical review. Monthly Weather Review, 120, 2, pp. 326-344

Jacob, D et al. (2013) EURO-CORDEX: new high-resolution climate change projections for European impact research. Regional Environmental Change, pp. 1-16.

The design and interpretation of RCM ensembles: lessons from GCM simulations in the Coupled Model Intercomparison Project

Jouni Räisänen and Jussi. S. Ylhäisi

Department of Physics, University of Helsinki, Finland (jouni.raisanen@helsinki.fi)

1. Introduction

Simulations by Regional Climate Models (RCMs) provide a means to examine future climate and weather phenomena at scales that are too fine to be resolved by Global Climate Models (GCMs). Yet, the RCMs are strongly dependent on their boundary conditions, and thus the larger-scale behavior of the GCMs. Therefore, studies based on GCM ensembles bear potentially important lessons for the design of RCM ensembles and the interpretation of the RCM results.

Here, we use simulations from the Coupled Model Intercomparison Project, CMIP (Meehl et al. 2000). This data set allows not only an intercomparison between different models, but also an inspection of how model development during the past 10-15 years has affected the simulation of climate changes. Specifically, we will focus on CO_2-induced climate change in northern Europe. To the extent that time allows, we will also try to discuss some more generic issues associated with ensemble design and model weighting.

2. CO_2-induced climate change in northern Europe

The last three phases of CMIP – CMIP2 (Covey et al. 2003), CMIP3 (Meehl et al. 2007) and CMIP5 (Taylor et al. 2012) – have all included an idealized climate change simulation with atmospheric CO_2 doubling in 70 years. This allows a comparison between different model generations without the complication arising from emission scenario differences.

Figure 1 shows changes in temperature and precipitation in northern Europe at the doubling of CO_2 (years 61-80) in the three ensembles. The variation between the individual models is substantial and has not changed much from CMIP2 to CMIP5. Differences in ensemble mean climate changes are much smaller, despite a small increasing trend in warming and a decreasing trend in precipitation increase when proceeding from CMIP2 towards CMIP5.

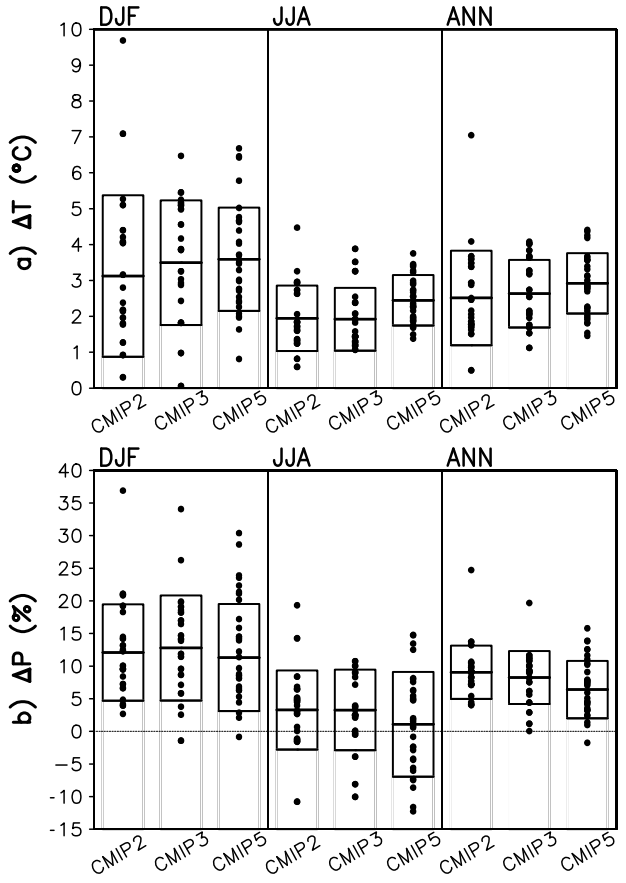


Figure 1. Changes in (a) temperature and (b) precipitation in northern Europe (land within 53.75N-71.25°N and 3.75-41.25°E) induced by a gradual doubling of CO_2. In each case, the bar shows the ensemble mean change ± one standard deviation, whereas the small closed circles show changes in individual models. DJF = December-January-February; JJA = June-July-August; ANN = annual mean. 20 / 20 / 32 models are included for CMIP2 / CMIP3 / CMIP5. The ensemble statistics are calculated with the "one vote per one institute" principle.

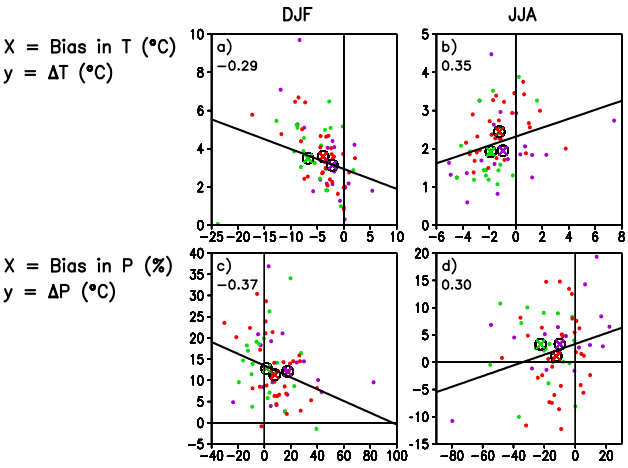


Figure 2 (in the right column). Scatter plots of (a)-(b) temperature bias versus temperature change and (c)-(d) precipitation bias versus precipitation change in the CMIP2 (purple), CMIP3 (green) and CMIP5 (red) ensembles. The circled crosses give the mean values for the three ensembles. The correlation coefficient and the least-square linear regression line are also indicated.

3. Relationships between present-day climate and climate changes

It is sometimes assumed that the large variation in the model-simulated climate changes might be reduced by eliminating badly performing models. This may be true, but to avoid circular reasoning, the "bad" models should be identified by a criterion that is not directly related to their simulated climate changes. Biases in present-day climate are an obvious candidate. However, as shown in Fig. 2, climate changes may vary substantially even in models with near-zero present-day biases. Nevertheless, when they exist, relationships between present-day biases and climate changes may still carry useful information. For example, in northern Europe in winter, the simulated warming tends to decrease with increasing present-day temperature (Fig. 2a; the correlation would be stronger if one outlier with an extreme cold bias and negligible warming were excluded). Together with the prevailing cold bias in the models, this suggests that the ensemble mean changes might give a positively biased best estimate of the CO_2-induced winter warming.

4. What about performance-based model weighting?

Performance-based weighting of model simulations is a very complicated issue, both because there are myriads of ways in which the weighting could be made and because its ability to improve the resulting climate change projections is unclear. If models are weighted based on some aspect of their present-day climates, but this aspect bears no relationship with the simulated climate change, the decrease in effective sample size caused by the non-uniform weighting tends to deteriorate the climate change projection (Weigel et al. 2010). Improvement is only expected if the relationship between present-day climate and the climate changes is strong enough.

Räisänen et al. (2010) showed, by using intermodel cross validation within the CMIP3 ensemble, that a suitably designed weighting scheme might indeed improve climate change projections. However, the potential improvement seems to be modest, and it is unclear whether it outweighs the additional complexity associated with the use of such a weighting scheme. Moreover, while cross validation seems a necessary tool for testing weighting schemes, it is still prone to a selection bias. When a large number of potential ways of performing the weighting are tested and the one with the best cross validation statistics is chosen, it is unlikely that this particular choice would work as well for an independent model data set or for the real world.

Regardless of its connection to the simulated climate changes, the magnitude of present-day biases may matter in climate impact assessment: the larger the biases, the larger and more problematic the bias corrections that need to be applied when climate model data are used to drive impact models. Climate models with very large biases might therefore be useless for some types of impact research, even if their simulated climate changes were no less accurate than those in other models.

5. Implications for RCM ensembles

Regarding the design and use of RCM ensembles, studies based on the CMIP simulations have at least three implications:

1. Inter-GCM variability in large-scale climate change remains substantial, but the ensembles might still not capture all uncertainty in climate change (e.g. van Oldenborgh et al. 2013). The best an RCM ensemble can do is to retain this variability, by including driving GCMs (and RCMs) with sufficiently different behavior.
2. When trying to identify the types of biases that are important for simulated climate change, intermodel comparison between present-day biases and climate changes may give useful clues.
3. Model weighting is at an exploratory stage of development and (somewhat like fusion energy?) will probably remain so for a long time to come. It is an interesting research topic, but the probability that a universally accepted weighting scheme for global or regional climate model simulations could be developed in the near future appears very small.

References

Covey C, AchutaRao KM, Cubasch U, Jones P, Lambert SJ, Mann ME, Phillips TJ, Taylor KE (2003) An overview of results from the Coupled Model Intercomparison Project. Global Planet. Change, 37, pp. 103-133

Meehl GA, Boer GJ, Covey C, Latif M, Stouffer RJ (2000) The Coupled Model Intercomparison Project (CMIP), Bull Amer Meteor Soc, 81, pp. 313-318

Meehl GA, Covey C, Delworth T, Latif M, McAvaney B, Mitchell JFB, Stouffer RJ, Taylor KE (2007) The WCRP CMIP3 multimodel dataset: A new era in climate change research. Bull. Amer. Meteor. Soc., 88, pp. 1383-1394

Räisänen J, Ruokolainen L, Ylhäisi J (2010) Weighting of model results for improving best estimates of climate change, Climate Dyn., 35, pp. 407-422

Taylor KE, Stouffer RJ, Meehl GA (2012) An overview of CMIP5 and the experiment design, Bull. Amer. Meteor. Soc., 93, pp. 485-498

van Oldenborgh GJ, Doblas-Reyes FJ, Drijfhout SS, Hawkins E (2013), Reliability of regional climate model trends, Env. Res. Lett., 8(1), 014055

Weigel AP, Knutti R, Liniger MA, Appenzeller C (2010) Risks of model weighting in multimodel climate projections, J. Climate, 23, pp. 4175–4191

South America regional temperature and precipitation projections for the end of XXIst century from CLARIS-LPB ensemble of RCMs

E. Sanchez[1], S. Solman[2], P. Samuelsson[3], R. da Rocha[4], L. Li[5], J. Marengo[6], A. Remedio[7], H. Berbery[8]

[1] UCLM, Toledo, Spain (e.sanchez@uclm.es)
[2] CIMA/CONICET-UBA, Buenos Aires, Argentina
[3] SMHI, Rossby Centre, Norrköping, Sweden
[4] USP, Sao Paulo, Brazil
[5] IPSL, CNRS, Paris, France
[6] INPE, Sao Paulo, Brazil
[7] MPI, Hamburg, Germany
[8] U. Maryland, USA

1. Introduction

The first ensemble of regional climate models simulating the whole South America continent has been obtained in CLARIS-LPB EU project (www.claris-eu.org). This region is, at the same time, an are affected with several and complex climatic phenomena. Global climate model projections described in IPCC2013 (Christensen et al., 2013) indicate that temperatures very likely will increase during the XXIst century for the whole continent, specially over the southern Amazonia, and precipitation with present a more complex behaviour, with areas with increases and decreases. In that report, just regional climate model simulations obtained by individual models are analzed. Thus, this ensemble of RCM simulations is a challenging opportunity to improve our understanding of the regional characteristics of the region for present and future conditions.

2. Methodology

A first evaluation of the capability of seven RCMs at 50km horizontal resolution to properly describe the different and complex climatic features of the continent was analyzed in Solman et al. 2013, for present climate period, as forced with ERAinterim perfect boundary conditions. Some sistematic biases are also found. Once those regional models have been proved to describe the main climatic characteristics of the region, future climate regional projections are performed, both for near future conditions (2011-2040) and for far future period (2071-2100), as forced by several global climate models under A1B SRES emissions scenarios and three different CMIP3 GCMs

3. Results for (2071-2100) period

Seasonal (DJF) mean temperature and precipitation changes for each of the ten RCM simulations performed in CLARIS-LPB for (2071-2100) period are shown in figures 1 and 2 as an example of the overall climate change response obtained for the whole continent. The mean DJF seasonal temperature change shows a consistent warming (ranging from 2 to 7ºC) over the whole continent for all the GCM/RCM combinations, with more warming over tropical South America than over the southern part of the continent. Precipitation changes are both positive or negative, depending on the region and regional model. Paraguay and Up-Parana show almost no change in precipitation with time, Uruguay and Low-Parana regions show in general an increase of precipitation, while SACZ and Southern Amazonia show a small negative trend in precipitation into the future. Temperature changes are more similar for different RCMs forced with different GCMs, whereas precipitation changes are more similar for a certain RCM being forced with different GCMs. A complete analysis of these regional climate change projections is expected to be submitted in the following months, with some results already shown (Samuelsson et al., 2013)

References

Christensen, J.H., et al., 2013: Climate Phenomena and their Relevance for Future Regional Climate Change. In: Climate Change 2013: The Physical Science Basis. Contribution of Working Group I to the Fifth Assessment Report of the Intergovernmental Panel on Climate Change [Stocker, T.F., D. Qin, G.-K. Plattner, M. Tignor, S.K. Allen, J. Boschung, A. Nauels, Y. Xia, V. Bex and P.M. Midgley (eds.)]. Cambridge University Press, Cambridge, UK and New York, NY, USA.

Samuelsson, P., S. Solman, E. Sanchez, R. Rocha, L. Li, J. Marengo, A. Remedio, H. Berbery (2013). Regional climate change projections over South America based on the CLARIS-LPB RCM ensemble, Geophys. Res. Abs., 15, 15, EGU2013-5800

Solman, S., E. Sanchez, P. Samuelsson , R. Da Rocha, L. Li , J. Marengo, N. Pessacg, A.R.C. Remedio , S. C. Chou, H. Berbery, H. Le Treut, M. De Castro and D. Jacob (2013). Evaluation of an ensemble of regional climate model simulations over South America driven by the ERA-Interim reanalysis: Models performance and uncertainties. Climate Dynamics, 41 , 1139-1157.

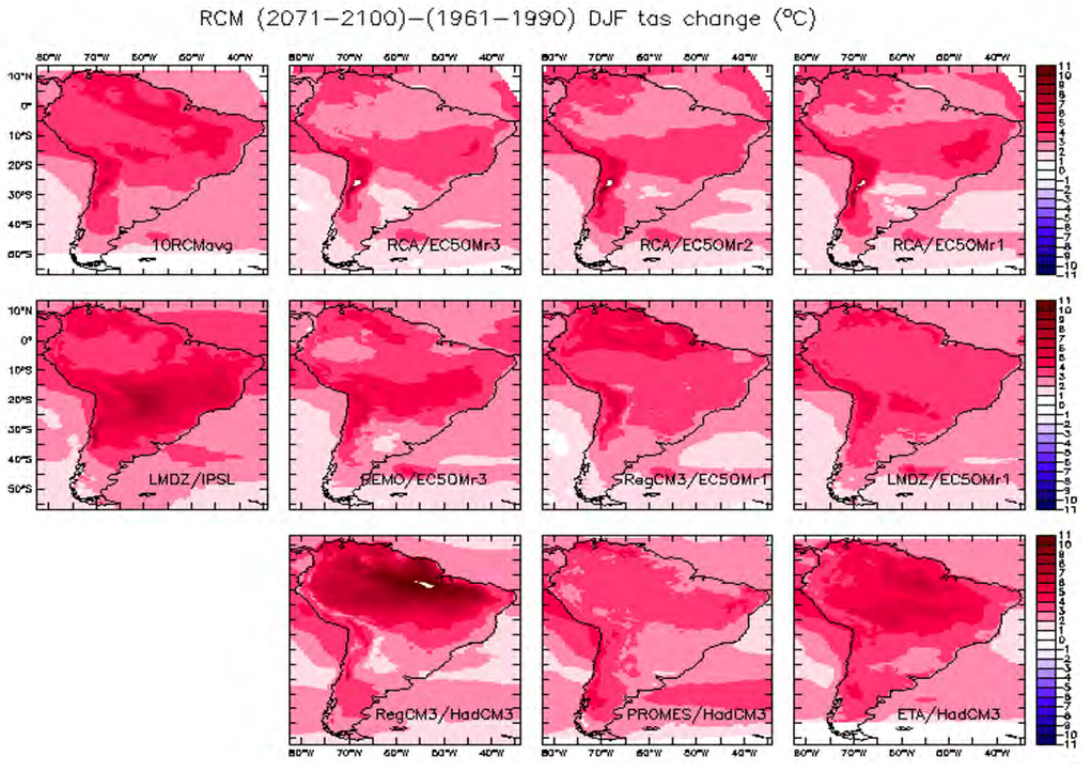


Figure 1. Temperature difference (in ºC) between future (2071-2100) and control period (1961-1990) for DJF season

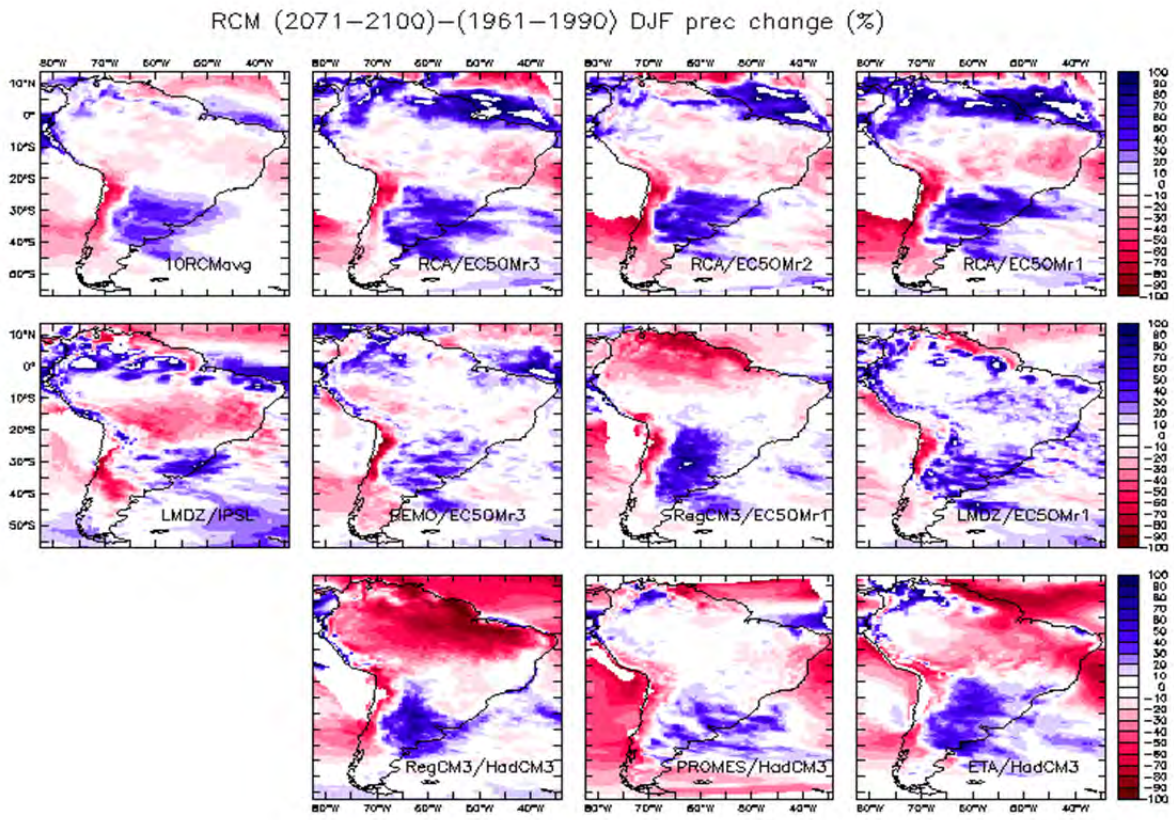


Figure 2: Precipitation difference (%) between future (2071- 2100) and control period (1961-1990) for DJF season

Using a Circulation Type Classification to Investigate the Internal Variability in Regional Climate Model Simulations over Europe

Kevin Sieck[1,2], Daniela Jacob[1,2]

[1] Max-Planck-Institut für Meteorologie, Hamburg, Germany (kevin.sieck@mpimet.mpg.de)
[2] Climate Service Center, Hamburg, Germany

1. Introduction

Regional climate models are frequently used and widely accepted tools for current climate simulations and future climate change projections because of their consistent representation of physical processes at a high resolution. These models are integrated on a limited domain and obtain their initial and boundary conditions from global climate models or gridded analysis of observations. In this way, a regional climate model acts as a magnifying glass to deliver climate information on the regional to local scale that are often needed in, e.g., climate change impact studies. To deliver robust information, it is of importance to study their uncertainties. Apart from uncertainties introduced by the boundary conditions and model formulations, it has been shown that regional climate models are subject to uncertainties that stem from processes intrinsic to the model (see, e.g., Laprise et al., 2008, 2012, and references therein). In this study, this form of uncertainty, referred to as the internal variability of a regional climate model, is investigated for a domain located over Europe.

2. Method and Experimental Set-up

All numerical simulations used in this study were carried out with the hydrostatic version of the RCM REMO (Jacob et al., 2001) in version 5.0. Target area of all simulations is Europe covered by a domain with 81x91 grid points on a rotated grid with a horizontal resolution of 0.5° (~ 55 km) and 20 levels in the vertical. The internal variability is estimated from the variance of a time-lagged initial condition ensemble after Alexandru et al. (2007) and Lucas-Picher et al. (2008) that has been run for a ten year period (1979-1988) forced by ERA-40 re-analysis data. The analysis is based on daily data of the internal variability. To investigate the influence of boundary forcing variability on the internal variability, a circulation type classification using the SANDRA method (Phillip et al., 2007) of the boundary data has been performed. To account for the flow in the vicinity of the model domain, the domain for the circulation type classification is extended by 30 grid boxes in the zonal and 20 grid boxes in the meridional direction at each boundary.

3. Results

It is shown that internal variability of a regional climate model applied over Europe is similar to other regions in the northern hemisphere mid-latitudes. Specifically the episodic character of internal variability with strong and weak phases are similar. But there are also important differences. In Europe the peak internal variability for mean-sea-level pressure and near-surface temperature are found in spring and winter, respectively (see Figure 1). The internal variability of precipitation in turn shows more the behavior expected from earlier studies with weak internal variability in winter and strong internal variability in summer. This rather mixed picture in annual cycle leads to the conclusion that internal variability for different variables is differently influenced by the large scale forcing (or circulation type).

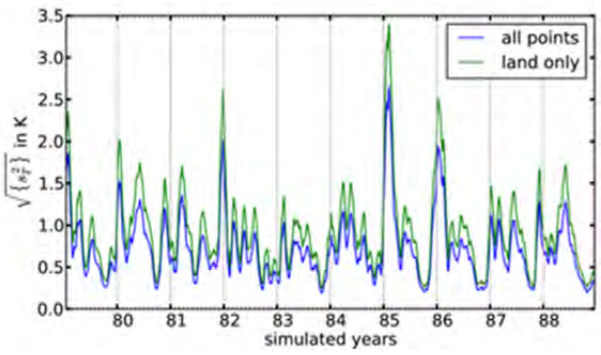


Figure 1: The blue line depicts the square root of area averaged daily internal variability of near-surface temperature over the entire domain (excluding the sponge zone) for the entire simulation period. The green line shows the same but only for land-points. A 30 day moving average has been applied to each line.

To understand the influence of circulation types on the internal variability, a circulation type classification of the lateral boundary forcing has been performed. It shows that the episodic behavior of internal variability can be related to the variability of the boundary forcing as already proposed by Laprise et al. (2012). This is especially the case for the winter season. In winter, NAO-like patterns have the strongest influence on the strength of internal variability inside the domain, with high (low) internal variability for NAO negative (positive) like circulation types (see Figure 2). This can be explained by the strength of the westerly flow that is stronger in NAO positive compared to NAO negative phases. For summer the weakest influence of circulation types on the strength of internal variability is found, which leads to similar conclusions drawn by Caya and Biner (2004) and Christensen et al. (2001) that internal variability in summer is closely related to local processes. The transition seasons spring and autumn show a mixed behavior. In both seasons circulation types with strong

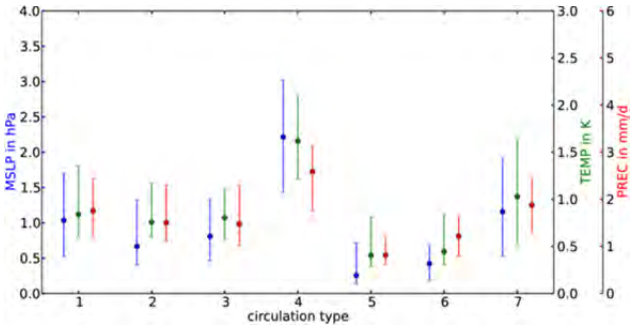


Figure 2: Level of internal variability for mean-sea-level pressure (MSLP, blue), near-surface temperature (TEMP, green), and precipitation (PREC, red) given for each winter circulation type. Dots indicate the median internal variability and error-bars the corresponding interquartile range. Two prominent types are circulation type 4 and 6 that can be associated with NAO negative and positive phases, respectively.

westerly flows show in general weaker internal variability and vice versa. This effect, however, becomes weaker for parameters that are more related to local processes like precipitation.

4. Conclusions

A comprehensive circulation type classification has been used to investigate the internal variability in a regional climate model simulation over Europe. Results suggest that NAO positive and negative like circulation types are linked to the strength of internal variability inside the domain during winter. Summer circulation types only marginally modulate the internal variability and thus the main origin of internal variability in summer are most likely local processes such as local scale variations in convection, and condensation between members of the ensemble as shown in a case study by Nikiema and Laprise (2011). The transition seasons spring and autumn show a mixed behavior, but significant differences in the strength of internal variability for NAO-like circulation types can been found.

5. Outlook

In this study, the internal variability on a daily basis has been presented. The internal variability of the climate (i.e., on longer time scales) on the investigated domain is rather small for most variables after one season and does not play a role after one year. This means that internal variability of a regional climate model on the current domain is small compared to other sources of uncertainty such as scenario uncertainty. However, internal variability grows with the model domain and internal variability of the climate can be important on very large domains used by Lucas-Picher et al. (2008) at least on the time scale of a decade. For some variables such as precipitation on the catchment scale, the internal variability of the regional climate model even plays an important role in the uncertainty of the climate change signal. This has been recently shown by Braun et al. (2012) for the North-East of Canada. For Europe internal variability seems to be even more important, because it is already quite large in the comparably small domain used in this study. On bigger domains with more grid points and higher resolution (e.g., the domains used in MiKlip or EUROCORDEX), the strength of internal variability is expected to be larger and internal variability on climatic time-scales may contribute significantly to the overall uncertainty on a European domain at least on decadal time scales. This will be investigated in a follow up study.

References

Alexandru, A., R. de Elia and R. Laprise (2007). Internal variability in regional climate downscaling at the seasonal scale. Monthly Weather Review, 135(9), 3221–3238.

Braun, M., D. Caya, A. Frigon and M. Slivitzky (2012). Internal Variability of the Canadian RCM's Hydrological Variables at the Basin Scale in Quebec and Labrador. Journal of Hydrometeorology, 13(2), 443–462.

Caya, D. and S. Biner (2004). Internal variability of RCM simulations over an annual cycle. Climate Dynamics, 22(1), 33–46.

Christensen, O. B., M. A. Gaertner, J. A. Prego and J. Polcher (2001). Internal variability of regional climate models. Climate Dynamics, 17(11), 875–887.

Jacob, D., B. J. J. M. Van den Hurk, U. Andrae, G. Elgered, C. Fortelius, L. P. Graham, S. D. Jackson, U. Karstens, C. Kopken, R. Lindau, R. Podzun, B. Rockel, F. Rubel, B. H. Sass, R. N. B. Smith and X. Yang (2001). A comprehensive model inter-comparison study investigating the water budget during the BALTEX-PIDCAP period. Meteorology and Atmospheric Physics, 77(1-4), 19–43.

Laprise, R., R. de Elia, D. Caya, S. Biner, P. Lucas-Picher, E. Diaconescu, M. Leduc, A. Alexandru and L. Separovic (2008). Challenging some tenets of Regional Climate Modelling. Meteorology and Atmospheric Physics, 100(1-4), 3–22.

Laprise, R., D. Kornic, M. Rapaic, L. Separovic, M. Leduc, O. Nikiema, A. D. Luca, E. Diaconescu, A. Alexandru, P. Lucas-Picher, R. de Elia, D. Caya and S. Biner (2012). Climate Change, chapter Considerations of Domain Size and Large-Scale

Driving for Nested Regional Climate Models: Impact on Internal Variability and Ability at Developing Small-Scale Details, p. 244. Springer-Verlag Wien.

Lucas-Picher, P., D. Caya, R. de Elia and R. Laprise (2008). Investigation of regional climate models' internal variability with a ten-member ensemble of 10-year simulations over a large domain. Climate Dynamics, 31(7-8), 927–940.

Nikiema, O. and R. Laprise (2011). Diagnostic budget study of the internal variability in ensemble simulations of the Canadian RCM. Climate Dynamics, 36(11-12), 2313–2337.

Improvement of Climate Projections and Reduction of their Uncertainties Using a Sequential Learning Algorithm

Ehud Strobach and Golan Bel

Department of Solar Energy and Environmental Physics, Blaustein Institutes for Desert Research, Ben-Gurion University of the Negev, Sede Boqer Campus, Israel

1. Introduction

Ensembles of climate models can improve climate predictions and reduce their uncertainties [Krishnamurti *et.al.* (2000)]. Here, we introduce a new method, adopted from the field of game theory [Cesa-Bianchi *et.al.* (2006)], to weight the ensemble members.

The weights are generated by comparing the hindcasts of climate models with reanalysis data (considered here as true values) during a learning period.

We show that this method improves the predictions of global climate models and reduces their uncertainties on a decadal time scale.

2. Basic Concept

The *forecaster* is a mathematical algorithm that takes advantage of several available climate model predictions (*experts*) and the knowledge of their past performance to generate a set of improved predictions in a sequential manner as illustrated in Figure 1.

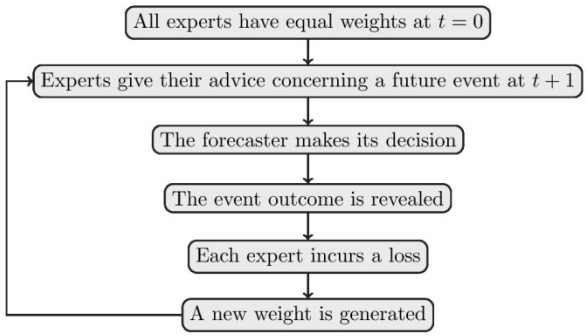


Figure 1. Flow chart of the forecaster algorithm during the learning period.

The forecaster's goal is to minimize the cumulative regret with respect to each one of the climate models. This is defined, for expert E, by the quantity:

$$\mathrm{R_{E,t}} \equiv \sum_{\mathrm{n=0}}^{\mathrm{t}} \left(\mathrm{l}(\hat{p}_t, \mathrm{y_t}) - \mathrm{l}(\mathrm{f_{E,t}}, \mathrm{y_t})\right) \equiv \mathrm{L_t} - \mathrm{L_{E,t}}$$

l - Loss function, a measure of the difference between the predicted and the true values.

t – Discrete time.

$\mathrm{y_t}$ - True value at time t.

$\hat{p}_t$ - Predicted value, by the forecaster, for time t.

$\mathrm{f_{E,t}}$ - Predicted value, by the expert E, for time t.

L - Cumulative loss function.

The outcome of the forecaster is a weighted average of the climate models in the ensemble, that is:

$$\hat{p}_\mathrm{t} \equiv \sum_{\mathrm{E=1}}^{\mathrm{N}} \mathrm{W_{E,t-1}}\left(\mathrm{R_{E,t-1}}\right) \cdot \mathrm{f_{E,t}}$$

$\mathrm{W_{E,t-1}}$ - Weight of expert E based on the regret up to time $\mathrm{t}-1$.

3. Forecasting Methods

We defined the loss function as:

$$l_{E,t}(f_{E,t}, y_t) \equiv \left(f_{E,t} - y_t\right)^2.$$

Two forecast methods were tested. The first is the exponentiated Weighted Average (EWA):

$$\hat{p}_t \equiv \frac{\sum_{E=1}^{N} e^{-\eta L_{E,t-1}} \cdot f_{E,t}}{\sum_{i=1}^{N} e^{-\eta L_{i,t-1}}},$$

$$L_{E,t} \equiv \sum_{j=1}^{t} l_{E,t}(f_{E,t}, y_t).$$

The second is the Exponentiated Gradient Average (EGA)

$$\hat{p}_t \equiv \frac{\sum_{E=1}^{N} e^{-\eta L'_{E,t-1}} \cdot f_{E,t}}{\sum_{i=1}^{N} e^{-\eta L'_{i,t-1}}},$$

$$l'_{E,t}(\hat{p}_t, y_t) \equiv \nabla l_{E,t}(\hat{p}_t, y_t) = \frac{\partial l_{E,t}(\hat{p}_t, y_t)}{\partial \mathrm{W_{E,t-1}}} = 2 \cdot (\hat{p}_t - y_t) \cdot f_{E,t},$$

$$L'_{E,t} \equiv \sum_{j=1}^{t} l'_{E,t}\left(f_{E,t}, y_t\right).$$

There is a conceptual difference between the two methods which is illustrated in Figure 2. The EWA converges to the best expert while the EGA converges to the true value.

4. Experimental Setup

- Results of eight climate models from the CMIP5 decadal project for the period (1981-2011) [Taylor et.al (2012)].
- NCEP reanalysis data considered as true values [Kalnay et.al. (1996)].
- Calculated monthly averages of the surface temperature.
- 25-year learning period (during which the weights are updated every month).
- Five years of validation of the forecasters (the weights are constant).

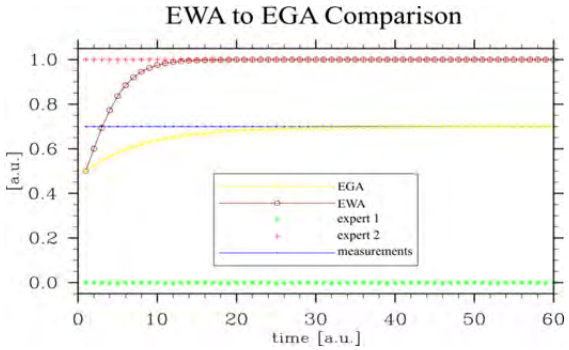


Figure 2. An ideal experiment with two experts. One always predicts zero and the second always predicts one. The true value is always 0.7. The EWA forecaster converges to the best model while the EGA converges to the true value.

5. Results

Figure 3 shows the average absolute anomaly of the monthly mean surface temperature for the five years of the validation period. The results are presented for three forecasting methods EWA, EGA and simple average. Both EWA and EGA improve the predictions compared with the simple average which is, by itself, better than each one of the models. The EGA shows slightly better predictions than the EWA.

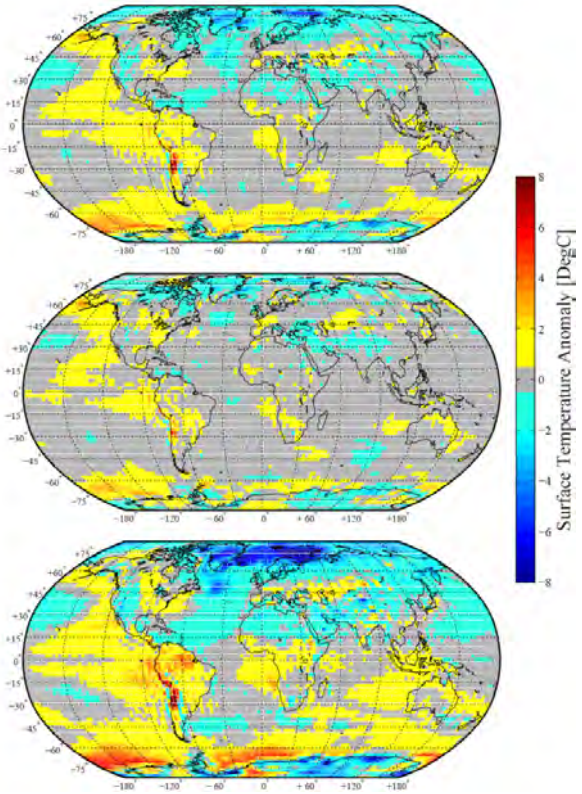


Figure 3. Average absolute anomaly of the monthly mean surface temperature for the five years of the validation period--Jan 2005-Dec 2010--and for three cases: (a) EWA forecaster, (b) EGA forecaster, and (c) simple average. Both forecasters seem to perform better than the simple average.

Figure 4 shows the average standard deviation of the monthly mean surface temperature for the five years of the validation period. It is shown that both forecasting method provide smaller uncertainty than the simple average with the EWA providing the minimal uncertainty.

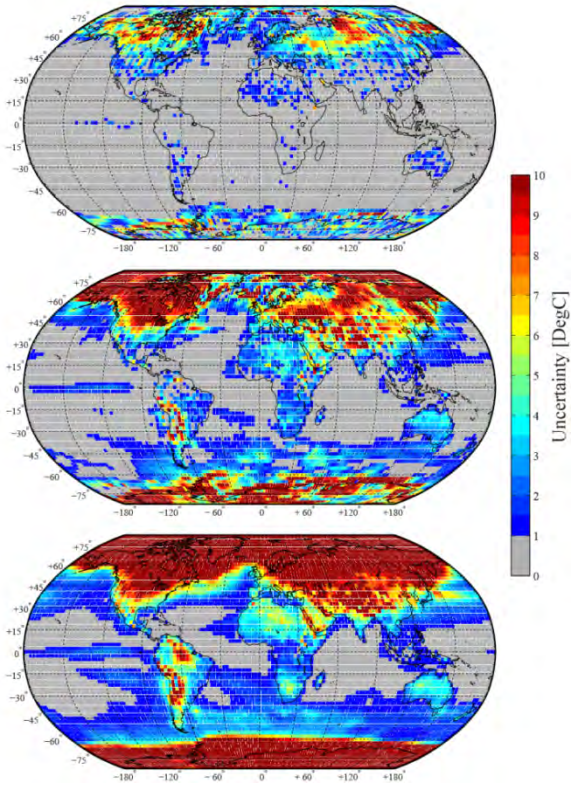


Figure 4. Average standard deviation of the monthly mean surface temperature for the five years of the validation period--Jan 2005-Dec 2010--and for three cases: (a) EWA forecaster, (b) EGA forecaster, and (c) simple average. Both forecasters reduce the uncertainties below the simple average; however, the EWA shows considerably better results.

5. Conclusions

- Two mathematical models were used to improve climate predictions and reduce their uncertainties.
- One model (EGA) is provides better predictions of future climate, and the other (EWA) provides smaller uncertainties.
- Both methods give better results than a simple average.

References

T. N. Krishnamurti, C. M. Kishtawal, Z. Zhang, T. LaRow, D. Bachiochi, E. Williford, S. Gadgil, S. Surendran (2000) Multi-model ensemble forecasts for weather and seasonal climate. Journal of Climate, 13(23):4196–4216.

N. Cesa-Bianchi, G. Lugosi (2006) Prediction learning, and games. Cambridge University Press, 2006.

Karl E. Taylor, Ronald J. Stouffer, Gerald A. Meehl (2012) An overview of CMIP5 and the experiment design. Bulletin of the American Meteorological Society, 93(4):485, 2012.

E. Kalnay, M. Kanamitsu, R. Kistler, W. Collins, D. Deaven, L. Gandin, M. Iredell, S. Saha, G. White, J. Woollen, Y. Zhu, A. Leetmaa, R. Reynolds, M. Chelliah, W. Ebisuzaki, W. Higgins, J. Janowiak, K. C. Mo, C. Ropelewski, J. Wang, Roy Jenne, Dennis Joseph (1996) The NCEP/NCAR 40-Year Reanalysis Project. Bulletin of the American Meteorological Society, 77(3):437–471.

An overview of the SOUSEI multi GCM/RCM dynamical downscaling ensemble

Asuka Suzuki-Parker[1], Izuru Takayabu[2], Ryo Mizuta[2], Hiroyuki Kusaka[3], Koji Dairaku[4], Suryun Ham[5], Sachiho A. Adachi[6], and Noriko N. Ishizaki[6]

[1] Graduate School of Life and Environmental Sciences, University of Tsukuba, Tsukuba, Japan (suzuki.asuka.fp@u.tsukuba.ac.jp)
[2] Meteorological Research Institute, Japan Meteorological Agency, Tsukuba, Japan
[3] Center for Computational Sciences, University of Tsukuba, Tsukuba, Japan
[4] Department of Integrated Research on Disaster Prevention, National Research Institute for Earth Science and Disaster Prevention, Tsukuba, Japan.
[5] Atmosphere and Ocean Research Institute, University of Tokyo, Kashiwa, Japan
[6] Japan Agency for Marine-Earth Science and Technology, Yokohama, Japan

1. Introduction

Today, there are a number of multiple GCM/RCM dynamical downscaling (DDS) ensemble projects throughout the world. These projects include ENSEMBLES, NARCCAP, and CORDEX series to name a few. Selections of GCMs and RCMs have depended on projects' goals and technical aspects (e.g., GCM data availability GCM-RCM compatibility, and computational resources, etc.). However, there are emerging evidences that in comparison to RCMs, variations in GCMs contribute to the ensemble spread more than those in RCMs (e.g., Deque et al. 2007). Yet how best to select GCMs for ensemble downscaling experiments remain as a very active discussion point within the DDS community. The authors have been conducting the SOUSEI multi GCM/RCM DDS experiments for Japan. In our project, GCM selection is made based on a cluster analysis of tropical SST change in CMIP5 GCMs. In this presentation, we will provide an overview of the SOUSEI multi DDS experiment, including GCM selection and its consequences, and some preliminary results from downscaling.

2. Experimental design

The SOUSEI multi GCM/RCM downscaling ensemble is comprised of three GCMs (MIROC5, MRI-CGCM3, and CCSM4) and four RCMs (MRI-NHRCM, NIED-RAMS, Tsukuba-WRF, and AORI-RSM) (Figure 1). Domain configuration is commonly set as Japan and its vicinity at 20km horizontal resolution (Figure 2). Simulation periods are also the same for all ensemble members; 1981-2000 under AR5 historical scenario, and 2081-2100 under RCP4.5 scenario.

SST changes are considered to be important for regional climate changes. From this reason, we selected GCMs based on a cluster analysis on SST future change in CMIP5 GCMs. Here, GCMs are classified into three clusters according to their spatial distribution of tropical SST change under RCP4.5 scenario (Figure 3). For the SOUSEI DDS ensemble, one GCM is selected from each of the three SST clusters. SST change in MIROC5 is characterized by a profound increase in eastern tropical Pacific, whereas MRI-CGCM3 has higher increase in Indian ocean and western tropical Pacific. CCSM4 has relatively more uniform SST increase throughout the tropics. Summer-time future precipitation change in these GCMs around Japan also exhibits marked differences.

3. Lookout

The SOUSEI DDS simulations are still underway. Our ensemble design, with all of the three GCMs downscaled by all RCMs resulting a "filled GCM/RCM matrix", allows us use Analysis of Variance (ANOVA) to attribute GCM and RCM variations to the ensemble spread. Some preliminary analysis, depending on the data availability, will be given using the downscaled seasonal mean temperature and precipitation.

Acknowledgment

This work was supported by the SOUSEI Program of the Ministry of Education, Culture, Sports, Science, and Technology. The CCSM4 data was obtained from the Research Data Archive at the National Center for Atmospheric Research, Computational and Information Systems Laboratory, Boulder, CO [available online at http:/dx.doi.org/10.5065/D6TH8JP5.] Accessed July-August 2014.

References

Deque, M., D. Rowell, D. Luthi, F. Giogi, J. Christensen, B. Rockel, D. Jacob, E. Kjellstrom, M. Castro, and B. Hurk, 2007: An intercomparison of regional climate simulations for Europe: assessing uncertainties in model projections. Climatic Change. 81 (S1), 53-70.

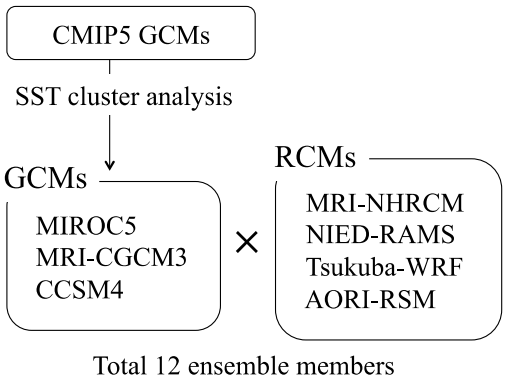


Figure 1. Schematic diagram of the SOUSEI multi DDS experiment.

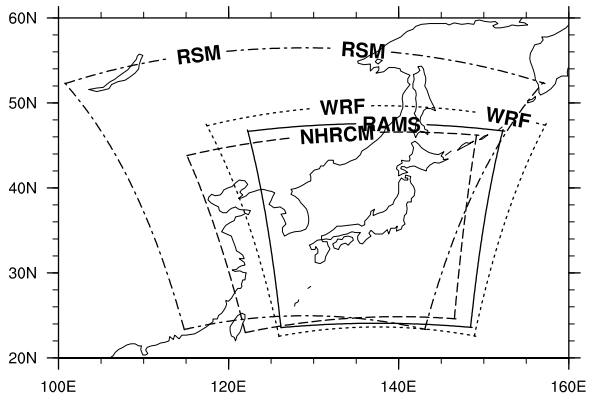


Figure 2. RCM domains for the SOUSEI multi DDS experiment.

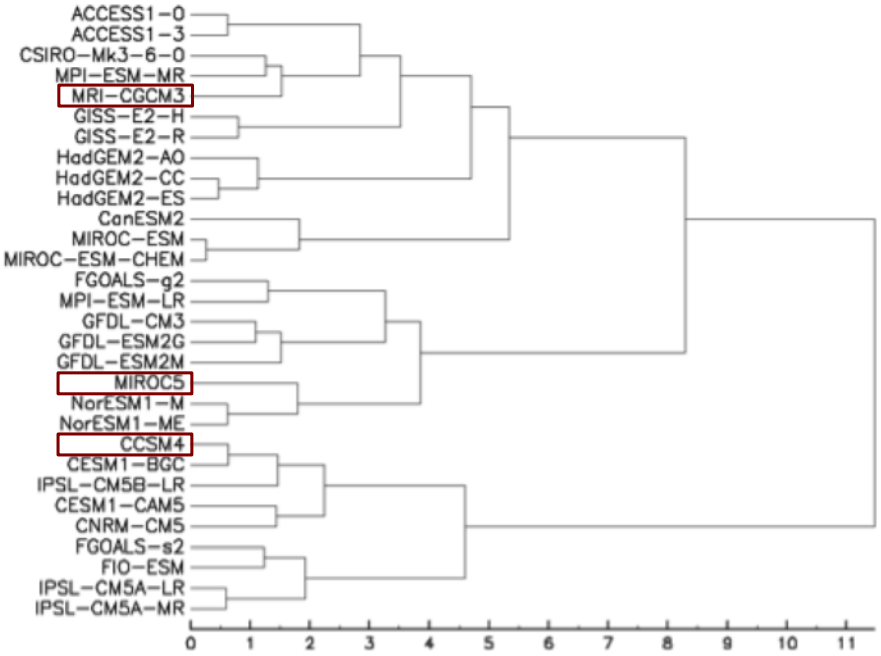


Figure 3. Cluster tree diagram for future tropical SST change in CMIP5 GCMs under RCP4.5 scenario

Sampling downscaling method and its application to Hokkaido summer climate

Y Tamaki[1], M Inatsu[2], N Nakano[3] and R Kuno[4]

[1] Hokkaido University, Sapporo, Japan (tmk-esker@ec.hokudai.ac.jp)

[2] Hokkaido University, Sapporo, Japan

[3] Tohoku University, Sendai, Japan

[4] ARK Information Systems, Yokohama, Japan

1. Introduction

In recent years, it is required to use the results of global warming projection for application fields such as agriculture, civil engineering, and socio-economy. However, general circulation models (GCMs) still run with coarse resolution in climate simulation, because it is difficult to perform a long-term integration of a high-resolution GCM with super computer. The dynamical downscaling (DDS) technique to make a spatially fine dataset from GCM outputs is then necessary to rationally fill the gap of resolution between GCM simulation and application-side requirement.

Kuno and Inatsu (2014) recently proposed the idea named sampling downscaling (SmDS), in which DDS is performed for selected years based on a statistical relation between global and regional climatic variables. They applied this method to wintertime Hokkaido climate and suggested that, to some extent, SmDS is effective under the assumption that local variables are mostly controlled by global variables. However, SmDS has not been tested in another climate condition yet, so that it is still uncertain that SmDS effectively reduces the computational cost of DDS in any cases with a small estimation error.

The purpose of this study is to apply SmDS to summertime precipitation over Hokkaido to investigate the robustness of the SmDS and to develop the error estimation theory to know the error of statistics for estimates by the SmDS.

2. Procedure

Singular value decomposition (SVD) analysis is performed from 1981 to 2010 in June-July-August (JJA) months to identify highly correlated spatial pattern between global and local variables. We chose moisture flux convergence in Northeast Asia as the former and precipitation over Hokkaido as the latter. Next, moisture flux convergence in GCMs of MIROC-hires, MPI/ECHAM5 and NCAR1/CCSM3 is projected onto the heterogeneous spatial pattern obtained from the SVD analysis. We then sample top and bottom two years from the projected time-series data. Finally we conduct the DDS for these sampling years using a regional atmospheric model of JMA/MRI-NHM (Saito et al., 2006). In this paper, we conduct the DDS for 30 years under both the current climate and the future climate conditions in advance to compare the conventional DDS (full DDS) result with the SmDS result as in Kuno and Inatsu (2014). It is remarked that the current climate period is 1990-1999, and the future climate period is 2050-2059 for MIROC, 2060-2069 for MPI, and 2080-2089 for NCAR, during which the global-mean surface temperature increases 2 K.

3. The error estimation theory of SmDS

We have developed the error estimation theory for the SmDS. The mean estimate of the SmDS is unbiased with a possible error range within

$$\pm t_\alpha(2M)\sqrt{\frac{(1-r^2)}{2M}}\sigma_p$$

where $t_\alpha(2M)$ is a t-value with the degree of freedom of 2M at the significant level of 2α; r is correlation coefficient between global and local variables; σ_p is variance of the local variable.

4. Result

a. SVD analysis

Figures 1a,b show a set of heterogeneous maps for the leading SVD mode. Precipitation is large in southern Hokkaido when the moisture flux are converges in northern Japan. The correlation coefficient is 0.87 (Fig. 1c) and the fraction of variance is 43.8% for local precipitation. Regression of sea level pressure (SLP) on the leading SVD mode (Fig. 1d) indicates that quasi-stationary cyclone anomaly is sandwiched between two anticyclone anomalies extended from east to west over northern Japan. The quasi-stationary cyclone anomalies correspond to the Baiu front [See Sampe and Xie (2010)]. Therefore the leading SVD mode explains that the northward/southward shift of the stationary Baiu front controls the precipitation over southern Hokkaido.

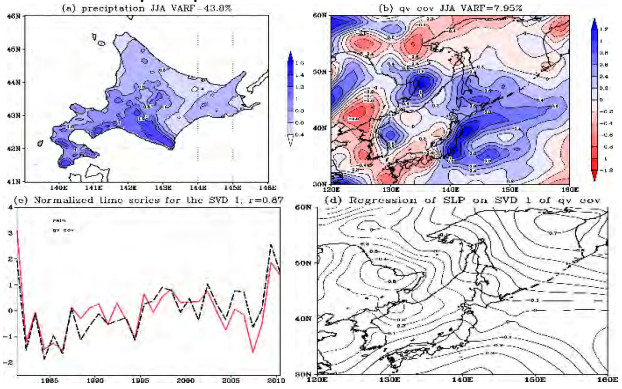


Figure 1: (a) Heterogeneous map of precipitation (mm/day) and (b) that of vertically integrated moisture flux convergence (mm/day) for the leading SVD mode. (c) Normalized time-series of (red) precipitation and (black) moisture flux convergence. (d) The linear regression of sea level pressure on time-series of moisture flux convergence. Contour interval is 0.1 hPa.

b. Comparison with full DDS

Figure 2 shows the SmDS and the full DDS results on daily precipitation and standard deviation of daily precipitation over Hokkaido for the current GCM simulation. Climatological precipitation for the full DDS indicates more than 6 mm/day in southern area and less than 4 mm/day in northeast area along the Sea of Okhotsk (Fig. 2a). The standard deviation for the full DDS indicates high values more than 25 mm/day in southern area. SmDS provides a similar spatial pattern of precipitation to the full DDS result (Figs. 2a,b), but it underestimates the amount all over Hokkaido especially in Okhotsk area. The standard deviation of precipitation for the SmDS is also similar to that for the full DDS with a bit underestimation (Figs. 2c,d).

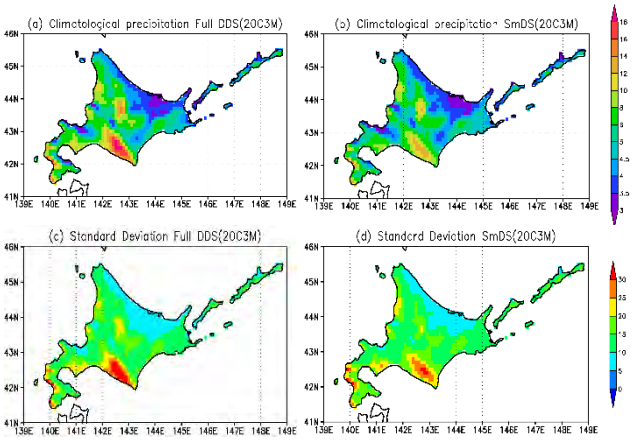


Figure 2: (a,b) Climatological precipitation (mm/day) under 20C3M for (a) the full DDS and (b) the SmDS. (c,d) Standard deviation of precipitation (mm/day) under 20C3M in (c) the full DDS and (d) the SmDS.

Figure 3 shows the full DDS results for the future climate. The SmDS result reproduces similar spatial distribution to the full DDS result, though it slightly exaggerates peaks in average. Consequently, SmDS almost reproduced the statistics of precipitation in the full DDS even in summer season in Hokkaido.

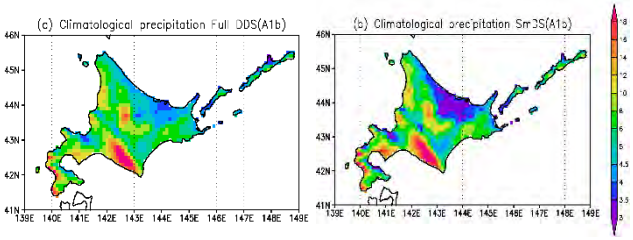


Figure 3: Same as Figs. 2a,b, but for GCM under SRES A1b scenario condition.

c. Comparison with SmDS theory

Figures 4a,b show the relative error of the SmDS estimation to the full DDS one and the correlation coefficient between statistical and dynamical estimations for local precipitation over Hokkaido in the current climate. The relative error is fallen within $\pm 10\%$ though SmDS underestimates the mean more than 30% in southern area. The relative error is less than $\pm 10\%$ in the area where the correlation coefficient indicates more than 0.5 (Figs. 4a,b). This is consistent with the error estimation theory of the SmDS. In the future climate, the relative error (Fig. 4c) ranges within $\pm 20\%$ and the correlation coefficient (Fig. 4d) is less than 0.4 in almost all areas.

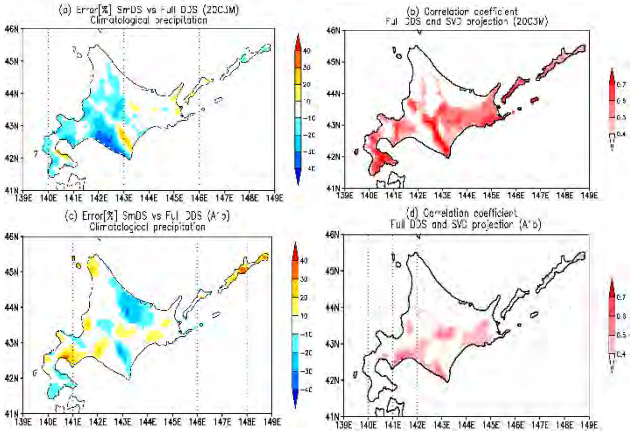


Figure 4: (a) Relative error of the SmDS to the full DDS in climatological precipitation. (b) Correlation coefficient between the statistical and DDS estimations for the climatological precipitation over Hokkaido under the current climate condition. (c,d) Same as (a,b), but for GCM under the future climate condition, respectively.

5. Conclusion

We have attempted to apply SmDS to summertime precipitation over Hokkaido. Comparing with the result based on DDS for the full period, the SmDS result almost reproduced a spatial distribution of average and fluctuation of precipitation under both the current and the future climate conditions.

We have also developed the error estimation theory for the SmDS. An estimate error for the average is related to how many samples we take and how much the local variable is controlled by the global variable. Consistent with theoretical consideration, the error in summertime precipitation climatology is actually small where correlation coefficient is large.

Acknowledgement

This study is supported by the Research Program on Climate Change Adaptation in Ministry of Education, Culture, Sports, Science and Technology.

References

Kuno R, Inatsu M (2014) Development of sampling downscaling: a case for wintertime precipitation in Hokkaido, Clim Dyn, in press.

Sampe T and Xie S.-P (2010) Large-scale dynamics of meiyu-baiu rainband: Environmental forcing by the westerly jet. J.Clim 23: 113-134.

Saito K et al (2006) The operational JMA nonhydrostatic mesoscale model. Mon Wea Rev 134: 1266-1298.

Estimation of the probability distribution of monthly mean temperature by a regression model

Genta Ueno[1], Yukito Iba[1], Koji Dairaku[2] and Izuru Takayabu[3]

[1] The Institute of Statistical Mathematics, 10-3 Midori-cho, Tachikawa, Tokyo 190-8562, Japan (gen@ism.ac.jp)
[2] National Research Institute for Earth Science and Disaster Prevention, Tsukuba, Ibaraki 305-0006, Japan
[3] Meteorological Research Institute, Tsukuba, Ibaraki 305-0052, Japan

We are studying how to evaluate climate ensemble experiments and to construct probability distribution from the ensemble. In the present study we estimate the probability distribution of monthly mean temperature. We have developed a regression model in which we treat reanalysis data and global atmospheric models (MRI-AGCM and CMIP3) as the response variable and the explanatory variables, respectively (Figures 1 and 2). With the regression model we can estimate the model error from the reanalysis data and do not need to prescribe the value in advance. Moreover, we can avoid introducing an emulator, which is too simple to describe the physical consistency. With the regression model (Figure 3) we estimated probability distribution of the monthly mean temperature in Tokyo (Figure 4), and found that inter-annual variations of the temperature in future climate are expected to become large in winter and spring, while those in summer become small.

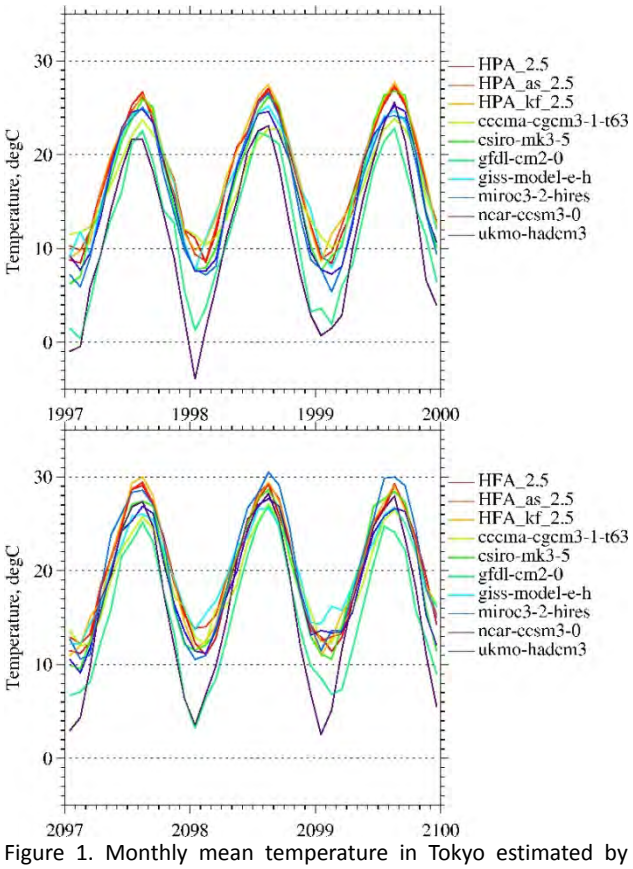


Figure 1. Monthly mean temperature in Tokyo estimated by GCMs in (top) 1997-1999 and (bottom) 2097-2099.

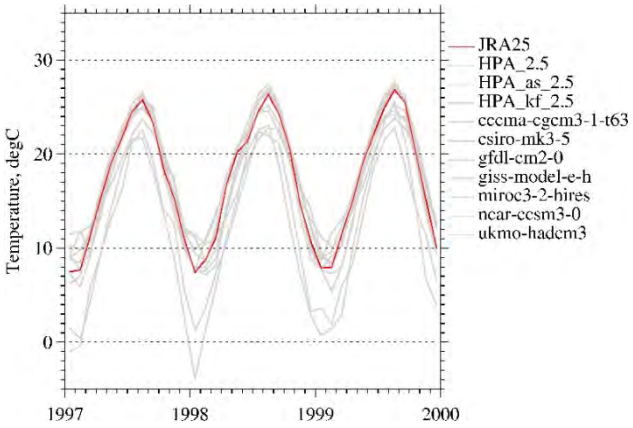


Figure 2. Monthly mean temperature in Tokyo by the JRA reanalysis data (red) and by GCMs (gray) in 1997-1999.

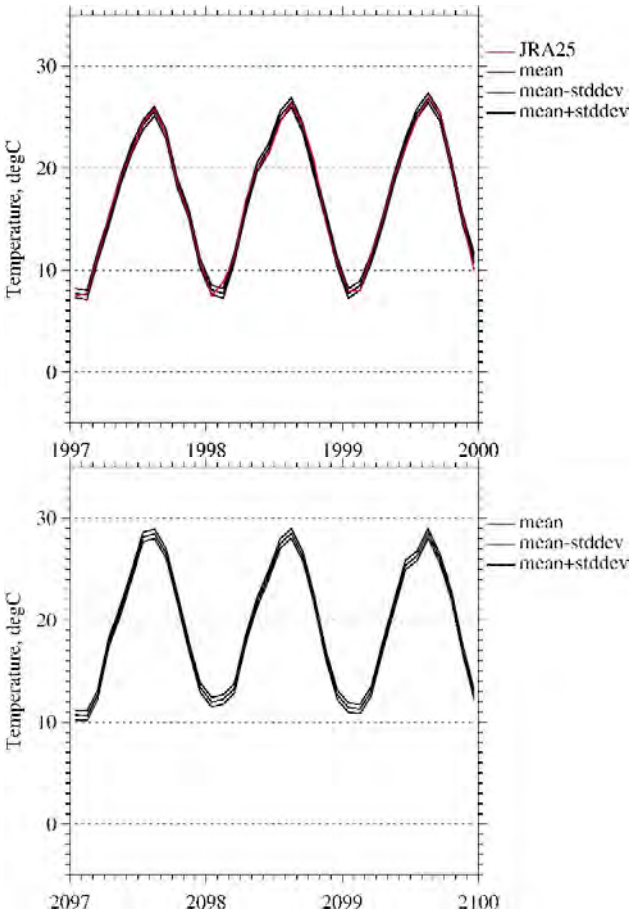


Figure 3. Estimated regression models for monthly mean temperature in Tokyo using a regression model. Mean of the regression model and standard deviations are shown.

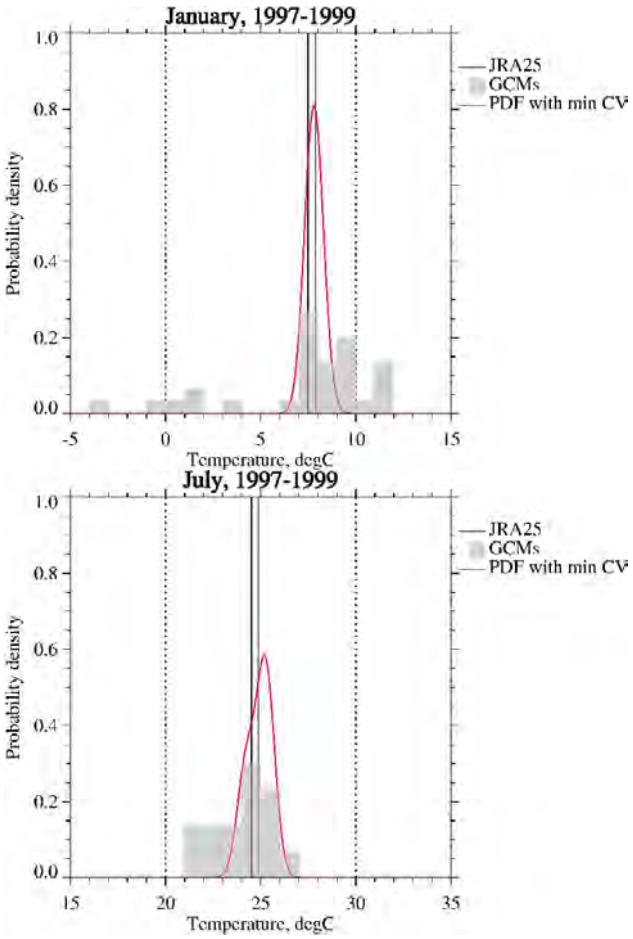


Figure 4. Estimated probability distribution of monthly mean temperature in Tokyo (red), reanalysis data (solid vertical lines), and GCM outputs (gray) in 1997-1999. Upper panel for January, lower for July.

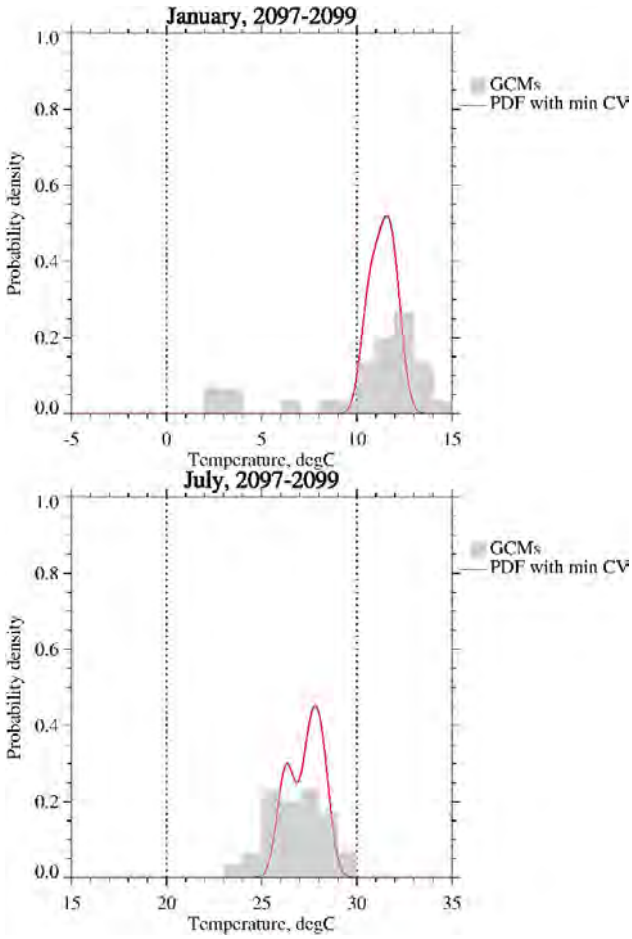


Figure 5. Same for Figure 4 but in 2097-2099.

Regional modeling approaches to study the recent shift in East African long rains

Nicolas Vigaud, Andrew Robertson and Bradfield Lyon

International Research Institute for Climate and Society, Earth Institute, Columbia University, USA (vigaud@iri.columbia.edu)

1. Introduction

The successive failure of East African short (October-December) and long (March-May) rains in 2010-11 led to a severe drought over the region. While poor short rains in 2010 were anticipated given the linkage with La Niña conditions in the Pacific, the long rains do not exhibit such predictability. Recent works from Lyon and DeWitt (2012) support the idea that the failure of the long rains was associated with a recurrent large-scale precipitation pattern following their abrupt decline in 1999. Further, both observations and GCM experiments suggest the dominant role of abrupt changes in sea surface temperatures (SSTs) in the tropical Pacific. The use of a Regional Climate Model (RCM) could help provide local scale climate information and allow studying processes entering into play over the region. However, the study of large-scale teleconnections including the effect of climate change might be challenging using a limited area approach. These issues will be documented through different modeling exercises in the first part of this paper. The usefulness of some methodologies developed recently within the RCM community to disentangle large-scale versus local-scale contributions will be discussed, in particular (i) the interest of regional ensemble simulations generated using perturbed initial conditions and (ii) the advantages and performance of a climate-mode approach already referenced through different regional modeling studies over the continent (Patricola and Cook, 2010; Cook and Vizy, 2013). The final part of this study will present some experimental setups using the Weather Research and Forecasting (WRF) model which might be more relevant to investigate large-scale teleconnections. Multi-scale modeling will then be discussed as it represents a very attractive alternative to examine large-scale influences and local mechanisms associated with the recent shift in East African long rains.

2. RCMs and regional climate information

Dynamical downscaling challenges and limitations will be illustrated through the use of WRF to spatially disaggregate large-scale GCMs output over the continent. In particular the ability of a regional model to reduce large-scale GCMs biases regarding local atmospheric circulation will be investigated together with the uncertainties associated with some of these biases propagating in the regional simulations.

Designing regional experiments to examine synoptic processes will then be documented through a study of tropical-temperate troughs (TTTs) using WRF over southern Africa (Vigaud et al., 2012). These results will be discussed to emphasize the advantages of ensemble experiments and the potential of coupling internally an oceanic mixed layer to study intra-seasonal climate variability and the role of the nearby ocean (Fig.1).

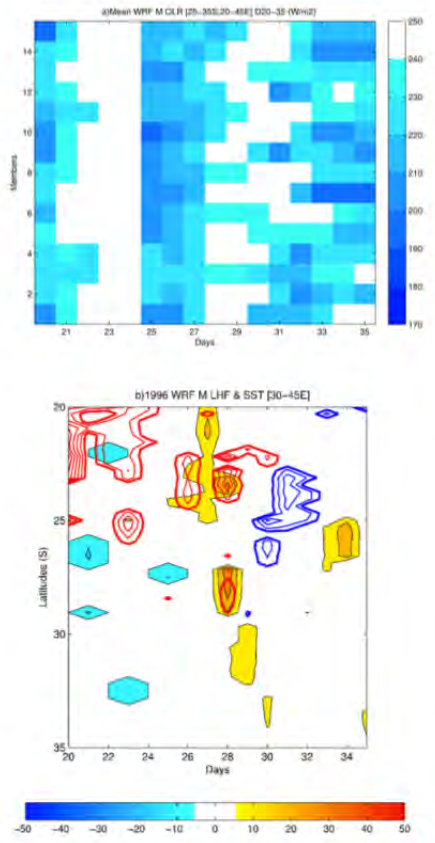


Figure 1. (a) Mean OLR averaged over [25–35S;20–45E] from day 20 to 35 of 1996/1997 austral summer (November–February) for fifteen WRF members using an oceanic mixed layer coupled internally to WRF, (b) Mean WRF sea surface temperatures (blue/red contours starting at and every 0.25C) and latent heat flux (shaded contours in W/m2) differences averaged off southern Africa east coast (30–45E) between the five members simulating the longest-lived TTT events and the five members characterized by the shortest episodes. Warmer SSTs over the Agulhas current region of the Indian Ocean appear to trigger increased latent heat exchange from the Ocean to the atmosphere favoring baroclinic instability and thus convection within TTT systems (Vigaud et al., 2012).

3. Climate-mode experiments for regional studies

Recent studies have shown that forcing a RCM with climatological fields from re-analyses produces reasonable regional climate information for tropical and subtropical regions of Africa at low computational costs (Patricola and Cook, 2010, 2011). This climate-mode methodology is here illustrated through WRF experiments performed to examine East African long rains daily statistics and their recent shift (Fig.2).

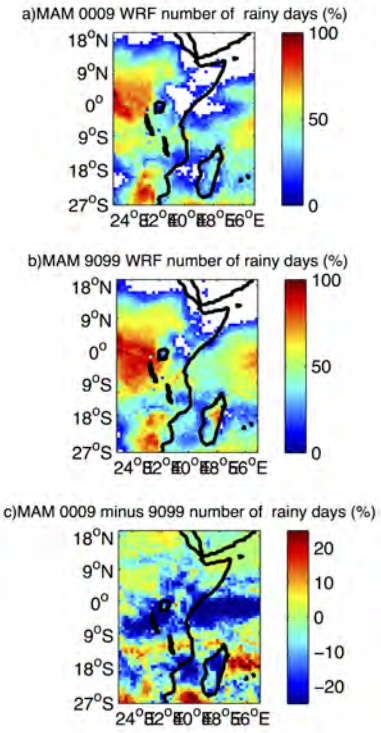


Figure 2. MAM number of rainy days simulated by WRF in climate-mode experiments over Africa at 90km resolution for the 2000-09 (a) and 1990-99 (b) periods together with their differences (c) in % showing their recent decrease since 1999.

4. Towards a global modeling framework

The limited area approach favored in most standard regional modeling exercises can be by itself a substantial limitation. Large-scale variability is assumed to be integrated through lateral boundary forcings, however teleconnections are not systematically and satisfactorily represented even in the case of ENSO (Boulard et al., 2012), which is the main mode of interannual variability in the Earth system.

The non-global modeling framework could be one of the reasons for such discrepancies in reproducing the sign, strength and phasing of large-scale climate signals at local scale. This is an obstacle to be addressed in the case of East African long rains, their recent shift being associated with large-scale teleconnections (Lyon and DeWitt, 2012; Lyon et al., 2013). In this respect different approaches can be developed, in particular tropical band and quasi-global experiments done with WRF. The advantages these offer will be discussed again in regards to daily rainfall statistics (Fig.3).

In parallel, the recent public release of the Model for Prediction Across Scales (MPAS) developed at NCAR (Skamarock et al., 2012) might be an elegant way forward. It would allow the exploration of regional-scale climate processes while maintaining a global modeling framework. Experiments with a high-resolution zoom over East Africa, forced for example by decadal averages of observed SSTs for two contrasting periods before and after 1999 would aid the investigation of the abrupt shift in long rains, while ensemble or multi-season runs will be useful to estimate internal variability.

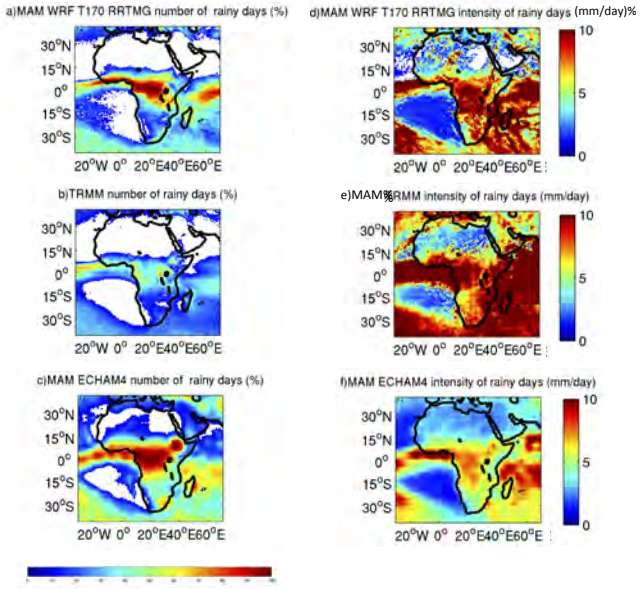


Figure 3. 1982-2009 MAM number of rainy days and their intensities simulated by Global WRF in climate-mode experiments at 75km resolution (a and d), from TRMM (b and e) and ECHAM4.5 forced by climatological SSTs at T42 resolution over the same period (c and f) in %. This illustrates the added value from Global WRF compared with coarser GCM output in terms of daily rainfall statistics.

References

Boulard D., Pohl B., Crétat J., Vigaud N. (2013) Downscaling large-scale climate variability using a regional climate model: the case of ENSO over southern Africa, *Clim Dyn*,, DOI10.1007/s00382-012-1400-6

Cook K.H. and E.K. Vizy (2013) Projected changes in East African rainy seasons, Clim Dyn, 26, 5931-5948

Lyon, B. and D.G. DeWitt (2012) A recent and abrupt decline in the East African long rains, *Geophys. Res. Lett.*, DOI:10.1029/2011GL050337

Lyon B., Barnston A.G., DeWitt D.G. (2013) Tropical Pacific forcing of a 1998-99 climate shift: Observational analysis and climate model results for the boreal spring, *Clim Dyn*, DOI10.1007/s00382-013-1891-9

Patricola C.M. and K. Cook (2010) Northern African climate at the end of the twenty-first century: an integrated application of regional and global climate models, *Clim Dyn*, 35,193-212

Patricola C.M. and K. Cook (2011) Sub-Saharan Northern climate at the end of the twenty-first century: forcing factors and climate change processes, *Clim Dyn*, 37,1165-1188

Skamarock W.C.,, Klemp J.B., Duda M.G., Fowler L.D., Park S.-H. (2012) A multiscale nonhydrostatic atmospheric model using centroidal Voronoi tessellations and C-grid staggering, Mon Weath Rev, 140, pp. 3090-3105

Vigaud N., Pohl B., Crétat J. (2012) Tropical-temperate interactions over southern Africa simulated in a regional model, *Clim Dyn*, DOI10.1007/s00382-012-1314-3

A stochastic regional scale climate change projection experiment using incremental dynamical downscaling and analysis system

Yasutaka Wakazuki[12], Masayuki Hara[2] and Fujio Kimura[2]

[1] University of Tsukuba, Tsukuba, Japan (ywakazki@gmail.com)

[2] Japan Agency for Marine-Earth Science and Technology, Yokohama, Japan

1. Introduction

Regional scale climate change projections play an important role in assessments of influences of global warming and include statistical (SD) and dynamical downscaling (DD) approaches. One of DD methods named as the "incremental dynamical downscaling and analysis system (InDDAS)" is newly developed in this study basing on the pseudo-global-warming (PGW) method developed by Kimura and Kitoh (2007). In the presentation, details of InDDAS and an experiment with the target regions of the Kanto District, Japan and the mountainous area in the central part of Japan would be introduced.

2. Higher approximation

In general, DD uses regional climate model (RCM) with lateral boundary data. In PGW method, the climatological mean difference estimated by GCMs are added to the objective analysis data (ANAL), and the data are used as the lateral boundary data in the future climate simulations. The ANAL is also used as the lateral boundary conditions of the present climate simulation. One of merits of the PGW method is that influences of biases of GCMs in RCM simulations are reduced. Here, the PGW method is regarded as the approximation method to control lateral boundary conditions of RCM runs in the future climate. Only the mean climatological increments of monthly averaged variables estimated by GCM runs are trusted and treated in PGW method. Higher order approximation information of climate changes of GCMs, such as climate changes in relative humidity, year-to-year variation, and short-term disturbances are not considered in PGW method. On the other hand, the developed InDDAS treat climate changes in relative humidity and year-to-year variations. To treat climate changes in relative humidity, a new humidity variable "modified relative humidity" developed by Wakazuki (2013) is introduced. Climate changes in year-to-year variation is introduced by Wakazuki et al. (2010).

3. Multi-GCM treatment

Uncertainties of climate change projections estimated by many GCMs are large and are not negligible. Thus, stochastic regional scale climate change projections are expected for assessments of influences of global warming. Many RCM runs must be performed to make stochastic information. However, the computational costs are huge because grid size of RCM runs should be small to resolve heavy rainfall phenomena. Therefore, the number of runs to make stochastic information must be reduced. In InDDAS, climatological differences added to ANAL become statistically pre-analyzed information. The climatological differences of many GCMs are divided into mean climatological difference (MD) and departures from MD. The departures are analyzed by singular vector decomposition, and positive and negative perturbations (positive and negative singular values multiplied by departure patterns (singular vectors)) with multi modes are added to MD. Consequently, the most likely future states are calculated with climatological difference of MD. Figure 1 shows that temporal variation of temperature for 1st and 2nd mode perturbation from ensemble mean. For example, future states in cases that temperature increase is large and small are calculated with MD plus positive and negative perturbations of the 1st mode. The patterns of higher modes are mainly associated with the variations of atmospheric circulations.

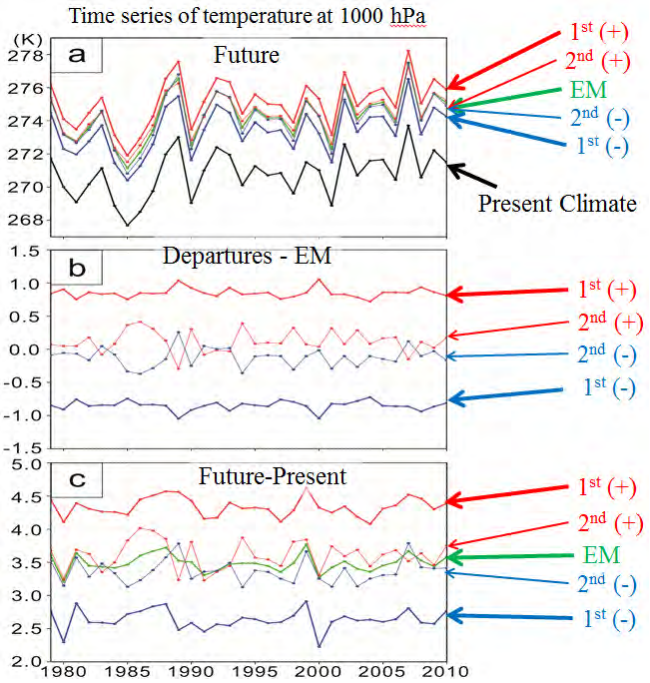


Figure 1. Temporal variation of (a) temperature, (b) the departure from ensemble mean, and (c) the climatological increments at 1000 hPa for 1st and 2nd modes estimated by 19 CMIP-3 GCMs with the target region around Japan.

4. A stochastic RCM experiment

Multi-GCM stochastic runs using InDDAS are performed with the target region in the central part of Japan. To estimate climate changes in heavy precipitation and snowpack, high-resolution simulation with the grid size of 6 km using WRF version 3.3.1 are calculated for 31 years. Various climate changes and their uncertainties are

estimated. Temporal shift of snow melting toward the earlier direction, decrease of maximum snow depth, intensification of precipitation, and increase of temperature are projected. From three RCM runs for a mode, variability of results is able to be estimated. Here, the statistical locations of the three runs are determined beforehand. The intervals among the results of three runs are mostly constant. Therefore, the results of RCM runs are able to be expressed by the Gaussian probability density function. However, for some variables such as precipitation amount, non-Gaussian functions for stochastic information might be appropriate.

5. Summary

The new dynamical downscaling method InDDAS is developed for approximated and stochastic regional climate change projections. The development includes (i) higher order approximation schemes for boundary data of RCM and (ii) stochastic projection schemes. For (i), InDDAS is able to treat climate changes in year-to-year variation and relative humidity of GCMs. However, the methods to treat climate change in short-term disturbances are not still developed. For (ii), many projections of GCMs are statistically analyzed before the RCM downscaling runs, and the number of runs is reduced. The results of runs are analyzed to make stochastic information, because the statistical locations of the runs are determined.

References

Wakazuki, Y., 2013: Modified relative humidity using the Johnson's SB distribution function. SOLA, 9, 111-114, doi:10.2151/sola.2013-025

Wakazuki, Y., M Hara, F Kimura, 2010: A method to treat climate changes of year-to-year variations in the pseudo-global-warming method as a dynamical downscaling. American Geophysical Union 2010 Fall Meeting. San Francisco USA.

Reducing model ensemble size for climate change impact application – a case study

Renate A. I. Wilcke[1], Lars Bärring[1,3] and Thomas Mendlik[2]

[1] Rossby Centre, Swedish Meteorological and Hydrological Institute, Norrköping, Sweden (renate.wilcke@smhi.se)
[2] Wegener Center for Climate and Global Change, University of Graz, Austria
[3] Centre for Environment and Climate Research, Lund University, Sweden

1. Introduction

Model inter-comparison experiments as well as regional downscaling experiments produce large matrices of GCM-RCM combinations. Such ensembles intend to sample a range of model assumptions and possible future climates. For climate change impact studies, it is not always feasible to use all GCM-RCM scenarios. Therefore, the question of selecting an optimum of representative subset of models needs to be answered.

Mendlik and Gobiet (2014, sub.) proposed a method to aids the user to select an optimum subset of climate scenarios which covers the spread of the full ensemble with scenarios being as independent as possible. The method is based on hierarchical clustering of loadings from a PCA on various climate change signals.

Here we apply this method in a case study to reduce the EURO-CORDEX (EUR-11 and EUR-44) ensemble for different climate impact applications. The focus is on analysing the sensitivity of the scenario selection process on variables and indices used for the ensemble reduction.

2. Study outline

The idea behind ensemble reduction is to save computational costs in impact studies while conserving the spread in climate change signals (ccs) and in realisations of climate by the scenarios to be analysed. The spread in ccs is multidimensional and includes models, variables, temporal and spatial components. The dimension of variables can be expanded including uni- and multivariate climate indices in the analyses. The ccs of those indices can differ substantially from the ccs of the variables they are derived from.

In this study standard climate model output like temperature (mean, max, min), precipitation, humidity, and wind are used and indices like degree days and temperature-humidity index are derived.

The spatial variability in ccs is covered by using six separate regions in northern Europe. The ccs of variables is calculated for the four seasons separately. The model dimension is spanned by nine GCMs used to force RCA4 (Samuelsson et al., 2011).

Figure 1 shows an exemplary clustering of 9 models using the ccs (2069-2098 minus 1971-2000) of mean temperature (T), maximum temperature (Tmax), 'Beetle Degree Day', BDD, degree day threshold from a spruce bark beetle study (Jönsson and Bärring, 2011), and number of days when temperature exceeds a certain threshold (ET).

Preliminary results are presented, showing the differences in the clustering for different input variables and indices.

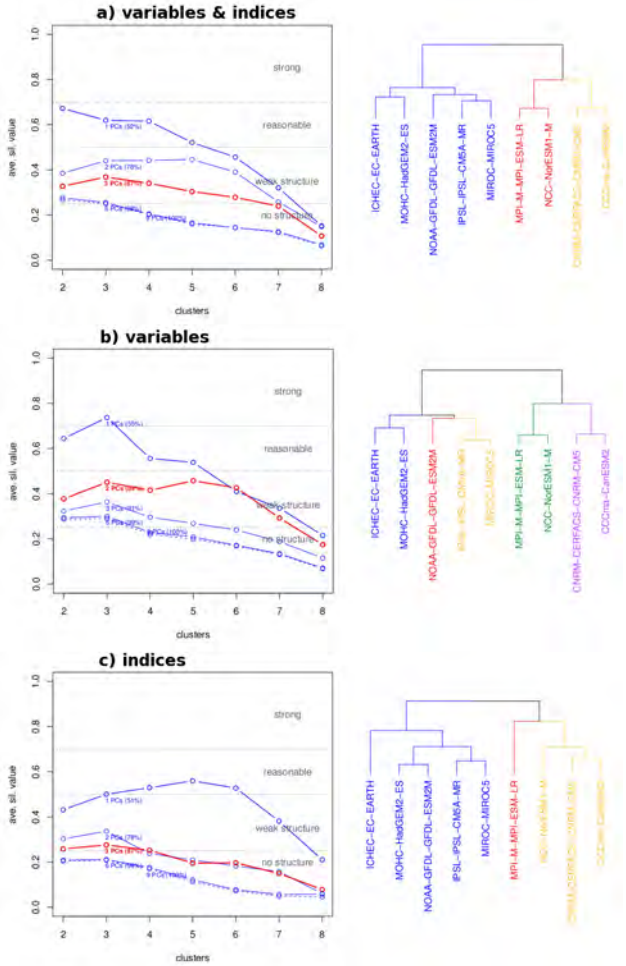


Figure 1. Silhouette plots and hierarchical clustering for 9 models (CORDEX EUR-44 rcp 8.5 using the ccs (2069-2098 minus 1971-2000) of a) T, Tmax, BDD, ET and b) T, Tmax and c) BDD, ET calculated for 6 regions in Northern Europe. The red lines in the silhouette plots indicate the number of PC explaining more than 80% of the variability. Those PCs have been chosen for the clustering.

Acknowledgement

This work is supported by the European project CLIP-C and the Swedish research programme Mistra-SWECIA

References

Jönsson, A.M., Bärring, L. (2011) Future climate impact on spruce bark beetle life cycle in relation to uncertainties in regional climate model data ensembles, Tellus A, 63, 158-173.

Mendlik, T., Gobiet A. (2014) Selecting climate simulations for impact studies based on multivariate patterns of climate change, Climatic Change, submitted.

Samuelsson, P., Jones, C.G., Willén, U., Ullerstig, A., Gollvik, S., Hansson, U., Jansson, C., Kjellström, E., Nikulin, G., Wyser, K. (2011) The Rossby Centre Regional Climate model RCA3: model description and performance, Tellus A, 63, 4-23.

Climate change scenarios over complex topography: assessing the added value of dynamical downscaling

Elias M. Zubler, Friederike Fröb, Andreas M. Fischer, Mark A. Liniger and C. Appenzeller

Federal Office of Meteorology and Climatology MeteoSwiss, Zurich, Switzerland (elias.zubler@meteoswiss.ch)

1. Introduction

There is a growing demand for reliable and up-to-date climate change information at local to regional scale in order to effectively manage future climate risks. The provision of climate change scenarios is a highly challenging task mainly due to the cascade of uncertainties ranging from emission uncertainties over model uncertainties down to uncertainties arising from natural fluctuations.

To sample part of these uncertainties, climate change scenarios are commonly constructed based on the joint evaluation of several future model projections. Moreover, since the information provided by general circulation models (GCMs) is too coarse for many applications, a subsequent downscaling step is necessary. This is often accommodated by running regional climate models (RCMs) driven by GCMs at their lateral boundaries.

In Switzerland, the RCM-GCM model suite of the EU project ENSEMBLES was the basis for generating the climate change scenarios "CH2011" (CH2011, 2011). Temperature and precipitation changes were evaluated as seasonal means for five regions and three future scenario periods. Uncertainties were assessed based on a Bayesian multi-model combination algorithm (Buser et al. 2009, Fischer et al. 2012). One limitation in the CH2011 scenarios is the way model and emission uncertainty is represented in the regional projections (in essence, too few GCMs are involved and all models run according to the A1B emission scenario only).

This study is part of the ELAPSE project which is related to the COST Action VALUE (http://www.value-cost.eu) and which aims at exploring the uncertainty in the existing Swiss scenarios. We inter-compare the regional climate change responses separately in the RCMs and in their driving GCMs. The ultimate goal is to derive scaling relationships that can be applied to GCM projections lacking an explicit dynamical downscaling step such as the CMIP5 model experiments (Taylor et al. 2009, 2012). If successful, this would allow expanding on the model sample size and emission scenarios.

2. Data & Method

Seasonal mean temperature and precipitation changes over the Alpine region defined in the PRUDENCE project (Christensen et al. 2007) are evaluated in two configurations of ENSEMBLES model projections: (a) in 14 coupled RCM-GCM projections at 25 km resolution and (b) in their driving GCM data at about 2.5° resolution (6 simulations). The projected changes and associated uncertainties (for the A1B emission scenario) are further compared to model projections from CMIP5. These GCM simulations run at horizontal resolutions between 1.8° and 3.75° depending on the model and in total comprise a number of 20 simulations according to the RCP6.0 scenario (comparable to A1B). The analysis is performed for 30-year scenario periods across the 21st century. As reference period we use 1980-2009 as in CH2011 (2011). In order to model projection uncertainty and internal decadal variability, we will apply the same Bayesian multi-model combination as described in Fischer et al. (2012).

3. Preliminary Results

First results show consistent climate change signals over the whole Alpine region for the two emission scenarios A1B (ENSEMBLES) and RCP6.0 (CMIP5). These scenarios lead to roughly the same cumulative carbon emissions over the course of the 21st century and are thus directly comparable. The largest differences between the data sets are found for summer temperature and precipitation change. Here, uncertainties are derived from the empirical distributions rather than through Bayesian statistics.

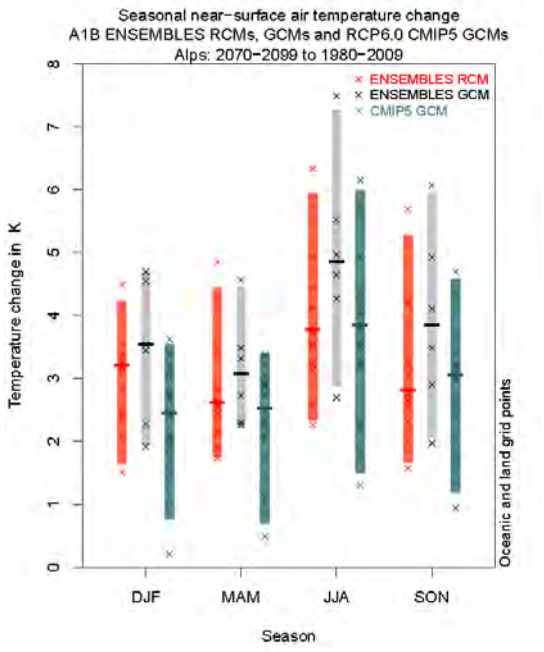


Figure 1. Expected seasonal temperature change (°C) over the Alpine region for the scenario period 2070-2099 using 3 different multi-model sets. Bars indicate the 95% confidence interval. The crosses correspond to individual model projections. Number of models: 14, ENSEMBLES RCMs, 6 GCMs, 20 CMIP5 GCMs.

Whereas the ENSEMBLES GCMs project a warming in summer of up to about 7°C for 2070-2099 with respect to 1980-2009, about 1.3°C less is obtained by the ENSEMBLES RCMs and the more recent GCM simulations within CMIP5 (Fig. 1). In all seasons, the Alpine warming is smaller in ENSEMBLES RCMs and CMIP5 than in the ENSEMBLES GCMs. Surprisingly the ENSEMBLES RCMs do not reflect the signal of their driving GCMs but rather agree with the CMIP5 multi-model ensemble.

In case of precipitation (Fig. 2), the ENSEMBLES RCMs as well as the driving GCMs project a statistically significant drying in summer at the end of the 21st century (down to -40% in case of the ENSEMBLES GCMs). This expected drying is much less clear in the case for the larger ensemble of CMIP5 models. They project an ensemble mean precipitation change of about -8% but uncertainties range between -30% and +20%. Hence precipitation may increase or decrease even in summer. For the other seasons result are roughly comparable.

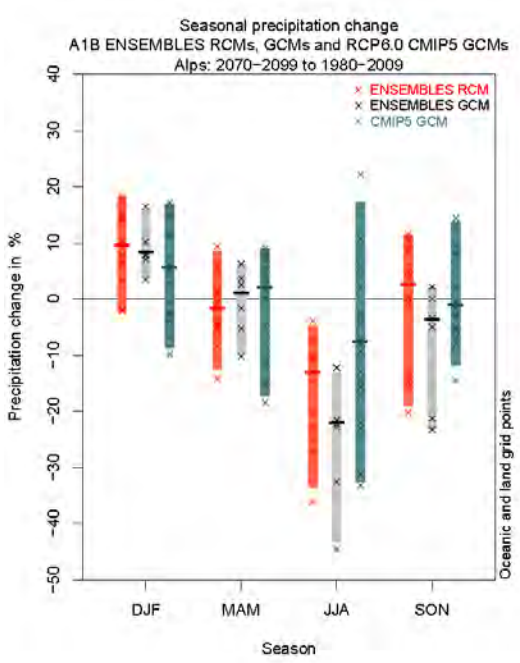


Figure 2. Same as Fig. 1, but for relative precipitation change (%).

4. Summary and Outlook

A first insight into the relationship of the climate change signal from RCM projections and from its driving GCM projections could be gained with the help of raw model output. Strongest differences were detected in summer for both precipitation and temperature.

This analysis is the basis for subsequent studies aiming to test whether robust scaling factors among the joint multi-model projections can be derived and to quantify what the associated uncertainties are. In this way, the so-derived (probabilistic) regional climate response could largely extend our model data basis and uncertainty estimates of regional climate change. To this stage, clear differences were found between the different multi-model settings. It remains unclear if similar relationships exist for other parameters besides temperature and precipitation.

References

Buser, C. M., Künsch, H. R., Lüthi, D., Wild, M., Schär, C. (2009). Bayesian multi-model projection of climate: bias assumptions and interannual variability. Climate Dynamics, 33(6), 849-868.

CH2011 (2011), Swiss Climate Change Scenarios CH2011, published by C2SM, MeteoSwiss, ETH, NCCR Climate and OcCC, Zurich, Switzerland, 88 pp, ISBN: 978-3-033-03065-7.

Christensen, J. H., Carter, T. R. , Rummukainen, M., Amanatidis, G. (2007). Evaluating the performance and utility of regional, climate models: the PRUDENCE project. Climatic Change 81, 1-6.

Fischer, A. M., Weigel, A. P., Buser, C. M., Knutti, R., Künsch, H. R., Liniger, M. A., Appenzeller, C. (2012). Climate change projections for Switzerland based on a Bayesian multi-model approach. International Journal of Climatology, 32(15), 2348-2371.

Taylor, K. E., Stouffer, R. J., Meehl, G. A. (2009). A Summary of the CMIP5 Experiment Design. Retrieved November 2013, from CMIP5 Coupled Model Intercomparison Project: http://cmip-pcmdi.llnl.gov/cmip5/experiment_design.html.

Taylor, K. E., Balaji, V., Hankin, S., Juckes, M., Lawrence, B., Pascoe, S. (2012). CMIP5 Data Reference Syntax (DRS) and Controlled Vocabularies. Retrieved from CMIP5 Coupled Model Intercomparison Project: http://cmip-pcmdi.llnl.gov/cmip5/.

Baltic Earth

Baltic Earth - Earth System Science for the Baltic Sea Region

An open research network to achieve an improved Earth system understanding of the Baltic Sea region

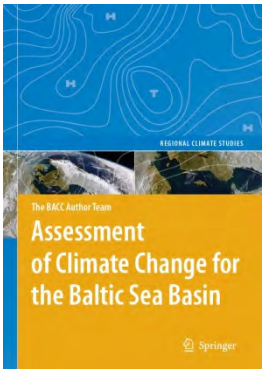
H. E. Markus Meier[1], Anna Rutgersson[2], Marcus Reckermann[3] and the Baltic Earth Interim Science Steering Group

[1] Swedish Meteorological and Hydrological Institute, Norrköping, Sweden,
and Department of Meteorology, Stockholm University, Sweden (markus.meier@smhi.se)
[2] Department of Earth Sciences, Uppsala University, Uppsala, Sweden
[3] International Baltic Earth Secretariat, Helmholtz-Zentrum Geesthacht, Germany

Extending the knowledge of the regional Earth system in the Baltic Sea region

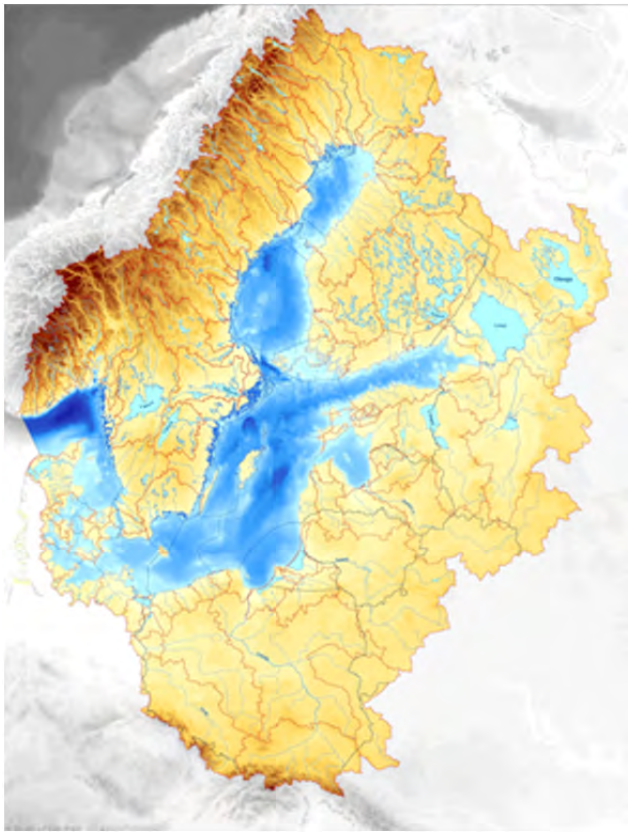
The goal of Baltic Earth is to achieve an improved Earth system understanding of the Baltic Sea region. Baltic Earth is the successor to BALTEX that was terminated in June 2013 after 20 years and two successful phases. The research components of BALTEX continue to be relevant, but now have a more holistic focus encompassing processes in the atmosphere, on land and in the sea, as well as processes and impacts related to the anthroposphere. Specific interdisciplinary research challenges have been formulated by the Baltic Earth Interim Science Steering Group to be approached by the new programme in the coming years. The continuity in basic research fields, structure (secretariat, conferences, publications) and the international network (people and institutions) is symbolized by the logo, which is similar but still distinctly different from the BALTEX logo.

Scientific assessments and Grand Challenges



A major means of achieving the goals of Baltic Earth will be scientific assessments of particular research topics to be prepared by expert groups. Similar to the BACC approach, the assessments shall help to identify gaps and inconsistencies in the current knowledge. A Baltic Earth Science Plan will be established by mid 2014, with a definition of core research questions, so-called “Grand Challenges”. They are currently:

1. Salinity dynamics in the Baltic Sea
2. Land-Sea biogeochemical feedbacks in the Baltic Sea region
3. Natural hazards and extreme events in the Baltic Sea region
4. Understanding sea level dynamics in the Baltic Sea
5. Understanding regional variability of water and energy exchanges



The Baltic Sea catchment basin

The Grand Challenges are intended as flexible, regularly updated research topics and will be dealt with by specific working groups. In addition, the BALTEX Working Groups on the “Utility of Regional Climate Models”, and “Assessment of Scenario Simulations for the Baltic Sea 1960-2100 “ will continue in Baltic Earth. Dedicated working groups have also been established on “Outreach and Communication” and “Education”.

The human impact shall be assessed at all levels, wherever possible and reasonable. New Grand Challenges and modifications of existing ones can be implemented by the steering committee and the working groups, by using the assessments of existing research and knowledge, and the open discussions at conferences and workshops. The Grand Challenges are foreseen as research foci for periods of about 3-4 years (then

terminated or updated). It is envisaged that Baltic Earth will be internationally embedded in a similar manner as was BALTEX.

Baltic Earth intends to provide a “service to society” in the respect that the assessments may provide an overview of knowledge gaps, and the communication with different stakeholders may help to identify open scientific questions relevant for society, which could be approached by funded research projects.



Baltic Earth will also be committed to educational activities with the establishment of regular Baltic Earth Summer Schools, the first of which is intended to take place in 2015. The first dedicated Baltic Earth Conference is planned for 2016.

“Products” of Baltic Earth will include:

- Conferences
- Workshops
- Assessment Projects
- Research Projects
- Summer Schools

References

Meier H.E.M., Rutgersson A. and Reckermann M. (2014) An Earth System Science Program for the Baltic Sea Region. Eos Vol. 95, No. 13, 109-110.

www.baltic-earth.eu

International Baltic Earth Secretariat Publications

ISSN 2198-4247

No. 1 Programme, Abstracts, Participants. Baltic Earth Workshop on ”Natural hazards and extreme events in the Baltic Sea region”. Finnish Meteorological Institute, Dynamicum, Helsinki, 30-31 January 2014. International Baltic Earth Secretariat Publication No. 1, January 2014.

No. 2 Conference Proceedings of the 2nd International Conference on Climate Change - The environmental and socio-economic response in the Southern Baltic region. Szczecin, Poland, 12-15 May 2014. International Baltic Earth Secretariat Publication No. 2, May 2014.

No. 3 Workshop Proceedings of the 3rd International Lund Regional-Scale Climate Modelling Workshop ”21st Century Challenges in Regional Climate Modelling”. Lund, Sweden, 16-19 June 2014. International Baltic Earth Secretariat Publication No. 3, June 2014.

For a list of International BALTEX Secretariat Publications (ISSN 1681-6471), see www.baltex-research.eu/publications

International Baltic Earth Secretariat Publications
ISSN 2198-4247